

1995104178

NASA Conference Publication 3266

303180

Ozone in the Troposphere and Stratosphere Part 1

(NASA-CP-3266-Pt-1) OZONE IN THE
TROPOSPHERE AND STRATOSPHERE, PART
1 (NASA, Goddard Space Flight
Center) 475 p

N95-10590
--THRU--
N95-10694
Unclas

H1/47 0018651

*Proceedings of the
Quadrennial Ozone Symposium 1992
held in Charlottesville, Virginia, U.S.A.
June 4-13, 1992*



NASA Conference Publication 3266

Ozone in the Troposphere and Stratosphere Part 1

Edited by
Robert D. Hudson
University of Maryland
College Park, Maryland

Proceedings of the
Quadrennial Ozone Symposium 1992
held in Charlottesville, Virginia, U.S.A.
June 4-13, 1992



National Aeronautics
and Space Administration

Goddard Space Flight Center
Greenbelt, Maryland 20771

1994

This publication is available from the NASA Center for AeroSpace Information,
800 Elkridge Landing Road, Linthicum Heights, MD 21090-2934, (301) 621-0390.

International Ozone Commission

President: Gerard J. Megie

Vice-President: Alvin J. Miller

Secretary: Rumen Bojkov

Scientific Program Committee Members

Co-Chairmen:

G. J. Megie, France

R. D. Hudson, USA

R. D. Bojkov, Canada

D. H. Ehhalt, FRG

S. Liu, USA

J. B. Kerr, Canada

Y. Khattatov, USSR

A. W. Matthews, NZ

A. J. Miller, USA

T. Ogawa, Japan

S. A. Penkett, UK

H. Reichle, USA

U. Schmidt, FRG

R. S. Stolarski, USA

B. Subbaraya, India

A. Thompson, USA

Sponsors

Alternative Fluorocarbons Environmental Acceptability Study

American Geophysical Union

American Meteorological Society

Environmental Protection Agency

National Aeronautics and Space Administration

National Oceanic and Atmospheric Administration

National Science Foundation

University of Virginia

Virginia Space Grant Consortium

World Meteorological Organization

PREFACE

The 1992 Quadrennial Ozone Symposium was held from June 4 to 13 at the University of Virginia in the United States of America. This was the seventeenth symposium organized by the International Ozone Commission and was equal in size to the symposium held in 1988. The symposium was devoted to all aspects of atmospheric ozone, covering both the troposphere and stratosphere. Almost 500 scientists from 35 countries participated in this international event. Over 400 papers were presented orally or as posters. The oral papers were divided into the following sessions:-

Troposphere

- (a) Ozone Trends and Climatology
- (b) Global and Regional Modeling
- (c) Ozone: The Human Impact

Stratosphere

- (a) Ozone and Climate
- (b) Measurements
- (c) Results from Upper Atmosphere Research Satellite
- (d) The Arctic
- (e) The Antarctic
- (f) Trends
- (g) Theory and Modelling
- (h) Volcanic Effects

Published in these two volumes are two hundred and thirty two of the presented papers. All papers have passed an initial review process. However, in order to produce this publication as quickly as possible, it was left to the authors to accommodate the reviewer's comments without editorial scrutiny of their final submission. These papers have been divided into sections that do not necessarily follow those of the oral presentations. This is due partly to the fact that some presented papers were not submitted for publication, and partly because the poster papers did not always fit into the categories used for the oral papers.

The Editor wishes to acknowledge the assistance rendered by many colleagues who responded with time and effort to review the numerous manuscripts.

Robert D. Hudson
College Park
Maryland

C O N T E N T S

PART I

TROPOSPHERE

OZONE TRENDS AND CLIMATOLOGY

Trends in Surface Ozone Over Europe, 1978-1992 <i>P.S. Low, P.M. Kelly and T.D. Davies</i>	3
Tropospheric Ozone at 45°S <i>W.A. Matthews</i>	7
Measurements of Lower Tropospheric Ozone at Mid-Latitudes of the Northern and Southern Hemisphere <i>H.E. Scheel, R. Sladkovic, E.G. Brunke, W. Seiler</i>	11
Analysis of a 7 Year Tropospheric Ozone Vertical Distribution at the Observatoire De Haute Provence <i>M. Beekmann, G. Ancellet and G. Megie</i>	15
Ozone Measurements from a Global Network of Surface Sites <i>S.J. Oltmans, H. Levy II</i>	19
Broad Features of Surface Ozone Variations Over Indian Region <i>R.R. Shende, K. Jayaraman, C.R. Sreedharan and V.S. Tiwari</i>	24
Tropospheric Ozone Measurements at the Equatorial Region (1980-88) <i>M. Ilyas</i>	33
Specific Features of Space-Time Variations of Ozone During The Development of Intensive Tropical Disturbances <i>A.F. Nerushev and V.I. Vasiliev</i>	37
Annual Variability of Ozone Along Alpine Hillsides <i>E. Putz and W. Kosmus</i>	41
The Vertical Distribution of Ozone at Pretoria from July 1990 to June 1991 and its Changes <i>M. Zunckel, R.D. Diab, C.B. Archer and M.W.J. Scourfield</i>	45
Seasonal Budgets of Ozone and Oxidant Precursors in an Industrial Coastal Area of Northern Italy <i>T. Georgiadis, L. Alberti, P. Bonasoni, F. Fortezza, G. Giovanelli and V. Strocchi</i>	48

GLOBAL AND REGIONAL MODELING

Tropospheric Ozone in the Western Pacific Rim: Analysis of Satellite and Surface-Based Observations Along With Comprehensive 3-D Model Simulations <i>Y. Sunwoo and G.R. Carmichael</i>	53
Simulations of Isoprene - Ozone Reactions for a General Circulation/Chemical Transport Model <i>P.A. Makar and J.C. McConnell</i>	57
Ozone Formation During an Episode Over Europe: A 3-D Chemical/Transport Model Simulation <i>T. Berntsen and I.S.A. Isaksen</i>	62
Estimates of the Changes in Tropospheric Chemistry Which Result From Human Activity and Their Dependence on NO _x Emissions and Model Resolution <i>M. Kanakidou, P.J. Crutzen and P.H. Zimmermann</i>	66
Comparison and Analysis of Aircraft Measurements and Mesoscale Atmospheric Chemistry Model Simulations of Tropospheric Ozone <i>J.E. Pleim and J.K.S. Ching</i>	70
Sources and Distribution of NO _x in the Upper Troposphere at Northern Midlatitudes <i>F. Rohrer, D.H. Ehhalt and A. Wahner</i>	74
A Global Numerical Study of Radon ²²² and Lead ²¹⁰ in the Atmosphere Using the AES and York University CDT General Circulation Model, (AYCG) <i>S.R. Beagley, J. de Grandpre, J.C. McConnell, R. Laprise and N. McFarlane</i>	78
On the Transport of Trace Gases by Extra-Tropical Cyclones <i>M.A.F. Allaart, L.C. Heijboer and H. Kelder</i>	82
An Analysis of the Impacts of Global Climate and Emissions Changes on Regional Tropospheric Ozone <i>K. John, K.C. Crist and G.R. Carmichael</i>	85
Estimates of Ozone Response to Various Combinations of NO _x and VOC Emission Reductions in the Eastern United States <i>S.J. Roselle, K.L. Schere and S-H. Chu</i>	89
Modeling Ozone Episodes in the Baltimore-Washington Region <i>W.F. Ryan</i>	93
Numerical Simulation of the Interaction of Transport, Diffusion and Chemical Reactions in an Urban Plume <i>B. Vogel, H. Vogel and F. Fiedler</i>	97

A Trajectory Modeling Investigation of the Biomass Burning - Tropical Ozone Relationship <i>K.E. Pickering, A.M. Thompson, D.P. McNamara, M.R. Schoeberl, L.R. Lait, P.A. Newman, C.O. Justice and J.D. Kendall.....</i>	101
Enhancement of Free Tropospheric Ozone Production by Deep Convection <i>K.E. Pickering, A.M. Thompson, J.R. Scala, W.K. Tao, R. Dickerson and J. Simpson.....</i>	105
The Sensitivity of Tropospheric Chemistry to Cloud Inter- actions <i>J.E. Jonson and I.S.A. Isaksen.....</i>	109

MEASUREMENTS

Tropospheric Ozone and Aerosol Variability Observed at High Latitudes with an Airborne Lidar <i>E.V. Browell, C.F. Butler, M.A. Fenn, S.A. Kooi and W.B. Grant.....</i>	115
Direct Measurement of Tropospheric Ozone using TOMS Data <i>R.D. Hudson and J-H. Kim.....</i>	119
Ozone Transport During a Cut-Off Low Event Studied in the Frame of the TOASTE Program <i>G. Ancellet, M. Beekmann, A. Papayannis and G. Megie....</i>	122
A Novel Ozone Sensor for Various Environmental Applications <i>H. Gusten G. Heinrich, R.W.H. Schmidt and U. Schurath... </i>	127
Surface Ozone Variability at Kislovodsk Observatory <i>N.F. Elansky, O.V. Makarov and I.A. Senik.....</i>	130
Carbon Monoxide Measurements at Mace Head, Ireland <i>B.G. Doddridge, R.R. Dickerson, T.G. Spain, S.J. Oltmans and P.C. Novelli.....</i>	134
Episodes of Vertical and Horizontal Ozone Transport Monitored at Italy's Mt. Cimone Observatory <i>T. Colombo, V. Cundari, P. Bonasoni, M. Cervino, F. Evangelisti, T. Georgiadis and G. Giovanelli.....</i>	138
Evaluation of the Production and the Destruction of Ozone in the Lower Atmosphere <i>H. Muramatsu.....</i>	142
Determination of Dry Deposition of Ozone: Comparison of Different Measuring Techniques <i>I. Colbeck and A. Simmons.....</i>	146

Turbulent Transport and Production/Destruction of Ozone in a Boundary Layer Over Complex Terrain <i>G.K. Greenhut, A.M. Jochum, and B. Neininger.....</i>	150
Transport into the Troposphere in a Tropopause Fold/Cut-Off Low System <i>G. Vaughan, J.D. Price and A. Howells.....</i>	154
Large-Scale Circulation Patterns Associated with High Concentrations of Tropospheric Ozone in the Tropical South Atlantic Ocean <i>K.M. Fakhruzzaman, J. Fishman, V.G. Brackett, J.D. Kendall and C.O. Justice.....</i>	158
Airborne Measurements of Biomass Burning Products over Africa <i>G. Helas, J. Lobert, J. Goldammer, M.O. Andreae, J.P. Lacaux and R. Delmas.....</i>	162
Long Path Monitoring of Tropospheric O ₃ , NO ₂ , H ₂ CO and SO ₂ <i>A.C. Vandaele, M. Carleer, R. Colin and P.C. Simon.....</i>	166
Results of Ozone Measurements in Northern Germany - A Case Study - <i>M. Schmidt.....</i>	170
The Gradient of Meteorological and Chemical Variables across the Tropopause <i>R.R. Dickerson, B.G. Doddridge, O. Poulida and M.A. Owens.....</i>	174

STRATOSPHERE

TRENDS

Long-Term Observed Ozone Trends in the Free Troposphere and Lower Stratosphere <i>J. London.....</i>	181
Trend Analysis of the Long-Term Swiss Ozone Measurements <i>J. Staehelin, J. Bader and V. Gelpke.....</i>	186
On Long-Term Ozone Trends at Hohenpeissenberg <i>H. Claude, W. Vandersee and K. Wege.....</i>	190
Total Ozone Trends over the U.S.A. During 1979-1991 from Dobson Spectrophotometer Observations <i>W.D. Komhyr, R.D. Grass, G.L. Koenig, D.M. Quincy, R.D. Evans and R.K. Leonard.....</i>	195

Ozone Trends Estimated from Umkehr Observations Made at Edmonton, Alberta, Canada <i>C.T. McElroy, E.W. Hare and J.B. Kerr</i>	199
Statistic Analysis of Annual Total Ozone Extremes for the Period 1964-1988 <i>J.W. Krzyscin</i>	203
Long-Term Changes in the Statistical Distribution of Dobson Total Ozone in Selected Northern Hemisphere Geographical Regions <i>J.W. Krzyscin</i>	207
Recalculated Values of the Total Ozone Amount Over Oslo, 60° N, for the Period 1979-1992 <i>S.H.H. Larsen, T. Svendby, F. Tonnessen and A. Dahlback</i> .	211
TOMS Total Ozone Data Compared With Northern Latitude Dobson Ground Stations <i>B. Heese, K. Barthel, and O. Hov</i>	215
Systematic Comparison Between the Ground Based Automated Dobson of the Observatory of Haute-Provence and TOMS Since 1983 <i>M.F. Merienne, A. Barbe and P. Da Conceicao</i>	219
Total Ozone Change Estimations for Different Time Intervals <i>V.E. Fioletov</i>	223
Difference Between Recalculated and Original Dobson Total Ozone Data From Hradec Kralove, Czechoslovakia, 1962-1990 <i>K. Vanicek</i>	226
Comparison of Recalculated Dobson and TOMS Total Ozone at Hradec Kralove, Czechoslovakia, 1978-1990 <i>M. Stanek and K. Vanicek</i>	229
Fractal Characteristics of Ozonometric Network <i>A.N. Gruzdev</i>	232
Characterization and Analysis of the Nimbus-7 SBUV Data in the "Non-Sync" Period (February 1987 - June 1990.) <i>J.F. Gleason, R.D. McPeters and J.R. Herman</i>	236
Revision of the Dobson Total Ozone Series at Hohenpeissenberg <i>U. Kohler</i>	240
The Global Distribution of Ozone Destruction Rates Obtained from 13 Years of Nimbus/TOMS Data (1979-1991) <i>J.R. Herman, R.S. Stolarski, R. McPeters and D. Larko</i>	244

Depletions in Winter Total Ozone Values over Southern England A. Lapworth.....	249
Stable Ozone Layer in Norway and USSR K. Henriksen, T. Svenoe, E.I. Terez, G.A. Terez, V. Roldugin and S.H.H. Larsen.....	254
Long-Term Trend of Selected Halogenated Hydrocarbons R. Borchers, R. Gunawardena and R.A. Rasmussen.....	259
Status of the Dobson Total Ozone Data Set W.G. Planet and R.D. Hudson.....	263
Results of International Dobson Spectrophotometer Calibrations at Arosa, Switzerland, 1990 R.D. Grass, W.D. Komhyr, G.L. Koenig and R.D. Evans.....	266
Deformation of the Total Ozone Content Field in the Tropical Zone V.I. Vasiliev.....	271
Total Ozone Trend over Cairo G.K.Y. Hassan.....	275

THEORY AND MODELING

Three Dimensional Model Calculations of the Global Dispersion of High Speed Aircraft Exhaust and Implications for Stratospheric Ozone Loss A.R. Douglass, R.B. Rood, C.H. Jackman and C.J. Weaver.....	281
Qualitative Study of the Behavior of Minor Species During a Stratospheric Warming with a 3-D Model R. Ramaroson, M. Pirre, and D. Cariolle.....	285
Connection Between Total Ozone Fields and Lower Stratospheric Dynamics G. Vaughan, A. Howells and J.D. Price.....	290
Model/Data Comparisons of Ozone in the Upper Stratosphere and Mesosphere D.E. Siskind, E.E. Remsberg, R.S. Eckman, B.J. Connor, J.J. Tsou and A. Parrish.....	294
On the Relevance of the Methane Oxidation Cycle to "Ozone Hole" Chemistry R. Muller and P.J. Crutzen.....	298

Effects of Stratospheric Aerosol Surface Processes on the LLNL Two-Dimensional Zonally Averaged Model <i>P.S. Connell, D.E. Kinnison, D.J. Wuebbles, J.D. Burley, and H.S. Johnson</i>	302
Evolution of Chemically Processed Air Parcels in the Lower Stratosphere <i>R.S. Stolarski, A.R. Douglass and M.R. Schoeberl</i>	307
Observational Evidence and Dynamical Interpretation of the Total Ozone Variations in the Equatorial Region <i>M. Shiotani and F. Hasebe</i>	310
A 3-D Model Study of Ozone Eddy Transport in the Winter Stratosphere <i>N.C. Hsu and D.M. Cunnold</i>	314
Impact of Supersonic and Subsonic Aircraft on Ozone: Including Heterogeneous Chemical Reaction Mechanisms <i>D.E. Kinnison and D.J. Wuebbles</i>	318
An Investigation of the Processes Controlling Ozone in the Upper Stratosphere <i>K.O. Patten, Jr., P.S. Connell, D.E. Kinnison, D.J. Wuebbles, J. Waters, L. Froidevaux and T.G. Slanger</i>	322
A New Mathematical Formulation of the Line-By-Line Method in Case of Weak Line Overlapping <i>A.G. Ishov and N.V. Krymova</i>	326
The Chemistry of Bromine in the Stratosphere: Influence of a New Rate Constant for the Reaction $\text{BRO} + \text{HO}_2$ <i>M. Pirre, F.J. Marceau, G. Le Bras, F. Maguin, G. Poulet and R. Ramaroson</i>	330
The Ozone Depletion Potentials of Halocarbons: Their Dependence of Calculation Assumptions <i>I.L. Karol and A.A. Kiselev</i>	334
Model Evaluation of the Radiative and Temperature Effects of the Ozone Content Changes in the Global Atmosphere of 1980-IES <i>I.L. Karol and V.A. Frolkis</i>	338
A Search for Relativistic Electron Induced Stratospheric Ozone Depletion <i>A. C. Aikin</i>	342
Impact of Stratospheric Aircraft on Calculations of Nitric Acid Trihydrate Cloud Surface Area Densities Using NMC Temperatures and 2D Model Constituent Distributions <i>D.B. Considine and A.R. Douglass</i>	347

The Response of Middle Atmospheric Ozone to Solar UV Irradiance Variations with a Period of 27 Days <i>L. Chen, G. Brasseur and J. London</i>	351
What Can We Learn from Relaxation Measurements of a Laser-Perturbed Atmosphere? A Modeling Study <i>A. Clericetti, H. van den Bergh and M.J. Rossi</i>	355
A Detailed Evaluation of Heating Processes in the Middle Atmosphere <i>M. Mlynczak and S. Solomon</i>	359
Effective UV Radiation from Model Calculations and Measurements <i>U. Feister and R. Grewe</i>	363
Impact of Stratospheric Aircraft Emissions on Ozone: A two Dimensional Model Study <i>M. Natarajan, L.B. Callis, R.E. Boughner and J.D. Lambeth</i>	367
Ozone and Stratospheric Height Waves or Opposite Phases of the QBO <i>K.C. Mo and J.Nogues-Paegle</i>	370
Infrared Absorption Cross Sections of Alternative CFC's <i>C. Clerbaux, R. Colin and P.C. Simon</i>	374
Distribution of Ozone Between 60 degrees North and 60 Degrees South <i>E. Mravlag and M.W.J. Scourfield</i>	378
Ozone Maxima Over Southern Africa: A Mid-Latitude Link <i>J. Barsby and R.D. Diab</i>	382
Efficient Ozone Generator for Ozone Layer Enrichment from a High Altitude Balloon <i>I.V. Filiouguine, S.V. Kostiouchenko, N.N. Koudriavtsev and S.M. Starikovskaya</i>	386
On Ozone Correlation with Meteofields in the Northern Hemisphere <i>T.V. Kadygrova and V.E. Fioletov</i>	390
Manifestation of Quasi-Biennial Oscillation in Ozone Vertical Distribution <i>S.A. Sitnov and A.N. Gruzdev</i>	393
Quasi-Bennial Oscillation in Total Ozone: Global Behaviour Derived from Ground-Based Measurements <i>A.N. Gruzdev and I.I. Mokhov</i>	397

Total Ozone Seasonal and Interannual Variations in the Principal Air Masses of the Northern Hemisphere in 1975-1990 I.L. Karol, L.P. Klyagina, A.M. Shalamyansky and S.V. Jagovkina.....	401
Solar Proton Effects on Austral Ozone During the Final Months of 1989 J.A.E. Stephenson and M.W.J. Scourfield.....	405
Model Evaluation of the Radiative and Temperature Effects of the Ozone Content Change in the Global Atmosphere of 1980-IES I.L. Karol and V.A. Frolkis.....	409
Temperature Dependent Absorption Cross-Sections of HNO ₃ and N ₂ O ₅ O.V. Rattigan, M.H. Harwood, R.L. Jones and R.A. Cox....	413
Radiative Forcing Perturbation due to Observed Increases in Tropospheric Ozone at Hohenpeissenberg W-C. Wang, R.D. Bojkov and Y.C. Zhuang.....	417
Temperature Dependence of Ultraviolet Absorption Cross-Sections of Alternative Hydrochlorofluorocarbons D. Gillotay, P.C. Simon and L. Dierickx.....	421
Ultraviolet Absorption Cross-Section of some Carbonyl Compounds and their Temperature Dependence D. Gillotay, P.C. Simon and L. Dierickx.....	425
Climate-Chemical Interactions and Greenhouse Effects of Trace Gases G-Y. Shi and X-B. Fan.....	429
A General Circulation Model Study of the Climatic Effect of Observed Stratospheric Ozone Depletion Between 1980 and 1990 M.P. Dudek, W-C. Wang, X.Z. Liang and Z. Li.....	433

APPENDIX

Author Index.....	A-1
-------------------	-----

PART II

STRATOSPHERE

RESULTS FROM THE UPPER ATMOSPHERE RESEARCH SATELLITE

- Measurements of Stratospheric NO, NO₂ and N₂O₅ By ISAMS:
Preliminary Observations and Data Validation
*B.J. Kerridge, J. Ballard, R.J. Knight, A.D. Stevens,
J. Reburn, P. Morris, J.J. Remedios and F.W. Taylor.....* 439
- Measurements of Stratospheric Constituents By ISAMS
*C.D. Rodgers, F.W. Taylor, J.J. Barnett, M. Corney,
A. Dudhia, M.A. Lopez-Valverde, C.J. Marks, P. Morris,
T. Nightingale, J.J. Remedios, D. Roisin, R.J. Wells,
J. Ballard, B.J. Kerridge, R.J. Knight, A. Chu,
B.J. Connor and C. Scheuer.....* 444
- Comparison of NOAA/NMC Stratospheric Wind Analyses with UARS
High Resolution Doppler Imager Wind Measurements
A.J. Miller, P.B. Hays, V. Abreu, C. Long and D. Kann... 448
- The Validation of Ozone Measurements from the Improved
Stratospheric and Mesospheric Sounder
*B.J. Connor, C.J. Scheuer, D.A. Chu, J.J. Remedios,
C.J. Marks, C.D. Rodgers and F.W. Taylor.....* 452
- ISAMS Observations of Stratospheric Aerosol
*A. Lambert, J.J. Remedios, A. Dudhia, M. Corney,
B.J. Kerridge, C.D. Rodgers and F.W. Taylor.....* 456
- Preliminary Results from the ISAMS NO Channel: Thermospheric
Radiances
J. Ballard, B.J. Kerridge and F.W. Taylor..... 459

THE ARCTIC

- Simulations of Arctic Ozone Depletion with Current and
Doubled Levels of CO₂
N. Butchart, J. Austin and K.P. Shine..... 467
- Laboratory Measurements of Polar Stratospheric Cloud Rate
Parameters
R.D. Kenner, I.C. Plumb and K.R. Ryan..... 471
- Laboratory Simulations of NAT Formation Approaching
Stratospheric Conditions
J. Marti and K. Mauersberger..... 475

Arctic Polar Stratospheric Cloud Measurements By Means of a Four Wavelength Depolarization Lidar	
<i>L. Stefanutti, F. Castagnoli, M. del Guasta, C. Flesia, S. Godin, J. Kolenda, H. Kneipp, E. Kyro, R. Matthey, M. Morandi, P. Rairoux, V.M. Sacco, B. Stein, V. Venturi, D. Weidauer, J.P. Wolf, L. Woeste and L. Zuccagnoli.....</i>	479
Measurements of Stratospheric Ozone and Aerosols above Spitsbergen	
<i>R. Neuber, G. Beyerle, O. Schrems, R. Fabian, P. von der Gathen and B.C. Kruger.....</i>	483
Balloon-Borne Measurements of the Ultraviolet Flux in the Arctic Stratosphere During Winter	
<i>C. Schiller, M. Muller, E. Klein, U. Schmidt and E-P. Roth.....</i>	488
Calculations of Arctic Ozone Chemistry using Objectively Analyzed Data in a 3-D CTM	
<i>J.W. Kaminski, J.C. McConnell and J.W. Sandilands.....</i>	492
Three-Dimensional Modelling of Trace Species in the Arctic Lower Stratosphere	
<i>M. Chipperfield, D. Cariolle, P. Simon and R. Ramarosan.....</i>	496
Investigation of the Structure and Dynamics of the Ozone Layer in the Eastern Arctic Region During EASOE Campaign	
<i>V. Khattatov, V. Yushkov, V. Rudakov, I. Zaitsev, J. Rosen and N. Kjome.....</i>	500
Temporal Development of the Correlation Between Ozone and Potential Vorticity in the Arctic in the Winters of 1988/89, 1989/90 and 1990/91	
<i>B. Knudsen, P. von der Gathen, G.O. Braathen, R. Fabian, T.S. Jorgensen, E. Kyro, R. Neuber and M. Rummukainen.....</i>	504
Modelling Stratospheric Polar Ozone Using Objective Analysis	
<i>J.W. Sandilands, J.W. Kaminski, J.C. McConnell, S.R. Beagley and N. McFarlane.....</i>	508
Intercomparison Between Ozone Profiles Measured Above Spitsbergen by Lidar and Sonde Techniques	
<i>R. Fabian, P. von der Gathen, J. Ehlers, B.C. Kruger, R. Neuber and G. Beyerle.....</i>	512
Lidar Measurements of Ozone and Aerosol Distributions During the 1992 Airborne Arctic Stratospheric Expedition	
<i>E.V. Browell, C.F. Butler, M.A. Fenn, W.B. Grant, S. Ismail and A.F. Carter.....</i>	516

Stratospheric OClO and NO ₂ Measured by Groundbased UV/VIS-Spectroscopy in Greenland in Jan/Feb 1990 and 1991 <i>A. Roth and D. Perner</i>	520
Column Amounts of Trace Gases from Ground Based FTIR Measurements in the Late North Polar Winters 1990 and 1991 <i>G. Adrian, T. Blumenstock, H. Fisher, E. Frank, L. Gerhardt, T. Gulde, G. Maucher, H. Oelhaf, P. Thomas, and O. Trieschmann</i>	524
Stratospheric Minor Species Vertical Distributions During Polar Winter By Balloon Borne UV-VIS Spectrometry <i>J-P. Pommereau and J. Piquard</i>	528
Average Ozone Vertical Distribution at Sodankyla Based on the 1988-1991 Ozone Sounding Data <i>E. Kyro, M. Rummukainen, P. Taalas and A. Supperi</i>	532
The Evolution of Synoptic Ozone Anomalies During the European Arctic Stratospheric Ozone Experiment in Winter 1991/92 <i>C.S. Zerefos, D.S. Balis, A.F. Bais, I.C. Ziomas, K. Tourpali, C. Meleti, P. Tzoumaka, H.T. Mantis, C.C. Repapis, V.E. Fioletov, V.U. Khattatov, and R.D. Bojkov</i>	535
Measurements of the Vertical Profile Diurnal Variation, and Secular Change of ClO in the Stratosphere Over Thule, Greenland, February-March, 1992 <i>R.L. de Zafra, L.K. Emmons, J.M. Reeves and D.T. Shindell</i>	540
Observed Changes in the Vertical Profile of Stratospheric Nitrous Oxide at Thule, Greenland, February-March, 1992 <i>L.K. Emmons, J.M. Reeves, D.T. Shindell and R.L. de Zafra</i>	543
Ozone Laminae Near the Edge of the Stratospheric Polar Vortex <i>S.J. Reid and G. Vaughan</i>	546
Ozone, Aerosols and Polar Stratospheric Clouds Measurements During the EASOE Campaign <i>S. Godin, G. Megie, C. David, V. Mitev, D. Haner, Y. Emery, C. Flesia, V. Rizi, G. Visconti and L. Stefanutti</i>	550

THE ANTARCTIC

Reinterpretation of Ozone data from "Base Roi Baudouin" <i>H. Kelder and C. Muller</i>	557
---	-----

Systematic Stratospheric Observations on the Antarctic Continent at Dumont D'Urville <i>S. Godin, A. Sarkissian, C. David, G. Megie, J-P. Pommereau, F. Goutail, P. Aumedieu, J. Piquard, E. La Bouar, L. Stefanutti, M. Morandi, and M. del Guasta.....</i>	561
Observation of Ozone and Aerosols in the Antarctic Ozone Hole of 1991 under the Polar Patrol Balloon (PPB) Project- Preliminary Result <i>M. Hayashi, I. Murata, Y. Iwasaka, Y. Kondo and H. Kanzawa.....</i>	565
Year-Round Measurements of Ozone at 66°S with a Visible Spectrometer <i>H.K. Roscoe, D.J. Oldham, J.A.C. Squires, J-P. Pommereau, F. Goutail and A. Sarkissian.....</i>	569
Ground Based NO ₂ and O ₃ Measurements by Visible Spectrometer at Syowa Base (69°S), Antarctica <i>Y. Kondo, W.A. Matthews, P.V. Johnson, M. Hayashi, M. Koike, Y. Iwasaka, A. Shimizu, A. Budiyo, T. Yamanouchi and S. Aoki.....</i>	573
Ozone Vertical Profile Changes Over South Pole <i>S.J. Oltmans, D.J. Hofmann, W.D. Komhyr and J.A. Lathrop.....</i>	578
Quantitative Characterization of the Antarctic Ozone Hole <i>T. Ito, Y. Sakoda, K. Matsubara, T. Takao, K. Akagi, Y. Watanabe, S. Shibata and H. Naganuma.....</i>	582
PSC and Volcanic Aerosol Routine Observations in Antarctica by UV-Visible Ground-Based Spectrometry <i>A. Sarkissian, J-P. Pommereau and F. Goutail.....</i>	586
Ozone Profiles Over McMurdo Station, Antarctica, during August, September, and October of 1986-1991 <i>T. Deshler and D.J. Hofmann.....</i>	590
An Observational Study of the Ozone Dilution Effect : Ozone Transport in the Austral Spring Stratosphere <i>R.J. Atkinson and R.A. Plumb.....</i>	594
Long-Term Ozone and Temperature Correlations above Sanae, Antarctica <i>G.E. Bodeker and M.W.J. Scourfield.....</i>	598
Four Years of Ground-Based Total Ozone Measurements by Visible Spectrometry in Antarctica <i>F. Goutail, J-P. Pommereau and A. Sarkissian.....</i>	602

Trajectory Analysis of Polar Patrol Balloon (PPB) Flights in the Stratosphere over Antarctica in Summer and Spring: A Preliminary Result	
<i>H. Kanzawa, R. Fujii, K. Yamazaki and M.D. Yamanaka</i>	606

Measurements of Stratospheric Odd Nitrogen at Arrival Heights, Antarctica, in 1991	
<i>J.G. Keys, P.V. Johnson, R.D. Blatherwick and F.J. Murcray</i>	610

VOLCANIC EFFECTS

NO ₂ Column Changes Induced by Volcanic Eruptions	
<i>P.V. Johnston, J.G. Keys, and R.L. McKenzie</i>	615

Modulations of Stratospheric Ozone by Volcanic Eruptions	
<i>C. Blanchette and J.C. McConnell</i>	619

Effects of the Mt. Pinatubo Eruption on the Radiative and Chemical Processes in the Troposphere and Stratosphere	
<i>D.E. Kinnison, K.E. Grant, P.S. Connell and D.J. Wuebbles</i>	623

UV Spectral Irradiance Measurements in New Zealand: Effects of Pinatubo Volcanic Aerosol	
<i>R.L. McKenzie</i>	627

Volcanic-Aerosol-Induced Changes in Stratospheric Ozone Following the Eruption of Mt. Pinatubo	
<i>W.B. Grant, E.V. Browell, J. Fishman, V.G. Brackett, M.A. Fenn, C.F. Butler, D. Nganga, A. Minga, B. Cros, S.D. Mayor, G.D. Nowicki, R.E. Veiga, L.L. Stowe, and C.S. Long</i>	631

Stratospheric Aerosol Increase after the Eruption of Pinatubo Observed with LIDAR and Aureolemeter	
<i>S. Hayashida, Y. Sasano, H. Nakane, I. Matsui and T. Hayasaka</i>	635

GROUND-BASED MEASUREMENTS

Checking Ozone Amounts by Measurements of UV-Irradiances	
<i>G. Seckmeyer, C. Kettner and S. Thiel</i>	641

Results from Two Years of Ozone Data Taken with a New, Ground-Based Microwave Instrument: An Overview	
<i>A. Parrish, B.J. Connor, J.J. Tsou, I.S. McDermid, W.P. Chu and D.E. Siskind</i>	645

LIDAR Measurements of Stratospheric Ozone at Table Mountain, California, Since 1988 <i>I.S. McDermid, M. Schmoe and T. D. Walsh.....</i>	649
Airmass Dependence of the Dobson Total Ozone Measurements <i>M. Degorska and B. Rajewska-Wiech.....</i>	653
UV-B Radiation Amplification Factor Determined based on the Simultaneous Observation of Total Ozone and Global Spectral Irradiance <i>T. Ito, Y. Sakoda, K. Matsubara, R. Kajihara, T. Uekubo, M. Kobayashi, M. Shitamichi, T. Ueno and M. Ito.....</i>	657
Visible Light Nitrogen Dioxide Spectrophotometer Intercomparison: Mt. Kobau, British Columbia July 28 to August 10, 1991 <i>C.T. McElroy, A. Elokhov, N. Elansky, H. Frank, P. Johnston and J.B. Kerr.....</i>	663
The Daytime Course of Total Ozone Content Caused by Cloud Convection <i>A. G. Ishov.....</i>	667
Measurements of Stratospheric Composition Using a Star Pointing Spectrometer <i>D.J. Fish, R.L. Jones, R.A. Freshwater, H.K. Roscoe, and D.J. Oldham.....</i>	671
Measurements of the Total Column Amount of NO ₂ at "Kislovodsk" Observatory in 1979-1990 <i>N.F. Elansky, A. Y. Arabov, O.V. Makarov, V.V. Savastyuk and I.A. Senik.....</i>	675
Polarimetric Method of Estimation of Vertical Aerosol Distribution in Application to Observations of Ozone and NO ₂ <i>N.F. Elansky, E.A. Kadyshevich and V.V. Savastyuk.....</i>	679
Near Simultaneous Measurements of NO ₂ and NO ₃ Over Tropics by Ground Based Absorption Spectroscopy <i>M. Lal, D.K. Chakrabarty, J.S. Sidhu and S.R. Das.....</i>	683
Derivation of Water Vapour Absorption Cross-Sections in the Red Region <i>M. Lal and D.K. Chakrabarty.....</i>	687
First Measurements of the New 110-mm-Wave Sounder at the Jungfraujoeh Alpine Station <i>L. Gerber and N. Kampfer.....</i>	691
Total Ozone and Total NO ₂ Latitudinal Distribution Derived from Measurements in the Atlantic Ocean in May 1988 <i>A.S. Elokhov and A.N. Gruzdev.....</i>	695

Variation of Stratospheric NO ₂ During the Solar Eclipse <i>N.F. Elansky and A.S. Elokhov</i>	699
The Determination of HNO ₃ Column Amounts from Tunable Diode Laser Heterodyne Spectrometer Spectra Taken at Jungfrauoch, Switzerland <i>P.F. Fogal, D.G. Murcray, N.A. Martin, N.R. Swann, P.T. Woods and C.T. McElroy</i>	703
Ozone Ground-Based Measurements by the "GASCOD" Near-UV and Visible DOAS System <i>G. Giovanelli, P. Bonasoni, M. Cervino, F. Evangelisti and F. Ravegnani</i>	707
Quality Control Concept and Recent Developments of the Light Climatic Observatory at Arosa - Ozone Measuring Station of the Swiss Meteorological Institute (LKO) <i>B. Hoegger, P. Viatte, G. Levrat, J. Bader, P. Ribordy, H. Schill and J. Staehelin</i>	711
Ozone and NO ₂ Measurements from Aberystwyth and Lerwick <i>L.M. Bartlett and G. Vaughan</i>	715
A New High-Sensitivity Superconducting Receiver For mm-Wave Remote-Sensing Spectroscopy of the Stratosphere <i>R.L. de Zafra, W.H. Mallison, M. Jaramillo, J.M. Reeves L.K. Emmons and D.T. Shindell</i>	719
Continuous Measurements of the Total Ozone Content in the Full Moon Period <i>A.G. Ishov</i>	723
Detection of Stratosphere Troposphere Exchange in Cut-Off Low Systems <i>J.D. Price and G. Vaughan</i>	727
A Star-Pointing UV-Visible Spectrometer for Remote-Sensing of the Stratosphere <i>H.K. Roscoe, R.A. Freshwater, R.L. Jones, D.J. Fish J.E. Harries, R. Wolfenden and P. Stone</i>	731
Possibility to Sound the Atmospheric Ozone by a Radiosonde Equipped With Two Temperature Sensors, Sensitive and Non-Sensitive to the Long Wave Radiation <i>T. Kitaoka and T. Sumi</i>	735
Seasonal Cycle in Atmospheric HCl at 45°S <i>W.A. Matthews, N.B. Jones, P.V. Johnson, C.P. Rinsland and A. Goldman</i>	739

UV-Observations with a Brewer Spectrophotometer at Hohenpeissenberg <i>W. Vandersee and U. Kohler</i>	742
O ₃ , SO ₂ , NO ₂ and UVB Measurements in Beijing and Baseline Station of Northwestern Part of China <i>G. Song, Z. Xiuji and Z. Xiaochun</i>	746
An Automated Optical Wedge Calibrator for Dobson Ozone Spectrophotometers <i>R.D. Evans, W.D. Komhyr and R.D. Grass</i>	749
The Updated Statistical Inversion Technique to the Evaluation of Umkehr Observations <i>A.D. Frolov and S.P. Obrazcov</i>	754
Ozone Height Profiles Using Laser Heterodyne Radiometer <i>S.L. Jain</i>	758
Ozone and Nitrogen Dioxide above the Northern Tien Shan <i>V.N. Aref'ev, O.A. Volkovitsky, N.E. Kamenogradsky, V.K. Semyonov and V.P. Sinyakov</i>	762
Ambient Temperature Effects on Broadband UV-B Measurements Using Fluorescent Phosphor (MgWO ₄)-Based Detectors <i>B.K. Dichter, D.J. Beaubien and A.F. Beaubien</i>	766
Comparison Between Brewer Spectrometer, M 124 Filter Ozonometer and Dobson Spectrophotometer <i>U. Feister</i>	770
The Measurement of Ultraviolet Radiation and Sunburn Time Over Southern Ontario <i>W.F.J. Evans</i>	774
The Ground-Based Measurement of Ozone in the 9.6 Micron Band <i>W.F.J. Evans and E. Puckrin</i>	778
Lidar measurements and Umkehr Observations of the Ozone Vertical Distribution at the Observatoire de Haute Provence <i>A-M. Lacoste, S. Godin and G. Megie</i>	782
Comparison of UV-B Measurements Performed with a Brewer Spectrophotometer and a New UVB-1 Broad Band Detector <i>A.F. Bais, C.S. Zerefos, C. Meleti and I.C. Ziomas</i>	786
Inclusion of the Second Umkehr in the Conventional Umkehr Retrieval Analysis as a Means of Improving Ozone Retrievals in the Upper Stratosphere <i>K. Gioulgkidis, R.P. Lowe and C.T. McElroy</i>	790

The Canadian Ozone Watch and UV-B Advisory Programs
J.B. Kerr, C.T. McElroy, D.W. Tarasick and D.I. Wardle.. 794

SAGE II-Umkehr Case Study of Ozone Differences and Aerosol
Effects from October 1984 to April 1989
M.J. Newchurch and D.M. Cunnold..... 798

AIRCRAFT, BALLOON, AND SONDE MEASUREMENTS

The 1991 WMO Ozone Sonde Intercomparison
*J.B. Kerr, C.T. McElroy, H. Fast, S.J. Oltmans,
J.A. Lathrop, E. Kyro, A. Paukkunen, H.J. Claude,
U. Kohler, C.R. Sreedharan, T. Tako and Y. Tsukagoshi... 807*

Measurements of Stratospheric Ozone by Rocket Ozonesondes
in Japan
T. Watanabe and T. Ogawa..... 811

The Discrepancy Between Stratospheric Ozone Profiles From
Balloon Soundings and From Other Techniques: A Possible
Explanation
D. De Muer and H. De Backer..... 815

Stratospheric Ozone Measurements at the Equator
M. Ilyas..... 819

Vertical Distribution of CH₄ and N₂O Over the Tropical Site
Hyderabad
S. Lal, B.H. Subbaraya, P. Fabian and R. Borchers..... 823

1990 Vertical Distribution of Two Important Halons - F-12B1
and F-13B1 - in the Tropics
*O.N. Singh, R. Borchers, S. Lal, B.H. Subbaraya,
B.C. Kruger and P. Fabian..... 827*

Balloon Measurements of Stratospheric HCl and HF By Far
Infrared Emission Spectroscopy
*K. Shibasaki, K.V. Chance, D.G. Johnson, K.W. Jucks
and W.A. Traub..... 831*

Universal Trace Pollutant Detector for Aircraft Monitoring
of the Ozone Layer and Industrial Areas
I.V. Filiouguine, S.V. Kostiouchenko, N.N. Koudriavtsev. 835

First Ozone Profiles Measured with Electrochemical and
Chemiluminescent Sondes, Developed in Russia
A.M. Zvyagintsev, S.P. Perov and Y.A. Ryabov..... 839

The MIPAS Balloon Borne Trace Constituent Experiment <i>H. Oelhaf, Th.V. Clarmann, H. Fischer, F. Friedl-Vallon, Chr. Fritzsche, Chr. Piesch, D. Rabus, M. Seefeldner and W. Volker.....</i>	842
Local Fluctuations of Ozone From 16 km to 45 km Deduced from in Situ Vertical Ozone Profile <i>G. Moreau and C. Robert.....</i>	846
Aircraft Measurements of NO and NO _y at 12 km Over the Pacific Ocean <i>M. Koike, Y. Kondo, Y. Makino and Y. Sugimura.....</i>	849
On the Laminated Structure of Ozone in the Sub-Tropical Atmosphere <i>C. Varotsos, P. Kalabokas and G. Chronopoulos.....</i>	854
The Latitudinal Distribution of Ozone to 35 km Altitude From ECC Ozonesonde Observations, 1982-1990 <i>W.D. Komhyr, S.J. Oltmans, J.A. Lathrop, J.B. Kerr and W.A. Matthews.....</i>	858
Lidar Observation of Ozone Over Tsukuba (36°N, 140°E) <i>H. Nakane, S. Hayashida, I. Matsui, N. Sugimoto, A. Minato and Y. Sasano.....</i>	863
On Vertical Profile of Ozone at Syowa <i>S. Chubachi.....</i>	867
Investigation of Catalytic Reduction and Filter Techniques for Simultaneous Measurements of NO, NO ₂ and HNO ₃ in the Stratosphere <i>J. Wendt, P. Fabian, G. Flentje and K. Kourtidis.....</i>	870

SATELLITE MEASUREMENTS

Global Ozone Data from the Meteor-3/TOMS Ultraviolet Spectrometer <i>J.R. Herman, A. Krueger, C. Cote, Z. Ahmad, M. Foreman, C. Wellemeyer, W. Byerly, L. Pan, G. Jaross, R. Hudson, V. Dosov, R. Salichov, Y. Borisov, A. Kondratiev, B. Kugaenko and H. Samvelyn.....</i>	877
Status of the Shuttle SBUV (SSBUV) Calibration of the NOAA SBUV/2 Operational Ozone Sounders and the Detection of Trends <i>E. Hilsenrath, R.D. McPeters and R.P. Cebula.....</i>	883
Ozone Determinations with the NOAA SBUV/2 System <i>W.G. Planet, J.H. Lienesch, H.D. Bowman, A.J. Miller and R.M. Nagatani.....</i>	887

SPEAM-II Experiment for the Measurement of Stratospheric NO ₂ , O ₃ and Aerosols <i>C.T. McElroy, L.J.B. McArthur, J.B. Kerr, D.I. Wardle, D. Tarasick and C. Midwinter.....</i>	891
Mesospheric Ozone Measurements by SAGE II <i>D.A. Chu and D.M. Cunnold.....</i>	895
An Asymptotic Method for Estimating the Vertical Ozone Distribution in the Earth's Atmosphere from Satellite Measurements of Backscattered Solar UV-Radiation <i>A. G. Ishov.....</i>	899
A New Method for Monitoring Long Term Calibration of the SBUV and TOMS Instruments <i>Z. Ahmad, C. Seftor and C.G. Wellemeyer.....</i>	903
Profile Shape Dependence in Backscattered Ultraviolet Satellite Retrievals of Total Ozone <i>S.L. Taylor, C.J. Seftor, C.G. Wellemeyer, K. Klenk and R.D. McPeters.....</i>	907
External Comparisons of Reprocessed SBUV/TOMS Ozone Data <i>C.G. Wellemeyer, S.L. Taylor, R.R. Singh and R.D. McPeters.....</i>	911
Effect of Stratospheric Aerosol Layers on the TOMS/SBUV Ozone Retrieval <i>O. Torres, Z. Ahmad, L. Pan, J.R. Herman, P.K. Bhartia and R. McPeters.....</i>	915
Effect of Partially-Clouded Scenes on the Determination of Ozone <i>C.J. Seftor, S.L. Taylor, C.G. Wellemeyer and R.D. McPeters.....</i>	919
Procedures to Validate/Correct Calibration Error in Solar Backscattered Ultraviolet Instruments <i>S.L. Taylor, R.D. McPeters and P.K. Bhartia.....</i>	923
Changes in Photochemically Significant Solar UV Spectral Irradiance as Estimated by the Composite MG II Index and Scale Factors <i>M.T. Deland and R.P. Cebula.....</i>	927
Performance Evaluation of the Solar Backscatter Ultraviolet Radiometer, Model 2 (SBUV/2) Inflight Calibration System <i>H. Weiss, R.P. Cebula, K. Laamann and R.D. McPeters.....</i>	931
The Accuracy of Temperature Distributions Used to Derive the Net Transport for a Zonally Averaged Model <i>E.E. Remsberg and P.P. Bhatt.....</i>	934

The Use of Visible-Channel Data From NOAA Satellites to Measure Total Ozone Amount Over Antarctica <i>R.D. Boime, S.G. Warren and A. Gruber.....</i>	938
Post Launch Performance of the METEOR-3/TOMS Instrument <i>G. Jaross, Z. Ahmad, R.P. Cebula and A.J. Krueger.....</i>	942
SSBUV Middle Ultraviolet Solar Spectral Irradiance Measurements <i>R.P. Cebula and E. Hilsenrath.....</i>	946
GOMOS-Global Ozone Monitoring by Occultation of Stars <i>G.W. Leppelmeier, E. Kyrola, R. Pellinen, P. Merat, S. Korpela, J.L. Bertaux, E. Chassefiere, F. Dalaudier and G. Megie.....</i>	950
Simulation and Data Processing of GOMOS Measurements <i>E. Krola, E. Sihvola, L. Oikarinen, J. Tamminen and H. Haario.....</i>	954
Ozone Profile Retrievals from the ESA GOME Instrument <i>R. Munro, B.J. Kerridge, J.P. Burrows and K. Chance.....</i>	958
Ground-Based Intercomparisons of SBUV/2 Flight Instruments, the World Standard Dobson Spectrophotometer 83 and Overpass Observations from Nimbus-7 TOMS and NOAA-11 SBUV/2 <i>D.F. Heath, Z. Ahmad, O. Torres, R.D. Evans, R.D. Grass, W.D. Komhyr and W. Nelson.....</i>	962

APPENDIX

Author Index.....	A-1
-------------------	-----

TROPOSPHERE

OZONE TRENDS AND CLIMATOLOGY

303132

1995104179

TRENDS IN SURFACE OZONE OVER EUROPE, 1978-1990

Pak Sum Low*, P. Michael Kelly and Trevor D. Davies**
 Climatic Research Unit, **School of Environmental Sciences,
 University of East Anglia, Norwich NR4 7TJ, United Kingdom.

*Present address: Ozone Secretariat, UNEP, P.O. Box 47074, Nairobi, Kenya

ABSTRACT

It has been suggested that surface ozone concentrations in rural areas of Europe have been increasing at a rate of 1 to 3% per year over the past two to three decades, presumably due to human influences (Feister and Warmbt, 1987; Bojkov, 1988; Penkett, 1989). Recently, we have analyzed surface ozone data from 20 European stations of differing character (remote, rural, suburban and urban) for a common period of 1978-1988 (Low *et al.*, 1992). It was found that there were pronounced annual and seasonal variations in the linear trends in different areas, and there was no dominant region-wide trend. In spring and, most notably, summer, stations on the maritime fringe of the network generally exhibited negative trends whilst those located further into the continental interior exhibited positive trends. In winter, most of the stations in the network exhibited positive trends. Relatively few of these trends were statistically significant. This paper updates our earlier analysis by extending the data sets of the network up to the year 1990. The spatial variations in surface ozone trends over the extended period 1978-1990 are examined and discussed in comparison to the 1978-1988 patterns. The update confirms the overall conclusions of the earlier analysis, specifically that caution should be exercised in interpreting the results of trend analyses based on station data representative of a limited period of time and/or geographical area.

1. INTRODUCTION

During an investigation of the links between surface ozone concentrations and atmospheric circulation in Europe, time series of surface ozone data from over 130 stations have been collected (Davies *et al.*, 1990). Most stations had a time series of less than ten years. Of those with longer periods of data, 20 stations were selected and linear trends in surface ozone concentration were determined for the common period 1978-1988. The statistical significance of the trends was tested taking into account autocorrelation in the data. The results are detailed in Low *et al.* (1992).

Recently we have updated the network time series to the year 1990. The spatial variations in surface ozone trends over the extended period 1978-1990 are examined in this

paper and comparison is made with the patterns for the period 1978-1988.

2. THE NETWORK OF STATIONS

The stations and their site characteristics are listed in Table 1 and their locations are shown in Figure 1a. Most stations are classified as "rural" with a few classified "suburban" and two "remote" (these latter stations are located over 1750m above sea level). London is the only station classified as "urban". Neuglobsow and Wank are WMO Background Air Pollution Monitoring Network (BAPMoN) stations.

3. SURFACE OZONE TRENDS

The linear trends in the annual and seasonal data for each station are given in Table 2 for the periods 1978-1988 and 1978-1990. The trends are expressed in terms of percentage change per year.

It is notable that the number of statistically significant trends is greater over the longer period. Moreover, most of the trends that are statistically significant in one or both periods remain of similar value, although others change markedly. This latter result is not surprising given that we are attempting to define trends over a short period of data. Sensitivity to the period of analysis has been well illustrated by Low *et al.* (1990, 1991).

The general conclusions reached in Low *et al.* (1992) are confirmed:

(1) Pronounced annual and seasonal variations are apparent in the trends in different areas.

(2) Relatively few of the trends are statistically significant.

(3) There is no dominant region-wide trend, although most of the stations in the network exhibit positive trends in the winter average data.

There are certain changes in the spatial character of the seasonal trends over the extended period (Figure 1b-f). We noted in Low *et al.* (1992) that over the period 1978-1988 there was evidence of a contrast between the trends over the continental interior and those over the maritime fringe of the network. Most marked in the summer data, stations on the maritime fringe of the network generally exhibited negative

Table 1 Surface ozone monitoring stations used in this study.

Country	Station	Location	Height (m asl)	Site class	Record	Meas. tech.	Comments
Former GDR	Arkona	54.68N 13.43E	42	rural	1956-90	I	BAPMoN; coastal; SO ₂ filter from 1972; continuous since 1982
	Dresden	51.12N 13.68E	246	suburban	1972-90	I	SO ₂ filter from 1972; continuous since 1981
	Fichtelberg	50.43N 12.95E	1213	rural	1970-90	I	Continuous recording since 1982
	Neuglobsow	53.15N 13.03E	62	rural	1978-90	I	BAPMoN; continuous since 1982
	Schmücke	50.65N 10.77E	937	rural	1978-90	I	Continuous since 1982
FRG	Hamburg	53.65N 10.12E	49	suburban	1976-90	I	
	Hohenpeissenberg	47.80N 11.02E	975	rural	1971-90	I/C	SO ₂ filter from 1976
	Garmisch-Partenkirchen	47.48N 11.07E	740	rural	1978-90	C	Valley station
	Wank	47.52N 11.15E	1780	remote	1978-90	C	BAPMoN; mountain station
	Zugspitze	47.42N 10.98E	2964	remote	1978-90	C	Mountain station
United Kingdom	Bottesford	52.93N 0.82W	32	rural	1978-90	C	1 km south of motorway
	Central London	51.50N 0.08W	20	urban	1972-90	C	City centre (Victoria)
	Sibton	52.30N 1.47E	46	rural	1977-90	C	Open flat cereal farmland; woodland to the northwest
	Stevenage	51.88N 0.20W	90	suburban	1977-90	C	Edge of industrial estate; 100 m east of motorway
The Netherlands	Balk	52.92N 5.57E	1	rural	1978-90	C	Data interruption in 1986
	Biddinghuizen	52.42N 5.59E	-5	rural	1978-90	C	Station moved about 200 m in 1986
	Brandwijk	51.89N 4.80E	-0.5	suburban	1978-88	C	Data interruption in 1985; record ended in 1988
	Cabauw	51.97N 4.93E	-0.5	suburban /rural	1978-90	C	
	Hellendoorn	52.38N 6.40E	20	rural	1978-90	C	Data interruption in 1985
Kloosterburen	53.40N 6.41E	1	rural	1978-90	C	Coastal	

Although changes in instrumentation have occurred at some of the stations, the quality of these data is considered to be good over the period of record analysed. The site classification follows that of the original observers and may not be based on entirely comparable criteria. All available data are used. For further details, see *Low et al.* (1991).

Key: Meas. tech., Measurement technique; BAPMoN, WMO Background Air Pollution Monitoring Network station; GDR, German Democratic Republic; FRG, Federal Republic of Germany; I, Iodometric; C, Chemiluminescent.

trends whilst those located further into the continental interior exhibited positive trends. Over the period 1978-1990, this pattern becomes clearer in other seasons. Stations on the maritime fringe of the network generally exhibit negative trends in the annual, spring and autumn data. Those located further into the continental interior exhibit positive trends in the annual, spring and summer data. This clustering of trends with similar signs in regional groupings does suggest a common causal mechanism, lack of statistical significance notwithstanding.

The variations in the trends at different locations reflect the complexity and diversity of the processes that control ozone formation, transport and destruction. The factors which influence the nature of the trend at a particular station have been discussed by *Low et al.* (1992). They include:

(1) The specific geographical or topographical location of the station. This will determine, for example, the effectiveness of the surface destruction of ozone (*Galbally and Roy, 1980*).

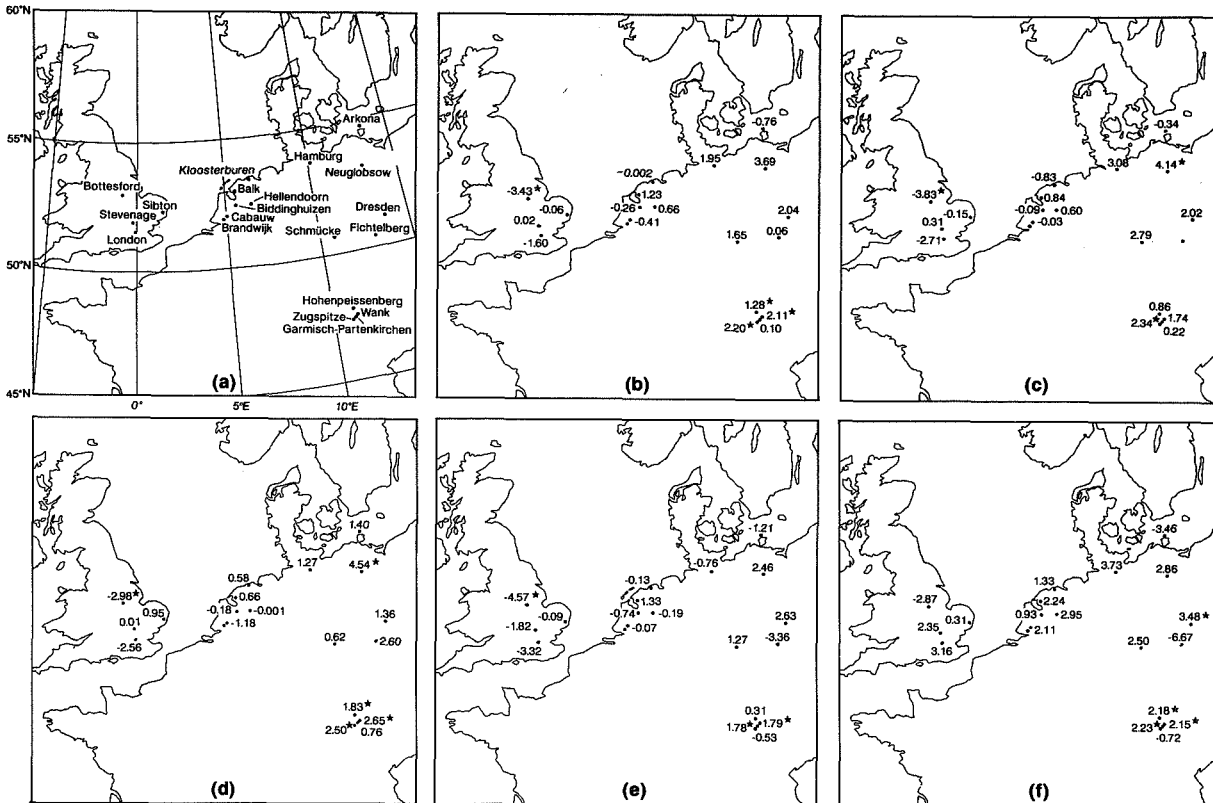


Figure 1 Station locations (a) and linear trends in surface ozone concentration over the period 1978-90, expressed as percentage change per year, for the (b) annual, (c) spring, (d) summer, (e) autumn and (f) winter data. * indicates statistical significance at the 5% level, after allowing for autocorrelation.

(2) Horizontal and vertical variability in the amount of solar radiation reaching the surface (Feister *et al.*, 1989; Schmidt, 1989). This is dependent on topography and fluctuations in cloudiness and, perhaps, the concentration of aerosols (Feister *et al.*, 1989).

(3) The influence of local emission sources as well as the medium- and long-range transport of pollutants from elsewhere. These determine the distribution of the concentrations of precursors, particularly NO_x , and, hence, the photochemical production and destruction of ozone (Liu *et al.*, 1987).

(4) Natural climate variability, such as changes in the atmospheric circulation. This can affect ozone concentration on the interannual and longer time scales (Davies *et al.*, 1992).

(5) Station elevation. The higher-elevation stations at Wank and Zugspitze, for example, which exhibit positive trends annually and in all seasons (all but one statistically significant), may be reflecting free tropospheric conditions to a much greater extent than the other stations at lower elevations.

(6) Local climatological factors, such as the frequency of nocturnal inversions and local circulations (Janach, 1989).

For certain stations which exhibit a negative trend in ozone concentration (such as Arkona), it should be noted that the trend is, to a large extent, the result of the marked and rapid decline in ozone concentration that occurred during the early 1980s. At other stations showing a negative trend (such as London and stations in the Netherlands), the observed increase in the concentration of NO_x (particularly NO) may be pertinent as it is an important ozone sink (Low *et al.* 1992).

The positive trends observed in winter at most stations are consistent with the prediction of a gradual increase of background ozone in that season because of the longer photochemical lifetime of ozone and the more efficient accumulation process of newly-produced ozone (Liu *et al.*, 1987).

4. CONCLUSIONS

Given the diversity of the trends reported here and the complex influences on surface ozone concentrations, we

Table 2 Linear trends in the seasonal and annual average data over the periods 1978-88 and 1978-90, expressed as percentage change per year. * indicates statistical significance at the 5% level.

Station	Spring		Summer		Autumn		Winter		Annual	
	78-88	78-90	78-88	78-90	78-88	78-90	78-88	78-90	78-88	78-90
Arkona	-2.85	-0.34	-2.07	1.40	-4.52	-1.21	-6.30	-3.46	-3.19	-0.76
Dresden	1.57	2.02	0.45	1.36	1.89	2.63	1.57	3.48*	1.28	2.04
Fichtelberg	-4.17	0.76	0.02	2.60	-5.87	-3.36	-12.02*	-6.67	-4.12	0.06
Neuglobsow	4.55*	4.14*	3.76	4.54*	2.58	2.46	3.37	2.86	3.86*	3.69
Schmücke	1.02	2.79	1.03	0.62	-0.41	1.27	-1.36	2.50	-0.32	1.65
Hamburg	3.16	3.08	1.42	1.27	-0.06	-0.76	5.86	3.73	2.46	1.95
Hohenpeissenberg	0.43	0.86	1.13	1.83*	-0.44	0.31	0.91	2.18*	0.56	1.28*
Garmisch-Partenkirchen	0.93	0.22	0.62	0.76	-0.46	-0.53	0.68	-0.72	0.48	0.10
Wank	2.53	1.74	2.68	2.65*	2.12	1.79*	2.22*	2.15*	2.41	2.11*
Zugspitze	2.76*	2.34*	2.59*	2.50*	2.00	1.78*	2.45	2.23*	2.40	2.20*
Bottesford	-3.16	-3.83*	-3.20	-2.98*	-5.05*	-4.57*	-3.30	-2.87	-3.38*	-3.43*
Central London	-5.59	-2.71	-2.30	-2.56	-3.87	-3.32	4.32	3.16	-2.75	-1.60
Sibton	-0.33	-0.15	-0.08	0.95	-1.54	-0.09	-1.19	0.31	-1.26	-0.06
Stevenage	0.65	0.31	-0.12	0.01	-2.89	-1.82	2.64	2.35	-0.17	0.02
Balk	0.66	0.84	0.04	0.66	0.44	1.33	3.84	2.24	0.86	1.23
Biddinghuizen	-1.07	-0.09	-1.36	-0.18	-2.02	-0.74	1.95	0.93	-1.12	-0.26
Brandwijk	-2.86		-4.61*		-1.02		5.08		-2.34*	
Cabauw	-1.10	-0.03	-2.21	-1.18	-1.90	-0.07	0.56	2.11	-1.67	-0.41
Hellendoorn	-0.39	0.60	-0.86	0.00	-1.45	-0.19	4.24	2.95	0.11	0.66
Kloosterburen	-1.50	-0.83	0.59	0.58	-1.83	-0.13	0.91	1.33	-0.59	0.00

think it would be inappropriate to use surface ozone data directly to infer any large-scale tropospheric ozone increase or decrease, unless it is certain that the air sampled at the surface ozone station is representative of that in the free troposphere. The mountain stations such as Wank and Zugspitze may be the most representative of all, although even at these stations the possibility of local anthropogenic influence cannot be excluded.

This analysis of the extended data set confirms the general conclusions reached by Low *et al.* (1992). First, it would be unwise to assume that the trends derived from a limited number of longer surface ozone records are necessarily representative of a wider area. Second, the occurrence of marked short-term variability means that conclusions concerning long-term trends drawn from records of limited duration may well be misleading.

REFERENCES

- Bojkov, R.D., 1988: Ozone changes at the surface and in the free troposphere. In *Tropospheric Ozone* (edited by I.S.A. Isaksen), pp. 83-96, D. Reidel, Hingham, Mass., USA.
- Davies, T. D., P. M. Kelly, P.S. Low, and C. E. Pierce, 1990: *Surface Ozone in Europe: Trends and Links to Atmospheric Circulation*, Report No. RK 4244, Climatic Research Unit, University of East Anglia, Norwich, pp.284.
- Davies, T. D., P. M. Kelly, P. S. Low, and C. E. Pierce, 1992: Surface ozone concentrations in Europe: Links with the regional-scale atmospheric circulation, *J. Geophys. Res.*, 97(D9), 9819-9832.
- Feister, U. and Warmbt, W., 1987: Long-term measurements of surface ozone in the German Democratic Republic. *J. Atmos. Chem.* 5, 1-21.
- Galbally, I. E. and C. R. Roy, 1980: Destruction of ozone at the earth's surface, *Quart. J. Royal Met. Soc.*, 106, 599-620.
- Janach, W. E., 1989: Trend details, seasonal variations, and interpretation, *J. Geophys. Res.*, 94(D15), 18289-18295.
- Liu, S. C., M. Trainer, F. C. Fehsenfeld, D. D. Parrish, E. J. Williams, D. W. Fahey, G. Hübler, and P. C. Murphy, 1987: Ozone production in the rural troposphere and the implications for regional and global ozone distributions, *J. Geophys. Res.*, 92(D4), 4191-4207.
- Low, P. S., T. D. Davies, P. M. Kelly, and G. Farmer, 1990: Trends in surface ozone at Hohenpeissenberg and Arkona, *J. Geophys. Res.*, 95(D13), 22441-22453.
- Low, P. S., T. D. Davies, P. M. Kelly, and R. Reiter, 1991: Uncertainties in surface ozone trend at Hohenpeissenberg, *Atmos. Environ.*, 25A(2), 511-515.
- Low, P. S., T. D. Davies, and P. M. Kelly, 1991: *European Surface Ozone Data Manual (First Edition)*, National Power Contract No. LC/3/0020, Climatic Research Unit, University of East Anglia, Norwich NR4 7TJ, pp. 131.
- Low, P.S., P.M. Kelly and T.D. Davies, 1992: Variations in surface ozone trends over Europe. *Geophys. Res. Lett.*, 19, 1117-1120.
- Schmidt, M, 1989: Relationships between tropospheric ozone and global solar radiation in Germany. In *Ozone in the Atmosphere - Proceedings of the Quadrennial Ozone Symposium 1988 and Tropospheric Ozone Workshop* (edited by R. D. Bojkov and P. Fabian), pp.447-450), A. Deepak, Hampton, Va.
- Penkett, S.A., 1989: Trends in atmospheric trace gases. In *Atmospheric Ozone Research and its Policy Implications* (edited by T. Schneider *et al.*), pp.159-166, Elsevier Science, Amsterdam.

N95- 10592

303136

TROPOSPHERIC OZONE AT 45°S

W. Andrew Matthews

National Institute of Water and Atmospheric Research (NIWAR)
Atmospheric Division, Lauder, Central Otago, New Zealand

Abstract:

In August of 1986 a programme was initiated to measure atmospheric ozone profiles at mid-latitudes in the Southern Hemisphere by flying ECC ozonesondes on a regular basis from the DSIR Physical Sciences Atmospheric Laboratory at Lauder, New Zealand, 45°S. Flights since that time have been performed on a regular basis at the rate of two flights per week during the 5 month period August to December, the time of maximum variability at mid-latitudes, and once per week for the remainder of the year.

These data, consisting now of more than 400 profiles has been analysed and the free tropospheric portion of the profiles binned as 1km slabs. These data have then been combined to form a seasonal average values for each season of each year in 2 km slabs and the variation observed in these seasonal averages is the basis of this paper. A biennial component is apparent in these data and the lack of any increasing trend over this 5 year period is contrasted with that measured at similar latitudes in the Northern Hemisphere over the same period.

Introduction:

Tropospheric ozone can be produced by *in situ* chemistry (Crutzen, 1973; Chameides and Walker, 1973; Fishman and Crutzen, 1978) or by transport down from the stratosphere in a process that is considered to provide the "natural" or classical sink for stratospheric ozone.

It has recently been suggested however that the large reductions in stratospheric ozone observed in the lower stratosphere over the last decade, could result in a significant increase in tropospheric ozone and OH, (Schnell et al, 1991). Recent other work considering the influence of sulphate particles on climate change processes suggests that by increasing the backscattered short wave radiation, anthropogenic sulphur emissions may in fact have counteracted climate warming from the increased emissions of greenhouse gases, (Wigley, 1991). Since over 90% of the anthropogenic sulphur release to the atmosphere occurs in the Northern Hemisphere, and since the atmospheric lifetime of SO₂ and sulphate is less than one week in the troposphere,

this process should be limited to the Northern Hemisphere. In fact, this latter effect is so significant that Charlson (1991) suggests that anthropogenic sulphur enhances the hemispherically reflected solar radiation to such an extent that it masks the expected warming through the growth of CO₂ in the Northern Hemisphere. Such an effect could also have a direct bearing on the oxidising capacity of the troposphere as it may also work to reduce the formation of OH in the troposphere.

Staehelin and Schmid, (1991) have found a significant increase of in tropospheric ozone from their balloon sounding program at Payerne (Switzerland). They report an increase that on average amounts to more than 1% per year over the last 20 years. It is against this background that it is interesting to consider what is happening to tropospheric ozone at similar latitudes in the Southern Hemisphere.

Database and Analysis:

In August of 1986, an ozonesonde sounding program was instituted at Lauder, New Zealand, 45°S. Lauder itself is located in the southern centre of the South Island of New Zealand and is 40km away from the nearest population "centre", Alexandra (population 4000). The site is 150km from the ocean and has been chosen as the Mid-latitude Southern Hemisphere Charter site for the international 5 station Network for the Detection of Stratospheric Change (NDSC).

Flights using regular type 4A ECC ozonesondes in conjunction with Phillips radiosondes operating at 1680MHz were flown on the regular basis of one flight per week augmented by an extra flight per week in the spring early summer period (August through December). The resulting chart records were then interpreted manually. At the end of 1989, a change was made to a fully digital system incorporating type 5A ECC ozonesondes and Vaisala RS80 radiosondes. This system was interfaced using a microprocessor controlled multiplexer board from TMax back to the Vaisala transmitter so that the hex-ASCII serial data stream can be transmitted to the ground station at 403MHz and is directly accessible by a PC. Ozone, pressure, ambient temperature and humidity were analysed from each

flight record. The measured ozone amounts were corrected for variations in the pump temperature, which was monitored directly and for pump efficiency, where an empirical correction was applied. The ozone measurement accuracy has been assessed in many studies and has found to be $\pm 10\%$ in the troposphere, $\pm 5\%$ in the stratosphere to 10hPa and ± 5 to $\pm 20\%$ between 10 and 3hPa, Hilsenrath et al., (1986).

The Lauder data series, consisting now of more than 400 profiles has been analysed and a subset of flights was then selected where there was a single well marked tropopause. This method was used to minimise the influence of stratospheric "contamination" of the tropospheric data by direct stratospheric / tropospheric exchange. The free tropospheric portion of the profiles was then binned in 1km slabs. These data have then been combined to form a seasonal average values for each season of each year in 2 km slabs. The number of flights used in each compilation for each season is given in Table 1.

Table 1

Number of Flights in each Season					
Month	FMA	MJJ	ASO	NDJ	Total
1986			22	14	36
1987	10	13	20	13	56
1988	12	13	19	12	56
1989	9	11	23	16	59
1990	11	10	21	16	58
1991	10	12	24	20	66

The each data point in the series of figures that follow represents an average of 6 individual measurements for each 2km slab per flight in the analog data set and an average of 36 measurements for the digital data set. The 1 sigma error bars are shown in each figure.

Results and Discussion:

In the series of figures that follow, the 2km bin data is presented as a function of season for each year. The 'seasons' have been chosen through consideration of the phase of the annual cycle in total ozone at mid-latitudes. The grouping of months February, March and April (FMA) coincide with the total ozone minimum in the Southern Hemisphere, while the grouping August, September and October (ASO) coincide with ozone maximum.

Figures 1(a) to 1(d) show the temporal variation in tropospheric ozone over Lauder in the November, December and January, (NDJ), period for the available time series. The data centered at each 5, 6, 7 and 8kms all show the same form. There is evidence of a 2 year periodicity and a slight downward trend. The summer period typically has a higher

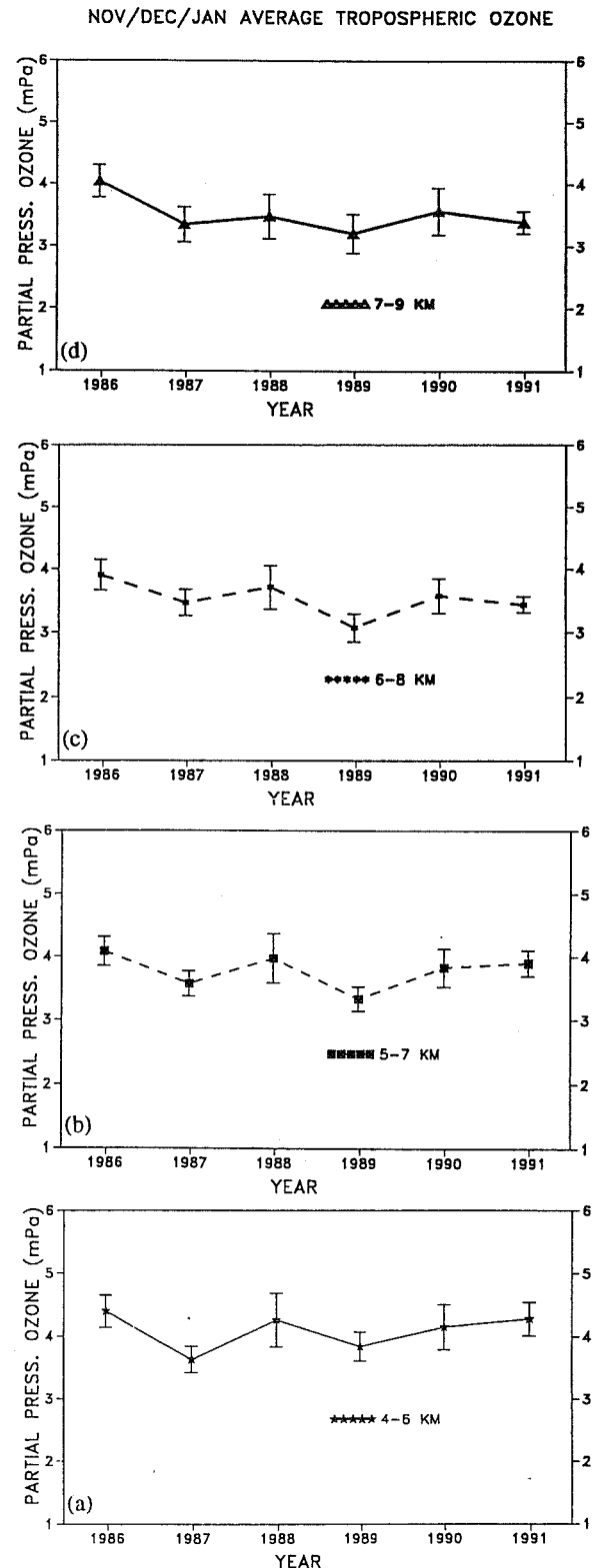


Figure 1: The temporal variation in ozone in a 2km slab over Lauder, centered at (a) 5km, (b) 6km, (c) 7km and (d) 8 km respectively is shown for the November, December, January, (NDJ) period from 1986.

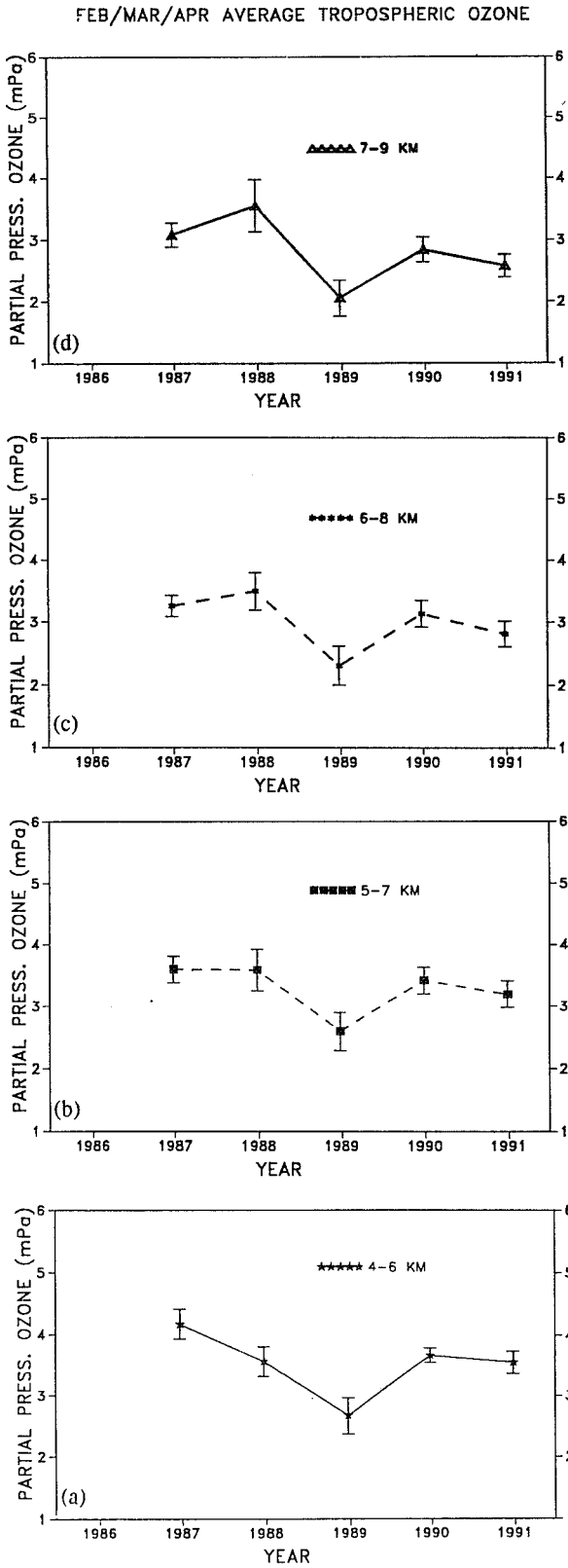


Figure 2: Same as for Figure 1 but for the February, March, April (FMA) period from 1987.

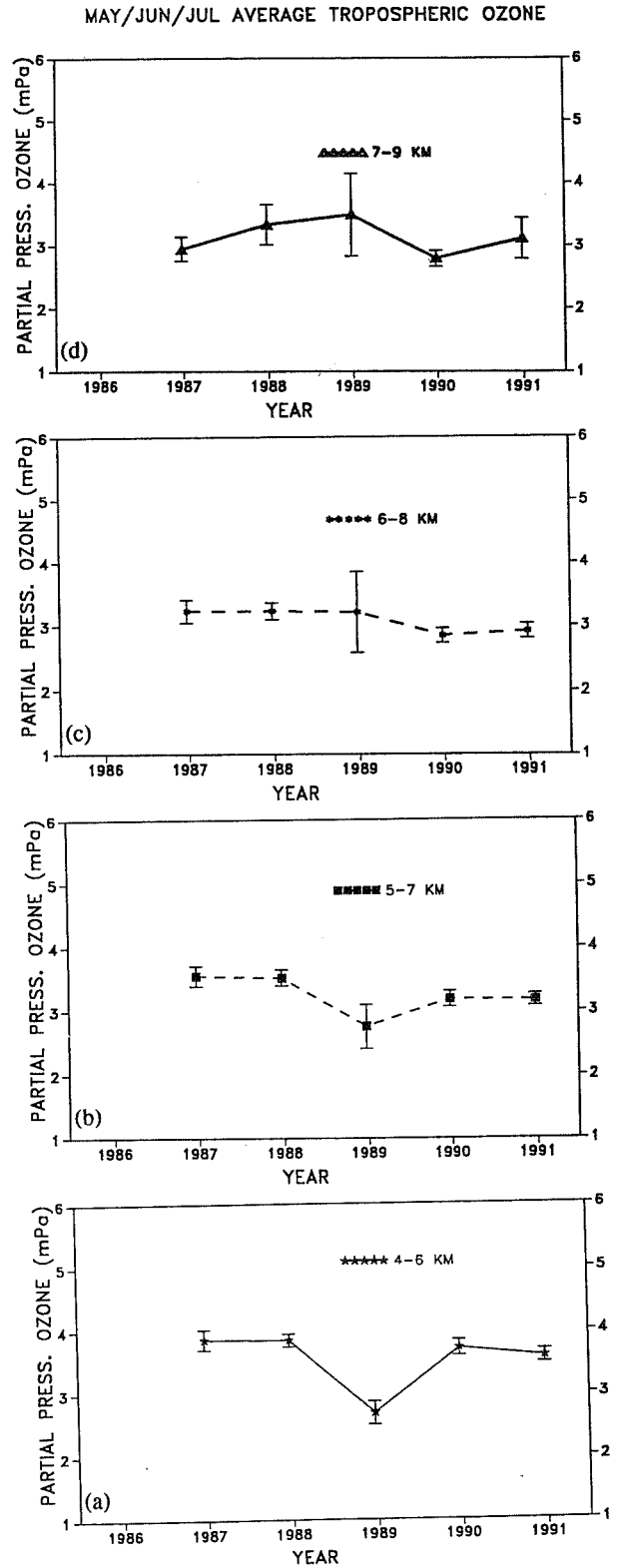


Figure 3: Same as for Figure 1 but for the May, June, July (MJJ) period from 1987.

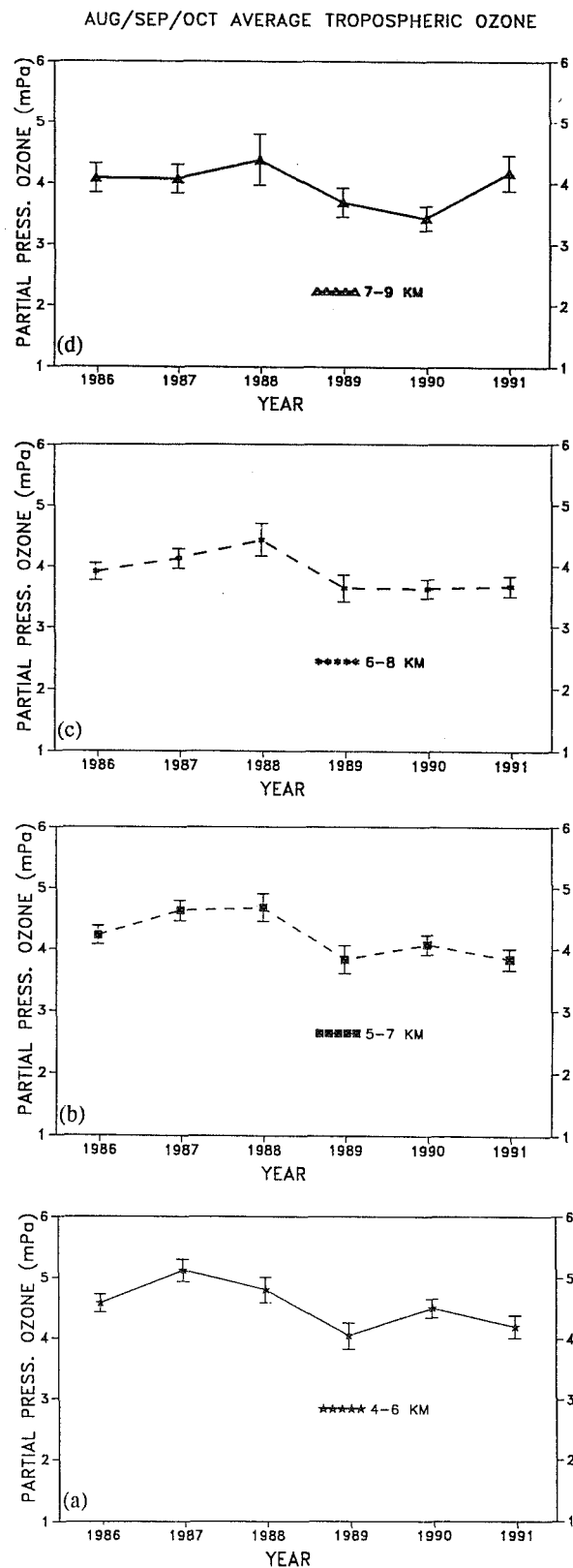


Figure 4: Same as for Figure 1 but for the August, September, October, (ASO) period from 1986.

tropopause and hence there is no evidence of stratospheric exchange processes interfering with even the 7-9km bin at this time of the year. The FMA data, figures 2(a) to 2(d), also show a similar 2 yearly feature, especially in the upper troposphere but the marked feature in these figures are the much lower values recorded in 1989. There is again a suggestion that the tropospheric levels have decreased over the period. The MJJ data, figures 3(a) to 3(d), again show that the tropospheric values in 1989 were much lower than in any other year in the period. The lower tropopause in winter and the occasional folding observed at this time of the year has possibly influenced the data in the 7-9km bin, figure 8, and hence this graph shows a shape that differs from the rest of the series. The period ASO in the spring, figures 4(a) to 4(d), is the time of ozone maximum in the column and also when the highest tropospheric concentrations are observed. It is also the time of greatest variability as evidenced by the larger standard deviations despite the larger data sample. A longer term oscillation is also evident in these data as well as a slight downward trend.

This 5 year data series from mid-latitudes in the Southern Hemisphere demonstrates that over this period, tropospheric ozone levels have not risen at a rate seen in the Northern Hemisphere and in fact there is a suggestion that tropospheric ozone levels may have reduced. A longer time series will in the future establish whether this change is significant and has been sustained.

Acknowledgements:

From 1986 to 1989, the logistical component of the ozonesonde program at Lauder was supported by the Chemical Manufacturers Association whose assistance is greatly appreciated. The assistance with the establishment of this program and initial data analysis by Walter Komhyr is also gratefully acknowledged as is the work by Tracy Beck, Des Rowles and Brian McNamara at Lauder.

References:

- Chameides W.L. and J.C.G. Walker, *J. Geophys. Res.*, **78**, 8751-8760, 1973.
- Charlson, R.L., J. Langner, H. Rodhe, C.B. Leovy and S.G. Warren, *Tellus*, **43A-B**, 4, 152-163, 1991.
- Crutzen, P., *Pure App. Geophys.*, **106-108**, 1385-1399, 1973.
- Fishman J. and P. Crutzen, *Nature*, **274**, 855, 1978.
- Hilsenrath, E., W. Attmannspacher, A. Bass, W. Evans, R. Hogemeyer, R.A. Barnes, W. Komhyr, K. Mauseberger, J. Mentall, M. Proffitt, D. Robbins, S. Taylor, A. Torres and E. Weinstock, *J. Geophys. Res.*, **91**, D12, 13,137-152, 1986.
- Schnell, R.C., S.C. Lui, S.J. Oltmans, R.S. Stone, D.J. Hofmann, E.G. Dutton, T. Deshler, W.T. Sturges, J.W. Harder, S.D. Sewell, M. Trainer and J.M. Harris, *Nature*, **35**, 726-729, 1991.
- Staehelin, J. and W. Schmid, *Atmos. Envir.*, **25a**, 1739-1749, 1991.
- Wigley, T.M.L., *Nature*, **349**, 503-506, 1991.

303142

MEASUREMENTS OF LOWER TROPOSPHERIC OZONE AT MID-LATITUDES OF THE NORTHERN AND SOUTHERN HEMISPHERE

Hans-Eckhart Scheel¹, Rudolf Sladkovic¹, Ernst-Günther Brunke², Wolfgang Seiler¹

¹: Fraunhofer Institute for Atmospheric Environmental Research (IFU),
D-8100 Garmisch-Partenkirchen, Germany

²: APMA-EMATEK, Council for Scientific and Industrial Research,
Faure 7131, South Africa

ABSTRACT

Ground-based measurements of ozone have been carried out at three stations in the German alps (47°N, 11°E, altitudes 740, 1776 and 2962 m a.s.l.) as well as at the coastal station Cape Point (34°S, 18°E). For the mountain sites (at 1776 and 2962 m), trend calculations based on monthly means have yielded O₃ growth rates of 0.8 and 0.9 ppbv yr⁻¹, respectively, over the period 1978-91. Seasonally differentiated data sets have yielded higher rates for summer than for winter. The impact of near-ground photochemical O₃ production on the observed O₃ concentration is shown. No significant long-term O₃ trend has been observed at 740 m (valley floor) as well as at the southern hemispheric station Cape Point. Evidence exists for a close relationship between the amplitude variations of the annual cycles of O₃ and CO at Cape Point.

1. INTRODUCTION

The existence of a long-term rising trend of lower tropospheric ozone over large parts of the Northern Hemisphere seems to be evident (Penkett, 1991 and references therein). However, the observed growth rates differ considerably among the different sites of observation (see e.g. Low et al., 1992), which is at least partly due to specific characteristics of the individual locations, such as influences from local meteorology. It is assumed that enhanced photochemical ozone production in the lower troposphere is responsible for the increase in O₃ observed during the last decades (Logan, 1985). For the Southern Hemisphere, long-term O₃ records are only available from a few sites. At none of these sites has a significant increase in O₃ been observed. For Antarctica even a decrease in O₃ has been reported (Schnell et al., 1991).

We report here on in-situ measurements of ozone performed at three neighboring stations in the German alps (47°N, 11°E) as well as at a coastal station in the southeastern part of Africa (34°S, 18°E). The alpine sites are located at elevations of 740 m a.s.l. (station Garmisch, on the floor of the valley), 1776 m a.s.l. (station Wank, ca. 1100 m above ground) and 2962 m a.s.l. (station Zugspitze, ca. 2200 m above ground). Details of the alpine sites and the O₃ measurements have been described by Reiter et al. (1987). Information on geographic location and instrumentation of the coastal station Cape Point has been given by Seiler et al. (1984) and Brunke et al. (1990).

2. NORTHERN HEMISPHERIC RESULTS

Figure 1 shows the monthly means of ozone for Zugspitze together with trend estimates. The time series is composed of seasonal variations, pronounced interannual variability, and a long-term trend. The rates of increase were highest during the period 1978-82. Thereafter the increase in O₃ was considerably slower. This is assumed to be at least partly related to changes in meteorological conditions, in particular to periods of enhanced cloudiness. The average growth rate for the period 1978-91 amounts to 0.9 ppbv yr⁻¹. A time series of similar shape and comparable trend has been obtained for the station Wank (growth rate 0.8 ppbv yr⁻¹). Near the ground, at Garmisch, no trend is indicated. Similar to Zugspitze (cf. Fig. 1) interannual variations with a period of 4 - 5 years are also present in the time series of the two lower-laying stations. The ozone concentrations observed on the floor of the valley are the result of source and sink relations that are strongly influenced by local meteorology. This is evidenced by Figure 2, where the average diurnal cycles for the individual stations are shown.

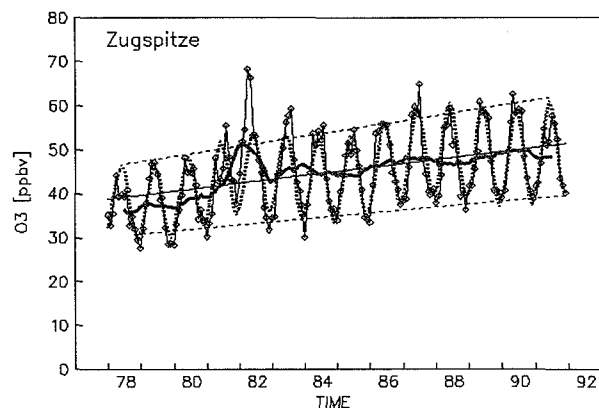


Fig. 1. Monthly mean values of O₃ at Zugspitze and 12-month moving averages (thick curve) together with trend estimates. The slope of the straight solid line corresponds to an average growth rate (1978-91) of 0.92 ppbv yr⁻¹. The non-linear regression function (dotted line) indicates an increase in seasonal amplitudes with growth rates of 1.2 and 0.7 ppbv yr⁻¹ obtained for the summer maxima and winter minima, respectively (slope of dashed lines).

In contrast to the valley, at the station Zugspitze local influence on the diurnal shape of ozone is only observed during spring and summer. For most of the time, the O₃ concentrations at this site can thus be regarded as representative of ozone levels characteristic of the lower free troposphere.

A temporal increase in the seasonal amplitudes is expected as a consequence of the seasonal dependence of photochemical ozone production. In order to test whether such an increase was reflected by the monthly means, a non-linear regression function with a linear gain term for the amplitudes was applied to the data. The resulting least squares fit has indicated an increase in seasonal amplitudes (peak-to-peak) of 4.6 ppbv over the whole time period. Moreover, for Zugspitze the calculations have suggested an average cycling time of 5.6 years for the interannual variations.

For a more detailed study of the impact of lower tropospheric photochemical O₃ production at the mountain sites, trend estimates have been performed on seasonally differentiated percentiles (5th, 25th, 50th (=median), 75th, and 95th) using linear regression. Figure 3 summarizes the results. Under conditions of enhanced photochemical O₃ production, i.e. is for spring and summer, the high ozone concentrations, as characterized by the 95th percentiles, have been increasing at a rate which is nearly twice the rate of the low concentrations. Accordingly, the rate of increase estimated for high summer concentrations is considerably greater than the rate determined for high winter concentrations (Fig. 3).

In Figure 4 the seasonal variations of O₃ at Zugspitze are depicted. The maximum of the seasonal cycle is observed in spring, which is in agreement with observations reported from other European locations (cf. Logan, 1985). For the first half of the measuring period, the seasonal amplitude is smaller than for the second half. From a different approach this confirms the above finding that the amplitudes of the annual cycle have been increasing due to enhanced concentrations in spring and summer.

The strong impact of solar radiation and thus of photochemistry on the ozone concentrations can be seen from Figure 5. Daily maxima have been classified according to the relative sunshine duration (RSD). Under conditions of cloudy sky (RSD < 1 % of the time), the annual cycles at the mountain stations show similar levels.

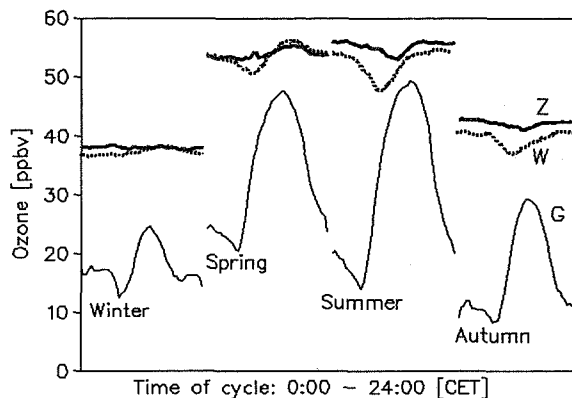


Fig. 2. Average diurnal cycle of O₃ (1986-88) at the stations Garmisch, Wank, and Zugspitze for the different seasons.

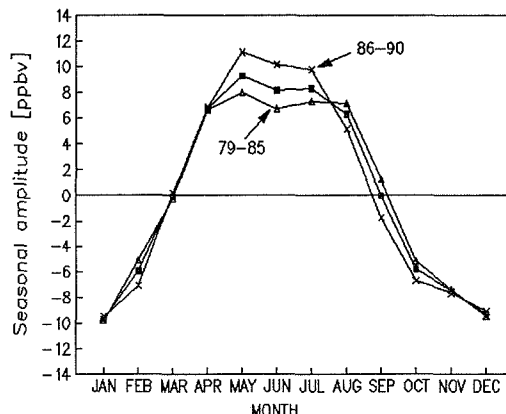


Fig. 4. Average seasonal variations (calculated from the difference between monthly mean value and 12-month moving average) of O₃ at Zugspitze for different time periods (79-90; 79-85 and 86-90).

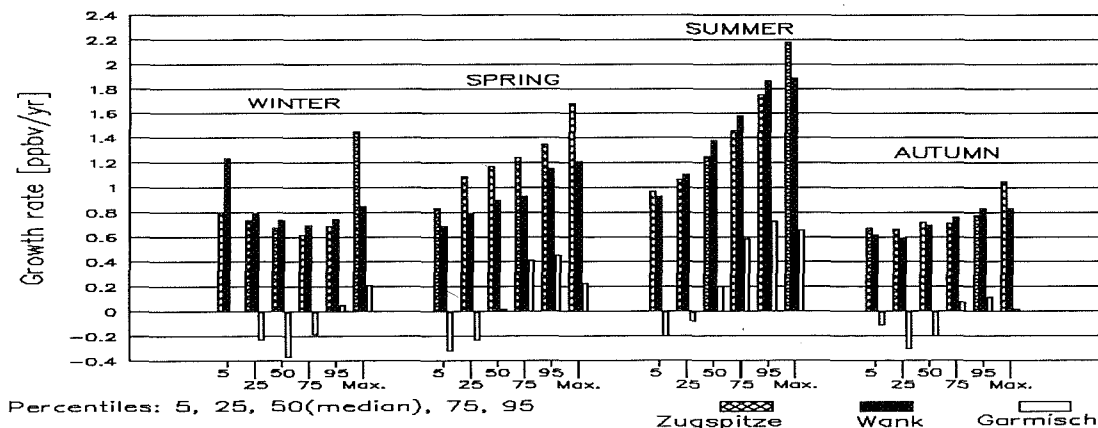


Fig. 3. Ozone trend (1978-90) at the mountain sites (Zugspitze, Wank) as a function of season and statistical parameters. For Garmisch (floor of the valley) none of the rates shown by the bars is statistically significant.

Peak ozone levels in the valley (at Garmisch) are lower by about 12 ppbv. In contrast, under conditions of intense solar radiation ($RSD > 80\%$), the peak of the distribution for Garmisch even surpasses the one for Zugspitze, which reflects a significant contribution from locally produced ozone. For $RSD > 80\%$, however, highest O_3 concentrations are observed at Wank, i.e. at an elevation of about 1000 m above ground. This supports the finding from model calculations (McKeen et al., 1989) that optimum conditions for photochemical ozone production can be expected around this altitude.

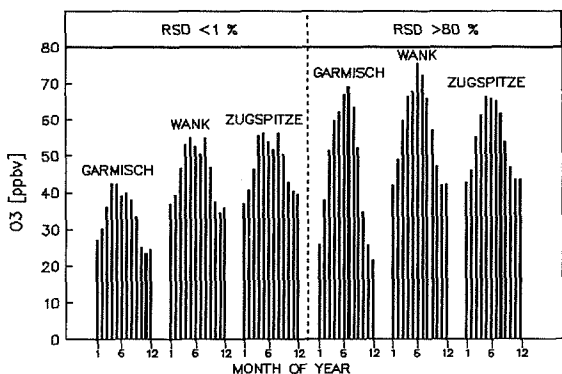


Fig. 5. Average annual distributions of daily O_3 maxima (1978-91) for low and high relative sunshine duration ($RSD < 1\%$ and $> 80\%$).

3. SOUTHERN HEMISPHERIC RESULTS

The time series of O_3 at Cape Point as given by the monthly means (Oct. 82 - Dec 91) is shown in Figure 6. The shape is characterized by both seasonal cycling and great interannual variability. Maximum O_3 concentrations occur in austral winter (July) and minima in summer (January). The annual means of O_3 center around 21 ppbv with average seasonal amplitudes of about ± 7 ppbv. So far, the monthly means do not indicate any long-term trend of O_3 at Cape Point. This is confirmed when the monthly means for the individual seasons are considered separately. However, in view of the strong interannual variability and the severe data gaps, the results obtained so far should be regarded as preliminary.

In Figure 7 the average annual cycle of ozone is shown. As is generally assumed for these southern latitudes, the cycle of surface ozone is mainly controlled by two types of processes, i.e. stratosphere/troposphere exchange (Liu et al., 1980) as well as photochemical ozone destruction (Fishman et al., 1979). The latter process, which is closely related to the annual cycle of solar UV radiation (Fig. 7), is assumed to lead to the O_3 minima observed around January. In contrast to the rather symmetric shape of the UV cycle, the ozone distribution with its maximum in July shows a slight shoulder between August and November.

The ozone distribution thus suggests that additional processes might contribute to its shape. One such process could possibly be biomass burning. This seems to be implicated by the following findings: Firstly, carbon monoxide, which has been measured at Cape Point since 1978 (Seiler et al., 1984; Brunke et al., 1990), shows an annual

distribution with a maximum around September/October (Fig. 7). The CO maximum thus coincides with the shoulder observed in the O_3 distribution during austral spring. After various interpretations have been put forward to explain the annual cycle of CO (Khalil and Rasmussen, 1984; Seiler et al., 1984; Fraser et al., 1986), recent publications have largely attributed the occurrence of the CO maximum to biomass burning (Heintzenberg and Bigg, 1990; Fishman et al., 1991, and reference therein). Secondly, Fishman et al. (1991), who studied upper tropospheric ozone from satellite data, have shown that ozone which originates from biomass burning also displays annual cycling with increasing concentrations from July to November. According to the results presented by Fishman et al. (1991), the rise of integrated O_3 in the troposphere over Cape Point partly parallels the shape of the CO distribution observed at ground-level, but is not in phase with the surface ozone observed at Cape Point (maximum in July). We thus speculate that the seasonal increase in ozone in the upper troposphere, which originates from biomass burning, does put its mark on the distribution of surface O_3 at Cape Point during the months August to November.

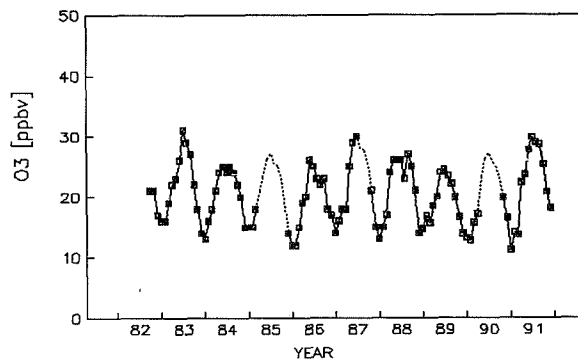


Fig. 6. Monthly means of O_3 as obtained for Cape Point ($34^\circ S$, $18^\circ E$) between Oct. 82 and Dec. 91. Periods of data loss, which are due to instrumental failures, have been interpolated by values from the average annual cycle (dotted line).

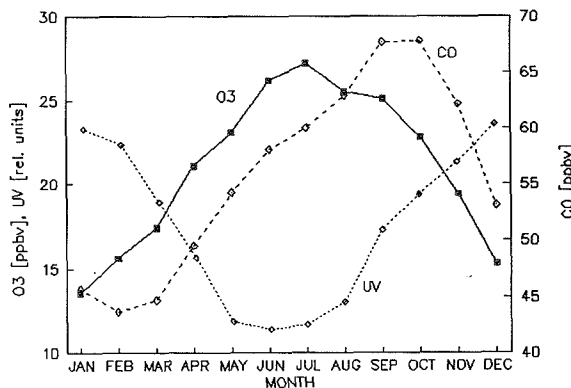


Fig. 7. Average annual cycles of O_3 (1983-91), UV radiation (1989-91) and CO (1979-91) at Cape Point.

At Cape Point, the annual peak-to-peak amplitudes of O₃ and CO (Fig. 8) show a close relationship (correlation coefficient of 0.9). This result has not yet been analyzed in detail; nonetheless it seems to support the view of either partly common sources or partly common transport mechanisms for O₃ and CO. Interestingly, the highest amplitudes were observed for El-Niño years, when among others the tropical meteorology and thus transport processes are strongly affected. Such a possible impact of El-Niño events on trace gas levels observed at Cape Point seems to merit further attention when more data are available.

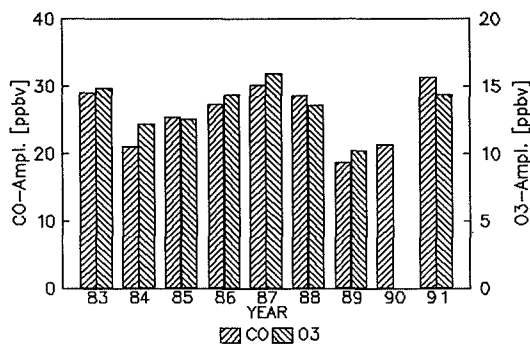


Fig. 8. Comparison between the annual peak-to-peak amplitudes of O₃ and CO at Cape Point. The data yield a correlation coefficient of 0.9.

REFERENCES

- Brunke, E.-G., H.E. Scheel, and W. Seiler, 1990: Trends of tropospheric CO, N₂O and CH₄ as observed at Cape Point, South Africa. *Atmos. Environ.* 24A, 585-595.
- Fishman, J., S. Solomon, and P.J. Crutzen, 1979: Observational and theoretical evidence in support of a significant in-situ photochemical source of tropospheric ozone, *Tellus* 31, 432-446.
- Fishman, J, K. Fakhruzzaman, B. Cros, and D. Nganga, 1991: Identification of widespread pollution in the Southern Hemisphere deduced from satellite analyses. *Science* 252, 1693-1696.
- Fraser, P.J. and P. Hyson, 1986: Methane, carbon monoxide and methychloroform in the Southern Hemisphere. *J. Atmos. Chem.* 4, 3-42.
- Heintzenberg, J. and E.K. Bigg, 1990: Tropospheric transport of trace substances in the southern hemisphere. *Tellus* 42B, 355-363.
- Khalil, M.A.K. and R.A. Rasmussen, 1984: Carbon monoxide in the earth's atmosphere: increasing trend. *Science* 224, 54-56.
- Liu, S.C., D. Kley, M. McFarland, J.D. Mahlmann, and H. Levy II, 1980: On the origin of tropospheric ozone. *J. Geophys. Res.* 85, 7546-7552.
- Logan, J.A., 1985: Tropospheric ozone: Seasonal behavior, trends, and anthropogenic influence. *J. Geophys. Res.* 90, 10463-10882.
- Low, P.S., P.M. Kelly, and T.D. Davies, 1992: Variations in surface ozone over Europe. *Geophys. Res. Lett.* 19, 1117-1120.
- McKeen, S., D. Kley, and A. Volz, 1989: The historical trend of tropospheric ozone over Western Europe: A model perspective. In "Ozone in the Atmosphere", R.D. Bojkov, P. Fabian (eds.), pp. 552-556.
- Penkett, S.A., 1991: Changing ozone - Evidence for a perturbed atmosphere. *Environ. Sci. Technol.* 25, 631-635.
- Reiter, R., R. Sladkovic, and H.-J. Kanter, 1987: Concentration of trace gases in the lower troposphere, simultaneously recorded at neighboring mountain stations, Part II: Ozone. *Meteorol. Atmos. Phys.* 37, 27-47.
- Schnell, R.C., S.C. Liu, S.J. Oltmans, R.S. Stone, D.J. Hofmann, E.G. Dutton, T. Deshler, W.T. Sturges, J.W. Harder, S.D. Sewell, M. Trainer and J.M. Harris, 1991: Decrease of summer tropospheric ozone concentrations in Antarctica. *Nature* 351, 726-729.
- Seiler, W., H. Giehl, E.-G. Brunke, and E. Halliday, 1984: The seasonality of CO abundance in the Southern Hemisphere. *Tellus* 36B, 219-231.

ANALYSIS OF A 7 YEAR TROPOSPHERIC OZONE VERTICAL DISTRIBUTION AT THE OBSERVATOIRE DE HAUTE PROVENCE

Matthias Beekmann, Gérard Ancellet and Gérard Mégie

Service d'Aéronomie du CNRS, Université Paris 6, Paris, France

Abstract

A seven year (1984-90) climatology of tropospheric vertical ozone soundings, performed by electrochemical sondes at the OHP (44°N, 6°E, 700m ASL) in Southern France, is presented. Its seasonal variation shows a broad spring/summer maximum in the troposphere. The contribution of photochemical ozone production and transport from the stratosphere to this seasonal variation are studied by a correlative analysis of ozone concentrations and meteorological variables, with emphasis on potential vorticity. This analysis shows the impact of dynamical and photochemical processes on the spatial and temporal ozone variability. In particular, a positive correlation ($r = 0.40$, significance >99.9%) of ozone with potential vorticity is observed in the middle troposphere, reflecting the impact of stratosphere-troposphere exchange on the vertical ozone distribution.

1. Introduction

The European project TOR (Tropospheric Ozone Research) aims at establishing the tropospheric ozone budget on a regional, European scale. The core of the project is a network of 39 surface stations measuring ozone, related trace constituents (NO_x, hydrocarbons), and radiative and meteorological parameters, and of 7 stations for vertical ozone sounding. The goal of the surface measurements is to evaluate the impact of photochemical ozone production in the boundary layer on a regional scale. The vertical ozone soundings provide information on the photochemical ozone production in the free troposphere and the transport of ozone both from the stratosphere and the boundary layer. The Observatoire de Haute Provence (OHP, 44°N, 6°E, 700m ASL) in Southern France is part of the TOR network and vertical tropospheric ozone sounding is performed there both with a UV-DIAL lidar system and with electrochemical sondes. In this paper, the tropospheric ozone climatology obtained at OHP with Brewer-Mast sondes between 1984 and 1990, is presented. By relating the ozone data to meteorological variables, the relative importance of

dynamical and photochemical processes for the spatial and temporal ozone variability will be studied.

II. The tropospheric ozone climatology at OHP between 1984 and 1990

Between 1984 and 1990, 140 ozone profiles up to approximately 30 km altitude have been performed at OHP, using balloon-borne electrochemical Brewer-Mast sondes. The OHP is a rural site, the largest nearby urban agglomeration (Marseille) being located at 150 km distance in a south-west direction. From the instrument error analysis and two intercomparison campaigns involving several measuring techniques, it is concluded that our time series of ozone measurements is too short to derive an annual ozone trend with sufficient statistical significance [Beekmann, 1992], but that Brewer-Mast sondes are well suited to match the temporal variability of tropospheric ozone on a timescale of some days (20%) or of one year (40%). Furthermore, the spatial ozone variability (typically 20% in the Western Europe free troposphere) can be correctly assessed if stations using the same measurement technique (here Brewer-Mast sondes) are taken into account.

The ozone climatology at the OHP shows a broad spring and summer maximum in the troposphere (fig.1), as expected for a northern mid-latitude station. This seasonal variation is similar for the other stations in Western Europe. Figure 1 indicates however a meridional gradient of ozone in Western Europe, with larger values at the more northerly stations Uccle and Jülich (51°N), compared to the more southerly stations OHP (44°N) and Pic de Midi (43°N). These differences become more pronounced with increasing altitude. There might also be systematic differences depending on the continental character of a station: at Hohenpeissenberg (48°N, 11°E), located at about the same latitude as Payerne (47°N, 7°E), but more in the east, the larger ozone values are found. This analysis raises thus the question of whether first the spring-summer maximum and second spatial gradients are caused either by photochemical ozone production or by transport from the stratosphere.

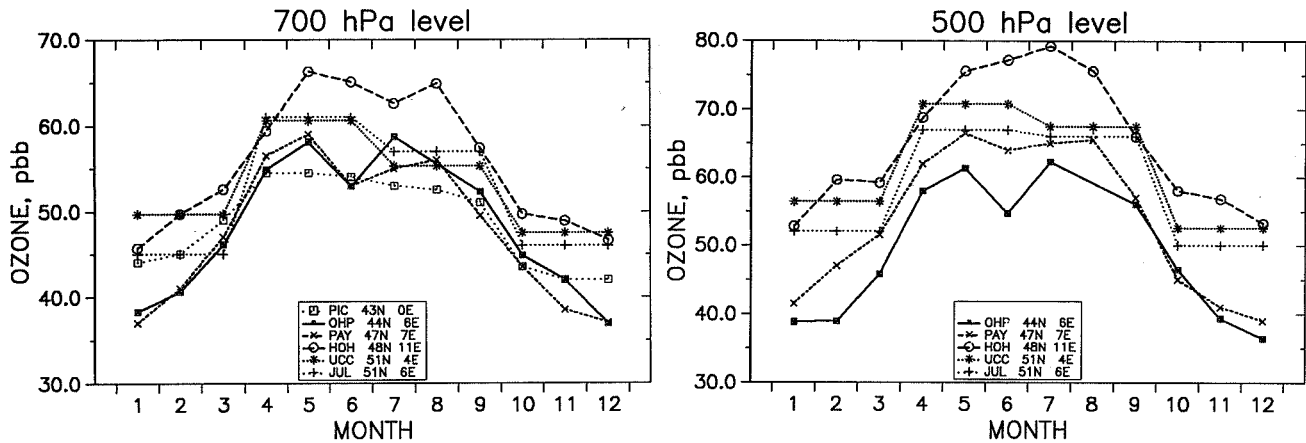


fig.1 : seasonal variation of tropospheric ozone at different Western European sounding stations,

station	location	period	instrument	reference
PIC	Pic de Midi 43°N, 0°E, 3000m ASL	1982-84/90-91	UV-photometer	Nedelec, 1991
OHP	Obs. de Haute Provence 44°N, 6°E, 670m ASL	1984-90	Brewer-Mast	Beekmann, 1992
PAY	Payerne 47°N, 7°E, 490m ASL	1982-88	Brewer-Mast	Stachelin et al., 1991
HOH	Hohenpeissenberg 48°N, 11°E, 980m ASL	1985-89	Brewer-Mast	Sonderbeobachtungen 86-90
UCC	Uccle 51°N, 4°E, 100m ASL	1984-88	Brewer-Mast	Bull. trimestr. 1985-89
JUL	Jülich 51°N, 6°E, 100m ASL	1989-91	ECC	Smit et al., 1991.

III. Analysis of ozone with respect to meteorological data

A first approach to relate the observed ozone variability at OHP to physico-chemical and dynamical processes, is to perform a statistical analysis of ozone concentrations with respect to meteorological data such as potential vorticity, humidity, geopotential height and trajectories. Contrary to concentrations of ozone precursors (NO_x, hydrocarbons), these data are available in the free troposphere for each ozone profile, either directly from sonde measurements (pressure, temperature, humidity) or from meteorological models, providing objectively analysed temperature and wind fields for potential vorticity and trajectory calculations.

In this paper, we focus on the analysis of potential vorticity, which is a tracer of stratospheric air masses transported into the troposphere. In the absence of a vertical gradient of diabatic heating and in the absence of frictional forces, potential vorticity is a conserved quantity. Due to the similar vertical gradients of ozone mixing ratios and potential vorticity (PV) in the lower stratosphere, a positive correlation of ozone and PV in this region is expected. This is verified for the OHP ozone data base at the 225 hPa level, where a strong and significant correlation between both variables is found ($r=0.82$, significance > 99.9%). At the 500 hPa level, a significant, but weaker, positive correlation between ozone concentrations and potential vorticity is observed ($r=0.40$, significance > 99.9%). This positive correlation reflects the impact of stratosphere-troposphere exchange on the ozone variability in the middle troposphere. The correlation is weaker for the mid-troposphere than for the lower stratosphere, because in the troposphere ozone and PV are

partially decorrelated by photochemical processes on one hand, acting on ozone, and by diabatic processes on the other hand, acting on PV (e.g. latent heat release, radiative processes including the interaction with clouds, sensible heat flux at ground). The ozone/PV correlation is most pronounced in the period spring/early summer (tab.1), indicating a larger importance of stratosphere-troposphere exchange during this period. The correlation coefficients are almost unchanged if one considers ozone concentrations and potential vorticity without their seasonal variation (residuals of monthly means), which means that the variability of both values is also correlated for timescales smaller than one month.

	r	p
225 hPa, all seasons	0.83	>99.9%
500 hPa, all seasons	0.40	>99.9%
mar. - july	0.49	>99.9%
aug. - oct.	0.27	93%
nov. -feb.	0.40	98%

tab.1 : correlation coefficients r between ozone and potential vorticity; $1 - p$ is the probability that a higher correlation coefficient than r would have been obtained if both data sets were completely uncorrelated (exactly valid only for binormal distributions).

The knowledge of potential vorticity offers the possibility to sort the ozone profiles into two classes: one with air masses of larger PV values, affected by recent stratospheric ozone intrusions, the other with air masses of

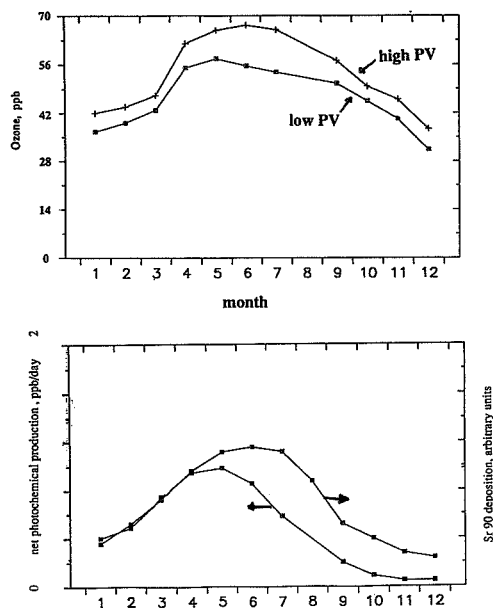


fig.2 : above: seasonal variation of ozone profiles of the high and the low potential vorticity class at 500 hPa, below: seasonal variation of the net photochemical ozone production at 50°N and 4 km height [Isakson, 1988], Sr 90 surface deposition in Southern France [Marenco and Fontan, 1974].

smaller PV values, which are then, in the absence of recent stratosphere-troposphere exchange, representative of the photochemical ozone source. PV values, which are more than 0.1 PV-units above their monthly mean at the 500 hPa level and which are larger than 0.8 PV-units at the 350 hPa level (i.e. near the dynamical tropopause of 1.6 PV-units), belong to the high PV-class (1 PV unit = $1.10 \cdot 10^{-6} \text{ K m}^2 / \text{kg s}$). Figure 2 shows a similar seasonal variation of ozone for both classes at the 500 hPa level. The seasonal variation of the high PV-class compares well with that of the deposition of Sr 90 in Southern France at the end of the sixties [Marenco et al., 1974]. Sr 90 is a fission product released during atmospheric nuclear bomb tests and was widely used as a tracer of stratospheric air. Furthermore, the seasonal variation is in good agreement with that of the frequency of occurrence of cut-off lows, which is maximum in June [United Kingdom Photochemical Oxidants Review Group, 1987]. The seasonal variation of the low PV-class corresponds well to that of the seasonal variation of the net photochemical ozone production at 50°N and at 4 km height, as computed by a 2D-model [Isaksen, 1988]. The larger amplitude in the seasonal variation of the ozone sources than in the seasonal variation of the ozone concentrations is explained by the larger deposition rates during the period spring/summer [Liu et al., 1987]. Thus, although a quantitative determination of the respective contribution of the two ozone sources is not possible by this analysis, it supports nevertheless the seasonal variation of the ozone sources, derived by photochemical modeling and by other tracers of stratosphere-troposphere exchange (Sr 90 deposition, cut-off lows).

The simultaneous knowledge of ozone and PV values allows to determine the ozone/PV ratio and its seasonal and altitude dependence at the OHP. The exact knowledge of this ratio allows the initialisation of ozone fields of models from PV fields and to calculate ozone fluxes from PV fluxes. At the OHP, the values of the ozone/PV ratio are much higher in the mid-troposphere than in the lower stratosphere (fig.3). They show a spring maximum at the levels 500 hPa and at 225 hPa and an early summer maximum at 350 hPa. The higher tropospheric values of the ozone/PV ratio are explained by a decrease of the potential vorticity in the troposphere due to diabatic processes and an increase of ozone due to photochemical production, particularly in the period spring/summer.

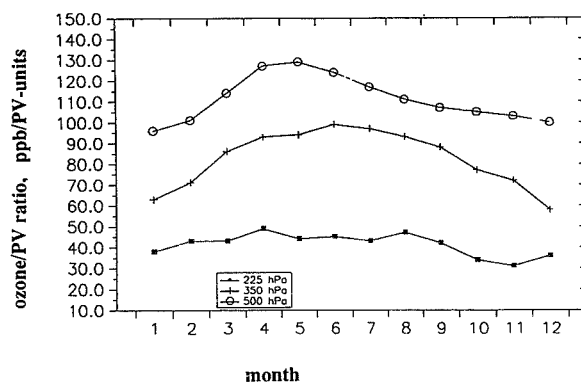


fig.3 : ozone / potential vorticity ratio at OHP for 500 hPa (upper curve), 350 hPa and 225 hPa.

A comparison of the ozone/PV ratios for a northern and a southern station (Uccle, 51°N, OHP, 44°N), shows only small differences compared to the error bars of the ratios (tab.2). As a consequence, the meridional ozone gradient in Western Europe is related to a similar gradient of potential vorticity, which shows the importance of dynamical effects (e.g. lower tropopause height at Uccle) for the spatial distribution of ozone in the upper and middle troposphere.

level	500 hPa		300 hPa	
station	OHP 44°N	Uccle 51°N	OHP 44°N	Uccle 51°N
ozone [ppb]	49.6 ± 4.6	61.8 ± 4.6	58.3 ± 7.7	99 ± 7.7
potential vorticity (PV-units)	0.45 ± 0.02	0.61 ± 0.05	0.95 ± 0.05	1.8 ± 0.2
ozone/PV ratio [ppb/PV-unit]	110 ± 15	101 ± 15	61 ± 11	55 ± 11

tab.2: comparison of the ozone / potential vorticity ratio at Uccle (51°N) and at OHP (44°N)

We now make use of the established correlations between ozone and potential vorticity and also between ozone and relative humidity at the 850 hPa level ($r = -0.38$, significance $> 99.9\%$), in order to determine the part of a potential ozone trend due to dynamical processes. For the OHP data set between 1984 and 1990, a considerable variability of relative humidity and potential vorticity has been observed which would yield ozone trends between -2.7% and $+1.2\%$ for different pressure levels (tab.3). It is clear that these dynamical induced ozone changes have to be taken into account, if one wants to deduce accurately the ozone trend due to anthropogenic activities.

level	850 hPa	500 hPa	350 hPa
annual trend of relative humidity (84-89)	-4.5 $\pm 1.4\%$		
annual trend of potential vorticity (84-89)		-2.0 $\pm 2.2\%$	-11.8 $\pm 5.2\%$
annual ozone trend induced by meteorological variables	+1.2 $\pm 0.4\%$	-0.5 $\pm 0.7\%$	-2.7 $\pm 1.2\%$

tab.3 : the impact of the interannual variability of potential vorticity and relative humidity on a possible ozone trend.

4. Summary and future work

The tropospheric ozone climatology obtained at the OHP in Southern France between 1984 and 1990 shows a seasonal variation characterized by a clear spring/summer

References :

Beekmann M., Bilan de l'ozone troposphérique aux moyennes latitudes: analyse climatologique et variabilité spatio-temporelle de la distribution verticale, *Thesis at University Paris 6*, France, 1992.

Bulletin trimestriel, Observations d'Ozone, Institut Royal Météorologique de Belgique, 1985-1989.

Isaksen, I.S.A., Is the oxidising capacity of the atmosphere changing ? in *The Changing Atmosphere*, F.Rowland, I.S.A.Isaksen, (ed.), Dahlem Workshop Reports, p.141-158, J.Wiley and Sons, Chichester, 1988.

Liu, S.C., M.Trainer, F.C.Fehsenfeld, D.D.Parrish, E.J.Williams, D.W.Fahey, G.Hubler and P.C. Murphy, Ozone production in the rural troposphere and implications for regional and global distributions, *J. Geophys. Res.* 92, 4191-4207, 1987.

Marengo, A. and J.Fontan, Etudes des variations des Be7, P32, Sr90, Pb210, et Po210 dans la troposphère, *Tellus* 26, 118-135, 1974.

maximum of ozone concentrations. A statistical analysis of the ozone profiles together with meteorological variables, especially with potential vorticity, shows that this maximum is both due to transport from the stratosphere and to photochemical production. This is in good agreement with the ozone sources derived from model calculations (photochemical production) and from independent tracers of stratosphere-troposphere exchange (Sr 90 deposition, cut-off lows). We can also show the notable impact of dynamical processes on the meridional ozone gradient in Western Europe and on an interannual ozone trend.

The future work has to be devoted to a more particular analysis of the photochemical source of ozone, using the surface data of ozone precursors (NO_x, hydrocarbons), which are now available in the TOR-database. Trajectory analysis, taking into account the photochemical transformation of air masses (Lagrangian modeling), could be used to relate the surface emissions of ozone precursors to the vertical ozone profiles, in order to establish the impact of the enhanced emissions of ozone precursors over Europe on the strength of the photochemical ozone production in the free troposphere.

Acknowledgements: This work has been supported by the French Ministry of Environment. M.Beekmann held a doctoral fellowship from Gottlieb Daimler und Karl Benz Stiftung and from the Environmental Protection Program of the CEC. The ECMWF is acknowledged for providing the temperature and wind field analysis.

Nedelec P., Mise au point d'un analyseur d'oxides d'azote à haute sensibilité, application à l'étude de l'ozone et de ses précurseurs dans la troposphère, *Thesis at University Paul Sabatier, Toulouse*, France, 1991.

Sonderbeobachtungen des Meteorologischen Observatoriums Hohenpeissenberg, Nr. 53 - 62, Deutscher Wetterdienst, 1986-1991.

Smit, H.G.J., W.Sträter, H.Loup and D.Kley, Ozone Profiles at Jülich and Schauinsland, *Berichte der KfA Jülich*, 1991.

Stahelin, J. and W.Schmid, Trend analysis of tropospheric ozone concentrations utilizing the 20 year ozone data set over Payerne (Switzerland), *Atmos. Env.* 25A, 1739-1749, 1991.

United Kingdom Photochemical Oxidants Review Group, Ozone in the United Kingdom, *Dep. Envir. Publ.*, Middlesex, England, p15, 1987.

**OZONE MEASUREMENTS FROM A GLOBAL NETWORK
OF SURFACE SITES**

Samuel J. Oltmans

Climate Monitoring and Diagnostics Laboratory, NOAA/ERL
Boulder, Colorado 80303, U.S.A.

Hiram Levy II

Geophysical Fluid Dynamics Laboratory, NOAA/ERL
Princeton, New Jersey 08542, U.S.A.

ABSTRACT

From a network of surface ozone monitoring sites distributed primarily over the Atlantic and Pacific Oceans, the seasonal, day-to-day, and diurnal patterns are delineated. At most of the NH (northern hemisphere) sites there is a spring maximum and late summer or autumn minimum. At Barrow, AK (70°N) and Barbados (14°N), however, there is a winter maximum, but the mechanisms producing the maximum are quite different. All the sites in the SH (southern hemisphere) show winter maxima and summer minima. At the subtropical and tropical sites there are large day-to-day variations that reflect the changes in flow patterns. Air of tropical origin has much lower ozone concentrations than air from higher latitudes. At the two tropical sites (Barbados and Samoa) there is a marked diurnal ozone variation with highest amounts in the early morning and lowest values in the afternoon.

At four of the locations (Barrow, AK; Mauna Loa, HI; American Samoa; and South Pole) there are 15- through 20-year records which allow us to look at longer term changes. At Barrow there has been a large summer increase over the 20 years of measurements. At South Pole, on the other hand, summer decreases have led to an overall decline in surface ozone amounts.

1. INTRODUCTION

As part of the Climate Monitoring and Diagnostics Laboratory, surface ozone measurements have been made for a number of years at four sites. Beginning in 1988 the number of sites has been expanded as part of the Atmosphere/Ocean Chemistry Experiment (AEROCE). Information on the location and period of data record is summarized in Table 1. In the discussion of the seasonal cycle, monthly mean data from three locations in the SH are taken from the literature to give better geographic coverage.

2. SEASONAL VARIATION

Figure 1 displays the monthly median ozone and its dispersion for eight sites spanning the latitude range 71°N-14°N. At all but the most northerly (Barrow) and southerly

Table 1: Elevation, location, and period of observation for surface ozone measurement stations.

Station	Elev.	Lat.	Long.	Period of Observ.
Barrow, AK	11m	71°N	157°W	3/73-2/92
Reykavik, Iceland	60m	64°N	22°W	9/91-5/92
Mace Head, Ireland	30m	53°N	10°W	7/89-4/92
Niwot Ridge, CO	3000m	40°N	106°W	7/90-5/92
Bermuda	40m	32°N	64°W	10/88-5/92
Izana, Canary Is.	2360m	28°N	16°W	5/87-10/89
Mauna Loa, HI	3397m	20°N	156°W	10/73-3/92
Barbados	45m	13°N	59°W	4/89-5/92
Samoa	82m	14°S	171°W	1/76-12/91
Cape Point, S. Africa	75m	34°S	18°E	1/83-6/88
Cape Grim, Australia	94m	41°S	145°E	1/82-12/86
Syowa, Antarctica	21m	69°S	40°E	2/89-1/90
So. Pole, Antarctica	2835m	90°S	--	1/75-2/92

(Barbados) there is a spring maximum. At high arctic locations such as Barrow at the surface, the expected spring maximum is missing because of strong ozone depletion that is linked to the presence of high bromine concentrations. (Barrie et al., 1988, Oltmans, 1991). In fact immediately above the boundary layer, there is a spring maximum (Oltmans, 1991). At Barbados the maximum in early winter is a result of the cutoff of flow from northerly mid-latitudes that occurs much earlier in the year at low latitudes than it does at Bermuda for instance (Oltmans and Levy, 1992). Niwot Ridge, Mauna Loa, and Izana are all high altitude sites at elevations of ~3,000 m. Expectedly, these sites have the highest ozone concentrations.

The largest seasonal variation is at Bermuda. During the winter and especially in the spring, there are numerous events where transport from mid-tropospheric levels over North America reaches Bermuda (Oltmans and Levy, 1992). During these events, hourly average ozone mixing ratios fall in the 50-70 ppb range. During the summer, however, flow from more southerly latitudes dominates with concentrations of 15-25 ppb. At the higher altitude site of Izana near the same latitude, summer values do not dip nearly so low

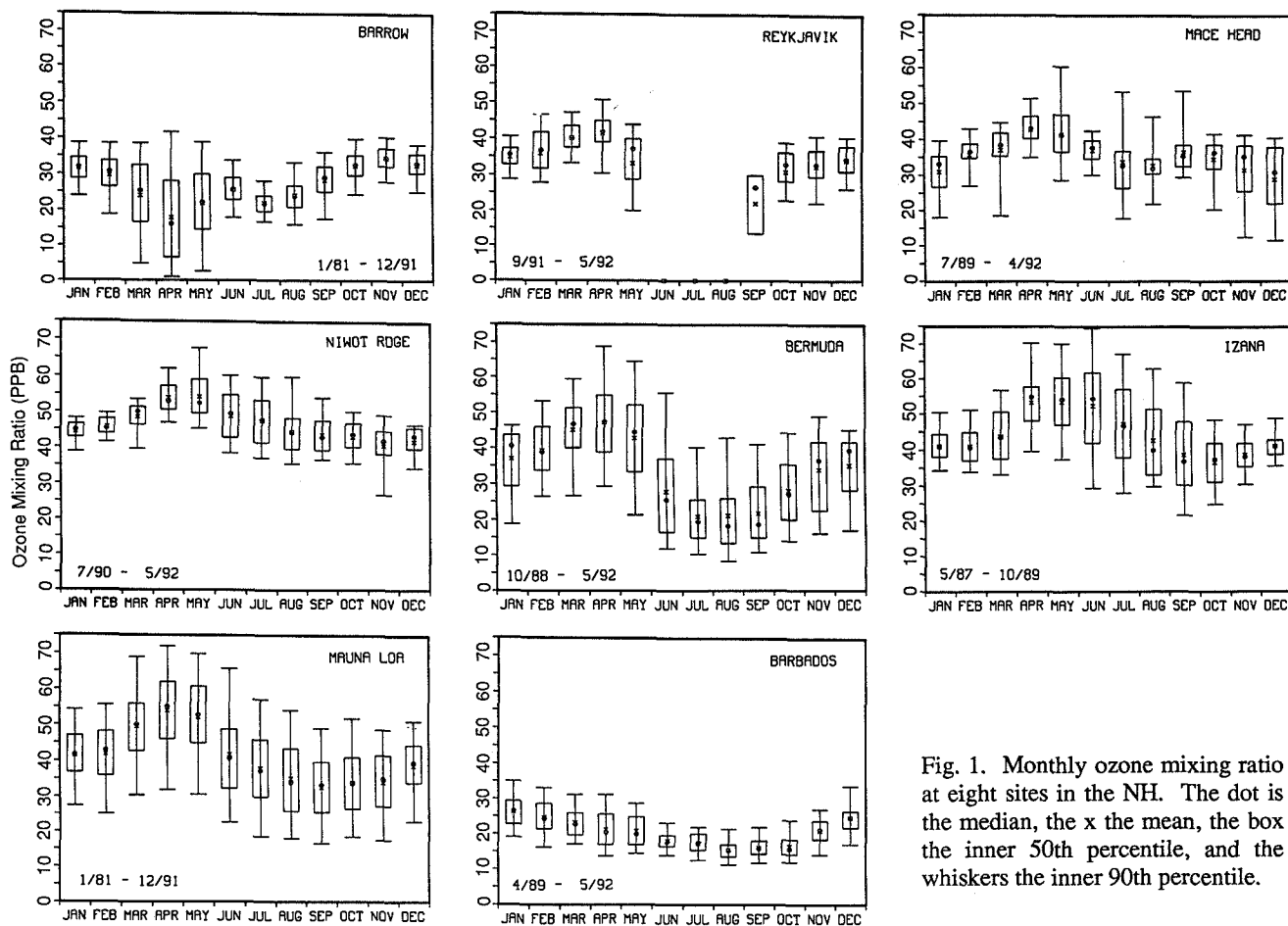


Fig. 1. Monthly ozone mixing ratio at eight sites in the NH. The dot is the median, the x the mean, the box the inner 50th percentile, and the whiskers the inner 90th percentile.

indicating much of the loss may result from ozone destruction in the boundary layer (Oltmans and Levy, 1992).

At Izana, unlike Mauna Loa, the spring maximum extends well into the summer. This difference results from transport from continental Europe to Izana (Schmitt et al., 1988). Generally the more southerly sites in the NH have larger seasonal variations. This is because the subtropical sites in particular are influenced in the winter and spring by flow from more northerly latitudes while during the summer are under the influence of more tropical flow with correspondingly lower ozone (see data for Barbados).

In the SH (Figure 2) there is a clear winter maximum and summer minimum at all locations from 14°S-90°S. At Cape Grim the maximum extends into early spring. There is a relatively smooth gradient from lower to higher values going from tropical to polar latitudes. South Pole is at an altitude of ~2800 m so cannot be compared directly with the other sites which are at sea level. Comparison of sites in the SH with locations at similar latitudes and altitudes in the NH shows higher concentrations in the NH (Fishman et al., 1979; Oltmans et al., 1989).

The phasing of the seasonal cycle is also different in the two hemispheres with the exception of Samoa and Barbados where the two stations are exactly six months out

of phase with both having winter maxima and summer minima. This seems to be at least partially related to the strong photochemical ozone destruction in the boundary layer in the tropics, with the greater ozone destruction during times of greatest solar UV input.

3. DIURNAL VARIATION

In some cases the character of the diurnal variation is useful in determining to what extent the site experiences photochemical production or destruction during the day. At two of the high altitude sites (Mauna Loa and Izana) the mountain wind regime gives highest ozone amounts at night associated with downslope flow. At Mace Head and Niwot Ridge there is often a strong diurnal variation during the summer with the largest values of the year seen during the daylight hours. Such events are typical of conditions with ozone production from anthropogenic precursor emissions. At Barbados and Samoa, on the other hand, there is a very regular diurnal variation at all times of the year with a maximum early in the morning and minimum in the afternoon. This is consistent with a low nitrogen oxides regime in which ozone is destroyed during the day (Oltmans, 1981; Oltmans and Levy, 1992). At Bermuda the pattern

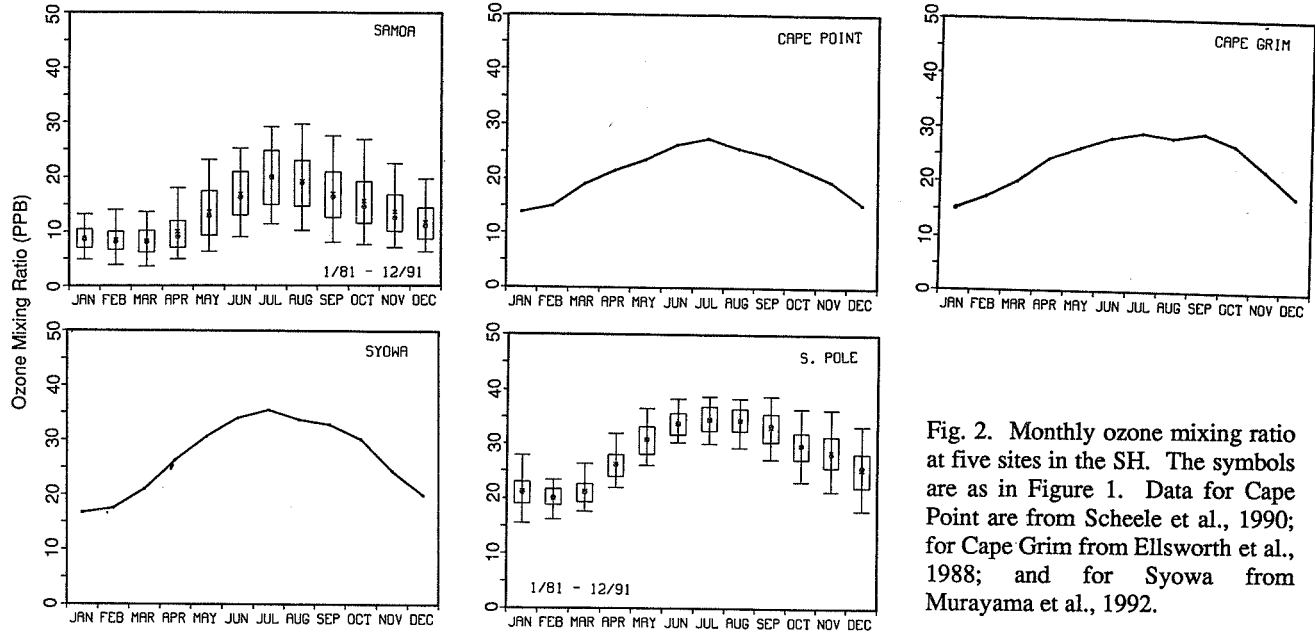


Fig. 2. Monthly ozone mixing ratio at five sites in the SH. The symbols are as in Figure 1. Data for Cape Point are from Scheele et al., 1990; for Cape Grim from Ellsworth et al., 1988; and for Syowa from Murayama et al., 1992.

appears to be similar but the much larger day-to-day variability makes the result less definitive. At Barrow and South Pole there is no discernable diurnal variation.

4. LONG-TERM VARIATIONS

At Barrow (Figure 3a) there has been a significant overall increase in surface ozone that has been driven primarily by the large ($1.73 \pm 0.58\%/yr$) summer (JUL-AUG-SEP) increases. By contrast there has been little change during the winter. Smaller, statistically non-significant increases are seen in spring and autumn (Table 2). The observed increases are consistent with the increase in petroleum extraction activities on Alaska's North Slope (Jaffe, 1991).

At Mauna Loa (Figure 3b) there has been a small but marginally significant increase over the nearly 20 years of measurement. No individual season shows a statistically significant increase but during the half-year from DEC-MAY the increase is $0.58 \pm 78\%/yr$. In recent years (beginning in 1984) the overall increase has been small ($0.10 \pm 0.71\%/yr$) but the spring increase has continued ($1.15 \pm 2.42\%/yr$) though over this short period the increase is not statistically

significant. The Mauna Loa trend prior to 1984 was influenced strongly by the anomalously high winter and spring values during the 1982-83 ENSO event but the 20-year trend computed when omitting this period is little affected except to decrease the variance. Since spring is the seasonal maximum, the increases may be linked to processes responsible for this peak.

There is no overall long-term trend at Samoa (Figure 3c). The summer decrease is fairly large ($-0.82 \pm 1.36\%/yr$) but not statistically significant. The smoothed monthly anomalies at Samoa (Figure 3d) show a nearly 2-year fluctuation with a peak-to-peak amplitude of ~ 2 ppb which is about 15% of the mean value and about 15% of the average seasonal variation. The maximum in surface ozone follows the maximum in the stratospheric east wind component (largest negative zonal wind) at 30 mb over Singapore by approximately 6 months. For the six QBO cycles covered, this relationship fails only during 1982-83 when the maximum in surface ozone is delayed about 6 months. This may be related to the effect of the very strong warm event of the ENSO that occurred during this time.

South Pole surface ozone amounts have declined significantly during the 16 years of observations. The drop

Table 2: Trends in deseasonalized surface ozone mixing ratio in percent per year. Ninety-five percent confidence interval is based on Student's t-test.

Station	Period	Annual	Winter	Spring	Summer	Autumn
Barrow	3/73-2/92	0.67 ± 0.30	-0.07 ± 0.81	0.85 ± 1.26	1.73 ± 0.58	0.50 ± 0.61
Mauna Loa	10/73-3/92	0.37 ± 0.26	0.56 ± 0.67	0.49 ± 0.98	0.28 ± 0.88	0.04 ± 0.63
Samoa	1/76-12/91	0.03 ± 0.44	0.22 ± 0.86	0.00 ± 0.94	-0.82 ± 1.36	0.22 ± 1.35
So. Pole	1/75-2/92	-0.68 ± 0.23	-0.22 ± 0.56	-0.66 ± 1.03	-1.42 ± 0.72	-0.66 ± 0.73

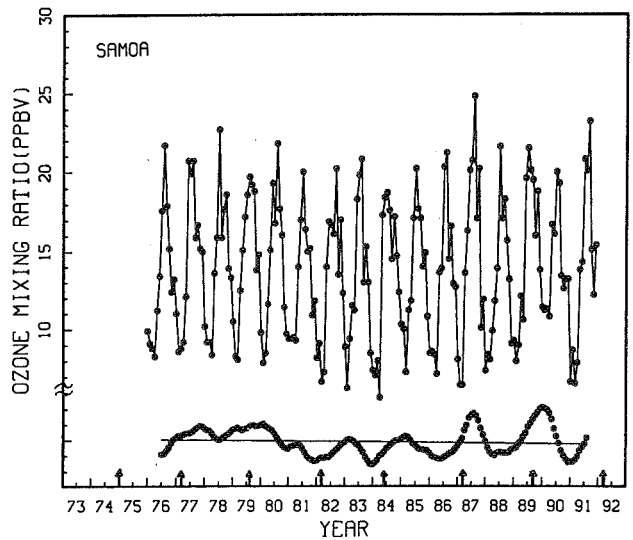
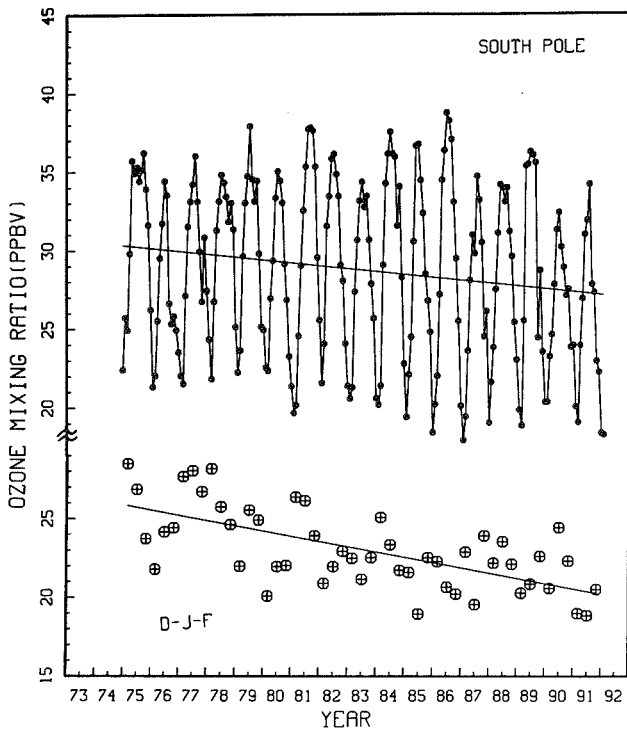
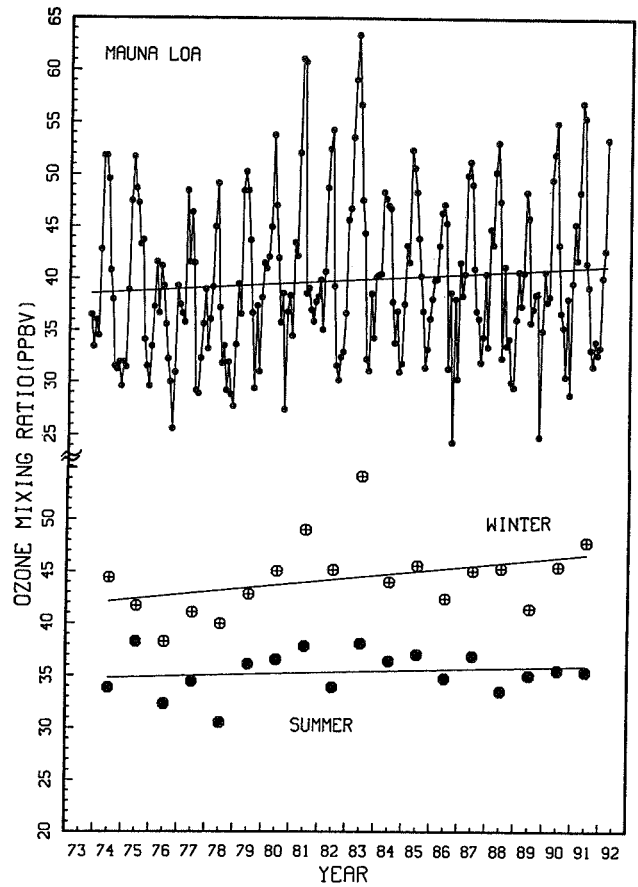
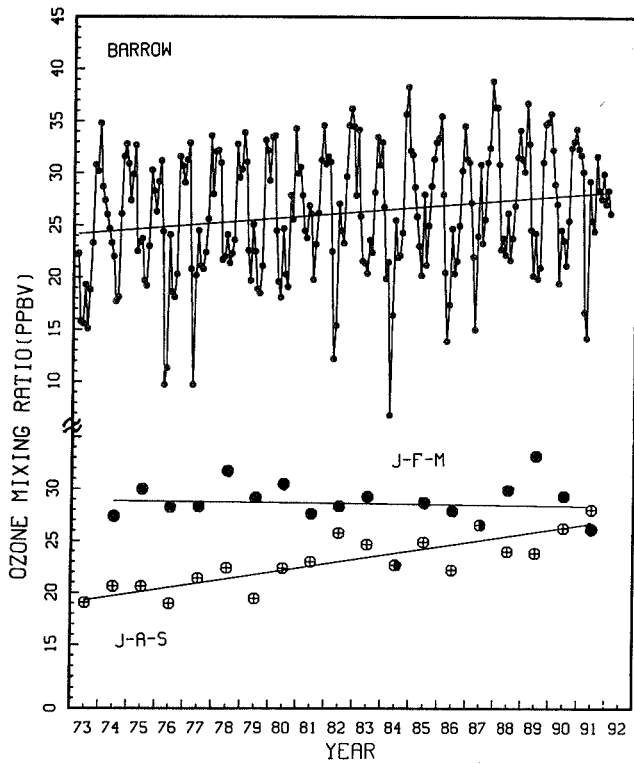


Figure 3. Monthly surface ozone mixing ratios with linear least squares trend derived from monthly anomalies. For Barrow, Mauna Loa, and South Pole various seasonal values and trends are shown. For Samoa the smoothed monthly anomalies are shown with the time of the Singapore 30 mb east wind maximum marked with an arrow.

has been very significant during the summer (Figure 3d, Table 2) with each of the months (DEC-JAN-FEB) showing significant declines (-1.44, -1.45, -1.32%/yr). This represents a nearly 25% decrease for this season over the measurement period. Two processes seem to be at work producing this decline (Schnell et al., 1991). The decline in stratospheric ozone in the spring which persists well into the summer allows for greater penetration of UV to the surface leading to enhanced surface ozone loss for the very low NO_x(NO+NO₂) conditions prevailing in this region. Secondly, enhanced transport from the coast of Antarctica increases the number of events of lower ozone that reach South Pole (Schnell et al., 1991).

The trend results from this network can be compared with some of the long-term results reported from Europe (Low et al., 1992). In particular the results from the high altitude site at the Zugspitze can be compared with those at Mauna Loa. The increase is much larger over Europe, and at both sites there has been some moderation of the rise after about 1983.

5. CONCLUSIONS

All of the surface ozone records presented here show strong seasonal variations. In the NH, for a variety of locations, spring maxima and autumn minima prevail. The largest seasonal variation is in the subtropics. In the SH there is a consistent winter maximum and summer minimum at all latitudes. Surface ozone mixing ratios in the NH are consistently higher than for the corresponding latitude in the SH.

At tropical latitudes of both hemispheres there is a regular diurnal variation with highest amounts early in the morning and minima in the afternoon. This is consistent with a low NO_x regime and ozone photochemical loss during daylight hours.

In the polar regions, there have been large summer increases at Barrow while at South Pole summer ozone amounts have declined by nearly 25% over the 17-year measurement period. A smaller but significant increase at Mauna Loa, a location generally representative of lower free tropospheric air in the region, has occurred primarily in the spring during the time of the annual maximum. At Samoa there is a small but detectable quasi-biennial variation which is closely related to the stratospheric wind QBO.

REFERENCES

- Barrie, L.A., J.W. Bottenheim, R.C. Schnell, P.J. Crutzen, and R.A. Rasmussen, 1988: Ozone destruction and photochemical reactions at polar sunrise in the low arctic atmosphere. *Nature*, **334**, 138-41.
- Ellsworth, C.M., I.E. Galbally, and R. Paterson, 1988: Ozone in near surface air in *Baseline 86*, B.W. Forgan and P.J. Fraser (eds.), Bureau of Meteorology, Melbourne, 60.
- Fishman, J., S. Solomon, and P.J. Crutzen, 1979: Observational and theoretical evidence in support of a significant in-situ photochemical source of tropospheric ozone. *Tellus*, **31**, 432-446.
- Jaffe, D.A., 1991: Local sources of pollution in the Arctic: From Prudhoe Bay to the Taz Peninsula in *Pollution of the Arctic Atmosphere*, W.T. Sturges (ed.), Elsevier, New York, 255-287.
- Low, P.S., P.M. Kelly, and T.D. Davies, 1992. Variations in surface ozone trends over Europe. *Geophys. Res. Lett.*, **19**, 1117-1120.
- Murayama, S., T. Nakazawa, M. Tanaka, S. Aoki, and S. Kawaguchi, 1992: Aircraft measurements of tropospheric ozone concentration over the Antarctic region. *Atmos. Environ.* (submitted).
- Oltmans, S.J., 1981. Surface ozone measurements in clean air. *J. Geophys. Res.*, **86**, 1174-1180.
- Oltmans, S.J., 1991: Arctic ozone chemistry in *Pollution of the Arctic Atmosphere*, W.T. Sturges (ed.), Elsevier, New York, 185-215.
- Oltmans, S.J. and H. Levy II, 1992: Seasonal cycle of surface ozone over the western North Atlantic. *Nature*, (in press).
- Oltmans, S.J., W.D. Komhyr, P.R. Franchois, and W.A. Matthews, 1989: Tropospheric ozone: Variations from surface and ECC ozonesonde observations in *Ozone in the Atmosphere*, Proceedings of the Quadrennial Ozone Symposium 1988 and Tropospheric Ozone Workshop, R.D. Bojkov and P. Fabian (eds.), A. Deepak, Hampton, VA, 539-543.
- Scheel, H.E., E.-G. Brunke, and W. Seiler, 1990: Trace gas measurements at the monitoring station Cape Point, South Africa, between 1978 and 1988. *J. Atmos. Chem.*, **II**, 197-210.
- Schmitt, R., B. Schreiber, and I. Levin, 1988: Effects of long range transport on atmospheric trace constituents at the Baseline Station Tenerife (Canary Islands). *J. Atmos. Chem.*, **1**, 335-351.
- Schnell, R.C., S.C. Liu, S.J. Oltmans, R.S. Stone, D.J. Hofmann, E.G. Dutton, T. Deshler, W.T. Sturges, J.W. Harder, S.D. Sewell, M. Trainer, and J.M. Harris, 1991. Decrease of summer tropospheric ozone concentrations in Antarctica. *Nature*, **351**, 726-729.

303/52

BROAD FEATURES OF SURFACE OZONE VARIATIONS OVER INDIAN REGION

R.R. Shende, K. Jayaraman, C.R. Sreedharan and V.S. Tiwari
Instruments Division, India Meteorological Department, Pune, India

ABSTRACT

Surface ozone concentration at three Indian stations - New Delhi (28.6°N), Pune (18.5°N) and Thiruvananthapuram (formerly Trivandrum) (8.3°N) - has been measured since 1973 with the help of an electrochemical continuous ozone recorder. These stations show diurnal, seasonal and annual cycles in surface ozone. Daily changes show that the minimum value occurs at sunrise and maximum in the afternoon. As regards seasonal variations, Thiruvananthapuram and Pune have a minimum value during monsoon season (June to August) while at New Delhi the minimum value occurs in January. However, New Delhi also records low ozone amount during monsoon season identical to the amounts shown at Thiruvananthapuram and Pune. The annual cycles at these stations have been compared with similar measurements in the northern and southern hemispheres. The Indian measurements agree well with the annual cycles at these stations. Further, the analysis of the Indian data indicates that the major contribution in surface ozone comes from the natural sources like stratospheric-tropospheric exchange, turbulence and mixing in the boundary layer; however, a small contribution from anthropogenic sources cannot be ruled out at Pune and probably at New Delhi, especially in winter and summer seasons.

1. INTRODUCTION

The importance of ozone measurement near the ground and in the troposphere has been realised in last two decades. Ozone is one of the most important trace species in the troposphere, which can directly affect climate through the absorption of infra-red radiation (Fishman et al., 1979). Increasing concentration of tropospheric ozone has been reported, especially in the northern hemisphere, in recent times (Logan (1985), Angell et al. (1983), Oltmans and Komhyr (1986), Bojkov (1986), Penkett (1988)). Ozone as a greenhouse gas is influencing the outgoing radiation budget and as a consequence the climate. There is much discussion on the relative contributions to the surface ozone concentration, from the stratosphere due to natural processes and from the troposphere due to human activities (Levi et al., 1985).

Surface ozone measurements have been made and examined by various workers, Oltmans and Komhyr (1986) at four land-based stations of Barrow, Alaska (71°N); Mauna Loa, Hawaii (19.5°N); American Samoa (14°S) and the South Pole (90°S), Low P.S. (1990) at Hohenpeissenberg and Arkona in Germany and Galbally et al. (1980) in Australia. Measurements of surface ozone concentration over ocean have been reported by Routhier et al. (1980), Liu et al. (1983) and Piotrowicz (1986).

Surface ozone measurements using an electrochemical continuous ozone sensor (Sreedharan and Tiwari, 1971) were started at Pune (18.5°N, 73.8°E) in 1970 and the diurnal, seasonal and short-term variations have been described on the basis of records obtained during 1972-73 (Tiwari and Sreedharan, 1973). Since 1973, the measurements were extended to two more stations namely, New Delhi (28.6°N, 77.2°E) and Thiruvananthapuram (8.3°N, 76.6°E). Hourly data at these stations have been computed from the continuous records of 1973, 1974 and 1975 and again for 1983, 1984 and 1985. Broad features of the surface ozone concentration as related to seasonal (winter, summer, monsoon and post-monsoon), diurnal, latitudinal and time-scale changes over the Indian region are described and the possible causes of these variations discussed in the present paper. The contribution of tropospheric production, if any, has also been examined from the above data.

2. VARIATION IN SURFACE OZONE CONCENTRATION OVER INDIAN REGION

Tropospheric ozone absorbs the outgoing longwave radiation from the earth, thereby contributing to the greenhouse effect. Till sixties, the tropospheric concentration of ozone was very low and its contribution to greenhouse warming was thought to be insignificant. It was also generally accepted until sixties that the main source of tropospheric ozone is from the middle and the upper stratosphere where it is produced by the photochemical reaction of ultraviolet radiation with the oxygen molecules. From the stratosphere, this heavier gas trickles down through the tropopause by various mixing processes associated with cyclonic circulations, jet streams and through tropopause breaks. Junge

(1962) showed that the rate of production of ozone in the stratosphere and its rate of destruction near the ground are same, thereby supporting that the stratosphere is the main source of tropospheric (surface) ozone.

In recent years, increasing trends in surface ozone concentrations have been reported at Hohenpeissenberg (47.8°N) and Arkona (54.7°N) by Low P.S. (1990). Bojkov (1988) and Penkett (1988) have also reported that over most of the northern hemisphere surface ozone concentrations have increased. This increase in surface ozone is attributed to increasing anthropogenic sources. Over Indian subcontinent, the daily and seasonal variations in surface ozone indicate a good correlation with changes in wind speed, surface temperature and overall mixing conditions in the boundary layer. However, some contribution by man-made sources cannot be ruled out especially after 1980.

2.1 Seasonal changes at the Indian stations

Before describing the seasonal behaviour at Thiruvananthapuram, Pune and New Delhi, it would be appropriate to describe the topography and surroundings of these stations. New Delhi is a densely populated city in the plains of northern India and is affected by extreme summer and winter climates. Pune is situated on the Deccan Plateau on the eastern side of Western Ghats, at a height of about 600 m (asl) with moderate climate changes throughout the year. The city is relatively clean, but Bombay - a highly industrialised and populated city - is located about 200 km away in West-North-West direction. The industrial belt at Pune extends in N-NE sector about 5 km away from the observational site. Thiruvananthapuram is a tropical coastal station with natural green surroundings with less population and few industries. This can be treated as a background unpolluted station. Fig. 1 shows the geographical locations of the three stations in the Indian subcontinent.

Fig. 2 shows the hourly variations of surface ozone at New Delhi, Pune and Thiruvananthapuram for the four seasons - summer

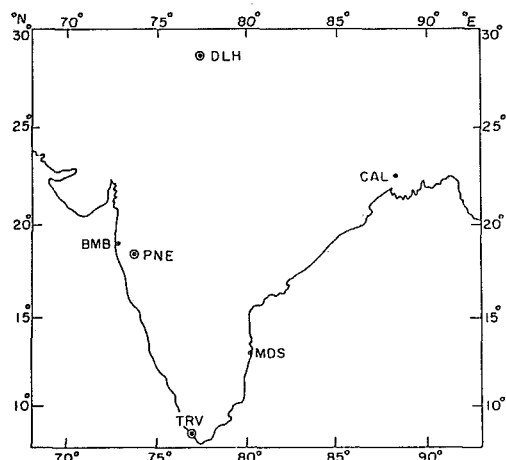


FIG.1 - GEOGRAPHICAL LOCATION OF OBSERVING STATIONS

(March-May), monsoon (June-August), post-monsoon (September-November) and winter (December-February). The hourly values have been averaged for each month and the mean hourly values for the four seasons computed from three years' data (1983, 1984 and 1985) have been plotted. The graphs for all the three stations clearly bring out that a minimum concentration of surface ozone is attained in the morning around 0700 (LST) coinciding with sunrise and a maximum is attained in the afternoon between 1400 and 1600 (LST). The occurrence of daily minimum and maximum ozone amount coincides with the lowest and the highest convection and turbulent mixing in the boundary layer respectively. Lowest values at Pune and Thiruvananthapuram are of the order of 5 to 8 ppbv, while night time value at New Delhi is lower compared to Pune and Thiruvananthapuram with minimum value up to 5 ppbv.

2.1.1 Hourly variation during summer season

Mean hourly changes in surface ozone during summer season are shown in Fig. 2a. Night time values are uniformly low at New Delhi and are varying between 5 and 7 ppbv. Thiruvananthapuram night time values are also low, about 10 ppbv, while Pune shows higher ozone concentration, of the order of 15 ppbv or more, during night hours. Day time values are the highest at Pune (30-34 ppbv) followed by New Delhi (25-29 ppbv) and the lowest value is observed at Thiruvananthapuram (20-22 ppbv). Further, the gradient of forenoon rise is the highest at Pune followed by New Delhi and is the lowest at Thiruvananthapuram. Pune and New Delhi forenoon records indicate that a cool and stable layer is formed near the ground preventing the free mixing across it. Pune record has one peculiarity that maximum value is observed around 1800 h. in the evening. The wind speed record also indicates an increase in the evening hours associated with ozone maxima. This maximum value around 1800 h. can be due to subsidence of tropospheric air on account of sudden cooling or due to air blowing from a highly polluted area and hence having high value of ozone concentration.

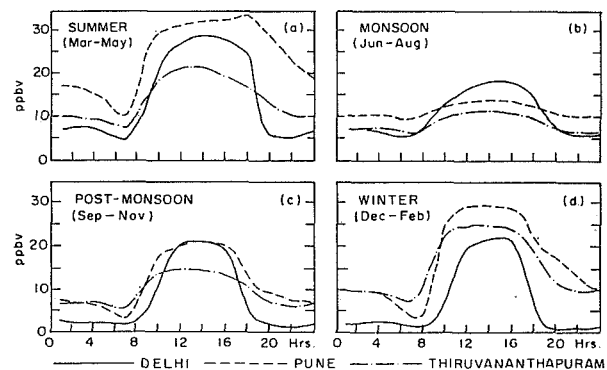
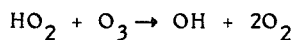
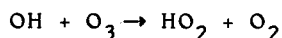
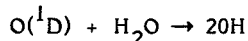
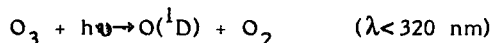


FIG.2 - HOURLY VARIATION IN SURFACE OZONE OVER INDIAN REGION DURING DIFFERENT SEASON (1983-1985)

2.1.2 Hourly changes during monsoon season

Ozone concentration during monsoon season (June-August) depicts low ozone value with decreased diurnal changes (Fig. 2b). The lowest value in the morning at all the three stations is between 5 and 10 ppbv but the highest value in the afternoon shows higher value with increasing latitude. During monsoon season, the air circulation over the Indian subcontinent is prevailing south-westerly flow from Arabian Sea and is redirected from SE direction in the Bay of Bengal along monsoon trough. The tropospheric airmass over the entire country is the monsoonal flow from low latitudes and partly from the southern hemisphere. The low concentration of ozone may be due to destruction by H₂O molecules which are available in abundance during this season by following reactions (Fishman et al. (1977), Logan et al. (1981):



The low ozone concentration may also be due to the effect of air from the southern hemisphere tropics, which is poor in ozone (Winkler P., 1989).

2.1.3 Hourly changes during post-monsoon season

After the monsoon season, diurnal changes have started increasing (Fig. 2c). All the three stations show higher difference between night and day values; night time values have decreased and the day time values increased. Night value is the lowest at New Delhi followed by Thiruvananthapuram and is the highest at Pune. Day time values are the lowest at Thiruvananthapuram while the concentrations at New Delhi and Pune are almost equal (however, day mean value is higher at Pune).

2.1.4 Hourly changes during winter season

Hourly changes in surface ozone during winter season (December-February) are shown in Fig. 2d. New Delhi shows near zero value (about 2 ppbv) throughout the night; so also the day time value is low, about 22 ppbv, followed by Thiruvananthapuram, while both day and night ozone amounts are the highest at Pune.

Day and night low values at New Delhi can be expected from the fact that during winter season it experiences extreme cold climate and the maximum temperature during winter is nearly equal to the minimum temperature obtained at the other two stations, Pune and Thiruvananthapuram. The difference between day's maximum and minimum ozone amounts is the highest at Pune (about 25 ppbv). The trend of decreasing

ozone concentration in the evening hours at Pune is not as sharp as at Thiruvananthapuram and New Delhi, indicating thereby that the replenishment of ozone near the ground continues at a faster rate during evening and early part of the night at Pune compared to New Delhi and Thiruvananthapuram. This appears to be due to its location on a plateau 600 m high and its nearness to the top of the boundary layer. Only in early hours between 0600 and 0800 it shows that the supply from the free troposphere is cut off on account of formation of cool and stable layer and during that time ozone values at Pune, New Delhi and Thiruvananthapuram are identical. This behaviour in ozone changes at Pune is further confirmed from the record of summer season (Fig. 2a). The trend in ozone changes at Pune during winter and summer seasons, especially the slow fall in the evening and early part of night, calls for a subsidence motion or transport of ozone rich air from polluted atmosphere.

To summarise the seasonal changes, the three years' (1983-1985) mean data has been examined pertaining to seasonal mean value (Fig. 3a), day time value (0800 to 1900 h.) (Fig. 3b), night time value (2000 to 0700 h.) (Fig. 3c) and the difference between day and night values (diurnal change) (Fig. 3d). These values are plotted corresponding to the respective latitudes of the three stations.

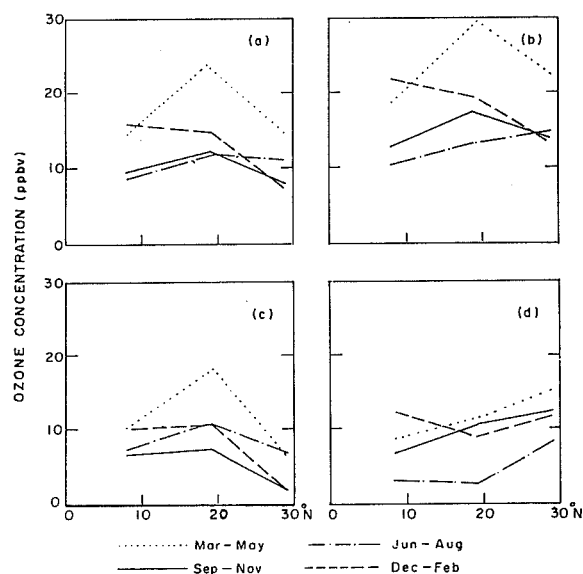


FIG. 3 - LATITUDINAL VARIATION OF SURFACE OZONE DURING FOUR SEASONS (1983-1985 Mean) (a) Seasonal mean, (b) Day time value, (c) Night time value, (d) Diurnal change.

The seasonal mean (Fig. 3a) shows that during monsoon months there exists a latitudinal gradient between Thiruvananthapuram and Pune (from 8° to 18°N); thereafter the value is same up to 28°N (New Delhi). During winter, there appears to be a reversal of surface ozone

gradient from 30°N to 8°N, i.e. the daily mean surface ozone decreases as latitude increases. During post-monsoon and summer seasons, Thiruvananthapuram and New Delhi show identical trends but Pune shows a higher concentration, the mean value during post-monsoon being lower than summer at all the three stations. Further, the absolute value of surface ozone at Thiruvananthapuram and New Delhi varies between 8 and 15 ppbv while at Pune the variation is from 12 to 24 ppbv.

The average concentration during day (mean of hourly values between 0800 and 1900 h.) shows a linear latitudinal gradient during monsoon season and a reversed latitudinal gradient during winter, while during rest of the seasons Pune has the highest value, Thiruvananthapuram and New Delhi have nearly same value in post-monsoon, but a slight higher value is seen at New Delhi during summer. Day values at New Delhi range between 12 and 22 ppbv, at Thiruvananthapuram from 10 to 19 ppbv and at Pune from 17 to 30 ppbv (Fig. 3b).

Night values (mean of 2000 to 0700 h.) show a reversal of latitudinal gradient between Thiruvananthapuram and New Delhi with exception of higher value at Pune during all seasons. The night values range between 6 and 10 ppbv at Thiruvananthapuram, between 2 and 7 ppbv at New Delhi and at Pune between 7 and 27 ppbv (Fig. 3c).

The difference between day and night values is shown as diurnal change in Fig. 3d. This depicts that the day minus night value at Thiruvananthapuram and Pune is same during monsoon, but higher at New Delhi. During winter, diurnal change is the highest at Thiruvananthapuram and the lowest at Pune. In post-monsoon and summer, the day-night difference increases with latitude. In this case, the range of variation is from 2 to 15 ppbv.

3. ANNUAL CYCLE OF SURFACE OZONE OVER INDIA

Mean monthly ozone values for the three stations are plotted in Fig. 4a. It is seen from the figure that the annual maximum at New Delhi is attained in May-June and minimum value in January. From August to December the surface ozone amount is very low and steady, around 8-9 ppbv, with slight increase in October. From January the mean surface ozone value starts increasing from 6 ppbv attaining the highest value, about 19-20 ppbv, in May. From July, the surface ozone amount starts decreasing approaching a near minimum value in August.

The annual cycle at Pune shows a minimum value in July, August and September, the value being about 9 ppbv, from September the concentration starts increasing gradually up to December followed by a sharp increase from January reaching the maximum value in April

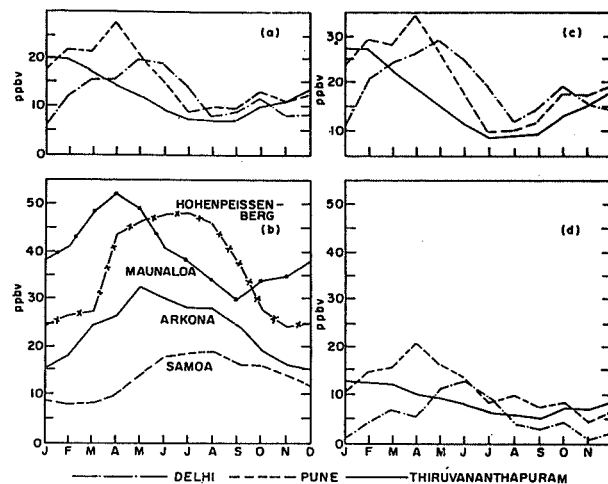


FIG. 4 - ANNUAL VARIATION IN SURFACE OZONE (1983-1985 Mean)
(a) INDIAN STATION, (b) SOME OTHER STATION FOR COMPARISON.
(c) DAY TIME AND (d) NIGHT TIME OZONE AMOUNT.

(25-26 ppbv). Again from April to July, there is almost a linear decrease. Similar to record of Delhi, Pune also shows a small increase in October.

The record of annual cycle at Thiruvananthapuram shows a smooth variation with maximum amount (19-20 ppbv) in January-February and a minimum (7-8 ppbv) in July-August-September. One noteworthy feature, as evident from the annual cycle at the three stations, is that during monsoon months July, August and September, the concentrations at all three stations are nearly equal and very low. The highest value at Thiruvananthapuram is attained in January-February, at Pune in March-April and at New Delhi in May-June. Thus the highest value in ozone occurs during dry months when the day's temperature is also maximum.

The low ozone amount during monsoon season points towards the ozone destruction by water vapour molecules and also towards a uniform mixed tropospheric air over the Indian subcontinent. The sharp increase beginning from January gives credence to stratospheric-tropospheric exchange through the discontinuity between the subtropical and tropical tropopause breaks and across the winter jet stream (sub-tropical jet stream) located at 300 hPa level. The increasing day temperatures also indicate more vertical mixing through deeper tropospheric layers. Thus the changes in surface ozone over Indian region are broadly explained by stratospheric-tropospheric exchange and change in mixing conditions in the boundary layer.

3.1 Comparison with annual variation at other stations

In Fig. 4b, annual cycles in surface ozone measured at Hohenpiessenberg (47.8°N, 11°E), Arkona (54.7°N, 13.4°E), Mauna Loa (19.5°N, 155.4°E) and Samoa (14°S, 170.3°E) have been shown. Concentration at Mauna Loa shows the maximum value (about 52 ppbv) during April and a minimum value (30 ppbv) in September. The gradient of increasing and decreasing trend from September to April and from April to September respectively is almost linear. The Mauna Loa observatory is located at an altitude of 3400 m. asl, above the trade wind inversion, and is more representative of the clean and free tropospheric ozone concentration. The highest and the lowest values can be taken to be representative of natural annual variations in tropospheric ozone. Mauna Loa record is very well compared with the records of Indian stations. The period of occurrence of maximum ozone at Mauna Loa and Pune (located in nearly same latitudinal belt) is in April, so also the absolute value at Pune is half of that observed at Mauna Loa. The range of annual cycle at New Delhi and Thiruvananthapuram is also well within the natural accountable limits as seen from Mauna Loa annual cycle.

The annual cycle of surface ozone at Arkona (Germany), a WMO Background Air Pollution Monitoring Network (BaPMON) station located on a bluff (42 m. asl), shows maximum value (32 ppbv) in May and minimum value (15 ppbv) in December. Comparing the annual variation over Indian stations, the values measured at New Delhi, Pune and Thiruvananthapuram are well below the ozone concentration recorded at Arkona.

Samoa, a coastal island station located in southern hemisphere tropics (14°S) near the sea level, shows that the maximum surface ozone (19 ppbv) occurs during July-August while minimum value (8 ppbv) is attained in February-March. From marine boundary layer ozone measurements from 32 ship cruises in the Atlantic Ocean between 80°N and 80°S, Winkler (1988) reported a northern hemisphere ozone concentration maximum of 30 ppbv between 25°N and 65°N. He also found a small maximum in the southern hemisphere of about 17 ppbv and a small minimum at the equator of about 14 ppbv. The low ozone amount at Samoa fits well with the above measurement in the SH tropics.

The record at Hohenpiessenberg shows very high value of surface ozone from March to November, the amount ranges between 25 and 48 ppbv and is certainly not accountable by natural processes but only by photochemical production in the troposphere.

3.2 Mean annual variation during day versus night time ozone amount

The mean monthly value for the day time (0800 to 1900 h.) and night time value (2000 to 0700 h.) have been plotted in Figs. 4c and 4d.

Day time values at New Delhi, Pune and Thiruvananthapuram show that the maximum value at Thiruvananthapuram is attained during January-February (about 26-27 ppbv) and the minimum occurs during July-September (9-10 ppbv). At New Delhi maximum value (about 29 ppbv) occurs during May and minimum (around 11 ppbv) in January. At Pune day time value shows the highest concentration (34 ppbv) in April while minimum occurs during July-August (about 10 ppbv). The annual cycle of day time ozone concentration (Fig. 4c) shows identical behaviour as depicted by monthly mean (day and night including) at the respective stations indicating that the major contribution towards daily mean comes from day time concentration.

Night time monthly variation at Thiruvananthapuram is similar to day time changes with maximum and minimum values of 12 ppbv and 5 ppbv respectively (Fig. 4d). At New Delhi, the minimum value (about 1 ppbv) occurs during November and January while maximum concentration during night (about 12 ppbv) occurs in June. At Pune minimum (about 4 ppbv) occurs in November while maximum occurs in April (about 20 ppbv). Night time changes in surface ozone show that the maximum value during night takes place in those months when the annual cycle also shows the highest value. But the night time minimum at New Delhi and Pune occurs in those months when the layers near the ground are cool and calm (probably associated with a temperature inversion) and they do not coincide with minimum of annual ozone cycle. But at Thiruvananthapuram maxima and minima in day and night time occur in same month and also coincide with the occurrence of the highest and the lowest values in annual cycle. This supports the view that near the equator the effect of stable surface layers is least or, in other words, the formation of stable and stratified layers near the ground is very rare in equatorial latitude.

3.3 Ozone amount in the free troposphere above the boundary layer

In order to have a rough estimate of ozone amounts in the free troposphere over Indian region, the day's maximum value (representative of free tropospheric ozone) and minimum value (representative of destruction near ground) has been plotted in Fig. 5 for the three Indian stations during 1983. Here again the near equatorial coastal station Thiruvananthapuram shows that the highest and the lowest ozone amount curves are almost parallel to mean. The minimum ozone shows the lowest value in July-August but this also is about 1.5 to 2 ppbv, while the highest value in the afternoon is obtained in the month of April, about 28 ppbv.

The envelopes of maximum and minimum ozone amount at Pune show one peak during February to April and another in November, the

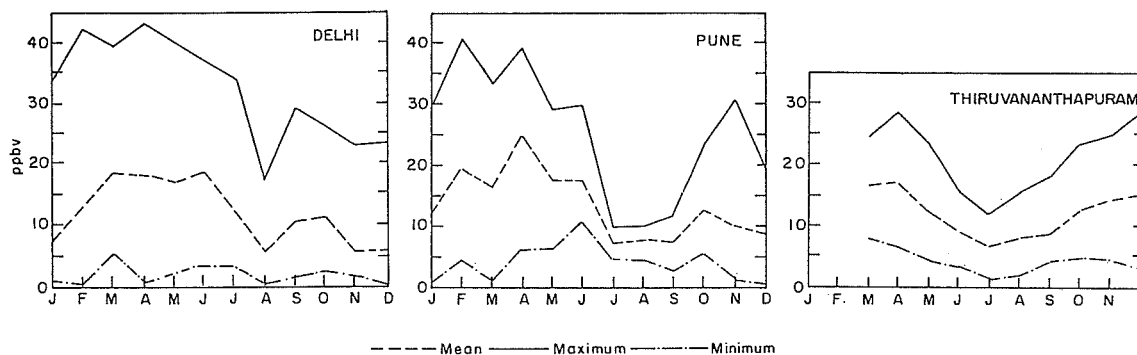


FIG. 5-- RANGE OF MEAN, MAXIMUM AND MINIMUM SURFACE OZONE AMOUNT DURING 1983.

values being of the order of 35 to 40 ppbv and 30 ppbv respectively. The profile of minimum ozone shows near zero value in December-January and higher night values from March to October with peak in June, about 10 ppbv.

The record at New Delhi shows that the free tropospheric ozone peak occurs from February to May, the value being about 40 ppbv accompanied by a sharp fall in August. But the decrease from April to November is linear except for August (low concentration during monsoon). The ozone profile of New Delhi indicates much better response to the injection of ozone rich stratospheric air into the troposphere during February to May months, due to its proximity near subtropical jet stream and tropopause break between the tropics and subtropics. In fact, New Delhi experiences double tropopause during winter season and the behaviour of ozone changes coincides roughly with the occurrence of maxima and minima in surface ozone in mid latitudes, e.g. Arkona. The profile of minimum ozone at New Delhi shows near zero night value from December to February and low value about 2 to 4 ppbv in other months.

The comparison of records at New Delhi, Pune and Thiruvananthapuram shows that both day and night values are higher at Pune. Though the Mauna Loa ozone amounts, representative of free tropospheric values in tropics, are still higher, but the sharp increase in ozone amount at Pune during April (seen in mean annual cycle - Fig. 4a) points to some tropospheric source. This point will be discussed further in next section.

4. TREND IN SURFACE OZONE VARIATION

From the hourly records of surface ozone, mean concentration for each month has been worked out at Thiruvananthapuram, Pune and New

Delhi for the years 1973, 1974 and 1975 and again for the years 1983, 1984 and 1985. These monthly mean values are plotted in Fig. 6. The period with no data has been shown by dotted curve in the figure.

It is seen from the figure that there are year to year variations at all the three stations, especially during 1984 when all the three stations recorded higher ozone concentration. Thiruvananthapuram and New Delhi also showed sharp fluctuations from month to month during 1974.

Year to year variations at Thiruvananthapuram from 1973 to 1985 indicate that both the lowest and the highest values during every year remained fairly stable. Thiruvananthapuram is a coastal station with lush green surroundings and devoid of heavy industries. Surface ozone record for the period gives an additional support that tropospheric ozone has not increased during these years. The highest value was around 17 ppbv and the lowest around 5-6 ppbv. New Delhi records show that annual maximum had remained steady at about 15 ppbv and the minimum 4-5 ppbv from 1973 to 1975. But from 1983 to 1985, the ozone amount shows a marginal increase in both minima and maxima values. The records at Pune also show that during 1973-74 maximum and minimum values were stable at 20 ppbv and 8 ppbv respectively. However, a slight increase in maximum value during 1975 is indicated though minimum value remained nearly same. The record from 1983 to 1985 does clearly bring out a gradual increase in the maxima and minima ozone amounts at New Delhi and Pune from year to year.

The increased industrialisation and human activities have resulted in increasing concentration of NO_x , CH_4 , CO and non-methane hydro-

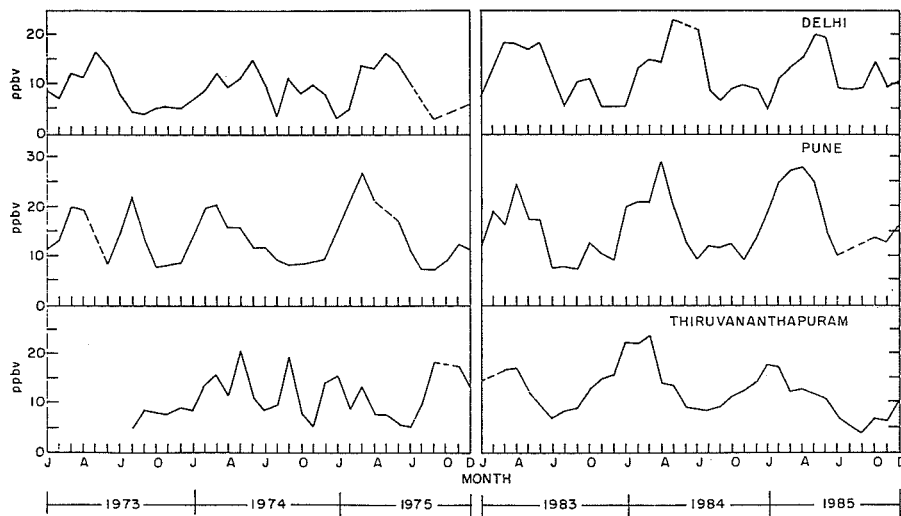


FIG. 6 - TREND IN SURFACE OZONE AT INDIAN STATIONS

carbons (NMHC). The enhanced photochemical production in an atmosphere containing abundance of these anthropogenic gases is largely responsible for the increase in surface ozone concentrations (Penkett, 1984; Logan, 1985; Bojkov, 1986; Crutzen, 1988). Over New Delhi and Pune, the combustion processes and automobile exhaust produce large amounts of NO_x and other anthropogenic gases which help in photochemical production of ozone. Therefore, the year to year increase may be associated with tropospheric production. It was generally thought that Pune, by virtue of its location on a plateau at a height of 600 m asl, is a comparatively clean city but the surface ozone records show that the ozone amounts are higher at Pune compared to New Delhi. The high concentration of ozone during winter and summer seasons at Pune and the occurrence of maximum value in the evening hours (1800 LST) and quite high concentration up to midnight during summer point to transport of ozone rich air from some polluted site. From the wind speed and wind direction records at Pune, it is observed that wind speeds are quite high from 1700 to 2000 h. and the wind is blowing predominantly from WNW direction. This probably indicates transport of polluted air from industrial areas of Bombay.

The surface ozone data pertaining to three years 1983-85 is too small to fit a regression curve and to compute a quantitative value for trend analysis. This is more difficult because over and above the normal trend there are superimposed year to year variations. But three years' data from 1983 to 1985 show a positive (increasing) trend in surface ozone amount at Pune and New Delhi.

5. DISCUSSION AND CONCLUSION

5.1 The analysis of surface ozone data at the three Indian stations do indicate a diurnal and seasonal variation. The daily hourly data show that the minimum value in surface ozone is observed between 0700 and 0800 (LST) and the maximum value between 1400 and 1600 (LST). The night values are higher at Thiruvananthapuram but the day night difference is the lowest.

Ozone measurements at most rural continental stations show a diurnal cycle with sunrise minima and afternoon maxima (Parrish et al., 1986; Fehsenfeld et al., 1983). The diurnal variation observed at Indian stations follows similar pattern. Johnson et al. (1990) suggest that this diurnal cycles are driven by photochemical ozone production in daylight hours with loss to surfaces dominating at night. The diurnal change at Indian stations is presumed to be mainly due to meteorological processes, i.e. the convection currents set in during day time, causing greater mixing in the tropospheric layers near the ground. The mixing layer and the turbulence extend to higher tropospheric layers in the afternoon giving rise to higher surface ozone concentration. Even the turbulence caused by changes in wind speed during night or day is very well reflected in surface ozone records (Tiwari and Sreedharan, 1973). Higher ozone concentration during night at Thiruvananthapuram (though the average ozone is low) and near zero ozone value at New Delhi during night indicate the predominant role of turbulence and mixing processes.

5.2 The seasonal variations show that during monsoon season (June-August) the average ozone concentration is low and the values at all the

stations are almost identical (between 9 and 11 ppbv). The low concentration may be due to destruction by water vapour or be the result of low ozone air from the southern hemisphere. Low values associated with less diurnal change at Thiruvananthapuram and Pune, where the monsoon activity is for longer period and more vigorous than at New Delhi, suggest that the destruction by water vapour is important.

During winter season, the ozone amount at New Delhi is the lowest and that at Thiruvananthapuram the highest. This also supports the dominance of mixing processes over photochemical production, if any. During post-monsoon and summer seasons, Pune shows a higher concentration than New Delhi and Thiruvananthapuram. The highest value at Pune during summer occurs around 1800 h. and the pattern of decrease up to midnight suggests the transport of ozone rich air from an area of anthropogenic ozone production. The seasonal mean values at New Delhi and Thiruvananthapuram are almost identical varying between 8 and 16 ppbv in different seasons while the value at Pune shows a higher concentration, especially during post-monsoon and summer; the summer value is about 25 ppbv. The higher ozone value observed during summer at Pune indicates the possibility of tropospheric production due to anthropogenic gases.

5.3 Annual cycle over India shows that the maximum value (about 20 ppbv) at Thiruvananthapuram is attained in January-February, at Pune (about 27 ppbv) in April and at New Delhi (about 20 ppbv) in May-June, while the minimum values at Thiruvananthapuram (about 8 ppbv) and at Pune (9 ppbv) occur during monsoon season (June to August) and at New Delhi in January (about 6 ppbv). Comparison of the annual cycle at Indian stations with Mauna Loa (19.5°N) shows that the time of occurrence of maximum value coincides with Pune (18°N) in April while the minimum value at Mauna Loa occurs in September, but at Pune and Thiruvananthapuram it occurs during rainy season. The occurrence of maximum and minimum ozone amounts at New Delhi agree with that of Arkona (54°N). The ozone amount at Indian stations is less than half of the value observed at Mauna Loa and is well below the value found at Arkona. The concentration at Samoa (14°S) is comparable with the value measured at Thiruvananthapuram and also at New Delhi with phase lag in the time of occurrence.

Arpe et al. (1986) computed the turbulent kinetic energy (KE) distribution with respect to height, latitude and season from a long series of atmospheric data produced by ECMWF model. They showed that KE had two maxima in the NH summer but only a single maximum during austral summer at 30°S. In the NH a spring maximum is observed in all latitudes between equator and 80°N. For latitudes between 0° and 60°N, the

peak appears during May while north of 60°N the peak shifts to June and even to July (70°N). The minimum concentration occurs during fall or winter in most latitudes. North of the Polar front (60°N) there is an indication of higher winter concentration (Winkler P., 1989).

From the foregoing discussions it appears more logical that the annual cycle in ozone variation over Indian station is due to the natural cycle of stratospheric tropospheric exchange and the change of turbulent kinetic energy in the troposphere. However, some abrupt rise in surface ozone concentration at Pune (the maximum value in April) shows the contribution of tropospheric production.

5.4 Latitudinal variation over the Indian region is not very well demonstrated. During monsoon season there appears a slight positive gradient between Thiruvananthapuram (8°N) and New Delhi (28°N) but during winter season this gradient is reversed, indicating a rather well mixed troposphere (Fig. 3a) where the variation is governed by mixing conditions in the boundary layer. Winkler (1989) has shown from the result of 32 cruises that surface ozone has a positive gradient in the NH with minimum near the equator and higher value between 30°N and 50°N and another maximum between 60°N and 70°N.

5.5 Tropospheric production

the surface ozone records at three stations over India bring out the predominant role of meteorological factors and turbulent mixing processes in the diurnal, seasonal and annual cycles. But from the comparison of year to year data from 1973 to 1975 and from 1983 to 1985, there appears to be slow increase in year to year surface ozone amounts at Pune and New Delhi. However, the record at Thiruvananthapuram does not indicate any change from 1973 to 1985. Some sharp increase in ozone amount recorded at Pune during March-April calls for additional source of production in the troposphere. The forenoon maximum is associated with a temperature inversion near the ground, trapping the gases from the automobile exhaust and factory products. With the sunrise and breaking up of inversion, a maximum in the ozone amount is observed due to in situ production of ozone. It is noted that in case of anthropogenic production, the forenoon maximum becomes the main maximum of the day and occurs near the local noon. The seasonal maxima at Pune during summer at 1800 (LST) appear to be due to transport of air from a polluted site.

REFERENCES

- Angell, J.K. and J. Korshover, 1983: Global variation in total ozone and layer mean ozone: An update through 1981. J. Climat. Appl. Meteorol., 22, 1611-1627.

- Arpe, K., C. Brancovic, E. Oriol, and P. Speth, 1986: Beitr. Phys. Atm., 59, 321-355.
- Bojkov, R.D., 1986: Surface ozone during second half of the nineteenth century. J. Climatol. Appl. Meteorol., 25, 343-352.
- Bojkov, R.D., 1988: A critical assessment of published total ozone data and the need for re-evaluation. Proc. Ozone. Symp.
- Crutzen, P.J., 1988: Tropospheric ozone, an overview in tropospheric ozone, regional and global scale interactions. NATO ASI Ser., edited by ISA Isaksen, Mass.
- Fehsenfeld, F.C. et al., 1983: A study of ozone in the Colorado mountains. J. Atmos. Chem., 1, 87-105.
- Fishman, J. and P.J. Crutzen, 1977: A numerical study of tropospheric photochemistry using a one dimensional model. J. Geophys. Res., 82, 5897-5906.
- Fishman, J., V. Ramanathan, P.J. Crutzen, and S.C. Liu, 1979: Tropospheric ozone and climate. Nature, 282, 818-820.
- Galbally, I.E., and C.R. Roy, 1980: Destruction of ozone at the earth's surface. QJRM Soc., 106, 599-620.
- Johnson, J.E. et al, 1990: Ozone in the marine boundary layer over Pacific and Indian Oceans: Latitudinal gradients and diurnal cycles. J. Geophys. Res., 95(D8), 11847-11856.
- Junge, C.E., 1962: Global ozone budget and exchange between stratosphere and troposphere. Tellus, 14, 363-377.
- Levy, H., J.D. Mahlman, and W.J. Moxim, 1985: Tropospheric ozone: The role of transport. J. Geophys. Res., 90, 3753-3772.
- Liu, S.C. et al., 1983: Tropospheric NO_x and O_3 budgets in the equatorial Pacific. J. Geophys. Res., 88, 1360-1368.
- Logan, J.E., M.J. Prather, S.C. Wofsy, and M.B. McElroy, 1981: Tropospheric chemistry: A global perspective. J. Geophys. Res., 86, 7210-7254.
- Logan, J.A., 1985: Tropospheric ozone: Seasonal behaviour, trends and anthropogenic influence. J. Geophys. Res., 90, 10463-10482.
- Low, P.S., 1990: Trends in surface ozone at Hohenpeissenberg and Arkona. J. Geophys. Res., 95(D13), 22441-22453.
- Oltmans, S.J., and W.D. Komhyr, 1986: Surface ozone distribution and variations from 1973-1984 measurements at the NOAA geophysical monitoring for climate change baseline observatories. J. Geophys. Res., 91, 5229-5236.
- Parrish, D.D. et al., 1986: Background ozone and anthropogenic ozone enhancement at Niwot Ridge, Colorado. J. Atmos. Chem., 4, 63-80.
- Penkett, S.A., 1984: Ozone increase in ground-level European air. Nature, 311, 14-15.
- Penkett, S.A., 1988: Indication and causes of ozone increase in the troposphere in the changing atmosphere. 38-48, John Wiley, N.Y.
- Piotrowicz, S.R., D.A. Boran, and C.J. Fischer, 1986: Ozone in the boundary layer of equatorial Pacific Ocean. J. Geophys. Res., 91, 13113-13119.
- Piotrowicz, S.R., R.A. Rasmussen, K.J. Hanson, and C.J. Fischer, 1990: Ozone in the boundary layer of equatorial Atlantic Ocean. Tellus.
- Routhier, F.R. et al., 1980: Free tropospheric and boundary layer airborne measurements of ozone over the latitude range of 58°S to 70°N. J. Geophys. Res., 85, 7307-7321.
- Sreedharan, C.R., and V.S. Tiwari, 1971: The use of a Brewer bubbler as a continuous ozone sensor. J. Phys. E. Sci. Inst., 706-707.
- Tiwari, V.S., and C.R. Sreedharan, 1973: Ozone concentration studies near the ground at Poona - Part I: Diurnal, seasonal and other time variations and ozone flux measurements. Ind. J. Met. Geophys., 24(4), 353-362.
- Winkler, P., 1988: Surface ozone over the Atlantic Ocean. J. Atmos. Chem., 7, 73-91.
- Winkler, P., 1989: Meridional distribution of surface ozone over the Atlantic (83°N76°S). Ozone in the Atmosphere, 423-425.

TROPOSPHERIC OZONE MEASUREMENTS AT THE EQUATORIAL REGION (1980-88)

Mohammad Ilyas

Astronomy and Atmospheric Research Unit
University of Science Malaysia,
11800 USM, Penang, Malaysia.

ABSTRACT

Results from surface ozone measurements at Penang ($5.5^{\circ}\text{N}, 100^{\circ}\text{E}$) over 1980-88 period are presented. The study indicates the ozone concentrations undergoing significant diurnal and seasonal variations. The peak concentration are observed at around mid-day (up to 35 nb) but the O_3 concentration generally drops to zero level in the early evening and remains unchanged until mid-morning. Monthly-averaged daily 1-h average concentrations are generally small (4-13 nb) and decrease continually from the early part of the year to the end. Frequently, varying local weather conditions seem to influence the O_3 concentrations.

1. INTRODUCTION

The natural ozone content of the troposphere is mainly determined by the rate of supply from the stratosphere and the rate of destruction on the earth's surface (Junge, 1962; Van Dop et al., 1977). Natural O_3 is also produced and destroyed within the troposphere by chemical reactions involving free radicals (Crutzen, 1974; Levy, 1988; Logan, 1985; Galbally and Roy, 1991). Besides the natural origin, surface O_3 can be produced photochemically due to the presence of NO_x and reactive HCs in association with high levels of solar near-ultraviolet (u.v.) radiation (Kirchhoff, 1988). Many of the industrial situations (including high emissions from motor vehicles) may result in photochemically produced surface O_3 and the O_3 levels can be of serious health and environmental consideration as elevated concentrations of ozone in the near surface air are damaging to vegetation and human health due to its toxicity. Also, ozone is a strong absorber of infrared radiation and large tropospheric concentrations

may have adverse greenhouse warming effect on the earth's climate.

In non-industrial locations, free of relevant chemical pollutants, the information on surface O_3 distribution is helpful in studying the natural production and transport mechanisms as well as in providing benchmark data for future comparisons. In view of these considerations, tropospheric and surface O_3 measurements under different local conditions have been made (e.g. Ogawa and Miyata, 1984; Attmannspacher and Hartmannsgruber, 1981; Oltmans and Komhyr, 1986; Chatterjee et al., 1982). Despite considerable effort on obtaining atmospheric O_3 measurements, there is a serious paucity in surface O_3 and vertical O_3 data for the equatorial region. In view of this, a comprehensive observational programme, involving surface O_3 , O_3 soundings, solar u.v. radiation and other related parameters, was initiated at the University of Science at Penang (Malaysia). Some initial results from this programme have appeared elsewhere (e.g. Ilyas, 1987a, b; Ilyas and Barton, 1983). The purpose of this paper is to report the results from the surface O_3 study for the 1980-1988 period incorporating the previously published results covering 1980 - 83 period (Ilyas, 1987a).

2. EXPERIMENTAL AND DATA ANALYSIS

The Island of Penang ($5.5^{\circ}\text{N}, 100^{\circ}\text{E}$) where the University of Science Malaysia is located is ideal for equatorial measurements. The air is reasonably clean from industrial polluting chemicals and the climate is moderate due to land and sea breezes and the centrally running (N-S) hill which passes by the West side of the campus. The instrument used for surface O_3 measurements, is a wet-chemical (KI solution) Brewer type, used in several studies for such measurements. The

instrument was activated in late 1980 and was operational through 1988 but malfunctioned in end 1981, 1982 and some other periods, which gave rise to some discontinuities in the data. In 1985 the ozone calibration source was sent for re-calibration at CSIRO (Australia).

The instrument produces an analog signal suitable for recording on an x-t plotter. Using the equal area averaging method, one-hour (1980-83) and half-hour (1984-88) averages were obtained for the daytime (0930-2100hrs). Also, due to generally small signals, single entries for the remaining night-end (2100-2400) and morning end (2400-0930) were recorded. These hourly/half-hourly averages were then machine processed to form (horizontal) hourly averages for daytime (AVD), night-end (AVN), morning-end (AMN) and day-night time (AVA) for each operational day. Strictly speaking, AVA should represent the hourly average for the day by averaging the hourly/half-hourly totals for the entire day over total day-hours (i.e. 24 hours). However, as before (Ilyas, 1987a) we have averaged it over 12 hours because most of the contribution comes from day-time 12-hours and only occasionally a small contribution may come from the morning and night components. The averaging over 12 hours provides the day-time average concentrations which is what we would experience and is the quantity directly relevant for air-toxicity considerations. But, if the daily concentrations, averaged over 24 hours, is desirable, this can be easily done by reading the scale/numbers to half the indicated values. If on any day, a partial data loss occurred (e.g. power loss), no period-averages were formed.

The hourly/half-hourly averages for each time-interval were processed to produce monthly averages and daily-hourly averages for the specific hours as well as monthly averages thus completing a monthly summary.

3. RESULTS

The diurnal and seasonal ozone variability is shown in Figs. 1 and 2. In a typical diurnal behaviour, the O₃ flux increases from the zero level at around 9 a.m. (solar time) to a maximum value slightly before noon (true mean noon at 1320 hrs). It maintains the high level in the early afternoon and slowly decreases to zero level again in the later part of the evening. There are, however, significant variations to this pattern depending upon weather conditions which undergo rapid changes over the period of a day. Occasionally

an O₃ level of as much as 5-10 nb may be maintained right through the night to the morning. Although night-time concentrations are usually zero level, on nights with significant thunderstorm activity (usually in the early mornings), traces of O₃ concentrations are recorded on the chart indicating O₃ levels increase during these activities.

SURFACE OZONE AVERAGE FOR 1/2-HOURLY PERMONTH 1985

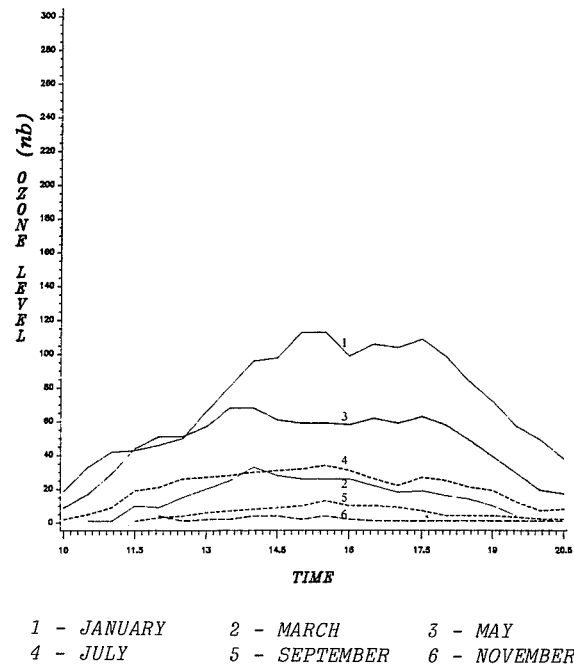


Fig. 1. Average monthly means of hourly-average ozone data as a function of local stands data; mean (local noon at 1320 local time) to show diurnal variability for different months for 1985.

The curves in Fig. 2 show seasonal variations using monthly averages of daytime hourly averages (AVA) for different years. The ozone concentrations usually drop to zero level in the late evening and maintains this level until late in the mid-morning.

Although the daytime 1-h average concentrations (partial pressure in nanobars) are relatively low (4-13 nb), the average-hourly maximum concentrations were found to be significantly higher (10-20nb),

SURFACE OZONE
DAILY HOURLY AVERAGE FOR THE MONTH
1980 - 1988

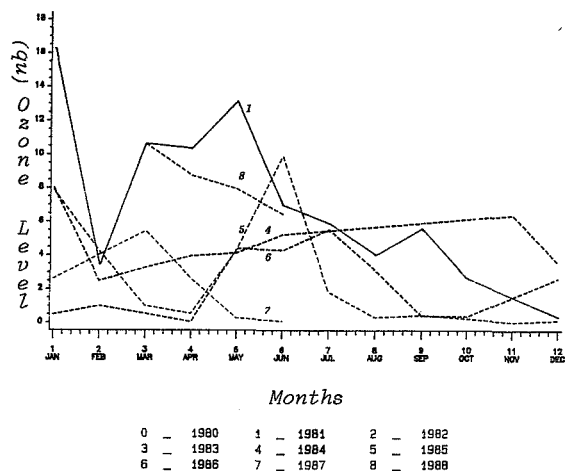


Fig. 2. Seasonal variability of monthly means of hourly-average ozone concentrations for the 1980-88 period.

especially in the early part of the year. Occasionally, the instantaneous (and 1-h average) values on individual days were found to reach as high as 35 nb. The data (Fig. 2) show a narrow dip around February which is the post-monsoon period. The prevailing synoptic situation (circulations) for the region is such that the wind direction changes over Peninsular Malaysia from North Easterly in January to approaching Westerly (April) and South-Westerly (July and October) over the northern part of Peninsular Malaysia including Penang. Although there is a gradual post-monsoon build up of the Westerlies, the general trend in April shows Easterlies able to penetrate the West coast of Peninsular Malaysia including Penang Island. An examination of the wind data taken at Penang indicated a swift change in wind direction from NE in January to NW in February (and October) which together with a weakening in the winds seems to be associated with the observed variation in O_3 flux (Ilyas, 1987a).

To study the other factors affecting the seasonal behaviour, the daytime average data were compared with seasonal trend of several other parameters based on many years of data at Penang as shown earlier (Ilyas, 1987a). The general trend of decreasing O_3 concentrations seems to be well matched (inversely) with the seasonal variability of several inter-related meteorological factors (sunshine-hours, solar radiation, wind speed, cloud cover and rainfall) (Fig.

3). However, the data for solar u.v.-A radiation and erythmal solar u.v.-B do not seem to show any clear impact of these two components on this seasonal O_3 trend.

4. DISCUSSION

The monthly averages (Fig. 2) clearly show a significant downward trend in 1982 believed to be due to instrument sensitivity changes and may not be used in year to year variability study. Examination of the diurnal monthly averages e.g. data for 1981 and 1988, 1987, 1986, 1985 indicated that the average 1/2-hourly averages and peak values were about the same for these years and thus the monthly-hourly averages in these years are primarily affected by the changes in weather and environmental conditions rather than by

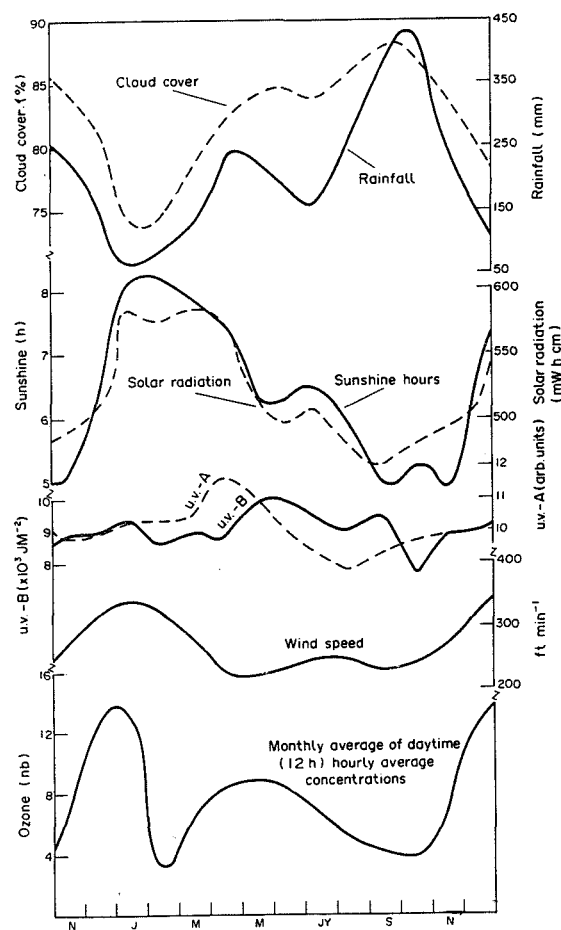


Fig. 3. Seasonal variability of surface ozone with other meteorological factors.

the instrumental sensitivity as in case of 1982.

Based on our experience with this instrument, we find two major maintenance problems. Firstly, the analyser calibration depends on the stability of the ozone source. The calibrator we used employs an opening-control which degrades with time as shown by a re-calibrator at CSIRO, Australia in 1985. The second source of problem comes from the frequent degradation and need for replacement of the air pump. On the whole, this instrument is very demanding in maintenance for the desired high precision data. In view of this, in 1988, we decided to discontinue the use of this instrument at the present location. It is our intention to establish a better type of instrument under a new broad programme at our recently built observatory and take other operational precautions. Despite the above mentioned sources of error, the overall seasonal and diurnal trends are clearly reflected in the Figs.

On the whole, considering the rather low O₃ levels and the absence of significant industrial sources, the surface O₃ in this region at present is considered to be essentially of natural origin and forms a background to possible future build up due to increasing industrial activities.

ACKNOWLEDGEMENTS

Valuable support in data processing was provided by Rahmita Wirza. The Analysis phase was partly supported through funds under National IRPA Grant from Ministry of Science, Technology and Environment, Malaysia. A grant from the Alternative Fluorocarbons Environmental Acceptability Study (SPA-AFEAS) enabling the author's participation in the Ozone Symposium is gratefully acknowledged. Balkis Abdul Rahman and Azlina Ali provided useful support towards the preparation of this paper.

REFERENCES

- Attmannspacher, W. and Hartmannsgruber, R. 1981: Trend and extreme values of 8 years continuous measurements of ozone near the surface at the Met. Observatory Hohenpeissenberg. In: Proc. Quad. Int Ozone Symp., Boulder 1980 (NCAR:Boulder), pp. 492-497.
- Chatterjee, K., Chandrasekharan C.K. and Verma V.P. 1982: Boundary layer studies conducted at Gadag during the total solar eclipse of 16 February 1980, Proc. Indian Nat. Sci. Acad., 43A (Suppl. 3), 254-259.
- Crutzen, P. J. 1974: Photochemical reactions initiated by and influencing ozone in unpolluted tropospheric air, Tellus, 26, 47.
- Galbally, I. E. and Roy, C. R. 1991: Ozone in the tropical troposphere: Overview, In: Ozone Depletion: Implications for the Tropics (Ed.: M. Ilyas), University of Science Malaysia, Penang/United Nations Environment Programme, Nairobi, pp. 139-158.
- Ilyas, M. 1987a: Equatorial measurements of surface ozone, Atmosph. Env., 21, 1799-1803.
- Ilyas, M. 1987b: Effect of cloudiness on solar ultraviolet radiation reaching the surface, Atmospheric Environment, 21, 1483-1484.
- Ilyas, M. and Barton, I.J. 1983: Surface dosage of erythemal solar ultraviolet radiation near the equator, Atmospheric Environment, 17, 2069-2073.
- Junge, C. E. 1962: Global ozone budget and exchange between stratosphere and troposphere, Tellus, 14, 363.
- Kirchhoff, V. W. J. H. 1988: Surface ozone measurements in Amazonia, J. Geophys. Res., 93, 1469-1476.
- Levy, H. II 1988: Global Transport of ozone, In Tropospheric Ozone, Isaksen I.S.A. (ed.), pp. 319-325, D. Reidel, Dordrecht.
- Logan, J. A. 1985: Tropospheric ozone: seasonal behaviour, trends and anthropogenic influence, J. Geophys. Res., 90, 10, 463-10, 482.
- Ogawa, T. and Miyata, A. 1984: Seasonal behaviour of the tropospheric ozone in Japan, In: Atmospheric Ozone, pp. 754-758, Reidel: Dordrecht.
- Oltmans, S.J. and Komhyr, W. D. 1986: Surface ozone distributions and variations from 1973-1984 measurements at the NOAA geophysical monitoring for climatic change baseline observatories, J. Geophys. Res., 91, 5229-5236.
- Van Dop H., Guicherit, R., and Lanting, R. W. 1977: Some measurements of the vertical distribution of ozone in the atmospheric boundary layer, Atmospheric Environment, 11, 65-71.

303160

**SPECIFIC FEATURES OF SPACE-TIME VARIATIONS OF OZONE DURING
THE DEVELOPMENT OF INTENSIVE TROPICAL DISTURBANCES**

Alexander F. Nerushev & Victor I. Vasiliev

Institute of Experimental Meteorology
82 Lenin Avenue, Obninsk, Kaluga Region 249020, Russia

ABSTRACT

Presented is an analysis of specific features of space-time variations of ozone in the tropical area which has been performed on the basis of processing of the results of special expedition studies in the Atlantic and Pacific in 1987-1990 and the data of observations at the stations of the world ozonometric network over the 25-year period. The existence of a cause-and-effect relation has been revealed between the processes determining tropical cyclone (TC) development, and specific features of variations of the total content of ozone (TCO) and the vertical distribution of ozone (VDO) in the regions of TC action. Characteristic features of day-to-day and daily variations of TCO during TC development have been found. On the periphery of a developing TC, 1-4 days before it reaches the stage of storm, TCO increases, on average, by 5-8%, and a substantial increase in the concentration of ozone occurs in the middle and upper troposphere. The most probable physical mechanisms relating the observed specific features of ozone variations to TC evolution have been suggested. A hypothesis of the possibility of using ozone as an indicator for early prediction of TC development has been substantiated.

1. INTRODUCTION

Space-time variations of the total content of atmospheric ozone (TCO) and its vertical distribution (VDO) in the tropical area are still not clearly understood. Meanwhile, dynamic processes in the tropics, and first of all, intensive vortex disturbances, namely, tropical cyclones (TC), cause

considerable deformations of the ozone layer (in some cases, up to several tens of percent). This paper presents a systematized information about specific features of space-time variations of ozone in the regions of TC formation and development, based on the results of special expeditions in the Atlantic and Pacific in 1987-1990 and the analysis of observational data from the stations of the world ozonometric network over the 25-year period (1957-1982) (Nerushev, 1991; Nerushev et al., 1986; 1989; 1990).

2. EXPERIMENTAL DATA AND METHODS OF THEIR ANALYSIS

In order to determine statistical mean characteristics of the space-time variation of ozone in the regions of TC formation and development, we used the data from 15 ozonometric stations in the Pacific and 7 stations in the Atlantic from monthly bulletins (Ozone Data for the World, 1957-1982), as well as the information on tracks and characteristics of 315 Pacific TC and 78 Atlantic TC over the same period.

For the purpose of separating out the TCO variations due to the processes associated with TC formation and development, as well as eliminating the latitudinal and seasonal variations of TCO, we calculated the value $\Delta x = x - \bar{x}$ for each observation, where x and \bar{x} are the daily mean and monthly mean of TCO, respectively.

As indicated by the analysis, the dependences $\Delta x(R, \varphi, t)$, where t is its life time in days, R is the distance from the ozonometric station to the TC center, and φ is the azimuthal angle, are of a great variety. For revealing general regularities, a compositing technique was used, in which individual dependences $\Delta x(R, \varphi, t)$ were averaged. In this case, different stages of TC development were

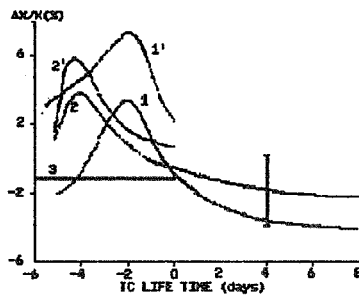


Fig. 1. The averaged time dependence of relative TCO variations during the life cycle of Atlantic (1, 1') and Pacific (2, 2') TC in the area with radius $R = 1000$ km (1) and 1500 km (2) from their centers, and in the external area at a distance of $500 \text{ km} < R < 1000 \text{ km}$ (1') and $600 \text{ km} < R < 1500 \text{ km}$ (2'); 0 - the day of depression intensification into storm, 3 - nondeveloping depression.

considered individually. Note that depending on the maximum wind speed at sea level (V_m), TC can be subdivided into tropical depressions (TD), with $V_m < 17$ m/s; tropical storms (TS), with $17 \text{ m/s} \leq V_m < 33$ m/s; and hurricanes or typhoons (T), with $V_m \geq 33$ m/s.

The day-to-day and daily variations of TCO were measured in expeditionary conditions in the Atlantic (is. Cuba, 1987 and 1989) and in the Pacific (1990) by automated ozonometer M-124 with wide-band filters, which had a single TCO measurement error of about 6%. The instrument made it possible to measure TCO at 1-min intervals, thus increasing substantially the accuracy of determining the TCO daily mean values.

3. TCO AND VDO VARIATIONS DURING THE LIFE CYCLE OF TC

The above-mentioned investigations revealed the existence of a cause-and-effect relation between the observed specific features of TCO and VDO variations in the areas of TC action, and the dynamic processes of different space-time scale which determine TC development or characterize its internal structure. The most essential of these features are as follows.

1. The nature of anomalies of the TCO daily mean field (Δx) around non-developing depressions differs noticeably from that of depressions

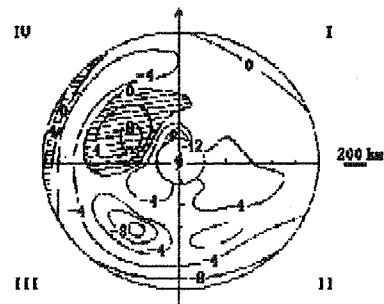


Fig. 2. A compositing space structure of the distribution of TCO daily mean deviations from the background values (in Dobson units) around the centers of Pacific storms and typhoons (the motion direction is indicated by an arrow).

developed to the storm stage. Two to four days before the depression intensification into tropical storm (when the wind speed is as great as 17 m/s), the TCO values on its periphery at a distance 500 to 1200 km to the north of the center increase, on the average, by 5-8%. Fig. 1 plotted by the compositing technique for the whole life cycle of TC, i.e., from depression to hurricane (typhoon), illustrates this specific feature for 78 Atlantic TC and 315 Pacific TC. The concentration of ozone in the middle and upper troposphere increases in the stage of depression intensification into storm by several tens of percent.

2. In the areas of action of a developed TC, i.e., a storm or a hurricane (typhoon) at a distance of up to 1500 km from its center, the space distribution of disturbances of the ozone layer is of a complicated nature. Fig. 2 shows a compositing pattern of anomalies of the TCO daily mean field around the TC center (with Δx in Dobson units) from the data on 315 TC in the western North Pacific (about 2500 TCO values). In this case, space averaging was performed over the distance intervals $|\Delta R| = 200 \text{ km}$ and the azimuthal angle $|\Delta \varphi| = 45^\circ$ in the coordinate system related to the direction of TC motion. Little data are available for an area of radius $R < 200 \text{ km}$ around TC. Note that Fig. 2 depicts the averaged space structure of the TCO anomaly field around TC. In some TC, positive and negative TCO anomalies can differ essentially from the averaged ones and amount to as much as several tens of percent.

3. In the stage of tropical storm and hurricane, characteristic oscillations with periods of 3-4 min. and

10-12 min. appear in the spectrum of short-period TCO variations. The nature of such short-period TCO variations is yet to be explained. They may be partly accounted for by internal gravity waves (IGW) generated in the atmosphere by a developing TC (for example, as cumulus congestus clouds break through the tropopause).

4. Based on the satellite data, the American scientists (Rodgers et al., 1990) found increased TCO values in the area of TC eye associated with the intrusion of stratospheric air rich in ozone.

4. PHYSICAL MECHANISMS DETERMINING THE OBSERVED TCO AND VDO VARIATIONS

In our opinion, the nature of the space-time distribution of TCO and VDO anomalies in the area of TC and its surroundings characterizes a complicated pattern of the interaction between the dynamic processes of different space-time scale from long waves ($10^3 - 10^4$ km) to convective cells (1 - 10 km).

For developing tropical depressions (TD), storms (TS) and typhoons (T) the characteristic feature is the presence of the upper-tropospheric trough (UTT) at levels of 300 and 200 hPa to the north-east (for TD) or north-west (for TS and T) of their centers, and the upper-tropospheric eastern jet (UTEJ) with speeds of 15-20 m/s in the 200-100 hPa layer with the axis at a level of 150 hPa at a distance of 1000-1500 km to the south of their centers (Bokhan, 1987).

The interaction of UTT with developing TC, which contributes to its intensification, leads to the enhancement of meridional exchange and the arrival of air masses of the moderate latitudes at the periphery of TC. As evident from the estimates, this mechanism may cause an increase of TCO by 8-20% in the typhoon season (May-November) to the north-east of the TD center or to the north-west of the center of TS and T. By virtue of its location, UTEJ is bound to lead to a small decrease of TCO ($|\Delta x|/x \leq 8\%$) at a distance of up to 1000-1500 km to the south of the centers of TD, TS and T.

A comparison of the above qualitative pattern of the TCO field deformation around the TC center under the influence of large-scale systems with the experimental data presented in Fig. 2, taking into consideration the mean direction of TC motion to the west-north-west, enables us to state that on the whole, the large-scale features of the TCO field deformation around TC are most probably due to the action of UTT and UTEJ. The observed increase of TCO on

the periphery of TD in the stage of its intensification into storm also can be fully explained by the above mechanism of meridional exchange (interaction of TC with UTT, invasions of cold air).

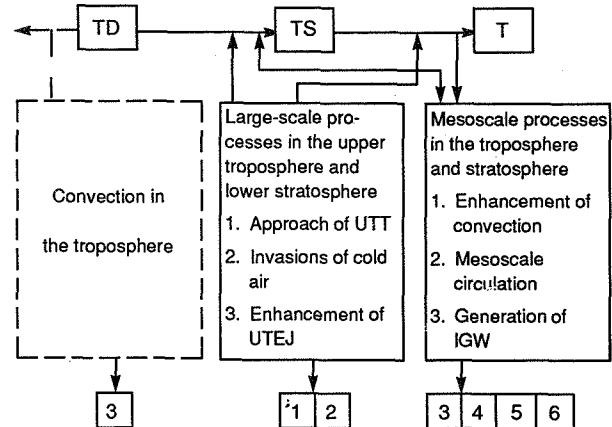


Fig. 3. The main observed TCO and VDO anomalies and their most probable origin.

- 1 - increase of TCO and ozone concentration in the upper troposphere and lower stratosphere to the north of the center of TD and TS;
- 2 - decrease of TCO and ozone concentration in the upper troposphere and lower stratosphere to the south of the center of TD and TS;
- 3 - decrease of TCO and ozone concentration in the troposphere in the active area and on the periphery;
- 4 - local increase of TCO and ozone concentration in the lower stratosphere and troposphere in the active area and on the periphery;
- 5 - increase of TCO in the "eye" of TC;
- 6 - short-period oscillation of TCO ($T < 10$ min.).

The circulation systems of the TC itself create small-scale disturbances of the ozone field showing themselves against the background of the anomalies which are due to the influence of the large-scale processes. In this case, as shown in our studies (Nerushev et al., 1986), the vertical ordered motions in the upper troposphere and lower stratosphere of mesoconvective scale ($10 - 10^2$ km) and of cloud cluster scale ($10^2 - 10^3$ km) play a leading role. Depending on their space distribution,

sign and value, both a decrease and an increase of TCO may occur in the active area (up to several tens of percent) and on the periphery of TC, as well as substantial changes of VDO of the corresponding sign.

Fig. 3 presents a simple schematic of cause-and-effect relations between the main specific features of TCO and VDO variations during TC development from depression to hurricane (typhoon), and the dynamic processes which, in our opinion, determine these features.

A qualitative assessment of the sign and value of the TCO field anomalies (Δx in Dobson units) around TC occurring under the influence of the dynamic processes of different space scale is given in the table, based on the published experimental data on TCO variations in the area of TC action. Considerable TCO anomalies in the active area of TC ($|\Delta x| < 100$ Dobson units) observed in individual intensive cyclones apparently indicate that the stratospheric layers are drawn into the circulation system of TC.

From the results presented we can conclude that the use of the data on TCO and VDO variations as indicators for early prediction of TC development is very promising and feasible. It is best to obtain the required information on TCO and VDO by remote space techniques.

Table. Approximate values of TCO anomalies (Δx in Dobson units) around TC occurring under the influence the dynamic processes of different space scale.

Dynamic process, characteristic size	Area of TC, stage of development			
	Active area E<300km		Periphery 500km<E<1500km	
	TD	TS,T	TD	TS,T
Long waves 10 ³ -10 ⁴ km			0< ΔX <60 (north of the center) -20< ΔX <0 (south of the center)	
Cloud clusters 10 ² -10 ³ km	$ \Delta X < 30^*)$		$ \Delta X < 20^*)$	
Mesoconvective 10-10 ² km	$ \Delta X < 30^*)$	$ \Delta X < 100^*)$ (in the 'eye' $\delta X > 0$)	$ \Delta X < 20^*)$	

*) The sign of Δx is dependent on the direction of vertical velocity in the stratosphere.

REFERENCES

- Bokhan, V.D., 1987: The structure of the tropical atmosphere in different stages of typhoon development. In: Tropical Meteorology. Proceedings of the Third International Symposium. L., Gidrometeoizdat, p. 164-169.
- Nerushev, A.F., 1991: Ozone as an indicator of tropical cyclogenesis. Trudy IEM (Transactions of the Institute of Experimental Meteorology, issue 54 (151), p. 87-101.
- Nerushev A.F., I.G. Anisova, and V.I. Vasiliev, 1990: Some specific features of space-time variations of the total content and vertical distribution of ozone in the tropics. Proceedings of the All-Union Conference on Atmospheric Ozone. M., Gidrometeoizdat, p. 114-120.
- Nerushev A.F., and E.K. Kramchaninova, 1986: An approximate model of the tropical cyclone influence on the ozonosphere. Trudy IEM, issue 39(122), p. 96-106.
- Nerushev A.F., S.S. Khmelevtsov, O.N. Belinsky et al., 1989: Preliminary results of research in the variability of ozone, water vapour and stratospheric aerosol during the complex expedition "Caribe-87". In: Tropical Meteorology. Proceedings of the Fourth International Symposium. L., Gidrometeoizdat, p. 233-247.
- Ozone Data for the World, 1957-1982: Toronto. Dep. Transport.
- Rodgers E.B., J. Stout, J. Steranka, and S.W. Chang, 1990: Tropical cyclone/upper-atmospheric interaction as inferred from satellite total ozone observations. J. Appl. Meteor., vol. 29, N 9, p. 934-957.

ANNUAL VARIABILITY OF OZONE ALONG ALPINE HILLSIDES

Erich Putz

Institut for Meteorology and Geophysics

Walter Kosmus

Institute for Analytical Chemistry

Karl-Franzens University of Graz, A-8010, Austria

ABSTRACT

Over a period of more than two years (March 1989 till June 1991) ozone and nitrogen dioxide have been monitored along twelve alpine hillsides in the Austrian alps. The profiles had a height-resolution of 100 m and cover a range between 400 m and 1800 m asl, that is 100 m to 1100 m above the bottom of the valleys. They were situated in remote rural areas as well as in the vicinity of polluted urban and industrial areas. Both trace gases were monitored by means of integral chemical (SAM-surface active monitor) methods with a measuring cycle of two weeks.

The concentration of ozone exhibits a substantial annual variation over the entire height range. In summer highest ozone levels are observed near ground and the top of the mountains, whereas in winter the maxima are found mainly in the crest regions. The overall ozone burden shows a relative maximum near the temperature inversion layer in the valleys and an absolute maximum at the crest.

1. INTRODUCTION

By the end of the 1970's there was growing recognition, that air pollution was threatening the alpine ecosystem. Reports on damaged forests were published and the public realized, that not only some regions in the vicinity of powerplants or heavy industry were affected, but more or less the whole alpine region. Acid rain was

the cause identified first. Actions for a reduction of sulphurdioxide emissions were set up, but soon it became clear that other pollutants and photochemical reaction products may play a more pronounced role. Investigations of forest authorities showed, that even in remote rural areas forests were damaged at a great pace. One striking feature is that the severest problems occur in distinct heights.

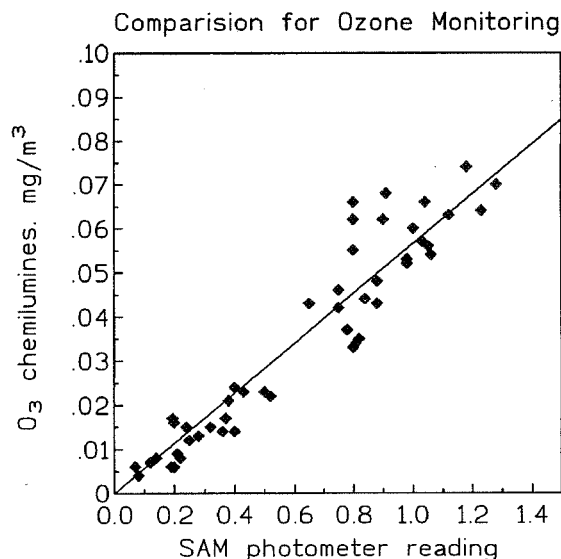
Like other alpine countries Austria has crowded populated valleys and basins combined with heavy transit traffic. More than two third of a year these basins are not ventilated very well. Although the emission controls are more rigorous nowadays we are faced with increasing air pollution.

By the mid 1980's the implementation of an air pollution monitoring network was still in its beginnings, especially in remote rural areas. Although there were indications, that Central Europe and especially the alpine regions are exposed to higher ozone concentrations as compared to other regions in Europe, the knowledge of the spatial distribution of NO_x and ozone burden in inneralpine valleys was not sufficient to decide if ozone was a threat or not. Reiter et al.(1987) and Paffrath and Peter (1988) observed higher ozone concentrations in the height range of 400m - 1400 m above ground and Broder and Gyax (1985) and other authors investigated the gradient of ozone in northern alpine regions. All investigations were limited in time, using airborne or balloon measurements or limited in space with instruments fixed on cablecars. It was not clear if these observations can be generalized for most inneralpine valleys or not. Moreover there was and is still a lack of regional models fitting such complex

terrain to decide whether local conditions, i.e. wind systems and emissions have significant influence on vertical ozone profiles or not. For economical reasons it is impossible to gain a sufficient spatial data coverage using sophisticated instruments, therefore it is necessary to utilize inexpensive passive samplers. To study the variability of ozone with height we set up profiles ascending twelve alpine hillsides in the province of Styria in the southeastern part of Austria, ozone was monitored for more than two years starting March 1989.

2. PASSIVE SAMPLERS FOR OZONE MONITORING

It is obvious that monitoring of air pollutants at a large number of sites to cover a large region with a dense grid could not be performed with sophisticated instruments due to the high costs of each device. Simple and therefore inexpensive techniques were developed to cover this demand. One possibility is the use of passive samplers. One particular type belongs to the group of the so-called surface active monitors (SAM). Based on the very specific reaction of ozone with the blue dye indigo to the red isatin, we developed such a sampler (Remler and Kosmus, 1988). The preparation is very simple. 2 g of indigo are dispersed in distilled water by means of an ultrasonic bath and with this dispersion of very fine dye particles chromatographic paper is impregnated two times. In between and at the end of this procedure the paper is dried at 80° C in an oven. This paper of about 10 x 10 cm in size is fixed on the surface of a cylindrical body and is exposed to the ambient air during a period of several days. The whole device is covered by a bell shaped shelter to protect it from rain. Ozone molecules reaching the surface of this paper can react with the exposed indigo. Constant deposition velocity assumed this amount should be proportional to the number of molecules in the volume of ambient air or in other terms, the number of deposited molecules should be proportional to the concentration (mg) of ozone per volume (m³). This proportionality is given by the amount of the reaction product isatin. After exposure the paper is extracted with ethanol and the isatin is measured photometrically. The validation of this method consists mainly of the exposure of SAM's in the vicinity of permanent instrumental monitors based on chemiluminescence. The mean of the measured ozone concentration during the exposure period is compared with the photometric absorption of the isatin concentration. The following figure 1 shows such a comparison. This is a result for a 2-week exposure at two different monitoring sites for 24 periods. For higher ozone concentrations the period has to be shortened to one week or the paper has to be soaked in a mixture of glycerol-phosphate buffer at the beginning to reduce the reaction rate. There are many advantages to apply SAM's in a large number, such



as simplicity and no maintenance and power is required, but with the loss of real time data, only average concentrations are given over the whole sampling period. The precision is mainly lost with rapidly changing or even fluctuating concentrations. It depends on the analytical problem if this could be accepted.

3. OBSERVATIONS AND RESULTS

The profiles have a resolution in altitude of 100 m and cover a range between 400 m and 1800 m above sea level, that is from the bottom of the valley up to the crest, which is in most cases 1100 m above ground. They are situated in remote rural areas as well as in the vicinity of polluted urban and industrial areas. Nearby continuous measuring instruments based on chemiluminescence supply additional data for comparison and verification. A measuring cycle of two weeks was applied, therefore our method can not exhibit short term variations. Apart from the changing weather pattern (global radiation, wind, humidity, precipitation, temperature etc) and smallscale meteorological effects (local valley wind systems), micrometeorological conditions due to varying deposition environment such as vegetation and snowcover play an important role for the quantification of the results. Because it is out of the scope of this short paper to discuss the characteristic pattern of each individual profile, some common behaviour concerning annual variability and dependence with height could be deduced.

As an example the following figure 2 shows the time series from one specific hillside. Near ground we

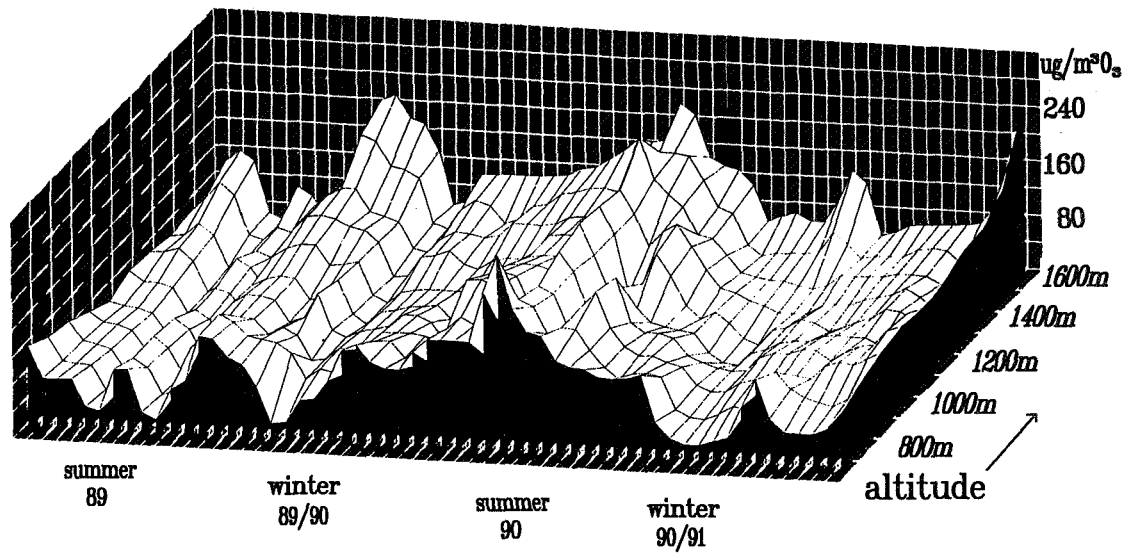


Fig. 2. Seasonal behaviour and dependence with height (asl) of ozone concentration.

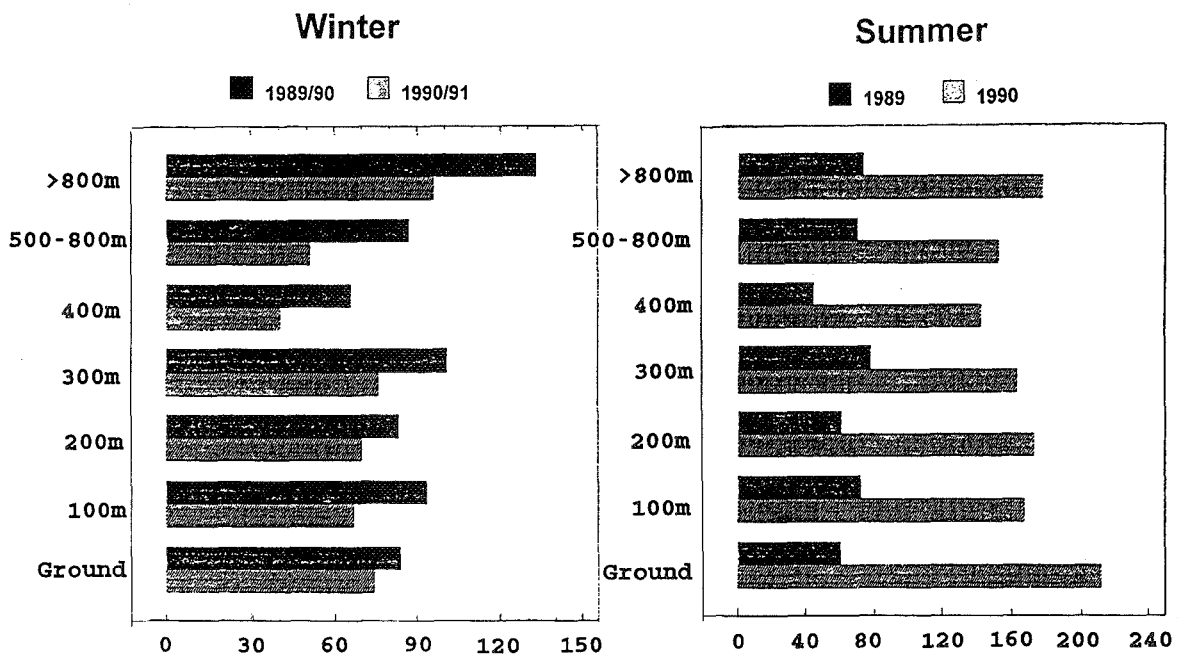


Fig. 3. Overall ozone burden ($\mu\text{g}/\text{m}^3$) in different altitudes for winter and summer

observe the highest values during autumn 1989 and summer 1990 which is attributed to the exceptional high sunshine duration in both seasons. The differences between the two summers 1989 and 1990 is attributed to a very rainy summer in the first year. The relative high values in winter 1989/90 might also be due to the exceptional high sunshine duration, a record since more than a century, leading to high local traffic to skiing resorts. The increased emission of ozone precursors results in an accumulation of ozone in high altitudes.

To demonstrate the different course of ozone with altitude more precisely we show in figure 3 the average ozone burden in two different seasons, winter and summer 1989 and 1990 from the same hillside. For the winter seasons we observe an increase from the ground up to a local maximum at about 300m above ground. From the minimum at 400m the concentration of ozone increases up to a maximum at the top of the mountain. The minimum coincides with the average height of the temperature inversion layer in alpine valleys. In the summer we observe the maximum at or near the bottom of the valley, a minimum around 400 m or 500 m above and again a maximum at the crest. The height of the minimum varies slightly from one hillside to the other, depending on local conditions, local wind systems, etc.

In spring and autumn the profiles exhibit either winter or summer behaviour, depending on the prevailing weather pattern. It is interesting to add, that the intervariance of the height-profiles is a minimum in winter 89/90 and summer 1990, i.e. low variability between individual heights, time and sites and a maximum in summer 1989 and winter 90/91. This shows the over all dominant influence of macroscale high pressure systems over central Europe for the production of ozone. In periods which are dominated by low pressure systems, increased convection and rapid changes of air masses the differences between the individual profiles appear more pronounced. For this investigation

and even more general for the whole alpine region we have take into account that the mountain barrier acts as a weather divide. As a result we can distinguish for the ozone different behaviour for inner alpine basins, valleys at the northern and southern part.

REFERENCES

- Broder B., H.A. Gygax , 1985: The influence of locally induced wind systems on the effectiveness of nocturnal dry deposition of ozone. Atmos. Environment 19,1627-1637
- Paffrath D., W. Peters, 1988: Betrachtungen der Ozonvertikalverteilung im Zusammenhang mit den neuartigen Waldschäden. Forstw. CBL. 107, 152-159.
- Reiter R., R. Sladkovic and H.J. Kanter, 1987: Concentration of trace gases in the lower troposphere, simultaneously recorded at neighboring mountain stations. Part II: Ozone. Meteorol. Atmos. Phys. 37,27-47.
- Remler, P., W. Kosmus, 1988: Integrale Langzeitmethode zur Bestimmung von Ozon in der Atmosphäre. Fresenius Z. Anal. Chem., 329, 871-874

THE VERTICAL DISTRIBUTION OF OZONE AT PRETORIA
FROM JULY 1990 TO JUNE 1991 AND ITS CHANGES

Mark Zunckel
Weather Bureau,
Private Bag X97, Pretoria,
0001 South Africa

Roseanne D Diab
Dept of Geographical and Environmental Sciences,
University of Natal,
King George V Avenue, Durban
4001 South Africa

Cal B Archer
Weather Bureau,
Private Bag X97, Pretoria,
0001 South Africa

Malcolm W J Scourfield
Space Physics Research Institute,
Dept of Physics,
University of Natal,
King George V Avenue, Durban
4001 South Africa

ABSTRACT

Total ozone and the vertical distribution of ozone were measured at Pretoria between 1965 and 1968. Total ozone measurements recommenced in Pretoria in August 1989, and measurements of the vertical distribution of ozone near Pretoria recommenced in July 1990. Relative to the earlier data, mean monthly total ozone values are significantly higher in all months, with a mean annual relative increase of 12%. The recent profiles show a significant increase in the mean monthly concentration of ozone in the lowest 12 km. Concurrent to this increase a relative decrease in ozone concentration is shown between 12 and 42 km.

The increased ozone concentration in the lower troposphere may be related to urbanization and the increase in ozone-forming nitrogen oxides over the last two decades. It is suggested that the decreased ozone concentration in the stratosphere and upper troposphere is evidence of the global decrease in the mid-latitudes of the Southern Hemisphere.

INTRODUCTION

Pretoria is situated at 25°44'S and 28°11'E, at an elevation of about 1500 m

above sea level, in South Africa's Transvaal province, the industrial and financial nucleus of the country where 60% of the approximate 30 million strong nation live and work.

In April 1964 total ozone was measured above Pretoria using a Dobson spectrophotometer and in May 1965 measurements of the Umkehr effect commenced, providing measures of the vertical distribution of ozone. Both of these measurements continued on a regular basis until February 1972. In 1989 the Dobson spectrophotometer was refurbished and calibrated at the NOAA laboratory in Boulder and measurements of total ozone resumed again in Pretoria in August 1989. In June 1990 the Dobson was relocated to the Irene Weather Office, 20 km south of Pretoria, where Umkehr measurements commenced in July 1990 and these were supported in October 1990 by weekly ozonesonde soundings.

BACKGROUND OZONE PROFILES

From the period May 1965 to December 1968, 645 Umkehr profiles were computed and averaged to obtain mean monthly vertical ozone profiles (Zunckel et al, 1992). These profiles showed ozone concentrations to increase steadily with height from partial pressure values of less than 1 mPa near ground level to values of about

14 mPa between 24 and 30 km altitude. Above this level the concentration decreases again to values approaching zero above 54 km altitude.

Large variability in ozone concentration in the vicinity of the tropopause suggests an interaction between the troposphere and stratosphere and a possible source of stratospheric ozone into the troposphere. Small variability in ozone concentration and a systematic decrease in concentration downward from the stratosphere suggests that sources of tropospheric ozone, other than stratospheric, were not significant.

These early ozone data are considered fundamental and represent the ozone situation over the central parts of South Africa before the main onset of stratospheric ozone depletion, and before large-scale industrialization and urbanization in the Pretoria area. They provide an ideal background against which current and future ozone values may be compared

CURRENT OZONE PROFILES

For the 12-month period July 1990 to June 1991, 75 Umkehr profiles were computed and averaged to obtain mean monthly vertical ozone profiles. These current profiles show ozone concentration to increase with height from partial pressure values of between 2 and 3 mPa near ground level to values of between 13 and 14 mPa in the layer between altitudes of 24 and 30 km. Above this level ozone concentration decreases towards zero above 54 km asl.

Large variability in concentration exists in the vicinity of the tropopause and in the layer from ground level to an altitude of 6 km, suggesting a stratospheric source of tropospheric ozone as well as a source of ozone near ground level.

COMPARISON OF OZONE PROFILES

Annual mean total ozone during the earlier period was 259 DU and the corresponding mean for the current period is 290 DU (Bruitjes et al, 1990). This represents a relative increase in total ozone of 12%. In investigating the apparent increase in total ozone, mean monthly values of ozone concentration in nine layers from ground level up to an altitude of 54 km at 6 km intervals were examined. The relative changes in each layer are listed in Table 1, from layer 1 extending from ground level to 6 km altitude up to layer 9 extending from 48 to 54 km altitude.

TROPOSPHERIC OZONE

The significant increase in tropospheric ozone can largely be attributed to a steady increase in electricity production in coal fired power stations within a 200 km arc to the east and southeast of Pretoria and a steady increase in the number of motor vehicles on Pretoria's roads. Motor vehicle numbers have quadrupled in Pretoria since 1966 and the national electricity, mostly in coal fired stations, has increased by five fold since 1965. These increases imply an increase in the concentration of ozone precursor gases in the troposphere and an increase in tropospheric ozone concentration.

Table 1: The mean annual change in ozone concentration in the nine atmospheric layers.

Layer	Background (mPa)	Current (mPa)	Percentage change
1	0.4	2.7	575
2	2.1	3.2	52
3	4.8	4.1	-15
4	10.3	9.4	-9
5	14.1	13.4	-5
6	9.4	9.1	-3
7	4.7	4.4	-6
8	1.90	1.87	-
9	0.55	0.59	-

STRATOSPHERIC OZONE

Since conditions suited to chlorine destruction of ozone do not readily occur in the relatively warm Pretoria stratosphere it is felt that the most feasible explanation for the relative decreases in concentration found in the stratosphere can largely be attributed to dilution. Air above Pretoria that is relatively rich in ozone may be diluted by ozone-poorer Antarctic air after the break down of the polar vortex in late spring.

REFERENCES

- Zunckel, M., Scourfield, M.W.J. and Diab, R.D., 1992: Vertical distribution of ozone above Pretoria from 1965 to 1968, South African Journal of Science, in print.
- Bruitjes, R.T., Archer, C.B. and Zunckel, M., 1990: Daily and seasonal variation in the atmospheric ozone over Pretoria between April 1964 and

February 1972, South African Journal
of Science, 86, 419-425.

Note: M Zunckel now at CSIR (Ematek), P O
Box 395, Pretoria, 0001 South Africa, from
1 June 1992.

303166

SEASONAL BUDGETS OF OZONE AND OXIDANT PRECURSORS IN AN INDUSTRIAL COASTAL AREA OF NORTHERN ITALY

T. Georgiadis*, L. Alberti⁺, P. Bonasoni*, F. Fortezza⁺,
G. Giovanelli* and V. Strocchi⁺

(*) FISBAT-C.N.R., via Castagnoli 1, 40126 Bologna, Italy

(⁺) P.M.P.-USL 35, via Alberoni 5, 48100 Ravenna, Italy

ABSTRACT

The seasonal budgets and evolution of photochemical oxidants reported for greater Ravenna's urban-industrial area in the present study were calculated using the combined data from on-site systematic surveys (1978-1989) and from the monitoring network of the local environmental authorities. The notable differences in the concentrations of ozone and nitrogen oxides depended on season, and meteorological variables showed a marked correlation to the seasonal budget of trace constituents. The weak local circulation, the land-sea breeze system, and high solar radiation in summer, which may persist at length because of the anticyclonic conditions, can produce episodes of intense photochemical reactions. In winter, by contrast, low solar radiation and the absence of the breeze system result in very different evolutions of both pollutant concentrations and their seasonal budget.

1. INTRODUCTION

Oxidant concentrations in the lower atmospheric levels close to industrial sites are the result of emissions, chemical reactions and transport mechanisms. Local concentration values and their diurnal variations are highly dependent on solar radiation and the emission of primary pollutants such as nitrogen oxides and hydrocarbons. In addition to the atmospheric chemical reactions that occur in the presence of specific emissions by industrial or power-plants, topographic discontinuities like coastlines can induce peculiar anemologic circulation systems in which pollutants are transported (Giovanelli *et al.*, 1985).

Geographically and climatically part of the Po valley, Greater Ravenna (Figure 1) is bordered on the east by the upper Adriatic Sea and features an extensive seaboard industrial belt (petrochemical and chemical plants, an electric power station and other industries). These plants produce large amounts of oxidant precursors whose concentrations levels show that the entire coastal area is affected by chemical pollution (Bonasoni *et al.*, 1991). The city proper, located a few kilometers inland, is characterized by congested viability and the resulting accumulation of motor vehicle pollutants.

Ozone concentration readings taken since 1978 by the air quality network show values of hourly concentration several-fold greater than those of Italy's national health standards (Fortezza *et al.*, 1986). The total emissions in the Ravenna area of certain pollutants from industrial, traffic and domestic production are reported in Table 1.

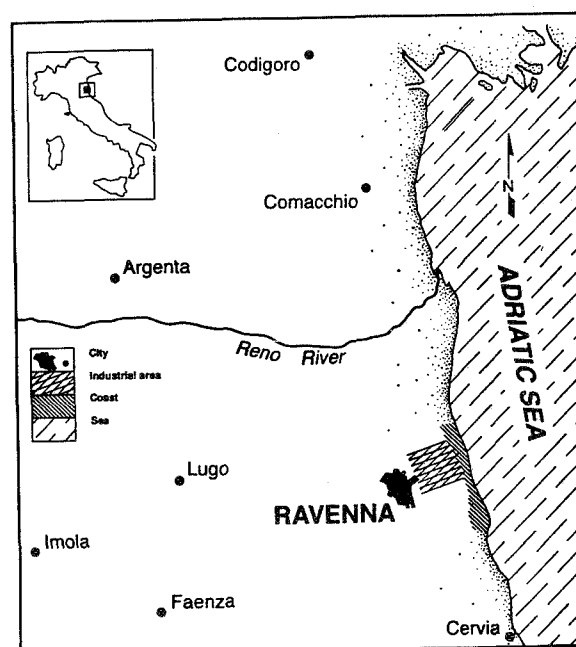


Fig. 1. Map of the Ravenna area.

2. DATA ANALYSIS AND DISCUSSION

Measurements were performed at an environmental protection network station equipped with the Philips analyzers PW9760 for NO_x (from 1986 monitored with an Environment AC30M) and PW9771 for O₃; meteorological sensors were placed at a representative site of the area under investigation. The solar radiation intensity was measured by a Kipp & Zonen AL4-MICROVA.

Figure 2 shows the average daily solar radiation for the period 1978-1989. Note the well-defined trend due to the sharp differentiation of the local climate at the change of seasons. Figure 3 has the average daily ozone concentration for the same period. Its seasonal variation is not so well defined throughout the period as that of solar radiation. The periods corresponding to zero value of O₃ concentrations are due to analyzer malfunction. Figure 4 shows the average diurnal NO_x concentration; the maxima correspond to the winter season.

Compound	Amount (T/Y)
SO _x	42,095
NO _x	13,053
CO	28,760
Particles	7,003
Hydrocarbons	3,026

Table 1. Yearly emissions from Ravenna area (industrial, civil and traffic)

The lengthy time span of this data set makes it possible to calculate the seasonal diurnal variation of O₃ and NO_x concentrations and of solar radiation with high statistical confidence. The seasonal trends were computed by averaging the half-hourly measurements collected in three-month periods. Figure 5 shows seasonal diurnal variations of solar radiation and figure 6 the seasonal diurnal variation trends of ozone concentration. A comparison of the summer and winter peaks reveals that the value of the former is three times higher than the latter. The spring and autumn concentration levels exhibit trends quite similar to each other over the day, noticeable differences appearing only in the tails of the trends corresponding to the late night and early morning hours. The relative maximum values are found about halfway between those of summer and winter.

Focusing on the position of the maximum it is possible to note during summer and spring high concentration values for many hours of the day and in the summer a secondary peak appears around 7:00 p.m..

This phenomena must be ascribed to transport mechanisms: in the warmer seasons the local prevailing circulation is driven by land-sea breeze system in which air masses rich in pollutants are transported out to sea in the morning, where they undergo photochemical reactions with subsequent ozone formation, and in the afternoon are transported back to the coast by the sea breeze, thereby causing persistent high concentration levels.

Figure 7 shows the seasonal diurnal variation trends of NO_x concentration. Note the strong decrease in values during the middle hours of the day due to photochemical reactions and turbulent diffusion in the increasing height of the mixing layer. The relative seasonal intensities are reversed compared to the ozone's, with high concentrations values recorded in winter rather than in summer.

During the coldest months the less dispersive condition of the atmosphere causes pollutant enrichment close to the emission sites, and the reduced incoming solar radiation prevents marked photochemical reactions and consequent NO_x depletion.

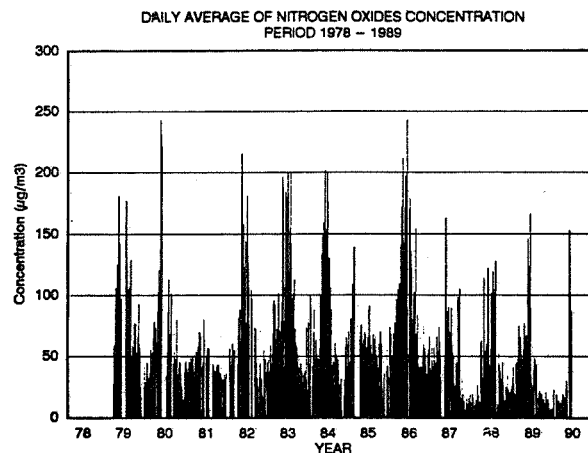


Fig. 2. Daily averages of solar radiation (1978-1989)

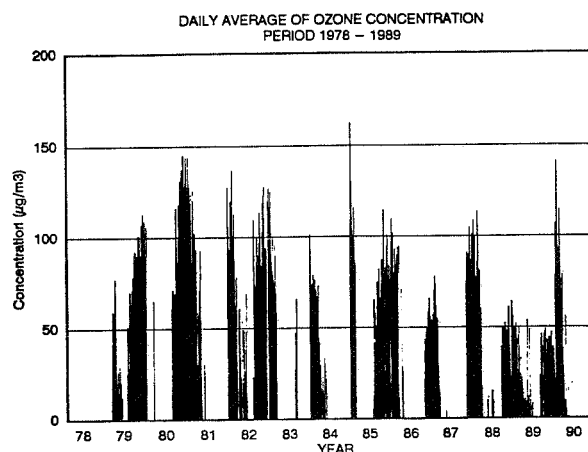


Fig. 3. Daily averages of ozone concentration (1978-1989).

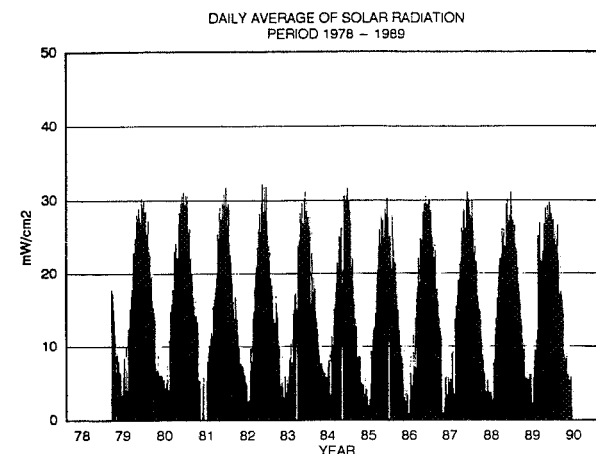


Fig. 4. Daily averages of nitrogen oxides concentration (1978-1989)

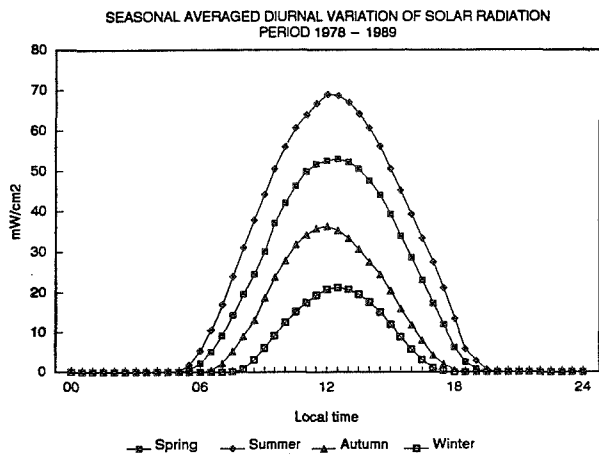


Fig. 5 Seasonal diurnal variation of solar radiation.

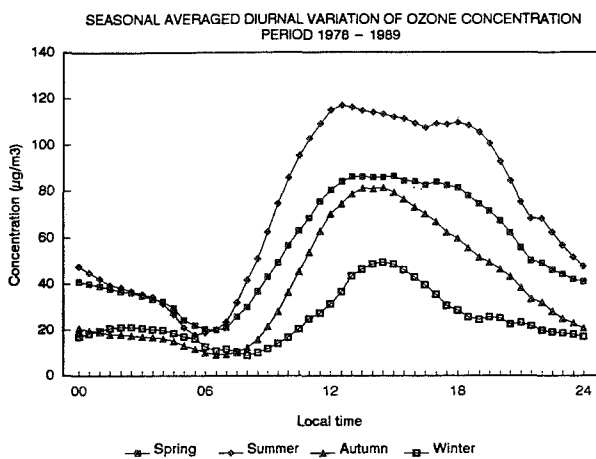


Fig. 6. Seasonal diurnal variation of O₃ concentration.

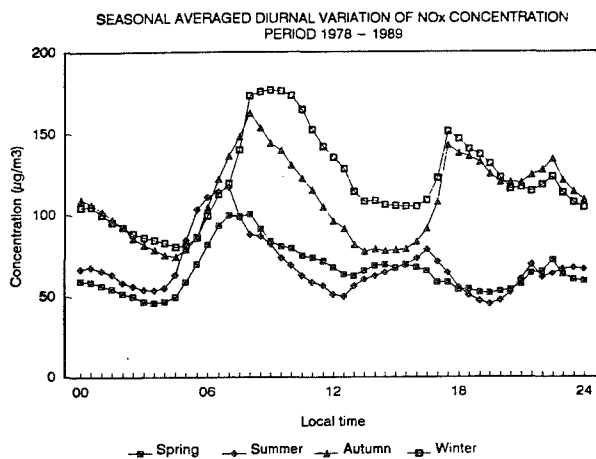


Fig. 7. Seasonal diurnal variation of NO_x concentration.

3. CONCLUSIONS

The high summer values of ozone concentration in Ravenna's industrial region, are to a great extent determined by emission of such pollutants as nitrogen oxides in conjunction with remarkable amount of solar radiation. The strong correlation of O₃ concentrations to the latter and the comparison with relative intensities indicate that solar radiation rather than high concentrations of primary pollutants drives the formation of ozone. Transport phenomena due to the presence of topographic discontinuities can notably alter the duration of high level concentrations in this area.

Budgets show how during the warm seasons the air quality is subject to frequent episodes of photo-oxidation reactions, resulting in high concentration values of secondary pollutants. The simultaneous presence of hydrocarbons and ozone in atmosphere which can produce free radicals, is more likely in the summer.

ACKNOWLEDGEMENT

This study has been supported by the CNR-ENEL Project - Interaction of energy systems with human health and environment - Rome Italy. The authors thank D. Cavallini for data processing and V. Gnani for network assistance.

REFERENCES

- Bonasoni, P., Fortezza, F., Georgiadis, T., Giovanelli, G., and V. Strocchi, 1991: Formation and transport of oxidants over a highly populated coastal area. *Chemrawn VII, The Chemistry of the Atmosphere*, December 2-6, Baltimore, Maryland, USA.
- Fortezza, F., Strocchi, V., Fariselli, G., Gnani, V., Signorini, T., Georgiadis, T., and G. Giovanelli, 1986: Analisi dei dati acquisiti in 7 anni di rilevamento dell'inquinamento atmosferico nell'area di Ravenna. In: *Analisi e gestione della qualità dell'aria a Ravenna*, edited by Amm. Prov. Ravenna, pp. 268.
- Giovanelli, G., Georgiadis, T., Fortezza, F. and V. Strocchi, 1985: Transport of photochemical ozone along the western Adriatic shore near a petrochemical plant. *Il Nuovo Cimento*, V. 8, 6: 727-742.

TROPOSPHERE

GLOBAL AND REGIONAL MODELING

**TROPOSPHERIC OZONE IN THE WESTERN PACIFIC RIM : ANALYSIS OF
SATELLITE AND SURFACE-BASED OBSERVATIONS ALONG WITH
COMPREHENSIVE 3-D MODEL SIMULATIONS**

Young Sunwoo and Gregory R. Carmichael

Department of Chemical and Biochemical Engineering
Center for Global and Regional Environmental Research
The University of Iowa
Iowa City, Iowa 52242, USA

ABSTRACT

Tropospheric ozone production and transport in mid-latitude eastern Asia is studied. Data analysis of surface-based ozone measurements in Japan and satellite-based tropospheric column measurements of the entire western Pacific Rim are combined with results from three-dimensional model simulations to investigate the diurnal, seasonal and long-term variations of ozone in this region. Surface ozone measurements from Japan show distinct seasonal variation with a spring peak and summer minimum. Satellite studies of the entire tropospheric column of ozone show high concentrations in both the spring and summer seasons. Finally, preliminary model simulation studies show good agreement with observed values.

1. INTRODUCTION

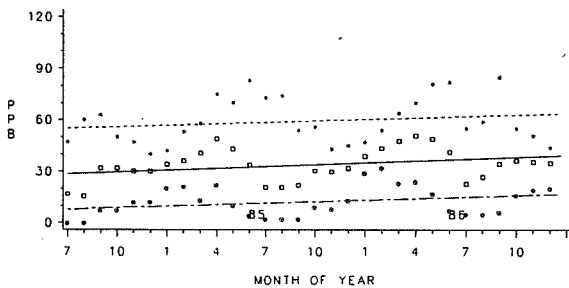
The characteristics of tropospheric ozone production and transport in the middle latitudes of the western Pacific Rim region are being studied. This region, which includes the countries of China, Japan, and Korea, is undergoing accelerated economic growth and industrial expansion resulting in, among other things, unprecedented increases in the anthropogenic emissions of ozone precursors such as nitrogen oxides and hydrocarbons. It has already been shown that this region of Asia has the highest tropospheric ozone column values anywhere on earth (Fishman et al., 1990). Thus, the effects of tropospheric ozone in this region are clearly significant and, furthermore, its impact on the global troposphere remains unquantified. In this paper results from both satellite and surface data analyses and those from preliminary three-dimensional simulations on a regional scale using a detailed tropospheric trace gas model (i.e., the STEM-II model) are presented.

2. SURFACE DATA ANALYSIS

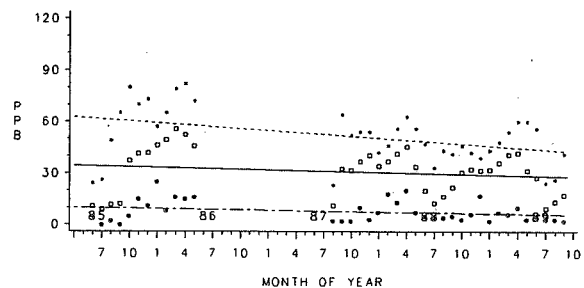
The surface-based observations of ozone are from the Background Surface Ozone Monitoring Network of Japan which was established in the 1980's (NIES Reports, 1989). There are over ten monitoring stations dispersed throughout Japan mostly at sites such as mountain tops and remote islands. The time span of data collection varies with station ranging from six years to three months of hourly values. Over the entire sampling period, about half of the stations, most of them from the island of Honshu, show an

increase of 1-5% in the monthly average of hourly measurements while the rest of the stations show no visible trend in either direction. Figure 1 shows the monthly maximum, average and minimum values and a simple linear regression of the three parameters for two different stations for approximately a three year period. Hourly values have been averaged for each month. Figure 1(a) is data collected at Mt. Tokusagamine in Yamaguchi prefecture on the southern tip of Honshu, the main island of Japan, while the measurements in Figure 1(b) are from the Amami station, located on a small island several degrees to the south of Kyushu island. The former station shows a small uniform increase in the average values as well as the maximum and minimum values. This station is at an elevation of about 500 (m) above sea level and its geographic location makes it susceptible to influences of transport of anthropogenic precursors of ozone such as nitrogen oxides and of ozone itself. The remoteness of the Amami station most likely keeps it away from much anthropogenic influence. Figure 1(b) shows a very slight decrease in all three indices but there is a gap in the data from the summer of 1986 to spring of 1987 which is not taken into account. Though the maximum hourly value of the month has decreased with time the trend is not statistically significant.

The seasonal variation for these two stations is common to all the other background stations in Japan showing a peak in the spring and a minimum in the summer. Amami reaches its peak in late March or early April while Yamaguchi has its peak in late April/ early May. The maximum in spring is slightly earlier compared to similar stations in the eastern United States and western Europe which usually have their maximums in late spring and summer (Logan, 1989). Some have attributed this relatively early spring maximum to natural peaks in the stratospheric intrusion process during this season (Ogawa and Miyata, 1984). The higher frequency of stratospheric-tropospheric exchange during this season bring higher ozone concentrations into the upper troposphere. Others claim a photochemical explanation (Liu et al., 1987). Colder temperatures during winter and early spring allow for longer transport distances and accumulation for ozone and its precursors followed by peaks in concentration due to warmer temperatures and increased photochemical activity. The summer minimum may be possibly attributed to a shift in the dominant meteorology over the region from continental northeasterly winds from China brought on by the Aleutian low-pressure system in the winter season to



(a)



(b)

Figure 1. (a) Monthly maximum, average and minimum surface ozone values for Yamaguchi Station. Elevation : 530 (m) (b) Monthly maximum, average and minimum surface ozone values for Amami Station. Elevation : 300 (m)

mostly southerly winds bringing moist air from the lower latitudes in the summer (Whelpdale and Moody, 1990).

Figure 2(a) shows a plot of daily average ozone and temperature at Happo in the heart of Japan for a period of five months in 1987. The drop-off of the ozone concentration in early July is very clearly shown while the surface temperature continues to rise as the summer develops. Happo is located at an elevation of about 1800 (m), essentially in the free troposphere, and the simultaneous measurements of ozone, dust, temperature, pressure and relative humidity is providing valuable insights into deciphering the sources of ozone, whether it be local sources, long range transport from urban centers, in situ photochemical production, or downward transport from the stratosphere and the upper troposphere. At this stage of the analysis, positive correlations between ozone and dust concentration peaks in the spring season, along with the corresponding meteorological conditions, seem to show that a combination of a passing cold front followed by general subsidence under a stagnant high-pressure system over Japan result in downward transport of ozone-rich, dust-rich mid-troposphere air and increases in photochemical activity causing higher production of ozone.

Similar plots for Amami and Yamaguchi (for years 1988 and 1986, respectively) are shown in Figure 2(b). As discussed above, Amami reaches its spring peak sooner and the summer minimum also arrives earlier, the latter most likely due to its southerly location making it more susceptible to relatively early influences from clean lower latitude air. The overall values of ozone concentration are lower for Yamaguchi relative to Happo, and Amami lower still. Site elevation and proximity to sources are the primary reasons behind these differences.

3. SATELLITE ANALYSIS OF TROPOSPHERIC COLUMN

To study the trends and regional distribution of the entire tropospheric column in the western Pacific Rim, satellite analyses have been performed utilizing the TOMS instrument on board the Nimbus-7 satellite which measures the total ozone column using back scattered UV-radiation and the SAGE-II, charting the vertical distribution of ozone in the stratosphere and above by the solar occultation

method, on the Earth Radiation Budget Satellite (Fishman and Larsen, 1987). Data from the years of 1985-87 for the region covering 20-50° N and 100-160° E have been analyzed by subtracting the integrated SAGE-II measurements above the tropopause from the total column data provided by TOMS. It should be pointed out that though the concept is very simple, there are still some uncertainties in the actual implementation of this methodology such as the accuracy of the TOMS instrument itself (especially in the treatment of clouds), inherent problems of the analysis such as the time difference of the TOMS and SAGE-II measurements (local noon versus local sunrise/sunset), and application to the relatively unstable midlatitude circulations, particularly with front and jet stream activity.

Results show a peak for the tropospheric column in East Asia in the spring and summer seasons of over 40 Dobson units as is seen in Figure 3 (averaged for all three years). An accurate interpretation of the data is hampered by the missing months of June and August, for which the number of data points were too few to be considered significant. However, it is clear that the tropospheric column values for the summer season are much more prominent when compared to the very low values obtained from surface measurements during this season in Japan. The regional distribution of the tropospheric column ozone shows good correlation with the prevailing seasonal wind patterns for the middle to upper troposphere. For example, the seasonal peak locations are downwind of heavy emission areas. There is also some evidence that the production and transport of tropospheric ozone in the upper half and lower half of the covered region of 20-50° N latitude are predominantly governed by differently weighted combinations of influencing factors, both meteorological and photochemical. The relatively small number of overlapping "points" between the two satellite instruments is still a substantial problem but with continued data collection expanding the data base this methodology should prove invaluable in studying the tropospheric column ozone behavior in the upcoming years.

4. PRELIMINARY 3-DIMENSIONAL SIMULATION

The STEM-II model (Carmichael et al., 1986) is

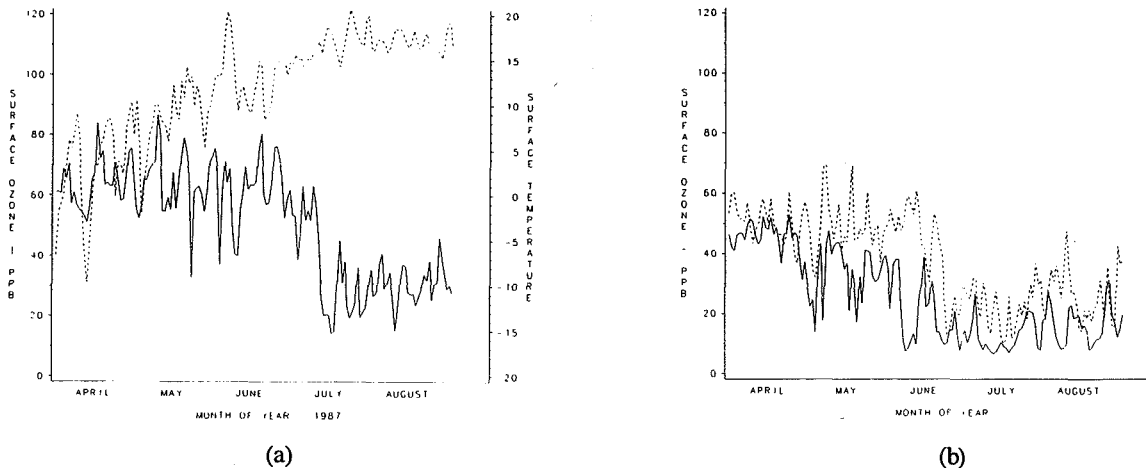


Figure 2. (a) Daily averages of surface ozone and temperature at Happo station, elevation 1800 (m), during five months of 1987. The units for ozone is ppb and that for temperature is °C. Ozone is the solid line and temperature is the dashed line. (b) Daily averages of surface ozone for Amami (for 1988; solid line) and Yamaguchi (for 1986; dashed line)

being utilized to conduct three-dimensional simulations of tropospheric ozone transport, both horizontal and vertical, and photochemistry in the study region of the western Pacific Rim. The STEM-II is a comprehensive three-dimensional, transport/chemistry/removal model. The current version of the model uses the photochemical mechanism of Lurmann et al. (1986), which includes 112 chemical reactions and 53 chemical species. This mechanism is best suited for analysis of trace gas cycles under conditions where NO_x levels are > 0.1 ppb. In order to extend the mechanism to lower NO_x conditions and to explicitly include the role of isoprene chemistry this mechanism has been modified as discussed in Jacob and Wofsy (1988). The complete mechanism includes 70 species and 200 reactions. In addition to gas phase photochemistry, the model treats cloud chemistry, and cloud micro-physics. A dust transport and chemistry module has been added to look more closely at the problem of "yellow sand" transport that is quite prevalent in East Asia. This phenomenon is thought to significantly influence the atmospheric chemistry and trace gas budgets of this region. Preliminary results show good agreement between simulated and observed data.

A springtime episode in May of 1987 is used to investigate the characteristics of tropospheric ozone production and transport during this season, including diurnal cycles. Figures 4 (a) and (b) show the results of a preliminary simulation. Both figures display ozone concentrations at surface level in ppb for the fourth day of simulation, one at 8 AM and the other at 8 PM local time. The first plot shows low values of surface ozone on the continent while the pocket of high ozone lies in south central Honshu with peak values of 80-100 ppb. This region of high ozone moves to north central Japan after a 12-hour period under the influence of a south-southeasterly wind and also grows in size. Also prominent is the 50-80 ppb region on the northern Chinese coastal areas at this time. The peak values in the early afternoon reaches values of over 100 ppb for the simulation results. Finally, slightly higher level

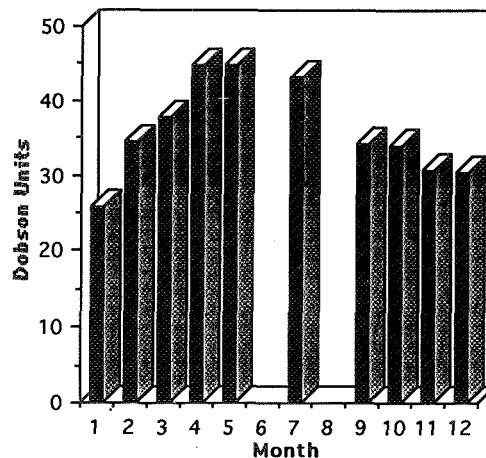


Figure 3. Monthly averages of tropospheric ozone residual column values in Dobson units (2.69×10^{16} molecules/cm²). Averaged over the three years of 1985-87. June and August missing due to insufficient data. Overall region covered is 20-50°N and 100-160°E.

ozone concentrations reach 60-70 ppb at elevations of 1000 (m) above Japan while above the Chinese continent values of 50 ppb can be seen.

5. CONCLUDING REMARKS

The production and transport characteristics of tropospheric ozone in East Asia is being comprehensively studied utilizing three different methods. Each methodology gives a different perspective of the phenomenon and together they are adding to our insight of the tropospheric ozone production, transport and destruction pathways. The

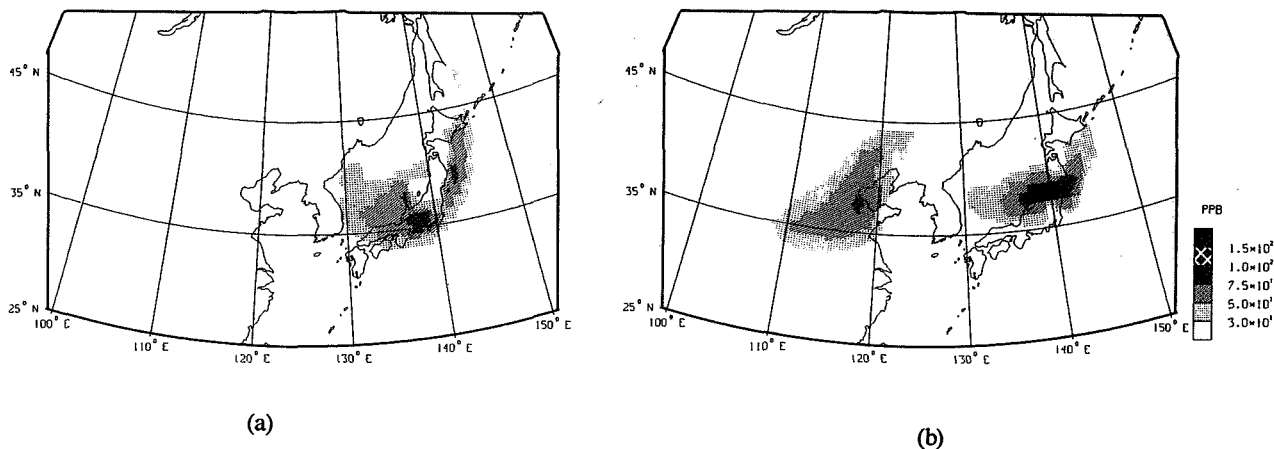


Figure 4. (a) Simulated results of surface ozone on 8 AM of May 11, 1987 (Day 4 of simulation). (b) Simulated results of surface ozone on 8 PM of May 11, 1987 (Day 4 of simulation).

continuous monitoring of background surface ozone in Japan is proving quite valuable and though the time span covered is too short to state conclusively, a uniform trend in either direction is not seen. Both downward transport of ozone-rich upper atmosphere air and accumulation and production of ozone and its precursors over the winter are possible explanations for the consistent spring peak in ozone concentration. However, the summer minimum is most likely brought about by dynamic influences of the southerlies dominating this season. Tropospheric column values show high values for the summer season along with the spring. The discrepancy in the summer may be caused by differences in dynamic regimes. Finally, preliminary simulations show that the model does a relatively good job in following the movement of pockets of elevated ozone concentrations. A more detailed and comprehensive simulation is currently under way. Also, a more rigorous statistical study of the satellite data is currently being conducted and results of an in-depth look into the surface ozone data is presented elsewhere (Sunwoo et al., 1992).

Acknowledgments

The authors wish to acknowledge the contributions made to this study by Dr. Hiromasa Ueda, Kyushu University. The satellite ozone data and the surface ozone data was obtained from the National Space Science Data Center, USA and the National Institute of Environmental Research, Japan. This research was supported in part by the NASA Global Change Fellowship Program and NASA Research Grant #NAGW-2428.

REFERENCES

- Carmichael, G.R., L. Peters, and T. Kitada. "A Second Generation Model for Regional-Scale Transport /Chemistry /Deposition", *Atmospheric Environment*. 20: 173-188 (1986)
- Fishman, J. and J.C. Larsen. "Distribution of Total Ozone and Stratospheric Ozone in the Tropics: Implications for the Distribution of Tropospheric Ozone", *Journal of Geophysical Research*. 92: 6627-6634 (1987)
- Fishman, J., C.E. Watson, J.C. Larsen, and J.A. Logan.

"Distribution of Tropospheric Ozone Determined from Satellite Data", *Journal of Geophysical Research*. 95: 3599-3617 (1990)

- Jacob, J.J. and S.C. Wofsy, "Photochemistry of biogenic emissions over the Amazon forest", *Journal of Geophysical Research*. 93:1477-1486 (1988)
- Liu, S.C., M. Trainer, F.C. Fehsenfeld, D.D. Parrish, E.J. Williams, D.W. Fahey, G. Hubler, and P.C. Murphy. "Ozone Production in the Rural Troposphere and the Implications for Regional and Global Ozone Distributions", *Journal of Geophysical Research*. 92: 4191-4207 (1987)
- Logan, J.A. "Ozone in the Rural Areas of the United States", *Journal of Geophysical Research*. 94: 8511-8532 (1989)
- Lurmann F.W., A.C. Loyd, and R. Atkinson, "A chemical mechanism for use in long-range transport/acid deposition computer modeling", *Journal of Geophysical Research*. 91:10905-10936 (1986)
- NIES (National Institute of Environmental Studies, Japan) Reports. "Studies on the Methods for Long-term Monitoring of Environmental Pollutants in the Background Regions and Atmospheric Pollutants on the Remote Island and Mountains: Concentrations and Variations, Research from the National Institute for Environmental Studies, Japan", #R-123. (1989)
- Ogawa, T. and A. Miyata. "Seasonal Behavior of the Tropospheric Ozone in Japan", in *Atmospheric Ozone*, Proceedings of the Quadrennial Symposium organized by the International Ozone Commission(IAMAP) held in Halkidiki, Greece, 3-7 September 1984, (C.S. Zerefos and A. Ghazi, ed.) D. Reidel Publishing Company, Boston pp. 754-758 (1985)
- Sunwoo, Y., G.R. Carmichael and H. Ueda. "Characteristics of Background Surface Ozone in Japan", submitted to *Atmospheric Environment*. (1992)
- Whelpdale, D.M. and J.L. Moody. "Large-Scale Meteorological Regimes and Transport Processes", in *The Long-Range Atmospheric Transport of Natural and Contaminant Substances*. (A.H. Knap, ed.) Kluwer Academic Publishers, pp. 3-36 (1990)

303/69

**SIMULATIONS OF ISOPRENE - OZONE REACTIONS
FOR A
GENERAL CIRCULATION/CHEMICAL TRANSPORT MODEL**

P. A. Makar and J.C. McConnell
CRESS, York University, Toronto, Canada, M3J 1P3

Abstract:

A parameterized reaction mechanism has been created to examine the interactions between isoprene and other tropospheric gas-phase chemicals. Tests of the parameterization have shown that its results match those of a more complex reaction set to a high degree of accuracy. Comparisons between test runs have shown that the presence of isoprene at the start of a six day interval can enhance later ozone concentrations by as much as twenty-nine percent. The test cases used no input fluxes beyond the initial time, implying that a single input of a biogenic hydrocarbon to an air mass can alter its ozone chemistry over a time scale on the order of a week.

Introduction:

Various studies (cf. Jacob and Wofsy, 1988, Trainer et al., 1987) have suggested that fluxes of terpenes such as isoprene may be responsible for enhanced ozone concentrations in the lower troposphere. The full reaction mechanisms for these gases are too complex for use in chemical transport models, due to the memory space required to store all species, and the computation time needed to predict future concentrations. The present work discusses the parameterization of one of these mechanisms (that of isoprene) into a simplified form. The effect of an initial input of isoprene on later ozone chemistry was studied as part of the parameterization process.

Constructing the Parameterization.

In the following discussion, reference will be made to three reaction sets; "no isoprene", "parameterization" and "full isoprene". The first is a simplified tropospheric reaction set, following Lurmann et al. (1986) and DeMore et al. (1990). The "full isoprene" set includes the no isoprene reactions and the detailed isoprene system of Lurmann et al. (1986), and incorporates some of the changes suggested by Jacob and Wofsy (1988). The "parameterization" is the simplified isoprene mechanism, designed to have the same effect on the simple troposphere as the full isoprene set, yet using fewer species to accomplish this goal. The parameterized reaction mechanism and its rates are given in Appendix I.

The parameterization was constructed by eliminating unimportant reaction pathways and lumping species with similar chemistry together. In summary, the changes were:

(1) Criegee - type radicals MVKO, MAOO, and MCRG were lumped together as "CREB". The products of the oxidation of CREB by NO were determined by adding the three oxidation reactions of CREB's components.

(2) Radicals MAN₂ and MVN₂ (produced via NO₃ oxidation of methacrolein and methyl vinyl ketone, respectively) were lumped together as "MBN₂". The

product coefficients for the subsequent reaction of MBN₂ with NO were derived by examining the amount of MBN₂ resulting from each of the methacrolein and methyl vinyl ketone paths.

(3) Radicals MRO₂ and VRO₂ (produced via OH reactions with MACR and MVK, respectively) were lumped together as "BRO₂", with product species and reaction coefficients adjusted as in step (2).

(4) The cycles for the natural acetyl nitrate species IPAN and MPAN were lumped together into the PAN cycle. The products leaving the cycle via oxidation of the lumped carbonate by NO are dependant on the concentrations of MACR and MVK. With this change, CH₃CHO and HOCH₂CHO are lumped as a single higher aldehyde, CH₃CO₃ and MAO₃ are similarly lumped, and the total acetyl-nitrate is the sum of PAN, IPAN, and MPAN concentrations. The reaction rates used were those of the normal PAN cycle, but the products and their coefficients were changed to reflect the new sources of total PAN.

(5) Product species IPN₄, MGLO, pyruvic acid and methyl acrylic acid were dropped from the parameterization, as were the reactions for the production of ozonides.

Numerical Tests of the Parameterization:

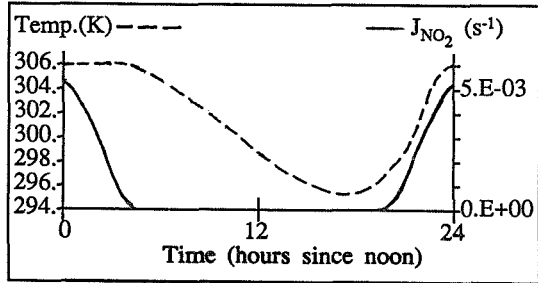
Nine test simulations were performed, each simulation spanning six days of diurnally varying photochemistry. No fluxes or deposition were allowed after the initial start-up of the box model. The initial conditions for these tests are given in Table 1. Most of the chemicals had the same initial concentration regardless of the test. The only species with different concentrations at the initial time were NO₂, NO, O₃, PAN, and isoprene. NO_x, ozone and PAN started at three levels, representing background, rural and polluted urban air. Isoprene was set at three levels. The combinations of the three NO_x scenarios with the three isoprene levels resulted in the nine test cases. Similarly, the level of NO_x and isoprene are the only possible causes of the differences between the simulations.

Reaction rates were calculated assuming sea-level pressures at the equator close to equinox. Photochemical rates were calculated using a detailed one-dimensional model (Henderson et al., 1987). The diurnal temperature profile and an example photochemical rate are given in Figure 1.

Simulations began at noon on the first day, with the noon-to-noon diurnal profile in rates repeating during the subsequent five days.

Two types of analysis were made with the resulting data. The effect of isoprene reactions on the model atmosphere were shown by comparing no isoprene and full isoprene simulations. The parameterization results were compared to the full isoprene results in order to gauge the usefulness of the former in simulating isoprene chemistry.

Figure 1. Temperature profile and J_{NO_2} .



Only a few species will be shown and discussed, due to the large amount of data resulting from these simulations and the limited space for this presentation. Researchers interested in obtaining the data files or plots of the results should contact the authors at the above address.

The O_3 results for each test are given in Fig. 2. Each graph shows the concentrations (ppbv) as functions of time, and are labeled according to the initial concentration scenario giving rise to the data. As can be seen from the graphs, the ozone concentration is enhanced by the addition of isoprene if the initial NO_x level is high or medium, and is depleted if the initial NO_x is low. The largest O_3 increase is for the case (high initial NO_x , high initial isoprene), in which the ozone maximum is 25 ppbv higher after the addition of isoprene (maximum of 83.8 ppbv without isoprene, and

108.3 ppbv with initial isoprene), an enhancement of 29%. The parameterization's O_3 values were within a few percent of those from the full isoprene mechanism for all test runs. The parameterization would appear to be suitable for O_3 simulations, with the caveat that ozone may be overpredicted by up to 5 ppbv.

The cause of the O_3 enhancements are explained via the relative steady state between O_3 and NO_x . Steady state ozone concentrations are roughly proportional to the ratio of NO_2 to NO ($O_3 \approx J_1 \cdot NO_2 / (k_{14} \cdot NO)$). Reactions that bias this NO_x ratio in favour of NO_2 therefore result in higher ozone concentrations.

Two processes cause such a bias. The first is the reaction of NO with RO_2 radicals to produce NO_2 . These radicals (RIO_2 , INO_2 , VRO_2 , MVN_2 , MRO_2 , and MAN_2) originate from isoprene's oxidation by OH and NO_3 . The reaction rates for the first hour of the "high NO_x - high Isoprene" scenario have shown that 43% of the net (positive) rate of change of NO_2 is due to production of NO_2 via the RO_2 reactions. The addition of isoprene causes the NO_2/NO ratio to move from 8.13 to 9.09.

This process is short-lived due to the rapid oxidation of isoprene and its product ketones within the first few hours of the simulation (example isoprene concentrations are given in Figure 3). This removes the source term for the RO_2 radicals. The second increase in O_3 , between hours 18 and 24 (6 am and noon) is due to the release of NO_2 from the cycles of peroxyacetyl nitrate (PAN), MPAN, and

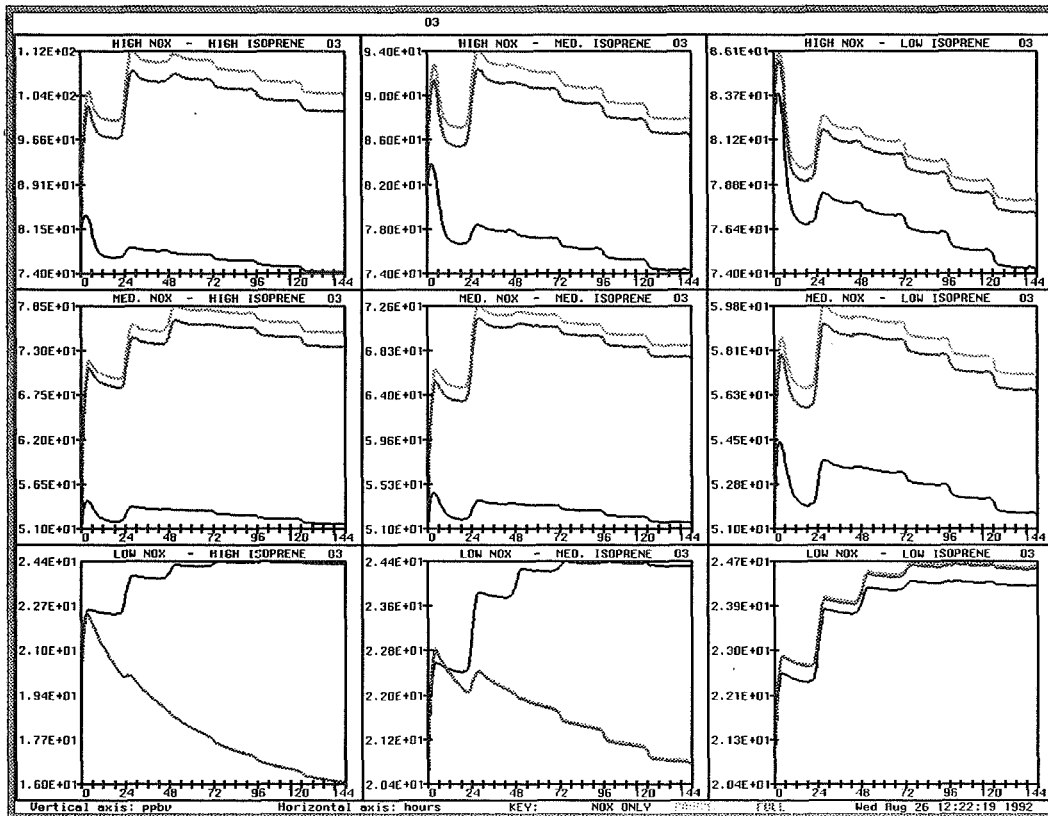


Figure 2. O_3 Concentrations, Nine test cases. Light grey, dark grey, and black lines correspond to parameterization, full isoprene, and no isoprene values, respectively.

IPAN. These species have very similar reaction chemistry (hence their combination in the parameterization); production is via reaction of a peroxyacetyl radical with NO_2 , and loss is via thermal dissociation of the compound back into NO_2 and the radical. The colder temperatures during the night (hours 6 to 18) thus resulted in a buildup of the PAN-type species. The increase of temperatures on the dawn of the second day caused the release of NO_2 stored during the night as PAN, MPAN and IPAN. These processes have a magnitude sufficient to account for the entire net rate of change of NO_2 at 11:30 am on the second day.

The enhancement of O_3 due to PAN-type compounds from isoprene oxidation has important implications with regards to ozone production far from the source region. For example, NO_x produced in a region of biomass burning (a high NO_x , high isoprene source region), if carried aloft a few kilometres (a temperature contrast equivalent to the day/night one used here) could be stored as PAN and related organic compounds. Later heating of the airmass far downwind from the source would result in strongly enhanced ozone. Such a mechanism may be responsible for the "Ozone high" in the troposphere over the South Atlantic, mentioned in other papers in these Proceedings.

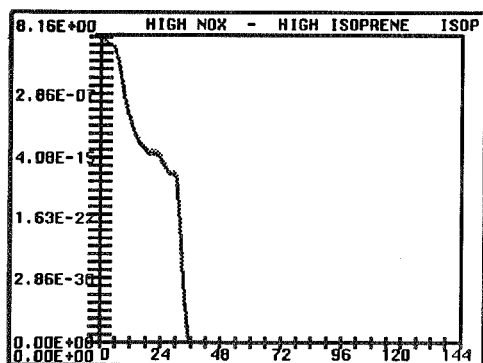


Figure 3. Isoprene Concentration, High NO_x - high isoprene. Light grey lines are parameterization results, dark grey are full isoprene mechanism.

The mechanism responsible for ozone depletion in the "low NO_x " simulations is that of removal by isoprene. Initial NO_x levels are sufficiently low so that the $(\text{RO}_2 + \text{NO})$ ozone source fails to compensate for the loss of ozone due to isoprene oxidation. During the first nightfall, isoprene removal of ozone dominates the other loss terms by about two orders of magnitude. Thereafter the curve describing ozone concentrations closely follows that of isoprene, with a gradual decrease in both species.

Total lumped PAN's for high NO_x - high isoprene are given in Figure 4. Total PAN has increased by about an order of magnitude for the high and medium NO_x scenarios. The increase is smaller for the low NO_x case, and almost non-existent for the case of low- NO_x , high-isoprene. The enhancement of total PAN's is due to the addition of the biogenic MPAN and IPAN to peroxyacetylnitrate. These species increase in concentration until the middle of the second day, when the concentrations of their ketone precursors have become depleted. The enhanced PAN cycle is one of the primary causes of the ozone enhancement noted above.

Methane, ethane and propane all have a "staircase" pattern of decreasing concentration (ethane is given as an example, Figure 5). The most rapid removal (steep parts of the steps) occurs during the day, when the oxidant, OH, is highest in concentration. The differences in the rate of alkane removal between isoprene and no isoprene cases thus reflect differences in OH concentrations. Ethane removal is enhanced by the addition of isoprene in the high and medium NO_x scenarios (ie. higher OH). In the low NO_x scenario, the addition of isoprene results in a decrease in the ethane removal rate (ie. lower OH). The OH values are a direct reflection of the NO_x changes discussed above. In the high NO_x - high isoprene case, daytime OH concentrations are enhanced by higher O_3 and thus higher $\text{O}(\text{D})$ values. In the low NO_x - high isoprene case, daytime OH is inhibited by removal by the as yet undepleted isoprene. At hour 24 for this scenario, the loss rate of OH due to isoprene alone is 4.2 times the combined loss rates due to CO and

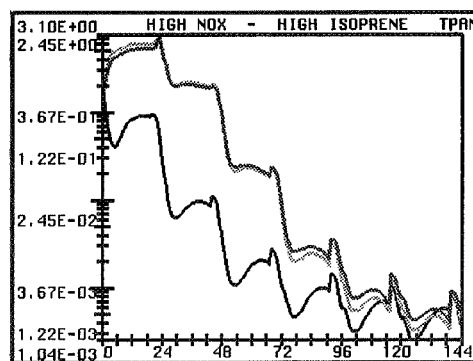


Figure 4. Total PAN (= PAN + MPAN + IPAN) Concentrations.

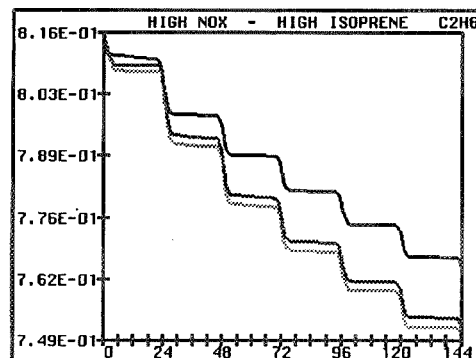


Figure 5. Ethane Concentrations.

CH_4 oxidation. When combined with the effects of its ketone products, methacrolein and methyl vinyl ketone, the isoprene-caused OH loss rate is 5.2 times the combined CO and CH_4 loss rate. In regions where the isoprene concentration is high (eg. close to the source) it will be the main chemical determining OH concentrations.

Formic acid values are given in Figure 5 (again, high NO_x - high isoprene is used as an example). The production of formic acid is greatly enhanced by the introduction of isoprene for all test cases. This is due to the addition of the cregee biradical CREA (CH_2O_2) as a source of formaldehyde.

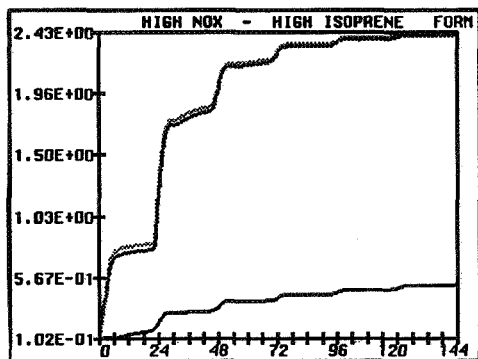


Figure 6. Formic Acid Concentrations.

Conclusions:

The isoprene parameterization derived in this work has been compared to a more detailed reaction mechanism, and has been found suitable for use in applications in which the number of chemicals are limited by computational memory and processing time. The parameterization uses 14 less species than the full mechanism, yet produces essentially the same results for the most important tropospheric gases.

The effect of isoprene on tropospheric chemistry depends on both the initial NO_x and isoprene levels. Ozone was found to either increase or decrease in concentration depending on the initial NO_x values. Increases were due to conversion of NO to NO_2 , with the causes of this conversion being RO_2 reactions with NO_x and release of NO_2 from PAN-type compounds. Similar effects were shown for the other species studied. The lack of deposition or sources after the initial time showed that the injection of isoprene into an air mass can have a long term effect on the chemistry of that air mass, long after the precursor hydrocarbon has been totally oxidized.

Table 1: Initial Concentrations

Species	Concentration (ppbv)	Concentration (molecules cm^{-3})
NO_2	0.1 / 3.0 / 8.0	0.25 / 7.4 / 20.0 ($\times 10^{10}$)
NO	0.02 / 1.0 / 1.8	0.05 / 2.5 / 4.4 ($\times 10^{10}$)
O_3	20. / 50. / 80.	50. / 125. / 200. ($\times 10^{10}$)
NO_3	0.04 pptv	10^6
N_2O_5	0.04 pptv	10^6
PAN	0.01 / 0.3 / 8.0	0.25 / 7.5 / 20. ($\times 10^9$)
HNO_2	0.2	$5.0 (\times 10^9)$
HNO_3	2.0	$5.0 (\times 10^{10})$
HNO_4	1.0 pptv	$2.5 (\times 10^7)$
CH_4	1.67 ppmv	$4.185 (\times 10^{13})$
HCHO	2.0	$5.0 (\times 10^{10})$
MCHO	0.5	$1.25 (\times 10^{10})$
MCO_3	0.04 pptv	10^6
MOOH	0.2	$5.0 (\times 10^9)$
MO_2	0.04 pptv	10^6
MO	0.04 pptv	10^6
CO	200	$5.0 (\times 10^{12})$
CO_2	343 ppmv	$8.575 (\times 10^{15})$
C_2H_6	0.8	$2.0 (\times 10^{10})$
C_2H_4	0.2	$5.0 (\times 10^{10})$
ETO ₂	0.04 pptv	10^6
H_2O_2	0.5	$1.25 (\times 10^{10})$
HO_2	0.04 pptv	10^6
OH	0.04 pptv	10^6
FORM	0.1	$2.5 (\times 10^{10})$
AHO ₂	0.04 pptv	10^6
O ^{(1)D}	$4.0 (\times 10^{-10})$	10^1
LOSS	$4.0 (\times 10^{-10})$	10^1
H_2O	1.5 %	$3.829 (\times 10^{17})$
O_2		$5.131 (\times 10^{18})$
M		$2.45 (\times 10^{19})$

Full Isoprene Mechanism Initial Conditions:

Species	Concentration (ppbv)	Concentration (molecules cm^{-3})
ISOP	0.5 / 3.1 / 8.2	1.23 / 7.50 / 20.0 ($\times 10^{10}$)
MACR	0.2	$5.0 (\times 10^{10})$
MVK	0.2	$5.0 (\times 10^{10})$
RIO_2	0.04 pptv	10^6
INO_2	0.04 pptv	10^6
MGGY	4 pptv	10^6
IPAN	4 pptv	10^6
MPAN	4 pptv	10^6
HAC	0.01	$2.5 (\times 10^9)$
PYRU	0.04 pptv	10^6
	(all remaining species, same as PYRU)	(all remaining species; MAAC, VRO ₂ , MAN ₂ , MVN ₂ , MRO ₂ , IPN ₂ , CREA, MVKO, MAOO, MCRG, MGLO, HACO, MAO ₃ , and OZID, start at 10^6 molecules cm^{-3} .)

Parameterization: ISOP, MACR, MVK, RIO₂, INO₂, MGGY, CREA are same as above. The radicals CREB, MBN₂, and BRO₂ all start at 10^6 molecules cm^{-3} . The lumped PAN has initial concentrations of 4.5×10^4 , 7.7×10^9 , and 2.02×10^9 molecules cm^{-3} , for low, medium and high NO_x scenarios. The lumped MCHO concentration is 1.275×10^{10} molecules cm^{-3} .

Appendix I: Reaction Mechanisms

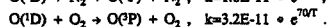
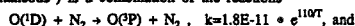
No Isoprene Reaction Mechanism	k_1	k_2	TYPE	SOURCE
1 $\text{NO}_2 + \text{hv} \rightarrow \text{NO} + \text{O}_3$			1	a
2 $\text{O}_3 + \text{hv} \rightarrow \text{O}(\text{D}) + \text{O}_2$			1	a
3 $\text{H}_2\text{O}_2 + \text{hv} \rightarrow 2 \text{OH}$			1	a
4 $\text{HCHO} + \text{hv} \rightarrow \text{H}_2 + \text{CO}$			1	a
5 $\text{HCHO} + \text{hv} \rightarrow 2 \text{HO}_2 + \text{CO}$			1	a
6 $\text{MOOH} + \text{hv} \rightarrow \text{MO} + \text{OH}$			1	a
7 $\text{N}_2\text{O}_5 + \text{hv} \rightarrow \text{NO}_2 + \text{NO}_3$			1	a
8 $\text{HNO}_3 + \text{hv} \rightarrow \text{OH} + \text{NO}_2$			1	a
9 $\text{MCHO} + \text{hv} \rightarrow \text{MO}_2 + \text{HO}_2 + \text{CO}$			1	a
10 $\text{NO}_3 + \text{hv} \rightarrow \text{NO} + \text{O}_2$			1	a
11 $\text{NO}_3 + \text{hv} \rightarrow \text{NO}_2 + \text{O}_3$			1	a
12 $\text{O}(\text{D}) + \text{M} \rightarrow \text{O}_3 + \text{M}$		special function	4	a
13 $\text{O}(\text{D}) + \text{H}_2\text{O} \rightarrow 2 \text{OH}$	2.2E-10		3	a
14 $\text{O}_3 + \text{NO} \rightarrow \text{NO}_2 + \text{O}_2$	2.0E-12	1.4E+03	2	a
15 $\text{O}_3 + \text{OH} \rightarrow \text{HO}_2 + \text{O}_2$	1.6E-12	9.4E+02	2	a
16 $\text{O}_3 + \text{HO}_2 \rightarrow \text{OH} + 2 \text{O}_2$	1.1E-14	5.0E+02	2	a
17 $\text{O}_3 + \text{NO}_2 \rightarrow \text{NO}_3 + \text{O}_2$	1.2E-13	2.45E+03	2	a
18 $\text{OH} + \text{H}_2\text{O}_2 \rightarrow \text{HO}_2 + \text{H}_2\text{O}$	2.9E-12	1.6E+02	2	a
19 $\text{OH} + \text{NO} \rightarrow \text{HNO}_2$		special function	4	b
20 $\text{OH} + \text{NO}_2 \rightarrow \text{HNO}_3$		special function	4	a
21 $\text{OH} + \text{HNO}_3 \rightarrow \text{NO}_3 + \text{H}_2\text{O}$		special function	4	a
22 $\text{OH} + \text{CO} \rightarrow \text{HO}_2 + \text{CO}_2$		special function	4	a
23 $\text{OH} + \text{CH}_4 \rightarrow \text{MO}_2 + \text{H}_2\text{O}$	2.3E-12	1.7E+03	2	a
24 $\text{OH} + \text{HCHO} \rightarrow \text{HO}_2 + \text{CO} + \text{H}_2\text{O}$	1.0E-11		3	a
25 $\text{OH} + \text{MOOH} \rightarrow \text{MO}_2 + \text{H}_2\text{O}$	3.8E-12	-2.0E+02	2	a
26 $\text{OH} + \text{MCHO} \rightarrow \text{MCO}_3 + \text{H}_2\text{O}$	6.9E-12	-2.5E+02	2	b
27 $\text{HO}_2 + \text{NO} \rightarrow \text{NO}_2 + \text{OH}$	3.7E-12	-2.4E+02	2	a
28 $\text{HO}_2 + \text{OH} \rightarrow \text{H}_2\text{O} + \text{O}_2$	4.8E-11	-2.5E+02	2	a
29 $2 \text{HO}_2 \rightarrow \text{H}_2\text{O}_2 + \text{O}_2$	2.3E-13	-6.0E+02	2	a
30 $\text{HO}_2 + \text{MO}_2 \rightarrow \text{MOOH} + \text{O}_2$	3.3E-13	-8.0E+02	2	a
31 $\text{HO}_2 + \text{MCO}_3 \rightarrow \text{LOSS}$	3.0E-12		3	b
32 $\text{HO}_2 + \text{NO}_2 \rightarrow \text{HNO}_4$		special function	4	b
33 $\text{NO}_2 + \text{NO}_3 \rightarrow \text{N}_2\text{O}_5$		special function	4	a
34 $\text{NO}_2 + \text{NO}_3 \rightarrow \text{NO} + \text{NO}_2 + \text{O}_2$	2.5E-14	1.23E+03	2	b
35 $\text{N}_2\text{O}_4 \rightarrow \text{NO}_2 + \text{NO}_3$		special function	4	b
36 $\text{NO}_3 + \text{NO} \rightarrow 2 \text{NO}_2$	8.0E-12	-2.5E+02	2	b
37 $\text{NO}_3 + \text{HCHO} \rightarrow \text{HNO}_3 + \text{HO}_2 + \text{CO}$	3.2E-16		3	b
38 $\text{NO} + \text{MO}_2 \rightarrow \text{NO}_2 + \text{MO}$	4.2E-12	-1.8E+02	2	b
39 $\text{NO}_2 + \text{MCO}_3 \rightarrow \text{PAN}$	4.7E-12		3	b
40 $\text{NO} + \text{MCO}_3 \rightarrow \text{MO}_2 + \text{CO}_2 + \text{NO}_2$	4.2E-12	-1.8E+02	2	b
41 PAN $\rightarrow \text{MCO}_3 + \text{NO}_2$	1.95E+16	9.0E+02	2	a
42 $\text{MO} + \text{O}_3 \rightarrow \text{HCHO} + \text{HO}_2$	3.94E-14	9.0E+02	2	a
43 $\text{N}_2\text{O}_5 + \text{H}_2\text{O} \rightarrow 2 \text{HNO}_3$	1.3E-21		3	b
44 $\text{C}_2\text{H}_6 + \text{OH} \rightarrow \text{ETO}_2 + \text{H}_2\text{O}$	1.7E-11	1.232E+03	2	b
45 $\text{ETO}_2 + \text{NO} \rightarrow \text{MCHO} + \text{HO}_2 + \text{NO}_2$	4.2E-12	-1.8E+02	2	b
46 $2 \text{ETO}_2 \rightarrow 1.6 \text{MCHO} + 1.2 \text{HO}_2$	5.0E-14		3	b
47 $\text{ETO}_2 + \text{HO}_2 \rightarrow \text{LOSS}$	3.0E-12		3	b
48 $\text{C}_2\text{H}_6 + \text{OH} \rightarrow \text{ETO}_2$	1.18E-11	6.79E+02	2	b
49 MCHO $+ \text{NO}_3 \rightarrow \text{MCO}_3 + \text{HNO}_3$	1.4E-12	1.9E+03	2	a
50 $\text{HNO}_4 \rightarrow \text{NO}_2 + \text{HO}_2$		special function	4	b
51 $\text{HNO}_4 + \text{hv} \rightarrow \text{NO} + \text{OH}$	0.205 x	J(NO ₂)	1	b
52 $\text{HCHO} + \text{HO}_2 \rightarrow \text{AHO}_2$	1.0E-14		3	b
53 $\text{AHO}_2 + \text{NO} \rightarrow \text{FORM} + \text{HO}_2 + \text{NO}_2$	4.2E-12	-1.8E+02	2	b
54 $\text{AHO}_2 + \text{HO}_2 \rightarrow \text{FORM} + \text{H}_2\text{O} + \text{O}_2$	2.0E-12		3	b
55 $2 \text{AHO}_2 \rightarrow 2 \text{FORM} + 2 \text{HO}_2 + 2 \text{O}_2$	1.0E-13		3	b
56 $\text{FORM} + \text{OH} \rightarrow \text{HO}_2 + \text{H}_2\text{O} + \text{CO}_2$	3.2E-13		3	b

Comments:

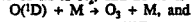
- (1) Photolysis rates from detailed model results at 0 km (see text).
- (2) Temperature dependant rates, $k = k_1 \times \exp(-k_2/T)$, T = temp. in K.
- (3) Constant rates.

(4) Special functions for given reactions:

(12) The reaction $O(^1D) + M \rightarrow O(^3P) + M$ (the products are actually $O(^3P) + M$, but the conversion to O_3 is assumed to be "instantaneous") is a combination of the reactions



If 80 % of M is N_2 and 20 % is O_2 , then the net reaction is



$$k_{net} = 1.44E-11 \cdot e^{-1107/T} + 6.4E-12 \cdot e^{-707/T}$$

$$(19) \quad k = \left(\frac{A \cdot T^B \cdot [M]}{1 + A \cdot T^B \cdot [M]} \right) \cdot 0.6 \left(1 + \left(\frac{A \cdot T^B \cdot [M]}{C \cdot T^D} \right)^2 \right)^{-1}$$

$$A = 1.0E-22, B = -3.3, C = 9.0E-09, D = -1.0$$

$$(20) \quad k = \left(\frac{A \cdot [M]}{1 + A \cdot [M]} \right) \cdot 0.6 \left(1 + \left(\frac{A \cdot [M]}{B} \right)^2 \right)^{-1}$$

$$A = 2.6E-30 \cdot (T/300)^{-3.2}, B = 2.4E-11 \cdot (T/300)^{-1.3}$$

$$(21) \quad k = A + \frac{C \cdot [M]}{1 + C \cdot [M]}, \quad A = 7.2E-15 \cdot \exp(-785/T),$$

$$B = 4.1E-16 \cdot \exp(1440/T), C = 1.9E-33 \cdot \exp(725/T).$$

$$(22) \quad k = 1.50E-13 \cdot (1 + 0.6 \cdot [M] \cdot T \cdot 1.36E-16 / 1.013E+06)$$

$$(32) \quad k = \left(\frac{6.9E-33 \cdot [M] \cdot e^{1007/T}}{1 + 4.86E-12 \cdot [M] \cdot e^{1007/T}} \right)$$

(33) (same formula as reaction 20),

$$A = 2.2E-30 \cdot (T/300)^{-3.2}, B = 1.5E-12 \cdot (T/300)^{-0.5}$$

$$(35) \quad k = k_{33} \cdot 7.5E+26 \cdot (300/T)^{0.32} \cdot e^{-110807/T}$$

$$(50) \quad k = (4.9E-06 \cdot [M] \cdot \exp(-10015/T)) / (1 + 4.86E-12 \cdot [M]^{0.61})$$

In the above, [M] is the total number density in molecules cm^{-3} , and T is the temperature in degrees Kelvin.

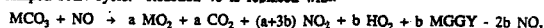
Sources: (a) DeMore et al, 1990, (b) Lurmann et al., 1986

Parameterization Reactions:

57	ISOP + O ₃	→ 0.5 HCHO + 0.2 MVK + 0.30 MACR + 0.2 CREA + 0.06 HO ₂ + 0.5 CREB	7.0E-15	1.9E+03	2
58	MVK + O ₃	→ 0.5 HCHO + 0.2 CREA + 0.21 HO ₂ + 0.2 CREB + 0.15 MCHO + 0.5 MGGY	4.0E-15	2.0E+03	2
59	MACR + O ₃	→ 0.5 HCHO + 0.2 CREA + 0.21 HO ₂ + 0.15 MO ₂ + 0.5 MGGY	4.4E-15	2.5E+03	2
60	ISOP + OH	→ RIO ₂	1.5E-11	-5.0E+02	2
61	RIO ₂ + NO	→ 0.9 NO ₂ + 0.45 MVK + 0.45 MACR + 0.9 HO ₂ + 0.9 HCHO	4.2E-12	-1.8E+02	2
62	INO ₂ + NO	→ 2.0 NO ₂ + HCHO + 0.5 MVK	4.2E-12	-1.8E+02	2
63	INO ₂ + NO ₂	→ LOSS	4.2E-13	-1.8E+02	2
64	ISOP + NO ₂	→ INO ₂	3.23E-13		3
65	CREA + H ₂ O	→ FORM + H ₂ O	4.0E-18		3
66	CREA + NO	→ HCHO + NO ₂	7.0E-12		3
67	CREA + NO ₂	→ HCHO + NO ₂	7.0E-13		3
68	CREB + H ₂ O	→ LOSS + H ₂ O	4.0E-18		3
69	CREB + NO	→ 0.33 MVK + 0.33 MACR + 0.33 MGGY + NO ₂	4.2E-12	-1.8E+02	2

70	CREB + NO ₂	→ 0.33 MVK + 0.33 MACR + 0.33 MGGY + NO ₂	4.2E-13	-1.8E+02	2
71	RIO ₂ + HO ₂	→ LOSS	3.0E-12		3
72	INO ₂ + HO ₂	→ LOSS	3.0E-12		3
73	MACR + NO ₂	→ MBN ₂	6.7E-15		3
74	MVK + NO ₂	→ MBN ₂	6.0E-14		3
75	MBN ₂ + NO	→ 2.0 NO ₂ + 0.45 MCO ₃ + 0.55 MGGY + HCHO + 0.45 HO ₂	4.2E-12	-1.8E+02	2
76	MACR + NO ₂	→ MCO ₃ + HNO ₃	3.3E-15		3
77	MGGY	→ MCO ₃ + HO ₂	0.15	xJ(NO ₂)	
78	MGGY + OH	→ MCO ₃	1.7E-11		3
79	MACR + OH	→ BRO ₂	3.86E-12	-5.0E+02	2
80	MACR + OH	→ MCO ₃	1.02E-11		
81	MVK + OH	→ BRO ₂	3.0E-12	-5.0E+02	2
82	BRO ₂ + HO ₂	→ LOSS	3.0E-12		3
83	BRO ₂ + NO	→ 0.9 NO ₂ + 0.625 HO ₂ + 0.625 HCHO + 0.625 MGGY + 0.275 MCO ₃ + 0.275 MCHO	4.2E-12	-1.8E+02	2
84	MBN ₂ + HO ₂	→ LOSS	3.0E-12		3

Comments: (1) The first 56 reactions are those of the "No Isoprene" set, with the exception of reaction 40, which has been altered to reflect the lumped PAN cycle. Reaction 40 is replaced with:



$$b = \frac{k_{74}(MACR)(NO_2) + k_{75}(MACR)(OH)}{(k_{74}(NO_2) + k_{75}(OH))(MACR) + (k_{79}(NO_2) + k_{76}(OH))(MCHO) + 0.15 k_{78}(MVK)(O_3) + (0.45 k_{73}(MBN_2) + 0.275 k_{83}(BRO_2))(NO) + (k_{77} + k_{78})(MGGY)}$$

and $a = 1.0 - b$. In the parameterization, "MCO₃", "MCHO", and "PAN" refer to the lumped peroxyacetyl radical, lumped higher aldehyde and lumped acetyl nitrate species, respectively.

(2) Temperature dependant rates: $k = k_0 \exp(-k_a/T)$, T = temperature in degrees K.

(3) Constant rates.

REFERENCES

- DeMore, W.B., S.P. Sander, D.M. Golden, M.J. Molina, R.F. Hampson, M.J. Kurylo, C.J. Howard, A.R. Ravishankara, 1990: Chemical Kinetics and Photochemical Data for Use in Stratospheric Modelling. J.P.L. Publication 90-1, 1990, Jet Propulsion Laboratories, California Institute of Technology, Pasadena, California.
- Henderson, G.S., W.F.J. Evans, J.C. McConnell and E.M.J. Templeton, 1987: A Numerical Model for One Dimensional Simulation of Stratospheric Chemistry. Atmosphere - Ocean, 25, 427 - 459.
- Jacob, D.J., and S.C. Wofsy, 1988: Photochemistry of Biogenic Emissions Over the Amazon Forest. J. Geophys. Res., 93, D4, 1,477 - 1,486.
- Lurmann, F.W., A.C. Lloyd, and R. Atkinson, 1986: A Chemical Mechanism for Use in Long-Range Transport/Acid Deposition Computer Modeling. J. Geophys. Res., 91, D10, 10,905 - 10,936.
- Trainer, M., E.Y. Hsieh, S.A. McKeen, R. Tallamraju, D.D. Parrish, F.C. Fehsenfeld, and S.C. Liu, 1987: Impact of Natural Hydrocarbons on Hydroxyl and Peroxy Radicals at a Remote Site. J. Geophys. Res., 92, D10, 11,879 - 11,894.

308171

**OZONE FORMATION DURING AN EPISODE OVER EUROPE :
A 3-D CHEMICAL/TRANSPORT MODEL SIMULATION**

Terje Berntsen and Ivar S. A. Isaksen

Institute of Geophysics,
University of Oslo,
P.O.Box 1022, Blindern,
N-0315 Oslo, Norway

ABSTRACT

A 3D regional photochemical tracer/transport model for Europe and the Eastern North Atlantic has been developed based on the NASA/GISS CTM. The model resolution is 4x5 degrees latitude and longitude with 9 layers in the vertical (7 in the troposphere). Advective winds, convection statistics and other meteorological data from the NASA/GISS GCM are used. An extensive gas-phase chemical scheme based on the scheme used in our global 2D model has been incorporated in the 3D model. In this work ozone formation in the troposphere is studied with the 3D model during a 5 day periode starting June 30. Extensive local ozone production is found and the relationship between the source regions and the downwind areas are discussed. Variations in local ozone formation as a function of total emission rate, as well as the composition of the emissions (HC/NO_x ratio and isoprene emissions) are elucidated. An important vertical transport process in the troposphere is by convective clouds. The 3D model includes an explicit parameterization of this process. It is shown that this process has significant influence on the calculated surface ozone concentrations.

1 Introduction

Ozone formation in the troposphere over Europe and other industrialized regions leading to ambient concentrations well above health standards during perodes with high pressure weather situations, is now a well established fact (Guicherit; 1988). The increase is observed at urban as well as rural locations. Measurements (Kley et al.; 88) show that typical ozone values have increased from 5-15 ppbv at turn of the century, to 30-40 ppbv at present most probably due to increased man made emissions of NO_x and hydrocarbons.

Several model studies have been performed to study this effect. This include box models, 1D and 2D eulerian models. Up to recently, lack of computer resources has put severe restrictions on the chemical scheme as well as the area and resolution of the models. The approach has been either to do regional studies with rather comprehensive chemical schemes (Chang et al.; 87), or global studies with simpler schemes (Crutzen and Zimmermann ; 91). This paper presents results from a 3D model with an extensive chemical scheme covering an area from 25°W to 55°E and 24°N to 76°N. The model is intended to be extended to a global scale after development and testing on less computer costly scales.

2 Model description

2.1 Transport

The model was originally developed by Prather et al.(87) to simulate global distribution and temporal variability of CFCs. As consistent global data sets with real-time meteorological data from numerical weather prediction models are not available, the model is set up to use data from the free running NASA/GISS general circulation model (GCM).

In this study calculations are done for a European "window" (25°W to 55°E and 24°N to 76°N) with a resolution of 5° longitude and 4° latitude. In the vertical there are 9 layers (σ -coordinates, $\sigma = (P - P_T)/(P_s - P_T)$) between the surface and 10 hPa. Table 1 gives the vertical resolution.

σ	1.0	.95	.87	.73	.55
P (hPa)	984	934	854	720	550
Z (km)	0.0	0.5	1.2	2.7	4.9
σ	0.39	0.25	0.14	0.061	0.0
P (hPa)	390	255	150	70	10
Z (km)	7.4	10.3	13.7	18.5	31.2

Table 1: *Horizontal boundaries of the 9 layers in the model. P_s = 984 hPa is the mean surface pressure in the GCM.*

The meteorological data consist of 4 hour integrated values of horizontal mass fluxes and surface pressure, total optical depth, surface precipitation and number of convective events (see Prather et al.;87). Temperature, humidity, precipitation (from cumulus convection and large scale precipitation) are given as 5 day averages from the GCM. Tracer transport due to convection is calculated by a mass flux scheme which divide the convection into three classes (dry, moist/shallow and moist/deep).

The advection of tracers are solved numerically by the method of conservation of second order moments (Prather; 86). A timestep of one hour is applied in calculation of the advective transport.

2.2 Chemistry

The model has been expanded to include an extended ozone chemistry scheme. It includes a gas-phase chemistry with first order scavenging of water soluble species. The scheme follows the basic pattern of the scheme developed for use in our global 2D model (Isaksen and Hov; 87), with recent updates of reaction mechanisms and rates according to IUPAC (89),

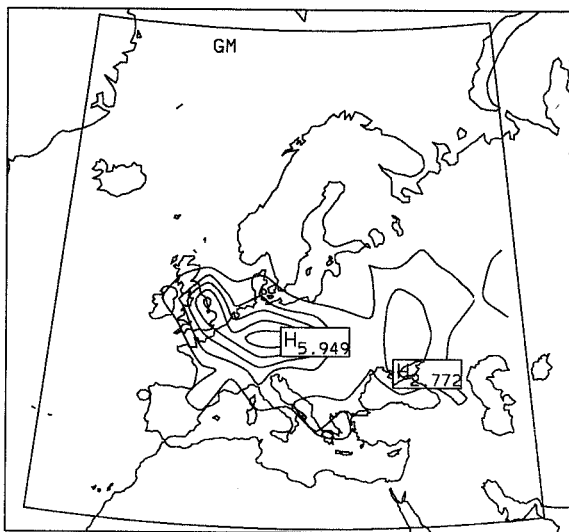


Figure 1: Relative distribution of NO emissions. Numbers give percentage pr. grid square of the total NO-emission which is 9.35 Tg/y as NO.

NASA/JPL (90) and Atkinson (90). The scheme includes 45 components, 16 photolytical reactions and 91 thermal reactions. The quasi steady state approximation (QSSA) of Hesstvedt et al. (78) is applied to solve the scheme, with a timestep of one hour.

Photolysis rates are calculated by the two-stream approximation method of Isaksen et al. (77) with corrections for diffusive scattering (Jonson and Isaksen ; 91) for a clear sky situation. Modifications of photolysis rates due to clouds are calculated according to the parameterization given by Chang et al.(87). To run a 5 day simulation on a DEC-station 5000/200 takes about 45 minutes CPU-time.

2.3 Emissions

Reasonable emission rates of primary pollutants are crucial if the model shall be able to simulate the real atmosphere. Table 2 gives the emission rates of the primary pollutants (except isoprene). Emission rates and geographical distribution of NO_x and hydrocarbons are derived on the basis of data from EMEP (D.Simpson,private com.) and EPA (Watson et al.;91). In the EMEP data hydrocarbon emissions are given as total man made VOC, while the EPA data divide the VOC emissions into groups such as paraffins, olefins, aromats, etc., but on a much courser grid (10° × 10°). The total VOC emissions were therefore taken from EMEP, while the spieciation was done according to the EPA data. However there was considerable differences between the total emission rates in the two sets of emission data, which means that this is a very significant source to uncertainties in the results. Fig. 1 and 2 show the relative distribution of NO and C₂H₆ emissions applied in the model. In this study no daily variation in the emissions are included (except for isoprene), nor any emissions from sources above the ground (airplanes and lightning).

Isoprene emissions are parameterized as a function of sunlight, surface temperature and deciduous forest cover according to Lubkert and Schopp (1989) and Veldt (1988):

$$E(\text{kg}/\text{h} * \text{km}^2) = 10^{(0.1 * T_s - 2.15)}$$

E is the hourly emission rate of isoprene in kg km⁻² h⁻¹ during

NO	NO ₂	CO	C ₂ H ₆	C ₄ H ₁₀
9.4	0.44	124.0	10.9	6.5
C ₆ H ₁₄	C ₂ H ₄	C ₃ H ₆	m-Xylene	HCHO
4.3	4.4	1.9	4.5	0.67

Table 2: Total emission rates applied in the model (except for isoprene). All values are in Tg/y of the emitted species.

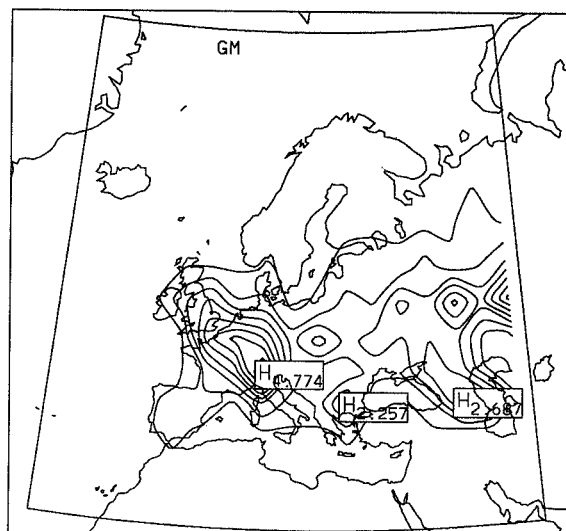


Figure 2: Relative distribution of C₂H₆ emissions. Numbers give percentage pr. grid square of the total C₂H₆-emission which is 10.9 Tg/y.

daytime, and T_s is the ambient temperature in deg. C.

The data from the NASA/GISS GCM only include 5 day averaged temperatures, so a daily variation in the surface temperature (T_s) as a function of the local time (lt), with an amplitude of 10 deg. C has been included

$$T_s = 5.0 * \text{SIN}(\text{MOD}((lt + 24 - 10), 24) * 2\pi/24.0) + T(\text{GCM})$$

Fig. 3 shows the calculated relative distribution of isoprene emissions at 15 GMT. The very pronounced maximum results from a combination of very dense forest cover and high surface temperature during the 5 day period. As isoprene emissions are highly uncertain this maximum can at least serve as sensitivity test of the impact of biogenic emissions.

2.4 Boundary conditions and initialization

With such a limited model area, the results will be very sensitive to the fluxes across the vertical boundaries of the model.

The boundary concentration of the species are obtained from results from a 2D channel model (Solberg et al.; 89) covering a zonal band between 30°N and 60°N, and a 2D zonally averaged global model (Isaksen and Hov; 87). The results from the channel model are distributed latitudinally according to the relative latitudinal distribution in the 2D global model to obtain a 3D distribution wich can be used to initiate the model, and as boundary conditions. To account for the possibility of a polluted air mass being transported out of the model area and back

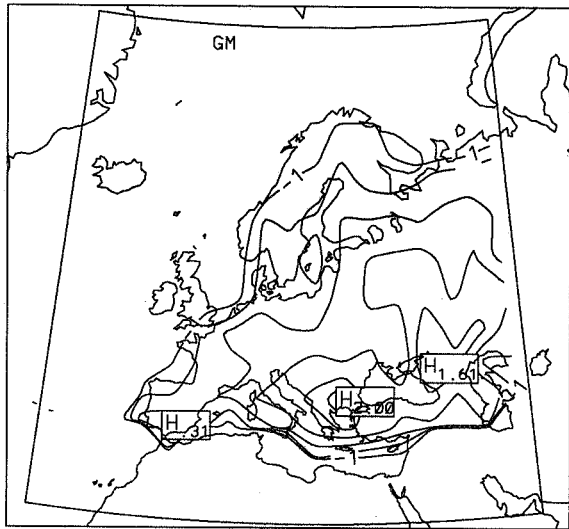
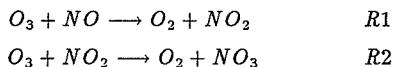


Figure 3: Relative distribution (%) at 15 GMT of the surface flux of isoprene. Numbers are on logarithmic scale relative to the grid cell with largest flux ($2.9 \cdot 10^{11}$ molec/($\text{cm}^2 \text{ s}$))

again due to a sudden shift in the wind direction, the boundary concentrations approach the upwind concentrations during out-flow and return to the original concentrations during a 12 hour relaxation period.

3 Results

The model has been run for a 5 day period starting at midnight GMT June 30. Fig. 4 shows the calculated surface concentration of ozone at 13 GMT the 5th day of the simulation. There is a broad maximum of about 70 ppbv over Northwestern Europe and the British Isles, and a secondary maximum over Eastern Europe. Earlier in the day the maximum is shifted towards the east with maximum values at about the same level (table 3) Fig. 5 shows the calculated ozone concentrations (mean of the two lowest layers in the model) at 4 different locations during the 5 day period. In the main source regions ozone concentrations show a very pronounced diurnal variation with a maximum concentration occurring usually before noon. The most important reason for the night time reduction is surface deposition ($\geq 50\%$ of the loss) and reactions with NO_x ($R1 \approx 20\%$ and $R2 \approx 25\%$ in the regions with large NO_x emissions).



The maximum surface concentration is very sensitive to the ventilation of the boundary layer through convective transport. As convective transport is only calculated every 4th hour, primary pollutants and their products (ozone, PAN etc.) are allowed to build up during the intervals between the convective events. This effect might give rise to regular over and under predictions, especially in the lowest layer of the model.

The surface ozone concentration and in particular the daily maximum is to a large degree determined by the composition of the emissions. To analyse the sensitivity of the model to variations in the emission rates and composition, several perturbations have been performed. Table 3 shows the maximum ozone concentration during the 5th day of the simulation at 4 locations. The locations were chosen to represent typical source regions.

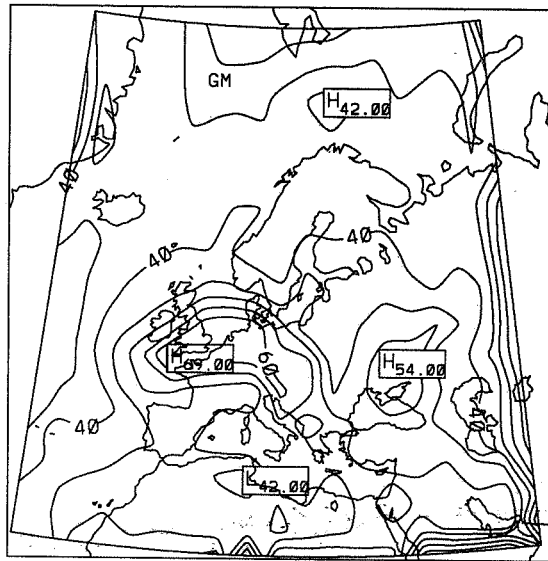
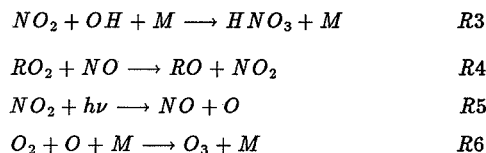


Figure 4: Calculated surface concentration (ppbv) of ozone at 13 GMT on 5th day of the simulation.

Over Western Europe, represented in fig.5 and table 3 by the grid cell located at 50°N and 5°E , NO_x emissions are large and the potential for further photochemical ozone production if NO_x emissions increase is low. In some cases it might even be negative, because reaction R1 followed by R3 consumes O_3 (and OH) faster than it is produced by R4-R6. The limiting factor for ozone production is then the abundance of RO_2 radicals (organic peroxy radicals and HO_2) which is produced by oxidation of hydrocarbons and CO by the OH radical.



In a region with a larger fraction of hydrocarbons in the emissions (42°N , 25°E) there is a large potential for further ozone production if NO_x emissions are increased. In this gridcell surface NO_x concentration stay around 0.5 ppbv during the periode from 10 am to 8 pm, while at the more polluted area over the Netherlands the corresponding NO_x concentration is around 2.5 ppbv. Table 3 shows that an increase of 50% in the NO_x emissions gives rise to an increase in the calculated surface ozone of 15%.

Over Eastern Europe (50°N , 25°E) the ratio HC/NO_x in the emissions are higher than in the west. It is therefore a potential for further ozone production if NO_x emissions are increased. A 13% increase in daily maximum ozone at the surface is calculated for a 50% increase in the NO_x emissions.

At the Scandinavian site (62°N , 15°E) there are small diurnal variations in the ozone concentration after the first day, and the concentration is virtually insensitive to the various perturbations of the emissions. Analysis show that there is net in situ loss of ozone all the time during this periode, and a steady-state situation between the local loss processes and transport is established within a few days. However this probably points to an underestimation of the emissions of precursors in this region as observations show evidence of significant ozone production at Scandinavian stations (Grennfeldt et al.,87).

Perturbation	O ₃ (ppb) at (°N, °E)			
	50,5	42,25	50,35	62,15
Reference	65	79	56	38
CH ₄ conc. = 0	61	78	55	38
Isoprene em. = 0	64	61	55	38
NMHC em. * 2	74	83	66	39
NO _x em. * 1.5	65	90	63	38
NO _x em. * 0.5	63	65	56	38

Table 3: Maximum calculated concentration of ozone (ppbv) in the lowest level during the 5 th day at 4 locations.

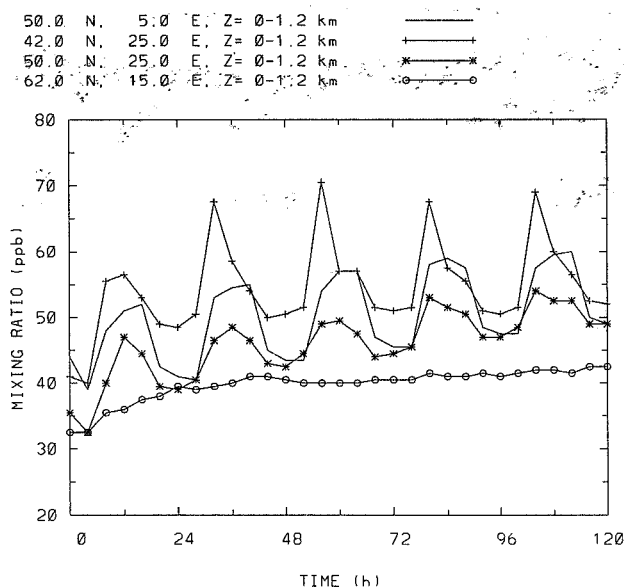


Figure 5: Calculated time development of ozone in the two lowest layers ($Z \approx 0-1.2$ km) at four locations during the 5 day simulation.

4 Conclusion

We have developed a 3D chemical tracer model based on the NASA/GISS CTM (Prather et al.; 87) for an extended European region with a comprehensive chemical scheme developed to study formation of photochemical oxidants. The model has been run for a 5 day period in the beginning of July, and the results are in general agreement with observations of ozone typical for this time of the year. Several perturbations have been performed, and the sensitivity of the model is consistent with other model studies. With some refinements of the model (especially with respect to convection) and improvement of the emission database, the model should be well suited to study the processes governing the formation of photochemical oxidants on regional scales.

Acknowledgement

This project was supported by BP-Norway Limited U.A. Contract No. C-550088-1-AL.

5 References

- Atkinson R., D.L. Baulch, R.A. Cox, R.F. Hampson Jr., J.A. Kerr and J. Troe Evaluated kinetic and photochemical data for atmospheric chemistry: Supplement III, *J. Phys. Chem. Ref. Data* 18, pp 881-1097, 1989.
- Atkinson R. Review article: Gas-phase chemistry of organic compounds: a review. *Atmos. Environment* Vol. 24A, No. 1, pp 1-41, 1990.
- Chang J.S., R.A. Brost, I.S.A. Isaksen, S. Madronich, P. Middleton, W.R. Stockwell and C.J. Walcek A three-dimensional acid deposition model; Physical concepts and formulation. *J. Geoph. Res.* Vol. 92, No. D12, pp. 14,861-14,700, 1987.
- Crutzen P.J. and P.H. Zimmermann The changing photochemistry of the troposphere *Tellus*, Vol 43 A, pp.136-151, 1991.
- Grennfeldt P., J. Saltbones and J. Schjoldager Oxidant data collection in OECD-Europe 1985-1987 (OXIDATE). NILU report, OR 22/87, Lillestrøm, Norway, 1987.
- Guicherit R. Ozone on an urban and regional scale, with special reference to the situation over the Netherlands. *Tropospheric ozone*.(ed.Isaksen I.S.A.). NATO ASI Series C, vol.227, pp.49-63, D.Reidel Publishing Company, Dordrecht, 1988.
- Hesstvedt E., Ø Hov and I.S.A. Isaksen Quasi steady-state approximation in air pollution modelling: Comparison of two numerical schemes for oxidant prediction. *Int. Journal of Chem. Kinetics*, Vol X, pp 971-994, 1978.
- Isaksen I.S.A., K.H. Midtbø, J. Sunde and P. Crutzen A simplified method to include molecular scattering and reflection in calculations of photon fluxes and photodissociation rates. *Geophysica Norvegica* Vol. 31, No. 3, 1977.
- Isaksen, I.S.A. Ø. Hov Calculations of trends in the tropospheric concentrations of O₃, OH, CO, CH₄ and NO_x. *Tellus*, Vol 39B, pp.271-283, 1987.
- Jonson J.E. and I.S.A. Isaksen The impact of solar flux variations on the tropospheric ozone chemistry. *Institute report no. 81 Inst. for Geophysics, University of Oslo*, 1991.
- Kley D., A. Volz og Mülheims F. Ozone measurements in historic perspective. *Tropospheric ozone*.(ed.Isaksen I.S.A.). NATO ASI Series C, vol.227, pp.63-72, D.Reidel Publishing Company, Dordrecht, 1988.
- Lubkert B. and W. Schopp A model to calculate natural VOC emissions from forests in Europe. *International Institute for applied system analysis*. Working paper WP-89-082.
- Prather M. Numerical advection by conservation of second-order moments. *J. Geoph. Res.* Vol. 91, No. D6, pp 6671-6681, May 1986.
- Prather M., M. McElroy, S. Wofsy, G. Russel and D. Rind Chemistry of the global troposphere: fluorocarbons as tracers of air motion. *J. Geoph. Res.* Vol. 92, pp 6579-6613, 1987.
- S.Solberg, I.S.A. Isaksen and R.B. Chatfield Design of a channel model to assess mid-latitude pollution effects. *Proceedings of International Ozone Symposium 1988*. pp 548-551, A. Deepak publ., Virginia, USA, 1989.
- Veldt C. Inventing natural VOC emissions for the CONAIR project. *TNO-report 88-275*, 1988.
- Watson R.T., M.J. Kurylo, M. Prather and F.M. Ormond Present state of knowledge of the upper atmosphere 1990: An assessment report. *NASA reference publication*, 1242, Sept. 1990.
- Watson J.J., J.A. Probert, S.D. Piccot, J.W. Jones Global inventory of volatile organic compound emissions from anthropogenic sources. *EPA-report EPA-600/8-91-002*, 1991.

303/73

ESTIMATES OF THE CHANGES IN TROPOSPHERIC CHEMISTRY WHICH RESULT FROM HUMAN ACTIVITY AND THEIR DEPENDANCE ON NO_x EMISSIONS AND MODEL RESOLUTION

Maria Kanakidou

Centre des Faibles Radioactivités, Laboratoire mixte CNRS/CEA, Domaine du CNRS, F-91198 Gif-sur-Yvette Cedex, France.

Paul J. Crutzen and Peter H. Zimmermann

Max Planck Institute for Chemistry, Atmospheric Chemistry Division, P.O.Box 3060, D-6500 Mainz, Germany.

ABSTRACT

As a consequence of the non-linear behavior of the chemistry of the atmosphere and because of the short lifetime of nitrogen oxides (NO_x), two-dimensional models do not give an adequate description of the production and destruction rates of NO_x and their effects on the distributions of the concentration of ozone and hydroxyl radical.

In this study, we use a three-dimensional model to evaluate the contribution of increasing NO_x emissions from industrial activity and biomass burning to changes in the chemical composition of the troposphere. By comparing results obtained from longitudinally-uniform and longitudinally-varying emissions of NO_x, we demonstrate that the geographical representation of the NO_x emissions is crucial in simulating tropospheric chemistry.

1. INTRODUCTION

The impact of anthropogenic trace gas emissions on ozone (O₃) and hydroxyl radical (OH) concentrations and generally on the oxidizing efficiency of the troposphere is a matter of great concern. There have been many modeling efforts devoted to simulating tropospheric chemistry and examining trends in the atmospheric concentrations of important trace gases (e.g. Isaksen and Hov, 1987; Crutzen and Zimmermann, 1991). However, the ability of models to adequately account for non-linear chemical interactions affecting the distributions of nitrogen oxides (NO_x), O₃ and OH needs to be examined carefully.

In this study, we use a three-dimensional model to evaluate the contribution of increasing NO_x emissions from industrial activity and biomass burning to changes in the

chemical composition of the troposphere. By comparing results obtained from longitudinally-uniform and longitudinally-varying emissions of NO_x, we demonstrate that the geographical representation of the NO_x emissions is crucial in simulating tropospheric chemistry.

2. MODEL DESCRIPTION

The model used is a climatological three-dimensional global model of the troposphere with a 10° latitude x 10° longitude spatial resolution. It contains 10 vertical layers from the surface to 100 hPa. The model design is described in detail by Zimmermann et al. [1989] and Crutzen and Zimmermann [1991]. The parametrization of deep cumulus convection, which is of particular importance for short-lived tracers, is described by Feichter and Crutzen [1990]. In its current form, the model is coupled with a chemical scheme containing about 100 photochemical reactions describing the O₃ - OH - NO_x - CO - CH₄ - C₂H₆ - C₃H₈ chemistry. The transport of 20 species in the troposphere is considered, whereas transport processes are neglected for another 31 species which are assumed to be in photochemical steady-state [Kanakidou et al., 1991]. A time step of 2 hours is used.

In the present study downward fluxes of O₃ at 100 hPa that vary monthly and latitudinally are adopted totalling approximately 300 Tg-O₃/yr. Global NO_x emissions amount to 34 Tg-N/yr. Their adopted distribution is discussed later. We also adopted CO surface emissions that vary monthly (including indirect CO emissions by oxidation of the NMHC other than C₂H₆ and C₃H₈) totalling about 1700 Tg CO/yr. C₂H₆ and C₃H₈ emissions amount to 15 Tg-C₂H₆/yr and 17 Tg-C₃H₈/yr, respectively, and vary by longitude, latitude, and month. CH₄ volume mixing ratios at the lower boundary are assigned, according to observations (Steele et al., 1987). Other

features of upper and lower boundary conditions used in the model are described in Crutzen and Zimmermann [1991] and Kanakidou et al. [1992].

Case Studies.

We will concentrate on the impact of NO_x emissions from industry and biomass burning on the oxidizing efficiency of the atmosphere. We will then evaluate uncertainties in the computed concentrations of OH radicals and in the net chemical production of O_3 related to the distribution of NO_x emissions.

For this purpose, 5 different scenarios of longitudinally and latitudinally varying NO_x emissions have been considered: In the base case, NO_x industrial emissions of 20 Tg N/yr are distributed proportional to the industrial CO_2 emissions [Marland and Rotty, 1984] and when possible readjusted to fit the NO_x emission data published by World Resources Institute [1990]. Tropical NO_x emissions of 6 Tg N/yr from biomass burning are spatially distributed according to the analysis of Hao et al. [1990]. These emissions occur mainly during the dry season in the tropics and subtropics. NO_x emissions from lightning totalling 5 Tg N/yr were varied spatially and temporally and are based on flash frequency observations [Turman and Edgar, 1982]. Another 4 Tg N/yr released by soils are distributed as a function of soil productivity [Crutzen and Zimmermann, 1991]. In the other 4 cases, we adopted the emissions of NO_x from industry and biomass burning shown in Table 1. The NO_x emissions by lightning and by soils are the same as in the base case.

3. RESULTS AND DISCUSSION

Changes in the chemical composition of the atmosphere due to increasing NO_x emissions from industry and biomass burning.

The chemical production and destruction of O_3 in the troposphere and the global tropospheric annual mean diurnal-average OH concentration computed for each of the 5 case studies are presented in Table 1.

Focusing on the chemical production and destruction of O_3 in the troposphere computed when NO_x emissions by industry are neglected and those computed for the present day, we can derive that 26% of the present day net chemical production of O_3 (664 Tg- O_3 /yr) in the troposphere could be due to NO_x emissions by industrial activity. This is the net result of increasing both chemical production (+17%) and chemical destruction of O_3 (+14%) when NO_x emissions are increasing (from 0 to 20 Tg-N/yr).

Table 1. Adopted global NO_x emissions by industry (E_I) and biomass burning (E_B) (in Tg N/yr). Chemical production (PO_3), chemical destruction (DO_3) and net chemical production ($\text{PO}_3 - \text{DO}_3$) of O_3 in the troposphere (in Tg O_3 /yr) and global tropospheric annual mean diurnal average OH concentration (in 10^6 cm^{-3}).

E_I	E_B	PO_3	DO_3	$\text{PO}_3 - \text{DO}_3$	OH
20	6	3013	2349	664	0.83
0	6	2511	2020	491	0.72
20	0	2837	2222	615	0.76
40	6	3275	2518	757	0.89
20	12	3113	2405	708	0.85

The difference in the net chemical production of O_3 calculated without consideration of NO_x emissions by biomass burning (615 Tg- O_3 /yr) from that calculated for the base case (644 Tg- O_3 /yr) shows that only about 5% could be due to emissions by biomass burning. Similarly, NO_x industrial emissions may explain up to 13% of the changes in the global tropospheric mean OH concentration whereas the impact of biomass burning NO_x emissions on this OH concentration reaches 8%. Note however that in this study we do not take into account changes in the emissions of NMHC and CO or the concentrations of CH_4 .

Doubled industrial emissions of NO_x will perturb the OH global mean value by only 7% ($0.89 \cdot 10^6 \text{ cm}^{-3}$ instead of $0.83 \cdot 10^6 \text{ cm}^{-3}$ in the base case) and the O_3 net chemical production by about 14% (757 Tg- O_3 /yr compared to 664 Tg- O_3 /yr). This percent change is about half the present day effect of NO_x emissions by industry on the net chemical production of O_3 , which as above mentioned, is 26%. This clearly demonstrates that the effect of NO_x emissions on tropospheric chemistry is not directly proportional to the amount of NO_x emitted into the atmosphere.

Doubled NO_x emissions from industry or biomass burning do not imply a double impact of NO_x on tropospheric chemistry. These calculations suggest that the changes in the chemical composition of the atmosphere are not linearly related to the changes in NO_x emissions.

Differences between results obtained with longitudinally-uniform and varying emissions of NO_x .

Kanakidou and Crutzen [1992] demonstrated by running a three-dimensional model both with longitudinally-uniform (2-D) and varying (3-D) NO_x and NMHC input rates that the use of varying input rates leads to significantly lower O₃ and OH concentrations.

Here we examine the differences between results computed with "2-D" distribution of NO_x emissions and those computed with "3-D" distribution of NO_x emissions and in addition to the earlier study we discuss the dependence of these differences on the amount of NO_x emitted by industry and by biomass burning. We produced a second series of 5 simulations using a longitudinally-uniform distribution of NO_x emissions summing up at each latitude to those used in the previous cases, respectively. This second series of simulations should reproduce the main features of the results which are obtained with two-dimensional models. A direct comparison between two-dimensional and three-dimensional models is not strictly possible because of non-equivalent transport formulation.

We compare the results obtained with longitudinally-uniform NO_x emissions to those obtained with longitudinally-varying NO_x emissions. In Table 2 we report the percent differences for the 5 studied scenarios of NO_x emissions from industry and biomass burning.

Table 2. Differences (in percent) between values computed with longitudinally-uniform (2-D) and those computed with longitudinally-varying (3-D) NO_x emissions ($[2-D - 3-D] / 3-D \times 100$) for the 5 scenarios of NO_x emissions by industry (E_I) and by biomass burning (E_B).

E _I	E _B	% in the O ₃ net chem. production	% in the OH global annual mean
a. Industrial emission scenarios *			
0	6	16	16
20	6	16	14
40	6	16	14
b. Biomass burning emission scenarios **			
20	0	13	12
20	6	16	14
20	12	18	17

* in increasing order of industrial emissions of NO_x.

** in increasing order of biomass burning emissions of NO_x.

The results of this comparison agree well with the earlier study by Kanakidou and Crutzen, [1992] and the reader is referred to this paper for further information regarding the spatial and temporal variation of the computed differences in O₃, NO_x and OH concentrations.

We focus here on the dependence of the degree of non-linearity (i.e. of the computed differences between "2-D" and "3-D" global tropospheric amounts) on the amount of NO_x emitted in the atmosphere. As shown in Table 2, increasing emissions of NO_x by biomass burning lead to an increase in the differences between the computed "2-D" and "3-D" O₃ net chemical production and OH global tropospheric mean concentration. This is not the case for increasing NO_x emissions from industry mainly in the northern hemisphere where zonal mixing by the winds is more effective than at the equator. The strong dependence of the computed results on the strength of the NO_x source in the tropics is probably due to the relatively small zonal mixing by the winds, implying that the assumption of longitudinally-uniform emissions of NO_x leads to large inaccuracies in the computed O₃ and OH concentrations in this region.

Furthermore, the difference between the results computed with longitudinally uniform and those computed with longitudinally varying emissions depend also on the adopted CO levels. For instance, a preliminary test of sensitivity of these differences to CO emissions shows that a reduction on the surface CO emissions by a factor of 3 (to about 500 Tg/yr instead of about 1700 Tg/yr adopted in this study) leads to a higher degree of non-linear dependence of the net chemical production of O₃ on NO_x emissions (up to 23% compared to 18%) but simultaneously to smaller differences between the 2-D and 3-D computed OH concentrations (9% to 12%).

4. CONCLUDING REMARKS

These results clearly show that O₃ and OH concentrations computed with longitudinally-uniform emissions of NO_x are higher than those computed with longitudinally-varying emissions. However, the relationship between the overestimation of the computed O₃ and OH concentrations and the adopted distribution and strength of the NO_x atmospheric sources is not straightforward. Thus, the accuracy in NO_x emissions data is crucial to simulating changes in tropospheric chemistry resulting from human activity.

REFERENCES

- Crutzen P. J., 1988: Tropospheric Ozone: An overview, in Tropospheric Ozone, I. S. A. Isaksen (ed.), D. Reidel Publ., 3-32.
- Crutzen P. J., and P. H. Zimmermann, 1991: The changing photochemistry of the troposphere, Tellus, **43AB**, 136-151.
- Feichter J., and P. J. Crutzen, 1990: Parametrization of vertical tracer transport due to deep cumulus convection in a global transport model and its evaluation with ²²²Radon measurements, Tellus, **42B**, 100-117.
- Hao W.M., M. H. Liu, and P. J. Crutzen, 1990: Estimates of annual and regional releases of CO₂ and other trace gases to the atmosphere from fires in the tropics, based on the FAO statistics for the period 1979-1980, in Fire in the tropical Biota, edited by J. G. Goldammer, Springer-Verlag, New York, pp. 440-462.
- Houghton, J. T., G.F. Jenkins, and J. J. Ephraums (eds), 1990: Report of Working Group, Intergovernmental Panel on Climate Change (IPCC), WMO/UNEP, New York.
- Isaksen I. S. A. , and O. Hov, 1987: Calculations of trends in the tropospheric concentrations of O₃, OH, CO, CH₄, and NO_x, Tellus, **39B**, 271-285.
- Kanakidou M., H. B. Singh, K. M. Valentin, and P. J. Crutzen, 1991: A two-dimensional study of ethane and propane oxidation in the troposphere, J. Geophys. Res., **96**, 15,395 - 15,413.
- Kanakidou M., P. J. Crutzen, P. H. Zimmermann, and B. Bonsang, 1992: A 3-dimensional global study of the photochemistry of ethane and propane in the troposphere: Production and transport of organic nitrogen compounds, Proceeding of the NATO/CCMS 19th ITM on Air Pollution Modelling and its Application, Ierapetra, Greece, 29 Sep. - 4 Oct., H. van Doop Editor, in press.
- Kanakidou M., and P. J. Crutzen, 1992: Scale problems in global tropospheric chemistry modeling: Comparison of results obtained with a three-dimensional model, adopting longitudinally uniform and varying emissions of NO_x and NMHC, Chemosphere, in press.
- Lin X., M. Trainer, and S. C. Liu, 1988: On the nonlinearity of the tropospheric ozone production, J. Geophys. Res., **93**, 15,789-15,888.
- Marland G., and Rotty R. M., 1984: Carbon dioxide emission from fossil fuels: A procedure for estimation and results for 1950-1982, Tellus, **36B**, 232-261.
- Steele L. P., P. J. Fraser, R. A. Rasmussen, M. A. K. Khalil, T. J. Conway, A. J. Crawford, R. H. Gammon, K. A. Masarie, and K. W. Thoning, 1987: The global distribution of methane in the troposphere, J. Atmos. Chem., **5**, 125-171.
- Turman B. N., and B. C. Edgar, 1982: Global lightning distribution at dawn and dusk, J. Geophys. Res., **87**, 1191-1206.
- Zimmermann P. H., J. Feichter, H. K. Rath, P. J. Crutzen, and W. Weiss, 1989: A global three-dimensional source receptor model investigation using ⁸⁵Kr, Atmos. Environ., **23**, 25-35.

COMPARISON AND ANALYSIS OF AIRCRAFT MEASUREMENTS AND MESOSCALE ATMOSPHERIC CHEMISTRY MODEL SIMULATIONS OF TROPOSPHERIC OZONE

Jonathan E. Pleim* and Jason K.S. Ching*

National Oceanic and Atmospheric Administration, Air Resources Laboratory
Atmospheric Sciences Modeling Division, RTP, NC

N95-10606

303176

ABSTRACT

The Regional Acid Deposition Model (RADM) has been applied to several of the field experiments which were part of the Acid Models Operational and Diagnostic Evaluation Study (Acid MODES). The experiment which was of particular interest with regards to ozone photochemistry involved horizontal zig-zag flight patterns (ZIPPER) over an area from the eastern Ohio River valley to the Adirondacks of New York. Model simulations by both the standard resolution RADM ($\Delta x = 80$ km) and the nested grid RADM ($\Delta x = 26.7$ km) compare well to measurements in the low emission regions in central Pennsylvania and upstate New York, but underestimate in the high emission upper Ohio River valley. The nested simulation does considerably better, however, than the coarse grid simulation in terms of horizontal pattern and concentration magnitudes. Analysis of NO_x and HO_x concentrations and photochemical production rates of ozone show that the model's response to large point source emissions is very unsystematic both spatially and temporally. This is due to the models inability to realistically simulate the small scale (subgrid) gradients in precursor concentrations in and around large point source plumes.

1. INTRODUCTION

Photochemical Eulerian grid models are being increasingly relied upon for understanding, assessment, and regulation of meso-scale and regional ozone problems. Therefore, it is extremely important to understand the realism and limitations of these models. It is often assumed that if grid resolution is made sufficiently small the model can realistically simulate the complex interactions of photochemistry and dynamic transport and dispersion processes. This is true only where the grid can sufficiently resolve the gradients of reacting chemical species. As modeling emphasis shifts from small urban areas to larger regions (e.g. Southern Oxidant Study, Lake Michigan Ozone Study, San Joaquin Air Quality Study), models with coarser grid resolution are being applied to photochemical problems. These modeling efforts are complicated by the presence of very large point source plumes which dominate NO_x emissions in many areas. Ozone formation associated with power plant plumes has been observed many times (Davis et al., 1974; Miller et al., 1978; Gillani and Wilson, 1980). Since ozone photochemistry is a notoriously non-linear process, the ability of Eulerian grid models to simulate ozone production in the vicinity of large point source plumes, where gradients of precursor concentrations are particularly severe, needs to be assessed.

2. DESCRIPTION OF AIRCRAFT MEASUREMENTS

The specific measurements involved in this study were made by two specially instrumented aircraft on August 31, 1988 as part of AcidMODES. Two types of flight patterns, designed to diagnose various aspects of RADM

performance under clear sky conditions, were flown in a corridor extending from the eastern Ohio River Valley to northeastern New York. This study focuses on the ZIPPER flights, a horizontal zig-zag pattern flown within the mixed layer (about 1300 m AGL), in order to discern horizontal spatial patterns and gradients. Both aircraft recorded continuous measurements of gaseous SO_2 , NO , NO_2 , NO_y , O_3 , H_2O_2 , and CO as well as ambient temperature, moisture, pressure, and winds.

3 DESCRIPTION OF MODEL

The Regional Acid Deposition Model (RADM) is a comprehensive Eulerian atmospheric chemistry grid model which includes state-of-science representations of gas-phase chemistry, advective transport, subgrid vertical mixing, dry deposition and cloud processes including aqueous chemistry, convective mixing, and wet deposition (Chang et al., 1991). The modeling system incorporates hourly emission inventories, both anthropogenic and biogenic, land-use information, and gridded hourly meteorological fields provided by simulations of the Mesoscale Meteorological Model, Version 4 (MM4) with 4-D data assimilation (Stauffer et al., 1990). In addition to the standard regional scale version of RADM which has a horizontal grid cell size of 80 km, a nested grid version of RADM (Pleim et al, 1991) which increases horizontal resolution by a factor of 3 ($\Delta x = 80 \text{ km}/3 = 26.67$ km) is used in this study in an attempt to investigate the effects of model resolution on mesoscale ozone simulation. A revision to the model since the description by Chang et al. (1991) is the addition of a non-local closure scheme for subgrid vertical transport in the convective boundary layer called the Asymmetric Convective Model (Pleim and Chang, 1992).

4. COMPARISON OF MEASURED AND MODELED OZONE CONCENTRATIONS ON A REGIONAL SCALE

Figure 1 shows the horizontal spatial distribution of ozone measured along the ZIPPER flight path (zig-zag line in Fig 1) and interpolated between the flight legs using a simple inverse distance weighting technique. In order to facilitate comparison with model simulations, the measured and interpolated values are spatially averaged onto the same grid used by the nested grid model ($\Delta x = 26.7$ km). Direct comparison to model simulations is complicated by the fact that the ZIPPER aircraft measurements took almost 4 hours to complete (1530 - 1920 GMT). Model simulations of this period, however, showed only small changes with time. Therefore, ozone concentrations at 18 GMT as simulated by the nested and coarse grid models are shown in Figure 2 for comparison to Figure 1. Model level 5 (~600-900 m) was used for comparison to the aircraft measurements even though the aircraft's altitude was mostly in level 6 because the current model generally underestimated the height of the convective mixed layer and level 5 is the highest model layer which was

*On assignment to the Atmospheric Research and Exposure Assessment Laboratory, U.S. Environmental Protection Agency.

entirely within the model's mixed layer for the duration of the flight.

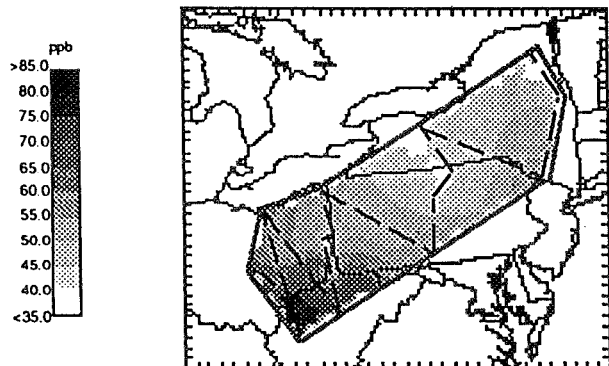


Figure 1. Airborne ozone concentration (ppb) measurements along ZIPPER flight path and interpolated between legs. Data is averaged onto a grid with 26.7 km grid cells (same as nested grid model).

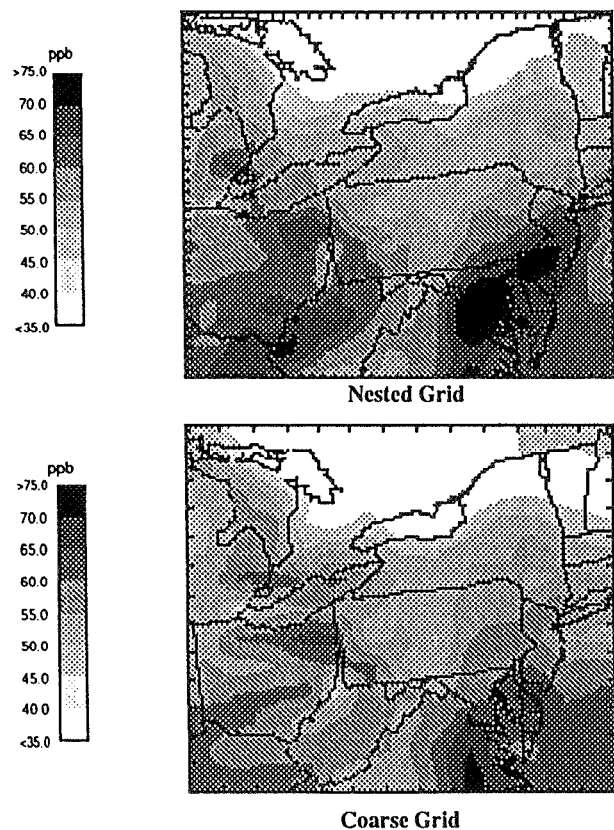


Figure 2. Ozone concentration (ppb) simulated by the nested RADM ($\Delta x = 26.6$ km) and coarse grid RADM ($\Delta x = 80$ km) in level 5 (~600-900m AGL) at 18 GMT.

Both nested and coarse grid model results (Figure 2) show very good similarity in terms of both spatial pattern and concentration magnitude to the measurements in the low emission regions in the northeastern portion of the ZIPPER. Throughout central and eastern PA and NY both model simulations are mostly within about 5 ppb of the measurements. In the higher NO_x emission region near the eastern Ohio River valley, however, the two simulations diverge significantly from each other and the measurements. For example, the location of the pronounced depression in the ozone concentration field near the OH-PA-WV border was simulated with much better accuracy by the nested model but the depth of the hole was

more closely simulated by the coarse grid model, although some 80-90 km to the south. The ozone maximum measured at the southmost ZIPPER corner near the Ohio river and into West Virginia (Figure 1) shows a broad area of concentrations in the 80-85 ppb range with a peak at about 85 ppb. The nested model simulation shows peak concentrations in this same area of 70-75 ppb at 18 GMT while the coarse grid simulation shows concentrations of 55-60 ppb in this area increasing to 60-65 ppb to the southwest (downwind). In general the nested model shows a marked improvement over the coarse grid simulation in the high emission Ohio River Valley region but is still unable to simulate the peak measured values.

5. ANALYSIS OF OZONE FORMATION IN THE OHIO VALLEY REGION

In this section the high ozone concentration region encountered by the aircraft near the southern end of the last corner in the ZIPPER flight path is further examined in an attempt to understand how the model simulates ozone formation in the vicinity of very large NO_x emitting elevated point sources. This section of the flight (~100 km long), where the aircraft crosses the Ohio River into WV and then doubles back into Ohio, is shown as a time series of 5 second average ozone and NO_y concentration data in Figure 3. The two peaks in the NO_y

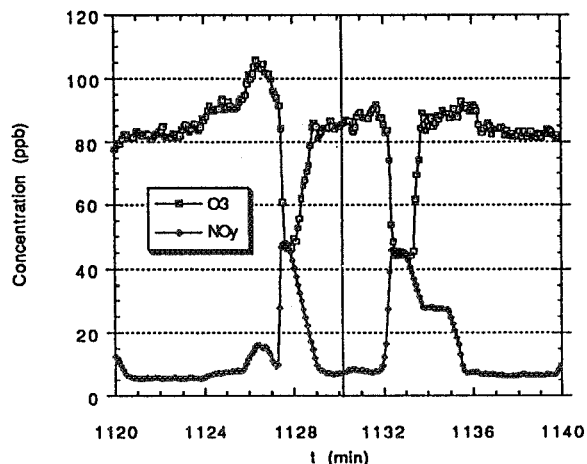


Figure 3. Time series of aircraft measurements of ozone and NO_y during ZIPPER flight when the G-1 aircraft flew through the same plume in western WV twice. The vertical line through the middle of the plot indicates where the aircraft made a 180° turn.

concentration which coincide with sharp holes in the ozone field are clear indications that the aircraft flew through freshly emitted plumes. In fact, since the aircraft turned around at the southern corner of the ZIPPER (western WV) in the middle of this time series (indicated by the vertical line in Figure 3), the two NO_y peaks are actually the same plume sampled twice. Using data from the navigational system onboard the aircraft the source of the plume was identified as a power plant which emits about 50,000 tons/year of NO_x located in southwestern West Virginia near Charleston. During the first pass the aircraft was about 3 km from the source and about 6 km on the second pass. The location of the ozone depression corresponds very closely with the NO_y peak due to the deple-

tion of ozone by reaction with freshly emitted NO in the plume. The peak in ozone concentration, up to 105 ppb on the first pass, immediately to the northwest of the ozone hole indicates photochemical production of ozone at the periphery of the plume where ambient air with VOCs and radicals is rapidly mixed with the NO_x emissions. The smaller peak in the NO_y profile which coincides with the ozone peak in the first pass through the plume suggests that this is a more dilute portion of the plume which broke away from the main plume and mixed more quickly with background air.

These measurements are an example of photochemical ozone production occurring very close to the source in large point source plumes. Plume photochemistry can be understood in terms of three stages (Gillani and Wilson 1980). The first stage is characterized by very concentrated NO causing a distinct depression in the background ozone field. In stage two, ozone starts to be photochemically produced at the plume edges where the NO_x has been sufficiently diluted with background VOCs and radicals to not only cause ozone levels to recover their background concentrations but to exceed them. A plume is in stage three when the ozone depression in the plume center, which still exists at stage two, is no longer evident. The aircraft measurements shown in Figure 3 seem to be an example of the early phases of a stage 2 plume since the plume core still shows a significant ozone deficit while the edges, particularly the north side of the first pass, show ozone excess.

The simulation of plume photochemistry by Eulerian grid models is quite different from the three stages described above. The evolution of plume chemistry is closely coupled to plume dispersion, however, this entire process is subgrid to models which have grid cell sizes on the order of tens of kilometers. Therefore, by examining the nested model simulation in this same area we hope to learn more about the model's response to plume photochemistry. Figure 4 shows several chemical quantities as simulated by the nested grid model at 17 GMT. The first plot (top) shows NO_x concentration at level 5 (~900 m). NO_x is clearly dominated by urban areas and the many coal-fired power plants along the upper Ohio River. The second plot (middle) shows HO_x (HO+HO₂) concentrations which very closely anti-correlate with NO_x concentration. This is because the radical termination reactions are proportional to NO_x concentration while radical initiation reactions are not, thereby resulting in net radical depletion where NO_x concentrations are high. For this discussion, the HO_x field is used as a surrogate for total radicals. Similarly, the rate of reaction between NO and HO₂, which is shown in the third plot (bottom), should be a good surrogate for photochemical ozone production by both HO₂ and RO₂ reactions. This plot shows peaks of ozone formation rates in regions of moderate NO_x concentration such as southwestern WV and near Washington DC. Where NO_x is highest, such as near the OH-PA-WV border and the western tip of Lake Erie, the radicals have been terminated to such a degree that the NO-radical reactions are relatively slow. Therefore, ozone formation is slower than ozone titration by NO emissions resulting in relative minima in the ozone field. Near the plume in southwest WV, on the other hand, NO_x concentrations are considerably lower and HO_x concentration much higher resulting in a favorable mix for ozone production. Note that, the greater amount of ozone formation in the Washington area (see the ozone plots in Figure 2) may be due to the greater amounts of

VOC's in the urban plumes and the more diffuse nature of the NO_x emissions (mostly area rather than point sources).

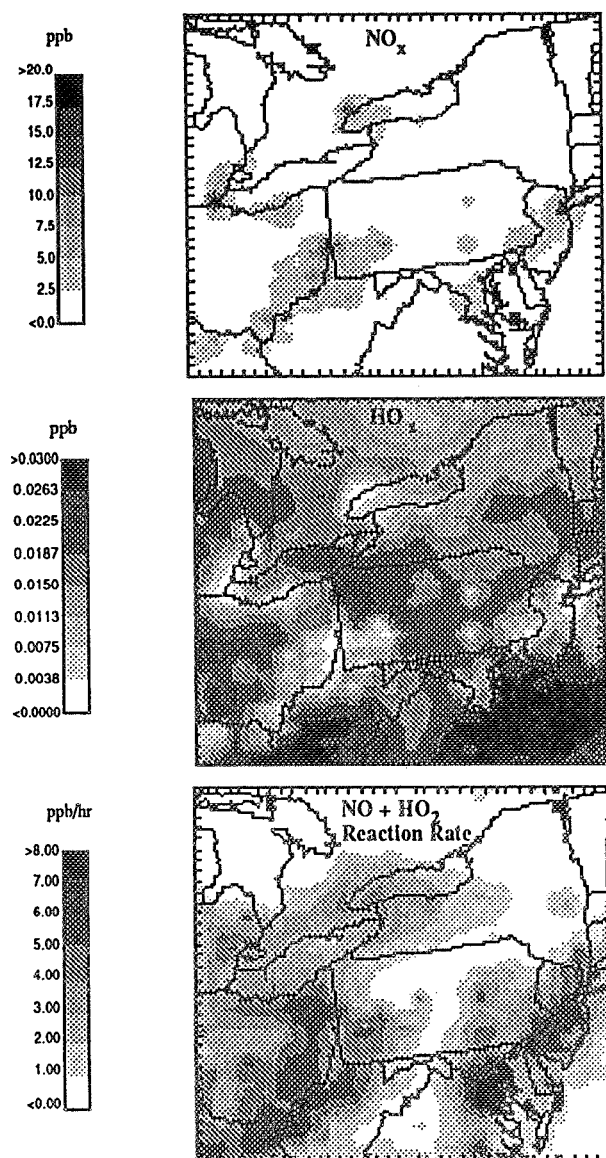


Figure 4. Nested model simulations in level 5 at 17 GMT on August 31, 1988 of NO_x concentration (top), HO_x concentration (middle), and rate of reaction between HO₂ and NO (bottom).

In order to further investigate the model's behavior, a set of time series for the grid cell in southwest WV where the nested simulation shows an isolated peak in ozone formation are shown in Figure 5. The plots are for model level 1 (~0-80 m) where hours 0-31 correspond to 00 GMT 8/31/88 - 07 GMT 9/1/88. The daytime rise in ozone concentration of about 40 ppb from hour 11 to hour 13 is coincident with a peak in the reaction rate between NO and HO₂ at 12 GMT of about 20 ppb/hr thereby showing the ozone increase to be primarily photochemical. The reason for this sharp peak in ozone formation can be understood through examination of NO and HO_x concentrations. NO concentrations begin increasing at 11 GMT (7 am EDT), probably from the morning rush hour in nearby cities such as Charleston, WV, while HO_x concentration initially rises in the morning, peaking at 12 GMT, then plunges to a minimum at 15 GMT. Therefore, the rapid

ozone formation at 12 GMT results from the combination of the onset of significant photochemistry, causing an increase in HO_x concentration, and increasing NO emissions. These favorable conditions, however, are short lived since the continuing rise in NO concentration leads to a decrease in HO_x , and by analogy other radical species. Thus, the phenomena of isolated peaks of ozone production, which was seen in the spatial model fields, is also evident in the temporal dimension such that ozone production during a single hour can dominate when conditions are most favorable.

6. DISCUSSION AND SUMMARY

In general, whether a particular grid cell containing a large point source plume results in an overestimation or underestimation of ozone production depends on a variety of factors such as emission rate, grid cell size, dispersion (wind speed and mixing height), and chemical background (VOCs and radicals). Thus, for the same conditions, models of different grid resolution may result in quite different simulations. The problem is the grid model's inability to simulate the subgrid processes of plume chemistry. The particular case discussed here suggests that increasing grid resolution from 80 km to 26.7 km improves the simulation of ozone formation. The highest ozone concentrations observed by the ZIPPER flights in the area downwind of the large point source plumes in the eastern Ohio Valley, however, were significantly underestimated even by the nested model. Analysis of the nested model simulation of this area shows that just a few grid cells, which happened to have a favorable mix of precursors, were responsible for the bulk of the ozone formed in this region. In addition, the time series in Figure 5 show that in these grid cells ozone formation occurred very sporadically when changing concentrations were briefly favorable for ozone formation. To improve model performance subgrid plume chemistry should be simulated either by a reactive plume/puff model or through parameterization of subgrid chemistry based on emissions, chemical and meteorological conditions.

REFERENCES

- Chang J. S., Principal Author. (1991) The Regional Acid Deposition Model and Engineering Model. NAPAP State of Science/Technology Report 4; In: National Acid Precipitation Assessment Program: Acid Deposition State of Science and Technology, Volume I. NAPAP, Washington, DC.
- Davis D. D., Smith G. and Klauber G. (1974) Trace gas analysis of power plant plumes via aircraft measurement: O_3 , NO_x , SO_2 chemistry. *Science*, 186, 733-736.
- Gillani N. V. and Wilson W. E. (1980) Formation and transport of ozone and aerosols in power plant plumes. *Annals N.Y. Acad. Sci.*, 338, 276-296.
- Miller D. F., Alkezweeny A. J., Hales J. M. and Lee R. N. (1978) Ozone formation related to power plant emissions. *Science*, 202, 1186-1188.
- Pleim, J. E., Chang J. S., and Zhang K. (1991) A nested grid mesoscale atmospheric chemistry model, *J. Geophys. Res.*, 96, 3065-3084.
- Pleim, J. E. and Chang J. S. (1992) A non-local closure model for vertical mixing in the convective boundary layer. *Atmos. Environ.*, 26A, 965-981.

Stauffer D. R. and Seaman N. L. (1990) Use of four-dimensional data assimilation in a limited-area model. Part I: Experiments with synoptic scale data. *Mon Wea. Rev.*, 118, 1250-1277.

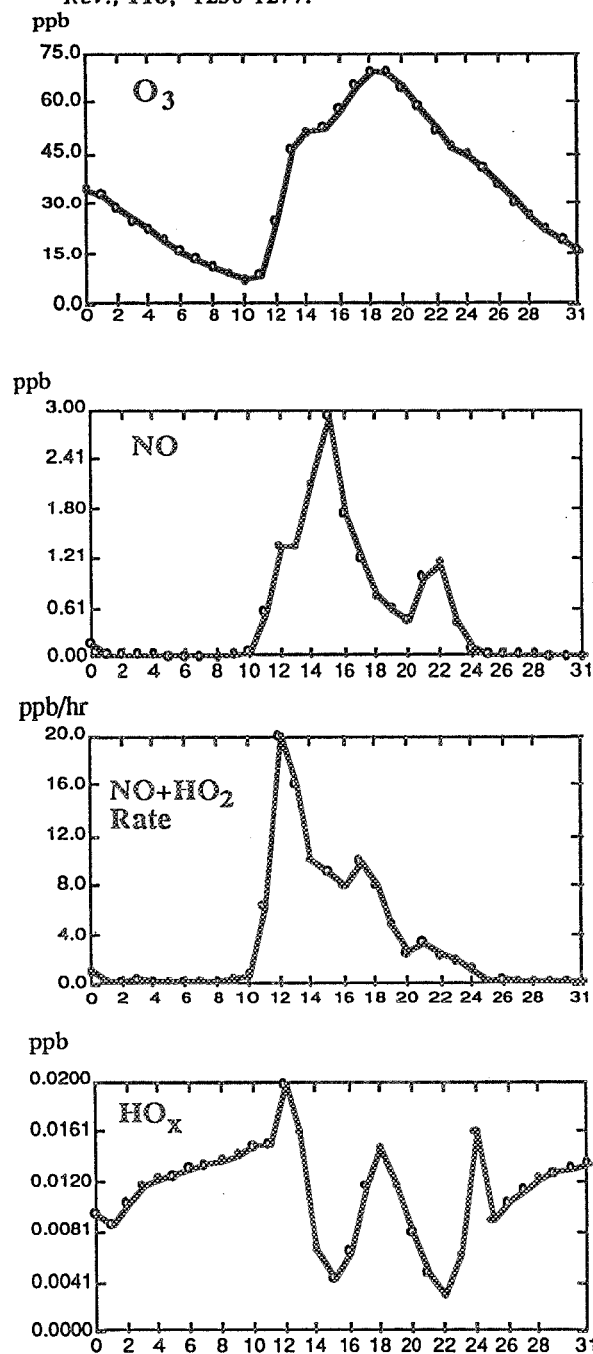


Figure 5. Time series (00 GMT 8/31/88 - 07 GMT 9/1/88) of nested model simulations in the grid cell corresponding to the plume encountered by the G-1 aircraft shown in Figure 3. From the top, the plots show O_3 , NO , rate of the reaction between HO_2 and NO , and HO_x in model level 1 (~0-80 km).

DISCLAIMER

This paper has been reviewed in accordance with the U.S. Environmental Protection Agency's peer and administrative review policies and approved for presentation and publication. Mention of trade names or commercial products does not constitute endorsements or recommendation for use.

303180

SOURCES AND DISTRIBUTION OF NO_x IN THE UPPER TROPOSPHERE AT NORTHERN MIDLATITUDES

Franz Rohrer, Dieter H. Ehhalt and Andreas Wahner

Institut für Atmosphärische Chemie
Forschungszentrum Jülich
Postfach 1913, D-5170 Jülich

ABSTRACT

A simple quasi 2-D model is used to study the zonal distribution of NO_x. The model includes vertical transport in form of eddy diffusion and deep convection, zonal transport by a vertically uniform wind, and a simplified chemistry of NO, NO₂ and HNO₃. The NO_x sources considered are surface emissions (mostly from the combustion of fossil fuel), lightning, aircraft emissions, and downward transport from the stratosphere. The model is applied to the latitude band of 40°N to 50°N during the month of June; the contributions to the zonal NO_x distribution from the individual sources and transport processes are investigated. The model predicted NO_x concentration in the upper troposphere is dominated by air lofted from the polluted planetary boundary layer over the large industrial areas of Eastern North America and Europe. Aircraft emissions are also important and contribute on average 30 %. Stratospheric input is minor about 10 %, less even than that by lightning. The model provides a clear indication of intercontinental transport of NO_x and HNO₃ in the upper troposphere. Comparison of the modelled NO profiles over the Western Atlantic with those measured during STRAT0Z III in 1984 shows good agreement at all altitudes.

1. INTRODUCTION

A major fraction of the available measurements of NO in the upper troposphere were made during the Stratospheric Ozone aircraft campaign STRAT0Z III in June 1984 (Drummond et al., 1988). The flight track of that campaign was placed mainly along the coastlines of North America, South America, western North Africa and Europe between 70°N and 60°S latitude and from 0 to 12 km altitude. The most conspicuous feature in the individual vertical profiles (see for example figure 1) and in the two dimensional representation of all measurements (figure 2) is the large hump of high NO-Concentrations in the upper troposphere at 10-11 km altitude extending all over the northern hemisphere.

To explain this result, all possible NO-sources must be considered, namely stratospheric input, emissions by high flying aircraft, lightning and fast vertical transport from the planetary boundary layer. Unfortunately, the observed patterns in the NO-distribution were by themselves not sufficient to provide a quantitative estimate of the contribution of the various sources. Also the hope of using correlations with the concentrations of other trace gases measured during STRAT0Z III, like O₃ and CO, proved vain so far. So we attempted to use a simple quasi

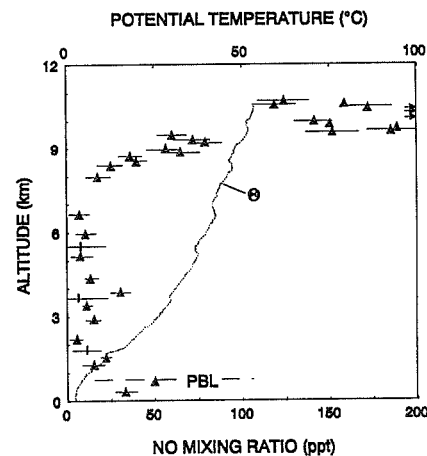


Fig. 1 Vertical profile of NO measured during STRAT0Z III near Halifax

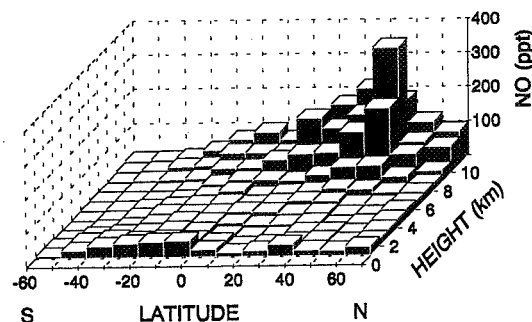


Fig.2 Meridional representation of the average NO mixing ratios measured during STRAT0Z III

2-D model to quantify the impact of the sources mentioned. The present paper summarizes the salient findings of our earlier work (Ehhalt et al., 1992).

2. MODEL DESCRIPTION

The model includes three types of transport : vertical transport by deep convection and eddy diffusion, and horizontal transport by vertically uniform wind. The fast vertical transport induced by deep convection is treated like a random process and superimposed onto a continuous transport by eddy diffusion. Selected by a random number, a fixed fraction of air at a specific altitude level is replaced by air from the boundary layer followed by a downward shift from each of the lower levels to the next one to maintain mass balance. This random process is adjusted such that the product of transport frequency and exchanged air fraction matches the exchange rate profiles (fig. 3) taken from the convection statistics of the GCM developed at the Goddard Institute of Space Studies (M. Prather, private communication 1990).

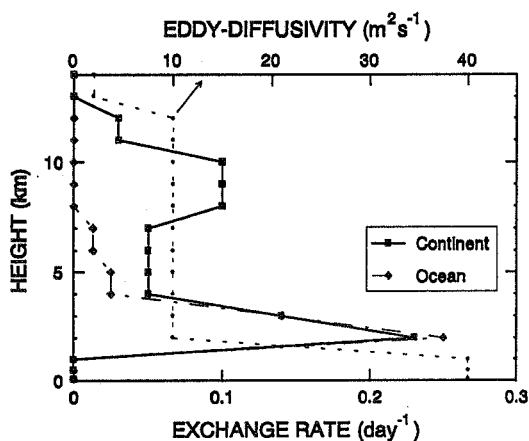
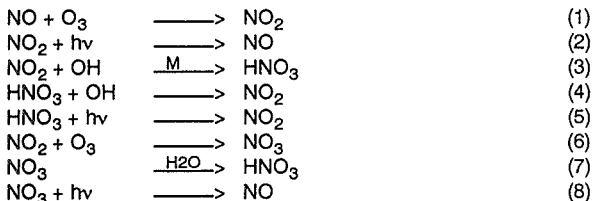


Fig. 3 Vertical profiles of the exchange rates of the fast vertical transport and of eddy diffusivity

Horizontal transport is introduced by moving the whole air column (0-14 km altitude) with a horizontal displacement given by a 8 ms^{-1} westerly wind (Houghton, 1985). The tropopause is located at 12 km altitude. Temperature and density profiles used are those of the U.S. Standard Atmosphere (1976). All parameters apply to the summer month at 40° - 50° N latitude.

The model allows the nitrogen compounds $\text{NO}_x = \text{NO} + \text{NO}_2$ and HNO_3 to be transported. Those species are interlinked by reactions (1) to (8).



The vertical concentration profiles of OH (Volz et al., 1981) and O_3 (Marengo and Said, 1989) and of the photolysis rates (Roeth, 1986) are held fixed at their diurnally averaged values. The rate constants used are those in Jet Propulsion Laboratory (JPL 1990).

The nitrogen compounds are removed from the atmosphere by dry and wet deposition. HNO_3 is deposited on all surfaces with a deposition velocity of 2 cm s^{-1} (Huebert and

Robert, 1985), NO_2 only on land surfaces with 0.5 cm s^{-1} (Boettger et al., 1978). Wet deposition of HNO_3 occurs in two modes. One is associated with the fast vertical transport events which are thought to proceed through convective clouds removing half of the HNO_3 lofted by the event. Additionally, HNO_3 is removed with a time constant of 10 days at altitudes of 1-12 km and with a time constant of 2 days below 1 km.

The emission rates of NO_x listed in Table 1 were calculated from Ehhalt and Drummond (1988) and Ehhalt and Drummond (1982). The emissions by lightning were coupled to the fast vertical transport by convective clouds allowing NO_x -injection for transport events which exceeded 8 km over the continents and 4 km over the oceans. The total emission rate by lightning was adjusted to match the value given in table 1.

Table 1 : NO_x Emissions in 40° - 50° N, June 1984

Source	Emission Rate 10^6 t N/yr
Surface source	
total	8.63
fossil fuel burning	7.45
Lightning	0.29
Aircraft, civil	0.081
Stratosphere	0.037

The aircraft emissions were derived from an average emission index of $10 \text{ g NO}_2/\text{kg fuel}$ and a fuel consumption in 1984 of $113 \cdot 10^6 \text{ t fuel/yr}$ (Nuesser and Schmitt, 1990). The vertical and longitudinal distribution was adopted from the Climatic Impact Assessment Program (CIAP, 1975).

3. RESULTS

The model was allowed to cycle three times around the globe to assume steady state. The zonal two dimensional distribution of NO and two sequences of vertical profiles of NO and NO_y are shown in figures 4 and 5. The contributions of the various sources in figure 5 were derived by model runs in which the individual source was switched off. Both figures demonstrate the development of a maximum in NO concentration at 10 km altitude as the air column passes over strong continental source areas. This maximum is a result of high surface concentrations carried upward by the fast vertical transport process. When the air column moves from a high surface source area out over the ocean (figure 5b), NO and NO_y are very quickly removed from the lower troposphere, but remain in the upper troposphere due to their long lifetime of about 10 days at those altitudes.

These results were tested against experimental results from Drummond et al. (1988). Figure 6 shows the comparison of the model predictions for the vertical NO-profiles at 50° W, 40° - 50° N and an average of the NO measurements between 50° N and 40° N about the south bound leg of STRATOZ III. The two profiles agree surprisingly well indicating that all four sources are needed to produce the high NO-concentrations observed in the upper troposphere.

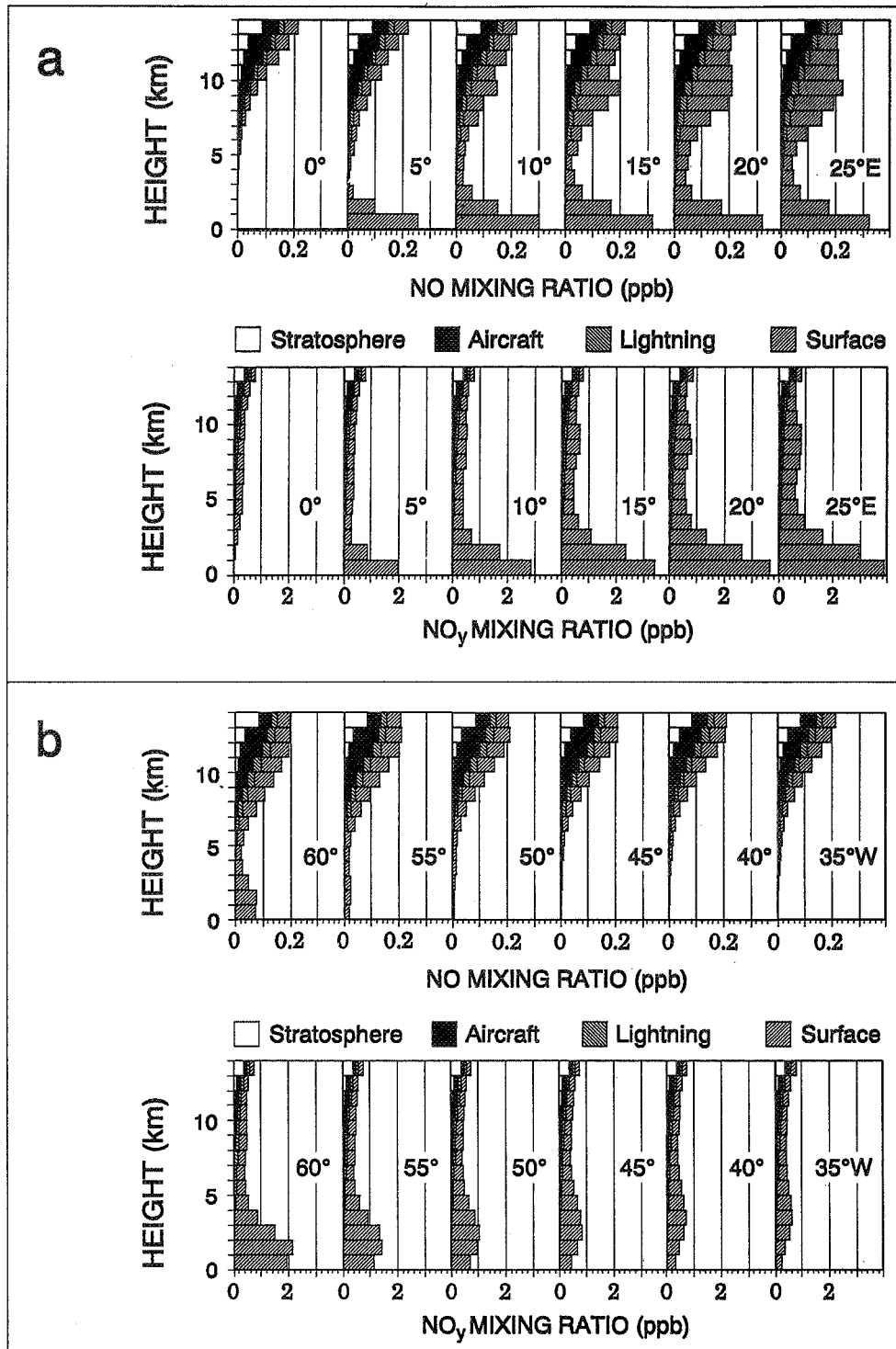


Fig 5 Calculated vertical mixing ratio profiles of NO and NO_y.
 a : over continental western Europe
 b : over the western North Atlantic

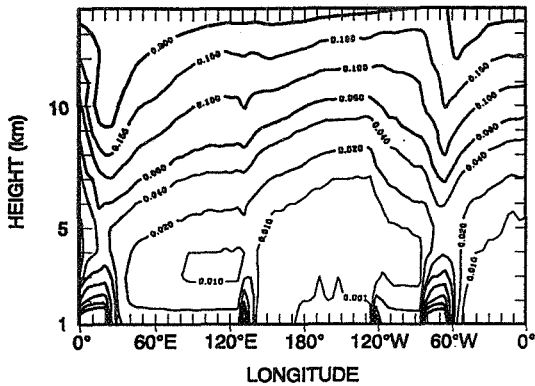


Fig. 4 Contour plot of the zonal two dimensional distribution of NO at 40°-50°N. Contours in ppb at 0.001, 0.01, 0.02, 0.04, 0.06, 0.1, 0.15 and 0.2

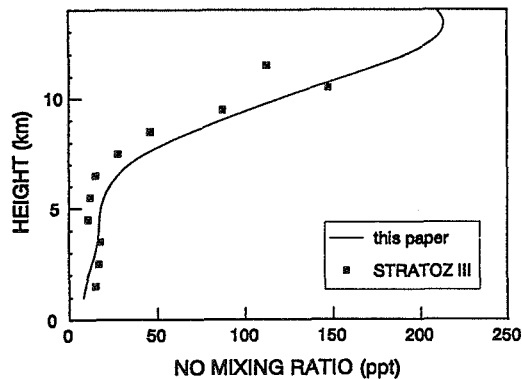


Fig. 6 Vertical profiles of the NO mixing ratio near 50°W, 40°-50°N, solid curve : model calculation, solid squares : averaged profiles measured during STRAT0Z III

4. CONCLUSIONS

Despite its simplicity the model used is capable of obtaining results similar to the salient features of the observed vertical NO-profiles at 40°-50°N in June 1984. In particular, it reproduces the high values and relative maxima in the vertical NO-profiles in the upper troposphere over coastal areas. The reason for this may be that for these latitudes and this time of year processes are indeed simple. The model facilitates a first examination of the contributions from various sources to the NO_x concentration in the upper troposphere. Aircraft emissions which contribute on average about 30% and NO_x lofted from the planetary boundary layer are the major sources of NO_x in the upper troposphere at northern mid-latitudes during summer. The quantitative conclusions are of course uncertain. They depend on the assumed source strength which have errors of the order of a factor of 2. Work which has been done by using an improved 2-D model showed that the qualitative and quantitative conclusions given here did not depend on the assumption of vertically uniform wind speed or on the lack of horizontal eddy diffusion.

REFERENCES

- Boettger, A., D.H. Ehhalt and G. Gravenhorst
KFA Juel Bericht 1558, p 1-96, Forschungszentrum Jülich, 1978
- Climatic Impact Assessment Program (CIAP) 1975,
Monograph 2, Rep.DOT-TST-75-52,
U.S. Dep. of Transp., Washington, D.C., 1975
- Drummond, J.W., D.H. Ehhalt and A. Volz
J.Geophys.Res. 83, 15831-15849, 1988
- Ehhalt, D.H. and J.W. Drummond
Proceedings of NATO Advanced Study Institute, Corfu, Greece,
edited by H.W. Georgii and G. Jäschke, pp. 219-251, D.Reidel, Norwell,
Mass., 1982
- Ehhalt, D.H. and J.W. Drummond
In Tropospheric Ozone, edited by I.S.A Isaksen, pp. 217-237, D.Reidel,
Norwell, Mass., 1982
- Ehhalt, D.H., F. Rohrer and A. Wahner
J.Geophys.Res. 97, 3725-3738, 1992
- Houghton, D.D.
Handbook of Applied Meteorology, John Wiley, New York, 1985
- Huebert, B.J., and C.H. Robert
J.Geophys.Res. 90, 2085-2090, 1985
- Jet Propulsion Laboratory (JPL), Evaluation 9, JPL 90-1, 1990
- Marenco, A., and F. Sald
Atmos.Environ. 23, 201-214, 1989
- Nuesser, H.-G., and A. Schmitt
In Air Traffic in the Environment - Background, Tendencies and Potential
Global Atmospheric Effects, edited by U. Schumann, pp. 1-11, Springer
Verlag, New York, 1990
- Roeth, E.P.
KFA Juel Bericht 2098, p 1-171, Forschungszentrum Jülich, 1986
- Volz, A., D.H. Ehhalt and R.G. Derwent
J.Geophys.Res. 86, 5163-5171, 1981

303183

A GLOBAL NUMERICAL STUDY OF RADON²²² AND LEAD²¹⁰
IN THE ATMOSPHERE USING THE AES AND YORK UNIVERSITY
CDT GENERAL CIRCULATION MODEL, (AYCG).

Stephen R. Beagley¹, Jean de Grandpré¹, John C. McConnell¹, René Laprise², Norman McFarlane³.

Department of Earth and Atmospheric sciences, York University, North York, Ont., Canada M3J 1P3.¹
Département de physique, Université du Québec à Montréal, Montréal, Québec, HC3 3P8.²
Canadian Climate Centre, The Atmospheric Environment Service, North York, Ontario, Canada.³

Abstract.

The Canadian Climate Centre (CCC) GCM has been modified to allow its use for studies in atmospheric chemistry. The initial experiments reported here have been run to test and allow sensitivity studies of the new transport module. The impact of different types of parameterization for the convective mixing have been studied based on the large scale evolution of Rn²²² and Pb²¹⁰. Preliminary results have shown that the use of a scheme, which mixes unstable columns over a very short time scale, produces a global distribution of lead that agrees in some aspects with observations. The local impact of different mixing schemes on a short lived tracer like the radon is very important.

1. Introduction.

Recently the modeling of chemistry has moved to the global scale, permitting the assessment of the multitude of chemical reactions within a global atmospheric model. The model described herein, the AES and York University Chemistry and General Circulation model, is a version of the Canadian Climate Centre General Circulation Model, (GCM). The model used is the operational version of the CCC spectral GCM (McFarlane et al, 1992). Initial experiments were aimed at examining the use of the spectral method for tracer transport and assessing the transport module. This module includes, multi-tracer advection, convective and boundary layer mixing, wet deposition, vertical and horizontal diffusion. This work describes some experiments on radon and lead tracers chosen to assess the part played by convective mixing in the transport of species within the GCM.

The current results are for T32 resolution and the model time step is 20 minutes. At this resolution the model resolves synoptic and planetary scale motions, however sub-grid meteorology which impacts on these scales are absent.

We have chosen Rn²²² as being representative of species with short chemical lifetimes such as isoprene and propane, and Pb²¹⁰ as being representative of a longer lived species,

e.g. CO and O₃. Very simplistically we are equating Rn²²² with a precursor chemical like NO_x or hydrocarbons which have short lifetimes, while the lead is equated to the longer lived chemical products, whose presence in the upper troposphere can only be achieved if its precursors are transported rapidly from their surface source regions. In addition, radon tests the impact of a simple surface source while the Pb²¹⁰ production is distributed throughout the troposphere.

2. The Radon Experiment.

As a first test of the model and transport module, a number of paired Rn²²² and Pb²¹⁰ like tracers were used. This allowed several convective mixing schemes to be considered and a general assessment to be made of the overall use of the spectral GCM as an online tracer advection model. A test of the mixing, rainout and spectral advection plus a first check on mass conservation and other numerical problems associated with sharp tracer gradients modeled in a spectral model was thus possible.

Initially, radon was distributed uniformly in the horizontal, with a fixed vertical profile, decreasing exponentially with height. The ground level value of 100 pCi/m³ STP was chosen based upon typical observed surface radon measurements. Lead was set as a low background which would be dominated rapidly by the radon decay source. Due to its short lifetime, the radon rapidly reached a global balance between the model source and decay within the first month and was largely unaffected by the initial state thereafter. For the lead, a global mass equilibrium state was not expected within the first several months due to its longer tropospheric lifetime. Since the radon surface flux is confined to the continent, the sharp boundaries and the hemispheric gradient, due to the source distribution, provide test problems for the model transport and analysis. The radon source was modeled by assuming a constant surface flux of 1 atom/sec/cm² from all non-ice covered land on the globe. The radon sink due to radioactive decay was obtained using a tendency based on the tracers 5.5 day e-folding time. Thus excluding the transport, the budget for Rn²²² is described

in equation 1,

$$\frac{\delta\chi_r}{\delta t} = -\frac{\chi_r}{\tau} + F_g \quad (1)$$

where χ_r = Rn²²² tracer mass mixing ratio, τ = radon e-folding time, and F_g = surface flux of radon. The Pb²¹⁰ was assumed as the only decay product of the radon so that the sink of radon in molecules was the same as the source of Pb²¹⁰ in molecules. Its sink was modeled using a simple rainout scheme, proportional to the local column rainfall amount and the local tracer mixing ratio (Mahlman and Moxim, 1978). Thus the budget for Pb²¹⁰ is;

$$\frac{\delta\chi_p}{\delta t} = \frac{\chi_r M_p}{\tau M_r} - \frac{\chi_p}{\tau_{ro}} \quad (2)$$

where χ_p = Pb²¹⁰ tracer mass mixing ratio, M_p = molecular mass of Pb²¹⁰, M_r = molecular mass of Rn²²² and τ_{ro} = rainout e-folding lifetime as defined below as;

$$\tau_{ro} = \frac{\tau_w(k) \cdot \langle P \rangle}{P} \quad (3)$$

where τ_w = wet deposition lifetime (as a function of height, k), P = local average precipitation amount ($mm s^{-1}$), and $\langle P \rangle$ = the global average precipitation amount ($mm s^{-1}$).

Convective mixing of tracer from the boundary layer into the free troposphere has been identified as an important component in a complete transport description of the troposphere. Tracer mixing schemes that have been used for radon include those of Jacob and Prather (1990), Feichter and Crutzen (1990) and Brost and Chatfield (1989). These schemes vary in complexity with a balance being struck between detailed model description and expense. However due to the large scale of the GCM's horizontal grid, parameterizations are, at best, highly approximate. Such a position poses a serious difficulty in global modeling and requires careful assessment and observational basis before interpretation can be considered valid.

It was decided to test two schemes in parallel using fundamentally different transport assumptions. The two basic schemes used are; a) a direct relocation scheme and b) a diffusive scheme. The direct relocation scheme is based on the scheme described in Prather et al. (1987), which assumes that within a model grid box a fraction of tracer mass is directly advected from the convection base to the top of the convectively unstable column. Continuity then requires an instantaneous subsidence to move tracer from the top down to the next lower box, throughout the column. Thus total mass is conserved in the column while redistributing tracer. The diffusive scheme was based upon the convective adjustment used in the GCM for convective parameterization of heat and moisture and in this sense, it is internally consistent with the dynamics. The diffusive scheme is different from that of the direct relocation, in that it tests adjacent points in a column and mixes between them if an instability exists. This process is done from the ground up so it is possible for tracer to slowly

'diffuse' up through the column. The two schemes are fundamentally different and will have significantly different impacts upon the transport of tracers with different lifetimes.

3. Results.

Due to its relatively short life time, the radon is on average mostly concentrated over the land area. Figure 1 shows the mass mixing ratio of radon at the surface, averaged over the second month, on which can be seen many features associated with the large scale circulation. In the tropics, zonal transport produced by the trade winds is evident as well as the impact of the tropical circulation due to the presence of the high pressure belt in the southern hemisphere. The persistence of such an anticyclonic circulation over the tropical ocean produces surface winds following the west coast of Africa and south America causing a strong gradient on the edge of both continents. Average surface concentrations of radon obtained over most of the northern continents range from 100-300 pCi/m³ which fall in the range of what is currently observed (Liu et al., 1984). However, spatial and temporal variability of radon is such that comparison between observation and model results over specific regions would necessitate further analysis (Feichter, 1988; Jacob, 1990).

At mid- and high-latitude in the winter season, the impact of convective mixing is weak no matter which scheme is used. Tropical regions are however strongly affected by the choice of parameterization and show highly localized spatial and temporal variations. To illustrate the differences between the schemes, Figures 2b and c show time snap-shots of the radon distributions for the two different parameterizations, for 71° West at model day 33, 00:00 GMT. Figure 2a shows, for comparison, the result achieved when no convective mixing is applied. The 'diffusive' and non-convective mixing variants are very similar with only a slight spread of tracer due to diffusion from the tracer plumes generated by synoptic scale ascent. This indicates that the 'diffusive' technique spreads tracer slowly to high altitudes but has little power to inject tracer higher due to the relatively short lifetime of radon. The 'relocation' scheme however is strikingly different producing a high level tracer maxima in the tropics right up to the tropopause and lower stratosphere. In addition, without convective mixing the model tracer (due to the source at the ground) builds up strong gradients in the lowest levels (Figure 2a), producing numerical problems at land-sea boundaries and above continents.

The mean residence time of lead in the stratosphere is considerably higher than in the troposphere, where the lead is washed out by precipitation. Previous studies have shown that the quantity of lead in the stratosphere is a significant fraction of the total (Moore, 1973) and could correspond to 33% of the global mass of lead in the atmosphere (Lambert, 1982). Our results show that such a reservoir can be approached by using the relocation technique

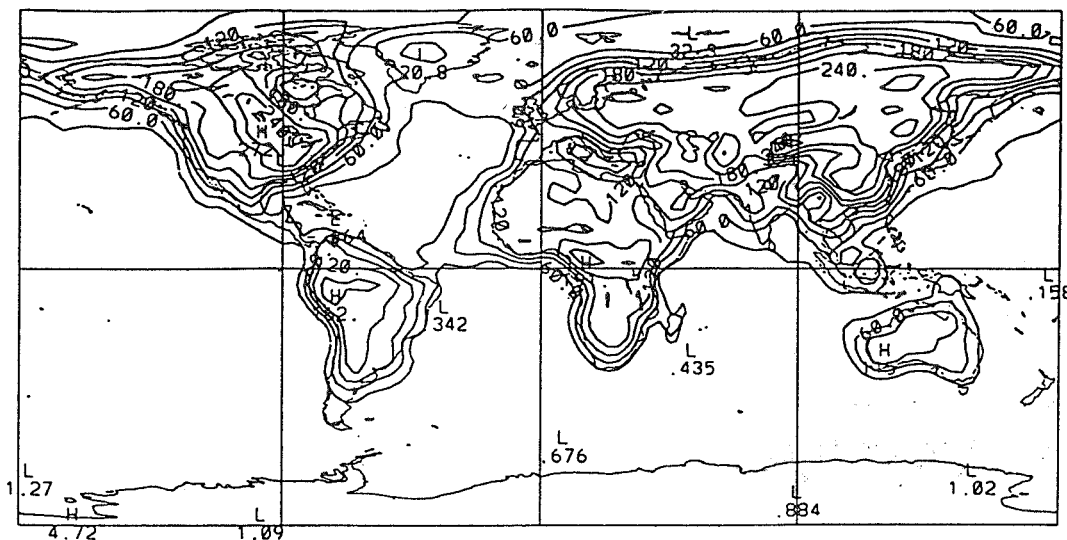


Figure 1 : Radon²²² surface mass mixing ratios, (pci/m³ at STP), for Radon variant ii) 'Diffusive' convective mixing, Monthly averaged data for February.

which gives a stratospheric mass fraction of 25% at quasi-steady state. The fraction given by the diffusive mixing scheme is of the order of 5-10% which is significantly lower.

In spite of the slowness of the diffusive scheme, it still contributes to the transport of species into the higher troposphere. Budget analyses show in fact that close to 30% of the transport of radon to the tropopause could be attributed to this process. To allow the tracer to go further into the stratosphere, an additional type of parameterization could be needed in that case to represent the exchange of tracer that occurs across the tropopause.

Part of the aim of these experiments was to determine the capabilities and limitations of the spectral technique. Initial model experiments reveal the model conserves mass well, giving a maximum global mass variation of 0.1 percent in 2 months. Running at T32 resolution the radon and lead tracers together with the convective mixing schemes give rise to strong gradients locally, regionally and globally. Despite the noisy nature of the convection and the permanent strong land-sea gradients which arise the total global magnitude of the numerical errors remain small, less than 0.25 percent of the global mass being used to remove negative values in the tracer field. For Radon the combined impact of the ground source and the convective mixing is a relatively severe test on the use of the spectral advective scheme. Consequently sharp gradients and low background values will be produced and numerical problems be more likely. A surprising bonus of the convective mixing has been its ameliorating effect upon the need for hole-filling in the model. As the result of active convection, the gradients of Rn²²² are no longer so sharp and trapping in the lower model levels is reduced.

A number of tracers in future studies will be like Rn²²² in having a source restricted to over land. This creates a

tracer distribution with steep horizontal gradients at the continental boundaries. Such a distribution must be modeled by the advection scheme, maintaining the gradients, to be accurate. Figure 1 illustrates the spectral model's description of Rn²²² near the surface, with strong gradients in the horizontal, with the tracer mass predominantly 'clinging' to the land surfaces. Future tracers will also have detailed geographical source distributions, e.g. dependent on terrain characteristics. The impact of similar sources varying on very small model scales (sometimes below the models $3 - 4\Delta x$ limit) will be partially tested as a result of the 'noisy' nature of the convective mixing which to the upper troposphere is acting like a highly variable source function in both space and time. With these types of additional requirement for advecting chemical tracers, the spectral technique is one among many alternative schemes proposed. GCMs using the spectral technique at low resolution cannot resolve strong gradients. Other alternatives exist including semi-Lagrangian and second-order moment techniques which can provide more accurate advection but normally at the expense of more computational effort and sometimes poorer mass conservation properties.

The radon distributions exhibit strong transport of tracers into the upper troposphere particularly in the tropics both via synoptic and subgrid motions. The consequences of this transport are important in any study of tracers whose source is the troposphere but whose sink lies in the stratosphere. With this type of transport scenario in mind the radon and lead tracers have been examined to view how the model moves tracers to the upper troposphere and across the tropopause into the lower stratosphere. The impact of the 'relocation' convective mixing and large synoptic ascent upon the redistribution of radon from the boundary layer to the upper troposphere is considerable. It could have also an important effect, in the long term, upon the cross equatorial transport of long lived tracer.

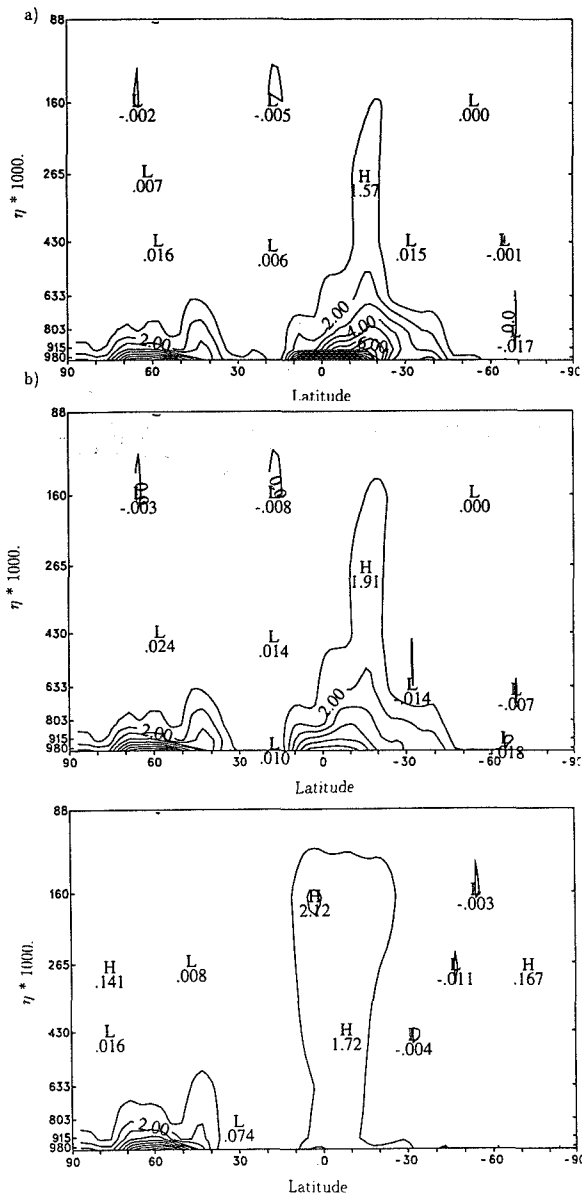


Figure 2 : Radon²²² mass mixing ratio constant longitude cross-sections, longitude 71° West, for variants: a) No convective tracer mixing, b) 'Diffusive' convective tracer mixing, and c) 'direct-Relocation' convective tracer mixing, for Day 33, 00:00 GMT. (Scaled by $1.0e^{19}$) Vertical axis shows data on model hybrid levels, where $\eta = f(p, \sigma)$.

4. Conclusions

A level 0 online tracer-model is now complete and testing indicates that mass conservation and negatives are not significant problems but that a better advection scheme may be needed if sharp gradients produced dynamically and chemically are to be maintained accurately. However the spectral technique with sufficient resolution is still a powerful and viable alternative. Sensitivity studies reveal

the importance of the parameterization of convective mixing on tropospheric tracer modeling. The model's convective mixing has maximum impact over the equatorial continents, with very small effect in the winter hemisphere higher latitudes. In terms of global impact, the parameterization of convective mixing based on the relocation technique appears to be more efficient in representing adequately the transport of long lived tracers into the lower stratosphere. However, the local impact of both schemes over specific regions still needs to be assessed with more analysis. It has been also noted that convective mixing acts to reduce spectral problems due to its diffusive effect on tracer gradients. Strong synoptic vertical motions produce important transport of radon into the tropical upper troposphere, greatly increasing the potential pool of tracer available for transport into the lower stratosphere. The convective mixing parameterizations used are relatively simple and questions on the degree of entrainment throughout the column, fraction of mass 'relocated' and the height of the ensemble average convection within a GCM grid box remain outstanding. Future modeling is intended using alternative and more complex schemes in order to assess and improve our ability to parameterize and interpret subgrid mixing within global models.

Acknowledgements: We would like to thank the Natural Sciences and Engineering Research Council of Canada for their support.

References

- Brost, R.A. and Chatfield, R.B., Transport of Radon in a 3D subhemispheric model, *J. Geophys. Res.*, **94**, 5095-5119, 1989.
- Feichter, J. and P.J. Crutzen, Parameterization of vertical tracer transport due to deep cumulus convection in a global transport model and its evaluation with Radon²²² measurements, *Tellus*, **42B**, 100-117, 1990.
- Jacob, D.J. and M.J. Prather, Radon 222 as a test of convective transport, *Tellus*, **42B**, 118-134, 1990.
- Lambert, G., Polian, G., Sanak, J., Ardouin, B., Buisson, B., Jegou, A., and Rouley, J.C., Cycle du Radon et de ses descendants: application à l'étude des échanges troposphère-stratosphère. *Ann. Géophys.*, **38**, 497-531, 1982.
- Liu, S.C., J.R. McAfee, and R.J. Cicerone, Radon 222 and tropospheric vertical transport, *J. Geophys. Res.*, **89**, 7291-7297, 1984.
- Mahlman, J.D., and Moxim, W.J., Tracer simulation using a GCM: results from a Mid-latitude instantaneous source experiment, *J. Atmos. Sci.*, **35**, 1340-1374, 1978.
- McFarlane, N.A. G.J. Boer, J.-P. Blanchet, and M. Lazare, The Canadian Climate Centre second generation GCM and its Equilibrium Climate, *J. Climat.*, to be published, 1992.
- Moore, H.E., S.E. Poet, and E.A. Martell, Rn²²², Pb²¹⁰, Bi²¹⁰, Po²¹⁰ Profiles and aerosol residence times versus altitude, *J. Geophys. Res.*, **78**, 7065-7075, 1973.
- Prather, M.J., M. McElroy, S. Wofsy, G. Russell, D. Rind, Chemistry of the global troposphere: Fluorocarbons as tracers of air motion, *J. Geophys. Res.*, **92**, 6579-6613, 1987.

ON THE TRANSPORT OF TRACE GASES BY EXTRA-TROPICAL CYCLONES

Marc A.F. Allaart, Lodewijk C. Heijboer and Hennie Kelder
Royal Netherlands Meteorological Institute,
De Bilt, The Netherlands

ABSTRACT

Extratropical cyclones are able to transport trace gases through the whole troposphere and lower stratosphere. At midlatitudes most of the ozone transport from the lower stratosphere down into the troposphere is accomplished by depressions. The changing total ozone contents, associated with the variable tropopause heights, are shown to be clearly visible in satellite ozone data.

1. INTRODUCTION

The transport of trace gases in the atmosphere takes place on different spatial and time scales. It ranges from small scale transport by turbulent diffusion to large scale organised transport in the migrating cyclones and baroclinic waves. At midlatitudes one of the most important contributors to transport are depressions. Large cyclones extends from the surface upto the lower stratosphere. Cyclones are effective and rapid both for vertical and horizontal transport. The outer scales are thousands of kilometers while the inner scales go down to hundreds of meters in the instabilities in the depression. Moreover, the vertical transport is largest in the small horizontal scales.

In this paper an analytical model of a cyclone (Heijboer

and Kelder, 1991) is used to get an impression of the exchange between the stratosphere and troposphere and to understand the corresponding changes of the tropopause height.

The exchange between the troposphere and the stratosphere takes place in the tropopause foldings which are partly irreversible. The tropopause is pushed up ahead of the depression and torn down behind it. This causes high total ozone values at the reverse of the depression and low values in front of the depression. This was already known for more than forty years (Reed, 1950). Here, one event is studied in detail to demonstrate this picture.

2. AN ANALYTICAL MODEL OF A CYCLONE AND THE CORRESPONDING FLOW REGIMES

An analytic conceptual model of an extratropical cyclone was developed recently (Heijboer and Kelder, 1991). It consists of a highly truncated solution of the quasi-geostrophic or semi-geostrophic equations. The simple model reveals the main characteristics of the cyclone as is shown in figure 1. Several different flow regimes can be distinguished. Ahead of the depression a warm moist conveyor belt is transporting boundary layer air upto the upper troposphere. The ascending movement is accelerated by the release of latent heat. The cold moist conveyor belt is ascending upto the middle troposphere

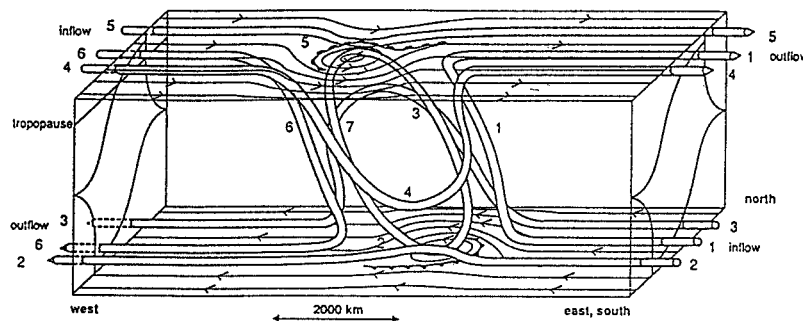


Fig. 1. Relative trajectories within and around a standard moving extratropical cyclone.

1. Warm moist conveyor belt
2. Low tropospheric flow of the environment
3. Cold moist conveyor belt
4. Descending stratospheric air overrunning the warm moist conveyor belt
5. Stratospheric flow of the environment
6. Descending stratospheric air into the troposphere
7. Circulating air in the centre of the depression moving with the speed of the depression

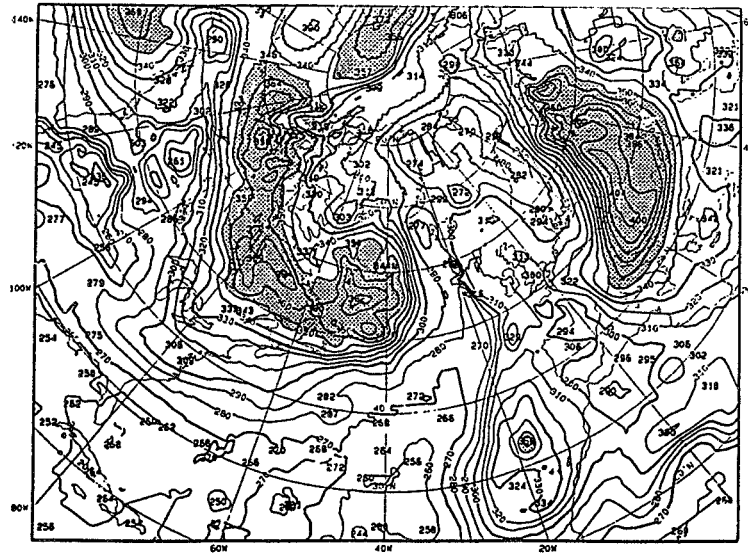


Fig. 2. The TOVS total ozone values for the Northern Hemisphere valid for 6 December, 1991. Areas with total ozone values over 350 Dobson units are shaded.

and is turning around the core of the depression before descending. Both conveyor belts are characterised by clouds and precipitation. Away from the depression the tropospheric flow is only little affected by the depression. At the back partly irreversible downward movement of lower stratospheric air takes place in channel 6. The downward movement in channel 4 of lower stratospheric air to the middle troposphere and back is in principle reversible. But this air is overrunning the warm moist conveyor belt and through shear and convective instabilities strong mixing takes place between these flows. The flow in the lower stratosphere and upper troposphere away from the depression is nearly undisturbed. In the core air of stratospheric and tropospheric origin is thoroughly mixed.

3. ESTIMATION OF THE TRANSPORT OF TRACE GASES

The analytical model suggests that the downward fluxes of trace gases takes place in three ways.

In channel 6 the air is transported from the lower stratosphere into the lower troposphere. The dimensions of the channel of a characteristic cyclone are about 800 km width and about 1.5 km thickness and the velocity with respect to the cyclone is assumed to be of the order of 10 m/s. If a concentration of $n \text{ mol/m}^3$ is assumed, then per second $n \times 1.2 \times 10^{10}$ molecules are transported downwards. The lifecycle of a cyclone is four to five days of which during about two days effective downward transport takes place. The total transport for one cyclone amounts to $n \times 2.1 \times 10^{15}$ molecules.

In channel 4 lower stratospheric air descends to the middle troposphere and back. The ascending air overruns the moist conveyor belt and convective and shear instabilities are causing strong mixing of the air in both channels. It is assumed that about half of the air from stratospheric origin remains by mixing in the troposphere and this contributes to $n \times 1.3 \times 10^{15}$ molecules.

Mixing in the core of stratospheric and tropospheric air is a third way of exchange. If the cyclone is dying out the deformed tropopause in the core will be restored and is closing above the core. If the core has a radius of 500 km and the

stratospheric part a thickness of about 1.5 km per depression $n \times 1.2 \times 10^{15}$ molecules are transported in this way. One cyclone amounts to $n \times 4.6 \times 10^{15}$ molecules.

Assuming 4 separate depressions per 4 days in the midlatitudes of the Northern Hemisphere leads to a total of $n \times 1.7 \times 10^{18}$ molecules per year. For ozone at 300 hPa, 50° N the concentration is about $3 \times 10^{18} \text{ mol/m}^3$ and the mean downward flux becomes 5.0×10^{36} molecules ozone per year. The mean vertical flux for the Northern Hemisphere becomes $6.2 \times 10^{14} \text{ molecules m}^{-2} \text{ s}^{-1}$. This is in the range of other estimates (e.g. Ebel et al., 1991).

In the same way upward fluxes can be determined. In channel 1, the warm moist conveyor belt, air is transported from the boundary layer air into the upper troposphere and lower stratosphere. This air, containing gases with residence times of hours to days like NO_x , SO_2 , HNO_3 etc., is taking part in the chemistry of the upper troposphere. The air is processed in ascending by clouds, precipitation and mixing with dry air from stratospheric origin. In the midlatitudes above the Atlantic Ocean in the belt of 40° N to 60° N upper tropospheric air is replaced intermittently by marine boundary layer air (Ehhalt et al., 1991).

4. CHANGES IN TROPOPAUSE HEIGHT AND TOTAL OZONE

Strong interrelation exists between midlatitude cyclones and total ozone.

1. In midlatitude cyclones ozone is transported from stratosphere into the troposphere.
2. The (column) total ozone-content can be a useful tool to unravel the structure of midlatitude cyclones.

Ozone trapped in a tropopause fold will of course show up on the total ozone picture. This ozone will eventually mix through the troposphere and break down by chemical destruction or by deposition in the boundary layer.

Figure 2 shows the TOVS total ozone values for December 6, 1991; Figure 3 shows the tropopause pressures for the same date. Steep gradients indicate tropopause folds.

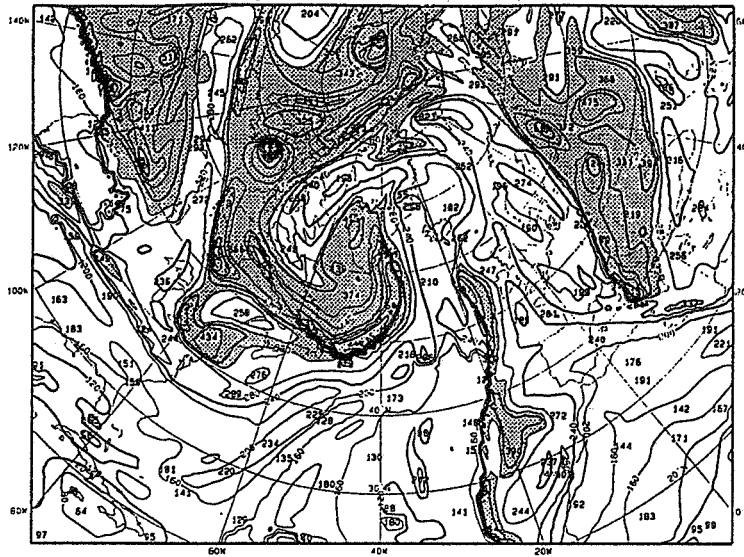


Fig. 3. Tropopause pressures valid for 6 December, 1991. Areas with tropopause pressures over 320 hPa are shaded.

5. SUMMARY AND DISCUSSION

In the paper it was argued that cyclones have a large impact on the transport of trace gases at midlatitudes. Most of the downward ozone transport from the stratosphere to the troposphere is accomplished by cyclones. With a simple model of a depression a conceptual view of the main flow regimes in and around a depression was obtained. The importance of the transport by cyclones for the budgets of total ozone was discussed.

The conclusion is that part of the short term fluctuations in total ozone is due to migrating cyclones. This idea was already formulated more than 40 years ago (Reed, 1950) but with the analyses of the ECMWF model and the satellite observations of total ozone now, it is possible to quantify his idea more accurately.

REFERENCES

- Ebel, A., H. Hass, H.J. Jakobs, M. Laube, M. Memmesheimer, A. Oberreuter, H. Geiss, and Y.-H. Kuo, 1991: Simulation of ozone intrusions caused by a tropopause fold and cut-off low. *Atmos. Environm.*, 25, 2131-2144.
- Ehhalt, D.H., F. Rohr, and A. Wahner, 1992: Sources and distributions of NO_x in the upper troposphere at Northern mid-latitudes. *J. Geophys. Res.*, 97, 3725-3738.
- Heijboer, L.C., and H. Kelder, 1991: An analytic conceptual model of extratropical cyclones. Submitted to *Quart. J. Roy. Meteor. Soc.*
- Hoskins, B.J., M.E. McIntyre, and A.W. Robertson, 1985: On the use and significance of isentropic potential vorticity maps. *Quart. J. Roy. Meteor. Soc.*, 111, 877-948.
- Komhyr, W.D., S.D. Oltmans, P.R. Franchois, W.F.J. Evans, and W.A. Matthews, 1989: The latitudeinal distribution of ozone to 35 km altitude from ECC ozone-sonde observations. 1985-1987. In: *Ozone in the Atmosphere*. Bojkov and Fabian Eds., 147-150.
- Reed, R.J., 1950: The role of vertical motions in ozone-weather relationships. *J. Meteorol.*, 7, 263-267.
- Vaughan, G., and J.D. Price, 1991: On the relation between total ozone and meteorology. *Quart. J. Roy. Meteor. Soc.*, 117, 1281-1298.

AN ANALYSIS OF THE IMPACTS OF GLOBAL CLIMATE AND EMISSIONS CHANGES ON REGIONAL TROPOSPHERIC OZONE

Kuruville John, Kevin C. Crist, and Gregory R. Carmichael

Department of Chemical and Biochemical Engineering
The University of Iowa
Iowa City, Iowa 52242, USA

ABSTRACT

Many of the synergistic impacts resulting from future changes in emissions as well as changes in ambient temperature, moisture, and uv flux have not been quantified. A three-dimensional regional-scale photo-chemical model (STEM-II) is used in this study to evaluate these perturbations to trace gas cycles over the eastern half of the United States of America. The model was successfully used to simulate a regional-scale ozone episode (base case - June 1984) and four perturbations scenarios - viz., perturbed emissions, temperature, water vapor column, and incoming UV flux cases, and a future scenario (for the year 2034). The impact of these perturbation scenarios on the distribution of ozone and other major pollutants such as SO₂ and sulfates were analyzed in detail. The spatial distribution and the concentration of ozone at the surface increased by about 5-15% for most cases except for the perturbed water vapor case. The regional scale surface ozone concentration distribution for the year 2034 (future scenario) showed an increase of non-attainment areas. The rural areas of Pennsylvania, West Virginia, and Georgia showed the largest change in the surface ozone field for the futuristic scenario when compared to the base case.

INTRODUCTION

A growing concern over global climate change has been instrumental in focusing the scientific community's attention toward the need to study its varied impacts. Issues pertaining to global warming, loss of stratospheric ozone, and their respective influences on human activities and the surrounding environment have become more important topics of research. Recent studies¹ seem to focus on the impacts of trace gases on possible climate change. There are, however, limited studies that address the issue of the impacts of a possible climate change scenarios on the trace gas distribution of the troposphere. Under a changed climate scenario, the tropospheric trace gas distribution would significantly alter. An increase in surface temperature (corresponding to global warming) would cause an increase in the water vapor concentration in the atmosphere. An increased water vapor concentration would then amount to an increase in the H₂O₂ and OH concentrations and a subsequent decrease in the ozone concentration field.² This would, thus, affect the oxidative capacity of the atmosphere. Moreover, due to anthropogenic and/or natural causes the atmospheric composition would change over a period of

time. Such changes in atmospheric levels of certain pollutants (NO_x, NMHC, CO, etc.) have the potential to affect the rate of tropospheric ozone formation and the abundance of the free radical oxidant OH on a global scale. Perturbations to stratospheric O₃ and climate (temperature and moisture) can also influence the rates of key photochemical processes affecting tropospheric O₃, H₂O₂, and OH. Since these species are the principal tropospheric oxidants, the above mentioned changes may alter the overall oxidizing capacity of the atmosphere.

A few studies^{3,4,5}, using one-dimensional models, have attempted to better understand these impacts on the complex tropospheric chemistry. Such studies, however, are limited and their authors recommend that the sensitivities/changes should be evaluated using a three-dimensional model because O₃ is sufficiently long-lived to have a widespread effect on the tropospheric chemistry.

The impact of various perturbations due to global climate change coupled with changes in emissions can be studied in detail using a comprehensive regional-scale photochemical model. In this paper, the author will make an attempt to address various issues pertaining to these climate and emission change attributes and their impact on the tropospheric trace gas distribution by utilizing STEM-II photochemical model.⁶

STEM-II APPLICATION

For a detailed study of the possible perturbations to the trace gas distribution over eastern U.S.A. due to the anticipated changes in global climate attributes and the regional-scale emissions, a three-dimensional regional-scale comprehensive photochemistry model (viz., the STEM-II)⁶ was used in this study. The modeling domain comprised of 22x28x11 grid points and the horizontal grid spacing was 80 km and the vertical resolution being 500m. This study domain covers the entire eastern United States. The 1985 NAPAP emissions inventory⁷ was used in this study. The episode selected as the base case was clear-sky summer-time conditions on 7th - 11th June, 1984.⁸ During this period, the entire modeling domain was under the influence of a high pressure system centered over the Atlantic Ocean off the coast of South Carolina. Most of the region was under clear sky during the event. This was a typical high-pressure

dominated stagnant summer event over eastern United States that results in high photochemical oxidant episodes. Shin⁸ provides a detailed description of the grid setup, emissions and the meteorological inputs.

In order to simulate a future scenario for the year 2034, large number of gas-phase-only simulations were performed using meteorological and emissions data for the base year of 1984. Table 1 shows the different scenarios simulated to study the impact of perturbations to key parameters on regional-scale trace gas distribution. The climate scenarios are consistent with present climate change scenarios (Intergovernmental Panel on Climate Change),⁹ while those for the emissions are estimated from EPA,¹⁰ OTA,¹¹ and Kavanaugh.¹² There, however, remains a large uncertainty in the projections of future NO_x and NMHC emissions. Each simulation consisted of a 48-hour run for initialization using the meteorological inputs of June 5-6, 1984. This provided us with the initial distributions consistent with the emissions and meteorological fields. Following this, a 5-day (108 hours) simulation was conducted and the results analyzed over a broad spectrum of pollutant species and their behavior. The impact on the trace gas distribution of all perturbation scenarios listed in Table 1 are analyzed.

Table 1 : List of Scenarios Simulated

(a)	Base Case with biogenic emissions and diurnal dry deposition incorporated
(b)	Perturbed Emissions scenario for the year 2034 : 33% increase in NO _x during 1984-2034 due to an increase in automobiles/highway miles and a simultaneous increase in stationary sources. 25% decrease in SO _x corresponding to a realistic decrease in sulfur sources subject to the 1990 Clean Air Act requiring a 50% cut in sulfur emissions from power plants.
(c)	Perturbed Surface Temperature and Vertical Temperature profile scenario approx. a 3K change in surface areas for the mid-litudinal areas ¹³
(d)	Perturbed water vapor scenario approx. 20 - 27% increase in the lower troposphere corresponding to an increase of surface temperature of 3 K ²
(e)	Perturbed uv flux scenario approx. a 10% increase in uv flux was accounted for the decrease in the stratospheric ozone
(f)	Total Perturbation scenario - Overall projected scenario for the year 2034 from a combination of cases (b) through (e)

RESULTS AND DISCUSSION

The STEM-II model was successfully used to simulate an actual episode (base case - year 1984), a future scenario (year 2034), and four perturbation scenarios to test the sensitivity of tropospheric trace gas distribution to perturbations to global climate attributes and emissions

change. The trace gas distribution of selected species (including ozone) were studied in detail and the impacts fully analyzed for all the above mentioned cases.

The spatial distribution of ozone at the surface increased for most cases except for the perturbed water vapor case. Figures 1(a) through 1(e) represent the percent change of ozone concentrations at the ground level, for each perturbation case, over the entire study domain. In the case of perturbed emissions, (see Figure 1a), the ozone concentrations increased by about 5-10% over the eastern land mass. However, the upper midwest regions encompassing Indiana, Michigan, and Ohio, and the urban centers in New Jersey and New York showed an actual decrease in ozone (-5 to -15%) at the surface. This can be explained by the already low hydrocarbon/NO_x ratios in those regions. By increasing the NO_x values to even higher levels, while the tropospheric hydrocarbon levels remain constant due to low biogenic sources and constant anthropogenic emissions, puts the photochemistry in the regime where formation of nitric acid (terminating reaction) becomes an important sink for all available HO_x. Consequently, any further increase in NO_x decreases the urban ozone concentrations.

In the case of perturbed temperature (+3 K) scenario (see Figure 1b), where the emissions were retained to the base levels, the regional-scale ozone concentration increased by about 5 - 15% over most of the domain. The effect of temperature on ozone is primarily due to the effect on the lifetime of PAN and its homologues.

In the case of perturbed water-vapor case (see Figure 1c), where the emissions and temperatures were retained to the base levels, the regional-scale ozone showed very little change. An increase in water vapor suggests an increase in the hydroxyl radical pool and a decrease in the ozone concentration.

In the case of an increase in the UV flux (~10%) (see Figure 1d), the regional ozone values increased by about 5-15%. This is accounted primarily by the daytime photochemistry and its subsequent carryover of higher values into the night time.

In the event of the total perturbation scenario (see Figure 1e), where all of the above perturbations were accounted to hypothetically simulate the year 2034, overall increase of surface ozone concentration was noted to be in the range of 10-25%. This implies an increase in the number of the non-attainment areas within the study domain.

The regional-scale surface ozone concentration predicted for the year 2034 (viz., total perturbation case) showed an increase of non attainment areas with the greatest changes observed in certain rural areas including the ones in Pennsylvania, West Virginia, and Georgia. Figure 2 highlights this feature by comparing the total perturbation case (2034) to the base case.

The diurnal variations of the ozone cycle remained similar and the differences between rural and urban profiles were essentially retained in all cases. Within the lower troposphere, the ozone profile showed a large change for the perturbed emissions and the total perturbation case. Rural values of ozone were most affected by these perturbations.

Two points were selected within the study domain representing an urban and a rural area in Georgia. Figure 3 (a and b) gives the percent change in the ozone concentrations at the ground level, for each perturbation with

respect to the base case, at these two sites. The percent change over the base case is computed for a 24-hour period. As seen in the graph, the surface values of ozone in the rural Georgia area increased significantly for the total perturbation case. Increase in the temperature also had a large effect on the ozone values. The other perturbations caused small increases in the ozone concentrations. However, the changes in the ozone concentrations in the urban Georgia site were relatively smaller. The constraint here could be the low hydrocarbon/NO_x ratio in the urban regions when compared to higher hydrocarbon/NO_x ratios in the rural areas.

In conclusion, this study has demonstrated that significant changes in trace gas and photochemical oxidant cycles can be anticipated under global climate change scenarios. Increases of upto 40% in ozone concentrations are predicted as a direct impact of changes in climate attributes and emissions. Such increases in tropospheric ozone could possibly have feedback effects on the regional climate. Rural areas and areas downwind of pollution hotspots would experience significant changes in the tropospheric composition. Regional-scale photochemical models, such as STEM-II, serve as invaluable tools in detailed studies of tropospheric trace gas distribution. This brief introduction to the sensitivity of trace gas distribution to global climate change and emission change should provide a basic insight into similar research endeavors.

ACKNOWLEDGMENT

The authors acknowledge the financial and computational support extended by Bergen Scientific Centre (IBM), Bergen, Norway, during our stay at BSC as visiting scientists.

REFERENCES

1. D. J. Wuebbles, K. E. Grant, P. S. Connell, and J. E. Penner, "The Role of Atmospheric Chemistry in Climate Change", *JAPCA*, 39 (1): 22 (1989).
2. A. M. Thompson and R. J. Cicerone, "Possible Perturbations to Atmospheric CO, CH₄, and OH", *J. Geophys. Res.*, 91: 10853 (1986).
3. A. M. Thompson, R. W. Stewart, M. A. Owens, and J. A. Herwehe, "Sensitivity of Tropospheric Oxidants to Global Chemical and Climate Change", *Atmos. Envir.*, 23 (3): 519 (1989).
4. A. M. Thompson, M. A. Huntley, and R. W. Stewart, "Perturbations to Tropospheric Oxidants, 1985-2035: Calculations of Ozone and OH in Chemically Coherent Regions", *J. Geophys. Res.*, 95: 9829 (1990).
5. P. J. Drivas, A. P. Toole, and S. C. Gnewuch, "The Effects of Global Warming and Increased UV Radiation on Urban Ozone Concentrations", Paper No. 40c, presented at the *AICHE Summer National Meeting* (1990).
6. G. R. Carmichael, L. K. Peters, and T. Kitada, "A Second Generation Model for Regional-Scale Transport / Chemistry / Deposition", *Atmos. Environ.*, 20, 173 (1986).
7. M. Saeger, J. Langstaff, R. Walters, L. Modica, D. Zimmerman, D. Fratt, D. Dulleba, R. Ryan, J. Demmy, W. Tax, D. Sprague, D. Mudgett, and A. S. Werner, "The 1985 NAPAP Emissions Inventory

(version 2): Development of the Annual Data and Modeler's Tapes", EPA-600/7-89-102a, Applied Technologies Corp., Chapel Hill, N.C., 1989.

8. W. C. Shin, "Comprehensive Air Pollution Modeling on Multiprocessing Environments: Application to Regional-Scale Problems", Ph. D. thesis, University of Iowa, Iowa City, 1990, pp 50-66.
9. Intergovernmental Panel on Climate Change, 1990, "Climate Change - The IPCC Scientific Assessment", J. T. Houghton, G. J. Jenkins, and J. J. Ephraums, Eds., Cambridge University Press, Cambridge, 1990.
10. EPA, "National Air Quality and Emissions Trends Report, 1990", EPA-450/4-91-023, Technical Support Division, Office of Air Quality Planning and Standards, U.S.E.P.A., Research Triangle Park, N.C., 1991.
11. OTA, "Catching Our Breath - Next Steps for Reducing Urban Ozone", Office of Technology Assessment, Congress of the United States, Washington, D.C., 1989.
12. M. Kavanaugh, "Estimates of Future CO, N₂O, and NO_x Emissions from Energy Combustion", *Atmos. Envir.*, 21 (3): 463 (1987).
13. V. Ramanathan, R. J. Cicerone, H. B. Singh, and J. T. Kiehl, "Trace Gas Trends and Their Potential Role in Climate Change", *J. Geophys. Res.*, 90, 5547 (1985).

Fig. 1a

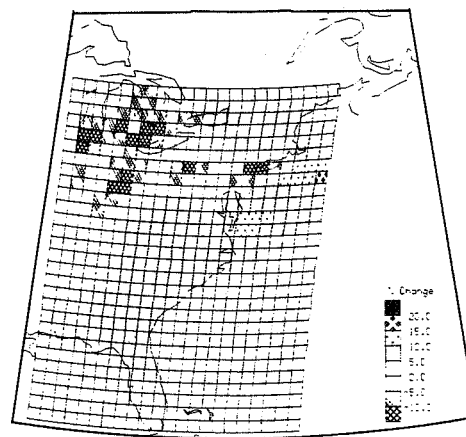


Fig. 1b

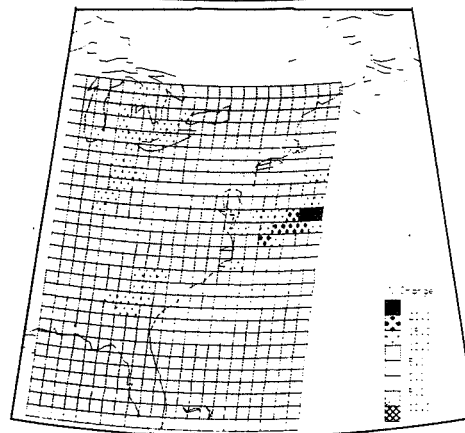


Fig. 1c

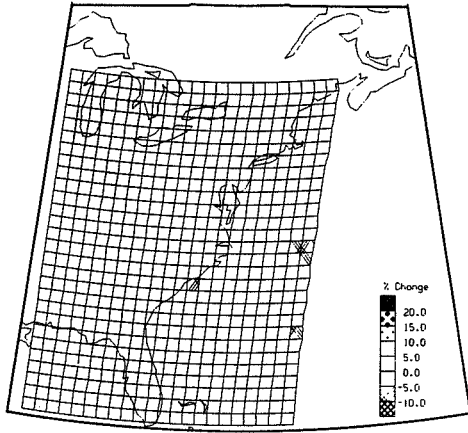


Fig. 1d

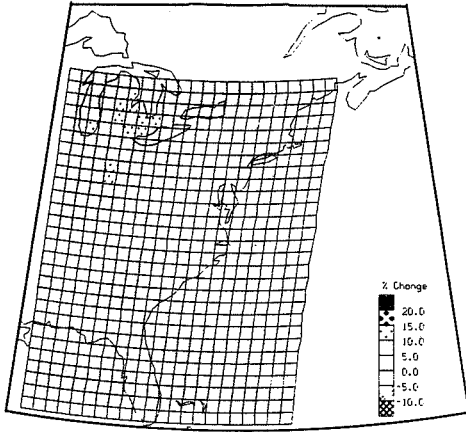
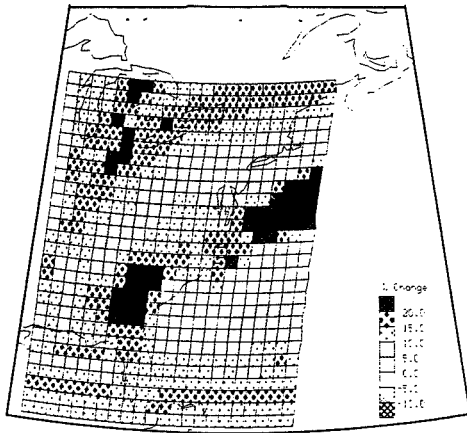
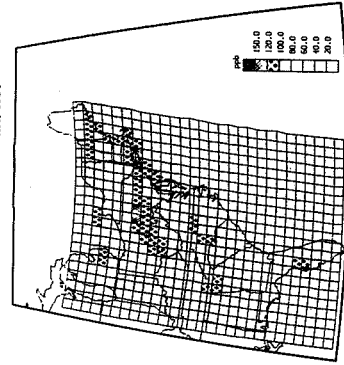


Fig. 1e



GAS PHASE OZONE CONC. AT THE SURFACE
TOTAL PERTURBATION CASE
June, 2004
1500 EST



GAS PHASE OZONE CONC. AT THE SURFACE
BASE CASE
June 10, 1984
1500 EST

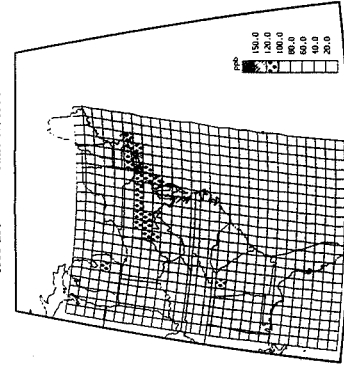
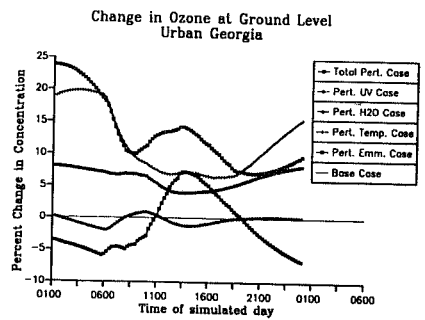
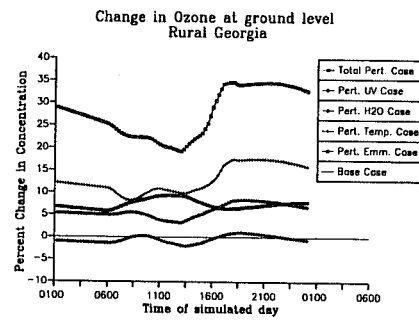


Fig. 2

Fig. 3



303246

**ESTIMATES OF OZONE RESPONSE TO VARIOUS COMBINATIONS OF
NO_x AND VOC EMISSION REDUCTIONS IN THE EASTERN UNITED STATES**

Shawn J. Roselle,† Kenneth L. Schere,*† and Shao-Hang Chu‡*

*Atmospheric Sciences Modeling Division, Air Resources Laboratory, National Oceanic and Atmospheric Administration, Research Triangle Park, North Carolina 27711; †On assignment to the Atmospheric Research and Exposure Assessment Laboratory, U.S. Environmental Protection Agency; ‡Office of Air Quality Planning & Standards, U.S. Environmental Protection Agency, Research Triangle Park, North Carolina 27711

ABSTRACT

There is increasing recognition that controls on NO_x emissions may be necessary, in addition to existing and future VOC controls, for the abatement of ozone (O₃) over portions of the United States. This study compares various combinations of anthropogenic NO_x and VOC emission reductions through a series of model simulations. A total of 6 simulations were performed with the Regional Oxidant Model (ROM) for a 9-day period in July 1988. Each simulation reduced anthropogenic NO_x and VOC emissions across-the-board by different amounts. Maximum O₃ concentrations for the period were compared between the simulations. Comparison of the simulations suggests that (1) NO_x controls may be more effective than VOC controls in reducing peak O₃ over most of the eastern United States; (2) VOC controls are most effective in urban areas having large sources of emissions; (3) NO_x controls may increase O₃ near large point sources; and (4) the benefit gained from increasing the amount of VOC controls may lessen as the amount of NO_x control is increased.

This paper has been reviewed in accordance with the U.S. Environmental Protection Agency's peer and administrative review policies and approved for presentation and publication. Mention of trade names or commercial products does not constitute endorsement or recommendation for use.

1. INTRODUCTION

Feasible solutions to the tropospheric ozone (O₃) problem have evaded scientists and policy makers for many years. Emissions which are precursors to O₃ formation, volatile organic compounds (VOC) and nitrogen oxides (NO_x), have to be controlled to reduce O₃ concentrations. The relationship between precursor controls and actual reductions in O₃ concentrations is highly nonlinear. Historically, efforts to reduce O₃ concentrations have focused primarily on VOC emissions. Recent modeling studies (Trainer et al., 1987; Sillman et al., 1990; McKeen et al., 1991) have characterized much of the eastern United States as NO_x-limited, suggesting that NO_x controls may be more effective. However, certain areas such as New York City may be VOC-limited (EPA, 1991), where NO_x emission controls may be counter-productive in reducing O₃ concentrations in the local area. Selection of VOC or NO_x controls (or a combination of the two) will probably vary spatially, depending on the chemical regime of the location.

Previous studies, such as EPA (1991), have examined combinations of emission reductions and have provided valuable insight into the effectiveness of different controls. However, scientific understanding of the results of these studies has been hampered because of the spatial variability in emission reductions. There is a clear need for a systematic examination of NO_x and VOC emission reductions to provide a basis for more effectively formulating future control strategies.

This study examines the response of maximum ozone concentrations to uniform spatial and temporal reductions in VOC and NO_x emissions. The Regional Oxidant Model (ROM) (Lamb, 1983; Young et al., 1989) was used to simulate the July 2-10, 1988 period of high O₃.

2. PROCEDURE

A total of twenty-five simulations are planned for this study. Six have been completed, including simulations with the following sets of anthropogenic emissions (the same set of biogenic emissions were used for each simulation): (1) Base case; (2) 25% VOC and 25% NO_x controls; (3) 75% VOC and 25% NO_x controls; (4) 50% VOC and 50% NO_x controls; (5) 25% VOC and 75% NO_x controls; (6) 75% VOC and 75% NO_x controls. Simulations were performed with ROM version 2.2. ROM simulates most of the physical and chemical processes responsible for the buildup of O₃ on regional scales (~10⁶ km²). Detailed descriptions of the model can be found in Lamb (1983); Young et al. (1989); and Roselle et al. (1991). For this study, the modeling domain was chosen to cover the eastern United States, consisting of 16,128 grid cells within each vertical layer. The grid size was (1/4)^o longitude × (1/6)^o latitude, or approximately (18.5 km)². The model uses 3 dynamic vertical layers to represent the planetary boundary layer and capping inversion. During an entire simulation period, horizontal advection, diffusion and gas-phase chemistry for specified pollutants are modeled prognostically in the 3 vertical layers. Meteorological fields are derived by objective analysis of observed data from both surface and upper-air stations. The chemistry mechanism incorporated in the model is the Carbon-Bond Mechanism IV (Gery et al., 1989), which consists of 83 reactions and 33 individual species. In all simulations, relatively clean air ([O₃] = ~30 ppb) was assumed for both the initial and lateral boundary conditions. The O₃ boundary condition for the top of the model was ~40 ppb. It should be noted that there are limitations to the ROM, which include the inability to resolve sub-

grid processes, uncertainties in the input data, crude treatment of point sources, and relatively coarse horizontal and vertical resolution. Evaluations of the ROM (Schere and Wayland, 1989; Pierce et al., 1990a; Roselle, 1992) have shown that the model does well in positioning most of the major O₃ plumes, but tends to underpredict concentrations when observed values are above 70-80 ppb, and overpredict values below this level. For the current simulation, the model underpredicted maximum O₃ concentrations over the episode by 17 ppb (11%), on average.

Anthropogenic emissions were derived from the 1985 National Acid Precipitation Assessment Program (NAPAP) inventory (Saeger et al., 1989), which included emissions of VOC, NO_x, and CO (carbon monoxide). Major point, area, and mobile source emissions were considered in the inventory with day of the week (Saturday, Sunday, and weekday) and hourly variations on the emission rates. Additionally, mobile source evaporative emissions were adjusted for daily temperature variations using the empirical model MOBILE4.2 (EPA, 1989). For each emission reduction simulation, the emissions from all anthropogenic sources were reduced uniformly in space and time. Biogenic emissions were provided by the Biogenic Emissions Inventory System (BEIS) of Pierce et al. (1990b). Biogenic emissions were the same in each simulation.

3. DISCUSSION AND RESULTS

3.1 Base Case Simulation

Figure 1a presents the maximum hourly-averaged predicted O₃ concentrations for each grid in ROM's lowest vertical layer (100-300 m deep) for the 9-day period July 2-10, 1988. Maximum concentrations over the entire episode were chosen for this analysis because of their importance in determining if a location has exceeded the National Ambient Air Quality Standard (NAAQS) for ozone. In this plot, lower concentrations are denoted with lighter shades and higher concentrations with darker shades. High concentrations of ozone (> 120 ppb) were predicted over a large area in association with a stagnating high pressure system. Anticyclonic circulation around the high pressure system dominated the Great Lakes, Ohio Valley, and mid-Atlantic States. The Northeast Corridor (the extended overlapping urban areas from Washington, D.C. through Boston), however, experienced flow from the southwest in association with a low pressure trough along the East Coast. High O₃ concentrations extended from central Georgia to Lake Huron, and from St. Louis, Missouri to the coast of Maine. Much of this area was predicted to have O₃ in excess of 120 ppb. Concentrations above 180 ppb were predicted near Chicago, Lake Michigan, Lake Erie, Washington, D.C., Philadelphia, and New York City. Concentrations above 150 ppb were predicted for Atlanta, Lake Ontario, Pittsburgh, Charleston (West Virginia), and along a small segment of the Ohio River. The highest predicted hourly-average O₃ concentration was 262 ppb, which occurred over Lake Michigan. The average peak O₃ concentration across the domain was 75 ppb. Predicted concentrations were relatively low (< 60 ppb) over other areas, although smaller composite (over the episode) urban plumes were apparent in Texas, Oklahoma, and Louisiana.

3.2 Comparison of Simulations

25% VOC, 25% NO_x Reductions. Compared to the base case (fig. 1b), predicted O₃ was reduced by 5%-15% across most of the Eastern United States for this control strategy. Ozone decreased by the largest amount (> 15%) in an area over Lake Michigan, which had high concentrations in the base case. To the north and south of this area, the model predicted an increase (> 5%) in O₃ for this control strategy. Areas with an increase in O₃ were widely-scattered across the domain and were primarily located near emission source regions. The spatial extent of these areas was limited to just a few grid cells.

75% VOC, 25% NO_x Reductions. Figure 1c shows that for this strategy, O₃ was reduced by 15% to 30% in many areas of the Northeast, the Great Lakes, and over Texas and Louisiana. In composite urban plumes from New York City, Toronto, Montreal, Detroit, Cleveland, Chicago, and Houston, O₃ decreased by more than 30%. Other areas of the domain saw O₃ reductions on the order of 5%-15%. The largest reduction in O₃ was 56%, which occurred over Lake Michigan.

Comparing results from the simulations with 25% VOC, 25% NO_x controls and 75% VOC, 25% NO_x controls (fig. 1b and c) shows the relative benefit of adding more VOC controls to a NO_x control of 25%. Increasing VOC controls had the greatest impact on the Northeast, the Great Lakes area, and the western Gulf Coast states, as evidenced by the large areas with 15%-30% reductions in O₃. Additionally, with higher VOC controls, there were fewer grid cells showing an increase in O₃ over the base case simulation. Very little additional reduction in O₃ was predicted for the Southeast.

50% VOC, 50% NO_x Reductions. In this simulation, O₃ decreased by 15%-30% over most of the model domain (fig. 1d). Over Lake Michigan and scattered over the Southeast, O₃ decreased by more than 30%. On average, peak O₃ concentrations decreased by 17%. There were a few locations with higher O₃ concentrations following the emissions reduction; the spatial extent of these regions was limited to only a few grid cells, located near large NO_x point sources.

In a similar modeling study, McKeen et al. (1991) also examined O₃ sensitivity to 50% reductions in both VOC and NO_x emissions. Their results are consistent with this study, showing a decrease in afternoon ozone concentrations of 12% to 16% across much of the eastern United States, but an increase in some grid cells which had high NO_x emissions.

25% VOC, 75% NO_x Reductions. In this simulation, O₃ was reduced by more than 30% across much of the domain (fig. 1e). The controls reduced O₃ by 29% on average. Ozone decreased by more than 50% across the Southeast. There were a few grid cells near large NO_x sources which had higher O₃ in this simulation than in the base case. Some of the specific locations included Toronto, Chicago, Tampa, Houston, Baton Rouge, and New Orleans. The locations with an increase in O₃ were generally limited in spatial extent to the core urban area.

75% VOC, 75% NO_x Reductions. This simulation compares well to the simulation with 25% VOC and 75% NO_x controls. Ozone decreased substantially with the emission reductions (fig. 1f); much of the East was predicted to have O₃ reduced by more than 30%. The Southeast had the largest reductions in O₃, however, the spatial extent of the area with > 50% decrease in O₃ was smaller than in the simulation with 25% VOC and 75% NO_x reductions. Additionally, there were

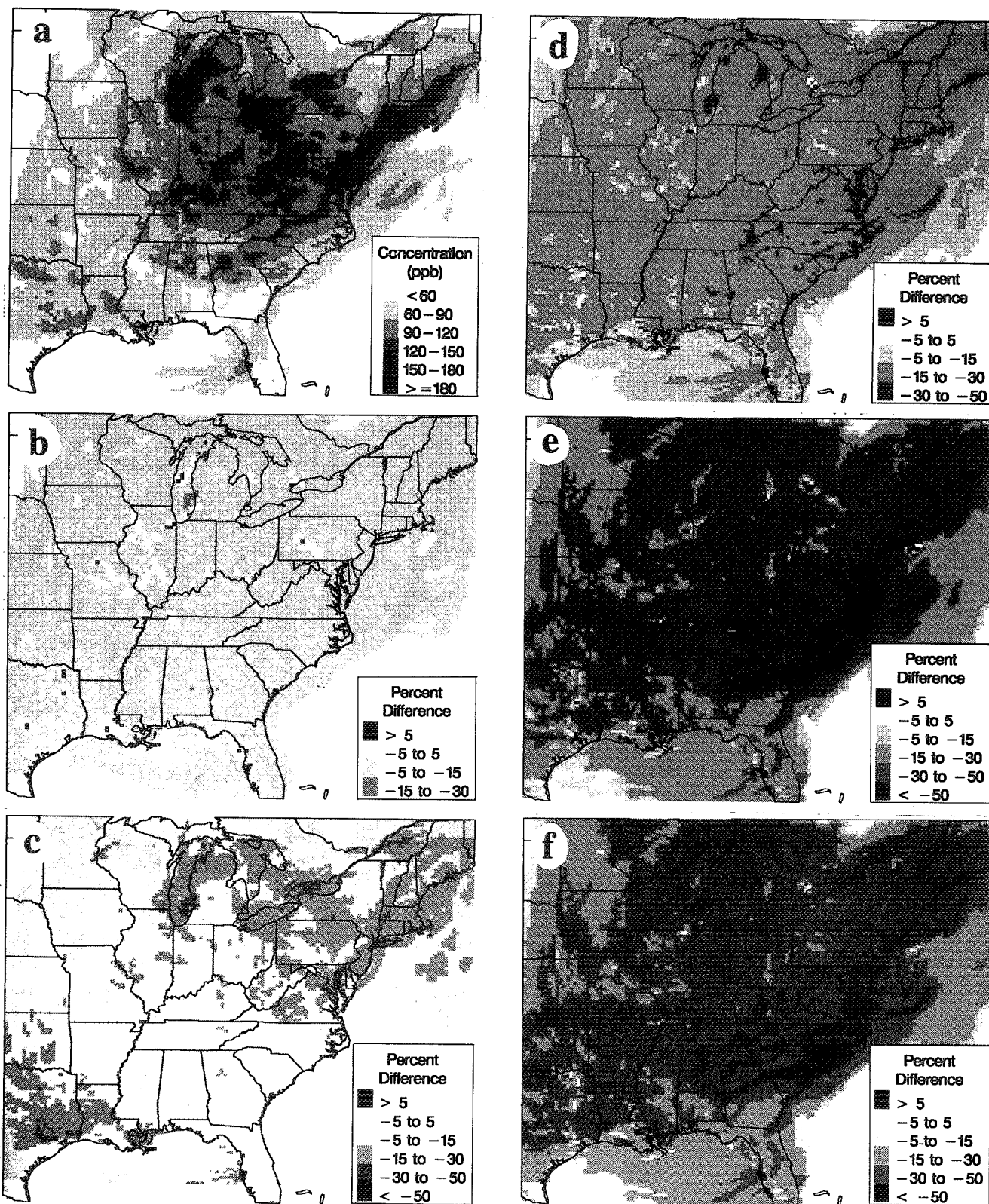


Fig. 1. (a) Episode maximum hourly-average O₃ (ppb) in layer 1 for the base case simulation. (b-f) Percent difference in episode maximum O₃ (layer 1) between the base case and simulations with anthropogenic emission reductions of: (b) 25% VOC, 25% NO_x, (c) 75% VOC, 25% NO_x, (d) 50% VOC, 50% NO_x, (e) 25% VOC, 75% NO_x, and (f) 75% VOC, 75% NO_x.

fewer grid cells in this simulations which had higher O₃ than the base case. The additional VOC controls examined in this simulation further improved O₃ in many of the major urban plumes, but hindered improvements in the Southeast where large NO_x controls were highly effective.

4. SUMMARY AND CONCLUSIONS

Simulations of the eastern United States were performed with the ROM for 6 different levels of anthropogenic emissions. The period of July 2-10, 1988 was studied because of the extremely high O₃ concentrations that occurred over the area. Initial results have been analyzed (summarized in Table 1) and have provided preliminary indications of the effects of different levels of emission controls. VOC controls benefit urban plumes near their sources, including the cities of Chicago, Detroit, Cleveland, Toronto, New York, Houston, and Dallas. NO_x controls produced widespread reductions in ozone. Controlling NO_x by 75% (with limited VOC control) made a much larger impact than 75% VOC control (with limited NO_x control). Reducing VOC emissions caused almost no increase in O₃, whereas NO_x controls did increase O₃ near large sources. The predicted behavior of O₃ suggests that much of the eastern United States is NO_x-limited, which is in agreement with modeling studies by Sillman et al. (1990) and McKeen et al. (1991).

As in most modeling studies, there are uncertainties that should be emphasized. In regards to scale, the ROM grid size may be too coarse to adequately resolve the fast chemical reactions which occur near large emission sources, and therefore the accuracy is reduced in model estimates of near-urban increases in O₃ due to NO_x controls. Uncertainty in model inputs is also a very important issue. It is generally accepted that anthropogenic VOC emissions are underestimated in the current inventories. For example, Fujita et al. (1992) suggest that mobile source VOC emissions are 2-3 times higher than the current estimates. Correction of the inventories for this underestimation of VOC's will only increase the preference for NO_x controls.

Further analysis will be performed on these simulations, and on the 19 simulations to be performed in the future. This paper examined only maximum predicted O₃ concentrations. The final objectives in this study are to develop response surfaces (isopleth plots) for various pollutants as a function of VOC and NO_x controls. Analysis of the response surfaces will then be performed on chemically-coherent subregions of the model domain. Upon completion, this research should provide

policy makers with detailed information on the predicted chemical nature of the eastern U.S. and may provide additional guidance for developing control strategies.

REFERENCES

- EPA, 1989: User's Guide to MOBILE4, EPA-AA-TEB-89-01, U.S. Environmental Protection Agency, Office of Mobile Sources, Ann Arbor, MI.
- EPA, 1991: Regional Ozone Modeling for Northeast Transport (ROMNET), edited by N.C. Possiel, L. Milich, and B. Goodrich, EPA-450/4-91-002a, U.S. Environmental Protection Agency, Office of Air Quality Planning and Standards, Research Triangle Park, NC.
- Fujita, E.M., B.E. Croes, C.L. Bennett, et al., 1992: Comparison of emission inventory and ambient concentration ratios of CO, NMOG, and NO_x in California's South Coast Air Basin, *J. Air & Waste Manag. Assoc.*, 42, 264-276.
- Gery, M., G. Whitten, J. Killus, et al., 1989: A photochemical kinetics mechanism for urban and regional scale computer modeling, *J. Geophys. Res.*, 94, 12,925-12,956.
- Lamb, R.G., 1983: A regional scale (1000 km) model of photochemical air pollution: Part 1. Theoretical formulation, EPA-600/3-83-035, U.S. Environmental Protection Agency, Research Triangle Park, NC.
- McKeen, S.A., E.-Y. Hsie, and S.C. Liu, 1991: A study of the dependence of rural ozone on ozone precursors in the eastern United States, *J. Geophys. Res.*, 96, 15,377-15,394.
- Pierce, T.E., K.L. Schere, D.C. Doll, et al., 1990a: Evaluation of the Regional Oxidant Model (version 2.1) using ambient and diagnostic simulations, EPA/600/3-90-046, U.S. Environmental Protection Agency, Research Triangle Park, NC.
- Pierce, T.E., B.K. Lamb, and A.R. Van Meter, 1990b: Development of a biogenic emissions inventory system for regional scale air pollution models, in Proceedings of the 83rd Air and Waste Manag. Assoc. Annual Meeting, Pittsburgh, PA.
- Roselle, S.J., T.E. Pierce, and K.L. Schere, 1991: The sensitivity of regional ozone modeling to biogenic hydrocarbons, *J. Geophys. Res.*, 96: 7371-7394.
- Roselle, S.J., 1992: Sensitivity of modeled ozone concentrations to uncertainties in biogenic emissions, EPA/600/R-92/067, U.S. Environmental Protection Agency, Research Triangle Park, NC.
- Saeger, M., J. Langstaff, R. Walters, et al., 1989: The NAPAP emissions inventory (version 2): Development of the annual data and modeler's tapes, EPA-600/7-89-012a, U.S. Environmental Protection Agency, Research Triangle Park, NC.
- Schere, K.L., and R.A. Wayland, 1989: EPA Regional Oxidant Model (ROM 2.0): Evaluation on the 1980 NEROS data bases, EPA-600/3-89-057, U.S. Environmental Protection Agency, Research Triangle Park, NC.
- Sillman, S., J.A. Logan, and S.C. Wofsy, 1990: The sensitivity of ozone to nitrogen oxides and hydrocarbons in regional ozone episodes, *J. Geophys. Res.*, 95, 1837-1851.
- Trainer, M., E.J. Williams, D.D. Parrish, et al., 1987: Models and observations of the impact of natural hydrocarbons on rural ozone, *Nature*, 329, 705-707.
- Young, J., M. Aissa, T. Boehm, et al., 1989: Development of the Regional Oxidant Model version 2.1, EPA-600/3-89-044, U.S. Environmental Protection Agency, Research Triangle Park, NC.

Table 1. Statistics on Episode Maximum Ozone*

Reduction Strategy	Mean Conc. (ppb)	Mean difference from base case	
		(ppb)	(%)
Base Case	75	-	-
25% NO _x 25% VOC	69	-6	-7
25% NO _x 75% VOC	66	-9	-10
50% NO _x 50% VOC	60	-15	-17
75% NO _x 25% VOC	49	-26	-29
75% NO _x 75% VOC	49	-26	-29

* Computed for model layer 1 over the entire domain (N=16,128 grid cells).

MODELING OZONE EPISODES IN THE BALTIMORE-WASHINGTON REGION

William F. Ryan

University of Maryland, Department of Meteorology,
College Park, MD 20742, USA

ABSTRACT

Surface ozone (O_3) concentrations in excess of the National Ambient Air Quality Standard (NAAQS) continue to occur in metropolitan areas in the United States despite efforts to control emissions of O_3 precursors. Future O_3 control strategies will be based on results from modeling efforts that have just begun in many areas. Two initial questions that arise are model sensitivity to domain-specific conditions and the selection of episodes for model evaluation and control strategy development. For the Baltimore-Washington region (B-W), the presence of the Chesapeake Bay introduces a number of issues relevant to model sensitivity. In this paper, the specific questions of the determination of model volume (mixing height) for the Urban Airshed Model (UAM) is discussed and various alternative methods compared. For the latter question, several analytic approaches (cluster analysis and classification and regression tree (CART) analysis) are undertaken to determine meteorological conditions associated with severe O_3 events in the B-W domain.

1. INTRODUCTION

Many major metropolitan areas in United States have been unable to comply with the NAAQS for O_3 set by the Clean Air Act (CAA). Many explanations have been advanced for this (1) failure to reduce emissions to extent proposed (rule efficiency); (2) underestimation of emissions, including biogenic emissions, and errors in the speciation of hydrocarbons; and (3) overly simplistic modeling approaches which have overestimated the effectiveness of proposed control strategies (*National Research Council, 1991*).

The 1990 amendments to the CAA mandate further use of photochemical modeling to demonstrate that control strategies will result in the future attainment of the O_3 NAAQS. This paper will provide a brief overview of the photochemical model in use in the B-W domain, the UAM, as well as critical U.S. Environmental Protection Agency (EPA) recommendations configuring the UAM for regulatory use. In addition, model sensitivity questions that have a domain-specific facet will be discussed along with the selection of historical O_3 episodes for modeling.

2. THE URBAN AIRSHED MODEL

The UAM is presently the only EPA-approved three-dimensional photochemical model for O_3 regulatory modeling. The UAM was first developed for use in

the Los Angeles Basin (*Reynolds, et al., 1973*) and the 1988 edition is in use in the B-W domain (*Morris et al., 1990*). In order to efficiently manage the numerous evaluation and control strategy model runs that are required, the input and archival processes are controlled by a software shell specially developed for the UAM (*Batch Processing System (BPS), John Haus*).

The UAM is a gridded Eulerian model, with three-dimensional cells having fixed horizontal and variable vertical dimensions. The vertical layers vary in space and time as a function of the height of the planetary boundary layer (PBL), generally referred to in UAM studies as the "mixing height". The UAM simulates spatially varying transport, diffusion, chemical transformation, deposition and emissions distributions within an area by solving the governing equations for particular processes. Atmospheric constituents are dispersed evenly within each cell. Surface removal is parameterized by deposition velocity which depends, generally, on surface concentration, roughness and type. The 1988 version of the UAM was updated to include the Carbon-Bond Mechanism IV (*Gery, Whitten and Killus, 1985*) and the Smolarkiewicz algorithm for the numerical approximation of horizontal advection terms in the species conservation equations.

The size of the domain (*Figure 1*) is determined by the expected distance that local emissions will be transported during an average day (*EPA, 1991*). This reflects the relatively slow process of photo-chemical O_3 production. The B-W domain is 250 km north-to-south and 230 km east-to-west and contains several unique aspects (1) the Chesapeake Bay dominates the center of the domain and introduces discontinuities in the surface heating and surface roughness fields; (2) the domain includes two urban cores and four states which introduces difficulties in emissions inventory development and model initialization; and (3) the extension of the domain boundaries to the north, to include portions of Greater Philadelphia as well as the Atlantic coast, introduces boundary condition problems.

The EPA recommends that the grid cells be no larger than 5 x 5 km. The UAM grid size can be varied to reflect emissions gradients and density and should bear some association to the resolution of the input data. The resolution of meteorological data, of course, is much coarser than 5 x 5 km and air quality data resolution can vary widely.

3. MODEL SENSITIVITY ANALYSIS

Model sensitivity issues can be roughly divided into universal or domain-specific categories. Chemical

mechanisms and reaction rates are examples of issues that are relatively independent of the model application. In the latter group are local effects such as unique meteorological or topographical conditions. In this paper domain-specific meteorological phenomena related to the model volume will be discussed. Results of earlier model sensitivity analyses with the UAM are contained in *Seigneur, et al. [1981]*; *Dennis and Downton [1984]*; *Seinfeld [1988]*.

The UAM is vertically described by model layers broken up into two regimes, with differing diffusion characteristics, separated by the "diffusion break", or mixing height. The model layers expand and contract evenly with the height of the diffusion break. In general, the layers below the diffusion break are assumed to be well-mixed with a homogeneous wind field and capped by an inversion. This idealized version of turbulent processes within the PBL reflects the origin of the UAM in Los Angeles applications where a strong subsidence inversion is frequent (*Taylor and Marsh, 1991*). It is not clear that this concept is as physically accurate in the B-W domain and early sensitivity work, using a simplified data base in this domain, showed that peak O₃ concentrations are very sensitive to variations in the height of mixed layer. As a baseline, a 50% reduction in mixing height increased peak O₃ by 33% (*M. Jorquera, personal communication*).

The hourly evolution of the mixing height (model volume) is determined via interpolation from minimum and maximum mixing height values calculated by an EPA algorithm (*Kelly, 1981*). The EPA algorithm uses potential temperature profiles, calculated from radiosonde data, and a static stability analysis to determine the extent of buoyant overturning of surface-based parcels of air. This analysis assumes that the air near the surface cools adiabatically as it rises so that θ is conserved. The maximum depth of the mixed layer is the height at which the ambient potential temperature (θ_2) is equal to or greater than surface potential temperature (θ_0).

This method for estimating mixing heights raises several questions. First, the timing of the radiosonde launches (0000 Universal Coordinated Time (UTC) and 1200 UTC) are early morning (0800 EDT) and early evening (2000 EDT) in the B-W domain and are not optimal for observing either mid-day maximum or early morning minimum mixing height. To account for this, the EPA algorithm replaces the surface temperature at the time of the sounding with the morning minimum and afternoon maximum surface temperature. The simulation of mid-day temperature profiles is reasonable given the relatively poor conductivity of air but will fail in conditions of synoptic-scale temperature advection. For a severe O₃ event (July 6, 1988) using the 1200 UTC and 0000 UTC soundings results in a 36% difference in maximum mixing height.

Second, θ profiles are most useful in dry environments and in situations where buoyancy forces driven by the earth's heating dominate over larger scale forces, such as convergence associated with approaching fronts, which can induce upward motion. The eastern U.S. is quite moist in the summer months and the mixing ratio of water is not constant with altitude. In these cases, a measure which accounts for the presence of moist air, virtual potential temperature (θ_v), is more useful (*Stull, 1991*). For a three day episode in July, 1988, the θ_v profiles of mixing height at three stations averaged 338 m or 21.4% higher than the θ profiles.

Finally, mixing heights calculated from a specific sounding station must be extrapolated to other locations within the domain. Dulles International Airport (IAD) is the only upper air station within the B-W domain.

The two nearest stations (Wallops Island, VA and Atlantic City, NJ) are liable to coastal effects, especially in the planetary boundary layer. Horizontal interpolation is accomplished by a proportional variation in mixing height based on temperature differences, or the entire sounding can be applied to surface temperatures at other stations. This is a particular problem with respect to Chesapeake Bay and coastal locations within the B-W domain. Previous studies have shown that the mixing height can vary significantly in this area (*Segal et al., 1982*).

The sparseness of meteorological data and the sensitivity of the UAM to input parameters such as mixing height, and wind fields, suggest that regulatory applications of the UAM should be confined to O₃ episodes characterized by uniform meteorological fields. That is, the cases should be as "model-tractable" as possible.

4. EPISODE SELECTION

EPA has recommended that several groups of historical severe O₃ episodes be modeled with each group, or regime, representative of a "distinctly different source-receptor relationship" (*EPA, 1991*). The selection of specific cases must then be made from the most severe O₃ episodes in each regime. Identifying discrete transport regimes in the context of severe O₃ episodes is a difficult process. Severe O₃ events in the eastern U.S. are typically associated with slow-moving, or stagnant, surface anticyclones (*Vukovich et al., 1977*; *Vukovich and Fishman, 1986*). Light and variable surface winds are associated with anticyclonic flow, especially near the center of the anticyclone. As a result, the likelihood of strong surface wind signals for distinct types of O₃ events are slight. In the B-W domain, there is an additional complicating factor in the strong bay breeze signal associated with weak synoptic forcing (*Schofield and Weiss, 1977*). This effect is often not seen in the synoptic-scale observation network. Surface wind rose calculations carried out in accordance with EPA recommendations show that for all types of conditions there is a single strong WSW signal. This suggests that there is only one transport regime associated with strong O₃ events or that this method is not effective.

In order to determine if there is a useful alternative classification strategy, three approaches were undertaken (1) cluster analysis; (2) classification and regression tree (CART) analysis; and (3) subjective meteorological analysis of severe O₃ events. The cluster analysis seeks to determine weather patterns using a set of meteorological data from a single location in a particular season. The shortcoming of this approach is that weather patterns, expressed in terms of meteorological variables, are generally homogeneous and categorization results in a loss of information as cases are forced into a Procrustean bed of clusters. In this study, summer season (June, July and August) data at Baltimore-Washington International Airport (BWI) for the period from 1983-1990 was used. Surface data consist of four times daily (10, 14, 18 and 2200 UTC) pressure, temperature, dew point temperature, wind velocity and sky cover. Upper air data (850 and 700 mbar) from the closest upper air station (IAD), was also included and consist of 1200 UTC geopotential height, temperature, moisture (expressed as dew point temperature) and wind velocity.

The cluster analysis consisted of two steps: First, principal components analysis (PCA) was applied to the original data matrix (*Kalkstein and Corrigan, 1986*). The cluster analysis is performed on the matrix of component scores using the average linkage method (*Kalk-*

stein et al., 1987). As expected, the bulk of the total variance is determined by temperature, pressure and sky cover. Of the ten total clusters, two contain the bulk of the most severe O₃ cases and are distinguished by hot and moist conditions (Cluster 3) or stagnant surface conditions (Cluster 9). In terms of source-receptor relationships, both clusters exhibit light WNW upper air winds.

To further analyze local effects, the CART analysis was used (*California Statistical Software, 1991*). This type of analysis has been used for O₃ studies (*Horie, 1987*) and general weather forecasting (*Burrows, 1991*) and has been recommended for use in regulatory applications (*National Research Council, 1991*). The CART technique operates by a binary splitting of data into groups that are more homogeneous (*Breiman, et al., 1984*). A succession of binary splits results in a "tree" whose final "branches", or terminal nodes, represent distinct classes, or categories of data. In this case, the predictand is domain mean maximum O₃ for the period JJA 1983-1990. The predictors consist of surface variables as in the cluster analysis. The observed upper air variables are expanded to include data at 50 mbar intervals between 950 and 650 mbar.

The majority of the strong O₃ cases are grouped in two of the five CART terminal nodes. The non-O₃ nodes are easily filtered out by mid-day surface temperature of less than 86°F. The two high O₃ nodes are distinguished by a linear combination dominated by midday temperature. The cases in the strongest O₃ node are characterized by lower morning temperature, higher pressure and higher afternoon temperatures. Wind directions are highly variable within each node and do not contribute significantly to differences at this level. Winds at the surface in the strong O₃ nodes are generally west (W) with west-northwest (WNW) winds aloft. In terms of episode selection, the results of the CART analysis can separate the weak O₃ cases but cannot further distinguish regimes within the high O₃ cases.

A second series of runs was undertaken using a subset of 195 strong O₃ cases in which domain mean O₃ exceeded 90 ppbv or in which the NAAQS was violated. In the cluster analysis the major components are essentially the same as in the initial run except that three additional components are added that include combinations of surface and upper air winds, afternoon sky cover and upper air temperatures. The two strongest O₃ sub-clusters are similar to the major clusters above with one cluster characterized by extremely hot and moist conditions with WNW winds aloft and afternoon southerly surface winds and a second sub-cluster characterized by stagnant conditions. The remaining sub-clusters, which have less severe average O₃, but contain a smattering of severe cases, are variations on the hot and moist sub-cluster with differences based on wind direction.

A second CART analysis using the subset of strong O₃ cases was also undertaken. The key variables responsible for the distinction between terminal nodes in this analysis are upper air temperature and the θ_v gradient. The strongest, in terms of O₃, node is characterized by high temperature at all levels with a weak gradient in θ_v . The remaining nodes are characterized by strong θ_v gradients but cooler temperatures. An inference that may be drawn from this distinction is that CART distinguishes between "hot" cases in which high temperature and low sky cover drive strong local O₃ chemistry and cases in which stable lower tropospheric conditions trap emissions into a smaller volume.

The subjective analysis investigated multi-day O₃ episodes for the 1983-1990 period (N=159). Multi-day events represent the bulk (83%) of the extreme O₃ cases from which the episodes must be selected. This

analysis classified cases by the position of the nearest surface anticyclone, the position of surface fronts and the upper air transport pattern as evidenced by 850 mbar height patterns. This process was able to successfully classify 86% of the cases included in multi-day O₃ events and was more successful (95%) with the most extreme twenty events. The subjective classification grouped the cases into four classes based mainly on differences in upper air height fields. Class 1 contains cases with northerly upper air winds and a surface anticyclone to the southwest. Class 2 contains similar surface conditions, although with a higher incidence of lee troughs (*Pagnotti, 1987*), but westerly winds aloft. Class 3 is characterized by a surface anticyclone to the SE, often near Cape Hatteras, and SW flow aloft.

This class is typical of O₃ events in the northeastern U.S. Finally, Class 4 contains cases in which stationary fronts, or slow-moving cold fronts are present in, or just south of, the domain.

When the subjective classifications are compared to the results of the cluster analysis using the subset of 195 cases and focusing on the classification of the fifteen strongest O₃ episodes there is some consistency. The sub-clusters with northerly winds and stagnant conditions are both associated with Class 1 (northerly air flow) in the subjective analysis. The hot sub-cluster with WNW upper air and WSW surface winds is associated with Class 2 and the sub-cluster with southwesterly winds is associated with Class 3. A similar comparison with the CART terminal nodes is less successful. The cases from Classes 1 and 2 in the subjective analysis are typically grouped together by the CART analysis. Cases with southerly air flow (Class 3) are successfully separated into another node by CART. However, when all multi-day events are compared, there is very little coherence between the cluster, CART and subjective analyses.

5. CONCLUSION

Due to the unique topography of the B-W domain, variations in mixing heights are expected to be large. The UAM is sensitive to variations in mixing heights and different analyses used to create mixing height fields result in significant variations. Given the UAM sensitivity to meteorological input fields, O₃ episodes to be analyzed for regulatory purposes should exhibit relatively uniform, or model-tractable, meteorological fields. Clustering techniques and subjective meteorological analysis are able to provide some evidence of distinct weather regimes associated with severe O₃ events in the B-W regime. The subjective analysis can also provide insight into the most model-tractable episodes. However, the EPA regulations relating to episode selection require that the final selections be limited to the most extreme O₃ events in each regime. These cases often exhibit unusual meteorological conditions such as lee trough formation.

REFERENCES

- Breiman, L., et al., *Classification and Regression Trees*, Wadsworth, 1984.
- Burrows, W.R., Objective guidance for 0-24-hour and 24-48-hour mesoscale forecasts of lake-effect snow using CART, *Wea. Forecasting*, 6, 357-378, 1991.
- California Statistical Software, *CART*, Lafayette, CA, 1991.
- Dennis, R.L., and M.W. Downton, Evaluation of urban photochemical models for regulatory use, *Atmos. Environ.*, 18, 2055-2069, 1984.
- Douglas, S.G., R.C. Kessler, and E.L. Carr, *User's Guide for the Urban Airshed Model, Volume 3: User's Manual for the Diagnostic Wind Model*, EPA-450/4-90-007A, U.S. Environmental Protection Agency, Research Triangle Park, NC, 1990.
- EPA, *Guidelines for Regulatory Application of the Urban Airshed Model*, EPA-450/4-91-013, U.S. Environmental Protection Agency, Research Triangle Park, NC, 1991.
- Gery, M.W., G.Z. Whitten, and J.P. Killus, *Development and Testing of the CBM-IV for Urban and Regional Modeling*, EPA-600/3-88-012, U.S. Environmental Protection Agency, Research Triangle Park, NC, 1988.
- Horie, Y., *Ozone Episode Representativeness Study for the South Coast Air Basin*, Valley Research Corp., prepared for the South Coast Air Quality Management District, El Monte, CA, 1987.
- Kalkstein, L.S., and P. Corrigan, A synoptic climatological approach for geographical analysis: Assessment of sulfur dioxide concentrations, *Annals Assoc. Amer. Geograph.*, 76, 381-395, 1986.
- Kalkstein, L.S., G. Tan, and J.A. Skindlov, An evaluation of three clustering procedures for use in synoptic climatological classification, *J. Clim. Appl. Meteor.*, 26, 717-730, 1987.
- Kelly, R.F., *User's Manual for Mixing Height Computer Program*, EPA-450/4-81-022, U.S. Environmental Protection Agency, Research Triangle Park, NC, 1981.
- Morris, R.E., and T.C. Myers, *User's Guide for the Urban Airshed Model, Volume 1: User's Manual for UAM (CB-IV)*, EPA-450/4-90-007A, U.S. Environmental Protection Agency, Research Triangle Park, NC, 1990.
- National Research Council, *Rethinking the Ozone Problem in Urban and Regional Air Pollution*, National Academy Press, Washington, D.C., 1991.
- Pagnotti, V., A meso-meteorological feature associated with high ozone concentrations in the northeastern United States, *J.A.P.C.A.*, 37, 720-722, 1987.
- Reynolds, S.D., J.H. Seinfeld, and P.M. Roth, Mathematical modeling of photochemical air pollution - I. Formulation of the model, *Atmos. Environ.*, 7, 1033-1061, 1973.
- Scofield, R.A. and C.E. Weiss, A report on the Chesapeake Bay Region Nowcasting Experiment, *Technical Memorandum NESS 94*, National Oceanic and Atmospheric Administration, Washington, D.C., 1977.
- Segal, M., et al., Numerical model simulation of the regional air pollution meteorology of the Greater Chesapeake Bay Area-Summer day case study, *Atmos. Environ.*, 16, 1381-1397, 1982.
- Seigneur, C., et al., Sensitivity of a complex urban air quality model to input data, *J. Clim. Appl. Meteor.*, 20, 1020-1040, 1981.
- Seinfeld, J.H., Ozone air quality models: A critical review, *J.A.P.C.A.*, 38, 616-645, 1988.
- Stull, R.B., Static stability - An update, *Bull. Amer. Meteor. Soc.*, 72, 1521-1527, 1991.
- Taylor, G.H., and S.L. Marsh, Jr., An inversion climatology for the Los Angeles Basin, *Preprints, 7th Joint Conference on Applications of Air Pollution Meteorology*, American Meteorological Society, Boston, MA, 294-297, 1991.
- Vukovich F.M., and J. Fishman, The climatology of summertime O₃ and SO₂ (1977-1981), *Atmos. Environ.*, 20, 2423-2433, 1986.
- Vukovich, F.M., W.D. Bach, Jr., B.W. Crissman, and W.J. King, On the relationship between high ozone in the rural surface layer and high pressure systems, *Atmos. Environ.*, 11, 967-983, 1977.

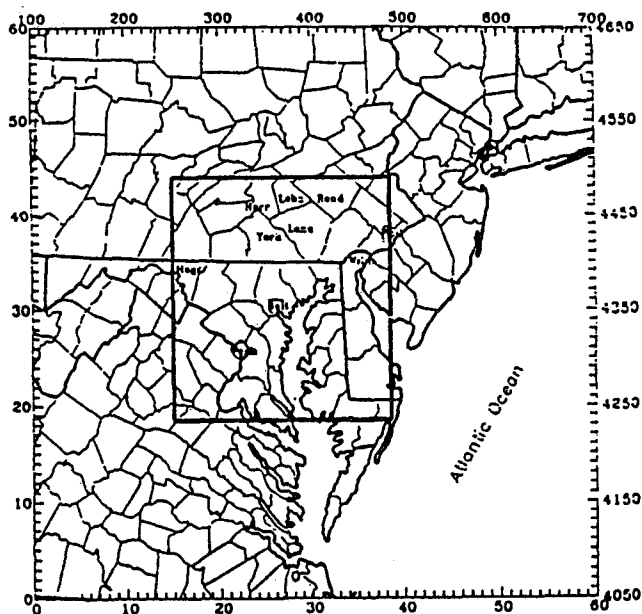


Fig. 1. UAM domain for Baltimore-Washington region.

NUMERICAL SIMULATION OF THE INTERACTION OF TRANSPORT, DIFFUSION AND CHEMICAL REACTIONS IN AN URBAN PLUME

Bernhard Vogel, Heike Vogel, Franz Fiedler

Institut für Meteorologie und Klimaforschung
Kernforschungszentrum Karlsruhe/Universität Karlsruhe
Postfach 3640, D-7500 Karlsruhe 1

ABSTRACT

A model system is presented that takes into account the main physical and chemical processes on the regional scale here in an area of 100x100 km². The horizontal gridsize used is 2x2 km². For a case study it is demonstrated how the model system can be used to separate the contributions of the processes advection, turbulent diffusion and chemical reactions to the diurnal cycle of ozone. In this way typical features which are visible in observations and are reproduced by the numerical simulations can be interpreted.

1 INTRODUCTION

Concentration levels of reactive trace gases observed in nature at any specific point of time and space are determined by a number of physical and chemical processes. In the case of a cloud free atmosphere these processes are the transport by the mean wind field, the diffusion caused by atmospheric turbulence and the chemical reactions. The mean wind field and the atmospheric turbulence field are remarkably influenced by the topography on the regional scale. Chemical reactions make the set of differential equations describing the temporal and spatial variation of the different air constituents nonlinear. The nonlinearity of the chemical reactions rises a number of problems. One is that it is impossible to derive simple emitter-receptor relations.

If in a highly industrialized region the behaviour of trace gases is to be studied, it is necessary to achieve a high temporal and spatial resolution, a requirement which can be fulfilled by measurements only during short periods. Such measuring activities were carried out e.g. by Becker et al. (1979) and during the TULLA-experiment (Fiedler, 1987).

Another possibility to study the involved processes with the relevant resolution in space and time arises by the use of a numerical simulation model.

In order to be able to apply a model for realistic conditions the most important processes must be included. In addition it also should be tested against measurements of a variety of atmospheric conditions.

With respect to atmospheric research there exist two main areas of interest. The first is connected to air quality studies where the most important problem is to keep concentration levels below a certain value or to reduce concentration levels. In this sense numerical simulation models can be used to develop efficient strategies for emission reductions.

The second area of interest, which will be focused on in this paper, is devoted to studies of the interaction of the different processes (advection, diffusion and chemical reactions) and to quantify the contributions of these processes to the time and spatial variation of the ozone concentration. The separation of the different processes from measurements alone is rather troublesome and is often not possible due to the lack of information. This is especially true if only measurements are available at a specific point and no information about the spatial variation of the variables is given. In many cases this lack of information is the reason for speculative interpretations.

Therefore models can be used to support the interpretation of measurements and to better understand the observed features.

2 THE MODEL SYSTEM

The nonhydrostatic mesoscale model KAMM (Adrian, Fiedler; 1991) coupled with a diffusion model and the RADM chemical transformation mechanism (Chang et al., 1987; Stockwell, 1986) is used to calculate the time variation of the three-dimensional distribution of the meteorological variables wind, temperature, humidity and turbulence and a number of chemical species on the regional scale. The model

system which takes into account the topography and the different land use includes a soil-vegetation model (Schädler, 1990) and a detailed parameterization of the dry deposition (Baer, Nester; 1992). With a method developed by Adrian (1987) it is possible to determine the basic state and the forcing of the model system from operational numerical weather forecast. Results of the model system were already compared with observations, for example by Vogel, H. (1991). Figure 1 shows the structure of the model and the input data which are necessary.

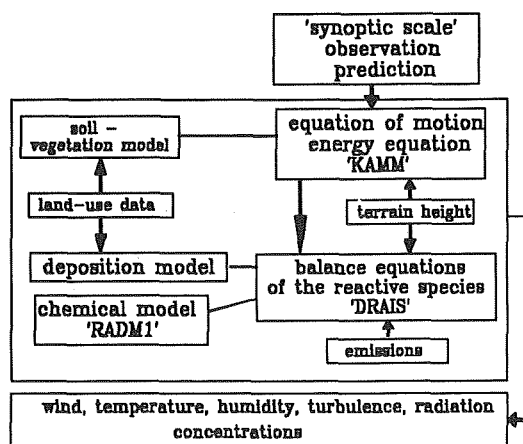


Figure 1. : The structure of the mesoscale model system developed at the 'Institut für Meteorologie und Klimaforschung' in Karlsruhe.

For this case study, only the emissions of the area sources of Heilbronn, a small city in the south-western part of Germany, are taken into account. The emission area is indicated by a rectangular in Figures 2-6. The emission data were taken from the emission data base determined for the time period of the TULLA experiment (Obermeier et al. 1989). The emission data are available with a spatial resolution of 1x1 km² and a temporal resolution of one hour. For the initial background concentrations, measurements are used. The horizontal grid size is 2 km, the vertical grid size differs from 18 m close to the surface up to 600 m at the top of the model which is 8 km above sea level. A geostrophic wind from north-west with 7.5 m/s is chosen for this simulation. Two complete diurnal cycles are calculated for a typical summer day.

In order to better understand the observed diurnal cycles the model is used to calculate the contributions of the relevant processes (advection, turbulent diffusion and chemistry) to the spatial and temporal variation of the O₃ concentration and to study their interaction.

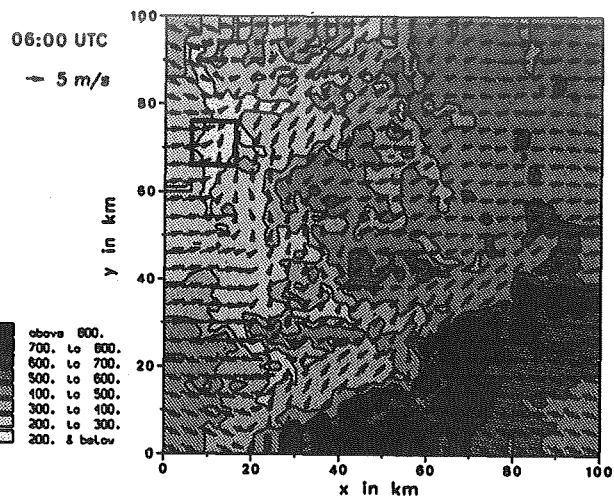


Figure 2: Topography and simulated windfield 18 m above ground (day 2, 06:00 UTC). The rectangular shows the area where the emissions are taken into account.

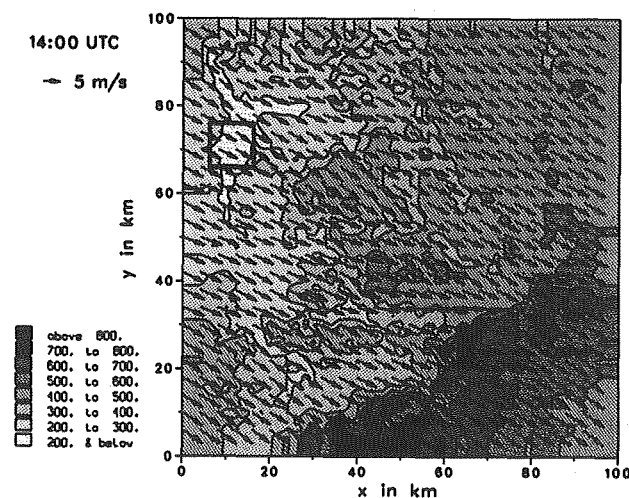


Figure 3: Topography and simulated windfield 18 m above ground (day 2, 14:00 UTC).

3 RESULTS

- The results show a strong modification of the flow field during the diurnal cycle caused by the topography. Therefore the city plume is also remarkably influenced (Figures 2-6).
- The simulated diurnal cycles of ozone show typical features for urban and rural areas (A,B in Fig. 7) which are in good agreement with measurements. These features are: First, concentrations close to zero are found during night in urban areas and therefore a high amplitude of the diurnal cycle. Second, much higher concentrations during night are found in rural areas and therefore a small amplitude of the diurnal cycle.

- There is a buildup region of ozone due to chemical reactions in the city plume about 50 km behind the source area (Fig. 6).
- At points A and B, the total hourly variations of ozone are in the same order of magnitude in spite of the fact that the order of magnitude of the single processes at both points are quite different (Fig. 8 and 9).
- In the urban area (Point A) the increase of ozone between sunrise and the early afternoon is mainly caused by turbulent diffusion (Fig. 8).

- The simulation shows that the secondary maximum of the ozone concentration after midnight at point A is caused by reduced chemical destruction and the advection of ozone from outside into the city (Fig. 8). Such a secondary maximum commonly can be recognized in the observations of many urban stations.
- During night the ozone distribution close to the surface is controlled by the interaction of turbulent diffusion and dry deposition (Figures 10-11). Low turbulence together with low windspeed results in low ozone concentrations (Point C). In contrast at elevated sites enhanced turbulence compensates the deposition (Point D).

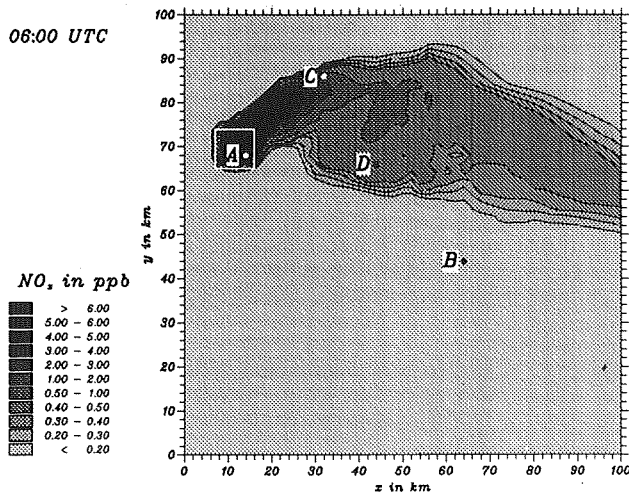


Figure 4: Simulated NO_x —distribution 18 m above ground (day 2, 6:00 UTC).

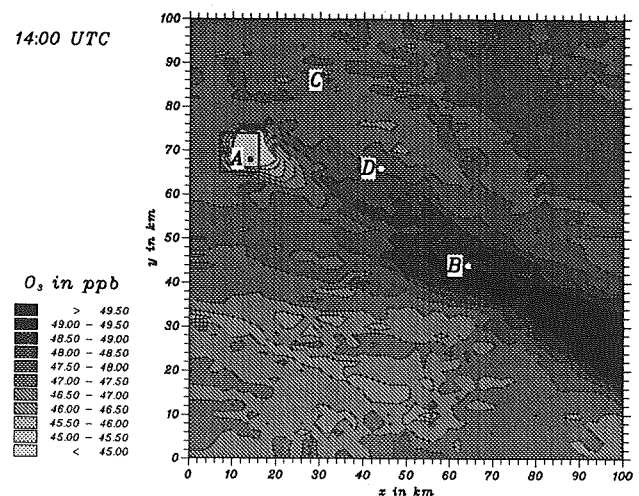


Figure 6: Simulated O_3 —distribution 18 m above ground (day 2, 14:00 UTC).

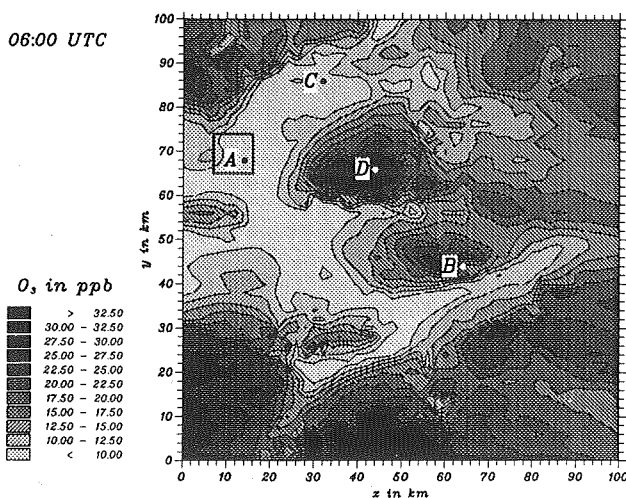


Figure 5: Simulated O_3 —distribution 18 m above ground (day 2, 6:00 UTC).

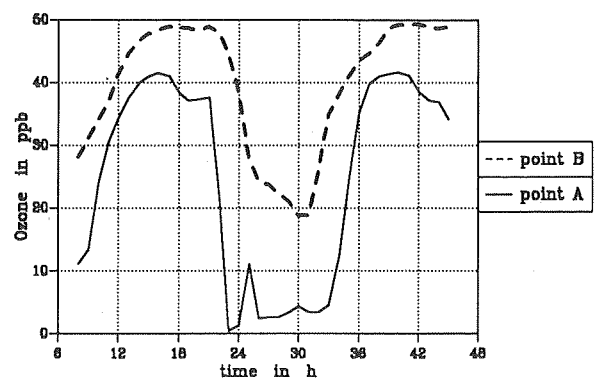


Figure 7. : Simulated diurnal cycles of the ozone concentration 18 m above ground at points A and B.

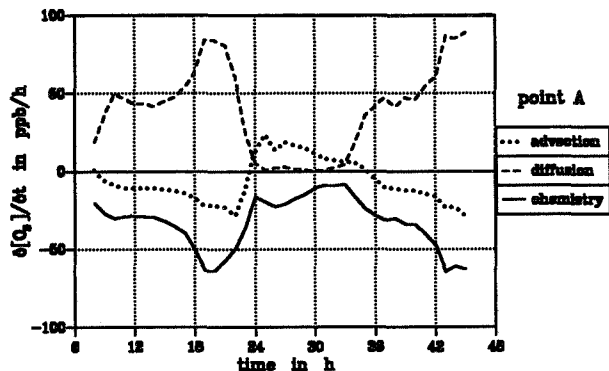


Figure 8. : Contributions of the different processes to the hourly variation of the ozone concentration 18 m above ground at point A.

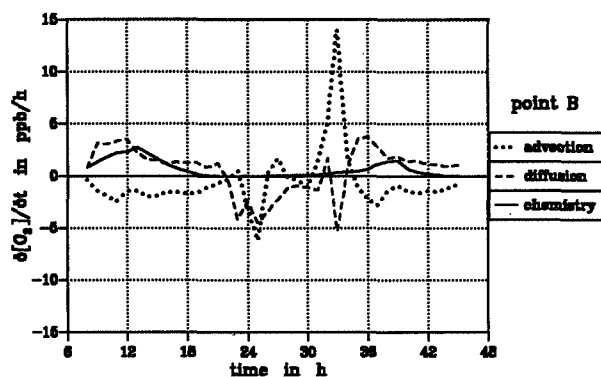


Figure 9. : Contributions of the different processes to the hourly variation of the ozone concentration 18 m above ground at point B.

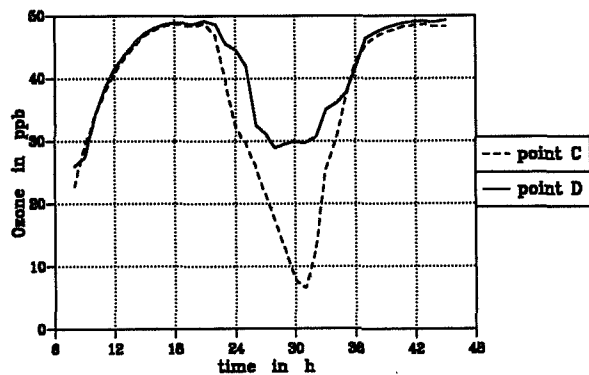


Figure 10. : Simulated diurnal cycles of the ozone concentration 18 m above ground at points C and D.

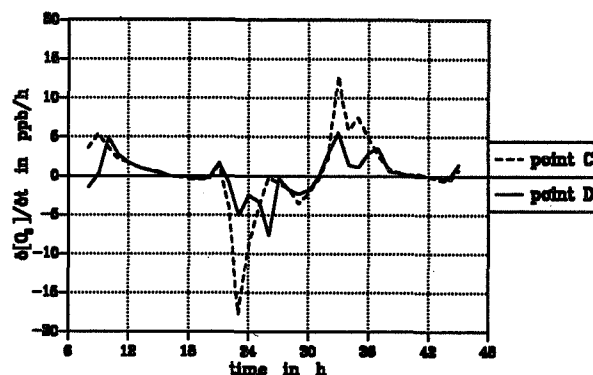


Figure 11. : Contributions of the turbulent diffusion including dry deposition to the hourly variation of the ozone concentration at the surface at points C and D.

REFERENCES

- Adrian G.,1987: Determination of the basic state of a numerical mesoscale model from operational numerical weather forecast. *Beitr. Phys. Atmosph.* , 60, 361 - 370.
- Adrian, G., F. Fiedler,1991: Simulation of unstationary wind and temperature fields over complex terrain and comparison with observations. *Beitr. Phys. Atmos.* 64 , 27-48
- Baer, M., K. Nester,1992: parameterization of trace gas dry deposition velocities for a regional mesoscale diffusion model. Accepted for publication by *Annales Geophysicae* .
- Becker, K.H., U. Schurath, H.W. Georgii, M. Deimel,1979: Untersuchungen über Smogbildung, insbesondere über die Ausbildung von Oxidantien als Folge der Luftverunreinigung in der Bundesrepublik Deutschland. *Forschungsbericht 79-10402502/03/04 für das Umweltbundesamt* .
- Chang, J.S., R.A. Brost, I.S.A., Isaksen, S. Madronich, P. Middleton; W.R. Stockwell, C.J. Walcek, C.J.1987: A three-dimensional Eulerian acid deposition model: Physical concepts and formulation. *J. Geophys. Res.* 92, 14681-14700 .
- Fiedler, F.,1987: Atmospheric transport of air pollutants in the mesoscale over hilly terrain: A review of the TULLA - experiment. S. Sandroni (ed.), *Regional and Long - Range Transport of Air Pollution: Lectures of a Course* , Elsevier Science Publ. B.V., Amsterdam, 337 - 353
- Obermeier, A., R. Friedrich, A. Voss,1989: Zeitlicher Verlauf und räumliche Verteilung der Emissionen von flüchtigen organischen Verbindungen und Kohlenmonoxid in Baden-Württemberg. 5. *Statuskolloquium des PEF. KfK-PEF 50*
- Schädler, G.,1989: Numerische Simulationen zur Wechselwirkung zwischen Landoberflächen und atmosphärischer Grenzschicht. *Wiss. Ber. Inst. f. Meteor. u. Klimaforschung Nr. 13*
- Stockwell, B.W.,1986: A homogeneous gas phase mechanism for use in a regional acid deposition model. *Atmos. Environ.*, 20, 1615-1632
- Vogel, H.,1991: Verteilungen reaktiver Luftbeimengungen im Lee einer Stadt - Numerische Untersuchungen. *Wiss. Ber. Inst. f. Meteor. u. Klimaforschung Nr. 15*

303249

A TRAJECTORY MODELING INVESTIGATION OF THE BIOMASS BURNING - TROPICAL OZONE RELATIONSHIP

Kenneth E. Pickering¹, Anne M. Thompson², Donna P. McNamara³,
Mark R. Schoeberl², Leslie R. Lait¹, Paul A. Newman²,
Christopher O. Justice⁴, Jacqueline D. Kendall⁵

¹Universities Space Research Association, NASA/GSFC, Greenbelt, MD 20771 USA

²NASA/Goddard Space Flight Center; ³Applied Research Corporation

⁴Dept. of Geography, Univ. of Maryland; ⁵Science, Systems, and Applications, Inc.

ABSTRACT

The hypothesis that tropical total O₃ maxima seen by the TOMS satellite derive from African biomass burning has been tested using isentropic trajectory analyses with global meteorological data fields. Two case studies from the 1989 biomass burning season demonstrate that a large fraction of the air arriving at the location of TOMS O₃ maxima passed over regions of intense burning. Other trajectories initiated at a series of points over Africa and the Atlantic suggest flight strategies for field studies to be conducted in September 1992.

1. INTRODUCTION

Biomass burning in the tropics has been increasing in recent years with the demand for agricultural land. The consequences of increased burning for atmospheric chemistry and global climate are being investigated at monitoring sites and in field missions (Cros et al., 1992; DECAFE issue JGR, 97, D6, 1992). A major concern is that biomass fires are contributing to tropospheric O₃ formation because biomass fires are rich sources of NO_x, CO and hydrocarbons.

Fishman et al. (1990, 1991) inferred enhancements in tropospheric O₃ over the South Atlantic by analysis of satellite data. The tropical O₃ maximum appears in the months of August - November in both TOMS total O₃ fields and in what Fishman et al. (1990) call the "tropospheric O₃ residual." The tropospheric residual is obtained by subtracting stratospheric O₃ (derived from SAGE I and II) from the TOMS total column O₃. Fishman et al. (1990) hypothesized the maximum comes from biomass burning emissions, primarily in southern Africa. Local enhancements in ozone have been observed in ozonesonde profiles taken at Brazzaville, Congo, and at Ascension Island in the Atlantic. The ozonesondes reveal seasonally elevated peaks of O₃ in the lower troposphere, presumably resulting from low-level transport of O₃ and precursor gases when there is burning on the African continent (Fishman et al., 1991; Cros et al., 1992).

Despite evidence for the hypothesis that "biomass burning causes tropical O₃ maxima," there has not been a detailed study using trajectory analysis to prove or disprove the linkage between biomass burning regions and the appearance of the South Atlantic maximum in the O₃ residual. The objective of this study is to examine that linkage. Specifically, we have performed case studies to determine the extent to which short-term (days) tropospheric O₃ maxima observed from TOMS can be linked to regions of extensive burning in Africa, as defined by AVHRR fire count data.

The first part of this paper is a preliminary report, focusing on links between TOMS O₃ and fires for two one-week periods in September and October 1989 for which fire counts have just become available. The second part of the paper describes results for trajectory analyses that look at flow regimes over the tropical South Atlantic on a larger scale. The aim is to anticipate conditions over South America, Africa, and the South Atlantic that are likely to be encountered during 1992 field campaigns (SAFARI = Southern Africa Fire Atmosphere Research Initiative and NASA/GTE/TRACE-A = Global Tropospheric Experiment/Transport and Atmospheric Chemistry Near the Equator - Atlantic). Methods and data sets are first described.

2. METHODS AND DATA SETS

TOMS Data. Gridded TOMS data (Version 6.0) are used to identify episodes of persistent high O₃ during the period August-October 1989. Tropical maxima in total O₃ that appeared unrelated to the major stratospheric horizontal gradient in the middle latitudes were identified and assumed to be tropospheric features. Fishman et al. (1990) have shown a very high correlation between total O₃ and the tropospheric O₃ residual in the tropics. Two O₃ maxima from early October 1989 were selected as likely candidates for having a biomass burning source (Figure 1).

AVHRR Fire Counts. Regions of burning each day were defined by fire count data derived from AVHRR imagery. Fires radiate at very high temperatures and their signature appears as a spike in the 3.55 to 3.93 micron channel (channel 3) of AVHRR, but has much less effect on the 10.3 to 11.3 micron channel (channel 4). The algorithm counts fires by looking for pixels with high channel 3 values and large differences between channels 3 and 4 relative to their immediate background values (Matson et al., 1987). The method performs well over uniform terrain, but is complicated by background differences (e.g., coastlines, rivers, burnscars, etc.) and very hot ground temperatures. Furthermore, deriving fire count estimates from AVHRR is complicated by smoke or fire-induced clouds that conceal fires and by uncertainty about fire size. One satellite pass over Africa per day is processed, but the orbital swath is not as wide as southern Africa. Therefore, the data are not complete enough to permit quantification of emissions. Instead, regions with large numbers of fires are identified for possible connection with high O₃.

Trajectory Model. An isentropic trajectory model developed for use in stratospheric analyses (e.g., Schoeberl et al., 1992) has been used. The model requires global gridded

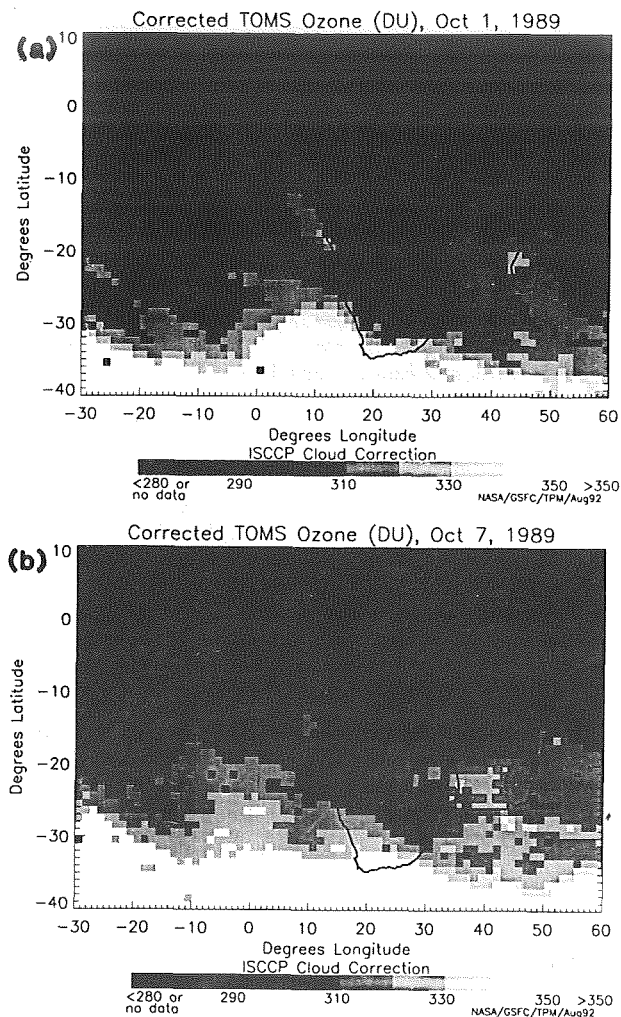


Fig. 1. TOMS total column ozone on a $1^\circ \times 1.25^\circ$ grid for (a) October 1, 1989, and (b) October 7, 1989. Note that prior to selection of these O_3 maxima data west of Africa were corrected for anomalously high O_3 over marine stratocumulus clouds (see Thompson et al, *this volume*).

fields of temperatures, u and v wind components, and potential vorticity. The gridded wind fields are first interpolated to user-selected isentropic surfaces and then interpolated temporally and spatially. A time step of 0.01 days (~15 min) is used. Temperature is interpolated onto the parcel path from the gridded data and used with an assumption of potential temperature conservation along the trajectory to compute the pressure at each successive parcel position. Model output for each parcel consists of a file containing a time series of parcel positions (x, y, p), temperatures, solar zenith angles, and potential vorticity. Plots of trajectories are prepared with parcel positions indicated every 12 hours. Both backward and forward trajectories have been constructed with the model.

Two different sets of meteorological data fields have been used in the trajectory model. The National Meteorological Center (NMC) 1200 UTC global analyses of temperature and geopotential height, along with balanced winds computed from the height fields were retrieved for September and October, 1989, from the archive at NASA

Goddard. The NMC data (on 18 standard pressure surfaces from 1000 to 0.4 mb) were interpolated to $2^\circ \times 2.5^\circ$ latitude/longitude grids. Twice-daily (0000 and 1200 UTC) analyzed fields from the European Center for Medium-range Weather Forecasting (ECMWF) were also acquired for days covering specific case study periods. These $2.5^\circ \times 2.5^\circ$ gridded fields are available for seven standard pressure surfaces from 1000 to 100 mb.

3. RESULTS: BACK TRAJECTORIES FROM O_3 MAXIMA

1 October 1989. The TOMS image for 1 October 1989 (Julian Day 274) showed total O_3 off the coast of Angola to have two grid cells with total O_3 at 330-340 DU and a much larger region with 320-330 DU (Figure 1a). Therefore, we have run backward trajectories from 1200 UTC on October 1 from an array of 11 air parcel arrival points ranging from $10^\circ S$ to $20^\circ S$ and from 0° longitude to $14^\circ E$, using the ECMWF fields.

The trajectories were computed for constant potential temperature surfaces ranging from 308 K to 324 K, yielding a total of 99 trajectories with arrival pressures ranging from 519 to 815 mb. Figure 2a shows that for all surfaces except 308 K the vast majority of the trajectories originate from the continent of Africa. For all surfaces combined, a total of 80 of 99 eight-day trajectories originate over the continent. While some flow off the continent may exist on the 308 and 310 K surfaces, the existence of considerable elevated terrain in Southern Africa (large regions > 1000 m elevation, corresponding to potential temperatures of 300 to 310 K) makes the surfaces 312 K and higher more likely to contain the bulk of the biomass burning emissions. Seventy of 77 trajectories on these surfaces arrive from the African continent. All 70 trajectories passed over regions with at least some burning, based on the fire data (Figure 3a) totaled over the week prior to October 1.

Several of the trajectory paths computed on the 312, 314, and 316 K surfaces (arrival pressures 649 to 763 mb) have been plotted in Figure 3a. For these three surfaces 31 of 33 trajectories originated over African burning regions, and nine trajectories passed over grid cells each containing more than 1750 pixels indicating fires. Therefore, flow characteristics in this case show that appreciable biomass burning emissions could have been transported to the region of the near-Angola 1 October TOMS total O_3 maximum.

7 October 1989. On October 6 (Julian Day 279) an O_3 maximum appeared over Zimbabwe and by October 7 (Figure 1b) had drifted to near the coast of Mozambique. The maximum column O_3 value was in the 330-340 DU range. We ran back trajectories on the 308-324K surfaces from 1200 UTC on October 7 from an array of 9 air parcel arrival points ranging from $20^\circ S$ to $24^\circ S$ and from $32^\circ E$ to $40^\circ E$.

The arrival pressures of the 81 trajectories ranged from 467 to 840 mb. Figure 2b shows that the source regions were quite diverse in this case. No one source region dominated on any of the isentropic surfaces. Overall, 24 trajectories arrived from the Indian Ocean or Madagascar and 57 trajectories passed over the African continent. Comparison with the fire data (Figure 3b) shows that the 57 trajectories passed over regions with at least some burning. Twenty-two of the 57 trajectories were in westerly flow sufficiently strong to have passed over South America during the eight-day trajectory duration. In general, flow arrived from the east at the more northerly points in the array and from the west at points further south. Several of the trajectories on surfaces arriving near 700 mb (310 - 314 K) are also displayed in Figure 3b. On these surfaces 15 out of the 27 trajectories were from the African

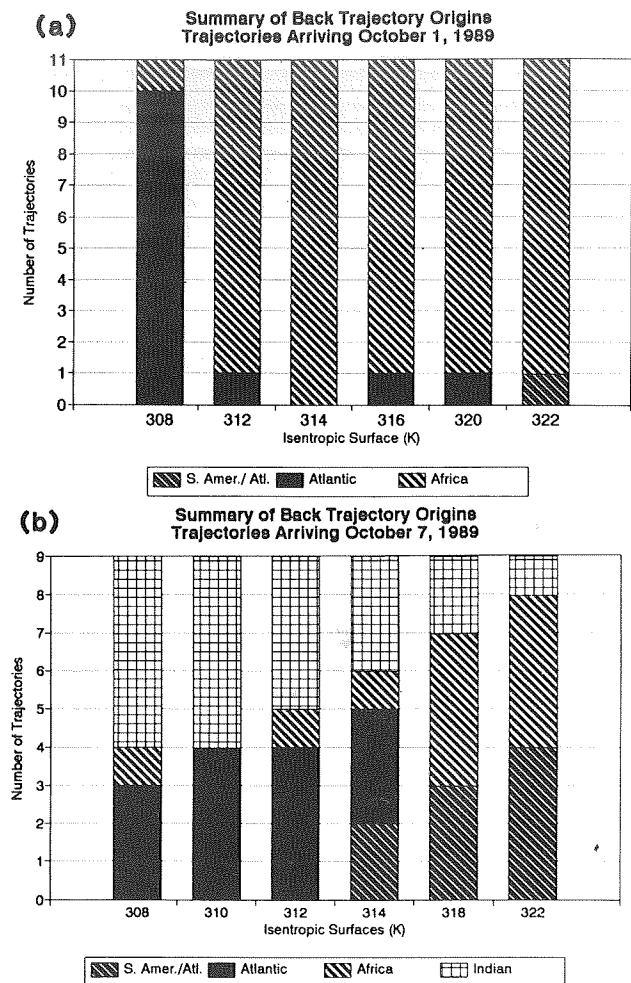


Fig. 2. Summary of back trajectory origins for six isentropic surfaces. (a) Trajectories arriving at TOMS O₃ maximum on October 1, 1989; (b) Trajectories arriving on October 7, 1989.

burning regions and eight of the remaining 12 trajectories passed over Madagascar where burning is also likely occurring (although no data for Madagascar are available at present). Particularly on the 310 and 314 K surfaces, several trajectories passed over African grid cells containing between 1000 and 1750 fire pixels. Therefore, large quantities of biomass burning emissions were likely transported to the case study region.

4. SUMMARY OF SEPTEMBER 1989 TRAJECTORIES

Trajectories based on the NMC analyses with balanced winds for September and early October 1989 were run to examine the larger-scale flow patterns. Forward trajectories were initiated every third day between September 11 and September 28, 1989, from an array of 15 points located from the equator to 30°S over the African continent. Trajectories that intersect the elevated terrain were not used. Backward trajectories were initiated every third day between September 19 and October 6, 1989, from an array of 19 points located from the equator to 25°S over the South Atlantic.

Eight-day forward trajectories from points on the African continent from the equator to 20°S show flow toward

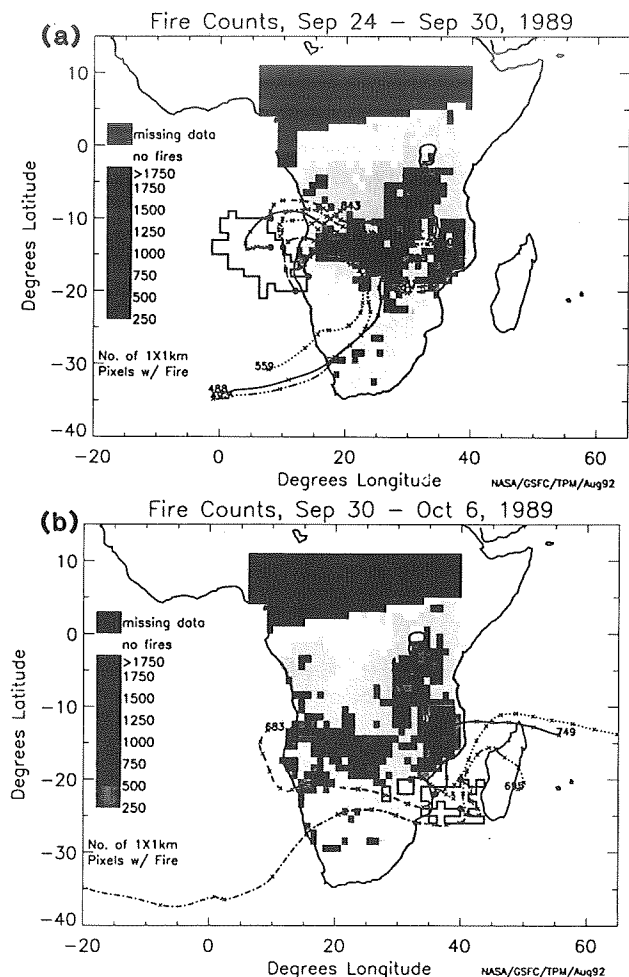


Fig. 3. Total biomass fire counts (derived from AVHRR imagery) for (a) September 24 - September 30, 1989; and (b) September 30 - October 6, 1989. The data displayed are counts of the number of 1.1 x 1.1 km pixels that have fires for each 1° latitude by 1° longitude grid cell. Superimposed are selected back trajectories and the TOMS maxima. In (a) trajectories are on the 312, 314, and 316 K surfaces and in (b) on the 310, 312, and 314 K surfaces. Numbers at the trajectory origins are pressures in millibars.

the South Atlantic at the low levels ($\theta < \sim 315\text{K}$, i.e., below ~ 700 mb). At points further south flow is toward the Indian Ocean. At higher altitudes ($\theta > 320\text{K}$; i.e., pressures $< \sim 500$ mb) trajectories go toward the Indian Ocean from points as far north as 15°S. In mid September extreme variation in the flow patterns was observed over a period of just a few days. Trajectory characteristics varied widely. In one case all the flow on the 316K surface from points at or south of 15°S headed for the Indian Ocean; three days later on the same surface almost all the flow was toward the South Atlantic.

Table 1 summarizes all the forward trajectories initiated in September from two specific points where controlled burns will be carried out in September 1992. These are Etosha National Park in Namibia (20°S, 15°E) and Kruger National Park in South Africa (25°S, 30°E). In both cases, flows are predominantly to the Indian Ocean, with a greater fraction of

Table 1. Number of Forward Trajectory Destinations
September 11-28, 1989

Destination	Isentropic Surface (K)					
	308	310	312	314	316	318 320
	Starting point 20°S, 15°E					
Atlantic Ocean	0	0	1	1	2	1 1
Africa	0	0	1	1	2	3 4
Indian Ocean	0	0	0	2	5	4 4
	Starting point 25°S, 30°E					
Atlantic Ocean	0	0	0	0	1	0 0
Africa	0	0	1	1	1	3 3
Indian Ocean	4	4	3	5	5	4 4

Table 2. Number of Backward Trajectory Origins
(Direction of Origin Relative to Arrival Point)
September 19 - October 6, 1989

Direction	Isentropic Surface (K)				
	308	310	315	320	325
	Arrival point 10°S, 0° long.				
East	7	7	7	7	6
West	0	0	0	0	0
	Arrival point 20°S, 0° long.				
East	0	1	2	1	1
West	5	6	5	5	5

the total number of trajectories from the Kruger area (38/39) than from the Etosha area (26/32) reaching that ocean. Virtually none of the trajectories from the Kruger region in 1989 went over the Atlantic.

Back trajectories from points in the South Atlantic show flow from the African continent arriving at the more northerly and easterly points in the array and flow from the South American continent arriving at the more southerly and westerly points. Trajectories on the 308K surface show the most air arriving from Africa and the least from South America. With increasing potential temperature more of the air arrives from South America. At 325K, for example, air arrives from South America as far north as 10°-15°S.

Table 2 summarizes the backward trajectory origins for two specific points over the South Atlantic (10°S, 0° and 20°S, 0°). The results are strikingly different for these two points. At the more northerly point all of the trajectories arrive from the easterly sectors (ie., likely African origin), whereas at 20S the majority of the trajectories arrive from westerly sectors (ie., likely South American origin).

5. DISCUSSION

The controlled burns of September 1992 in Etosha and Kruger National Parks will be the focus of intensive measurements during the TRACE-A and SAFARI experiments. During TRACE-A the NASA DC-8 aircraft will be flown to measure O₃, CO, hydrocarbons, NO_x, and meteorological data. Flight tracks will be directed along African coastlines to characterize outflow from the continent to the oceans.

If the results of 1989 are any indication of typical flow patterns for this region and time of year (they agree in general with longer-term climatologies), our trajectory results strongly suggest that most of the burning emissions from southern Africa (south of 20°) will be transported off the eastern coast. Flight tracks should be included over the Indian Ocean.

In terms of identifying sources of high O₃ episodes over the tropical Atlantic, the back trajectories underscore the need for flights planned to measure outflow from South America as well as Africa.

6. CONCLUSIONS

We have performed trajectory analyses to explore linkages between biomass burning emissions in Africa and tropical O₃ maxima seen by the TOMS satellite instrument.

(1) Back trajectory analyses in two case studies show that a significant fraction of the air arriving at locations of TOMS total O₃ maxima near the coasts of Africa passed over regions of intense burning during the prior eight days. Therefore, ozone generated from the precursor emissions could have contributed to the total O₃ maxima measured by the satellite.

(2) Examination of 1989 trajectories throughout the month of September shows that points of intense burning in southern Africa will tend to export fire emissions to both the Atlantic and Indian Ocean regions. Backward trajectories computed for an array of points over the Atlantic have suggested significant influences by burning occurring on the African and South American continents.

(3) These results suggest that research flights off southern Africa to capture outflow from burning regions include sampling along both eastern (Indian Ocean) and western (Atlantic) coasts. Characterization of tropical O₃ maxima west of Africa also requires flights along South America.

(4) There are several caveats regarding the analyses performed to date. The fire data do not cover all of southern Africa on any given day. In addition, the representativeness of the 1989 fire data will not be known until more years are processed. Even after performing a correction of regions of marine stratocumulus clouds, there remains considerable uncertainty in interpreting the TOMS measurements in cloudy and partly cloudy regions. The meteorological fields are uncertain because of the scarcity of observations over Africa and the tropical Atlantic. There is also uncertainty in using the isentropic trajectory technique over tropical Africa where the temperature profile frequently approaches adiabatic and where clouds may produce important diabatic effects. However, the consistency of the transport characteristics over a deep isentropic layer suggests robustness in the results.

Acknowledgments. This work was sponsored under the NASA Tropospheric Chemistry Program and through an EOS Interdisciplinary Investigation. Fire count data were generated under funding from NASA's Process Studies Program Office.

REFERENCES

- Cros, B., D. Nganga, A. Minga, J. Fishman, V. Brackett, The distribution of tropospheric ozone at Brazzaville, Congo, determined from ozonesonde measurements, *J. Geophys. Res.*, **97**, 12869-12875, 1992.
- Fishman, J., C. E. Watson, J. C. Larsen, and J. A. Logan, The distribution of tropospheric ozone determined from satellite data, *J. Geophys. Res.*, **95**, 3599-3617, 1990.
- Fishman, J., K. Fakhruzzaman, B. Cros, D. Nganga, Identification of widespread pollution in the Southern Hemisphere deduced from satellite analyses, *Science*, **252**, 1693-1696, 1991.
- Matson, M., G. Stephens, and J. Robinson, Fire detection using data from the NOAA-N satellites, *Int. J. Remote Sens.*, **8**, 961-970, 1987.
- Schoeberl, M. R., L. R. Lait, P. A. Newman, J. E. Rosenfield, The structure of the polar vortex, *J. Geophys. Res.*, **97**, 7859-7882, 1992.
- Thompson, A. M., K. E. Pickering, D. P. McNamara, Effect of marine stratocumulus on TOMS ozone in the tropical eastern Atlantic, *1992 Quadrennial Ozone Symposium*, Charlottesville, VA, 1992.

ENHANCEMENT OF FREE TROPOSPHERIC OZONE PRODUCTION BY DEEP CONVECTION

*Kenneth E. Pickering¹, Anne M. Thompson², John R. Scala¹
Wei-Kuo Tao², Joanne Simpson²*

¹ Universities Space Research Association, NASA/GSFC,
Greenbelt, MD 20771 USA

² NASA/Goddard Space Flight Center

ABSTRACT

It is found from model simulations of trace gas and meteorological data from aircraft campaigns that deep convection may enhance the potential for photochemical ozone production in the middle and upper troposphere by up to a factor of 60. Examination of half a dozen individual convective episodes show that the degree of enhancement is highly variable. Factors affecting enhancement include boundary layer NO_x mixing ratios, differences in the strength and structure of convective cells, as well as variation in the amount of background pollution already in the free troposphere.

1. INTRODUCTION

It has been observed that deep convective clouds are a major means of transporting insoluble trace species such as CO, NO_x, O₃, and hydrocarbons from the boundary layer to the middle and upper troposphere (Dickerson et al., 1987). Ozone precursor gases, once detrained from a convective cloud, can react and produce O₃ photochemically in the free troposphere downwind from a convective system. Ozone produced in the free troposphere has a much longer lifetime than O₃ produced photochemically in the boundary layer, thereby allowing it to be transported large distances from the precursor source region. Another consequence of deep convection is that O₃ production in the boundary layer may actually become more efficient following dilution of polluted boundary layer air with cleaner air descending from aloft in convective downdrafts. More ozone may be produced in the boundary layer, thereby enhancing the ozone production potential of the entire tropospheric column.

These conclusions are based on a series of model analyses to estimate the downwind perturbation in tropospheric O₃ production in convective outflow using airborne trace gas observations from convective events that occurred during NASA- and NSF/NOAA-sponsored field programs. This paper describes the analytical method and major results from this series of model simulations. We present a summary of O₃ production enhancements for six studies completed to date and a discussion of how chemical and dynamical characteristics contributed to the degree of enhancement in each event.

2. METHOD

The analysis procedure consists of three steps: (1) The convective system is simulated with a two-dimensional cloud

dynamical and microphysical model (e.g., Tao et al., 1991) initialized with a sounding of temperature, moisture, and winds.

(2) The wind fields produced in this simulation are used in a tracer transport model to redistribute trace gases measured from aircraft that can, as a first order approximation, be considered conserved during rapid convective transport (O₃, NO_x, CO, and many nonmethane hydrocarbons).

(3) Profiles representing "undisturbed" and "cloud-processed" trace gas composition are selected from the resulting 2-D trace-gas fields and used to constrain a one-dimensional photochemical model (Thompson and Cicerone, 1986; Pickering et al., 1990; 1991) to calculate O₃ production rates for the 24-hour period following the convective event.

These 24-hour averaged rates are designated the "ozone production potential". We have defined a "convective enhancement factor" (CEF) which is the ratio of column ozone production potential in cloud-processed air to that in undisturbed air. The column is chosen based on the vertical extent of the free tropospheric cloud-outflow layer in each convective event.

3. RESULTS AND DISCUSSION

Table 1 lists the convective events analyzed with their convective enhancement factors. The results and discussion are grouped by geographic region.

Oklahoma - PRESTORM

We have simulated two vigorous thunderstorm events from the Oklahoma PRESTORM experiment of June 1985 (Studies 1 and 5). The O₃ production rates for the June 15 mesoscale convective complex were calculated (Pickering et al., 1990) with only the photochemical model using direct aircraft observations to distinguish undisturbed and cloud-processed air (ie., without using the cloud simulation), whereas the June 10 squall line was simulated (Pickering et al., 1992a) with the full procedure described in the previous section. The June 15 cloud-processed observations (Dickerson et al., 1987) reflect the effects of convective redistribution and lightning on a typical rural central U. S. NO_x profile; a CEF of ~4 was computed. Rural NO_x mixing ratios also characterized the June 10 event, but the O₃ production calculations were performed with the simulated NO_x redistribution with no additional NO_x from lightning. The resulting CEF was 2.5. The June 10 storm later passed over the Oklahoma City region, entraining the urban plume. When measured trace gas mixing ratios characteristic of the Oklahoma City plume (50 km downwind of the city) were redistributed by the simulated

Table 1. Convective Ozone Production Enhancement

Study	Description	CEF	Reference
1	Okla. PRESTORM, 15 June 85	4	Pickering et al (1990)
2	ABLE 2A, 3 August 85 P(O ₃)	-- +	Pickering et al (1991)
2A	ABLE 2A, 3 August 85 dynamics Savanna burning Forest burning	53 59	Pickering et al (1992b)
3	ABLE 2B, 6 May 87	~1	Scala et al (1990)
4	ABLE 2B, 26 April 87 Unpolluted Urban plume	2.5 35	Pickering et al (1992a)
5	Okla. PRESTORM, 10 June 85 Rural Urban plume	2.5 3.9	Pickering et al (1992a)
6	STEP/EMEX, 2 Feb. 87	< 1	Pickering et al (1992d)

storm, the CEF increased to 3.9.

Amazon Basin - ABLE 2A and 2B

Studies 2 through 4 were conducted for convective events that occurred during the NASA Global Tropospheric Experiment Amazon Boundary Layer Experiment (ABLE 2A and ABLE 2B) in Brazil. The dry season case (August 3, 1985 - Study 2) included observations of low NO_x and hydrocarbons (primarily isoprene), causing a net loss of O₃ in the undisturbed free troposphere (Pickering et al., 1991). Following the convective event, the cloud-processed air contained sufficient NO_x vented from the boundary layer to allow net O₃ production to occur in the free troposphere. The integrated ozone production potential in the 5-13 km cloud-outflow layer changed from net destruction to net production as a result of convective transport. The simulation of the August 3 squall line shows efficient transport of boundary layer air to the upper troposphere in relatively undilute core updrafts (a "hot tower" as shown by the trajectories in Figure 1).

In a sensitivity study of ozone production potential (Pickering et al., 1992b), the August 3, 1985, cloud dynamics were assumed to apply to regions in Brazil affected by intense pollution from biomass burning (Study 2A). When the simulated squall line redistributed the trace gases (Figure 2) over these regions, pollution plumes were introduced into a pristine free troposphere, enhancing the ozone production potential by a factor of between 50 and 60. The CEF for redistribution of forest burning emissions is slightly higher than that for savanna burning because of the presence of isoprene over the forest. Figure 3 shows the profile of ozone production potential in cloud processed and undisturbed air for the forest burning case.

We have extrapolated our cloud-scale CO convective transport results to the regional-scale for an area intensely polluted by biomass burning. Using the convective transport in the August 3 event as a prototype, along with satellite-derived convective cloud climatology and areal extent of biomass burning pollution, we have estimated (Pickering et al., 1992c) that 10 - 40% of CO emissions from biomass burning may be rapidly transported to the free troposphere

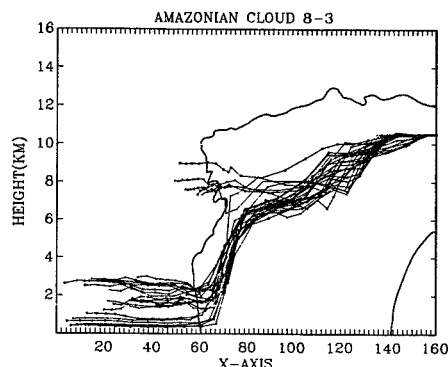


Fig. 1. Set of back trajectories simultaneously arriving at 26 horizontal positions at 10.5 km at the rear of the August 3, 1985 Amazonian squall line. Horizontal scale shows grid points at 0.5-km intervals. Heavy line is approximate outline of cloud (after Pickering et al. (1991), copyright American Geophysical Union).

over the major region of deforestation in the Amazon Basin. This result suggests that a significant fraction of the O₃ precursors generated from forest burning in Brazil may actively generate O₃ in the free troposphere where O₃ has a much longer lifetime than in the boundary layer.

In the wet season over the Amazon Basin, NO_x concentrations in unpolluted air are even lower than in the dry season and the ozone production potential was very close to zero (May 6, 1987 event - Study 3, Scala et al, 1990). Convective transport to the free troposphere was considerably less than in the August 3, 1985, dry season case, due to much overturning and midlevel detrainment of air from the storm. The well-mixed moist troposphere in which the squall line developed may have hindered strong updraft and downdraft development. Parcel trajectory analyses show that more than 50% of the air transported to the anvil region of the storm originated above 6 km, not from the boundary layer via undilute cores, as in the dry season event. The resulting CEF

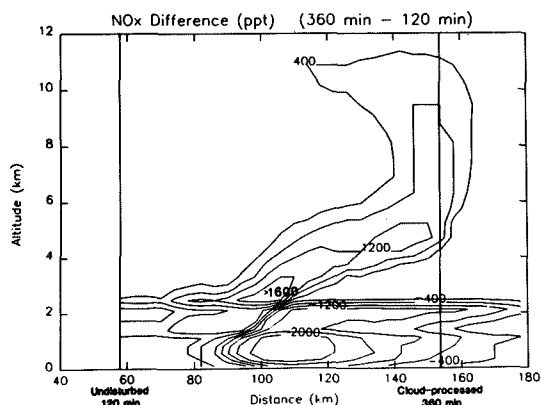


Fig. 2. Difference in tracer mixing ratios computed by subtracting undisturbed fields from cloud-processed fields, showing the magnitude of trace gas redistribution when biomass burning pollution encounters a convective storm such as the August 3, 1985, event. NO_x difference, contour interval 400 pptv (after Pickering et al. (1992b), copyright Kluwer Academic Publishers).

was very close to 1.

In a second wet season case (April 26, 1987 - Study 5), the NO_x was slightly greater and the convection more vigorous, producing a CEF of about 2.5 (Pickering et al., 1992a). This squall line also entrained the urban plume from the city of Manaus, containing similar NO_x , CO, and hydrocarbon levels to those in the Oklahoma City plume (Study 5). Because of the much cleaner free troposphere over Brazil, the CEF for this case was 35, compared to only 3.9 for convective redistribution of the Oklahoma City urban plume. This contrast demonstrates the importance of the amount of background pollution already in the free troposphere in determining the degree of convective enhancement. The CEF computed for the entire tropospheric column in the redistributed Manaus plume shows that convection increased column ozone production potential by almost 50%. In addition to the greater O_3 production in the middle and upper troposphere, O_3 production efficiency per molecule of NO in the boundary layer increased by 60% as cleaner air descended to dilute the more polluted air (Figure 4).

Marine tropics - STEP/EMEX

Simulation of a convective event off the northern Australian coast (Study 6 - February 2, 1987; Pickering et al., 1992d) showed relatively weak vertical transport. This event occurred during the Stratosphere-Troposphere Exchange Project (STEP) and the Equatorial Mesoscale Experiment (EMEX). Low NO_x marine air was transported upward from the lower troposphere, resulting in a CEF < 1 in the cloud outflow. Both observations and the simulation showed that the cloud was relatively deep (15-16 km), but vertical velocities did not exceed 10 m s^{-1} . Forward trajectories (Figure 5) constructed from model-computed wind fields showed boundary layer air not reaching altitudes higher than 12 km with substantial mid-level detrainment.

As in the Study 3 wet season ABLE 2B event (May 6, 1987), the troposphere was already quite well mixed prior to the event, as evidenced by the profile of equivalent potential temperature shown in Figure 6. The convective transport characteristics of the STEP/EMEX case and of Study 3 are in sharp contrast to those of the Amazon dry season event

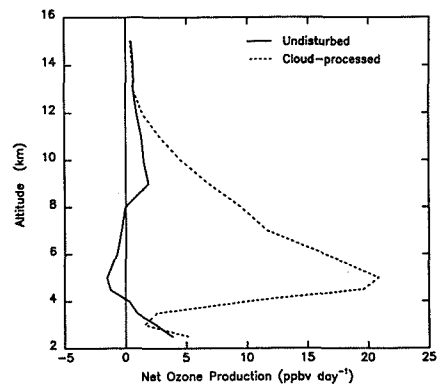


Fig. 3. Diurnally-averaged ozone production potential for the 24 hours following the redistribution of pollution from forest burning by the August 3, 1985, convective event (after Pickering et al. (1992b), copyright Kluwer Academic Publishers).

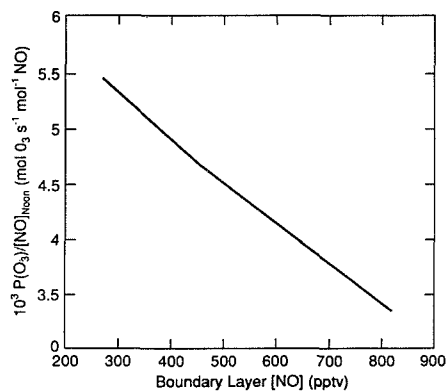


Fig. 4. Ozone production efficiency in the boundary layer as a function of NO for the April 26, 1987, ABLE 2B convective event. The highest value of NO existed in the undisturbed urban air and the lower values are representative of the cleaner air that descended into the boundary layer during the storm (after Pickering et al. (1992a), copyright American Geophysical Union).

(August 3, 1985, Studies 2 and 2A) which showed little entrainment or detrainment in the middle troposphere. The equivalent potential temperature profile for the August 3 event (also in Figure 6) shows a very pronounced midtropospheric minimum. These findings agree with the conclusion reached by Scala et al. (1990) that showed that the up and downdraft structure of tropical convective storms may depend largely on the shape of the equivalent potential temperature profile prior to the storm.

4. CONCLUSIONS

The analyses summarized in Table 1 are the beginning of a global climatology of the effects of deep convection on tropospheric chemistry. The major factors affecting the degree of enhancement of O_3 production by convection are the available boundary layer NO_x , strength and structure of the convective cells, and the amount of background pollution in the free troposphere.

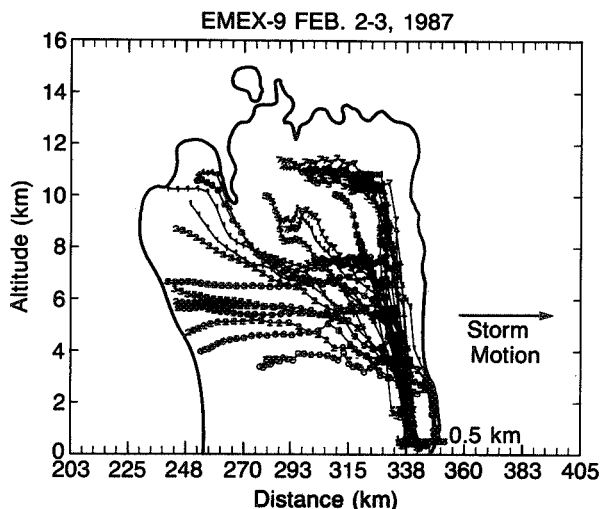


Fig. 5. Set of forward trajectories simultaneously beginning at 26 horizontal positions at an altitude of 0.5 km at the forward edge of the February 2, 1987, STEP/EMEX convective system.

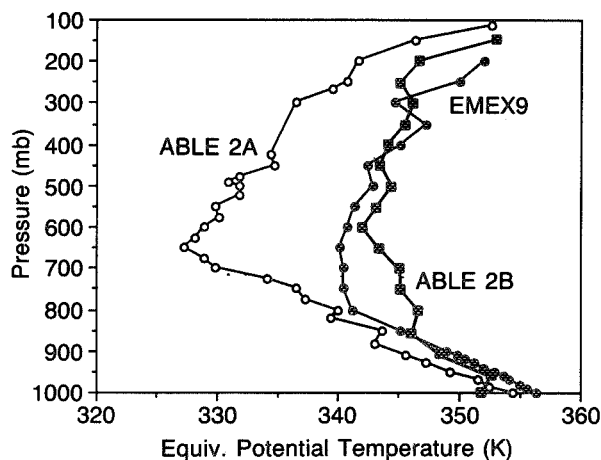


Fig. 6. Profiles of equivalent potential temperature observed prior to the August 3, 1985, ABL2A squall line and the February 2, 1987, STEP/EMEX convective event.

Major conclusions that we have reached from our series of analyses are as follows:

(1) The maximum convective enhancement of O_3 production in the free troposphere occurred with the redistribution of intense boundary layer biomass burning pollution into a pristine free troposphere by a storm with undilute updrafts. At the other extreme a small decrease in the ozone production potential of the free troposphere has been computed for a marine low NO_x event with very weak vertical transport.

(2) Convective transport characteristics appear to correlate with how well mixed the troposphere is prior to a convective event. Therefore, the efficiency of vertical transport of ozone precursors to the middle and upper troposphere might be predictable from the equivalent potential temperature profile prior to a storm.

(3) In addition to pumping O_3 precursors into the free troposphere, a convective system may also bring air with lower NO_x mixing ratios into a polluted boundary layer. The

efficiency of O_3 production per molecule of NO_x in the boundary layer increases, and the total tropospheric column ozone production potential is enhanced.

(4) When considered on a regional basis over a season, deep convection may vent a significant fraction of biomass burning emissions to the free troposphere over parts of the Amazon Basin, enhancing the free tropospheric ozone production potential over broad areas. Our results show that it is critical that parameterizations of deep convective transport be improved in 3-D global and regional chemical models.

The CEF's for ozone production in cloud outflow are derived from model calculations initialized with observations in undisturbed air. More research flights are needed to confirm our model predictions of convective transport and of O_3 production rates in cloud-processed air. Measurements of ozone precursors are required in outflow layers immediately downwind of storms, as well as measurements of O_3 in the first several hundred kilometers of downstream transport.

Acknowledgments. This work has been supported under the NASA Tropospheric Chemistry Program, the NASA Radiation, Dynamics, and Hydrology Program, and the NASA Atmospheric Chemistry Modeling and Analysis Program. Support has also been provided by the EPA Global Tropospheric Chemistry Program.

REFERENCES

- Dickerson, R. R., et al., Thunderstorms: An important mechanism in the transport of air pollutants, *Science*, 235, 460-465, 1987.
- Pickering, K. E., et al., Model calculations of tropospheric ozone production potential following observed convective events, *J. Geophys. Res.*, 95, 14049-14062, 1990.
- Pickering, K. E., et al., Photochemical ozone production in tropical squall line convection during NASA Global Tropospheric Experiment/Amazon Boundary Layer Experiment 2A, *J. Geophys. Res.*, 96, 3099-3114, 1991.
- Pickering, K. E., et al., Free tropospheric ozone production following entrainment of urban plumes into deep convection, *J. Geophys. Res.*, in press, 1992a.
- Pickering, K. E., et al., Ozone production potential following convective redistribution of biomass burning emissions, *J. Atmos. Chem.*, 14, 297-313, 1992b.
- Pickering, K. E., et al., A regional estimate of convective transport of CO from biomass burning, *Geophys. Res. Lett.*, 19, 289-292, 1992c.
- Pickering, K. E., et al., Upper tropospheric ozone production following mesoscale convection during STEP/EMEX, *J. Geophys. Res.*, submitted, 1992d.
- Scala, J. R., et al., Cloud draft structure and trace gas transport, *J. Geophys. Res.*, 95, 17015-17030, 1990.
- Tao, W.-K., J. Simpson, and S.-T. Soong, Numerical simulation of a subtropical squall line over Taiwan Strait, *Mon. Wea. Rev.*, 119, 2699-2723, 1991.
- Thompson, A. M. and R. J. Cicerone, Possible perturbations to atmospheric CO, CH₄, and OH, *J. Geophys. Res.*, 91, 10853-10864, 1986.

THE SENSITIVITY OF TROPOSPHERIC CHEMISTRY TO CLOUD INTERACTIONS.

Jan E. Jonson and Ivar S. A. Isaksen

Institute of Geophysics,
University of Oslo,
P.O.Box 1022, Blindern,
N-0315 Oslo 3, Norway

ABSTRACT

Clouds, although only occupying a relatively small fraction of the tropospheric volume can have a substantial impact on the chemistry of the troposphere. In newly formed clouds, or in clouds with air rapidly flowing through, the chemistry is expected to be far more active than in aged clouds with stagnant air. Thus frequent cycling of air through shortlived clouds, i.e. cumulus clouds, is likely to be a much more efficient media for altering the composition of the atmosphere than an extensive cloud cover i.e. frontal cloud systems.

The impact of clouds is tested out in a 2-D channel model encircling the globe in a latitudinal belt from 30 to 60°N. The model contains a detailed gas phase chemistry. In addition physiochemical interactions between the gas and aqueous phases are included. For species as H₂O₂, CH₂O, O₃ and SO₂, Henry's law equilibria are assumed, whereas HNO₃ and H₂SO₄ are regarded as completely dissolved in the aqueous phase. Absorption of HO₂ and OH is assumed to be mass-transport limited.

The chemistry of the aqueous phase is characterized by rapid cycling of odd hydrogen (H₂O₂, HO₂ and OH). O₂⁻ (produced through dissociation of HO₂) reacting with dissolved O₃ is a major source of OH in the aqueous phase. This reaction can be a significant sink for O₃ in the troposphere. In the interstitial cloud air, odd hydrogen is depleted, whereas NO_x remains in the gas phase, thus reducing ozone production due to the reaction between NO and HO₂. Our calculations give markedly lower ozone levels when cloud interactions are included. This may in part explain the overpredictions of ozone levels often experienced in models neglecting cloud chemical interactions.

In the present study the existence of clouds, cloud types and their lifetimes are modelled as pseudo random variables. Such pseudo random sequences are in reality deterministic and may, given the same starting values, be reproduced. The effects of cloud interactions on the overall chemistry of the troposphere will be discussed. In particular, tests are performed to determine the sensitivity of cloud frequencies and cloud types.

1. INTRODUCTION.

Measurements indicates that since the turn of the century there has been a marked increase in tropospheric ozone levels particularly over northern mid latitudes (Bojkov, 1986; Kley et al., 1988). The increase is a result of man made emissions of hydrocarbons and NO_x (NO and NO₂) compounds (Crutzen, 1988). Tropospheric ozone is an active greenhouse gas, and thus increased ozone levels, particularly in the Northern Hemisphere could contribute to global warming.

Several past model studies of tropospheric ozone have had a tendency to overpredict ozone (i.e. Isaksen et al., 1989; Jonson and Isaksen, 1992a). Lelieveld and Crutzen (1990, 1991) proposed that clouds may act as an efficient sink for ozone, predominantly through the aqueous phase reaction with O₂⁻. In fact, they found this reaction to be so fast that without a fixed ozone value, ozone levels would have become unrealistically low. Jonson and Isaksen (1992b) calculate a much smaller, but nonetheless, significant impact of clouds on ozone levels. They found that about half of the ozone reductions could be attributed to indirect effects on the gas phase chemistry, the other half to the aqueous phase reaction with O₂⁻.

Lelieveld and Crutzen (1990, 1991) and Jonson and Isaksen (1992b) used crude parameterizations for clouds. Lelieveld and Crutzen (1990, 1991) assumed average cycling times in and out of clouds based on lagrangian statistics. Jonson and Isaksen (1992b) assumed stationary clouds with the air flowing through. The present study applies the same model, but a more flexible cloud parameterization is used. Based on statistics for the fractional cloud cover, clouds are distributed according to a pseudo random function.

Several species will reach concentrations in the aqueous phase several orders of magnitude higher than in the gas phase. Provided fast aqueous phase reactions occur, several soluble species are rapidly removed in clouds. Thus, important aqueous phase processes are likely to become far less important with increasing residence time for air in clouds.

2. DESCRIPTION.

The model covers the latitudinal belt from 30 - 60°N. The horizontal resolution is 10° longitude and the vertical resolution 500 m from ground level to 3 km and 1 km from 3 to 16 km, the upper boundary of the model. The timestep is 1 hour, and the model is run for 30 days. Mid-april conditions are simulated. The zonal distributions of both natural and anthropogenic emissions of NO_x (NO+NO₂), non-methane hydrocarbons and CO are taken from Isaksen et al. (1989), while emissions of SO₂ are from Jonson and Isaksen (1992a). For the advection, seasonally averaged wind fields are used (Oort, 1983). The advection equation is solved by an upwind scheme with corrections for numerical dispersion (Smolarkiewicz, 1983). In the vertical, the eddy diffusion is separated into a slow diffusive transport, and a rapid cloud transport. The cloud transport is a combination of direct transport from cloud base to any layer between cloud base and cloud top, and a slower compensating subsidence to the layer below. This method was first described by Chatfield and Crutzen (1984). Cloud transport takes place at every longitude, regardless of whether cloudy or cloud free conditions, as described below, are assumed. However, in clouds, the cloud transport is multiplied by 1.6, outside clouds by 0.2, emphasizing cloud advection where the bulk of the clouds are assumed to be concentrated. The advection, eddy diffusion and cloud transport are described in more detail by Solberg (1989).

Whether a grid rectangle will be in clouds (cloud mode) or not is determined by a pseudo random function. Each grid rectangle is assigned a probability for cloud based on statistics for the fractional cloud cover (Gordon et al., 1984). Whenever the cloud mode is selected by the random function, the model has a choice of 4 cloud categories. Each cloud category is assigned a probability and a corresponding residence time. Probabilities for the 4 cloud categories, their residence times and their height intervals and optical thickness are listed in Table 1. If a clear sky situation is selected, a choice is made between 4 residence times. The probability for a residence time of 31 hours is 0.1, a residence time of 6 hours, 0.2, a residence time of 2 hours, 0.4, and of 1 hour, 0.3. The overall probability for the individual cloud categories and for the length of the clear sky periods are determined by the product of the probabilities and their residence times. When selected the average residence times for clear sky and cloud events are equal. The overall probabilities for clouds are thus determined by the cloud fractions. This pseudo random sequence can be reproduced given the same starting values. Different sets of dissociation rates are calculated for the 4 cloud categories and for clear sky conditions (Jonson and Isaksen, 1992b).

The chemistry (gas- and aqueous- phase) has been described by Jonson and Isaksen (1992b). In clouds, we assume that H₂SO₄ and HNO₃ are completely absorbed by the droplets. For H₂O₂, SO₂, O₃, HCHO and HCOOH, equilibrium between the gas- and liquid- phase, determined by Henry's law constants and equilibrium constants, are

applied. The fraction of the total (gas and liquid) concentration dissolved in the aqueous phase is defined as

$$f = \frac{1}{1 + (LH_{eff}RT)^{-1}}$$

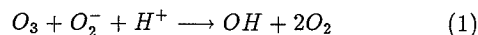
where L is the volume ratio between gas and liquid water, H_{eff} is the efficient Henry's constant (taking into account the effect of dissociation), R is the universal gas constant and T the temperature. In clouds, the aqueous phase concentration is then calculated as f multiplied by the total (gas and liquid) concentration, and the gas phase concentration as (1-f) multiplied by the total concentration. The mass-transfer of OH and HO₂ is assumed to be mass-transport limited, and is calculated as described by Schwartz (1986). In the previous study (Jonson and Isak-

Cat.	Prob.	Res.	Height (km)	Opt.
1	0.1	3	0 - 0.5	see caption
2	0.2	10	7 - 8(9)	5
			5 - 7	15
			0.5(2) - 4	20
3	0.2	8	2.5 - 5	30
4	0.5	3	0.5(2)-6(7)	30

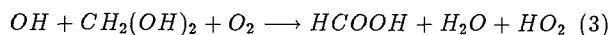
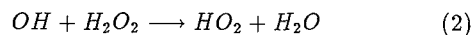
Table 1: When cloud mode is selected, Prob. denotes the probability for a cloud category, Res. the residence time in hours of the cloud event, Height, denotes the height interval(s) for the cloud layer(s) and Opt., the optical thickness of the cloud. For category 1, J-values for clear sky are multiplied by a factor 1.5 in the lowest layer. Numbers in brackets denote cloud-base and cloud-top heights over land.

sen, 1992b), we showed that aqueous phase chemistry has a substantial impact on the composition of the gas phase. The processes were studied with clouds fixed in space and time. This simple approach has the advantage of providing stable conditions where the individual reactions can be studied in more detail. Two processes, resulting in reduced ozone levels compared to gas-phase chemistry only, were identified:

The first process is the aqueous phase loss through the reaction:



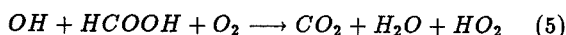
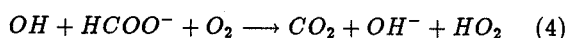
Although ozone has a low solubility in water, the reaction is nonetheless a significant sink for ozone. This reaction is also a major source of OH in the aqueous phase. The sources of O₂⁻ ⇌ HO₂ are absorption from the gas phase and recycling of hydrogen from OH through the aqueous phase reactions:



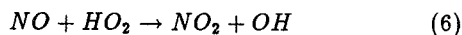
Long.	short cycling				long cycling			
	fc	P	Q_g	Q_{aq}	fc	P	Q_g	Q_{aq}
150°W	0.63	1.8E+6	1.1E-6	7.5E-7	0.7	2.0E+6	1.2E-6	6.2E-7
80°W	0.74	6.8E+6	5.0E-7	2.3E-7	0.69	6.5E+6	5.4E-7	2.2E-7
30°W	0.7	2.5E+6	1.4E-7	3.3E-7	0.72	2.4E+6	1.5E-6	2.4E-7
20°E	0.48	6.8E+6	5.0E-7	2.1E-7	0.41	6.7E+6	6.0E-7	2.1E-7
mean	0.38	4.3E+6	8.7E-7	4.4E-7	0.39	4.7E+6	9.9E-7	3.4E-7

Table 2: Ozone production and loss terms for selected longitudes and mean values for the whole model volume. *fc* is the fractional time in the cloud mode. *P* is the production of ozone in molecules $cm^{-3}s^{-1}$, and Q_g and Q_{aq} the gas- and aqueous- phase loss of ozone in s^{-1} averaged over a 30 day period for the lowest 6750 meters of the troposphere.

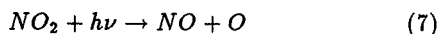
Formic acid partially evaporates, but it also contributes to the cycling of hydrogen:



The second process which leads to reduced ozone levels is due to reduced gas phase production through the reaction sequence:



In sunlight NO_2 is photolyzed:



O rapidly combines with O_2 giving ozone. Whereas most of the odd hydrogen (OH , HO_2 and H_2O_2), and thereby HO_2 , resides in the aqueous phase, NO_x has a low solubility, and will remain in the gas phase. The effect is reduced ozone production.

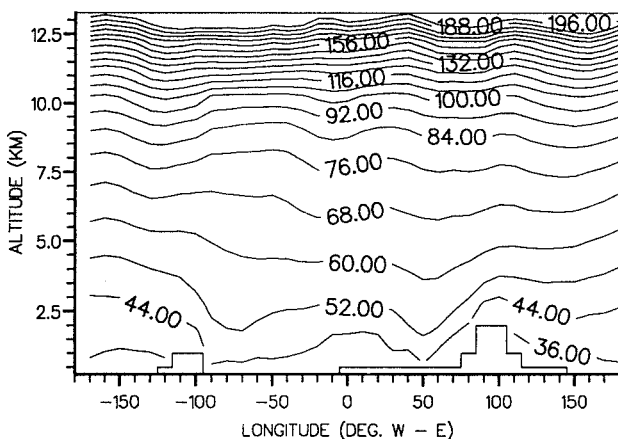


Figure 1: Diurnally averaged ozone concentrations for the Northern mid- latitudes as a function of latitude and altitude. Concentrations are given in parts per billion (ppb).

In the gas phase, ozone is destroyed by a number of species, including HO_2 .

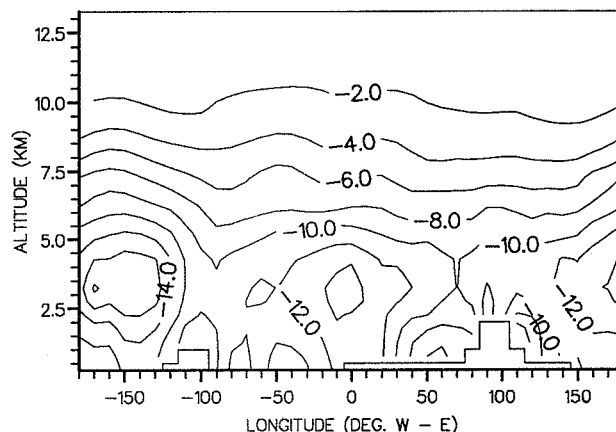
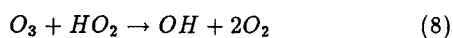


Figure 2: Percentage difference in ozone concentrations between model runs without cloud chemistry and with cloud chemistry as a function of longitude and altitude.

3. COMPUTATIONAL RESULTS.

In this study we are interested in quantifying the effects of different cloud representations rather than to study the individual reactions in detail. In Figure 1 ozone concentrations are shown with random clouds as described above. Figure 2 shows the percentage difference between concentrations calculated with no cloud chemistry (but with identical dissociation rates) and calculations with cloud chemistry. With cloud chemistry included, concentrations are lower throughout the troposphere. Ozone produced over polluted continents (North America, Europe and East Asia) is transported eastwards. During transport ozone is destroyed in clouds. In particular, large differences are found at the eastern rim of the Atlantic and Pacific oceans, downwind from North America and East Asia respectively.

Figure 3 shows the percentage difference in ozone concentrations between a model run with residence times doubled, and a run where residence times have been approximately halved. Effects on ozone are generally small, and are slightly negative over polluted continents, most likely due to changes in the NO_x distribution. In Table 2, ozone production and loss rates are shown. The tabulated values are averages for the whole period studied, with both cloudy and cloud free periods included. The effect of long and

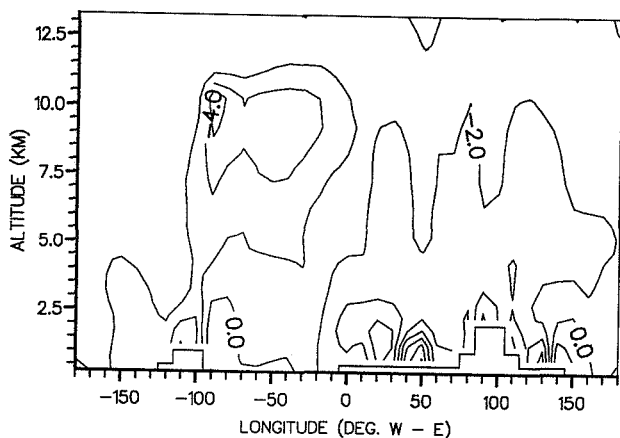


Figure 1: Percentage difference in ozone concentrations between model runs with long and short residence times for clouds.

short cloud cycling times are compared. Production rates (reaction 6) and loss rates for ozone reacting with HO_2 in both gas and aqueous phase (reaction 8 and 2 respectively) are tabulated. Over the polluted continents (80°W and 20°E) production rates are about a factor of 10 higher than over remote oceanic sites (150°W and 30°W). With short residence times the aqueous phase loss (reaction 2) is about 30% higher averaged over the whole model volume. This is compensated for by lower loss rates in the gas phase (reaction 8). However, Figure 3 show that ozone concentrations generally are lower in calculations with short cloud cycling times. These changes are caused by indirect effects on the NO_x chemistry and distribution rather than changes in aqueous phase destruction.

4. CONCLUSIONS.

Aqueous phase chemistry can reduce ozone concentrations in the troposphere significantly. Two mechanisms are identified by which ozone is reduced. Ozone absorbed in the droplets are consumed by a reaction with O_2^- . Secondly HO_2 and NO are separated in the clouds, as HO_2 is absorbed by the droplets whereas NO is virtually insoluble, thus slowing ozone production. Variations in residence times for cloud events does not alter the ozone concentrations by more than a few percent. With such a low sensitivity to cloud cycling parameterization, it is justified to apply the proposed mechanism even in models with low resolution where individual clouds, or even entire cloud systems are not properly resolved.

Acknowledgement: This work is sponsored by the Norwegian Research Council for Science and Humanities under grant 447.90/016b.

5. REFERENCES.

- Bojkov R.D. (1986) Surface ozone during the second half of the nineteenth century. *J. Chem. Appl. Meteor.*, Vol. 25, pp 343-352.
- Chatfield R.B. and Crutzen P. (1984) Sulfur dioxide in remote oceanic air. Cloud transport of reactive precursors. *J. Geophys. Res.*, Vol. 89, pp 7111-7132.
- Crutzen P.J. (1988) Tropospheric ozone: an overview. *Tropospheric Ozone - Regional and Global Scale Interactions*, edited by I.S.A. Isaksen. NATO ASI Series c, D Reidel, Dordrecht, The Netherlands, Vol. 227, pp 3-33.
- Gordon C.T., Hovaneč R.D., Stern W.F. (1984) Analyses of monthly mean cloudiness and their influence upon model-diagnosed radiative fluxes. *J. Geophys. Res.*, Vol. 89, pp 4713-4738.
- Isaksen I.S.A., Jonson J.E., Reeves C.E., Solberg S., Chatfield R. (1989) Model studies of free tropospheric ozone formation from pollution sources. *Proceedings of the 4'th Quadrennial Ozone Symposium*. Ed. by R. D. Bojkov and P. Fabian A. DEPAK Publishing, pp 544-548.
- Jonson J.E., Isaksen I.S.A. (1992) Parameterization of episodic cloud and rainout events in large-scale atmospheric chemistry models. *Atmospheric Environment*. Vol. 26A, No. 11, pp. 2019-2029.
- Jonson J.E., Isaksen I.S.A. (1992) Tropospheric ozone chemistry: The impact of cloud chemistry. Accepted by *J. Atm. Chem.*
- Kley D., Volz A., Mulheims F. (1988) Ozone measurements in historic perspective, *Tropospheric Ozone - Regional and Global Scale Interactions*, edited by I.S.A. Isaksen. NATO ASI Series c, D Reidel, Dordrecht, The Netherlands, Vol. 227, pp 63-72.
- Lelieveld J. and Crutzen P.J. (1990) Influences of cloud photochemical processes on tropospheric ozone. *Nature*, Vol. 343, pp. 227-233.
- Lelieveld J. and Crutzen P.J. (1991) The role of clouds in tropospheric photochemistry. *J. of Atm. Chem.* Vol. 12, pp 229-267.
- Oort A.H. (1983) Global atmospheric circulation statistics, 1958 - 1973, NOAA professional paper 14.
- Schwartz S.E. (1986) Mass-transport considerations pertinent to aqueous phase reactions of gases in liquid-water clouds. *Chemistry of multiphase atmospheric systems*. Ed. by W. Jaeschke, Springer-Verlag, Berlin, pp 415-471.
- Smolarkiewicz P.K. (1983) A simple positive definite advection scheme with small implicit diffusion. *Monthly Weather Rev.*, Vol 111, pp 476-487.
- Solberg S., Isaksen I.S.A., Chatfield R. (1989) Design of a channel model to assess mid-latitude pollution effects. *Proceedings of the 4'th Quadrennial Ozone Symposium*. Ed. by R.D. Bojkov and P. Fabian A. DEPAK Publishing, pp 548-552.

TROPOSPHERE

MEASUREMENTS

TROPOSPHERIC OZONE AND AEROSOL VARIABILITY OBSERVED AT HIGH LATITUDES WITH AN AIRBORNE LIDAR

Edward V. Browell¹, Carolyn F. Butler², Marta A. Fenn², Susan A. Kooi², and William B. Grant¹

¹NASA Langley Research Center, Atmospheric Sciences Division, Hampton, Virginia 23681

²Science Applications International Corporation, Hampton, Virginia 23666

ABSTRACT

Large-scale summertime (July-August) distributions of O₃ and aerosols were observed in a broad range of atmosphere conditions over the tundra, ice, and ocean regions near Alaska in 1988 and over the lowlands and boreal forests of Canada in 1990. The tropospheric O₃ budget in the high-latitude regions was found to be strongly influenced by stratospheric intrusions, and deposition at the surface was found to be the main sink for O₃ in the troposphere. Enhanced levels of O₃ were observed in plumes from fires in Alaska and Canada. This paper discusses the large-scale variability of O₃ and aerosols observed in the high-latitude regions during these field experiments.

1. INTRODUCTION

The NASA Atmospheric Boundary Layer Experiment (ABLE-3A) was conducted near Barrow and Bethel, Alaska, from July 10 to August 12, 1988, and a second field experiment (ABLE-3B) was conducted over eastern Canada from July 6 to August 16, 1990. The primary objective of these experiments was the investigation of the sources and sinks for tropospheric ozone (O₃) in the high-latitude regions of North America. During these field experiments, the NASA Langley Research Center's airborne Differential Absorption Lidar (DIAL) system [Browell et al., 1983; Browell, 1989] was flown on the NASA Wallops Electra aircraft to provide simultaneous remote measurements of O₃ and aerosols above and below the aircraft from near the surface to above the tropopause. An O₃ measurement accuracy of less than 10% or 3 ppbv (parts per billion by volume), whichever is larger, was obtained [Browell et al., 1983, 1985]. In addition, comparisons between airborne DIAL and in situ O₃ measurements were made throughout the field experiments to verify that the DIAL accuracy was in agreement within the above stated accuracy. Detailed characteristics of the current airborne DIAL system and the O₃ DIAL technique are given by Browell [1989].

This airborne lidar system has been used in many previous experiments to study tropospheric O₃ and aerosol distributions [see e.g., Browell et al., 1987, 1988, 1990]. This paper discusses the results of the airborne DIAL measurements of O₃ and aerosols that were made during ABLE-3A&B in a broad range of atmospheric conditions over the ice, tundra, and ocean regions of Alaska and over eastern Canada.

2. ARCTIC AND SUBARCTIC MEASUREMENTS

A total of 33 missions were flown as part of ABLE-3A, including 23 flights in the vicinity of Barrow and Bethel, Alaska, and 10 survey flights between the NASA Wallops Flight Facility at Wallops Island, Virginia, and Barrow. The tropospheric O₃ budget in the summertime high-latitude regions near Alaska was found to be strongly influenced by stratospheric intrusions. Regions of low aerosol scattering and enhanced O₃ mixing ratios in the troposphere were usually correlated with descending air from the lower stratosphere. In the vicinity of Barrow, Alaska, O₃ was generally in the range of 20-30 ppbv below 2 km; however, air with O₃ >40 ppbv and low aerosol scattering was found as low as 1 km with continuity in air mass characteristics to the tropopause level. Ozone measurements in the vicinity of Barrow showed large regions where O₃ exceeded 45 ppbv extending down to about 1 km altitude. Using the zenith DIAL O₃ data, these regions of elevated O₃ were traced back to large-scale stratospheric intrusions that generally increased the O₃ levels in the upper troposphere [Shipham et al., 1992]. Ozone mixing ratios of over 100 ppbv were found as low as 6 km in the presence of strong intrusion events. The variability in O₃ in the mid to upper troposphere affects the O₃ distribution in the lower troposphere, and due to the frequency of the observed intrusions, this process plays an important role in the tropospheric O₃ budget at high latitudes.

Several cases of continental polar air masses were examined during this experiment. The aerosol scattering associated with these air masses was very low, and the atmospheric distribution of aerosols was quite homogeneous for those air masses that had been transported over the ice for at least 3 days. The average O₃ profile (Figure 1) derived from three cases of continental polar air masses had a nearly constant gradient of 7 ppbv/km from 30 ppbv at 600 m to 55 ppbv at 4 km. This distribution reflects the influence of downward transport of O₃ from the upper troposphere at high latitudes and the destruction of O₃ near the surface.

Five cases were studied to determine the average background O₃ profile over the tundra region of southwestern Alaska (Figure 2). Near the surface, the tundra and continental polar O₃ levels are about the same; however, the average O₃ value above 1.5 km is 10-20% less than for the continental polar cases. This is thought to be due to the influence of more frequent stratospheric intrusions at the higher latitudes associated with the continental polar air masses. Zenith O₃ profiles in the region of 56-62°N showed good agreement from 2.5-10.0 km in altitude with a

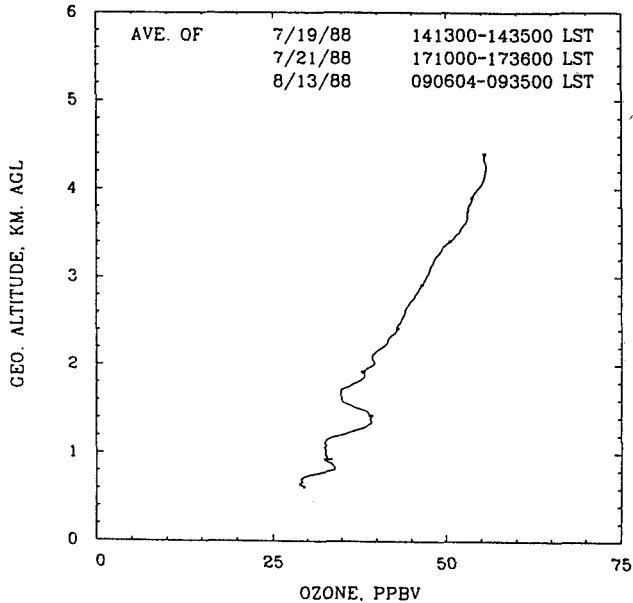


Fig. 1. Average continental polar O₃ profile derived from DIAL measurements on the dates shown.

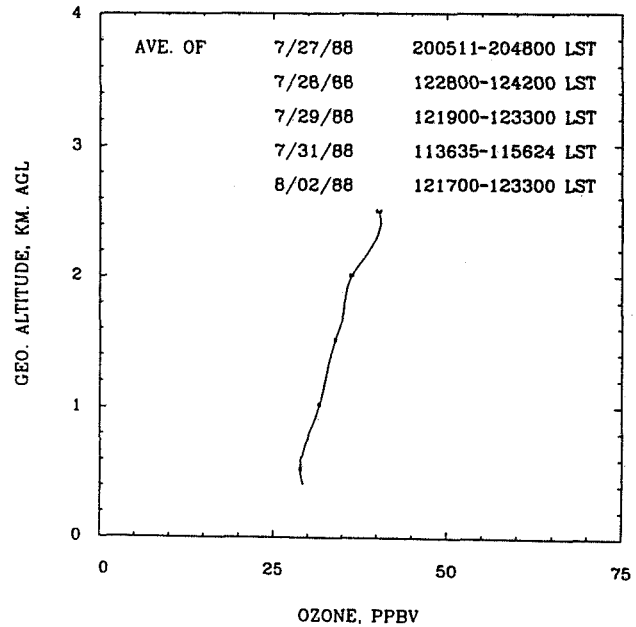


Fig. 2. Average tundra O₃ profile derived from DIAL measurements on the dates shown.

5.5 ppbv/km gradient determined below 2.5 km over the tundra.

Several cases of enhanced O₃ were observed during ABLE-3A in conjunction with enhanced aerosol scattering in layers in the free troposphere. Multiple aerosol layers were often observed coming from the many fires in Alaska. In some cases, O₃ in these layers was found to be more than 50% higher than the average background O₃ distribution over the tundra region. The products of biomass burning was found to significantly alter the chemical composition of the troposphere in the Arctic [Wofsy et al., 1992], as was shown to happen over the Amazon Basin during the dry season [Andreae et al., 1988].

An analysis of the percentage of the troposphere containing air having significantly different characteristics was conducted using the nadir and zenith DIAL data. The troposphere was found to contain air that fell into four general categories with the following properties: (1) mixed-layer air with enhanced aerosol scattering and with O₃ <30 ppbv; (2) plumes in the free troposphere with significantly enhanced relative aerosol scattering; (3) stratospheric intrusions in free troposphere with significantly enhanced O₃ levels and with low aerosol scattering;

and (4) background air in the free troposphere with none of the above characteristics.

An unperturbed background O₃ profile was defined as having a gradient of 5.2 ppbv km⁻¹ from 29 ppbv at 500 m to 68 ppbv at 8 km. Table 1 presents the results of an analysis of the DIAL data from ABLE-3A to determine the percentage of the troposphere containing the above types of air in particular altitude and latitude regions. The troposphere was divided into 2-km intervals from the surface to 8 km, and the data were grouped into two latitude intervals: a subarctic region (57-65°N) and an arctic region (>65°N).

Mixed-layer air was found to be contained almost entirely within the 0-2 km altitude range, and its vertical extent was a factor of 3 larger in the tundra region of southwestern Alaska than at higher latitudes (>65°N) with extensive regions of ice. Plumes were most often observed below 4 km where they accounted for almost 10% of the atmosphere. Plumes were sometimes found at the higher altitudes but with very reduced extent. The measured tropospheric extent containing plumes at

Table 1. Percentage of Troposphere in ABLE-3A Containing Different Air Types

Air Type	Altitude								Tropospheric Coverage	
	0-2 km		2-4 km		4-6 km		6-8 km		0-8 km	
	57-65	>65	57-65	>65	57-65	>65	57-65	>65	57-65	>65
Mixed Layer	17	6	0	0	0	0	0	0	4	1
Plumes	9	10	10	11	1	3	2	2	5	7
Strat. Int.	12	18	30	37	51	57	57	42	38	38
Backgnd (Free Trop)	62	66	60	52	48	40	41	56	53	54

high-latitudes ($>57^{\circ}\text{N}$) during ABLE-3A was 6% with a maximum of 11% for plumes in the 2-4 km range. While the percentage for plumes may be relatively small, they are a concentrated source of gases and aerosols that once mixed with the ambient air can significantly alter the chemical composition of the lower troposphere. The influence of stratospheric intrusions on the O_3 distribution in the troposphere increased with altitude over the entire high-latitude region investigated ($>57^{\circ}\text{N}$) from an average of 16% in the 0-2 km range to over 53% above 4 km. At the higher latitudes ($>65^{\circ}\text{N}$), the tropospheric extent of the intrusions was 18% below 2 km. The measured tropospheric extent containing stratospheric intrusions at high-latitudes ($>57^{\circ}\text{N}$) was 38% with a maximum extent of 53% in the 4-6 km range. The background air was defined as tropospheric air that did not fall into any of the above categories, and it accounted for 44-64% of the troposphere (0-8 km). When the extent of the types of air is compared in the two latitude regions ($57-65^{\circ}\text{N}; >65^{\circ}\text{N}$), there is no apparent trend in any of the categories, except for the mixed layer extent, which was discussed earlier.

3. MEASUREMENTS OVER EASTERN CANADA

During ABLE-3B, 22 flights were made in eastern Canada from bases in North Bay and Goose Bay, Canada. In addition to the types of air identified for ABLE-3A, two additional types of air were observed during ABLE-3B: (1) convective outflows in the free troposphere with significantly enhanced aerosol scattering and with O_3 lower than the background level at that altitude; and (2) low O_3 air with O_3 more than 20% below the background value at that altitude and with low aerosol scattering. Background O_3 profiles over Canada are shown in Figure 3 for the lower troposphere and in Figure 4 for the upper troposphere. An analysis similar to that conducted for ABLE-3A was done for the data collected during ABLE-3B. Table 2 presents the results of an analysis to determine the percentage of the troposphere containing different types of air during ABLE-3B. An additional category was added to the table to take into account the cases where the tropopause was below 12 km.

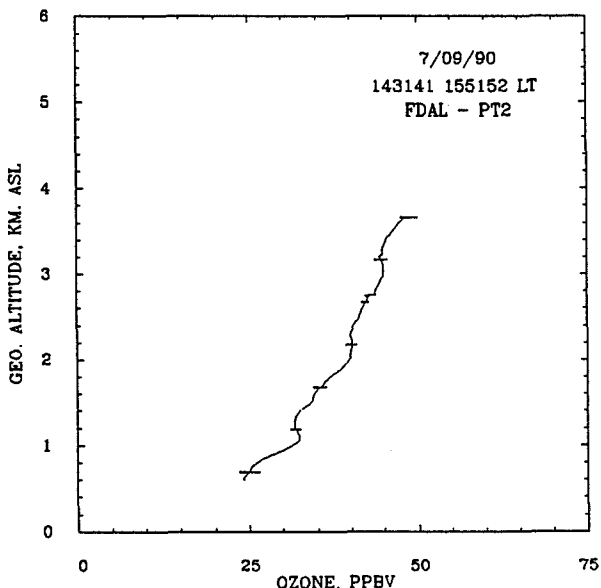


Fig. 3. Average background O_3 profile for lower troposphere observed over James Bay lowlands on July 9, 1990.

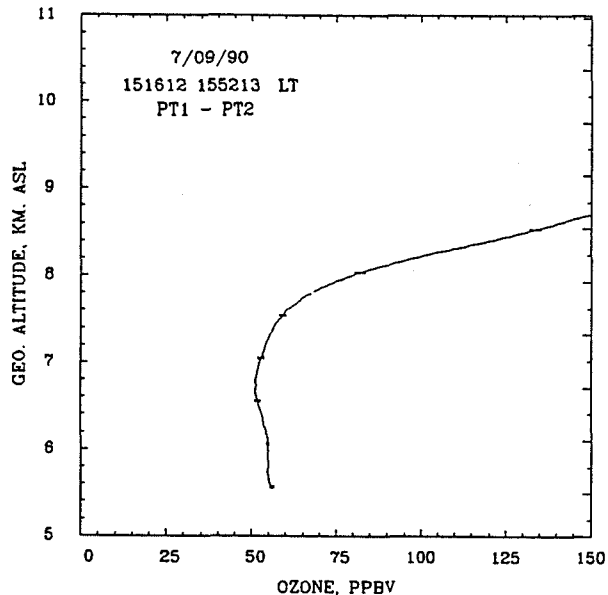


Fig. 4. Average background O_3 profile for upper troposphere observed over James Bay lowlands on July 9, 1990.

The mixed-layer air over the lowlands and boreal forests of Canada was found to cover over 25% of the 0-2 km altitude range. This is more than twice the area occupied by the mixed-layer air over the tundra in ABLE-3A. Plumes were most often observed below 4 km where they accounted for almost 25% of the atmosphere. The amount of plumes observed during ABLE-3B over Canada was more than 2.5 times the amount observed over the tundra regions of Alaska during 1988. Of the plumes observed over Canada, over 60% had elevated O_3 ($>20\%$ above the background O_3 level). While these plumes were old enough to exhibit substantial photochemical O_3 production, a significant number of young plumes from near-by fires were observed that did not have enhanced O_3 .

Stratospheric intrusions were observed on 68% of the missions flown during ABLE-3B, where they were found to significantly influence the O_3 distribution in the middle and upper troposphere. Over 40% of the atmosphere between 4-8 km had enhanced O_3 and low aerosol scattering associated with these intrusions. Even in the lower troposphere there was a substantial occurrence of intrusions. In the 45-55 $^{\circ}\text{N}$ latitude range, the area of the troposphere that contained intrusions was about 20% lower than the area containing intrusions at the higher latitudes in ABLE-3A. A combination of the lower tropopause, the influence of the polar jet, and the large-scale subsidence in the Arctic is thought to be the reason for the difference in the observations. Stratospheric intrusions represented 33% of the entire troposphere over Canada during ABLE-3B. This is only slightly lower than the 38% found during ABLE-3A in the Arctic and Subarctic.

Low O_3 air was observed on several occasions in the upper troposphere, and in total, it covered almost 20% of the atmosphere above 6 km. These air masses had their origins in the tropics according to their back trajectory analyses. An additional source of low O_3 to the free troposphere is associated with the vertical transport of boundary layer air resulting from cloud activity. The amount of air associated with convective outflows is generally less than 5%; however, this is probably an underestimate due to the limitation of having to make the lidar measurements outside of optically thick clouds.

Table 2. Percentage of Troposphere in ABLE-3B Containing Different Air Types

Air Type	Altitude Range						Tropospheric Coverage 0-12 km
	0-2 km	2-4 km	4-6 km	6-8 km	8-10 km	10-12 km	
Mixed Layer	36	8	0	0	0	0	7
Background (Free Trop.)	17	40	43	40	34	23	33
Plumes	26	24	2	2	2	1	10
Stratospheric Intrusion	8	24	45	41	31	51	33
Low Ozone Air	4	1	9	13	26	19	12
Convective Outflow	9	3	1	4	5	3	4
Low Tropopause	0	0	0	0	2	3	1

The background air accounted for 33% of the troposphere (0-12 km). This compares to 33% for stratospheric intrusions, which was the largest component of the troposphere. The low O₃ air, plumes, and boundary layer air all had comparable amounts of tropospheric coverage; however, each has distinctly different chemistry and influence of the troposphere.

4. CONCLUSIONS

The tropospheric O₃ budget in the Arctic was found to be strongly influenced by stratospheric intrusions. Regions of low aerosol scattering and enhanced O₃ mixing ratios were usually correlated with descending air from the upper troposphere or lower stratosphere. In continental polar air masses, the aerosol scattering was also low, and the average O₃ profile had a nearly constant gradient of 7 ppbv/km from about 30 ppbv at 600 m to 55 ppbv at 4 km. This distribution reflects the influence of downward transport of O₃ from the upper troposphere at high latitudes and the destruction of O₃ near the surface. Over the tundra of southwestern Alaska, the average O₃ level observed in the mixed layer was in the 25-35 ppbv range, and the average O₃ profile above the mixed layer was 10-20% lower than for the continental polar air masses, possibly due to fewer intrusions at lower latitudes. Several cases of enhanced O₃ were observed during ABLE-3A in conjunction with enhanced aerosol scattering in layers in the free troposphere. These layers were coming from regions where biomass burning was occurring.

The background O₃ level observed in the mixed layer over Canada during ABLE-3B was in the 20-30 ppbv range indicating that the wetlands and boreal forest regions of Canada provided a stronger surface sink for O₃ than the tundra regions of Alaska. Except for cases of biomass burning plumes, aerosols were generally negatively correlated with O₃, which indicates that their primary source was at the surface. As with ABLE-3A, numerous cases of stratospheric intrusions were observed with evidence that their effect extended well down into the lower troposphere. Deep convective cloud activity and associated outflows were found to be the primary mechanism for vertically transporting O₃-poor air from near the surface to the upper troposphere. Air containing abnormally low O₃ was observed on a number of missions, and some of these air masses were thought to have originated in the tropics. Plumes from near-by fires had enhanced aerosol loading without any significant increase in O₃ levels. Aged plumes had only slightly enhanced aerosol scattering; however, the O₃ was enhanced to greater than 50 ppbv due to photochemical O₃ production.

5. ACKNOWLEDGMENTS

The authors would like to thank Arlen Carter, Syed Ismail, Neale Mayo, William McCabe, Byron Meadows, and Jerry Williams of the Lidar Applications Group in the Atmospheric Sciences Division at the NASA Langley Research Center for their assistance in integrating the system into the Electra, operating the lidar in the field, and reducing the lidar data after the mission. This research was supported by NASA's Global Tropospheric Research Program.

REFERENCES

- Andreae, M. O., E. V. Browell, M. Garstang, G. L. Gregory, R. C. Harriss, G. F. Hill, D. J. Jacob, M. C. Pereira, G. W. Sachse, A. W. Setzer, P. L. Silva Dias, R. W. Talbot, A. L. Torres, and S. C. Wofsy, Biomass-burning emissions and associated haze layers over Amazonia, *J. Geophys. Res.*, **93**, 1509-1527, 1988.
- Browell, E. V., Differential absorption lidar sensing of ozone, *Proc. IEEE*, **77**, 419-432, 1989.
- Browell, E. V., A. F. Carter, S. T. Shipley, R. J. Allen, C. F. Butler, M. N. Mayo, J. H. Siviter, Jr., and W. M. Hall, NASA multipurpose airborne DIAL system and measurements of ozone and aerosol profiles, *Appl. Opt.*, **22**, 522-534, 1983.
- Browell, E. V., S. Ismail, and S. T. Shipley, Ultraviolet DIAL measurements of O₃ profiles in regions of spatially inhomogeneous aerosols, *Appl. Opt.*, **24**, 2827-2836, 1985.
- Browell, E. V., E. F. Danielsen, S. Ismail, G. L. Gregory, and S. M. Beck, Tropopause fold structure determined from airborne lidar and in situ measurements, *J. Geophys. Res.*, **92**, 2112-2120, 1987.
- Browell, E. V., G. L. Gregory, R. C. Harriss, and V. W. J. H. Kirchhoff, Tropospheric ozone and aerosol distributions across the Amazon Basin, *J. Geophys. Res.*, **93**, 1431-1451, 1988.
- Browell, E. V., G. L. Gregory, R. C. Harriss, and V. W. J. H. Kirchhoff, Ozone and aerosol distributions over the Amazon Basin during the wet season, *J. Geophys. Res.*, **95**, 16,887-16,901, 1990.
- Shipham, M. C., A. S. Bachmeier, D. R. Cahoon, Jr., and E. V. Browell, Meteorological overview of the ABLE-3A flight series, *J. Geophys. Res.*, **97**, in press, 1992.
- Wofsy, S. C., et al., Influence of natural fires and anthropogenic emissions on atmospheric chemistry in remote areas, *J. Geophys. Res.*, **97**, in press, 1992.

DIRECT MEASUREMENTS OF TROPOSPHERIC OZONE USING TOMS DATA

Robert D. Hudson and Jae-Hwan Kim
 Department of Meteorology, University of Maryland
 College Park, Maryland 20742, USA

ABSTRACT

Fishman and Larsen (1987) have proposed a new algorithm, called "tropospheric residual method", which retrieves the climatological tropospheric ozone by using SAGE (Stratospheric Aerosol and Gas Experiment) and TOMS (Total Ozone Mapping Spectrometer) data. In this paper, we will examine the feasibility of detection for tropospheric ozone using only TOMS data. From a case study over the Atlantic Ocean off coast of west Africa, it has been found that total ozone in the archived TOMS data has been overestimated over a region of marine-stratocumulus clouds.

INTRODUCTION

The TOMS total ozone data is derived from the backscattered ultraviolet radiances measured by the TOMS instrument on Nimbus-7 using an algorithm that was developed principally for measurements of stratospheric variability. In 1986, Fishman et al., used the TOMS total ozone data to determine tropospheric ozone fields in the tropics. They assumed that horizontal stratospheric gradients in the tropics are small, and used the TOMS relative total ozone field as a surrogate for the tropospheric ozone field. In 1987, Fishman and Larsen, extended this method, by using the SAGE profiles to determine the stratospheric ozone field, and then subtracted this quantity from the TOMS data. In this paper we examine the physics of the TOMS algorithm as it applies to the measurement of tropospheric ozone.

PRESENT ALGORITHM

A simplified schematic of the principle of the TOMS measurement is shown in Figure 1. This simple case assumes that the atmosphere does not scatter, and that the layer of ozone is confined to a narrow strip in the stratosphere. If the reflectivity of the ground is R, then the measured albedo A is given by:

$$A = R \exp(-\alpha\Omega s - \beta\Delta s) \quad (1)$$

where α is the ozone absorption cross section, Ω is the column content of the ozone layer, β is the Rayleigh scattering coefficient for the atmosphere, and Δ is the column content of the atmosphere. s , the path length, is given by:

$$s = 1/\cos(\theta) \quad (2)$$

θ is given in Figure 1. If we can measure the reflectivity, R, then the only unknown in equation (1) is Ω . In the TOMS algorithm, R is measured at another wavelength where the absorption due to ozone is negligible, the assumption being that in the ultraviolet R varies only slowly with wavelength.

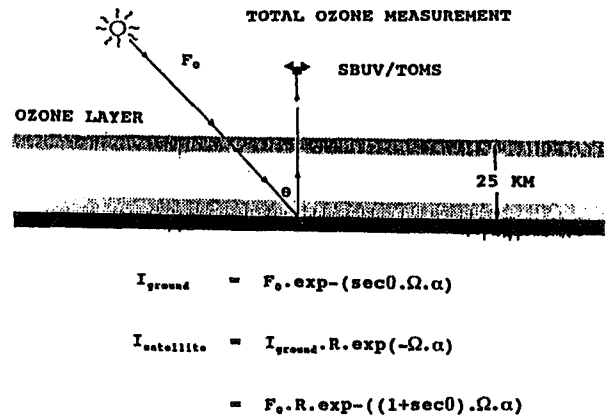


Fig. 1. Schematic diagram that shows how TOMS measures the backscattered radiation from reflecting surface. F_0 is the solar irradiance, I_{ground} is the intensity reaching to ground, I_{sat} is the measured intensity by TOMS, Ω is total ozone, and α is the ozone absorption coefficient.

Unfortunately for the simple method described above, the atmosphere does scatter, and thus the measured radiance at the instrument is the sum of the reflected sunlight plus the scattered sunlight from the atmosphere. However because the density of the atmosphere increases exponentially as the altitude decreases, almost all of the scattered radiation comes from the troposphere. Thus, if the ozone were confined to the stratosphere, as shown in the illustration, then one can derive an equation similar to (1), where R is replaced with the effective reflectivity of the ground plus the atmosphere. In reality, about 90% of the column ozone is in the stratosphere.

However it is the 10% in the troposphere which is of interest to us now. In the illustrations above, the total radiance, both reflected and scattered, passes through the entire ozone column, and thus the efficiency of detection of the ozone column is 100%. However if we now consider ozone in the troposphere, the outgoing scattered radiation from a particular altitude will not pass through any ozone below it, thus the efficiency of detection for tropospheric ozone will in general become less than 100%, and will get worse the lower the altitude of the ozone layer. Figure 2 gives the results of calculations of this efficiency as a function of the altitude of the ozone, and the reflectivity of the surface. Note that the efficiency becomes larger as the reflectivity of the surface increases, i.e. as the reflected sunlight becomes larger than the scattered sunlight. It should be noted that the efficiency can become larger than 100%. This is because multiple scattering at the lower boundary can increase the effective path length, and hence enhance the effect of the absorption due to ozone.

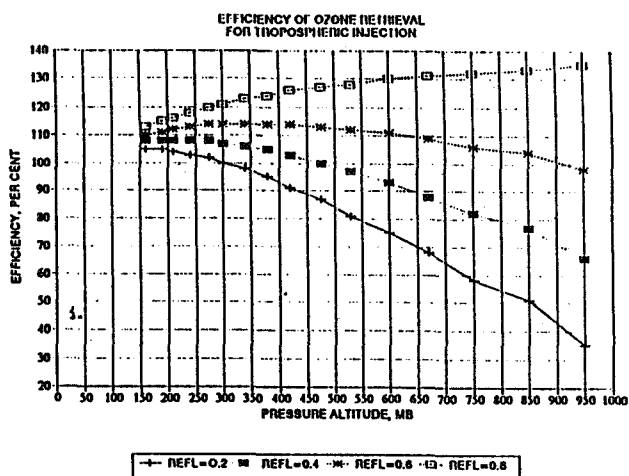


Fig. 2. The efficiency of detection for tropospheric ozone as a function of the altitude and the reflectivity of the surface (1000 mb). X-axis is the altitude in atmosphere, y-axis is the retrieval efficiency (sensitivity) of tropospheric ozone in percentage, and R is the reflectivity of the surface. The values are calculated at zero solar zenith angle, azimuthal angle, and scan angle.

There is another factor however which effects the derivation of tropospheric ozone, the height of the reflecting boundary within the TOMS footprint. The present algorithm assumes a cloud base if the derived reflectivity is 0.6 or greater (snow and ice is discriminated against by reference to other satellite data). The lower boundary is then obtained from a climatological table of mean cloud height versus latitude. If the reflectivity is less than 0.2, then the lower boundary is obtained from a table of terrain height versus latitude and longitude. If the reflectivity is between 0.2 and 0.6, then broken clouds are assumed, and the lower boundary is obtained by interpolation between the terrain height and the mean cloud height.

In general, of course, the cloud height is not at the mean. If the real cloud height is below the climatological mean, then the observed albedo will be larger than the expected albedo, and the algorithm will interpret this as additional ozone. The reverse is

true for a real cloud height greater than the climatological mean.

RESULTS

Figure 3-a shows a plot of the total ozone and Figure 3-b shows a plot of lower boundary reflectivity as retrieved by TOMS (archived TOMS data) for a region off the west coast of Africa, on October 14, 1989.

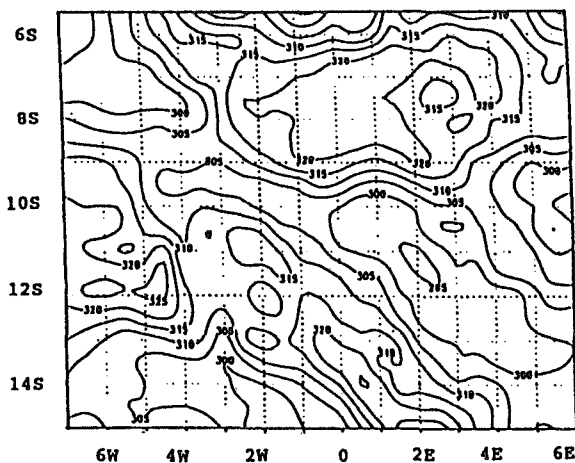


Fig. 3-a. Total ozone from the archived TOMS data on October 14, 1989. The unit is Dobson (D.U) and the interval is 5 D.U. X-axis is latitude and y-axis is longitude.

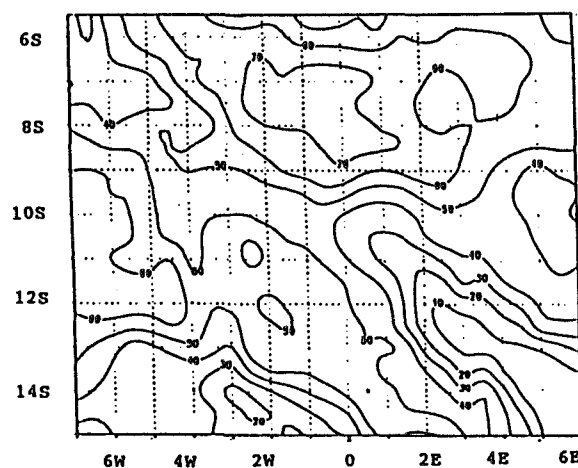


Fig. 3-b. Reflectivity from the archived TOMS data on October 14, 1989. The unit is percentage (%) and the interval is 10%. X-axis is latitude and y-axis is longitude.

In the region near 8S and between 0 to 6E, and near

between 9S and 14S and 3W and 7W the total ozone contours follow closely those of the reflectivity. This is a region of marine-stratocumulus clouds. The climatological cloud height is set at about 300 mb if reflectivity is greater than 0.6, whereas the measured height is about 810 mb. The algorithm is expected to retrieve higher ozone values over this region, and, for the reasons discussed above, it is also expected that the higher the reflectivity the greater the retrieved value because of the effect of multi-scattering at the reflecting boundary. If the cloud is at or near the climatological height, and the contribution from scattered radiation is small, hence little correlation is seen between the measured total ozone and the reflectivity. In general the regions over low reflectivity show lower total ozone values.

The data for the area near 8S and 0 to 6E has been reanalysed using the measured radiances, assuming the following:

- (a) The real cloud height
- (b) That the measured reflectivities represent a real change in cloud reflectivities (Satellite pictures do not indicate broken clouds over this region)
- (c) The standard altitude profiles used in the TOMS retrievals.

The results of this analysis are shown in Figure 4. As can be seen, the correlation between the reflectivity and the total ozone field has been removed. From a comparison between Fig 3-a and Fig 4, we can see that total ozone in the archived TOMS data has been overestimated over marine-stratocumulus cloud.

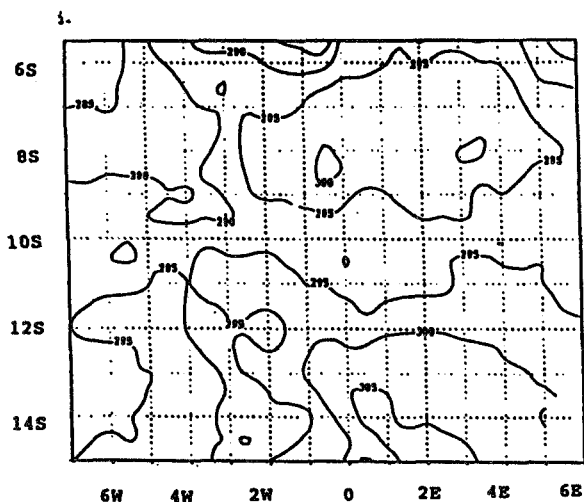


Fig. 4. Corrected total ozone over cloud whose reflectivity is greater than 45% on October 14, 1989. The unit is D.U and the interval is 5 D.U. X-axis is latitude and y-axis is longitude.

Perhaps what is more important, is that the apparent high ozone levels shown in Figure 3-a, which would be interpreted as high tropospheric levels if one subtracts a uniform stratospheric level, are removed.

CONCLUSIONS

This preliminary analysis has shown that there is indeed information in the TOMS data on levels of tropospheric ozone. However, in the region of clouds, great caution should be exercised in the use of the archived total ozone data from TOMS.

ACKNOWLEDGEMENTS

This research was supported by grant number NAGW-2696 from the National Aeronautics and Space Administration.

REFERENCES

- Dave, J.V., Meaning of successive iteration of the auxiliary equation in the theory of radiative transfer, *Astrophys. J.*, 140, 1292-1303, 1964.
- Dave, J.V., Effect of aerosols on the estimation of total ozone in an atmospheric column from the measurement of its ultraviolet radiance, *J. Atmos. Sci.*, 35, 899-911, 1978.
- Dave, J.V., and C.L. Mateer, A preliminary study on the possibility of estimating total atmospheric ozone from satellite measurements, *J. Atmos. Sci.*, 24, 414-427, 1967.
- Fishman, J., K. Fakhruzzaman, B. Cros, and D. Nganga, Identification of widespread pollution in the Southern Hemisphere deduced from satellite analyses, *Science*, 252, 1693-1696, 1991.
- Fishman, J., P. Minis, and H.G. Reichle, Jr., The use of satellite data to study tropospheric ozone in the tropics, *J. Geophys. Res.*, 91, 14451-14465, 1986.
- Fishman, J., and J.C. Larsen, Distribution of total ozone and stratospheric ozone in the tropics: implication for the distribution of tropospheric ozone, *J. Geophys. Res.*, 91, 14451-14465, 1987.
- Fishman, J., C.E. Watson, J.C. Larsen, and J.A. Logan, The distribution of tropospheric ozone determined from satellite data, *J. Geophys. Res.*, 95, 3599-3618, 1990.
- Mateer, C.L., D.F. Heath, and A.J. Krueger, Estimation of total ozone from satellite measurements of backscattered ultraviolet earth radiance, *J. Atmos. Sci.*, 28, 1307-1311, 1971.

**OZONE TRANSPORT DURING A CUT-OFF LOW EVENT
STUDIED IN THE FRAME OF THE TOASTE PROGRAM**

G. Ancellet, M. Beekmann, A. Papayannis, G. Megie

Service d'Aeronomie du CNRS, Universite Paris 6
Paris, France

Abstract

A study of ozone transfer to the troposphere has been performed during two phases of the evolution of a cut-off low using both ozone vertical profiles and objective analysis of the ECMWF to compute potential vorticity distributions and air mass trajectories. Ozone profiles were measured by a ground based lidar system at the Observatoire de Haute Provence (OHP, 43°55N, 5°42E). A stratospheric ozone transport into the troposphere has been observed during a tropopause fold which occurred at the beginning of the cut-off low formation and during the erosion phase of the cut-off low. From the estimate of the maximum ozone content transferred to the troposphere, both mechanisms have the same order of magnitude of influence on the ozone flux to the troposphere. On a time scale of a few days, the correlation is very good between the potential vorticity and the ozone time evolution in the vicinity of the upper level frontal system.

1. Introduction

Air mass exchanges between the stratosphere and the troposphere must be understood to improve our knowledge of the tropospheric ozone budget. New progress in this field is dependent on the availability of experimental data of meteorological parameters and tracers like ozone. The european TOASTE experiment (Transport of Ozone and Stratosphere Troposphere Exchange) took place in 1990-1991 and aims at providing to modelling work a complete ensemble of experimental data obtained in meteorological systems which are likely to generate Stratosphere Troposphere Exchanges (STE). In this paper, we present ozone vertical profiles performed at the Observatoire de Haute Provence (OHP, 670 m, 43°55N, 5°42E) and meteorological analyses for one of the TOASTE case study to illustrate the impact of cut-off lows on STE. The role of cut-off lows is twofold: ozone transfer within the frontal system associated with the low and small scale mixing at the tropopause level over the whole surface of the low. The first mechanism was studied at the beginning of the TOASTE campaign (November 22nd to 25th, 1990) and the second one

during the erosion phase of the cut-off low (November 27th to 30th, 1990).

2. The meteorological situation

The evolution of the meteorological situation during this campaign is illustrated by the 300 hPa maps of the geopotential heights (Fig.1). They show that a low pressure system developed over France on November 22nd with the associated trough located over southern Spain at midnight. On November 23, a new low appeared south of Iceland causing a northward motion of the trough over Spain along a line going from Spain to Germany. The axis of the trough passed over the OHP during the afternoon of November 23rd and was directed on a line from Corsica to Paris. The circular motion of the two lows induced the formation of a large low pressure system over western Europe on November 24th. On the following days, this system moved southward and cut from the main jet stream on November 27th. The resulting cut-off low remained over France for 4 days before it reconnected to the general circulation flow.

3. Ozone Transfer within the frontal system

The ozone vertical distribution was measured by a UV DIAL lidar [Ancellet, 1989] almost continuously on November 23rd. The OHP lidar system uses two recording modes corresponding to two different altitude ranges: 4 - 7 km (analog mode), 7 - 13 km (photocounting mode). The maximum range is reduced to 11 km during daytime when the noise due the background light increases. Measurements within cloud layers are not included owing to the large aerosol interferences in the cloud. Although ozone concentrations larger than 1.0×10^{12} mol/cm³ (100 ppb) have been measured during the night at 350 hPa (7.8 km), no clear evidence of ozone transport to the troposphere is shown on the lidar results. During the day, the time evolution resembles to a vertical cross section through a tropopause fold passing over the OHP near 18 UT (Fig.2). At the 450 hPa level (6 km) ozone values about 0.65×10^{12} mol/cm³ (46 ppb) are not very high, but remain significantly larger than average values outside of the fold 0.4×10^{12} mol/cm³ (30 ppb).

Using the European Center for Meteorological Weather Forecasting (ECMWF) analysis with the highest resolution $1.1^\circ \times 1.1^\circ$, a vertical cross section of the isentropic potential vorticity (IPV) was calculated for the 18 UT time periods (Fig.3). The section was taken transverse to the minimum of the trough where the jet curvature is maximum. Air masses with high IPV ($> 1.2 \times 10^{-6} \text{ K m}^2 \text{ s}^{-1} \text{ kg}^{-1} = 1.2 \text{ PV}$) supports the presence of a fold over the OHP extended down to 450 hPa. The resolution of the ECMWF analysis is still too coarse to fully resolve the fold below 450 hPa but IPV distribution is in good agreement with the ozone data between 450 hPa and 350 hPa. The ozone to IPV ratio is 38 ppb/PV at 450 hPa where IPV is 1.3 PV, and is 29 ppb/PV at 350 hPa where IPV is 3.4 PV. The air mass trajectories (Fig.4) shows clearly the stratospheric origin of the air masses, and indicates also that a large part of the air in the fold is transferred to the troposphere at low altitudes after turning around the developing low pressure system over Western Europe. This can also be supported by the presence of a dry (specific humidity of 150 ppm) and stable layer (potential temperature gradient of 25 K/100 hPa) observed at 600 hPa on the November 26 by radiosoundings performed at Gibraltar.

To estimate the number of ozone molecules that can be transferred to the troposphere, one can use the ozone content of the fold which is derived from the lidar measurements, and the horizontal distribution of the IPV on the 450 hPa surface to determine the horizontal extent of the fold. On a 1 or 2 day time scale, the ozone to IPV ratio can be taken constant in the free troposphere between 40°N and 50°N since ozone can be considered as a passive tracer within the fold. Therefore the area covered by air masses with IPV larger than 1 PV represents the possible extent of the fold which is approximately located in a $500 \text{ km} \times 2200 \text{ km}$ rectangle (Fig.5). Using a 2 km vertical width for the intruded air mass where ozone is of the order of $0.55 \times 10^{12} \text{ mol/cm}^3$, one obtains a value of 1.2×10^{33} molecules which can be transferred to the troposphere. This value is 3 times smaller than a similar estimate for a tropopause fold observed at the OHP during the spring period [Ancellet et al, 1991]. Although it is difficult to derive a general behavior from some case studies in March and in November, it supports the seasonal variation of the climatological mean of the stratospheric air flux proposed by Danielsen which shows a spring flux 4 times larger than the fall flux [Danielsen et al, 1977].

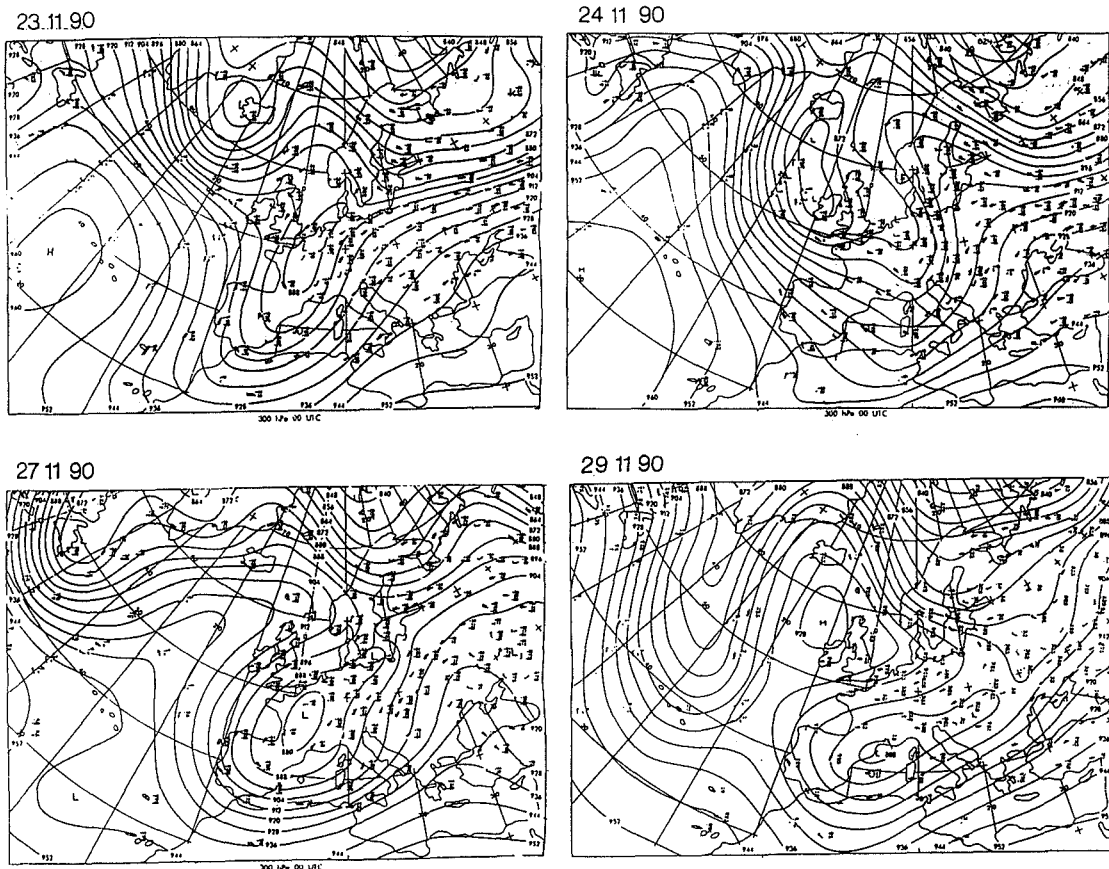


Fig.1 : Meteorological maps of the geopotential height and the wind vector on the 300 hPa surface from November 23rd 00 UT to November 29th 00 UT.

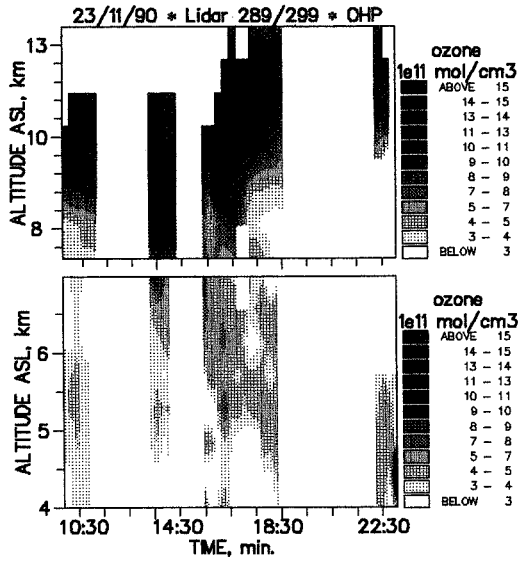


Fig.2 : Ozone concentration time series measured by lidar from 10:30 UT to 22:00 UT on November 23rd. The lower and higher parts correspond respectively to the analog and photocounting recording mode

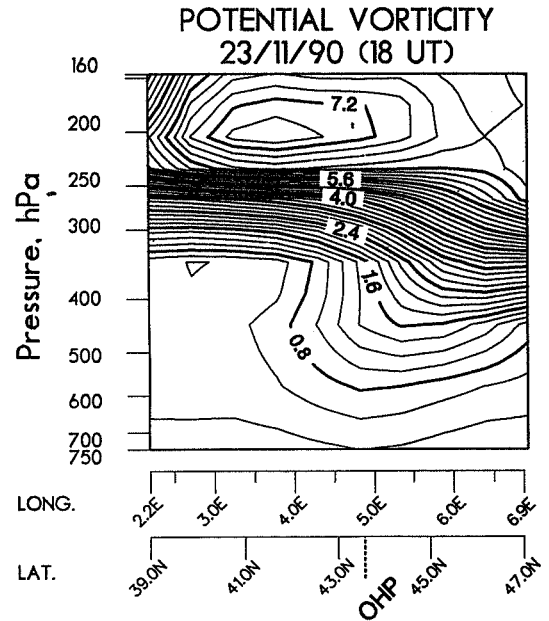


Fig.3 : Vertical cross section of the potential vorticity in PV units, for November 23rd at 18 UT.

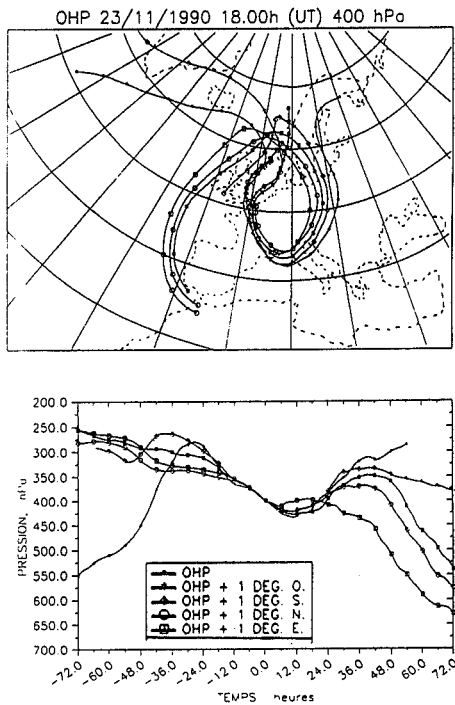


Fig.4 : Horizontal and vertical motions of air masses passing at 400 hPa above the OHP and above four points located 1° away from the OHP, for November 23rd at 18 UT.

4. Evolution of the cut-off low

Ozone was measured on November 27th after 16:00 UT and on November 29th in the afternoon, two time

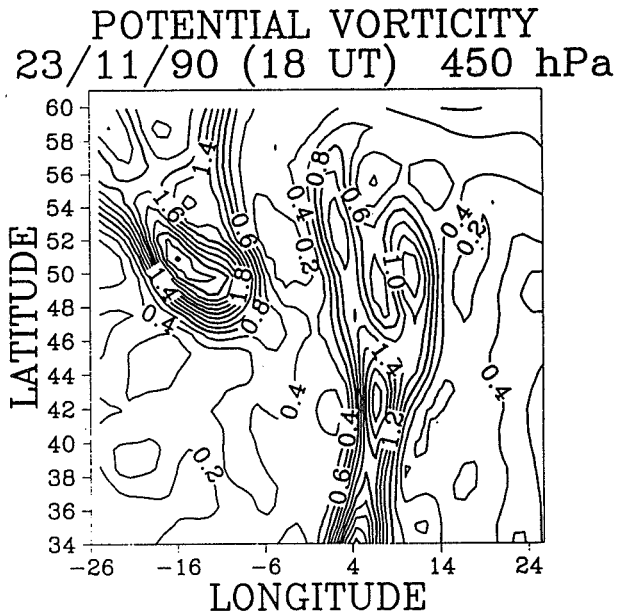


Fig.5 : Potential vorticity in PV unit on the 450 hPa surface on November 23rd 18 UT.

periods for which the OHP was located within the cut-off low. A continuous coverage was not possible owing to the large cloudiness level and rainfall within the low. The ozone temporal evolutions for these two days indicate a large ozone

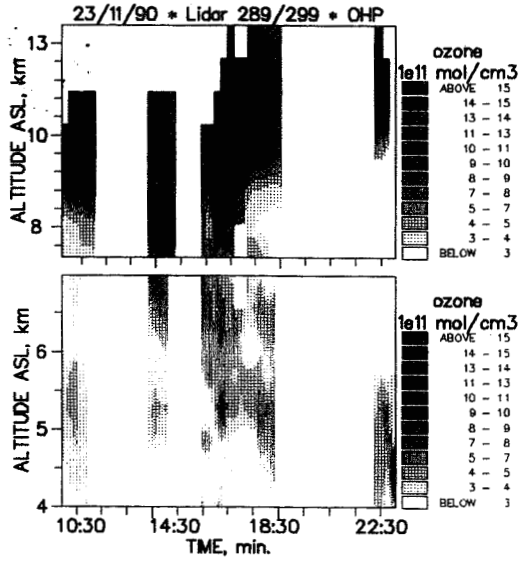


Fig.2 : Ozone concentration time series measured by lidar from 10:30 UT to 22:00 UT on November 23rd. The lower and higher parts correspond respectively to the analog and photocounting recording mode

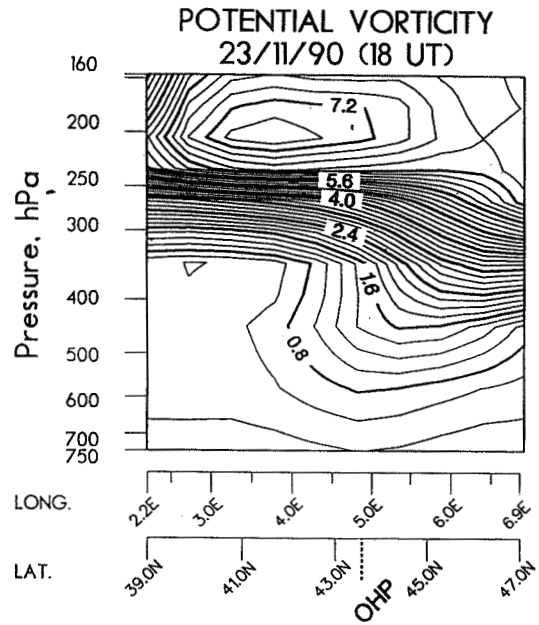


Fig.3 : Vertical cross section of the potential vorticity in PV units, for November 23rd at 18 UT.

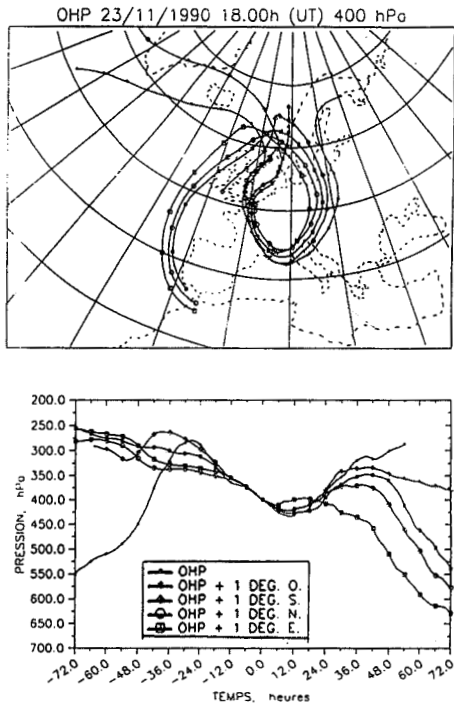


Fig.4 : Horizontal and vertical motions of air masses passing at 400 hPa above the OHP and above four points located 1° away from the OHP, for November 23rd at 18 UT.

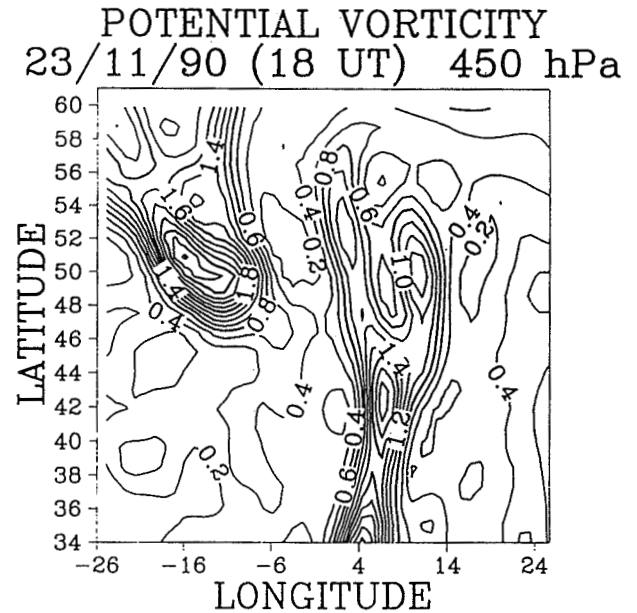


Fig.5 : Potential vorticity in PV unit on the 450 hPa surface on November 23rd 18 UT.

4. Evolution of the cut-off low

Ozone was measured on November 27th after 16:00 UT and on November 29 th in the afternoon, two time

periods for which the OHP was located within the cut-off low. A continuous coverage was not possible owing to the large cloudiness level and rainfall within the low. The ozone temporal evolutions for these two days indicate a large ozone

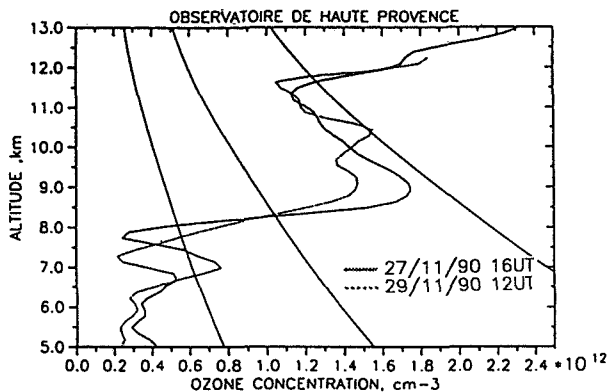


Fig.6 : One hour average ozone profiles measured on November 27th at 16 UT and November 29th at 12 UT.

gradient remaining at 8 km which corresponds to the tropopause altitude measured for these two days at the nearby Nîmes radiosounding station. The one hour average ozone profiles for November 27th at 18 UT and November 29th at noon (Fig.6) shows that the ozone gradient at 8 km is weaker on November 29th than on November 27th while the position of the OHP respect to the center of the low is similar for these two time periods. The tropospheric ozone values between 6 and 8 km on November 27th may be slightly overestimated due to the presence of a cloud layer at 7 km. As a consequence ozone transfer to the troposphere by small scale processes cannot be accurately estimated from the ozone change in this region, but we can use the ozone decrease above the tropopause (between 8.5 and 10.5 km) to estimate this effect during the evolution of the low. The ozone transferred to the troposphere from November 27th to November 29th corresponds then to the variation of the integrated ozone between 8.5 km and 10.5 km assuming that small scale mixing at the upper boundary remains small. Indeed the ozone gradient measured by the lidar at 10.5 km does not change significantly during the two day time period. It is not surprising since the climatological mean of the exchange coefficient in the low stratosphere is generally of 3-4 times smaller than at the tropopause level [Warneck, 1988]. In addition this ozone variation is not related to a tropopause altitude change, since the latter remains constant during these two days.

The ozone flux through the tropopause is then of the order $2.8 \cdot 10^{12} \text{ cm}^2 \text{ s}^{-1}$ associated to an integrated ozone decrease of $4 \cdot 10^{16} \text{ cm}^2$. If one extends this flux to the $1500 \times 1000 \text{ km}$ surface of the cut-off low, one obtains a value of $1.0 \cdot 10^{33}$ molecules transferred to the troposphere in two days. The contribution to the stratospheric air flux is then of the same order of magnitude or even larger than a direct transfer of ozone present in tropopause folds.

5. Conclusion

In this work, stratospheric ozone transfer to the troposphere was studied using both ozone vertical profiles and objective analysis of the ECMWF model to derive

potential vorticity distribution and air mass trajectories. We have shown by this study that:

- the ozone variations observed in the vicinity of frontal systems are well correlated with potential vorticity variations, supporting similar results obtained over continental U.S. [Browell, 1987]. The ozone to potential vorticity ratio of the order of 30 ppb/PV for air masses with potential vorticity larger than 1.2 PV is in good agreement with the November climatological mean of the this ratio obtained from the 1984-1990 OHP ozone data set considering air masses of similar potential vorticity [Beekmann, 1992].
- the ozone potentially transferred from the tropopause fold in the region of maximum jet stream curvature and the ensuing cut-off low development can increase the tropospheric ozone content of $1.2 \cdot 10^{33}$ molecules in a two or three day time scale.
- the small scale mixing taking place at the tropopause level within the observed cut-off low reduces the ozone gradient and leads to an ozone transfer almost equivalent to the transfer by tropopause folding.

Acknowledgements: This work has been supported by the STEP program of the CEC. M.Beekmann held a doctoral fellowship from Gottlieb Daimler und Karl Benz Stiftung and from the Environmental Protection Program of the CEC. The ECMWF is acknowledged for the temperature and wind field analysis.

References

- Ancellet, G., A.Papayannis, J.Pelon, G.Megie, DIAL Tropospheric Ozone Measurement Using a Nd:YAG Laser and the Raman Shifting Technique, *J.Atm.Ocean.Tech.*, 6, 5, 832-839, 1989
- Ancellet, G., J.Pelon, M.Beekmann, A.Papayannis, G.Megie, Ground based lidar studies of ozone exchanges between the stratosphere and the troposphere, *J.Geophys.Res.*, 96D12, 22401-22421, 1991
- Beekmann, M., G.Ancellet, G.Megie, Analysis of a 7 year tropospheric ozone vertical distribution at the Observatoire de Haute Provence, *Proc. Quadrennial Int. Ozone Symp.*, (this issue), 1992.
- Browell, E., E.Danielsen, S.Ismail, G.Gregory, S.Beck, Tropopause fold structure determined from airborne lidar and in situ measurements. *J.Geophys.Res.*, 92D2, 2112-2120, 1987.
- Danielsen, E., and V.Mohnen, Project Dustorm Report: Ozone transport, in situ measurements and meteorological analyses of tropopause folding, *J.Geophys.Res.*, 82(37), 5867-5877, 1977.
- Warneck, P., Chemistry of the natural atmosphere, International Geophysics Series Vol 41, Academic Press San Diego, 1988.

A NOVEL OZONE SENSOR FOR VARIOUS ENVIRONMENTAL APPLICATIONS

H. Güsten, G. Heinrich,
 Institut für Meteorologie und Klimaforschung
 Kernforschungszentrum Karlsruhe/Universität Karlsruhe
 Postfach 36 40, 7500 Karlsruhe, Germany

R.W.H. Schmidt and U. Schurath
 Institut für Physikalische und Theoretische Chemie,
 Universität Bonn, 5300 Bonn, Germany

ABSTRACT

A small, lightweight and fast-response ozone sensor for various environmental applications is described. At a flow rate of 100 l min^{-1} the ozone sensor has a response time of significantly better than 0.1 s with a detection limit lower than 100 pptv. The ozone sensor was successfully tested in various environmental applications, i.e. in measuring directly the vertical ozone flux onto agricultural land utilising the eddy correlation or covariance technique and in monitoring horizontal and vertical ozone profiles in the troposphere and stratosphere.

1. INTRODUCTION

Despite the various ozone analysers which are commercially available, there is an obvious need for

a small, light-weight ozone sensor, which combines simplicity with low cost and low electric power consumption. Furthermore, the commercial ozone analysers feature fairly slow response times of approximately 10 seconds and a detection limit of about one ppb. For various applications such as the eddy correlation technique or aircraft measurements, fast and more sensitive ozone sensors are needed. We will present here various applications of a novel, fast and sensitive ozone sensor.

2. EXPERIMENTAL

The measuring principle of the novel ozone sensor is the chemiluminescence of an organic dye adsorbed on dry silica gel in the reaction with ozone. Details about the prototype ozone sensor and its application are given in Refs. 1 and 2.

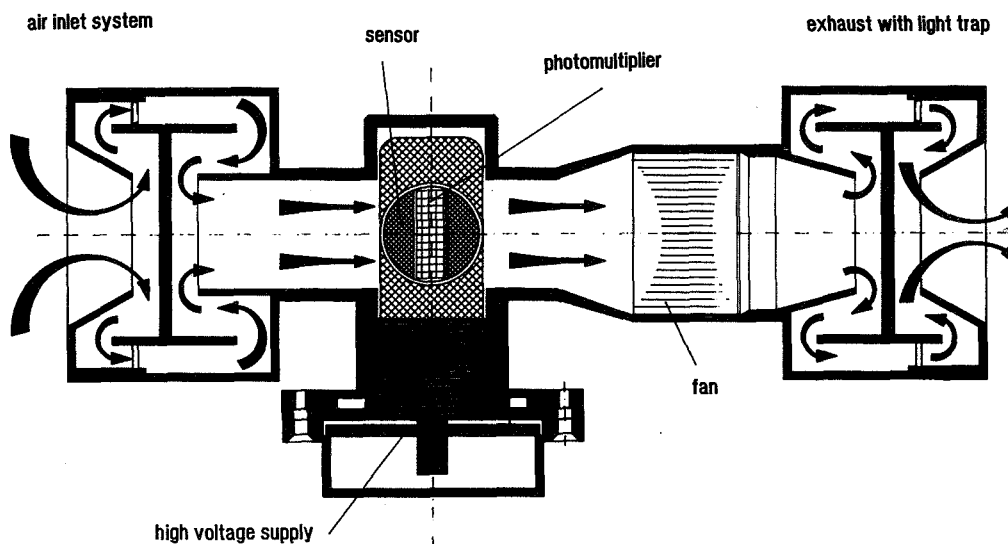


Fig. 1 Schematic of the novel ozone sensor (GFAS Corporation, Germany).

The novel ozone sensor* which is now commercially available, is depicted in Fig. 1. Its basic features are a cheap, blue-sensitive side-window photomultiplier, a high-performance miniature fan producing a rate of air flow through the detector of more than 100 liter min⁻¹, and a thin chemiluminescent disc.

All three components are housed in a black metal rod equipped with light and aerosol traps. A fast flow of air is sucked through the narrow gap between the photomultiplier and the disc surface. The intensity of the chemiluminescence light is directly proportional to the ambient ozone concentration. For various applications in the environment, e.g. eddy correlation technique, aircraft or balloon-based measurements of vertical or horizontal ozone profiles, different versions of the ozone sensor* are available.

The advantages of the novel ozone sensor over conventional ozonometers are:

- a detection limit lower than 100 ppt,
- a response time significantly better than 0.1 second,
- no interference from other atmospheric trace gases like NO_x, H₂O₂ and PAN,
- its small size, light weight (< 1 kg) and ease of handling.

3. ENVIRONMENTAL APPLICATIONS

Continuous eddy flux measurements of ozone on towers over long periods [2,3,4] or on aircrafts

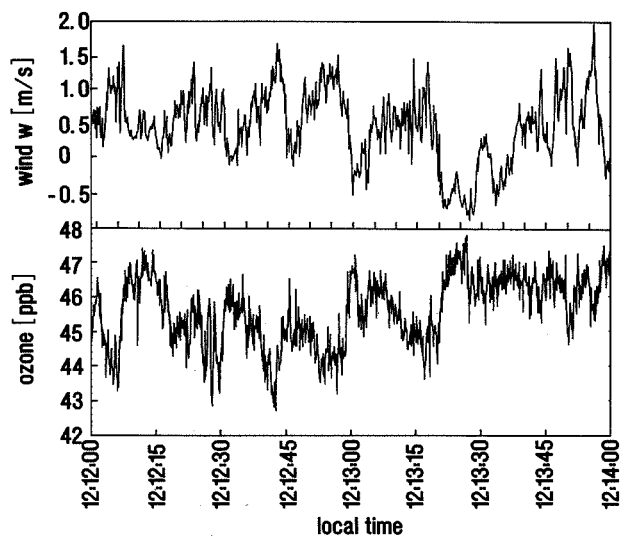


Fig. 2 Time series of vertical wind velocity and ozone concentration, simultaneously measured with 10 Hz resolution.

In Figure 2 a time series of the vertical wind and ozone concentration simultaneously measured with 10 Hz resolution over a wheat field demonstrates the excellent resolution of the signals around a mean

value of about 0.5 m s⁻¹ and 45 ppb, respectively. The vertical ozone flux is computed as the covariance of the fluctuations of both entities [2,3].

Aircraft-based measurements of vertical ozone profiles in the troposphere

Figure 3 displays the vertical ozone and temperature profiles below and above the atmospheric boundary layer, measured on board of a small airplane over the Rhine valley and the Black Forest on January 30, 1992. In the Rhine valley a distinct lamination of the ozone profile within the boundary layer can be observed.

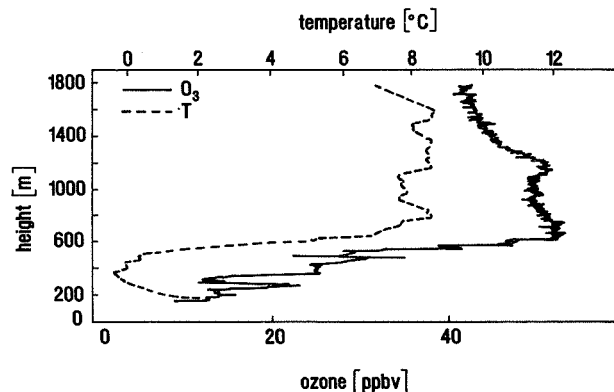


Fig. 3 Vertical ozone and temperature profiles in the lower troposphere, measured on board of a small airplane over the Rhine Valley and the Black Forest on January 30, 1992.

Monitoring vertical ozone profiles in the stratosphere

Figure 4 shows the vertical ozone profile in the stratosphere, measured during a balloon flight launched from Hohenpeißenberg Meteorological Observatory on October 23, 1989 [1].

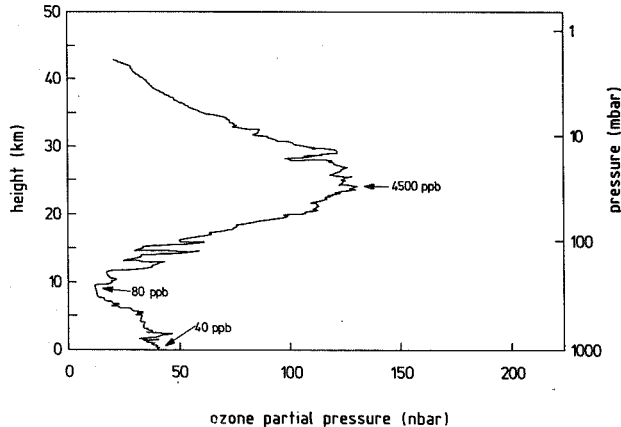


Fig. 4 Vertical ozone profile in the stratosphere, measured during a balloon flight launched from Hohenpeißenberg on October 23, 1989.

*Licensee: Fa. GFAS, Fritz-Kopp Str. 2, D-7997 Immenstaad, Germany.

The ozone profile nicely demonstrates a pronounced laminar structure in the lower stratosphere, a recently much discussed phenomenon [5].

Due to the fast response time, the ozone profiles obtained in a tandem balloon flight with a Brewer-Mast ozone sensor display a better spatial resolution in comparison to the latter sensor [6].

REFERENCES

1. Schurath, U., Speuser, W., and Schmidt, R., 1991: Principle and Application of a Fast Sensor for Atmospheric Ozone. *Fresenius J. Anal. Chem.* **340**, 544-547.
2. Güsten, H., Heinrich, G., Schmidt, R. and Schurath, U., 1992: A Novel Ozone Sensor for Direct Eddy Flux Measurements. *J. Atmos. Chem.* **14**, 73-84.
3. Ernst, N., Güsten, H., Heinrich, G., Mönnich, E., and Weppner, J., 1991: Measurement of the Dry Deposition of Ozone onto Agricultural Land. in: *Proc. EUROTRAC Symposium '90*, P. Borrell et al., eds., pp. 127-129, SPB Academic Publ. bv, The Hague, The Netherlands.
4. Güsten, H., Ernst, N., and Heinrich, G., 1992: Kontinuierliche Bestimmung der turbulenten Ozonflüsse in der bodennahen Luftschicht. *Ann. Meteorol.* **27**, 84-85.
5. Reid, S.J., and Vaughan, G., 1991: Lamination in Ozone Profiles in the Lower Stratosphere. *Q.J.R. Meteorol. Sci.* **117**, 825-844.
6. Speuser, W., Sahand, S., and Schurath, U., 1989: A Novel Fast-response Chemiluminescence Sonde for Routine Soundings of Stratospheric Ozone up to 1.5 mbar. in: *Ozone in the Atmosphere*, pp. 747-750, R.D. Bojkov and P. Fabian, eds., Deepak, Hampton, Virginia.

303268

SURFACE OZONE VARIABILITY AT KISLOVODSK OBSERVATORY

*Nikolay P. Elansky , Oleg V. Makarov
and Irina A. Sentik*

Institute of Atmospheric Physics,
Pyzhevsky per. 3, Moscow 109017,
Russia

ABSTRACT

The results of the surface ozone observations at the Observatory "Kislovodsk", situated in the North Caucasus at the altitude 2070 m a.s.l., are given. The observatory is in the background conditions and the variations of the surface ozone are determined by the natural dynamic and photochemical processes. The mean value of the concentration and its seasonal variations are very near to those obtained at the high-mountain stations in Alps (Reiter, 1987). The daily variations have the features, which remain stable during all warm period of the year (April-October). These features, including the minimum of the surface ozone at noon, are formed by the mountain-valley circulation. The significant variations of the surface ozone are connected with the unstationary lee waves.

1. INTRODUCTION

The long-term observations of ozone concentrations in the troposphere on the set of the ozonometric stations show that there is a positive trend of the troposphere ozone in the middle latitudes of the North hemisphere.

The tropospheric ozone has two sources: transport from the stratosphere and the photochemical generating in the polluted air. Their interaction determines the main features of the ozone behavior. It is difficult to divide their influence for the stations which are situated in the industrial area. Therefore the data got at the high-mountain stations are of the great value, as the local photochemical processes and any antropogenic factors play the insignificant role (Reiter, 1987). These data are the most informative for the analysis of the trends.

In April 1989 the regular measurements of the surface ozone concentrations at the "Kislovodsk"

Observatory were started. The Observatory is situated in the North Caucasus (43,7°N, 42,7°E, 2070 m a.s.l.) on the plateau in the zone of the alpine grasslands. The altitude of the plateau increases in the direction from N-E to S-W. The resort town Kislovodsk is situated 18 km away to the North. 48 km to the South there is the mountain Elbrus which together with the nearest mountain chains forms the local system of the air flows and is the source of the internal gravity waves. The prevailing air flow is of the western direction and is more strongly pronounced in winter. In summer and during the warming up in other seasons the active mountain-valley circulation is acting.

The Observatory is situated in clean background conditions. The only large source of the pollution in its environs is the town of Kislovodsk (800-870 m a.s.l.). Observations of nitrogen oxides (NO_x) concentration with the help of the gas analyzer Antechnica AC-30 during 5 months in 1989 and 1990 gave their mean level below the level of the instrument's sensitivity which is 1ppb. In the present work the time variability of the surface ozone concentration in the mountains and the causes of these variations are analyzed.

2. OBSERVATIONS

The measurements of the ozone concentration were carried out with the help of the gas analyzer Dasibi 1008-AH which works on the base of the absorption of the UV-radiation. The precision of the measurements is about 1-2 ppb. The air was sampled on the level of 2,5 m above the ground.

The measurements are being carried out twenty-four-hour with the periodical switching off for the preventive inspection and because of the unfavorable meteo conditions: the intensive precipitations or the dense fog.

The analogous instrument was used for measurements of the ozone concentration in the south part of the town of Kislovodsk. The measurements there were carried out less regularly mostly in the daytime.

Both instruments were calibrated with the help of the ozone generator and compared with each other. The correlation coefficient between the instruments output was 0,98. The mean differences of the absolute values was 1 ppb.

The main information about the mean characteristics of the time variation of the ozone concentration at the Kislovodsk observatory are given in Tabl.1.

Tabl. 1. Mean values of the ozone concentration (ppb) at the station Kislovodsk.

Month 1989- 1990	Monthly means	Daily means		Hourly means	
		max	min	max	min
Apr	43 ± 3	46	30	56	33
May	44 ± 4	49	35	55	32
Jun	46 ± 6	55	39	59	35
Jul	41 ± 6	53	31	60	24
Aug	47 ± 4	56	41	61	32
Sep	41 ± 5	52	30	59	22
Oct	36 ± 2	40	32	42	28
Nov	32 ± 4	36	24	42	20
Dec	34 ± 3	39	26	40	21
Jan	32 ± 3	41	21	46	24
Feb	38 ± 4	48	26	51	23
Mar	42 ± 5	52	33	63	30
Apr	42 ± 6	56	33	57	21
May	44 ± 4	52	35	64	29
Jun	41 ± 5	49	29	63	29
Jul	44 ± 7	55	20	65	20

The averaged over year (April 1989-March 1990) ozone concentration was 39.7 ppb. It is approximately coincides with the mean values 40-42 ppb, got obtained Reiter et al. (1987) at the high-mountain stations in FRG Wank Peak, 1780 m a.s.l. and Zugspitze Peak, 2964 m a.s.l. (48 N) and slightly less than got at the high-mountain stations of the Japan at 32 N and 41 N - (45-47 ppb) (Tsuruta et al., 1989).

Hourly means of the ozone concentration during the same period varied within the limits of 20-65 ppb. The concentration equal or more 60 ppb were registered in total for 33 ours (only 9 days). During the day the hourly means vary insignificantly: minimum variation is 1 ppb, maximum - 25 ppb. Monthly means varied from 32 to 47 ppb. In Fig.1 the decade means of the ozone concentration at the Kislovodsk observatory are shown. Their values and seasonal variations are very similar to the data, given by Reiter et al. (1987) for the high-mountain stations in the Alps. The time of the

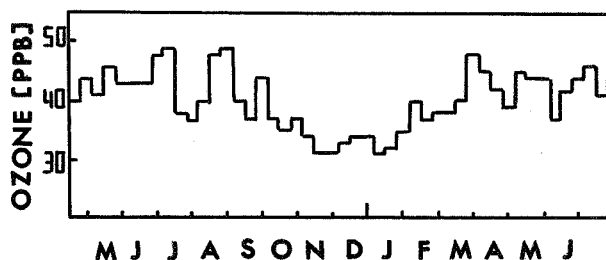


Fig. 1. The decade mean surface ozone concentration at the Kislovodsk observatory.

year maximum (May-August) and minimum (December-January) practically coincide as well.

At the stations situated below 1000m such as Kislovodsk town, Hohhenpeissenberg Garmich-Partenkirchen (Reiter et al., 1987; Volz et al., 1989) the absolute values of the ozone concentration (yearly means - 24-32 ppb) and their variations differ significantly from the given above. The influence of the atmospheric pollution is noticeable there already.

The daily variations of the ozone concentration at the Kislovodsk Observatory (Fig. 2) is characterized by the small variations and high stability of the characteristic features from month to month. In contrast to the plain stations the stable minimum of the ozone concentration is registered there at the near noon time. This minimum is more deep (4-5 ppb) in June-July and disappears only in winter. Monthly mean time of the minimum existence varies from 11 hours (local time) in June to 13 hours in April and October. There can be two cause of such stable and characteristic daily variations of the ozone concentration. The first one is the action of the photochemical processes in conditions of the low content of the nitrogen oxides (NO_x) in the surface layer. The second one

supposes the action of the dynamic mechanisms - the transport of ozone by system of the mountain - valley circulation in presence of the positive altitude gradient of the ozone concentration.

To our opinion, the daily variations can be explained in that way. The decreasing of the ozone concentration after the sunrise begins just as the N and N-E flows which moves upward the slope are formed. After the meteorological data the reiteration of the winds of these directions before noon during the warm period of the year make up 65%. In average, in 1-2 hours the air from the region of the higher border of the planetary boundary layer comes to the

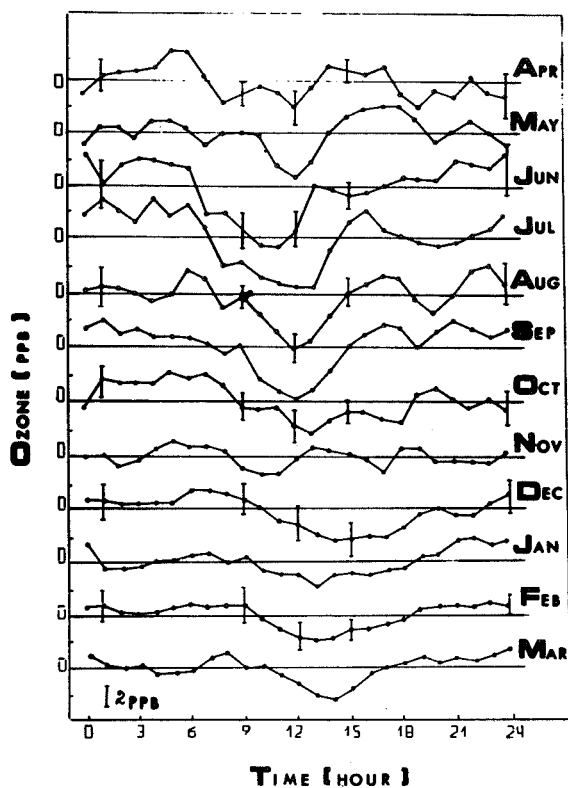


Fig. 2. Daily variations averaged by month for the period April 1989-March 1990.

observatory. This border is localized during the period from April to October at the mean altitude 1700 m. At all monthly mean diurnal profiles at this time the weak maximum of ozone is registered. The subsequent ascent of the air up the slope brings more poor by ozone but more polluted air from the valley and sometimes from Kislovodsk town. In this time the minimum of ozone is observed. When this air mass is rich with NO_x the intensive production of ozone under the influence of the sunlight is going on and the ozone concentration is increasing. This is demonstrated in Fig. 3. It is seen, that the daily variation of the ozone concentration at the Observatory got by averaging over the days when the direction of the wind was from Kislovodsk town is approximately the same as in the town after the noon. To the evening with the weakening of the photochemical processes the ozone concentration is decreasing but after the development of the downward flow is again increasing and stays on high level till the morning.

The unregular variations of the surface ozone are connected with the different meteorological processes: the

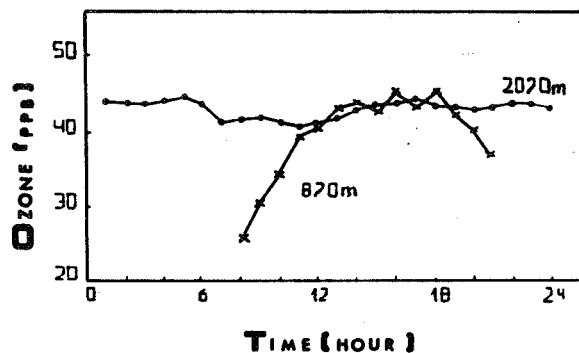


Fig. 3. The averaged over the period April-July 1989 (for the days with the North wind) daily variations of the ozone concentration at Kislovodsk town and the Kislovodsk observatory.

passing of the fronts, the intensive precipitations, fogs. In whole, the value and the character of such variations repeat the well known data for the plain stations. The characteristic features of the time variability of the ozone concentration at the observatory is the short-time (from 3 to 20 min) increasing up to 75-120 ppb and more. There was 6 such events in 1989. For these events the existence of the intensive jet streams in the upper troposphere the descending moving and internal gravity waves (IGV)

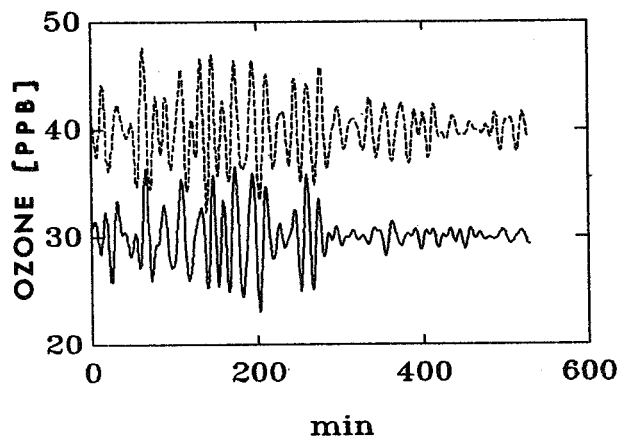


Fig. 4. The variations of the ozone concentration in 2 sites which are 250 m away from each other.

is characteristic . It says about the high probability of the descent of the stratospheric air in the zone of the tropopause break.

IGV of the orographic origin and from the developed convection play the significant role in the time variability of the surface ozone. The most characteristic periods of oscillations are 5-8; 12-16; 25-35 min. Unstationary waves reveal themselves in the observations in different sites. In Fig. 4 the example of such measurements carried out with the help of the chemoluminescent gasanalyzers in the points which are 250 m away from each other. The spectral analysis gives the periods of oscillations in each of these points 21 and 14 min and high values of coherency (0,8-0,9). The deviation of the phase of the oscillations corresponds to the time deviation 1-2 min. The vertical profile of the Brant-Vaisil frequency, got from the aerological data, says about the presence of the favorable conditions for the existing of the IGV with the periods 12-20 min in the layer 1.5-3 km.

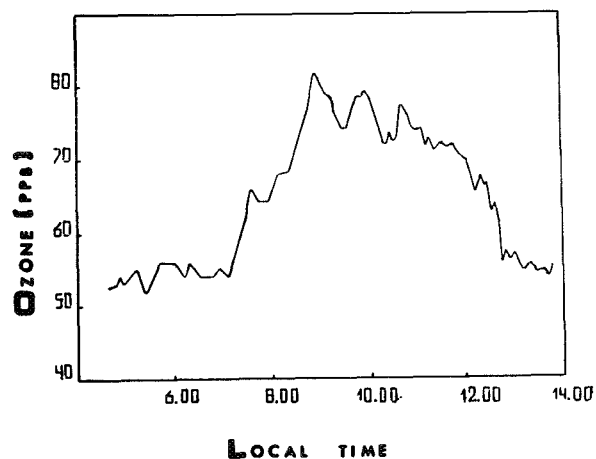


Fig. 5. The influence of the forest fire on the surface ozone concentration on 27 March 1991.

In Fig. 5 the great and prolonged increasing of the ozone concentration on 21 March 1991 is shown. It is connected with the violent forest fire 4-5 km away from the observatory. On this sunny day the concentration increased after the coming of smoke to the observatory and restored down to the normal level after the change of the wind direction.

References

- Reiter, R., R. Sladkovic, H.J. Kanter, 1987: Concentration of trace gases in the lower troposphere, simultaneously recorded at neighboring mountain stations. Part II: Ozone. Meteorol. Atmos. Phys., 37, 37-47.
- Tsuruta, H., K. Shinya, T. Mizoguchi, T. Ogawa, 1989: Seasonal behavior of the troposphere ozone in rural Japan. Proc. of the Quadr. ozone symp. 1988 and Troposph. ozone workshop. A DEEPAK Publ., 433-436.
- Liu, S.C., D. Kley, M. McFarland, J.D. Mahlman and H.L. Levy II, 1980: On the origin of tropospheric O₃. J. Geophys. Res., 85, 7546-7552.
- Analytical Review of the atmospheric pollution with sulphur and nitrogen compounds and assessment of their deposition in background areas in the East-European CMEA members - countries (1982-1987), 1988: Hidromet, Moscow, 77p.
- Volz, A., H. Geiss, S. McKeen, D. Kley, 1989: Correlation of ozone and solar radiation at Montsouris and Hohenpeissenberg: indications for photochemical influence. Proc. of the Quadr. Ozone symp. 1988 and Troposph. ozone workshop. A. DEEPAK Publ., 447-450.

303271

CARBON MONOXIDE MEASUREMENTS AT MACE HEAD, IRELAND

Bruce G. Doddridge, Russell R. Dickerson
Department of Meteorology, University of Maryland
College Park, Maryland 20742, USA

T. Gerard Spain
University College Galway
Co. Galway, Ireland

Samuel J. Oltmans
NOAA/CMDL
Boulder, Colorado 80303, USA

Paul C. Novelli
NOAA/CMDL and CIRES
Boulder, Colorado 80309, USA

ABSTRACT

The North Atlantic Ocean is bordered by continents which may each, under the influence of seasonal weather patterns, act as sources of natural and anthropogenic trace gas and particulate species. Photochemically active species such as carbon monoxide (CO) react to form ozone (O₃), a species of critical importance in global climate change. CO is sparingly soluble in water, and the relatively long lifetime of CO in the troposphere makes this species an ideal tracer of air masses with origin over land. We have measured CO using a nondispersive infrared gas filter correlation analyzer at Mace Head on the west coast of Ireland nearly continuously since August 9, 1991. Measurements of CO were acquired at 20-sec resolution and recorded as 60-sec averages. Daily, monthly, and diurnal variation data characteristic of CO mixing ratios observed at this site are reported. Depending on source regions of air parcels passing over this site, 60-min concentrations of CO range from clean air values of ~90 ppbv to values in excess of 300 ppbv. Data characterizing the correlation between 60-min CO and O₃ mixing ratio data observed at this site are reported also.

1. INTRODUCTION

Any meaningful assessment of the impact of continental emissions on chemical processes in the atmosphere and characterization of the climatology of tropospheric O₃ over the North Atlantic Ocean rely heavily on the acquisition of a large data base containing continuous and time-averaged values for a variety of species. Carbon monoxide has natural and anthropogenic sources contributing to observed concentrations in the atmosphere; nearly all major sources are, however, of continental origin. Carbon monoxide may act as a precursor to photochemical O₃ by reaction with the hydroxyl radical, the primary removal process for CO in the atmosphere. Carbon monoxide is sparingly soluble in water and the relatively long lifetime of CO in the troposphere makes this species an ideal tracer

of air masses with origin over land. The importance of CO in the global carbon cycle and implications for global climate change is the subject of an excellent review by Khalil and Rasmussen (1990). Our research site at Mace Head, Ireland (53°19'N, 9°54'W), has an excellent westerly exposure to the North Atlantic Ocean, and suffers little by way of interferences from ship or air traffic. The site has been described in detail previously (Jennings et al., 1991). An understanding of the sources, abundance, and seasonal behavior of this species over the North Atlantic Ocean is essential to gain valuable insight into delicate biogeochemical cycles in this region, and changes in the global environment.

2. EXPERIMENTAL TECHNIQUE

For continuous measurements of ambient CO we use a commercial nondispersive infrared (NDIR) gas filter correlation analyzer (Thermo Environmental Corporation, Franklin, MA; Model 48), modified for increased sensitivity (Dickerson and Delany, 1988), equipped with a Nafion[®] drying tube (Perma Pure, Toms River, NJ, Model PD-625-12PS) for sample air stream drying, and a heated (to 250°C) Pd on alumina catalyst (type E 221 P/D, Degussa Corp., Plainfield, NJ) (Parrish et al., 1991) as a chemical zero for CO. A Teflon filter (5–10 μm pore size; Shelby Jones, Upper Derby, PA) is used upstream of the analyzer to keep out large particles. Laboratory and field studies of the Pd/alumina catalyst indicate that the catalyst is 100% efficient at 250°C over the dynamic range of CO mixing ratio expected at a North Atlantic regional site. We calibrate the instrument (for ~1 hr) weekly using a cylinder of compressed air of known concentration (referenced to a NIST/SRM CO standard). At intervals of six months the instrument is compared also to a NIST/SRM (1677c 9.97 ppmv CO in nitrogen, certified; NIST, Gaithersburg, MD) and a number of secondary standards (~5 ppmv CO in nitrogen; Matheson Gas, East Rutherford, NJ) referenced previously to the NIST/SRM. Measurements of ozone are provided by a commercial optical instrument using absorp-

tion of UV radiation at 254 nm (Monitor Labs Model 8810; Enviro Technology, Gloucestershire, UK). Both ozone and CO are sampled at a height of 10 m.

A digital data acquisition system (Hewlett Packard, Loveland, Colo.; Model 3421A, with HP-41CV driver and HP-9114B floppy disk drive) provide 1-min mean (of 3x20-s data) CO and ozone data. Data are stored on 3.5" floppy disks prior to further processing into calibrated time series of CO and ozone mixing ratios.

3. RESULTS

Carbon monoxide has been measured at Mace Head since August 9, 1991. Table 1 shows statistical data on 60-min means generated from the 1-min data from that time to January 17, 1992. Data arising from local sources,

Table 1. Project data summary

	Aug	Sep	1991 Oct	Nov	Dec	1992 Jan
Maximum	358	421	447	239	367	333
75th.Perc.	122	238	137	143	212	170
Median	107	123	123	134	182	153
25th.Perc.	99	114	118	128	138	147
Minimum	73	65	80	105	94	132
Mean	132	170	153	138	182	168
$\pm 1\sigma$ †	65	73	70	16	53	39
Total Data‡	466	682	741	407	628	276

† Standard deviation in the 60-min mean

‡ Total 60-min means used (computed from 1-min data)

as characterized by relatively high frequency peaks on the CO mixing ratio time series, and data during periods of analyzer malfunction or calibration, as documented by the site operator, have been removed. Fig. 1 shows a time series of daily mean CO mixing ratio observed at Mace Head during this period. One sees a number of periods of elevated CO, over a steadily rising baseline due to the natural seasonal variation expected for Northern Hemisphere CO mixing ratio (see Khalil and Rasmussen, 1990).

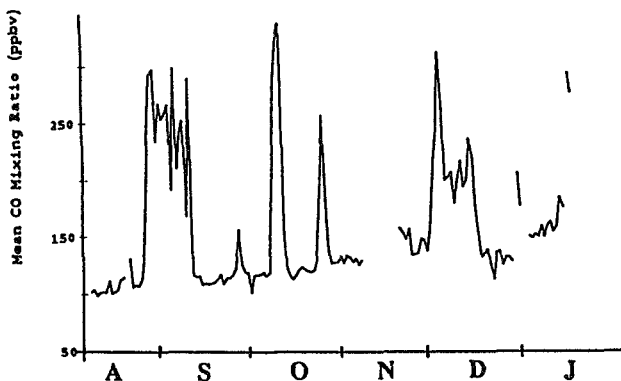


Fig. 1. Daily CO mixing ratio data from Mace Head for the period 91/08/10 – 92/01/17. Daily mean is the average of 1-min data.

On the basis of isentropic back-trajectories used for source attribution to Mace Head (Merrill, unpublished data 1992), we find that for the most part, elevated CO daily mean mixing ratios can be attributed to source regions in Europe, while westerly flow accounts for most of the baseline data.

A comparison of weekly NOAA/CMDL CO flask measurement data (analyzed using a GC/mercuric oxide reduction technique) from Mace Head with our own data has been performed. Fig. 2 shows the results of this inter-comparison through the period 91/08/12 – 92/01/06 of their (grab can) data with our own (60-min mean) CO data. The

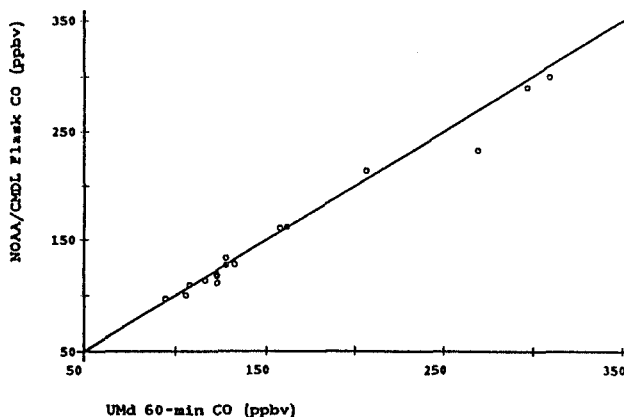


Fig. 2. Intercomparison of NOAA/CMDL calibrated flask CO data with U. Md. 60-min mean CO data from Mace Head, over the period 91/08/12 – 92/01/06. Open circles indicate data pairs and the solid line indicates 1:1 agreement between the data sets.

agreement between the two data sets is quite good, with a linear least-squares fit of the data in fig. 2 having a slope of 0.931 ± 0.034 ($r = 0.991$). This excellent comparison with these independent data gives us a high degree of confidence in our results.

The mean data in Table 1 seem biased by some high-[CO] data, presumably European in origin. Fig. 3 shows the upper and lower quartiles, mean, and median 60-min CO data, for each month processed thus far. A trend toward higher ambient CO mixing ratio at this site

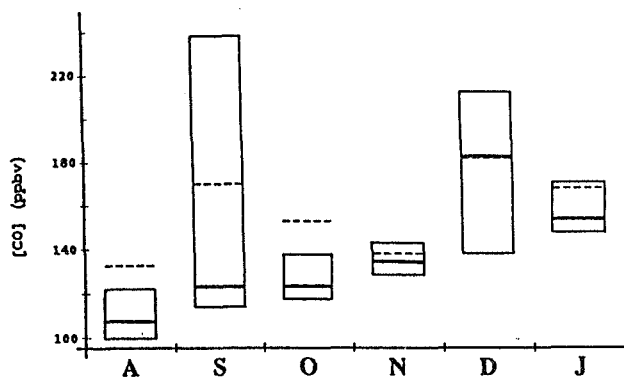


Fig. 3. Monthly variation in CO mixing ratio at Mace Head. Boxes define the upper and lower quartiles; the solid line within each box represents the median; and the dashed line represents the mean.

during winter is apparent. This fits the expected chemistry, as the primary sink for CO in the troposphere, the hydroxyl radical (OH), is most abundant during the summer months. Fig. 4 shows the monthly diurnal variation in median 60-min CO mixing ratio observed at this site. The lack of

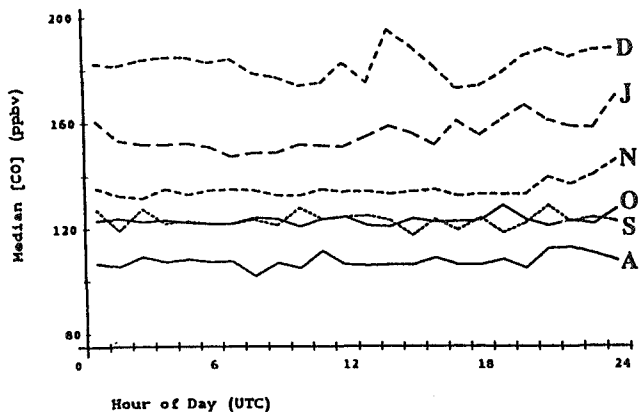


Fig. 4. Diurnal variation in 60-min median CO mixing ratio at Mace Head. Each month is indicated at right; time of day is (UTC).

diurnal variation shown in these data indicate that the origin of periods of high CO are regional in scale; local sources would be expected to show a diurnal cycle due to traffic patterns or boundary layer dynamics.

Analysis of CO data for one complete season, being Fall (September–November), is now complete. Fig. 5 shows a histogram of the Fall 60-min CO data. One

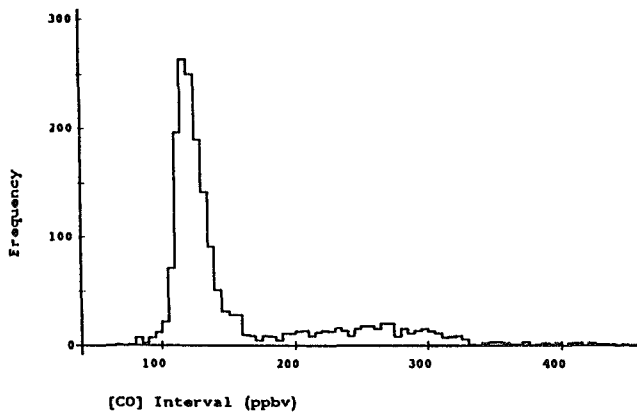


Fig. 5. Histogram of 60-min mean CO mixing ratio data for the Fall season, subject to a CO interval of 5 ppbv.

observes two distinct distributions within these data with a division at ~180 ppbv; air with origin over the North Atlantic Ocean with a median CO mixing ratio of ~120 ppbv accounting for 78% of the data, and (presumably) European air with median CO mixing ratio ~260 ppbv making up the other 22%. A study by Piotrowicz et al. (1990) of CO over the mid-latitude North Atlantic Ocean

during late-summer and early-fall indicated an average CO mixing ratio of ~124 ppbv under conditions of westerly flow, which is consistent with our interpretation. We have made a comparison of 60-min mean CO data with hourly mean ozone data from Mace Head for the Fall season, and the resulting scatter plot is shown in fig. 6. Most of the data can be placed in a box bounded by CO 100–150 ppbv and O₃ 25–45 ppbv, and these data appear anticorrelated;

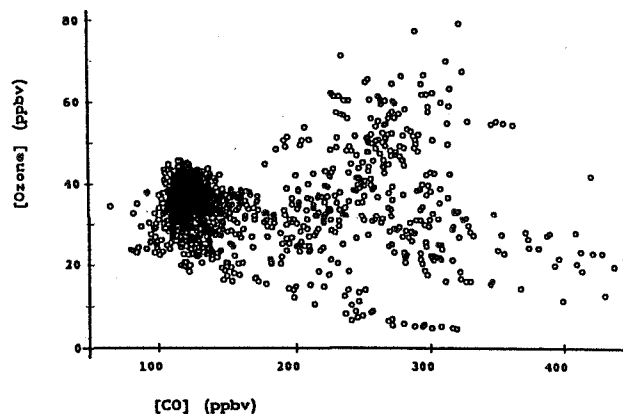


Fig. 6. Comparison of observed 60-min CO and O₃ data from Mace Head, for the Fall season. Data pairs are shown as open circles.

most of these data are certainly of North Atlantic origin. At higher CO mixing ratios there is some indication of two processes operating, ozone destruction by titration with NO and hydrocarbons (indicated by negative correlation), and photochemical ozone production (positive correlation), but without a detailed analysis of back-trajectory data, it is not possible to resolve these regimes at this stage. A conditional mean (Poulida et al., 1991) of the Fall CO data, relative to 1-ppbv intervals of ozone mixing ratio, is more instructive, and is shown in fig. 7. We see three distinct

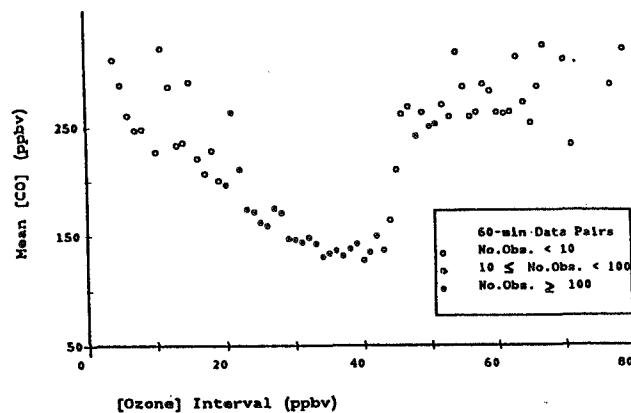


Fig. 7. Conditional mean of 60-min CO mixing ratio relative to 1-ppbv interval of O₃ at Mace Head, for the Fall season. The number of individual CO data averaged to produce that mean for each O₃ interval is indicated by the figure legend.

regimes in these data. For $O_3 < \sim 25$ ppbv, the curve has a large negative slope, representative of periods of relatively high CO input, presumably European in origin, to the area. For $O_3 > \sim 45$, the curve has a positive slope, indicative of photochemical ozone production. At intermediate levels of O_3 , the curve is relatively flat, with a slope near zero, suggesting that photochemical production and loss are similar in magnitude, and probably both slow in this season of sparse solar radiation.

We have just begun using isentropic back-trajectory analysis data (Merrill, unpublished data 1992) to determine if a valid correlation exists between air mass origin and observed CO mixing ratios at Mace Head, even from as far away as North America. As an example, fig. 8 shows two back-trajectories, with arrival times at Mace Head 24 hr apart, but with differing source regions on the North American continent. The 60-min mean CO mixing ratio

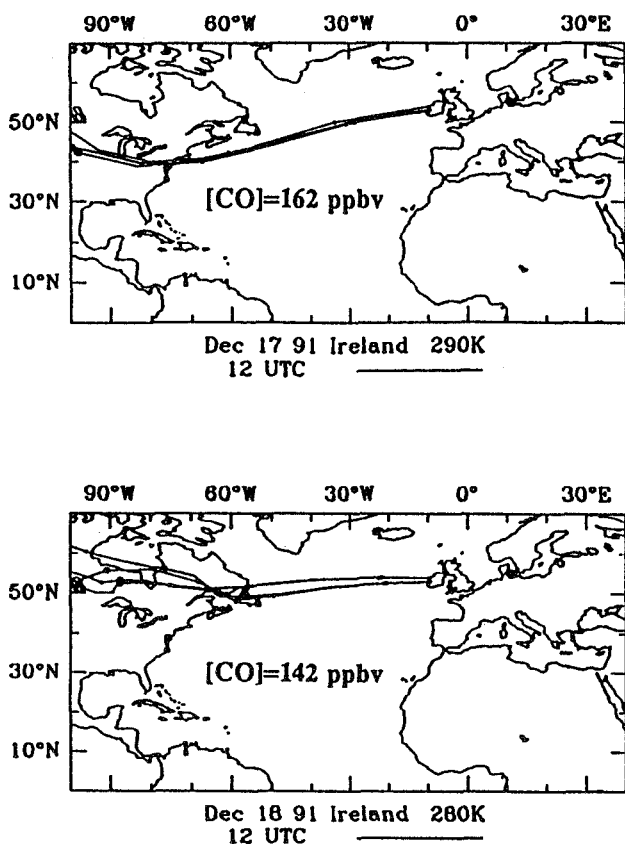


Fig. 8. Isentropic back-trajectories to Mace Head, Ireland, and observed 60-min mean CO mixing ratios at arrival times of 12 UTC on 12/17/91 and 12/18/91. Trajectories supplied by Merrill (unpublished data 1992).

observed at Mace Head at 12 UTC on 12/17/91 was 162 ppbv, with the trajectory passing over heavily industrialized regions of the northeastern U.S. A significantly lower CO mixing ratio of 142 ppbv was observed at 12 UTC on 12/18/91, with the trajectory passing over sparsely populated areas of northern Canada and Newfoundland. In contrast, a trajectory arriving at Mace Head at 00 UTC on

12/05/91, of European origin as shown in fig. 9, is characterized by a much higher observed CO mixing ratio of 306 ppbv.

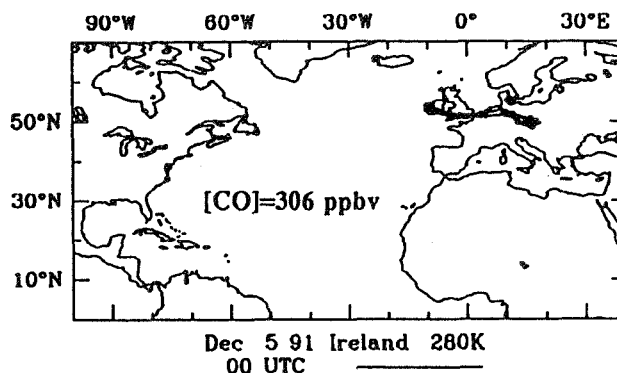


Fig. 9. Isentropic back-trajectory to Mace Head, Ireland, and observed 60-min mean CO mixing ratio at an arrival time of 00 UTC on 12/05/91. Trajectory supplied by Merrill (unpublished data 1992).

ACKNOWLEDGMENTS

BGD and RRD wish to acknowledge support from NOAA (Grant NA16RC0463) and NSF (Grant ATM-90-14841). The views expressed herein are those of the authors and do not necessarily reflect the views of NOAA. We wish to thank University College, Galway, and AEROCE for the use of the Mace Head site and associated facilities. The ozone instrument is provided by Warren Spring Laboratory, UK. The authors thank J. Merrill for kindly providing back-trajectories to us prior to publication. We are grateful to J. Bower, F. Fehsenfeld, G. Jennings, H. Maring, D. Parrish, J. Prospero, H. Schiff, and P. Simmonds for helpful assistance and collaboration.

REFERENCES

- Dickerson, R. R., and A. C. Delany, 1988: Modification of a commercial gas filter correlation CO detector for enhanced sensitivity, *J. Atmos. Ocean. Technol.*, 5, 424-431.
- Jennings, S. G., C. D. O'Dowd, T. C. O'Connor, and F. M. McGovern, 1991: Physical characteristics of the ambient aerosol at Mace Head., *Atmos. Environ.*, 25A, 557-562.
- Khalil, M. A. K., and R. A. Rasmussen, 1990: The global cycle of carbon monoxide: Trends and mass balance, *Chemosphere*, 20, 227-242.
- Parrish, D. D., M. Trainer, M. P. Buhr, B. A. Watkins, and F. C. Fehsenfeld, 1991: Carbon monoxide concentrations and their relation to concentrations of total reactive oxidized nitrogen at two rural U.S. sites, *J. Geophys. Res.*, 96, 9309-9320.
- Piotrowicz, S. R., C. J. Fischer, and R. S. Artz, 1990: Ozone and carbon monoxide over the North Atlantic during a boreal summer, *Global Biogeochem. Cycles*, 4, 215-224.
- Poulida, O., R. R. Dickerson, B. G. Doddridge, J. Z. Holland, R. G. Wardell, and J. G. Watkins, 1991: Trace gas concentrations and meteorology in rural Virginia 1. Ozone and carbon monoxide, *J. Geophys. Res.*, 96, 22,461-22,475.

**EPISODES OF VERTICAL AND HORIZONTAL OZONE TRANSPORT
MONITORED AT ITALY'S MT. CIMONE OBSERVATORY**

T. Colombo and V. Cundari
Italian Meteorological Service, 41029 Sestola (MO), Italy

P. Bonasoni, M. Cervino, F. Evangelisti, T. Georgiadis and G. Giovanelli
FISBAT-C.N.R. Institute, Bologna, Italy

ABSTRACT

Variations in the concentration of surface ozone measured at a pollution-free mountain site from March 1991 to March 1992 are reported and discussed. Two of the ozone-transport episodes are presented in this case study: a stratospheric intrusion recorded in November 1991 and a horizontal transport in August 1991.

1. INTRODUCTION

A great deal of attention has been focused in recent years on the tropospheric ozone concentration, which has doubled in the northern hemisphere over the last century (Bojkov, 1986). A high surface concentration is not only harmful to human health and toxic to vegetation but contributes, along with other trace gases such as CO₂, CH₄, and CFCs, to produce the greenhouse effect - a fact that has important climatic implications. The present study, which is based on measurements of mid-latitude ozone taken at a mountain site in the northern hemisphere far from sources of anthropogenic pollution, provides a brief overview of the seasonal variations in surface-ozone concentration and focuses on two transport episodes. The first deals with a case of vertical transport of stratospheric origin and the second with a horizontal transport of man-made, photochemical ozone that occurred over the Po valley.

2. SITE AND INSTRUMENTATION

The Mt. Cimone Meteorological Observatory (44°12' N, 10° 42' E, 2,165 m asl) is situated atop the highest peak in Italy's north-central Apennines and divides the Po valley from the Tyrrhenian Sea's Gulf of La Spezia (Fig.1). It is accessible by vehicle only via a private road that begins at 1,500 m asl (timberline is at 1,600 m asl) and ends at the entrance to a cable-railway within the mountain itself that covers the final 300 m. The closest inhabited areas are small villages situated 15 km from and about 1,200 m below the Observatory; the large towns are situated in the lowlands about 70 km away. In comparison to the other weather stations in Italy, Mt. Cimone features the highest recorded wind values (yearly average wind speed about 16 knots). It is thus a privileged vantage point for measuring meteorological parameters and monitoring atmospheric trace compounds (Cundari et al., 1986).

Apart from collecting the usual meteorological data, it has been used since 1979 to measure atmospheric CO₂ in baseline conditions and, since March 1991, for continuous monitoring of surface ozone concentration via a UV Dasibi 1108 photometer. The teflon sampling line runs to the heated

air intake 7 m above the ground. The VDC signal is processed by PC via an A/D card converter. An original software package continuously logs concentrations on the hard disk and transforms the data in one-minute averages so as to generate therecorded ten-minute and hourly averages.

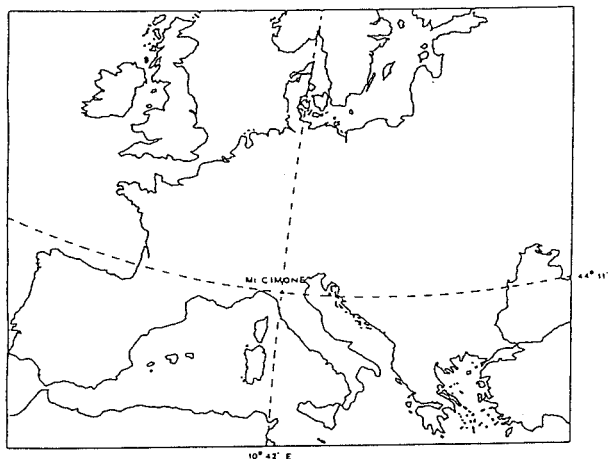


Fig. 1. Measurement site .

3. TRANSPORT PHENOMENA

The reported surface-ozone time series is for continuous measurements taken from March 1991 to March 1992. The monthly averages of O₃ concentrations (fig. 2) clearly evince the yearly variation, which is marked by a main peak in August, a secondary one in May and a minimum in December. The spring peak can likely be attributed to a stratospheric air intrusion, a frequently occurring phenomenon at mid-latitudes at this time (Bojkov, 1985), whereas the summer peak is the result of transport phenomena associated with photochemical production (Austin et al., 1991; Bonasoni et al., 1991) of anthropic emissions in Po valley. The hourly seasonal averages of the ozone concentrations were also plotted (fig. 3): the readings for late spring and summer show the typical night-maximum and day-minimum pattern. This daily swing in ozone concentration is likely due both to diurnal updrafts, which peak at noon and lift ozone-poor air from the valley woodlands, a trend similar to that recorded at Mauna Loa and at a mountain station in Japan (Oltmans, 1981; Tsuruta et al., 1989), and to the nocturnal

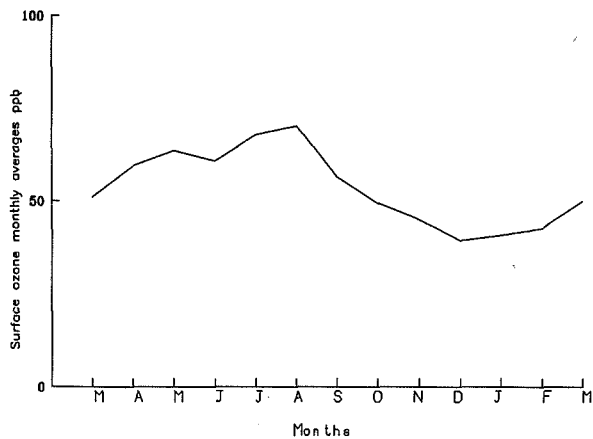


Fig. 2. Yearly trend of surface ozone from March 1991 to March 1992.

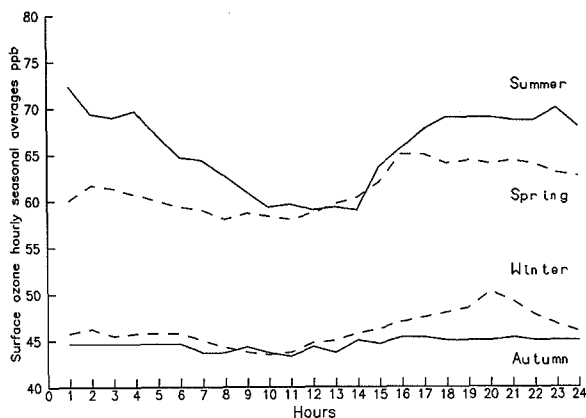


Fig. 3. Hourly seasonal average.

downdrafts, which are marked by prevailing free tropospheric air and background ozone concentrations. The air samples from Mt. Cimone are thus a mixture of free tropospheric air and air masses from the underlying local valleys, although in high pressure conditions persistent inversions confine surface air below the observatory in late autumn, winter and early spring. Daily variability is lower than 5 ppb over the given time span when the mountain's slopes are covered with snow as ozone destruction is held to be slight in snowy conditions (Hakola et al., 1991). By contrast, the daily swing in late spring, summer and early autumn peaks at 20 ppb. A similar, seasonally oriented daily swing is also found upon analysis of the twelve-year data for CO₂ concentration values registered at Mt. Cimone, a pattern resulting from the effect on mid-day values of vegetative uptake from the surrounding valleys (Cundari et al., 1986).

An examination of the hourly average surface-ozone values shows two types of event: rapid consistent increases in concentration (two-four orders of magnitude) as compared to the seasonal average associated with stratospheric intrusions linked to upper tropospheric lows, and concentration

increases more limited in extent yet of greater duration that are linked to horizontal transport phenomena occurring mainly in summer in conjunction with high pressure and temperature. An intrusion of stratospheric air is usually associated with a surface cold front stemming from a cyclonic vortex. The air from such an intrusion is marked by high values of both potential vorticity and ozone and low values of water vapour with respect to upper tropospheric air (Danielsen et al., 1968; 1987; Buzzi et al., 1984; Hoskins et al., 1985; Appenzeller et al., 1992).

Several of these stratospheric intrusions were registered over the survey year but did not occur in any one particular season. One such episode of a rapid increase of ozone concentration is here examined by correlating it to the overall meteorological situation in Europe at the time of the event, to the potential vorticity (PV) map of 350° K isentropic surface, to an image of radiance measurement in the water vapour band, and to local wind speed and direction.

This first event covered the period from 24 to 26 November 1991, which was characterized by the presence in the Mediterranean Basin of a cut-off low moving slowly northeastward that retained its intensity throughout the monitored period. The meteorological picture on 24 November 1991 at 300 hPa (fig.4) shows the cut-off low in southern Europe: the ozone values registered at Mt. Cimone on this date rose abruptly to a peak of 120 ppb on 25 November. Figure 5 shows the hourly average surface ozone, along with synoptic measurements of wind speed and prevailing direction, as measured at Mt. Cimone.

An analysis of these data indicates the drop in ozone concentration and the sudden shift of the prevailing wind direction associated with high speed values. The PV map for 24 November shows a zone of high PV, about 700 1E-8 K m² Kg⁻¹ s⁻¹ (fig. 6), extending eastward of the low (Knudsen, 1992): this value is typical for air stemming from the lower stratosphere (Keyser et al., 1986). On the same date the dry stratospheric air slanted several kilometers into the troposphere: this is shown in fig. 7 by the water vapour image (5.7-7.1 μm band, supplied by METEOSAT 4) where a dark dry band with a vortex-like structure appears as an effect of the altered radiance properties of part of the low. The contemporary events recorded over the same period clearly indicate the occurrence of a stratospheric air intrusion.

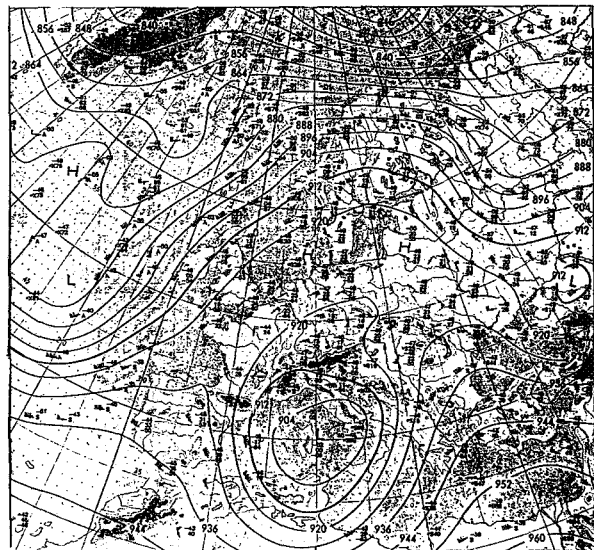


Fig. 4. Meteorological chart on 24 November at isobar 300 hPa, Deutscher Wetterdienst.

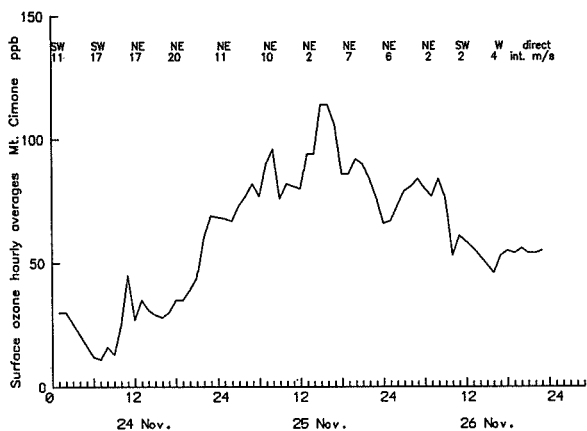


Fig. 5. Ozone concentration recorded on 24-26 November 1991 and synoptic measurements of wind direction and speed recorded at Mt. Cimone observatory.

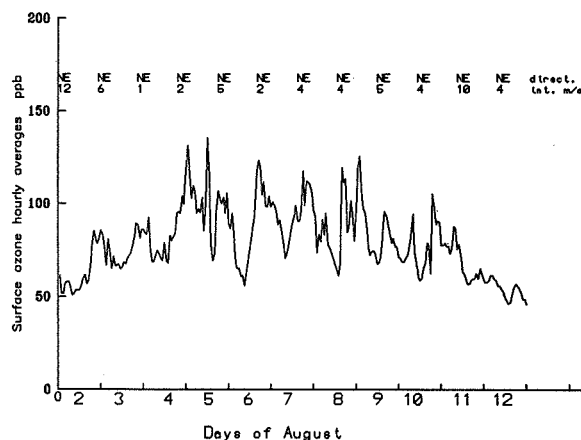


Fig. 8. Ozone trend, wind direction and speed recorded from 2-12 August 1991 at Mt. Cimone observatory.

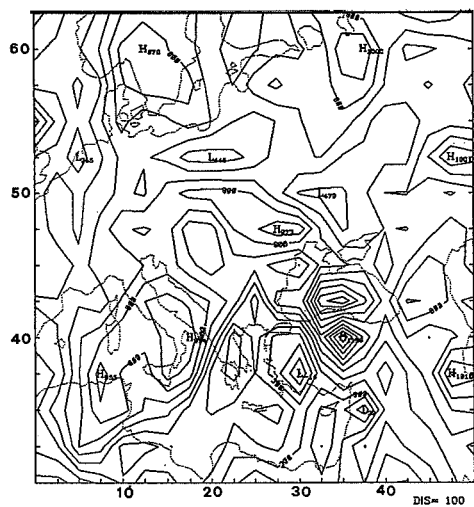


Fig. 6. Potential vorticity distribution on the 350 °K isentropic surface in central and eastern Europe (as 100 contour spacing; $1 \text{ E-}8 \text{ K m}^2 \text{ Kg}^{-1} \text{ s}^{-1}$ measurement unit) on 24 November 1991.

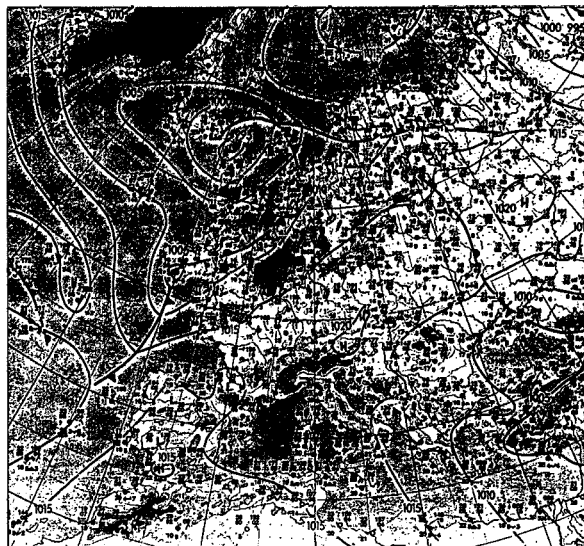


Fig. 9. Meteorological surface chart on 6 August 1991, Deutscher Wetterdienst.

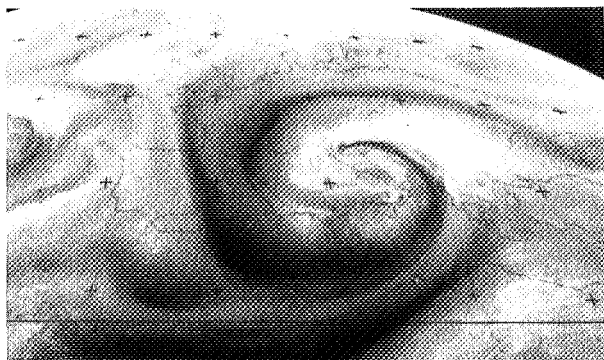


Fig. 7. Map of radiance in the water vapor band ($5.7\text{-}7.1 \mu\text{m}$) coded in grey-scale for Europe at 12:00 GMT on 24 November 1991.

A marked increase in ozone (fig. 8) over the seasonal average (fig.3) was recorded at Mt. Cimone from 2-12 August 1991. Of the concomitant factors contributing to the interpretation of this episode, the stationary high pressure system extending in the surface chart (fig. 9) from southern to northeastern Europe, with a peak northeast of Italy, is the most essential. Accompanied by high values of solar radiation intensity, it produced high readings of ozone concentration over the Po valley (Giovanelli et al., 1985; Bonasoni et al., 1991; Georgiadis et al., 1992), a source of anthropogenic pollution in northern Italy. Fig. 10 shows that at the San Pietro Capofiume (45°N , 12°E , 10 m asl) station in the Po valley the ozone sounding for 5 August 1991 exhibits a distinct shift from the yearly average trend, the peak surge occurring at about 2 km in height - a level that coincides with the altitude of the Mt. Cimone site. This ozone-rich air was transported over the Mt. Cimone station by the weak north-east air circulation (fig. 8). At the same time, the daily swing of the ozone concentration registered at Mt. Cimone shows a nocturnal peak, which is probably due to the daily alternating of up- and downdrafts (*supra* and Oltmans, 1981).

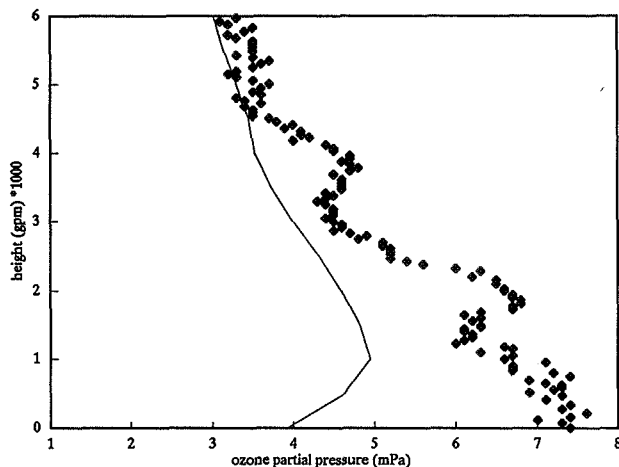


Fig. 10. Ozone concentration profile as measured at San Pietro Capofiume (45°N, 12°E), Po valley, Italy. Dots: 5 August 1991 ozonesounding. Solid line: yearly average over 1991-1992.

4. CONCLUSIONS

The extent to which the surface ozone concentrations recorded at Mt.Cimone are similar to other readings from mountainous, pollution-free stations (Oltmans, 1981; Tsuruta et al., 1989) is such that the former can be considered a baseline station for the monitoring of trace gases. The only exception would be the concentrations registered in summer that are affected by local diurnal mixing with ozone-poor low tropospheric air upwelling at noon (removal of these influences by excluding mid-day values so as to yield free tropospheric ozone concentrations will be undertaken).

Given its location in a cyclogenetic area like the Mediterranean Basin, Mt. Cimone can also be considered a suitable station for monitoring stratospheric air intrusion. This because episodes of high surface-ozone concentrations from stratospheric air intrusions are most likely to occur when cyclonic activity over southern Europe, i.e. autumn, winter and spring, is most likely to occur. By contrast, in summer, when extensive and persistent high-pressure systems are most frequent, it is horizontal transport phenomena that increase ozone concentrations.

5. ACKNOWLEDGEMENTS

This study has been supported by the CNR-ENEL Project-Interaction of energy systems with human health and environment - Rome Italy. The authors are indebted to Dr. B. Knudsen, who made available potential vorticity data, Dr. V. Levizzani, who made available the water vapour map, and Mr. A. Capasso for his assistance in computing Mt. Cimone ozone values.

REFERENCES

- Appenzeller C. and Davies H.C., 1992: Structure of stratospheric intrusion into the troposphere. *Nature*, 358, 570-572.
- Austin J.F. and Follows M.J., 1991: The ozone record at Pajeme: an assessment of the cross-tropopause flux. *Atmos. Envir.*, 25A, 9, 1873-1880.
- Bonasoni P., Fortezza F., Georgiadis T., Giovanelli G. and Strocchi V., 1991: Formation and transport of oxidants over a highly populated coastal area. Chemrawn VII, *The chemistry of the atmosphere*, December 2-6, Baltimore, Maryland, USA.

- Buzzi A., Giovanelli G., Nanni T. and Tagliazucca M., 1984: Study of high ozone concentration in the troposphere associated with lee cyclogenesis during ALPEX. *Beitr. Phys. Atmosph.*, 57, 3, 380-392.
- Bojkov, R.D., 1985: Lectures presented at the WMO Technical Conference on Observation and Measurement of Atmospheric Contaminants, Vienna, 17-21 October 1983, Spec. Environ. Rep. 16, 94 -127, WMO, Geneva.
- Bojkov, R.D., 1986: Surface ozoneding during the second half of the nineteenth century. *J. Clim. Appl. Meteor.*, 25, 343 - 352.
- Cundari V. and Colombo T., 1986: Atmospheric carbon dioxide measurements at Mt.Cimone, Italy (1979-1983). *Annales Geophysicae*, 4, B, 1, 13 - 20.
- Danielsen E.F., 1968: Stratospheric-Tropospheric exchange based on radioactivity ozone and potential vorticity. *J. Atmos. Sci.*, 25, 502-518.
- Danielsen E.F., Hipskind R.S., Gaines E., Sachse G.W., Gregory G.L. and Hill G.F., 1987: Three-dimensional analysis of potential vorticity associated with tropopause folds and observed variations of ozone and carbon monoxide. *J. Geophys. Res.*, 92, 2103-2111.
- Georgiadis T., Alberti L., Bonasoni P., Fortezza F., Giovanelli G. and Strocchi V., 1992: Seasonal budgets of ozone and oxidant precursors in an industrial coastal area of northern Italy. *Proceedings of the Quadrenn. Ozone Symp. 1992*, this issue.
- Giovanelli G., Georgiadis T., Fortezza F. and Strocchi V., 1985: Transport of photochemical ozone along the western Adriatic shore near a petrochemical plant. *Il Nuovo Cimento*, 8, 6, 727-742.
- Hakola H., Joffre S., Lattila H., and Taalas P., 1991: Transport, formation and sink processes behind surface ozone variability in North European conditions. *Atmos. Environ.*, 25A, 8, 1437 - 1447
- Hoskins B.J., McIntyre E. and Robertson A.W., 1985: On the use and significance of isentropic potential vorticity maps. *Q. J. R. Meteorol. Soc.*, 111, 470, 877-946.
- Keyser D. and Shapiro M.A., 1986: A review of the structure and dynamics of upper-level frontal zones, *Mon. Weather Rev.*, 14, 452-499
- Knudsen B., PV value maps 1992 in: NADIR, NILU Atmospheric Database for Interactive Retrieval, EASOE Campaign, Lillestrom, Norway.
- Oltmans, S.J., 1981: Surface ozone measurements in clean air. *J. Geophys. Res.*, 86, 1174 - 1180.
- Tsuruta H., Shinya K., Mizoguchi T. and Ogawa T., 1989: Seasonal behavior of the troposphere ozone in rural Japan. *Proceedings of the Quadrenn. Ozone Symp. 1988 and Tropospheric Ozone Workshop*: R.D.Bojkov and P.Fabian, Eds., 433- 436.
- Viney P. A., Businger S., Li Z., Claiborn C. S. and Murthy A., 1991: Ozone climatology at high elevations in the southern Appalachians. *J. Geophys. Res.*, 96, 1007 - 1021.

EVALUATION OF THE PRODUCTION AND THE DESTRUCTION
OF OZONE IN THE LOWER ATMOSPHERE

H. Muramatsu

Disaster Prevention Research Institute,
Kyoto University, Gokasho, Uji, Kyoto 611, Japan

ABSTRACT

Observed surface ozone mixing ratio X_{ob} is partitioned into two parts; X_{tr} , transported from the free troposphere and X_{ch} , chemically produced or destructed in the boundary layer. X_{tr} is estimated from the ozone concentration in the free troposphere and the wind speed. The ozone in the free troposphere estimated from surface ozone observations is consistent with that of ozonesonde data.

X_{ch} is obtained from the difference between X_{ob} and X_{tr} . X_{tr} increases with wind speed, while X_{ch} shows maximum at hourly wind speed of 1-2 m/s in the daytime. Contribution of X_{tr} to X_{ob} is larger than X_{ch} except for a short period in summer. X_{ch} is positive for April-October, but X_{ch} can be negative in winter, showing the net chemical destruction in the boundary layer. X_{ch} increases linearly with solar radiation, and is negative for daily global solar radiation below 8 MJ/m², which is about equal to the monthly mean in winter.

1. INTRODUCTION

Year-to-year variations of ozone at the surface and tropospheric levels are in general agreement with very few exceptions (Bojkov, 1988). But the ozone at the surface and in the lower troposphere show complex seasonal trends and correlations with solar radiation. An increase in lower tropospheric ozone is obvious (Logan, 1985; Bojkov, 1988; Wege et al., 1989). The summertime concentrations of ozone near the surface in rural areas of Europe and central and eastern United States may have increased by approximately 6-22 ppbv since 1940's (Logan, 1985). Bojkov (1988) showed that at rural stations the ozone increasing rate is greater in the lower troposphere than at the surface, and surface ozone during November-January is increasing at a greater rate than during May-October. Wege et al. (1989) have reported that the trends in ozone at Hohenpeissenberg show increases in winter and spring but trends are not significant in summer and autumn, and a trend is not present in data from recent years. At an urban station (Delft) ozone concentration shows no trend or at most a slight downward one (Guicherit, 1988).

The relation between the surface ozone concentration and the solar radiation is expected since solar radiation determines the photochemical reactions. The positive correlations between peak hourly ozone and total insolation and hours of sunshine are obtained at rural sites (Colbeck and Harrison, 1985a). Monthly means of ozone show good correlation with monthly values of sunshine at Hohenpeissenberg (Volz et al., 1989). The correlations between ozone and solar radiation are different for each stations and depend on height and geographical conditions such as north/south and rural/industrial area (Schmidt, 1989). Although no direct relationship between annual totals of solar radiation and surface ozone are shown, trend of both parameters are either positive (Dresden, Fichtelberg) or negative (Arkona) (Feister et al., 1989).

To apportion the relative contributions to ground level ozone concentrations from the stratosphere/troposphere and man-induced processes in polluted areas is a complex matter. It is essential to know the relationship between the ozone variation at the surface and in the lower troposphere. In this report, we estimate the ozone transported from the free troposphere. Then we obtain chemically produced or destructed portion of ozone in the boundary layer and show its correlation with wind speed and solar radiation.

2. VERTICAL TRANSPORT OF OZONE IN
BOUNDARY LAYER

When the photochemical production and destruction are neglected, ozone concentration near the surface is determined by transport from the free troposphere and its destruction at the surface. For stationary and horizontally homogeneous conditions the vertical ozone flux F in the boundary layer is given by :

$$F = D\rho(dX/dz) = q\rho_0X_0 \quad (1)$$

where D is eddy diffusivity, ρ air number density, X ozone volume mixing ratio, q ozone destruction velocity at the surface, z height, ρ_0 and X_0 values at the surface. Vertical change of D is assumed :

$$D = u_*k(z + z_0)\beta / \{1 + u_*k(z + z_0)\beta / D_0\} \quad (2)$$

where u_* is the friction velocity, z_0 the roughness length, k von Karman's constant and β parameter introduced to take account of stability. Above the surface layer we assume D approaches a constant value D_0 (Fabian and Junge, 1970). In the surface layer u_* can be obtained by logarithmic wind profile

$$u_* = ku / \ln\{(z_u + z_0)/z_0\} \quad (3)$$

where u is the wind speed at the level z_u which is the height of observation above the surface.

From Eqs.(1)-(3), we can obtain ozone mixing ratios, X_{tr} , at the level z_u and $X(z_h)$ at the top of the boundary layer z_h . The ratio $X_{tr}/X(z_h)$ is given by :

$$X_{tr}/X(z_h) = (1/C_2)(qC_0 + u)/(qC_1/C_2 + u) \quad (4)$$

where $C_0 = (1/\beta k^2)[\ln\{(z_u + z_0)/z_0\}]^2$, $C_1 = 1/(\beta k^2) \ln\{(z_u + z_0)/z_0\} [\ln\{(z_h + z_0)/z_0\} + z_h/H]$, $C_2 = 1 + (qz_h/D_0)\{1 + z_h/(2H)\}$, and H is the scale height of the lower atmosphere. Eq.(4) shows that $X_{tr}/X(z_h)$ is determined by the wind speed and supplemental parameters of z_h , q , D_0 and β .

3. OZONE IN THE FREE TROPOSPHERE AND TRANSPORT TO THE SURFACE

Surface ozone has been monitored at Uji (34.9°N, 135.8°E), a suburb of Kyoto, by u.v. absorption type instrument (Dasibi, Model 1006-AHJ) since May 1990 at the height of about 10 m above the surface together with meteorological parameters. On days when the maximum hourly wind speed exceeds 3.5 m/s and the daily global solar radiation is below 13 MJ/m², hourly ozone mixing ratio X_{tr} determined by vertical transport is given by the experimental equation :

$$X_{tr} = A(u - 0.30)/(u + 0.34) \quad (5)$$

where u is wind speed (m/s), and A corresponds to $X(z_h)/C_2$ defined in Eq.(4). Observed surface ozone tends to zero at $u = 0.3$ m/s, and it is very rare when $u < 0.3$ m/s. An example is given in Fig.1, showing the relation between the wind speed and the ozone concentration observed or estimated by Eq.(5). When hourly wind speed is 5 m/s observed ozone concentration is 85% of the upper limit A . Guicherit (1988) has shown that the monthly ozone concentration increases with wind speed and saturates at 12 m/s.

The combination of parameters z_h , D_0 , q and β is determined so that Eq.(4) agrees with experimental Eq.(5), with replacement of u in Eq.(4) by $u - u_0$, where u_0 is the correction term. For $z_h = 1000$ m, 1500 m and 2000 m the degree of coincidence was tested for ranges $D_0 = 1 - 20$ m²/s, $q = 0.001 - 0.01$ m/s, and $\beta = 0.1 - 1.0$. Satisfactory agreement was obtained for the combinations; for $z_h = 1000$, $D_0 = 20$, $q = 0.004$, $\beta = 1.0$ and for $z_h = 2000$, $D_0 = 20$, $q = 0.0025 - 0.0010$, $\beta = 0.3 - 0.6$, with $C_2 = 1.11 - 1.28$. The best fit is for $z_h = 2000$ m,

$D_0 = 20$ m²/s, $q = 0.0025$ m/s and $\beta = 0.6$ with $C_2 = 1.28$. In the following analysis we adopt this combination of parameters.

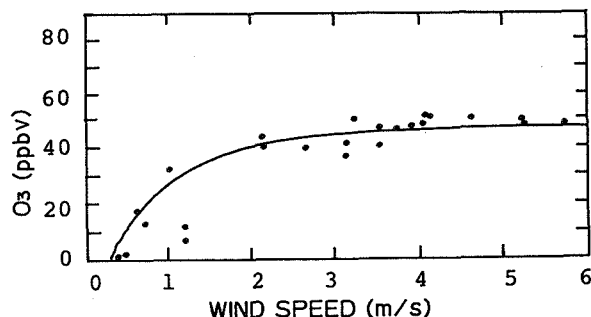


Fig. 1 Surface ozone and wind speed. Dots show the observed value and solid curve is estimation by Eq.(5) with $A = 55$ ppbv, on 8 May 1991. Total global solar radiation is 5.5 MJ/m².

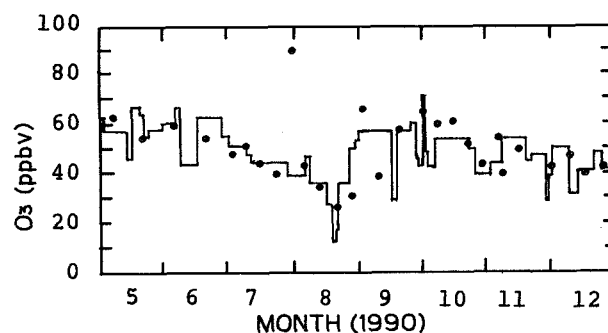


Fig. 2 Ozone in the free Troposphere. Solid line shows the estimated daily $X(z_h)$ values and dots represent ozonesonde data at 700 hPa at Tsukuba for May - December 1990.

More than four samples of $X(z_h)$ per month are obtained, with the condition of maximum wind speed and global solar radiation as stated before. Fig. 2 shows the daily $X(z_h)$ estimated from surface ozone and the ozone mixing ratio at 700 hPa level by ozonesonde data at Tsukuba/Tateno (36.0°N, 140.1°E) about 40 km east of Uji. The same daily value of $X(z_h)$ is adopted until a new sample is obtained. Apart from a few exceptions, the agreement is reasonable. Monthly mean values show better agreement, and it is recognized that the ozone in the free troposphere $X(z_h)$ has two maxima in spring and autumn, and minima in winter and summer. This seasonal variation in the lower troposphere is due to the transport from the stratosphere.

The ozone mixing ratio determined by vertical transport X_{tr} is estimated from wind speed by Eq.(5) applying the $X(z_h)$ obtained above. Denoting the observed ozone at the

surface as X_{ob} , the difference between X_{ob} and X_{tr} , i.e., $X_{ch} = X_{ob} - X_{tr}$, is interpreted as the part produced from chemical reactions in the boundary layer apart from the destruction at the surface.

Monthly means of X_{ob} and X_{tr} in the daytime are shown as a function of wind speed in Figs. 3(a) and 3(b) for summer and winter, respectively. In summer the difference between observed and transported ozone i.e., the photochemical effect is positive and maximum at wind speed 1-2 m/s, and vanishes above 5 m/s (Fig.3(a)). In winter, the net photochemical effect is very small with negative effect for wind speed below 0.5 m/s.

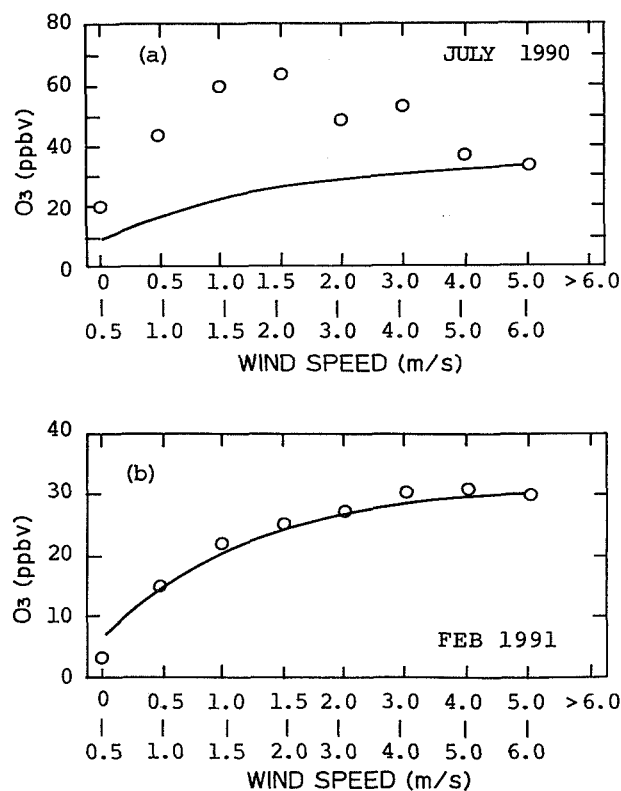


Fig. 3 Monthly means of observed and transported ozone as a function of wind speed in the daytime. Circles show observed ozone X_{ob} averaged over hourly wind speed intervals 0.5 m/s or 1.0 m/s, and solid curve shows the transported ozone X_{tr} . Summer case (a) for July 1990 and winter case (b) for February 1991 are shown.

4. SEASONAL VARIATIONS OF TRANSPORTED OZONE AND CHEMICAL EFFECTS

Fig. 4 shows the seasonal variations of $X(z_h)$, X_{ob} , X_{tr} and X_{ch} in the daytime. X_{tr} has the maximum in spring corresponding to the $X(z_h)$, with higher value in 1991 than

1990. Small humps (secondary maxima) are seen for both $X(z_h)$ and X_{tr} . X_{ch} has the maximum in summer, and the minimum in winter. In winter X_{ch} is nearly zero or negative, which shows net chemical destruction.

In 1990, observed ozone X_{ob} shows the maximum in July due to the large chemical effect, while the maximum is in May in 1991 due to the strong transport from the free troposphere. During the night (not shown) X_{tr} is 12 - 27 ppbv with weak seasonal variation. X_{ob} is lower than X_{tr} by 10 ppbv at most, showing net chemical destruction in all months.

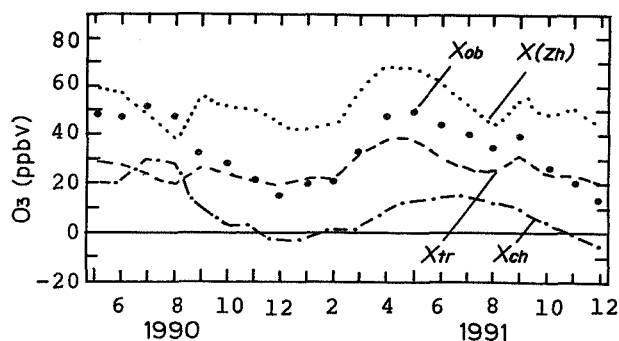


Fig. 4 Variation of monthly mean ozone in the daytime. Dotted line shows ozone mixing ratio in the free troposphere $X(z_h)$; Filled circles, observed surface ozone X_{ob} ; Broken line, transported X_{tr} ; Dash-dot line, chemically produced X_{ch} .

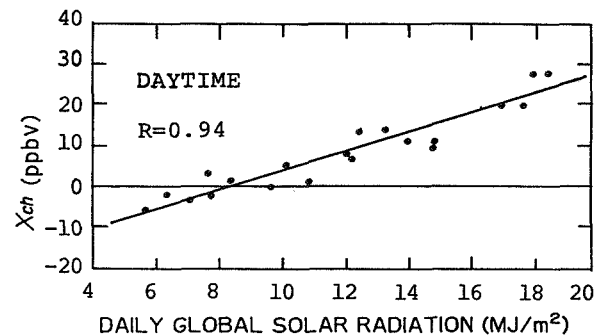


Fig. 5 Global solar radiation and X_{ch} . Monthly means of X_{ch} in the daytime are plotted against the the monthly means of daily global solar radiation. The regression line is shown with the correlation coefficient $R=0.94$.

5. SOLAR RADIATION AND X_{ch}

Monthly means of X_{ch} in the daytime are closely correlated with those of global solar radiation as shown in Fig. 5. The correlation coefficient is 0.94. It is seen that below about 8 MJ/m² per day X_{ch} is close to zero or negative, showing net chemical destruction. Above 8 MJ/m²

per day (April-September), net chemical production is observed, amounting to 30 ppbv which is more than half of X_{ob} in summer months.

6. DISCUSSION

The parameters z_h , D_0 , q and β in Eq.(4) determined to satisfy the experimental Eq.(5) are kept fixed throughout the period. It means to use the mean values for parameters and for C_2 . This assumption is justified as the ozone in the free troposphere $X(z_h)$ shows good agreement with ozonesonde data as shown in Fig. 2. Estimated ozone destruction velocity, $q = 0.001 - 0.008$ m/s over land with grass obtained directly (Aldaz, 1969; van Dop et al., 1977; Garland and Derwent, 1979; Galbally and Roy, 1980; Lenschow et al., 1981; Colbeck and Harrison, 1985b).

Photochemical effect on surface ozone would be highest in summer as shown by X_{ch} in Fig. 4. But it does not necessarily lead to the summer maximum in X_{ob} . Surface ozone X_{ob} shows the maximum in May in 1991 at Uji due to strong transport from the free troposphere. Singh et al. (1978) showed the model wherein photochemical effect at remote sites is recognized from June to October, but the net photochemical production is observed from April to October in the daytime at Uji, a suburb of Kyoto.

Monthly means of daily averaged X_{tr} show the seasonal variation ranging from 20 to 30 ppbv (not shown). Corresponding value of X_{ch} is positive in summer season and negative in winter season, deviations being less than ± 10 ppbv. So the effect of X_{ch} on X_{ob} is relatively small, which means surface ozone is close to that transported from the free troposphere in yearly mean as suggested by Galbally et al. (1986) for rural sites.

It is usual to study the correlation between global solar radiation or u.v. radiation and surface ozone X_{ob} (Colbeck and Harrison, 1985a; Volz et al., 1989; Schmidt, 1989). It is more reasonable to adopt X_{ch} instead of X_{ob} .

REFERENCES

- Aldaz, L., 1969: Flux measurements of atmospheric ozone over land and water, *J. Geophys. Res.*, **74**, 6943-6946.
- Bojkov, R.D., 1988: Ozone changes at the surface and in the free troposphere, in *Tropospheric Ozone*, I.S.A. Isaksen, ed., D.Reidel, Dordrecht, 83-96.
- Colbeck, I. and R.M. Harrison, 1985a: The frequency and causes of elevated concentrations of ozone at ground level at rural sites in north-west England, *Atmos. Environ.*, **19**, 1577-1587.
- Colbeck, I. and R.M. Harrison, 1985b: Dry deposition of ozone: Some measurements of deposition velocity and of vertical profiles to 100 metres, *Atmos. Environ.*, **19**, 1807-1818.
- Fabian, P. and C.E. Junge, 1970: Global rate of ozone destruction at the earth's surface, *Arch. Met. Geoph. Biokl., Ser.A*, **19**, 161-172.
- Feister, U., K.-H. Grasnack and G.Jakobi, 1989: Surface ozone and solar radiation, in *Ozone in the Atmosphere*, R.D. Bojkov and P. Fabian, eds., A. Deepak Publishing, Hampton, Virginia, 441-446.
- Galbally, I.E. and C.R. Roy, 1980: Destruction of ozone at the earth's surface, *Quart. J. R. Met. Soc.*, **106**, 599-620.
- Galbally, I.E., A.J. Miller, R.D.Hoy, S.Ahmet, R.C.Joynt and D.Attwood, 1986: Surface ozone at rural sites in the Latrobe Valley and Cape Grim, Australia, *Atmos. Environ.*, **20**, 2403-2422.
- Garland, J.A. and R.G. Derwent, 1979: Destruction at the ground and the diurnal cycle of concentration of ozone and other gases, *Quart. J. R. Met. Soc.*, **105**, 169-183.
- Guicherit, R., 1988: Ozone on an urban and regional scale - with special reference to the situation in the Netherlands -, in *Tropospheric Ozone*, I.S.A. Isaksen, ed., D.Reidel, Dordrecht, 49-62.
- Lenschow, D.H., R.Pearson, Jr., and B.B.Stankov, 1981: Estimating the ozone budget in the boundary layer by use of aircraft measurements of ozone eddy flux and mean concentration, *J. Geophys. Res.*, **86**, 7291-7297.
- Logan, J.A., 1985: Tropospheric ozone: Seasonal behavior, trends, and anthropogenic influence, *J. Geophys. Res.*, **90**, 10463-10482.
- Schmidt, M., 1989: Relationships between tropospheric ozone and global solar radiation in Germany, in *Ozone in the Atmosphere*, R.D. Bojkov and P. Fabian, eds., A. Deepak Publishing, Hampton, Virginia, 451-454.
- Singh, H.B., F.L. Ludwig and W.B. Johnson, 1978: Tropospheric ozone: Concentrations and variabilities in clean remote atmospheres, *Atmos. Environ.*, **12**, 2185-2196.
- van Dop H., R. Guicherit and R.W. Lanting, 1977: Some measurements of the vertical distribution of ozone in the atmospheric boundary layer, *Atmos. Environ.*, **11**, 65-71.
- Volz, A., H. Geiss, S. McKeen, and D. Kley, 1989: Correlation of ozone and solar radiation at Montsouris and Hohenpeissenberg: Indications for photochemical influence, in *Ozone in the Atmosphere*, R.D. Bojkov and P. Fabian, eds., A. Deepak Publishing, Hampton, Virginia, 447-450.
- Wege, K., H. Claude, and R. Hartmannsgruber, 1989: Several results from 20 years of ozone observations at Hohenpeissenberg, in *Ozone in the Atmosphere*, R.D. Bojkov and P. Fabian, eds., A. Deepak Publishing, Hampton, Virginia, 109-112.

303276

**DETERMINATION OF DRY DEPOSITION OF OZONE :
COMPARISON OF DIFFERENT MEASURING TECHNIQUES**

I COLBECK and A SIMMONS

Institute of Aerosol Science
University of Essex, Colchester CO4 3SQ
UK

ABSTRACT

Five methods were used to investigate the deposition of ozone. The measurements of the eddy diffusivity of heat using the Bowen ratio technique, were slightly higher than but closely matched the measurements made for the momentum eddy diffusivity, measured simultaneously, using the profile technique. Similar flux values were obtained by the profile and eddy correlation method. Deposition velocities determined using the box method were higher than those calculated using an open top chamber.

through the removal of important precursor species eg NO₂, HNO₃ and PAN.

In studies of dry deposition the rate of transfer, or deposition velocity, v_g is often expressed by

$$v_g(z) = F/c(z) = 1/(r_a + r_b + r_s)$$

where F is the downward flux of the pollutant, which is related to the eddy diffusivity, and c is its concentration at height z. As indicated above, the total resistance to transport to the surface can be written as the sum of the resistances from each of the processes involved where r_a is the aerodynamic resistance, r_b is the resistance in the laminar sublayer next to the surface and r_s is the resistance controlled by the surface itself.

1. INTRODUCTION

The destruction of ozone at the earth's surface plays an important role in the budget of tropospheric ozone. Dry deposition is the direct absorption/destruction of a gas at the ground. This distinguishes it from removal by precipitation, although water surfaces as well as vegetation and soil may participate. Deposition requires the transfer of ozone through the lower part of the boundary layer to the surface followed by decomposition or chemical reaction on contact with the surface. The first part of the deposition process depends on the nature of the boundary layer whereas the second part depends on the chemical reactivity of the surface with respect to ozone. Not only does dry deposition deplete ozone concentrations directly, but also indirectly

There are several methods routinely used to measure dry deposition in the field and each has its own advantages and disadvantages (Colbeck and Harrison, 1985; Dolske and Gatz, 1985; Kramm et al., 1991). We selected several micrometeorological techniques and the flux chamber method to measure ozone deposition over various types of surface (Simmons, 1992). The micro-meteorological methods chosen were the gradient, Bowen ratio and eddy correlation techniques. Both open- and closed-top chambers were studied.

2. TECHNIQUES

In suitable conditions, micro-meteorological methods permit the vertical flux of species to be determined from measurements made above a surface, by considering the turbulent transfer of that species. The

profile method is based on vertical gradients of windspeed, temperature and concentration (Colbeck and Harrison, 1985). In order to calculate deposition velocities this method assumes that in turbulent flow, where mechanical mixing dominates, an eddy transfers atmospheric properties equally so that exchange of all gases, vapours, heat and momentum are expected to be similar. Eddy diffusivities are evaluated as a function of momentum flux, surface roughness and atmospheric stability, which are derived from supporting meteorological data (Hicks et al., 1980). The profile method is straightforward in neutral stability, when profiles of only windspeed and concentration are required. Outside such conditions the wind profile must be corrected, empirically, for the effects of thermal buoyancy. The accepted corrections appear valid over short crops but are less accurate over tall rough crops.

The Bowen ratio determination of flux is derived from the energy balance of the underlying surface. The eddy diffusivities are assumed to be the same as for sensible heat or water vapour and is determined from measurements of vertical gradients of temperature, humidity and ozone concentration as well as the net radiation and soil heat flux. For a flux to be estimated with any accuracy using this technique substantial net radiation fluxes ($>50 \text{ W m}^{-2}$) are required. At night, during Winter or in cloudy conditions the available net radiation is often too small for accurate flux determination.

Both the profile and Bowen ratio method are indirect methods of determining the flux since they rely on the measurement of mean potentials and their gradients in the atmosphere. Eddy correlation is a direct method (Monteith and Unsworth, 1990) and requires simultaneous measurement of rapid fluctuations of vertical windspeed in the constant flux region of the surface boundary layer and the associated fluctuations in gas concentration, temperature or humidity. Only stress of the horizontal wind on a horizontal surface together with a mean vertical velocity of zero is assumed. This method requires an extensive uniform upwind fetch so that the flux has equilibrated over the surface being investigated.

The box or decay method enables the surface resistance to ozone uptake of various surfaces to be measured. An inert box, containing a known concentration of ozone is placed with one open side over the surface to be investigated. The rate of decrease of ozone concentration within the box is assumed to be equal to its destruction rate at the surface. Unless atmospheric conditions are simulated in the box, deposition velocities found in this way cannot be compared with field studies. Surface resistances can be compared and, in this case, were obtained by measuring the total surface resistance before and after coating the surface with potassium iodide solution (Simmons and Colbeck, 1990). This has the effect of making the surface resistance negligible. Measurements were made in a $0.5 \times 0.5 \times 0.5 \text{ m}$ teflon lined box. Closed top chambers alter the environment in ways that probably affect the action of pollutant concentrations on the receptor plants (eg raised temperatures within the chamber), however open top chambers provide more natural conditions. The deposition velocity may be determined by the equilibrium method which involves filling the chamber with ozonated air and measuring the ozone concentration entering the chamber and that of the equilibrium mixture. The chamber used had a volume of 1.52 m^3 and the surface area of the base was 0.95 m^2 . The advantage of this method is that it can be used under any atmospheric stability. The main disadvantage is that ozone concentrations higher than ambient have to be used in the chamber, to achieve a significant difference in the two concentrations that are measured.

3. RESULTS

Full details of the measurement sites, averaging times, meteorological data (including atmospheric stability) and data selection/rejection criteria are given in Simmons (1992). Of particular importance is the strict requirement on the nature of the upwind fetch. At all sites the fetch was uniform for a sufficient upwind distance to ensure that the boundary layer had equilibrated over the surface of interest. For the profile technique, results were only used when the Richardson number was in the range -0.1 to 0.01 .

Figure 1 shows the values of surface resistance obtained by both the profile and box techniques over three days. There is reasonable agreement between the methods although the profile values are highly variable. Measurements were made over short (3

cm), dry grass. For the profile method, the averaging period was 30 minutes. From a detailed examination of the data (Simmons, 1992) it was concluded that the box was a better method than the profile method for measuring r_s , but $r_a + r_b$ was more accurately measured by the profile technique. Over vegetation it was found that the performance of the box method varied, depending on whether the box significantly altered the temperature and humidity within it. If the internal environment changes greatly, the stomata will react and any results will not be representative of the vegetation outside the box.

The measurements of the eddy diffusivity of heat (K_h) using the Bowen ratio technique, were slightly higher than but closely matched the measurements made for the momentum eddy diffusivity (K_m), measured simultaneously, using the profile technique. The values of K_h and K_m converged slightly as the atmospheric stability increased, adding substance to the theory that the properties of heat and momentum are transported differently in unstable conditions.

Figure 2 shows the correlation between the profile and eddy correlation methods for deposition over barley. It can be seen that the two sets of fluxes (given as 10 minute averages) are similar, and not consistently lower by either method. The average deposition velocities over the daytime period were 1.9 cm s^{-1} and 1.0 cm s^{-1} for the profile and eddy correlation technique respectively. The higher deposition velocity was measured at a height of 1 m whilst the lower value was measured at 5.6 m.

Figure 3 shows the results of simultaneous box and open-top chamber experiments over grass. Measurements were made over both wet and dry grass (9 cm long). The average deposition velocity, obtained using the open-top chamber, was 0.27 cm s^{-1} and 0.59 cm s^{-1} over wet and dry grass respectively. Although the observed deposition velocity was found to be similar, the actual values calculated using the box method were higher than those calculated using the chamber method. This could have been due to elevated levels of ozone in the chamber having a biological effect on the grass causing the stomata to close. It was observed that measurements made over a glass surface by these two methods

yielded similar values for both the surface resistance and deposition velocity.

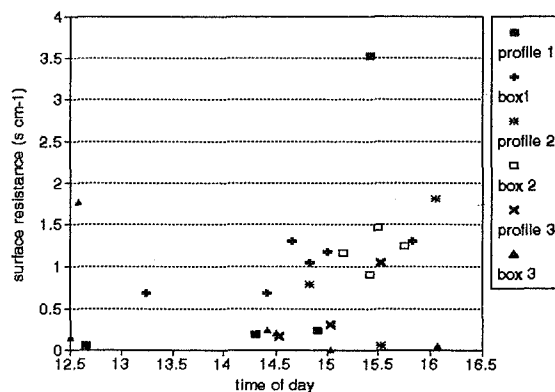


Figure 1. Comparison of surface resistances measured by the profile and box method on three separate occasions.

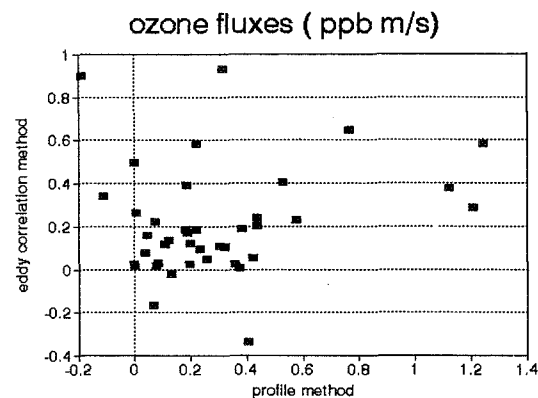


Figure 2. Comparison of ozone flux as measured by the profile and eddy correlation techniques.

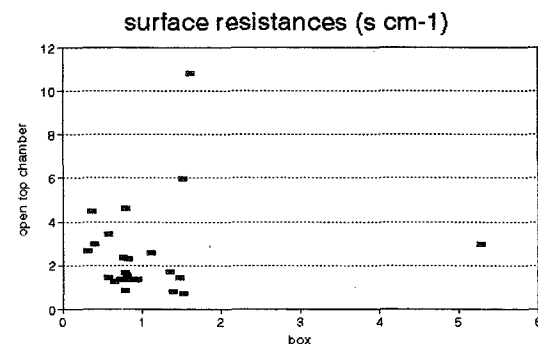


Figure 3. Comparison of surface resistances as measured by the box and open-top chamber.

REFERENCES

- Colbeck I. and Harrison R.M. (1985) Dry deposition of ozone : some measurements of deposition velocity and of vertical profiles to 100 metres, *Atmos. Environ.*, 19, 1807-1818.
- Dolske D.A. and Gatz D.F. (1985) A field intercomparison of methods for the measurement of particle and gas dry deposition, *J. Geophys. Res.*, 90, 2076-2084.
- Hicks B.B., Wesely M.L. and Durham J.L. (1980) Critique of methods to measure dry deposition, EPA-600/9-80-050.
- G., Muller H., Fowler D., Hofken K.D., Meixner F.X. and Schaller E. (1991) A modified profile method for determining the vertical fluxes of NO, NO₂, ozone and HNO₃ in the atmospheric surface layer, *J. Atmos. Chem.*, 13, 265-288.
- Monteith J.L. and Unsworth M.H. (1990) *Principles of Environmental Physics*, 2nd edition, Edward Arnold, London.
- Simmons A. and Colbeck I. (1990) Resistance of various building materials to ozone deposition, *Environ. Tech.*, 11, 973-978.
- Simmons A. (1992) *Studies of ozone deposition*, PhD Thesis, University of Essex.

**TURBULENT TRANSPORT AND PRODUCTION/DESTRUCTION OF OZONE
IN A BOUNDARY LAYER OVER COMPLEX TERRAIN**

Gary K. Greenhut

Forecast Systems Laboratory, NOAA/ERL, Boulder, Colorado 80303, USA

Anne M. Jochum

Institute of Atmospheric Studies, DLR, Oberpfaffenhofen, Germany

Bruno Neininger

Laboratory for Atmospheric Physics, LAPETH, Duebendorf, Switzerland

ABSTRACT

The first Intensive Observation Period (IOP) of the Swiss air pollution experiment POLLUMET took place in 1990 in the Aare River Valley between Bern and Zurich. During the IOP, fast response measurements of meteorological variables and ozone concentration were made within the boundary layer aboard a motorglider. In addition, mean values of meteorological variables and the concentrations of ozone and other trace species were measured using other aircraft, pilot balloons, tether sondes, and ground stations.

Turbulent flux profiles of latent and sensible heat and ozone are calculated from the fast response data. Terms in the ozone mean concentration budget (time rate of change of mean concentration, horizontal advection, and flux divergence) are calculated for stationary time periods both before and after the passage of a cold front. The source/sink term is calculated as a residual in the budget, and its sign and magnitude are related to the measured concentrations of reactive trace species within the boundary layer. Relationships between concentration ratios of trace species and ozone concentration are determined in order to understand the influence of complex terrain on the processes that produce and destroy ozone.

1. INTRODUCTION

POLLUMET is an ongoing air pollution and meteorology experiment in Switzerland that focuses on interdisciplinary studies of emissions, transport, and atmospheric chemistry in the boundary layer on distance scales ranging from regional to international and time scales ranging from hours to days (Neininger and Dommen, 1990). In the summer of 1990, aircraft of the Deutsche Forschungsanstalt fuer Luft- und Raumfahrt (DLR: German Aerospace Research Establishment) participated in the first

Intensive Observation Period of POLLUMET, collecting data on boundary layer turbulence (motorglider) (Willeke et al., 1991), trace gas mean concentrations (Queen Air) (Paffrath et al., 1991), and winds and other meteorological parameters (King Air and pilot balloons) (Enderle et al., 1991; Hoelle et al., 1991).

2. FLUX MEASUREMENTS AND THE BUDGET OF MEAN OZONE CONCENTRATION

On three days in July 1990, the motorglider flew 20-km legs in a T-pattern at various altitudes within the boundary layer centered about 30 km northeast of Bern, Switzerland, in the vicinity of the Aare Valley. The complex terrain under the flight legs is shown in fig. 1. The motorglider flew at an air speed of 35 m s⁻¹. Fast-response data were sampled at a rate of 10 Hz. The flight data analyzed in this paper were obtained between 1200 and 1530 LT (local time) (1000 and 1330 GMT), which corresponds approximately to the midday stationary time period in the evolution of the daytime boundary layer.

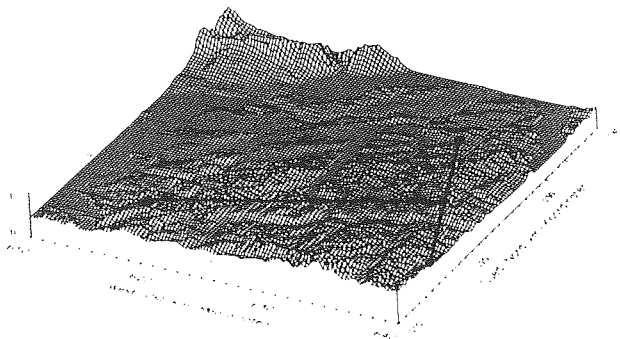


Fig.1. Terrain under the T-pattern flown by the motorglider during the Intensive Observation Period of POLLUMET 1990.

The profiles of potential temperature, specific humidity, ozone concentration, and the fluxes of sensible and latent heat and ozone are shown in figs. 2, 3 and 4 for 27, 28 and 30 July, respectively. There was only one motorglider flight on 29 July, when a cold front passed through the region, and the data from this flight are not included here.

The motorglider flew at the height of the inversion (z_i) on both 27 and 28 July, as evidenced by large, intermittent nonstationarities in the time series caused by sampling both above and below z_i . Although the data from the flights at these levels cannot be used for flux computations, the flight altitudes are denoted by z_i in figs. 2 and 3. The points in figs. 2, 3 and 4 are averages over five legs at each height (ten legs at the lowest level on 30 July) in the T-pattern, and the error bars are the standard deviations of the mean.

The fluxes of ozone were upward (positive) at a height of approximately 0.5 z_i on 27 and 28 July. More typical ozone fluxes were obtained on 30 July after the passage of the cold front, with downward (negative) values observed throughout the boundary layer, decreasing in magnitude up to the height of the inversion, which was at approximately 1300 m MSL (above mean sea level) on this day. (It was substantially higher on 27 and 28 July.) The average height of the terrain under the T-pattern was approximately 700 m MSL.

The budget of mean ozone concentration, neglecting horizontal flux divergence, is given by (Lenschow et al., 1981)

$$\frac{\partial c}{\partial t} = - \frac{\partial}{\partial z} (\overline{w'c'}) - V \cdot \nabla c + S$$

where the term on the left is the local time rate of change of ozone concentration, and the terms on the right are vertical flux divergence, horizontal advection, and boundary layer source/sink, respectively. Data from the motorglider, Queen Air, King Air, and pilot balloons were used to calculate the terms in the ozone concentration budget, except the source/sink term, which was obtained as a residual. The results are given in Table 1.

Although there are large uncertainties in the values of the source/sink terms in Table 1, the chemical processes in the boundary layer appear to change from a sink of ozone before the cold front passage on 29 July to a source of ozone afterward. The change in sign of the source/sink term is governed mainly by the change in sign of the flux divergence term, which is directly related to the change in direction of the mid-boundary layer ozone fluxes.

Along with the passage of a cold front, it is possible that the change in the sign of the source/sink term is

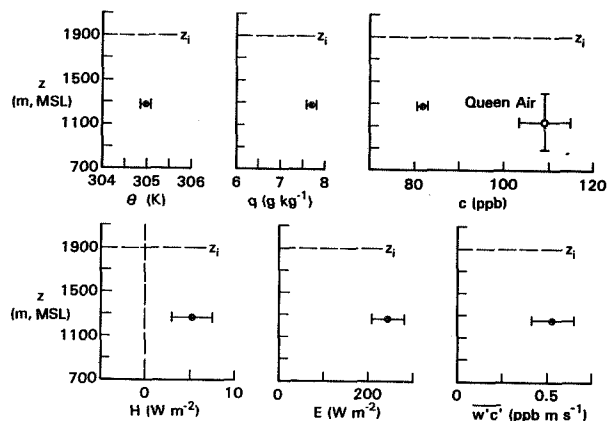


Fig. 2. Potential temperature (θ), specific humidity (q), ozone concentration (c), and the fluxes of sensible heat (H), latent heat (E) and ozone ($\overline{w'c'}$) measured aboard the motorglider and Queen Air on 27 July 1990.

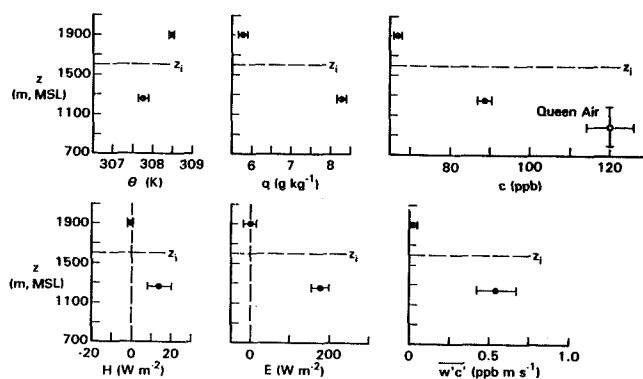


Fig. 3. Same as fig. 2 for 28 July 1990.

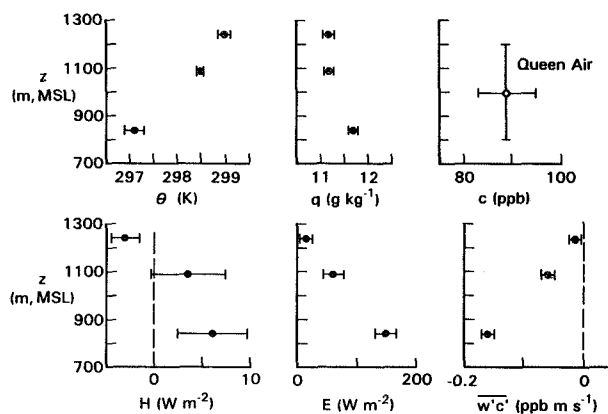


Fig. 4. Same as fig. 2 for 30 July 1990.

associated with the timing of the flights: the midpoint of the flight on 30 July was 3 hours earlier than the midpoints of the flights on 27 and 28 July.

From the data taken aboard the Queen Air (discussed below), the only large change that occurred in mean meteorological variables and trace gas concentrations after the passage of the cold front was in average relative humidity, which increased by about 35% in the morning and 24% in the afternoon from before to after the passage of the front. The average pre- to post-frontal temperature change was approximately -3 deg. C in both the morning and afternoon; the average pre- to post-frontal change in ozone concentration was -4 ppb (parts per billion) in the morning (93 to 89 ppb) and -17 ppb in the afternoon (114 to 97 ppb).

Thus, in terms of mean quantities, conditions in the boundary layer were not changed very much by the frontal passage. The change in the boundary layer from being a sink of ozone to being a source, and the related change in the sign of the flux divergence, may therefore be at least partly due to the earlier time in the day for the flight of the motorglider after the frontal passage.

3. DAYTIME VARIATIONS OF METEOROLOGICAL VARIABLES AND CONCENTRATIONS OF CHEMICAL TRACE SPECIES

On 27, 28, and 30 July, the Queen Air flew at two levels within the boundary layer (at approximately 90 m and 550 m above the surface) in the morning and in the afternoon. The mean quantities measured during each flight were averaged over the three days. The results are shown in Table 2.

The distribution of meteorological quantities and concentrations of chemical species within the boundary layer

	27 July 1990	28 July 1990	30 July 1990
$\frac{\partial c}{\partial t}$	-2.7 ± 2.7	3.4 ± 3.4	1.9 ± 1.1
$\frac{\partial(\overline{w'c'})}{\partial z}$	-3.1 ± 0.7	-5.8 ± 1.4	1.3 ± 0.3
$V \cdot \nabla c$	-1.7 ± 0.7	-2.5 ± 3.0	-2.2 ± 1.2
S	-7.5 ± 4.1	-4.9 ± 7.8	1.0 ± 2.6
local flight time (midpoint)	1530	1530	1230

Table 1. Terms in the ozone mean concentration budget calculated from data obtained aboard the motorglider, Queen Air, and King Air, and from pilot balloon soundings. The source/sink term (S) is calculated as a residual. Units are ppb h-1.

can be inferred from the averaged Queen Air data in Table 2. Potential temperature, specific humidity, and the concentration of ozone were well-mixed in the boundary layer in both the morning and the afternoon. Temperature and ozone concentration increased and relative humidity decreased from morning to afternoon. Visibility decreased with height in the morning, but was approximately uniform in the boundary layer in the afternoon.

The profiles of the concentrations of NO₂, NO, and SO₂ had large vertical gradients within the boundary layer in the morning. The concentrations of NO₂, NO, and SO₂ at the upper level in the boundary layer remained relatively small from morning to afternoon. However, there was a marked decrease in the concentrations of these species at the lower level in the afternoon, resulting in a decrease in the vertical gradients.

4. PRODUCTION/DESTRUCTION RELATIONSHIPS BETWEEN TRACE SPECIES

A comparison was made between the coincident variations in the concentrations of ozone, NO₂, NO, and SO₂, and visibility over all 11 flights of the Queen Air, and also over the 5 low-level flights, on 27, 28, and 30 July. The resulting correlation coefficients are given in Table 3.

Although the number of flights is small, six correlation coefficients in Table 3 are significant at or above the 95% level. Ozone concentration was negatively correlated with the concentrations of NO₂, NO, and SO₂ and with visibility, with larger correlation coefficients occurring at the lower level in the boundary layer. The correlation coefficients between the concentrations of NO₂, NO, and SO₂ and visibility were all positive, with the strongest correlations occurring between NO₂ and SO₂, and between NO₂ and visibility.

The correlation coefficients in Table 3 indicate that the production (destruction) of ozone in the boundary layer

	local time (midpoint)	altitude (m, ASL)	T (°C)	RH (%)	O ₃ (ppb)	NO ₂ (ppb)	NO (ppb)	SO ₂ (ppb)	visibility (10 ⁻⁴ m)
morning lower level	1156	750	20	58	84	6.3	1.6	2.6	1.3
morning upper level	1141	1230	18	57	97	1.3	0.1	0.8	0.8
afternoon lower level	1653	830	25	43	111	2.8	0.7	1.3	0.9
afternoon upper level	1653	1270	21	46	106	1.4	0.4	0.4	1.0

Table 2. Mean meteorological variables and mean concentrations from flights of the Queen Air averaged over 27, 28, and 30 July 1990.

was directly related to the destruction (production) of NO₂, NO, and SO₂. High concentrations of the latter three chemical species occurred low in the boundary layer (approximately 90 m above the surface) in the late morning (at about 1150 LT; see Table 2). These concentrations were reduced by a factor of 2 to 3, with a corresponding increase in ozone concentration by about 30% by mid-afternoon (at about 1650 LT).

At the upper level (550 m above the surface), the production/destruction relationships between ozone and NO₂, NO, and SO₂ are not as clear. From Table 2, between late morning and mid-afternoon, the ozone concentration at the upper level increased slightly (by about 10%), while the NO₂ concentration remained constant, the (small) NO concentration increased by a factor of 4, and the (small) SO₂ concentration decreased by a factor of 2.

5. DISCUSSION

Jumps in the magnitude of potential temperature, specific humidity, and ozone concentration indicate the presence of well-developed capping inversions at the top of the boundary layer on each observation day. For 27 and 28 July, these jumps were determined from the large, intermittent non-stationarities in the time series obtained during the flights of the motorglider at the height of the inversion (zi), and from the jumps in the profiles of mean quantities across the inversion (28 July only, fig.3).

Representative changes in mean quantities from below to above the inversion were, for potential temperature, +0.4 deg C and +0.8 deg C; specific humidity, -2.4 g kg⁻¹ and -3.1 g kg⁻¹; and ozone concentration, -16 ppb and -30 ppb, for 27 and 28 July, respectively. A temperature jump similar

	O ₃	NO ₂	NO	SO ₂	visibility
O ₃ :	—	-0.49	-0.61	-0.44	-0.51
NO ₂ :	-0.76	—	0.68	0.88	0.70
NO :	-0.72	0.35	—	0.46	0.56
SO ₂ :	-0.61	0.92	-0.08	—	0.44
visibility :	-0.94	0.88	0.74	0.68	—

Table 3. Correlation coefficients for variations of mean concentrations and visibility from data obtained during flights of the DLR Queen Air within the boundary layer on 27, 28, and 30 July 1990. The coefficients above the diagonal are for all 11 flights; those below the diagonal are for the 5 low level flights (approximately 90 m above the surface) only. Highlighted correlation coefficients are significant at or above the 95% level.

to those on 27 and 28 July was seen in profile data from the King Air obtained on 30 July. (No other inversion jump data are available for this day.)

The presence of a well-defined capping inversion on each day, combined with the presence of anthropogenic sources and sinks at the surface and the complex terrain associated with the Aare Valley (fig. 1), tended to trap pollutants in the experimental region. Interactions between these pollutants gave rise to the production/destruction relationships between ozone and NO₂, NO, and SO₂ discussed in the previous section.

REFERENCES

- Enderle, K. H., Chr. Balle, H. Giehl, G. Rackl, H.-G. Tremmel, J. Werhann, K. Wohlfahrt, A. Hoff, D. Brunner, L. Goedeke, R. Jeske, and Th. Wede, 1991: Flugzeugmessungen im Rahmen von POLLUMET. Tiel 2: King Air. DLR/POLLUMET Technical Memo.
- Hoelle, K., J. Sedlmeir, and A. Bruenner, 1991: Pilotballonmessungen in Rahmen von POLLUMET. Tiel 4. DLR/POLLUMET Technical Memo.
- Neininger, B., and J. Dommen, 1990: POLLUMET: Luftverschmutzung und Meteorologie in der Schweiz. POLLUMET-Koordination publication.
- Lenschow, D. H., R. Pearson, and B. B. Stankov, 1981: Estimating production of ozone in the boundary layer by use of aircraft measurements of ozone eddy flux and mean concentration. J. Geophys. Res., 86, 7291-7297.
- Paffrath, D., H. Schlager, M. Krautstrunk, M. Bruenner, M. Petz, G. Uhlemann, F. M. Roesler, H. Gnatz, G. Koerner, H. Jesse, H.-G. Tremmel, and K. Wohlfahrt, 1991: Flugzeugmessungen im Rahmen von POLLUMET. Tiel 1: Queen Air. DLR/POLLUMET Technical Memo.
- Willeke, H., N. Enstrasser, and A. M. Jochum, 1991: Flugzeugmessungen im Rahmen von POLLUMET. Teil 3: Motorsegler. DLR/POLLUMET Technical Memo.

303519

TRANSPORT INTO THE TROPOSPHERE IN A TROPOPAUSE FOLD / CUT-OFF LOW SYSTEM

G. Vaughan, J. D. Price and A. Howells

Physics Dept., University of Wales, Aberystwyth, UK.

ABSTRACT

A tropopause fold developed on the western flank of a trough in the 300mb flow on 6th October 1990. Radiosonde ascents over western Europe showed very dry stable layers beneath the jet stream in the potential temperature range 310-315K. These were evident on profiles from 12h on the 6th to 00h on the 8th October. ECMWF model assimilations were examined for this period to determine how well the model represented the radiosonde observations. Humidity fields were found to give better agreement than potential vorticity, probably because the PV is affected by the limited vertical resolution of the model.

Isentropic trajectories were calculated for the air in the fold as represented by the ECMWF assimilation at 00h on 7th. Those on the western edge of the fold split from the main flow and transferred to the troposphere, while those on the eastern side ended up in the cut-off low. A lower bound of 1.1×10^{14} kg is estimated for the amount of stratospheric air transferred into the troposphere by this fold.

1. INTRODUCTION

The synoptic development of the tropopause fold/cut-off low system began over the Atlantic on 6th October 1990, as a trough in the 300 mb flow propagated eastwards, extending southward as it did so. By 00h on the 7th (fig. 1a) it lay over the UK, with a northerly jet streak over Ireland containing peak winds in excess of 60 ms^{-1} . By 12h on the 7th (fig. 1b) the trough had extended down to 45°N and formed a small cut-off region, which enlarged and moved southwards on the 8th. This cut-off low remained over the western Mediterranean until 00h on 12th October.

This study is aimed at determining the evolution of the fold from radiosonde profiles, and using this information to determine how well the ECMWF operational assimilation represented the fold. The assimilation fields are then used to estimate the amount of stratospheric air irreversibly transferred into the troposphere by the fold.

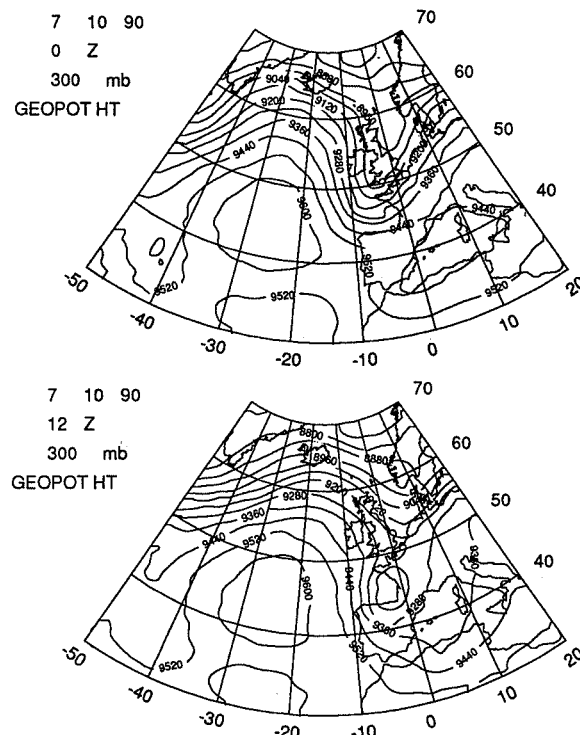


Fig.1: 300 mb geopotential height charts, 00h and 12h, October 7th 1990.

2. IDENTIFICATION OF THE TROPOPAUSE FOLD IN RADIOSONDE DATA

One of the characteristics of tropopause folds (indeed, the characteristic by which they were originally identified) is the presence of a very dry stable layer in the free troposphere at potential temperatures around 310-320K (i.e. those that span the midlatitude troposphere and polar lower stratosphere). This corresponds to the frontal zone beneath the polar jet stream, and therefore slopes downward on the equatorward side of the jet. Typically, folds occur on the western flank of deepening troughs in the upper tropospheric flow (Danielsen 1968), as occurred on 6-8 October 1990.

Radiosonde ascents for this period from western European stations were examined for the presence of such layers. Air was deemed to be stratospheric if the potential vorticity, calculated from the radiosonde stability and ECMWF analysis absolute vorticity (see 3a) exceeded $1.5 \times 10^{-6} \text{ Km}^2(\text{kgs})^{-1}$. The results are shown in fig.2. They show that a fold began near Iceland at 12h on 6th, extended along the whole western edge of the trough from near Iceland to north-west Spain at 00h on 7th, then propagated around the cut-off low and dissipated over southern Spain early on 8th October. This analysis, of course, cannot give a complete picture of the fold since there were very few radiosonde ascents over the ocean, but it does serve to delineate its overall development, and gives a good estimate of its depth (about 800m near 500 mb and nearer 500 m at lower levels, especially during the dissipating phase).

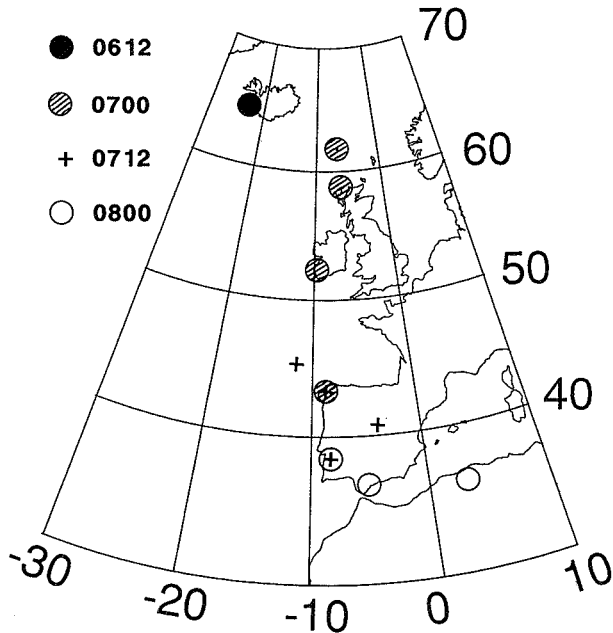


Fig.2: Extent and development of the fold as revealed at 12-hourly intervals by radiosonde profiles, from 12h on the 6th October (0612) to 00h on 8th (0800).

3. REPRESENTATION OF THE FOLD IN ECMWF ANALYSES

Model assimilation fields containing winds, temperature, geopotential height and specific humidity were available at 6-hourly intervals with a horizontal resolution of 1.5° and 12 vertical levels (1000, 850, 700, 500, 400, 300, 250, 200, 150, 100, 70 and 50 mb), from 00h on 6th onwards.

a) Potential Vorticity

Stratospheric air is distinguished from tropospheric air by high values of potential vorticity ($> 2 \times 10^{-6} \text{ Km}^2(\text{kgs})^{-1}$). Isentropic maps of PV were derived from the model vorticity and static stability fields and compared with spot values derived using the radiosonde stability (sect. 2). The main PV anomaly propagating into the trough and the cut-off low was well represented on these charts, but the fold which formed its western edge was poorly defined: the model did not show high PV values dipping down sufficiently far into the troposphere. This may be attributed to its coarse vertical resolution: the fold was considerably thinner than the 2.5 km separating the model fields at 700 and 500mb.

b) Humidity fields

As previously mentioned, stratospheric air is also distinguished by being very dry. Specific humidity values were available directly from the model assimilation; thus, cross-sections of humidity perpendicular to the flow were examined for evidence of the fold. It was found that the model did indeed generate folded structures in its humidity assimilation between 310 and 315K, in the region below the jet stream, with tongues of very dry air ($< 100 \text{ ppmm}$) extending into the troposphere. The horizontal extent of these features is shown in fig.3. Several points may be made regarding these cross-sections:

i) The model began generating a fold at 12h on 6th, but did not show a tongue of very dry air extending into the

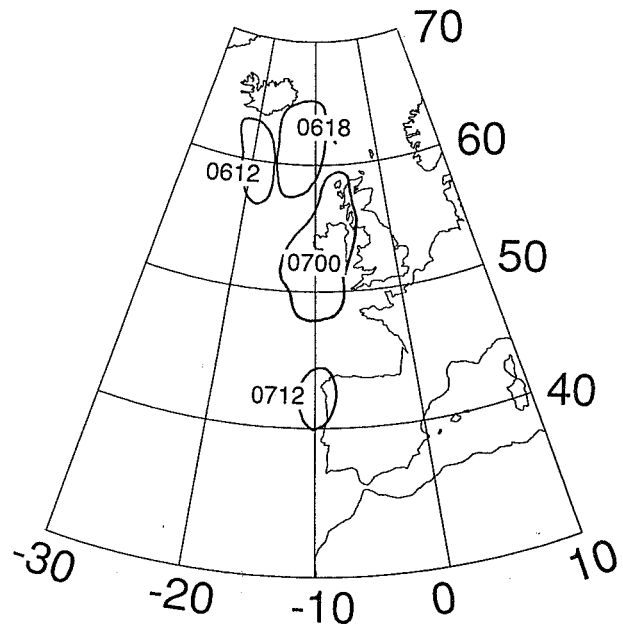


Fig.3: Development of the fold in the model humidity assimilations from 12h on 6th (0612) to 12h on 7th (0712).

troposphere - unlike the Keflavik radiosonde ascent at this time.

ii) The area of folded humidity contours propagated southwards more quickly than the PV anomaly, overtaking it by 12h on 7th.

iii) The model depicted a large fold at 18h on 6th, when radiosonde measurements would not have been available. This feature was larger than its counterpart at 12h. Thus, the dry tongues were not simply passive features of the assimilation, but were produced (or at least enhanced) by the model dynamics.

iv) No folds were produced in the model assimilation for 06h on 7th, and only a very small area of limited folding at 12h (at the time of a very prominent fold in the Coruna radiosonde ascent at 43.3°N, 8.4°W). During this period the base of the trough was cutting off and the fold (as shown by the radiosonde analysis) was propagating around the base of the low and dissipating. Thus the model humidity field did not represent the dissipating phase of the fold.

v) At 00h on 7th, the area of folded humidity contours extended over a considerably smaller latitude range than the fold depicted in the radiosonde analysis, which extended from just south of Iceland to Coruna.

vi) The model humidity field represented the fold more realistically than the derived PV. A similar result was shown in WMO (1986, Chapt.5). In fact, it appeared sufficiently realistic for the humidity field to be used to define the folded region at 00h on 7th October when estimating the amount of stratosphere-troposphere exchange in the episode.

The conclusion from this analysis is that the ECMWF assimilation represented the growth phase of the fold rather well (although, understandably, underestimating its extent), but that the decay phase was less well represented.

c) Trajectory analyses

Kinematic air parcel trajectories were carried out on the 310 and 315K surfaces for the air in the model-resolved fold at 00h on 7th. The results are summarised in fig.4 for 310K, where the horizontal locations of five groups of air parcels are shown at 00h on the 7th and after 24 and 48 hours. The evolution of these groups can be summarised as follows:

- 1) the westernmost group (no shading) began near 4.5 km altitude, and descended 700m before turning anticyclonically and rising. This group had descended by 2 km in the previous 24 hours.
- 2) trajectories immediately to the east of group 1 (diagonal shading), beginning near 4.8km, also descended by 700m,

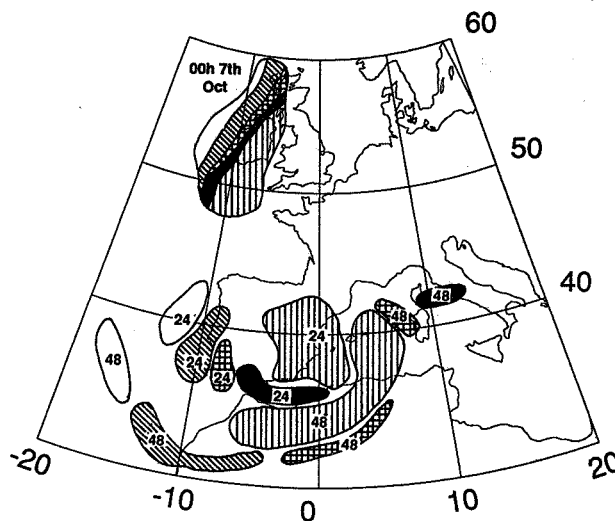


Fig. 4: Evolution of groups of trajectories over 48 hours, beginning in the model fold at 00h on 7th over Ireland. The shading differentiates between groups as defined in the text: group 1 (no shading) is the westernmost and group 5 (vertical hatching) the easternmost at 00h on 7th. The diagram shows end-points after 24 and 48 hours, identified by the appropriate numeral. Groups 1 and 2 transfer into the troposphere, groups 3 and 5 enter the cut-off low while group 4 continues flowing downstream beneath the jet.

but travelled southward towards the subtropics and continued to descend. Back-trajectories from this group showed that they had descended 2.2 km from their stratospheric origin at 00h on the 6th.

- 3) to the east of group 2, a strip of trajectories beginning at 5.4 km entered the cut-off low near 4.8 km early on 9th October (cross-hatched shading). These had descended by 2 km in the previous 24 hours,
- 4) further east again, trajectories originating near 5.7 km continued downstream beneath the jet at an altitude of 4.5-4.8 km (solid shading). These had descended by 1.9 km in the previous 24 hours.
- 5) the easternmost (and largest) group (vertical shading) had returned to the stratosphere in the base of the cut-off low by 00h on the 8th. All these trajectories started at heights between 5.8 and 6.1 km, and had descended by 1.5 km or less in the past 24 hours (700 m in the case of the easternmost trajectories near the Irish coast). Their heights within the cut-off low varied between 5 and 5.5 km. Some of them left the low in a second folding event at 06h on the 8th, associated with the injection of group 3 into the low 12 hours later.

The extent of the fold at 00h on 8th as shown on fig.4

closely matches the radiosonde observations (fig.2), lending support to the trajectory calculations. Additionally, isobaric specific humidity fields for 700mb at 12h on the 8th and 00h on the 9th (ie 36 and 48 hours along the trajectories) showed low humidity values near 35°N and 30°N respectively - corresponding to the group 2 trajectories at 310K.

d) Estimate of the irreversible STE in the fold.

The trajectories in groups 1 and 2 represent irreversible transfer of air from stratosphere to troposphere (air in the other groups returned, at least initially, into the stratosphere on the eastern side of the trough or in the cut-off low). The area of these regions at 00h on 7th was 120,000 and 140,000 km² respectively. The depth of the fold for the group 2 trajectories may be directly measured from the Valentia and Stornoway radiosonde profiles at 00h; this yields 550m (at 500 mb). The group 1 trajectories passed near a ship at 46°N, 11°W 12 hours later, where the fold was 450 m deep (at 650 mb); this was taken as the depth of this region at 00h. Group 1 therefore contained 4.3×10^{13} kg and group 2, 6.7×10^{13} kg of air: a total irreversible transfer of 1.1×10^{14} kg. In fact, the radiosondes show that the fold was about twice as long as the model representation, suggesting that this figure should be increased, perhaps by a factor of around 2. It is also entirely likely that the true fold extended westwards of that shown by the model, again increasing the estimate of the mass of air transferred.

An estimate of the total amount of ozone transferred may be made by reference to the PV in groups 1 and 2. According to Beekmann et al (1992) the ratio between ozone mixing ratio and PV in the lower stratosphere is about 40 ppb/PV unit. From the radiosonde-derived PV fields at 00h and 12h, the PV in group 2 was estimated as 2.9 PV units and that in group 1 as 1.8 PV units. Thus the total no. ozone molecules contained in these two regions was 2.2×10^{32} - an excess of 8×10^{31} molecules over a normal tropospheric background of 50 ppbv (Beekmann et al, 1992).

4. CONCLUSIONS

The main objective of this case study was to study the potential application of ECMWF operational analysis fields to the study of stratosphere-troposphere exchange, and in particular tropopause folds. By using cross-sections from the model, specific humidity fields and an extensive trajectory analysis, it was seen that the model did resolve the growth phase of a fold which developed in a southward plunge of the polar jet stream over Ireland. Representation of the dissipating phase was less satisfactory. Careful analysis of radiosonde data is clearly essential when studying folds with the ECMWF model.

The value of around 2×10^{14} kg of stratospheric air irreversibly transferred into the troposphere in this event is rather small compared to previous studies (e.g 6×10^{14} kg by Reiter and Mahlman, 1965). However, further potential for stratosphere-troposphere exchange is revealed by the trajectories in categories 3 and 5: some of the air which formed the base of the cut-

off low had passed through the fold. Small-scale mixing is prevalent in baroclinic zones due to the low Richardson number, so that air returning to the stratosphere contains a mixture of the two air masses - exactly as observed in the base of a cut-off low by Bamber et al (1983). Furthermore, the injection of group 3 trajectories into the low was connected with a second fold along its western flank and the transfer of further air parcels into the troposphere.

ACKNOWLEDGEMENTS

We thank Keith Shine for providing ECMWF analyses and Barbara Naujokat for radiosonde data. This work was carried out as part of the TOASTE programme, funded by the CEC.

REFERENCES

- Beekmann, M., G. Ancellet and G. Megie. 'Analysis of a 7-year tropospheric ozone vertical distribution at the Observatoire de Haute Provence'. This volume.
- Bamber, D. J., P. G. Healey, B. M. Jones, S. A. Penkett, A. F. Tuck and G. Vaughan. 'Vertical profiles of tropospheric gases - chemical consequences of stratospheric intrusions' *Atmos. Environ.*, **18**, 1759-1766, 1984.
- Danielsen, E. F. 'Stratospheric-tropospheric exchange based on radioactivity, ozone and potential vorticity' *J. Atmos. Sci.*, **25**, 502-518, 1968.
- Reiter, E. R. and J. D. Mahlman. 'Heavy radioactive fallout over the southern United States, November 1962'. *J. Geophys. Res.*, **70**, 4501-4520, 1965.
- WMO. 'Atmospheric Ozone 1985'. Global ozone research and monitoring project report 16, 1986.

303527

LARGE-SCALE CIRCULATION PATTERNS ASSOCIATED WITH HIGH CONCENTRATIONS OF TROPOSPHERIC OZONE IN THE TROPICAL SOUTH ATLANTIC OCEAN

*K. M. Fakhruzzaman*¹, *J. Fishman*, and *V. G. Brackett*¹
 Atmospheric Sciences Division (Mail Stop 401A)
 NASA Langley Research Center
 Hampton, Virginia 23681-0001 U. S. A.

*J. D. Kendall*² and *C. O. Justice*³
 NASA Goddard Space Flight Center, Greenbelt, Maryland 20771 U.S.A.

ABSTRACT

Several years of satellite observations indicate the presence of enhanced amounts of tropospheric ozone over the tropical South Atlantic during the austral springs. Widespread biomass burning is prevalent over Africa and South America during the same time of the year. Another recent satellite technique has identified the locations of fires over the continents. In this study, we present an analysis of the prevailing meteorological conditions when the highest amounts of tropospheric ozone are present.

1. INTRODUCTION

Recently, a methodology has been developed at the NASA Langley Research Center for the indirect measurement of the tropospheric ozone (known as tropospheric residual) using observations of two satellite instruments (Total Ozone Measurement Spectrometer [TOMS] and Stratospheric Aerosol and Gas Experiment [SAGE], Fishman et al., 1990). The tropospheric residual ozone was obtained by subtracting stratospheric ozone measured by SAGE instruments from the total column of atmospheric ozone measured by TOMS. The analysis of several years of satellite observations indicates that large amounts of tropospheric ozone are often present over the trop-

pical South Atlantic Ocean (Fishman et al., 1991). The highest amounts of ozone are generally observed during austral spring (September-November). Based on these analyses, the figure below shows the annual average of the global distribution of tropospheric ozone (Fig. 1).

INTEGRATED TROPOSPHERIC OZONE (1979-1990)

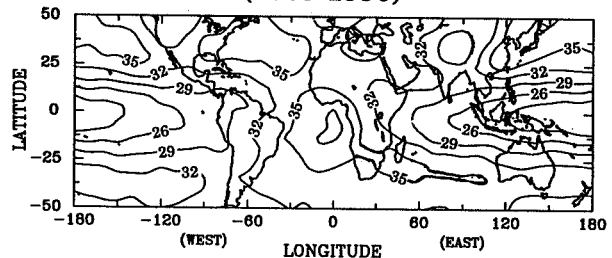


Figure. 1

In this study, we present a case study analysis of the prevailing meteorological conditions when high tropospheric amounts are present. Another technique has been developed to identify hotspots and thus anthropogenic origin of greenhouse gases by using Advanced Very High Resolution Radiometer (AVHRR) satellite imagery. Using these techniques, we have located the regions of highest ozone concentration and their relationship to the source regions using isentropic trajectory analyses. A case study of a fire in the Okavango River delta in northern Botswana is shown below.

Though isobaric surfaces are a conventional way of most meteorological analyses, the quasi-conservative three-dimensional

¹ Science Application International Corporation.

² Science Systems Application Incorporated.

³ University of Maryland, College Park.

airflow takes place quite closely on the surfaces of equal potential temperature (Danelsen, 1961). Therefore, we have chosen isentropic surfaces for prevailing meteorological analysis (Haagenson and Shapiro, 1979). The use of an isentropic trajectory model unveils a complex three-dimensional flow regime over the tropical South Atlantic Ocean of continental origin which is typical during the burning season.

Utilizing all these analyses, we will determine the relative contributions from tropospheric sources in both Africa and South America, as well as attempt to quantify how much ozone in the troposphere had been recently transported from the lower stratosphere and upper troposphere. Our analyses also have utilized observations from ozonesonde launches (Cros et al., 1992; Fishman et al., 1992) made simultaneously at Ascension Island (8° S, 15° W) and Brazzaville, Congo (4° S, 15° E).

2. OZONESONDE OBSERVATIONS AND TRAJECTORIES

The ozonesonde measurements at two stations reveal high ozone during the burning season of equatorial southern sub-tropical Africa. Typically ozone maxima in Ascension Island are lower in concentration and at a higher altitude than at Brazzaville, Congo (Fig. 2).

TYPICAL BURNING SEASON OZONE PROFILE

Ascension Island, (12 Sept., 1990),
and Brazzaville, Congo, (19 Sept., 1990)

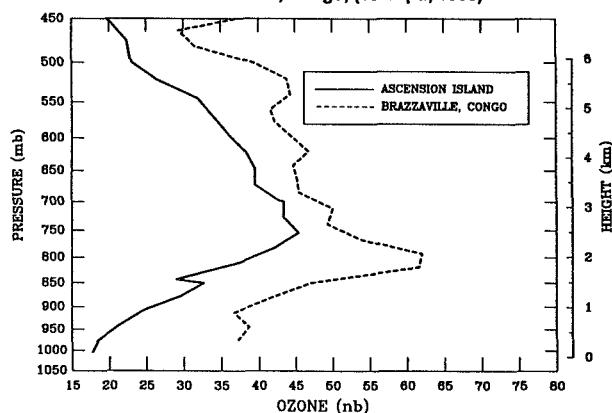


Figure 2

The isentropic trajectories of air parcels from equatorial Africa confirmed that ozone-rich air ascends slowly during westward transit across the Atlantic by the prevailing trade-winds (Fig. 3). The Montgomery stream functions generated by the isentropic analyses indicate the flow pattern of the region on the given potential temperature surfaces.

Backward Trajectories From Ascension Island Theta Level = 312 K

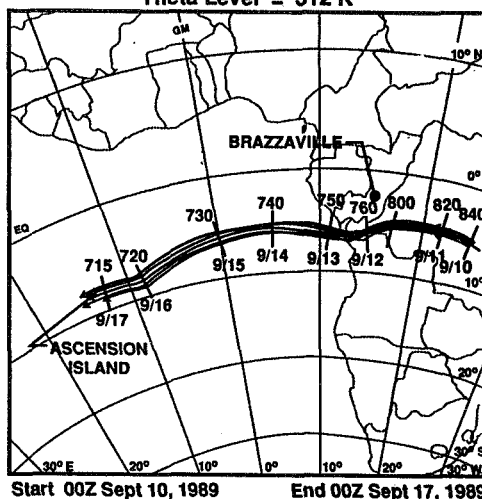


Figure 3

3. CASE STUDY: OKAVANGO DELTA FIRE

Our analyses of AVHRR imagery can be used to identify active fires, smoke, and the burn scars during the case study (Mason and Dozier, 1981; Thomas and Tag, 1990). For our case of study, we have analyzed ozone, meteorological and AVHRR data in conjunction with widespread burning taking place in near the Okavango River delta.

The progress of the fire fronts, the development of the burn scars, and the plumes of smoke indicated at least three different directions of air flow in this region during the time of the fire (Fig. 4). The forward trajectories from the delta region confirmed the three different directions of transport of trace gases (Fig. 5). Allowing the time and suitable condition of photochemical production of ozone, a significant

increase in the tropospheric ozone was found along the trajectories as shown in figure 6.

regime that consists of air originating from South America as well as from southern Africa.

Okavango River Delta Fire, September 3, 1989

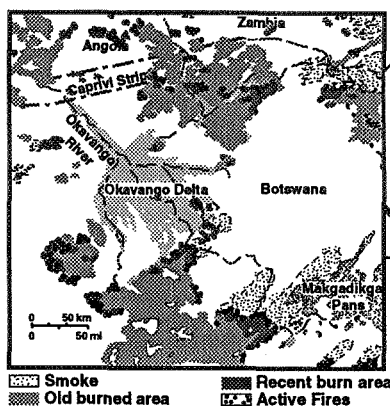
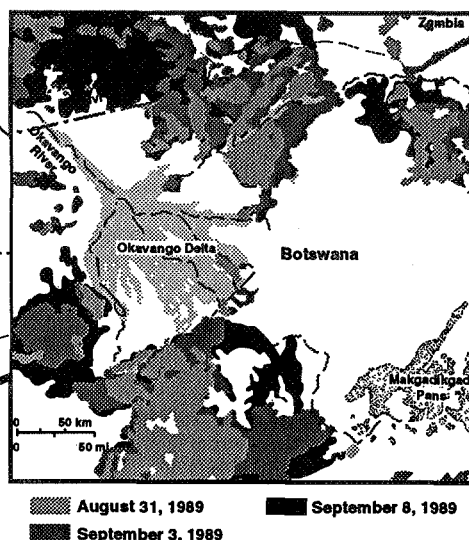


Figure 4

Progression of Biomass Burning, Okavango River Delta



Forward Trajectories From Okavango Delta, Botswana
Theta Level = 320 K

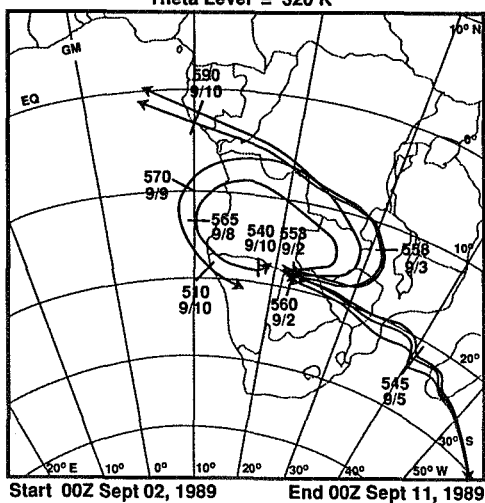


Figure 5

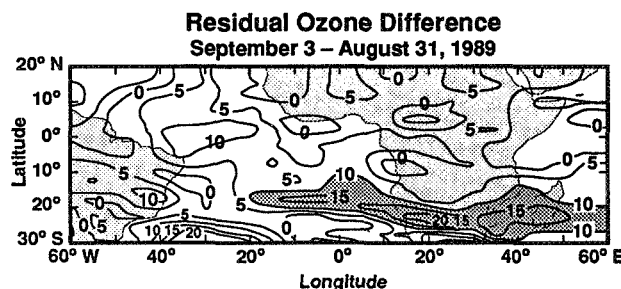


Figure 6

4. THREE-DIMENSIONAL FLOW REGIME

We have constructed a generalized three-dimensional flow regime of atmospheric circulation over the tropical South Atlantic Ocean for the month of September, 1989 by calculating bulk isentropic trajectories of continental air parcels that originated over the regions of biomass burning (Fig. 7). This analysis suggests that the source of ozone-rich air off the coast of Angola is result of a fairly complex flow

5. CONCLUSION

Recent scientific interest on global warming and pollution highlights the need to understand atmospheric chemistry and biomass burning in the tropics. The subsequent transport of trace gases is also an important issue, along with the photochemistry. At the present time very little is known about the tropical meteorology of this region of the world.

This study of the three dimensional flow regime in the southern tropics is among the first of its kind (Fig. 7). These analyses show that the circulation pattern is more

Middle and Lower Tropospheric Flow Regime (September, 1989)

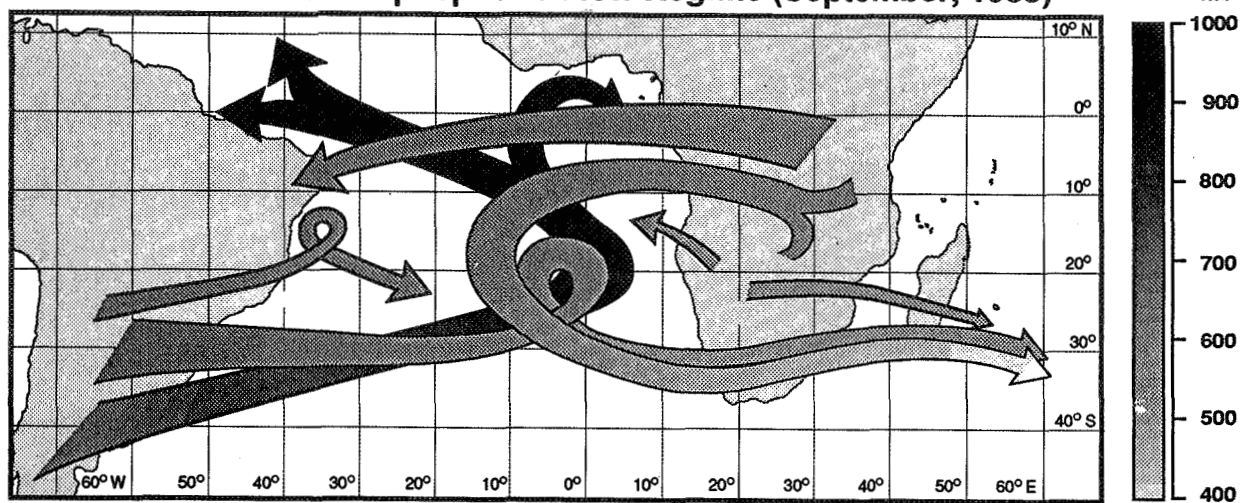


Figure 7

complex than previously thought. The elevation of the African landmass and the presence of a semi-permanent high pressure system, in addition to the migration of the Inter-Tropical Convergence Zone (ITCZ) and subtropical jet stream greatly complicate the observed circulation pattern. Further studies are needed to understand fully the dynamics of this region.

Tropical meteorologists, atmospheric chemists and environmentalists are now enthusiastic about the study of this region. It is expected that considerable insight will come forth as a result of the upcoming Transport and Atmospheric Chemistry near the Equator -- Atlantic (TRACE-A) mission which is scheduled in August-October, 1992..

5. ACKNOWLEDGMENT

The authors thank P. Haagenson for developing the NCAR's isentropic trajectory model which has been used in this study.

6. REFERENCES

Cros, B., D. Nganga, A. Minga, J. Fishman, and V. Brackett, Distribution of tropospheric ozone at Brazzaville, Congo, determined from ozonesonde measurements, *J. Geophys. Res.*, **97**, 12869-12876, 1992.

Danielsen, E. F., Trajectories: isobaric, isentropic and actual, *J. Meteor.*, **18**, 470-486, 1961.

Fishman, J., C. E. Watson, J. C. Larsen, and J. A. Logan, The distribution of tropospheric ozone determined from satellite data, *J. Geophys. Res.* **95**, 3599-3617, 1990.

Fishman, J., K. Fakhruzzaman, B. Cros, and D. Nganga, Identification of widespread pollution in the southern hemisphere deduced from satellite analyses, *Science*, **252**, 1693-1696, 1991.

Fishman, J., V. Brackett, and K. Fakhruzzaman, Distribution of tropospheric ozone in the tropics from satellite and ozonesonde measurements, *J. of Atmos. Terr. Phys.* **54**, 589-597, 1992.

Haagenson, P. and M. Shapiro, Isentropic trajectories for derivation of objectively analyzed meteorological parameters, *NCAR Technical Note. NCAR/TN-149+STR*, Boulder, CO., 30 pp., 1979.

Matson, M. and J. Dozier, Identification of sub-resolution high temperature sources using a thermal IR sensor, *Photo. Eng. and Remote Sensing*, **47**, 1312-1318, 1981.

Thomas F. L. and P. M. Tag, Improved Detection of Hotspots using the AVHRR 3.7- μ m Channel, *Bull. Amer. Meteor. Soc.*, **71**, 1722-1730, 1990.

N95-10629

303528

AIRBORNE MEASUREMENTS OF BIOMASS BURNING PRODUCTS OVER AFRICA

Günter Helas, Jürgen Lobert⁺, Johann Goldammer, Meinrat O. Andreae
Max Planck Institute for Chemistry, Biogeochemistry Department
POB 3060, D-6500 Mainz, F.R.G.

⁺ present address: NOAA-CMDL, Boulder, CO, U.S.A.

J. P. Lacaux

Centre de Recherche atmosphérique de CNRS, Campistrous, F-65300 Lannemezan, France

R. Delmas

Laboratoire d'Aérodologie, Université Paul Sabatier, F-31062 Toulouse, France

SUMMARY

Ozone has been observed in elevated concentrations by satellites over hitherto believed "background" areas. There is meteorological evidence, that these ozone "plumes" found over the Atlantic ocean originate from biomass fires on the African continent. Therefore we have investigated ozone and assumed precursor compounds over African regions. The measurements revealed large photosmog layers in altitudes between 1.5 and 4 km. Here we will focus on some results of ozone mixing ratios obtained during the DECAFE 91/FOS experiment and estimate the relevance of biomass burning as a source by comparing the strength of this source to stratospheric input.

Key words: Ozone, biomass burning, Africa

INTRODUCTION

It was already realized in the late 70's, that biomass fires emit the same ingredients that can form photosmog as urban pollution does (Evans et al., 1974; Evans et al., 1977). This was deduced from prescribed fires, which were set to reduce the density of flammable undergrowth. The technique is practiced in many regions of the world (Goldammer, 1990). Together with incidental fires and those induced by lightning, they influence ecosystems in several ways. They reduce vegetation, change patterns of succession and biodiversity, and have a global impact on climate and soil. In respect to the last issue, changes in soil hydrology and atmospheric moisture are anticipated as well as alteration of the budgets of atmospheric trace gases on a global scale. For the present approximately 40% of global CO₂-emissions are

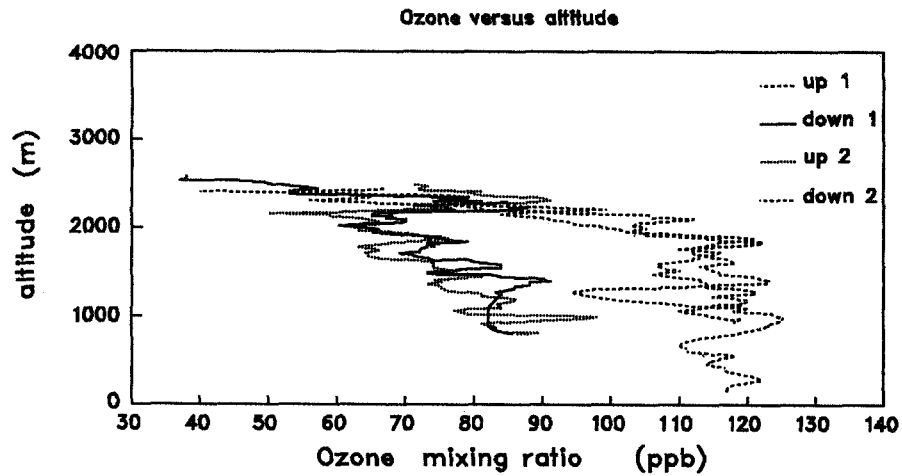
estimated to be due to biomass burning (Crutzen and Andreae, 1990). The production of ozone in the emission plumes of vegetation fires follows the same rules as the wellknown formation of photosmog in cities as the ingredients are the same. Biomass fires produce nitrogen oxides and unsaturated hydrocarbons, which, with sunlight yield ozone. Mixing ratios of up to 100 ppbv ozone frequently are encountered (Delany et al., 1985; Browell et al., 1988; Helas et al., 1989; Andreae et al., 1992). Not only that these elevated mixing ratios can be harmful, a main concern is that ozone acts as a powerful greenhouse gas, especially in the upper troposphere.

As the results of DECAFE 88 (Dynamique et Chimie de l'Atmosphère en Forêt Equatoriale), which took place over forested areas of central Africa, pointed to the fact that most of the assessed airmasses originated from savanna areas, we surveyed in a second experiment DECAFE 91/FOS (Fire of Savannas) savanna areas of western Africa.

EXPERIMENTAL

We have measured ozone with an UV-absorption instrument, e.g. a Thermo Electron 49. For other compounds which were measured in parallel, IR-absorption (CO₂), wet chemiluminescence (NO₂), and gas chromatographic techniques have been applied (CO, CO₂, CH₄). Measurements were made from a Beechcraft Bonanza. Flight patterns were chosen to probe air ranging from local background to directly contaminated by the flames of the vegetation fires. The field campaign was carried out in the Ivory coast between Bouaké and Lamto in January 1991 during the local dry season.

Cote d'Ivoire 1991



DECAFE 91 Flight No 1 (OH) over Bouaké; 2^o sounding

Figure 1:
Mixing ratios of ozone measured over the savanna between Bouaké and Lamto, Ivory Coast on Jan. 10th, 1991.

Cote d'Ivoire 1991

Bouaké, Flight 2, up2

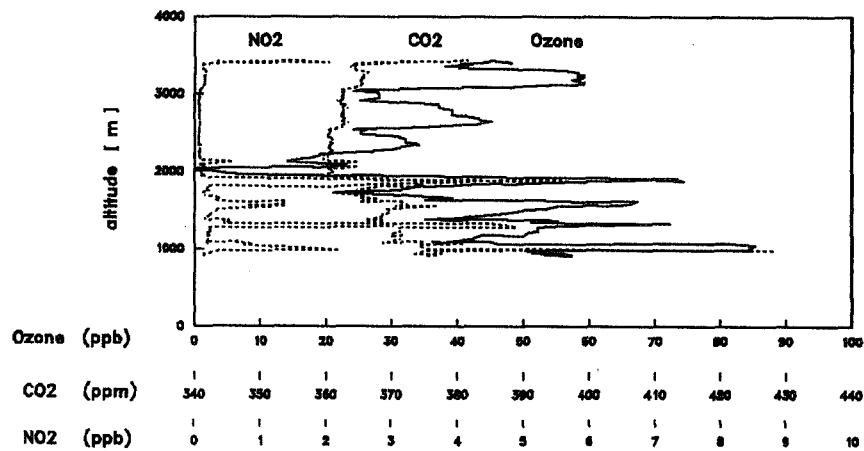


Figure 2:
Mixing ratios of O_3 , CO_2 and NO_2 measured over the savanna between Bouaké and Lamto, Ivory Coast on Jan. 11th, 1991.

Comparison of production ratios

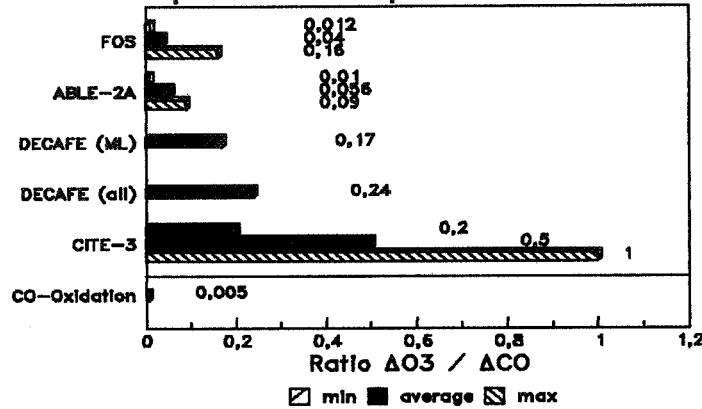


Figure 3: Comparison of production ratios of delta O₃ to delta CO as determined during different field assessments of biomass burning. The ratios are ordered in an approximate plume age with FOS ca. hours to CITE-3 ca. 1 week. Details see text.

TABLE 1: Comparison of biomass burning as a source for tropospheric ozone to input from the stratosphere.

Biomass burning			
	CO	--->	O ₃
	Tmol / year		Tmol / year
Logan et al. (1981)	23		8.1
Seiler and Conrad (1987)	36		12.6
Crutzen and Andreae (1990)	26		9.1
Stratospheric input--			
	Hemisphere		
data taken from Warneck (1988)	North	South	
in Tmol / year			
Fabian and Pruchniewics	8.9	5.7	
Mohnen	8.2	-	
Nastrom	5.2	-	
Gidel and Shapiro	6.5	3.3	
Warneck I	8.1	-	
Warneck II	10	-	

RESULTS AND DISCUSSION

We found elevated mixing ratios of ozone in air masses above the savanna area of western Africa. As is shown in Figure 1 the mixing ratios extended up to 100 ppbv. The most striking feature, however, is the distinct layering of the

atmosphere as is visible in the concentrations. This behavior is also reflected in the concentrations of the concurrent measured CO₂ and NO₂, which we show here in Figure 2 for a single ascent. Obviously the individual plume air parcels are not as well mixed as was observed during DECAFE 88 (Helas et al., 1989; Andreae et al., 1992), though

convective mixing in the area clearly was visible from the cloud formation during the sampling.

In order to assess the importance of vegetation fires as a source for tropospheric ozone we determined the production ratio of delta O₃ to delta CO. The delta indicates enhancement of trace components above background. This value ranged from 0.012 to 0.16 with an average of 0.04. When comparing this ratio to those determined during other field assessments on biomass burning as is shown in Figure 3, we find a distinct increase with plume age. While the air masses probed during DECAFE 91/FOS were approximately 1 hour old, meteorological evidence shows that the plumes of ABLE-2A (Andreae et al., 1988) and DECAFE 88 in the monsoon layer were in the order of a day, while the average of all data of DECAFE 88 together were derived from ages of several days (Andreae et al., 1992). Finally the plume surveyed during CITE-3 was estimated to be a week old (Andreae et al., 1990). In this latter plume the production ratio ranged from 0.2 to 0.5 with excursions up to 1. This development of delta O₃ to delta CO is also expected from the model calculations of Chatfield and Delany (1990), who showed that the concentration rise of ozone produced by the ingredients of vegetation fires develops particularly rapid in the first few days after dilution of the initial plumes. Based on the comparison shown in Figure 3 we predict that the delta O₃ to delta CO determined during DECAFE91/FOS of 0.04 will increase by a factor of ten during the transport from the source region to the remote troposphere.

As we find that the biomass burning plumes can survive over an extended period of time, we have chosen for further calculation as a conservative value an average production ratio of O₃ to CO of 0.35 and multiplied this value with estimates of CO production due to biomass burning found in the literature (Logan et al., 1981; Seiler and Conrad, 1987; Crutzen and Andreae, 1990). The data used are compiled in Table 1. With these data we calculate a production rate of approximately 10 Tmol ozone per year. We compare this source strength to the yearly input of ozone from the stratosphere downward. This is shown in the lower part of Table 1, which is taken from Warneck (1988). Several estimates are compiled from literature together with two assessments, which are denoted as Warneck I and Warneck II. We find both sources for ozone, biomass burning and stratospheric input, to be similar in strength. Thus the input of ozone from biomass burning on a global scale cannot be neglected.

ACKNOWLEDGEMENTS

We are grateful for the help of J. Baudet of the University of Abidjan, Côte d'Ivoire. We also thank the Air Force of the Côte d'Ivoire for support.

REFERENCES

- Andreae, M.O., E.V. Browell, M. Garstang, G.L. Gregory, R.C. Harriss, G.F. Hill, D.J. Jacobs, M.C. Pereira, G. Sachse, A.W. Setzer, P.L. Silva Dias, R.W. Talbot, A.L. Torres, and S.C. Wofsy, 1988. Biomass-burning emissions and associated haze layers over Amazonia. *J. Geophys. Res.* 93, 1509-1527.
- Andreae, M.O., B.E. Anderson, J.E. Collins, G.L. Gregory, G.W. Sachse, M.C. Shipham, J.D. Bradshaw, D.D. Davis, V.W.J.H. Kirchhoff, 1990. Influence of plumes from biomass burning on atmospheric chemistry over the equatorial Atlantic during CITE-3. *EOS Trans. AGU.* 71, 1255.
- Andreae, M.O., A. Chapuis, B. Cros, J. Fontan, G. Helas, C. Justice, Y.J. Kaufman, A. Minga, and D. Nganga, 1992. Ozone and Aitken nuclei over equatorial Africa: Airborne observations during DECAFE 88. *J. Geophys. Res.* 97, 6137-6148.
- Browell, E.V., G.L. Gregory, R.C. Harriss, and V. Kirchhoff, 1988. Tropospheric ozone and aerosol distribution across the Amazon basin. *J. Geophys. Res.* 93, 1431-1451.
- Chatfield, R.B., and A.C. Delany, 1990. Convection links biomass burning to increased tropical ozone: however, models will tend to over-predict O₃. *J. Geophys. Res.* 95, 18473-18488.
- Crutzen, P.J., and M.O. Andreae, 1990. Biomass burning in the tropics: Impact on atmospheric chemistry and biogeochemical cycles. *Science* 250, 1669-1678.
- Delany, A.C., P. Haagensohn, S. Walters, A.F. Wartburg, and P.J. Crutzen, 1985. Photochemically produced ozone in the emission of large scale tropical vegetation fires. *J. Geophys. Res.* 90, 2425-2429.
- Evans, L.F., N.K. King, D.R. Packham, and E.T. Stephens, 1974. Ozone measurements in smoke from forest fires. *Environ. Sci. Technol.* 8, 75-76.
- Evans, L.F., I.A. Weeks, A.J. Eccleston, and D.R. Packham, 1977. Photochemical ozone in smoke from prescribed burning of forests. *Environ. Sci. Technol.* 11, 896-900.
- Goldammer, J., Ed.: *Fire in the tropical biota. Ecosystem processes and global challenges.* Springer-Verlag, Berlin, 1990.
- Helas, G., M.O. Andreae, J. Fontan, B. Cros, and R. Delmas, 1989. Ozone measurements in equatorial Africa during DECAFE 88. In R.D. Bojkov and P. Fabian, eds.: *Ozone in the atmosphere*, A. Deepak Publishing, p. 430-432.
- Logan, J.A., M.J. Prather, S.C. Wofsy, and M.B. McElroy, 1981. Tropospheric chemistry: A global perspective. *J. Geophys. Res.* 86, 7210-7254.
- Seiler, W., and R. Conrad, 1987. Contribution of tropical ecosystems to the global budgets of trace gases. In *Geophysiology of Amazonia*, ed.: R. Dickinson, Wiley, New York.
- Warneck, P., 1988, *Chemistry of the Natural Atmosphere*, Academic Press, San Diego.

303509

Long Path Monitoring of Tropospheric O₃, NO₂, H₂CO and SO₂A.C. Vandaele¹, M. Carleer², R. Colin², P.C. Simon¹

¹ Institut d'Aéronomie Spatiale de Belgique, 3 av. Circulaire, 1180 Brussels, Belgium,
Tel.: +32-2-3751579, Fax: +32-2-3748423

² Université Libre de Bruxelles, Laboratoire de Chimie Physique Moléculaire, CP 160,
50 av. F.D. Roosevelt, 1050 Brussels, Belgium,
Tel.: +32-2-6502415, Fax : +32-2-6504232,

Concentrations of tropospheric O₃, NO₂, H₂CO and SO₂ have been measured on the Campus of the "Université Libre de Bruxelles" on a routinely basis since October 1990. The long path system (see Figure 1) consists of a source lamp, a first 30 cm f/8 Cassegrain type telescope which collimates the light onto a slightly parabolic mirror placed on the roof of a building situated 394 m away from the laboratory. The light is sent back into a second 30 cm Cassegrain telescope. This telescope has been modified so that the output beam is a 5 cm diameter parallel beam. This beam is then focused onto the entrance aperture of the BRUKER IFS120HR Fourier Transform Spectrometer. The two telescopes are mounted on alignment devices and the external mirror is equipped with a driving system operated from the laboratory. The choice of the light source (either a 1000 W high pressure "ozone free" Xenon lamp or a 250 W Tungsten filament) and of the detector (either a solar blind UV-diode or a Silicon diode) depended on the spectral region studied. These regions lie respectively from 26000 cm⁻¹ to 30000 cm⁻¹ (260-380 nm) and from 14000 cm⁻¹ to 30000 cm⁻¹ (330-700 nm). The spectra have been recorded at the resolution of 16 cm⁻¹ and with a dispersion of 7.7 cm⁻¹. They have been measured during the forward and the backward movements of the mobile mirror, in double sided mode; each spectrum is an average of 2000 scans. The time required to record a spectrum is about 45 minutes. The shape of the raw spectra in the two investigated regions are represented in Figure 2.

The concentration of the measured constituents are deduced from the experimental spectra using the Beer-Lambert law :

$$I = I_0 e^{-n \Delta \sigma d}$$

where I is the measured intensity, I_0 the measured intensity from which all absorption structures have been

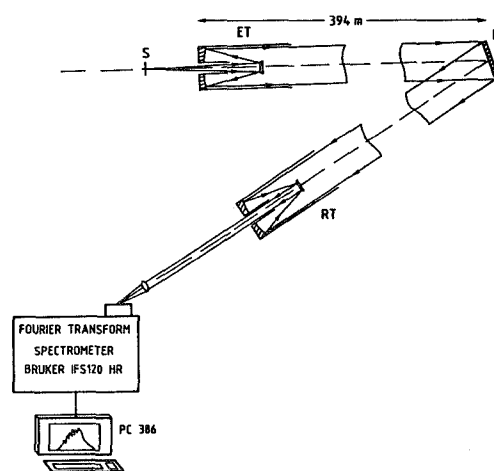


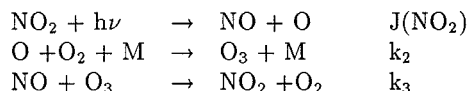
Fig. 1 : Experimental set-up : S = Source Lamp, ET = Emitting Telescope (30 cm ϕ). RT = Receiving Telescope (30 cm ϕ), M = Long Focal Retroreflector Mirror

removed, n the concentration, d the optical path length and $\Delta \sigma$ the differential absorption cross section of the molecule. Numerous methods for determining I_0 exist. Fourier transform filtering has been used in this work. This method defines I_0 as the inverse Fourier transform of the lower frequencies portion of the power spectrum of the experimental data. A least squares procedure is then applied in order to determine the concentration of the desired molecules. Cross sections of O₃ and H₂CO have been taken from the literature (Daumont et al., 1992; Moortgat et al., 1989). The cross sections of SO₂ and NO₂ have been measured in the laboratory with the same spectrometer (Carleer et al., 1992). These cross sections have been

recorded in the UV and visible regions at different resolutions (2,4,8 and 16 cm^{-1}) and at room temperature. The gas is introduced in a 20 cm long absorption cell; the partial pressure of the gas is measured with a Baratron gauge; air is then added to obtain a total pressure of 1 atmosphere. The temperature is measured with a conventional sensor. Two blanks were taken before and after each measurement. The experimental conditions for the measurement of the cross sections are identical to those used for the atmospheric spectra, except that each spectrum is an average of 4000 scans, instead of 2000 scans, in order to improve the signal to noise ratio. Absolute cross sections of SO_2 and NO_2 at the resolution of 16 cm^{-1} are plotted in Figures 3 and 4. The accuracy on the cross sections of SO_2 is of the order of $\pm 2\%$ and of the order of $\pm 5\%$ for NO_2 .

The absolute cross sections measured in this work have been compared to data from the literature (Schneider et al., 1987; Thomsen, 1990). The absolute cross sections of NO_2 are in good agreement in the wavenumber range 30800 - 34000 cm^{-1} (better than 5%), however discrepancies of about 10% appear in the 23800 - 30800 cm^{-1} range. Below 23500 cm^{-1} the cross sections measured by Schneider et al. present some anomalies regarding the wavelength calibration. The comparison between the cross sections of SO_2 of this work and of Thomsen, shows that the data are in good agreement (better than 5%).

Diurnal variations of SO_2 , NO_2 , O_3 and H_2CO concentrations measured on the Campus of the "Université Libre de Bruxelles" for February, 27, 1992 and April 29, 1992 are reported in Figure 5. SO_2 does not show any clear diurnal cycle and its variation is mostly due to climatic parameters such as the wind velocity and direction. H_2CO was found to be often below the detection limit. O_3 and NO_2 show strongly anti-correlated cycles, with O_3 increasing between 7 pm and 12 pm, then decreasing till 19 am, increasing again till 2 pm. As NO_2 and O_3 seem to be chemically correlated, NO concentrations have been deduced from the Leighton photochemical reaction scheme, which is only valid when photochemical equilibrium has been reached (daytime conditions, except at sunrise or sunset):



The NO concentration is given by

$$[\text{NO}] = \frac{J(\text{NO}_2)}{k_3} \frac{[\text{NO}_2]}{[\text{O}_3]}$$

where $k_3 [\text{cm}^3/\text{molec sec}] = 2.0 \cdot 10^{-12} \exp(-\frac{1400}{T})$ (DeMore et al., 1990) and the photodissociation rate $J(\text{NO}_2)$ is calculated using the empirical relation given by Parrish (Parrish et al., 1986).

Results for February 27, 1992 are plotted in Figure 6. NO concentrations measured by the Institute for Hygiene and Epidemiology (IHE, Brussels) are also reported. The station of the IHE is located at Uccle, 3 km away from the Campus of the ULB and uses a chemical technique to measure NO.

The detection limits of these constituents are listed in Table 1.

Table 1 : Detection limits

	$\bar{\nu}$ (cm^{-1})	S/N	Detection Limit (ppb)
SO_2	33340	3200	0.1
NO_2	28710	500	5.8
	22300	4000	0.3
O_3	35305	1700	1.6
H_2CO	29514	1000	5.2

Acknowledgments

This project has been supported by the Belgian State - Prime Minister's Service - Science Policy Office and the "Fonds National de la Recherche Scientifique". We would like to also thank D. De Muer (Koninklijke Meteorologische Instituut) and the Institute for Hygiene and Epidemiology for the data they have provided.

References

- Carleer M., Colin R., Vandaele A.C. and Simon P.C., in press
- Daumont D., Barbe A., Brion J. and Malicet J., submitted for publication in J. Atm. Chem. (1992)
- Moortgat G.K., Raber W., Reinholdt K., Meller R., Schneider W., LACTOZ (EUROTRAC) Annual Report (1989)
- Schneider W., Moortgat G., Tyndall G., Burrows J., J.Photochem. and Photobiol., **40A**, 195 (1987)
- Thomsen O., GKSS-Forschungszentrum, GKSS 90/E/36 (1990)
- DeMore W.B., Sander S.P., Golden D.M., Molina M.J., Hampson R.F., Kurylo M.J., Howard C.J. and Ravishankara A.R., Publication No 90-1, January 1 (1990)
- Parrish D.D., Murphy P.C., Albritton and D.L., Fehsenfeld F.C., Atmos. Environ., **17**, 1365 (1986)

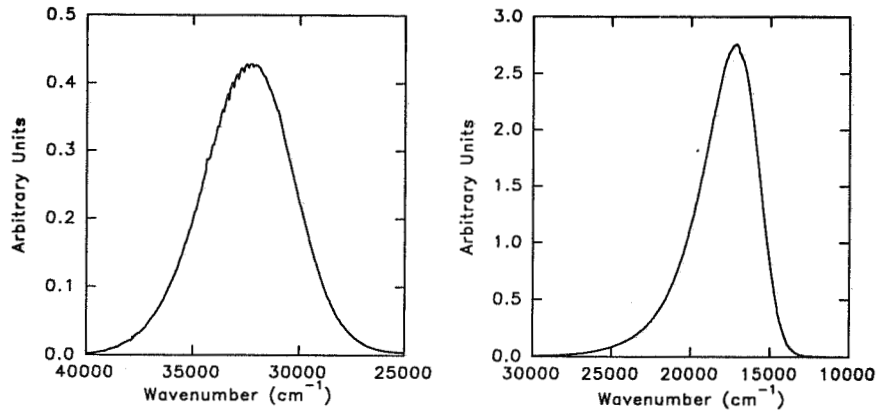


Fig. 2 : Experimental spectra in the two investigated regions

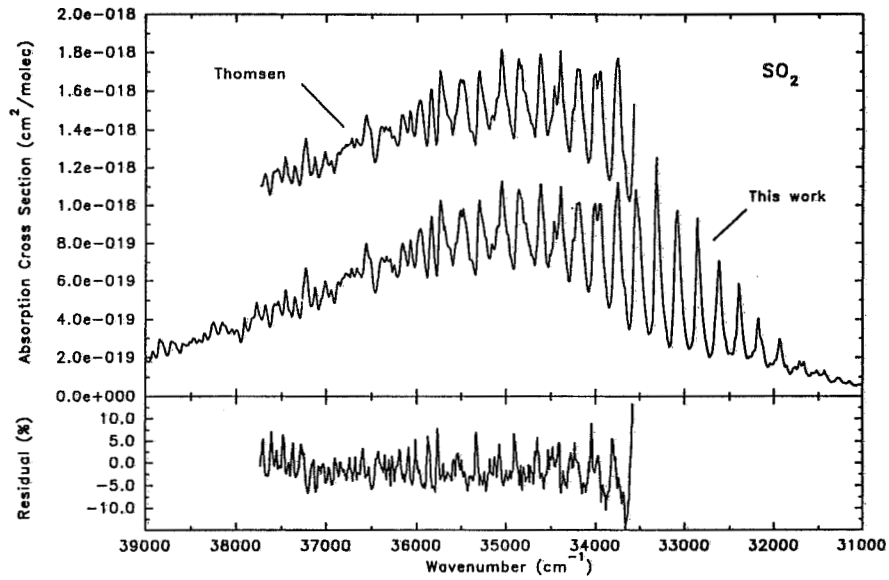


Fig. 3 : Absolute absorption cross sections of SO_2 between 31000 and 39000 cm^{-1} . The values of Thomsen (1990) have been displaced by $7 \cdot 10^{-19} \text{ cm}^2/\text{molec}$ for comparison purposes.

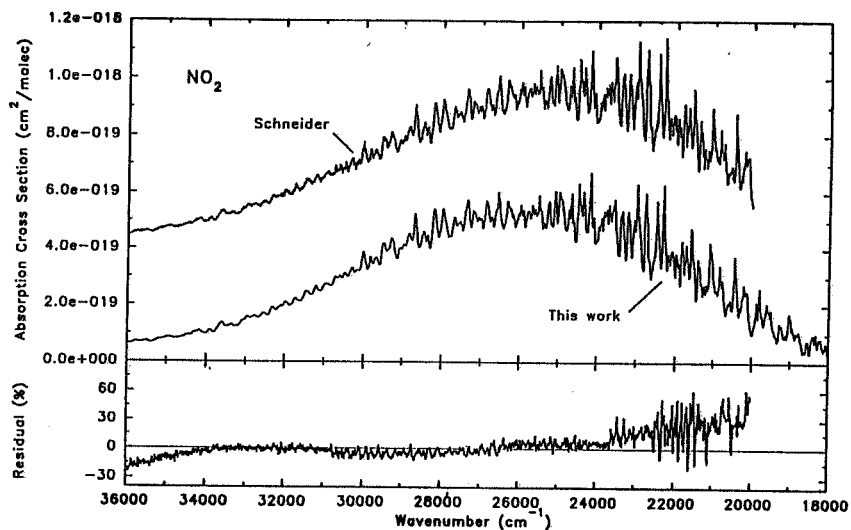


Fig. 4 : Absolute absorption cross sections of NO_2 between 18000 and 36000 cm^{-1} . The values of Schneider et al. (1987) have been displaced by $4 \times 10^{-19} \text{ cm}^2/\text{molec}$ for comparison purposes.

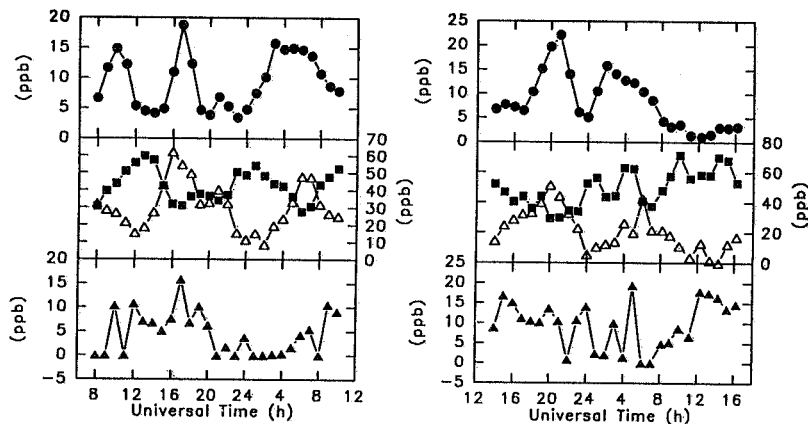


Fig. 5 : Diurnal variations of SO_2 (\bullet), O_3 (\blacksquare), NO_2 (\blacktriangle) and H_2CO (\blacktriangle) measured at the ULB on the February 27, 1992 and April 29, 1992.

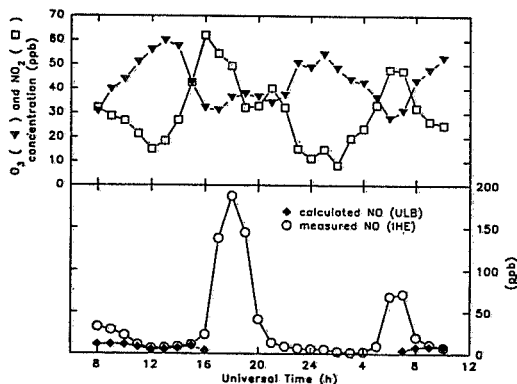


Fig. 6 : Comparison between calculated NO and measured NO for February 27, 1992.

303530

RESULTS OF OZONE MEASUREMENTS IN NORTHERN GERMANY
- A CASE STUDY -

Manfred Schmidt

Max-Planck-Institut für Aeronomie
D-3411 Katlenburg-Lindau, Germany

ABSTRACT

At most of the German ozone recording stations which have records over a sufficiently long period, the results of the summer months 1989 showed the highest values since the beginning of the measurements. One of the reasons for this phenomenon was the high duration of sunshine in that summer; for example, in Potsdam near Berlin in May 1989 the sunshine duration was the highest in May since the beginning of the records in 1893. For that reason we selected this summer for a case study.

The basis for the study was mainly the ozone measuring stations of the network of Lower Saxony and the Federal Office of Environment (Umweltbundesamt). The results of these summer measurements point to intense sources of ozone, probably in form of gaseous precursors, in the Middle German industrial areas near Leipzig and Halle and in Northwestern Czechoslovakia, with coal-mining, chemical and petrochemical industries, coking plants and others. The maps of average ozone concentrations, number of days with high ozone maxima, ozone-windroses of the stations etc., suggest that these areas could be a main source of precursors and of photochemical ozone production in summer smog episodes in Central Europe.

Stations on the North Sea coast, at which early ozone measurements were made by our institute in 1973/74 are compared with similarly located stations of the Lower Saxon network in 1989 and the results show a reversal of the ozone-windroses. In 1973/74, the highest ozone concentrations were correlated with wind directions from the sea while in 1989 these concentrations were correlated with directions from the continent. In the recent years, photochemical ozone production on the continent is probably predominant, while in former years the higher ozone content of the maritime subpolar air masses has been explained by stratospheric-tropospheric exchange.

1. INTRODUCTION

Figure 1 shows the summer ozone concentration averages (May-August) of some stations in Germany with

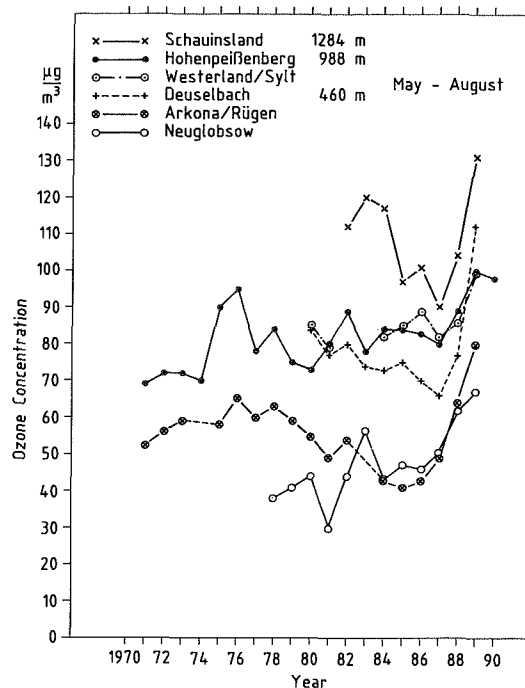


Fig. 1 Average ozone concentrations in the summer months May-August of 6 German stations, 1971-1989

longest duration of records; the longest series are at Arkona on the coast of the Baltic Sea (since 1956) and at Hohenpeißenberg in southern Germany (since 1971) [e.g. Low et al., 1990]. The geographical positions of these stations, and others considered in this paper, are plotted in Fig. 2. The most striking features in Fig. 1 are the very high O_3 values in the summer of 1989, at all stations without exception. These are the highest average concentrations since beginning of the records. The 1989 summer in Germany was dry and the recorded sunshine durations and global radiations were far above normal (up to 120-140% sunshine duration). If we consider sufficient concentrations of gaseous precursors, NO_x , CO , CH_4 and non-methane hydrocarbons (NMHC), an increased photochemical produc-



Fig. 2 Map of Germany with relevant ozone measuring stations, and the location of important industrial areas. Stations in Lower Saxony are considered especially

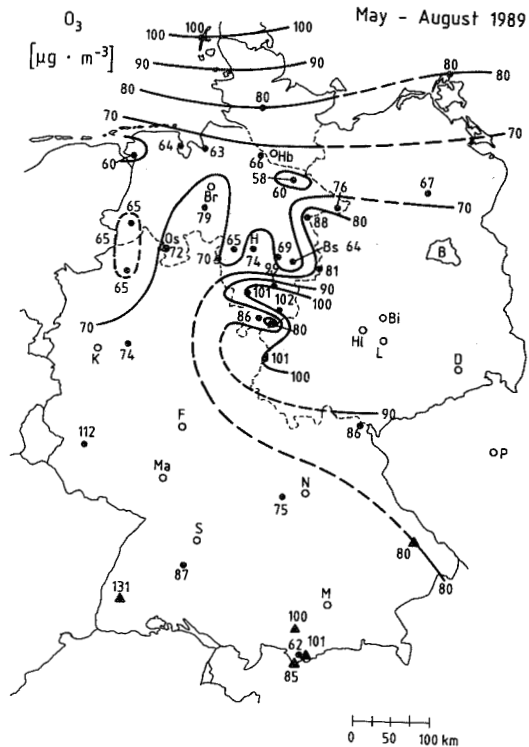


Fig. 3 Average ozone concentrations May-August 1989 of the stations in Fig. 2

tion of ozone during these enhanced radiation conditions with simultaneously increased UV radiation is to be expected [Schmidt, 1989]. A further reason for choosing the 1989 summer months for a case study was the unusually high ozone concentration at all stations in the southern part of Lower Saxony, the district which contains the city of Göttingen and the location of our institute. This is the main point of discussion in this paper.

We have, therefore, concentrated on air quality measurement data from the 17 stations in the Federal State Lower Saxony, in addition to the 15 stations of the Federal Office of Environment, and the two WMO Background Air Pollution Monitoring stations of the former GDR (names and positions in Fig. 2). Wind direction measurements have been taken from suitable stations of the German Weather Service.

2. RESULTS

In Fig. 3, we have plotted the average ozone concentrations for May-August 1989 from all stations mentioned and indicated in Fig. 2. To a careful first approximation, we have also included isolines. Unexpectedly, "a priori", the highest ozone concentrations $> 100 \mu\text{g}/\text{m}^3$ appeared in districts north and southeast of Göttingen, > 90 and $> 80 \mu\text{g}/\text{m}^3$ in the adjacent regions, all situated near the border to the former GDR. Similar high concentrations were

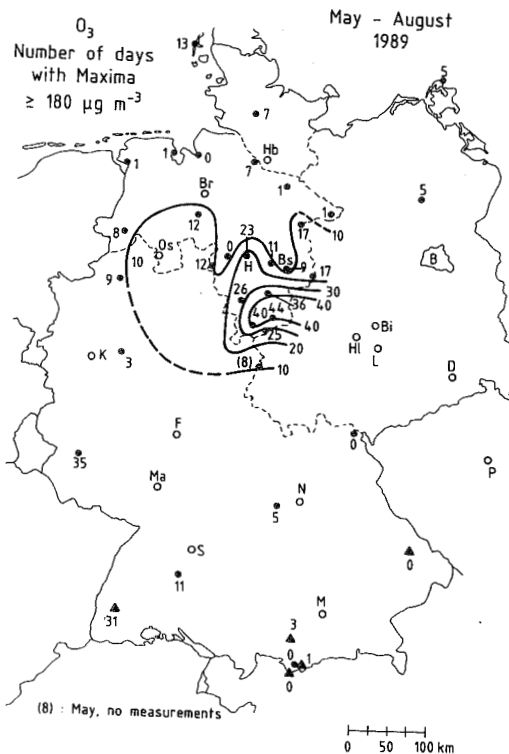


Fig. 4 Number of days with ozone maxima $\geq 180 \mu\text{g}/\text{m}^3$ in May-August 1989. Ozone stations of Fig. 2

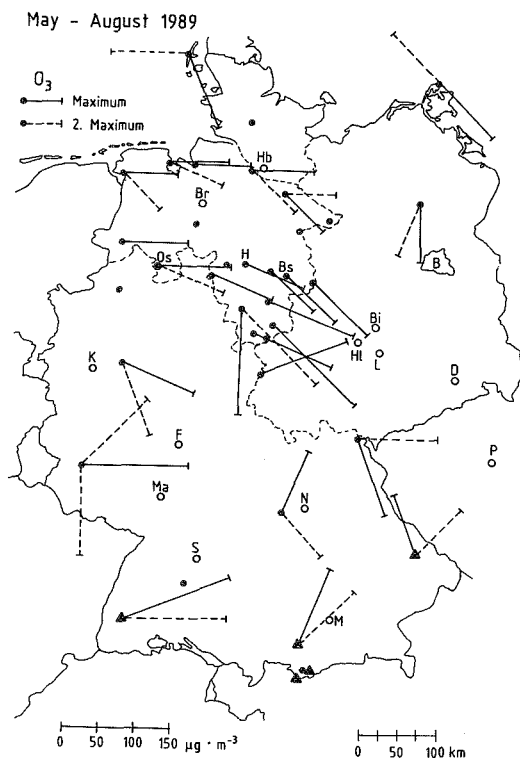


Fig. 5 Direction and amount of maximum and 2nd maximum of the ozone-windroses, epoch May–August 1989

found in the northernmost parts of Germany, at and near the North Sea and the Baltic Sea coasts, and again at elevated places in Southern Germany. The highest average concentration of $130 \mu\text{g}/\text{m}^3$ was measured at the peak of Schauinsland in the Black Forest, 1284 m a.s.l. At this mountain station, the O_3 concentrations are normally the highest of all stations, also during other periods – months and seasons –, a fact, which should be investigated further on. Very surprising and impressive are supporting results, shown in Fig. 4, the number of days with O_3 maxima $> 180 \mu\text{g}/\text{m}^3$ at the stations considered. This value is an upper limit during summer smog episodes, from which the authorities disseminate warnings to patients and persons with diseases affected by high ozone concentrations and other poisonous substances in the photochemical smog. In the southeastern part of Lower Saxony and probably to the east we find the highest number of such days, more than 20 to 40, in the summer of 1989. Similar high values, 31 and 35 days, appeared at two further stations, Schauinsland (1284 m) and Deuselbach (460 m a.s.l.), the latter probably influenced by two other industrial centers (Fig. 5 and section 3).

In Fig. 5, we have plotted the directions and amounts of the maximum and 2nd maximum of the ozone windroses of nearly all of the stations. These ozone-wind vectors are the key to an explanation of the results in Figs. 3 and 4.

3. DISCUSSIONS

The results given in Figs. 3, 4 and 5, notably in Fig. 4, suggest that the sources of these unusually high ozone concentrations may be in the strongly polluted industrial areas of the former GDR, in the district Halle–Leipzig–Bitterfeld (at the time of these measurements, 1989, HL, L, Bi in Figs. 3–5). Nearly all maximum ozone-wind vectors of nearby stations in Fig. 5 point in this direction. Similar strongly polluted industrial areas are also located in the northwestern part of CSFR (Fig. 2), indicated by an extension of the vectors above. Even the vectors of the station Brotjacklriegel in the Bavarian Forest and one vector of the station Hof point in this direction.

The industrial areas just mentioned are, admittedly, the highest polluted areas in Central Europe, particularly with regard to the SO_2 emission. One of the reasons for this is the almost exclusive use of the pit-brown coal for energy production, raw material for chemical and petrochemical industries and for coke production. The most important chemical factories of the former GDR are located in the district Halle–Bitterfeld. One of these factories was the largest factory of all kinds in the GDR. These factories mainly produced fuels of all kinds, acids, nitrogen fertilizers, technical gases, chemicals, medicaments and plastics. One of these factories was the greatest producer of calcium carbide CaC_2 in Europe, made from brown coal and lime, with water transformed into acetylene C_2H_2 , and finally used as a basic substance via other NMHC's for the production of plastics. From extended artificial mud pools containing the remaining $\text{Ca}(\text{OH})_2$, large amounts of residual C_2H_2 must surely have escaped into the atmosphere, to be converted there into further NMHC's. Sources of precursors are to be expected from parts of the gas, escaping from coking plants operated there. Coke-oven gas mainly contains tar vapour, H_2 , CH_4 , NMHC's, N_2 , CO , CO_2 and others, most of them being precursors for photochemical O_3 production. Unfortunately, no direct measurements of trace gases including ozone are available from these areas before the time of unification of the German states. Our results are supported by some other observations. Kourtidis [1991] published results of PAN measurements, made in the spring of 1989 at our institute in Katlenburg-Lindau near Göttingen. His PAN windroses point with the maxima in the same directions, East to South, like our windrose vectors in Fig. 5. In the 3 summers prior to 1989, 1986 – 1988, the numbers of half-hour averages of O_3 concentrations $> 120 \mu\text{g}/\text{m}^3$ and $> 180 \mu\text{g}/\text{m}^3$ were highest at the two Lower Saxon stations Dassel and Oker, compared with 4 further stations in the North, Hanover, Braunschweig, Wilhelmshaven and Emden. All stations attained maxima in 1989. Even the annual O_3 means of Dassel and Oker in the years 1986–1988 show higher values than those of Hanover and Emden. In these years, the number of stations was still reduced.

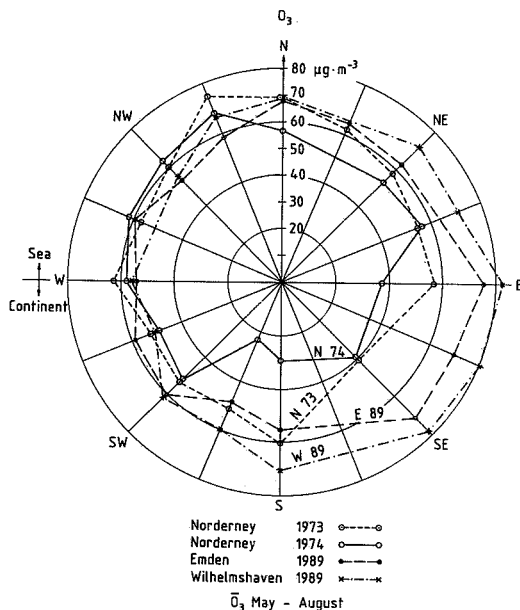


Fig. 6 Ozone-windroses May–August of 3 nearby located stations at the German coast of North Sea; Norderney 1973 and 1974, (N73, N74), Emden (E89) and Wilhelmshaven 1989 (W89). Locations see Fig. 2. Sunshine duration: 942 (N73), 973 (N74), 949 (E89) and 951 (W89) hours

The maximum ozone vectors in Fig. 5 of station Deuselbach, with similar high values in Figs. 3 and 4, point in directions where the chemical industries in the area Mannheim–Ludwigshafen–Frankfurt are located and, furthermore to the South, in the direction of the coal mining and coal manufacturing districts in the Federal State of Saar. The vector of Schauinsland, mentioned in section 2, point to the densely populated area of Stuttgart, the vectors of Hohenpeißenberg to the similarly populated district of Munich [like Wege and Vandersee, 1991]. In the northernmost part of Germany, the ozone concentrations in Fig. 3 increase towards the North, up to $100 \mu\text{g}/\text{m}^3$ at station Westerland. The vectors of the 2nd ozone maximum in Fig. 5 point to the West in Westerland and to the Northwest in Arkona. These facts suggest that the ozone concentrations at such rural stations near the Middle European sea shores are, at least partially, composed of ozone, transported by subpolar air masses and coming from stratospheric-tropospheric exchange processes, if the wind is blowing from the North towards the stations. This also should be the subject of further investigation.

An interesting result, regarding this question, is plotted in Fig. 6. During project “Tropospheric Ozone” in the seventies [e.g. Schmidt, 1981], our institute operated an ozone measuring station at Norderney, in the same coastal area as the stations Emden and Wilhelmshaven of the recent Lower Saxon network (Fig. 2). At station Norderney increased ozone concentrations were found in all seasons during wind directions from the Southwest via North

to the Northeast, i.e. from the North Sea and Baltic Sea, and decreased concentrations from all other directions, i.e. from the European continent. Fig. 6 shows two examples in the summers of 1973 and 1974 (N73,74). On the other hand, the nearby located stations Emden (E89) and Wilhelmshaven (W89) show the highest O_3 concentrations 15 years later in the summer of 1989 during wind directions from the continent, with slightly lower concentrations when the wind was from the North Sea, W to NNW. The total sunshine durations during each of these 3 summers were nearly the same, as indicated in Fig. 6 below. An explanation of these contrary results could be that, in recent years, the photochemical ozone production on the European continent was predominant, especially in the summer months, and caused by a distinct increase of anthropogenic gaseous precursors; this is also suggested by measurements. In former years, the higher ozone content of the subpolar air masses correlated with wind directions from the northern sector; this was explained by stratospheric-tropospheric exchange and demonstrated in a series of papers [e.g. Fabian and Pruchniewicz, 1977; Schmidt and Fabian, 1980].

4. CONCLUSIONS

The assumption is justified, the industrial areas in Eastern Germany and CSFR have been important sources of precursor gases for the ozone production in summers such as 1989 with its relatively strong UV radiation. Since some of these factories are now obsolete and have since been closed (for renewal), further investigations of ozone during sunny summers in the future should consider, whether or not the ozone concentrations will now decrease in these locations.

REFERENCES

- Fabian, P. and P.G. Pruchniewicz: Meridional Distribution of Ozone in the Troposphere and Its Seasonal Variations. *J.G.R.* **82**, 2063-2073, 1977
- Kourtidis, K.: Analysis of PAN (Peroxyacetylnitrate) in the Atmosphere. PhD Thesis, Aristoteles-University of Thessaloniki, Greece, 1991
- Low, P.S., T.D. Davies, P.M. Kelly and G. Farmer: Trends in Surface Ozone at Hohenpeißenberg and Arkona. *J.G.R.* **95**, 22441-22453, 1990
- Schmidt, M. and P. Fabian: Relationships Between Tropospheric Ozone Concentration and the General Weather Situation. *Contr. Atm. Phys.* **53**, 63-73, 1980
- Schmidt, M.: Further Results from the MPAE-Project “Tropospheric Ozone”. *Proc. Quadr. Intern. Ozone Symp.*, Boulder, 4-9 Aug. 1980, 454-461, Boulder/Col. 1981
- Schmidt, M.: Relationships Between Tropospheric Ozone and Global Solar Radiation in Germany. In: Bojkov R.D. and P. Fabian (Eds): *Ozone in the Atmosphere*, 451-454, Deepak Publ., Hampton, VA, 1989
- Wege, K. und W. Vandersee: Ozonbeobachtungen am Nordrand der Alpen. *Met. Rundschau* **44**, 138-146, 1991

THE GRADIENT OF METEOROLOGICAL AND CHEMICAL
VARIABLES ACROSS THE TROPOPAUSE

Russell R. Dickerson, Bruce G. Doddridge, Olga Poulida
Department of Meteorology, University of Maryland
College Park, MD 20742, USA

Melody A. Owens
Chemical Physics Program, University of Maryland
College Park, MD 20742, USA

ABSTRACT

The downward transport of air through the tropopause can bring substantial amounts of ozone and reactive nitrogen into the upper troposphere. In this cold region of the atmosphere, O_3 is particularly effective as a greenhouse gas. As part of the North Dakota Thunderstorm Project in June 1989, the NCAR Sabreliner made five flights through the tropopause. We measured ozone, nitric oxide (NO), total reactive nitrogen (NO_y), carbon monoxide (CO), and water vapor (H_2O), and took grab samples for hydrocarbon (HC) analysis. Hydrocarbons, CO , and H_2O , species with sources primarily at the Earth's surface, showed a strong concentration decrease with increasing altitude, while O_3 and NO_y , species with a source in the stratosphere showed a strong concentration increase with increasing altitude. Stratospheric concentrations of NO_x , NO_y , and H_2O were all high relative to winter observations made during NASA's AASE. We suggest that mid latitude thunderstorms may inject wet, NO -rich air into the lower stratosphere. Calculation based on measured ratios of NO_x and NO_y to O_3 , yield a total flux of reactive nitrogen from the Northern Hemisphere stratosphere into the troposphere of 1 to 2 $Tg(N) yr^{-1}$ with about 8% in the form of NO_x . This value is higher than reported estimates of total stratospheric nitrogen fixation.

1. INTRODUCTION

The principal natural source of tropospheric ozone is downward transport from the stratosphere in extratropical regions (Junge, 1962). Much of this transport is associated with tropopause folding events occurring on the cyclonic generally poleward side of the jet streams (see WMO, 1986 for a review). Carried along with this ozone are reactive nitrogen compounds that can lead to in situ photochemical ozone production in the upper troposphere (Liu et al., 1980). Ozone is particularly effective at greenhouse warming at this altitude because it is the coldest part of the troposphere.

Published estimates of the flux of ozone from the stratosphere into the troposphere range from about 4 to 8×10^{10} molec. $cm^{-2}s^{-1}$ for the Northern Hemisphere (see Fishman, 1985 and WMO, 1986 for reviews). From measured ratios of reactive nitrogen to ozone, one can estimate the flux of nitrogen species to the troposphere. Nitric oxide, NO and nitrogen dioxide, NO_2 , (together referred as

NO_x) play the most active role in photochemical ozone production. NO_x can exist as several reservoir species; total reactive nitrogen, NO_y , is composed of NO , NO_2 , NO_3 , $2xN_2O_5$, $HONO$, HNO_3 , HO_2NO_2 , $ClONO_2$, PAN (peroxy acetylnitrate), $RONO_x$ (organic nitrates and nitrites), and small nitrate particles. In several recent NASA programs (see Murphy et al., 1993), ozone and reactive nitrogen species were measured in the lower stratosphere, but data are still sparse and there are no reports in the literature of simultaneous measurements of NO , or NO_y and O_3 in this region of stratospheric egress. Here we report such measurements and use the results to estimate the flux of NO_x and NO_y from the stratosphere into the Northern Hemisphere troposphere.

2. EXPERIMENTAL METHODS

The research aircraft, the NCAR Sabreliner, is a small, twin engine jet, the capabilities of which are described by Pickering et al. (1989) and Luke et al. (1992).

Ozone was measured with a modified UV absorption instrument that gives a response time of about 10 s (Model 49, ThermoEnvironmental Corp. Franklin, MA). Water vapor was measured with a liquid nitrogen-cooled dew point detector developed at NCAR (Spyres-Duran, 1990).

Nitric oxide was measured by chemiluminescence (Dickerson et al., 1984) with a detection limit ($\pm 2\sigma$) of about 10 ppt (parts per 10^{-12} by volume) for a 20 s integration time. Total reactive nitrogen, NO_y , is detected by reduction to NO on $375^\circ C$ Mo. The converter housing, attached directly to the top of the aircraft, has a very short (ca 5 cm) quartz inlet that prevents loss of reactive species such as HNO_3 (Luke et al., 1992).

Carbon monoxide, CO , was measured by IR absorption (Dickerson and Delany, 1988) that provided a detection limit ($\pm 1\sigma$) of about 12 ppb (parts per billion by volume) with a response time of 60 s. For the low mixing ratios encountered in the stratosphere, several 1-min values were averaged together. Mixing ratios were corrected for a 1.4% interference from ozone. Nonmethane hydrocarbons (NMHC), were measured in grab samples taken during the flights. These samples were later analyzed by gas chromatography with a flame ionization detector (Greenberg and Zimmerman, 1984). The NO_2 and O_3 photolysis rate coefficients were derived from Eppley UV radiometer signals as described by Dickerson et al. (1982). Experimental uncertainty is discussed in the Appendix.

3. RESULTS

The aircraft experiment described here was conducted as part of the North Dakota Thunderstorm Project (NDTP) with the primary objective of understanding convective clouds. On two ferry flights between NCAR/RAF in Broomfield, CO and Bismarck, ND, and on three flights over North Dakota we were able to characterize the air in the upper troposphere and lower stratosphere (Fig. 1). North Dakota is frequently located north of the jet stream where the tropopause is relatively low and stratospheric intrusions are common.

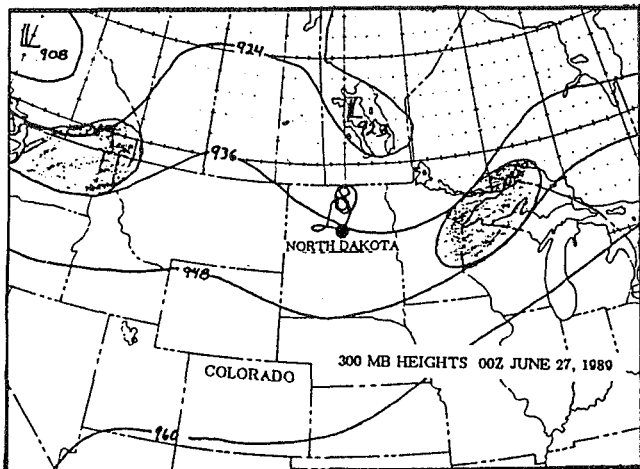


Fig. 1. Analysis of 300 mb heights (dm) for 00 UCT 27 June 1989. Operations were based in Bismarck, ND (indicated by a filled circle). The flight track for R7, conducted between 1612 and 1838 CDT (2112 and 2338 UCT) June 26, 1989, is shown north of Bismarck. The jet stream is indicated by the shaded areas. Skies over the flight region were cloud-free at this time -- note the region of upper level divergence over Montana.

The flight conducted on June 26, 1989 provides a good case study. Four constant-altitude legs were flown to the north of Bismarck (Fig. 1). Above the tropopause, located at about 10.5 km, O_3 and NO_y showed a rapid increase, reflecting strong sources in the stratosphere. Water vapor and carbon monoxide showed the opposite effect, reflecting their origin at the Earth's surface (Table 1). In the upper troposphere leg (260 mb), the NO and CO mixing ratios are relatively high. A thin cirrus cloud was present just below this altitude, suggesting outflow from a thunderstorm upstream. Examination of flow fields and radar summaries confirms the existence of convective clouds over the northwestern US at the appropriate time.

Details of the flight leg at 216 mb (11.3 km) show considerable variation in potential temperature (Θ), O_3 , and dew point with time, even though the altitude was constant to within about 20 m (Fig. 2). Ozone and Θ are positively correlated, and dewpoint is anticorrelated. This shows that transport of air occurs more along levels of constant potential temperature (entropy) than along constant altitude, (e.g. WMO, 1986). Even the fine structure shows the strong correlative nature of these three variables. Each symbol represents a 10-s average, and the peak at 17:20 has a half width corresponding to about 1.5 km.

Correlation coefficients for all level flight legs (Table 2) generally show that species with an origin in the stratosphere, O_3 and NO_y , have strong positive correlations with each other and with Θ .

TABLE 1. MEAN PROPERTIES OF THE ATMOSPHERE MEASURED NEAR THE TROPOPAUSE

Pres. mb	Date mo/day	Temp. K	Θ K	H_2O ppmv	CO ppb	NO ppb	NO_y ppb	O_3 ppb	Alt. km
198	6/13	221.9	352.6	21	37	0.188	NA	454	11.3
198	6/26	221.4	351.5	6.5	34	0.189	5.15	417	11.8
216	6/26	219.3	340.0	24	76	0.202	3.75	236	11.3
217	6/13	228.2	338.6	80	55	0.180	NA	267	11.3
218	6/12	219.5	339.1	NA	75	0.330	2.54	182	11.2
237	6/26	219.8	331.6	41	113	0.163	1.52	128	10.7
238	6/30	229.4	345.5	31	83	0.100	4.49	171	10.7
238	6/22	227.3	342.4	8	38	0.093	0.51	383	10.7
239	6/13	217.4	327.4	80	113	0.151	4.86	88	10.7
260	6/26	223.1	328.3	55	119	0.309	1.51	88	10.1
359	6/13	240.8	322.7	336	119	0.016	2.84	66	7.9
376	6/22	237.1	313.6	130	101	0.032	2.43	56	7.6

Dates are month/day of 1989. Each entry represents a flight segment of approximately 20 min. duration.

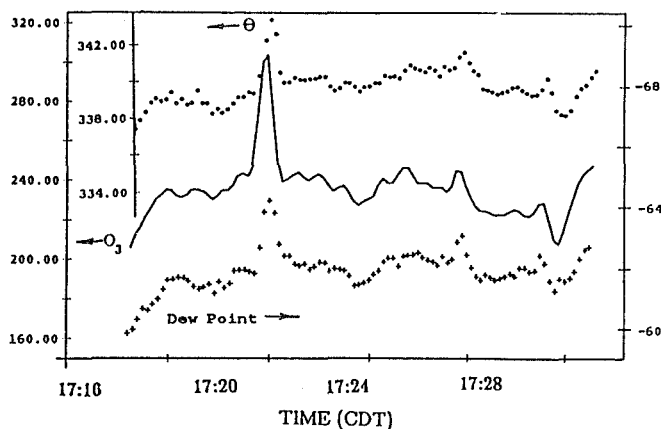


Fig. 2. Time series of in lower stratosphere June 26, 1989 at a constant altitude of 11.29 ± 0.02 km (216 mb) about 800 m above the tropopause. Equivalent potential temperature (top) in K, with the scale on the insert. Ozone, continuous line in middle, in ppb. Dew point, bottom in $^{\circ}C$; note sign. These results demonstrate that potential temperature rather than altitude defines chemically coherent layers in the lower stratosphere.

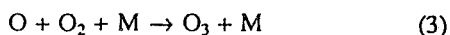
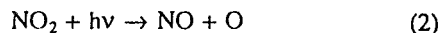
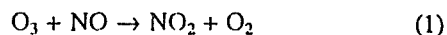
TABLE 2. CORRELATION COEFFICIENTS FOR FLIGHTS NEAR THE TROPOPAUSE

	H_2O	CO	NO	NO_y	O_3
Θ	-.60	-.76	.37	.48	.85
H_2O		.53	-.60	-.18	-.55
CO			-.12	-.83	-.95
NO				-.40	.19
NO_y					.76

Species with an origin at the Earth's surface, CO and H_2O , show a positive correlation with each other, but a negative correlation with Θ . Both the stratosphere and lightning are strong sources for NO in this data set; if the points showing greatest NO production by lightning (260 mb on 6/26) are omitted, the NO/NO_y correlation coefficient changes from -0.40 to 0.04. The strongest correlation coefficient, -0.95, is observed for CO and O_3 . The product of the mixing ratios (in ppb) of CO and O_3 is remarkably constant at about 15×10^3 ; analysis of stratospheric data reported by Hipskind et al. (1987) shows the same value.

4. DISCUSSION

In order to calculate the fraction of NO_y in the form of NO_x , we must convert measured concentrations of NO into NO_x . This is achieved through the assumption of a photostationary state in which the following reactions dominate.



Ozone and NO are measured directly, thus we can express NO_x as follows.

$$[\text{NO}_x] = [\text{NO}] + \frac{k[\text{NO}][\text{O}_3]M}{j(\text{NO}_2)} \quad (\text{E1})$$

Where k is the rate coefficient for Reaction 1 ($2.0 \times 10^{-12} e^{-1400/T} \text{ cm}^3 \text{ s}^{-1}$); the ambient temperature, T , is measured directly. The coefficient for NO_2 photolysis, $j(\text{NO}_2)$, is obtained from the output of upward- and downward-looking Eppley UV radiometers (Dickerson et al., 1982).

Our observations (Table 3) can be profitably compared to those obtained on the Airborne Arctic Stratospheric Expedition (AASE). We observed stratospheric NO_x mixing ratios range from about 0.17 to 0.44 ppb. Carroll et al. (1990) measured fairly constant stratospheric mixing ratios of 0.10 ppb during winter near 40°N , and even less in the Arctic.

TABLE 3. RATIOS OF REACTIVE NITROGEN TO OZONE MEASURED NEAR THE TROPOPAUSE

Pres. mb	Date mo/day	$j(\text{NO}_2)$ $\text{s}^{-1} \times 10^3$	NO_x ppb	NO_x/NO_y ppb/ppb	O_3/NO_x ppb/ppm	O_3/NO_y ppb/ppm
198	6/13	10.2	0.203	NA	0.65	NA
198	6/26	11.6	0.346	0.067	0.83	12.3
216	6/26	12.0	0.206	0.079	1.25	15.9
217	6/13	18.4	0.238	NA	0.89	NA
218	6/12	13.3	0.441	0.173	2.42	13.9
237	6/26	12.0	0.209	0.137	1.66	12.0
238	6/30	5.5*	0.205	0.046	1.20	26.3
238	6/22	15.2	0.168	0.018	0.44	25.0
239	6/13	19.3	0.168	NA	1.92	NA
260	6/26	12.6	0.378	0.250	4.29	17.2
359	6/13	19.2	0.019	NA	0.29	NA
376	6/22	14.4	0.040	0.016	0.71	43.6

See text for explanation of how NO_x is calculated.
*Zenith angle greater than 80° and $j(\text{NO}_2)$ highly uncertain.

On the NDTP, NO_y values range from about 1.5 to 9.5 ppb. On AASE Kawa et al. (1990) measured 1-2 ppb at similar potential temperatures near 60°N in December. Hübner et al. (1990) measured 1.5 to 1.9 ppb NO_y with occasional excursions to over 10 ppb attributed to nitric acid-containing falling from above. Kondo et al. (1990) measured 2 to 3.5 ppb at about 15 km ($\Theta = 380 \text{ K}$).

Ratios of trace gas concentrations can also be instructive. If we consider only flights on the cyclonic side of the jet stream, and clearly in the stratosphere as indicated by ozone mixing ratios above 100 ppb, we arrive at the following mean (median) ratios.

$$[\text{NO}_x]/[\text{O}_3] = 0.83(.89) \text{ ppb/ppm}$$

$$[\text{NO}_y]/[\text{O}_3] = 14.9(13.9) \text{ ppb/ppm}$$

$$[\text{NO}_x]/[\text{NO}_y] = .075(.079) \text{ ppb/ppb}$$

The range of values for the NO_x ratios is about a factor of two, while that for NO_y is about 30%. On the AASE project, stratospheric NO_x/NO_y ratios measured near 40°N were very similar to those reported here. Both data sets show higher ratios in the troposphere, and AASE showed lower ratios in the Arctic. AASE ratios of NO_y/O_3 , however, were lower (4 to 10 ppb/ppm) than those observed in the NDTP.

More NO_x in the mid latitude summer than in the Arctic winter is expected due to more active photochemistry. Higher NO_y , however, cannot be explained on the basis of stratospheric photochemistry. The origin of the relatively high NO_x and NO_y concentrations observed in the lower stratosphere on the NDTP may be the active convection characteristic of summer on the Great Plains. As evidence, consider the water vapor mixing ratios (Table 1.). In AASE the mean value was near 5 ppm, typical of the stratosphere (WMO, 1986), but on the NDTP, water vapor mixing ratios were several times higher. The injection of NO must have occurred a day or more before we sampled the air, because under these conditions the lifetime of NO_x with respect to HNO_3 is about a day, and the observed ratio of NO_x/NO_y is not unusually high.

The NO_y is unlikely to result from upward transport of polluted boundary layer air — the CO levels were typical of the stratosphere. Hydrocarbon levels were likewise low; on the 11.8 km (198 mfb) on 6/13 we detected ethane (0.320 ppt), propane (60 ppt), and *i*-butane (10 ppt). When high NO_y comes from convective transport of boundary layer air, CO and NMHC are elevated (e.g. Dickerson et al., 1987).

From the estimated flux of O_3 into the Northern Hemispheric troposphere of 4 to $8 \times 10^{10} \text{ molec. cm}^{-2} \text{ s}^{-1}$ we estimate the range of NO_x flux as 0.06 to $0.13 \text{ Tg(N) yr}^{-1}$, and the range of NO_y flux as from 1.1 to $2.2 \text{ Tg(N) yr}^{-1}$. These values exceed the rate of nitrogen fixation in the global stratosphere calculated by Kasibhatla et al. (1991) of $0.64 \text{ Tg(N) yr}^{-1}$, and may be inflated by lightning-produced NO . The results indicate clearly that downward transport of reactive nitrogen can be important for the photochemistry of the upper troposphere, but not for the lower troposphere over the continents or for nitrogen deposition to the continents.

5. CONCLUSIONS

- Θ , O_3 , and NO_y are positively correlated.
- CO and H_2O are anticorrelated with O_3 and Θ .
- High NO_x , NO_y , and H_2O concentrations were observed in the stratosphere on the cyclonic side of the jet stream.
- Implied NO_y flux into Northern Hemisphere troposphere is 1 to 2 Tg(N) yr^{-1} with 8% as NO_x ; this exceeds some estimates of global stratospheric NO_y production.
- Observed trace gas concentrations suggest that thunderstorms inject water and NO produced by lightning into the lower stratosphere.

ACKNOWLEDGMENTS

The authors wish to thank the NCAR RAF for support in this project, especially G. Kok who supplied the ozone instrument, P. Spyres-Duran who developed the cryogenic dew pointer, and V. Glover, M. Heiting, and J. Ragni for field-support. C. Selleck helped collect and analyze the data. G. Greenberg and P. Zimmerman per-

formed hydrocarbon analyses. This experiment was conducted as part of the NDTP (supported by NOAA, NSF, and USBR), and was supported primarily by NSF Grant ATM-86-19491. NCAR is supported by NSF.

APPENDIX: EXPERIMENTAL UNCERTAINTY

Several factors contribute to the uncertainty in the calculated $[\text{NO}_x]$. Our technique for calculating $j(\text{NO}_2)$ gives results equivalent within experimental uncertainty to those obtained using the technique described by Madronich (1987), however no direct calibration of radiometers with chemical actinometers has ever been performed for these conditions. We have ignored other species such as HO_2 that can oxidize NO to NO_2 , but these should play a relatively minor role in the lower stratosphere. Measurements of NO under field conditions carry an uncertainty of about $\pm 15\%$, and errors in the other factors in Equation 1 are small. Calculation of $j(\text{NO}_2)$ at the surface can be performed with an uncertainty of about $\pm 10\%$, but for our aircraft observations, the uncertainty is more likely $\pm 20\%$. The calculation of $[\text{NO}_x]$ is still robust, however, because NO is typically about 70% of NO_x ; an error of 20% in the estimate of $j(\text{NO}_2)$ would lead to an error of only about 7% in $[\text{NO}_x]$.

The estimated absolute accuracy (95% confidence) of the NO_y measurements in the stratosphere is about $\pm 30\%$. The molybdenum converter releases NO when first exposed to high levels of ozone, and the low ambient pressures reduce the flow and thus the sensitivity of the instrument. The estimated absolute accuracy in the CO measurements is ± 10 ppb or $\pm 5\%$ whichever is greater. Total uncertainty ($\pm 1\sigma$) in the reported frost points is ± 0.43 K (Spyres-Duran, 1990)

REFERENCES

- Carroll, M. A., D. D. Montzaka, G. Hübler, K. K. Kelly, and G. L. Gregory, 1990: In situ measurements of NO_x in the Airborne Arctic Stratospheric Expedition, *Geophys. Res. Lett.*, **17**(4), 493-496.
- Dickerson, R. R., D. H. Stedman, and A. C. Delany, 1982: Direct measurements of ozone and nitrogen dioxide photolysis rates in the troposphere, *J. Geophys. Res.*, **87**(7), 4933-4946.
- Dickerson, R. R., A. C. Delany, and A. F. Wartburg, Further modification of a commercial NO_x detector for high sensitivity, *Rev. Sci. Instr.*, **55**(12), 1995-1998, 1984.
- Dickerson, R. R. and A. C. Delany, 1988: Modification of a commercial gas filter correlation CO detector for enhanced sensitivity, *J. Atmos. Oceanic Tech.*, **5**, 3, 424-431.
- Fishman, J., 1985: Ozone in the troposphere, in *Ozone in the Free Atmosphere*, R. C. Whitten and S. S. Prasad, eds., Van Nostrand Reinhold, New York, 161-194.
- Greenberg, J. P. and P. R. Zimmerman, 1984: Non-methane hydrocarbons in the remote tropical, continental and marine atmospheres, *J. Geophys. Res.*, **89**(3), 4767-4778, 1984.
- Hipskind, R. S., G. L. Gregory, G. W. Sachse, G. F. Hill, and E. F. Danielsen, 1987: Correlations between ozone and carbon monoxide in the lower stratosphere, folded tropopause, and maritime troposphere, *J. Geophys. Res.*, **92**(2), 2121-2130.
- Hübler G., et al., 1990: Redistribution of odd nitrogen in the lower stratosphere, *Geophys. Res. Lett.*, **17**(4), 453-456.
- Kasibhatla, P. S., H. Levy II, W. J. Moxim, and W. L. Chameides, 1991: The relative impact of stratospheric photochemical production on tropospheric NO_y levels: A model study, *J. Geophys. Res.*, **96**(10), 18631-18646.
- Kawa, S. R., D. W. Fahey, L. C. Anderson, M. Loewenstein, and K. R. Chan, 1990: Measurements of total reactive nitrogen during the Airborne Arctic Stratosphere Expedition, *Geophys. Res. Lett.*, **17**(4), 485-488.
- Kondo, et al., 1990: Balloon-borne measurements of total reactive nitrogen, nitric acid, and aerosol in the cold Arctic stratosphere, *Geophys. Res. Lett.*, **17**(4), 437-440.
- Liu, S. C., D. Kley, M. McFarland, J. D. Mahlman, and H. Levy II, 1980: On the origin of tropospheric ozone, *J. Geophys. Res.*, **85**, 7546-7552.
- Luke, W. T., R. R. Dickerson, W. F. Ryan, K. E. Pickering, and L. J. Nunnermacker, 1992: Tropospheric chemistry over the lower Great Plains of the United States 2: Trace gas profiles and distributions, *J. Geophys. Res.*, **97**(18), 20,647-20,670.
- Madronich, S., 1987: Intercomparison of NO_2 photodissociation and UV radiometer measurements, *Atmos. Environ.*, **21**(3), 569-578.
- Murphy, D. M., D. W. Fahey, M. H. Proffitt, S. C. Liu, K. R. Chan, C. S. Eubank, S. R. Kawa, and K. K. Kelly, 1993: Reactive nitrogen and its correlation with ozone in the lower stratosphere and upper troposphere, *J. Geophys. Res.*, **98**(5), 8751-8773.
- Pickering, K. E., R. R. Dickerson, G. J. Huffman, W. T. Luke, and L. J. Nunnermacker, 1989: Clear-sky vertical profiles of trace gases as influenced by upstream convective activity, *J. Geophys. Res.*, **94**(12), 14,875-14,892.
- Spyres-Duran, P., 1990: The Airborne Cryogenic Frost Point Hygrometer Users Guide, NCAR-TN-347+IA.
- World Meteorology Organization, 1986: Atmospheric Ozone 1985, 1195 pp., Geneva.

STRATOSPHERE

TRENDS

PRECEDING PAGE BLANK NOT FILMED

LONG-TERM OBSERVED OZONE TRENDS IN THE FREE
TROPOSPHERE AND LOWER STRATOSPHERE*Julius London*Department of Astrophysical, Planetary, and Atmospheric Sciences,
University of Colorado, Boulder, Colorado 80309-0391

ABSTRACT

The vertical distributions of ozone trends in the free troposphere and lower stratosphere were derived from ozonesonde observations taken over an average period of ~20 years. The results for the annual trends show a consistent pattern of increased ozone of ~1%/yr to 2%/yr up to ~300 mb and decreased ozone of ~-0.6%/yr from ~100 to 50 mb.

Statistically significant positive trends found in mid-troposphere (~500 mb) at a set of representative stations in the Northern Hemisphere have little apparent seasonal variation. Negative trends are generally strongest at 50-70 mb with a tendency to be larger during spring. A highly significant negative trend of ~-5%/yr is found near 100 mb over Syowa (69°S) during spring.

INTRODUCTION

Documentation of the three-dimensional distribution of atmospheric ozone in the troposphere and lower to middle stratosphere and its time variations have been matters of some concern because of, among other things, its dominant role in regulating the UVB irradiance at the ground and its potential role in problems of climatic change (WMO, 1989; IPCC, 1990).

Direct measurements of the ozone concentration up to ~30 km have been made routinely with the aid of balloon-borne instruments since about 1962 (see, for instance, London and Liu, 1992). It has been shown from data derived from these ozonesonde measurements in the global observing network that during the past 20 or so years there has been a statistically significant negative annual ozone trend in the lower stratosphere and a positive trend in the mid-troposphere (e.g., WMO, 1989). Here, we discuss the annual and seasonal variations of these trends as observed at a few stations with relatively long periods of observations. The types of instruments used at these stations and the time periods of the observations up to 1988 are given in London and Liu (1992). In this paper the data set is generally extended to 1990.

The results from three different groups of stations are discussed below. These results are based on observations from two stations in Central Europe (Hohenpeissenberg and Payerne), a station in the Antarctic (Syowa), and a composite from four stations in Canada. In each case the annual and seasonal trends have been analyzed except for Syowa, where data were sufficiently available for analysis only for the spring season (i.e., September, October, and November).

DATA ANALYSIS

For the annual trends all observations for each month were averaged first, and then the 12 monthly values were averaged for each year. For the four quarterly trends all observations for each quarter were averaged separately for each year. Quarter 1 covered December, January, and February; quarter 2 covered March, April, and May, etc. For the four Canadian stations we assumed that the observed data were taken from a common population; therefore, all observations for monthly or quarterly periods were grouped together as a Canadian composite. The four Canadian stations for which there were relatively long periods of ozonesonde observations are Resolute (75°N, 1966-1990), Churchill (59°N, 1974-1990), Edmonton (53°N, 1973-1990), and Goose (53°N, 1970-1990). The starting period for each of the Canadian stations was different. The composite analysis period started in 1973, the year when three of the four stations were operative.

Ozonesonde observations from two representative European stations with long periods of available data sets were used. These stations are Hohenpeissenberg (48°N, 1967-1990) and Payerne (47°N, 1969-1988).

The only station in the Southern Hemisphere for which there is an available quasi-continuous set of measurements is Syowa (69°S, 1966-1990), and even here the observing series is adequate for analysis only during the spring (September, October, and November) season. Trends were calculated for 11 standard levels for which ozonesonde data are available from the World Ozone Data Center, Atmospheric Environment Service, Canada. Values from Payerne were interpo-

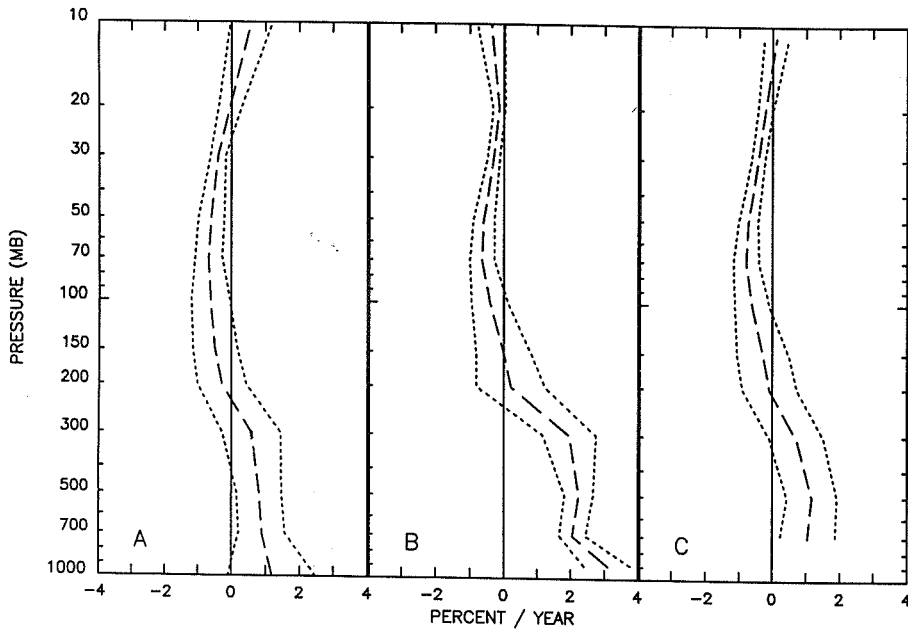


Fig. 1. Annual ozone trends.
 (A) Canadian composite, 1973-90.
 (B) Hohenpeissenberg, 1967-90.
 (C) Payerne, 1969-88.

lated to these levels from the mean layer data supplied to us by J. Staehelin.

RESULTS

Annual Trends

The annual ozone trends (dashed lines) are given in Fig. 1 for the Canadian composite (1973-1990), Hohenpeissenberg (1967-1990), and Payerne (1969-1988). The dotted lines represent the standard error ($\pm 2\sigma$) of the individual annual trend values for the periods as indicated. The vertical distributions of the annual trends for this representative set are very similar to other pub-

lished results, generally for shorter periods (e.g., Tiao et al., 1986; Wege et al., 1989; Staehelin and Schmid, 1991; Stolarski et al., 1992; McCormick et al., 1992).

Large, significant positive ozone trends of $\sim 1\%/yr$ to $2\%/yr$ are found in mid-troposphere (500-700 mb), and significant negative trends, $-0.6\%/yr$ to $-0.7\%/yr$, are found at 50-70 mb. The crossover from positive to negative trends occurs at a pressure level of ~ 200 mb, in the region of the diffuse tropopause layer at these latitudes. Inspection of the annual negative trends in the lower and middle stratosphere for each of the four Canadian stations (not shown here) indicates almost

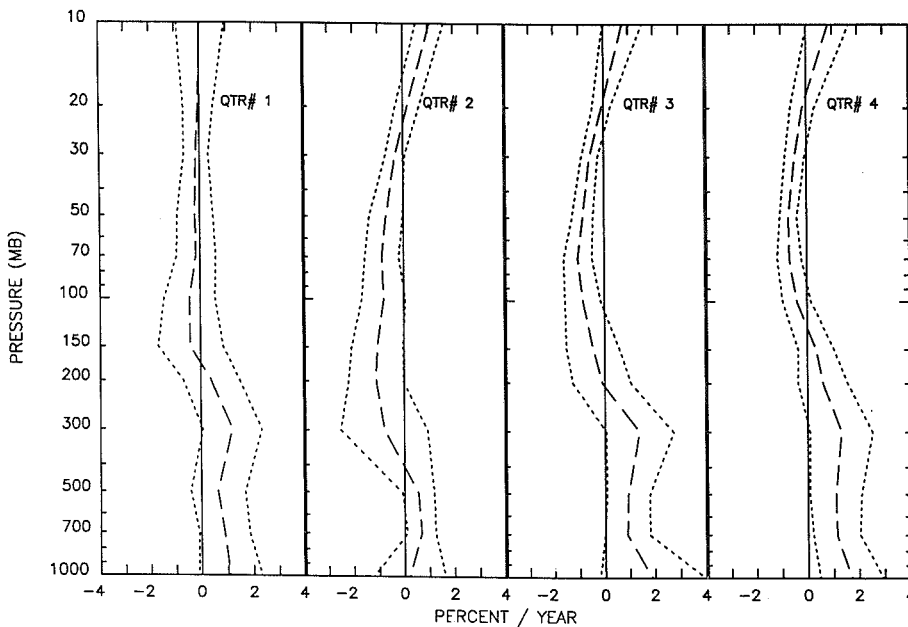
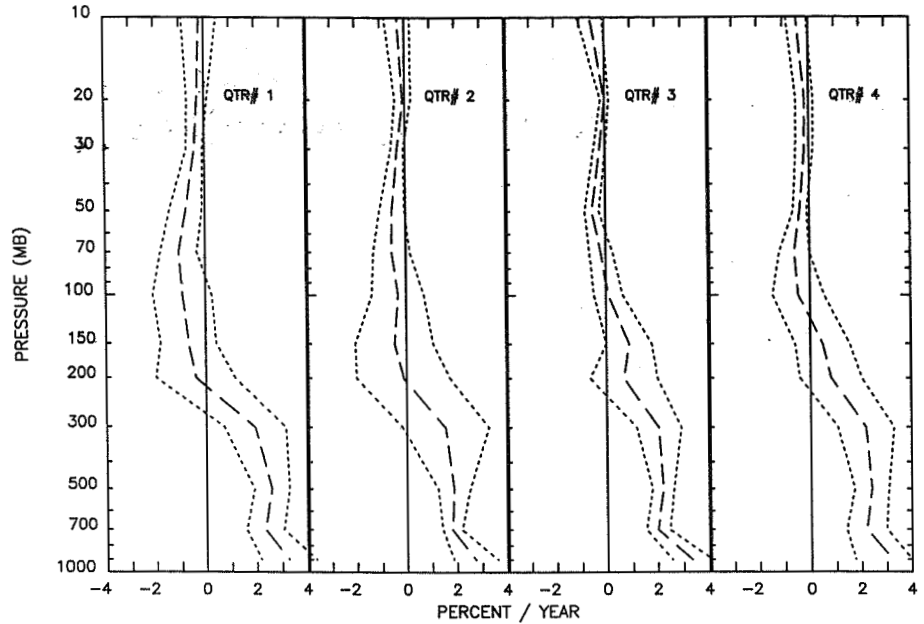


Fig. 2a. Ozone trends (quarterly), Canadian composite, 1973-90.

Fig. 2b. Quarterly ozone trends, Hohenpeissenberg (48°N), 1967-90.



the same values. However, the mid-tropospheric positive trends have some differences indicating year-to-year local influences, both chemical and dynamic, affecting the tropospheric trends. The largest standard errors associated with the trend values are generally found at the surface and in the upper troposphere at ~300 mb.

Seasonal Variations

The seasonal trends for the Canadian composite values are given in Fig. 2a. Although the ozone trends in the troposphere are positive (~1.0%/yr) during all seasons, the trends are just barely statistically significant.

There are, however, large significantly negative trends between 50 and 200 mb in spring and between 30 and 100 mb in summer and fall. Note that the ozone trends over Canada in winter (quarter 1) are close to zero. This is true for three of the four stations in the composite set. The crossover level from positive to negative trends varies with the seasons from ~175 mb during winter to 400 mb in spring and then to lower pressures (~125 mb) in fall similar to the seasonal shift of tropopause height at these latitudes.

The calculated seasonal trends for Hohenpeissenberg and Payerne (Figs. 2b, 2c) show very similar distri-

Fig. 2c. Quarterly ozone trends, Payerne (47°N), 1969-88.

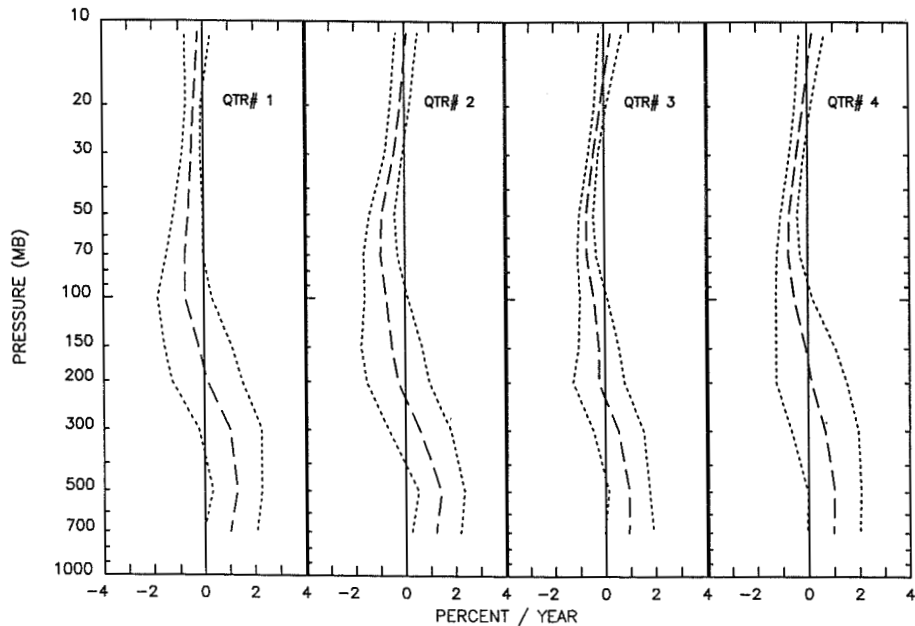
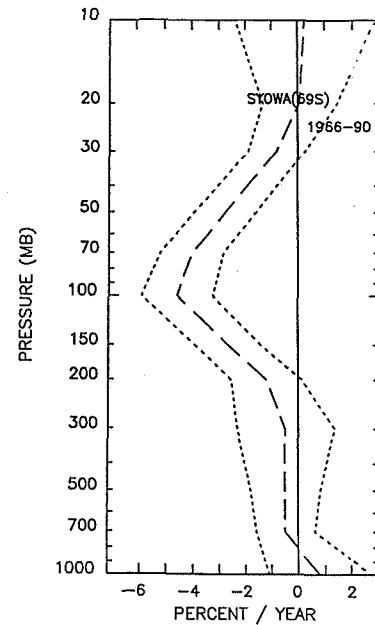


Table 1. Ozone Trends (% per year)

Level (mb)	Annual	Qtr. 1	Qtr. 2	Qtr. 3	Qtr. 4
Canadian Composite (1973 - 1990)					
Surface	1.19	1.10	0.21	1.89	1.70
700	0.88	0.88	0.68	0.90	1.12
500	0.81	0.64	0.58	0.94	1.09
300	0.58	1.20	-0.79	1.40	1.32
200	-0.28	0.40	-1.11	-0.10	0.60
150	-0.48	-0.40	-1.06	-0.45	0.34
100	-0.61	-0.43	-0.80	-0.85	-0.40
70	-0.67	-0.15	-0.86	-1.04	-0.69
50	-0.59	-0.20	-0.70	-0.85	-0.72
30	-0.39	-0.15	-0.32	-0.56	-0.46
20	-0.04	-0.06	0.17	-0.09	-0.15
10	0.59	0.03	1.09	0.77	0.86
Hohenpeissenberg (1969 - 1988)					
Surface	3.03	2.72	2.58	3.29	3.46
700	2.13	2.14	1.98	1.94	2.46
500	2.34	2.69	1.82	2.17	2.89
300	2.03	2.91	1.20	1.95	2.13
200	0.10	0.23	-0.33	0.60	0.35
150	-0.09	-0.41	-0.62	1.08	0.12
100	-0.39	-0.84	-0.20	-0.01	-1.04
70	-0.67	-0.81	-0.87	-0.14	-0.91
50	-0.61	-0.75	-0.74	-0.48	-0.58
30	-0.32	-0.48	-0.30	-0.19	-0.32
20	-0.23	-0.53	-0.13	0.00	-0.29
10	-0.51	-0.47	-0.45	-0.66	-0.40
Payerne (1969 - 1988)					
Surface	--	--	--	--	--
700	1.05	1.03	1.22	0.94	0.98
500	1.17	1.30	1.44	0.95	1.02
300	0.70	1.03	0.58	0.53	0.65
200	-0.09	0.11	-0.29	-0.25	0.13
150	-0.29	-0.24	-0.54	-0.25	-0.09
100	-0.61	-0.76	-0.75	-0.44	-0.53
70	-0.79	-0.76	-0.98	-0.71	-0.75
50	-0.73	-0.61	-0.91	-0.73	-0.72
30	-0.43	-0.49	-0.44	-0.44	-0.42
20	-0.22	-0.40	-0.18	-0.16	-0.17
10	0.11	-0.20	-0.10	-0.27	-0.19

Fig. 3. Quarter 4 ozone trends for Syowa (69°S), 1966-90.



butions particularly for the stratosphere. The positive trends in the troposphere found over Hohenpeissenberg are very strong, $\sim 2\%/yr$ to $3\%/yr$, and occur during all seasons. At Payerne, the positive trends are $\sim 1\%/yr$ and are barely significant. In both cases the maximum positive trends are found at ~ 500 mb during all seasons. In the stratosphere the strongest negative trends ($-0.9\%/yr$) occur during spring and fall over Hohenpeissenberg and during spring over Payerne.

The overall patterns of the ozone trends at mid-latitude and subpolar-latitude stations discussed above are generally consistent, but details of the seasonal variations show differences, particularly in the troposphere, that certainly reflect local influences.

Individual seasonal trend values are listed for the Canadian composite, Hohenpeissenberg, and Payerne in Table 1. The calculated trends for the Hohenpeissenberg and Payerne shown in Table 1 cover the same 20-year period (1969-1988) for comparison purposes. Note that there are no trend values given for the surface at Payerne. For the Canadian composite data, the largest positive annual trend is at the surface ($1.2\%/yr$), and the largest negative annual trend ($-0.7\%/yr$) is found in the stratosphere at 70 mb. The positive trends in the troposphere are significantly different from zero (2σ). In the stratosphere the negative trends are statistically significant (2σ) at levels from 30 to 100 mb. The largest positive trends occur during winter, summer, and fall and are generally found in mid-troposphere. Al-

though there are large positive trends indicated at the surface, they are frequently not statistically significant. Significant, negative trends in the stratosphere ($-0.7\%/yr$ to $-1\%/yr$) occur during spring, summer, and fall but not during winter. The trends are largest during spring, and the pressure level for the large negative trends decreases from 200 mb in spring to 50 mb in fall.

At Hohenpeissenberg the strong positive trends in the troposphere are present during all seasons of the year. In mid-stratosphere, however, the negative trend is just statistically significant (2σ) at 50-70 mb during spring and fall. The maximum positive trends at Payerne occur at ~ 500 mb and also do not show much seasonal variation. The negative trends in the stratosphere ($-0.7\%/yr$ to $-0.9\%/yr$) are again found at ~ 50 -70 mb. The seasonal variation of crossover level from positive to negative trends for Hohenpeissenberg and Payerne is similar to that found for the Canadian composite. This level occurs at the highest pressure generally during spring (or winter-spring as is the case for Hohenpeissenberg) and at the lowest pressure during fall (or summer-fall at Hohenpeissenberg). It is clear that the long-term patterns of ozone variations at these stations in mid-latitudes to polar latitudes of the Northern Hemisphere respond to different photochemical and dynamic influences in the troposphere and lower stratosphere (e.g., Liu et al., 1987; Austin et al., 1991).

Only one station in the Southern Hemisphere (Syowa, $69^\circ S$) has a sufficiently long period of available ozone-sonde observations to determine tropospheric and lower stratospheric trends. Even so the data set is adequate for only the spring season (September, October, and November) when the Antarctic ozone hole has become progressively more intense. The vertical distribution of the ozone trend at Syowa is shown in Fig. 3. The

trend in the troposphere is slightly negative but is not significantly different from zero, even at the 1σ level. It is important to note that the lack of a tropospheric ozone trend in the Antarctic region is in contrast to the strong positive trend in the troposphere found for Northern Hemisphere mid- and polar-latitude stations. This is an indication of the minimum effect of low tropospheric photochemical influences in the Southern Hemisphere at high latitudes far removed from precursor pollutant sources. In the stratosphere, however, the negative trend from 40 to 200 mb is everywhere statistically significant ($>2\sigma$) and at 100 mb reaches a value of $\sim -5\%/yr$.

CONCLUSIONS

Analysis of the long-term ozone data at mid- to polar-latitude stations of the Northern Hemisphere shows a distinct pattern of increasing ozone in mid-troposphere and decreasing ozone in the lower to mid-stratosphere. This pattern occurs during all seasons, but the stratospheric decreases seem to be larger and generally more significant during the spring. The crossover from positive to negative ozone trends occurs in the upper tropospheric and lower stratospheric regions at the time of the largest exchange between the two regions.

What are the associated atmospheric effects of these trends? The major ozone decreases in the stratosphere occur at levels of highest ozone concentrations. Thus the negative stratospheric trends are reflected in negative trends of total ozone. Also, it has been shown that the observed stratospheric ozone trends are associated with observed and calculated negative trends in temperature above ~ 15 km (e.g., Miller et al., 1992). It is clear that a total ozone loss will increase the transmittance of UV and visible irradiance to the surface and lower troposphere. However, the optical depth of ozone in the IR ($9.6 \mu m$) in the troposphere is relatively small as compared with the optical depth at the ozone peak. Thus, surface radiation to space would normally increase as the ozone peak gets thinner. On the other hand, if the lower tropospheric ozone concentration continues to increase, the downward irradiance in the IR window is increased, leading to a contribution to a greenhouse-type warming. Simple 1-D radiative equilibrium models using typical observed vertical distributions of ozone variations are best suited to test the effectiveness of these variations as potential greenhouse contributions.

ACKNOWLEDGMENTS

I thank Larry Morrison who made available corrected ozonesonde data archived by the World Ozone Data Center. I would also like to acknowledge the programming assistance given by Mary Eberle and Delbert Wagner. Support for this study was provided through the Upper Atmosphere Research Program of NASA under Contract No. NAS5-27263.

REFERENCES

- Austin, J. F., and M. J. Fellows, The Ozone Record at Payerne: An Assessment of the Cross-Tropopause Flux. *Atmospheric Environment*, 25A, pp. 1873-1880, 1991.
- IPCC, *Climate Change—The IPCC Scientific Assessment*, J. T. Houghton, G. J. Jenkins, and J. J. Ephraums (eds.). Cambridge University Press, Cambridge, U.K., 362 pp., 1990.
- Liu, S. C., M. Trainer, F. C. Fehsenfeld, D. D. Parrish, E. J. Williams, D. W. Fahey, G. Hübler, and P. C. Murphy, Ozone Production in the Rural Troposphere and the Implications for Regional and Global Ozone Distributions. *Journal of Geophysical Research*, 92, pp. 4191-4207, 1987.
- London, J., and S. C. Liu, Long-Term Tropospheric and Lower Stratospheric Ozone Variations from Ozonesonde Observations. *Journal of Atmospheric and Terrestrial Physics*, 54, pp. 599-625, 1992.
- McCormick, M. P., R. E. Veiga, and W. P. Chu, Stratospheric Ozone Profile and Total Ozone Trends Derived from the Sage I and Sage II Data. *Geophysical Research Letters*, 19, pp. 269-272, 1992.
- Miller, A. J., R. M. Nagatani, G. C. Tiao, X. F. Niu, G. C. Reinsel, D. Wuebbles, and K. Grant, Comparisons of Observed Ozone and Temperature Trends in the Lower Stratosphere. *Geophysical Research Letters*, 19, pp. 929-932, 1992.
- Stahelin, J., and W. Schmid, Trend Analysis of Tropospheric Ozone Concentrations Utilizing the 20-Year Data Set of Ozone Balloon Soundings over Payerne (Switzerland). *Atmospheric Environment*, 25A, pp. 1739-1749, 1991.
- Stolarski, Richard, Rumen Bojkov, Lane Bishop, Christos Zerefos, Johannes Stahelin, and Joseph Zawodny, Measured Trends in Stratospheric Ozone. *Science*, 256, pp. 342-349, 1992.
- Tiao, G. C., Reinsel, G. C., Pedrick, J. H., Allenby, G. M., Mateer, C. L., Miller, A. J., and DeLuisi, J. J., A Statistical Trend Analysis of Ozonesonde Data. *Journal of Geophysical Research*, 91, pp. 13121-13136, 1986.
- Wege, K., H. Claude, and R. Hartmannsgruber, Several Results from 20 Years of Ozone Observations at Hohenpeissenberg, in *Ozone in the Atmosphere*, R. D. Bojkov, and P. Fabian (eds.). A. Deepak Publishing Company, Hampton, Virginia, pp. 109-111, 1989.
- WMO, Scientific Assessment of Stratospheric Ozone, 1989. 1, *Global Ozone Research and Monitoring Project Report No. 20*, pp. 231-234, 1989.

**TREND
ANALYSIS OF THE LONG-TERM SWISS OZONE MEASUREMENTS**

Johannes Staehelin and Juerg Bader
Atmospheric Physics, ETH-Hoenggerberg
CH-8093 Zürich, Switzerland

Verena Gelpke
Statistics, ETH-Zürich,
CH-8092 Zürich, Switzerland

ABSTRACT

Trend analyses, assuming a linear trend which started at 1970, were performed from total ozone measurements from Arosa (Switzerland, 1926-1991). Decreases in monthly mean values were statistically significant for October through April showing decreases of about 2.0-4% per decade. For the period 1947-91, total ozone trends were further investigated using a multiple regression model. Temperature of a mountain peak in Switzerland (Mt. Säntis), the F10.7 solar flux series, the QBO series (Quasi Biennial Oscillation) and the southern oscillation index (SOI) were included as explanatory variables. Trends in the monthly mean values were statistically significant for December through April.

The same multiple regression model was applied to investigate the ozone trends at various altitudes using the ozone balloon soundings from Payerne (1967-1989) and the Umkehr measurements from Arosa (1947-1989). The results show four different vertical trend regimes: On a relative scale changes were largest in the troposphere (increase of about 10% per decade). On an absolute scale the largest trends were obtained in the lower stratosphere (decrease of approximately 6% per decade at an altitude of about 18 to 22 km). No significant trends were observed at approximately 30 km, whereas stratospheric ozone decreased in the upper stratosphere.

1. INTRODUCTION

A multiple regression model, similar to a previously used model by Bojkov *et al.*, 1990 and the OTP, 1989, was applied to calculate ozone trends from the long term Swiss ozone measurements. They include the world's longest total ozone series (Arosa), ozone balloon soundings (Payerne) and one of the most extensive data sets of Umkehr measurements (Arosa).

2. MEASUREMENTS

The total ozone series from Arosa (monthly mean values) adjusted to the Dobson world standard instrument (Hoegger *et al.*, 1992) was used.

The Umkehr measurements (wavelength pair C) have been processed using the program of Mateer (Mateer, 1965) and the aerosol correction of J. DeLuisi (pers. commun.).

The ozone balloon sondes (Brewer mast sondes) were launched from Thalwil (near Zürich) during the first 2 years (1967-1969) and thereafter from Payerne, which is about 200 km to the west of Arosa. Three ascents per week were planned from the beginning, the number of the successful ascents and their data quality is described in Staehelin and Schmid, 1991.

3. TREND ANALYSES OF TOTAL OZONE

We first present the results of a trend model which only includes total ozone (monthly means) using a linear trend which started at 1970.

$$Y_t = \mu + \sum_{i=1}^{i=12} \mu_i I_{it} + \sum_{i=1}^{i=12} \beta_i I_{it} R_t + N_t \quad (1)$$

Y_t : Ozone monthly mean at the month t

μ : overall mean of ozone

μ_i : deviation of ozone of the i -th month of the year from the overall mean; $\sum_i \mu_i = 0$

I_{it} : 1 if month t corresponds to i -th month of the year, otherwise 0

β_i : trend for the i -th month of the year

R_t : linear ramp function: $R_t = (t-t_0)/12$ if $t > t_0$ (t_0 : Dec. 1969) and 0 = if $t < t_0$

Summation goes over $i=1$ to 12.

The month to month correlation in ozone, which is present after the elimination of seasonal and other effects, was modelled by an autoregressive series of second order (AR(2)):

$$N_t = \phi_1 N_{t-1} + \phi_2 N_{t-2} + \epsilon_t \quad (2)$$

We first included in eq.(2) the values back to the sixth month, but the results showed that an AR(2)-model is appropriate to treat the data. We used maximum likelihood fitting of model (1) assuming Gaussian errors ϵ_t . The variances for each month were estimated, then model (1) was calculated again using weighted least squares. This procedure did not yield new results and was therefore not applied in the further calculations.

Fig. 1a shows the seasonal variation of total ozone at Arosa. The total ozone decrease is much stronger during winter time (see Fig. 1b). The results are consistent with results from more sophisticated models in which shorter time periods have been used (OTP, 1990, Bojkov *et al.*, 1990, Stolarski *et al.*, 1992).

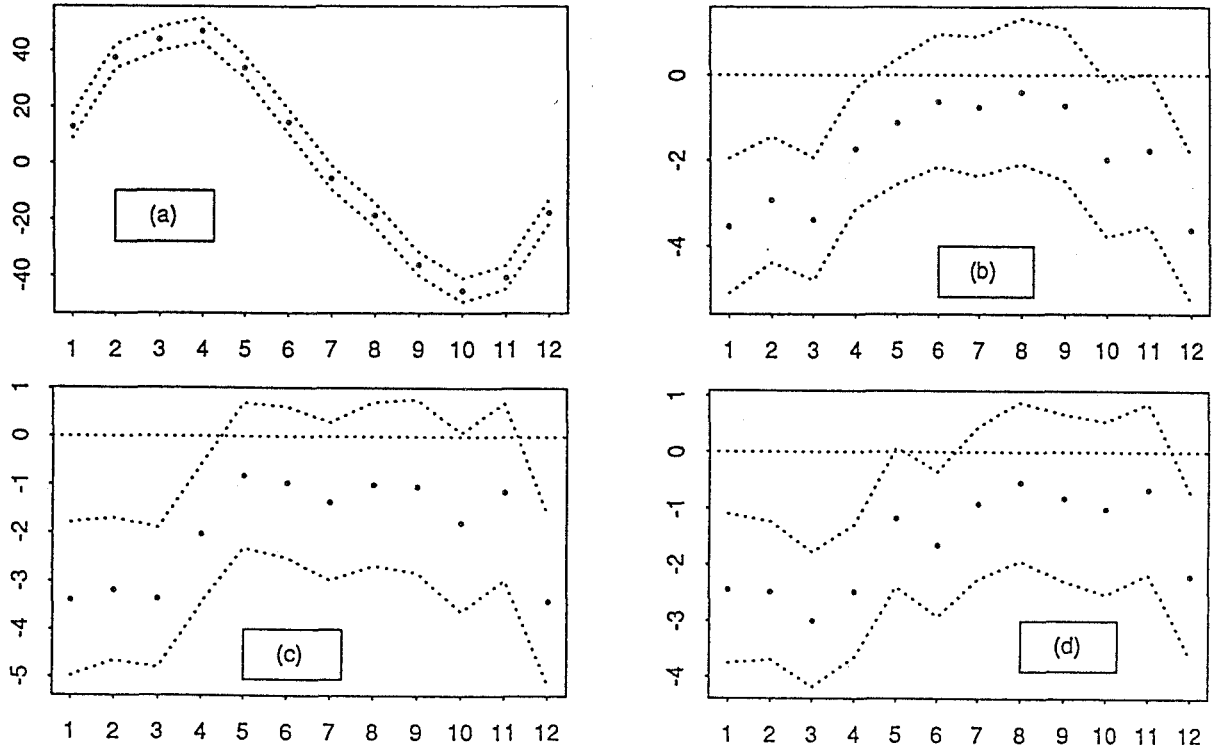


Figure 1: Total ozone series of Arosa. Labels of the abscissa: number of the calendar month. (a): Deviation of the monthly mean values (in D.U.) from the long-term annual mean value (332 D.U.). The dashed lines include the 95% confidence intervals of the monthly deviations. (b)-(d): Trends in the monthly mean values (in % per decade). The dashed lines include the 95% confidence intervals for the calculated trends which were assumed to start in Jan. 1970. (b): Model of eq. (1), ozone series 1926-91. (c): Model of eq. (1), ozone series 1947-91. (d): Model of eq. (3), ozone series 1947-91, including temperature of Mt. Säntis and the F10.7 solar flux as explanatory variables.

4. INFLUENCE OF EXPLANATORY VARIABLES

The following multiple regression model is an extension of the model described in Bojkov *et al.*, 1990. We added the SOI (Southern Oscillation Index, used e.g. by Zerefos *et al.*, 1992) and the temperature from a mountain peak in Switzerland representing the temperature in the free troposphere as potential explanatory variables. Because some variables were not available before 1957 the model was applied for the later measurements.

$$Y_t = \alpha + \sum_{i=1}^{i=12} \mu_i I_{it} + \sum_{i=1}^{i=12} \beta_i I_{it} R_t + \sum_{i \in K_1} \gamma_k \log(F10.7)_{t-k} + \sum_{i \in K_2} \delta_k T_{t-k} + \sum_{i \in K_3} \eta_k QBO_{t-k} + \sum_{i \in K_4} \xi_k SOI_{t-k} + N_t \quad (3)$$

Where:

Summation: $i: 1 \dots 12$ and $k: k \in K_i$

α : Intercept

$F10.7_{t-k}$: solar 10.7-cm flux series with time lag k and associated coefficient γ_k

T_{t-k} : deseasonalized temperature at Mt. Säntis with time lag k and associated coefficient δ_k

QBO_{t-k} : QBO time series with time lag k and associated coefficient η_k

SOI_{t-k} : Southern Oscillation Index series with time lag k and associated coefficients ξ_k

N_t : noise series, AR(2)

K_i ($i = 1 \dots 4$): Sets of time lags at which the different variables influence total ozone at Arosa

We tried to evaluate the appropriate time lags using the lagged regression model of Shumway (Shumway, 1988). Temperature influences ozone strongly with a time lag of zero. The calculations of the other variables did not indicate any clearly evident pattern of time lags. Some sensitivity runs, including different time lags of the explanatory variables, indicated that the QBO- and ENSO series did not significantly influence the results of the trend calculations. However, the F10.7 significantly influences total ozone at Arosa (time lag of 0 month). We therefore included in the calculations of total ozone trends temperature of Mt. Säntis and F10.7. The calculated trends of the period 1947-91 are stronger in May and June using model of eq (3) than model of eq (1), otherwise the results of the two models are very similar (see Fig. 1c and 1d).

Dütsch and Staehelin, 1989, have shown that the negative correlation between total ozone at Arosa and the temperature record of Mt. Säntis can be interpreted by the transport of ozone rich air masses from the polar region to midlatitudes by polar cyclones, i.e. regional weather influences. Dütsch *et al.*, 1992, have used a similar model including the total ozone from 1926 to 1989, the temperature of Mt. Säntis, and the solar cycle which was described by the sunspot number. In this study, the influence of the solar cycle on total ozone was statistically significant (at 5%) only if the temperature of Mt. Säntis was included in the analysis (1.26% or 4.4D from minimum to maximum of the solar cycle, in good agreement with previous studies of the worldwide Dobson network (WMO, 1989)).

5. RESULTS OF THE TREND ANALYSES CONSIDERING THE VERTICAL DISTRIBUTION OF OZONE

A similar type of multiple regression model (eq. (3)) was used to elucidate the vertical distribution of the trends. In a pre run the autocorrelations were calculated. Based on the results of the calculations of total ozone (see 4) we included the time lags of zero in this model. A strong dependency between the temperature at Mt. Säntis and ozone was found for most altitudes (see Fig. 2). The strongest signal of QBO was found for an altitude of approximately 22.5 km, which is about the altitude of the ozone maximum layer, where ozone concentration is most strongly influenced by the transport from the tropics. The influence of SOI on ozone concentration is generally weak, but noticeable at the altitude of about 19 km. Similarly, the influence of the solar cycle is weak for most altitudes and only weakly statistically significant at an altitude of about 30 km, which already has been described in Dütsch *et al.*, 1992.

Four different regimes of trends can be distinguished in the vertical (see Fig. 3a-3d):

- On a relative scale, changes are strongest in the troposphere showing strongly increasing ozone concentrations especially during the eighties (Staehelin and Schmid, 1991). This is most probably attributable to the tropospheric air pollution by nitrogen oxides, hydrocarbons and carbon monoxide.
- On an absolute scale trends are strongest in the lower stratosphere. In this region, ozone decrease was faster in winter (about 10% per decade), than in summer and in autumn (approximately 5% per decade). The altitude where the ozone decrease was strongest was at approximately 16 km in winter and at approximately 20 km during summer and autumn.
- No trends were observed at an altitude region of 30 km.
- The Umkehr measurements indicate decreasing trends of ozone in the upper stratosphere.

The trends in the upper stratosphere can be explained by the gas phase ozone destruction. However, at the altitude of the strongest stratospheric trends heterogeneous processes destroying stratospheric ozone are probably important.

ACKNOWLEDGEMENTS

The authors acknowledge the advise of H. Künsch (Sem. Statist., ETH-Z) and are grateful to W. Stahel and R. Dixon for reviewing the manuscript (Sem. Statist., ETH-Z). The authors further acknowledge the careful performance of the ozone measurements by the coworkers of the Swiss Meteorological Institute (SMI). We are grateful to C. Zerefos and L. Bishop for providing us the data of ENSO, QBO and F10.7.

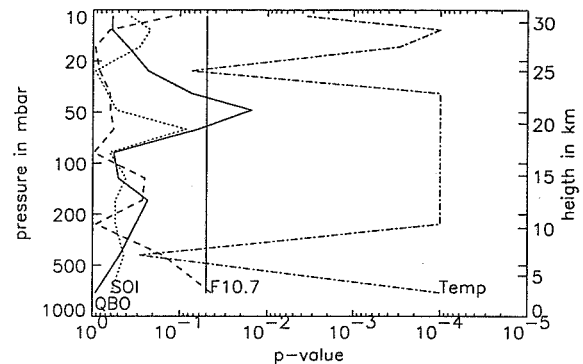


Figure 2: Significance, given as error probabilities (p-values), of the dependence of the ozone concentration on the used explanatory variables as function of the altitude. The p-value in this case is the probability that the standardized regression coefficient is smaller than the estimated value.

REFERENCES

- Bojkov, R., Bishop, L., Hill, W.J., Reinsel, G.C., and Tiao, G.C. (1990): A statistical trend analysis of revised Dobson total ozone data over the Northern Hemisphere, *J. Geophys. Res.*, **95**, 9785-9807.
- Dütsch, H.U. and Staehelin, J. (1989): Discussion of the 60 year total ozone record at Arosa based on measurements of the vertical distribution and a meteorological parameter, *Planet. Space Sci.*, **37**, 1587-1599.
- Dütsch, H.U., Bader J. and Staehelin, J. (1992): Separation of solar effects on ozone from anthropogenically produced trends, *J. Geomagn. Geoelectr.*, in press.
- Hoegger, B., Viatte, Levrat, G., Bader, J., Ribordy, P., Schill, H. and Staehelin, J. (1992): Quality control concept and recent developments of the Light Climatic Observatory at Arosa - Ozone measuring station of the Swiss Meteorological Institute (LKO), this conference.
- Mateer, C. (1965): On the information content of Umkehr observations, *J. Atmos. Sci.*, **22**, 370-381.
- OTP (1990): Report of the International Ozone Trends Panel: 1988, *World Meteorological Organization, Global Research and Monitoring Project Report*, No. 18, World Meteorological Organization, Geneva, Switzerland.
- Shumway, R.H. (1988): Applied statistical time series analysis, Prentice-Hall International Editions, p.203-213.
- Staehelin, J. and Schmid, W. (1991): Trend analysis of tropospheric ozone concentrations utilizing the 20-year data set of ozone balloon soundings over Payerne (Switzerland), *Atm. Env.*, **25A**, 1739-1749.
- Stolarski, R., Bojkov, R., Bishop, L., Zerefos, C., Staehelin, J., and Zawdony, J. (1992): Measured trends in stratospheric ozone, *Science*, **256**, 342-349.
- WMO (1989): Scientific assessment of stratospheric ozone, Vol.I, **165**, 194-234.
- Zerefos, C.S., Bais, A.F. and Ziomias, I.C. and Bojkov, R.D. (1992): On the relative importance of QBO and ENSO in the revised Dobson total ozone records. *J. geophys. Res.*, in press.

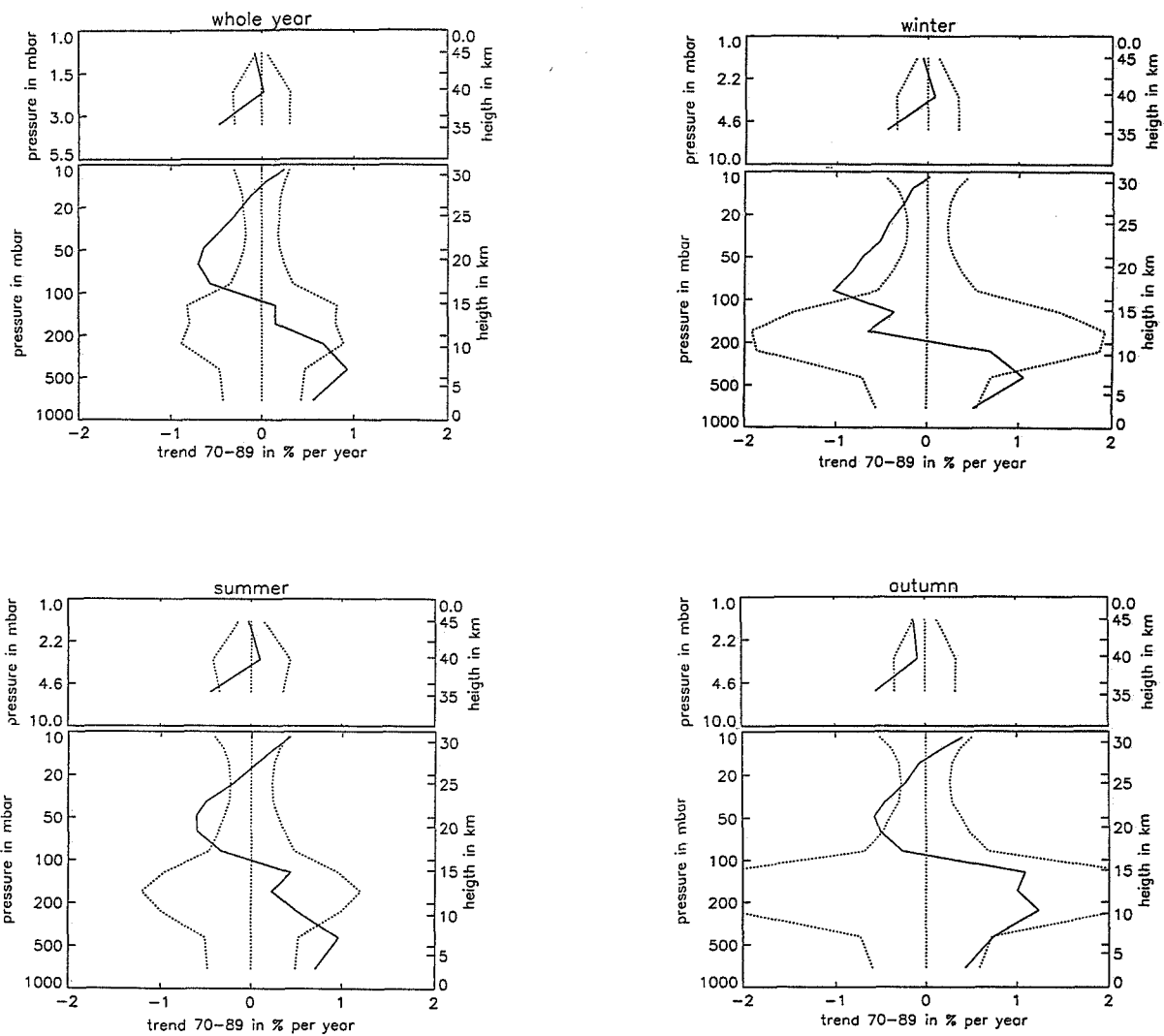


Figure 3: Trends for different altitudes deduced from the ozone balloon soundings from Payerne (1967-89) and the Umkehr-measurements from Arosa (1956-89), calculated using model of eq. (3). Trends are assumed to start on Jan., 1970. The dashed lines describe $\pm 2s$ (s is the standard deviation of the trends). Thus points outside the dashed line indicate trends, which are statistically significant according the t-test for regression coefficients approximately at the 5% level. a: Year around trends; b: Trends for winter (Dec. to March); c: Trends for summer (May to Aug.); d: Trends for fall (Sept. to Nov.).

303535

ON LONG-TERM OZONE TRENDS AT HOHENPEISSENBERG

H. Claude, W. Vandersee, and K. Wege

DWD, Meteorologisches Observatorium Hohenpeissenberg, Germany

ABSTRACT

More than 2000 ozone soundings and a large number of Dobson observations have been performed since 1967 in a unique procedure. The achieved very homogeneous data sets were used to evaluate significant long-term trends both in the troposphere and the stratosphere. The trend amounts to about +2% per year in the troposphere and to about -0.5% per year in the stratosphere.

Extremely low ozone records obtained during winter 1991/92 are discussed in the light of the long term series. The winter mean of the ozone column is the lowest one of the series. The ozone deficit occurred mainly in the lower stratosphere. One cause may be the Pinatubo cloud. Even compared with the extreme winter mean following the El Chichon eruption the ozone content was lower. Additionally ozone was reduced by dynamical effects due to unusual weather situations.

1. INTRODUCTION

The main goal of this paper is to investigate the long-term changes in ozone based on the Hohenpeissenberg long-time series. These time series have been examined in the past (*Attmannspacher* et al. 1984, *Bojkov* et al. 1990, *Wege* et al. 1989) and although the previously detected trends have been repeatedly confirmed, new investigations are nevertheless valuable. The data set has grown longer and the strength of the resulting conclusions is considerably more reliable. The statistical processes used allow a refinement of the almost 25-year data set so that the spatial and temporal course of ozone concentration can be more precisely examined. Further, an estimation of the low ozone concentration during winter 1991/92 is only possible in view of this long data set. The initial effects of the eruption of the Mount Pinatubo can certainly be demonstrated in this case. However the data can also be used to show that this volcanic eruption, the greatest of this century, cannot totally be responsible for the reduction in ozone concentration.

2. DATASET

Measurements of the vertical ozone have been made since 1967 with electrochemical Brewer Mast sondes on every Wednesday. Since 1977 the sounding frequency has been twice a week during the summer and three times a week during the winter. The careful pre-flight preparation of the sondes has never changed and is described in *Claude* et al. 1987. The measured ozone raw data has been corrected for decreasing pump efficiency and other sources of errors. The integrated column amount of ozone from each sounding was ratioed with the column amount measured by a Dobson spectrophotometer to calculate a correction factor, which has been applied to all ozone values. The so-called normalization is in any case an improvement of the ozone sonde data and identifies totally erroneous soundings. On the other hand a miscalibration of the Dobson instrument has an influence on the sonde data. A change in the absorption coefficients, for example, implemented on January 1, 1992, shifts the sonde data if this correction is applied. The Hohenpeissenberg data set is not completely free of such influences either, but great care has been taken in the past to minimize them. All total column ozone data are based on "the old" absorption coefficients according to *Vigroux*, so that both the total ozone data and the sonde data are very homogeneous.

Nevertheless, how much the applied Dobson normalization affects detected trends in an ozone data set requires clarification, whereby each of the over 2000 profiles used was an individual measurement. Figure 1 shows an inter-comparison of two such data sets with the vertical distribution of ozone trends 1967 - 1990 at Hohenpeissenberg. It is obvious that within the troposphere there is almost no difference between corrected and uncorrected data. The relative tropospheric trend is approximately +2.2% per year, significant at the 99.9% level. The largest difference between the normalized and the raw data appears within the lower stratosphere below the ozone maximum at 22 km. Within the stratosphere this is the range with the most pronounced trend amounting to approximately -0.5% per year.

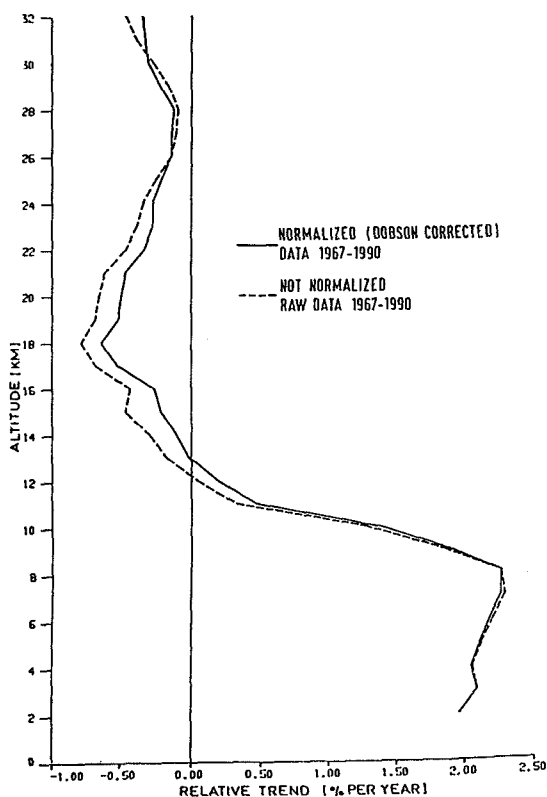


Figure 1: Mean trend profiles based on balloon sonde data.

The evaluation of the raw data reveals a very similar trend profile with a slightly stronger ozone decrease in that range. This examination shows that the fundamental trends in the Hohenpeissenberg sonde data are practically independent of the Dobson normalization. The following investigations are based on the normalized data.

3. TROPOSPHERIC OZONE

Time series of tropospheric ozone have been investigated repeatedly in the past (Logan 1985; Bojkov 1988; Staehelin and Schmid 1991). Almost without exception a trend of increasing ozone at rates of about 1% per year or more was found, most pronounced within the lower troposphere.

Figure 2 shows annual means at 2, 4, 6, and 8 kilometers a.s.l. above Hohenpeissenberg with corresponding regression lines from 1967 - 1990. The calculated correlation coefficients of ozone versus time are highly significant at between 0.94 and 0.96. The regression analysis reveals a significant increase of more than 2% per year throughout the whole troposphere. Compared with other stations this is one of the strongest tropospheric trends but it is in remarkable agreement with the +2.2% per year observed

at the summit of the Zugspitze (42 km south of Hohenpeissenberg, 2964m a.s.l.) for the period 1978 - 1989 (Schneider, 1992).

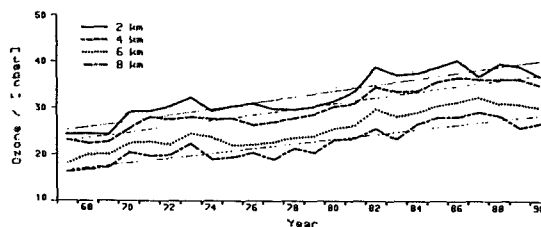


Figure 2: Annual means of ozone at different altitudes within the troposphere with regression lines.

About 50 years ago Ehmert (1949/50) described ozone measurements on an aircraft over Bavaria using Regener's (1938) potassium iodide method. The partial pressures of that time were between 2 and 9 nbar throughout the whole troposphere. Figure 3 shows an attempt to combine these observations with our tropospheric ozone records. The extrapolated regression lines of the corresponding present data agree with the very low ozone data of that time. Even if such intercomparisons are problematical because of uncertainties they point out that our strong tropospheric ozone increase might be the effect of a marked change in human activities within the last decades.

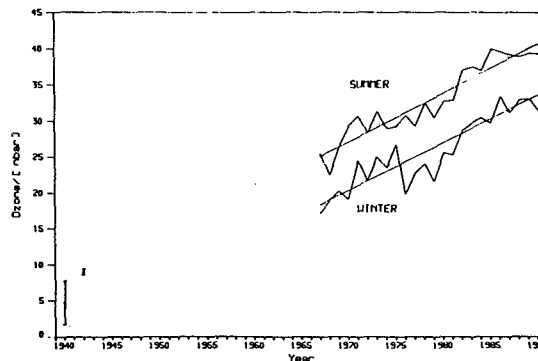


Figure 3: Course of tropospheric ozone at Hohenpeissenberg with regression lines extrapolated back to the forties when Ehmert performed measurements on aircraft.

4. STRATOSPHERIC OZONE

Figure 1 reveals the vertical trend distribution. Besides the tropospheric increase mentioned above, a stratospheric decrease clearly dominates. It is significant only between 17 and 25 km. In regard to the long term mean this -0.7 nbar per year corresponds to approximately -0.5% per year (Wege et al., 1989).

To gain more insight into the temporal and spatial course of the ozone trend, a dynamic trend analysis was performed (fig. 4). It was carried out by shifting a 10-year time span along the entire period year by year. The trend was calculated for each of these 10-year windows. Hatched and cross-hatched areas represent time-altitude ranges where trends are statistically significant at the 2 and 3 σ -level respectively. It reveals that stratospheric regions with significant trends are exposed to marked spatial and temporal changes. During the first years the largest decreases were observed below 26 km, prevailing at around 20 km and between 12 and 15 km.

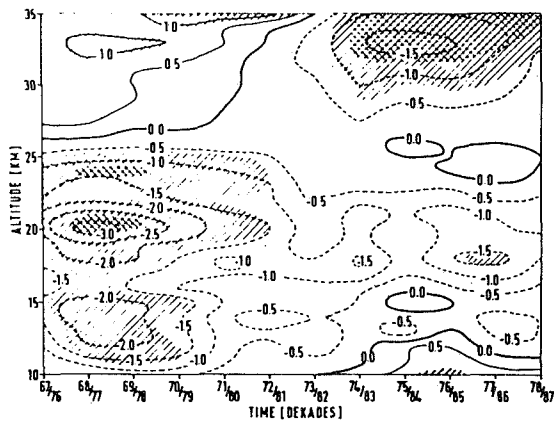


Figure 4: Time-height cross-section of the stratospheric ozone trends at Hohenpeissenberg. The units on the contours are nbar/year.

This decrease became smaller in the following years and reached significance only at the 2 σ -level in the period from 1977 to 1986 at approximately 18 km. The centre of ozone decrease seems to be shifted to higher altitudes at levels above 30 km. However, it must be considered that the sonde reliability decreases generally at those altitudes.

5. TOTAL COLUMN OZONE

The long-term series of total ozone measured with the Dobson 104 (fig. 5), exhibits a relative change of approximately -0.1% per year, i.e. almost no trend. Significance tests prove negative here. The reason for this lies in the counteraction of stratospheric ozone decrease by tropospheric ozone increase, which amounts to about 45% since 1967. That is, there has been a shift of the proportion of ozone between the stratosphere and the troposphere. Whereas in 1967 the tropospheric ozone made up only about 7% of the total ozone, the value today is 10%.

In addition figure 5 also displays a very pronounced year to year variability. For example the years 1975, 1983, and 1990 exhibit very conspicuous minima. The minima in 1975 and 1983 can almost certainly be connected with the volcanic eruptions of Fuego and El Chichon.

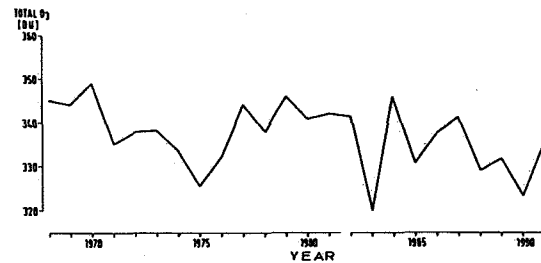


Figure 5: Course of total ozone based on annual means.

This connection can also be identified in the longer total ozone series from Arosa (Dütsch, 1984). The counteractions between volcanic products and ozone are not yet completely understood, possible causes for the reduction in ozone concentration could be:

1. direct ozone destruction due to injected chlorine.
2. heterogeneous processes involving long-living stratospheric aerosols.
3. dynamic processes due to the warming of the aerosol-loaded stratosphere, associated with a shift in the circulation pattern.

6. RECORD OZONE LOWS FOLLOWING THE MOUNT PINATUBO ERUPTION

During the whole of the winter of 1991/92 very low ozone values were measured at Hohenpeissenberg. This led, as figure 6 shows, to the lowest total ozone winter mean of the series, a decrease of about -9.7% compared with the long-term winter mean, and -1.6% lower than the minimal values of the winters of 1974/75, 1982/83, and 1989/90.

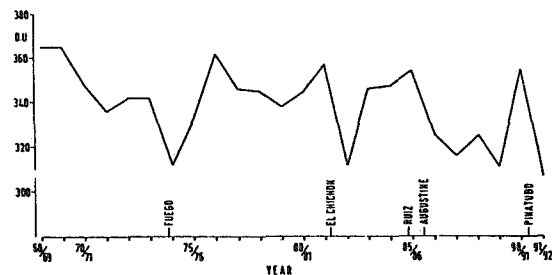


Figure 6: Course of total ozone winter means with marked volcanic eruptions.

The low values measured in the winter of 1989/90 and indeed the whole of 1990 (fig. 5) can hardly be directly related to a large volcanic eruption, unlike the other "minimal" years. It is doubtful whether the two weak volcanic events indicated have any appreciable influence.

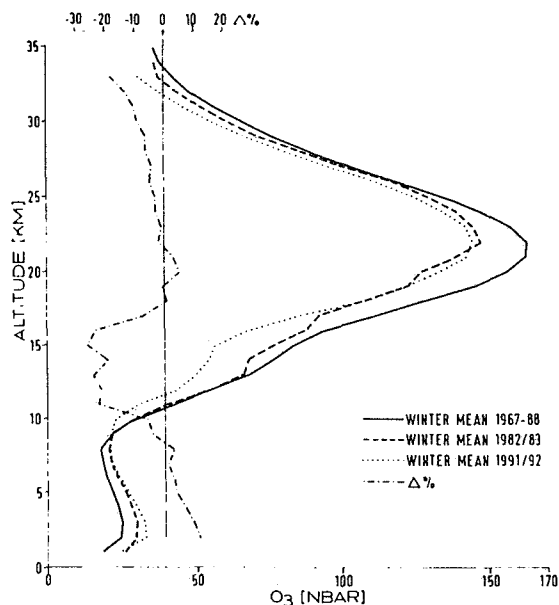


Figure 7: Mean ozone profiles for the winter months December - February and relative difference between winter 91/92 and 82/83.

Figure 7 shows the mean ozone profiles for several winters. As well as the long-term mean for 1967-88, the means for the winter of 1982/83 after the El Chichon eruption, and that for the past winter were chosen.

It is obvious that almost the complete ozone profile between 9 and 33 km for the last winter lies well below that of the long-term mean profile. Even compared with the extreme El Chichon winter, the ozone concentration was vastly reduced at most altitudes. This is pointed out by the relative difference profile $\Delta\%$, i.e., in the lower stratosphere between 11 and 16 km an especially great reduction of 20-30% compared to 1982-83 occurred.

Moreover, the altitudes above the main maximum show a conspicuous decrease compared to the winter of 1982/83. Because of the height this can hardly be attributed to a direct effect of Pinatubo aerosols. Here again the question arises as to other additional causes.

The soundings show, besides the extremely low ozone values, very low temperatures in almost the whole stratosphere. Figure 8 shows the temperature profiles analogously to the last figure. It can be seen that the past European winter was very unusual. Just as in the ozone profiles, the temperatures at altitudes between 9 and 33 km were very low, so that at an altitude of approximately 26 km a reduction in temperature of 5 K occurred. This is very extreme for a 3-month average.

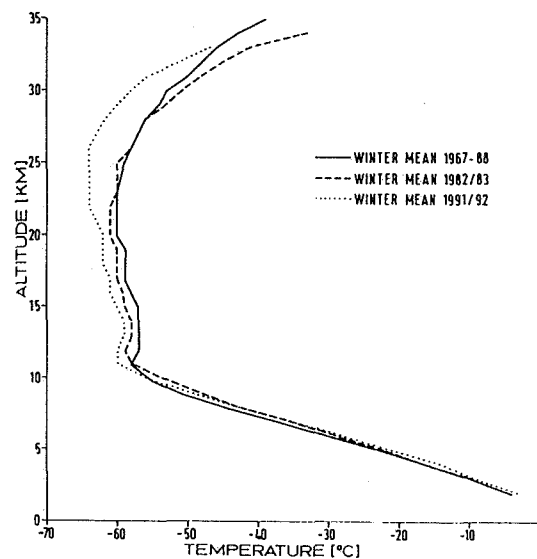


Figure 8: Mean temperature profiles for the winter months December - February.

Therefore, it must be assumed that, besides the direct ozone reduction by volcanic products, other ozone-reducing processes are involved, whereby the dynamic processes must be given primary consideration. The past winter has been distinguished by almost persistent pressure and temperature anomalies over vast areas of Europe (Geb and Naujokat, 1991/92). Because of the superimposition of the Pinatubo effects and the dynamic processes the individual causes cannot be separated or determined quantitatively. In addition it must be remembered that the long-term downwards trend in the stratosphere favours the minima. This trend might be the anthropogenic component of the observed stratospheric ozone loss over Europe during the last winter.

7. CONCLUSIONS

The long-term sounding data from Hohenpeissenberg exhibit pronounced ozone trends. Both increase in tropospheric ozone and decrease in stratospheric ozone are highly statistically significant. However, the long-term record of total column ozone shows practically no trend. The past winter is distinguished by record low values in both total column ozone as well as stratospheric ozone profiles.

The causes of this are recognized, however, the size of the effect of each cause cannot be determined. Nevertheless, it is certain that the eruption of Mount Pinatubo and abnormal dynamic processes played the dominant roles.

8. REFERENCES

- Attmannspacher, W., R. Hartmannsgruber, P. Lang, Langzeitendenzen des Ozons aufgrund der 1967 begonnenen Ozonmeßreihen am Meteorologischen Observatorium Hohenpeißenberg, Meteorol. Rdsch., 37, 193-199, 1984.
- Bojkov, R. D., Ozone Changes at the Surface and in the Free Troposphere, in: Tropospheric Ozone, Ed. Isaksen, I.S.A., 83-96, D. Reidel Publishing Company, 1988.
- Bojkov, R. D., L. Bishop, W. J. Hill, G. C. Reinsel, G. C. Tiao, A Statistical Trend Analysis of Revised Dobson Total Ozone Data over the Northern Hemisphere, J. Geophys. Res., 95, 9785-9807, 1990.
- Claude, H. J., R. Hartmannsgruber, U. Köhler, Measurement of Atmospheric Ozone Profiles Using the Brewer/Mast Sonde. Preparation, Procedure, Evaluation, WMO-Report No. 17, 1987.
- Dütsch, H. U., Total ozone trend in the light of ozone soundings, the impact of El Chichon, in: Atmospheric Ozone, Proc. Quadr. Ozone Symp., D. Reidel, P. 263-268, 1984.
- Ehmert, A., Über das troposphärische Ozon, Vorträge und Diskussionen anlässlich der Sondertagung "Ozon" am 17. und 18.04.1944 in Tharandt. in: Ber. d. Deutschen Wetterdienstes in der US-Zone, 2.Bd, 26-28, 1949/50.
- Ehmert, A., Über den Ozongehalt der unteren Atmosphäre bei winterlichem Hochdruckwetter nach Messungen im Flugzeug, Forschungs- und Erfahrungsberichte des Reichswetterdienstes No.13, 1941. in: Ber.d. Deutschen Wetterdienstes in der US-Zone, 2.Bd, 63-66, 1949/50.
- Geb, M. and Naujokat B., Beilagen zur Berliner Wetterkarte, Nordhemisphärische Klimaberichte, November 1991 - Februar 1992.
- Logan, J. A., Tropospheric Ozone: Seasonal Behavior, Trends, and Anthropogenic Influence, J. Geophys. Res., 90, 10463-10482, 1985.
- Regener, V. H., Messungen des Ozongehaltes der Luft in Bodennähe, Meteo. Z., 55, 459-462, 1938.
- Schneider, U., Die Verteilung des troposphärischen Ozons im bayerischen Nordalpenraum, thesis, Mainz 1992.
- Staelin, J., W. Schmid, Trend Analysis of Tropospheric Ozone Concentrations Utilizing the 20 Year Data Set of Ozone Balloon Soundings over Payerne (Switzerland), Atmos. Environ., 25A, 1739-1749, 1991.
- Wege, K., H. Claude, R. Hartmannsgruber, Several Results from 20 Years of Ozone Observations at Hohenpeißenberg, in: Ozone in the Atmosphere, Ed. Bojkov, R.D., P. Fabian, 109-112, Deepak Publishing, 1989.

**TOTAL OZONE TRENDS OVER THE U.S.A. DURING 1979-1991
FROM DOBSON SPECTROPHOTOMETER OBSERVATIONS**

Walter D. Komhyr, Robert D. Grass, Gloria L. Koenig
NOAA/ERL Climate Monitoring and Diagnostics Laboratory
Boulder, Colorado 80303

Dorothy M. Quincy, Robert D. Evans, R. Kent Leonard
Cooperative Institute for Research in Environmental Sciences
Boulder, Colorado 80309

ABSTRACT

Ozone trends for 1979-1991, determined from Dobson spectrophotometer observations made at eight stations in the United States, are augmented with trend data from four foreign cooperative stations operated by NOAA/CMDL. Results are based on provisional data archived routinely throughout the years at the World Ozone Data Center in Toronto, Canada, with calibration corrections applied to some of the data. Trends through 1990 exhibit values of -0.3% to -0.5% yr^{-1} at mid-to-high latitudes in the northern hemisphere. With the addition of 1991 data, however, the trends become less negative, indicating that ozone increased in many parts of the world during 1991. Stations located within the $\pm 20^\circ\text{N-S}$ latitude band exhibit no ozone trends. Early 1992 data show decreased ozone values at some of the stations. At South Pole, Antarctica, October ozone values have remained low during the past 3 years.

1. INTRODUCTION

NOAA's Climate Monitoring and Diagnostics Laboratory (CMDL) currently operates 16 Dobson spectrophotometer stations, some of which have records dating back to the early 1960's. Since inception of the program, all field instruments have been calibrated relative to a single "world standard" Dobson spectrophotometer No. 83, whose long-term ozone measurement precision has been maintained at better than $\pm 1\%$ [Komhyr et al., 1989]. Of the 16 operating stations, 4 are foreign cooperatives: Haute Provence, France; Huancayo, Peru; Lauder, New Zealand; and Perth, Australia. We present trend data for 12 of the stations for 1979-1991, a time interval approximating that of the operating interval of the National Aeronautics and Space Administration's TOMS and SBUV ozone spectrometers aboard the Nimbus 7 satellite. Also presented are total ozone data for South Pole, Antarctica, for October months of 1962-1991. Results are expressed in the new Bass-Paur [1985] ozone absorption coefficient scale adopted for use world-wide January 1, 1992 [Hudson et al., 1991]. The new scale yields ozone values about 2.6% smaller than did the Vigroux [1953] ozone absorption coefficient scale used during July 1, 1957-December 31, 1991.

absorption coefficient scale used during July 1, 1957-December 31, 1991.

2. OZONE TRENDS

Figures 1 and 2 plot total ozone anomaly data (i.e., monthly mean ozone deviations from monthly normals for the periods of record shown) for five stations on the United States mainland; two stations in Alaska; Mauna Loa Observatory, Hawaii; American Samoa, South Pacific; and three foreign cooperative stations. Data used in the analysis are provisional, archived at the World Ozone data Center in Toronto, Canada, except that Mauna Loa and Samoa data were provisionally reprocessed in the past through July 1987, and corrections of 0 to -1.7% were applied to Wallops Island data for May 1985 to September 1991 based on recalibration of the instrument in Boulder in 1991. (Provisionally reprocessed data have mean calibration corrections applied; additional small corrections that are air mass dependent may be necessary for portions of the record). Not used in the analysis are available data from Nashville, Tennessee, and Perth, Australia, which require re-evaluation, as well as data from Tallahassee, Florida, where observations were terminated in late 1989, but resumed in April 1992. Data shown in Figures 1 and 2 are de-seasonalized. No attempt has been made to remove from the data ozone variations due to the 11-year solar cycle, the Quasi-biennial Oscillation (QBO), and El Niño phenomena, or the effects of volcanic stratospheric aerosols.

Least squares linear regression lines fitted to the ozone anomaly data of Figures 1 and 2 through 1991 exhibit several interesting features. The two most northerly stations, Point Barrow and Poker Flat show non-significant downward ozone trends of -0.3 and -0.5% yr^{-1} , based on sparse data obtained during spring to autumn seasons of years when observations were made. Stations Bismarck, Caribou, Haute Provence Observatory, and Boulder, located between 40° and 50°N latitudes show downward ozone trends of about -0.4% yr^{-1} , statistically significant at the 95% confidence level (t-statistic) except in the case of the short Haute Provence Observatory record. At Wallops Island (38°N), the downward ozone trend

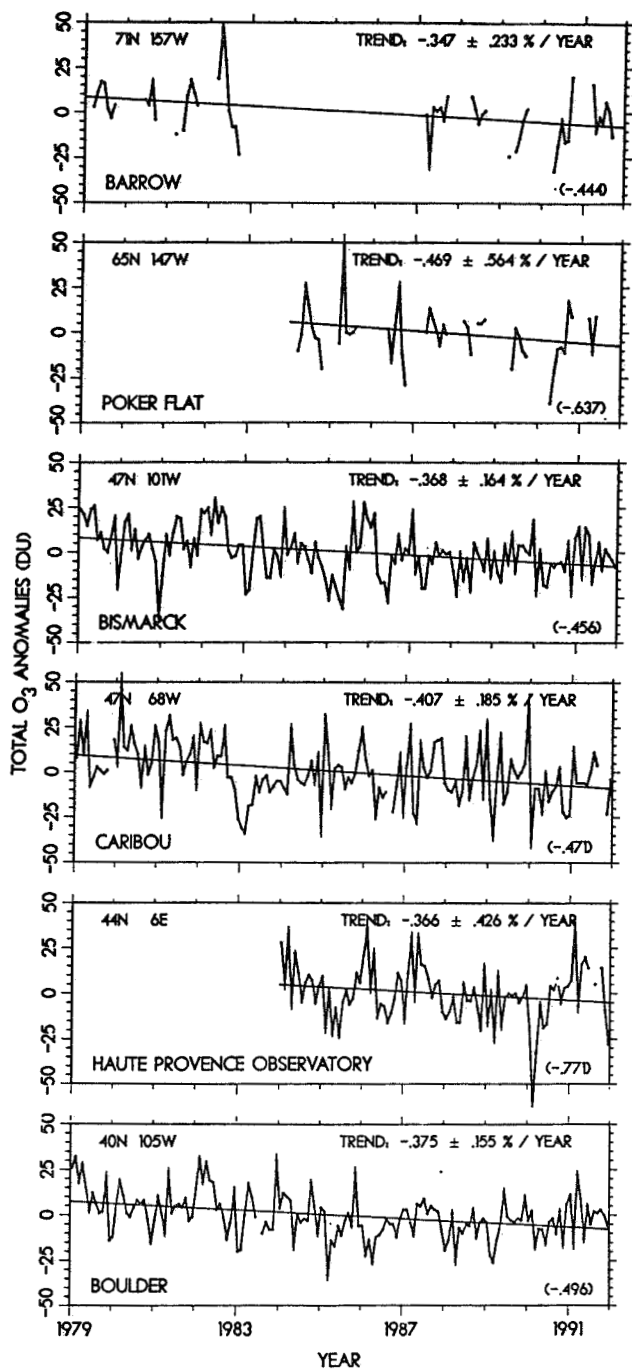


Fig. 1. Provisional total ozone anomaly data derived from Dobson spectrophotometer observations made at BRW, Poker Flat, Caribou, Bismarck, Boulder, and Haute Provence observatories. Least-squares linear regression lines are fitted to data obtained through 1991. Uncertainties in indicated ozone trends are 95% confidence intervals (t-statistic). The values in brackets in the lower right-hand corner of each plot is the ozone trend derived from data obtained only through 1990.

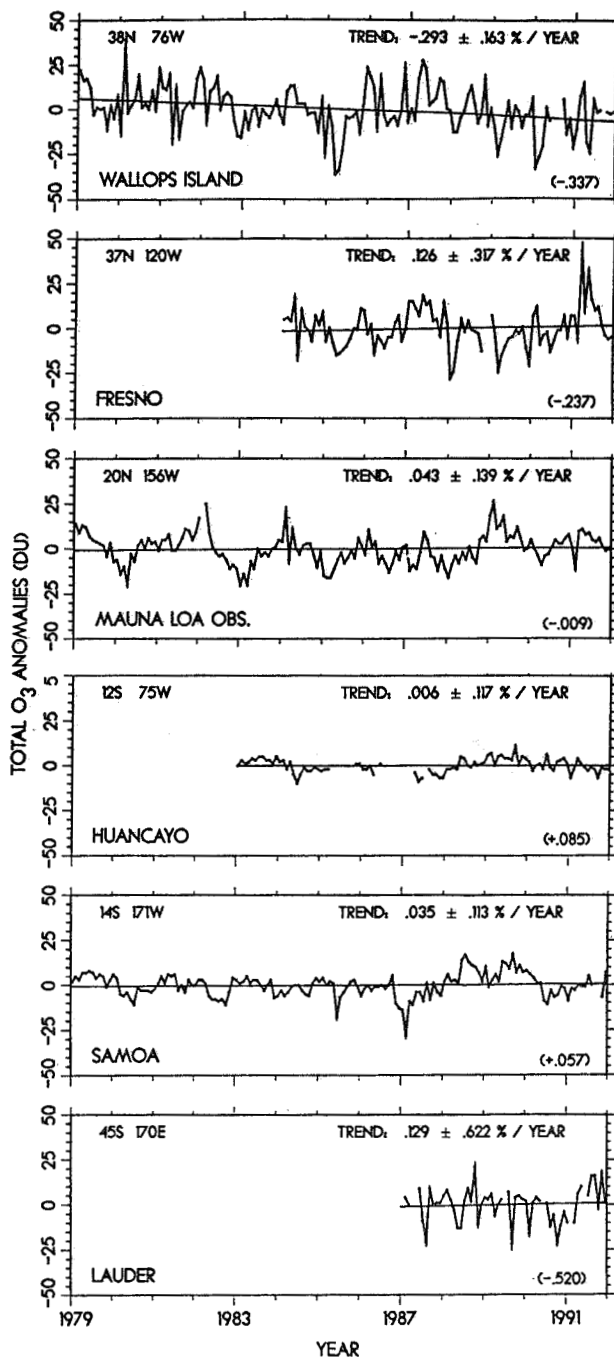


Fig. 2. Provisional total ozone anomaly data obtained from Dobson spectrophotometer observations made at Wallops Island, Fresno, MLO, Huancayo, Samoa, and Lauder. Least-square linear regression lines are fitted to the data obtained through 1991. Uncertainties in indicated ozone trends are 95% confidence intervals (t-statistic). The value in brackets in the lower right-hand corner of each plot is the ozone trend derived from data obtained only through 1990.

TABLE 1. Comparison of Ozone Trends Through 1990 and 1991, for Data Shown in Figures 1 and 2

Station	Lat./Long.	O ₃ Trend* (% yr ⁻¹) 1979-1991	O ₃ Trend* (% yr ⁻¹) 1979-1990
Pt. Barrow	71°N, 157°W	-0.35 ± .23	-0.44 ± .27
Poker Flat	65°N, 147°W	-0.47 ± .56	-0.64 ± .63
Bismarck	47°N, 101°W	-0.37 ± .16	-0.46 ± .19
Caribou	47°N, 68°W	-0.41 ± .19	-0.47 ± .21
Haute Prov.	44°N, 6°E	-0.37 ± .43	-0.77 ± .47
Boulder	40°N, 105°W	-0.38 ± .16	-0.50 ± .17
Wallops Is.	38°N, 76°W	-0.29 ± .16	-0.34 ± .18
Fresno	37°N, 120°W	+0.13 ± .32	-0.24 ± .33
Mauna Loa	20°N, 75°W	+0.04 ± .14	-0.01 ± .16
Huancayo	12°S, 75°W	+0.01 ± .12	+0.09 ± .14
Samoa	14°S, 171°W	+0.04 ± .11	+0.06 ± .13
Lauder	45°S, 170°E	+0.13 ± .62	-0.52 ± .80

*Indicated uncertainties are 95% confidence interval errors (t-statistic). The records are not all of uniform length.

TABLE 2. Percent Ozone Changes in 1992 January-April Monthly Means Relative to Monthly "Normals" Based on Data Records of Figures 1 and 2

Station	Latitude	1992			
		Jan.	Feb.	March	April
Pt. Barrow	71°N	-	-	-3.7	-2.5
Poker Flat	64°N	-	-	[-5.9]	-3.9
Bismarck	47°N	-1.7	-5.1	-4.6	-5.4
Caribou	47°N	-2.9	-7.1	-4.7	-2.4
Haute Prov.	44°N	[-11.8]	-4.0	-7.9	-3.6
Boulder	40°N	+2.4	-0.8	-3.0	-7.4
Wallops Is.	38°N	-1.6	-2.2	-2.3	-7.5
Fresno	37°N	+2.0	+1.6	+4.2	[-8.5]
Mauna Loa	20°N	-1.3	+4.7	+1.3	-0.4
Huancayo	12°S	-2.6	-1.3	[-2.1]	-
Samoa	14°S	+2.2	+2.7	+1.7	-2.5
Lauder	45°S	+3.4	+1.9	+3.4	-3.4

Values in brackets in the body of the table represent record ozone lows.

is about -0.3% yr⁻¹. Mauna Loa Observatory, Huancayo, and Samoa, located within the ±20°N-S latitude band, exhibit essentially zero trends in ozone. At Lauder (45°S), where the record length is only 5 years, the trend is slightly positive, through not statistically significant.

We are currently engaged in a program to reprocess total ozone data from our stations, with application of detailed instrument calibration corrections. Trends computed from recently reprocessed 1979-1991 data from Caribou, Fresno, and Wallops Island, are not different from values shown in Figures 1 and 2 by more than ±0.1% yr⁻¹.

Numbers in brackets in the lower right-hand corners of the plots of Figures 1 and 2 are the ozone trends computed only through 1990. Note that through 1990 (see also Table 1), computed trends are in most cases considerably more negative than trends determined through 1991. The large downward trend through 1990 at Haute Provence Observatory resulted largely from unusually low ozone values at Haute Provence in February 1990. Most stations (see especially Fresno and Lauder) show more ozone in 1991 than in 1990, indicating that ozone increased over many parts of the world in 1991.

Because of high ClO values reported at mid-to-high latitudes of the northern hemisphere in early 1992 [NASA headquarters, 1992], as well as possible ozone destruction by Mt. Pinatubo stratospheric aerosols, there has been considerable speculation about a possible increase in ozone depletion rate early in 1992. In Table 2, we present percent changes in ozone for the NOAA/CMDL station network for the months of January-April 1992 relative to "normal" values for these months derived from the data records depicted in Figures 1 and 2. Record low monthly means in Table 2 are denoted by bracketed percent changes in ozone. Thus, the March 1992 monthly mean total ozone at Poker Flat was nearly 6% lower than March values observed in the past, though this result may not be significant due to the sparsity of the Poker Flat data. The January 1992 Haute Provence Observatory ozone value was lower by nearly 12% than the average of 1984-1991 January values. (Contrast this with the Haute Provence February 1990 ozone mean (not shown) which was 18% lower than the 1984-1991 "normal" value). The Fresno April 1992 monthly mean ozone value was nearly 9% lower than the mean 1984-1991 April ozone value. But in 1991 (not shown), March total ozone was higher at Fresno than the 1984-1991 "normal" March value by 13%. Note also (Table 2) that relatively low ozone values occurred during April 1992 at Bismarck, Boulder, and Wallops Island. These resulted most likely from anomalous air flow patterns, which brought ozone-poor air from equatorial regions during April 1992 northward to higher latitudes.

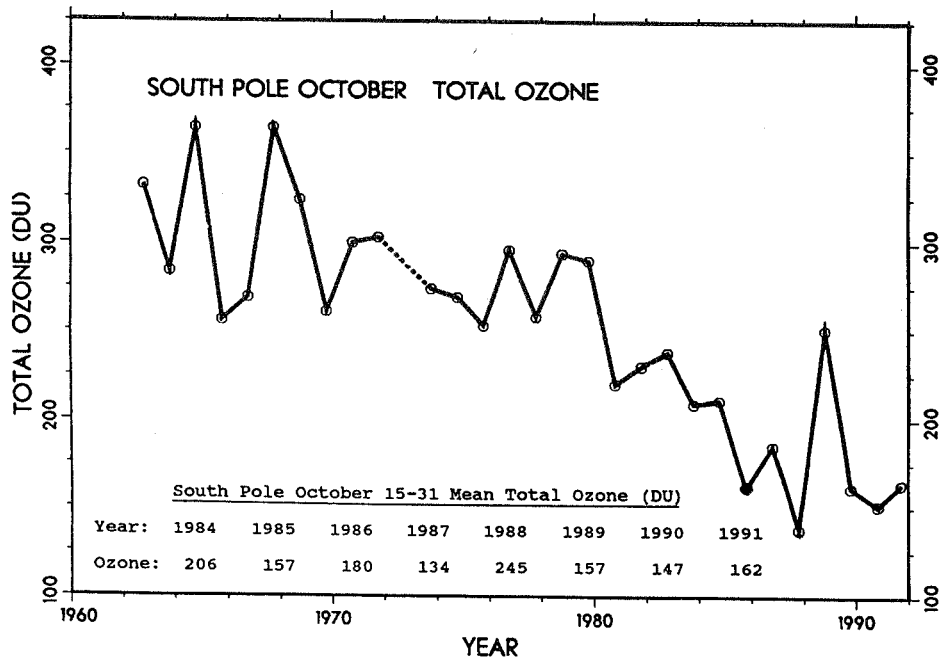


Fig. 3. South Pole mean total ozone amounts for October 15-31 time intervals of 1962-1991.

3. OCTOBER TOTAL OZONE AT SOUTH POLE

Figure 3 plots mean October 15-31 total ozone for South Pole, Antarctica, for 1962-1991. (October 15 is the time each spring when Dobson spectrophotometer observations first became possible following the polar night.) To date the record low October mean ozone value occurred at South Pole in 1987, though similar low ozone values occurred in succession also during the past 3 years. Komhyr et al. [1991] related low October South Pole total ozone values to anomalously warm sea surface temperatures in the eastern equatorial Pacific during June-August months. Considering that the current El Niño is still in progress, we expect a deep total ozone low at South Pole again in October 1992, barring undue atmospheric circulation perturbation effects by Mt. Pinatubo stratospheric aerosols.

4. ACKNOWLEDGMENTS

Appreciation is expressed to the observers at the various stations who made the observations throughout the years. Observations at the foreign cooperative stations of Haute Provence, Huancayo, and Lauder were conducted, respectively, under the supervision of Alain Barbe, Carlos Nickl Wanka, and W. Andrew Matthews.

REFERENCES

Bass, A.M., and R.J. Paur, The ultraviolet cross-sections of ozone, I. The measurements, in *Atmospheric Ozone*, edited by C.S. Zerefos and A. Ghazi, pp. 606-610, Reidel, Boston, 1985.

Hudson, R.D., W.D. Komhyr, C.L. Mateer, and R.D. Bojkov, Guidance for use of new ozone absorption coefficients in processing Dobson and Brewer spectrophotometer total ozone data beginning January 1, 1992, Ozone Commission of IAMAP (IUGG), Geneva, Switzerland, 6 pp., December 19

Komhyr, W.D., R.D. Grass, and R.K. Leonard, Dobson spectrophotometer 83: A standard for total ozone measurements, 1962-1987, *J. Geophys. Res.*, 94(D7), 9847-9861, 1989.

NASA Headquarters, End of Mission Statement Second Airborne Arctic Stratospheric Expedition AASE-II, 20 pp, 30 April 1992.

Vigroux, E., Contribution à l'étude expérimentale de l'absorption de l'ozone, *Ann. Phys.*, 8, 709-762, 1953.

Komhyr, W.D., S.J. Oltmans, R.D. Grass, and R.K. Leonard, Possible influence on long-term sea surface temperature anomalies in the tropical Pacific on global ozone, *Canadian J. Physics*, 69(8 and 9), 1093-1102, 1991.

**OZONE TRENDS ESTIMATED FROM UMKEHR OBSERVATIONS
MADE AT EDMONTON, ALBERTA, CANADA**

C.T. McElroy, E.W. Hare and J.B. Kerr

Atmospheric Environment Service
4905 Dufferin Street
Downsview, Ontario, M3H 5T4

ABSTRACT

A Brewer Ozone Spectrophotometer has been in service at the Canadian Ozone monitoring station at Stony Plain (53.55° N, 114.10° W), near Edmonton, Alberta, since 1984. During that time, the instrument has been operated in a fully automated mode that includes the collection of morning and evening Umkehr observations. Some 197 Umkehr observations have been analyzed to make an estimate of the temporal trend in ozone amount at high altitude over the station during the last 8 years. This work has shown that at 40 km the trend in the ozone concentration has been observed to be 0.14±0.10 percent per year.

1 INTRODUCTION

Trends in the global ozone amount have been estimated by several independent methods. These have included the estimate of trends in high level ozone using the Dobson Spectrophotometer Umkehr results [DeLuisi and Nimira, 1979], the TOMS data set [Stolarski et al., 1989], and values estimated using the global total ozone data set [Bojkov and Mateer, 1984]. The TOMS data set is nearly independent of the ground-based measurements of ozone in the Version 6.0 form, since the values have been recalculated using an algorithm which suppresses the effects of diffuser degradation [Herman et al., 1991]. The Brewer Umkehr data set offers an additional, independent method for the estimation of ozone trends at high altitude.

The Brewer Ozone Spectrophotometer has been in commercial production for 10 years. During that time a large number of ozone observations have been made at Canadian ozone monitoring sites. A Brewer spectrophotometer has been in service at Toronto since 1982, and at Edmonton since 1984. Umkehr observations [Gotz, 1930; Mateer, 1984; McElroy, 1988] are made automatically as part of the daily Brewer observation schedule. Since 1984 over 500 (see Table 1) Umkehr observations have been attempted at Edmonton (in the first quarter of each year). Many of these were unsuccessful because of the variability in light level which occurs during cloudy weather, but a large number are available for analysis.

The Edmonton data have been chosen to make an ozone trend estimate for several reasons. The Umkehr series from Edmonton is among the longest Brewer data set available, the Edmonton weather conditions are quite good, there is access to good correlative data (ozonesondes), and the Edmonton Dobson data have already been analyzed to determine an ozone trend [Mateer, 1984].

2 DATA COLLECTION

The Umkehr data are collected by turning the Brewer instrument sun director prism toward the zenith and observing the intensity of light scattered vertically downward by the sky at 8 wavelengths in the ultraviolet. The Brewer is designed to make nearly simultaneous measurements at 5 different wavelengths using time multiplexing [Kerr et al., 1980]. Depending on the setting of the spectrometer diffraction grating angle, observations are made at 306.3, 310.1, 313.5, 316.8, 320.1 nm or 316.5, 320.1, 323.2, 326.4 and 329.5 nm. Measurements are made alternately at these two settings during sunrise or sunset. Data from three wavelength pairs are simultaneously fitted in the analysis process.

The Brewer instrument is equipped with a polarizer which is mounted in the foreoptics. Measurements of the strong polarization component of the zenith sky light are made by properly orienting the instrument. The whole spectrometer is rotated in azimuth under computer control to maintain the direction of polarization during the Umkehr period (60 to 90 degrees solar zenith angle).

The data collected each day at the observation site are stored on a floppy disk by the instrument control software. Floppy disks are filled and duplicated at the rate of 1 per week and the copied data are sent to Toronto where they are loaded onto the Brewer data base computer. The results presented here were analyzed after retrieval from the data base.

3 DATA ANALYSIS

The data collected by the Brewer are analyzed using software based on the algorithm of Mateer [1984] (the "short Umkehr method") which uses the technique of Rodgers [1976] to make an optimal estimate of the ozone profile based on both the Umkehr data and a knowledge of ozone climatology based on the analysis of a large ozonesonde data set Mateer et al. [1980].

In the analysis, the data are first preprocessed to produce interpolated intensity values at the Mateer "standard Umkehr angles" (60.0, 65.0, 70.0, 74.0, 77.0, 80.0, 83.0, 85.0, 86.5, 88.0, 89.0, 90.0 degrees solar zenith angle).

The processing includes correcting the data for instrument dark count, non-linearity, and interpolating by a least-squares spline algorithm at the standard angles. The data in the longer and shorter wavelength sets are interpolated to the same angles (see Figure 1). The preprocessing stage also includes looking up the appropriate

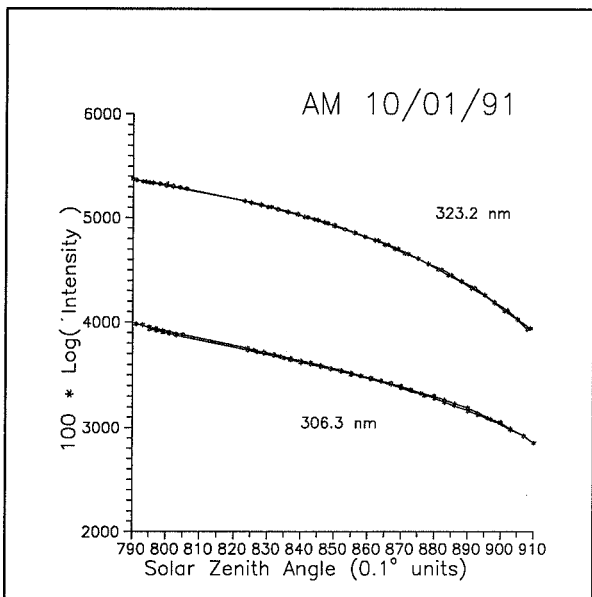


Figure 1 This figure shows the fitted curve and the raw data points output by the preprocessor for the longest and shortest wavelengths observed by the Brewer spectrophotometer.

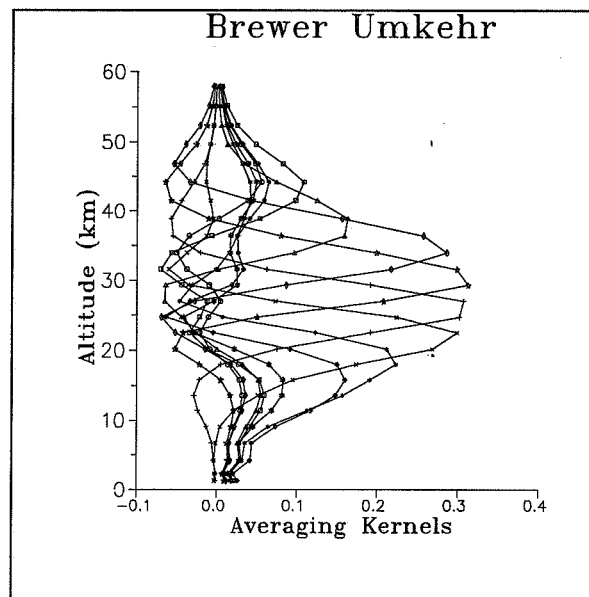


Figure 2 The averaging kernels for the Brewer Umkehr inversion algorithm. Note that the performance of the algorithm is best between 20 and 40 km.

ozone value for each Umkehr curve from the total ozone file for the observing station. All these data are written out in a terse format for further analysis by the Umkehr inversion software. A file is written for each day and instrument, and includes both a morning and evening Umkehr curve.

Quality control is done both at the preprocessing stage and at the Umkehr analysis step. The output from the preprocessor is examined for those days where the spline fitting process does not yield a good estimate of the observed data because of large variations between successive data points. If the RMS error between the observed and the fitted data is excessive the Umkehr is rejected.

If the curves cannot be inverted in 2 or 3 iterations of the inversion algorithm, the results are also rejected. Excessive differences after the second inversion iteration indicates that the observations are not well described by the range of curves represented by the climatology (perhaps due to instrument problems or observing conditions).

4 RESULTS

Table 1 shows the statistics for the success rate for Umkehr observations at Edmonton during the first quarter of each year between 1984 and 1991 inclusive. Of the possible 1444 Umkehr hours which could have been observed, 518 were actually logged in the data base. Of these, 327 passed the preprocessing screening step, and 197 actually produced acceptable, inverted profiles. This success rate roughly parallels the "good data" days for Edmonton based on the success rate for total ozone observation attempts.

Table 2 shows the statistical report from the Umkehr analysis program for the data collected in 1991. For each year, all of the data collected in the first quarter were analyzed together to produce

a mean profile, and an estimate of the variability of the results for the quarter using the "good" Umkehr curves. Since the same collection criteria were used for all curves, the results for different years should be comparable.

The amount of ozone in each Umkehr layer is recorded as a function of year in Table 3. The averaging kernels [Rodgers, 1990] shown in Figure 2 indicate the height range over which the Umkehr method produces its best results. A profile typical of those inverted from the 1992 Umkehr data is shown in Figure 3. Also included in Figure 3 is the climatological profile which was used in the estimation of the inverted results. The calculated rates of change of ozone based on these data are presented in Table 4. These rates apply to the actual observed ozone amounts and have not been corrected for physical effects such as the solar cycle variation of the solar flux.

5 CONCLUSIONS

These results do not show a significant long-term change in ozone concentrations at high altitudes above Edmonton. The SAGE results presented elsewhere in this proceedings have indicated a small, but statistically insignificant trend [McCormick, this issue] which is consistent with the results presented here. However, they demonstrate the quality and quantity of data which are available using the Brewer in its fully automated mode. Based on the success of this analysis, it is recommended that Brewer Umkehr observations from all stations in the global network be analyzed with the current algorithm and published in Ozone Data for the World as soon as possible.

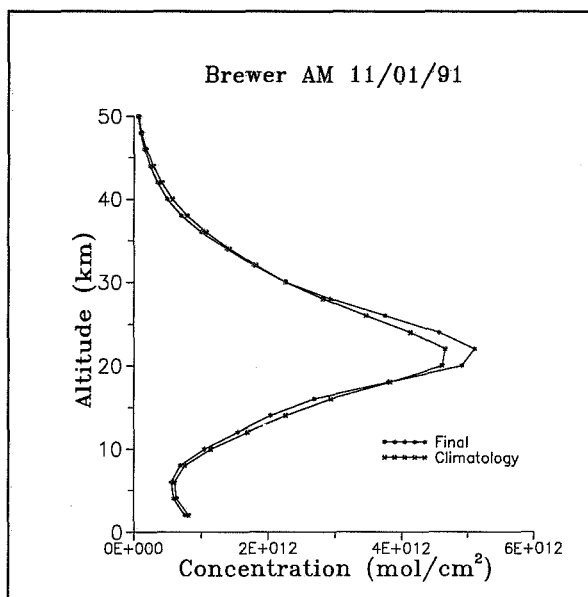


Figure 3 This is a sample of the output of the inversion algorithm presented as an altitude profile of ozone. Both the climatological "first-guess" and the retrieved profile are shown.

YEAR	Chances	Obs	Prepro	Complete	% Obs
1985	180	26	7	6	46.2
1986	180	12	1	1	8.3
1987	180	44	29	22	50.0
1988	182	48	30	19	22.9
1989	180	84	64	35	41.7
1990	180	76	56	40	52.7
1991	180	100	77	41	41.0
1992	182	128	63	33	26.0
Total	1444	518	327	197	38.0

Table 1. Observation statistics for Edmonton Umkehr observations.

Solution Statistics for 41 Profiles										
Ozone Obs.=0.3502±0.0438 Sol'n=0.3512±0.043										
Avg. Residual = 0.52±0.11 Iterations = 103										
Layer	10	9	8	7	6	5	4	3	2	1
AVG	1.5	4.0	11	21	35	63	92	64	34	26
RMS	.1	.3	1	2	4	9	11	13	9	2
% Err	19	17	15	11	11	11	11	13	16	19

Table 2. Statistics for the processing of 1991 Umkehr data from Edmonton.

Layer	1985	1986	1987	1988	1989	1990	1991	1992
10	1.55	1.41	1.54	1.59	1.52	1.50	1.53	1.52
9	4.23	3.49	4.13	4.24	3.97	4.01	3.95	3.99
8	11.5	9.52	11.3	10.6	10.9	11.5	10.5	10.7
7	22.0	19.6	22.3	20.4	22.4	23.5	21.4	21.7
6	35.0	36.3	36.7	34.3	37.2	37.4	35.1	34.9
5	60.5	73.2	67.7	62.4	63.7	64.8	62.6	59.7
4	86.7	98.4	95.1	90.9	88.4	92.9	91.5	88.6
3	70.8	69.0	69.5	66.6	66.4	72.2	64.4	70.1
2	41.9	38.4	40.1	36.7	37.0	41.1	34.1	38.4
1	29.0	27.5	28.1	27.4	27.1	28.1	26.3	27.5
Number	6	1	22	19	35	40	41	33

Table 3. Edmonton ozone amounts (in Dobson Units) in each of the Umkehr layers (see Table 4 for heights).

Layer	Altitude	Trend 1985-92 (%/year)	Trend 1987-92 (%/year)
8	37.7 - 42.8	0.14±0.10	-0.87±0.10
7	32.8 - 37.7	0.69±0.07	0.15±0.10
6	28.1 - 32.8	-0.06±0.05	0.51±0.12
5	23.6 - 28.1	-1.20±0.10	-1.70±0.10
4	19.1 - 23.6	-0.39±0.07	-0.82±0.06
3	14.7 - 19.1	-0.35±0.05	-0.09±0.10

Table 4. Ozone trends estimated using the data in Edmonton Umkehr data.

ACKNOWLEDGEMENTS

The authors wish to express sincere appreciation of the valuable comments contributed by the referees.

REFERENCES

- Bojkov, R.D. and C.L. Mateer, On the relative quality and performance of the Global Ozone Observing System - Total Ozone Measurements, *Proc. Quad. Ozone Symp.*, 335-340, 1984.
- DeLuisi, J.J., and J. Nimira, Preliminary comparison of seasonal variations of upper stratospheric ozone concentrations revealed by Umkehr and Nimbus 4 BUUV observations, *J. Geophys. Res.*, **84**, 3728-3732, 1979.
- Gotz, F.P.W., A.R. Meetham and G.M.B. Dobson, The vertical distribution of ozone in the atmosphere, *Proc. Roy. Soc. London, Ser. A*, **145**, 416-446, 1934.
- Herman, J.R., R. Hudson, R. McPeters, R. Stolarski, Z. Ahmad, X.-Y. Gu, S. Taylor, and C. Wellemeier, A new self-calibration method applied to TOMS and SBUV backscattered ultraviolet data to determine long-term global ozone change, *J. Geophys. Res.*, **96**, 7531-7545, 1991.
- Kerr, J.B., C.T. McElroy, and W.F.J. Evans, The automated Brewer ozone spectrophotometer for the measurement of SO₂, O₃, and aerosols, *Proc. Fifth Symp. on Meteor. Obs. and Instrumentation*, Toronto, Publ. by AMS, Boston, 1983.
- Mateer, C.L., J.J. DeLuisi, and C.C. Porco, The short Umkehr method, part 1: Standard ozone profiles by the inversion of short Umkehr observations, *NOAA Tech. Memo. ERL ARL-86*, 20 pp., NOAA Air Resources Laboratories, Silver Springs, MD, 1980.

- Mateer, C.L., J.B. Kerr, and W.F.J. Evans, Ozone profiles derived from Umkehr observations obtained with the Brewer Ozone spectrophotometer, Proc. Quad. Ozone Symp., 407-411, 1984.
- McElroy, C.T., C.L. Mateer, J.B. Kerr, D.I. Wardle, Umkehr observations made with the Brewer ozone spectrophotometer, Ozone in the Atmosphere, Eds. R.D. Bojkov, and P. Fabian, Publ. A. Deepak, pp. 725-727, 1989.
- Rodgers, C.D., Retrieval of atmospheric temperature and composition from remote measurements of thermal radiation, Rev. Geophys. and Space Phys., 14, 609-624, 1976.
- Rodgers, C.D., Characterization and error analysis of profiles retrieved from remote sounding measurements, J. Geophys. Res., 95, 5587-5595, 1990.
- Stolarski, R.S., A.J. Krueger and M.R. Schoeberl, Total ozone trends from TOMS data, Ozone in the Atmosphere, Eds. R.D. Bojkov, and P. Fabian, Publ. A. Deepak, 185-189, 1989.

**STATISTIC ANALYSIS OF ANNUAL TOTAL OZONE EXTREMES
FOR THE PERIOD 1964-1988**

Janusz W. Krzyścin

Meteorological Research Institute
1-1 Nagamine, Tsukuba, Ibaraki, 305 Japan
(Permanent affiliation: Polish Academy of Sciences, Institute of Geophysics)

ABSTRACT

Annual extremes of total column amount of ozone (in the period 1964-1988) from a network of 29 Dobson stations have been examined using the extreme value analysis.

The extremes have been calculated as the highest deviation of daily mean total ozone from its long-term monthly mean, normalized by the monthly standard deviations. The extremes have been selected from the direct-Sun total ozone observations only. The extremes resulting from abrupt changes in ozone (day to day changes greater than 20%) have not been considered.

The ordered extremes (maxima- in ascending way, minima - in descending way) have been fitted to one of three forms of the Fisher-Tippet extreme value distribution by the nonlinear least square method (Levenberg-Marguard method).

We have found that the ordered extremes from a majority of Dobson stations lie close to Fisher-Tippet type III.

The extreme value analysis of the composite annual extremes (combined from averages of the annual extremes selected at individual stations) has shown that the composite maxima are fitted by the Fisher-Tippet type III and the composite minima by the Fisher-Tippet type I. The difference between the Fisher-Tippet types of the composite extremes seems to be related to the ozone downward trend.

Extreme value prognoses for the period 1964-2014 (derived from the data taken at: all analyzed stations, the North American, and the European stations) have revealed that the prognostic extremes are close to the largest annual extremes in the period 1964-1988 and there are only small regional differences in the prognoses.

1. INTRODUCTION

Analyses of both ground-based [IOTP, 1990] and satellite ozone data [Stolarski et al., 1991] indicate statistically significant total ozone decline.

The potential effects of an increase in solar ultraviolet radiation on the biosphere have stimulated much of the concern about ozone depletion. Then, the estimation of future ozone changes is of special interest for human life.

In this paper we examine possibilities to implement the theory of extreme value to infer future total ozone extremes. Many extreme value analyses of

hydrological and meteorological variables have been undertaken in the past (for review, see Tabony, 1983). The method provides estimation of the highest and the lowest values which meteorological (or other) variable is likely to attain in a given number of years. The extreme value prognoses are based on the assumption that all factors determining changes in a prognostic variable have already appeared during the period of observations.

2. DATA

Total ozone extremes in the period 1964-1988 have been selected from a network of 29 Dobson stations. The names of the stations, index in the World Ozone Data Center, locations and the data periods are listed as follows:

1	Lerwick,	U.K.	43,	60°N,	1°W;	1/64-11/88
2	St.Petersburg	Russia	42,	60°N,	30°E;	8/68-12/88
3	Churchill,	Canada	77,	59°N,	94°W;	1/65-12/88
4	Edmonton,	Canada	21,	54°N,	114°W;	1/64-12/88
5	Belsk,	Poland,	68,	52°N,	21°E;	1/64-12/88
6	Bracknell,	U.K.	102,	51°N,	1°W;	1/69-12/88
7	Uccle,	Belgium	53,	51°N,	4°E;	2/71-12/88
8	Hradec K.,	Czech.	96,	50°N,	16°E;	1/64-12/88
9	Hohenpeiss.,	Germany	99	48°N,	11°E;	1/67-12/88
10	Caribou,	U.S.A.	20,	47°N,	68°W;	1/64-12/88
11	Arosa,	Switzerland	35,	47°N,	10°E;	1/64-12/88
12	Bismarck,	U.S.A.	19,	47°N,	101°W;	1/64-12/88
13	Toronto,	Canada	65,	44°N,	79°W;	1/64-12/88
14	Sapporo,	Japan	12,	43°N,	141°E;	1/64-12/88
15	Rome,	Italy	55,	42°N,	12°E;	1/64-12/88
16	Boulder,	U.S.A.	67	40°N,	105°W;	1/64-12/88
17	Cagliari,	Italy	38,	39°N,	9°E;	1/64-12/88
18	Wallops Is.,	U.S.A.	107,	38°N,	76°W;	1/70-12/88
19	Nashville,	U.S.A.	106,	36°N,	87°W;	1/64-12/88
20	Tateno,	Japan	14,	36°N,	140°E;	1/64-12/88
21	Srinagar,	India	13,	34°N,	75°E;	2/64-12/88
22	Kagoshima,	Japan	7,	32°N,	131°E;	1/64-12/88
23	Quetta,	Pakistan	11,	30°N,	67°E;	8/69-12/88
24	Cairo,	Egypt	152,	30°N,	31°E;	11/74-12/88
25	Naha,	Japan	190,	26°N,	128°E;	4/74-12/88
26	Mauna Loa,	U.S.A.	31,	19°N,	156°E;	1/64-12/88
27	Huancayo,	Peru	110,	12°S,	75°W;	2/64-12/88

28 Samoa, U.S.A. 191, 14°S, 171°W; 1/76-12/88
 29 Aspendale, Australia 26, 38°S, 145°E; 1/64-12/82

For each station, the annual extremes in total column amount of ozone have been calculated from the daily averages of total ozone published in Ozone Data for the World (ODW) journals. However, International Trend Panel-1988 [IOTP, 1990] have found strong incongruities in the published data of many ground-based stations due to instrument calibrations.

A provisionally revised data set (1957-1986) was prepared by the Panel, with the corrections being applied to the monthly averages of total ozone values.

Making use of the Panel's re-evaluated total ozone monthly means we convert all daily averages of total ozone values (calculated before Jan. 1987) to the provisionally corrected ones in the following way:

$$O_{3\text{ new}}(i, j, k, l) = O_{3\text{ old}}(i, j, k, l) \cdot \frac{M1(j, k, l)}{M2(j, k, l)}$$

where: $O_{3\text{ new}}(i, j, k, l)$, $O_{3\text{ old}}(i, j, k, l)$ - daily mean of total ozone on i -th day, j -th month, k -th year and at l -th Dobson station, provisionally revised and unrevised, respectively, $M1(j, k, l)$ - revised monthly mean of total ozone at l -station in j -th month and k -th year (data from IOTP, 1990), $M2(j, k, l)$ - monthly mean of total ozone derived from ODW data.

Provisionally corrected daily averages of total ozone values are transformed to the departures from the long-term monthly means (1964-1988) expressed in percents of the long-term monthly standard deviation. Finally, the annual extremes have been selected from the dimensionless daily averages of total ozone values.

ODW data from only a few stations (Belsk, Sapporo, Kagoshima, Tsukuba, Naha) could be accepted without any adjustment of the data, because original reported results of total ozone measurements were re-evaluated (and published in ODW) on daily basis taking into account all instrument's calibrations. Our correction method provides only a crude estimation of daily mean total ozone.

ODW data contain results from the various types of ozone observations among these the direct-Sun ozone observations provide the highest accuracy. Taking this into consideration, the extremes have been selected only from the direct-Sun observations. The extremes, which were formed as a result of abrupt changes in the ozone pattern (day-to-day change in total ozone more than 20%), have not been considered. Therefore, the extremes in total ozone, examined in this paper, are caused by processes with a time scale larger than a few days. Moreover, in the case when the day-to-day change in total ozone is very large there is a larger likelihood that this change is a result of erroneous observations.

3. THE EXTREME VALUE ANALYSIS

The theory of extreme value was first developed by Fisher and Tippett, [1928]. They showed that extremes taken from a sample containing N observations converge asymptotically towards one of only three forms as N increases. These are called Fisher-Tippett Type I, Type II and Type III. A general solution of the extreme value problem was obtained by Jenkinson [1955] in the form:

$$X = X_0 + a \frac{1 - \exp(-k Y)}{k} \quad [1]$$

where: X - extremes (ordered in ascending way),
 Y - reduced variate calculated from the equation:

$$F(X) = \exp(-\exp(-Y)),$$

$F(X)$ - empirical cumulative probability function, X_0 , a , and k constants to be calculated.

Fisher-Tippett types I, II, and III are characterized by their different shapes when plotted on a graph X against Y (see Fig.1). Type I corresponds to $k = 0$ and forms a straight line. Type II (bounded below but not above) and Type III (bounded above but not below) correspond to $k < 0$ and $k > 0$, respectively.

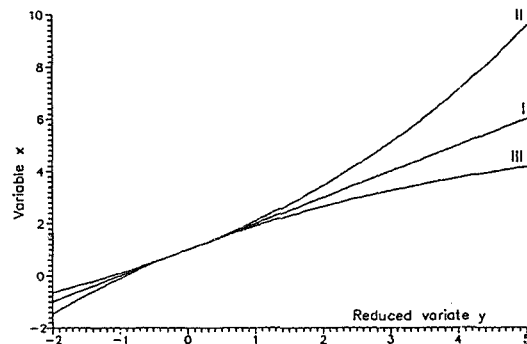


Fig.1. Fisher-Tippett distribution types I, II, III

4. RESULTS

In order to use extreme value method, the empirical cumulative distribution function of annual extremes (ECDFAE) has to be constructed. The annual extremes are ordered from the lowest X_1 (for minima we use absolute values) to the highest X_m , where m is the number of annual extremes. ECDFAE could be calculated by various formulas, we have chosen Beard's formula [Beard, 1943];

$$F(X_i) = (i - 0.31) / (m + 0.38)$$

Finally, one of the three Fisher-Tippett types has to be fitted to a set of (X_i, Y_i) points,

$$Y_i = -\ln(-\ln(F(X_i)))$$

In practice, after plotting the set of (X_i, Y_i) points on a graph X against Y , the Fisher-Tippett type of ECDFAE is determined "by eye" method and the parameters describing precisely the pattern of ECDFAE are calculated assuming that the type of ECDFAE is known. However, in our paper we use the nonlinear least square method (Levenberg-Margardt method) to find the model's constants:

X_0 , a , and k .

Then, both the values of k and the standard error of k let us determine the type of ECDFAE.

In Fig.2, the estimates of k from individual stations extremes data are presented. It is seen that Fisher-Tippett type III dominates.

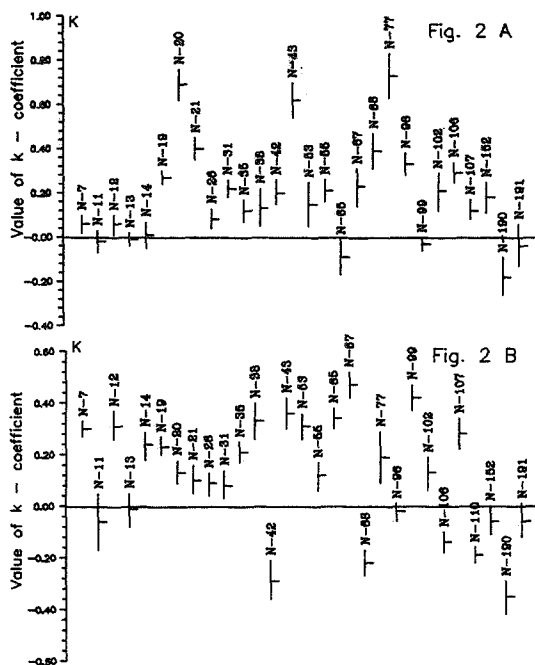


Fig.2. Values of k for annual maxima (Fig.2 A) and for annual minima (Fig. 2 B) derived from the annual extremes taken at the selected Dobson stations. Number above each point corresponds to the ODW station index. Vertical bars represent standard errors

When, the extremes lie close to the physically imposed bound, a type III distribution of the extremes maybe expected, but when the observed extremes fall far from their limit, they may appear to be fitted by types I or II. However, type III and II may appear erroneously if the extremes are selected from small population (too small number of direct-Sun measurements per year) or the data contain samples from various populations (extremes are caused by more than one mechanism). Type II can be form misleadingly if the data are contaminated by only a few very large extremes coming from erroneous observations.

Then, to determine the type of extremes from individual station data correctly we need to analyze a cause of the extremes appearance.

Examination of the composite extremes, combined from the annual extremes taken at each station, is an attempt to eliminate the observation errors. In Fig.3 we present result of extreme value analysis applied to the composite annual total ozone extremes.

Maxima are well fitted by Fisher-Tippet type III distribution, $k = 0.46 \pm 0.06$. The minima (absolute values) lie close to Fisher-Tippet type I distribution, $k = -0.02 \pm 0.06$. These findings imply that the future maxima with the values much larger than the largest maximum registered up to 1988 will not be expected (the highest maximum in the period 1964-1988 lies close to upper limit imposed by Fisher-Tippet III type), while more negative minima will be recorded (total ozone minima seem to be unbounded).

The difference between the Fisher-Tippet types obtained for the annual maxima and minima seems to

be related to decreasing tendency in atmospheric ozone. The ozone extremes have been calculated as the highest annual departures from the long-term (1964-1988) means. In the future, larger maxima (deeper minima) than the ones recorded up to 1988 will be unlikely (likely) because the negative trends in ozone attenuate the maxima (amplify the minima) relative to the ozone mean level in the period 1964-1988.

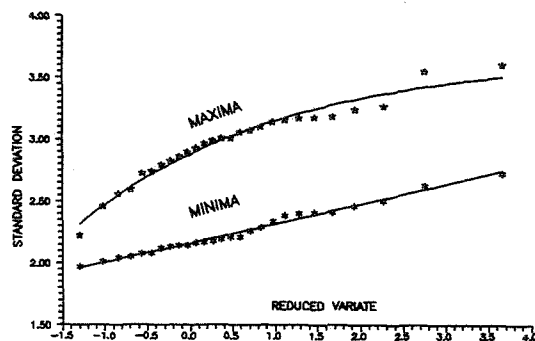


Fig.3. Empirical cumulative probability function of annual extremes (for minima we use absolute values) combined from the annual total ozone extremes taken at 29 Dobson stations.

The extreme value method provides the possibility to estimate the highest and the lowest values, which any meteorological (or other) variable is likely to attain in a given number of years. The estimation is obtained from the extrapolation of Fisher-Tippet distribution at a reduced variate value, which corresponds with a chosen period of prognosis.

Tab.1 shows results of extreme value prognosis in the period 1964-2014 for all Dobson stations listed in section 2 and for 10 European and 8 North American stations. We examine both provisionally revised data and non corrected ODW data.

Table 1. Extreme value prognoses (expressed in the standard deviations units) in the period 1964-2014 for 29 Dobson stations and for the European and the North American stations. Standard errors of the estimates in parentheses.

Class	D A T A			
	REVISED		NON-REVISED	
	MIN	MAX	MIN	MAX
All stat.	-2.79(0.02)	3.53(0.04)	-2.68(0.03)	3.55(0.04)
Europe	-2.80(0.03)	3.91(0.05)	-2.81(0.04)	3.90(0.05)
N.Amer.	-2.82(0.04)	3.47(0.04)	-2.79(0.03)	3.53(0.05)

Comparing the extreme value prognoses for the analyzed groups of ozone stations we have found that; provisionally revised data and non corrected ODW data give similar result, there are small regional differences in the prognoses. Prognoses for minima (absolute values) are lower than for maxima (this reflects positive asymmetry of the parent distribution).

In the period 1964-1988, the largest maximum (about 3.5 standard deviation) and minimum (about -2.6 standard deviation), calculated for the group of all the analyzed stations (see Fig.3), differ only slightly from the prognostic extremes for the period 1964-2014.

We estimate that 1 standard deviation for the group of all the analyzed stations equals about 10 Dobsons. Then, the predicted largest minimum (for the period 1964-2014) is only a few Dobsons lower than that observed in the period 1964-1988. Therefore, a downward trend in total ozone (about 1.5 % per decade for the region 30°N-60°N in the period 1970-1988, Krzyścin, 1992) will influence only a little the future largest extremes.

Almost all studies of the long-term variations in atmosphere ozone (especially the trend models) were limited to analyses based on the monthly means or the annual means of total ozone. Our paper reveals that the extreme value analysis provides a useful tool for the detection long-term changes in atmospheric ozone. The reliability of climatological statements based on the analysis of ozone extremes is clearly dependent upon quality of the data. Then, elimination of spurious extremes from the data seems to be the most important part of the analysis.

ACKNOWLEDGMENTS

This work was supported by the Science and Technology Agency of Japan Fellowship.

REFERENCES

- Beard, L.R., 1943: Statistical analysis in hydrology. *Tran. Am. Soc. Civ. Eng.*, 108, 1110-1160.
- Fisher, R.A. and L.H.C. Tippett, 1928: Limiting forms of the frequency distribution of the largest or smallest members of a sample. *Proc. Cambridge Philos. Soc.*, 24, 180-190.
- IOTP, 1990: Report of the International Ozone Trend Panel 1988, Vol.1. World Meteorological Organization Global Ozone Research and Monitoring Project. Report No. 18, WMO Geneva, Switzerland.
- Jenkinson, A.F., 1955: The frequency distribution of annual maximum (or minimum) values of meteorological elements. *Q. J. R. Meteorol. Soc.*, 81, 158-171.
- Krzyścin, J.W., 1992: Long-term changes in the probability density function of Dobson total ozone in selected northern hemisphere geographical regions. 1992 Quadrennial Ozone Symposium Proceedings.
- Stolarski, R.S., P. Bloomfield, R.D. McPeters, and J.R. Herman. 1991; Total Ozone Trends Deduced from Nimbus-7 TOMS Data. *Geophys. Res. Lett.*, 18, 1015-1018.
- Tabony R. C, 1983: Extreme value analysis in meteorology. *Meteorol. Mag.*, 112, 77-98.

303639

LONG-TERM CHANGES IN THE STATISTICAL DISTRIBUTION OF DOBSON TOTAL
OZONE IN SELECTED NORTHERN HEMISPHERE GEOGRAPHICAL REGIONS

Janusz W. Krzyścin

Meteorological Research Institute
1-1, Nagamine, Tsukuba, Ibaraki, 305-Japan
(Permanent affiliation: Polish Academy of Sciences, Institute of Geophysics, Warsaw, Poland)

ABSTRACT

The daily averages of total column amount of ozone taken in the period 1964-1988 at a network of 24 Dobson stations have been analyzed. Year-round data as well as summer data (May-Aug.) and winter data (Dec.-March) have been examined in the following regions: latitude bands (30°N-39°N, 40°N-52°N, 30°N-60°N), North America, Europe, Japan.

To find year-to-year changes in the shape of the annual statistical distribution of total ozone (ASDTO) for these regions, we analyze trends in the following statistic characteristics of ASDTO: mean, standard deviation, median, 10 and 90 percentiles. Time series of the statistical characteristics for the selected regions have been combined by averaging the individual stations values of these characteristics.

The trends have been calculated by the multiple regression model adjusted for: the 11-year solar cycle, the Southern Oscillations effects, and for serial correlations. We have found that:

a) in all regions (excluding Japan, North America), the shape of ASDTO has been drifting towards low ozone values. The drift seems to be not accompanied with a transformation in the shape of ASDTO.

The drift speed (the rate of decrease in the annual means of total ozone) is of order 1-3 % per decade (in the period 1970-1988).

b) the drift speed depends on the regions, the lowest one is in 30°N-39°N band.

b) in Japan, the interannual changes in the shape of ASDTO have not been revealed.

c) in North America, the drift of the year-round ASDTO (the year-round ASDTO comprises all the daily means of total ozone in a given year) has been accompanied with a transformation in the shape. The shape of the year round ASDTO becomes narrower.

d) in all regions, except Japan and the band 30°-39°N, the winter ASDTO (the winter ASDTO comprises the data taken in the period December in a given year through March next year) moves faster towards low ozone values than the summer ASDTO (the summer ASDTO comprises the data taken in the period May through August in a given year).

1. INTRODUCTION

Ozonetrend detection has been a subject of interest during the past decade (e.g. Reinsel *et al.*, 1981; Angell *et al.*, 1983; Hill *et al.*, 1986; Oehlert, 1986;

IOTP, 1990). Implications for UV radiation changes at the earth's surface have stimulated much of the concern about ozone downward trend.

Almost all studies of the long-term variations in the atmospheric ozone were carried using the monthly (or yearly) averages of ozone. In this paper, we analyze interannual changes in values of a few statistic characteristics of the annual statistical distribution of total ozone (i.e. mean value, standard deviation, median, 10 and 90 percentiles) to disclose the long-term variations in the shape of ASDTO in selected Northern Hemisphere regions

2. DATA

Dobson total ozone data have been analyzed from a network of 24 stations for the period 1964-1988. The names of the stations, locations and the data periods are listed below:

STATION	COUNTRY	LAT.	LON.	PERIOD
1 Lerwick,	U.K.	60°N,	1°W;	1/64-11/88
2 Leningrad,	Russia	60°N,	30°E;	8/68-12/88
3 Churchill,	Canada	59°N,	94°W;	1/65-12/88
4 Edmonton,	Canada	54°N,	114°W;	1/64-12/88
5 Belsk,	Poland	52°N,	21°E;	1/64-12/88
6 Bracknell,	U.K.	51°N,	1°W;	1/69-12/88
7 Uccle,	Belgium	51°N,	4°E;	2/71-12/88
8 Hradec K.,	Czechoslov.	50°N,	16°E;	1/64-12/88
9 Hohenpeiss.,	Germany	48°N,	11°E;	1/67-12/88
10 Caribou,	U.S.A.	47°N,	68°W;	1/64-12/88
11 Arosa,	Switzerland	47°N,	10°E;	1/64-12/88
12 Bismarck,	U.S.A.	47°N,	101°W;	1/64-12/88
13 Toronto,	Canada	44°N,	79°W;	1/64-12/88
14 Sapporo,	Japan	43°N,	141°E;	1/64-12/88
15 Rome,	Italy	42°N,	12°E;	1/64-12/88
16 Boulder,	U.S.A.	40°N,	105°W;	1/64-12/88
17 Cagliari,	Italy	39°N,	9°E;	1/64-12/88
18 Wallops Is.,	U.S.A.	38°N,	76°W;	1/70-12/88
19 Nashville,	U.S.A.	36°N,	87°W;	1/64-12/88
20 Tateno,	Japan	36°N,	140°E;	1/64-12/88
21 Srinagar,	India	34°N,	75°E;	2/64-12/88
22 Kagoshima,	Japan	32°N,	131°E;	1/64-12/88
23 Quetta,	Pakistan	30°N,	67°E;	8/69-12/88
24 Cairo,	Egypt	30°N,	31°E;	11/74-12/88

In this paper, we analyze the daily mean total ozone record published in "Ozone Data for the World" (ODW) journals. However, International Trend Panel-1988 [IOTP, 1990] found strong incongruities in the published data of many ground-based stations due to instrument calibrations.

For 31 Dobson stations, a provisionally revised data set (1957-1986) was prepared by the Panel, with the corrections being applied to the monthly averages of total ozone.

We examine results of the ozone observations taken at the stations selected by the Panel.

Making use of the Panel's re-evaluated total ozone monthly means we convert daily averages of total ozone (calculated before January 1987) to the provisionally corrected ones in the following way:

$$O_3 \text{ new}(i, j, k, l) = O_3 \text{ old}(i, j, k, l) \frac{M1(j, k, l)}{M2(j, k, l)}$$

where: $O_3 \text{ new}(i, j, k, l)$, $O_3 \text{ old}(i, j, k, l)$ - daily mean of total ozone on i -th day, j -th month, k -th year and at l -th Dobson station, provisionally revised and uncorrected, respectively, $M1(j, k, l)$ - revised monthly mean of total ozone [IOTP, 1990], $M2(j, k, l)$ - monthly mean of total ozone derived from ODW data.

Provisionally revised daily averages of total ozone have been transformed to the departures from the long-term monthly means (1964-1988) expressed in percents of the long-term monthly standard deviation.

Using $O_3 \text{ new}(i, j, k, l)$ and $O_3 \text{ old}(i, j, k, l)$ (since January 1987) we calculate a few characteristics describing the shape of ASDTO at station l in year k .

The following ones have been considered: mean value ($MEAN$), standard deviation (SD), median (MED), 90 percentile ($P90$), 10 percentile ($P10$). $P10$ and $P90$ estimate locations of the low values tail and the high values tail of ASDTO, respectively.

For selected northern hemisphere regions, the statistic characteristics of ASDTO in a given year have been estimated averaging the individual stations values of the statistic characteristics in that year.

The following regions have been considered: latitude bands ($30^{\circ}N-39^{\circ}N$, $40^{\circ}N-52^{\circ}N$, $30^{\circ}N-60^{\circ}N$), North America, Europe, Japan.

The statistic characteristics of ASDTO have been calculated from all daily averages of total ozone values in a given year. To find seasonal differences in the long-term changes of ASDTO, summer (May through Aug.) and winter (Dec. through March) values of the statistic characteristics have been examined also.

3. TREND MODEL

Trends in the statistic characteristics of ASDTO have been found by multiple regression model. The model has been adjusted for: the 11-year solar activity cycle, the long-term stratospheric circulation fluctuations (Southern Oscillations) effects, and the serial correlations.

Variations in total ozone related to the QBO have not been parameterized because the relatively high frequency of the QBO (there are about 12 cycles in the period 1964-1988) makes its inclusion in the ozone trend model (or exclusion) have a negligible effect on the trend estimates (IOTP, 1990).

Trends in the statistic characteristics of ASDTO have been modelled by means of the ramp trend model, i.e. we assume that the trend in ozone has formed after 1969:

$$y(t) = \alpha + \beta Sun(t) + \gamma Soi(t) + N(t), \quad t \leq 1969$$

$$y(t) = \alpha_1 + Tt + \beta Sun(t) + \gamma Soi(t) + N(t), \quad t > 1969$$

where: α , α_1 , β , γ - constants, T - rate of linear changes (trend), $Sun(t)$ - annual mean of Zurich sunspot number in year t , $Soi(t)$ - Southern Oscillation index (normalized pressure difference between Tahiti and Darwin). The noise term $N(t)$ is modeled as a first order autoregressive process, i.e. $N(t) = \delta N(t-1) + e(t)$, where $e(t)$ is a noise with normal distribution and zero mean.

In our model, we assume that declining tendency in total ozone has begun around 1970. This hypothesis was widely used in the trend modeling in the past decade (e.g. Reinsel *et al.*, 1981; IOTP, 1990).

We run the trend model using as $y(t)$ the composite time series of: $MEAN$, SD , MED , $P90$, and $P10$, combined from individual station values of these characteristics. Constants α , α_1 , β , γ , δ , T are derived by the least square fit.

For example, the comparison between observed and modeled time series of $MEAN$ for 10 European Dobson station (see section 2 for the names of these stations) is presented in Fig. 1. The correspondence between the long-term variations in the observed and modeled time series allows to state that the model reproduces adequately the long-term variations in total ozone.

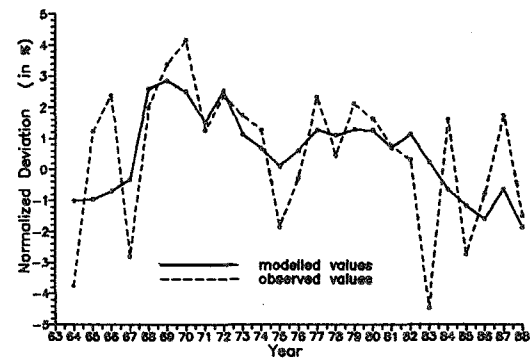


Fig.1 Observed and modelled departures of annual total ozone means from its long-term (1964-1988) mean (expressed in percent of the long-term mean) in the period 1964-1988 for European Dobson stations (see section 2 for the names of stations)

4. RESULTS

In Fig.2 we present an example of analyzed time series set. The annual values of the statistic characteristics have been combined from ten European Dobson stations. It is seen that the pattern of SD time series is almost constant during observation's period (1964-1988), but other time series ($MEAN$, $P90$, $P10$) show similar decreasing tendency. Moreover, variations in timeseries of $MEAN$, $P90$ and $P10$ seem to be highly correlated. The correlation coefficients between: $MEAN$ and $P90$, $MEAN$ and $P10$, $P90$ and $P10$ are equal 0.93, 0.93, 0.75, respectively.

These high correlations, similar negative trends in *MEAN*, *P10*, *P90*, and no trend in *SD* let us suggest that year-to-year variations in the shape of ASDTO are caused by a drift of the shape (towards low ozone values) rather than by a transformation of the shape (for example a change of the distribution type).

For the European stations, we have found that ASDTO is well approximated by the log-normal distribution. The long-term changes in the shape of ASDTO can be mathematically described as a translation of the distribution towards low ozone values because almost similar negative trends have been found in time series of *MEAN*, *P10* and *P90*, while no trend in *SD*.

For all analyzed northern hemisphere regions, the high correlations between *MEAN*, *P10* and *P90* have been detected. Then, the long-term changes in the shape of ASDTO have been deduced from the trend analyses of the following composite time series: *MEAN*, *SD*, *MEDIAN*, *P10*, *P90*. The results are presented in Tab. 1.

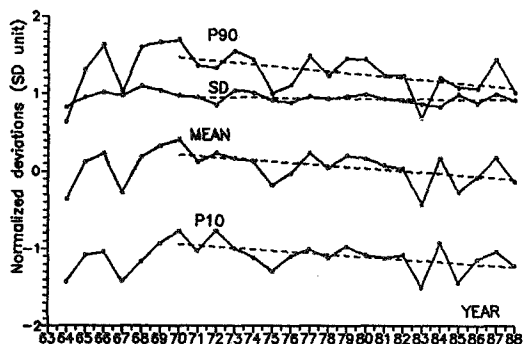


Fig. 2. Time series (1964-1988) of statistical characteristics (annual mean - *MEAN*, standard deviation - *SD*, 90 percentile - *P90*, 10 percentile - *P10*) of the distribution of total ozone combined from the individual station values of these characteristics. The analyzed time series have been obtained from the data taken at 10 European Dobson stations. Values of the characteristics are expressed in standard deviation unit. Dashed lines represent linear regression lines.

The main finding from Tab.1 is a drift of the shape of ASDTO towards low ozone values (only the results for Japan show that the shape remains constant in the period 1970-1988). We have found that the annual rates of the changes in selected statistical characteristics (*MEAN*, *MEDIAN*, *P90*, *P10*) of ASDTO are almost the same (within 2σ band) and the trends in *SD* are not statistically significant (except North America where the trend is negative). Therefore, it seems that the long-term changes in the shape of ASDTO in all the analyzed regions (except Japan, North America) are expressed simply as a translation of the shape towards low ozone values. The speed of this translation (the rate of decrease in the annual means of total ozone) depends on latitude (the lowest is found in the latitude band 30°N - 39°N) The speed varies with season also. For the winter ASDTO, which is built from the all daily means of total ozone in the period December-March, the speed is greater than the speed for the summer ASDTO (May through August daily means of total ozone have been used to prepare the summer ASDTO).

In North America, for the year round data, statistically significant trend in *SD* time series has been revealed. Therefore, the drift of the shape of the year-round ASDTO (the year-round ASDTO comprises all the daily means of total ozone in a given year) seems to be accompanied with a transformation of the shape. The shape of the year round ASDTO becomes narrower. There is a likelihood that the negative tendency in the annual standard deviations over North America, calculated from all the daily total ozone means in a given year, is forced by the large decline in the high value tail of ASDTO (see Table 1, section for North America, where a large difference between the trends in *P90* and *P10* can be seen).

Tab.1. Long-term trends (year-round, winter and summer trends in the period 1970-1988) in the characteristics of the annual statistical distribution of total ozone (in % per decade) for selected northern hemisphere regions: latitude bands (30°N - 39°N , 40°N - 52°N , 30°N - 60°N), North America, Europe, Japan.

For the period 1964-1986 provisionally revised daily averages of total ozone and for the period 1987-1988 the data published in Ozone Data for the World journals have been used. Errors (on 2σ level) are shown in parentheses. Statistical significant results are underlined

EUROPE			
Trends			
	Year-round	Winter	Summer
MEAN	<u>-2.10</u> (1.80)	-2.50 (2.89)	-1.11 (1.83)
SD	-1.64 (5.66)	2.54 (7.13)	-3.10 (7.20)
MED	<u>-1.98</u> (1.82)	-1.96 (2.99)	-1.20 (1.79)
P90	<u>-2.45</u> (2.32)	-2.17 (3.65)	-1.63 (2.29)
P10	<u>-1.99</u> (1.60)	<u>-3.33</u> (2.37)	-0.70 (1.72)
NORTH AMERICA			
Trends			
	Year-round	Winter	Summer
MEAN	<u>-2.60</u> (1.62)	<u>-3.83</u> (2.14)	<u>-2.03</u> (1.47)
SD	<u>-4.91</u> (3.38)	-1.44 (6.12)	-5.29 (5.87)
MED	<u>-2.70</u> (1.59)	<u>-3.65</u> (2.12)	<u>-2.17</u> (1.46)
P90	<u>-3.26</u> (1.98)	<u>-4.31</u> (2.80)	<u>-2.50</u> (1.98)
P10	<u>-1.95</u> (1.40)	<u>-3.70</u> (2.16)	<u>-1.37</u> (1.37)
JAPAN			
Trends			
	Year-round	Winter	Summer
MEAN	-0.70 (1.19)	-0.73 (2.01)	0.05 (1.68)
SD	0.59 (4.30)	-2.67 (9.14)	0.16 (4.61)
MED	0.16 (1.25)	-0.88 (2.12)	0.33 (1.78)
P90	0.06 (1.29)	-0.44 (2.80)	0.33 (2.10)
P10	0.14 (1.15)	-0.11 (1.89)	-0.07 (1.33)

B A N D: 40°N - 52°N			
Trends			
	Year-round	_Winter_	_Summer_
MEAN	-1.90 (1.35)	-2.33 (2.06)	-1.34 (1.23)
SD	-2.83 (5.12)	-3.18 (7.43)	-3.53 (6.24)
MED	-1.82 (1.34)	-2.11 (2.11)	-1.44 (1.20)
P90	-2.27 (1.77)	-2.21 (2.79)	-1.50 (1.65)
P10	-1.64 (1.12)	-3.01 (1.71)	-0.90 (1.23)

BAND: 30°N - 39°N			
Trends			
	Year-round	_Winter_	_Summer_
MEAN	-1.34 (1.13)	-1.52 (2.14)	-1.50 (1.50)
SD	-1.68 (4.36)	2.00 (5.93)	0.96 (5.62)
MED	-1.34 (1.19)	-1.51 (2.23)	-1.52 (1.52)
P90	-1.29 (1.27)	-0.84 (1.99)	-1.51 (1.66)
P10	-1.44 (1.00)	-1.45 (2.40)	-1.46 (1.30)

BAND: 30°N - 60°N			
Trends			
	Year-round	_Winter_	_Summer_
MEAN	-1.66 (1.18)	-2.30 (1.54)	-1.23 (1.21)
SD	-1.62 (3.25)	-0.45 (4.66)	-2.24 (3.25)
MED	-1.65 (1.18)	-2.14 (1.62)	-1.26 (1.24)
P90	-1.87 (1.44)	-2.16 (1.84)	-1.39 (1.44)
P10	-1.52 (0.96)	-2.46 (1.34)	-0.98 (1.01)

5. Discussion and Conclusion

We have found that the long-term changes in the shape of ASDTO, calculated for selected northern hemisphere geographical regions, have been expressed as a drift of the shape towards low ozone values. Some regional and seasonal peculiarities in the drift speed (the rate of decrease in annual means of total ozone) have been revealed.

The errors of the trend estimates in the statistical characteristics of ASDTO have been calculated too large to make conclusive statement about details of a transformation of ASDTO in the period 1964-1988. However, in all the analyzed regions (excluding Japan, North America), the high correlations between time series of *MEAN*, *P90* and *P10* and almost similar trends in these characteristics (while no trends in *SD*) let us suggest that the shape of ASDTO has been drifting towards low values without a transformation of the shape. Results for the North America stations show that the drift of the shape has been accompanied with a transformation of the shape. The rate of ozone loss found in the high values tail of ASDTO (*P90*) is greater than ozone loss in *MEAN*, and ozone loss in the low values tail of PDFTO (*P10*) is lower than the trend in *MEAN*. As the result of these changes, *SD* should show decreasing tendency. The trend analysis of *SD* time series reveals this tendency. It means that the shape of ASDTO becomes narrower during its drifting towards low ozone values.

The long-term trends (in the period 1970-1990) calculated from the monthly averages of Dobson

total ozone values (Stolarski *et al.*, 1992) are broadly consistent with the trends in *MEAN* derived from the interannual variations of ASDTO, i.e. there is a significant winter loss and a smaller summer loss in total ozone over the Northern Hemisphere, this difference is more pronounced at high and mid latitudes than at low latitudes.

The results of our trend model (for the variable *MEAN*) and the newest trend estimates in monthly means of Dobson total ozone by Stolarski *et al.* [1992] are almost the same. The differences between the ozone trends are lower than 0.6 % per decade for North America, Europe, and the northern temperate regions. For example, Stolarski *et al.* [1992] found the following trends over 26°N-64°N band in the period 1970-1990: year-round -1.8% per decade, winter - 2.7% per decade, summer -1.3% per decade. The errors in our trend estimates are larger, because relatively small number of data points (annual means) has been used in the trend detection.

In the last decade, the rate of ozone loss seems to be greater than that in the period 1970-1990, Stolarski *et al.* [1992]. We have tried to prove this hypothesis comparing the trends in the periods 1970-1986 and 1978-1988. The differences between the trends in the statistical characteristics of ASDTO calculated for these periods have been found statistically insignificant (limited number of the data points has been used to estimate trends, especially in the period 1978-1988). Then, the analysis of the interannual variations in ASDTO for the detection short-term trends (in the period of one decade) is not able to provide a support for the hypothesis probably due to large errors of the trend estimates.

ACKNOWLEDGMENTS

This work was supported by the Science and Technology Agency of Japan Fellowship.

REFERENCES

- Angell, J.K., J. Korshover, 1983: Global variations in total ozone and layer mean ozone: An update through 1981, *J. Clim. and Appl. Meteor.*, 22, 1611-1627
- Hill, W.J., G.W. Oehlert, and G.C. Reinsel, 1986: Trend analysis sensitivity studies of Dobson total ozone data through 1984, *J. Geophys. Res.*, 91, 14515-14520.
- IOTP, Report of the International Ozone Trend Panel 1988, 1990: Vol. 1. World Meteorological Organization Global Ozone Research and Monitoring Project. Report No.18, WMO Geneva, Switzerland.
- Oehlert, G., Trends in Dobson total ozone: An update through 1983, 1986: *J. Geophys. Res.*, 91, D2, 2675-2679,
- Reinsel, G.C., G.C. Tiao, M.N. Wang, R. Lewis, and D. Nychka, Statistical analysis of stratospheric ozone data for the detection trend, 1981: *Atmos. Environ.*, 15, 1569-1577.
- Stolarski, R.S, R. Bojkov, L. Bishop, Ch. Zerefos, J. Staehelin, J. Zawodny, Measured trends in Stratospheric Ozone, 1992: *Science*, 256,342-349.

303540

RECALCULATED VALUES OF THE TOTAL
OZONE AMOUNT OVER OSLO, 60° N,
FOR THE PERIOD 1979-1992

Søren H.H. Larsen, Tove Svendby, Finn Tønnessen,
Department of Physics, University of Oslo

Arne Dahlback
Norwegian Institute for Air Research, NILU

Abstract.

The total ozone amount over Oslo has been measured with the Dobson spectrophotometer No 56. The instrument was modified, calibrated and intercompared in 1977 in Boulder. A new intercomparison was made in 1986 in Arosa. Much work has been done to make the zenith charts reliable. A new method has been introduced where one takes into account the change in the shape of the zenith chart curves which is caused by a change of the ozone profile when the ozone amount changes. According to the conclusion derived from the intercomparison in Arosa 1986, the instrument has not been stable. The R-N tables had to be altered, but not the Q-tables. We have tried to account for this change in our handling of the observation data. No statistical analyses of these data has yet been made, but the monthly averages of the raw data show a negative linear trend of about 4% for the whole period.

1. INTRODUCTION

Dobson spectrophotometer No 56 has been operated at the University of Oslo since 1969 when we got it from The Norwegian Polar Institute. At that time the instrument required recalibration since the instrument had been damaged during an expedition to Antarctica some years before. In 1977 the instrument was sent to Boulder where W.D. Komhyr, R.D. Grass, and S.H.H. Larsen modified and re-aligned the instrument, which was in a bad shape. The optical wedge was recalibrated and a new photomultiplier was put in and adjusted. The prisms and mirrors were cleaned and the position adjusted. Also the positions of the slits and the slit-widths were checked. Afterwards the instrument was a part of an intercomparison campaign in Boulder, August 1977.

In Oslo the main observation series started in 1978. The zenith chart and the cloud correction charts had to be constructed, a task which had to take some time due to great changes in weather and ozone amount. We decided to depend on observations carried out with the C wavelength pair because we wanted to get as many observations as possible throughout the winter season

with low sun. Due to this the observations will suffer from large standard deviations because of change in the turbidity, SO₂ - amount, and clouds. The AD wavelength pair will give more accurate measurements when the sun is high enough, with an airmass less than 3.5. With lower sun, the internal scattering and skylight will influence and give too low ozone values.

In 1986 the instrument was in Arosa for a new intercomparison. In spite of satisfactory Hg-lamp tests new N-tables were required after the Arosa intercomparison. This resulted in an increase in the calculated ozone amounts after 1986 of about 3-4%. This may be caused partly of a change in internal scattering from all optical components and a change in the photomultiplier response.

The ozone data presented here are recalculated data. The relative large data set has made it possible to construct new zenith chart where model calculation and observations have been combined. A radiative energy transfer model for the atmosphere has been used, where primary and multiple scattering from the zenith sky, are derived. The ozone distribution in the model has been selected from ozone sonde ascents carried out near Oslo.

The cloud correction charts are constructed in a similar way by using a large particle scattering model and combine the model calculations with observations.

One has to trust the intercomparisons in 1977 and 1986 where the instrument has been compared directly to the world standard No 83. We first assumed a linear drift of the instruments calibration from 1977 to 1986 and afterwards a stable instrument. The data were recalculated with changing R-N tables incorporated in the computer program. We were not quite satisfied with this procedure. Being aware of the breakdown of the instruments electronics in 1980, which took the instrument out of operation several months in 1980-81, we decided to follow another course. The 1977 R-N tables were used for the data up to the end of 1980 and the 1986-tables were used from the summer 1981 and onward. The ozone data now derived, seem to agree well with the data from nearby stations as Norrköping, Copenhagen and Lerwick. The recalculated data also

agree well with the data derived from our Brewer instrument which we installed in 1990. In all our calculations we have used the ozone absorption and molecular scattering coefficients recommended by WMO, Ozone Commission, in December 1991. Our Brewer instruments calibration was checked against the travelling standard instrument in the summer 1991.

REVISION OF THE DATA SET

The measurements in Oslo, 60° N, carried out with the Dobson spectro-photometer No 56, were a supplement to the measurements which had been established in Tromsø, 70° N, in 1936 and in Longyearbyen at Spitzbergen, 78° N, in 1950. The behaviour of the atmospheric ozone over Oslo seems to be representative for the condition in the Arctic. A comparison between the winter values of the total ozone in Oslo and the mean values of 12 stations north of 58° N, agreed very well in the period 1978-1986. In 1986 the series of the 12 stations means were terminated (1,2).

After the dataset for Oslo has been revised, the ozone data should be more reliable and a more structural picture of the ozone behaviour appears. The variations in the ozone amount can be large and rapid and are well correlated with the movements of the polar front. This change in weather condition will influence the quality of the observations. In cloudy weather one has to depend on zenith light observations which are less accurate than the basic direct sun observations. A rapid change of weather may also alter the vertical ozone profile which introduces uncertainties in the method of observation. This is, however, the situation.

In order to improve the zenith sky method of observation, we plan to introduce another type of measurements. Our Brewer spectrophotometer, M4, measures the global UV irradiation. From a calculated or empirical constructed radiation chart, one can estimate the ozone values. This has been done in Antarctica and in Tromsø (3). It seems as if clouds will make very little influence.

Most of our direct sun measurements are made with the C wavelengthpair. Since 1990 the AD combination has been a regular routine in our observing program.

The AD measurements are recommended since they are least dependent of atmospheric scattering. However, our routine observing program is always, C, A, D, C and C'. This means C, A, D, C direct sun and CC' zenith sky observations. The difference between C and AD direct sun has decreased since we started to use the new absorption coefficients. The difference C-AD seems to have seasonal variations with a higher value in the Spring. If the C-AD difference is large, C direct sun usually gives a higher ozone amount than the corresponding zenith light observation when the revised zenith blue charts are used.

When the solar zenith angle is less than 75° we think that an AD measurement gives the true ozone value. For higher solar zenith angles, however, they may be too small due to the very low intensity in the A wavelength pair. In the autumn when the clear sky is more common, one would expect the C direct sun to give reliable ozone values for solar zenith angles up to 78°, and still higher with the focused image method. Due to this, the C direct sun measurements have been used to revise the zenith charts.

PRESENTATION OF THE RECALCULATED OZONE DATA IN OSLO

As declared, we decided to use two set of R-N tables. We used the 1977-tables for the data from February 1, 1978 to November 6, 1980. The 1986-tables were used from July 1, 1981 and onward. In the meantime we used the Dobson instrument no 14 which we had in Oslo at that time.

To get more reliable ozone values from the zenith sky observation, much work has been done to make the zenith charts better. We checked the quality of the zenith chart, by calculating the difference between zenith sky and direct sun measurements. The difference should be as near zero as possible.

The method used to obtain reliable ozone values from the zenith sky observations is to make the first attempt with chart No 1.

If the ozone value obtained is above 400 DU one goes to chart No 2 to derive the best value. If the ozone value is under 300, one goes to chart No 3 to get the best value. In this way one has counted for the fact that the vertical distribution of the atmospheric ozone changes when the total ozone amount increases or decreases. This method could be refined further. In figure 1 and 2 the ozone difference between zenith -and direct sun measurements for the two charts are shown.

With the new zenith charts applied, together with the revised cloud correction charts, revised ozone values over Oslo have been calculated. The data series cover the period from February 1978 to January 31, 1992. In figure 3 the monthly averages of total ozone are given in a diagram. The estimated linear trend is calculated. It is negative and it amounts to 4%. In the diagram in fig. 4 the TOMS monthly averages over Oslo are plotted. The linear trend is calculated. It is negative and it amounts to 10% (4).

A twelve months running mean for the Dobson measurements in Oslo has also been calculated and is plotted in the diagram in figure 5. The diagram gives an exaggerated picture of the ozone behaviour of the period around 1982 and probably the beginning of a period around 1991. Both periods will count heavily in any estimate of a trend in the ozone data.

The data set which is presented here is not ready to be used in a statistical model. There are still unsolved problems with the C direct sun and C zenith sky measurements, especially in Spring. However, the data set, which is available on disks, should be more reliable than the values given in the "Red Book", the ozone data for the world. In due time these will be revised.

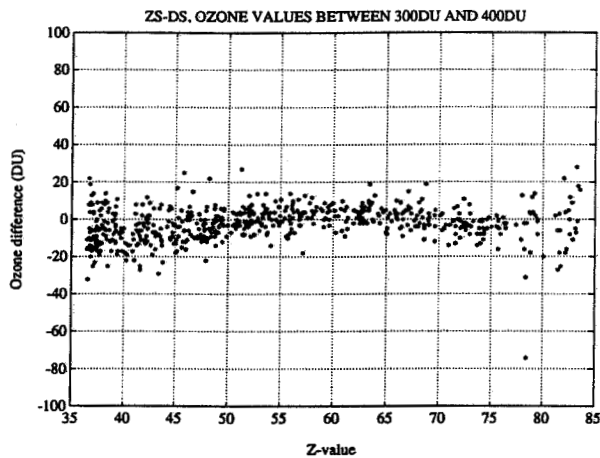


Figure 1: Ozone differences between zenith (zs) and direct sun (ds) measurements for ozone values between 300 and 400 DU. Chart No 1. (Z: solar zenith angle).

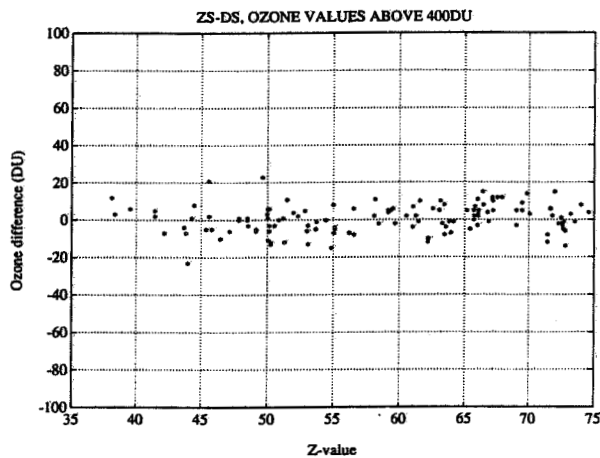


Figure 2: Ozone differences between zenith and direct sun measurements for ozone values above 400 DU.

MONTHLY AVERAGES
Dobson instrument no. 56, Oslo

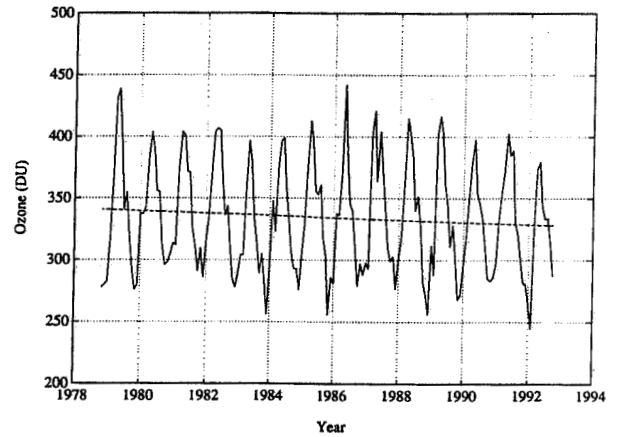


Figure 3: Total ozone amount at Oslo, monthly averages from Dobson measurements.

MONTHLY AVERAGES
TOMS satellite

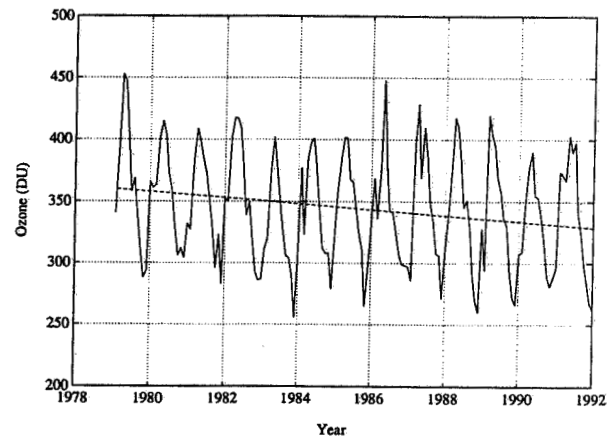


Figure 4: Total ozone amount at Oslo, monthly averages from TOMS data.

Dobson instrument no. 56, Oslo

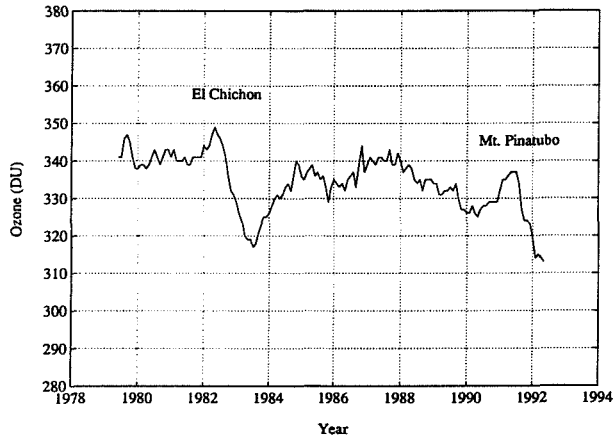


Figure 5: The twelve months running mean of the total ozone amount from Dobson measurements in Oslo.

REFERENCES

1. Bojkov, R.D., *Met. atmos. Phys.*, **38**, 117-127 (1988).
2. Larsen, S.H.H., Henriksen, T., *Nature*, Vol. 343, Jan. 124 (1990).
3. Stamnes, K. and Svenø. T., personal communication.
4. TOMS data are obtained from the data base at NILUm Norwegian Institute for Air Research,

303841

TOMS TOTAL OZONE DATA COMPARED WITH NORTHERN LATITUDE DOBSON GROUND STATIONS

B. Heese

Alfred-Wegener-Institut, Bremerhaven, Germany

K. Barthel, Ø. Hov

University in Bergen /Nansen Environmental and Remote Sensing Center, Bergen, Norway

ABSTRACT

Ozone measurements from the Total Ozone Mapping Spectrometer on the Nimbus 7 satellite are compared with ground-based measurements from five Dobson stations at northern latitudes to evaluate the accuracy of the TOMS data, particularly in regions north of 50°N. The measurements from the individual stations show mean differences from -2.5% up to +8.3% relative to TOMS measurements and two of the ground stations, Oslo and Longyearbyen, show a significant drift of +1.2% and +3.7% per year, respectively. It can be shown from nearly simultaneous measurements in two different wavelength double pairs at Oslo that at least 2% of the differences result from the use of the CC' wavelength double pair instead of the standard AD wavelength double pair. Since all Norwegian stations used the CC' wavelength double pair exclusively a similar error can be assumed for Tromsø and Longyearbyen. A comparison between the tropospheric ozone content in TOMS data and from ECC ozonesonde measurements at Ny-Ålesund and Bear Island shows that the amount of tropospheric ozone in the standard profiles used in the TOMS algorithm is too low, which leads to an error of about 2% in total ozone. Particularly at high solar zenith angles (>80°), Dobson measurements become unreliable. They are up to 20% lower than TOMS measurements averaged over solar zenith angles of 88° to 89°.

INTRODUCTION

At high latitudes, errors in TOMS total ozone are possibly larger than is generally assumed. The solar zenith angles are higher, and there are generally more variations in total ozone than at middle and low latitudes. When using TOMS data for studies of the ozone climatology and for correlations with synoptic meteorological parameters at northern latitudes it is important to know their accuracy. The objective of this study is to identify and possibly quantify errors in TOMS data by comparison with Dobson measurements at five stations at northern latitudes.

DATA AND METHOD

TOMS data exist in several versions, version 6 being the most recent. Relative to version 5, the version 6 data have been corrected for a drift caused by the degradation of the instrument's diffuser plate using the internal "pair-justification" technique. These data are in agreement within the error limits with the average of 39 ground-based Dobson stations [Herman et al., 1991]. The TOMS data were prepared

by the Ozone Processing Team of NASA Goddard Space Flight Center: J.R. Herman, R. Hudson, R.D. McPeters and R. Stolarski, Z. Ahmad, X.Y. Gu, S. Taylor, and C. Wellemeyer.

Ten years of GRID-TOMS version 5 data (1979 - 1988) and 4 years of version 6 data (1986 - 1989) have been compared with five Dobson stations at high latitudes: Oslo (59.5°N, 10.5°E), Tromsø (69.4°N, 18.6°E), Longyearbyen (78.1°N, 15.4°E), Reykjavik (64.1°N, 21.5°W), and Resolute (74.4°N, 94.6°W). The measurements at Tromsø and Longyearbyen began again in winter 1984 after a break in 1969, so that there are only 4 years for comparison. The 1979-1985 TOMS version 6 data became available in spring 1991 when most of the work for this study was done. Since the objective of this study is to find reasons for the differences between TOMS and Dobson ozone estimates and since the drift in the version 5 data for the respective years is small (0.25% per year from November 1978 to June 1982 and 0.51% per year from July 1982 to December 1985) [Fleig et al., 1988a], the version 5 data for the years 1979 to 1985 are sufficient for this purpose and can be used together with the version 6 data.

Errors of ± 2% for the TOMS data [Fleig, 1988b] and ± 3% for a typical good Dobson measurement [Basher, 1982] are assumed, so that the accuracy of this comparison is ±3.6% (rms).

RESULTS

Figures 1a and 1b show the monthly mean relative differences (Dobson - TOMS) / Dobson for Oslo and Reykjavik calculated for ground and satellite measurements taken on the same day during at least 13 days in the given month. The limit of 13 days per month is chosen to obtain a sufficient number of monthly mean values, particularly for the months around the polar night.

Almost all Dobson measurements at the five stations show greater annual mean ozone values than the TOMS total ozone of the version 5 data. Only the first 7 years at the Reykjavik station have differences less than or equal to zero (Table 1). If direct-overpass TOMS data, which have a higher resolution of about 50 km², are used instead of gridded TOMS data, their relative differences to Dobson measurements do not change significantly.

The relative differences at the stations with long measurement series show a significant annual drift of +1.0% at Oslo, +0.7% at Resolute, and +0.5% at Reykjavik, which is based upon the slope of a linear regression through the data. These individual drifts are comparable with the two-part linear fit to the drift found by Fleig et al. [1988a].

Table 2 shows the annual mean percentage differences between the ground measurements and the TOMS data of the version 6. Since the drift should be corrected in these TOMS

data, no drift should occur relative to stable ground stations. An observed drift in the relative differences at the ground stations in Oslo and Longyearbyen of +1.2% and +3.7% per year, respectively, or rather a shift from 1986 to 1987 of 2.5% and a small drift of 0.6% the following years at Oslo and a shift from 1987 to 1988 of 2.1% and 7.7% from 1988 to 1989 at Longyearbyen indicates a drift in these Dobson instruments or a shift in the observing routine at these stations. Tromsø, Reykjavik and Resolute show no significant drift, which is indicated by a low square correlation coefficient r^2 .

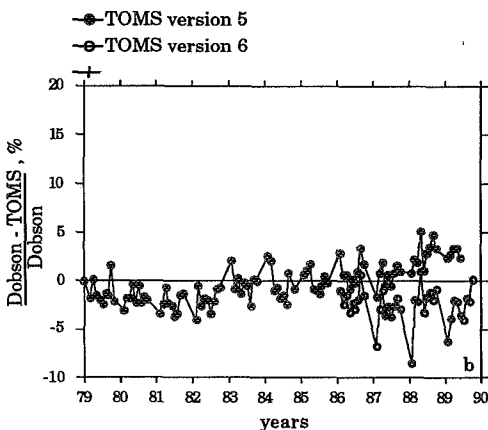
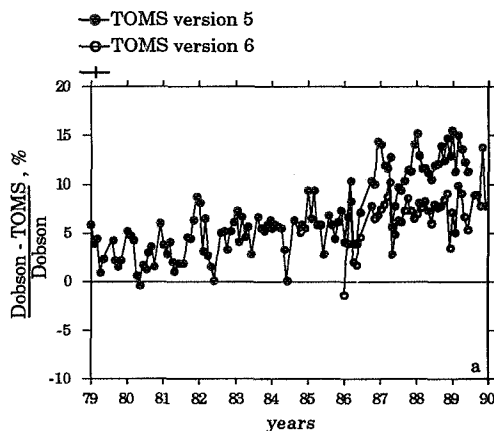


Fig. 1. Monthly mean relative differences (Dobson - TOMS) / Dobson at the ground stations in (a) Oslo and (b) Reykjavik. TOMS version 5 (solid circles) and version 6 (open circles), markers indicate new year.

For each station the relative mean difference to TOMS for the years 1986 to 1989 has been calculated from all monthly mean differences. It is as high as +6.9% and +8.3% at Oslo and Longyearbyen but lower at the other stations and within the accuracy of $\pm 3.6\%$ for this comparison: Tromsø has a mean difference of +2.9%, and Resolute has a mean difference of +1.2%, while Reykjavik is the only station with a negative mean difference of -2.5%.

TABLE 1.: Annual Mean Relative Differences Between Satellite and Ground-Based Measurements of Total Ozone: (Dobson-TOMS) / Dobson, (Version 5)

Year	Oslo	Tromsø	Longyb.	Reykjavik	Resolute
1979	3.1			-1.2	0.04
1980	2.9			-1.7	0.9
1981	3.8			-2.3	0.6
1982	4.3			-1.8	1.2
1983	5.6			-0.3	1.3
1984	5.0			-0.3	1.0
1985	6.5	7.4	9.8	0.02	4.6
1986	7.9	6.6	7.6	1.0	4.2
1987	10.9	5.7	8.4	0.5	3.5
1988	12.6	8.0	13.2	2.8	6.7

TABLE 2.: Annual Mean Relative Differences Between Satellite and Ground-Based Measurements of Total Ozone : (Dobson-TOMS) / Dobson, (Version 6)

Year	Oslo	Tromsø	Longyb.	Reykjavik	Resolute
1986	4.5	4.0	5.3	-1.8	1.7
1987	7.0	2.4	5.7	-3.1	0.1
1988	7.5	1.8	8.8	-2.3	2.3
1989	8.2	3.2	16.5	-2.8	0.5

All stations show individual differences relative to the TOMS version 6 data. While Tromsø, Reykjavik, and Resolute are within the error range of $\pm 3.6\%$ for this comparison, the difference between TOMS and Dobson at Oslo and Longyearbyen is greater than 3.6% and increases from 1986 to 1989, indicating a drift in these ground-based instruments. Some reasons for these differences have been studied for both the Dobson and TOMS measurements.

Since the relative differences are larger for all Norwegian stations, a common source of error may be present in the observation technique. Dobson measurements with the AD wavelength-pair at direct sun are standard, since they are least dependent on atmospheric scattering. The C wavelength pair is to be used together with the C' wavelength pair (332 nm, 453 nm) when clouds are present. Additionally, the pathway of the radiation through the atmosphere may be longer, which is quite important for observing stations in the north according to the relatively high solar zenith angles. However, the ozone values have to be taken from empirical charts derived from comparisons with AD measurements, since the algorithm is valid only for AD measurements [Basher, 1982]. These values may be less accurate, especially if the charts are not quite actual. All Norwegian stations measured exclusively with the CC' wavelength double pair until 1990 to obtain a homogeneous time series, while the other two stations also used the AD double pair if weather conditions permitted. This choice of the wavelength pair seems to produce errors.

Simultaneous measurements with the C wavelength pair (311 nm, 332 nm) and the AD double pair (305 nm, 325 nm; 317 nm, 339 nm) taken at direct sun in Oslo by S.H.H. Larsen, Physical Institute, from May until October 1990 show systematically higher monthly mean values in observed total ozone from the C wavelength pair between 9.1 and 21.1 DU. (Figure 2). These differences amount to 2% - 7% of the observed total ozone column. So the measurements with the CC' wavelength pair at the Norwegian stations cause an error of at least 2% in total ozone.

Thus one reason for the systematically higher Dobson ozone-values could be found in the permanent use of a different wavelength pair than the standard AD wavelengths. Since

1990 the Norwegian stations have also used the AD wavelength double pair if weather conditions permit (S.H.H. Larsen, personal communication, 1991) so this error should decrease in the measurements after 1989.

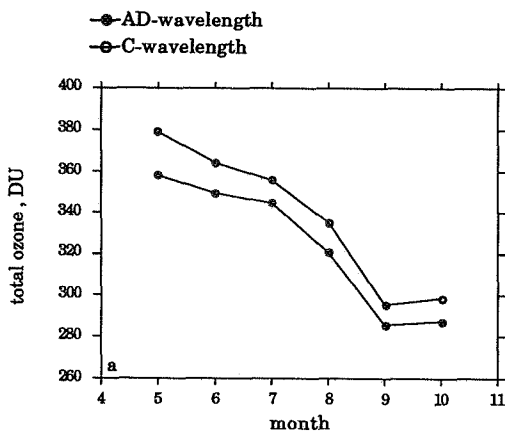


Fig. 2. Monthly mean total ozone from Dobson measurements at Oslo with the AD wavelength double pair (solid circles) and C wavelength pair (open circles) in 1990.

A second possible error source lies in the correction of TOMS measurements to tropospheric ozone, which is measured only partially because the effective reflecting surface for the backscattered radiance lies in the upper troposphere. So the amount below this layer, i.e., most of the tropospheric ozone, depends on the standard ozone profiles in the TOMS algorithm. These standards are fixed climatological, annual means. Thus seasonal and day to day variations up to 50% in tropospheric ozone and a long term trend of 0.5 - 1.0% per year observed by sonde measurements at several stations in the northern hemisphere [Bojkov, 1988] will not be measured by TOMS.

To study the resultant error, the ozone amount in the two lowest layers (up to 240 hPa) of the TOMS standard profiles were compared with the amount in the same layer measured by electrochemical concentration cell (ECC) ozonesondes at Ny-Ålesund and on Bear Island in 1989. The layers from ground up to 240 hPa represent the troposphere only roughly but allow for an approximation of the error size. ECC sonde frequency was irregular, in particular at Ny-Ålesund, and some sondes at both stations were destroyed at low altitude. They are omitted, and the remaining number of sonde measurements are 25 for Ny-Ålesund and 28 for Bear Island. The sonde data have been made available by the German Alfred Wegener Institute (AWI), the Norwegian Institute for Air Research (NILU), and the Norwegian Meteorological Institute (DNMI).

Figure 3 show that the tropospheric ozone of almost all ECC measurements at Ny-Ålesund are higher than in the TOMS standard profiles, especially in summer. The same was found for Bear Island. This shows that the seasonal variations of tropospheric ozone, i.e., the higher values in summer, were not measured by TOMS.

The resultant error in total ozone can be seen from the relative differences between TOMS and ECC sonde measurements (Figure 4). Averaged over all days with observations, the mean difference is +2.3% at Ny-Ålesund and

+0.8% at Bear Island. At these two stations, roughly 1 to 2% more total ozone is measured by the sondes than by TOMS. To find the part of this difference caused by the standard ozone profiles in the TOMS algorithm, the tropospheric ozone in TOMS total ozone is replaced by the value measured by the ECC sondes. Then the averaged relative difference in total ozone changes significantly at both stations by about -2% (Figure 4).

The ECC measurements are quite good in the troposphere, about ±2% error (Komhyr, 1985) Hence, the TOMS total ozone measurements are at least 2% too low and show seasonal variations because of the dependence of the tropospheric ozone amount in the standard ozone profiles in the algorithm.

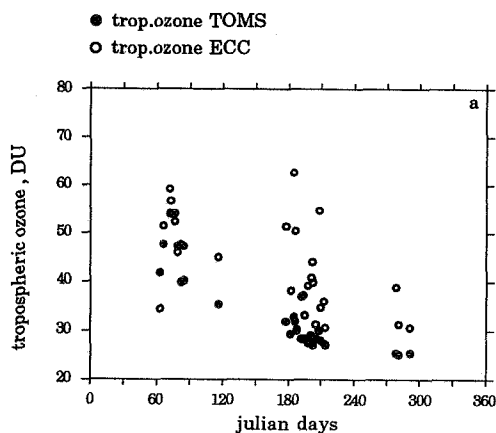


Fig. 3. Tropospheric ozone from TOMS standard profiles and ECC sonde measurements in Ny-Ålesund in 1989.

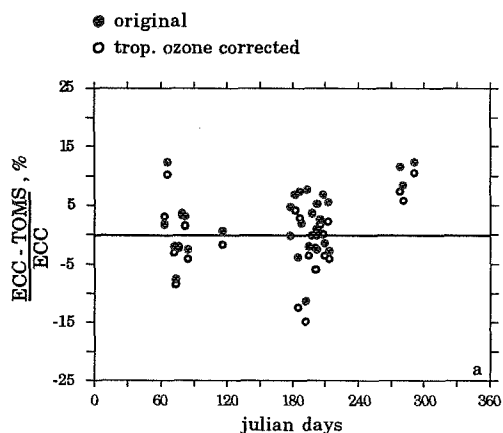


Fig. 4. Relative differences in total ozone between TOMS and ECC sonde measurements $(ECC - TOMS) / ECC$ in Ny-Ålesund. Original TOMS measurements (solid circles) and TOMS with tropospheric ozone corrected (open circles).

Another possible error source is the high solar zenith angle (SZA) at the time of observation. The relative differences between TOMS version 6 and Dobson measurements for the years 1986 to 1989 versus the TOMS SZA (Figure 5) show lower values as well as larger scatter at SZA greater than 80°. The larger scatter is probably caused by the higher dependence of TOMS total ozone on the standard vertical profile, since the reflecting surface moves upward into the ozone layer at high SZA [Dave and Mateer, 1967; Pommereau, 1989] and the path length of UV radiance through the atmosphere becomes greater.

At the Reykjavik station, three February mean relative differences in the 4 years of the version 6 data were as low as -6.7%, -8.6%, and -6.3% (Figure 1b). These negative difference may partly be caused by the relatively high number of measurements at high SZA in February. Large increase in TOMS data relative to Dobson for measurements at high SZA were found especially at Reykjavik (Figure 5) and Resolute. When averaged over 1° intervals of the SZA, the Dobson measurements at Reykjavik are up to 20% smaller than TOMS at SZA of 88° to 89°.

This is contrary to the results reported by Pommereau [1989], who found that the TOMS version 5 ozone content decreases relative to SAOZ (Système d'Analyse par Observation Zénithale) measurements at Dumont d'Urville and Greenland with increasing SZA. The SAOZ is constructed to measure at high SZA, so that these measurements should be more accurate and the error should lie in the TOMS data. Pommereau has found that the differences are largely reduced when using the TOMS version 6 data because of the additional standard profiles in the new algorithm for polar conditions (J.P. Pommereau, personal communication, 1991).

Since Dobson measurements are taken at SZA higher than 80° at the five stations, where they become unreliable [Komhyr, 1980], the results from Pommereau and from Figure 5 indicate that the Dobson measurements at SZA higher than 80° are particularly inaccurate.

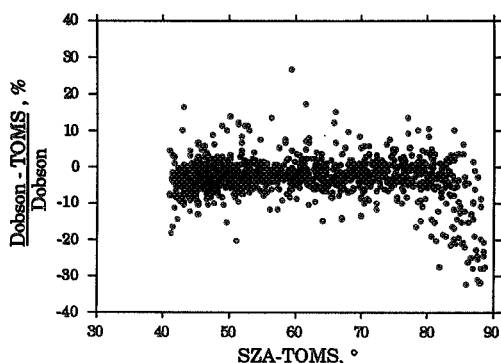


Fig. 5. Relative differences in total ozone at Reykjavik versus the solar zenith angle (SZA) at the time of TOMS measurements.

SUMMARY

The comparison between total ozone measurements from satellite (TOMS) and ground-based (Dobson) measurements show significant differences between the ground stations. For the years 1986 to 1989 the relative mean difference to TOMS can be calculated for each station. It is as high as +6.9% and +8.3% at Oslo and Longyearbyen but lower at the other stations

and within the accuracy of $\pm 3.6\%$ for this comparison: Tromsø has a mean difference of +2.9%, and Resolute has a mean difference of +1.2%, while Reykjavik is the only station with a negative mean difference of -2.5%.

A drift of +1.2% per year in Oslo and +3.7% per year in Longyearbyen is found in the relative differences. Since there is no drift in the TOMS data from the algorithm version 6, the observed drift may be due to some drift in the Dobson instrument at the ground stations.

It can be shown from nearly simultaneous measurements in two different wavelength double pairs in Oslo that at least 2% of the difference results from the use of the CC' wavelengths instead of AD wavelengths. Since all Norwegian stations have used the CC' wavelengths exclusively, a similar error can be assumed for Tromsø and Longyearbyen. Since 1990 the Norwegian stations have also used the AD wavelength double pair if weather conditions permit (S.H.H. Larsen, personal communication, 1991) so this error should decrease in the measurements after 1989.

Another error source is mainly caused by the use of standard ozone profiles in the TOMS algorithm. The comparison between the tropospheric ozone amount in these standard profiles and from ECC ozonesonde measurements shows that the tropospheric ozone in the standard profiles used in the TOMS algorithm is too low, and this leads to an error of about 2% in total ozone.

Solar zenith angles in northern latitudes are higher than 80° during a significant part of the year. The relative differences between TOMS and Dobson total ozone show a higher scatter at large SZA, so that daily ozone values, in particular, may be in error.

REFERENCES

- Basher, R.E., Review of the Dobson spectrophotometer and its accuracy, Rep. 13, Global Ozone Res. and Monit. Proj., World Meteorol. Organ., Geneva, 1982.
- Bojkov, R.D., Ozone changes at the surface and in the free troposphere, in *Tropospheric Ozone*, edited by I.S.A. Isaksen, pp. 83-96, D.Reidel, Norwell, Mass., 1988.
- Dave, J.V., and C.L. Mateer, A preliminary study on the possibility of estimating total atmospheric ozone from satellite measurements, *J.Atmos.Sci.*, 24, 414-427, 1967.
- Fleig, A.J., D.S. Silberstein, C.G. Wellemeyer, R.P. Cebula, and P.K. Bhartia, An assessment of the long-term drift in TOMS total ozone data, based on the comparison with the Dobson network, *Geophys.Res.Lett.*, 15(10), 1133-1136, 1988a.
- Fleig, A.J., A.J. Krueger, P.K. Bhartia, B.M. Schlesinger, R.P. Cebula, and C.G. Wellemeyer, Nimbus-7 total ozone mapping spectrometer (TOMS) data products users guide, *NASA Ref.Publ.* 1988b.
- Herman, J.R., R. Hudson, R. McPeters, R. Stolarski, Z. Ahmad, X.Y. Gu, S. Taylor, and C. Wellemeyer, A new self-calibration method applied to TOMS and SBUV backscattered ultraviolet data to determine long-term global ozone change, *J.Geophys.Res.*, 96(D4), 7531-7545, 1991.
- Komhyr, W.D., Operations handbook — Ozone observations with a Dobson spectrophotometer, Global Ozone Res. and Monit. Proj., Rep.6, World Meteorol. Organ., Geneva, 1980.
- Komhyr, W.D., S.J. Oltmans, A.N. Chopra, and P.R. Franchois, Performance characteristics of high-altitude ECC ozonesondes, in *Atmospheric Ozone*, edited by C.S. Zerefos and A.Ghazi, pp. 499-501, D. Reidel, Norwell, Mass., 1985.
- McPeters, R.D., and W.D. Komhyr, Long-term changes in the total ozone mapping spectrometer relative to the world primary standard Dobson spectrometer 83, *J.Geophys.Res.*, 96(D2), 2987-2993, 1991.
- Pommereau, J.P., Ground-based stratospheric monitoring by ultraviolet and visible spectrometry, paper presented at *Die nordpolare Stratosphäre im Winter 88/89*, BMFT-Workshop, Federal Min. for Res. and Techn., Bonn, Germany, June, 12-13, 1989.

SYSTEMATIC COMPARISON BETWEEN THE GROUND BASED AUTOMATED DOBSON OF THE
OBSERVATORY OF HAUTE-PROVENCE AND TOMS SINCE 1983

Marie-France Mérienne, Alain Barbe, Pierre Da Conceição

Groupe de Spectrométrie Moléculaire et Atmosphérique
URA D1434 - UFR Sciences 51062 REIMS - FRANCE

ABSTRACT

The total ozone quantity has been obtained since September 1983 at O.H.P. using the conventional AD wavelength technique. An average of 180 measurements per year is obtained with the Dobson n°85. Each of these daily total quantity is in fact an average of at least 5 measurements. The preliminary comparison with TOMS data show good agreement. We discuss systematic daily and monthly comparisons.

INTRODUCTION

The Dobson instrument based at Observatory of Haute-Provence was automated in 1983. It is considered to be very accurate, as confirmed by all the intercalibrations. It is then interesting to compare its results with those of the TOMS aboard Nimbus 7 up to 1992.

RESULTS

1. In order to have the most accurate results, we keep only AD direct sun measurements. For the same reason, only days with at least 5 measurements are compared with TOMS values.

In figure 1 the two sets of data for monthly mean total ozone are compared. A global agreement is easily observed. As an example the low observed value for february 1990 is obviously obtained by both instruments.

For further details we have undertaken a systematic daily and monthly comparison. We restrict our figures, examples and remarks to the year 1989, but all the comments are the same for other years.

In figure 2 monthly mean total ozone values for 1989 are plotted. The agreement is good for nine months, with a systematic discrepancy of -3 to -4% by TOMS due to the different cross-section values used for the two instruments. For other months differences can also be explained : for April, due to local weather conditions, only one measurements (in perfect agreement) is obtained by the Dobson between the first and 14th ; all the TOMS value during this period are lower than the monthly average. This explains the lower average for TOMS. In February the same explanation holds but in the opposite direction : values of TOMS without Dobson observations from the

16th to the 28th are higher than monthly average.

Daily values are plotted in figure 3. In figure 4 we have plotted the daily differences expressed as a percentage. The same global comments can be applied as mentionned above. If we take as an example the March values, we note a significantly larger value for the Dobson than for TOMS values on the 8th. The explanation is as follows :

TOMS has performed its measurements giving 367 Dobson units at 10H22. The Dobson instrument began 15 measurements (389 D.U. at 11H10 up to 402 D.U. at 12H53), followed by 7 measurements between 14H00 (432 D.U.) up to 11H23 (435 D.U.). Thus, it is shown that the extrapolation from Dobson values should give about the same total ozone (amount) as the TOMS at 10H22.

For a few days, for which differences are significant, we do not have specific explanations : for example, on March 13th, TOMS gave 374 D.U. at 10H50 and 25 measurements by Dobson showed no real diurnal variation : 20 measures from 10H20 (349 D.U.) up to 13H00 (355 D.U.) and 4 measures of 339 D.U. from 16H00 to 16H30. We note that on this day the sky was slightly hazy. For that reason, we are continuing this detailed comparison to look at possible problems in retrieval by TOMS when the sky is cloudy.

2. Relation with local meteorological conditions. Before comparing the results with satellite data, we note a quasi systematic correlation between large variations of total ozone and a strong local winds (Mistral). Because, this wind is tropospheric, it is interesting to consider the stratospheric dynamics, in order to explain these big variations. For example, on the February 25th 1988, the stratospheric wind trajectories obtained from french meteorology and european center for medium range weather forecasts clearly show north air masses arrivals coming from higher latitude. These air masses have a high ozone content. Figure 5 shows of the trajectories at ending pressure level 70hPa.

CONCLUSION

Systematic comparison between TOMS measurements and ground based Dobson value at OHP shows fairly good agreement. But in order to detect small trends (less than 0.4% per year), it is absolutely necessary to have very accurate measurements.

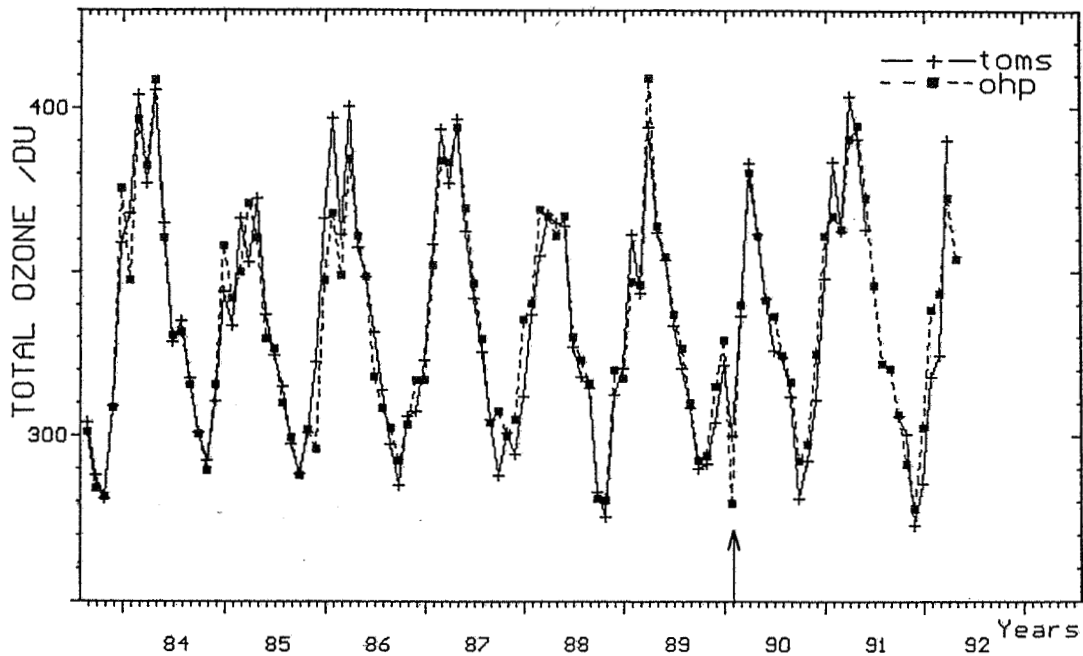


Fig 1 : Monthly mean Total Ozone : comparison between TOMS and DOBSON -OHP (September 1983 - April 1992)

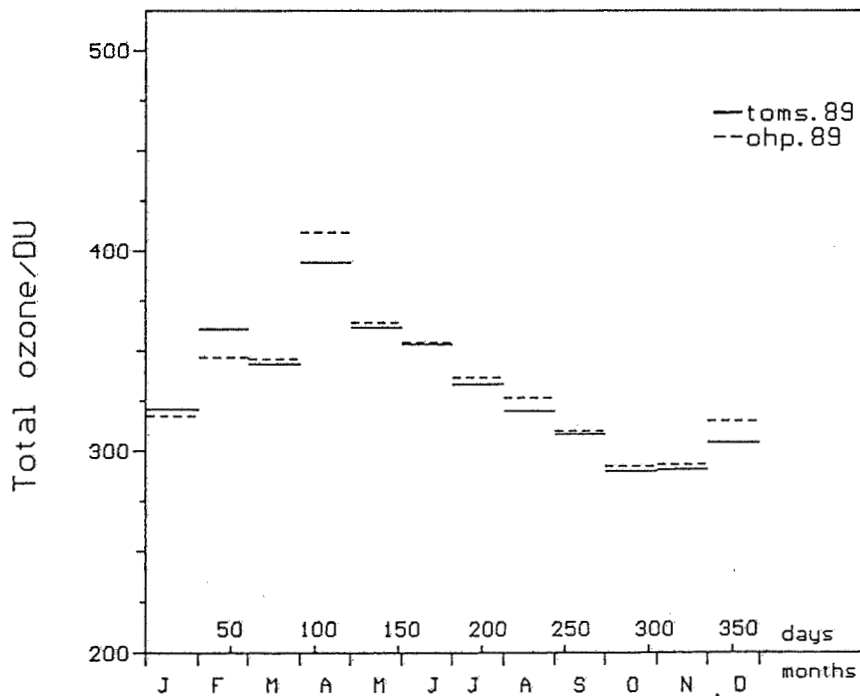


Fig 2 : Monthly mean Total Ozone: comparison between TOMS and DOBSON-OHP measurements in 1989

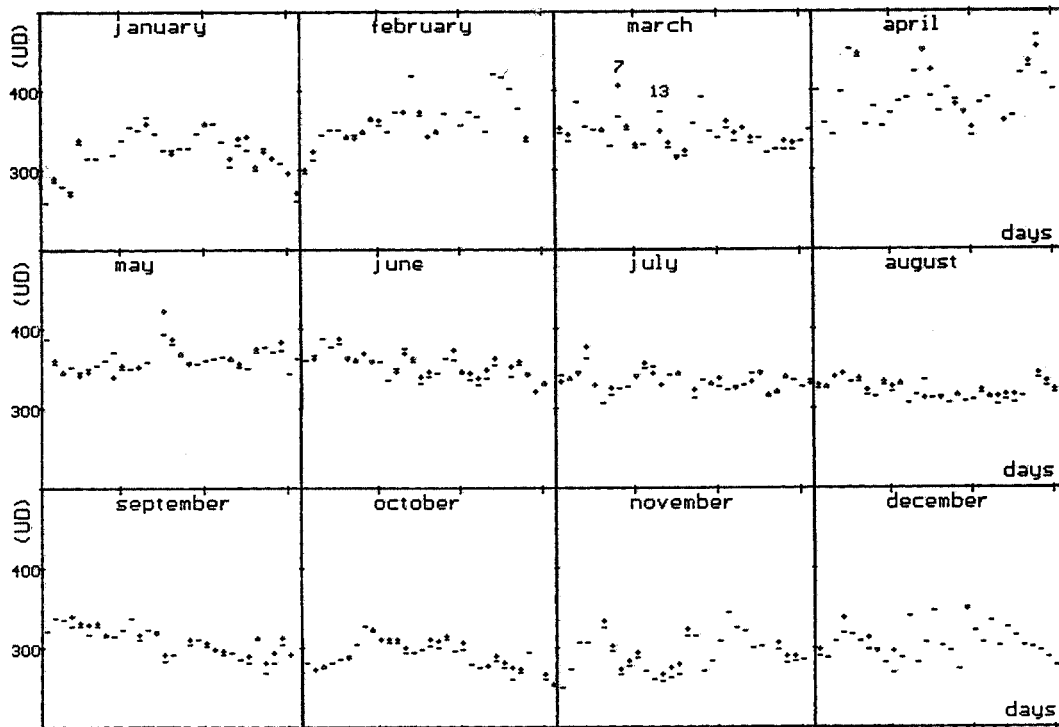


Fig 3 : Daily Total Ozone: comparison between TOMS (—) and DOBSON-OHP (+) measurements in 1989

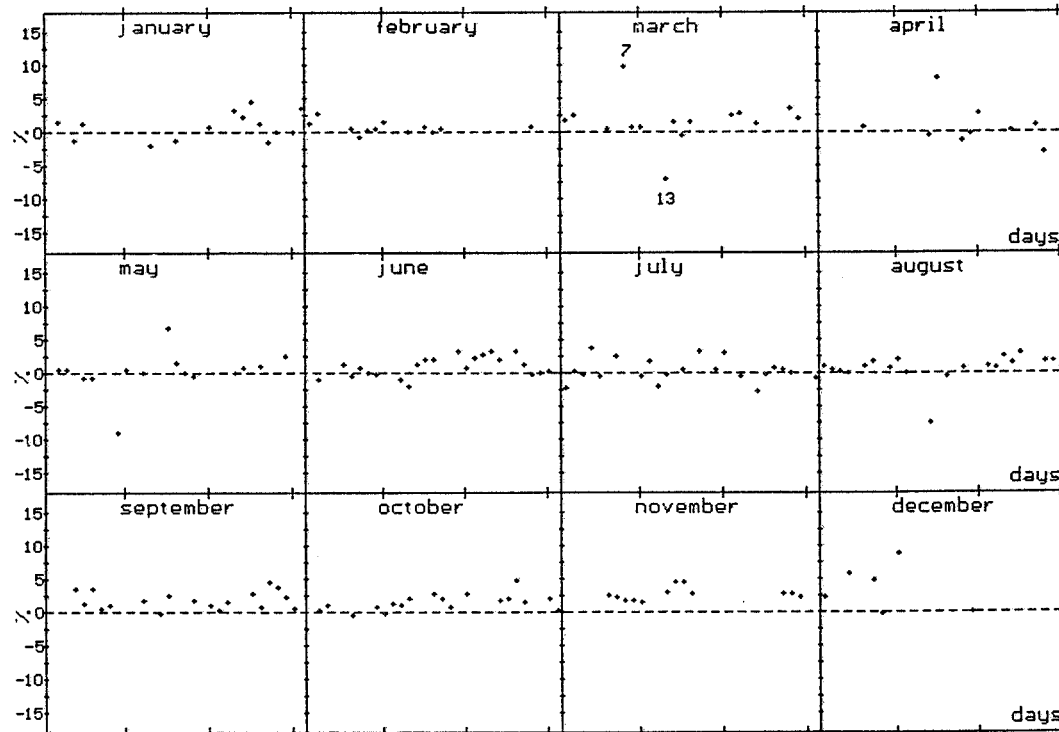


Fig 4 : Daily Total Ozone: Relative differences between TOMS and OHP in 1989. $(OHP - TOMS) / OHP$ (%)

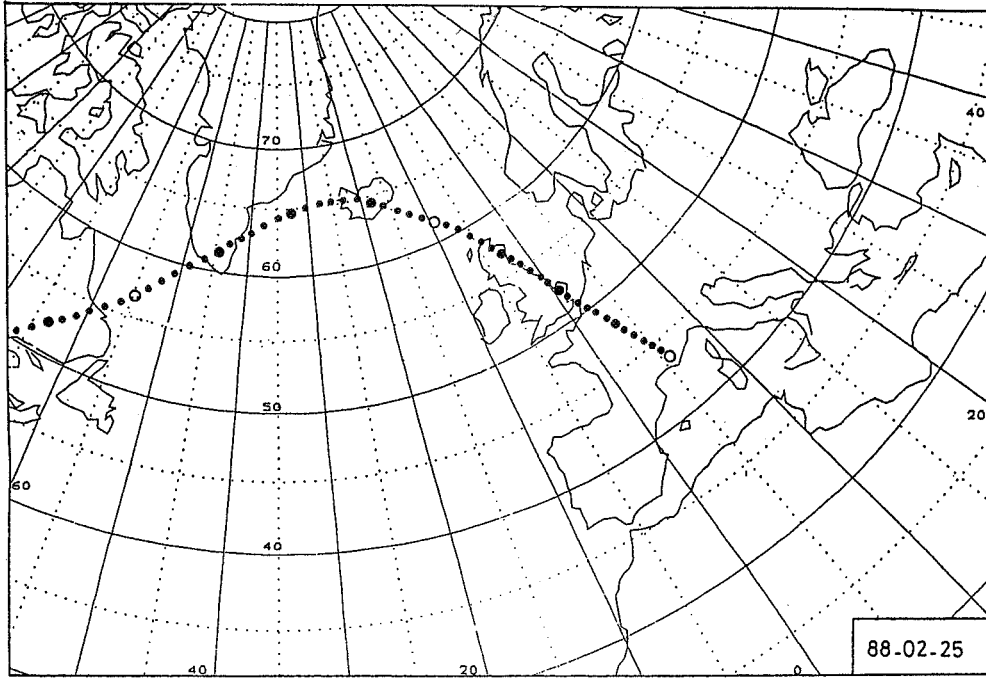


Fig 5 : Air mass backward trajectory ending at O.H.P.
 1988-02-25-12UT. Ending pressure level 70hPa. o-o: 24h ●-●: 6h - - -: 1h

303595

TOTAL OZONE CHANGE ESTIMATIONS FOR DIFFERENT
TIME INTERVALS

Vitali E. Fioletov

Central Aerological Observatory,
Dolgoprudny, Moscow Region, Russia

ABSTRACT

To investigate total ozone behavior in different time intervals for the 40°-52°N and 53°-64°N latitudinal bands sliding 11 year linear trends with the first interval from 1959 to 1969, and the final one from 1980 to 1990 were computed.

The most recent 11-year trends are negative and have larger absolute values than in the past. The trend values in the period from 1980 to 1990 in the 53°-64°N band are -4.3% (winter), -3.2% (summer), -3.8% (annual) per decade, and in the 40°-52°N band they are -5.9% (winter), -2.7% (summer), -3.6% (annual) per decade.

1. INTRODUCTION

A thorough investigation of the available data conducted by the NASA / WMO Ozone Trend Panel [1988] (OTP) has shown that in the winter time some ozone depletion occurs in the middle and high latitudes.

To examine the question of the starting of ozone depletion and its temporal variations considered are total ozone trends' estimations at various 11-year intervals in the middle (40°-52°N) and subpolar (53°-64°N) latitudinal zones using the Dobson and filter network data. The investigation was conducted with the linear and "hockey stick" trend functions. The analytical relationship between these two trend functions has been analyzed.

2. DATA SET

The data used in the analysis were monthly mean total ozone values with revisions done by Dr.R.Bojkov and by the national operating agencies for the period from January 1958 to March 1991. Besides the Dobson, the revised data of 29 stations of the USSR network (see Bojkov and

Fioletov, 1992) for the period from January 1973 to March 1991 were also used.

Before the zonal means calculation the annual circle was removed from the series of individual stations, and deviations from the annual circle at individual stations for each month were averaged over all the stations in the latitudinal belt.

The solar flux data at 10.7 cm wavelength were used as an indicator of the solar activity.

3. STATISTICAL MODEL

For obtaining trend estimates with minimum errors all the periodical constituents present in the series should be taken into account. For QBO-component isolation the Ormsby bandpass filter was used, which was applied by Hasebe [1980] to the total ozone series. The solar activity influence was isolated by the regression procedure.

A "hockey stick" dependence in the capacity of the trend function was offered by OTP: up to a certain moment this function is constant, and farther it grows linearly:

$$f(i) = \begin{cases} a, & -m+1 \leq i < 0 \\ a+ib, & 0 \leq i \leq n \end{cases}$$

In the OTP report point "zero" corresponds to December 1969; the data were analyzed for the period from December 1964 to November 1986. The "hockey stick" function use is possibly justified when we search for the freons influence on ozone, but this function is hardly suitable for the investigation of trends in total ozone behavior in various periods. For this purpose the linear trend function (1-trend) has been studied in the paper:

$$f(i) = a+ib_1, 0 < i \leq n.$$

Total ozone changes for the period of n years for s- and l-trends equal bn . The least squares method yields the following estimates for the total ozone changes :

- for l-trend (Δ_l):

$$\Delta_l = b_l = \frac{12 \sum_{i=1}^n (x_i - \bar{x}) i}{(n+1)(n-1)}$$

- for s-trend (Δ_s):

$$\Delta_s = b_s n = \frac{12(n+m) \sum_{i=1}^n (x_i - \bar{x}) i}{(n+1)(n^2 - n + 4nm + 2m)} + \frac{6(\bar{x} - \bar{\bar{x}}) nm}{(n^2 - n + 4nm + 2m)}$$

where

$$\bar{x} = \frac{1}{n} \sum_{i=1}^n x_i, \bar{\bar{x}} = \frac{i}{m} \sum_{m_i=-m+1}^0 x_i$$

Thus, Δ_s and Δ_l are related by the relationship:

$$\Delta_s = \Delta_l \left(1 - \frac{3m(n+1)}{n^2 - n + 4nm + 2m}\right) + \frac{6(\bar{x} - \bar{\bar{x}}) nm}{n^2 - n + 4nm + 2m}$$

4. THE TOTAL OZONE TRENDS ESTIMATIONS

In Figure 1 the estimations results of ozone changes for l- and s- trend functions

in the interval from December 1969 to November 1990 are shown; for s-function estimation all the data since December 1964 are being used. The discrepancy between the estimations is relatively small and is within the limit of one standard error. The filter data addition does not practically effect trend's estimation. Trends are negative practically in all month in both latitudinal belts.

To study total ozone behavior in different time intervals for the latitude bands $40^\circ - 52^\circ N$ and $53^\circ - 64^\circ N$ computed were sliding 11-year linear trends with the first interval from 1959 to 1969, and the final one from 1980 to 1990. The annual, winter (DJFM) and summer (MJJA) trends were computed (Figure 2). Standard errors of the trend estimations are, approximately, 2% per decade for winter trends, 1% for summer, and 0.7% for annual.

The results are little affected by the type of the data set used, irrespective of the fact either it is Dobson, or both Dobson and filter data. When computing the trends QBO and the solar cycle were taken into account.

The annual average trend is positive in the early part of the record in each of the two latitude bands. Since the 11 year period from 1965 to 1975 the trend at both latitudes has been consistently negative. The winter trend is also positive at the beginning of each record, more so in the $53^\circ - 64^\circ N$ band. The winter trend in the $40^\circ - 52^\circ N$ band is negative in every 11 year interval starting with 1962 through 1972. Till recently the maximum negative trend in this latitude band occurs in the 1966 to 1976 interval (4.7% per decade), also large

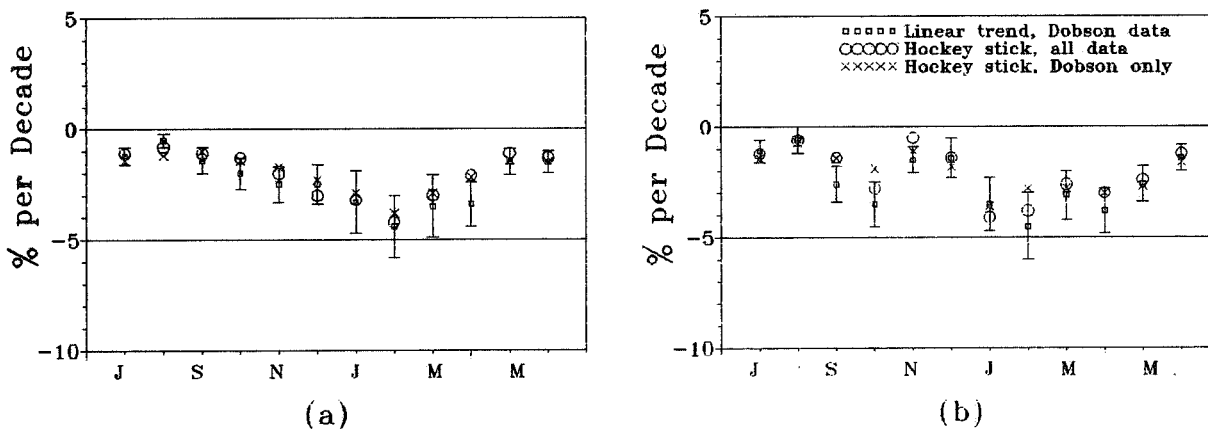


Fig. 1. Total ozone trends versus month for the period December 1969 - November 1990 on the $40^\circ - 52^\circ N$ (a) and $53^\circ - 64^\circ N$ (b) latitude bands for different data sets and trend functions. Bars show one sigma intervals for linear trend.

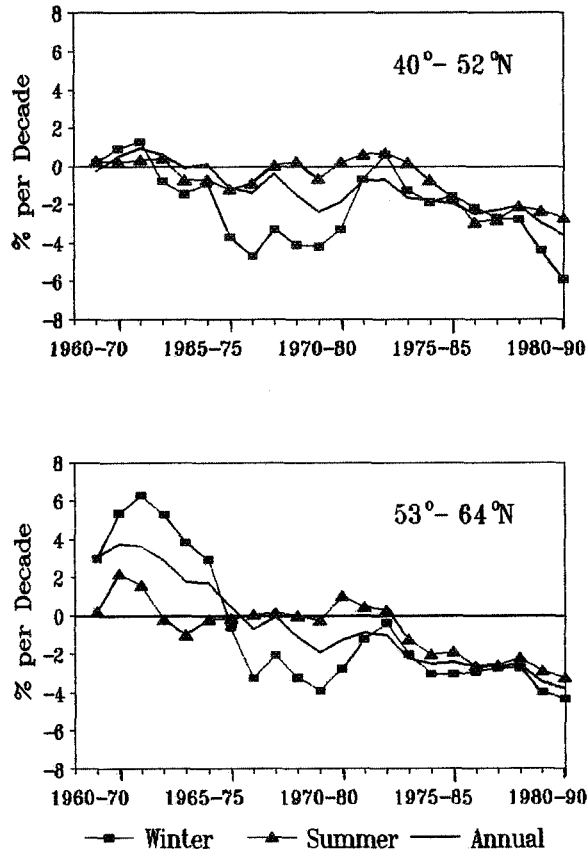


Fig. 2. Sliding 11-year trend determined for the latitude bands 40° - 52° N and 53° - 64° N (all data). Each point on the graph was obtained by fitting a linear 11-year trend through the given time period.

(>3% per decade) negative trends occur in all the 11-year periods ending in the 1975-1980 range. At this time the winter trends in the 53° - 64° N band are also negative (2%-3.9% per decade) with the maximum value in the 1969-1979 interval. The summer trends in both latitude bands are near zero over most of the record. The first 11-year period with a significant negative trend occurs in 1973-1983. The most recent 11-year trends have larger absolute values than in the past. The trend values in the period from 1980 to 1990 in the 53° - 64° N band are -4.3% (winter), -3.2% (summer), -3.8% (annual) per decade, and in the band 40° - 52° N they are -5.9% (winter), -2.7% (summer), -3.6% (annual) per decade.

5. SUMMARY AND DISCUSSION

The largest absolute values of negative trends take place in the last decades. Ozone decrease occurs in both latitudinal zones in winter as well as in summer months.

Large positive winter trends in the 60-s and early 70-s in the 53° - 64° N latitudinal belt are hardly trustworthy. In this period the zonal means were estimated from the data of three-four stations only.

Significant negative trends in the winter time in both zones in the intervals from 1966-1976 to 1970-1980 are probably connected with the relatively high ozone values in the winter time at the end of 60-s. It should be noted that between the ozone minima (or maxima) and the western (eastern, respectively) QBO phase there is a clear correlation. But in January 1968 and 1970 maxima were observed during the western QBO phase! At the same time in these months a sudden stratospheric warming occurred which is extremely seldom occurred during the western phase [Labitzke, 1982]. Only twice for all the observation period there occurred a stratospheric warming during the western phase in January. Stratospheric circulation changes during the period of warming lead to the penetration of the tropical and middle latitudes air, rich in ozone, into the polar regions, thus causing total ozone increase.

REFERENCES

- Bojkov, R.D., V.E. Fioletov, Ozone changes from Eastern Europe to Far East, Quadrennial Ozone Symposium, Charlottesville, Virginia, 1992, Abstracts, p. 185.
- Hasebe, F., A global analysis of the fluctuation of total ozone. II Non-stationary annual oscillation, quasi-biennial oscillation and long-term variation in total ozone, J. Meteorol. Soc. Japan, 58, 104-107, 1980.
- Labitzke, K., On the internal variability of the middle stratosphere during the northern winters, J. Meteorol. Soc. Japan, 60, 124-139, 1982.
- Reinsel, G.C., G.C. Tiao, S.K. Ahn, M. Pugh, S. Basu, J.J. DeLuigi, C.L. Mateer, A.J. Miller, P.S. Connell, and D.J. Wuebbles, An analysis of the 7-year record of SBUV satellite ozone data: global profile features and trends in total ozone, J. Geoph. Res., 93, 1689-1703, 1988.
- Watson, R.T., M. Prather, and M.J. Kurylo, Present state knowledge of the upper atmosphere 1988: An assessment report, NASA reference publication, 1208, 1988.

303697

DIFERENCES BETWEEN RECALCULATED AND ORIGINAL DOBSON TOTAL OZONE DATA FROM HRADEC KRALOVE, CZECHOSLOVAKIA, 1962-1990.

Karel Vanicek

Solar and Ozone Observatory, Czech Hydrometeorological Institute
Hvezdarna 456, 500 08 Hradec Kralove 8, Czechoslovakia

ABSTRACT

Backward re-evaluation of long-term total ozone measurements from the Solar and Ozone Observatory of Czech Hydrometeorological Institute at Hradec Kralove, Czechoslovakia, was performed for the period 1962-1990. The homogenization was carried out with respect to the calibration level of the World Primary Standard Spectrophotometer No.83 - WPSS by means of day-by-day recalculations of more than 25000 individual measurements using the R-N Tables reconstructed after international comparisons and regular standard lamp tests of the Dobson spectrophotometer No.74. The results showed significant differences among the recalculated data and those original ones published in the bulletins Ozone Data for the World. In the period 1962-1979 they reached 10-19 D.U. (3.0-5.5%) for annual averages and even 26 D.U. (7.0%) for monthly averages of total ozone. Such differences exceed several times accuracy of measuring and can significantly influence character of trends of total ozone in Central Europe. The refore the results from Hradec Kralove support the calls for re-evaluation of all historical Dobson total ozone data sets at individual stations of Global Ozone Observing System.

1. INTRODUCTION

Long-term ground-based measurements of total ozone in the Global Ozone Observing System (GOOS) of the World Meteorological Organization (WMO) enabled creation of the data sets which are important sources of information for monitoring and analyses of the ozone layer. Nevertheless, their reliable use requires above all individual homogenization so as the data series are comparable with one another. This is one of the most important conclusions, declared in the Report of the International Ozone Trends Panel 1988 [Bojkov,1988], and recommendations of WMO.

Establishment of the Dobson spectrophotometer No.83 as a World Primary Standard Spectrophotometer (WPSS) [Komhyr et al., 1989b] and realization of international comparisons of the spectrophotometers gave a possibility to the individual measuring stations to specify relations of their instruments towards the WPSS's calibration level and to do day-by-day backward recalculations of their data sets. Some basic information and results of such homogenization of the total ozone data at the Solar and Ozone Observatory of the Czech Hydrometeorological Institute in Hradec Kralove, Czechoslovakia, are given in this contribution.

2. MEASUREMENTS OF TOTAL OZONE AT HRADEC KRALOVE

Measurements of total ozone have been performed at Hradec Kralove since August 1961, when the Observatory was incorporated into GOOS, station No.96 [WMO-WODC]. The ozone data from Hradec Kralove are regularly submitted to the World Ozone Data Center (WODC) at

Toronto from the very beginning of the measuring. They are published in the bimonthly bulletins Ozone Data for the World and frequently used by scientists in various studies concerning total ozone.

Measurements of total ozone are carried out at Hradec Kralove with the Dobson spectrophotometer No.74 which is maintained with respect to the internationally adopted regulations and recommendations [Dobson,1957a,1957b,1962, Komhyr,1980]. The Direct Sun Ground Quartz Plate (DSGQP), Zenith Blue (ZB) and Zenith Cloudy (ZC) observations are performed on the wavelength pairs AD,CD and CC'.

The spectrophotometer No.74 was renovated and adjusted by the specialists from NOAA at Potsdam, Germany in 1979. In 1986 the instrument was compared side-by-side with the WPSS No.83 at Arosa, Switzerland. Stability of its calibration level was checked at the international comparison at Arosa in 1990 including calibration of absorption wedges and processing of new G-Tables. Comparisons of the spectrophotometer No.74 with WPSS and substandard No.65 (USA) at Arosa showed the differences of total ozone for various values of MU that did not exceed 0.35% and that confirmed its fairly good MU-dependence [Komhyr et al.,1989a,Komhyr 1990]. Since 1962 the instrument has been tested regularly while using the standard lamps 74-B, QJ-74-1,QJ-74-2 and the mercury lamp [Dobson,1957]. The results of international comparisons and standard lamp tests enabled homogenization of the total ozone data series from Hradec Kralove in the way described below.

3. METHODOLOGY OF HOMOGENIZATION

Creation of the total ozone data base at Hradec Kralove for the period 1962-1990 presented on the WPSS's calibration level and therefore being internationally comparable was the chief goal of homogenization. It was realized by means of backwards recalculations and complex assessment of all measurements of total ozone from the period under consideration. New R-N Tables of the spectrophotometer No.74 reconstructed for each year were applied in the data processing. The following principles were respected in recalculations.

- The R-N Tables were reconstructed on the basis of the results of the international comparisons at Potsdam 1979, Arosa 1986, Arosa 1990 and regular standard lamp tests as described by Komhyr [Komhyr,1980].

- The R-N Tables established at Arosa in 1986 after side-by-side comparison with WPSS were taken as a reference and modified for individual years by means of the correction factors given in Table 1.

- The absorption coefficients implemented by IAMAP in 1968 were used for the whole period of homogenization.

- Recalculations of DSGQP ozone values were made in the first step while the ZB and ZC ones in the end by means of correction factors established from parallel direct sun and zenith observations.

- The measurements made on the AD wavelength pair were taken as primary in the period from March to October while the CD wavelength pair was preferred in the winter period from November to February.

- The WPSS's calibration level accepted in 1986 was increased by 0.35 percent according to its shift declared at Arosa 1990 [Komhyr,1990].

More than 25000 individual measurements from the period 01. 01. 1962 - 31. 12. 1990 were recalculated in the course of homogenization and at least 60 percent of them were of Direct Sun type. In last twenty years total ozone was measured on more than 90 percent of days in a year at Hradec Kralove. After final check and assessment of the recalculated data altogether 22675 measurements were incorporated into the homogenized total ozone data base. These results were published together with detailed description of methodology of homogenization in the final report of the work [Vanicek,1991].

Table 1. Yearly averages of Standard Lamp readings and corrections of R-N Tables relative to 1986 values, Dobson spectrophotometer No.74, Hradec Kralove, 1962-1990.

YEAR	Standard Lamp Readings (°)				Corr. of R-N Tables		
	R _A	R _C	R _D	R _D -R _A	corr _{N_A}	corr _{N_C}	corr _{N_D}
1962	39.75	40.26	43.87	4.12	5.64	7.06	5.71
1963	39.70	40.23	44.06	4.36	5.69	7.09	5.52
1964	39.09	39.78	43.48	4.39	6.30	7.54	6.10
1965	39.19	40.16	43.92	4.73	6.20	7.16	5.66
1966	39.80	40.93	44.62	4.82	5.59	6.39	4.96
1967	41.23	42.54	46.18	4.95	4.16	4.78	3.40
1968	42.50	43.23	47.20	4.70	2.89	4.09	2.38
1969	41.87	43.44	46.85	4.98	3.52	3.88	2.73
1970	41.95	43.35	46.80	4.85	3.44	3.97	2.78
1971	41.80	43.30	46.60	4.80	3.59	4.02	2.98
1972	44.10	45.90	49.00	4.90	1.29	1.42	0.58
1973	39.90	41.80	45.84	3.94	5.49	5.52	5.74
1974	40.82	42.35	44.95	4.13	4.57	4.97	4.63
1975	42.25	43.50	46.15	3.90	3.14	3.82	3.43
1976	44.13	45.13	47.60	3.47	1.26	2.19	1.98
1977	44.75	45.70	48.00	3.25	0.64	1.62	1.58
1978	45.30	46.20	48.35	3.05	0.09	1.12	1.23
1979	45.68	46.62	48.63	2.95	-0.29	0.70	0.95
1979	43.76	45.97	48.76				
1979	26.66	31.76	37.13	10.47	1.63	1.35	0.82
1980	26.66	31.76	37.13	10.47	1.63	1.35	0.82
1981	26.99	32.01	37.25	10.26	1.30	1.10	0.70
1982	27.32	32.26	37.37	10.05	0.97	0.85	0.58
1983	27.64	32.50	37.50	9.86	0.65	0.61	0.45
1984	28.16	33.06	38.01	9.85	0.13	0.08	-0.06
1985	28.33	33.13	38.08	9.75	-0.04	-0.20	-0.13
1986	28.29	33.11	37.95	9.66	0.00	0.00	0.00
1987	28.36	33.33	38.03	9.67	-0.07	-0.22	-0.08
1988	28.59	33.48	38.08	9.49	-0.30	-0.37	-0.13
1989	29.14	34.00	38.53	9.39	-0.85	-0.89	-0.58
1990	28.70	33.65	38.16	9.46	-0.41	-0.54	-0.21

x Replacing of photomultiplier tube.
 xx Values before readjustment of the instrument, valid till 7/79.
 + Values after readjustment of the instrument (Potsdam, 7/79).
 ++ Extended 1980 values, valid since 7/79.
 o Reference values for corrections of R-N Tables.

4. RESULTS AND CONCLUSIONS

The main results of homogenization are demonstrated in Figure 1 and Figure 2 and in Table 2. The figures show the monthly averages of original and recalculated total ozone in spring (March), summer (June), autumn (September), winter (December) and the yearly averages in individual years. It is evident from the graphs that the original data published by WODC in the past are significantly different from those recalculated in

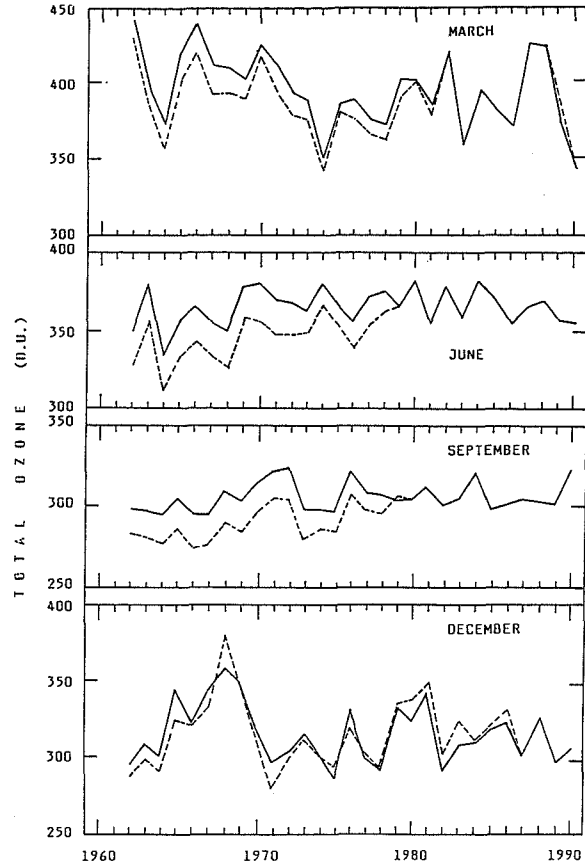


Fig. 1. Monthly averages of recalculated (full line) and original (dashed line) total ozone, Hradec Kralove, 1962-1990.

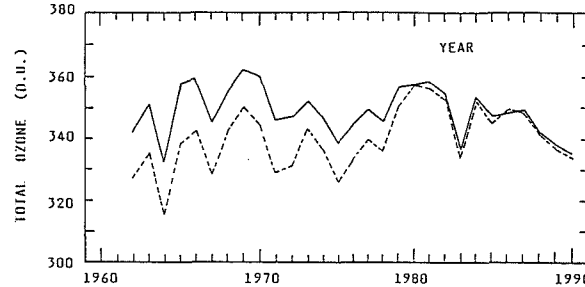


Fig. 2. Yearly averages of recalculated (full line) and original (dashed line) total ozone, Hradec Kralove, 1962-1990.

the period 1962-1979, except for the winter months. After readjustment and the first intercomparison of the spectrophotometer No.74 at Potsdam in June 1979 accuracy of measuring increased evidently at Hradec Kralove. This conclusion is demonstrated by the differences between original and recalculated monthly and yearly averages of total ozone given in Table 2 too.

The highest differences between original and recalculated values appear in the months April to October of the period 1962-1979. In the months November to February the differences are lower because of sub-

Table 2. Original minus recalculated monthly and yearly averages of total ozone (D.U.), Hradec Kralove, 1962-1990.

YEAR	MONTH												Year
	J	F	M	A	M	J	J	A	S	O	N	D	
1962	-24	-12	-15	-21	-23	-21	-24	-20	-17	-13	+1	-8	-15
1963	-11	-6	-14	-20	-22	-25	-19	-21	-19	-12	-7	-10	-16
1964	-4	-16	-18	-17	-22	-22	-20	-20	-20	-10	-10	-10	-17
1965	-11	-13	-19	-22	-23	-25	-24	-23	-20	-15	-13	-19	-19
1966	-6	-14	-19	-17	-24	-24	-25	-24	-22	-13	-11	-2	-17
1967	-7	-4	-20	-23	-25	-24	-25	-23	-21	-17	-4	-10	-17
1968	+23	-13	-17	-18	-25	-24	-26	-26	-22	-17	-8	+19	-13
1969	+15	+11	-14	-16	-25	-21	-22	-24	-20	-12	-8	-6	-12
1970	-5	-20	-8	-17	-19	-25	-24	-22	-21	-16	-13	-8	-16
1971	-8	-9	-19	-22	-17	-24	-21	-21	-18	-16	-14	-18	-17
1972	-1	-9	-16	-18	-19	-23	-25	-22	-22	-15	-10	-4	-16
1973	0	+5	-15	+5	-16	-16	-19	-18	-19	-18	-3	-3	-9
1974	+6	+2	-10	-16	-15	-16	-16	-17	-13	-16	-11	-3	-10
1975	-11	-21	-7	-18	-19	-23	-14	-16	-13	-12	+2	+7	-12
1976	+4	-1	-14	-17	-16	-18	-16	-18	-13	-9	0	-12	-11
1977	-2	-7	-10	-12	-18	-19	-18	-14	-13	-8	-5	+2	-10
1978	+8	+1	-10	-12	-14	-15	-17	-18	-13	-11	-8	0	-9
1979	-1	-16	-12	-14	-15	-1	+1	-1	+1	0	-3	+2	-5
1980	+3	-5	-1	+3	-1	0	+1	+3	-3	0	-5	+14	0
1981	+8	+10	-6	-4	0	-1	+3	+1	0	-3	+2	+6	+2
1982	+13	-2	-2	-2	-3	-1	-1	-2	-1	-1	-1	+8	+2
1983	+6	+1	+2	-1	+2	0	-1	0	+1	0	+2	+15	+2
1984	+3	+17	0	-1	-1	-4	-1	-2	-1	-1	-1	+5	+1
1985	+5	+6	0	0	+2	+1	-1	+1	+1	-1	+9	+3	+2
1986	-4	+2	-2	-1	0	0	-3	-1	-1	-1	+6	+4	-1
1987	+8	+6	+2	-1	-1	-1	-2	-2	0	+3	-1	+1	+1
1988	+4	+5	-1	-1	-1	-1	-1	-1	-1	-1	-1	-1	0
1989	-1	-1	-3	-1	-1	-1	-1	-1	-1	-1	-1	-1	-1
1990	-1	-1	-1	-1	-1	-1	-1	-1	-1	-1	-1	-1	-1
MEAN													
62-90	0	-4	-9	-10	-12	-13	-13	-12	-11	-9	-4	-1	-8
62-79	-2	-8	-14	-16	-19	-20	-20	-19	-17	-13	-7	-5	-13
80-90	+4	+4	-1	-1	0	-1	-1	0	-1	-1	+2	-4	+1

sequent preference of measurements on the wavelength pair CD which compensated changes due to corrections of the R-N Tables. In the years 1980-1990 the differences are generally small as a result of periodical corrections of the R-N Tables based on regular standard lamp tests of the instrument performed since 1980.

The analysis of the results of homogenization showed that accuracy of measuring of total ozone was fairly good at Hradec Kralove in the period 1980-1990 when technical condition of the spectrophotometer No.74 was stable. But significant differences were found in the years 1962-1979 reaching 10-19 D.U. (3.0-5.5%) for yearly averages and even

26 D.U. (over 7,0%) for monthly averages in the summer-season. Such differences highly exceed accuracy of measuring with the Dobson spectrophotometer and can significantly influence reliability of the data base and namely character of trends. Due to this fact the recalculated total ozone data were published separately [Vanicek,1991] again. In this way the data were made generally available for studies concerning variation of atmospheric ozone over Central Europe. The results given above evidently support the requirements for re-evaluation of historical total ozone data sets of the GOOS's stations as an important step for improvement of quality of long-term monitoring of the ozone layer.

REFERENCES

- Bojkov R.D., 1988: Ozone Trends Panel - Report, WMO Ozone Project Report No.18.
- Dobson, G.M.B., 1957a: Adjustment and calibration of the ozone spectrophotometer, Ann. Int. Geophys. Year,5, part 1, 90-113.
- Dobson, G.M.B., 1957b: Observers' handbook for the ozone spectrophotometer, Ann. Int. Geophys. Year,5, part 1, 46-89.
- Dobson, G.M.B. and C.W.B. Normand, 1962: Determination of the constants etc. used in the calculation of the amount of ozone from spectrophotometer measurements and of the accuracy of the results, Ann. Int. Geophys. Year, 16, part 2, 161-191.
- Komhyr, W.D., 1980: Operations handbook - Ozone Observations with a Dobson spectrophotometer, Global Ozone Res. and Monit. Proj. Rep.6, 125pp., World Meteorolog. Org., Geneva.
- Komhyr, W.D., R.D. Grass, R.D. Evans and R.K. Leonard, 1989a: Results of international Dobson spectrophotometer and Brewer spectrophotometer calibrations, Arosa, Switzerland, 1986, Proc. of the Quadrennial Ozone Sympos., Gottingen, FRG, 1988, 776-779.
- Komhyr W.D., R.D. Grass and R.K. Leonard, 1989b: Dobson Spectrophotometer 83: A Standard for Total Ozone Measurements, 1962-1989, Journ. of Geophys. Research, 94,D7, 9847-9861.
- Komhyr W.D., 1990: International Comparison of Dobson Spectrophotometers, Arosa, Switzerland - the preliminary results.
- Vanicek K., 1991: The Recalculated Total Ozone Data, Hradec Kralove, 1962-1990, Publications of Czech Hydrometeorological Institute, 1991.
- WMO-WODC: Ozone Data for the World - Catalogues of Published Data, Toronto, Canada.

303698

COMPARISON OF RECALCULATED DOBSON AND TOMS TOTAL OZONE AT HRADEC KRALOVE, CZECHOSLOVAKIA, 1978-1990

Martin Stanek and Karel Vanicek

Solar and Ozone Observatory, Czech Hydrometeorological Institute
Hvezdarna 456, 500 08 Hradec Kralove 8, Czechoslovakia

ABSTRACT

The re-evaluated Dobson total ozone data from Hradec Kralove, Czechoslovakia were compared with independent Total Ozone Mapping Spectrophotometer (TOMS) "version 6" data set. The comparison was performed by means of the parallel daily averages of ground-based and satellite total ozone pairs of the period November 1978 to December 1990. The comparison showed slight differences between both data series. Their average relative difference is 0.48%. The similar results have been reached for subsets of direct sun and zenith types of measurements as well. Their relative differences are 0.61% and 0.11% respectively. These facts indicate not only good mutual relation of both data sources but also reliability and accuracy of the zenith charts of the spectrophotometer No.74 used at Hradec Kralove. Preliminary assessment of seasonal MU-dependence of the differences between Dobson and TOMS data was made while using total ozones of winter and summer months representing values of $MU=2.70-5.20$ and $MU=1.12-1.30$ respectively. The results did not show systematic underestimation or overestimation of total ozone due to MU-dependence of the instrument at Hradec Kralove in both seasons.

1. INTRODUCTION

The total ozone data set created with the Dobson spectrophotometer No.74 at the Solar and Ozone Observatory (SOO) of the Czech Hydrometeorological Institute at Hradec Kralove, Czechoslovakia was homogenized using day-by-day method. The recalculations were performed on the calibration level represented by the World Primary Standard Spectrophotometer No.83 (WPSS). The recalculated data from the period 1962-1990 were published together with description of methodology of homogenization in 1991 [Vanicek,1991]. The experts from SOO decided to check the quality of these individually recalculated total ozone data by means of the independent satellite measurements performed with the Total Ozone Mapping Spectrophotometer (TOMS) in the similar way as it was done for preliminary re-evaluated total ozones in recent years [Bojkov,1988]. The TOMS data set was also used for assessment of seasonal MU-dependence of the instrument No.74 and reliability of its zenith charts. Accuracy of both direct sun and zenith measurements was checked in this way too.

2. SPECIFICATION OF THE DATA SETS

Daily averages of recalculated Dobson total ozone from Hradec Kralove of the period November 1978 to December 1990 published by SOO [Vanicek,1991] were taken as a data base for comparison. These data were compared with the TOMS total ozone data set "version 6" of the same period of time measured with this satellite system in the quadrant 2×5 deg. above the Observatory [Stolarski and McPeters,1991]. Both data series were arranged so that only the averages from days with parallel ground-

based and satellite measurements could be taken into consideration. The series containing 3505 doubled pairs of daily averages comparable with each other was created in this way and used for following processing. To show nearly steady distribution of occurrence of parallel measurements the Figure 1 presents number of the pairs in individual months and years. It is evident that there is no significant reduction of the number of the measurements in the period under consideration which could decrease reliability of the data series from the statistical point of view. Only the data from the months June 1979, August 1986 and August 1990 are missing due to participation of the spectrophotometer No.74 at the international comparisons at Potsdam 1979 and Arosa 1986 and 1990.

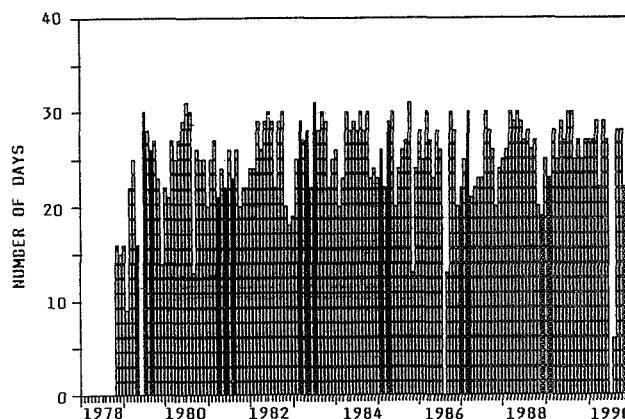


Fig.1. Number of days with parallel DOBSON and TOMS measurements in individual months of the period November 1978 to December 1990, Hradec Kralove.

3. COMPARISON OF MEASUREMENTS

In order to assess reliability of the Dobson data from Hradec Kralove and validity of the zenith charts the direct sun, zenith and all type of measurements were compared with the TOMS data separately. Comparison was performed by means of average relative differences of total ozones $100 \cdot (\text{DOBSON} - \text{TOMS}) / \text{DOBSON}$ calculated for all individual months of the period specified above. The results are shown in Figures 2,3,4 where the dotted lines express the averages and STDs typed over the curves.

It is obvious from the graphs that averages and STDs are not very different for all three groups of measurements. The averages do not exceed 0.62% and STDs are lower than 1.7% that is nearly equivalent to operational accuracy of the Dobson spectrophotometer. Moreover, the dif-

ferences between the ground-based-zenith and TOMS total ozones can be considered fully comparable with differences that have been got for direct sun measurements.

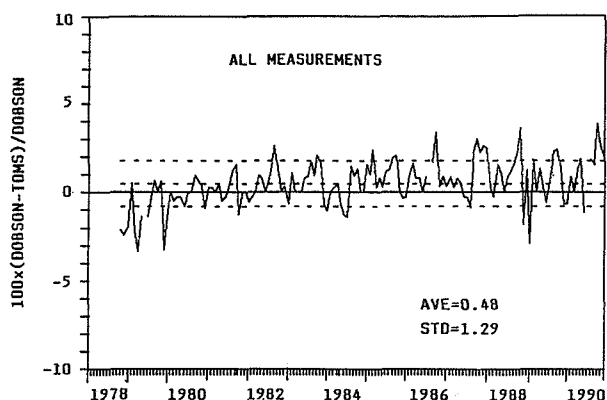


Fig. 2. Relative differences between Dobson and TOMS daily averages of total ozone in individual months (full line), AVE and STD (dashed lines) - all measurements.

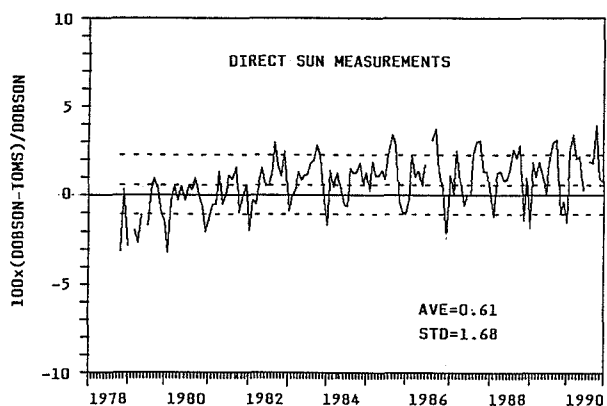


Fig. 3. Relative differences between DOBSON and TOMS daily averages of total ozone in individual months (full line), AVE and STD (dashed lines), Hradec Kralove - direct sun measurements.

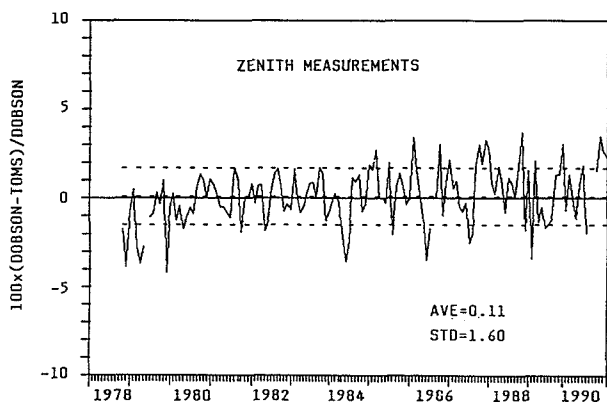


Fig. 4. Relative differences between DOBSON and TOMS daily averages of total ozone in individual months (full line), AVE and STD (dashed lines), Hradec Kralove - zenith measurements.

Zenith measurements of total ozone have been performed since 1967 at Hradec Kralove. The percentage of this type of measurements was about 40% in the period 1978-1990. The original zenith charts of the instrument No.74 (Chart AD, Chart CD, Chart C' and Chart for Cloud Corrections) [Komhyr,1980], approximated by polynomial regressions, are used in computer program for calculation of total ozone. In the final step of processing the zenith total ozones are corrected towards direct sun ground quartz plate AD standard values by means of the factors established from parallel direct sun and zenith measurements [Vanicek,1991]. Therefore it seems that the way of use of the zenith charts implemented at the Observatory does not require any change at present time.

4. MU-DEPENDENCE OF THE SPECTROPHOTOMETER NO.74

Side-by-side comparison of the spectrophotometer No.74 with the WPSS No.83 at Arosa, Switzerland in 1986 and 1990 gave the differences of total ozone for different values of MU. These deviations were generally lower than 0.4% and they show fairly low MU-dependence of the instrument No.74 for MU=1.15-4.00.

In order to assess MU-dependence in routine operation of the instrument the parallel satellite TOMS data mentioned above were used as a reference. The mean differences of total ozone in percents $100 \times (\text{DOBSON} - \text{TOMS}) / \text{DOBSON}$ in individual years were calculated for the seasons November, December, January - NDJ and May, June, July - MJJ. In these seasons the MU reaches maximum and minimum values $\text{MU} = 2.70 - 5.20$ and $\text{MU} = 1.12 - 1.30$ respectively at the latitude of Hradec Kralove. The results presented in Figure 5 show that the mean relative differences of total ozones are mostly lower than $\pm 1.5\%$ for both seasons. It is evident from the graphs that both in winter (NDJ) and in summer (MJJ) neither essential overestimation nor underestimation of ground-based total ozone appear. This conclusion confirms the fact that MU-dependence of the spectrophotometer No.74 has not affected significantly quality of routine ground-based measurements and therefore reliability of the total ozone data base at Hradec Králové at least since 1978.

5. CONCLUSIONS

Comparison of the homogenized total ozone data from Hradec Kralove with the independent satellite TOMS data set confirmed that the Dobson spectrophotometer No.74 does not show essential MU-dependence in the range of MU from 1.15 to 4.20 which is the typical one for its operation in Central Europe. Moreover, the comparison showed that quality of

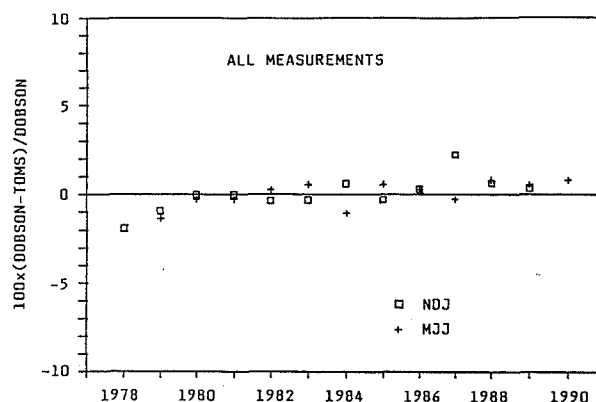


Fig. 5. Relative differences between DOBSON and TOMS averages of total ozone in the months NDJ and MJJ, Hradec Kralove - all measurements.

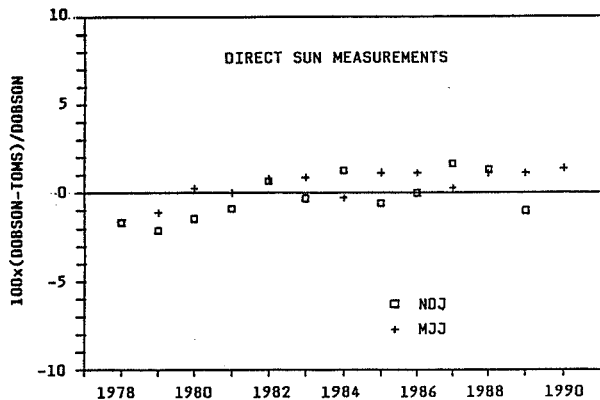


Fig. 6. Relative differences between DOBSON and TOMS averages of total ozone in the months NDJ and MJJ, Hradec Kralove - direct sun measurements.

zenith measurements is fully comparable with quality of direct sun ones. Therefore, the validity of the approximated zenith charts can be supposed to be acceptable for the next observations. These facts confirm reliability of the total ozone data base from Hradec Kralove as a whole and show the way how the satellite data can be used for checking and improving the quality of the data sets at individual stations of the Global Ozone Observing System.

ACKNOWLEDGMENTS

We would like to thank R. McPeters and R. Stolarski, NASA Goddard Space Flight Center for their help in provision of the TOMS total ozone data set, 1978-1990.

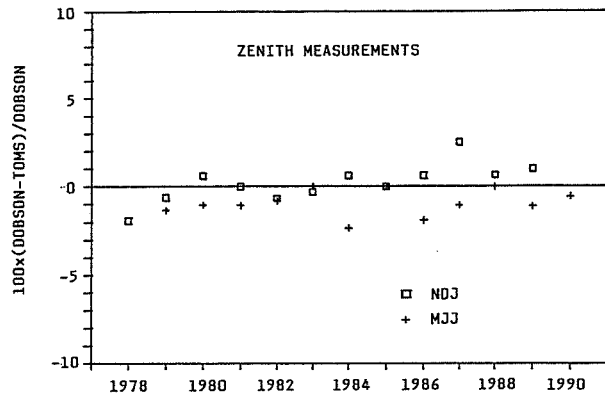


Fig. 7. Relative differences between DOBSON and TOMS averages of total ozone in the months NDJ and MJJ, Hradec Kralove - zenith measurements.

REFERENCES

- Bojkov, R.D., 1988: Ozone Trends Panel - Report, WMO Ozone Project Report No.18.
- Komhyr, W.D., 1980: Operations handbook - Ozone Observations with a Dobson Spectrophotometer, Global Ozone Res. and Monit. Proj. Rep. 6, 122pp., World Meteorolog. Org., Geneva.
- Komhyr, W.D., R.D. Grass, R.D. Evans and R.K. Leonard, 1989: Results of international Dobson spectrophotometer and Brewer spectrophotometer calibrations, Arosa, Switzerland, 1986. Proc. of the Quadrennial Ozone Symp., Gottingen, FRG, 1988, 776-779.
- Komhyr, W.D., Evans R., 1990: International Comparison of Dobson Spectrophotometers, Arosa, Switzerland, 1990 - the preliminary results.
- McPeters, R., Stolarski, R., 1991: Private communication.
- Vanicek, K., 1991: The Recalculated Total Ozone Data, Hradec Kralove, 1962-1990, Publications of Czech Hydrometeorological Institute.

303599

FRACTAL CHARACTERISTICS OF OZONOMETRIC NETWORK

Alexander N. Gruzdev

Institute of Atmospheric Physics
Russian Academy of Sciences, Pyzhevsky per.3, Moscow 109017, Russia

ABSTRACT

The fractal (correlation) dimensions are calculated which characterize the distribution of stations in the ground-based total ozone measuring network and the distribution of nodes in a latitude-longitude grid. The dimension of the ground-based ozonometric network equals 1.67 ± 0.1 with an appropriate scaling in the 60 - 400 km range. For the latitude-longitude grid two scaling regimes are revealed. One regime, with the dimension somewhat greater than 1, is peculiar to smaller scales and limited from a larger scale by the latitudinal resolution of the grid. Another scaling regime, with the dimension equaled 1.84, ranges up to 15,000 km scale. The fact that the dimension of a measuring network is less than 2, possesses problems in observing sparse phenomena. This has to have important consequences for ozone statistics.

1. INTRODUCTION

A geometrical set of points can be characterized by a dimension. There are different methods for estimating the dimension (Eckman and Ruelle, 1985). For example, the so-called correlation dimension, ν , can be calculated through:

$$\nu = \lim_{r \rightarrow 0} \frac{\langle \ln n(r) \rangle}{\ln r}, \quad (1)$$

where $n(r)$ is the number of points within the r -neighborhood of each point, r is the size (e.g. diameter) of the neighborhood, the angle brackets denote averaging over all points of a set. The existence of ν implies the existence of scaling (at small r):

$$\langle n(r) \rangle \sim r^\nu. \quad (2)$$

If the dimension is fractional it is

called the fractal dimension. In practice, r and the number of points in a set are limited, and dimension ν is determined as an angle coefficient in graph of $\ln \langle n(r) \rangle$ versus $\ln r$, and scaling (1) can exist at finite intervals of r .

If D is the dimension of a space including a point set, the density of a point set in this space is proportional to $r^\nu / r^D = r^{-c}$. Here $c = D - \nu$ is the co-dimension of a point set (Lovejoy and Schertzer, 1990). If $c = 0$, the density of a point set does not depend (on the average) upon the scale of r (in the scale range where (2) holds). If $c > 0$, the density of points decreases with a scale, i.e. points are concentrated on diminishing relative part of a space. Hence, the fractal dimension of a point set is a measure of sparseness of a set (Lovejoy and Schertzer, 1990).

2. FRACTAL STRUCTURE OF THE GROUND-BASED OZONOMETRIC NETWORK

Any ground-based measuring network is mainly distributed on continents, concentrating in densely populated regions. Hence, its surface distribution is highly inhomogeneous and has to have a fractal dimension. So, the global meteorological network has the fractal (correlation) dimension equaled 1.75 (Lovejoy et al, 1985; Lovejoy and Schertzer, 1990). The ground-based total ozone measuring network includes more than a hundred stations. Fig.1 shows the location of the 137 stations which worked during the last decade. Calculating the fractal dimension of the network, one should take into account the sphericity of the Earth's surface. Let r be the radius of the covering sphere, R be the radius of the Earth (Fig.2). Then $r = 2R \sin(\theta/2)$.

Fig.3 shows the graph of $\langle n(L) \rangle$ versus $L = 2r$. In the 60-400 km range the scaling (2) holds with $\nu = 1.67 \pm 0.1$. The

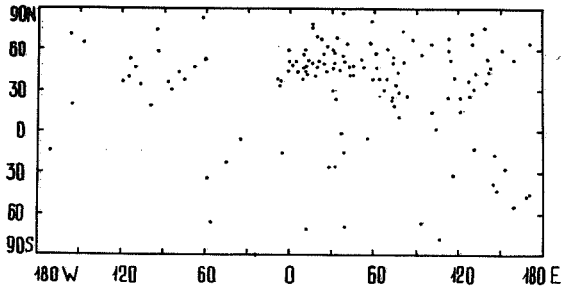


Fig.1. The location of 137 stations in the ground-based total ozone measuring network.

function $L^{1.67}$ is shown in Fig.3 by the straight line. Following Lovejoy et al (1986) one can estimate the greatest possible scale range, where the found scaling holds. Proceeding from the limited number of stations, one finds the minimum value, $\langle n(L) \rangle_{min} \sim 1/137 \sim 7.3 \cdot 10^{-3}$, and the maximum value, $\langle n(L) \rangle_{max} \sim 137/2 \sim 69$. The assumption that the scaling of $L^{1.67}$ holds in this range, gives $L_{min} \sim 50$ km and $L_{max} \sim 10,000$ km. Fig.3 shows that the lower limit of the scaling of the $L^{1.67}$ function coincides approximately L_{min} . However, this scaling is broken at $L > 400$ km. Perhaps, there is another scaling at $L > 1000$ km, but an appropriate reliable ν value cannot be determined because of insufficient number of stations and saturation of the $\langle n(L) \rangle$ function at large scales.

3. FRACTAL CHARACTERISTICS OF A GLOBAL LATITUDE-LONGITUDE GRID

Satellite measurements give more full and detailed information about the ozone global distribution. For different practical purposes, the information collected by a satellite during a lot of circuits may be considered as related to a single time moment. Necessarily, data of measurements can be brought to the standard times by interpolating in time and space, if one has wind data. In any case, satellite data are inhomogeneous, because satellite orbits are nearer each other over polar regions than over tropics. In order to estimate the fractal dimension of such a "network", let us consider it as a regular latitude-longitude grid with nodes denoting the sites of satellite measurements. Note that in different problems data of

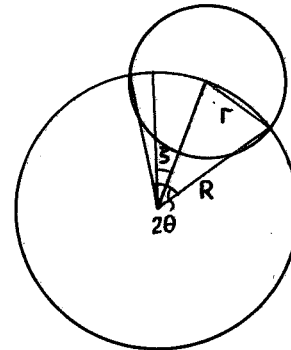


Fig.2. The geometry for calculating the correlation dimension of a point set on a sphere.

measurements are interpolated to such a grid.

3.1. Analytical consideration

Let $N_\varphi + 1$ be the number of nodes along meridian (including the poles), N_λ be the number of nodes along a circle of latitude. Then the density of nodes along meridian, $n_\varphi = N_\varphi / \pi R$, is constant, and the density of nodes along a circle, $n_\lambda = N_\lambda / (2\pi R \sin\varphi)$, depends upon latitude, φ . To simplify the analytical analysis let the grid be dense enough to replace summation by integration. The number of nodes within the θ -neighborhood of any node at the polar angle, ζ (see Fig.2), is

$$n = \int_{\varphi_1}^{\varphi_2} \int_{\lambda_1}^{\lambda_2} n_\varphi n_\lambda R^2 \sin\varphi \, d\varphi \, d\lambda, \quad (3)$$

where the integration limits satisfy the equation for the intersection of the two spheres. Calculating the integral (3), one should distinguish two cases: $\zeta \leq \theta$ and $\zeta > \theta$.

a) Case 1, the near-pole neighborhood: $\zeta \leq \theta$. Besides this, let $\theta \ll 1$ and, hence, $\zeta \ll 1$. In this case the integration of (3) gives:

$$n \approx 2R/\pi n_\varphi N_\lambda \theta E(\zeta/\theta) \quad (4)$$

where E is the full normal elliptical integral of the second type.

b) Case 2, the out-polar neighborhood: $\zeta > \theta$. Let also $\zeta \ll 1$ and, hence, $\varphi \ll 1$. Then the integration of (3) gives:

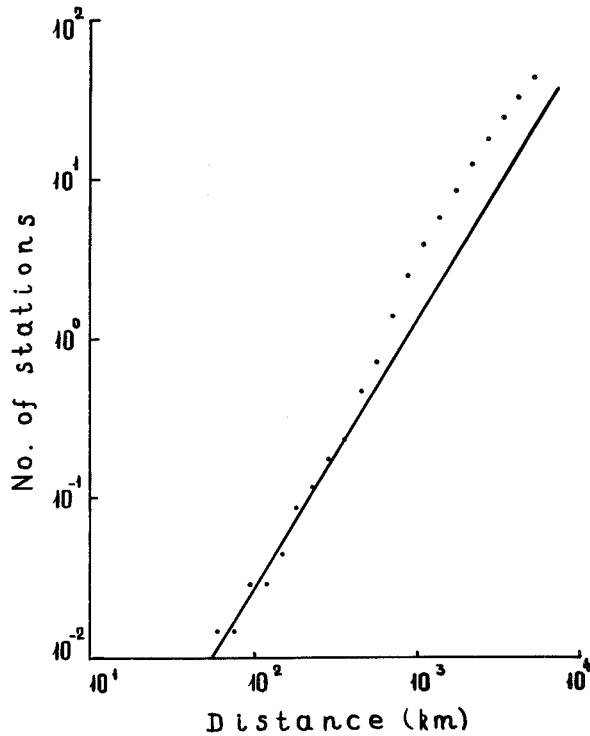


Fig.3. The average number of stations in the ground-based ozonometric network, $\langle n(L) \rangle$, within annuli of geometrically increasing radii. The straight line corresponds to scaling with an index equaled 1.67.

$$n \approx 2R/\pi n_\varphi N_\lambda \zeta \{E(k) - (1-k^2)K(k)\}. \quad (5)$$

Here K is the full normal elliptical integral of the first type, and $k = \sin \lambda_m$, where λ_m is determined through:

$$\cos \lambda_m = 1/\sin \zeta \sqrt{2 \cos \zeta (\cos \theta - \cos \zeta)}.$$

Now let ζ be arbitrary, but such that $\zeta \gg \theta$. Then

$$n \approx R/2 \sin \zeta n_\varphi N_\lambda \theta^2. \quad (6)$$

Let the local scaling of type (2) exist: $n(\theta) \sim \theta^\nu$. Transition from r to θ is correct, as $r \approx R\theta$ when $\theta \ll 1$. Then $\nu \approx (\theta/n)(dn/d\theta)$, if ν does not depend upon θ or ν is a slow function of θ . Under this condition one gets from (4) that for the near-polar region

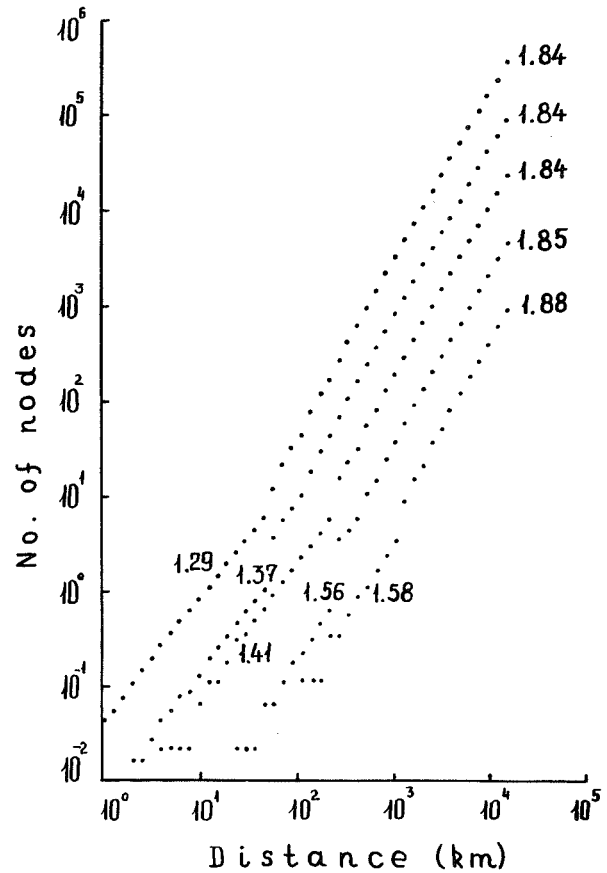


Fig.4. The average number of nodes in a latitude-longitude grid, $\langle n(L) \rangle$, within annuli of geometrically increasing radii, at different values of latitudinal, $\Delta\varphi$, and longitudinal, $\Delta\lambda$, resolutions. Five series of points correspond (from top to bottom) to: 1) $\Delta\varphi = \Delta\lambda = 0.25^\circ$; 2) $\Delta\varphi = 0.25^\circ$, $\Delta\lambda = 1^\circ$; 3) $\Delta\varphi = \Delta\lambda = 1^\circ$; 4) $\Delta\varphi = 1^\circ$, $\Delta\lambda = 5^\circ$; 5) $\Delta\varphi = \Delta\lambda = 5^\circ$. The numbers at series denote correlation dimensions.

$$\nu \approx 1 + 1/2 (\zeta/\theta)^2,$$

while for out-polar region (but at $\zeta \ll 1$)

$$\nu \approx 2 - 1/2 (\theta/\zeta)^2.$$

If ζ is large one gets from (6) that $\nu \approx 2$ with a high precision. Thus, the local fractal dimension of a latitude-longitude grid is a monotonous function of latitude and changes from 1 at the poles to 2 at the equator. It is evident that the correlation dimension (1) which

characterizes the global distribution of nodes of the grid, has to have an intermediate value.

3.2. Empirical fractal characteristics

In practice the distribution of the grid nodes is discrete. Fig.4 shows the calculated mean value, $\langle n \rangle$, as a function of L at different values of latitudinal and longitudinal resolutions. This function has two different scaling regimes. One regime is peculiar to smaller scales and limited from a larger scale by the latitudinal grid resolution. This regime is characterized by the small correlation dimension which decreases if the grid resolution improves. One can show that $\nu \rightarrow 1$ then. Another scaling regime ranges up to a global scale and is characterized by a correlation dimension equalled to 1.84 at sufficiently good resolution.

4. CONCLUDING REMARKS

The fact that the fractal dimension of ozone measuring network is less than the Earth's surface dimension (equalled 2), can have important consequences for ozone statistics. According to Lovejoy et al (1986), such a network is not able to detect phenomena with dimension $\nu_p < D - \nu$.

The detectability limits are: $\nu_p = 2 - 1.67 = 0.33$ for the ground-based ozonometric network, $\nu_p = 0.16$ for the latitude-longitude network at large scales, and $\nu_p \sim 0.4 \div 0.7$ for the latitude-longitude network at small scales. If one suppose the fractal dimension of ozone field to be decreasing function of ozone content (similar to the case of some meteorological fields, see e.g. Lovejoy et al., 1986; Lovejoy and Schertzer, 1990), then insufficiently large fractal dimension of ozone measuring network has to lead to biases in ozone statistics. In particular, this can lead to biases in the spatial averages.

REFERENCES

- Eckman, J.-P., and D. Ruelle, 1985: Ergodic theory of chaos and strange attractors. Rev. Mod. Phys., 57, 617-656.
- Lovejoy, S., and D. Schertzer, 1990: Our multifractal atmosphere: a unique laboratory for non-linear dynamics. Phys. Can., 46, 62-71.
- Lovejoy, S., D. Schertzer, and P. Ladoy, 1986: Fractal characterization of inhomogeneous geophysical measuring networks. Nature, 319, 43-44.

303600

Characterization and Analysis of the Nimbus-7 SBUV data in the "Non-Sync" Period (February 1987 - June 1990.)

James F. Gleason, Richard D. McPeters and Jay R. Herman

NASA/Goddard Space Flight Center, Mail Code 916,
Greenbelt MD, 207771

Introduction

The SBUV instrument, on Nimbus-7, measures the backscattered ultra-violet radiance at 12 wavelengths. The radiance data from these wavelengths was used to deduce the ozone profile and the total column ozone. In February 1987, there was an instrument malfunction. The purpose of this paper is to describe the malfunction, to determine the effect of the malfunction on the data quality and if possible, to correct for the effects of the malfunction on the data from the SBUV instrument.

Instrument Description

The SBUV instrument consists of both a monochromator for dispersing the light into the ozone wavelengths and a single wavelength photometer for monitoring the reflectivity of the Earth. The two parts share a common chopper wheel and counting electronics. The SBUV photometer measures the radiance at 343 nm, using a filter/photodiode combination. The photometer data are coincident with the data from each monochromator channel. The absolute reflectivity is derived from the 339.8nm monochromator channel and the photometer data to monitor the changes in the earth reflectivity as the instrument collects data at each wavelength channel. Additional instrumental details can be found in Appendix 1.

The SBUV chopper wheel chops the optical signal just prior to the entrance slit. This chopping enables the instrument to compensate for the background signal induced by the energetic particle radiation in the space

environment. The background signal gets significantly higher as the spacecraft passes through high radiation environments, e.g., the South Atlantic Anomaly. The lack of a chopped signal affected the data quality from the earlier Nimbus-4 BUUV instrument.

The chopper wheel was synchronized to the counting electronics. The counter would count up with the slit open and count down with the slit closed. Beginning February 13, 1987, the chopper wheel and the counting electronics started to become non-synchronized. By mid-summer 1987, the non-synchronization was complete and all the scans were taken with the chopper and the counter out of synchronization.

Assessing the Instrument in the Non-Sync Period

The SBUV instrument makes weekly solar flux measurements using the 12 ozone wavelengths. The photometer data are also collected during this set of measurements. The photometer solar flux at 343 nm should be constant during the measurement cycle (10 scans of 32 seconds each). The distribution or the variation of the solar flux data from the photometer should give us an idea of how "out of sync" the chopper wheel and the counting electronics really are. A time series of the discrete mode solar photometer measurements is shown in fig 1. The start of the non-sync period is easily observed in fig 1, in early 1987.

Diffuser plate calibration errors will cause a small variation in the photometer measurements. Note that after the start of non-sync, the distribution of the solar photometer data increases. The standard deviation of the monthly average solar photometer will give us a qualitative measure of the nonsync condition. The standard deviation

time series plot, fig 2, shows very stable standard

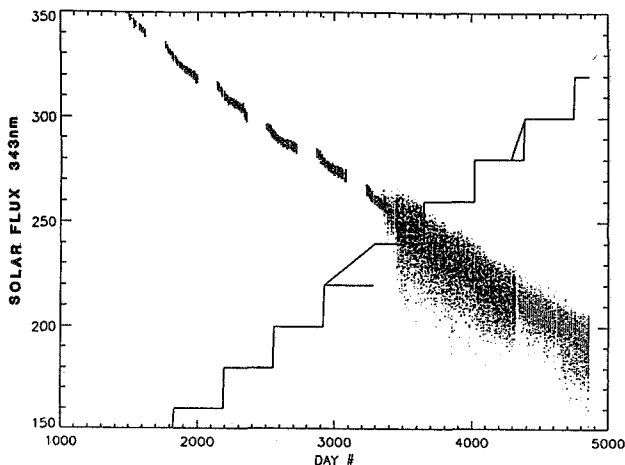


Figure 1: Solar photometer data at 343 nm for each wavelength for each scan for the months January to June, for the years 1983 to 1991.

deviation prior to February 1987, an increase in the standard deviation in 1987 as the out of sync rate approached 100%, then a plateau through the spring of 1990.

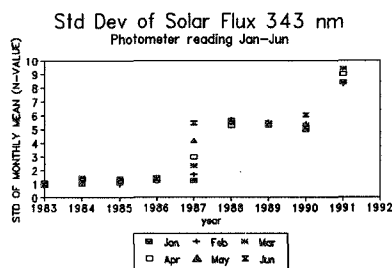


Figure 2: The standard deviation of the monthly mean solar photometer flux for the months January to June, for the years 1983 to 1991.

The consistency of the photometer solar flux standard deviations indicates that the instrument was fairly stable and that the amount of non-synchronization was not changing. In the summer of 1990, the TOMS instrument, which is attached to and shares common electronics with the SBUV, began to have non-sync problems. The occurrence of the TOMS non-sync was thought to be temperature related and SBUV was put in a different mode to add heat to the spacecraft, in an attempt to correct the TOMS problems. After normal SBUV operations were

resumed, the SBUV instrument was in a different state, as shown by the increase in the standard deviation of the solar photometer data.

The solar data indicate that the instrument had gone out of sync in Feb 1987 and reached a stable state where it remained until the summer of 1990. Since the out of sync condition appeared to be stable we believe that the earth radiance data can be corrected for the nonsync condition and more accurate ozone values can be retrieved from the SBUV instrument.

Correction of the Non-Sync Data

As the photometer and the monochromator view the same area, at the same time, at two different wavelengths, we can use these simultaneous measurements to compensate for the non-synchronous chopper wheel.

The photometer responds to changes in the earth's reflectivity at 343 nm. The reflectivity that the photometer measures should not change very much over a single SBUV scan, 1.5 sec between each of 12 wavelengths. Five consecutive photometer scans before the non-sync period are shown in fig 3, note the smooth, monotonic photometer signal within a single scan. A larger deviation will occur between consecutive scans due to the 12 second gap between them.

Five consecutive scans from the non-sync period are shown in fig 4, note random scatter within a single scan. The scatter observed in the photometer data is caused by the nonsynchronous chopper wheel and not by changes in the earth's albedo.

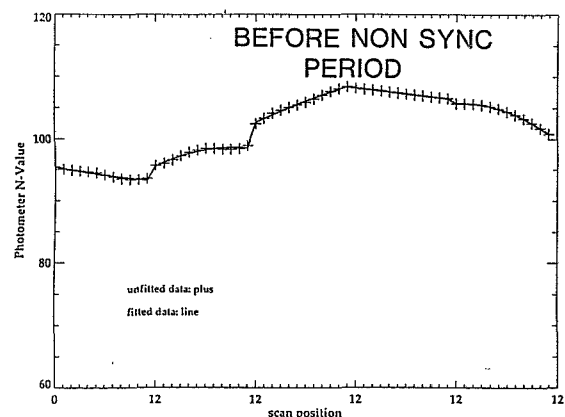


Figure 3: The equatorial photometer values from 5 scans before the start of the chopper wheel non-sync problem. The line is a quadratic fit through the 12 points of each of the scans.

Since the photometer and the monochromator view the same scene at the same time, the deviation in a single photometer reading will be proportional to the deviation in the simultaneously measured monochromator ozone wavelength. By smoothing the photometer data within a single scan, we can remove the variation caused by the nonsynchronous chopper wheel.

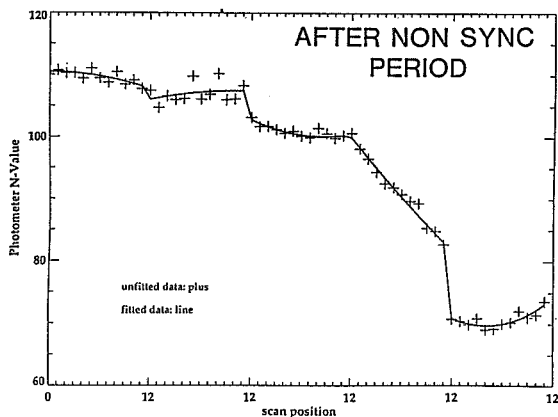


Figure 4: The equatorial photometer values from 5 scans after the start of the chopper wheel non-sync problem. The line is a quadratic fit through the 12 points of each of the scans.

The ratio of the smoothed to unsmoothed photometer data, from a single scan, can be used to correct the monochromator data from that scan.

Our correction technique consists of fitting a quadratic expression to each photometer scan. Any outlier, a point which is greater than 2 standard deviation from the fitted point, is replaced with the fitted value and the scan is quadratically fit again. The ratio between the fitted and the unfitted photometer data is used to correct the monochromator data for that scan.

Ratio = $1 - (\text{Photometer}_{\text{fit}} - \text{Photometer}_{\text{unfit}}) / \text{photometer}_{\text{unfit}}$
 For each scan, the photometer ratio is calculated at every wavelength, ratio at each wavelength is multiplied by the monochromator albedo from that wavelength. The corrected monochromator albedos are used in the inversion algorithm to calculate ozone profile and total column ozone.

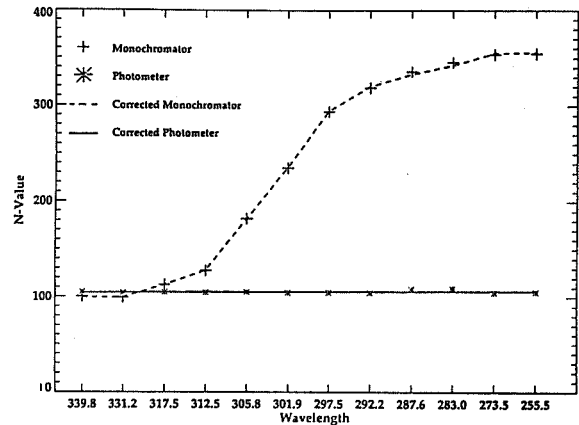


Figure 5: An example of a single scan showing the corrected and uncorrected photometer data with the corresponding monochromator data. **Ozone Results using the Corrected Data**

The corrected data had a dramatic effect on individual ozone profiles. The magnitude of the albedo corrections can be relatively small, and still have a significant impact on the retrieved ozone profile. In fig 5, the original and the corrected data are shown, and the corresponding ozone profiles are shown in fig 6.

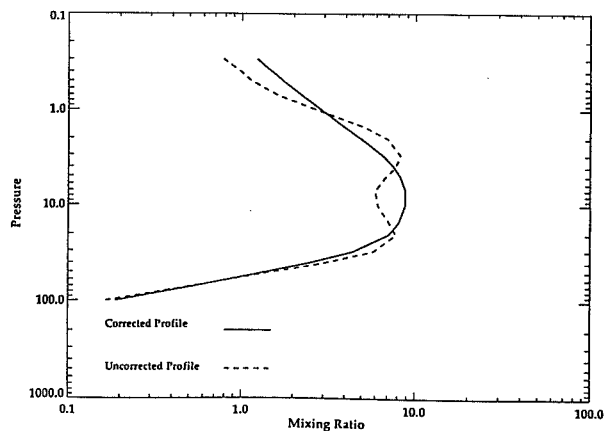


Figure 6: A single ozone profile retrieved from using the data in figure 5.

The zonal mean profile data also showed a significant improvement. The standard deviation of the monthly zonal means improved significantly. The results for May, 15S -15N, for Umkehr layers 4 to 9 are shown in figs 7 and 8.

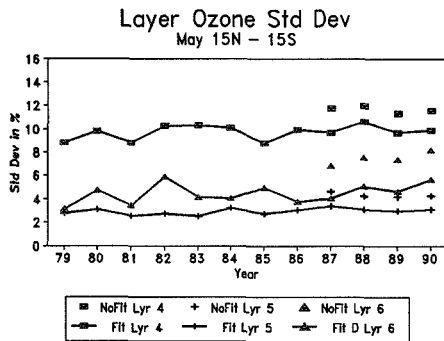


Figure 7: This shows the standard deviation in % of monthly zonal mean, for the month of May for layers 4,5, and 6. The standard deviation calculated using the uncorrected data is shown by symbols without the line drawn through them.

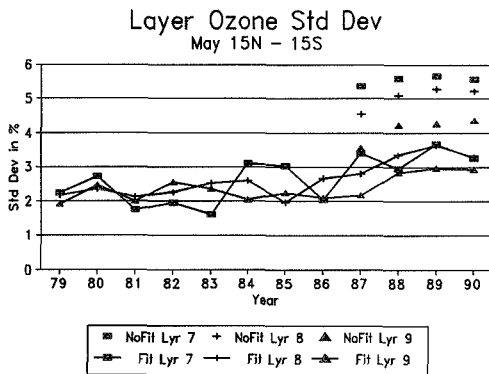


Figure 8: The same as above for layers 7,8, and 9.

There was a smaller improvement in the total ozone data. Since the total ozone is calculated using wavelength pairs, this partially compensated for the non-sync in the chopper wheel. The standard deviations in the zonal means improved slightly after using the corrected albedo data. Comparison of the SBUV data with the TOMS data, fig 9 and 10, does not show any bias introduced by using the corrected albedos in the non-sync period.

Conclusions

Using the smoothed photometer data to compensate for the non-synchronization between the chopper wheel and the counting electronics has improved the ozone data derived from the SBUV measurements.

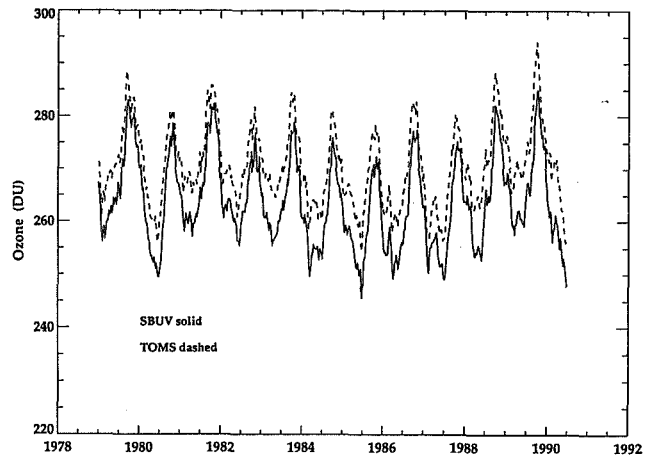


Figure 9: The weekly zonal average for TOMS and SBUV total ozone for the latitude band 20S to 10S. The TOMS is the dashed line and the SBUV is the solid line. The offset between the data sets is caused by initial calibration differences.

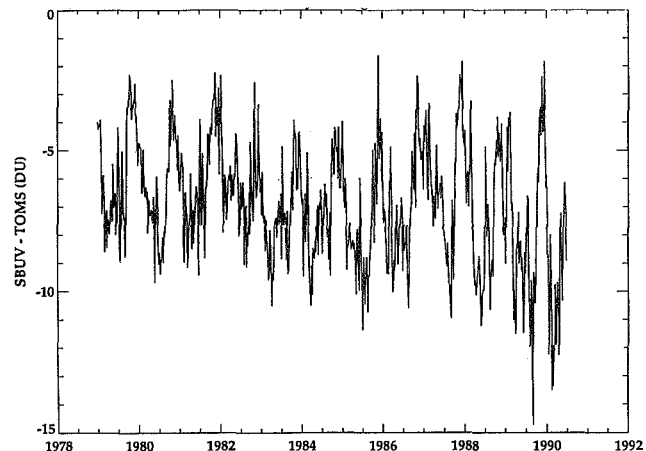


Figure 10: A time series of the difference between the SBUV and TOMS total ozone. Using the corrected albedos does not appear to have introduced a bias in the total ozone data.

Appendix 1

Instrument characteristics

Double Ebert-Fastie monochromator, 1 nm bandwidth
 12 Wavelengths (nm): 339.8, 331.2, 317.5, 312.5, 305.8, 301.9,
 297.5, 292.2, 287.6, 283.0, 273.5, 255.5
 Photometer Channel 343 nm, 3 nm bandwidth
 32 second measurement sequence
 12 channels (339.8 to 255.5) measured in 18 seconds

Orbital Characteristics

Sun-synchronous Polar orbit 13-14 orbits/day
 11.3° x 11.3° (200 km x 200 km) field of view
 each orbit separated by 26°
 footprint speed 6 km/sec

303601

REVISION OF THE DOBSON TOTAL OZONE
SERIES AT HOHENPEISSENBERG

U. Köhler

DWD, Meteorologisches Observatorium Hohenpeissenberg

Abstract

Total ozone measurements with the Dobson No. 104 (D 104) have been performed at the Meteorological Observatory Hohenpeissenberg since 1967.

A critical review of this time series and the comparison with other instruments like TOMS or Brewer spectrophotometer revealed some intervals with uncertainties. Especially in the early eighties a monthly mean bias of about -3% to TOMS-data with annual variations depending on the mean sun-height exists. An extreme amplitude of 5.6% occurs in 1980 with -0.76% (February) and -6.36% (July).

Two different methods were applied to reprocess the Dobson data set. A comparison of the differently recalculated data showed, that the application of N-corrections by means of the standard-lamp tests starting from the reference values of the Arosa Intercomparison 1986 yields better results than the N-corrections based on a Langley-plot of the Arosa Intercomparison 1978. The extreme amplitude of the year 1980 is now reduced to 3.02%.

There is still a slight drift in the monthly and yearly mean differences between TOMS and revised Dobson data. It cannot be excluded, that the satellite data may be responsible for the trend.

1. Introduction

During the last years great efforts have been done to enhance the quality of the Dobson total ozone network. Three Dobson intercomparisons took place in Arosa (Switzerland) in 1978, 1986 and 1990, in which the Observatory Hohenpeissenberg participated with its D 104. Especially the last two comparisons revealed, that it is possible to maintain the Dobson network in Europe in a good state (Komhyr et al., 1989; Komhyr et al., 1990/1991). On the other hand problems are reported on the '78-comparison in Arosa (Grasnick et al., 1991). These uncertainties are responsible for the D 104 - TOMS differences in the late seventies and early eighties.

Investigations by Fleig et al. (1983) and Bhartia et al. (1985) indicated, that there was obviously

a negative bias of some percent with a remarkable annual amplitude. Figure 1 shows these differences between the original D 104 data and the latest TOMS Version 6. A comparison with the Brewer No. 10 (Köhler, Attmannspacher, 1986), which was installed at Hohenpeissenberg in 1983, and a calibration check with traveling standard lamps (Grass, Komhyr, 1985) confirmed this calibration problem of D 104.

A first attempt to improve at least the actual data was made in 1985. By means of the well calibrated BR 10 the D 104 was recalibrated. Instead of the normal calibration (determining the extraterrestrial constants ETC of the Dobson) a new method using effective absorption coefficients EAC was applied (Kerr et al., 1985). The success of this first Dobson "improvement" is described in Köhler (1986) and can also be seen in Figure 1. The D 104 - TOMS differences are clearly reduced since March 1985.

After the successful intercomparison in Arosa 1986, it was decided to check and recalibrate the D 104 total ozone series. In the following the different attempts and methods are described.

2. Methods for data reprocessing

One main condition for the re-evaluation of a total ozone data set of a Dobson instrument is a complete documentation of all tests (at least standard- and mercury-lamp tests) and the computer availability of all raw data (R - or at least N - values). Furthermore it is necessary to have all former and actual R - N tables at one's disposal. An advantage would be to possess the records of all intercomparisons inclusively the wedge calibration data.

At Hohenpeissenberg all conditions except the raw data availability were existing. The time consuming transfer of the raw data from tables to a PC is at present done for the period 1/1978 - 12/1991 and it is planned to complete this task for the entire time series of Dobson total ozone observations. Unfortunately in the first period 1967 - 1977 only single total ozone values but no R- or N-values are available in tables. This data will be sufficient, if only an ETC-correction is necessary, which seems to be the case with Hohenpeissenberg Dobson during the concerning period.

The first attempt to re-evaluate the D 104 series was done by Bojkov and Hartmannsgruber (Bojkov, 1987/88). They used the TOMS observations as reference and determined monthly mean correction factors in order to adjust the Dobson to the TOMS. With this empirical correction method it is not possible to recalculate each single measurement but only the daily average, because the μ -depending ($\mu \approx 1/\cos(\text{solar zenith angle})$) bias during the diurnal course cannot be corrected. Preliminary results were published in Bojkov et al., 1988 and Bojkov et al., 1990.

The next step was the re-evaluation of the Arosa Intercomparison in 1978. Grasnick et al. (1991) described its results only as preliminary. Although both used standard Dobsons (No. 71 from the former GDR, No. 41 from U.K.) had participated in the Boulder Intercomparison 1977 they had a remarkable difference in the D-wavelength. The negative result for D 104 can be seen in Figure 1. Large differences to the TOMS up to -6.36% in July 1980 and an additional, large annual variation (5.6% in 1980) depending on the mean μ -range of the corresponding months confirm the miscalibration of the D 104. An additional trend of +0.55% p.a. is superimposed.

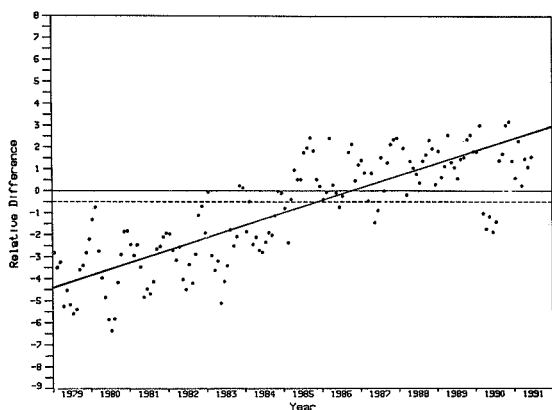


Fig. 1: Comparison Dobson 104 (orig. data) - TOMS (Vers. 6). Ordinate: Relative monthly mean differences (D104 - TOMS)/TOMS in %.

As no correction method using any standard instrument was possible, the only independent calibration method, the so-called Langley-plot was applied to determine better ETC's for D 104. The Na-, Nd and Nad-values (N-values for A, D and AD wavelength pairs) of the observations on August 24, 1978, were plotted versus the corresponding μ -values. The intercept of the linear regression curve as the best fit yields the correction values, which should be applied to the N-tables.

Thus the original Nad-correction of +9 was changed to 27.4. Figure 2 represents the effect of the modified ETC-values to the observations of August 24. The original total ozone (squares), with its obvious μ -depending trend is shifted to higher values (crosses) and the trend is significantly reduced. The daily mean changed from 302.5 D.U. (± 2.7 D.U. standard deviation) to 310.4 D.U. (± 1.3 D.U.).

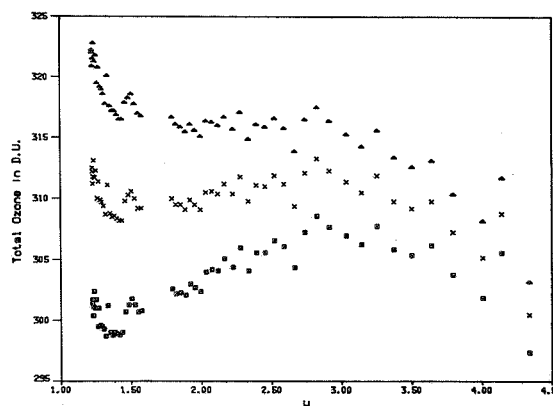


Fig. 2: Total ozone measurements of Dobson 104 in Arosa on August 24, 1978.

□ : original data
x : recal. data Vers.1 (Arosa '78 forward)
Δ : recal. data Vers.2 (Arosa '86 backward)

A further method is the use of a successful inter-comparison (in this case Arosa 1986) and the standard-lamp record. As a first step the initial ETC's of the D 104 were determined during this campaign by means of a comparison with the world standard Dobson. A set of reference standard-lamp values were measured at the same time. A new calibration of the optical wedge confirmed, that the original wedge calibration was still valid. Thus it was possible to use the historical standard-lamp tests for calculating ETC-corrections backward till 1978, which bases on the reference values of 1986.

This method follows the recommendations of the first International Dobson Instrument Data Workshop held in September 1991 in Lanham, Maryland, near Washington (Komhyr and Grass, 1991). It has already been applied by some Dobson scientists and the first results were presented at that workshop.

The Nad-correction for August 1978 after this method was +44, which causes another increase of the total ozone on August 24 (s. Figure 2) up to 317.6 D.U. (± 2.2). Now there is nearly no trend in the μ -range 1.5 - 3.0. The strong increase at small μ (high sun) in all three data sets may be natural, which means a real ozone increase, for example due to an air mass change. The general decrease at $\mu > 3.0$ is characteristic for almost each Dobson due to stray light problems etc.

3 Results of the different methods

The following discussion of the results will clarify, which correction method yields the best or most reasonable total ozone series. It should be mentioned, that in all drawings the dashed line represents the reference zero line taking into account the difference between the altitude of the Hohenpeissenberg (1000 m a.s.l.) and the mean altitude for the corresponding TOMS area (500 m a.s.l.). Nevertheless all previous and following values are related to the normal zero line.

Figure 3 and 4 show the comparisons of both correction methods (Arosa 78 used for recalculating forward = Version 1, Arosa 86 used for recalculating backward = Version 2) with the TOMS Version 6.

It is obvious, that both methods remarkably improve the data set. Version 1 reduces both the mean bias to TOMS and the annual amplitudes of the differences. In 1980 the extreme amplitude of 5.6% is diminished to 4.15%, generally the monthly mean bias amounts about -1% instead of -3% in the original data. Figure 3 also reveals, that this correction is not sufficient enough. There is still a trend in the monthly mean differences of about +0.33% p.a. with significantly lower values in 1979 - 1983 than in 1984 - 1991.

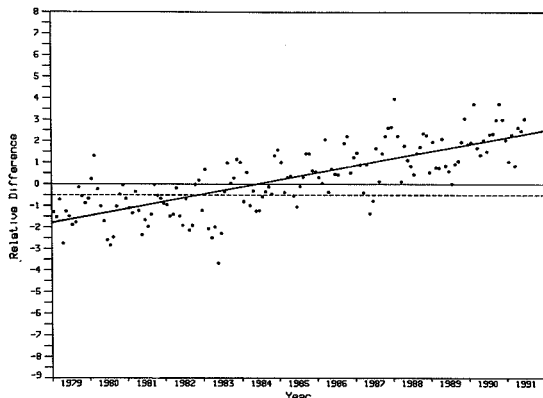


Fig. 3: Comparison Dobson 104 (recalc. data Vers.1) - TOMS (Vers. 6). Ordinate: Relative monthly mean difference (D104-TOMS)/TOMS in %.

Correction method Version 2 yields a further improvement. The largest amplitude of 5.6% in 1980 is once more reduced to 3.02% with extremes of -0.08% in July and +2.94% in February. Positive trends in the original and recalculated (Version 1) data sets (difference Dobson - TOMS) are replaced by a small decrease between 1979 - 1984 (-0.23% p.a.) and an increase between 1985 - 1990 in the same order of Version 1 with +0.35%.

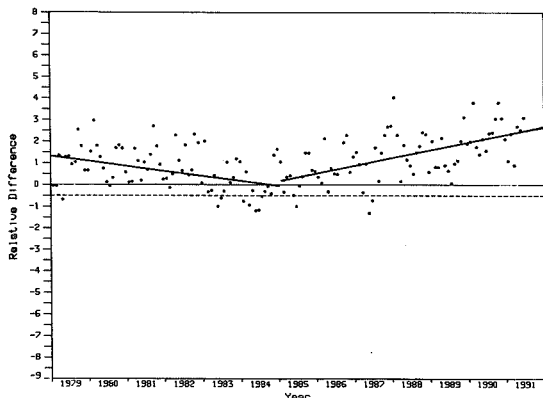


Fig. 4: Comparison Dobson 104 (recalc. data Vers.2) - TOMS (Vers. 6). Ordinate: Relative monthly mean difference (D104-TOMS)/TOMS in %.

It is not easy to clarify whether this oscillation is caused either by TOMS or by D 104. In some papers (Chesters and Neuendorffer, 1991; Herman et al., 1991; McPeters and Komhyr, 1991; Stolarski et al., 1991) it is claimed, that the last TOMS Version 6 should be free of any artificial trend, caused by e.g. instrumental degradation, but especially the comparison with selected Dobson stations (McPeters and Komhyr, 1991) does not exclude such a trend. In Herman et al. (1991) one possible reason for a trend especially during winter is given: The difference between the shape of the standard and the actual profile. Indeed the shape of the mean ozone profile has been changing during the last years. The ozone soundings of Hohenpeissenberg with the Brewer/Mast sonde yield a downward trend in the stratosphere of about -0.5% p.a. and an upward trend in the troposphere of +2% p.a. (Claude et al., 1992). These trends are changing the proportions stratosphere:troposphere from 93:7 to 90:10.

A further confirmation of the assumption, that the D 104 does not cause the above mentioned trend is the comparison between D 104 and BR 10 (Figure 5). The Brewer has been very stable since Arosa 1986. The linear regression using only the annual means yields +0.16% p.a. in the period 1986 - 1991 with a correlation coefficient of 0.443. This trend is obviously not significant. The large annual oscillations with amplitudes of 2.5 to 3% are caused by the mean sun height of the compared daily means. The Dobson observations are mainly performed at higher sun than the Brewer measurements during summer. A comparison only of simultaneous observations will clearly reduce these amplitudes.

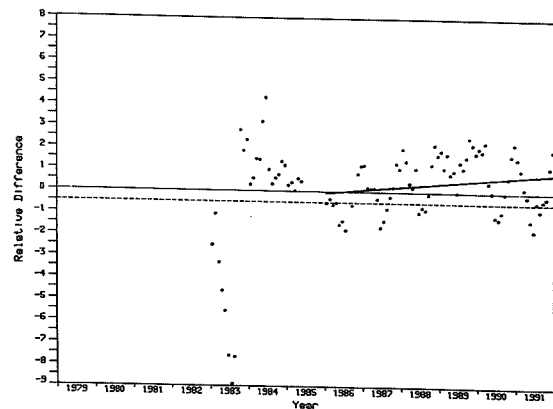


Fig. 5: Comparison Brewer 10 (orig. data) - Dobson 104 (recalc. data Vers. 2). Ordinate: Rel. monthly mean diff. (BR10-D104)/D104 in %.

Figure 6 represents the application of the new Bass and Paur absorption coefficients in the Dobson total ozone calculation (Vers. 3) instead of the Vitroux coefficients. The monthly averages are only shifted by about -2.6%, but the features are still the same.

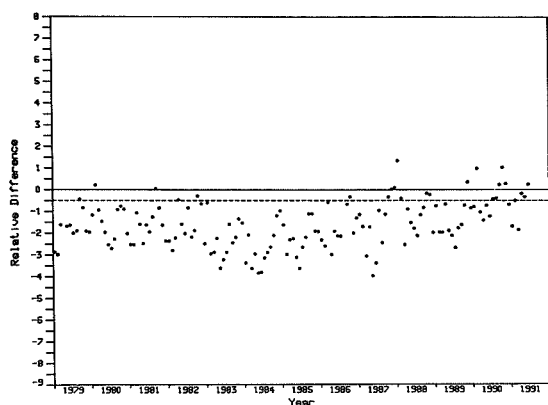


Fig. 6: Comparison Dobson 104 (recalc. data Vers.2 after Bass and Paur) - TOMS (Vers.6). Ordinate: Relative monthly mean differences (D104-TOMS)/TOMS in %.

4. Conclusion and outlook

The results of this investigation show that it will be possible to reprocess a Dobson total ozone series, if the records of raw data, tests and results of intercomparisons are available. Computer-availability of these data is a remarkable facilitation. The comparison with other instruments, especially satellite data, can be used to detect suspicious periods and to check, whether a re-evaluation is successful. They should not be used as a reference for the determination of corrections to the Dobson calibration. With this re-evaluation after method Version 2 the total ozone series of the Hohenpeissenberg D 104 is now homogeneous and reliable in the period 1978 - 1991.

It is planned to apply a similar correction to the data set of 1967 - 1977. Instead of the not available satellite or Brewer data the correlation between total ozone and 100 hPa-temperature will serve as test for the success of the re-evaluation. Additionally the Brewer/Mast-sonde correction factor from the Dobson total ozone, can be used as criterion for the homogeneity of the D 104 data set.

References

- Bhartia, P. K., Klenk, K. F., Gordon, D., Fleig, A. J.: Intercomp. of the NIMBUS 7 SBUV/TOMS total ozone data sets with Dobson and M 83 results. *J. of Geoph. Res.* 89, 5239-5247, (1985).
- Bojkov, R.: Private communication with Hohenpeissenberg (Wege, Hartmannsgruber), (1987/1988).
- Bojkov, R., Mateer, C. L., Hansson, A. L.: Comparison of Ground-Based and Total Ozone Mapping Spectrometer Measurements used in Assessing the Performance of the Global Ozone Observing System. *J. of Geoph. Res.*, 93, 9525-9533 (1988).
- Bojkov, R., Bishop, L., Hill, W. J., Reinsel, G. C., Tiao, G. C.: A statistical trend analysis of revised Dobson total ozone data over the Northern Hemisphere, *J. Geoph. Res.*, 95, 9785-9807, 1990.

- Chester, D., Neuendorffer, A.: Comparison between TOMS, TOVS and DOBSON observations: satellite and surface views of total column ozone. *Paleogeography, Paleoclimatology, Paleoecology (Global and Planetary Change Section)*, 90, p. 61-67, (1991).
- Claude, H., Vandersee, W. and Wege, K.: On long-term ozone trends at Hohenpeissenberg. Submitted for publication in the proceed. of the Quadrennial Ozone Symp., June 1992, Charlottesville, Virginia.
- Fleig, A. J., Bhartia, P. K., Klenk, K. F., Wong, C. K., Mateer, C. L.: Comparison of NIMBUS 7 TOMS and Ground Station Total Ozone Measurements, in *Ozone Data for The World, Catalogue of Ozone Stations and Catalogue of Ozone Data for 1980-1982, Index No. 17*, (1983).
- Grasnack, K.-H., Plessing, P., Feister, U.: Inter-comparison of Dobson Spectrophotometers within the Regional Association VI in 1978 and 1979. *Z. Meteorol.* 41, 4, 283-285, (1991).
- Grass, R. D., Komhyr, W. D.: Traveling standard lamp calibration checks on Dobson ozone spectrophotometers during 1981-83. *Atmospheric Ozone, proceed. of the Quadr. Ozone Symp. in Halkidiki, Greece, 1984.* Reidel, Dordrecht, Holland, 376-380, (1985).
- Herman, J. R., Hudson, R., McPeters, R., Stolarski, R., Ahmad, Z., Gu, X.-Y., Taylor, S., Wellemeyer, C.: A new selfcalibration method applied to TOMS and SBUV backscattered ultraviolet data to determine long-term global ozone change. *J. of Geoph. Res.*, 96, 7531-7545, (1991).
- Kerr, J. B., Evans, W. F. J., Asbridge, I. A.: Recalibration of Dobson Field Spectrophotometers with a Travelling Brewer Spectrophotometer Standard. *Atmospheric Ozone, proceed. of the Quadr. Ozone Symp. in Halkidiki, Greece, 1984.* Reidel, Dordrecht, Holland, 381-386, (1985).
- Köhler, U.: Recalibration of the Hohenpeissenberg Dobson Spectrophotometer 104 Presuming 'Effective Absorption Coefficients'. *J. of Atm. Chem.* 4, 359-374, (1986).
- Köhler, U., Attmannspacher, W.: Long Time Intercomparison Between Brewer and Dobson Spectrophotometer at the Hohenpeissenberg. *Contr. to Atm. Phys.*, Vol. 59, No. 1, 85-96, (1986).
- Komhyr, W. D., Grass, R. D., Evans, R. D., Leonard, R. K.: Results of International Dobson Spectrophotometer and Brewer Spectrometer Calibrations, Arosa, Switzerland, 1986. *Ozone in the Atmosphere, proceedings of the Quadrennial Ozone Symposium in Göttingen, Germany, 1988.* Deepak Publishing, Hampton, Va., 776-779., (1989).
- Komhyr, W. D., Grass, R. D.: Dobson Spectrometer Observations - Corrections To Existing Records. Paper, presented at the International Dobson Instrument Data Workshop, Lanham, Maryland, 1991.
- Komhyr, W. D., Evans, R. D.: Private communication with Hohenpeissenberg in 1990 and 1991.
- McPeters, R. D., Komhyr, W. D.: Long-Term Changes in the Total Ozone Mapping Spectrometer Relative to World Primary Standard Dobson Spectrometer 83. *J. of Geoph. Res.*, 96, 2987-2993, (1991).
- Stolarski, R. S., Bloomfield, P., McPeters, R. D.: Total ozone trends deduced from NIMBUS 7 TOMS data. *Geoph. Res. Letters*, 18, No. 6, 1015-1018, 1991.

303662

THE GLOBAL DISTRIBUTION OF OZONE DESTRUCTION RATES
OBTAINED FROM 13 YEARS OF NIMBUS/TOMS DATA (1979 - 1991)

JAY R. HERMAN, R.S. STOLARSKI, R. MCPETERS
Code 916, NASA/Goddard Space Flight Center
Greenbelt, MD 20771

D. LARKO
Hughes-STX Corporation, 4400 Forbes Road
Lanham, MD 20706

ABSTRACT

Long-term ozone trends (percentage change) have been computed from 13 years of Nimbus/TOMS (Total Ozone Mapping Spectrometer) data as a function of latitude, longitude, and month for the period January 1, 1979 to December 31, 1991. In both hemispheres, the ozone column content has decreased at latitudes above 30° by amounts that are larger than predicted by homogeneous chemistry models for the 13-year time period. The largest rates of ozone decrease occur in the southern hemisphere during winter and spring, with recovery during the summer and autumn. The large winter ozone loss rates are consistent with observed low stratospheric temperatures, ice-cloud formation, and heterogeneous chemistry at middle and high latitudes. There are similar, but smaller changes observed in the northern hemisphere. At midlatitudes (40°N to 50°N) there are increased zonal average ozone depletion rates that correspond to 5 geographically localized regions of increased ozone depletion rates. Only the equatorial band between ±20° shows little or no long-term ozone change since January, 1979. The long-term winter ozone depletion rate data for both hemispheres suggests that heterogeneous chemistry processes may operate over a wide range of latitudes during half of the year.

INTRODUCTION

Measured decreases in the global amount of ozone have exceeded the predicted amount based on a homogeneous chemistry model and the known injection rates of chlorine bearing compounds (mainly chloroflourocarbons) into the atmosphere. The discovery (Farman, et al., 1985) and evolution of the springtime Antarctic ozone hole represents the clearest evidence of accelerated destruction of ozone by heterogeneous chemistry involving chlorine. More recent evidence indicates that accelerated destruction of ozone occurs outside of the Antarctic regions (WMO, 1990; Stolarski, et al., 1991). This study extends the work to include details of the latitudinal variation of ozone trends (12-year percentage change in ozone amount) for each month of the year. The results provide evidence of heterogeneous chemistry processes operating during the winter and spring months over an extended latitude range.

The ozone data from Nimbus/TOMS (Total Ozone Mapping Spectrometer) have been analyzed for global

average trends (Herman et al., 1991b) showing a decrease of $3.2 \pm 1.6\%$ per decade. Removal of solar cycle effects reduced the global average rate of ozone decrease to $2.6 \pm 1.6\%$ per decade. The global average results agree with a statistical study of latitudinal and global changes by Stolarski et al. (1991). Zonal averages of the 12-year ozone trends for each month have shown that regions of accelerated ozone destruction can extend to midlatitudes during the winter and spring months. We show that the zonally averaged ozone depletion rate has a local maximum (7% to 10% per decade) in the 40°N to 50°N latitude range from January to March. In the southern hemisphere, we show that the large midlatitude and polar ozone depletion rates occur before the appearance of the Antarctic ozone hole, and therefore are not the result of backfilling into the polar region.

The TOMS ozone data set has been obtained from a six channel (312.5, 317.5, 331.2, 339.8, 360, and 380nm) Fastie-Ebert downward-viewing spectrometer on board the Nimbus-7 polar orbiting sun-synchronous satellite (see Herman et al. 1991a and b).

The TOMS ozone data are examined for long-term trends for the period from January 1, 1979 to December 31, 1991. The daily ozone data are grouped into 2° x 5° latitude-longitude bins and averaged for each month. The latitude coverage for each month is set to eliminate regions where there is no sunlight for part of the month. Some of the ozone data obtained near the day-night terminator has reduced accuracy when the solar zenith angle is greater than 82° (mostly during the winter months). For larger solar zenith angles, the underlying radiance data may be useable, but the inversion to obtain ozone is uncertain. Contributors to the uncertainty include; 1. non-Lambertian surface reflectivities, 2. cloud and aerosol effects, and 3. spherical geometry corrections for multiple scattering at zenith angles above 85°.

LATITUDINAL ZONAL AVERAGE OZONE TRENDS

The ozone trend within each 2° latitude band is obtained from a linear least squares fit to the zonally averaged ozone data after removing the seasonal variation (Herman et al., 1991b). The seasonal variation is removed by the following procedure. First, average the daily ozone values from each year to form an average annual ozone

(deseasonalized), and then averaged to form a monthly data set. "Months" consist of 4 or 5 whole weeks. The yearly pattern is 5 4 4 4 5 4 5 4 4 5 4 4 weeks per month, with the largest shift from the non-leap-year calendar being 4 days in January and February (shift = 4 4 1 -1 3 -1 3 0 -2 2 0 3 days/month). Next, the 12-year ozone trend was determined by using a linear least squares fit to the "deseasonalized" ozone data. Solar cycle effects could be removed by subtracting 0.33% PD from each ozone-trend cell. The QBO correction for the 12-year ozone time series is negligible.

The 12-years of ozone trend data were subdivided into monthly and seasonal groupings. The seasonal groupings are: 1. December, January, February, 2. March, April, May, 3. June, July, August, and 4. September, October, November, corresponding roughly to Northern hemisphere winter, spring, summer, and autumn. Data obtained during the summer months in both hemispheres can be analyzed for trends over the largest latitude range for which Nimbus/TOMS acquires data (0° to 90°). During the winter months, the range is restricted to approximately 0° to 65° . Linear least squares fits to the data within each 2° x 5° grid cell are made to determine the ozone trends from January 1, 1979 to December 31, 1990. Figure 2 contains the zonal average trends for each month as a function of latitude, and are grouped by season.

THE SOUTHERN HEMISPHERE OZONE DEPLETION

In the southern hemisphere, the computed 12-year ozone depletion rates increase steadily from the equator towards the Antarctic. The larger depletion rates are in the winter, spring, and early summer (June through December), with the largest depletion rates occurring in the spring in conjunction with the ozone hole formation over the Antarctic region. Ozone depletion rates are observed to be in excess of 7% per decade over populated regions in South America poleward of -45° S (southern Argentina and the tip of New Zealand) for 7 months of the year. At the southernmost portion of South America the zonally averaged depletion rate is about 15% per decade during October.

Between -60° S and the equator, the ozone depletion rates (-6% to 0% per decade) are almost independent of the season during most of the summer and autumn months. During the winter, there are large increases in depletion rates between -80° S and -30° S, prior to the formation of the ozone hole. These large long-term depletion-rate increase during the winter months, -13% at 65° S, compared to summer and autumn, -5% to -8% from January to April, indicates that rapid chemical ozone destroying processes (possibly heterogeneous chemistry) are operating during the winter and spring, but at a slower rate than those within the ozone hole region. The large fall and winter depletion rates are not a carryover from previous year's springtime ozone hole, since there is a summer recovery to -5% depletion rates in January and February.

Even though the high latitude 12-year ozone depletion rate is large from June to December, rapid decreases in Antarctic ozone are not observed by TOMS until September, so that the large winter depletion rates (June, July, and August) are not the result of backfilling of an ozone hole. However, the persistence of large rates of ozone decrease into the midlatitude springtime may be enhanced by mixing with the ozone poor air from the Antarctic region.

Low atmospheric temperatures, the availability of particulates, and the sunrise conditions after the long polar night can account for differences in the rate of ozone destruction between the regions inside and outside of the south polar vortex. For example, the appearance of lower temperatures and the formation of stratospheric clouds and polar stratospheric clouds (PSCs) is greatly increased over Antarctica (PSC's, McCormick et al., 1982) compared to midlatitude regions during the winter months. As spring starts in the Antarctic region, temperatures rise, and the amount of active chlorine compounds increases rapidly in the lower stratosphere while the amount of active nitrogen compounds remains low. Aircraft flights into this region show the sudden rise of ClO (Brune et al., 1988, 1990) and OCIO (Wahner et al., 1989) and depletion of NO_2 at the region's boundary (Lowenstein et al., 1989). The elevated amounts of active chlorine and reduced nitrogen oxides lead to the rapid destruction of ozone observed for two months each Antarctic spring. The TOMS instruments on both the Nimbus and Meteor satellites see the rapid formation of the ozone hole each year within the south polar vortex region. Observations of the daily variation of ozone amount from TOMS do not show any large regions in the southern hemisphere outside of the south polar vortex where there is a rapid ozone depletion beyond the normal seasonal cycle. However, the trends computed from the ozone data show definite enhanced long-term depletion rates during the winter and spring months.

NORTHERN HEMISPHERE OZONE DEPLETION

The long-term ozone depletion rates observed during the northern hemisphere winter and spring months appear to be similar to the larger long-term depletion rates in the southern hemisphere outside of ozone hole region. The similarity is primarily in the rapid change of ozone depletion rates as a function of season (see Figure 2). There are differences between some of the corresponding months (e.g., during December and June), and there is the absence of a north polar ozone hole during the spring. Two additional differences between the hemispheres are immediately apparent in Figure 2. First, the northern hemisphere long-term ozone depletion rate is smaller than the rate in the southern hemisphere, particularly during the winter and spring (6% to 8% at 55° N compared to 8% to 10% at -55° S). It is likely that the seasonal ozone depletion rate differences between the hemispheres are related to the different behavior of the winter-spring polar vortex winds

variation for each latitude band. Second, subtract the average annual ozone variation for each day from the corresponding ozone data within each latitude band. The net ozone trend in percent per decade (PD) is given in Figure 1.

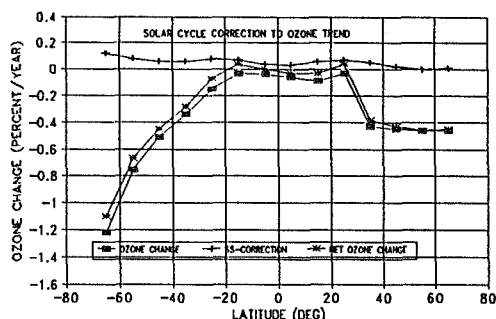


Figure 1. The zonally averaged ozone trend (percent loss per decade) as a function of latitude for the entire year. Also shown is an estimate of the solar cycle correction to the ozone trend of about +0.5% PD.

Each ozone time-series includes an apparent trend arising from solar cycle effects. For the 11.6-year time series considered in Herman et al. (1991b), the beginning time of the ozone data (November 1978) and the ending time (May 1990) are not symmetric with respect to the 10.7 cm solar radio flux ($F_{10.7}$) used as a surrogate for the solar ultraviolet variation (Bojkov et al., 1990). This effect can be removed from the ozone data by forming the fractional variation of $F_{10.7}$ and subtracting the results from the deseasonalized ozone data after the linear least squares trend has been removed (see equations 2, 3, and 4 of Herman et al., 1991). The solar correction at most latitudes is about 0.5% PD. This compares with the value computed for the global average data of 0.54% PD (see Figure 5 in Herman et al., 1991b). The apparent increase in the solar cycle correction near 65°S (1.2% PD) and the decrease near 65°N (0.1% PD) may not be significant because of the large seasonal and interannual variance at these latitudes. These results are in agreement with the statistical analysis of Stolarski et al. (1991). Similar asymmetry corrections have been computed for the 11- and 13-year ozone time series data. The results are 0.7% PD, 0.54% PD, 0.33, and 0.06% PD for 11-, 11.6-, 12-, and 13-year ozone time series, respectively.

The deseasonalized global average and zonal average ozone time series data show clear signs of wave structure of the same period as the 40 mb Singapore wind QBO (Quasi-biennial Oscillation) effect (see Herman et al., 1991b). The 40 mb Singapore winds show a 2% PD linear trend over the approximately 5 cycles between 1979 and 1991. Ozone time series can be reconstructed from the QBO and solar cycle terms and compared with the original deseasonalized ozone data (see Herman et al., 1991b).

Residual time series are obtained by subtracting the reconstructed time series from the original deseasonalized ozone time series for each latitude band. The results show that the small percentage change in the QBO signal does not contribute to a long-term ozone trend. However, there is a $\pm 1\%$ asymmetry effect with respect to the starting and ending points of the ozone time series relative to the phase of the QBO cycle at latitudes below 50°.

The trend analysis can be extended using more recent TOMS data (up to December 31, 1991). The extended period from May 1990 to December 1991 contains two periods of anomalous data. The first of these is related to an instrumental problem with the TOMS chopper wheel synchronization (see Herman et al., 1991a). The percentage of time that the chopper wheel was slightly out of synchronization increased to 70% (from the usual 1%) during the summer of 1990. The percentage returned to low values by October 1990 (less than 10%), and gradually returned to less than 1% for all of 1991. The effect on the ozone trend data was to slightly increase the noise content of the data and, therefore, the uncertainty of the trend determination. Since the period of time for the chopper wheel being out of synchronization was short (2 to 3 months), the effect of increased noise on the 12-year least squares fit to the deseasonalized data is much smaller than the total uncertainty of $\pm 1.4\%$ for the 1979 to 1990 period.

The second period of anomalous data is related to the Pinatubo volcanic eruption in June 1991. This eruption injected large amounts of SO_2 and dust into the stratosphere. The SO_2 is converted rapidly into small sulfuric acid aerosol particles that can remain resident in the stratosphere for many months. Adding this data to the ozone time series and computing long-term trends showed an apparent decrease in equatorial ozone between $\pm 15^\circ$ latitude. The equatorial ozone data measured by TOMS from June 1991 to November 1991 shows an aerosol scalloping effect centered on the 14 daily TOMS north-south orbital tracks. Based on radiative transfer calculations using the aerosol phase function (Torres et al., 1992), the zonal average values using all of the TOMS scan positions across an orbital track are very close to the correct values of zonal average ozone. Because of this, the effect of the Mt. Pinatubo aerosols on zonal average ozone trend determination is very small. Instead, most of the apparent decrease in equatorial ozone arises from the QBO driven wave structure in the ozone time-series data, and does not represent a long term ozone depletion effect.

MONTHLY LATITUDINAL VARIATION IN OZONE TRENDS

To investigate localized geographical patterns in the long-term behavior of ozone by month, the daily ozone data averaged for each week were grouped into $2^\circ \times 5^\circ$ (latitude \times longitude) cells over the latitude range $\pm 85^\circ$. For each grid cell, the average weekly variation was subtracted from the ozone data on a week-by-week basis

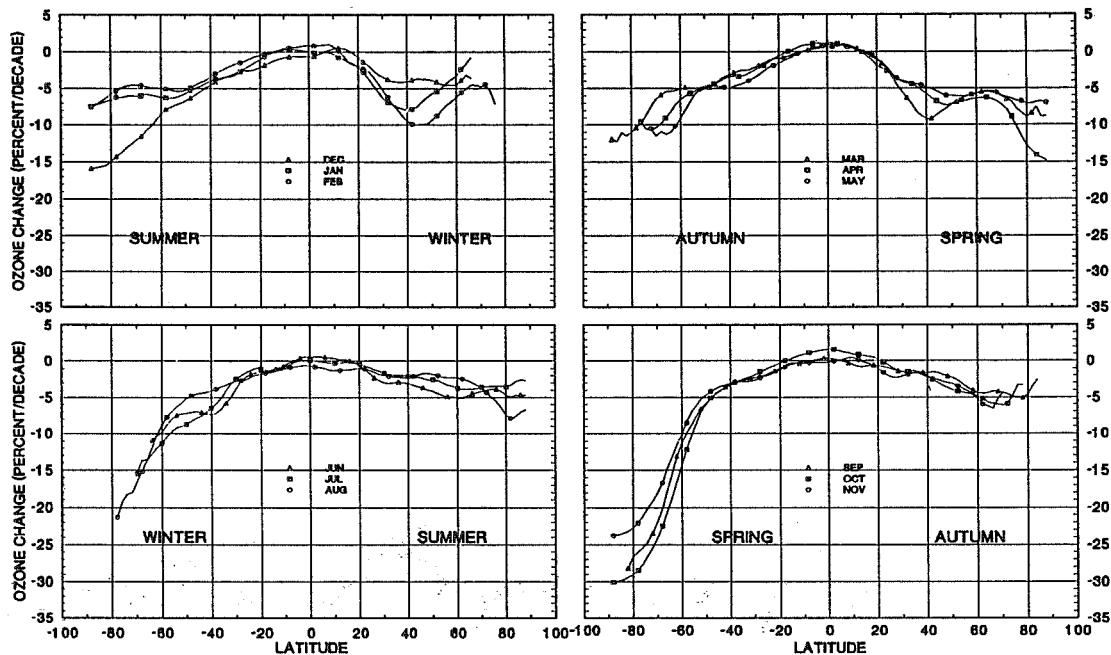


Figure 2. The zonal averages for long-term ozone percentage changes, from January 1, 1979 to December 31, 1990, computed for each month as a function of latitude. The ozone trend data were obtained from the daily TOMS measurements on a $2^{\circ} \times 5^{\circ}$ latitude by longitude grid, and then zonally averaged. The trend data was truncated as a function of latitude for those months where a portion of the period had days where there was no sunlight (e.g., polar winter).

and to the lower temperatures in the southern hemisphere winter causing the formation of more stratospheric ice particles.

Second, the winter-spring depletion rate maxima at 40°N to 50°N only appears as a small feature during the southern hemisphere winter. The local maxima do not appear in the estimates of northern hemisphere trends derived from the ground based Dobson spectrometer network (Bojkov, 1990) even though the general trends are consistent. These mid-latitude local maxima correspond to five regions of enhanced ozone depletion that appear in the northern hemisphere during the winter and spring months. The larger regions are located: 1. on the north-east coast of the United States, 2. on the north-west coast of the United States, 3. in the mid-Pacific ocean, and 4. over the northern portion of Russia. There is a geographically smaller region of enhanced depletion over the Scandinavian countries. It is unlikely that these local depletion regions signify any new depletion mechanisms, but rather are likely to be the result of long-term annually repeating transport of ozone-poor polar air to midlatitudes.

Northern hemisphere high latitude long-term ozone depletion rates, and the seasonal variation of these rates, are far larger than predicted using homogeneous chemistry models (Granier and Brasseur, 1992). Recent aircraft flights

into the Arctic have seen regions of enhanced ClO (Brune et al., 1988, 1990) and depleted NO_x (Kawa et al., 1990, and Wahner et al., 1990) in the lowest portions of the stratosphere. Satellite temperature measurements over the arctic (Newman et al., 1990) imply that PSC's can cover the region for periods on the order of weeks, and so provide the particulates for heterogeneous chemistry. Since Figure 2 shows that the long-term ozone depletion rate is smaller in the summer and autumn than in the winter and spring, the seasonal ozone destruction rate appears to be correlated with the onset of low temperatures and the appearance of stratospheric clouds. The long-term ozone depletion rate data are consistent with a reduced heterogeneous chemistry destruction rate for ozone (relative to the southern hemisphere) involving stratospheric particulates.

CONCLUSION

Long-term ozone trends (percent change) have been computed for 13 years of Nimbus/TOMS data as a function of latitude, longitude, and month for the period January 1, 1979 to December 31, 1991. Examination of the seasonal ozone trends for both the northern and southern polar regions reveal similarities and some differences in behavior. The most obvious difference between the two hemispheres is the much larger southern hemisphere decrease during the spring and winter. The large ozone

trend differences between the hemispheres probably arise from the different behavior of the north- and south-polar vortex winds, and the higher Arctic region winter temperatures. The result is that the Arctic depletion region is more irregular and smaller in magnitude than that in the Antarctic. The second major difference is the appearance of increased midlatitude ozone depletion rates in the vicinity of 30° to 50° during the winter and spring. These correspond to 5 localized depletion regions located: 1. on the north-east coast of the United States, 2. on the north-west coast of the United States, 3. in the mid-Pacific ocean, 4. over the northern portion of Russia, and 5. a smaller region of enhanced depletion over the Scandinavian countries. Since most of these are far south of the region where persistent stratospheric ice clouds, extremely low temperatures, and heterogeneous chemical reactions can produce long-term enhanced ozone depletion rates, they are likely to be the result of annually repetitive weather patterns involving the transport of high latitude air to midlatitudes. Until June, 1991, only the narrow region around the equator, between ±20°, had no significant long-term ozone change compared to the amount of ozone present in 1978, when the Nimbus-TOMS instrument began measurements. After June 1991, the ozone time series for the equatorial region appears to show a significant decrease that might be associated with the Mt Pinatubo injection of SO₂ into the stratosphere. However, zonal average ozone amounts are almost unaffected by the presence of aerosols.

REFERENCES

- Bojkov, R., L. Bishop, W.J. Hill, C. Reinsel, and G.C. Tiao, A statistical analysis of revised Dobson total ozone data over the northern hemisphere, *J. Geophys. Res.*, 95, 9785-9808, 1990.
- Brune W.H., D.W. Toohey, J.G. Anderson, W.L. Starr, J.F. Vedder, and E.F. Danielsen, In situ northern midlatitude observations of ClO, O₃, and BrO in the wintertime lower stratosphere, *Science*, 242, 558, 1988.
- Brune W.H., D.W. Toohey, J.G. Anderson, and K.R. Chan, In situ observations of ClO in the Arctic stratosphere: ER-2 aircraft results from 59°N to 80°N latitude, *Geophys. Res. Lett.* 17, 505, 1990.
- Farman, J.C., B.D. Gardiner, and J.D. Shanklin, Large Losses of Ozone in Antarctica Reveal Seasonal ClO_x/NO_x Interaction, *Nature*, 315, 207-210, 1985.
- Granier, C. and G. Brasseur, Impact of heterogeneous chemistry on model predictions of ozone changes, *J. Geophys. Res.*, 97, Accepted for publication, 1992.
- Herman, J.R., R. Hudson, R. McPeters, R. Stolarski, Z. Ahmad, X-Y Gu, S. Taylor, and C. Wellemeyer, A new self-calibration method applied to TOMS/SBUV backscattered ultraviolet data to determine long-term global ozone change, *J. Geophys. Res.*, 96, 7531-7545, 1991a.
- Herman, J. R., R. McPeters, R. Stolarski, D. Larko, and R. Hudson, Global Average Ozone Change From November 1978 to May 1990, *J. Geophys. Res.*, 96, 17279-17305, 1991b.
- Kawa, S.R., D.W. Fahey, and L.C. Anderson, Measurement of Total Reactive Nitrogen During the Airborne Arctic Stratospheric Expedition, *Geophys. Res. Letters*, 17, 485-488, 1990.
- Lowenstein, M., J.R. Podolske, K.R. Chan, and S.E. Strahan, Nitrous Oxide as a Dynamical Tracer in the 1987 Airborne Antarctic Ozone Experiment, *J. Geophys. Res.*, 94, 11589-11598, 1989.
- McCormick, M.P., H.M. Steele, P. Hamill, W.P. Chu, and T.J. Swisler, Polar Stratospheric Cloud Sightings by SAM II, *J. Atmos. Sci.*, 39, 1387-1397, 1982.
- McCormick, M.P., R.E. Veiga, and W.P. Chu, Stratospheric Ozone Profile and Total Ozone Trends Derived From the SAGE I and SAGE II Data, *Geophys. Res. Letters*, 19, 269-272, 1992.
- Newman, P.A., L.R. Lait, M.R. Schoeberl, and R.M. Nagatani, Stratospheric temperatures during the northern hemisphere winter, *Geophys. Res. Lett.* 17, 329-332, 1990.
- Stolarski, R.S., P. Bloomfield, R.D. McPeters, and J.R. Herman, Total Ozone Trends Deduced From Nimbus 7 TOMS Data, *Geophys. Res. Letters*, 6, 1015-1018, 1991.
- Stolarski, R.S., L. Bishop, R. Bojkov, M.L. Chanin, V. Fioletov, V. Kircchhoff, J. Zawodny, and C. Zerefos, Chapter 2. Ozone and Temperature Trends, in *Scientific Assessment of Ozone Depletion: 1991*, WMO Ozone Report No. 25, 1992.
- Torres, O. P.K. Bhartia, J.R. Herman, *Quadrennial Ozone Symposium*, This Volume, 1992.
- Wahner, A., R.O. Jakoubek, G.H. Mount, A.R. Ravishankara, and A.L. Schmeltekopf, Remote sensing observations of nighttime OClO during the Airborne Antarctic Ozone Experiment, *J. Geophys. Res.*, 94, 11405, 1989.
- WMO, Report of the International Ozone Trends Panel: 1988, World Meteorological Organization, Global Ozone Research and Monitoring Project-Report No. 18, Geneva, Switzerland, 1990.

303603

Depletions in winter total ozone values over Southern England

A.Lapworth
UK Meteorological Office,
England

1 Introduction

Total ozone observations have been made in southern England since Professor Dobson's original measurements at Oxford in the 1930's. However it is only since the 1960's that data from the Bracknell station has been regularly published in 'Total ozone data for the world' (the "red book"). The Bracknell station was closed in August 1989 and the Dobson instrument there was transferred to Camborne (a distance of some 340 kilometers) where observations have been continued to the present date.

The Bracknell station was one of those criticised in the report on an intercomparison between TOMS satellite and ground-based total ozone measurements by Bojkov et al in 1989. Errors of up to 7% or more were noted in sections of the data. As a result of this a re-evaluation was made of measurements and intercomparisons since 1979, the earliest time from which raw data was available, and the results republished in the "red book". It is only the measurements from this period of 1979 to the present that have been used in this study. In addition a survey was made of operating practices and improvements were made. It was as a result of this that the move to Camborne was made, as Bracknell was particularly subject to pollution and did not have as high a number of sunshine hours as Camborne. In addition Camborne was a sonde station from which local upper air data is regularly available and as will be seen below, use has been made of this. The nearest sonde station to Bracknell is Crawley, a distance of about 50km away.

A comparison of total ozone measurements made by the TOMS satellite over the Bracknell and Camborne sites has shown that there is an extremely high correlation between them, as might be expected from their proximity, and for the purposes of this study they have been treated as one station.

Dobson spectrophotometers have been used for

all total observations made at both these stations. For the period 1979 to mid-1990, Dobson No 2, Professor Dobson's own instrument, was the main spectrophotometer in use, with No 41 as a backup, while since then the majority of observations have been made by No 41, the U.K. standard instrument. For short periods since 1990, instruments Nos 32 and 35 have replaced No 41.

2 The annual ozone record

An examination of the re-evaluated ozone values over the period shows a seasonal variation typical of mid-latitude stations in which total ozone values rise from a minimum of about 290 Dobson units in autumn to a maximum of around 405 Dobson units in spring, after which there is a steady decline till autumn. The variability of total ozone amount is high during the winter when ozone amount is increasing, but low during summer when it is decreasing. Dobson (1930) and others have suggested that the annual ozone cycle is due to the transport of air with high ozone mixing ratios from over the equator to high latitudes by the vigorous winter-time stratospheric circulations. Apart from variability due to the global circulation of ozone, total ozone amount has a variation on the order of days that correlates well with locally measured meteorological quantities such as sea level pressure, tropopause height, or stratospheric temperatures. Dobson (1928,1946), Reed (1950), Ohring and Muench (1960), Schubert and Muntenanu (1987), and Vaughan and Price (1991) have shown that much of this correlation is related to ascending and descending motions in the lower stratosphere. Finally, total ozone measurements usually show a diurnal cycle, with higher ozone values during the afternoon caused by daytime increases in boundary layer ozone. There has been a decrease of yearly mean ozone values of -4.6% per decade, which is similar to that found at other stations.

3 Recent measurements

During the last three years, two periods of particularly low ozone monthly means have been measured in southern England. The first of these was during the early months of 1990. The resulting ozone deficit was so great that the annual mean for the year was the lowest recorded during the re-evaluated period 1979 to the present. The value obtained was 325 dobson units compared with a typical value in the past of around 348 dobson units. The satellite data confirms that this record is independent of the fact that the measurement was made at Camborne rather than Bracknell. Although no re-evaluation of the data for the previous decade has been performed, it is of interest to compare the 1990 value with published annual means for this period. There is reason to believe that the No 2 dobson in use suffered less from instrumental problems during this earlier period than during the 1979 to 1990 period when these problems were directly responsible for the poor performance. On average the annual mean values for 1969 to 1978 were higher than those for 1979 to 1991 and none were as low as that in 1990. The second period of reduced ozone values was in December 1991 and January 1992. The January 1992 monthly mean was an exceptional departure from the value over the last decade, having a value of 266 dobson units. This compares with an average value for the January mean over the past decade of 342 dobson units, and is 3.5 standard deviations beneath this value. The only monthly mean in the whole period which is lower than this was November 1988 when the value was 262 dobson units and which was measured at a time of year when low ozone values normally occur. The January 1992 value was so exceptional that a careful check was made of the data. The weather for much of January was overcast, with stratus under an intense anticyclone, so that many of the observations were of the zenith cloudy type. The zenith polynomials were recalculated from data over the past two years but the monthly mean was not significantly altered. In addition checks were made on three periods in January when direct sun measurements were made. These agreed with the zenith observations to within a few dobson units. It should be noted here that as part of the observation program, several observations are made on each day, with as many different observation types as can be fitted in. Another problem is the low sun angle in January, the 'nu' value for midday being between

2.5 and 3.0. Because of this, regular total ozone measurements use the CD wavelengths which are more prone to error than AD observations. This is particularly relevant because during this month observations by lidar at Aberystwyth university show that dust from the Pinatubo eruption covered the region (Vaughan - private communication). However these measurements had detected the dust layer in November and showed that it continued into February and later, which covers periods when AD and CD simultaneous measurements were available. A careful examination of these simultaneous measurements in November, February and March shows that apart from the odd isolated occasion, the AD and CD reading were rarely more than a few Dobson units different. It therefore seems unlikely that the January CD measurements would have been affected by dust relative to the AD standard. It should be noted that any sulphur dioxide accompanying the volcanic dust would have had the effect of increasing rather than decreasing the CD measurement relative to AD. As a final check, TOMS satellite measurements for the Camborne station have recently been sent to us by Dr R. McPeters and these agree within 2% for the January monthly mean.

It therefore appears that the January monthly mean was real rather than related to instrumental problems, and it is useful to consider possible causes of the anomaly.

4 Meteorological anomalies

There seem to be at least three possible causes for the anomalous total ozone values in January, and the first two of these are related to the presence in January of a prolonged anticyclone that covered North-west Europe for much of December and January. Unusually high sea-level pressures of around 1050 hPa were measured in some parts, although not at Camborne itself. Such a blocking feature may have three effects. It will reduce total ozone due to the related ascent of stratospheric air. This is a relatively local effect. As noted above, several meteorological variables are well correlated with total ozone values but this correlation falls off significantly with distance. The best correlated meteorological quantity is the 100 hPa temperature, being at a height of around 17km which is just below the maximum in stratospheric ozone and is the region where vertical air motions are expected to have their greatest effect. The correlation between total ozone value and lo-

cal 100 hPa temperature is about 60% at Camborne, which is typical of a mid-latitude station, but this correlation falls to 35% if ozone values at Bracknell, 340km distant, are correlated with Camborne 100hPa temperatures. Although vertical motions contribute a large part to this type of correlation, it is probable that other advective effects play a minor part.

The second effect of such a prolonged blocking pattern is the possible cutting off of the circulation supplying ozone from the production regions over the equator to middle latitudes that starts in late autumn. Such advective components are unlikely to be detected in the local meteorological correlations.

The third possible cause of ozone depletion is a chemical mechanism related to the reactions involved in the formation of the Antarctic ozone hole. Possible factors involved are the low Stratospheric temperatures necessary for the chemical reactions to take place and which may be found in a winter anticyclone and the volcanic dust veil mentioned above which may provide a surface area for heterogeneous chemistry to take place on (Hofmann and Solomon 1989).

It is not possible to differentiate between the last two depletion mechanisms from single station measurements, but it is possible to quantify the probable effect of vertical stratospheric air motions by making use of the time series of measured total ozone values together with simultaneous meteorological observations. A relation between the ozone values and meteorological variables can be derived from a correlation of past observations and this can be used to quantify the effects of weather systems on total ozone.

5 Meteorological correlations

The meteorological quantities used in the correlation studies described below were surface pressure, tropopause height, 100hPa temperature and 50hPa temperature. For the Camborne station these variables are all measured locally, but for the Bracknell station, upper air quantities were obtained from soundings at Crawley which reduced the correlations because of the separation of these two stations. For each meteorological quantity a linear regression was performed on two variables. The first variable was the deviation of daily total ozone values from either a filtered time series or a slightly filtered 12 year daily mean value. The second variable was the deviation of the meteorological quantity from either a filtered time series or a 12 year daily mean value.

The filters used had a half width of 60 days but the result was not found to be sensitive to the period chosen, and neither was it sensitive to whether the filtered series or 12 year mean was used. The linear regression coefficients were then applied to the difference between the daily values of the meteorological quantity and its 12 year daily mean to give an ozone adjustment which could then be applied to the measured total ozone value. The resulting adjusted ozone value can be considered as the total ozone value that would have been expected in the absence of an anomaly in the meteorological quantity. The linear regression coefficients for the whole time series, together with the correlation coefficients for the Camborne station are given in the table below. Also shown are the adjusted total ozone mean values for January 1992.

Met. Var.	Regress. Coeff.	Corr. Coeff.	Adj. ozone Camb. Jan.'92
Sea lev. Pres.	1.5 DU/hPa	-0.4	283 DU
Trop. Height	0.0145 DU/Dm	-0.55	282 DU
100 hPa Temp.	6.0 DU/deg C	0.6	285 DU
50 hPa Temp.	6.0 DU/deg C	0.55	292 DU

As has been found by previous workers, the 100hPa temperatures are the Meteorological variables best correlated with total ozone measurements, followed by tropopause height and 50 millibar temperatures, with sea level pressures the least well correlated. It is noticeable that the adjusted January 1992 monthly mean total ozone values all lie fairly close together between 282 and 293 Dobson units, with the value for the best correlated meteorological quantity, the 100hPa temperature being 285 Dobson units. This value is still considerably below the annual mean value for January of 348 Dobson units and is 2.5 standard deviations different. It therefore seems apparent that one or both of the other two mechanisms described above are necessary to explain the anomalous January value. However it should be noted that this analysis assumes that the correlation be-

tween meteorological variables and ozone amount is not itself significantly affected by the anomalous synoptic pattern.

6 Adjusted winter ozone values

The use of adjusted total ozone values has several advantages in the study of time series from a station. In general the standard deviation of adjusted daily ozone values is reduced by about 30% from that of non-adjusted values, and a graph of daily ozone values over a year shows a significantly reduced scatter. One particular application is in the comparison of total ozone time series with 100hPa temperatures. A technique often used (Bojkov - private communication) is to form an average annual time series of monthly means, the average being taken over a period of a decade or more. A time series of differences is produced by subtracting these averaged monthly mean values from the individual monthly means and normalising the differences by dividing by the standard deviation of the observations for a month. A similar series is then constructed for the 100hPa temperature observations and the two series are compared. However if ozone values adjusted for 100 hPa measurements as described above are used, there is no need to compare with the 100hPa series as the correlation is automatically included. The normalised difference series is found to have considerable less scatter and is much easier to use. This plot has applications in the detection of anomalies in total ozone values and can also be used in re-evaluation of instrument calibrations.

Another method of applying adjusted ozone values is by plotting a time series of a particular month in a year. This plot has been used for the Bracknell - Camborne time series and for all the plots, the adjusted ozone values show less scatter than the unadjusted values. As noted previously, the scatter is greater in the winter than in the summer months, and the plots show that, as is well known, part of this increased scatter is due to meteorological variations.

The plots for January show a continuous decline in total ozone amount over the last decade. This decline is pronounced only in the spring months and is a major component of the decrease in annual ozone mean values. Use of data published in the decade 1969 to 1979 shows that this decline spans both decades. There is a very pronounced drop in the monthly mean ozone value in January 1992, which is particularly clear in the adjusted

ozone plot. A drop in monthly mean ozone value is also evident in the plot for the previous month of December 1991. Looking back over the previous decade there are noticeable dips in adjusted ozone value in December 1982 and January 1983 although the reduction in ozone was not nearly so extreme in those cases as for 1991/1992. Several workers (e.g. Angell et al., 1985) have already noted a minimum in total ozone at several northern hemisphere stations in the winter of 1982/1983

These two winters have the following circumstance in common, that they were both preceded by a major northern hemisphere volcanic eruption in the previous late spring/early summer and in both cases the dust from the eruptions reached the United Kingdom during the autumn. The two eruptions were those of El Chichon and Pinatubo. No other major eruptions with dust significantly affecting the U.K. occurred during the decade. It is possible that the reductions in total ozone value noted during the winter months over southern England for these two years are in some way related to the two eruptions. As mentioned above, such an anomaly may have occurred either due to changes in the stratospheric circulation or by chemical processes or by a combination of these two effects. However it is also possible that the ozone reductions are unrelated and have different causes. In particular, there was a pronounced ENSO event in 1982 and several studies of the 1983 ozone minimum (e.g. Chandra and Stolarski 1991) indicate that much of that anomaly was related to the Quasi-Biennial Oscillation, although some may have been an effect of the volcano.

7 Conclusions

A study has been made of the recently re-evaluated time series of daily total ozone values for the period 1979 to 1992 for southern England. The series consists of measurements made at two stations, Bracknell and Camborne. The series shows a steady decline in ozone values in the spring months over the period, and this is consistent with data from an earlier decade that has been published, but not re-evaluated. Of exceptional note is the monthly mean for January 1992 which was very significantly reduced from the normal value, and was the lowest so far measured for this month. This winter was also noteworthy for a prolonged period during which a blocking anticyclone dominated the region, and the possibility existed that this was related to the ozone anomaly.

It was possible to determine whether the origin of the low ozone value lay in ascending stratospheric motions. A linear regression analysis of ozone value deviation against 100hPa temperature deviations was used to reduce ozone values to those expected in the absence of high pressure. The assumption was made that the normal regression relation was not affected by atmospheric anomalies during the winter. This showed that vertical motions in the stratosphere only accounted for part of the ozone anomaly and that the main cause of the ozone deficit lay either in a reduced stratospheric circulation to which the anticyclone may be related or in chemical effects in the reduced stratospheric temperatures above the high pressure area. A study of the ozone time series adjusted to remove variations correlated with meteorological quantities, showed that during the period since 1979, one other winter, that of 1982/3, showed a similar although less well defined deficit in total ozone values. It is possible that these two periods of low ozone amounts are related to the fact that large quantities of volcanic dust covered the region on these two occasions. However work that included a far greater area than a single station is necessary to show that such a correlation indeed exists. Previous work on the 1983 anomaly has indicated that much of the ozone reduction then may be attributable to non-volcanic causes.

8 Acknowledgements

I first of all wish to thank Dave Drew, Ivor Jones and the other observers who operate the Camborne station and also Mike Regan who was the principal operator of the Bracknell instrument from 1979 to 1989. Phil Hughes and Richard Smout are now responsible for collection of the ozone data and were very helpful in supplying it when required. Keith Grant supplied much of the upper air data. I am very grateful to Richard McPeters who has been extremely helpful in supplying TOMS version 6 data for a number of stations as soon as it was available whenever I asked for it. I would also like to mention Geraint Vaughan of Aberystwyth University for supplying unpublished lidar data, and who gave advice. Finally I would like to thank Rod Jones, Brian Gardener, and Paul Newman for useful conversations.

9 References

- Angell J.K., Korshover J., and Planet W.G., 1985 'Ground based and satellite evidence for a pronounced total-ozone minimum in early 1983 and responsible atmospheric layers' *Month. Wea. Rev.* **113**,641
- Bojkov R.D., Mateer C.L. and Hanson A.L., 1988 'Comparison of Ground-Based and Total Ozone Mapping Spectrometer Measurement used in assessing the performance of the Global Ozone Observing System' *J. Geophys. Res.* **93**,9525-9533
- Chandra S. and Stolarski R.S., 1991 'Recent trends in stratospherical total ozone: implications of dynamical and El Chichon perturbations' *Geophys. Res. Lett.* **18**,2277-2280
- Dobson G.M.B., Harrison D.N. and Lawrence J., 1928 'Measurement of the amount of ozone in the earth's atmosphere and its relation to other geophysical conditions' *Proc. Roy. Soc. London, A* **122**,456-486
- Dobson G.M.B. 1930 'Observations of the amount of ozone in the Earth's atmosphere and its relation to other geophysical conditions' *Proc. Roy. Soc. London, A* **120**,411
- Dobson G.M.B., Brewer A.W. and Cwilog B.M., 1946 'Meteorology of the lower stratosphere' *Proc. Roy. Soc. London, A* **185**,144-175
- Hofmann D.J. and Solomon S., 1989 'Ozone destruction through heterogenous chemistry' *J. Geophys. Res.* **94**,5029
- Ohring G. and Muench H.S., 1960 'Relationship between ozone and meteorological parameters in the lower stratosphere' *J. Meteorol.* **17**,195-206
- Reed R.J., 1950 'The role of vertical motions in ozone-weather relationships' *J. Meteorol.* **7**,263-267
- Schubert S.D. and Muntenau M.J., 1988 'An analysis of tropopause pressure and total ozone correlations' *Mon. weather Rev.* **116**,569-582
- Vaughan G. and Price J.D., 1991 'On the relation between total ozone and meteorology' *Q. J. R. Meteorol. Soc.* **117**,1281-1298

303604

STABLE OZONE LAYER IN NORWAY AND USSR

*K. Henriksen and T. Svenøe*The Auroral Observatory, University of Tromsø
Tromsø, Norway*E.I. Terez and G.A. Terez*
University of Simferopol
Simferopol, Ukraina*V. Roldugin*
Polar Geophysical Institute
Murmansk/Apatity, Russia*S.H.H. Larsen*
The Institute of Physics, University of Oslo
Oslo, Norway

ABSTRACT

Long-term column ozone density measurements have been carried out in Norway and USSR. Data from Tromsø and two meridional chains in USSR are analysed, and most of the stations show that no significant decreasing trend in ozone has occurred during the last two decades.

1. INTRODUCTION

In a recent statistical study of ground-based ozone data from 19° N to 64° N (Bojkov et al., 1990) results similar to those in the NASA/WMO report (1988) were obtained, but this study also reveals essential regional differences with no negative trend in Iceland and Mexico. The biggest negative trend, 3.5% per decade, was found at Uccle, Belgium. Subsequently the Belgian data were reanalysed by the scientists responsible for the data collection, and no negative trend was found. The reason for this change was the decreasing load of SO₂ content over Belgium during the two last decades. The results of this reanalysis were presented at a scientific meeting in Tromsø, Norway in June 1991 (De Backer and De Muer, 1991).

In accordance with the Belgian results it has been documented that there is no long term decrease of the ozone layer in the Scandinavian sector of the Arctic (Larsen and Henriksen, 1990; Henriksen et al., 1991,

1992). However, the Oslo data have been reanalysed using new charts for the zenith sky observations and correcting the data according to the results of the inter-comparison workshop in Arosa, Switzerland in 1986. These two factors result in a decrease of 7% during the period of the observation in Oslo from 1978 throughout 1991. It must be added that no correction for possible changes in SO₂ content over Oslo has been considered.

2. NORWEGIAN DATA

Ozone data from Tromsø and two meridional chains in USSR, comprising the period from 1973 to 1988, are used in this study. The Norwegian and Soviet stations are shown on the map shown in Fig. 1.

The ozone measurements in Tromsø started in 1935 but were interrupted from 1969 to 1984. The average ozone values for each year, having a complete record, are shown in Fig. 2. The average ozone value for the period 1935-1969 is 337 DU. In this period the release of CFC gases was negligible and similarly the ozone destruction due to anthropogenic sources is believed to be negligible. Fig. 2 also shows that the yearly average ozone values of the years 1985 through 1989 all lie above the average for the period 1936 to 1969. Statistical analysis of the data identify that ozone increase has occurred through July, August, and September months (Henriksen et al., 1991).

The Tromsø data were obtained with a Féry spectrograph from 1935 to 1939 and since 1939 with

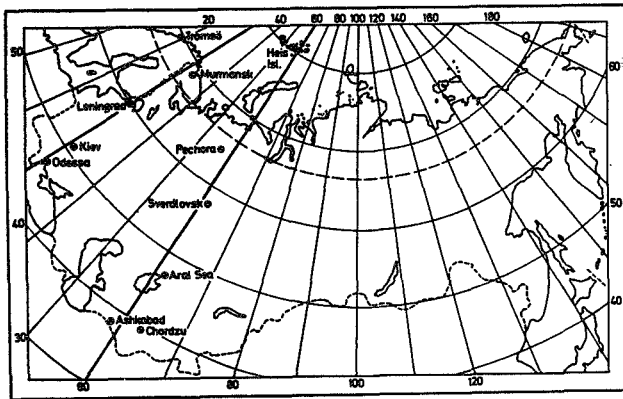


Fig. 1. Map of Europe and USSR pointing out the ozone observing stations used in this review.

x Mean yearly values of total ozone in Tromsø 1935 - 1989

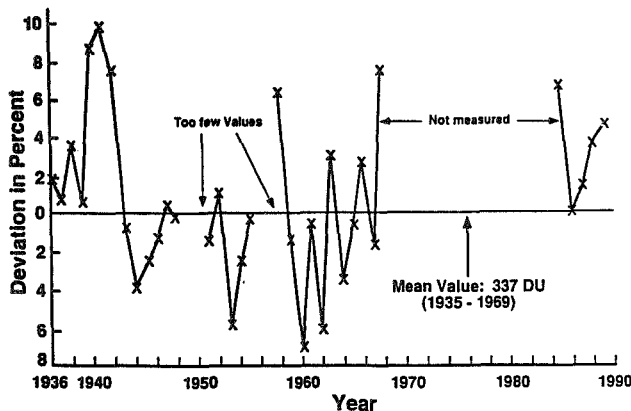


Fig. 2. Annual average ozone values in Tromsø for the periods 1935-1969 and 1984-1989. The deviations are given relative to the average value of the period 1936-1969, and this value is 337 Dobson Units (DU).

Dobson spectrophotometer no. 14. This instrument is a highly stable instrument calibrated three times in 1939, 1950, and 1954 against G.M.B. Dobson's calibration standard, in 1977 against Dobson spectrophotometer no. 83 in Boulder, USA, and in 1990 against Dobson spectrophotometer no. 65 in Arosa, Switzerland. There was a positive shift of 2.41 per cent in sensitivity for the C wavelength pair during the period from 1977 to 1990, but no correction for this minor shift is imposed on the data. The measurements in Tromsø have been carried out only with the C wavelength pair. The data were gathered by direct sun, zenith sky, and moon measurements, and during the polar night the most reliable data were obtained by the moon measurements. The sta-

bility of the instrument was checked monthly by a set of standard lamps.

The comparison between direct sun and zenith sky measurements has been made systematically in Tromsø through several years. Theoretical umkehr curves have been calculated to study how different ozone profiles influence the shape of the profiles and introduce uncertainties in calculations of the ozone values. In addition, one has to apply cloud corrections which is a great problem. Our cloud correction charts are based on years of gathered data.

Concerning moon measurements we have taken into account a correction for using focused image on the slit. Whenever possible, the night-time moon measurements have been compared with the daytime, direct sun measurements to assure that the moon measurements are reasonable. Comparison between the Tromsø instrument on the moon and ozone sonde ascents in Sodankylä, Finland has been carried out for the last three years, showing reasonable agreements although the distance between the two places is more than 150 km.

As anywhere else the direct sun method gives the fundamental data, and the other methods are adjusted relative to this method. Therefore no systematic deviations have occurred between the fundamental data and values obtained by zenith sky or moon measurements.

Due to the long record with a stable instrument a reference for an average annual variation of the thickness of the ozone layer is calculated from the measurements carried out during the period 1935-1969, shown in Fig. 3. An estimate of the standard deviation of single measurements is obtained from the measurements from 1984 to 1992, and the 99.87% confidence interval consists of the range comprised by \pm three times the standard deviation. The calculation of the confidence interval is based on the assumption that the daily measurements have a Gaussian distribution, and that they are independent. The large variation of ozone at Tromsø can be mainly due to changes related to meteorological factors such as low pressure centers and polar fronts, resulting in wide confidence limits. Therefore all the measurements obtained during the first months of 1992 are well within the limits, indicating that the variations of the ozone layer can be considered as stochastic.

3. SOVIET DATA

The Soviet data were obtained with the Soviet ozonometer M-124 since 1973. The calibration of each instrument were frequently updated by travelling standards and intercomparisons held at Feodosia (45° N) in Crimea. However, most of the routine measurements at these stations were initiated during IGY, 1956-1959 using another instrument, ozonometer M-83.

The measuring procedure of the Soviet ozonometers is outlined by Gushchin (1986), and these instru-

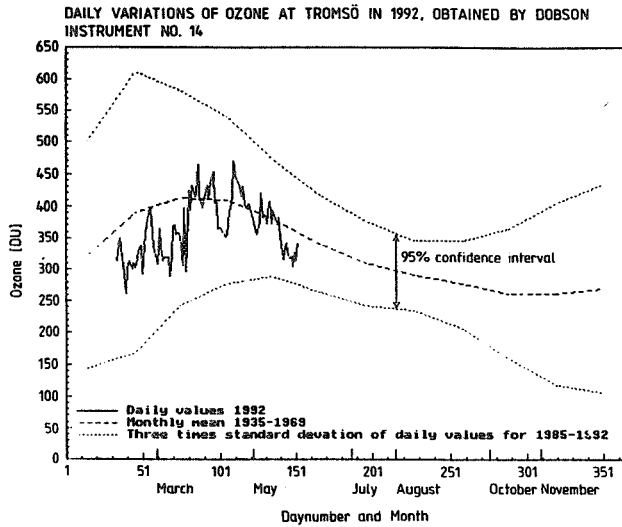


Fig. 3. Average annual ozone variation, dashed curve obtained from measurements throughout the reference period 1935-1969. An estimate of the standard deviation is obtained from single measurements during the period 1984-1992. The 99.87% confidence interval consists of the area of \pm three times standard deviation of the single, independent measurements. The continuous curve gives the existing daily ozone measurements in 1992. They are all well within the 99.87% confidence limits, indicating that all variation have been of statistical nature. Based on previous data such variations are to be expected.

ments are calibrated against the secondary calibration standard, Dobson spectrophotometer no. 108. These data are issued by The Main Geophysical Observatory (MGO), Leningrad in an annual data publication called *Total ozone and spectral transparency of atmosphere*, Leningrad Hydrometeoizdat 1975-1988 (in Russian). The statistical treatment of these data agrees fairly well with the results of the analysis of a large amount of Soviet data presented by Bojkov and Fioletov (1992), where certain amount of corrections of original data are carried out.

The main results of these two studies are negative ozone trends from 1 to 5% per decade. Some disagreements appear considering the confidence limits. Bojkov and Fioletov (1992) associate the observation with much smaller statistical uncertainties than our study and find that their calculated trends are significant.

The Soviet data are shown in Figs. 4 and 5, where monthly average ozone values from each station of both

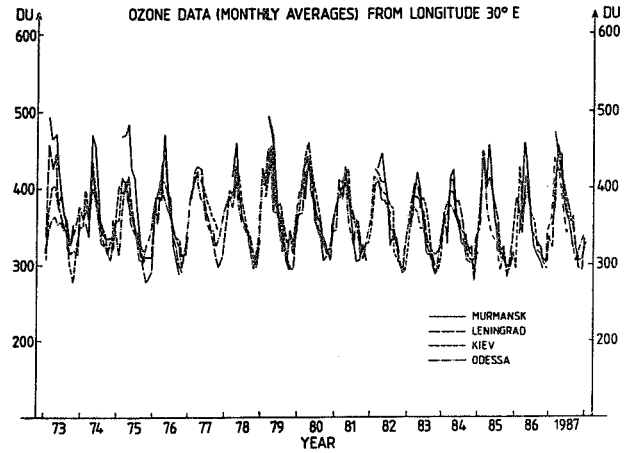


Fig. 4. Superposed ozone values for the ozone stations around the meridian 30° E.

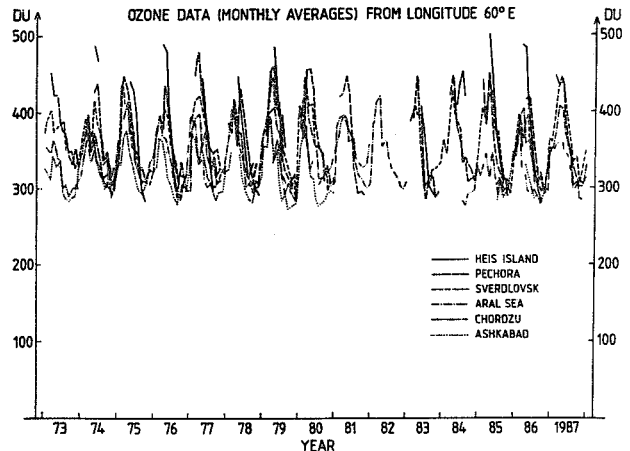


Fig. 5. Superposed ozone values for the ozone stations around the meridian 60° E.

meridional chains are superposed. One meridional chain is around longitude 30° E, containing the four stations Murmansk (69° N), Leningrad (60° N), Kiev (50° N), and Odessa (46° N). The other chain is situated around longitude 60° E, containing Heis Island (80° N), Pechora (65° N), Sverdlovsk (56° N), Aral Sea (46° N), Chordzu (39° N), and Ashkabad (37° N). The superposition of the Soviet data reveals a stationary ozone behaviour with maximum in March and minimum in October.

Due to the disagreements about statistical confidence limits mentioned above, the formulas used in this analysis will be given. The linear regression coefficients, a_n , and the related error, err_n , are calculated by the expression given by Box et al. (1978)

$$a_n = \frac{\sum_i (X_i - \bar{X}_n)(y_i - \bar{y}_n)}{\sum_i (X_i - \bar{X}_n)^2},$$

Table I.

STATION and LATITUDE	$a_n \pm err_n$				$\bar{y}_n \pm \sigma_n$
	YEAR	DEC-MAR	MAY-AUG	SEP-NOV	
MURMANSK (69° N)	-5.88±4.8	-5.69±14.7	-6.63±3.8	-3.92±5.1	370.4±15.88
LENINGRAD (60° N)	-1.01±2.5	-4.16±7.6	+1.66±3.8	+0.22±4.0	358.3±6.73
KIEV (50° N)	-3.37±5.5	-3.29±7.8	-0.90±5.4	-3.89±5.8	356.1±14.94
ODESSA (46° N)	-3.32±6.3	-1.24±7.2	-4.50±5.7	-5.28±3.8	352.6±16.77
30° meridian	-2.82±3.2	-2.83±5.4	-2.18±3.5	-3.16±3.0	358.4±9.29
HEIS ISLAND (80° N)	-1.19±10.3	no data	-0.31±8.4	-5.12±48.8	382.5±20.46
PECHORA (65° N)	-2.51±4.3	+0.45±10.4	-2.99±3.7	-5.25±3.8	364.3±11.74
SVERDLOVSK (56° N)	-1.46±4.0	-1.76±9.2	-2.11±5.0	-1.44±4.5	358.4±10.28
ARAL SEA (46° N)	-2.75±5.1	-3.39±9.5	-1.03±5.6	-4.88±2.9	342.4±11.02
CHARDZHOU (39° N)	-0.52±7.3	-0.38±6.1	+1.16±9.4	+0.53±5.6	324.9±15.13
ASHKHABAD (37° N)	-3.77±3.7	-2.35±9.1	-4.18±4.4	-2.90±5.6	318.2±7.77
60° meridian	-0.32±2.1	0.17±2.5	0.20±2.7	-2.18±2.1	346.5±5.16

and

$$err_n = t_{\alpha/2} \sqrt{\frac{\sum(y_i - \bar{y}_n)^2 - a_n^2 \sum(X_i - \bar{X}_n)^2}{(N-2) \sum(X_i - \bar{X}_n)^2}}$$

In these expressions X_i and y_i are the abscissa and ordinate of each measurement, N the total number of measurements at each station, $t_{\alpha/2}$ the quantile of Student's distribution for $(1-\alpha)$ probability, α being the probability outside the level of confidence. Only mean monthly values of ozone column densities are used in this analysis. The confidence interval for the regression coefficients, a_n , as indicated by the related errors, err_n , is 95%. The σ symbol indicates the standard deviation of the single values,

$$\sigma = \sqrt{\frac{\sum(y_i - \bar{y}_n)^2}{n-1}}$$

The results of the statistical analysis of the Soviet data set for the individual stations and each chain for the whole data set and separate seasons are carried out and shown in Table I together with the corresponding errors and uncertainties (err_n). The units are (percent/decade). In the table all the data from the two chains are used, and all the calculations are carried out using mean ozone data at the individual stations.

The coefficients are normally smaller than the uncertainties, and no all-year significant trend can be stated on the basis of this data set. However, for the sake of completeness it must be noted that three stations show downward trends in the fall, statistically significant on

the 95% confidence level, and such larger deviations can be expected from a statistical point of view.

In the last column of Table I it can be seen that the ozone content along the chains increases northwards, and therefore grouping of stations in latitudinal intervals may mask real gradients. The relatively large standard deviations, however, are mostly caused by averaging the inherent annual amplitude of 100 DU. It must be remarked that no trend is calculated for Heis Island during winter since there exist too little data.

The trends of the two chains are -2.8 ± 3.2 (percent/decade) for the 30° chain and -0.3 ± 2.1 (percent/decade) for the other chain. Therefore the summed data do not show any significant trend on the 95% confidence level during the period 1973-1987, and the result is in agreement with the trends obtained for the individual stations.

4. CONCLUDING REMARKS

The long-term data set from Tromsø and the extensive data set from Soviet do not show any significant decreasing trend of the measured ozone content when the complete data sets are examined by the methods outlined in this study. There are both longitudinal and latitudinal variations in the ozone content, which can obviously be of dynamical origin as shown by Rabbe and Larsen (1991). In order to find the effect of the physical processes, adequate statistical analysis of the measured variations must be carried out, deleting the well-documented annual variations, and making correla-

tions with meteorological data as wind and temperature in the stratosphere. The large ozone increase in the beginning of 1940's in Tromsø is also obvious in the data from Arosa (Dütsch and Staehlin, 1989), but the decreasing trend from the beginning of the 1950's in the Arosa data is not present in the Tromsø data.

It must be admitted that the small negative trend quoted by Bojkov and Fioletov (1992) in the Soviet data also appears from our analysis, but Bojkov and Fioletov (1992) find that the negative trend is significant while we do not. This disagreement with Bojkov and Fioletov (1992) can be due to the calculation and interpretation of the statistical uncertainty, and to some extent to their correction of the original Soviet ozone data. They postulate that the Soviet data are influenced by physical processes as quasi-biennial oscillations and solar activity and include several such driving forces into a regression model together with one term taking care of trends. The driving forces of the ozone layer and their effects are not sufficiently understood, and including such effects into a regression model introduces unpredictable uncertainties. It seems by this mathematics of Bojkov and Fioletov (1992) that the measured ozone variations are smoothed, and significant negative trends appear.

Our analysis, however, uses the original data as they are issued by MGO, Leningrad. Then trends are calculated both for the whole data set and for specific seasons, and the uncertainties and confidence limits are derived by well-known formulas. The over-all result indicates that the ozone layer is stable both in Norway and USSR.

REFERENCES

- Bojkov R., L. Bishop, W.J. Hill, G.C. Reinsel, and G.C. Tiao, 1990: A statistical trend analysis of revised Dobson total ozone data over the northern hemisphere. J. Geophys. Res., 95, 9785-9807.
- Bojkov, R.D. and V.E. Fioletov, 1992: Ozone changes from the eastern Europe to the far East, paper presented at 1992 Quadrennial Ozone Symposium, Virginia, USA.
- Box, G.E.P., W.G. Hunter, and J.S. Hunter, 1978: Statistics for experimenters. An introduction to design, data analysis, and model building. John Wiley & Sons, New York.
- De Backer H. and D. De Muer, 1991: Comparative analysis of revised total ozone time series as measured with Dobson no. 40 and Brewer no. 16 at Uccle (Belgium); Implications of SO₂ trends on total ozone trends, paper presented at the 18th Annual European Meeting on Atmospheric Studies by Optical Methods, Tromsø, Norway.
- Dütsch, H.U. and J. Staehlin, 1989: Discussion of the 60 year total ozone record at Arosa based on measurements of the vertical distribution and a meteorological parameter. Planet. Space Sci., 37, 1587-1599.
- Gushchin, G.P., 1989: Common content of atmospheric ozone and spectral transparency of atmosphere. Published by Hydrometeoizdat, ed. G.P. Gushchin, Leningrad.
- Henriksen K., T. Svenøe, and S.H.H. Larsen, 1992: On the stability of the ozone layer at Tromsø, J. Atm. Terr. Phys., 54, 1113-1117.
- Henriksen, K., E.I. Terez, G.A. Terez, V. Roldugin, T. Svenøe and S.H.H. Larsen, 1992: On the stationarity of the ozone layer in Norway and USSR. Accepted for publication in J. Atm. Terr. Phys.
- Larsen S.H.H. and T. Henriksen, 1990: Persistent Arctic ozone layer. Nature, 343, 124.
- NASA/WMO Ozone Trends Panel Report, 1988: Present state of knowledge of the upper atmosphere 1988: An assessment report, NASA Ref. Publ. 1208.
- Rabbe, Å. and S.H.H. Larsen, 1991: Ozone "minihole" over northern Scandinavia. Submitted to J. Atm. Terr. Phys.

303605

LONG TERM TREND OF SELECTED HALOGENATED HYDROCARBONS

R. Borchers,

Max-Planck-Institut für Aeronomie, 3411 Katlenburg-Lindau, Germany

R. Gunawardena and R.A. Rasmussen

Oregon Graduate Institute, Beaverton, Oregon, USA

ABSTRACT

The so-called "Library of Background Air" at the Oregon Graduate Institute was used to determine the trend in volume mixing ratios of selected halogenated hydrocarbons in the time period 1977-1989. This library consists of background air samples most of them taken at Cape Meares (Oregon). For storage stainless steel containers are used. Tests have shown the gases under consideration to be stable in these containers.

Analyses using a GC/MS-system were performed for the CFCs 11, 12, 12B1 (HALON 1211, CBrClF₂), 22, 113, 114 and CH₃Cl, CH₃Br, CH₃CCl₃, CCl₄. The advantage of this unique investigation: Different aged air samples are analysed at the same time with the same instrument. No calibrations or intercalibrations are needed. All data are presented in normalized mixing ratios versus time. We discuss the results, derive rate constants and we present a formula to describe the nonlinear increases.

1. INTRODUCTION

Halocarbons containing chlorine and bromine have been found to deplete ozone in the stratosphere. In addition they are important greenhouse gases [Climate change, 1990; WMO, 1990]. Since there is no significant tropospheric removal mechanism for the fully halogenated hydrocarbons, they are almost inert gases in the troposphere, where they accumulate. Transported into the stratosphere by various mechanism, they decompose by UV photolysis and by reacting with O(¹D), liberating chlorine and bromine. The overall lifetime of these CFC's is large, whereas the lifetime of partly halogenated hydrocarbons such as CHClF₂ (CFC-22) methyl chloride (CH₃Cl), methylbromide (CH₃Br) and methylchloroform (CH₃CCl₃) is relatively small and they are mostly removed in the troposphere. Nevertheless, the global release of CH₃Cl and CH₃CCl₃ is so large, that despite tropospheric removal, their contribution to the stratospheric chlorine budget is significant [Borchers et al., 1983, 1989; Fabian et al., 1981; Fabian 1986].

One of the important partly halogenated halocarbons of anthropogenic origin, CFC-22 (CHClF₂) is being seri-

ously considered to be a replacement substance for CFC-11 and CFC-12. But it should be pointed out that its lifetime is ~ 10-20 years, and is not low enough to prevent it from reaching to the stratosphere and augmenting its chlorine budget.

2. MEASUREMENTS

The growth rate of the tropospheric concentration of some of the important halogenated hydrocarbons, namely CFC-11, CFC-12, CFC-22, CFC-113, CFC-114, CFC-12B1, CH₃Cl, CH₃Br, CH₃CCl₃ and CCl₄ has been obtained by analysing air samples from the "Library of Background Air" at the Oregon Graduate Institute. The GC-MS-system equipped with a DB-1 capillary column has been used to analyse the air samples collected periodically during a time span of 13 years (1977-1989). All the analyses have been performed under exactly identical conditions. Considering these halogenated hydrocarbons to be stable under the storage in the stainless steel containers during the aforesaid time-frame - a plausible assumption - the data generated have been used to obtain the annual percentage growth rate by using a simple exponential formula.

RESULTS AND DISCUSSIONS

The volume mixing ratios of all these gases normalized to the value of 1989, have been plotted and are shown in Figs. 1-10. Considering the growth to be exponential and using the following expression

$$\text{VMR}_{\text{rel}} = A_0 e^{B(t-1976)}$$

[where A and B are constants and t denotes the year]

the relative growth rates have been calculated. These growth rates are tabulated in Table 1 and are also shown by the solid lines in all the figures [Figs. 1-10].

The atmospheric concentrations of CH₃Cl and CH₃Br have been found stable (long term behavior) indicating that they do not have any significant anthropogenic source

(Figs. 9 and 10). The current percentage increase evaluated for the other source gases at Cape Meares are also compared with the global growth rates of these species [Climate Change 1990, WMO, 1990].

Table 1. Growth rates obtained for different CFCs

Substance	A_0	$B[\text{year}^{-1}]$	Growth Rate [%/year]	
			Present Data	WMO 1990
CFC-11	0.584	0.04360	4.50	4
CFC-12	0.561	0.04730	4.80	4
CFC-12B1	0.306	0.09560	10.00	12
CFC-22	0.424	0.06930	7.20	8 *
CFC-113	0.133	0.10700	11.30	10
CFC-114	0.591	0.04080	4.20	()
CH_3CCl_3	0.629	0.04030	4.10	4
CCl_4	0.896	0.00944	0.95	1.5
CH_3Cl	-	-	-	-
CH_3Br	-	-	-	-

* Rasmussen, 1992 unpublished data

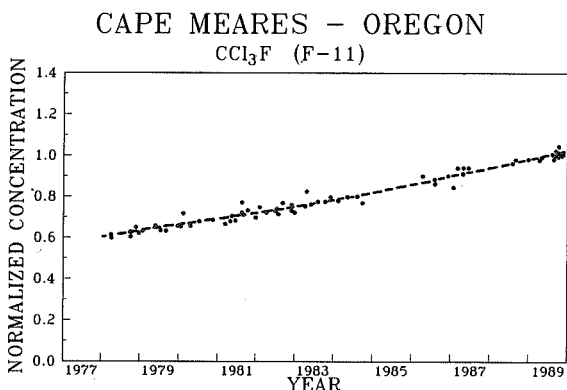


Fig. 1 Volume mixing ratios for CFC-11

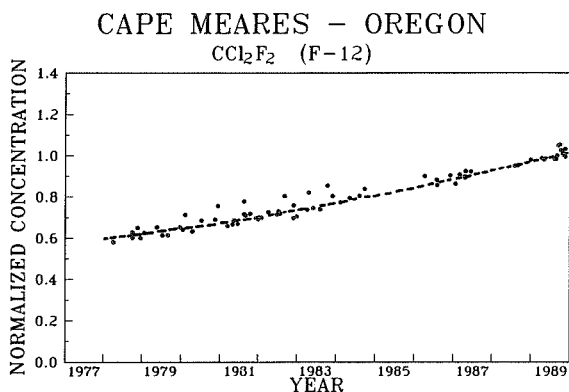


Fig. 2 Volume mixing ratios for CFC-12

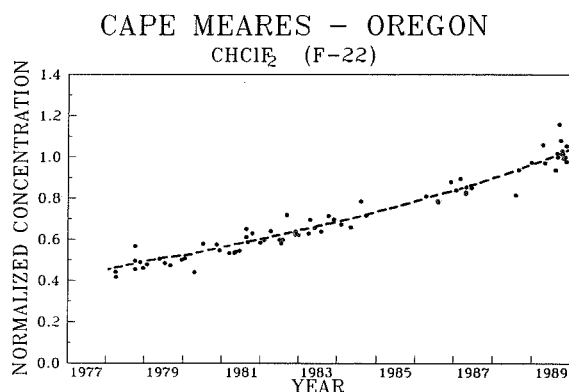


Fig. 4 Volume mixing ratios for CFC-22

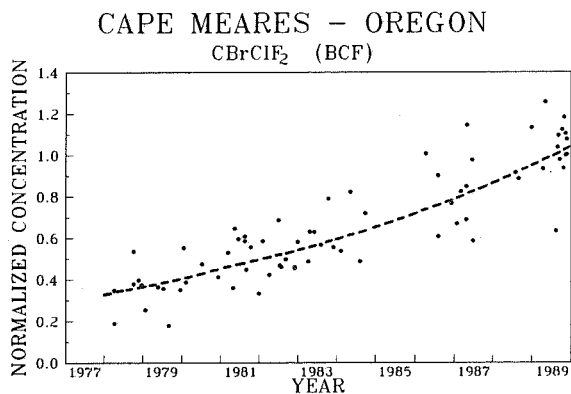


Fig. 3 Volume mixing ratios for CFC-12B1

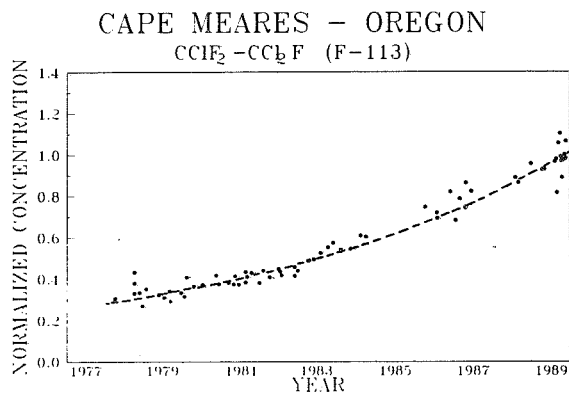


Fig. 5 Volume mixing ratios for CFC-113

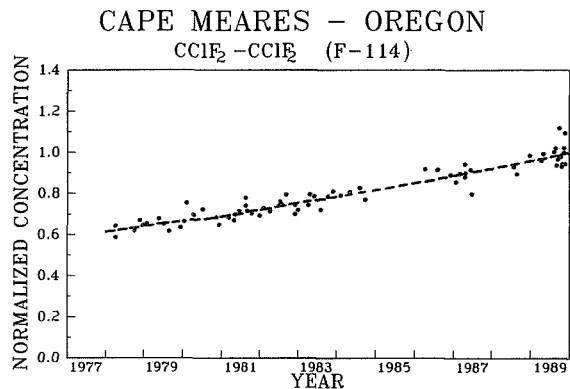


Fig. 6 Volume mixing ratios for CFC-114

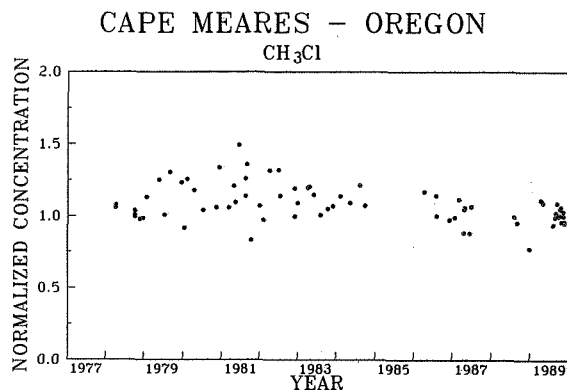


Fig. 9 Volume mixing ratios for CH₃Cl

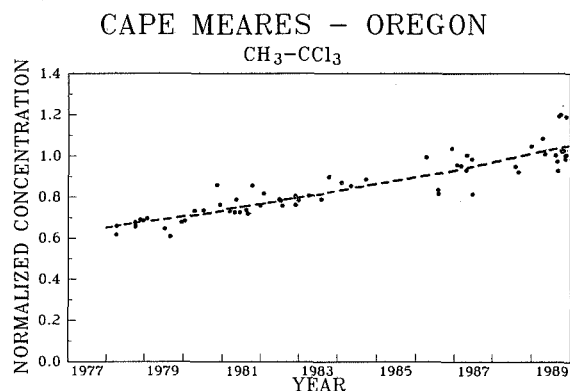


Fig. 7 Volume mixing ratios for CH₃CCl₃

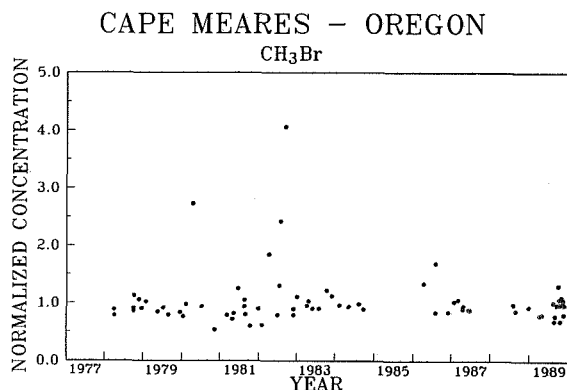


Fig. 10 Volume mixing ratios for CH₃Br

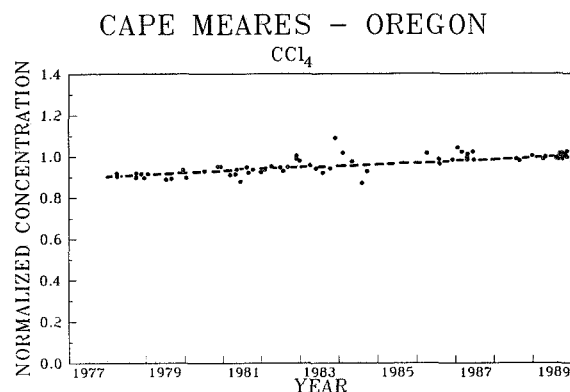


Fig. 8 Volume mixing ratios for CCl₄

This method is projected as a superior one for calculating the annual percentage increase volume mixing ratio of these trace gases on the following counts:

1. All the analyses could be carried out under identical conditions and more or less simultaneously.
2. The growth rates were evaluated without making an absolute calibration which can rather be tricky and at times uncertain.

It may be added that the percentage increase in the concentration of all these gases in the atmosphere of Cape Meares is more or less similar to their global growth rates. The variations in some cases may be natural because these measurements pertain to a particular region.

REFERENCES

Borchers R., Fabian, P., Penkett, S.A.: First measurements

of the vertical distribution of CCL_4 and CH_3CCl_3 in the stratosphere. *Naturwissenschaften* **10**, 14-16, 1983.

Borchers R., Fabian, P., Singh, O.N., Lal S., Subbaraya, B.H.: The Vertical Distribution of Source Gases at Tropical Latitudes. *Ozone in the Atmosphere*, 290-293. R.D. Bojkov and P. Fabian (Eds.): *Ozone in the Atmosphere*, Proceedings of the Quadrennial Ozone Symposium 1988 and Tropospheric Ozone Workshop, Göttingen, Federal Republic of Germany, 4-13 August 1988. A. Deepak Publishing, 101 Research Drive, Hampton, Virginia 23666, U.S.A., 1989.

Climate Change: The IPCC Scientific Assessment (Ed. Houghton, J.T., Jenkins, G.J. and Ephraums J.J.), Cambridge Univ. Press, 1990.

Fabian P., Borchers, R., Penkett, S.A., Prosser, N.J.: Halocarbons in the stratosphere. *Nature* **294**, 733-735, 1981.

Fabian P.: Halogenated hydrocarbons in the atmosphere. In: *Handbook of Environmental Chemistry* (O. Hutzinger, Eds.), Vol. 4, Part A, 23-51, Springer-Verlag Berlin-Heidelberg-New York, 1986

Rasmussen, R.A., Unpublished Data.

World Meteorological Organization (WMO), Scientific assessment of stratospheric ozone, 1989, Rep. 20, vol. 1 & 2, 1990.

303607

Status of the Dobson Total Ozone Data Set

Walter G. Planet
NOAA/NESDIS
Satellite Research Laboratory
Camp Springs, Maryland 20746, USA

Robert D. Hudson
Dept. of Meteorology
University of Maryland
Greenbelt, Maryland 20771, USA

1. INTRODUCTION

During deliberations of the International Ozone Trends Panel (IOTP) it became obvious that satellite determinations of global ozone amounts by themselves could not provide the necessary confidence in the measured trends. During the time of the deliberations of the IOTP, Bojkov re-examined the records of several North American Dobson stations and Degorska re-examined the records of the Belsk station. They were able to improve the quality of the data sets, thus improving the precision of their total ozone data sets.

These improvements showed the greater potential of the world-wide Dobson total ozone data set in two primary areas.

Firstly, the improvements showed that the existing data set when evaluated will become more valuable for comparisons with satellite determinations of total ozone. Secondly, the Dobson data set covers a greater period of time than the satellite data sets thus offering the possibility of extending improved information on ozone trends further back in time.

An International Dobson Workshop was convened in September, 1991, under the auspices of the NOAA Climate and Global Change Program. It was part of the Information Management element of the C&GC Program. Further, it was considered as a "data archaeology" project under the above. Clearly if the existing Dobson data set can be improved by re-evaluating all data records, we will be able to uncover the "true" or "best" data and fulfill the role of archaeologists.

2. DISCUSSION

Participants at the Workshop were asked to specifically address the following questions: 1. Could the precision of the data from Dobson stations other than those mentioned above be improved in a similar fashion?

2. What procedures should be employed in the reanalysis of the existing data?
3. Which stations should be reanalyzed first?

The breakdown of the participants contributing to the discussion is approximately as follows:

- o Dobson station operators - 9
- o Dobson data analysts - 8
- o Inter-sensor analysts - 8

Interdisciplinary scientists in addition to these brought the total attendance to more than thirty participants.

It was the unanimous feeling of the Workshop participants that certain stations had already shown the ability to produce a highly precise data set.

Additional support for this conclusion will be amply supplied by several speakers at this Symposium as they discuss reevaluation of several specific data sets. Speakers at the Workshop discussed several ways to identify inconsistencies in the published data sets. These include:

- (i) Examination of the station continuous record alone
- (ii) Re-examination of the instruments calibration history
- (iii) Comparison of the station record with those from nearby stations
- (iv) Comparison of the station record with nearby 100 mb temperatures
- (v) Comparison of the station record with satellite overpass measurements.

It is worth emphasizing that comparisons with external data sets such as noted in iii-v are useful in identifying possible inconsistencies in the data sets. They must not be used to correct or "tune" the data.

An extended discussion of these topics is given in Hudson and Planet (1992). Examples of some of these points are shown in Fig. 1-3. Figure 1 shows the time histories of the data from Potsdam and the fully revised data set from Belsk. While 600 km apart and having different ozone values over both stations, the time series should be

similar. Shifts in the records are seen. Figure 2 shows the time series of the Potsdam ozone data along with the 100 mb temperature over Berlin. Again, similarities and differences are noted in the comparison.

Figure 3 shows the monthly averages of the differences between the Oslo Dobson data and TOMS total ozone measurements, again showing marked differences in the data sets.

It is with comparisons such as these and undoubtedly others that the Dobson data sets can be initially screened for quality.

3. DATA QUALITY

The stability of Dobson instruments were discussed in IOTP (1988). For a well-run system, the error in the resulting trend in ozone was estimated to be 1.2% per decade; for a poorly run instrument, up to 3.8% per decade.

The status of the individual station records were discussed by the Workshop participants. The stations were identified in four categories. The status and the number of stations in each category are:

1. Stations with completely revised records - 10;
2. Stations that are undergoing data record reevaluation - 12;
3. Stations that are thought to have good records, but have not been completely revised - 10; and
4. Stations whose records need reevaluation - 40.

Clearly, much has yet to be done to bring the world-wide Dobson data set into a consistent and stable data set.

The need for a credible 35 year data set is critical for long-term trend studies as well as for supporting information for satellite data evaluation.

It should be noted that the data set maintained and published by the WODC contains provisional or upgraded data. Up to now, the WODC has precious few data sets that have been re-evaluated in the sense that we are talking about here. These are data from Belsk, Uccle, and for the stations maintained by Japan and the United Kingdom (for the ten years from 1979-1989). In addition the instrument at Bracknell has been relocated (Morrison, 1992). Guidelines for re-evaluation that were discussed by the Workshop participants are contained in Hudson and Planet (1992). Several documents are available that form the basis for understanding the Dobson instrument itself and its operation.

See, for example Dobson (1957), Komhyr (1980) and Basher (1982). In addition to these guidelines, there unquestionably are other procedures that

Dobson scientists have used and are not included in this discussion. It would be useful if a fourth report could be added to the library of Dobson references. This would be a "handbook" for reevaluating Dobson data records. In fact, this is precisely the agenda for the second Workshop held in June 1992, just before the main Symposium.

4. CONCLUSION AND RECOMMENDATIONS

It was the unanimous feeling of the Workshop participants that certain Dobson stations have already shown the ability to re-evaluate their data and produce higher-quality data sets. The major question is, what other stations should be reanalyzed and by what procedures?

The highest priority is the reanalysis of all stations with suitable calibration information. The procedures used to analyze retrospectively the existing data records should of course be applied to new data so that we can establish a long term data set based on common procedures and thus maintain the continuity of the Dobson ozone record.

On a scientific priority basis, knowledge of the stability of high latitude data is probably the most important in that significant decreasing ozone trends have been noted in those regions. Further, the high latitude data are acquired at large zenith angles which introduce retrieval uncertainties in the measurements themselves. Next would be Southern Hemisphere data. Outside of the Antarctic, few of the southern stations have been subjected to detailed re-evaluation. Next would be tropical stations. The fact that ozone changes in the tropics appear to be small at present require the best possible data set to accurately determine future trends in this region.

Finally, the northern stations require more analysis. Longitudinal variations in ozone have been observed and detailed analysis of the northern station data are needed for comparisons of data from the many stations in this latitude region.

A plan established from the Workshop can be described as follows:

1. Identify the priority stations
2. Advise the organizations responsible for the station operations of the need for re-evaluation of all Dobson data sets
3. Provide assistance to those stations that have not reanalyzed their data. This has led to the decision to conduct a second Workshop at which those scientists who have developed specific procedures to discuss the details for the benefit of those stations not yet covered.
4. Archive, in one place, all the results of each reanalysis, including

especially all calibration data.

5. SUMMARY

The establishment a long-term credible Dobson total ozone data base is critical to characterizing the trends of global ozone amount. This is an international problem and must be addressed in that vein. Much has been done by and through the WMO and some national station operations. A high level of cooperation must be maintained to reach the goal.

6. REFERENCES

Basher, R.E., 1982: Review of the Dobson Spectrophotometer and Its Accuracy, Global Ozone Research and Monitoring Project, Report No. 13.

Dobson, G.M.B., 1957: Observers Handbook for the Ozone Spectrophotometer, Ann. IGY, Vol. 5, pp 46-114.

Hudson, R.D. and G. Planet, 1992: International Dobson Data Workshop Report, NOAA Technical Report NESDIS 60.

IOTP, 1988: Report of the International Ozone Trends Panel: Global Ozone Research and Monitoring Project, Report NO. 18, World Meteorological Organization, Geneva.

Komhyr, W.D., 1980: Operations Handbook Ozone Operations with a Dobson Spectrophotometer, Global Ozone Research and Monitoring Project, Report No. 6.

Morrison, L., 1992: personal communication.

BELSK & POTSDAM

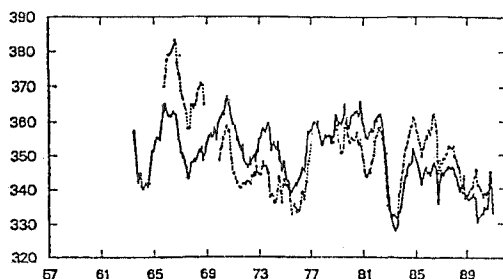


Fig. 1 The completely revised Belsk total ozone record (solid line) is plotted with the published Potsdam total ozone record (dotted line). Both series are shown as 12 month running means. The stations are about 600 km apart.

Potsdam

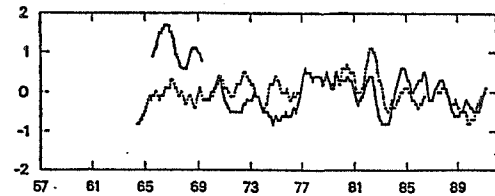


Fig. 2 The published Potsdam total ozone record (solid line) is plotted with the 100 mb temperature from Berlin (dotted line). Both series are shown as the normalized deviations from the long term monthly means and are smoothed.

Oslo

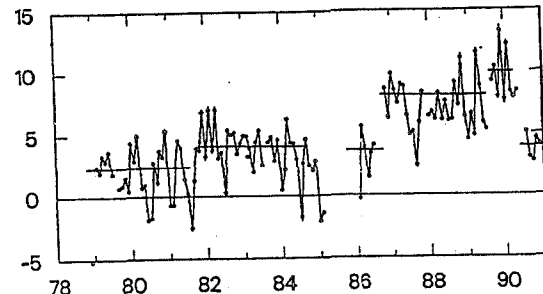


Fig. 3 The monthly mean difference between the total zone above Oslo measured by the TMS satellite instrument and the ground based Dobson instrument. The y-axis shows the absolute difference (Dobson minus TMS) multiplied by 100 and divided by the Dobson reading.

303609

RESULTS OF INTERNATIONAL DOBSON SPECTROPHOTOMETER
CALIBRATIONS AT AROSA, SWITZERLAND, 1990

R.D. GRASS, W.D. KOMHYR, AND G.L. KOENIG
NOAA Climate Monitoring and Diagnostics Laboratory
Boulder, Colorado, 80303, U.S.A.

R.D. EVANS
Cooperative Institute for Research in Environmental Sciences, University of Colorado
Boulder, Colorado, 80303, U.S.A.

ABSTRACT

An international comparison of Dobson ozone spectrophotometers, organized and partially funded by the World Meteorological Organization (WMO), was held at the Lichtklimatisches Observatorium (LKO) in Arosa, Switzerland, July-August 1990. Countries participating with a total of 18 Dobson instruments were Belgium, Czechoslovakia, Denmark, Germany, Greece, Hungary, Iceland, Norway, Poland, Portugal, Rumania, Spain, Switzerland, the United Kingdom, the United States, and the United Soviet Socialist Republics. The reference standard instrument for the comparison was U.S.A. Secondary Standard Dobson Spectrophotometer 65 maintained by the NOAA Climate and Monitoring and Diagnostics Laboratory, Boulder, Colorado. The mean difference in ozone obtained with the Dobson instruments relative to Dobson instrument 65, calculated from ADDSGQP observations in the air mass range 1.15-3.2, was -1.0 ± 1.2 (1σ) percent. The WMO Standard Brewer Spectrometer 39 also participated. In the mean, the Brewer instrument measured 0.6 ± 0.2 (1σ) percent more ozone than did Dobson instrument 65. Results are presented, also, of ozone vertical profile measurements made with the Dobson instruments, two Brewer spectrometers, a LIDAR, a balloon ozonesonde flown from Hohenpeissenberg, Germany, and balloon ozonesondes flown from Payerne, Switzerland.

1. INTRODUCTION

A program to calibrate Dobson ozone spectrophotometers of the global Dobson instrument station network, relative to United States standard Dobson instrument 83, began in the mid-1970s under auspices of the WMO. In 1980, the WMO designated Dobson instrument 83 as the Standard Dobson Spectrophotometer for the World. Long-term (1962-present) ozone measurement precision of this instrument has been maintained at better than $\pm 1\%$ [Komhyr *et al.*, 1989a]. Since the mid-1970s, virtually all global network Dobson instruments have been calibrated several times relative to instrument 83, either directly or

through secondary standard instruments having calibrations traceable to instrument 83. Eight such foreign secondary standards were established in 1977 [Komhyr *et al.*, 1980]. Two United States secondary standards, instruments 65 and 86, were established in the early 1980s.

The Arosa 1990 Dobson instrument calibrations were a continuation of an ongoing program of the WMO Dobson Spectrophotometer Central Laboratory, NOAA/ERL Climate Monitoring and Diagnostics Laboratory, Boulder, Colorado, to improve the quality of total ozone measurements throughout the world. It was held mid-July to mid-August at the Lichtklimatisches Observatorium with the aid of the Swiss Meteorological Institute (SMI), Payerne, and the Eidgenossische Technische Hochschule (ETH), Zurich. Purposes of the instrument intercomparisons were to certify the calibration levels of the participating instruments relative to a standard instrument, and to identify instruments with optical or electronic problems for repair. A total of 18 Dobson instruments from 16 countries participated (Table 1). Three of the instruments (50, 104, and 107) received some optical alignment, six (12, 14, 84, 118, 120, and 121) required various electronic repairs, while optical wedge calibrations were performed on eight instruments (15, 50, 74, 84, 92, 104, 110, and 118). The wavelength settings of all instruments were verified.

While enroute to Arosa, a stop was made at the Observatoire de Haute Provence (OHP), France, for calibration checks on Dobson instruments 49 and 85. Results obtained are also presented in Table 1.

Toward the end of the intercomparison campaign, Umkehr observations were made with the Dobson instruments to compare their performance when measuring ozone vertical distribution. Participating in these comparisons were Brewer spectrometers 39 and 40, the lidar at Hohenpeissenberg, Germany, and balloon-ozonesondes at Hohenpeissenberg and Payerne, Switzerland.

Procedures used in calibrating Dobson spectrophotometers relative to a reference instrument have been described by Komhyr *et al.* [1980, 1989b]. The reference instrument used at LKO and OHP was U.S.A. secondary standard spectrophotometer 65. It was calibrated against World Standard Dobson Spectrophotometer 83, May 21,

Table 1. Instruments and Participants of the 1990 LKO, Arosa, Dobson and Brewer Instrument Intercalibrations

Instrument Number	Country	Participants
<i>Dobson Instruments</i>		
13	Portugal	D. Henriques
14	Norway	K. Henriksen
15, 101	Switzerland	T. Svende
		K. Aeschbacher
40	Belgium	H. Schill
		H. DeBacker
41	England	R. DeMuer
		A. Lapworth
50	Iceland	B. Thorkeelson
64	Germany (Potsdam)	U. Feister
		P. Plessing
65	United States	W. Komhyr
		R. Grass
		R. Evans
		K. Vanicek
74	Czechoslovakia	M. Degorska
84	Poland	R. Rajewska-Wiech
		P. Eriksen
92	Denmark	R. Hartsmannsgruber
104	Germany (Hohenpeissenberg)	U. Kohler
		Z. Nagy
110	Hungary	F. Miskolczi
		G. Koksa
		C. Varotsos
118	Greece	D. Asimakopoulou
120	Spain	J. Cacho
121	Rumania	A. Diaz
		M. Frimescu
<i>Brewer Instrument</i>		
39	WMO	I. Asbridge

1990, and assigned a calibration scale dated May 21, 1990 F1. The F1 designation reflects a slight improvement in the 1962-1989 calibration level of World Standard Dobson instrument 83, amounting to an increase in measured ozone values of 0.3%. This change in the instrument 83 calibration scale stemmed from slightly improved computations of μ , the effective path length of light through the ozone layer.

Results of preliminary calibrations of the various Dobson instruments are shown in Table 2. Preliminary calibrations assess the "as is" status of the instruments, yielding information that may be used in correcting total ozone data obtained in the past. The last column in Table 2 shows mean percent differences in ozone measured by the various instruments within the air mass range 1.15-3.2, compared with ozone values measured with Dobson instrument 65. Columns 4-7 of Table 2 present similar data for narrower air mass observing ranges.

Table 2. Results of Initial Dobson Instrument Calibrations at Arosa in 1990 Relative to Secondary Standard Dobson Instrument 65*

Dobson Inst. Number	Last Calibration Date	Arosa Calibration Date	Test Instrument - Instrument 65 Total Ozone Difference in Percent				
			$\mu = 1.15-1.5$	$\mu = 1.5-2.0$	$\mu = 2.0-2.5$	$\mu = 2.5-3.2$	$\mu = 1.15-3.2$
13	10/20/87	08/02/90	0.9	0.6	-0.5	0.0	0.3
14	09/29/77	08/02/90	-0.5	-0.6	-1.5	-1.3	-1.0
15	07/18/90†	07/25/90	-6.4	-5.0	-3.5	-4.9	-5.0
40	08/15/86	08/02/90	-1.3	-0.9	-0.6	0.4	-0.6
41	09/17/85	07/25/90	-0.4	-0.5	-0.8	-0.7	-0.6
50	08/20/77	07/19/90	-2.7	-3.1	-3.4	-3.5	-3.2
64	08/21/86	07/25/90	0.2	0.1	-	0.3	0.2
74	08/15/86	07/19/90	-1.1	-0.6	-0.8	-0.1	-0.7
84	01/01/89	07/25/90	-0.3	0.1	0.9	0.7	0.4
92	08/15/86	07/25/90	-0.1	-0.1	-0.8	-1.1	-0.5
101	08/21/86	07/25/90	0.2	0.3	0.7	0.3	0.4
104	10/01/88	07/25/90	-1.7	-2.2	-2.9	-2.8	-2.4
107	09/08/88	07/25/90	-1.2	-1.0	-	-0.6	-1.0
110	06/16/88	07/25/90	0.3	0.7	1.4	1.3	0.9
118	-	07/25/90	-2.3	-	-	-	-2.3‡
120	11/04/89	08/05/90	-2.3	-2.5	-1.9	-1.0	-1.9
121	06/15/88	07/25/90	0.4	0.4	-0.1	0.5	0.3
49*	06/21/83	07/07/90	-1.6	-1.6	-1.4	-0.7	-1.3
85*	/83	07/07/90	-0.7	-0.4	0.0	0.4	-0.2

*Calibrations performed at OHP, France

†N-tables adjusted yearly by Langley plot method

‡Applies to μ range of 1.15-1.5 only

Final calibration data are shown in Table 3. These results were obtained after optical adjustments, wedge calibrations, and repairs were made to some of the instruments as indicated above. As in Table 2, performance of the instruments relative to instrument 65, is characterized in Table 3 as a function of air mass.

2. BREWER INSTRUMENT MEASUREMENTS

Dobson spectrophotometer 64 and Brewer spectrophotometer 39 were intercalibrated July 25, 1990. For observations on AD wavelengths the Brewer instrument measured higher ozone values than did the Dobson instrument by 0.1%, 0.3%, 0.8%, and 1.2% at effective ozone layer path lengths μ of 1.15-1.5, 1.5-2.0, 2.0-2.5, and 2.5-3.2, respectively, for a mean difference of 0.6%. Part of this difference stemmed from slightly different methods used for computing μ . Using μ values derived for the Dobson instrument observations in processing both sets of data, the discrepancy in the mean ozone difference for the two instruments decreased to 0.4%.

At higher μ , outside the range of normal AD-DSGQP observations, the Dobson instrument values fell more quickly with increasing μ than did the Brewer instrument values. In the μ range 3.2-4.0, for example, the Dobson instrument ozone values were lower by 2.9%. Considering direct sun observations on CD wavelengths within this μ range, both

Table 3. Results of Final Dobson Instrument Calibrations at Arosa in 1990 Relative to Secondary Standard Dobson Instrument 65*

Dobson Instrument Number	Date of Calibration N-Tables†	Test Instrument - Instrument 65 Total Ozone Difference in Percent				
		μ = 1.15-1.5	μ = 1.5-2.0	μ = 2.0-2.5	μ = 2.5-3.2	μ = 1.15-3.2
13	08/02/90	0.8	0.5	-0.5	0.0	0.2
14	08/02/90	1.3	0.8	-0.5	-0.5	0.2
15	No final calibration					
40	08/02/90	-0.6	-0.3	-0.3	0.7	-0.1
41	08/02/90	0.8	0.6	-0.2	-0.3	0.2
50	08/02/90	0.2	0.2	0.0	-0.1	0.1
64	08/02/90	-0.7	0.1	0.1	0.1	-0.1
74	08/02/90	-0.4	0.4	0.0	-0.1	0.0
84	08/02/90	-0.6	0.3	-0.1	0.2	0.0
92	08/02/90	-0.6	0.2	0.1	0.0	-0.1
101	08/02/90	0.1	0.6	0.2	-0.5	0.1
104‡	08/02/90	0.6	0.6	-0.1	0.3	0.2
107	08/09/90	0.3	-0.3	0.2	0.0	0.0
110	08/02/09	-1.3	-0.4	0.0	0.6	-0.3
118	08/05/90	0.2	0.4	0.0	-0.4	0.1
120	08/09/90	1.1	0.2	-0.2	-0.2	0.2
121	06/15/88	0.1	0.9	0.1	-0.6	0.1
49*	07/10/90	0.0	-0.3	0.0	0.1	0.0
85*	07/10/90	-0.5	-0.2	-0.2	0.5	-0.1

*Calibrations performed at OHP, France

†N-tables date is the date of final calibration, except for instrument 121 for which the existing 1988 tables were found to be acceptable.

‡Using wedge calibration of 06/28/91

instruments gave results in the mean that agreed to within 0.3%.

A second intercomparison of the Dobson and Brewer instruments August 2, 1990, yielded essentially identical results.

3. OZONE VERTICAL DISTRIBUTION MEASUREMENTS

On the morning of August 3, 1990, simultaneous Umkehr observations were made in Arosa with 14 newly calibrated Dobson instruments. Included in the intercomparisons, also, were Dobson instrument 15 routinely operated at LKO, as well as automated LKO Dobson instrument 51. Brewer spectrometers 39 and 40 also participated. Also that morning, the SMI facility at Payerne, Switzerland (200 km west), flew balloon ozonesondes at 0600 and 1200 hours UTC, and the Meteorological Observatory at Hohenpeissenberg, Germany (130 km northeast), flew an ozonesonde at 0128 UTC. Lidar ozone measurements were made at Hohenpeissenberg the night before at 2111 UTC and the night after at 2053 UTC.

Dobson instrument Umkehr observations were processed using C-wavelengths data and the conventional Umkehr inversion algorithm [Mateer and Düsch, 1964].

Brewer instrument data were processed using a short Umkehr inversion technique similar to that developed by DeLuisi [1979]. The method uses observations made on three Brewer instrument wavelength pairs similar to the Dobson instrument A, C, and D wavelength pairs.

Total ozone amount used in processing the Umkehr data was 319 DU, a value measured to within ±1% by 12 of the participating instruments. (Dobson instruments 50, 64, 74, and 110 measured 2% less ozone.) For data comparisons, ozonesonde ozone partial pressures were converted to Umkehr layer partial pressures. Lidar ozone data, normally expressed in molecules cm⁻³ as a function of altitude, were also converted to Umkehr layer ozone partial pressures using auxiliary Hohenpeissenberg rawinsonde data.

Table 4 presents mean ozone partial pressures in Umkehr layers 1-9 derived from measurements with the 16 Dobson instruments (see also Figure 1). Ozone partial pressure percent deviations from these means, for the individual Dobson instruments as well as for three ozonesonde soundings and two lidar soundings, are shown in Table 5. Salient features of the comparison data are described in section 4.

4. CONCLUSIONS

Results of the 1990 Arosa Dobson instrument calibrations were highly satisfactory. Of 17 Dobson instruments calibrated in Arosa, the calibration of 12 instruments agreed with that of WMO/U.S.A. secondary standard instrument 65 to within ±1%. Of the instruments exhibiting more discrepant calibration values, instrument 15 (Switzerland) is operated on its own calibration scale for consistency in its long-term ozone record; instrument 50 (Iceland) had not been calibrated in 13 years; instrument 104 (Germany) required some optical adjustments; instrument 118 (Greece) had not been previously calibrated relative to

TABLE 4. Mean Ozone Partial Pressures in Umkehr Layers 1-9 Derived August 2, 1990, at Arosa, Switzerland From Simultaneous Measurements With 16 Dobson Spectrophotometers*

Umkehr Layer Number	Pressure Range (mb)	Approx. Height (km)	O ₃ Partial Pressure (mb)
1	1000.0 - 250.0	5.1	28.8
2	250.0 - 125.0	12.5	45.8
3	125.0 - 62.5	16.9	74.4
4	62.5 - 31.2	21.4	124.4
5	31.2 - 15.6	25.9	125.9
6	15.6 - 7.8	30.4	90.1
7	7.8 - 3.9	35.0	46.9
8	3.9 - 1.96	40.0	17.2
9	1.96 - 0.98	45.2	5.4

*Dobson instruments used are identified in Table 5.

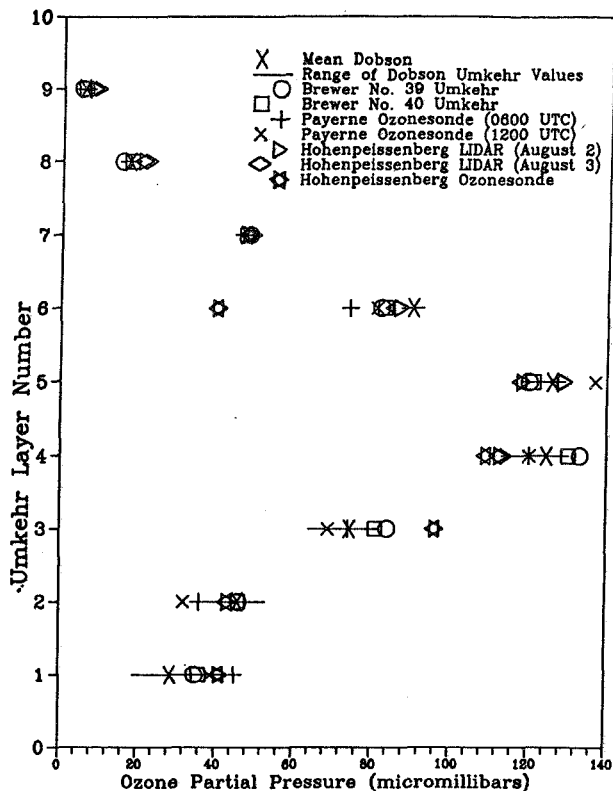


Figure 1. Ozone partial pressures in Umkehr layers 1-9 measured at Arosa, Switzerland, and vicinity August 3, 1990, with 16 Dobson instruments, 3 balloonborne ozonesondes, and an ozone lidar.

World Primary Standard Dobson Instrument 83; and instrument 120 (Spain) had an electrical problem that affected initial results.

Final instrument calibrations (Table 3) yielded calibration discrepancies, relative to the calibration scale of instrument 65, of only $\pm 0.2\%$. Note that instruments 14, 110, and 120 exhibit larger μ -dependent data than do the other instruments and may require further work to improve their performance.

Intercalibration of Dobson instrument 65 and Brewer instrument 30, gave results which agreed on average to within 0.6% for observations made on AD wavelengths in the μ range 1.15-3.2. Using the same method of computing μ for both instruments reduced the discrepancy to 0.4%. The Dobson instrument exhibited a slight μ dependency in measured ozone at $2.5 < \mu < 3.2$. No such μ dependency was observed for observations on CD wavelengths.

With regard to ozone vertical distribution comparison observations, note (Table 5) the highly satisfactory agreement in results obtained with 15 of the 16 Dobson

TABLE 5. Individual Dobson, Brewer, Ozonesonde, and Lidar Instrument Ozone Partial Pressure Percent Differences from Mean Ozone Partial Pressures in Umkehr Layers 1-9 Derived From Measurements With 16 Dobson Spectrophotometers August 3, 1990, at Arosa, Switzerland

Layer No.:	1	2	3	4	5	6	7	8	9	r*
<i>Dobson Instruments</i>										
13	-10	0	+1	0	+1	+2	+4	+1	+2	0.38
14	+4	-4	-1	0	0	0	0	-2	-6	0.26
15	+11	+14	-2	-4	-3	-2	-2	+1	+6	0.42
40	-27	-4	+9	+5	+2	0	+2	+6	+13	0.23
41	-6	+5	+3	+1	-1	-1	-2	-2	-2	0.23
50	+1	0	+1	0	+1	0	-4	-6	-9	0.21
51	+4	0	-1	0	+1	0	0	+2	+6	0.23
64	+15	-21	-6	0	+2	+2	+2	+3	+6	0.34
65	+4	+3	+1	0	0	-1	-4	0	-7	0.20
(standard)										
74	+1	+7	-1	-2	-2	0	+2	+1	+2	0.33
84	-3	0	+1	0	0	0	0	+1	+4	0.28
92	-6	0	+1	0	0	+1	+2	0	-2	0.24
101	+15	-10	-7	-1	+2	+1	-2	-2	0	0.39
104	-34	-2	+10	± 5	+2	+1	+2	+5	+9	0.35
110	-20	-4	+5	+3	+2	+1	+2	+2	+6	0.35
121	+5	+16	-14	-10	-6	-3	-6	-9	-15	0.33
<i>Brewer Instruments</i>										
39	+25	+3	+16	+10	-2	-7	+4	-8	-9	0.51
40	+28	+3	+12	+8	-2	-6	+2	-5	+6	0.39
<i>Payerne Ozonesondes</i>										
0600 UTC	+56	-21	-1	-4	+1	-18	-	-	-	-
1200 UTC	+35	-30	-7	-4	+9	-10	-	-	-	-
<i>Hohenpeissenberg Ozonesonde</i>										
0728 UTC	+42	-6	+29	-12	-6	-9	-	-	-	-
Lidar 1										
2111 UTC†	-	-	-	-5	+1	-9	-	-	-	-
Lidar 2										
2053 UTC	-	-	-	-3	-2	-9	-	-	-	-

*The factor "r" is a data quality control indicator. An ozone profile with "r" greater than 0.7 is considered unreliable.

†This lidar sounding made August 2, 1990.

instruments when measuring ozone in Umkehr layers 4-8, namely, $\pm 5\%$, $\pm 3\%$, $\pm 2\%$, $\pm 4\%$, and $\pm 6\%$, respectively. Discrepancies in results in Umkehr layers 1-3 and 9 are larger. The sonde and Brewer instrument ozone vertical distribution data indicate, furthermore, that ozone amounts were underestimated in Umkehr layer 1 but overestimated in layer 6 by the conventional Umkehr technique. This shortcoming of the conventional Umkehr inversion algorithm is likely to be remedied by the new-conventional method [Mateer and DeLuisi, 1992] that uses improved a priori ozone profile statistics and takes into account the temperature dependence of ozone absorption coefficients.

ACKNOWLEDGMENTS

The 1990 Arosa international Dobson spectrophotometer calibrations were conducted under the auspices and partial financial support of the WMO Global Ozone Research and Monitoring Project. Appreciation is expressed to Dr. B. Hoegger of the SMI for providing the LKO Arosa site for the calibrations, and to Dr. J. Staehelin of the Laboratory for Atmospheric Physics, ETH, for hosting the calibrations. Special thanks are given to I. A. Asbridge of Canada for assistance provided in calibrating the instruments.

REFERENCES

- DeLuisi, J.J., Shortened version of the Umkehr method for observing the vertical distribution of ozone, *Applied Optics*, 18, 3190-3197, 1979.
- Götz, F.W.P., A.R. Meetham, and G.M.B. Dobson, The vertical distribution of ozone in the atmosphere, *Proc. Roy. Soc., A*, 145, 416, 1934.
- Komhyr, W.D., R.D. Grass, and R.K. Leonard, WMO 1977 international comparison of Dobson ozone spectrophotometers, *Proc. of the Quarennial International Ozone Symposium*, Boulder, CO, August 4-9, National Center for Atmospheric Research, Boulder, 25-32, 1980.
- Komhyr, W.D., R.D. Grass, and R.K. Leonard, Dobson spectrophotometer 83: a standard for total ozone measurements 1962-1987, *J. Geophys. Res.*, 94(D7), 9847-9861, 1989a.
- Komhyr, W.D., R.D. Grass, R.D. Evans, and R.K. Leonard, Results of international Dobson spectrophotometer and Brewer spectrometer calibrations, Arosa, Switzerland, 1986, *Ozone in the Atmosphere*, R.D. Bojkov and P. Fabian (Eds.), A. Deepak, Hampton, VA, 776-779, 1989b.
- Mateer, C.L., and H.U. Dütsch, Uniform evaluation of Umkehr observations from the World Ozone Network: Part I, Proposed standard evaluation technique, National Center for Atmospheric Research, Boulder, CO, 105 pp., 1964.
- Mateer, C.L., and J.J. DeLuisi, A new Umkehr inversion algorithm, *J. Atmos. and Terrestrial Physics*, 54(5), 537-556, 1992.

DEFORMATION OF THE TOTAL OZONE CONTENT FIELD IN THE TROPICAL ZONE

Victor I. Vasilyev

Institute of Experimental Meteorology SPA "Typhoon"
Obninsk, 249020, Russia

ABSTRACT

Presented are the ozone investigation results obtained in the tropical zone. Measurements of the total ozone content (TOC) were carried out by the ozonometer M-124. The ozonometer was automated to investigate the ozone intradiurnal variations and to increase precision of the TOC measurements. Obtained results allowed to follow the effect of tropical cyclones (TC) on the TOC field. Several days before the TC formation the TOC increase is observed in daily mean course compared with the background one.

Three types of a trend can be singled out in the TOC intradiurnal course: zero, parabolic, quasi-linear. Maximum velocities of a trend are observed some days before the TC formation.

Analogous harmonic constituents are mainly presented in spectrum of daily means of ozone, mean and absolute velocities of trend and dispersion as well as in spectra of meteorological, hydrometeorological and actinometric values.

Revealed is a number of day-to-day ozone variations concerned with large-scale circulations, moisture content in the atmosphere.

Obtained are the data about short-period ozone waves, which period is less than a day.

Thin-film silver sensors were used to measure the vertical ozone distribution (VOD). Atmospheric aerosol and VOD measurements were carried out simultaneously, they gave data of the VOD layered structure, where the VOD local minima coincided with the position of aerosol layers' maxima.

1. INTRODUCTION

Experimental investigations of the ozone peculiar variations concerned with dynamical processes in the tropical zone

and hardware of these measurements were begun by the author in 1984. Reliable and detailed information about ozone is important for using it as indicator of dynamical processes in the atmosphere. During those years the studying of ozone was carried out in four tropical expeditions: 1984, 1987, 1989 and 1990. First three expeditions were on the Cuba island, the fourth one was in the north-west of the Pacific Ocean, where the ozone measurements were carried out using the scientific-research vessel "Ocean". The time of measurements involved end of summer, autumn and beginning of winter. The data of all expeditions include the TOC daily means, intradiurnal ozone variations and in 1987 and 1989 the vertical ozone distribution was also measured.

To measure the TOC and short-period variations the automated ozonometers M-124 were used (Vasilyev, 1989). The maximum frequency of the TOC determination was 1 min. Number of measurements per day varied from 600 to a less number. Switching time from the first light filter for the second was not more than 3 s. The recording of measurement results was produced on recorder and magnetic tape (Vasilyev et al., 1991).

To identify the discrepancies in determination of intradiurnal course and TOC values in the tropical zone in 1984 the long-period measurements were simultaneously carried out by several instruments. The instruments were set up close to each other, the measurements were at the TOC different daily means and cloud position in zenith. The results showed that in rare cases the maximum discrepancy in the TOC determination obtained by different instruments was 3.3% relative to the mean for a day. The characteristic of the TOC daytime course was repeated by all instruments with sufficient precision, the maximum departure from the curve of the TOC

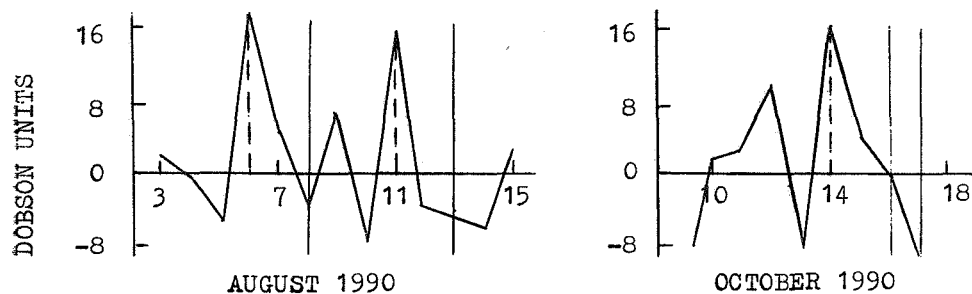


Fig.1. Random variations in the TOC daily means.

daily mean course was 3%. To compare precision of the TOC determination on zenith relative to the sun measurements, the simultaneous and long-period investigations for 120 days were carried out. As the result analysis showed the measurement error on zenith did not prevail 4% relative to the sun measurements. Normal precision of determination of the TOC on the sun was 4% compared to the standart.

The vertical ozone distribution (VOD) was obtained by MARZ radiosonde and thin-film silver sensors (Vasilyev et al., 1991). Ozonosensors were set up on a radiosonde instead of humidity sensor. To correlate ozonosensor with radiosonde the supplementary electronic block and power battery was set up in the radiosonde. The sensor was closed by glass cap to guard the ozonesensor from cloudiness and rain drops. The sensor disclosure was produced by a breaking device. Disclosure height and ozonometer sensitivity were positioned on the ground before the radiosonde launch. Precision of the VOD determination was 20%.

There were about 80 launches of radiosondes with ozonosensors during that period of time. Obtained were the results of 300 intradiurnal long-period observations of ozone and more then 600 TOC daily means (9 series). The TOC measurements were carried out simultaneously in several locations, therefore the space-time ozone relations could be investigated. During the given works besides ozone carried out was the study of integral content of water vapor and stratospheric aerosol (Nerushev et al., 1989).

2. DEFORMATION OF THE TOTAL OZONE CONTENT FIELD UNDER THE TROPICAL CYCLONE FORMATION

The space-time ozone variations in periods preceeding the TOC origination are of great interest. In July-October of 1990 the TOC observation was carried

out by the author in the tropics of the north-west of the Pacific Ocean by the scientific-research vessel "Ocean" using the automated ozonometer. During that period of time 14 TC were registered, it was a higher number than during the previous expeditions. Under tropical disturbance development from depression (TD) to a storm the TOC increased on the average of 5-8% compared to the background level before some days of TD transformation to TC. Such TOC disturbances were registered at a distance up to 300 km from observation site to TD, which later reached the TC stage. Random variations of the TOC daily means obtained by subtracting trend and periodic component from the initial series are shown in fig. 1. The vertical lines denote the days of TD transformation to TC.

The same ozone increase some days before TD transformation to TC was detected in the previous expeditions, fig. 2, (Arefyev et al., 1987).

The effect of processes favouring the TC formation is good visible on local minima in time course of the TOC daily means which appeared before the TC formation and were divided between each other and later changed by rather high minima. The analysis of synoptic situation allowed to conclude that the TOC increase was caused to a great extent by intrusion of cold air more enriched with ozone from the temperate latitudes. Such an intrusion promoted the cloud accumulation development and its transformation to TC. Analysis of the TOC latest results gave two peaks (maxima) divided between each other by the ozone minimum those were to be observed before the TC formation (fig. 2). The TOC first increase was as response to a formation or future formation of cyclonic circulation and cloud accumulation, the second ozone peak was response to TC future formation. The second ozone peak appeared in 1-5 (several) days before TC formation, but the first in 7-14 days i.e. some days

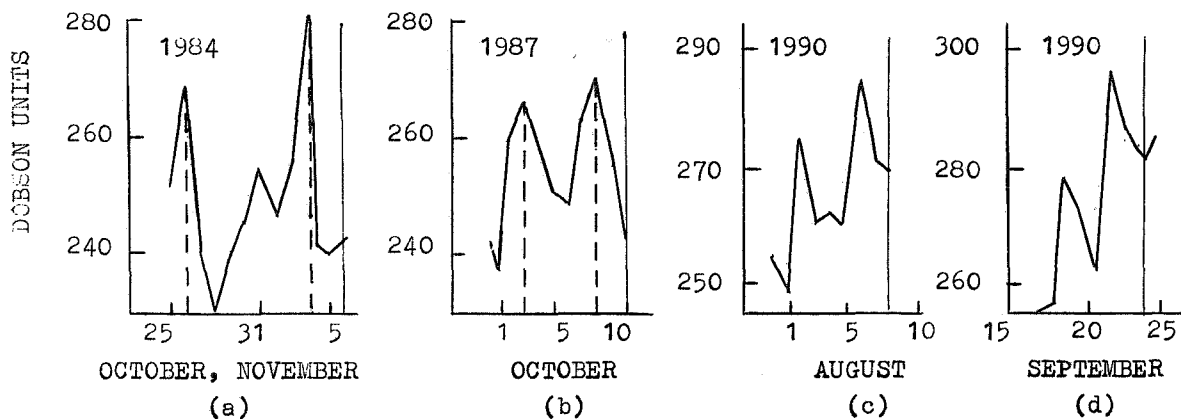


Fig.2. The TOC variation before the TC formation.

before formation of the second.

Atmosphere processes favoring TD transformation to TC, formation of cyclonic circulation, cloud accumulations and TD caused ozone increase in the region, which was registered by the ozonometers at a rather long distance from a place of the TC formation. Such an ozone increase was revealed in that region where an effect of extratropical zone of convergence presented. Local ozone peaks are good visible on the background of the TOC increase, that occurs due to an effect of extratropical zone of convergence (fig. 2d).

3. SOME PECULIARITIES OF DAY-TO-DAY OZONE VARIABILITY

The TOC daily means in the tropical zone variate every day. Besides the local maxima appeared are the days (rather prolonged time) with an increased ozone content relative to the TOC monthly means. An excess of the TOC monthly means during rather prolonged period of time is caused by predomination of meridional circulation, an effect of frontal systems, cold fronts on observation sites. It is caused by an intrusion of air masses from temperate latitudes with higher ozone content relative to the tropical air masses. The TOC increase was observed in passing the extratropical zone of convergence.

The TOC simultaneous measurements obtained in three sites at the distance 300-500 km from each other on the Cuba island show sequential appearance of the TOC local maxima in these observations over 1-3 days (Nerushev et al., 1989). It denotes the TOC relation with the circulation processes in the atmosphere. It is confirmed by correlation of time course of the TOC daily means and height of H_{200}

isobaric surface, comparison with synoptic situation effecting the observation sites and also dependence of the TOC variation and integral content of water vapor from the type of large-scale circulation in the atmosphere.

Local maxima are appeared one-several days before cold front passage. It is caused by cold front advance, when fall of temperature at great heights and consequently ozone increase begin earlier than near the Earth.

4. INTRADIURNAL COURSE OF THE TOTAL OZONE CONTENT

The TOC variations during a day have a complex structure: slow variations (trend) are superimposed by fast variations. Trend is determined as a process constituent, which period (peculiar time scale of constituent) exceeded a length of realization. To find a form of a diurnal trend the initial data bulk was approximated by polynomials. Polynomial coefficients were determined by the least-square method, a degree of polynomial was chose by the best approximation (the least mean-square method) to the initial data set.

In accordance with ozone variations during a day there were three types of trend changes: zero, when TOC variations occur over TOC certain value per day, parabolic with minimum or maximum during a day, peculiarity of trend variation is good described by polynomial in the 2-3 degree, quasi-linear when monotone increase or decrease of ozone occurs during a day (Vasilyev et al., 1988). All papers concerned with the ozone studying describe all three types of trend. Figure 3 shows peculiar type of a diurnal trend for the tropical zone. Parabolic type of trend was presented in a half of the TOC measurements (50%), then quasi-linear trend

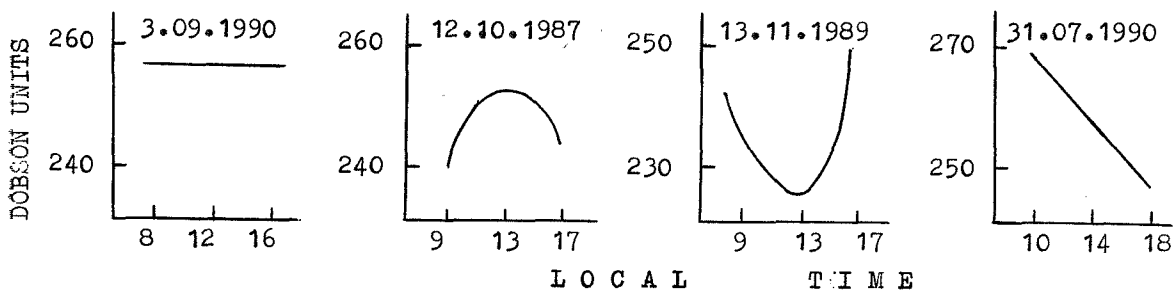


Fig.3. Types of diurnal trend for the tropical zone.

(29%) followed, it was close to the zero one (21%). Least of all there were the increased trends (21%), parabolic with maximum during a day and increased quasi-linear ones in the tropical zone. The present paper does not consider the zero trend with other types of trend which have low velocities of variations. Therefore, in most of cases the ozone was in "excited" state during a day, then it varied permanently and slowly. Parabolic type of trend was mainly observed in the day of TC formation. Besides, several days before it (fig. 1-2, dotted lines) registered were the maximum velocities of trend with parabolic form.

5. WAVE VARIATIONS OF THE DAILY MEANS OF THE TOTAL OZONE CONTENT

The presence of close relations of ozone with elements of the total circulation with meteorological, hydrometeorological and actinometric values in the tropical zone allows to propose that analogous periodic constituents to be present in these time series. As far as ozone is quasi-conservative constituent of the atmosphere, its variations and periodic constituents can account for some processes occurring in the atmosphere. As the ozone formation occurs in the tropics appeared is its permanent run-off to the poles, the studying of wave processes in this region more distinctly would clarify it. Ozone wave motions are to propagate from the tropical zone to the temperate latitudes and vice versa. The wave processes can be in some way a source of ozone removal from the tropical zone. All these reasons described above point to the fact that significant TOC spectrum to be observed in the tropical zone. An increase of wave variations must result from modulated interaction of waves of different scales, from interaction with waves of temperate latitudes. To identify the latent periodicities in a series of the TOC daily means the spectral analysis was carried out. It covered data with eliminated trend. 9 series of measurements have been

processed, each series included the TOC data of three months observations which were carried out almost in one and the same time. We can rather surely say about authenticity of the obtained calculations for the given period. The studies showed that in the energetic spectra of the TOC presented were mainly the analogous variations similar to those in meteorological, hydrometeorological and actinometric values. The analysis showed the presence of waves with the period of 4, 9, 11, 13, 15-16, 17-20, 36-39 days. Besides these wave processes discovered were the additional variations with period of 5-7, 8, 10, 12, 29-30, 42-45 days by measurements carried out in Cuba. The analogous wave processes are presented in a series of absolute and daily mean velocities of trend and in dispersion of the TOC daily means.

REFERENCES

- Arefyev, V.N., V.I. Vasilyev et al., 1987: Investigation of the total content of water vapor and ozone in the atmosphere above Cuba. Tropical Meteorology. Proceedings of the Third International Symposium. 455-464.
- Nerushev, A.F., S.S. Khmelevtsov, V.I. Vasilyev et al., 1989: Preliminary results of investigation of variability of ozone, water vapor and stratospheric aerosol in the complex expedition "Karibe-87". Tropical Meteorology. Proceedings of the Fourth International Symposium. 233-247.
- Vasilyev, V.I., Nerushev A.F., 1988: On daytime variations of the total ozone content in the atmosphere above Cuba. Trudy IEM, vyp. 45(135), 155-161.
- Vasilyev, V.I., 1989: Unit for automatic information recording from the ozonometer M-124. Trudy IEM, vyp. 20(140), 20-25.
- Vasilyev, V.I., A.S. Vasilyev, 1991: Peculiarities of using of measurer of the atmospheric ozone concentration with radiozonde MARZ. Trudy IEM, vip. 24(150), 69-70.
- Vasilyev, V.I., V.P. Solovyev, 1991: Information recording from the ozonometer M-124 to ML. Trudy IEM, vyp. 24(150), 67-68.

303613

TOTAL OZONE TREND OVER CAIRO

BY

G.k.Y.HASSAN

METEOROLOGICAL AUTHORITY OF EGYPT
KOURY EL QOUBBA, CAIRO, EGYPT

ABSTRACT:

A world wide interest in protecting ozone layer against manmade effect is now increasing. Assessment of the ozone depletion due to these activities depends on how much successful the separation of the natural variabilities from the data.

The monthly mean values of total ozone over Cairo (30 05N) for the period 1968-1988, have been analyzed, using the power spectral analysis technique. The technique used in this analysis does not depend on a pre-understanding of the natural fluctuations in the ozone data. The method depends on increasing the resolution of the spectral peaks in order to obtain the more accurate sinusoidal fluctuations with wave-length equal to or less than record length. Also it handles the possible sinusoidal fluctuation with wave length greater than the record length.

The results show that: It is possible to detect some of the well known national fluctuations in the ozone record such as annual, semiannual, quasi biennial and quasi-quadrennial oscillations, in addition to some waves as 18, 6 years which are not known.

After separation the natural fluctuations from the ozone record, the trend analysis of total ozone over Cairo show that a decrease of about of -1.2% per decade has occurred since 1979.

INTRODUCTION:

There have been many statistical studies of global total ozone trends. Detailed studies of the ozone trend Reinsel et al 1981, 1984, Bloomfield et al 1982, Bojkov et al 1984, 1987, Tiao et al 1986 and Degorska et al 1988)

indicate significant negative trend in winter at middle and high latitudes.

The statistical models used to obtain these trends are described in details in the Ozone Trend Panel (OTP) report. The models used to estimate ozone trend handled the regular variations, such as the annual cycle, the QBO, the solar cycle, etc. These known variations were eliminated from the data records by forcing an appropriate series to the data, for example Degorska (1988) forces a number of series to express seasonal, semi-annual, annual, quasibiennial and 11 years cycles to Belsk data in the statistical analysis for ozone trend. Accordingly the estimated trend depends in the first place on a pre-understanding of these variabilities. Even so, elimination of these waves in this way may effect the estimated trend, since the oscillation period of these wave, eg QBO differs from one cycle to another.

In the present paper, we used the power spectral model designed by Hassan (1989), to estimate the ozone trend over Cairo for the period 1968-1988.

DATA:

Ozone observations at Cairo (30 05 N) have been carried out on routine basis since October 1967 using Dobson ozone spectrophotometer number 96. The monthly averages of total ozone, used in this study have been calculated after the recomputation of the whole observations using the results of the international intercomparisons (Belsk 1974, Boulder 1977 and Arosa 1986) and by applying the new technique in estimating the total ozone from the zenith sky observations Hassan 1984.

STATISTICAL TREATMENT:

This method depends on handling the

data regardless of any pre-expected periodicities to separate two kinds of wave such as:

A- Waves with oscillation periods equal to or less than the length of the available record.

B - Waves with oscillation period longer than the length of the record.

The first kind of waves have been found through the analysis, using the variable record length method of Schickedanz et al (1975). Each time we get the waves with the largest contribution. From these waves, we consider the one with minimum root square mean error from the actual data as a real wave in the record. After subtracting this wave from the actual data the analysis is repeated again to obtain the next one. This analysis continue until it reaches to waves with negligible contributions to the record. After eliminating this kind of waves which are equal or less than the record length, a curve fitting using a third order equation is applied to the residual. The second order equation resulting from differentiating the third order equation has been examined from point of view of its real roots. The maximum and minimum values of the roots indicate to the presence of wave amplitude equal half the difference between them and with oscillation period twice their time difference. These values of amplitude and oscillation period are taken as a first guess for a natural waves with oscillation period greater than the record length.

An iteration procedure is then used to get the best values for this waves. Subtracting this waves from the residual and by repeating the analysis again to detect any other waves longer than the record length, the remainder can give indication of any anthropogenic influence in the data.

RESULTS AND DISCUSSIONS:

The procedure mentioned above has been used for separating natural variabilities in the record, Eight waves have been found to be of great contribution to the data, (12, 216, 88, 21, 8, 28, 56, 6 months), with amplitudes equal to 18.96, 8.51, 5.1, 4.3, 3.6, 3.3, 3.0, 2.6 D.U. respectively arranges in descending order according to their amplitudes. (see Figs.1a, 2a)

Figure 1 represent the monthly average of the actual total ozone data for 1968-1988. It is clear from the figure that the annual oscillation has the greatest amplitude. Also these waves have semi-annual, quasibiennial, and quasiquadrenial oscillations.

Figure 2 shows a summations of eight-

waves plus an over mean value.

Figure 3 and figure 4 show the twelve month running mean for both actual and estimated values. It is clear from the two figures that the actual data can be presented successfully by eight waves and a mean value.

Figure 5 shows the residuals, it is clear from the figure that there is a small negative trend in the record after 1979.

The above analysis shows that, there is a negative trend of about 1.2 percent per decade as from 1979. The value is comparable with the results obtained by Reinsel et al 1981, Bojkov et al 1984, 1989, and others for this latitudinal belt using different statistical models.

CONCLUSION:

In this paper we summarized the main conclusions as:

It is possible to detect some of the well known natural variations in the record such as, annual, semiannual, quasibiennial and quasiquadrenial oscillations, in addition to some waves (18 and 6.5 years), which are not known.

By separation the natural fluctuation mentioned above from the ozone data over Cairo, the analysis of trend shows that a decrease of about 1.2 percent per decade, has been found from 1979.

REFERENCES:

- Bloomfield, P., M.L. Thompson, and S. Zeger 1982: A Statistical analysis of Umkehr measurements of 32 - 46 km ozone. *J. Applied Met.* 12 1828-1937.
- Bojkov, R. D., and G. C. Reinsel, 1984 : Trends in tropospheric ozone concentration in eds. C.S. Zerfors and Ghazi, D. Reidal Publ. Co. Dordrecht, Holland, 775-761.
- Bojkov, R. D., The 1983 and 1985 anomalies in ozone distribution in respective, *Mon. Weather Rev.* 15, 2188-2201, 1987.
- Degorska, M. and Rajewska-Wiech B., 1987 The Ozone minimum observed in the north temperate ozone in 1982-1983
- Hassan, G. K. Y. : Construction Empirical Ozone Charts and Tables using the Multiple linear Regression technique, *Proc. of Quaddr. Ozone Symp. Hattidici., Greece, 1984.*
- Reinsel, G. C., G. C. Taio, A. J. Miller D. j. Waebbles, P.S. Connell, C.L. Mateer and J. J. Deluisci, 1987: Statistical analysis of total ozone and stratospheric Umkehr data for trends and Solar cycle relationship, *J. Geophys. Res.* 92

2201-2209.
 Reinsel, G. C., G. C. Tiao M. N. Wang r.
 Lewis and D. Nychka : Statistical
 analysis of stratospheric ozone
 data for the detection trends.
 Atmos. Environ. S. 15, 1569-1577
 1981.

Schickedanz, T. and E. G. Bowen 1975:
 Computation of climatological
 Power Spectra Using Variable re-
 cord length, Forth Conference
 on Probability and statistics in
 the atmospheric Science.

FIG.(1a) Waves 216, 88, 21, 8 Months
 of Total ozone over cairo

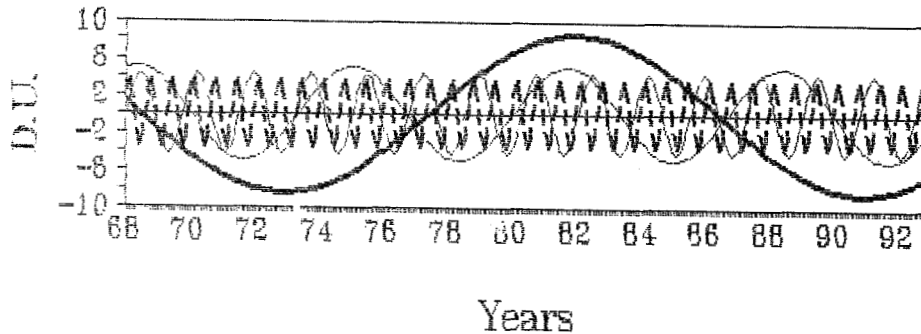


FIG.(2a) Waves 28, 56, 6 Months
 of Total ozone over cairo

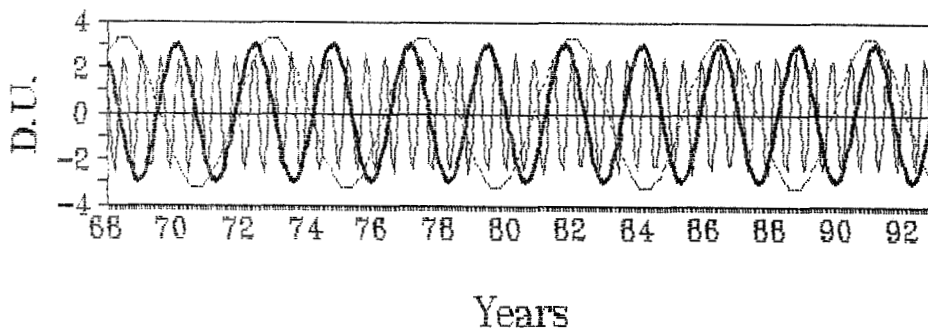


Fig.(1)The Monthly Average of Actual
 Data (1968-1988)

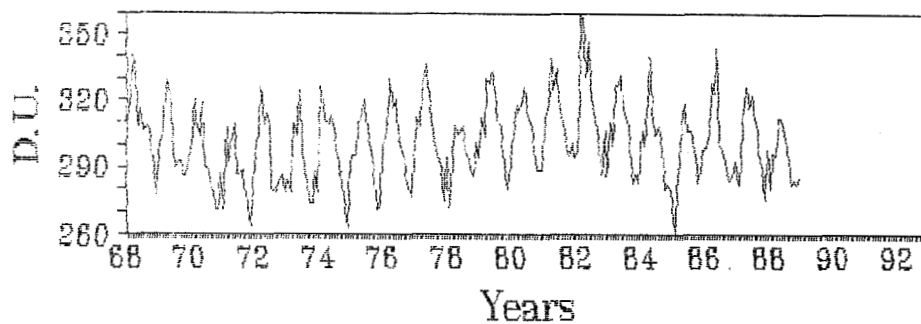


Fig.(2) Summation of Eight Waves Plus an Over Mean value

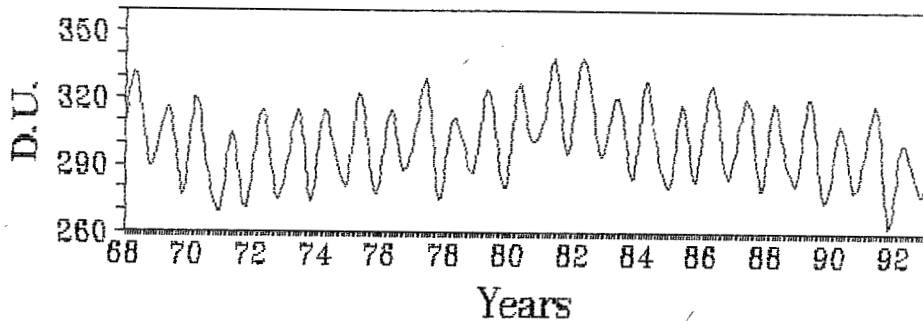


Fig.(3) Twelve Month Running Mean for The Actual Data

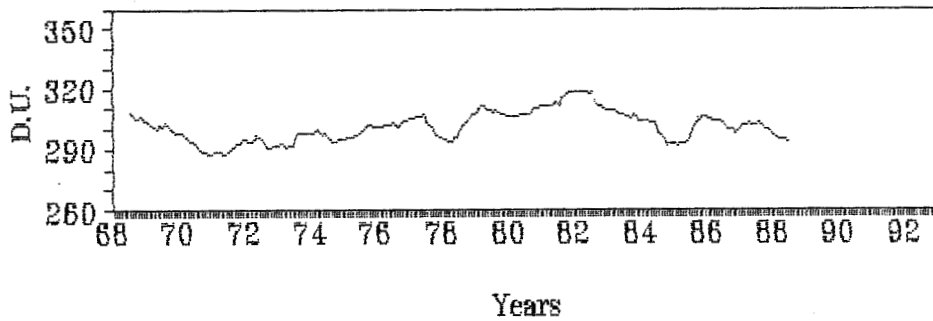


Fig.(4) Twelve Month Running Mean for The Forecast

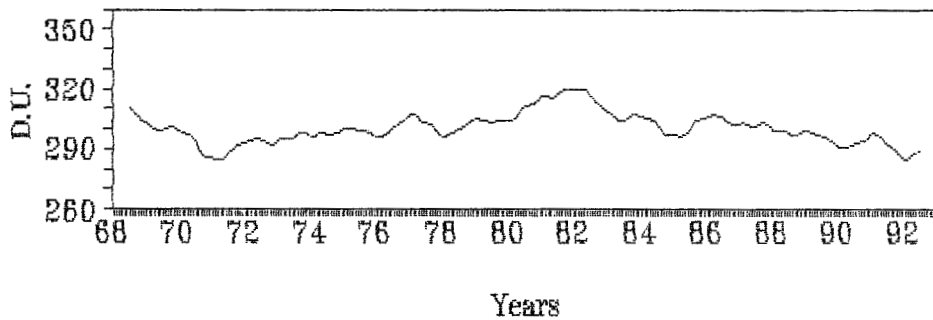
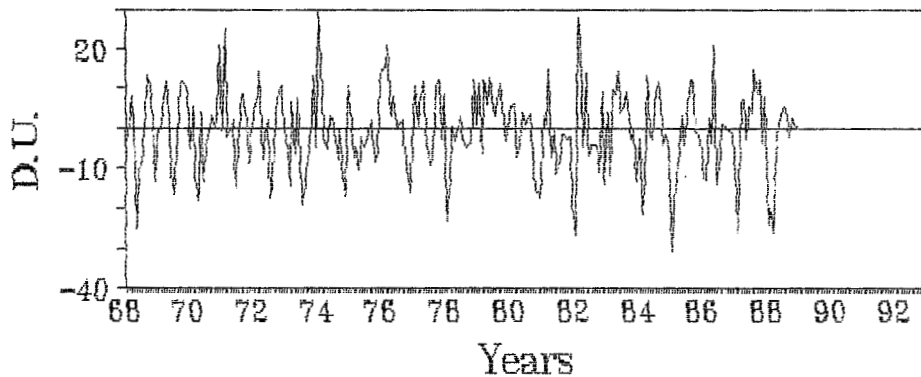


Fig.(5) The Residuals (Actual-Forecast)



STRATOSPHERE

THEORY AND MODELLING

THREE DIMENSIONAL MODEL CALCULATIONS OF THE GLOBAL DISPERSION
OF HIGH SPEED AIRCRAFT EXHAUST AND
IMPLICATIONS FOR STRATOSPHERIC OZONE LOSS

303615

Anne R. Douglass, Richard B. Rood, Charles H. Jackman
Mail Code 916, NASA/Goddard Space Flight Center
Greenbelt, Maryland 20771 USA

Clark J. Weaver
Applied Research Corporation
Landover, Maryland 20785 USA

ABSTRACT

Two-dimensional (zonally averaged) photochemical models are commonly used for calculations of ozone changes due to various perturbations. These include calculating the ozone change expected as a result of changes in the lower stratospheric composition due to the exhaust of a fleet of supersonic aircraft flying in the lower stratosphere. However, zonal asymmetries are anticipated to be important to this sort of calculation. The aircraft are expected to be restricted from flying over land at supersonic speed due to sonic booms, thus the pollutant source will not be zonally symmetric. There is loss of pollutant through stratosphere/troposphere exchange, but these processes are spatially and temporally inhomogeneous. Asymmetry in the pollutant distribution contributes to the uncertainty in the ozone changes calculated with two dimensional models.

Pollutant distributions for integrations of at least 1 year of continuous pollutant emissions along flight corridors are calculated using a three dimensional chemistry and transport model. These distributions indicate the importance of asymmetry in the pollutant distributions to evaluation of the impact of stratospheric aircraft on ozone. The implications of such pollutant asymmetries to assessment calculations are discussed, considering both homogeneous and heterogeneous reactions.

1. INTRODUCTION

Questions concerning the environmental impact of a fleet of supersonic aircraft operating in the lower stratosphere were first considered in the early 1970's (Johnston et al., 1989; Douglass et al., 1991 and references therein). Since then, there have been advances in engineering which may make it possible to develop aircraft engines which are ten times less polluting than engines which are currently available. There have also been improvements in the ability to model stratospheric transport which make it possible to determine the likely distribution and lifetime of aircraft exhaust pollutants. Improvements in the representation of photochemical processes in the lower stratosphere, validated by comparisons with aircraft, satellite, balloon and sonde measurements, make it possible to calculate the likely impact of the pollutants on stratospheric ozone.

Currently, evaluations of the ozone changes due to aircraft exhaust are made using two dimensional (2D) models. There are uncertainties in these model evaluations due to the parameterized transport of 2D models. In particular, stratosphere/troposphere (strat/trop) exchange, which is crucial to determining the pollutant lifetime in the lower stratosphere, is poorly represented in 2D models. There are also uncertainties which arise from the three dimensional nature of the pollutant source. Aircraft are expected to fly at supersonic speeds only over the oceans as sonic booms are not permitted over land. Thus the pollutant source is restricted to oceanic corridors. During northern hemisphere winter, there are quasi-stationary features (e.g., the Aleutian anticyclone) which may lead to pollutant concentrations in the corridor which substantially exceed the perturbation to the zonal mean. The importance of these uncertainties to 2D assessments of the impact of aircraft exhaust on stratospheric ozone is considered using a three dimensional (3D) model.

2. MODEL AND EXPERIMENT DESCRIPTION

Tracer experiments are carried out using the NASA/Goddard three dimensional chemistry and transport model (3DCTM). The tracer is injected in the model continuously in specified corridors; the tracer evolution is calculated using winds from the surface to 0.4 mb taken from the STRATAN data assimilation procedure (Rood et al., 1991). In the assimilation procedure (Baker et al., 1989) data are inserted at regular intervals into a general circulation model. The data are combined with model fields using an optimal interpolation analysis; the analysis fields become the initialization for a six hour integration. At the end of six hours, the model fields are the first guess for the optimal interpolation procedure as new data are inserted into the model. Simulations for species such as ozone calculated using these wind fields may be compared with satellite, aircraft, and sonde measurements (Rood et al., 1991). Comparisons of model fields with measurements indicate that the calculated ozone fields represent the synoptic and planetary scale features evident in the satellite fields. In particular, total ozone measurements suggest that the model faithfully represents the upper tropospheric disturbances which contribute to strat/trop exchange.

At this time, the 3DCTM does not provide a quantitative estimate of strat/trop exchange. On longer time scales, the ozone experiments deviate from measurements and indicate that the residual circulation associated with the assimilated wind fields is too strong. As a result of the continual data insertion in the assimilation procedure, the expected thermodynamic balance between the horizontal eddy heat flux convergence and the vertical heat transport is never achieved (Weaver et al., 1992), leading to excessively strong upwelling in the tropics and downward motion in midlatitudes. However, the good representation of synoptic and planetary scale events indicates that these model simulations may be useful in developing a qualitative picture of strat/trop exchange, and in examining horizontal transport and mixing.

The experiments here consider a passive tracer inserted continuously on great circle paths for three proposed aircraft routes: North Atlantic (Boston-London (BLO)); North Pacific (Los Angeles - Tokyo (TLA)), and Tropical (Los Angeles - Sydney (LAS)). Simulations were considered using STRATAN for Jan - Mar, 1989. STRATAN winds are not available for a full year, but assimilation wind fields from the European Centre for Medium-Range Weather Forecasts (ECMWF) analyses were available up to 10 mb. Since the ECMWF wind fields do not have the vertical range necessary to repeat the ozone experiments, the LAS calculation was repeated using ECMWF winds for transport to compare the two analyses. These two simulations showed remarkable agreement. Year long integrations were completed using ECMWF fields for each of the three corridors beginning October 1986.

3. RESULTS

a. Stratosphere/Troposphere Exchange

A qualitative picture of strat/trop exchange is produced by noting the correlation between areas of high tracer concentration at levels below the injection level and areas of low geopotential height on the 500 mb surface. An example of the tracer concentration at 250 mb for TLA is given in Figure 1(a); the 500 mb geopotential height is given in Figure 1(b). The high values of tracer are correlated with low values of 500 mb geopotential height. Comparison with Total Ozone Mapping Spectrometer (TOMS) data for the same period indicate that these highs in tracer are also correlated with highs in total ozone. This behavior is found for all tracer experiments, indicating that transport to the troposphere is associated with upper tropospheric synoptic scale features, and occurs primarily at middle latitudes (30°-60°).

The importance of this result is made clear by examining the time series of the fraction of the total pollutant mass which is found between the surface and the 250 mb pressure level for each of the three corridors (Figure 2). Transport to the troposphere is nearly equivalent for the two mid-latitude corridors and for the tropical corridor. For the tropical corridor, this transport is mainly associated with synoptic scale events poleward of the subtropical jets; the tropical troposphere remains largely tracer free.

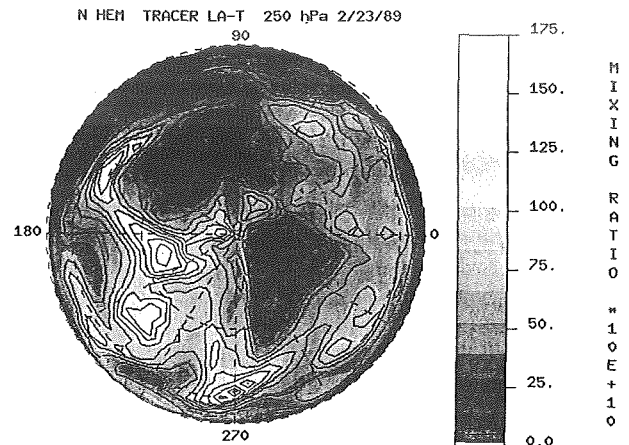


Fig. 1(a): The tracer mixing ratio at 250 mb (LA-T corridor) shows high values between 150°E and 180°E and near 270°E.

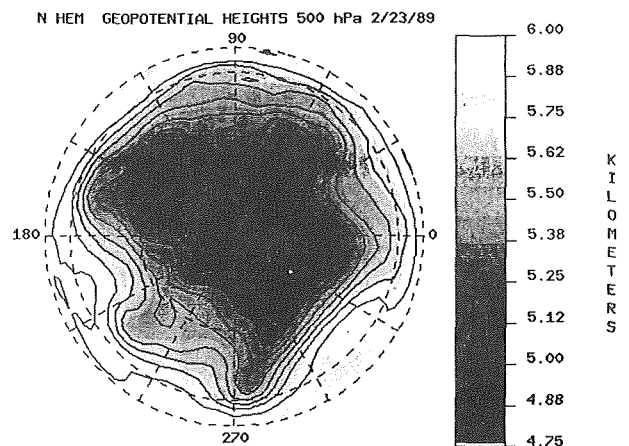


Fig. 1(b): The 500 mb geopotential height show troughs associated with the high tracer values at 250 mb in Fig.1(a).

The common time for strat/trop exchange for these corridors stands in sharp contrast to the 2D transport to the troposphere using the NASA/Goddard 2D model (Douglass et al., 1989) for a tropical source (30°S-30°N) compared to the 2D transport for a midlatitude source (40°N-50°N). The difference is emphasized by comparing the time series of the ratio of the fraction of pollutant in the troposphere for a midlatitude source to the fraction in the troposphere for a tropical source (Figure 3). The transport is much more rapid for the midlatitude source. In the 2D model, diffusive transport to the troposphere is independent of latitude, and advective transport takes place at mid to high latitudes (poleward of 40°). The tropical tracer must undergo significant horizontal transport before it can reach the troposphere. The maximum pollutant level for a tropical tracer is substantially higher for a 2D calculation than for a 3D calculation. The transport to the troposphere for a flight path in midlatitudes where most of the synoptic scale events associated with strat/trop exchange occur may also be underestimated by a 2D calculation.

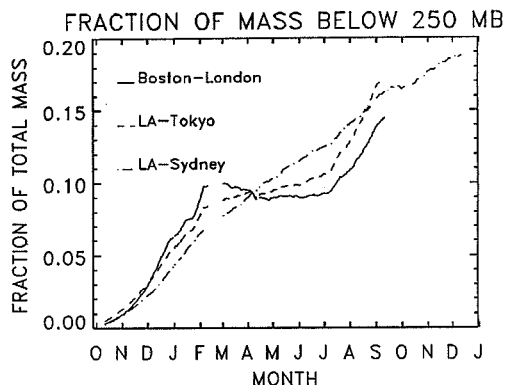


Fig. 2: The time series of the fraction of the total mass below 250 mb for tracer calculations for the 3 corridors shows no difference in the mass transported to the troposphere for a midlatitude or tropical route.

b. The corridor effect

Time series are given in Figure 4(a,b,c); the tracer maximum and minimum are indicated by solid lines; the zonal mean bounded by the standard deviation is indicated by the shaded areas for each of the 3 corridors. Generally, the maximum value for the midlatitude corridors exceeds the zonal mean by a factor of 2-4 in winter and a factor of 5-7 in summer. In the tropics, the zonal asymmetry is pronounced during the westerly phase of the quasi-biennial oscillation (QBO), and drops dramatically during the easterly phase. Studies with SAGE aerosols (Trepte and Hitchman, 1991) show that transport from the tropics to middle latitude occurs more during the westerly phase of the QBO than the easterly phase.

For all 3 corridors, because the tracer maximum is so much larger than the zonal mean, and the lower stratospheric turnover time is on the order of a few years at most, the zonal mean pollutant value will never be as large as the maxima. There will always be significant asymmetries and clearly defined corridors in experiments such as these. However, it should be noted that the tracer distribution for a combination of flight paths, such as Boston-London and LA-Tokyo, is more symmetric than that calculated for a single corridor. This indicates the importance of a good estimate of the probable city pairs and flight frequency to the assessment calculations.

4. DISCUSSION

The placement of strat/trop exchange in middle latitudes (30°-60°) by the 3D model through synoptic scale events contrasts with the mid to high latitude poleward of 40° placement of strat/trop exchange by the 2D model through latitude independent diffusion and mid to high latitude advection. This model result suggests that two dimensional models may underestimate the rate of return to the troposphere for tropical and midlatitude pollutant sources, leading to higher estimated pollutant values than would be

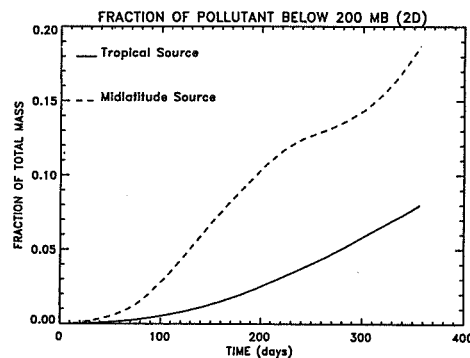


Fig. 3: The time series of the fraction of the total mass below 250 mb for tracer calculations using the NASA/GSFC 2D model shows transport to the troposphere is more rapid for a midlatitude injection than for a tropical injection.

realized. Conversely, they may overestimate the rate of return for a high latitude source. This result must be reconciled with results of 2D calculations of the behavior of measured tracers such as excess ^{14}C produced by atmospheric tests of nuclear weapons during the 1950's and 1960's; these calculations suggest that the return to the troposphere in 2D models is too rapid (Jackman et al., 1991). It is possible that the 2D models overestimate the rate of transport of ^{14}C to the troposphere because the most of the nuclear explosions which produced excess ^{14}C took place poleward of 60°N.

The corridor experiments indicate that pollutant levels in flight corridors may exceed the zonal mean perturbation by factors of 3-5 or more. For gas phase photochemistry, the loss of ozone is nearly a linear function of odd nitrogen, and zonal asymmetry in the perturbation would not impact the zonal average of the impact on ozone. However, the heterogeneous reaction of N_2O_5 with H_2O on background sulfate aerosols to produce HNO_3 has recently been found to be important to the lower stratosphere. This reaction would convert the odd nitrogen in the aircraft exhaust to the reservoir HNO_3 , and drastically reduce the impact of aircraft exhaust on the ozone layer (Weisenstein et al., 1991). However, in the corridor, this could lead to a very large increase in HNO_3 and H_2O , and a significant increase in the formation temperature for nitric acid trihydrate clouds (NAT). Heterogeneous reactions on the surfaces of these cloud particles involving chlorine reservoirs have been shown to be responsible for large scale ozone depletion in the Antarctic winter. The possibility of cloud formation within flight corridors and the importance of concurrent heterogeneous reactions involving chlorine species to assessment calculations is under consideration (Consideine et al., 1992). Preliminary results indicate that there would be a substantial increase in the probability of NAT formation, particularly near the edge of the north polar vortex.

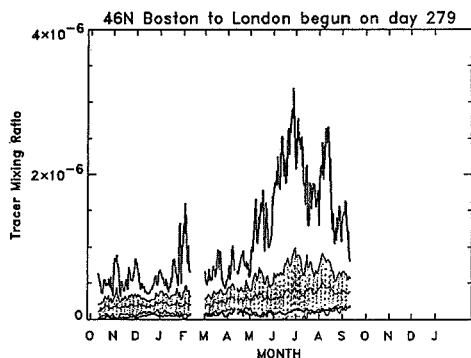


Fig. 4 (a): The maximum tracer value for the Boston-London corridor (bold line) is substantially larger than the zonal mean \pm sigma (shaded area).

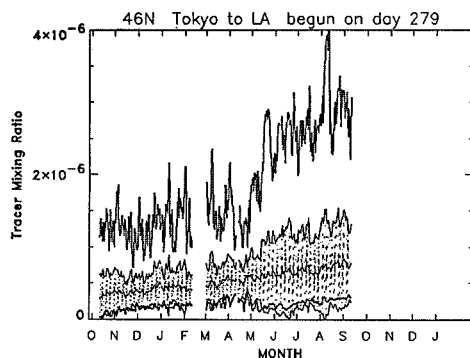


Fig. 4 (b): Same as (a) but for Los Angeles - Tokyo corridor

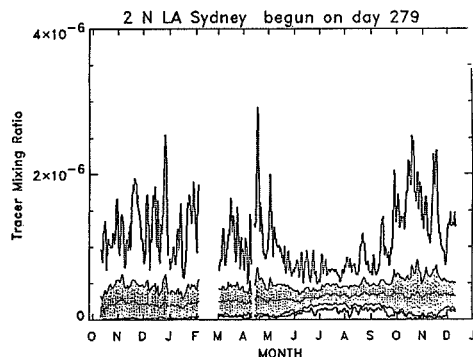


Fig. 4 (c): Same as (a) but for Los Angeles - Sydney. The period of near zonal symmetry during the summer and fall corresponds to the easterly phase of the QBO.

5. SUMMARY

The transport in 2D models may affect assessments of the impact of aircraft exhaust on stratospheric ozone. The 3D calculations indicate the importance of mid-latitude synoptic scale events to strat/trop exchange. The rate for return of tracer to the troposphere is comparable for a tropical and midlatitude corridor. In contrast, 2D model results indicate a longer perturbation lifetime for a tropical tracer source compared to a midlatitude source.

The results for three flight corridors show that substantial buildup of tracer compared to the zonal mean is possible. Such a buildup is important if non-linear chemical processes are important. In particular, it is possible that NAT clouds could form sporadically in the corridors, which could produce substantial ozone loss for current levels of inorganic chlorine and bromine.

REFERENCES

- Baker, W.E., S. C. Bloom, J. S. Woolon, M. S. Nestler, E. Brin, T. W. Schlatter and G. W. Brantstator, Experiments with a three-dimensional statistical objective analysis scheme using FGGE data, *Mon. Wea. Rev.*, **115**, 272-296, 1987.
- Considine, D. B., A. R. Douglass, and C. H. Jackman, 2D model sensitivity to heterogeneous reactions of the stratospheric sulfate aerosol layer: comparison of model results with observations, *Proceedings of Quad. Ozone Symp.*, 1992.
- Douglass, A. R., C. H. Jackman, and R. S. Stolarski, Comparison of model results transporting the odd nitrogen family with results transporting separate odd nitrogen species, *J. Geophys. Res.*, **94**, 9862-9872, 1989.
- Douglass, A. R. M. A. Carroll, W. B. DeMore, J. R. Holton, I. S. A. Isaksen, H. S. Johnston and M. K. W. Ko, The atmospheric effects of stratospheric aircraft: a current consensus, NASA Ref. Publication 1251, 1991.
- Jackman, C. H., A. R. Douglass, K. F. Brueske and S. A. Klein, The influence of dynamics on two-dimensional model results: simulations of ^{14}C and stratospheric aircraft NO_x injections, *J. Geophys. Res.*, **96**, 22559-22572, 1991.
- Johnston, H. S., D. E. Kinnison and D. J. Wuebbles, Nitrogen oxides from high-altitude aircraft: an update of potential effects on ozone, *J. Geophys. Res.*, **94**, 16351-16364, 1989.
- Rood, R. B., A. R. Douglass, J. A. Kaye, M. A. Geller, C. Yuechen, D. J. Allen, E. M. Larson, E. R. Nash, J. E. Nielsen, Three-dimensional simulations of wintertime ozone variability in the lower stratosphere, *J. Geophys. Res.*, **96**, 5055-5071, 1991.
- Trepte, C. R. and M. H. Hitchman, Tropical stratospheric circulation deduced from satellite aerosol data, *Nature*, in press, 1992.
- Weaver, C. J. A. R. Douglass and R. B. Rood, Thermodynamic Balance of Three-Dimensional Stratospheric winds derived from a data assimilation procedure, submitted to *J. Geophys. Res.*, 1992.
- Weisenstein, D. K., M. K. W. Ko, J. M. Rodriguez, and N-D Sze, Impact of heterogeneous chemistry on model calculated ozone change due to high speed civil transport aircraft, *Geophys. Res. Lett.*, **18**, 1991-1994, 1991.

303616

QUALITATIVE STUDY OF THE BEHAVIOR OF
MINOR SPECIES DURING A
STRATOSPHERIC WARMING WITH A 3-D MODEL

R. Ramaroson

Office National d'Etudes et de Recherches Aérospatiales,
BP 72, 92322 CHATILLON CEDEX, FRANCE

M. Pirre

CNRS/LPCE, 3a, avenue de la recherche scientifique,
45071 ORLEANS CEDEX 2, FRANCE

D. Cariolle

CNRM/EERM, Météorologie Nationale,
Mirail, avenue Gustave Coriolis, 31000 TOULOUSE,
FRANCE

INTRODUCTION

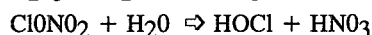
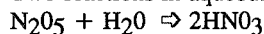
It is well-known that the behavior of the ozone layer depends upon the coupling between several processes in the atmosphere. Natural or anthropogenic pollutants emitted from the surface or injected directly at high altitude may affect this layer. Assessment studies for long-term change of the ozone layer are conducted with the aid of various two-dimensional models (Brasseur et al., 1990; Garcia and Solomon, 1983,...). These models describe the long-term and seasonal evolution of minor constituents and take into account the interaction between all processes. However, many limitations affect the self-consistency of these models *e.g.*: the circulation in these models is only meridional and vertical and is not able to represent all types of motion in the atmosphere. During a perturbed winter in the north polar regions, the vortex is displaced from the pole to lower latitude so that wind may be reversed at a given location. Perturbed air masses are transported outside the darkened regions and may mix with local air masses (Mc Intyre and Palmer, 1984). Three-dimensional models are the only tools which can describe correctly these sporadic phenomena.

1. THE MODEL AND THE INITIALISATION

In this work, we use an improved version of three-dimensional model described by Ramaroson et al., 1990. The model results from the on-line coupling between a general circulation model (T21 version) (Cariolle et al., 1990) and a photochemical box model (Ramaroson et al., 1991). The photochemical package includes species of O_x , HO_x , NO_y , Cl_y and Br_x families and other source molecules *e.g.*: H_2O , N_2O , CH_4 , CH_3Br , CO , CFM's and CFC's. In the box model, no photochemical equilibrium is assumed. Ozone is interactive in the radiative codes of the GCM and is a prognostic variable in the box model.

Photodissociation coefficients are computed using O_2 and O_3 as major absorbant. In the Schuman-Runge band, $J(O_2)$ is calculated with Frederick and Hudson method (1980). Rayleigh scattering and temperature dependence of cross-section of various species are taken into account. The four standard heterogeneous reactions occurring on PSC type I and II are taken into account. The condensation of HCl is parameterized as proposed by Marti and Mausberger (1991).

Two reactions in aqueous phase:



using a background profile of aerosol are added to the photochemical system, the surface area of aerosol varies between $10^{-10}cm^{-1}$ to $5.10^{-9}cm^{-1}$ from 12 km to 25 km. CFC's and CFM's are fixed in the box from a zonal distribution computed by a two-dimensional model (Brasseur et al., 1990). Thirty-one species are transported independently. No family approximations are made and full diurnal variations are calculated.

The model initialisation is done with the analysis of ECMWF for January 17, 1987. The initial distributions of all species are derived from the 2-D model. Quantitative results depend strongly on these initial conditions especially for long-lived species. The aim of the study is to analyze the behavior of various species. Integration are carried out over 15 days. For all stratospheric levels, the vortex is lightly symmetric and centered at the North pole.

2. RESULTS AND DISCUSSION

Fig. 1a shows the distribution of the calculated PV on January 19 at a potential temperature surface of 1390 K (close to 3 hpa, 40 km). A tongue of air with relatively low values of PV is transported over the polar region. A high

value of PV, associated with the vortex is now located at 70°N-10°E with a tongue spread over the North-America. On Fig. 1b, 2 days later, apparently no entire "breaking" occurs over the pole but the PV value is almost constant ($20.7 \cdot 10^{-4}$ USI).

Due to the number of species studied in this work, all results cannot be shown here. In order to discuss, with a preliminary approach, the dynamical behavior of the various species, we have plotted the distribution of the variables at a specific universal time (12 UT).

The NO₂ behavior during a stable winter has been described by Ramaroson et al. (1990). When darkness prevails, NO₂ is converted via NO₃ to N₂O₅. A minimum of the NO₂ mixing ratio is computed over the North pole associated with sharp gradients due to the dependence of the lifetime versus latitude. For the perturbed winter we are studying here, Fig. 2a illustrates the NO₂ behavior (January 19). The incursion over the pole of high NO₂ air masses modifies the non-perturbed situation. The NO₂ minimum is found over high PV regions, in the vortex. After 2 days the behavior of NO₂ is changed. Fig. 2b shows a high value (14 ppb), originating from lower latitude, and transported over polar regions, is now surrounded by a tongue of low NO₂ (7 ppb). (The minimum calculated for the January 21 is 2 ppb). This situation may be easily interpreted with the help of the geopotential field maps for 20 and 21 January (not shown). After 11 days, Fig. 2c indicates that the mixing over North America is finished and chemical relaxation is complete. Another incursion of low latitude NO₂ occurs at about 110°E-20 to 40°N. The corresponding geopotential field is indicated on Fig. 3 on which one can notice a rapid incursion of air from low latitude (from Europ).

At mid-latitudes chemical lifetime for ClO is short. ClO mixing ratio varies with the solar zenith angle at all levels. At 40 km, it decreases slowly at night, to reach a minimum before sunrise; it increases rapidly when the sun rises. The main losses for ClO is the reactions with NO, O, and NO₂. The first two reactions are more rapid than the last one (only a few days). On Fig. 4a, we can see that the air incursion, mentioned above, gives low ClO mixing ratio. Two cells with high mixing ratio are calculated, associated with low NO₂ mixing ratio inside the vortex (see Fig. 2a). At mid-latitude, diurnal variations are not disrupted by this dynamical dependence. Fig. 4b gives the ClO distribution corresponding to Fig. 2c for NO₂. The first minimum over North America is quasi-steady (intermediate results not shown here). The second minimum located at 60°N-120°E is a dynamical effect, coupled with chemistry (see Fig. 3). The large maximum is also quasi-steady and corresponds to the position of the vortex.

Fig. 5 shows the cross-section for HNO₃ (condensed and gas phase). The maximum at 60°N (day) - 35 hPa is due to the condensation of HNO₃ (NAT formation) and

conversion of ClONO₂ to Cl₂ and HNO₃ (solid) by reacting with HCl on the surface.

Fig. 6 illustrates the effects of PSC type I and II on the enhancement of ClO_x level (located approximately at 60N - 35hPa - > 0.4 ppb) by heterogeneous reactions. In the troposphere, cells of high ClO_x are due to reaction in aqueous phase which convert ClONO₂ to ClO_x.

The distribution of the temperature in Fig. 7 shows a strong cooling (about 185 K) at 60°N (day) - 35 hPa which occurs only during 3 days.

The behavior of HCl the 25 of January (Fig. 8) looks similar to that of HNO₃. However the main HCl production comes through the reaction with methane (CH₄ + Cl => HCl + CH₃), which is highly dependent on the temperature. At about 60°N 10 hPa (Fig. 8), the maximum of HCl (1.7 ppb) is associated with the incursion of CH₄ (Fig. 9) and high temperature (not shown but due to the warming about 246 K) At high latitudes, the reaction between HCl and OH is less effective due to the low concentration of OH. The inverse situation appears at 45°N. At these levels zonal winds are weak, the waves are broken and mixing may occur (Fig. 10).

CONCLUSION

Coupling between dynamics and chemistry is essential to understand the behavior of the different species. The 3D model which has been used in this work clearly shows the association of high vorticity with low NO₂, high HNO₃, HCl and ClO and a probable mixing during a wave breaking. The "normal" behavior during a stable winter is disrupted and high values of ClO and HNO₃ are transported with the vortex.

REFERENCES

Brasseur, G., M.H. Hitchman, M. Dymek, E. Falise and M. Pirre, An interactive chemical dynamical radiative two-dimensional model of the middle atmosphere, *J. Geophys. Res.*, 95, D5, 5639-5655, 1990.

Cariolle, D., A. Lasserre-Biggory, J.F. Royer and J.F. Geylein, A GCM simulation of the Springtime Antarctic Ozone Decrease and its impact on mid-latitudes, *J. Geophys. Res.*, 95, 1883-1898, 1990.

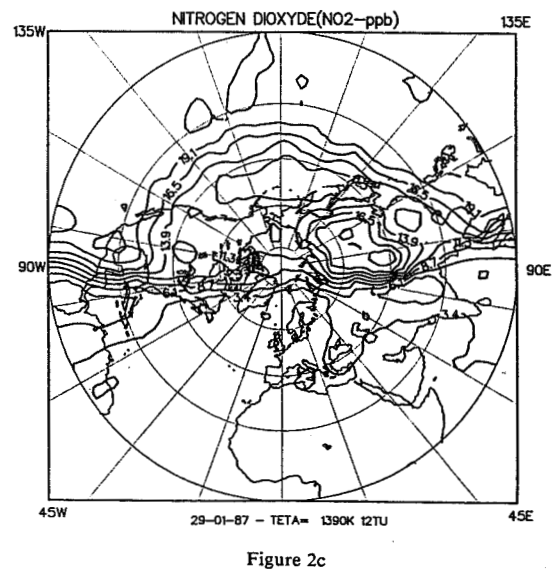
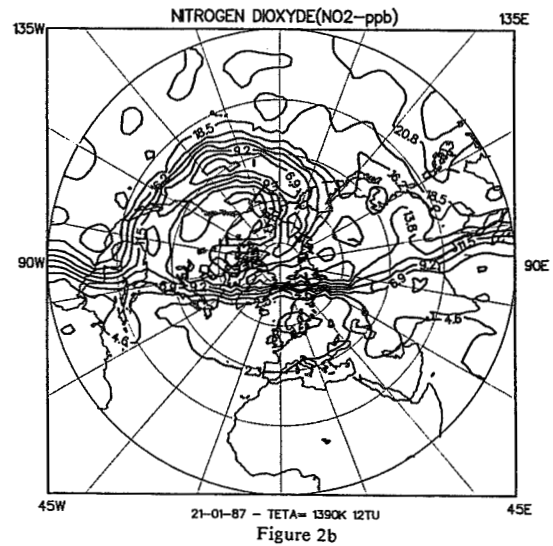
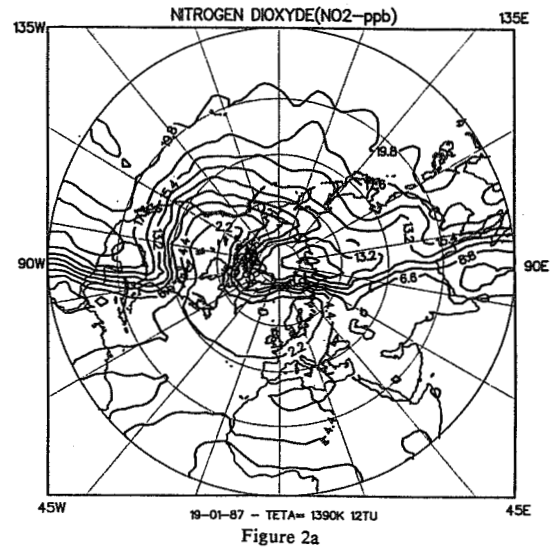
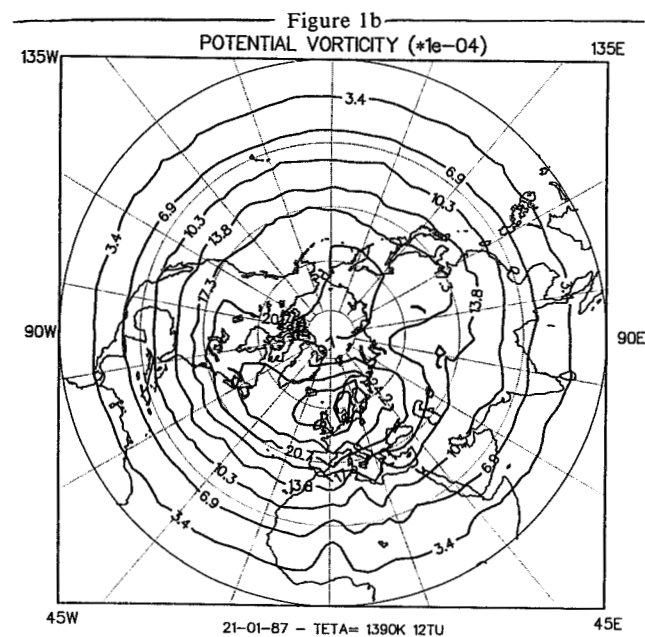
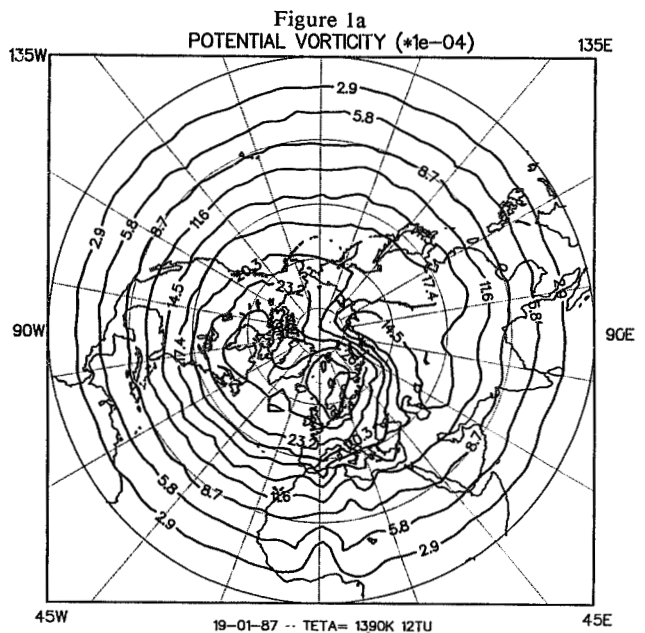
Frederick, J.E., and R.D. Hudson, Dissociation of molecular oxygen in the Schuman-Runge band, *J. Atmos. Sci.*, 37, 1099-1106, 1980.

Garcia and Solomon, A numerical model of the zonally averaged dynamical and chemical structure of the middle atmosphere, *J. Geophys. Res.*, 88, 1379, 1983.

Marti, J., and K. Mausberger, HCl dissolved in solid mixture of nitric acid and ice: Implantation for the polar stratosphere, *Geophys. Res. Lett.*, 18, 1861-1864, 1991.

Ramaroson, R., M. Pirre and D. Cariolle, A box model for on-line computations of diurnal variations in multidimensional models: Application to the one-dimensional case, *Ann. Geophys.*, 10, 416-428, 1992.

Ramaroson R., D. Cariolle and M. Pirre, Simulation of Noxon Cliff in a three-dimensional model with diurnal variations during an unperturbed winter, European Polar Ozone Workshop, Schliersee, October 3-5, 1990.



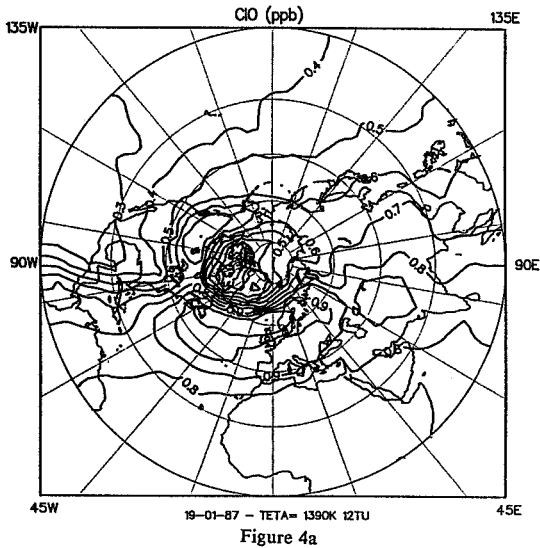
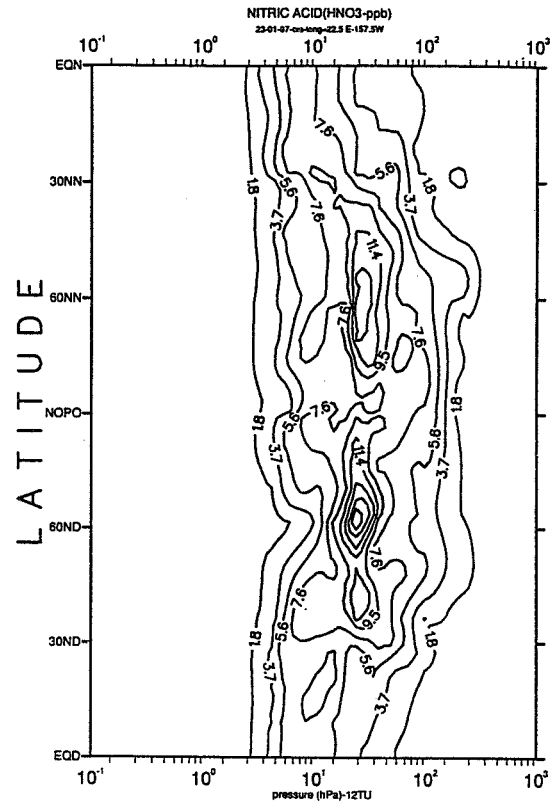
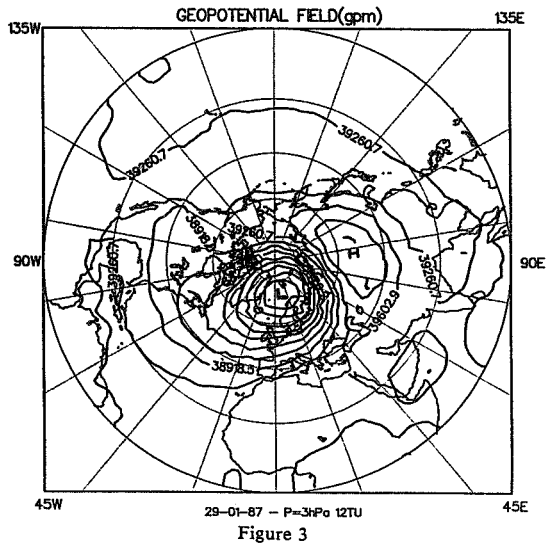
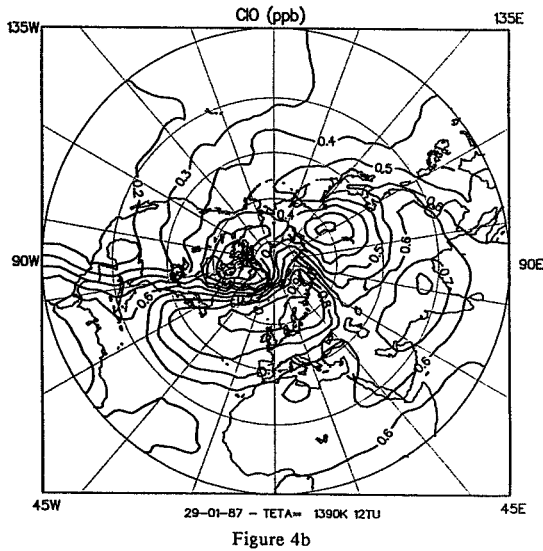
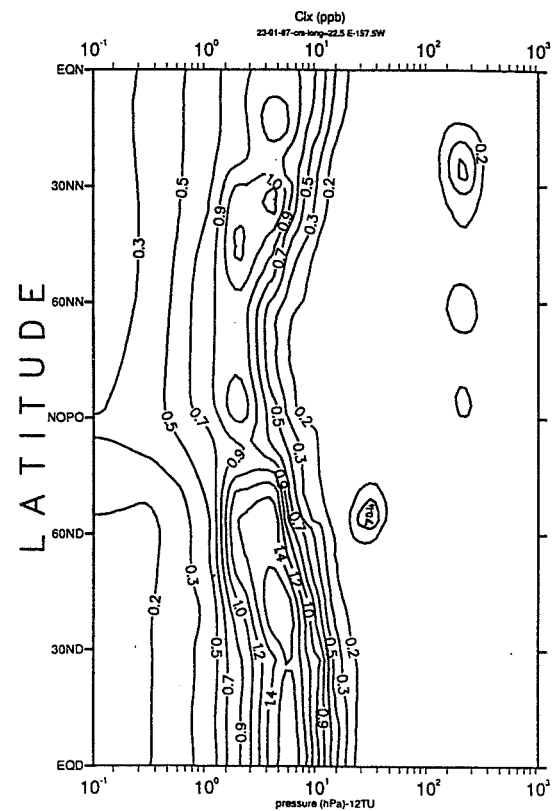


Figure 5



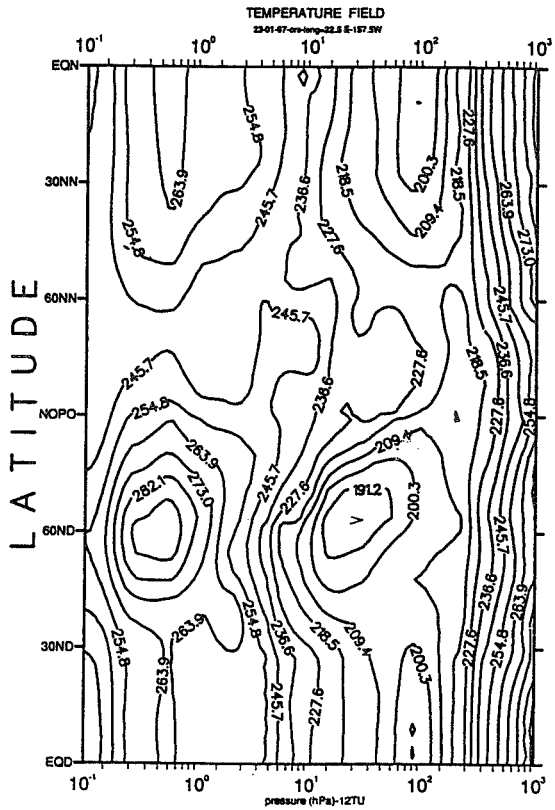


Figure 7

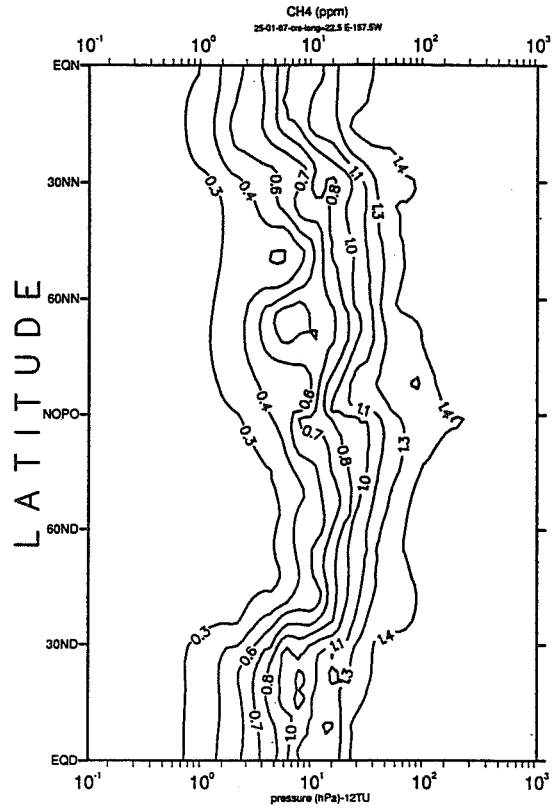


Figure 9

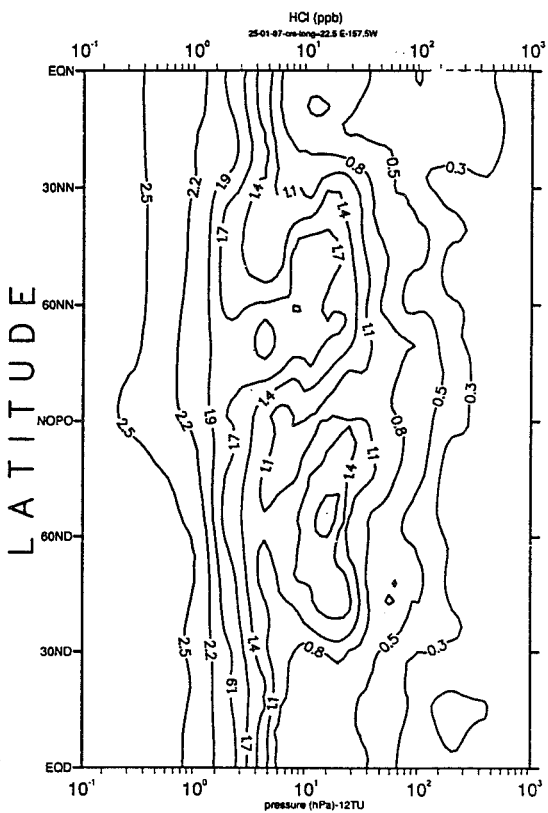


Figure 8

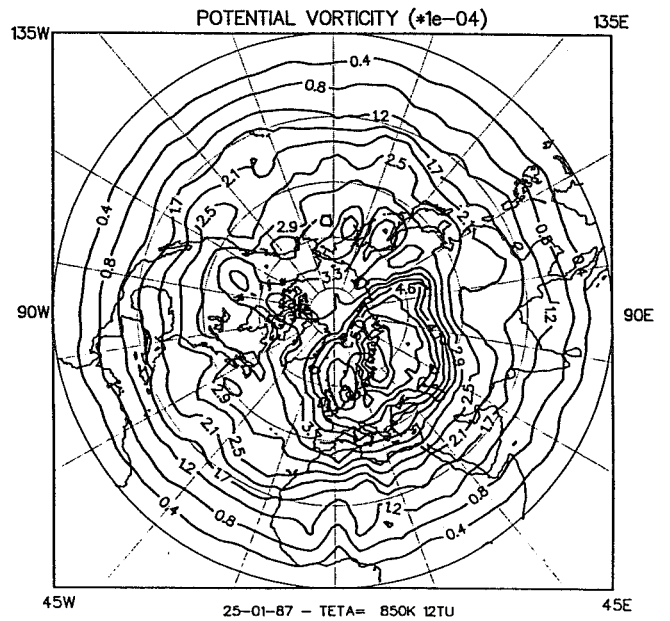


Figure 10

303617

CONNECTION BETWEEN TOTAL OZONE FIELDS AND LOWER STRATOSPHERIC DYNAMICS

G. Vaughan, A. Howells and J. D. Price

Physics Dept., University of Wales, Aberystwyth, UK

ABSTRACT

It is expected from theoretical considerations that synoptic-scale variations in total ozone should be correlated with the absolute vorticity field near the tropopause. This paper tests the theory, using TOMS total ozone fields and vorticity derived from ECMWF analyses. A good correlation is found, except during winter - suggesting that other sources of variability in total ozone are active at this time. The correlation with potential vorticity is also investigated. This shows two maxima in the correlation coefficient in winter and spring, one near the tropopause and the other in the region of 420K. A study of the residuals from a linear regression of vorticity with total ozone during January reveals a similar structure to the 450K potential vorticity field.

1. INTRODUCTION

The relation between total ozone and vorticity that forms the basis of this paper was derived by Vaughan and Price (1991). The total column of ozone in the atmosphere, N, may be written as

$$N = \int_0^{\infty} n(z) dz = - \int_{\theta_s}^{\infty} \frac{x(\theta)}{Mg} \frac{\partial p}{\partial \theta} d\theta$$

where n is the ozone number density, x its volume mixing ratio, M the mass of an air molecule, θ the potential temperature and θ_s its surface value. We can substitute for $\partial\theta/\partial p$ from the expression for potential vorticity Q, to obtain

$$N = \frac{1}{M} \int_{\theta_s}^{\infty} \frac{x(\theta)}{Q(\theta)} \xi_p d\theta \tag{1}$$

where ξ_p is the absolute vorticity on an isentropic surface. The ratio x/Q varies slowly with latitude and height since x and Q are strongly correlated between the tropopause and 21km (Danielsen, 1985; Gidel and Shapiro, 1980), where most of the ozone column is found. If the correlation holds up to a potential temperature θ_p ,

$$N = \frac{1}{M} \frac{\bar{x}}{[Q]} \int_{\theta_s}^{\theta_p} \xi_p d\theta + N_t + N_u \tag{2}$$

where θ_t is the potential temperature at the tropopause, N_t is the column of ozone in the troposphere and N_u is the residual column total above θ_p where x and Q are no longer positively correlated.

Synoptic-scale disturbances decay with height in the lower stratosphere, with no phase progression. Thus, variations in vorticity on this scale (and smaller) near the tropopause will be coherent with those at all heights in the lower stratosphere, provided there are no processes generating variability on such scales in the stratosphere itself. Consequently, total ozone should correlate with the isentropic vorticity at tropopause levels. This may be understood qualitatively by noting that air columns stretch on entering regions of high vorticity (such as troughs) because of the need to conserve potential vorticity (PV). They therefore present more total ozone to the TOMS instrument.

A further influence on total ozone columns is the height (or potential temperature) of the tropopause. Different air masses, with different depths of stratosphere, will contain different total ozone even though the absolute vorticity is the same. Air mass differences may be identified by differences in PV, therefore total ozone should also correlate with the PV distribution in the lower stratosphere. The purpose of this paper is to investigate the correlation of total ozone with potential and absolute vorticity. The study is based on GRID-TOMS ozone fields and meteorological data from ECMWF assimilation fields for mid-day. The latter provided winds and temperatures on 11 pressure levels extending up to 50 mb, with a horizontal resolution of 1.125°.

2. GRID CORRELATIONS BETWEEN ABSOLUTE VORTICITY AND TOTAL OZONE

Correlations were calculated every five days from 1st Jan to the 14th August 1987 for the region from 30°N to 60°N and 30°W to 30°E. The latitude range was chosen because equation (2) is not valid in the subtropics (Vaughan and Price 1991) and

TOMS measurements are unreliable poleward of 60°N in winter because of the high solar zenith angles. A restricted longitude range was chosen to ensure a close correspondence in time between the two data sets. GRID-TOMS data in this region were derived from three passes of the NIMBUS-7 satellite, within about 3 hours of 12h.

CORR. OF ABS. VORTICITY AND TOTAL OZONE

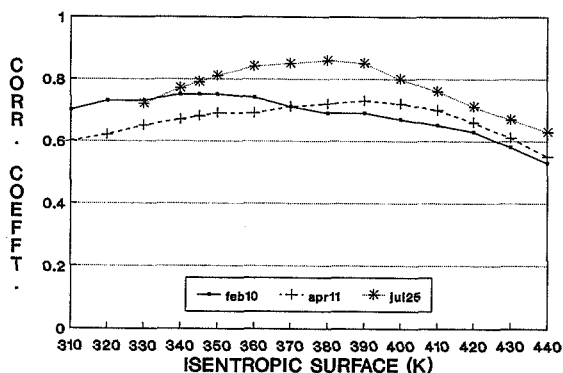


Fig. 1

Correlation coefficients were calculated for isentropic surfaces at 10K intervals between 310 and 440K (the latter was the highest surface remaining below 50 mb throughout the year). Examples are shown in fig.1, for 3 representative days. It is clear that the correlation coefficient varies slowly with height (consistent with the coherent decay of synoptic-scale disturbances in the lower stratosphere), and is higher in summer than in winter (exceeding 0.8 in July). This point is elaborated in fig.2, which shows how the correlation coefficient at three representative levels varied during the year. From March onwards, the values are roughly constant at 0.75 ± 0.07 , but the correlation in winter is poor. This is consistent with the theory outlined above: the lower stratosphere is itself dynamically active in winter and this destroys the correlation with synoptic-scale features.

CORR. OF ABS. VORTICITY AND TOTAL OZONE
JANUARY-AUGUST 1987

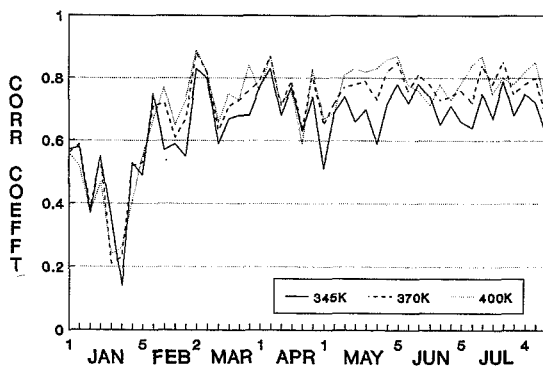


Fig. 2

3. GRID CORRELATIONS BETWEEN POTENTIAL VORTICITY AND TOTAL OZONE

The variation with height of the correlation coefficients between potential vorticity and total ozone is shown for four representative days in fig.3. In contrast to the absolute vorticity, there are very different patterns in summer and winter. In the

CORR. OF POT. VORTICITY AND TOTAL OZONE

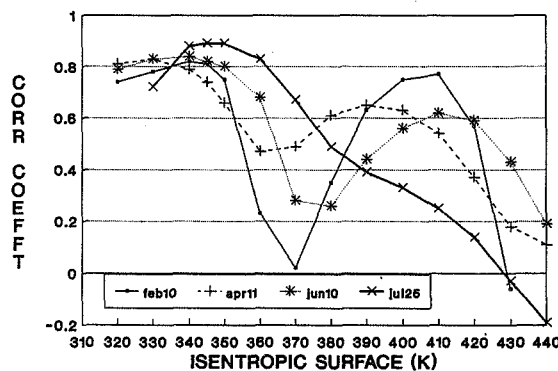


Fig. 3

summer case (July 25th) a maximum correlation of 0.85 occurs near 350K, then the correlation coefficients decrease steadily with height, becoming negative by 430K. In the other three examples a maximum correlation greater than 0.8 occurs between 330K and 340K, just above the tropopause, followed by a minimum near 370K and a second maximum near 400K. This pattern is most pronounced for the winter case (Feb 10th), where the correlation coefficient is not significantly different from zero at 370K, yet the second maximum is almost as large as the first. Above 420K in winter the correlation coefficient decreases sharply, becoming negative above 430K. The two spring profiles show a gradual evolution from the winter to the summer pattern, the latter being established by early July. This point is demonstrated more clearly by fig.4, showing the time

CORR. OF POT. VORTICITY AND TOTAL OZONE
JANUARY-AUGUST 1987

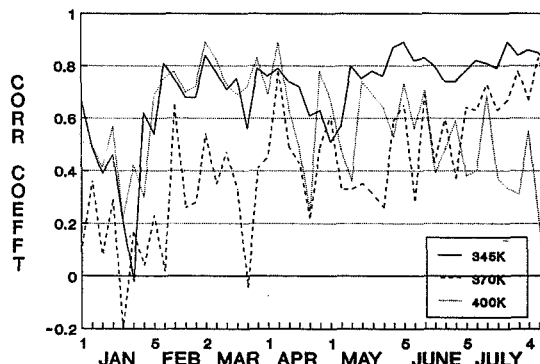


Fig. 4

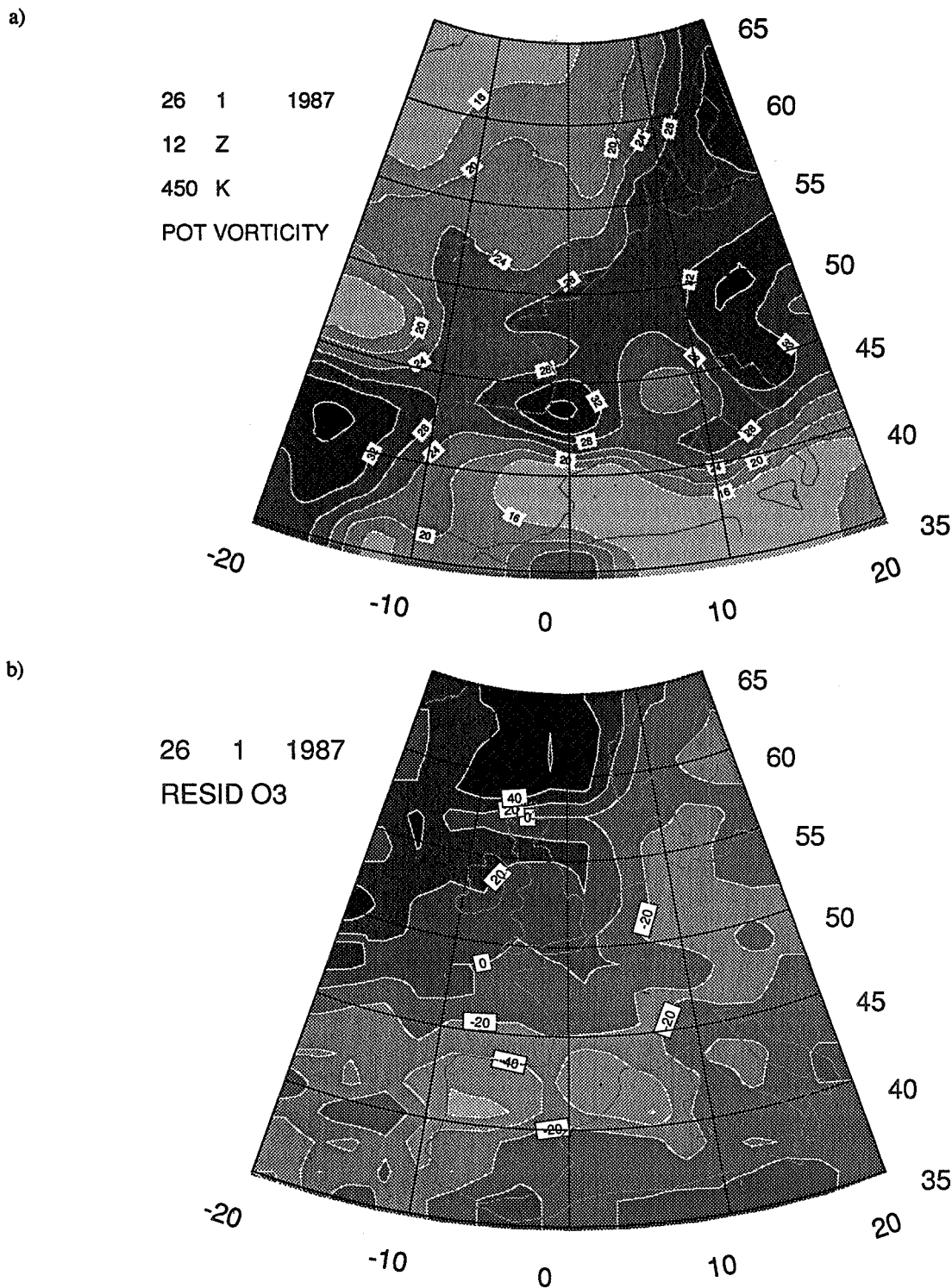


Fig.5 a) Potential vorticity field at 450 K potential temperature, 12h 26 Jan 1987 in units of $\mu\text{Km}^2(\text{kgs})^{-1}$, derived from ECMWF operational analyses. Note the tongue of high PV extending southwestwards between 40° and 50°N .
 b) Residual ozone field in DU for the same time. This was calculated by subtracting from the actual total ozone at each point (measured by TOMS) the value predicted from the regression equation between total ozone and absolute vorticity derived on the 17th January. Note negative residuals corresponding to the PV tongue in a); the polar vortex shows up as a region of lower total ozone once tropopause-level disturbances are removed.

series of correlation coefficients at three representative levels. As before, the values at 345K were low in winter (especially from 22-28th Jan, see below); but increased to around 0.75 in spring and 0.8 in summer. Values in the second maximum remained as large as those in the first until the beginning of April, by which time the minimum correlation near 370K had increased to roughly the same value.

These results may be explained as follows: below 345K good correlation is found throughout the year because these surfaces intersect the tropopause, and high PV is found on the cyclonic side of the jet stream where the tropopause is low and the stratosphere comparatively deep. The second maximum in winter and spring is then indicative of further air mass differences at a higher level - near the base of the stratospheric polar vortex. Around 360-370K in winter there is a transition region, below which isentropes slope downward towards the pole (corresponding to the low tropopause there) and above which they slope up into the polar vortex because of the strong diabatic cooling there. This will be particularly pronounced when the polar front jet stream lies below the stratospheric polar jet. In the transition region the static stability decreases poleward and tends to be anticorrelated with ξ_p (as was verified by direct calculation); thus, the correlation between total ozone and PV disappears at this level. The gradual decay of the second maximum in fig.4 is related to the time taken to mix out the inhomogeneities set up in winter; its disappearance coincided with the establishment of the easterly polar vortex at 50mb during June.

Independent confirmation that the pattern shown in figs. 3 and 4 is not an artifact of the ECMWF assimilation is provided by the study of Vaughan and Begum (1989), who correlated total ozone and PV over Asia. Although their vorticity values were derived from ECMWF analyses, their stability was calculated directly from radiosonde profiles (and so had better vertical resolution than the present study). Their distribution of correlation coefficients between 40° and 50°N is very similar to the present results, with a second maximum in winter and spring above 380K.

4. THE PERIOD 22-28 JANUARY 1987

This period is identified in figs. 2 and 4 as one where total ozone correlated very poorly with both potential and absolute vorticity. It corresponded to a major stratospheric warming over northern latitudes, when polar air throughout most of the stratosphere shifted equatorwards resulting in a significant distortion of the total ozone field due to a change in the term N_u in equation 2. The aim of this section is to isolate this change by removing the synoptic-scale features related to tropospheric weather systems.

The method used was to calculate the linear regression equation of total ozone on absolute vorticity at 345K over the region 35°-60°N, 20°W-20°E, and look at the map of residuals from this equation. Tests during summer showed that typical residuals of 20 DU were found; this value represents a 'noise' for the method. Correlation coefficients were calculated daily

from 17-30 January. The highest value (0.65) was found on 17th January, when the polar vortex was well away from the region of study. The regression equation derived for that day was then used to calculate residual fields for the rest of the period.

The results were compared with the PV fields at 450K derived from the ECMWF model (this surface was below 50 mb in winter). A reasonable agreement was found, with negative residuals corresponding to high PV at 450K, and therefore the polar vortex. An example is shown in fig. 5 for January 26. During this period a tongue of air was drawn off the vortex and moved to lower latitudes; this feature is well captured by the residual field.

5. CONCLUSIONS

This paper verifies the theoretical relationship derived by Vaughan and Price (1991) linking synoptic-scale disturbances in total ozone to the upper tropospheric absolute vorticity pattern. Additionally, correlations with potential vorticity reveal the influence of air mass differences on the ozone column: correlation coefficients from this study are high just above the tropopause at all times of the year, but show a distinct minimum near 370K and a second maximum near 400K in winter and spring. Above about 440K the correlation coefficients with PV become negative at all times of the year. A study of the residuals from a linear fit of total ozone with absolute vorticity during a stratospheric warming clearly identifies the removal of a tongue of ozone-poor air from the polar vortex, which correlates well with the 450K PV chart. Thus, TOMS data may be used to study transport processes in the stratosphere without the interference of tropospheric weather systems.

ACKNOWLEDGEMENTS

We thank Dr. A.J. Fleig, Dr. A. J. Krueger and members of the TOMS Nimbus experiment and ozone processing teams for supplying GRIDTOMS data and the Director of ECMWF, Reading for meteorological data. AH held a SERC studentship during the course of this work.

REFERENCES

- Danielsen, E. F. 'Ozone transport' in *Ozone in the free atmosphere*, ed. R. C. Whitten and S. S. Prasad, Van Nostrand Reinhold, 123-160, 1985.
- Gidel, L. T. and M. A. Shapiro. 'General circulation model estimates of the net vertical flux of ozone in the lower stratosphere and the implications for the tropospheric ozone budget' *J. Geophys. Res.*, **85**, 4049-4058, 1980.
- Vaughan, G. and D. A. Begum. 'Correlation between ozone and potential vorticity'. in 'Ozone in the atmosphere', ed. R. D. Bojkov and P. Fabian, A. Deepak, 91-4, 1989.
- Vaughan, G. and J. D. Price. On the relation between total ozone and meteorology. *Q. J. Roy. Met. Soc.*, **117**, 1281-1298, 1991.

303620

MODEL/DATA COMPARISONS OF OZONE IN THE UPPER STRATOSPHERE AND MESOSPHERE

David E. Siskind,¹ Ellis E. Remsberg, Richard S. Eckman, Brian J. Connor

Atmospheric Sciences Division, NASA Langley Research Center, Mail Stop 401B, Hampton, Virginia 23665-5225

J. J. Tsou

Lockheed Engineering and Sciences Company, Hampton, Virginia, 23666

Alan Parrish²

University of Massachusetts, Amherst, Massachusetts 01003

Abstract. We compare ground-based microwave observations of ozone in the upper stratosphere and mesosphere with daytime observations made from the SME satellite, with nighttime data from the LIMS instrument, and with a diurnal photochemical model. The results suggest that the data are all in reasonable agreement and that the model-data discrepancy is much less than previously thought, particularly in the mesosphere. This appears to be due to the fact that the latest data are lower than earlier reports and the updated model predicts more ozone than older versions. The model and the data agree to within a factor of 1.5 at all altitudes and typically are within 20%.

Introduction

A long standing problem in middle atmospheric science is the fact that photochemical models of ozone from 40 to 80 km have historically predicted significantly less ozone than is observed. In the review by Rusch and Clancy (1987), they state that the discrepancy is on the order of 30-50% in the upper stratosphere, increasing to a factor of 2-3 in the upper mesosphere. There have been a number of proposals advanced to try and reconcile the models and the observations. For example, it has been suggested that the catalytic cycles, such as that due to HO_x (Rusch and Eckman, 1985) which destroy ozone are less efficient than currently assumed. Others have suggested that larger O_3 photolysis cross sections are required (e.g. Allen and Delitsky, 1991). This would then increase the production of odd oxygen. Finally, there has also been considerable effort to try and identify a missing ozone source that is not included in the current chemical scheme (e.g. Slanger et al., 1988).

Recently, Natarajan and Callis (1989) have pointed out that the discrepancy in the upper stratosphere can be reduced somewhat if updated rate coefficients and solar fluxes are used in their model along with the somewhat lower total chlorine estimates obtained from the ATMOS data. On the other hand, Allen and Delitsky (1991) argue that by combining the analysis of stratospheric and mesospheric ozone from ATMOS, a consistent, significant discrepancy still exists.

In this paper we pursue the question of the model-data comparison using a variety of datasets including that from the Solar Mesosphere Explorer (SME) for the daytime mesosphere, from the Limb Infrared Monitor of the Stratosphere (LIMS) for the nighttime upper stratosphere and mesosphere and from ground-based microwave data which span the altitude region from 40 to 70 km for both day and night conditions.

Comparison of Observational Data

Figure 1 presents an overview of the ozone data used in our study. The data are all mean profiles for the month of March, at a latitude of 35N, and include both day and night conditions. Although the measurement set spans 12 years (1979 for LIMS, 1982 for SME, and 1991 for the microwave) these data were all obtained during comparable solar activity conditions, near the maximum of either cycles 21 or 22. The figure shows a consistent pattern in that the nighttime data exceed the daytime data, by an amount which increases with decreasing pressure. This reflects the well known mesospheric diurnal variation of ozone whereby atomic oxygen recombines after sunset to increase the ozone density (Zommerfelds et al., 1989). Specific features of these profiles will be discussed below.

The LIMS data that we used were described by Remsberg et al. (1984) and consist of zonal mean ozone data up to 0.1 mb. We have exclusively used nighttime data in order to avoid the non-LTE effects known to be present above about 0.5 mb in the daytime data (Solomon et al., 1986).

SME measured ozone from 1982 to 1986 using an ultraviolet absorption (UVS) technique from 1.0 to 0.1 mb (Rusch et al., 1984) and a near infrared (NIR) emission technique from 0.75 to 0.002 mb (Thomas et al., 1984). Both techniques are valid during daytime conditions only. The SME dataset was reprocessed in 1988 (WMO, 1988) and we used this dataset for our study.

The microwave data come from an instrument at the Table Mountain Observatory (34 deg N, 118 deg W). The instrument was developed at the Millitech Corporation and the data is processed at NASA's Langley Research Center. The data cover the altitude range from 20 to 70 km (.05 mb) and record an observation every 20 minutes. A complete description of the instrument, the observing tech-

¹now at Naval Research Laboratory, Code 4141, Washington DC, 20375

²Also at Millitech Corporation, Deerfield, MA, 01373

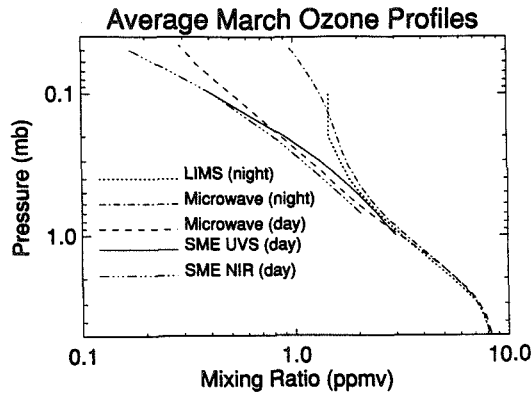


Fig. 1. Summary of monthly mean ozone datasets for 35N latitude. The LIMS data are from March 1979, the SME data from March 1982, and the microwave data from March 1991.

nique and calibration method are described in Parrish et al., (1992). The retrieval method is described by Connor et al., (1991). Comparisons of these data with other ground and satellite observations are given by Parrish et al., (1992, these proceedings). It is important to note that the microwave experiment has much lower vertical resolution than the limb scanning satellites (12-16 km for the microwave, 3-4 km for LIMS and SME). Thus, in the discussion which follows we will convolve the high resolution satellite data (as well as the photochemical model) with the microwave averaging kernels as described by Connor et al. (1991).

Figure 2 shows March mean daytime ozone profiles from the SME NIR instrument from 1982 and the ground based microwave from 1991. Both the SME and the microwave data are for 1500 hours local time. Also shown in the figure is the SME data after convolution with the microwave averaging kernel. The effect of the convolution process is most noticeable at the lowest pressure (.05 mb). The figure shows that the convolved SME agrees with the microwave to within the estimated errors of the two experiments (25% for the microwave at .05 mb, 15-20% for SME). It should be noted that the narrower pressure range covered by the UVS instrument (1.0 to 0.1 mb) precludes a direct inter-comparison with the low resolution microwave. On the other hand, in the next section we will compare all three daytime ozone profiles to a photochemical model.

Figure 3 shows the ratio of the nighttime LIMS to the nighttime microwave. Because the LIMS data only extend up to 0.1 mb, it is necessary to extrapolate the data up to 0.01 mb in order to convolve with the microwave averaging kernels. The three curves in Figure 3 show the results for three different extrapolations. The solid line uses a profile taken from the photochemical model (discussed below), normalizes it to the LIMS data at 0.1 mb and then is used to extend the data up to 0.01 mb. Using this extrapolation, we find that the LIMS and the microwave data agree to within 5% at all altitudes. The left dotted line simply assumes a constant mixing ratio from 0.1 to 0.01 mb, while the right dotted line uses the microwave a priori profile above 0.1 mb. The purpose of the two dotted curves

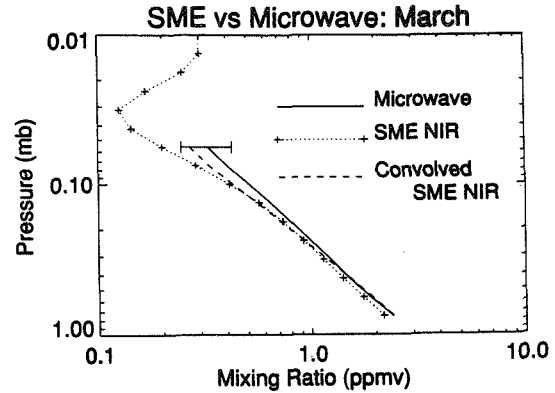


Fig. 2. Daytime ozone data. The dotted line is the SME NIR mean data for March 1982, the solid line is the mean microwave data for March 1991. The dashed curve is the SME data after convolving with the microwave averaging kernels.

is to show that although the agreement between LIMS and microwave is excellent everywhere, there is a mathematical uncertainty of $\pm 10\%$ at the top of the profile which results from the need to extrapolate the LIMS data.

Photochemical Model Calculations

The model we use is a one dimensional photochemical model of the middle atmosphere from 40 to 80 km. It has evolved from the model used by Rusch and Eckman (1985) to study daytime mesospheric ozone. For the present application we have expanded its capabilities in three ways. First, we now use complete spherical geometry to calculate the attenuation of the solar UV radiation by ozone and thus improve the O_2 and O_3 photolysis calculations during twilight. Second, while the previous model used the family method to combine O and O_3 as O_a , we now calculate the O and O_3 densities separately for altitudes greater than 60 km and for solar zenith angles greater than 92° . Third, we now account for the enhanced photolysis of O_3 and NO_2 at near UV and visible wavelengths by inputting a ta-

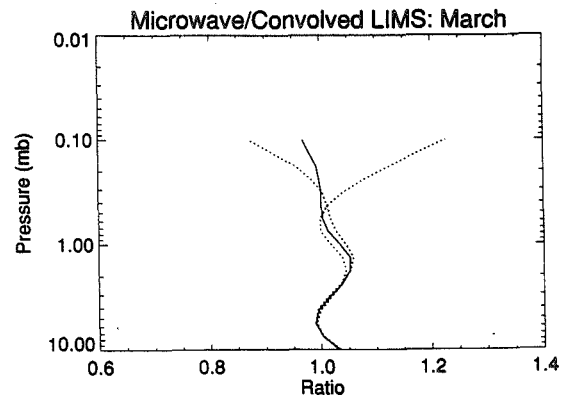


Fig. 3. Ratio of microwave to convolved LIMS. Three different assumptions were used to extrapolate the LIMS data above 0.1 mb when performing the convolution (see text).

ble of scattering enhancement factors which depend upon altitude and solar zenith angle.

The model uses fixed chlorine ($Cl_y = HCl + HOCl + ClO + Cl$), nitrogen ($NO_x = NO + NO_2$), and water vapor inputs. For Cl_y , we used a constant value of 2.2 ppbv for the comparison with the LIMS data, 2.4 ppbv for the comparison with SME, and 3.0 ppbv for the comparison with the microwave data. These chlorine quantities are consistent with that used by Natarajan and Callis (1989) and are lower than those used in earlier studies. For NO_x , we used a fixed value of 15 ppbv, except for the LIMS comparison where we used the LIMS nighttime NO_2 measurement as an indicator of the total NO_x . Our assumed water vapor profile is taken from the LIMS climatology (Remsburg et al., 1990) for the stratosphere and the microwave data of Bevilacqua et al. (1989) for the mesosphere. Finally, the model uses different temperatures when comparing with different datasets: for the LIMS comparison, simultaneously measured LIMS temperatures are used, for the microwave comparison, the temperatures are those used in the data processing, and for SME, the reference climatology of Cole and Kantor (1978) was adopted.

One limitation of the model is its neglect of vertical transport. While this will not be important for altitudes where the lifetime of ozone is short (< 75 km), it could introduce an uncertainty when comparing with the low resolution microwave data at 70 km. We therefore have limited our comparison of the microwave data and the convolved model to altitudes below 66 km (0.1 mb).

Figure 4a compares the ratio of the two nighttime datasets to either the model (in the case of LIMS) or the convolved model (for the microwave). A similar comparison with the March LIMS data was presented by Natarajan and Callis (1989); however, their analysis only went up to 0.5 mb (52 km). Here, we extend the comparison up to 0.1 mb. The figure shows that the data exceeds the model at all pressures, consistent with all previous studies of the problem. The detailed shape of the difference agrees very well with that seen by Natarajan and Callis in the pressure range where our two studies overlap, a minimum from 1.0 to 0.5 mb with a maximum at 3 mb. In addition, our analysis suggests that the discrepancy increases above 0.5 mb to reach a maximum of a factor of 1.3 at 0.1 mb. Also, the figure shows remarkable agreement between the LIMS and microwave comparisons, despite the different inputs to the model (described above) and the 12 year separation in the observations. Given the lack of other nighttime mesospheric ozone measurements, the combination of this comparison and that shown in Figure 3 serves as the first reliable validation of the LIMS nighttime ozone in the mesosphere.

Figure 4b presents a similar model-data comparison for the three daytime data sets. It shows the ratio of the three daytime datasets to either the model (in the case of SME) or the convolved model (for the microwave). At 1.0 mb, the UVS and the microwave data exceed the respective model by a factor of 1.15-1.20. At pressures below 1.0 mb, the discrepancy between the model and the UVS worsens to reach a factor of 1.35 at 0.3 mb. The discrepancy between the microwave and the SME NIR show somewhat different behavior and seem to agree slightly better. Above 0.1 mb

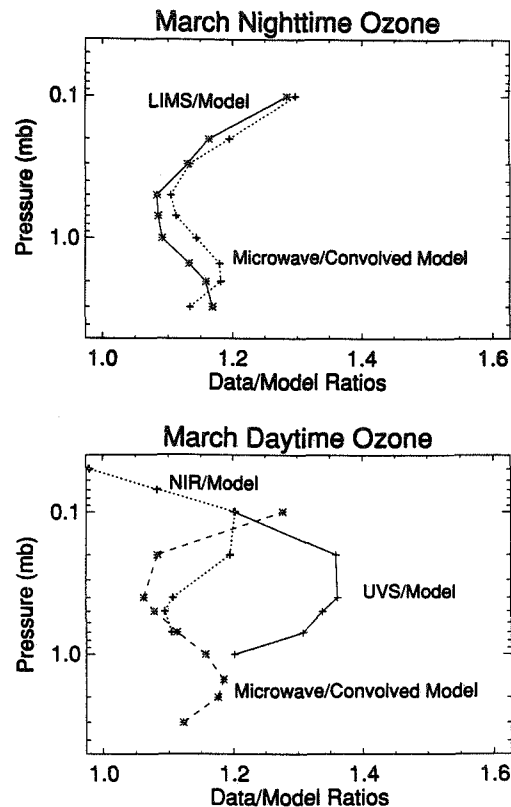


Fig. 4. (a) Ratio of March nighttime ozone to photochemical model (in the case of LIMS data- solid line) and convolved model (for the microwave- dotted line). (b) Ratio of March daytime ozone to photochemical model (solid line is for the SME UVS data, the dotted line is for the SME NIR data) and with convolved model (dashed line for the microwave data).

the model and the NIR data come into closer agreement. The pattern here is not as consistent as that seen in Figure 4a. Part of this undoubtedly reflects the 20% disagreement which exists between the two simultaneous SME measurements at certain pressures (e.g 0.4 mb). In addition the temperatures used in the comparison between the model and the SME datasets, which are from the Cole and Kantor (1978) climatology, may not be as realistic as those used in analysing the microwave data (from the National Meteorological Center analysis and the MAP climatology).

Discussion

In both Figures 4a and 4b, the data-model ratios are lower than previously reported. For example, using SME UVS data from 1983, Rusch and Eckman (1985) reported a discrepancy of 1.8 during March at 40 N, with a larger discrepancy during winter. Here, however, the peak discrepancy from all 5 ozone observations lies in the range 1.2 - 1.35. One reason for this change is that the model now uses a faster $OH + HO_2$ rate coefficient (see JPL90 for a discussion) and thus predicts less HO_x and about 1.15 times more ozone at 0.1 mb. Second, the reprocessed SME

data is generally lower than the original version used by Rusch and Eckman (1985). Some of this is discussed in the WMO (1988) report and is attributed to a removal of a calibration drift, corrections to the field of view and the determination of tangent point altitude as well as a 12% change in the absolute calibration of the NIR instrument (R. Thomas, private communication, 1992). An example of the difference is shown in Figure 5 which compares the new SME NIR data for March 1982 with the version 1 data as given in the MAP Handbook (1985). It can be seen that at 0.1 mb, the old data is more than 1.3 times greater than the new. The combination of the newer, lower data (factor of 1.2 - 1.4) and the higher model (factor of 1.10 - 1.15) leads to a significantly reduced discrepancy between model and data.

Summary

We have compared ground based microwave data with satellite observations from LIMS and SME. For both day and night, the observations agree to within 25%. When compared to photochemical model calculations, the data exceed the model at all altitudes, but by an amount which is much smaller than earlier reports. This is because the revised model predicts more ozone while the newer observations report less.

Acknowledgments. We acknowledge the National Space Science Data Center and Charles A. Barth, Principal Investigator, for supplying the SME data. We also thank R. Thomas and M. Callan for assistance in using this data.

References

Allen, M. and M. L. Delitsky, A test of odd-oxygen photochemistry using Spacelab 3 Atmospheric Trace Molecule Spectroscopy Observations, *J. Geophys. Res.*, **96**, 12,883, 1991.

Bevilacqua, R. M., J. J. Olivero, and C. L. Croskey, Mesospheric water vapor measurements from Penn State: Monthly-mean observations (1984-1987), *J. Geophys. Res.*, **94**, 12807, 1989.

Connor, B. J. A. Parrish, and J. J. Tsou, Detection of stratospheric ozone trends by ground-based microwave observations, *Proc. of SPIE conf. 1491*, Remote Sensing of Atmospheric Chemistry, Soc. of Photo-Opt. Instrum. Eng., Bellingham, Wash., 1991.

Cole, A. E. and A. J. Kantor, Air Force reference atmospheres, Rep AFGL-TR-78-0051, Air Force Geophys. Lab., Cambridge, Mass., 1978.

NASA-JPL, Chemical kinetics and photochemical data for use in stratospheric modeling, Evaluation No. 9, *JPL publication 90-1*, Jet Propulsion Laboratory, Pasadena, California, 1990.

Natarajan, M. and L. B. Callis, Examination of stratospheric ozone photochemistry in light of recent data, *Geophys. Res. Lett.*, **473**, 1989.

Parrish, A., B. J. Connor, J. J. Tsou, I.S. McDermid, W. P. Chu, Ground-based microwave monitoring of stratospheric ozone, *J. Geophys. Res.*, **97**, 2541-2546, 1992.

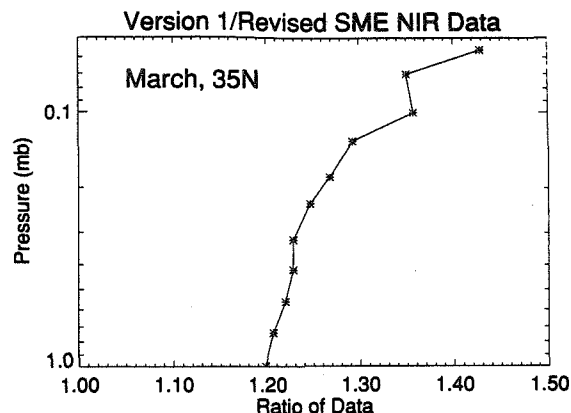


Fig. 5. A comparison of version 1 and the revised SME NIR for March 1982. The older dataset (version 1) contains larger values.

Remsberg, E. E., J. M. Russell, III, J. C. Gille, L. L. Gordley, P. L. Bailey, W. G. Planet, and J. E. Harries, The validation of Nimbus 7 LIMS measurements of ozone, *J. Geophys. Res.*, **89**, 5161, 1984.

Remsberg, E. E., J. M. Russell III, and C. -Y. Wu, An interim reference model for the variability of the middle atmosphere water vapor distribution, *Adv. Space Res.*, **10**, 51, 1990.

Rusch, D. W. and R. T. Clancy, Minor constituents in the upper stratosphere and mesosphere, *Rev. Geophys.*, **25**, 479, 1987.

Rusch, D. W. and R. S. Eckman, Implications of the comparison of ozone abundances measured by the Solar Mesosphere Explorer to model calculations, *J. Geophys. Res.*, **90**, 12991, 1985.

Rusch, D. W., G. H. Mount, C. A. Barth, R. J. Thomas, and M. T. Callan, Solar Mesosphere Explorer ultraviolet spectrometer: Measurements of ozone in the 1.0 to 0.1 mb region, *J. Geophys. Res.*, **89**, 11677, 1984.

Russell, J. M. III (Ed.), *Handbook for MAP*, **22**, 302pp., University of Illinois, Urbana, 1986.

Slinger, T. G., L. E. Jusinski, G. Black, and G. E. Gadd, A new laboratory source of ozone and its potential atmospheric implications, *Science*, **241**, 945, 1988.

Solomon, S., J. T. Kiehl, B. J. Kerridge, E. E. Remsberg, and J. M. Russell III, Evidence for nonlocal thermodynamic equilibrium in the ν_3 mode of mesospheric ozone, *J. Geophys. Res.*, **91**, 9865, 1986.

Thomas, R. J., C. A. Barth, D. W. Rusch, and R. W. Sanders, Solar Mesosphere Explorer near-infrared spectrometer: Measurements of 1.27 μm radiances and the inference of mesospheric ozone, *J. Geophys. Res.*, **89**, 9569, 1984.

WMO, Report of the international ozone trends panel 1988, *WMO Global Ozone Research and Monitoring Project Report No. 18*, WMO, Geneva, 1988.

Zommerfelds, W. C., K. F. Kunzi, M. E. Summers, R. M. Bevilacqua, D. F. Strobel, M. Allen, and W. J. Sawchuck, Diurnal variations of mesospheric ozone obtained by ground based microwave radiometry, *J. Geophys. Res.*, **94**, 12,819-12,832, 1989.

303621

ON THE RELEVANCE OF THE
METHANE OXIDATION CYCLE TO "OZONE HOLE" CHEMISTRY

Rolf Müller and Paul J. Crutzen

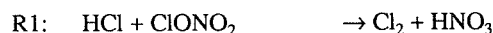
Max Planck Institute for Chemistry,
P.O. Box 3060, D-6500 Mainz, Germany

ABSTRACT

High concentrations of active chlorine are clearly responsible for the observed ozone depletion during the Antarctic polar spring. However, the mechanism behind the activation of chlorine from the reservoir species HCl and ClONO₂ and the maintenance of extremely high levels of active chlorine after polar sunrise is less well understood. Here, we focus on the influence of the methane oxidation cycle on "ozone hole" chemistry through its effect on HO_x and ClO_x radicals. We demonstrate the great potential importance of the heterogeneous reaction HCl + HOCl → Cl₂ + H₂O and the gasphase reaction ClO + CH₃O₂ → ClOO + CH₃O under sunlight conditions in polar spring. Under these conditions, the heterogeneous reaction is the main sink for HO_x radicals. Through this channel, the HCl reservoir may be almost completely depleted. The gas phase reaction may control the levels of the CH₃O₂ radical, provided that high levels of ClO exist. Otherwise this radical initiates a sequence of reactions leading to a considerable loss of active chlorine. Moreover, the production of HO_x radicals is reduced, and thereby the efficiency of the heterogeneous reaction limited. The two reactions together may accomplish the complete conversion of HCl into active chlorine, thereby leading to a rapid destruction of ozone.

1. INTRODUCTION

It is now well-established that high levels of active chlorine are responsible for the observed depletion in stratospheric ozone in Antarctic polar spring. This is mainly accomplished through the ClO-dimer cycle (Molina and Molina, 1987; Anderson et al., 1991). The activation of chlorine through heterogeneous reactions from the main reservoir species HCl is less well understood. Assuming that N₂O₅ is largely converted to HNO₃ through heterogeneous reaction on the background sulphate aerosol (Hanson and Ravishankara, 1991), then only the reaction



on nitric acid trihydrate (NAT) is known as a possible source of active chlorine during polar night. Thus ClONO₂ is titrated by HCl and a significant amount of gasphase HCl

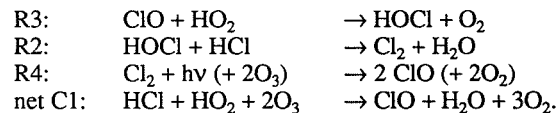
survives until sunrise after polar night. However, both high levels of observed ClO (Anderson et al., 1991) and very low HCl column amounts (Murcray et al., 1989; Toon et al., 1989) indicate, that most chlorine may already be in active form by the beginning of September in the lower stratosphere.

Both, ClONO₂ and HOCl (Hanson and Ravishankara, 1992; Abbatt and Molina, 1992) react rapidly with HCl on PSC surfaces, thus providing a channel for the fast removal of HCl. Therefore, in the presence of PSCs, ClONO₂ and HOCl should not be regarded as chlorine reservoirs. Rather, every ClONO₂ or HOCl molecule produced will react rapidly with HCl, thus providing a source of active chlorine.

However, ClONO₂ is an unlikely reaction partner since the necessary levels of ClONO₂ cannot be sustained as long as almost all of the active nitrogen is converted to HNO₃ and frozen out as NAT. Recently, Prather (1992) and Crutzen et al. (1992) have independently pointed out that the heterogeneous reaction



provides a much more efficient pathway for the completion of the liberation of the entire HCl reservoir after polar sunrise. Reaction R2 is efficient under sunlit conditions closing the reaction sequence (Crutzen et al., 1992)



For the very high ClO concentrations under "ozone hole" conditions, reaction R3 controls the HO₂ concentration; thus the net rate of cycle C1 may be expressed as:

$$-\frac{d(\text{HCl})}{dt} = \frac{d(\text{ClO}_x)}{dt} = P_{\text{OH}} \quad (1)$$

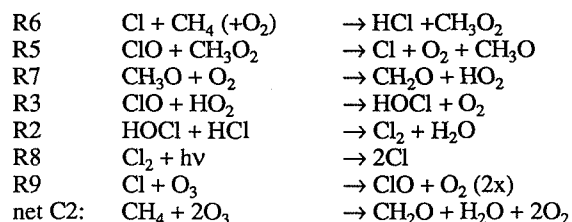
with P_{OH} denoting the production rate of OH and HO₂ radicals.

2. METHANE OXIDATION AND "OZONE HOLE" CHEMISTRY

The methane oxidation cycle and "ozone hole" chemistry are closely linked because many compounds participating in the methane oxidation cycle react rapidly with the Cl radical. Moreover the reaction proposed by Simon et al. (1989)

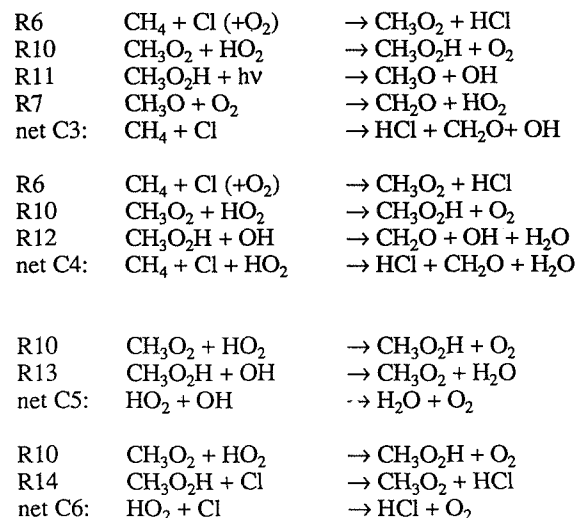


may constitute yet another link between these two systems. Crutzen et al. (1992) demonstrated that R5 strongly limits the effect of the deactivation of chlorine by formation of HCl through the reaction cycle:

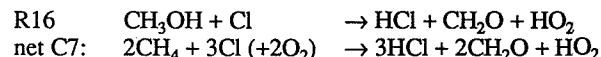
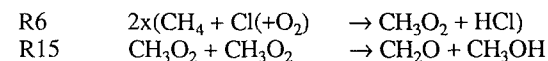


Under "ozone hole" conditions, R6 is the main source of CH_3O_2 due to the high Cl concentrations.

Reaction R5 is relevant here because it closes cycle C2 and thereby largely controls the fate of the CH_3O_2 radical. The latter would otherwise participate to a much larger extent in several cycles leading to a loss of both HO_x and active chlorine. Considering Eq. (1) it is clear that both the destruction of HO_x and the formation of HCl from Cl limit the amount of active chlorine under PSC conditions in Antarctic spring. Four parallel cycles are of importance under these conditions:

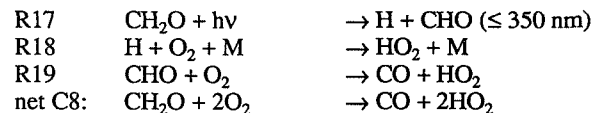


Moreover, the main channel for the CH_3O_2 self-reaction at low temperatures (Horie et al., 1990) and the methanol oxidation should be considered



It is assumed for all these cycles, that gasphase NO_x concentrations are extremely low and Cl levels considerably elevated.

The photochemical breakdown of formaldehyde to carbon monoxide occurs along four pathways. One of these, takes place with a probability of about 40% and leads to the production of two HO_2 radicals:



and thus strongly enhances cycle C1. Other channels for the decomposition of formaldehyde lead directly to the formation of CO without amplifying C1.

3. MODEL RESULTS

Calculations were performed (see Crutzen et al., 1992, for details) for conditions at 75°S near 70 mb, starting on August 20, at about the time sunlight returns after the polar night, and continuing for 55 days. Initial chemical conditions, except ozone and water vapour concentrations, were taken from 2D model results for the beginning of the polar night but shifted downward by several kilometers to take into account a general downward motion in the polar vortex, indicated by N_2O measurements (Fahey et al., 1990). Dehydration as observed by Kelly et al. (1989) and a 75 % denitrification (Fahey et al., 1990) were taken into account. A linear increase in temperature (Fig. 1) was estimated from the measurements of Deshler and Hofmann (1991) at McMurdo station, 78°S , in 1990. Initial chemical conditions were: O_3 1.6 ppmv (Deshler and Hofmann, 1991), H_2O 2.2 ppmv (Kelly et al., 1989), HCl 1.6 ppbv, ClONO_2 0.5 ppbv, HNO_3 2.1 ppbv. Further additional assumptions were made:

1. All NO_x gases, which were present at the onset of the polar night, were assumed to have been converted to HNO_3 by reactions on sulphate aerosol particles before PSC formation, thus they did not affect the conversion of HCl to ClO_x .
2. It was assumed that all ClONO_2 and HOCl had reacted with HCl during the polar night on the NAT and ice particles to yield Cl_2 . A reaction probability of $\gamma = 0.3$ for R1 and $\gamma = 0.2$ for R2 was adopted.
3. Whenever temperatures were low enough for NAT existence (Hanson and Mauersberger, 1988) HNO_3 was frozen out at a concentration of 1 particle/ cm^3 . The following calculations were performed:
 - (A) Both reactions R2 and R5 were included.
 - (B) Reaction R5 was not included, but reaction R2 was.
 - (C) Reaction R2 was not included, but reaction R5 was.
 - (D) Both reactions R2 and R5 were neglected.

Some results of the computer model runs on which this paper is based have already been discussed in Crutzen et al. (1992). The main findings are summarized in Fig. 1. Clearly in case D the HCl reservoir is not sufficiently

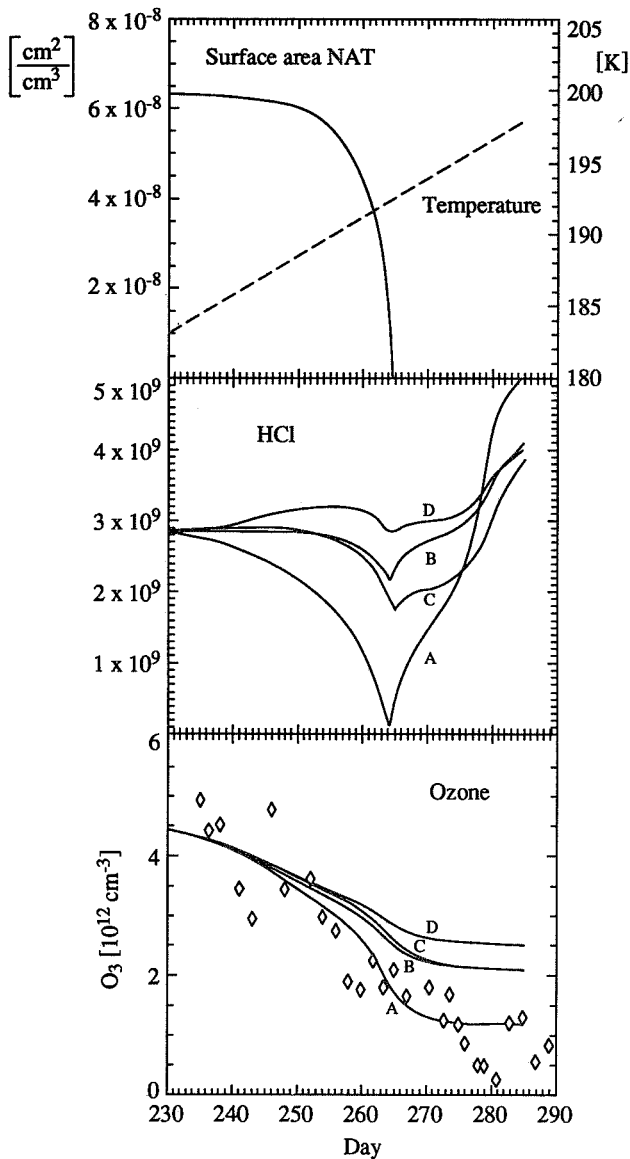


Fig. 1. The development of the surface area of NAT (in cm^2/cm^3) and temperature, upper panel; the concentration of HCl (in molecules/ cm^3), middle panel and the ozone concentration (in molecules/ cm^3) over the model period. Daily variation of ozone and HCl are smoothed. Initial day is August 20, height 70 mbar. Diamonds indicate ozone measurements at approximately 70 mbar (Deshler and Hofmann, 1991). Line A shows results for reactions R2 and R5 included, line B with R5 neglected, line C with R2 neglected and line D with both R2 and R5 neglected. The last NAT particles evaporate around day 265 bringing an end to ozone depletion.

activated to reproduce the ozone destruction recorded in the measurements (Deshler and Hoffman, 1991). When either reaction R2 or R5 is included (case B and C respectively) the results improve. However, only when both R2 and R5 are introduced, does the model produce a strong depletion in both ozone and HCl.

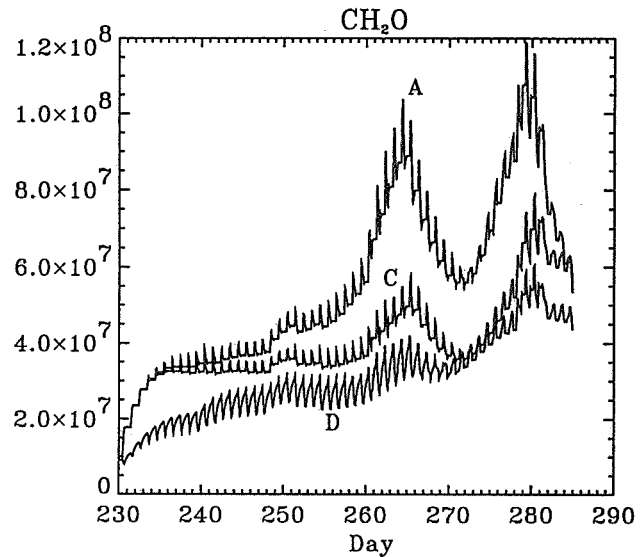


Fig. 2. The temporal evolution of the concentration of formaldehyde (in molecules/ cm^3) over the model period. Cases A, C, D are shown; case B (not shown) exhibits very similar, but slightly higher values than case D.

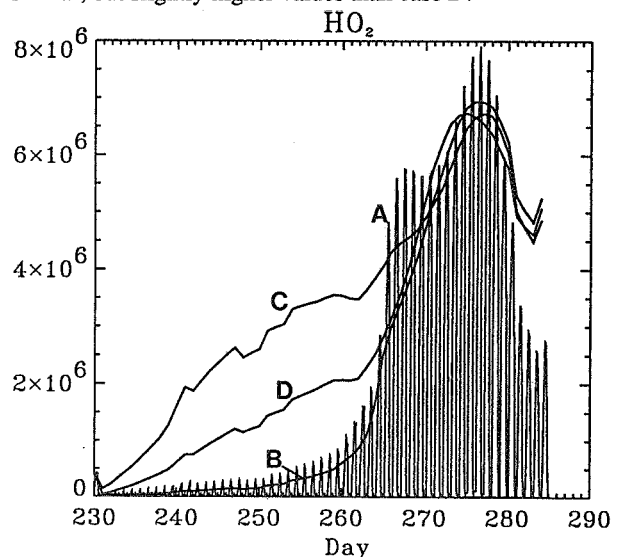


Fig. 3. As in Fig. 2, but for HO_2 concentrations in molecules/ cm^3 . Case A shows diurnal variation, cases B, C, D only daily maximum values.

Fig. 2 shows the variation of formaldehyde over the model period. Compared to case D concentrations of CH_2O are about a factor of two higher, when both reactions R2 and R5 are included. The cause is an enhanced production through cycle C2. Reaction R5 is particularly efficient in enhancing the production of CH_2O , as can be seen from the higher concentrations in case A and C compared to case D (Fig. 2). High levels of CH_2O produce high concentrations of HO_x through cycle C8.

HO_x radicals play a crucial role in the cycles discussed here. In Fig. 3, the efficiency of R2 in keeping HO_x at low levels (comp. A,B with D,C) under PSC conditions is evident. In case A, after the evaporation of the

NAT particles, a drastic increase in ClONO₂, HOCl (Crutzen et al., 1992) and HO₂ (Fig. 3) was observed. The Cl radicals (Fig. 4) exhibit a distinct behaviour. As long as PSCs exist (until day 264) the buildup of active chlorine is reflected in an increasing concentration in Cl. From day 264 to 270 Cl decreases much like the ClO (Crutzen et al., 1992). However, from day 270 to 278 Cl increases again in contrast to ClO. During this period the ClO/Cl ratio is shifted in favour of Cl by the increase in NO by a factor of 20 from day 270 to 280. Prior to day 270, NO_x (and thus NO) is kept at very low concentrations by the formation of ClONO₂ from ClO and NO₂ leading to the extremely high concentrations of ClONO₂ that peak around day 276. After day 278 Cl levels relax to background levels. High Cl concentrations enhance cycle C2 and thus HO_x production. Therefore, the double peak structure for Cl is also apparent for CH₂O (Fig. 2) and HO₂ (Fig. 3).

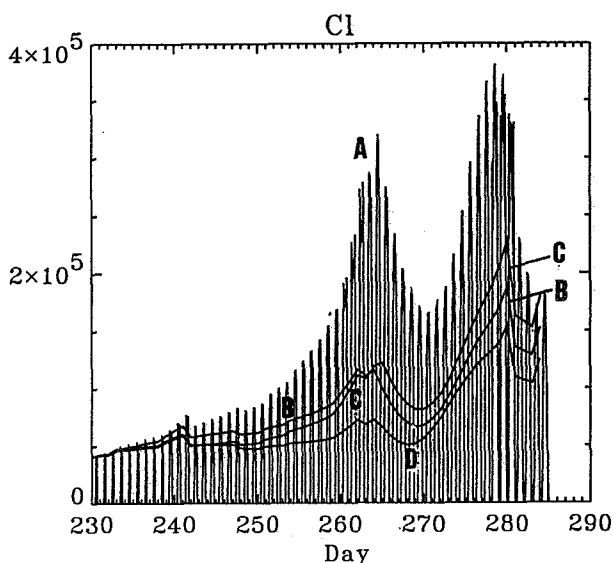


Fig. 4. As Fig. 3, but for Cl concentration in molecules/cm³. The extreme variability shown in case A represents the diurnal variation in Cl. For cases B, C and D only daily maximum values are shown.

CONCLUSIONS

We have underlined the importance of reactions R2 and R5 in "ozone hole" chemistry. In particular, under sunlight conditions reaction R2 is the main source of active chlorine and indirectly, through cycle C1, the main sink of HO_x as long as NAT surfaces are available to catalyse heterogeneous reactions. Also under these conditions, high levels of chlorine radicals lead to a significant replenishment of the HCl reservoir through reactions R6, R14, R16 and R21. However, reaction R5 would then control the levels of CH₃O₂ through cycle C2 and thereby strongly reduce the efficiency of the reactions producing HCl. Moreover, in cycle C2 CH₄ is oxidized to CH₂O without the loss of HO_x radicals. In contrast, in the competing cycles C4, C5 and C6, HO_x is lost. The decomposition of CH₂O to CO however, constitutes a considerable source of HO_x.

The drastic changes in ClONO₂, HOCl, HCl, CH₂O and HO₂ after evaporation of NAT predicted by the inclusion of reactions R2 and R5 should offer a focus for testing our theory. We therefore recommend both further investigation of the rate coefficients of R2 and R5 and atmospheric observations of the afore mentioned trace substances.

REFERENCES

- Abbatt, J.P.D. and M.J. Molina. The heterogeneous reaction HOCl + HCl → Cl₂ + H₂O on ice and nitric acid trihydrate: reaction probabilities and stratospheric implications, *Geophys. Res. Lett.*, **19**, 461-464, 1992.
- Anderson, J.G., D.W. Tooney and W.H. Brune. Free radicals within the Antarctic Vortex: the Role of CFCs in the Antarctic Ozone Loss, *Science*, **251**, 39-46, 1991.
- Crutzen, P.J., R. Müller, Ch. Brühl and Th. Peter. On the potential importance of the gas phase reaction CH₃O₂ + ClO → ClOO + CH₃O and the heterogeneous reaction HOCl + HCl → H₂O + Cl₂ in "Ozone Hole" chemistry, *Geophys. Res. Lett.*, **19**, 113-116, 1992.
- Deshler, T. and D.J. Hofmann. Ozone Profiles at McMurdo Station, Antarctica, The Austral Spring of 1990, *Geophys. Res. Lett.*, **18**, 657-660, 1991.
- Fahey, D.W., K.K. Kelly, S.R. Kawa, A.F. Tuck, M. Lowenstein, K.R. Chun and L.E. Heidt. Observations of denitrification and dehydration in the winter polar stratosphere, *Nature*, **344**, 321-324, 1990.
- Hanson, D.R. and K. Mauersberger. Laboratory studies of the nitric acid trihydrate: implications for the south polar stratosphere, *Geophys. Res. Lett.*, **15**, 855-858, 1988.
- Hanson, D.R. and A.R. Ravishankara. The reaction probabilities of ClONO₂ and N₂O₅ on 40 to 75% sulfuric acid solutions, *J. Geophys. Res.*, **96**, 17307-17314, 1991.
- Hanson, D.R. and A.R. Ravishankara. Investigation of the reactive and nonreactive processes involving ClONO₂ and HCl on water and nitric acid doped ice, *J. Phys. Chem.*, **96**, 2682-2691, 1992.
- Horie, O., J.N. Crowley and G.K. Moortgat. Methylperoxy self-reaction: Products and branching ratio between 223 and 333 K, *J. Phys. Chem.*, **94**, 8198-8203, 1990.
- Kelly, K.K. et al. Dehydration in the lower Antarctic stratosphere during late winter and early spring, 1987, *J. Geophys. Res.*, **94**, 11317-57, 1989.
- Molina, L.T. and M.J. Molina. Production of Cl₂O₂ from the self-reaction of the ClO radical, *J. Phys. Chem.*, **91**, 433-436, 1987.
- Murcray, F.J., A. Goldman and R. Blatherwick. HNO₃ and HCl amounts over McMurdo during spring of 1987, *J. Geophys. Res.*, **94**, 16615-16618, 1989.
- Prather, M.J. More rapid polar ozone depletion through the reaction of HOCl with HCl on polar stratospheric clouds, *Nature*, **355**, 534-537, 1992.
- Simon, F.G., J.P. Burrows, W. Schneider, G.K. Moortgat and P.J. Crutzen. Study of the Reaction ClO + CH₃O₂ → Products at 300 K, *J. Phys. Chem.*, **93**, 7807-7813, 1989.
- Toon, G.C., C. B. Farmer, L. L. Lowes, P. W. Schaper, J.-F. Blavier and R. H. Norton. Infrared Aircraft Measurements of Stratospheric Composition Over Antarctica During September 1987, *J. Geophys. Res.*, **94**, 16571-16596, 1989.

303625

EFFECTS OF STRATOSPHERIC AEROSOL SURFACE PROCESSES ON THE
LLNL TWO-DIMENSIONAL ZONALLY AVERAGED MODEL

Peter S. Connell, Douglas E. Kinnison, and Donald J. Wuebbles
Lawrence Livermore National Laboratory
Livermore, California 94550, USA

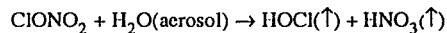
Joel D. Burley and Harold S. Johnston
Department of Chemistry, University of California, Berkeley
and
Chemical Sciences Division, Lawrence Berkeley Laboratory
Berkeley, California 94720, USA

ABSTRACT

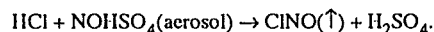
We have investigated the effects of incorporating representations of heterogeneous chemical processes associated with stratospheric sulfuric acid aerosol into the LLNL two-dimensional, zonally averaged, model of the troposphere and stratosphere. Using distributions of aerosol surface area and volume density derived from SAGE II satellite observations, we were primarily interested in changes in partitioning within the Cl- and N- families in the lower stratosphere, compared to a model including only gas phase photochemical reactions. We have considered the heterogeneous hydrolysis reactions



and



alone and in combination with the proposed formation of nitrosyl sulfuric acid (NSA) in the aerosol and its reaction with HCl



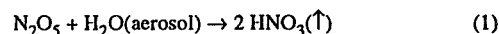
Inclusion of these processes produces significant changes in partitioning in the NO_y and ClO_y families in the middle stratosphere.

INTRODUCTION

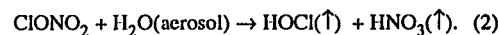
Numerical models of the troposphere and stratosphere including only gas-phase homogeneous photochemical processes can reproduce many of the observed features of trace constituent distributions. However, homogeneous models can not represent the chemical processes (Solomon, 1988) responsible for the observed lower stratosphere winter polar behavior of ozone and partitioning among the nitrogen and chlorine species. These processes require local temperatures low enough to condense water or a mixture of nitric acid and water into particles providing a surface for heterogeneous reactions which transform more stable chlorine reservoir species into more labile species.

Homogeneous models also fail to produce the bias toward nitric acid observed in the partitioning of the

nitrogen oxide family at mid and high latitudes in the winter hemisphere. Two reactions of importance that would take place on the surface of stratospheric sulfuric acid aerosol have been identified through laboratory investigation (Hofmann and Solomon, 1989, and WMO/UNEP, 1992)



and

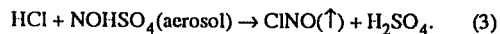


Both reactions convert NO_x to HNO_3 , supplementing the homogeneous termolecular reaction of OH with NO_2 .

In consideration of the upcoming availability of a vastly increased data base of stratospheric trace species from the Upper Atmospheric Research Satellite (UARS), we have investigated the effects, in a numerical atmospheric model, that the sulfuric acid aerosol reactions above would have on species distributions, compared to inclusion of only gas phase processes. In this model study we have used an aerosol burden representing a climatological average of several years of SAGE II satellite data (WMO/UNEP, 1992), but, in order to distinguish the effects of the sulfuric acid aerosol reactions, have not included processes related to polar stratospheric clouds (PSC). Future direct comparison to UARS observations will be done with inclusion of the observed aerosol burden as perturbed by the Mt. Pinatubo eruption, as well as with PSC processes.

We have also taken a preliminary look at the effects of an additional process proposed to occur in sulfuric acid aerosol of appropriate composition. Nitrosyl sulfuric acid (NOHSO_4) has been tentatively identified as a common constituent of stratospheric sulfuric acid aerosol (Farlow et al., 1977) and is known from bulk phase laboratory work to be capable of existence as an ionic solute or solid within a range of sulfuric acid concentration and temperature characteristic of stratospheric aerosol. Burley and Johnston (1992) have shown that, based on current thermodynamic knowledge of the system, it is

possible that gaseous HCl in the stratosphere could react with NSA present in aerosol to produce nitrosyl chloride



ClNO absorbs in the near ultraviolet with breaking of the Cl-N bond. Reaction (3), if it occurs, would then act to shift the partitioning of ClO_y toward Cl-containing radical species and temporary Cl reservoirs, such as ClONO_2 , and away from HCl. Its importance depends on its magnitude compared to the reaction of OH with HCl, which also releases Cl.

MODEL DESCRIPTION

The model used in this study is a version of the Lawrence Livermore National Laboratory (LLNL) two dimensional model of the troposphere and stratosphere, with about 10° latitude resolution and 3 km vertical resolution in the stratosphere extending from pole to pole and the surface to 60 km. The gas phase homogeneous photochemistry in the model encompasses about 50 species and 120 thermal and photolytic reactions, for which kinetic and spectral parameters are taken from current recommendations (NASA, 1990). The circulation in the model is calculated interactively from the net heating rates resulting from the modeled species distributions and a climatological temperature field. In order to isolate the local photochemical effects of, for example, additional reactions, the circulation can be fixed to a previously calculated result.

Reactions (1) and (2) are treated as kinetically controlled, where the rate of the reaction is proportional to the rate of collision through the dimensionless reaction probability γ . The first order rate constant for reaction is given by

$$k = \frac{\bar{v}}{4} \gamma \mathcal{S}$$

where \bar{v} is the average molecular velocity and \mathcal{S} is the aerosol surface area density. In this study, ν is taken to be 5200 cm s^{-1} for both N_2O_5 and ClONO_2 throughout the model domain. Based on laboratory results, the reaction probability for N_2O_5 is assigned 0.1. For ClONO_2 the reaction probability is given by

$$\gamma(2) = 0.006 \exp(-0.15(T - 200)),$$

where the temperature dependence arises from the dependence of the reaction probability on aerosol composition, which is in turn dependent on temperature.

Surface area density for this study is based on an analysis of SAGE II data by Poole et al. (WMO/UNEP, 1992) and is representative of an average atmosphere unperturbed by any major recent volcanic eruption. The prescribed values are functions of altitude, latitude, and, coarsely, season, extending from 12 to 32 km and pole to pole.

Minimum and maximum values are about 0.025 and $1.75 \times 10^{-8} \text{ cm}^2 \text{ cm}^{-3}$, respectively.

The rate constant for the proposed reaction of HCl with NSA dissolved or incorporated in the aerosol should depend on the NSA concentration in the aerosol, and may be controlled either by the collisional rate constant for HCl with the particle and an associated reaction probability, or by the Henry's Law solubility for HCl and a solution phase rate constant. The presence of NSA in the aerosol depends on the concentration of H_2SO_4 . According to Burley and Johnston (1992), NSA can be present at lower stratospheric temperatures when the H_2SO_4 weight per cent exceeds about 60%. The aerosol composition in the model was determined by interpolating from the tabulated results of Jaeger-Voirol (Jaeger-Voirol et al., 1990) for binary $\text{H}_2\text{O}/\text{H}_2\text{SO}_4$ mixtures, using the model temperature and water partial pressure. Fig. 1 below shows the calculated values for July. The modeled concentration is generally below 60% in the lowest portion of the aerosol distribution, but above 60% in the 15-30 km region of greatest importance to ozone controlling processes.

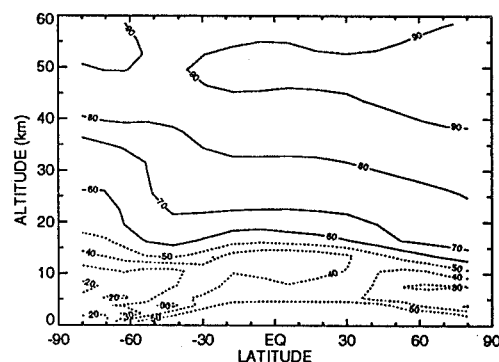
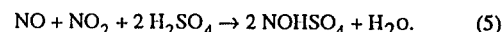


Figure 1. Derived composition of July stratospheric sulfuric acid aerosol in H_2SO_4 weight per cent. Solid contours are greater than 60 per cent. Dashed contours are smaller than 60 per cent.

Burley and Johnston (1992) propose several possible formation reactions for NSA, involving various NO_y species, including



and



Farlow et al (1977) tentatively observed solid NSA crystals in the collected aerosol, which would be formed when the NSA concentration in the aerosol exceeded its solubility in H_2SO_4 . A proper calculation of the NSA abundance would require representing the processes of aerosol formation, growth, and loss, as well as the heterogeneous NSA-forming reactions. In this preliminary study we have assumed that the processes forming and destroying NSA are rapid compared to its abundance, allowing

the use of a steady state expression for NSA abundance. The formation rate is taken as equal to the NO/aerosol collision rate times a reaction probability of 0.01, following Burley and Johnston (1992). The NSA loss rate is assumed to be the HCl/aerosol collision rate times a reaction probability representing the relative abundance of NSA to H₂SO₄ at the particle surface, so that the atmospheric concentration of NSA is

$$[\text{NSA}(ss)] \equiv \left(2 \cdot 0.01 \cdot [\text{NO}] \cdot \frac{V\{\text{H}_2\text{SO}_4\}^{3/2}}{[\text{HCl}]} \right)^{3/2}$$

V is the aerosol volume density and $\{\text{H}_2\text{SO}_4\}$ is the concentration of sulfuric acid in the aerosol. V is simply scaled from the surface area density assuming that the surface area in 1 cm³ of atmosphere is on one spherical particle. Fig. 2 shows the resulting atmospheric concentration of NSA when these assumptions are made. The values are typically a few per cent or less of the H₂SO₄ concentration.

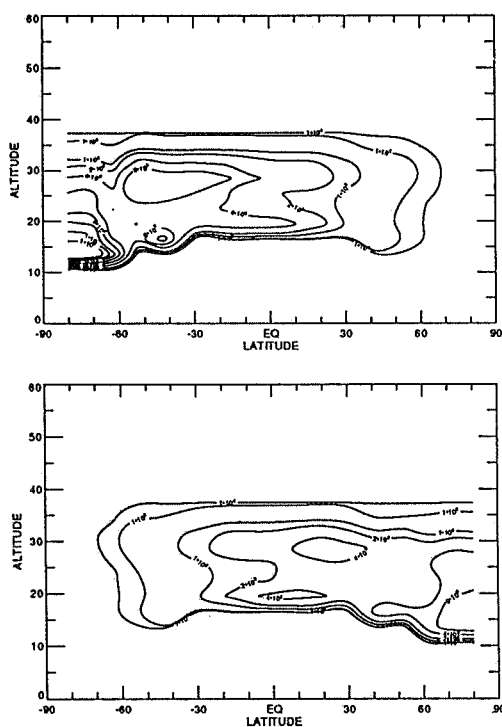


Figure 2. Calculated steady state concentration of NSA in mol cm⁻³. (a) December, (b) July.

Given these assumptions, the rate of HCl loss and ClNO production in reaction (3) is expressed as

$$\frac{d[\text{ClNO}]}{dt} = \frac{\bar{v}}{4} \frac{S}{(V\{\text{H}_2\text{SO}_4\})^{3/2}} [\text{HCl}][\text{NSA}(ss)].$$

The calculated rate of HCl + NSA is compared to the rate of OH + HCl in Fig. 3.

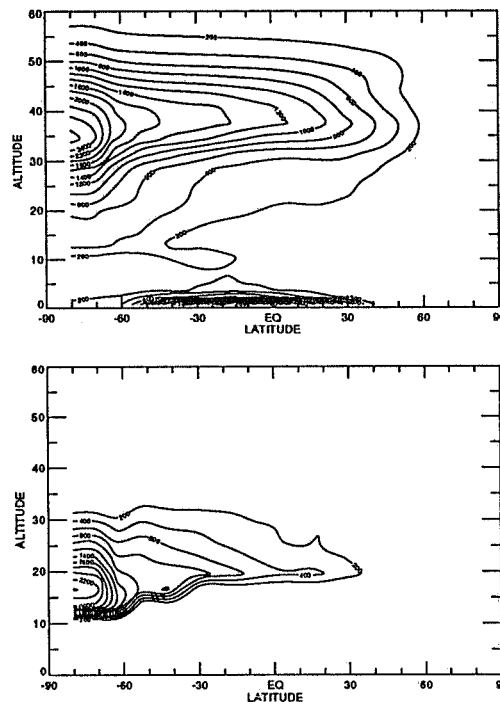


Figure 3. Calculated rates of reaction in December (molecules cm⁻³ s⁻¹) for (a) HCl + OH → Cl + H₂O, and (b) HCl + NSA → ClNO + H₂SO₄.

The model was integrated to steady state using 1990 ambient boundary conditions for the source species, establishing the circulation for the case including reactions (1)-(3). This circulation was then prescribed for integrations to steady state for the case including reactions (1) and (2) and for the case of only gas phase reactions.

RESULTS

An expected major effect of both reactions (1) and (2) is a large increase in HNO₃ (Fig. 4) at middle and upper latitudes particularly in winter and spring, where the rates of (1)+(2) become larger than the rate of OH + NO₂ + M. This is shown in Fig. 5, where in December, the heterogeneous processes dominate northward of about 30°.

As HNO₃ increases, other NO_y family members, particularly NO, NO₂, and N₂O₅, show a corresponding decrease. The abundance of ClONO₂ changes little because the γ for reaction (2) is fairly small except in the southern high latitude winter. The effect on ozone of reactions (1) and (2) is to increase the importance of the ClO_x destruction catalytic cycles while somewhat diminishing the dominant position of the NO_x cycle between 20 and 30 km. The net overall effect on ozone is a slight increase of

0.11% relative to the total abundance in the gas phase case.

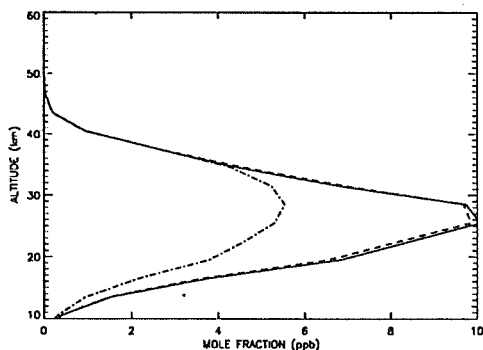


Figure 4. Derived HNO_3 mole fraction at 62°N in December. Solid line includes reactions (1) and (2), dashed line includes (1)-(3), dot-dash line includes only gas phase photochemistry.

The addition of reaction (3) and the associated NSA formation and ClONO photolysis reactions do not produce significant further changes in NO_y partitioning (Fig. 4). However, as expected, ClO and

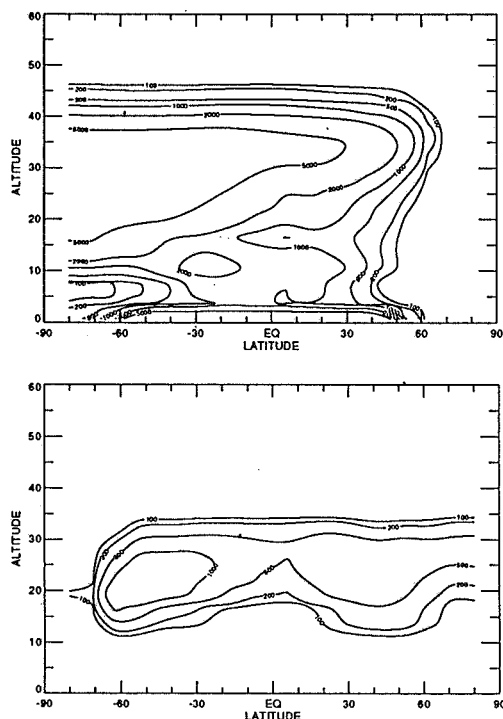


Figure 5. Calculated rates of HNO_3 production in December ($\text{mol cm}^{-3} \text{s}^{-1}$). (a) $\text{NO}_2 + \text{OH} + \text{M} \rightarrow \text{HNO}_3 + \text{M}$, (b) Sum of $\text{N}_2\text{O}_5 + \text{H}_2\text{O}(\text{aerosol}) \rightarrow 2 \text{HNO}_3$ and $\text{ClONO}_2 + \text{H}_2\text{O}(\text{aerosol}) \rightarrow \text{HOCl} + \text{HNO}_3$.

ClONO_2 are substantially increased between 20 and 30 km globally, while HCl decreases. Fig. 6 shows that in some regions of the stratosphere, with the

inclusion of reaction (3), ClONO_2 becomes the dominant inorganic Cl-containing species. Total ozone abundance is decreased by about 3% relative to the gas phase case, with the largest effects in regions where the photochemical ozone lifetime is long and the enhancement of ClO produces proportionately a larger reduction in local ozone abundance.

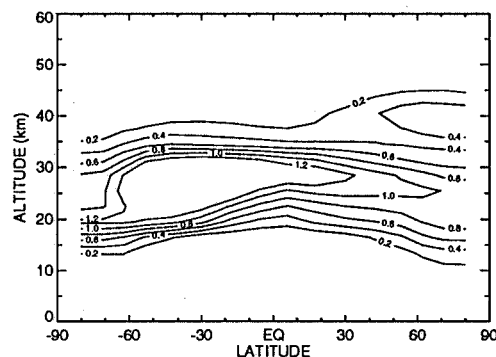


Figure 6. Calculated ratio of ClONO_2 to HCl in December with NSA included. Where the value exceeds 1, ClONO_2 is the dominant inorganic Cl species.

CONCLUSION

This preliminary study of the effects, on trace species distributions, of heterogeneous processes taking place on stratospheric sulfuric acid aerosol provides some guidance for consideration of observations of NO_y and ClO_y family members. A strong enhancement of HNO_3 in the partitioning in the NO_y family at winter high latitudes is an indicator of aerosol moderated hydrolysis of N_2O_5 , while NO , NO_2 , and N_2O_5 are substantially decreased. With the proposed NSA-related chemistry, ClONO_2 is made the major inorganic Cl-containing species in the 24-31 km region.

Future improvements in our knowledge of the thermodynamic and kinetic properties of the sulfuric acid aerosol/ $\text{H}_2\text{O}/\text{NO}_y$ system will allow better model representation of NSA and related chemistry than was attempted here.

Consideration of heterogeneous chemistry on or within sulfuric acid aerosol is important for understanding of natural and anthropogenic influences on the stratosphere. Comparisons to observations of the UARS satellite and other data may provide evidence for the importance of these processes.

ACKNOWLEDGMENTS

This work was performed under the auspices of the U.S. Department of Energy by the Lawrence Livermore National Laboratory under contract No. W-7405-Eng-48 and was supported in part by the NASA Upper Atmospheric Research Satellite Program.

REFERENCES

- Burley, J. D., and H. S. Johnston, 1992: Ionic Mechanisms for Heterogeneous Stratospheric Reactions and Ultraviolet Photo-absorption Cross Sections for NO_2^+ , HNO_3 , and NO_3^- in Sulfuric Acid Solutions. *Geophys. Res. Lett.* (in press).
- Burley, J. D., and H. S. Johnston, 1992: Nitrosyl Sulfuric Acid and Stratospheric Aerosols. *Geophys. Res. Lett.* (in press).
- Farlow, N. H., D. M. Hayes, and H. Y. Lem, 1977: Stratospheric Aerosol: Undissolved granules and physical state. *J. Geophys. Res.*, 82, 4921-4929.
- Hofmann, D. J., and S. Solomon, 1989: Ozone Destruction Through Heterogeneous Chemistry Following the Eruption of El Chichon. *J. Geophys. Res.*, 82, 4921-4929.
- Jaccker-Voirol, A. J., L. Ponche, and P. Mirabel, 1990: Vapor Pressures in the Ternary System Water-Nitric Acid-Sulfuric Acid at Low Temperatures. *J. Geophys. Res.*, 95, 11857-11863, 22565.
- NASA Panel for Data Evaluation, 1990: Chemical Kinetics and Photochemical Data for Use in Stratospheric Modeling. Evaluation No. 9, JPL Publication 90-1.
- Solomon, S., 1988: The Mystery of the Antarctic Ozone Hole. *Rev. Geophys.*, 26, 131-148.
- World Meteorological Organization, and United Nations Environment Programme, 1992: 1991: Scientific Assessment of Ozone Depletion. in press.

308627

EVOLUTION OF CHEMICALLY PROCESSED AIR PARCELS IN THE LOWER STRATOSPHERE

Richard S. Stolarski, Anne R. Douglass, and Mark R. Schoeberl

Laboratory for Atmospheres
NASA Goddard Space Flight Center
Greenbelt, Maryland 20771, USA

ABSTRACT

Aircraft, ground-based, and satellite measurements indicate large concentrations of ClO in the lower stratosphere in and near the polar vortex (Anderson, et al., 1989; Brune et al., 1990; de Zafra, et al., 1987; Waters et al., 1993). The amount of local ozone depletion caused by these large ClO concentrations will depend on the relative rates of ozone loss and ClO recovery. ClO recovery occurs when NO_x from HNO₃ photolysis, reacts with ClO to form ClONO₂. We show that air parcels with large amounts of ClO will experience a subsequent ozone depletion that depends on the solar zenith angle. When the solar zenith angle is large in the middle of winter, the recovery of the ClO concentration in the parcel is slow relative to ozone depletion. In the spring, when the solar zenith angle is smaller, the ClO recovery is much faster. After ClO recovery, the chlorine chemistry has not returned to normal. The ClO has been converted to ClONO₂. ClO production from further encounters with PSCs will be limited by the heterogeneous reaction of ClONO₂ with water. Large ozone depletions, of the type seen in the Antarctic, occur only if there is significant irreversible denitrification in the air parcel.

INTRODUCTION

We have developed a version of our photochemistry model (Douglass et al., 1989) to calculate chemical changes occurring along the path of a stratospheric air parcel. In this study we apply the model to the simple case of a parcel which is fixed at a given latitude and altitude; 50°N and 20 km. The chemistry of the parcel is initialized by assuming that the air has been fully processed by heterogeneous reactions on the surface of NAT particles; i.e. all of the reactive nitrogen is HNO₃ and all of the inorganic chlorine is ClO or Cl₂O₂ (Jones et al., 1990; Brune et al., 1990; Fahey et al., 1990). Parcels are started at the beginning of each month of the northern winter and spring (November through April) and are allowed to evolve chemically for 30 days. At this point, ozone loss greater than that expected from normal photochemistry has ceased. Details of the assumed initial conditions are shown in Table 1.

Starting Date	January 1 or April 1
Pressure	50 mbar
Temperature	210 K
ClO + 2Cl ₂ O ₂	2.5 ppbv
ClONO ₂	0.0
HCl	0.0
HNO ₃	15 ppbv
NO _x	0.0

Table 1. Parcel initialization conditions. Integration of the gas-phase chemical equations is carried out for 30 days from starting date.

MODEL RESULTS

Ozone loss calculated from two model runs are shown in Figure 1. One run begins January 1 while the other begins April 1. On the first day after initialization,

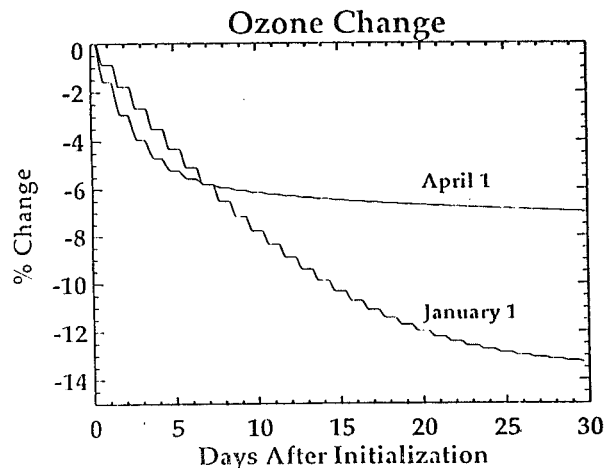


Fig. 1. Calculated ozone change as a function of time after parcel initialization. Results are shown for two parcels, one initialized on January 1, the other on April 1.

both parcels have about the same ClO concentration and lose ozone at the same rate. The parcel released on April 1 experiences a longer period of sunlight and thus loses more ozone. As the parcels evolve, the one released on April 1 exhibits a rapid recovery of ClO as illustrated in Figure 2. Thus, the rate of ozone loss for the April 1 parcel diminishes each day such that by day 4, the total ozone lost is the same as that lost by the January 1 parcel despite the difference in the length of day. By day 6, the cumulative ozone loss in each of the parcels is the same and on all succeeding days, the ozone loss is greater for the parcel released on January 1. The somewhat surprising result is that the parcel which was fully processed by January 1 lost 13% of its initial ozone, while the parcel which was fully processed on April 1 lost only 7% of its initial ozone.

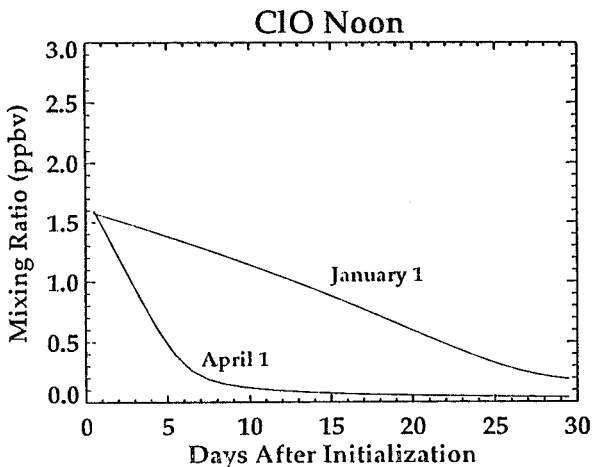


Fig. 2. Calculated noontime ClO mixing ratio as a function of time after parcel initialization. Actual calculated ClO exhibits a strong diurnal variation with a noon maximum.

The recovery of the ClO concentration is controlled by NO_x which is generated by the photolysis of HNO_3 . Because the parcel has a very high ClO concentration, the NO_x generated is rapidly converted to ClONO_2 . For the April 1 parcel, the ClONO_2 concentration rises rapidly to 2.5 ppbv, using up all of the available chlorine as illustrated in Figure 3. The January 1 parcel shows a slower rise, but still goes to 2.5 ppbv after 30 days. Figure 4 illustrates that the chlorine nitrate concentration rises at almost exactly the rate of the disappearance of HNO_3 . When the ClONO_2 concentration reaches 2.5 ppbv, no more ClO is available, and NO_x begins to accumulate. At the end of 30 days, the HCl concentration is barely more than 0.2 ppbv for the April 1 parcel and about 0.1 ppbv for the January 1 parcel.

The reason for the change in the relative efficiency of ozone loss to ClO recovery can be understood by examining the photolysis rates for Cl_2O_2 and HNO_3 . Figure

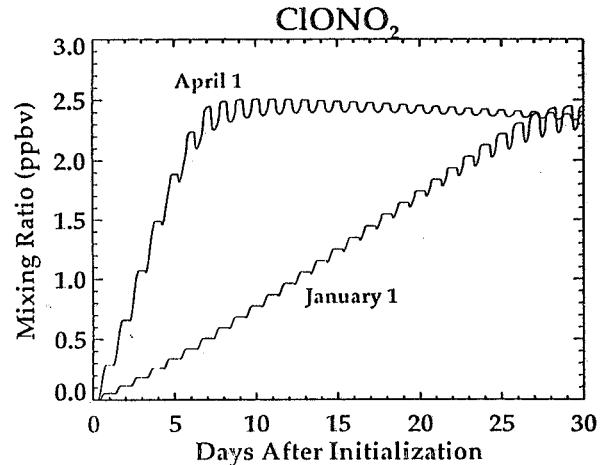


Fig. 3. Calculated ClONO_2 mixing ratio as a function of time after parcel initialization.

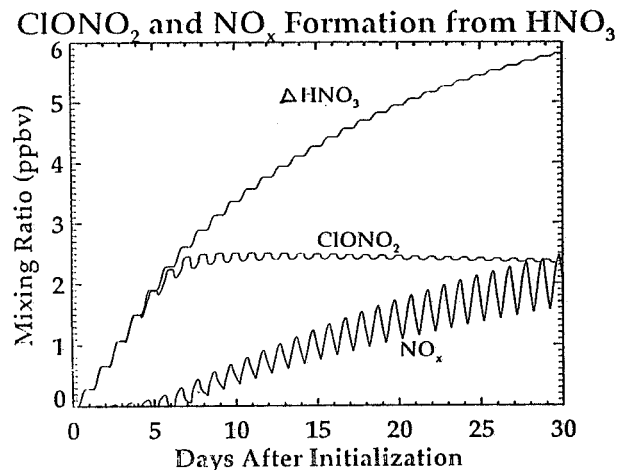


Fig. 4. Comparison of calculated ClONO_2 mixing ratio as a function of time with the rate of disappearance of HNO_3 . When all of the chlorine is used up to form ClONO_2 , the NO_x mixing ratio begins to rise.

5a shows the diurnal variation of the HNO_3 photolysis rate on January 1 compared to April 1. Figure 5b shows the same thing for the photolysis rate of Cl_2O_2 . Cl_2O_2 , because of its near uv absorption, is photolyzed about 70% as rapidly on January 1 as on April 1. HNO_3 , on the other hand, is photolyzed only about 35% as rapidly on January 1. For a given amount of ClO, the rate of ozone destruction by the ClO dimer cycle is determined by the Cl_2O_2 photolysis rate. It can be seen from Figure 5 that the sun effectively rises faster for ozone destruction than it does for ClO recovery.

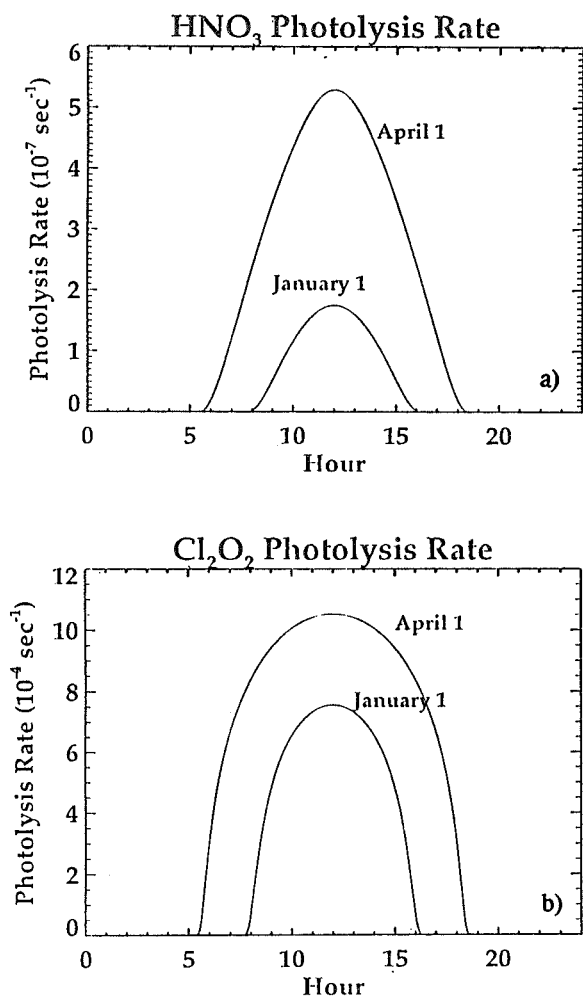


Fig. 5. a) Diurnal cycle of the HNO₃ photolysis rate for January 1 and April 1, b) same for Cl₂O₂.

CONCLUSION

Ozone depletion occurring in parcels of lower stratospheric air, which have been processed through a PSC, is limited by the recovery of the high ClO concentrations to chlorine nitrate. Parcels processed in the middle of winter showed more subsequent ozone depletion than those processed in the spring. A parcel which was initialized on January 1 with all of the chlorine as ClO and Cl₂O₂, and all of the reactive nitrogen as HNO₃, lost 13% of its ozone in the next 30 days. A parcel similarly initialized on April 1, lost only 7% of its ozone in 30 days. The explanation has been shown to be related to the relative photolysis rates of Cl₂O₂ and HNO₃, which govern the competition between ozone loss and ClO recovery.

If the chemically perturbed air from these parcels is processed through a subsequent PSC, reconversion of ClONO₂ to ClO cannot occur via reaction with HCl because of the slow recovery of HCl. The effect of further PSC processing will be limited by the reaction of ClONO₂ with water. However, if the air has been denitrified, large ozone depletions can occur because chlorine nitrate formation will be inhibited. In this case, recovery will be controlled by the resupply of active nitrogen to the parcel by mixing processes.

REFERENCES

- Anderson, J.G., W.H. Brune, S.A. Lloyd, D.W. Toohy, S.P. Sander, W.L. Starr, M. Loewenstein, and J.R. Podolske, 1989: Kinetics of O₃ destruction by ClO and BrO within the Antarctic vortex: An analysis based on in situ ER-2 data. *J. Geophys. Res.*, 94, 11480-11520.
- Brune, W.H., D.W. Toohy, J.G. Anderson, and K.R. Chan, 1990: In situ observations of ClO in the Arctic stratosphere: ER-2 Aircraft Results from 59°N to 80°N. *Geophys. Res. Lett.*, 17, 505-508.
- de Zafra, R.L., M. Jaramillc, A. Parrish, P. Solomon, B. Connor, and J. Barrett, 1987: High concentrations of chlorine monoxide at low altitudes in the Antarctic spring stratosphere: diurnal variation, *Nature*, 328, 408-411.
- Douglass, A.R., C.H. Jackman, and R.S. Stolarski, 1989: Comparison of model results transporting the odd nitrogen family with results transporting separate odd nitrogen species. *J. Geophys. Res.*, 94, 9862-9872.
- Fahey, D.W., S.R. Kawa, and K.R. Chan, 1989: Nitric oxide measurements in the Arctic winter stratosphere. *Geophys. Res. Lett.*, 17, 489-490.
- Jones, R.L., D.S. McKenna, L.R. Poole, and S. Solomon, 1989: Simulating the evolution of the chemical composition of the 1988/89 winter vortex. *Geophys. Res. Lett.*, 17, 549-552.
- Waters, J.W., L. Froidevaux, W.G. Read, G.L. Manney, L.S. Elson, D.A. Flower, R.F. Jarnot, and R.S. Harwood, 1993: Stratospheric ClO and ozone from the Microwave Limb Sounder on the Upper Atmosphere Research Satellite. *Nature*, 362, 597-602.

303628

OBSERVATIONAL EVIDENCE AND DYNAMICAL INTERPRETATION OF THE TOTAL OZONE VARIATIONS IN THE EQUATORIAL REGION

Masato Shiotani

Department of Geophysics, Faculty of Science
Kyoto University, Kyoto 606, Japan

Fumio Hasebe

Institute for Terrestrial and Planetary Atmospheres
State University of New York, Stony Brook, New York 11794-3800, USA

1 Introduction

The total ozone amount is sensitive to the general circulation changes in the lower stratosphere due to the photochemically inactive nature of ozone there. In the equatorial region, such circulation changes arise from the quasi-biennial oscillation (QBO) of the stratospheric zonal wind and the El Niño/Southern Oscillation (ENSO). In the first half of this study we present observational results of the long-term variations in the equatorial ozone field using the 11-year Total Ozone Mapping Spectrometer (TOMS) data, by paying special attention to the longitudinal structure. In the latter half we try to understand quantitatively these variations by using a simple mechanistic relationship. We hypothesize that the ozone modulating processes are attributable to two dynamical effects, the advection effect and tropopause effect, owing to the strong vertical stratification of ozone existing just above the tropopause. The advection effect comes from the vertical motion which maintains the temperature structure, compensating for the radiative damping. The tropopause effect is associated with the altitude change of the tropopause. The total ozone variations in the tropics is discussed in terms of these two dynamical processes with the aid of mechanistic equations combined with the wind and sea surface temperature (SST) observations. The interactions between tropical and extratropical latitudes are beyond the scope of this study. Photochemical effects are also neglected. Details of this study are given by Shiotani (1992) and Hasebe (1992).

2 Observational Evidence

2.1 Annual Variation

From Fig. 1, showing a time-longitude section of the monthly mean total ozone field, we see that an annual variation with a zonal wavenumber one component is prominent over the equator. The climatological features of the annual cycle are summarized as follows: (1) Zonal mean values are maximum around September and minimum around January. (2) All the year round, the zonal wavenumber one pattern is persistent with minimum values between 140°E and the date line. (3) The wave 1 amplitudes are maximum around September. The location of minimum total ozone around the western Pacific is suggestive of the vigorous convective activity there.

These features in total ozone are closely related to the temperature field in the lower stratosphere. By using the 100–50 mb layer mean temperature field estimated from the SSU (stratospheric sounding unit) thickness data for 1980 to 1989 (not shown), the climatological features of the annual cycle in the lower stratosphere temperature field are summarized as follows: (1) Zonal mean values are maximum around August and minimum around March. (2) The zonal wavenumber one pattern is persistent with minimum values between 140°E and the date line. (3) The wave 1 amplitudes show a semiannual variation with maximum values around July and December. The annual variation in the lower stratosphere temperature field is basically similar to that in the total ozone field, in the sense that cold (warm) temperature in space and time corresponds approximately to low (high) total ozone.

2.2 QBO

Though the total ozone variation has a clear annual component over the equator, the annual cycle is modulated by much longer time-scale variations. Fig. 2 shows a time-longitude section of the monthly mean anomaly field; the anomaly field was constructed by subtracting the climatological (11-year mean) annual cycle from the original data. There is a clear signal of the QBO in total ozone having a zonally uniform phase structure. The amplitude of the QBO variation is about 10 DU (Dobson unit), which is of comparable order to the annual variation. Because of its strong zonality, there have been many studies of the equatorial total ozone QBO on the basis of station data and/or zonal mean satellite data (e.g., Angell and Korshover, 1973; Oltmans and London, 1982; Hilsenrath and Schlesinger, 1981; Bowman, 1989). Thus, we will not make a detailed discussion here.

2.3 ENSO Cycle

Subtracting zonal mean values from Fig. 2 to see variations in longitudinal anomaly, there appears to be an east-west seesaw pattern with a nodal longitude around the date line (Fig. 3 (a)). This east-west variation has a characteristic time-scale of about 4 years, and is clearly related to the El Niño and the Southern Oscillation (ENSO) cycle. The Southern Oscillation is one of the prominent climate anomalies in the equatorial atmosphere, showing

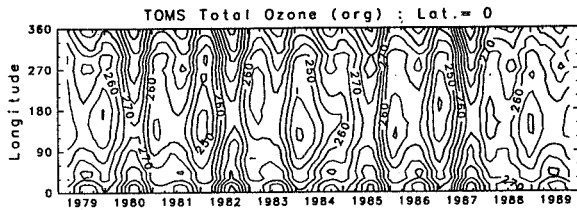


Fig. 1 Time-longitude section of the monthly mean total ozone field over the equator (contour interval 5 DU; Dobson unit); a 5-month running mean was applied.

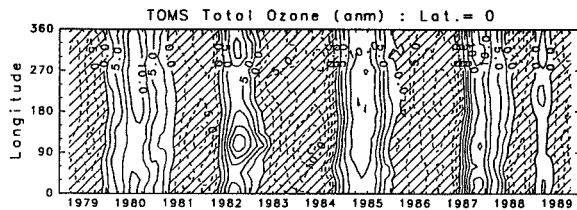


Fig. 2 Time-longitude section of the monthly mean anomaly field of total ozone over the equator (contour interval 2.5 DU, negative values are hatched); a 5-month running mean was applied.

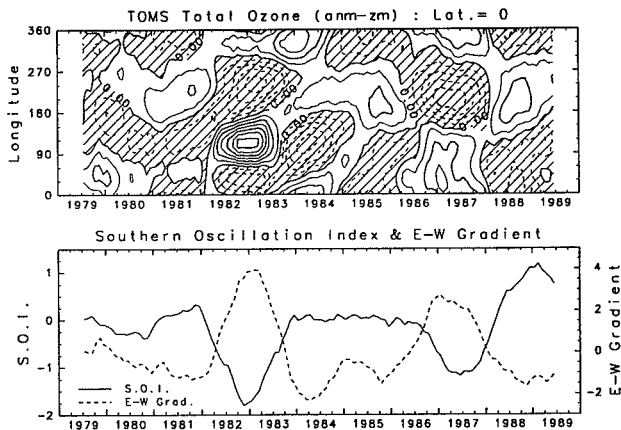


Fig. 3 (a) Time-longitude section of the monthly mean anomaly field of total ozone over the equator (zonal mean values are subtracted, contour interval 1 DU, negative values are hatched) and (b) line plots of the Southern Oscillation Index (solid line) and the east-west gradient of the total ozone anomaly field (dashed line); a 13-month running mean was applied. For definition, see text.

a standing variation of pressure anomalies between the Indian Ocean and the Pacific Ocean in an opposite sense. This variation is mutually coupled with the SST variation in the eastern Pacific Ocean, particularly with warm SST anomaly events: the so-called El Niño. As an index representing this fluctuation, we usually use the Southern Oscillation Index (S.O.I.) which is a measure of the pressure gradient between Tahiti (18°S, 150°W) and Darwin (12°S, 131°E). In Fig. 3 (b), the S.O.I. adopted from Monthly Report on Climate System by the Japan Meteorological Agency (1991) is plotted in solid line. Plotted in dashed line is the east-west gradient of the total ozone anomaly field defined by the difference between averages of the western Pacific region (60°- 165°E) and the eastern Pacific region (75°- 180°W). During the El Niño events (1982-83, 1986- 87) when the S.O.I. has large negative values, there are positive anomalies in the western Pacific and negative anomalies in the eastern Pacific, resulting in positive east-west gradient of the total ozone anomaly field; the anomaly pattern, thus the gradient, is reversed during the anti-El Niño events.

Because the sea surface temperatures in the eastern Pacific are higher during El Niño events than during anti-El Niño events, an active region of convective clouds moves relatively eastward; this must bring about a change in longitudinal structure of the tropopause height. According to Gage and Reid (1987), the tropopause potential temperature during El Niño events is warm at Koror (7°N, 134°E) as compared to Majuro (7°N, 171°E), and thus the difference in the tropopause potential temperature and also in the tropopause height between the two stations is correlated well with the S.O.I. These tropical tropopause properties related with the ENSO events support our results; the eastward movement of active convective region during the ENSO events should be accompanied with relatively higher tropopause in the eastern Pacific so as to reduce the total amount of ozone as followed by the mechanism introduced in the following section.

3 Dynamical Interpretation

3.1 Response to zonal wind QBO

The total ozone QBO in the tropics is believed to be driven by vertical ozone advection. On the time scale of the QBO, the geostrophic approximation is valid even quite near the equator. Then the vertical wind shear of the mean zonal wind is proportional to the meridional gradient of the zonal mean temperature as described by the thermal wind equation. This temperature structure is damped radiatively by infra-red cooling. The diabatic circulation driven by this radiative heating is a good approximation to the Lagrangian mean circulation (cf. Plumb and Bell, 1982). Owing to the strong vertical stratification of ozone, the time change of the zonal mean ozone is approximated by the vertical advection of the basic state ozone distribution. Assuming a Gaussian form for the meridional structures of zonal wind and temperature, a mechanistic equation for the total ozone QBO is derived on an equatorial beta-plane. This equation is combined with the zonal wind data provided by Naujokat (1986) to simulate the total ozone QBO. The results are shown together with observations in Fig. 4. We can see some systematic phase difference between the two time series. Our preliminary investigations suggest that the feedback of the ozone QBO to diabatic heating possibly resolves this disagreement.

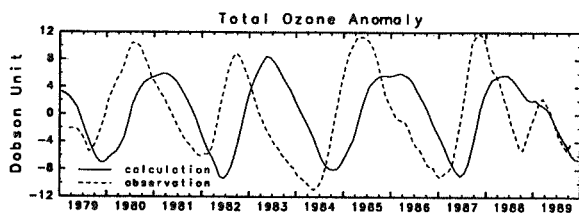


Fig. 4 Line plots of the total ozone QBO over the equator: derived values by using the observed zonal wind are plotted in solid line and zonal mean values in Fig. 2 are plotted in dashed line.

3.2 Response to ENSO time-scale SST

In section 2.3 we have revealed an east/west seesaw pattern of equatorial total ozone correlated with the Southern Oscillation Index. This is understood to be a reflection of the tropopause effect of SST variations. High SST's, for example, would give increased evaporation and cumulus convection, lift up the tropopause, and thus reduce the total ozone amount. Tropopause height changes are estimated from the Climate Analysis Center's monthly mean SST by using the equivalent potential temperature in the manner of Reid and Gage (1981). The associated total ozone variations are derived by applying small perturbations of the tropopause height to the basic state ozone profile. The results are shown in Fig. 5, which is the time-longitude section of the zonal wave component of tropical total ozone. The general agreement between Figs. 3 and 5, especially at the time of El Niño, indicates that the zonal wave component of equatorial total ozone on the ENSO time scale can be understood by the tropopause height modulation.

Zonal mean total ozone tends to show low (high) values about one year later than high (low) SST in the equatorial region (four year oscillation or FYO; Hasebe 1983). This is understood to be due to the advection effect of SST. The activated upward motion at the time of high SST would penetrate into the lower stratosphere. The air parcels cool adiabatically because of the lack of latent heat supply. Then, lower stratospheric temperature shows negative correlation with the SST (Reid *et al.*, 1989). If the vertical motion is maintained much longer than the radiative time-scale (≈ 1 month), the temperature anomalies are subject to radiative damping as in the case of the QBO. This diabatic heating must be coupled with the vertical motion. These processes are formulated into a mechanistic equation to model the total ozone variations associated with the advection effect of SST (See Hasebe, 1992, in detail). It should be noted that the tropospheric heating is proportional to the time derivative of ozone in the advection effect and to the ozone anomaly itself in the tropopause effect.

3.3 Annual cycle

The annual cycle of equatorial total ozone exhibits a maximum in September and a minimum in January accompanied by a stationary zonal wavenumber 1 structure with the phase of minimum located around 120°-150° E (Fig. 1). This component is tightly coupled with the altitude change of the tropopause. Although the location of the phase of minimum suggests the strong influence of SST on the

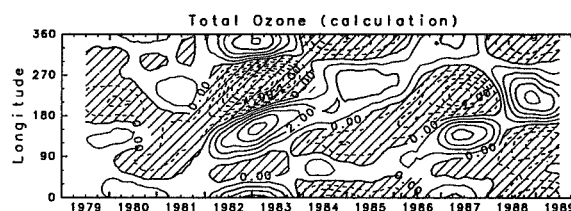


Fig. 5 Time-longitude cross section of the zonal wave component of total ozone fluctuations (contour interval 1 DU) along the equator based on estimation from SST; a 13-month running mean was applied.

tropopause height, the annual cycle of the tropopause height cannot be described solely by SST variations. Rather it is directly related to the lower stratospheric temperature field which may be understood by the asymmetrical seasonal variation of meridional heat transport by planetary waves. This suggests that the quasi-horizontal eddy transport responsible for the tropopause height changes also plays some role in the annual cycle of the equatorial total ozone.

4 Summary

Using the 11-year TOMS data we have found the following dominant long-term variations in the equatorial total ozone field, by paying special attention to the longitudinal structure.

Annual cycle: This variation has a longitudinal structure with a zonal wavenumber one pattern; the zonal mean values are maximum around September and minimum around January. The wave 1 pattern is persistent over the year with minimum values between 140°E and the date line. There is a synchronous variation in the lower stratosphere temperature, which is related to the variation in tropopause height (Reid and Gage, 1981). When the lower stratosphere temperature is lower, the tropopause is higher, then the erosion of the lower stratosphere ozone layer should give less total ozone. Thus, the annual variation in total ozone could be mainly attributed to that in tropopause height, although a mechanism of the tropopause height variation is not yet clear. The wave 1 structure can also be regarded as the tropopause height variation in longitudinal direction; this longitudinal structure should be produced by the active convective cloud system in the western Pacific, which brings about the higher tropopause there.

QBO cycle: This variation shows zonally uniform phase changes and is clearly coupled with the equatorial zonal wind QBO in the lower stratosphere. However, the vertical motions associated with the vertical shear of zonal wind (Plumb and Bell, 1982) need to be modified to fully describe the ozone advection.

ENSO cycle: In the longitudinal anomaly field, there is an east-west seesaw variation with a nodal longitude around the date line, having a characteristic time-scale of about 4 years. During the El Niño events, there are positive anomalies in the western Pacific and negative anomalies in the eastern Pacific; the anomaly pattern is reversed during the anti-El Niño events. The east-west seesaw pattern must be due to the longitudinal variation in the tropopause height associated with the convective cloud system in the ENSO cycle.

These variations of equatorial total ozone can be understood as being driven by two dynamical processes; the advection effect and the tropopause effect. The advection effect affects the zonal mean values of total ozone through vertical ozone advection by the diabatically driven mean meridional circulation. The diabatic heating comes from the radiational relaxation of temperature anomalies associated with the vertical gradients of mean zonal winds and the adiabatic ascent forced in the troposphere by latent heat release in convective systems. The tropopause effect affects the zonal wave component as well as the zonal mean value of total ozone by changing the altitude of the tropopause. Mechanistic equations which describe these dynamical processes are used together with the observed wind and SST to estimate total ozone variations. It is found that the zonal mean values of total ozone are dominated by the advection effect associated with the zonal wind QBO, although our preliminary investigations suggest that modification of the vertical velocity seems to be necessary by incorporating the feedback of the ozone QBO into diabatic heating. On the other hand, the zonal wave components are well described by the tropopause effect of SST. The annual cycle of equatorial total ozone can be understood by the tropopause height changes, although the annual cycle of tropopause height remains to be fully explained.

References

- Angell, J. K. and Korshover, J., 1973: *Mon. Wea. Rev.*, **101**, 426-443.
- Bowman, K. P., 1989: *J. Atmos. Sci.*, **46**, 3328-3343.
- Gage, K. S. and Reid, G. C., 1987: *J. Geophys. Res.*, **92**, 14197-14203.
- Hasebe, F., 1983: *J. Geophys. Res.*, **88**, 6819-6834.
- Hasebe, F., 1992: *J. Atmos. Sci.*, *accepted for publication*.
- Hilsenrath, E. and Schlesinger, B. M., 1981: *J. Geophys. Res.*, **86**, 12087-12096.
- Japan Meteorological Agency (JMA), 1991: Technical Note No. 34, 71 pp (in Japanese).
- Naujokat, B., 1986: *J. Atmos. Sci.*, **43**, 1873-1877.
- Oltmans, S. J. and London, J., 1982: *J. Geophys. Res.*, **87**, 8981-8989.
- Plumb, R. A. and Bell, R. C., 1982: *Q. J. R. Meteorol. Soc.*, **108**, 335-352.
- Reid, G. C. and Gage, K. S., 1981: *J. Atmos. Sci.*, **38**, 1928-1938.
- Reid, G. C., Gage, K. S. and McAfee, J. R., 1989: *J. Geophys. Res.*, **94**, 14705-14716.
- Shiotani, M., 1992: *J. Geophys. Res.*, **97**, 7625-7633.

303629

A 3-D MODEL STUDY OF OZONE EDDY TRANSPORT IN THE WINTER STRATOSPHERE

N. C. Hsu¹ and D. M. Cunnold²

¹ Science Application International Corp., Hampton, VA 23666

² School of Earth and Atmospheric Sciences, Georgia Institute of Technology, Atlanta, Ga 30332

Abstract

Calculations of the Northward eddy fluxes of stratospheric ozone in a three-dimensional chemical-dynamical model are discussed. It is shown that, although approximately 50% of the zonal mean flux is produced by stationary planetary wavenumbers 1 and 2, the wintertime flux due to the chemical eddies is substantially underestimated when a quasi-linear representation is used.

Introduction

The problem of modeling ozone of the middle atmosphere has been considered to be complex because of the coupling between radiation, dynamics and photochemistry. The eddy transport of ozone plays an important role in determining the stratospheric ozone distribution, especially in the winter. Based upon the linear wave theory, Hartmann and Garcia (1979) and Garcia and Solomon (1983) argued that the net eddy transport is significant only in the region where advective and photochemical time scales are comparable and that the zonal mean eddy flux might be approximated by including just the contribution by stationary wavenumber 1 based upon quasi-linear mathematics. On the other hand, using the LIMS satellite data, Leovy et al. (1985) showed that the ozone distribution is strongly influenced by irreversible deformation associated with planetary wave breaking, which is a highly nonlinear process. The purpose of this work is to study the effect of the nonlinear wave-wave interactions on ozone eddy fluxes using the results of a spectral global 3-D model.

Model Description

The model used in this study is an improved version of the 3-D GCM model by Cunnold et al. (1975). This model utilizes quasi-geostrophic governing equations (see Cunnold et al., 1975 for details). The vertical domain of integration extends from the ground to approximately 85 km in log-pressure altitude. In the horizontal plane, truncated series of spherical harmonics are used to represent the zonal and meridional structures up to wavenumber 18. This self-consistent 3-D model allows for full interaction between radiative heating, dynamics and photochemistry without much ad-hoc parameterization in either the dynamical or the chemical schemes.

Results

The model has been integrated for 18 months starting from December 1. The results discussed in this section are based upon the model output of the second January.

Figure 1 shows the calculated January monthly mean ozone map at 10 mb. A distinct region of strong ozone gradient spiraled westward and outward from the vortex between 50° and 60° N to the tropical region. Between the edge of the

vortex and the tropical branch of the spiral a prominent tongue of high ozone stretches inward toward the polar region near 60° N, 210° E. These features are consistent with the LIMS data analyzed by Leovy et al. (1985).

Figure 2 shows the model-generated amplitude and phase of the geopotential height of wavenumber one in January. Compared to the satellite observations analyzed by Labitzke et al. (1985), the location of the maximum amplitude of the model geopotential height disturbance is at a slightly lower altitude than the observed which is at about 65 degree north and 7 mb, and the measured magnitudes are underestimated by approximately 10% in the stratosphere and the polar night region. The phases of the model geopotential heights are generally in good agreement with the satellite data, which exhibit decreasing phase with increasing altitude and increasing phase with increase of latitude toward the north pole.

The comparison of the model temperature disturbances of wavenumber one with the satellite measurements by Labitzke et al. (not shown here) also indicates that the observed amplitude of temperature disturbance is characterized by a major maximum located at 62° N and 40 mb, which is about the same amplitude and location as the model predicted, and a minor maximum at 58° N and 2 mb, which is overestimated by approximately 40% in the model. The constant phase lines in both the model and the observations tilt equatorward and downward with magnitudes decreasing with height.

There are large interannual fluctuations of planetary wave activities from year to year. Although the model-predicted amplitudes of geopotential height and temperature of wavenumber 1 and 2 do not agree exactly with the multi-year averaged satellite measurements reported by Labitzke et al., they are within the range of the interannual variations given in the four-year NOAA/NMC observations (Geller et al., 1984). Therefore the perturbations of the winter middle atmosphere generated by the model are representative of the real atmosphere and can be used to study the ozone eddy transport in the stratosphere.

The Importance of The Nonlinear Terms In The Mass Continuity Equation

The complete Eulerian ozone eddy continuity equation can be written as follow:

$$\frac{\partial \chi'}{\partial t} + (\bar{u} + u') \frac{\partial \chi'}{\partial x} + v' \left(\frac{\partial \bar{\chi}}{\partial y} + \frac{\partial \chi'}{\partial y} \right) + w' \frac{\partial \chi_0}{\partial z} = S' \quad (1)$$

where χ is the ozone mixing ratio; S denotes the ozone production/loss rate; (u, v, w) are zonal, meridional and vertical velocities, respectively; overbars represent the zonal means of quantities and primes denote the departures from zonal averages.

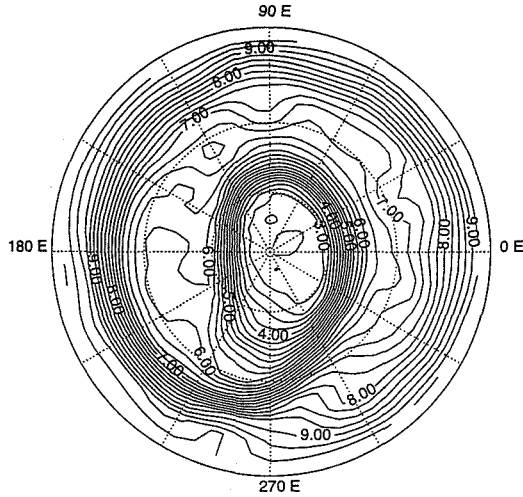


Figure 1 January monthly mean ozone (in ppmv) map at 10 mb

The nonlinear terms in equation (1) have been neglected in a number of studies concerning ozone eddy transport. The rationale for the neglect of the nonlinear transport depends on the validity of the linear wave theory which assumes that the wave amplitudes are small and thus the linear terms would be much larger than the nonlinear terms in the tracer eddy continuity equation. Using the satellite measurements, Douglass et al. (1985), however, pointed out that the nonlinear terms could be an important part of the net dynamical forcing in the winter stratosphere and the inclusion of these terms improved the agreement between the calculated ozone mixing ratios and the observations. To investigate the importance of the nonlinear terms in the net dynamical forcing, the nonlinear terms have been calculated at each timestep of the 3-D model and averaged over the simulated month of January.

Figure 3 (a) and (b) show the comparisons of the nonlinear terms against the linear terms at the Gaussian longitudes at 60° N and 42° N for wavenumber 1. For both wavenumber 1 and 2 (not shown) the nonlinear terms are small compared to the linear terms between 1 and 10 mb at 60° N, while at 42° N the nonlinear terms are comparable to or even larger than the linear terms in the altitudes between 1 and 10 mb.

Generally speaking, the region where the nonlinear terms are significant in the eddy ozone budget takes place at a lower latitude for wavenumber 2 than for wavenumber 1. The nonlinear terms are more important to the net dynamical forcing at midlatitudes than at high latitudes, implying that the ozone distribution is greatly influenced by the nonlinear wave interaction at some distance from the core of the polar night jet stream. This is consistent with the idea that wave breaking (i.e. strong nonlinear interaction) occurs in winter outside the polar vortex (e.g. McIntyre and Palmer, 1984).

The Roles of The Transient and The Nonlinear Terms on The Net Ozone Eddy Fluxes Due To Stationary Rossby Waves

Model calculation indicates that in the winter stratosphere about 50% of the model net ozone eddy fluxes are attributed to the contributions of stationary waves, while the contributions of planetary wavenumber 1 and 2 account for 90% of the model net ozone transport due to stationary waves. Therefore approximately half of the net ozone eddy transports result from the transports by stationary planetary wavenumber 1 and 2. The importance of wavenumber 1 has been noted

observationally by Wu et al. (1987). In this section, we will discuss the significance of the transient and nonlinear effects in calculating the net ozone eddy transport due to stationary wavenumber 1 and 2 using the output of the 3-D model.

Time averaging equation (1) and following Garcia and Solomon's procedures (1983), the net ozone eddy fluxes due to stationary waves can be represented as

$$\begin{aligned} \left(\frac{[\overline{v}][\overline{\chi}]}{[\overline{w}][\overline{\chi}]} \right)^{\text{NET}} &= \left(\frac{[\overline{v}][\overline{\chi}]}{[\overline{w}][\overline{\chi}]} - \frac{[\overline{v}][\overline{T}]}{\sigma} \frac{\partial \overline{\chi}_0}{\partial z} \right) \\ &= -\widehat{S}_1 \begin{pmatrix} [\frac{\partial \overline{\chi}}{\partial y}] \\ [\frac{\partial \overline{\chi}}{\partial z}] \end{pmatrix} - \widehat{S}_2 \begin{pmatrix} [\frac{\partial \overline{T}}{\partial y}] \\ \sigma \end{pmatrix} - \widehat{S}_3 + \widehat{S}_4 \quad (2) \end{aligned}$$

where

$$\begin{aligned} \widehat{S}_1 &= \begin{pmatrix} C_1 & A+B \\ A-B & C_2 \end{pmatrix} \\ \widehat{S}_2 &= \begin{pmatrix} \gamma \phi_2 [\overline{\eta}]^2 & \gamma (\phi_2 [\overline{\eta}][\overline{\zeta}] - \phi_1 i [\overline{\eta}][\overline{\zeta}]) \\ \gamma (\phi_2 [\overline{\eta}][\overline{\zeta}] + \phi_1 i [\overline{\eta}][\overline{\zeta}]) & \gamma \phi_2 [\overline{\zeta}]^2 \end{pmatrix} \\ \widehat{S}_3 &= \begin{pmatrix} \tau_D (\phi_1 [\overline{v}][\overline{D}'_x] - \phi_2 i [\overline{v}][\overline{D}'_x]) \\ \tau_D (\phi_1 [\overline{w}][\overline{D}'_x] - \phi_2 i [\overline{w}][\overline{D}'_x]) \end{pmatrix} \\ \widehat{S}_4 &= \begin{pmatrix} \gamma \tau_D^2 (\phi_2 [\overline{v}][\overline{D}'_T] + \phi_1 i [\overline{v}][\overline{D}'_T]) \\ \gamma \tau_D^2 (\phi_2 [\overline{w}][\overline{D}'_T] + \phi_1 i [\overline{w}][\overline{D}'_T]) \end{pmatrix} \\ A &= \frac{\phi_1}{\tau_D} [\overline{\eta}][\overline{\zeta}]; \quad B = \frac{(\phi_2-1)}{\tau_D} i [\overline{\eta}][\overline{\zeta}] - \frac{\tau_D}{\sigma} i [\overline{v}][\overline{D}'_T]; \\ C_1 &= \frac{\phi_1}{\tau_D} [\overline{\eta}]^2; \quad C_2 = \frac{\phi_1}{\tau_D} [\overline{\zeta}]^2; \\ \phi_1 &= \frac{(\overline{\tau}_c/\tau_D)}{1 + (\overline{\tau}_c/\tau_D)^2}; \quad \phi_2 = \frac{(\overline{\tau}_c/\tau_D)^2}{1 + (\overline{\tau}_c/\tau_D)^2}; \\ D'_x &= u' \frac{\partial \chi'}{\partial x} + v' \frac{\partial \chi'}{\partial y} + \bar{u}^* \frac{\partial \chi'^*}{\partial x} + v'^* \frac{\partial \chi'^*}{\partial y} + w'^* \frac{\partial \chi_0}{\partial z} \\ D'_T &= q' - u' \frac{\partial T'}{\partial x} - v' \frac{\partial T'}{\partial y} - \bar{u}^* \frac{\partial T'^*}{\partial x} - v'^* \frac{\partial T'^*}{\partial y} \end{aligned}$$

bracket [] denotes the time average, star * represents the deviation from the time average, τ_c is the chemical time

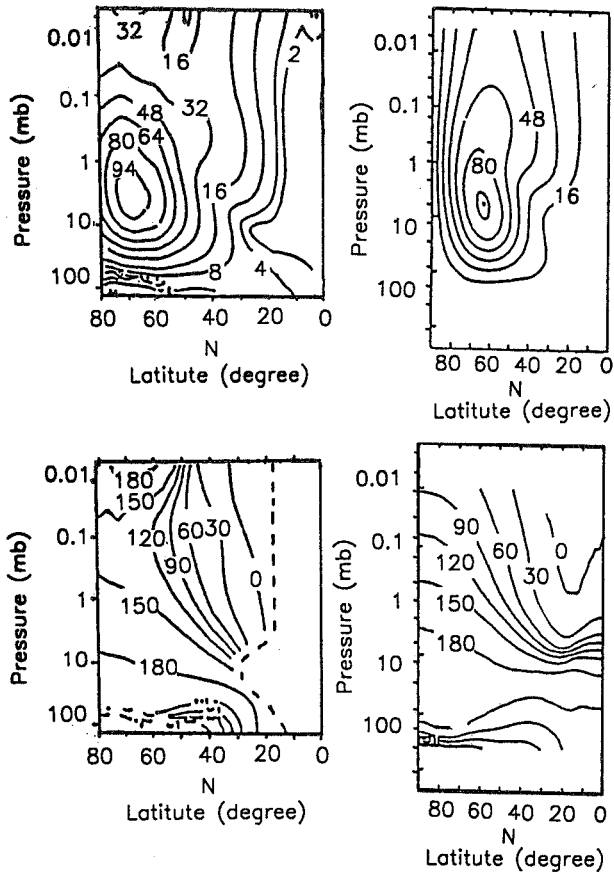


Figure 2 The monthly mean amplitude and phase of the model geopotential height of wavenumber one (on the right) for January with the observations analyzed by Labitzke et al. (1985) (on the left).

constant of ozone, τ_d is the advective time constant $[\text{ku}]^{-1}$, k is the wavenumber, σ denotes the static stability parameter and q is the heating rate perturbation.

The first two terms on the right hand side of (2) are similar to those derived based on a quasi-linear theory by Garcia and Solomon and many others, except that an extra term appears in the anti-symmetric components of the first term, which results from the effect of D_T' on the ozone eddy transport. This is compensated by the transports by the Eulerian mean motion. The last two terms are caused by the inclusion of D_X' and D_T' which represents the transient and nonlinear terms in the ozone continuity equation and the thermodynamic equation, respectively.

As depicted in figure 4, the chemically induced ozone eddy fluxes predicted by the quasi-linear theory (i.e. $D_X' = 0$ and $D_T' = 0$) substantially underestimate the model net ozone eddy fluxes for wavenumber 1 as well as wavenumber 2. Neither the magnitudes of the net ozone eddy fluxes nor their structures have been reproduced.

When the nonlinear terms and the linear transient terms in the ozone eddy continuity equation and the thermodynamic equation are included in the calculation of the net ozone eddy transport, the resulting net ozone eddy fluxes of wavenumber 1 and 2 calculated from (2), shown in Figure 5, are in remarkable agreement with those from the model except in the region south of 40°N , where the model mean zonal wind is

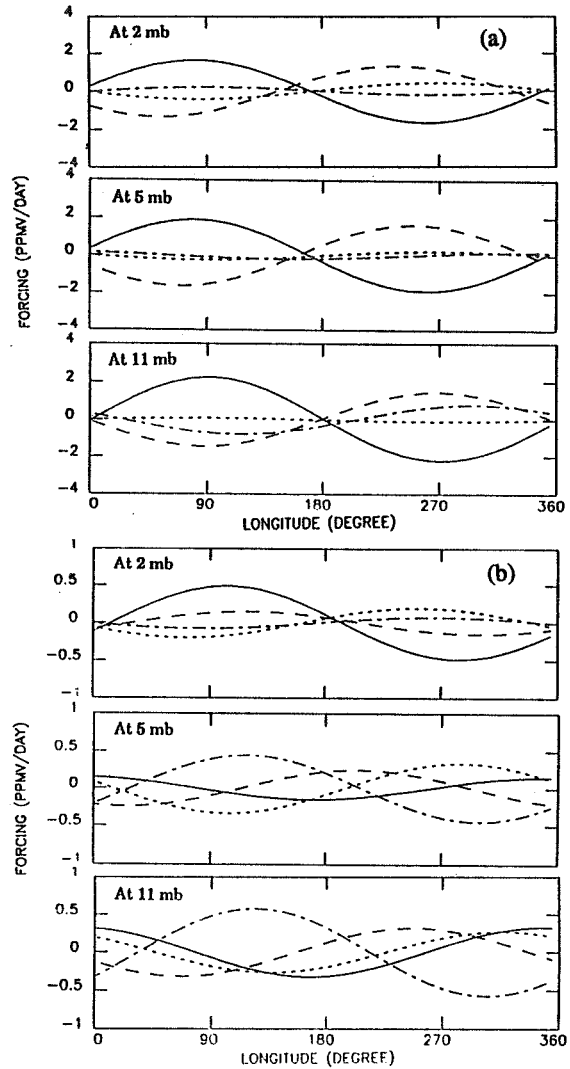


Figure 3(a) The comparison of the linear advection terms with the nonlinear advection terms for wavenumber 1 at 60°N for January. The solid line denotes the linear term $\bar{u} \frac{\partial \bar{X}'}{\partial x}$, the short-dashed line the nonlinear term $u' \frac{\partial \bar{X}'}{\partial x}$, the long-dashed line the linear term $\bar{v} \frac{\partial \bar{X}'}{\partial y}$, the dot-dashed line the nonlinear term $v' \frac{\partial \bar{X}'}{\partial y}$.

Figure 3 (b) As in Figure 3 (a) except for 42° latitude.

weak and the particle trajectories are quite variable. Obviously, the discrepancies between the net model ozone eddy fluxes and those calculated by the linearized formulation of Garcia and Solomon (1983) are caused by the neglect of the nonlinear terms and the linear transient terms.

The relative importance of the transient linear terms and the nonlinear terms was also investigated by comparing the net ozone eddy fluxes resulting from the nonlinear terms against those arising from the linear transient terms for wavenumber 1 and 2. For wavenumber 1, the linear transient forcings are prominent in the the upper stratosphere, while the effects of the nonlinear terms are dominant in the middle and lower stratosphere. For wavenumber 2, the net ozone eddy

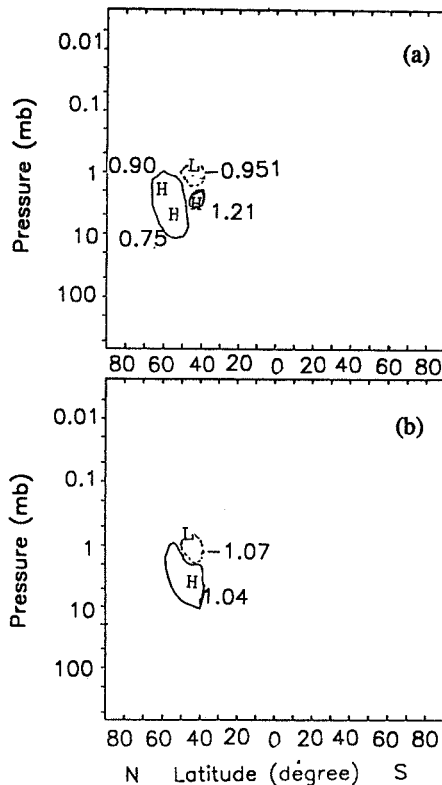


Figure 4 The chemical meridional ozone eddy fluxes, derived from the linear theory, due to (a) standing wavenumber 1; (b) standing wavenumber 2. Contour interval is 0.6 ppmv*m/s.

transports are almost completely controlled by the nonlinear processes.

Therefore the nonlinear process, such as planetary wave breaking, plays an important role in determining the net ozone eddy transport and consequently the mean ozone distribution in the transition region.

Concluding Remarks

The model results suggest that in the winter stratosphere the contribution of stationary waves accounts for more than 50% of the net ozone eddy fluxes and that the net ozone eddy transport contributed by stationary planetary wavenumber 2 may not be ignored, especially in the subtropical region where the nonlinear process is dominant in controlling ozone transport.

Calculations also indicate that the chemical ozone eddy fluxes of stationary wavenumber 1 and 2 estimated by the linearized tracer continuity equation, although significant, do not agree well with the net ozone eddy fluxes evaluated directly from the model for the month of January. The linear chemical transport is important only over a limited area near the edge of the polar vortex and even there it is no larger than the nonlinear contribution.

Acknowledgments

This work is supported by NASA contract NAS 5-27264 to Georgia Institute of Technology.

References

Cunnold, D., and F. Alyea, N. Philips, and R. G. Prinn, 1975: A three-dimensional dynamical-chemical model of atmospheric ozone, *J. Atmos. Sci.*, 32, 170-194.

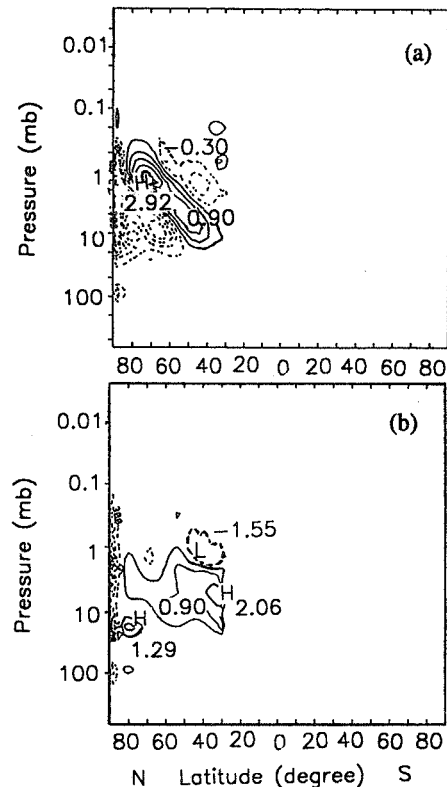


Figure 5 The calculated net meridional ozone eddy fluxes including the effects of the nonlinear terms and the transient terms, due to (a) standing wavenumber 1; (b) standing wavenumber 2. Contour interval is 0.6 ppmv*m/s.

- Douglass, A. R., R. B. Rood and R. S. Stolarski, 1985: Interpretation of ozone temperature correlations, 2, Analysis of SBUV ozone data, *J. Geophys. Res.*, 90, 10,693-10,708.
- Garcia, R. R. and S. Solomon, 1983: A numerical model of zonally averaged dynamical and chemical structure of the middle atmosphere, *J. Geophys. Res.*, 88, 1379-1400.
- Geller, M. A., M.-F. Wu, and M.E. Gelman, 1984: Troposphere-stratosphere (surface-55 km) monthly winter general circulation statistics for the northern hemisphere-interannual variations, *J. Atmos. Sci.*, 41, 1726-1744.
- Hartmann, D. L., and R. R. Garcia, 1979: A mechanistic model of ozone transport by planetary waves in the stratosphere, *J. Atmos. Sci.*, 36, 350-364.
- Labitzke, K., J. J. Barnett, and B. Edwards, 1985: Atmospheric structure and its variation in the region 20 to 120 km, draft of a new reference middle atmosphere, *Handbook for MAP*, Vol 16 SCOSTEP, Univ. of Illinois, Urbana-Champaign.
- Leovy, C. B., C.-R. Sun, M. H. Hitchman, E. E. Remsburg, J. M. Russell, III, L. L. Gordley, J. C. Gille and L. V. Lyjak, 1985: Transport of ozone in the middle stratosphere: Evidence for planetary wave breaking, *J. Atmos. Sci.*, 42, 230-244.
- McIntyre, M. E. and T. N. Palmer, 1984: The surf zone in the stratosphere, *J. Atmos. Terr. Phys.*, 46, 825-849.
- Wu, M.-F., M. A. Geller, J. G. Olson and E. M. Larson, 1987: A study of global ozone transport and the role of planetary waves using satellite data, *J. Geophys. Res.*, 92, 3081-3097.

303632

IMPACT OF SUPERSONIC AND SUBSONIC AIRCRAFT ON OZONE: INCLUDING HETEROGENEOUS CHEMICAL REACTION MECHANISMS.

Douglas E. Kinnison and Donald J. Wuebbles
Lawrence Livermore National Laboratory
Livermore CA 94550, USA

ABSTRACT

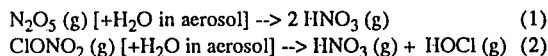
Preliminary calculations suggest that heterogeneous reactions are important in calculating the impact on ozone from emissions of trace gases from aircraft fleets. In this study, three heterogeneous chemical processes that occur on background sulfuric acid aerosols are included and their effects on O₃, NO_x, Cl_x, HCl, N₂O₅, ClONO₂ are calculated.

INTRODUCTION

The aircraft industry is showing interest in the development of supersonic, High Speed Civil Transports (HSCT's) for intercontinental passenger flights. The purpose of this study is to extend recent research (Johnston et al., 1989; Weisenstein et al., 1991; Kinnison and Wuebbles, 1991; and Jackman et al., 1991) examining global environmental effects from potential future emissions of commercial aircraft fleets. In addition to the gas-phase reaction mechanism believed to be important in the troposphere and stratosphere, three heterogeneous chemical processes that occur on and within the bulk of sulfuric acid aerosols are investigated. In this study the LLNL two-dimensional zonally averaged chemical-radiative-transport model of the troposphere and stratosphere is used to investigate the effects of NO_x emissions from future fleets of both subsonic and supersonic aircraft on ozone and other trace gas distributions. Recent uses of this model include those of Johnston et al., 1989 and Wuebbles et al., 1992. For a general description of the LLNL 2-D model, see Kinnison et al., 1992.

HETEROGENEOUS REACTIONS

In this study, we added the following reactions to the LLNL 2-D model chemistry package:



Since a complete treatment of these reactions would require a sophisticated aerosol microphysical model, which currently has both theoretical and practical limitation, we treated these reactions using the following relationship to calculate the two rate constants for the above cases.

$$K = (V)(\gamma)(\text{Surface Area Density})$$

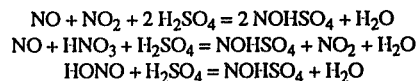
Surface area density (cm²/cm³) for the reference atmosphere is based on analysis of Sage II data by Poole, Thomason, and Yue (WMO/UNEP, 1992). This distribution is representative of an atmosphere that has not been influenced by a major volcanic eruption. The surface area density distribution has altitude (12-32 km), latitude (90N-90S), and temporal resolution. The effective collision velocity (V) is 5200 cm/s

for this study. The reaction probability per collision (γ) is based on laboratory measurements (WMO/UNEP, 1992). For N₂O₅ on sulfuric acid aerosols the reaction probability (γ_1) is set to 0.1 and does not have a temperature dependence. The reaction probability for ClONO₂ on sulfuric acid aerosols does have a temperature dependent expression:

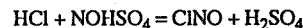
$$\gamma_2 = 0.006 \exp(-0.15(T-200)).$$

In addition, Burley and Johnston (1992), have proposed an additional heterogeneous chemical mechanism. This mechanism has the net effect of converting HCl into ClNO. A brief description of the major points about this mechanism are described below. For a more complete description of the modeling approach use in this study, see Connell et al., 1992.

- *Nitrosyl sulfuric acid (NSA) -- NOHSO₄ -- has been observed as a solid crystalline precipitate in the stratospheric sulfuric acid aerosol
- *NSA can be present in sulfuric acid solutions where the H₂SO₄ weight per cent is greater than 60 % at typical stratospheric temperatures, either as an ionic solid -- NO⁺HSO₄⁻ -- or as H₂ONO⁺ and HSO₄⁻ in solution
- *Potential NSA formation reactions (Burley and Johnston, 1992) on sulfuric aerosols include:



- *HCl reacts with NSA to form ClNO:



- *The ClNO produced is readily photolyzed to form Cl:



- *The overall process is the acid-catalyzed conversion of the chlorine reservoir species HCl to active atomic Cl

EMISSION SCENARIO FOR 2015 AIRCRAFT FLEET

Emission scenarios for this study are taken from a recent investigation conducted by the NASA High Speed Research Program (Prather et al, 1992). In these scenarios both subsonic and supersonic aircraft fleets are represented for the year 2015. The trace gas emissions for the 2015 subsonic scenario are based on the Boeing B6 scenario. The subsonic emission scenario was divided into two regions, flights under 400 miles or short range, and flights greater than 400 miles or long range. The total amount of fuel consumed is 20 x 10⁹ kg/year and 150 x 10⁹ kg/year for short and long range



flights respectively. The subsonic emission index for NO_x is 20.7 g/kg fuel consumed. The altitude of injection for short range flight is between 6.1 and 9.1 km and between 9.1 and 12.2 km for long range flights. For this study only the Mach 2.4 (16.8-19.8 km) airframe was considered. The total amount of fuel consumed for the supersonic scenario is kept constant at 70×10^9 kg/year, which represents approximately 500 aircraft. The supersonic emission index for NO_x is 15g/kg fuel consumed. For the above prototype, fuel use during take off, climb, and descent is ignored. In both the subsonic and supersonic emission scenarios, the NO_x emitted is 90% NO and 10% NO_2 on a molecular basis.

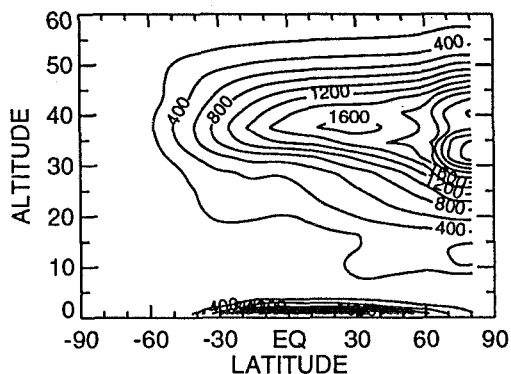


Figure 1: Rate of reaction of $\text{HCl} + \text{OH} = \text{Cl} + \text{H}_2\text{O}$ (molec. $\text{cm}^{-3} \text{s}^{-1}$) for an ambient 2015 atmosphere that includes N_2O_5 and ClONO_2 reactions on sulfuric acid aerosols; summer solstice.

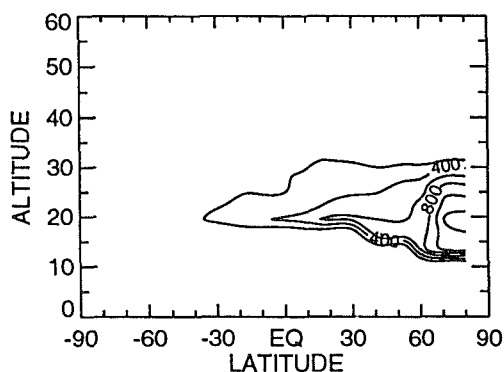


Figure 2: Rate of reaction of $\text{HCl} + \text{NSA} = \text{ClNO} (\text{g}) + \text{H}_2\text{SO}_4$ (molec. $\text{cm}^{-3} \text{s}^{-1}$) for an ambient 2015 atmosphere that includes NSA, summer solstice. Contour intervals are: 200, 400, 600... with a maximum of 1200.

RESULTS

In figure 1, the HCl and OH rate of reaction is shown for the ambient 2015 heterogeneous atmosphere that includes the reactions of N_2O_5 and ClONO_2 on sulfuric acid aerosols.

Figure 2 indicates the importance of the NSA mechanisms for converting HCl to reactive chlorine in the lower stratosphere. Including the NSA mechanism reduces HCl by up to 10-20 percent in the lower stratosphere, increasing the $\text{ClONO}_2/\text{HCl}$ ratio by 20-30 %; Cl_x ($\text{Cl} + \text{ClO}$) and NO_x ($\text{NO} + \text{NO}_2$) change by +50 to +200 % and -4 to +8 % respectively (see Connell et al., 1992 for more details on the impact of NSA on trace gas distributions). As NO_x is increased from the proposed aircraft scenario, the NSA concentration will increase which increases the NSA + HCl reaction rate, at high latitudes, Northern Hemisphere, from 1200 to 1800 molecules $\text{cm}^{-3} \text{s}^{-1}$. The HCl concentration decreases by another 15 percent in this region.

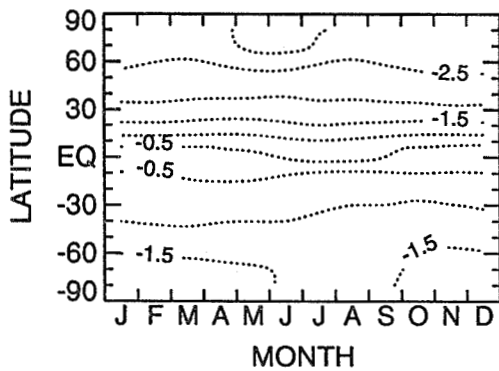
Table 1: Percent change in $\text{ClONO}_2/\text{HCl}$, Cl_x , and NO_x from the Mach 2.4 aircraft fleet emission of NO_x , at midlatitudes, in the Northern Hemisphere, July 15.

Chemistry Set	$\text{ClONO}_2/\text{HCl}$	Cl_x	NO_x
Gas-phase	-20 to -30	-50 to -60	+80
Heterogeneous	-4 to -8	-40	+60
Het. with NSA	+20 to +40	-20	+50

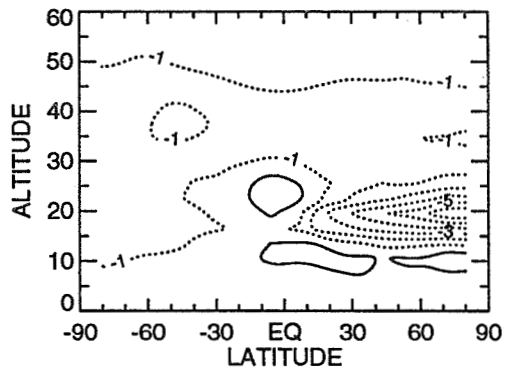
In figure 3, the percent change in column and local ozone is plotted for gas-phase, heterogeneous (N_2O_5 and ClONO_2 reactions) and heterogeneous (N_2O_5 and ClONO_2 reactions) with the NSA mechanism. Without the heterogeneous chemical reactions, the NO_x emissions decrease global annual-average column ozone by -1.4 %. This decrease is due to the 80 % increase in NO_x which increases the rate of odd oxygen loss from the NO_x catalytic cycles (table 1). Including both the N_2O_5 and ClONO_2 heterogeneous reactions decreases the effect on ozone of the Mach 2.4 scenario (figures 3b and 3c). The percent global annual-average column ozone change is -0.21 %. With the heterogeneous reactions present, the odd oxygen loss from the NO_x catalytic cycles are reduced and the Cl_x catalytic cycles are increased. As the emitted NO_x reacts with the enhanced Cl_x in the heterogeneous atmosphere, the local excess NO_x is reduced, minimizing the fleets impact on ozone. When the NSA mechanism is included, the change in global annual-average column ozone is -0.15 %. The net effect of the aircraft NO_x emissions is to increase the $\text{ClONO}_2/\text{HCl}$ ratio, but at least for this Mach 2.4 scenario, did not change ozone concentrations dramatically (compare figures 3c and 3e).

Derived local ozone increases in the troposphere when the heterogeneous reactions are present. This is not observed in the gas-phase case (compare figures 3b with 3d). Since the heterogeneous reactions decrease NO_x relative to the gas-phase only mechanism, additional input of NO_x is very efficient in producing ozone via the $\text{CH}_4\text{-NO}_x\text{-smog}$ reactions.

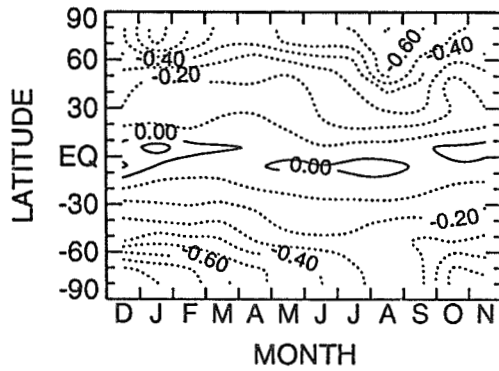
When emissions of the proposed subsonic fleet are included with the Mach 2.4 supersonic fleet, maximum local ozone changes in the troposphere are greater than 10 % for the heterogeneous case without NSA chemistry (figure 4). Approximately 3 percent (see figure 3d) of this change is from supersonic emissions and the rest is due to subsonic emissions. Both the heterogeneous with and without NSA showed similar increases in tropospheric ozone. The global



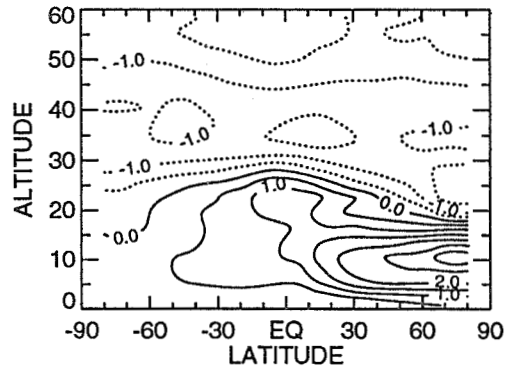
3 a



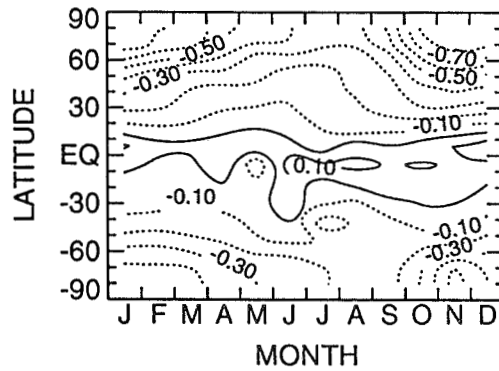
3 b



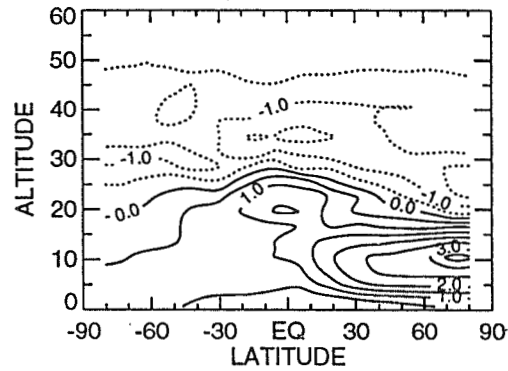
3 c



3 d



3 e



3 f

Figure 3: Percent change in ozone relative to an ambient atmosphere without aircraft for: a) column ozone, gas-phase reaction set; b) local ozone, gas-phase, July 15; c) column ozone, heterogeneous (i.e., N_2O_5 and $ClONO_2$ reactions); d) local ozone, heterogeneous, July 15; e) column ozone, heterogeneous with NSA; f) local ozone, heterogeneous with NSA, July 15. There are no subsonic emissions included in these cases.

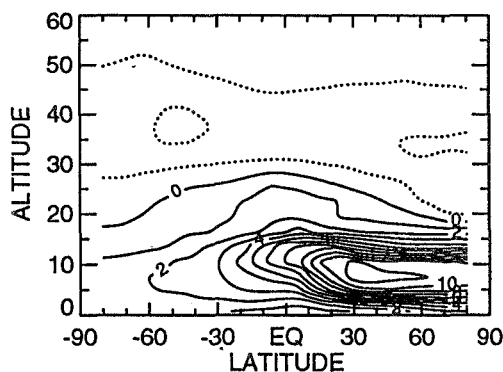


Figure 4: Percent change in local O_3 for an ambient 2015 atmosphere with both proposed subsonic and supersonic emissions of NO_x from aircraft, July 15 (relative to an atmosphere without aircraft). This scenario includes the N_2O_5 and $ClONO_2$ heterogeneous reactions.

annual-average change in ozone increases by 0.48 % and 0.32 % when both the proposed supersonic and subsonic aircraft fleets are included with and without NSA respectively.

CONCLUSIONS

- 1) The rate of $OH + NSA$ is comparable to $OH + HCl$ in the lower stratosphere (Figures 1 and 2).
- 2) With the gas-phase only chemistry mechanism, relatively large changes ($> 3\%$ column ozone change at high latitudes in the northern hemisphere) occur when the NO_x emissions from the proposed Mach 2.4 fleet are modeled (Figures 3a and 3b).
- 3) Including N_2O_5 and $ClONO_2$ reactions on sulfuric acid aerosols decreases the ozone loss relative to what was derived with a gas-phase only chemical mechanism (Figures 3c and 3d).
- 4) Including NSA chemistry with the N_2O_5 and $ClONO_2$ reactions does not change the net ozone production or loss from the aircraft scenario by a large amount from that derived with the N_2O_5 and $ClONO_2$ chemistry only case (Figures 3e and 3f).
- 5) When the heterogeneous reactions are included, there is a net increase in ozone in the troposphere. This is not observed with the gas-phase only case (compare figures 3b with 3d).
- 6) When subsonic emissions are included with the proposed HSCT fleet, large positive changes in tropospheric ozone are derived (Figure 4).

ACKNOWLEDGMENTS

The authors would like to thank Chi Tang for her contributions in analyzing and plotting the results for this study. This work was performed under the auspices of the U.S. Department of Energy by the Lawrence Livermore National Laboratory under contract No. W-7405-Eng-48 and was supported in part by the NASA High Speed Research Program.

REFERENCES

- Burley J. D., and H. S. Johnston, "Nitrosyl Sulfuric Acid and Stratospheric Aerosols", in press, *Geophys. Res. Lett.*, 1992.
- Connell, P. S., D. J. Wuebbles, and D. E. Kinnison, "Effects of Stratospheric Aerosol Surface Processes on the LLNL Two-Dimensional Zonally Averaged Model and Comparison to Potential Data from the Upper Atmospheric Research Satellite", Quadrennial Ozone Symposium, Charlottesville, VA, June 4-13, in press, 1992.
- Hofmann D. J., and S. Solomon, "Ozone Destruction through Heterogeneous Chemistry following the Eruption of El Chichon," *J. Geophys. Res.*, 94,5029-5041,1989.
- Jackman, C. H., A. R. Douglass, K. F. Brueske, and S. A. Klein, "The Influence of Dynamics on Two-Dimensional Model Results: Simulations of ^{14}C and Stratospheric Aircraft NO_x Injections," *J. Geophys. Res.*, 96, 22559-22572, 1991
- Johnston, H. S., D. E. Kinnison, and D. J., Wuebbles, "Nitrogen Oxides from High-Altitude Aircraft: An Update of Potential Effects on Ozone," *J. Geophys. Res.*, 94, 16351-16363, 1989.
- Kinnison, D. E., and D. J. Wuebbles, "Future Aircraft and Potential Effects on Stratospheric Ozone and Climate," 42nd Congress of the International Astronautical Federation, October 5-11, 1991, Montreal, Canada, Reference Number IAA-91-736, 1991.
- Kinnison, D. E., K. E. Grant, P. S. Connell, and D. J. Wuebbles, "Effects of the Mt. Pinatubo Eruption on the Radiative and Chemical Processes in the Troposphere and Stratosphere," Quadrennial Ozone Symposium, Charlottesville, VA, June 4-13, in press, 1992.
- Prather, M. J., H. L. Wesoky, R. C. Maike-Lye, A. R. Douglass, R. P. Turco, D. J. Wuebbles, M. K. W. Ko, and A. L. Schmeltekopf, "The Atmospheric Effects of Stratospheric Aircraft: A First Program Report, NASA Reference Publication 1272," NASA Office of Space Science and Applications, Washington, D.C., 1992.
- Weisenstein, D., M. K. W. Ko, J. M. Rodriguez, and N. D. Sze, "Impact of Heterogeneous Chemistry on Model-Calculated Ozone Change due to HSCT Aircraft," *Geophys., Res., Lett.*, 18,1991-1994, 1991.
- World Meteorological Organization, United Nations Environment Programme, 1991: Scientific Assessment of Ozone Depletion, in press, 1992.
- Wuebbles, D. J., D. E. Kinnison, K. E. Grant, and J. Lean, "The Effect of Solar Flux Variations and Trace Gas Emissions on Recent Trends in Stratospheric Ozone and Temperature," *J. of Geomagnetism and Geoelectricity*, in press, 1992.

303633

An Investigation of the Processes Controlling
Ozone in the Upper Stratosphere

Kenneth O. Patten, Jr., Peter S. Connell, Douglas E. Kinnison, Donald J. Wuebbles
Lawrence Livermore National Laboratory
Livermore, CA 94550, USA

Joe Waters, Lucien Froidevaux
Jet Propulsion Laboratory
Pasadena, CA 91109, USA

and
Tom G. Slanger
SRI International, Inc.
Menlo Park, CA 94025, USA

ABSTRACT

Photolysis of vibrationally excited oxygen produced by ultraviolet photolysis of ozone in the upper stratosphere is incorporated into the Lawrence Livermore National Laboratory 2-D zonally averaged chemical-radiative-transport model of the troposphere and stratosphere. The importance of this potential contributor of odd oxygen to the concentration of ozone is evaluated based upon recent information on vibrational distributions of excited oxygen and upon preliminary studies of energy transfer from the excited oxygen. When the energy transfer rate constants of previous work are assumed, increases in model ozone concentrations of up to 40 percent in the upper stratosphere are found, and the ozone concentrations of the model agree with measurements, including data from the Upper Atmosphere Research Satellite. However, the increase is about 0.4 percent when the larger energy transfer rate constants suggested by more recent experimental work are applied in the model. This indicates the importance of obtaining detailed information on vibrationally excited oxygen properties to evaluation of this process for stratospheric modeling.

INTRODUCTION

Simulations of stratospheric chemistry do not produce as large an ozone concentration as is experimentally found in the upper stratosphere. This difference has been known for at least 15 years (Butler, 1978; WMO, 1985). One of the possible explanations of this lower ozone concentration is that a source of odd oxygen is missing from the existing models. Slanger *et al.* (1988) have proposed a possible additional source of odd oxygen based on experiment. Photodissociation of ozone in the ultraviolet (200 to 310 nm) produces oxygen molecules in the ground electronic state. This oxygen carries a large vibrational excitation (Slanger *et al.*, 1988; Kinugawa *et al.*, 1990). The vibrationally excited oxygen (O_2^{\dagger}) then absorbs a second photon by its Schumann-Runge transition and dissociates to two O atoms. This second dissociation can occur with light considerably to the red of that which photolyzes thermal oxygen. In order to incorporate this mechanism into atmospheric models, the distribution of O_2^{\dagger} with respect to vibrational quantum number v and the rate constants for removal of vibrational quanta from O_2^{\dagger} by collisional quenching must be known.

Utilizing O_2^{\dagger} distributions from Kinugawa *et al.* (1990) and quenching rate constants for O_2^{\dagger} based on Rapp (1965), Toumi *et al.* (1991) found an enhancement of ozone concentration ranging from 13 to 60 percent for altitudes of 36 to 58 km in their atmospheric model. The 248 nm O_3 photolysis data of Slanger (private communication) indicate a different $O_2^{\dagger}(v)$ distribution, and preliminary collisional quenching data in the same study indicate a considerably higher rate constant than was used previously. Photolysis of O_2^{\dagger} has been incorporated into the LLNL global two-dimensional chemical-radiative-transport model, and this study compares the ozone concentrations calculated using both the earlier collisional quenching and the experimental quenching with observed ozone concentrations, including recent measurements from the Upper Atmosphere Research Satellite Microwave Limb Sounder (UARS MLS).

EXCITED OXYGEN CHEMISTRY

The LLNL 2-D model has been discussed previously (Johnston *et al.*, 1989). In addition to the standard model, the rate of photolysis of O_3 into the ground state oxygen channel ($O_2(^3\Sigma_g^-)$) is used to calculate O_2^{\dagger} processes. As is detailed below, the O_2^{\dagger} calculation internally performs three steps for each altitude-latitude combination. The nascent distribution of $O_2^{\dagger}(v)$ is first found from O_3 photolysis rates. Rate constants for O_2^{\dagger} photolysis are calculated from absorption cross sections. Finally, with the photolysis and energy transfer rate constants, the steady state concentration of $O_2^{\dagger}(v)$ is determined.

When O_3 is photolyzed, excess energy is distributed among translation (between the centers of mass of O_2 and O atom) and rotation and vibration of the O_2 fragment. Data obtained by Slanger indicate that a bimodal distribution of vibrationally excited O_2 arises when O_3 is photolyzed at 248 nm. The time-of-flight study of Kinugawa *et al.* (1990) shows two peaks of O atom with respect to translational energy when O_3 is photolyzed at 226 nm. The peak at higher O_2 vibrational quantum number is assigned as partially but not completely due to thermal decomposition of O_3 . We use a double Gaussian fit in the relative translational energy of photolysis fragments to approximate both the Slanger data and the Kinugawa *et al.* data. Since the vibrational energy in $O_2(^3\Sigma_g^-)$ is equal to the photolysis energy minus E_T except for the rotational energy in O_2 , the vibrational distribution can be calculated.

The O_2^{\ddagger} cross sections are calculated from wavefunctions for O_2 and the Schumann-Runge transition dipole moment function using equations based on those in Levine (1975) and Saxon and Slanger (1991). The wavefunctions for both the ground and excited electronic states are calculated from potential surfaces using the method of Kulander (1988). The Rydberg-Klein-Rees potential surfaces of ground O_2 (${}^3\Sigma_g^-$) and excited O_2 (${}^1\Sigma_u^-$) are from Krupenie (1972) extrapolated to $r = 1.0 \text{ \AA}$ and to $r = 11.0 \text{ \AA}$. The transition dipole moment function $D(r)$ is from Allison *et al.* (1986). The transition strengths produced agree to within 50% with the experimental transition strengths of Lewis *et al.* (1986) and calculated transition strengths of Allison *et al.* (1971). Cross sections agree reasonably with the $v = 12$ cross sections found by Saxon and Slanger (1991).

The removal of vibrational excitation from O_2^{\ddagger} involves multiple processes which ultimately must be distinguished from one another. The O_2^{\ddagger} may lose vibrational excitation by either transfer to translational and rotational energy or transfer to vibrational energy. Either transfer mechanism preferentially removes one quantum of vibrational energy; however, according to Slanger's preliminary observations on O_2^{\ddagger} collisions with nitrogen for $v = 18$ to 20, processes which remove two quanta of vibrational energy from O_2^{\ddagger} are also significant. Further work at $v = 22$ finds that nitrogen and oxygen have approximately the same rate constants for O_2^{\ddagger} quenching, so that v - t transfer must dominate there. A model proposed by Rapp and Englander-Golden (1964) and by Rapp (1965), as further expanded to multiple-quantum removal by Yardley (1980), provides the v - v energy transfer rate constants used in the O_2^{\ddagger} model. The v - t contribution chosen for compatibility with the Slanger *et al.* observations at $v = 22$ is $3.0 \times 10^{-15} \text{ molec cm}^{-3} \text{ s}^{-1}$ for all temperatures and for both $M = O_2$ and $M = N_2$; this is referred to as the "full k_c case" in the results. The sensitivity of the O_2^{\ddagger} processes to the choice of energy transfer rate constants must be determined due to the preliminary nature of the Slanger group results. A second

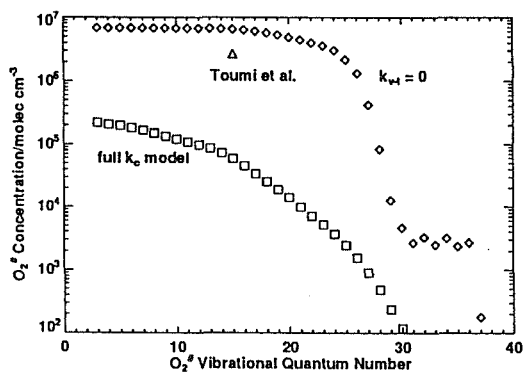


Figure 1. Steady state concentrations of vibrationally excited oxygen versus vibrational quantum number for 30° N , 44 km on the Autumn Equinox for both zero vibration-to-translation contribution (\diamond) and the full vibrational energy transfer model (\square) are compared with the result of Toumi *et al.* (1991) for $v = 15$ (Δ).

series of 2-D model runs is thus conducted with $k_{v,t}$ set to zero and $M = O_2$ alone; this lower limit to the uncertainty range of O_2^{\ddagger} energy transfer rate constants is referred to as the " $k_{v,t} = 0$ " case below. The rate constants of this case are similar to those used by Toumi *et al.* (1991).

O_2^{\ddagger} may be either deactivated by collisional energy transfer or photolyzed in the Schumann-Runge transition region. The lifetime of O_2^{\ddagger} is less than one hour, so that the instantaneous equilibrium or steady-state approximation may be applied to each of the species $O_2^{\ddagger}(v)$. Those equations are solved using the fact that O_2^{\ddagger} may not be produced with v greater than its dissociation limit of 38.

MODEL-DERIVED O_2^{\ddagger} AND O_3

Figure 1 illustrates steady state O_2^{\ddagger} concentrations (Equation 4) at noon on the Autumn Equinox (September 22) in the LLNL 2-D model with respect to vibrational quantum number. In the $k_{v,t} = 0$ model (diamonds), the concentration of O_2^{\ddagger} falls off rapidly for $v > 25$ from values of at least $5 \times 10^6 \text{ molec cm}^{-3}$ which remain nearly constant with v . Use of the full k_c model (squares) reduces the maximum O_2^{\ddagger} concentration to $2 \times 10^5 \text{ molec cm}^{-3}$ for $v = 3$, and the concentration decreases more steeply throughout the range of v , reaching $2 \times 10^3 \text{ molec cm}^{-3}$ at $v = 25$. The additional quenching of the full k_c model severely reduces the calculated O_2^{\ddagger} concentrations and will be shown to reduce the O_2^{\ddagger} effect upon odd oxygen considerably compared with that of Toumi *et al.* (1991). Toumi *et al.* (1991) provides $[O_2^{\ddagger}]$ only for $v = 15$ (triangle), which is slightly less than is the $[O_2^{\ddagger}(15)]$ for our $k_{v,t} = 0$ case in Figure 1.

The rate of O atom production from O_2^{\ddagger} also depends on the rate of O_3 photolysis, the solar flux, and the absorption cross section of O_2^{\ddagger} . For both k_c models, the rate of O_2^{\ddagger} photolysis in $\text{molec cm}^{-3} \text{ s}^{-1}$ (one half of the O atom production rate) at 30° N , Autumn Equinox noon is plotted against v in Figure 2. The O_2^{\ddagger} photolysis rate peaks at $2 \times 10^5 \text{ molec cm}^{-3} \text{ s}^{-1}$ for $v = 20$ in the $k_{v,t} = 0$ model, with considerable contributions for v down to 12 and up to 27. However, in the full

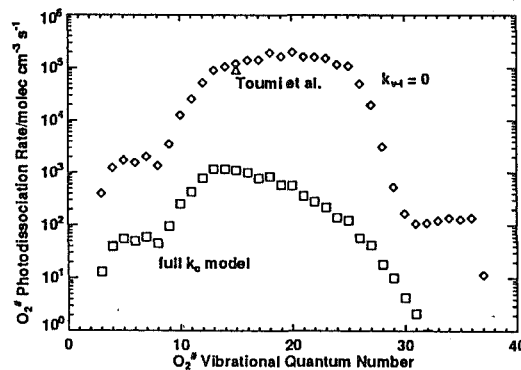


Figure 2. Rate of photolysis for vibrationally excited oxygen versus vibrational quantum number for 30° N , 44 km on the Autumn Equinox. Zero vibration-to-translation case: \diamond ; full vibrational energy transfer model: \square ; Toumi *et al.* (1991) for $v = 15$: Δ .

k_v model, the maximum contribution becomes 1×10^3 molec $\text{cm}^{-3} \text{s}^{-1}$ at $v = 12$, and the photolysis rate falls off more quickly with v to either direction. The strongest contribution to O atom production from O_2^+ comes from v in the range of 10 to 25, and the higher v are most severely affected by use of the full k_v quenching both in terms of concentration and in terms of photolysis rate.

Figure 3 illustrates the ratio of the O_2^+ dissociation rate to the thermal O_2 dissociation rate at the Autumn Equinox. The altitude shown is the log-pressure scaled altitude used in the 2-D model. Altitudes less than 30 km are omitted for this figure and Figure 4 since neither process is significant. In the $k_{v-1} = 0$ case (Figure 3A), the O_2^+ process contributes 10 percent as much odd oxygen as does thermal O_2 photodissociation around 35 km for all latitudes except the Antarctic region. The odd oxygen addition from O_2^+ increases with increasing altitude up to 55 km. Peak values of the ratio are greater than 50 percent at latitudes of 45 °S and 60 °N and 55 km altitude. Toumi *et al.* (1991) Table 2 shows an odd oxygen production ratio at 30 °N on the Autumn Equinox which increases monotonically from 13 percent at 36 km to 60 percent at 58 km, but with a leveling off of the rate of increase with altitude at the higher altitudes. Some quantitative differences in the production ratio exist between our model and that of Toumi *et al.*, but the qualitative features are mostly the same at 30 °N.

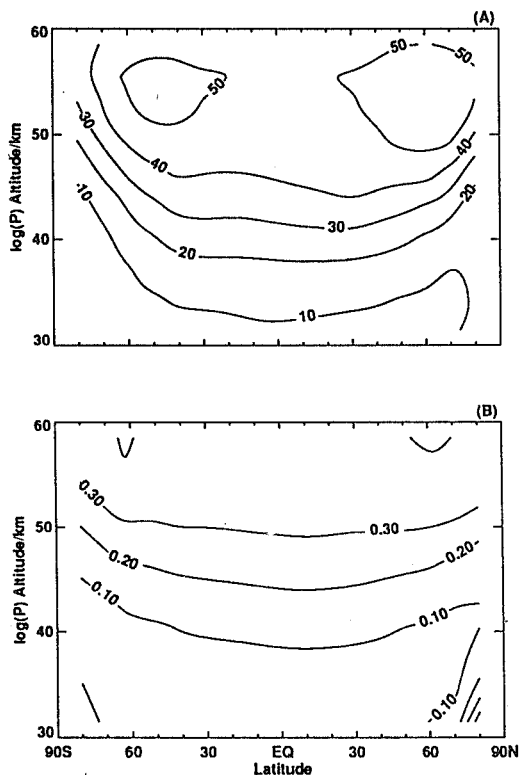


Figure 3. Ratio (percent) of rate of photolysis ($\text{molec cm}^{-3} \text{s}^{-1}$) of O_2^+ to that of thermal O_2 for (A) $k_{v-1} = 0$ case; (B) full k_v case.

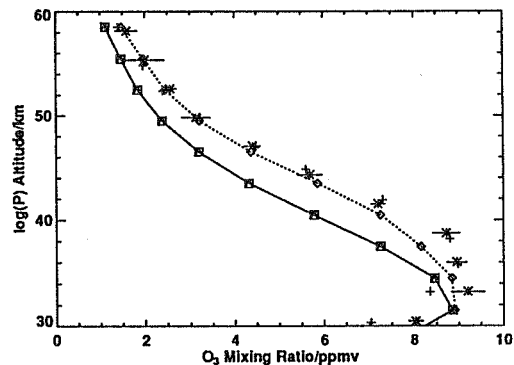


Figure 4. Comparison of LLNL 2-D model results with measurements of ozone concentration on the Autumnal Equinox at 30° N. * - UARS MLS (lines represent 1σ uncertainty); + - MAP recommended values (10 percent typical uncertainty); Δ - LLNL 2-D ambient atmosphere (no O_2^+); \diamond - LLNL 2-D model, $k_{v-1} = 0.0 \text{ cm}^3 \text{ molec}^{-1} \text{ s}^{-1}$, O_2 v-v transfer only; \square - LLNL 2-D model, $k_{v-1} = 3.0 \times 10^{-15} \text{ cm}^3 \text{ molec}^{-1} \text{ s}^{-1}$, N_2 and O_2 colliders.

The full k_v case (Figure 3B) reduces the odd oxygen percentage ratio from O_2^+ compared with thermal O_2 by two orders of magnitude for all latitudes and altitudes. Increased collisional quenching forces the maximum O_2^+ production upward (lower pressure), so that the maximum of 0.4 percent is located at 58 km, 60 °S or 60 °N; the upper limit of the model is at 58 km, so that this is not necessarily the overall maximum, but contributions for higher altitudes should not be markedly larger due to decreasing concentrations of O_3 . The contribution of O_2^+ below 58 km is sharply reduced at all latitudes toward a minimum of less than 0.1 percent about 40 km. O_3 concentrations for an ambient atmosphere in our 2-D model also typically change by 0.1 percent from year to year.

Addition of approximately half again as much O atom from O_2^+ as is produced by thermal O_2 photolysis in the $k_{v-1} = 0$ case to the upper stratosphere should produce a large increase in O_3 concentration. Figure 4 compares model O_3 concentrations on the Autumn Equinox at 30°N as a function of altitude with preliminary results from UARS MLS and the recommended zonal mean values of the Middle Atmosphere Program (Keating *et al.*, 1989). When $k_{v-1} = 0$ is used (diamonds), the O_3 concentration is markedly greater for all altitudes above 32 km than for the ambient atmosphere. The resulting concentrations are within the uncertainty limits of the preliminary measurements of the UARS MLS and are comparable to the MAP recommended values for September at 30 °N (crosses) for log-pressure altitudes down to 44 km. The MLS measurements are an average over 28 °N to 32 °N for September 21, 1991 for the 205 GHz O_3 band. Absolute accuracy of MLS is still under investigation, but the O_3 concentrations observed at these altitudes are not expected to vary significantly. The change between the LLNL 2-D model without O_2^+ processes (triangles) and for the O_2^+ full k_v case (squares) is insignificant on the scale of Figure 4.

CONCLUSIONS

Odd oxygen production from the photolysis of vibrationally excited oxygen (O_2^*) produced by ultraviolet photolysis of ozone (O_3) in the upper stratosphere has been incorporated in the LLNL 2-D global stratosphere-troposphere model. When quenching of O_2^* only by v-v collisional energy transfer to O_2 is considered, odd oxygen production rates throughout the upper stratosphere (>30 km) increase by up to 50 percent, with a corresponding increase in O_3 concentration, in qualitative agreement with the previous work by Toumi *et al.* (1991). Inclusion of an assumed v-t collisional energy transfer rate constant and of N_2 as a collider gas, indicated by recent preliminary experimental work, reduces the odd oxygen contribution from O_2^* processes to insignificance compared with thermal O_2 photolysis. The sensitivity of O_2^* processes in the stratosphere to detailed energy transfer rate constants is well demonstrated here; unfortunately, these constants are not yet well determined in the laboratory. Thus, this study shows the importance of obtaining detailed experimental information on the input parameters of O_2^* , particularly the rate constant for collisional energy transfer as a function of v, in order to judge the potential importance of O_2^* processes to stratospheric O_3 concentrations.

ACKNOWLEDGMENTS

This work was performed under the auspices of the U. S. Department of Energy by the Lawrence Livermore National Laboratory under contract No. W-7405-Eng-48 and was supported in part by the U. S. Department of Energy (DOE) Office of Health and Environmental Research's Environmental Sciences Division and by the National Aeronautics and Space Administration Upper Atmosphere Research Satellite program. KP also appreciates appointment to the Global Change Distinguished Postdoctoral Fellowships sponsored in part by the U. S. DOE, Office of Health and Environmental Research, and administered by Oak Ridge Associated Universities. We thank R. P. Saxon and D. L. Huestis at SRI International, Inc. for many helpful discussions concerning this study, and K. Kulander and B. P. Lengsfeld of LLNL for use of and guidance in their vibrational wavefunction code.

REFERENCES

- Allison, A. C., A. Dalgarno, and N. W. Pasachoff, 1971: Absorption by Vibrationally Excited Molecular Oxygen in the Schumann-Runge Continuum *Planet. Space Sci.* **19**, 1463-73.
- Allison, A. C., S. L. Guberman, and A. Dalgarno, 1986: A Model of the Schumann-Runge Continuum of O_2 *J. Geophys. Res.* **91**, 10,193-8.
- Butler, D. M., 1978: The Uncertainty in Ozone Calculations by a Stratospheric Photochemistry Model *Geophys. Res. Lett.* **5**, 769-72.
- Johnston, H. S., D. E. Kinnison, and D. J. Wuebbles, 1989: Nitrogen Oxides from High-Altitude Aircraft: An Update of Potential Effects on Ozone *J. Geophys. Res.* **94**, 16,351-63.
- Keating, G. M., M. C. Pitts, and D. F. Young, 1989: Ozone Reference Models for the Middle Atmosphere (New CIRA) in *Middle Atmosphere Program: Handbook for MAP 31*, G. M. Keating ed., pp. 1-36.
- Kinugawa, T., Sato, T., Arikawa, T., Matsumi, Y., and Kawasaki, M., 1990: Formation of $O(^3P)$ Photofragments from the Hartley Band Photodissociation of Ozone at 226 nm *J. Chem. Phys.* **93**, 3289-94.
- Krupenic, P. H., 1972: The Spectrum of Molecular Oxygen *J. Phys. Chem. Ref. Data* **1**, 423-534.
- Kulander, K. C., 1988: Spectroscopy of SO *Chem. Phys. Lett.* **149**, 392-6.
- Levine, I. N., 1975: *Molecular Spectroscopy* (John Wiley and Sons, New York), pp. 306-8.
- Lewis, B. R., L. Berzins, and J. H. Carver, 1986: Oscillator Strengths for the Schumann-Runge Bands of $^{16}O_2$ *J. Quant. Spectrosc. Radiat. Transfer* **36**, 209-32.
- Rapp, D., and P. Englander-Golden (1964): Resonant and Near-Resonant Vibrational-Vibrational Energy Transfer between Molecules in Collisions *J. Chem. Phys.* **40**, 573-5.
- Rapp, D., 1965: Interchange of Vibrational Energy between Molecules in Collisions *J. Chem. Phys.* **43**, 316-7.
- Saxon, R. P., and T. G. Slanger, 1991: Relative Contributions of Discrete and Continuum Absorption to the Photodissociation of Vibrationally Excited O_2 ($v = 12-20$) *J. Geophys. Res.* **96**, 17291-5.
- Slanger, T. G., L. E. Jusinski, G. Black, and G. E. Gadd, 1988: A New Laboratory Source of Ozone and Its Potential Atmospheric Implications *Science* **241**, 945-50.
- Toumi, R., B. J. Kerridge, and J. A. Pyle, 1991: Highly Vibrationally Excited Oxygen as a Potential Source of Ozone in the Upper Stratosphere and Mesosphere *Nature* **351**, 217-9.
- WMO, 1985: Comparison of Calculated and Observed Ozone Profiles in *Atmospheric Ozone 1985: Assessment of our Understanding of the Processes Controlling its Present Distribution and Change* (World Meteorological Organization Report Number 16), vol. 2, section 8.2, pp. 420-9.
- Yardley, J. T., 1980: *Introduction to Molecular Energy Transfer* (Academic Press, New York).

Note added in proof: After this work was presented, R. Toumi has published "An Evaluation of Autocatalytic Ozone Production from Vibrationally Excited Oxygen in the Middle Atmosphere" in *J. Atmos. Chem.* **15**, 69-77. That report incorporated past experimental quenching results and found ozone enhancements ranging from 0.4 to 11 percent for 40-60 km altitude, depending on various models of the nascent O_2^* distribution from O_3 photolysis.

303634

A NEW MATHEMATICAL FORMULATION OF THE LINE-BY-LINE METHOD
IN CASE OF WEAK LINE OVERLAPPING

Alexander G. Ishov, Natalie V. Krymova

Institute of Experimental Meteorology
249020 Obninsk, Kaluga Region, Lenin Street, 82, Russia

ABSTRACT

A rigorous mathematical proof is presented for a multiline representation of the equivalent width of a molecular band which consists in the general case of n overlapping spectral lines. The multiline representation includes a principal term and terms of minor significance. The principal term is the equivalent width of the molecular band consisting of the same n nonoverlapping spectral lines. The terms of minor significance take into consideration the overlapping of two, three and more spectral lines. They are small in case of the weak overlapping of spectral lines in the molecular band. The multiline representation can be easily generalized for an optically inhomogeneous gas media and holds true for combinations of molecular bands. If the band lines overlap weakly the standard formulation of line-by-line method becomes too labor-consuming. In this case the multiline representation permits line-by-line calculations to be performed more effectively. Other useful properties of the multiline representation are pointed out.

1. INTRODUCTION

As more complete and precise information about parameters of spectral lines becomes available (Rothman et al., 1987), the line-by-line method is used as a reference method in computation of the total vibration - rotation molecular and absorptance. This method assumes that the band consists in the general case of n overlapping spectral lines each of which is characterized by intensity S_i , half-width γ_i , frequency of line center ν_i^0 and line profile $\alpha(\nu_i^0 - \nu)$, $i=1, 2, \dots, n$. The equivalent bandwidth $W(n)$, used for a description of total absorptance of the molecular band in optically inhomogeneous gas media is given by

$$W(n) = \int \text{av} \left\{ 1 - \exp \left[- \sum_{i=1}^n \tau_i \alpha(\nu_i^0 - \nu) \right] \right\}, \quad (1)$$

where τ_i is optical depth at the central frequency of i -th line.

Line-by-line method assumes numerical integrating of the oscillating function, the number of the oscillations in the general case being equal to the number of spectral lines composing the band. In this case the calculation time rises with increasing of the oscillation magnitude of the absorption coefficient at line center, as the line overlapping is reduced. Thus, in the case of weak overlap-

ping of the lines in the band the line-by-line method becomes too labor-consuming and then a new approach is needed to calculate the total band absorptance. The following multiline representation can be taken as the basis of such an approach.

2. THE MULTILINE REPRESENTATION

The representation (Sakai et al., 1964) is known for the equivalent width $W(2)$ of the band consisting of two overlapping spectral lines:

$$W(2) \approx W_1 + W_2 - \int \text{dv} \prod_{i=1}^2 \left\{ 1 - \exp \left[-\tau_i \alpha(\nu_i^0 - \nu) \right] \right\}, \quad (2)$$

where

$$W_i = \int \text{dv} \left\{ 1 - \exp \left[-\tau_i \alpha(\nu_i^0 - \nu) \right] \right\}, \quad (3)$$

is the equivalent width of the i -th line. The relation (3) follows from the obvious identity $1 - \exp(-q_1 - q_2) = (1 - \exp(-q_1)) + (1 - \exp(-q_2)) - (1 - \exp(-q_1)) \times (1 - \exp(-q_2))$ which takes place for any material number q_1 and q_2 . It may be proved by means of the mathematical induction method with respect to n , that for $n \geq 2$ we have

$$1 - \exp \left(- \sum_{i=1}^n q_i \right) = \sum_{i=1}^n (1 - \exp(-q_i)) - \sum_{i_1, i_2}^{i_1 \neq i_2} \prod_{m=1}^2 (1 - \exp(-q_{i_m})) + \dots + (-1)^{n+1} \prod_{i=1}^n (1 - \exp(-q_i)).$$

Substituting in (1) and using $q_i = \tau_i \times \alpha(\nu_i^0 - \nu)$ we obtain the following representation for the equivalent bandwidth:

$$W(n) = \sum_{i=1}^n W_i - \sum_{i_1, i_2}^{i_1 \neq i_2} \int \text{dv} \prod_{m=1}^2 \left\{ 1 - \exp \left[-\tau_{i_m} \alpha(\nu_{i_m}^0 - \nu) \right] \right\} - \dots + (-1)^{n+1} \sum_{i_1, \dots, i_n}^{a \neq b} \int \text{dv} \prod_{m=1}^n \left\{ 1 - \exp \left[-\tau_{i_m} \times \alpha(\nu_{i_m}^0 - \nu) \right] \right\} + \dots + (-1)^{n+1} \int \text{av} \prod_{i=1}^n \left\{ 1 - \exp \left[-\tau_i \times \alpha(\nu_i^0 - \nu) \right] \right\}.$$

The first term in the right-hand side of (4) represents the equivalent bandwidth $W_N(n)$ in the nonoverlapping line approximation. In this approximation each line corresponds to its own ensemble of photons and these ensembles do not blend. The second term takes account of the overlapping of two lines or blending of the photons from two different ensembles, etc. By analogy with well-known problem of electrodynamic the proposed relation (4) can be referred to as multiline representation of the equivalent width of the band consisting in the general case of n overlapping spectral lines. In spite of its awkward form, multiline representation (4) has proved to be useful in practice for the following reasons. Representation (4) is an asymptotic series expansion for $W(n)$, from (1), in which the equivalent bandwidth $W_N(n)$ in the nonoverlapping line approximation is the principal term because the 1-th term in the right-hand side of (4) decreases as $\int dv \left(\prod_{m=1}^n \tau_m \alpha (v_m^0 - v) \right)$ with increasing of sufficiently large distances between the line centers and decreasing of sufficiently small optical depths in the line centers (i.e. as the nonoverlapping line approximation becomes more valid). Accordingly, the estimating of $W(n)$ by summarizing only few first terms of (4) will be more exact as the nonoverlapping line approximation becomes more valid, i.e. as the line-by-line method becomes more labor-consuming. Besides, as long as the minor terms of (4) in this case will make insignificant contribution, as compared to the principal term $W_N(n)$, it is possible to estimate them based on physical meanings.

3. APPROXIMATION FOR MINOR TERMS OF (4)

Let us arrange the band lines in the order of decreasing optical depths τ_i ($\tau_1 \geq \tau_2 \geq \dots \geq \tau_n$) and use approximate relation (Ishov et al., 1990):

$$\int dv \prod_{i=1}^n \left\{ 1 - \exp \left[-\tau_i \alpha (v_i^0 - v) \right] \right\} \approx \quad (5)$$

$$W_1 \prod_{i=2}^n \left\{ 1 - \exp \left[-\tau_i \alpha (v_1^0 - v_i^0 - v_i^0) \right] \right\}.$$

Then it may be shown with the mathematical induction method with respect to n that instead of (4) we have:

$$W(n) = W_N(n) - \Delta, \Delta \approx \quad (6)$$

$$\sum_{i=1}^{n-1} W_i \left\{ 1 - \exp \left[- \sum_{k=i+1}^n \tau_k \times \alpha (v_i^0 - v_k^0) \right] \right\}.$$

The approximate relation (5) is found to be useful in the case when radiative transfer occurs mainly at the frequencies of the spectral line with maximum τ_1 on a background of the comparatively smooth changing of the wings of other lines, included in the integral of (5), and for which $\tau_i \leq \tau_1$. Of course, one can construct other representations for Δ of (6). However, the above representation is preferable because in addition to elementary functions it contains

functions W_i only, describing isolated line absorptance, the values of which have already been calculated with calculating the principal term of multiline representation (4). Clearly, that other conditions being equal, relation (5) is worst satisfied when all $\tau_i = \tau_1$. Besides, with weak overlapping of spectral lines the overlapping occurs primarily in the line wings which according to the Voigt profile conception (i.e. given statistically independent Doppler and Collision mechanisms of the spectral line broadening) have the Lorentzian character. Therefore we can limit oneself to the Lorentz profile case when testing the approximate relation (6). It should also be noted that for real vibration-rotation bands the variations of the half-widths γ_i and the distances between neighbouring lines $|v_{i+1}^0 - v_i^0|$ are negligible in comparison with those of the intensities S_i (i.e. τ_i). Therefore it seems reasonable to illustrate the results obtained using the model critical case rather than single examples of the specific bands. The case is a band, consisting of n identical equidistant Lorentzian lines, which at $n \rightarrow \infty$ represents Elsasser model band. The testing results are shown in Fig. 1. It illustrates that using the approximate formula (6) significantly increases the accuracy of $W(n)$ calculations in comparison with $W_N(n)$. Furthermore, there is a "corridor" of values δ and τ , in which approximate representations (6) proves to be extremely accurate.

4. PRINCIPAL TERM OF (4)

The equivalent width of an isolated spectral line $W(\tau)$ with optical depth τ at the line center is expressed through dimensionless absorption function $M_O(\tau)$ and its derivatives $M_k(\tau)$ with respect to τ ($k=1, 2, \dots$) for Lorentz (L), Doppler (D) and Voigt (V) line profiles which are mathematically well-studied (Ivanov, 1973). High-precision calculation algorithms have been developed for $M_k^L(\tau)$ and $M_k^D(\tau)$ functions (Hummer, 1981, Ishov, 1982). For $M_k^V(\tau)$ functions we have power for $\tau \rightarrow 0$ and asymptotic for $\tau \rightarrow \infty$ ($a \rightarrow \infty$) series expansions (Ivanov, 1973; Hummer, 1982) and Chebyshev's polynomials series in which coefficients are expressed through $M_k^L(\tau)$ functions only (Ishov et al., 1989). Also it has been shown that all Lorentz functions $M_k^L(\tau)$ for $k \geq 2$ can be limited to calculations of the two first Lorentz functions $M_0^L(\tau)$ and $M_1^L(\tau)$ only (Ishov et al., 1989). Moreover, the method of the universal functions has been developed for rapid estimating of the principal term of multiline representation (4) (Shved et al., 1984, 1988; Ishov et al., 1988). This method is based on introducing special absorption functions for each type of molecules (linear molecule and spherical, symmetric and asymmetric tops). For all these functions power ($\tau \rightarrow 0$) as well as asymptotic ($\tau \rightarrow \infty$) series expansions managed to be obtained (Ishov, 1982). It was also shown that the universal functions for the Voigt line profile may be reduced to calculating corresponding functions for the Lorentz and Doppler profiles (Ishov, 1985).

Thus we can argue that high-precision and effective calculation of the principal term of multiline representation (4) is a solved problem. Although further study of mathematical properties of the absorption function $M_O^V(\tau)$ for the Voigt line profile is, certainly, of applied importance. The thing is that different asymptotic representations of $M_O^V(\tau)$ have irregular character with respect to the parameter a and do not cover the whole range of a and τ parameters with sufficiently accurate calculations of $M_O^V(\tau)$.

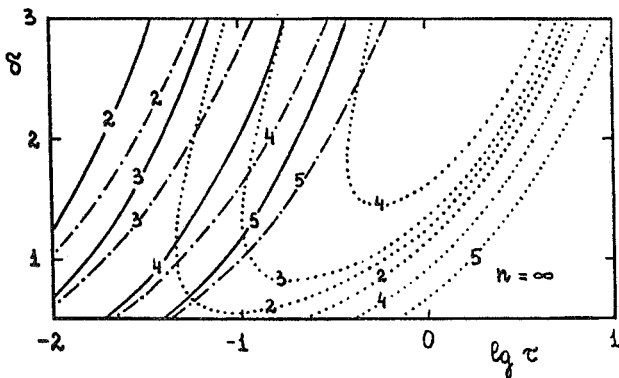
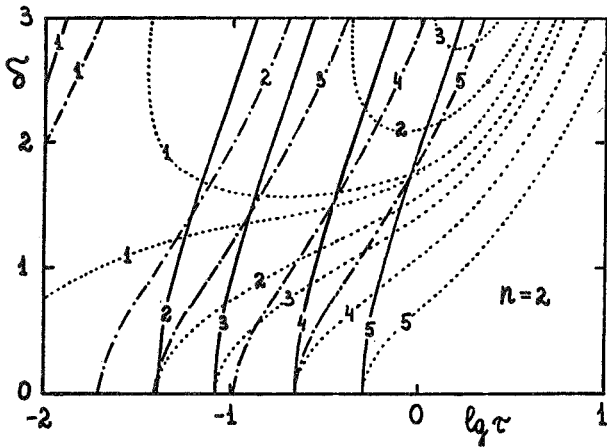


Fig. 1 Isolines of relative error of the approximations used with calculation of the equivalent width of the band consisting of $n=2, \infty$ identical equidistant overlapping Lorentz lines: — the isolated spectral line approximation, $\delta_1 = |W_N(n) - W(n)(1)|/W_N(n)$; ... - the approximate version (6) of multiline representation (4), $\delta_2 = |W(n)(1)|/W_N(n) + \Delta(6)/W_N(n)$; - - - $\delta_3 = \Delta(6)/W_N(n)$. Numbers are corresponding to: 1-0.1%, 2-1%, 3-2%, 4-5%, 5-10%. Approximate representation (6) becomes exact in the points of intersection of δ_1 and δ_3 isolines. δ is ratio of the distance between neighbouring line centers to the Lorentz half-width.

5. NEW REPRESENTATION OF $M_O^V(\tau)$

Multiline representation (4) has also proved to be useful for deriving new representations of the absorption function $M_O^V(\tau)$ for the Voigt line profile. Indeed, using the representation $\alpha^V = (1-\xi)\alpha^D + \xi\alpha^L$ (i.e. assuming the each Voigt line consists of two lines and one with the Doppler profile and another with the Lorentz one) it may be shown that the following approximate relation is valid:

$$M_O^V(\tau) \approx (1-\xi)qM_O^D(\tau) + \sqrt{2}\xi qM_O^L(\tau) + \tau[1 - q(1-\xi + \sqrt{2}\xi)], \quad (7)$$

where $q = H(O, \sqrt{2}a)/H(O, a)$, $\xi = \sqrt{2(1-q)}/(\sqrt{2}-1)$ and $H(x, a)$ is Voigt function. Relation (7) becomes exact as $a=0$ (Doppler profile case) and at $a=\infty$ (Lorentz a profile case) and has no peculiarities over the whole range of the a and τ parameters. Relation (7) is worst satisfied at $a \approx 1$, but even in this case it approximates the absorption function $M_O^V(\tau)$ much better then the two first terms of Taylor's series expansion.

6. OTHER PROPERTIES OF (4)

The multiline representation can be easily generalized for an optically inhomogeneous gas media: $\tau; \alpha(v_i^O - v) \rightarrow \int_0^l dz S_i(z) \alpha(v_i^O - v; z) n(z)$, where l is geometrical path length, $n(z)$ is absorbing molecule concentration at the point z . With traditional application of the line-by-line method, the multiline representation eliminates exact accounting for the contribution of weak lines to total absorptance due to dividing all the lines into two sub-bands: strong and weak nes. The multiline representation holds true for combinations of molecular bands.

7. CONCLUDING REMARKS

The present paper has revealed some basic properties of multiline representation (4) only. When calculating total absorptance in some spectral intervals covering spectral lines of several bands of various gases in different layers of the atmosphere, an alternative can arise within the framework of the proposed approach. Particular attention should be given to approximate version (6) for multiline representation (4). The formulas (6) are simple and feasible for calculations. Therefore, it is desirable that the band be dividing into sub-bands so that each of them hit in the "corridor" of values δ and τ shown in Fig. 1, in which approximate relations (6) becomes extremely accurate. Besides, when writing approximate relations (5), the weakest line may be preferred to the strongest. In this case relations (6) will have the same form but be satisfied more exactly.

REFERENCES

- Ishov, A.G., 1982: Research of functions describing radiative transfer in molecular bands. *Izvestia AN USSR, Physics of atmosphere and ocean*, 10, 1101-1105.
- Ishov, A.G., 1985: Universal functions for describing radiative transfer in molecular bands for the Voigt line profile. *Izvestia AN USSR, Physics of atmosphere and ocean*, 7, 788-791.
- Ishov, A.G., N.V. Krymova, 1989: About mathematical properties of functions used for describing radiative transfer in Lorentz profile line. *Atmospheric Optics* (Transactions of Institute of Experimental Meteorology), 20(140), 81-81. Moskow, Hidrometeoizdat.

- Ishov, A.G., N.V. Krymova, 1989: To the theory of line-by-line method of calculating total vibration-rotation band absorptance. First All-Union Symposium on radiative plasmodynamics, vol. 2, 64-65. Moskow, Energoatomizdat.
- Ishov, A.G., N.V. Krymova, 1990: Multiline representation for total band absorptance. *Optics of atmosphere*, vol. 3, No. 1, 79-82.
- Ishov, A.G., G.M. Shved, 1988: Universal functions for estimating total vibration-rotation band absorptance. III. Asymmetric tops. *J. Quant. Spectrosc. Radiat. Transfer*, vol. 39, No. 5, 399-407.
- Ivanov, V.V., 1973: *Transfer of Radiation in Spectral Lines* (translation edited by D.G. Hummer). National Bureau of Standards Special Publication 385 (U.S. Government Printing Office Washington D.C.).
- Hummer, D.G., 1981: Expressions for the computer—evaluation of the four kernel functions for line formation with Doppler and Lorentz profiles. *J. Quant. Spectrosc. Radiat. Transfer*, 26, No. 3, 187-195.
- Hummer, D.G., 1982: High order asymptotic expansions of the four kernel functions for line formation with the Voigt profile. *J. Quant. Spectrosc. Radiat. Transfer*, 27, 569-573.
- Rothman, L.S., R.R. Gamache, A. Goldman et al., 1987: The HITRAN database: 1986 edition. *Applied Optics*, vol. 26, No. 19, 4058-4097.
- Sakai, H., F.R. Stauffer, 1964: Equivalent width due to two overlapping lines. *J. Opt. Soc. Amer.*, vol. 54, No. 6, 759-761.
- Shved, G.M., A.G. Ishov, A.A. Kutepov, 1984: Universal functions for estimating total vibration-rotation band absorptance. I. Linear molecules and spherical tops. *J. Quant. Spectrosc. Radiat. Transfer*, vol. 31, No. 1, 35-55.
- Shved, G.M., A.G. Ishov, I.A. Podgorny, 1988: Universal functions for estimating total vibration-rotation band absorptance. IV. Extension of method and its applicability to the Doppler line shape. *J. Quant. Spectrosc. Radiat. Transfer*, vol. 40, No. 4, 539-551.

303636

THE CHEMISTRY OF BROMINE IN THE STRATOSPHERE:
INFLUENCE OF A NEW RATE CONSTANT FOR THE REACTION $\text{BrO} + \text{HO}_2$

Michel Pirre, François J. Marceau
Laboratoire de Physique et Chimie de l'Environnement, CNRS
45071 Orléans, France

Georges Le Bras, Françoise Maguin, Gille Poulet
Laboratoire de Combustion et Systèmes réactifs, CNRS
45071 Orléans, France

and Radiela Ramaroson
Office National d'Etudes et de Recherches Aéropatiales
92322 Châtillon, France

ABSTRACT

The impact of new laboratory data for the reaction $\text{BrO} + \text{HO}_2 \rightarrow \text{HOBr} + \text{O}_2$ in the depletion of global stratospheric ozone has been estimated using a one-dimensional photochemical model taking into account the heterogeneous reaction on sulphate aerosols which converts N_2O_5 into HNO_3 . Assuming an aerosol loading 2 times as large as the "background" and a reaction probability of 0.1 for the above heterogeneous reaction, the 6 fold increase in the measured rate constant for the reaction of BrO with HO_2 increases the computed depletion of global ozone produced by 20 ppt of total bromine from 2.01% to 2.36%. The use of the higher rate constant increases the HOBr mixing ratio and makes the bromine partitioning and the ozone depletion very sensitive to the branching ratio of the potential channel forming HBr in the $\text{BrO} + \text{HO}_2$ reaction.

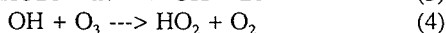
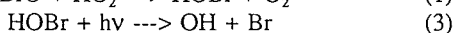
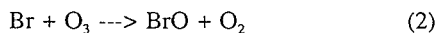
1. INTRODUCTION

Bromine compounds play a significant role in both the depletion of global stratospheric ozone (Wofsy et al., 1975), (Yung et al., 1980) and in the perturbed chemistry which leads to the ozone hole formation in polar stratospheric regions (Mac Elroy et al., 1986).

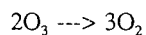
Assuming kinetic data available in 1980, Yung et al. (1980) concluded that the catalytic cycle involving the reaction $\text{BrO} + \text{ClO}$ was the main cycle involving bromine compounds to destroy odd oxygen in the lower stratosphere. More specifically, the rate constant they assume for the reaction:



was too low to make the following cycle significant:



net:



Recently, Poulet et al. (1992) have reported a rate constant for reaction (1) which has been measured at LCSR/CNRS to be 6 times higher than the preferred value given in the kinetic data bases (De More et al., 1990). The new value is $k_1 = 3.3 \cdot 10^{-11} \text{ cm}^3 \cdot \text{molecule}^{-1} \cdot \text{s}^{-1}$ instead of $k_1 = 5.0 \cdot 10^{-12} \text{ cm}^3 \cdot \text{molecule}^{-1} \cdot \text{s}^{-1}$. In their modelling of the influence of this new kinetic data on the stratospheric chemistry, they show that the reduction of global ozone column density produced by 20 ppt of bromine is increased from 1.14% to 1.45%. They conclude that the above cycle is no longer insignificant to deplete ozone. Besides, they point out that a possible channel for reaction (1) yielding HBr and O_3 as products could decrease significantly the ozone depletion assuming the new kinetic data. They found that with a 10% branching ratio for the HBr forming channel of reaction (1), 20 ppt of bromine would deplete the ozone column by only 0.6%. This channel may occur at low temperatures, but this has to be established by laboratory studies.

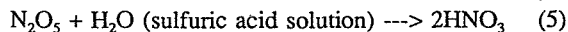
The present paper describes the impact of the new kinetic data on the bromine chemistry of the lower stratosphere in the presence of aerosols.

2. IMPACT OF THE $\text{BrO} + \text{HO}_2$ REACTION IN PRESENCE OF AEROSOLS

A 1D steady state photochemical model has been used to estimate the effect of the new kinetic data on both the bromine partitioning in the stratosphere and the global ozone depletion due to bromine compounds in the presence of an aerosol layer. This layer is assumed to reduce the concentration of the NO_x compounds. The effect of the possible occurrence of the HBr forming channel in reaction (1) is also investigated.

The 1D model has been recently described (Ramaroson et al., 1992). This model includes the species of the O_x , HO_x , NO_y , ClO_y and BrO_y families and the source species: N_2O , H_2O , CH_4 , CO , CFC_s , CH_3Cl and CH_3Br . The vertical temperature and total concentration profiles are taken from the U.S. Standard Atmosphere (1976). The kinetic and photochemical data used are essentially those recommended in the last NASA-JPL report (De More et al., 1990). Those concerning the bromine species are reported in Table I. The

following heterogeneous reaction on sulfate aerosols has been taken into account:



The reaction probability has been assumed to be $\gamma = 0.1$ which is consistent with measurements of Hanson and Ravishankara (1991). A sulfate aerosol area profile twice as high as the "background" 1979 values over Laramie, Wyoming (Hofmann and Solomon, 1989) has been adopted in the calculations (Rodriguez et al., 1991). The stratospheric aerosol layer is assumed to be saturated and all the HNO_3 produced in reaction (5) is immediately released in the gas-phase.

The steady-state vertical distribution of the source species and families are computed by iterations from 0 to 60 km, by step of 1 km. The diurnal averaged production and loss terms needed are calculated before each iteration, which

Table I: Reactions involving bromine compounds and rate coefficients

$\text{CH}_3\text{Br} + \text{hv} \rightarrow \text{CH}_3 + \text{Br}$	(a)
$\text{BrO} + \text{hv} \rightarrow \text{Br} + \text{O}$	(a)
$\text{BrONO}_2 + \text{hv} \rightarrow \text{Br} + \text{NO}_2$	(a)
$\text{HOBr} + \text{hv} \rightarrow \text{OH} + \text{Br}$	(a)
$\text{BrCl} + \text{hv} \rightarrow \text{Br} + \text{Cl}$	(a)
$\text{CH}_3\text{Br} + \text{OH} \rightarrow \text{products}^{\text{a}}$	$6.8 \cdot 10^{12} \exp(-850/T) \text{ cm}^3 \text{ molecule}^{-1} \text{ s}^{-1}$
$\text{Br} + \text{O}_3 \rightarrow \text{BrO} + \text{O}_2$	$1.7 \cdot 10^{11} \exp(-800/T) \text{ cm}^3 \text{ molecule}^{-1} \text{ s}^{-1}$
$\text{BrO} + \text{O} \rightarrow \text{Br} + \text{O}_2$	$3.0 \cdot 10^{11} \text{ cm}^3 \text{ molecule}^{-1} \text{ s}^{-1}$
$\text{BrO} + \text{ClO} \rightarrow \text{Br} + \text{ClOO}$	$2.9 \cdot 10^{12} \exp(220/T) \text{ cm}^3 \text{ molecule}^{-1} \text{ s}^{-1}$
$\text{BrO} + \text{ClO} \rightarrow \text{Br} + \text{OCIO}$	$1.6 \cdot 10^{12} \exp(430/T) \text{ cm}^3 \text{ molecule}^{-1} \text{ s}^{-1}$
$\text{BrO} + \text{ClO} \rightarrow \text{BrCl} + \text{O}_2$	$5.8 \cdot 10^{12} \exp(170/T) \text{ cm}^3 \text{ molecule}^{-1} \text{ s}^{-1}$
$\text{BrO} + \text{NO} \rightarrow \text{Br} + \text{NO}_2$	$8.8 \cdot 10^{12} \exp(260/T) \text{ cm}^3 \text{ molecule}^{-1} \text{ s}^{-1}$
$\text{BrO} + \text{BrO} \rightarrow \text{Br} + \text{Br} + \text{O}_2$	$1.4 \cdot 10^{12} \exp(150/T) \text{ cm}^3 \text{ molecule}^{-1} \text{ s}^{-1}$
$\text{Br} + \text{HO}_2 \rightarrow \text{HBr} + \text{O}_2$	$1.5 \cdot 10^{11} \exp(-600/T) \text{ cm}^3 \text{ molecule}^{-1} \text{ s}^{-1}$
$\text{HBr} + \text{OH} \rightarrow \text{Br} + \text{H}_2\text{O}$	$1.1 \cdot 10^{11} \text{ cm}^3 \text{ molecule}^{-1} \text{ s}^{-1}$
$\text{BrO} + \text{HO}_2 \rightarrow \text{HOBr} + \text{O}_2$	$5.0 \cdot 10^{12} \text{ cm}^3 \text{ molecule}^{-1} \text{ s}^{-1}$
$\text{BrO} + \text{OH} \rightarrow \text{Br} + \text{HO}_2$	$1.0 \cdot 10^{11} \text{ cm}^3 \text{ molecule}^{-1} \text{ s}^{-1}$
$\text{HBr} + \text{O} \rightarrow \text{Br} + \text{OH}$	$5.8 \cdot 10^{11} \exp(-1500/T) \text{ cm}^3 \text{ molecule}^{-1} \text{ s}^{-1}$
$\text{Br} + \text{CH}_3\text{O} \rightarrow \text{HBr} + \text{CHO}$	$1.7 \cdot 10^{11} \exp(-800/T) \text{ cm}^3 \text{ molecule}^{-1} \text{ s}^{-1}$
$\text{BrO} + \text{NO}_2 + \text{M} \rightarrow \text{BrONO}_2 + \text{M}^{\text{b}}$	$k_a = 5.2 \cdot 10^{-26} (T/300)^{-3.2} \text{ cm}^3 \text{ molecule}^{-2} \text{ s}^{-1}$ $k_b = 9.0 \cdot 10^{-11} (T/300)^{-2.2} \text{ cm}^3 \text{ molecule}^{-1} \text{ s}^{-1}$

(a): see text for the photodissociation rate calculations

(b): considered in the model as the limiting step for the Br production from CH_3Br

$$(c): k = \left(\frac{k_0[M]}{1 + k_0[M]/k_c} \right) 0.6 \left(1 + [\log_{10}(k_0[M]/k_c)]^2 \right)^{-1}$$

requires the diurnal evolution of the short-lived species. Starting with realistic vertical distributions, convergence is obtained after 12 iterations. In the calculations, a total chlorine content of 3.2 ppb and a total bromine content of 20 ppt have been used.

Figure 1 compares the computed vertical distributions of NO_2 , HO_2 and ClO at noon if reaction (5) is included in the photochemical scheme (case b) with the same vertical distributions if (5) is not included (case a). Reaction (5) leads to an important sink of NO_x ($\text{NO} + \text{NO}_2 + \text{NO}_3 + 2 \times \text{N}_2\text{O}_5$), as well as to an additional source of HO_x due to the subsequent photolysis of HNO_3 . Chlorine compounds are also affected by this reaction. High levels of HO_x , through the reaction of OH with HCl , increase the concentration of the reactive chlorine species ($\text{Cl} + \text{ClO} + \text{ClONO}_2$). Low values of NO_2 shift the partitioning between ClO and ClONO_2 in favour of ClO . Figure 1 shows that reaction (5) decreases the NO_2 concentration by 45% and increases the concentration of HO_2 and ClO by respectively 36% and 100%, at 20 km.

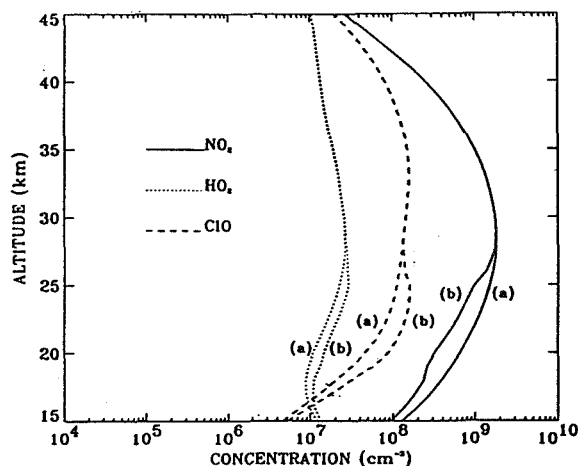


Figure 1: Vertical distribution, at noon, of the concentrations of NO_2 , HO_2 and ClO . Case (a): reaction (5) is not included. Case (b): reaction (5) is included.

These results are globally consistent with the 2D model calculations of Rodriguez et al. (1991). We may assume in consequence that the results of our 1D calculations concerning the influence of the new kinetic data for reaction (1) on both the partitioning of bromine and the ozone depletion are realistic at least globally.

Figure 2 shows the combined effect of the high rate constant k_1 and of the occurrence of reaction (5), on the diurnal averaged concentration of bromine species. Concentrations of BrO and BrONO_2 are mainly affected by reaction (5) in the same manner than chlorine compounds. HOBr is affected by both the reaction (5) and the high

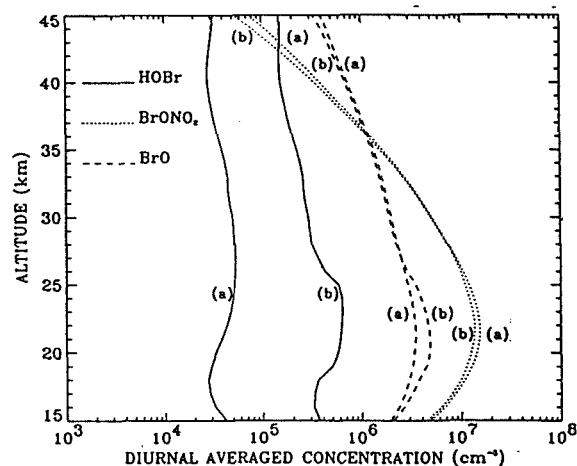


Figure 2: Vertical distribution of the diurnal averaged concentration of HOBr , BrONO_2 and BrO . Case (a): reaction (5) is not included and $k_1 = 5.0 \cdot 10^{12} \text{ cm}^3 \text{ molecule}^{-1} \text{ s}^{-1}$. Case (b): reaction (5) is included and $k_1 = 3.3 \cdot 10^{11} \text{ cm}^3 \text{ molecule}^{-1} \text{ s}^{-1}$.

constant k_1 . At 20 km its averaged concentration is increased

by a factor 20.

The effect of the new rate constant on the efficiency of the catalytic cycles involving bromine compounds to deplete global ozone has been also computed. Four cycles have been assumed: the two cycles already mentioned which involve $\text{BrO} + \text{ClO}$ (cycle I) and $\text{BrO} + \text{HO}_2$ (cycle II) together with those which involve $\text{BrO} + \text{BrO}$ (cycle III) and $\text{BrO} + \text{O}$ (cycle IV). Figure 3 shows the odd oxygen destruction rates by cycles I to IV using the new kinetic data for reaction (1). The odd oxygen destruction rate by all the other cycles is also shown for comparison. The calculations show that the new rate constant has no effect on cycles I, III

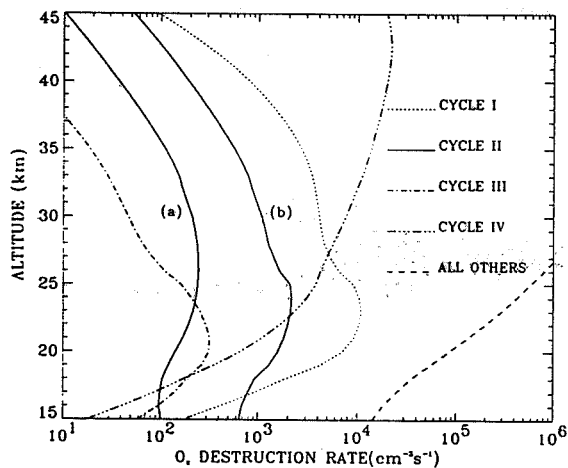


Figure 3: Odd oxygen destruction rate by catalytic cycles I, II, III and IV defined in the text, as a function of altitude, ALL OTHERS refers to the sum of the destruction rates due to the cycles which do not involve bromine species. Reaction (5) is included in the photochemical scheme. The destruction rates for cycles I, III, IV and ALL OTHERS are computed with $k_1 = 3.3 \cdot 10^{-11} \text{ cm}^3 \cdot \text{molecule}^{-1} \cdot \text{s}^{-1}$. For cycle II, case (a): $k_1 = 5.0 \cdot 10^{-12} \text{ cm}^3 \cdot \text{molecule}^{-1} \cdot \text{s}^{-1}$, case (b): $k_1 = 3.3 \cdot 10^{-11} \text{ cm}^3 \cdot \text{molecule}^{-1} \cdot \text{s}^{-1}$

and IV. Figure 3 shows that the rate of cycle II increases by a factor 6 similarly to the increase of the new rate constant. This was expected because reaction (1) is the limiting step of cycle II.

The destruction rate by cycle II is lower than the destruction rate by cycle I by about a factor 4.5 at 20 km. As it can be seen from Figure 4 in Poulet et al. (1992), this factor was only 3 when reaction (5) was not taken into account. The importance of cycle II to deplete ozone is therefore reduced by the presence of aerosols, relatively to cycle I. It remains nevertheless significant.

To quantify the impact of the new rate constant to deplete ozone, the percentage of ozone decrease versus altitude produced by 20 ppt of bromine has been calculated (Figure 4) using successively the low and the high value for the rate constant k_1 . From these calculations, it is found that the new rate constant leads to an increased reduction of the ozone column density from 2.01% to 2.36%. This is significantly higher than the reduction of 1.14% and 1.45%

reported by Poulet et al. (1992).

The channel of reaction (1) yielding HBr and O_3 is not unlikely, mainly at low temperature. Laboratory studies have to establish the branching ratio of this channel. As already pointed out (Poulet et al., 1992), even a small value of this ratio will lead to a large increase of the concentration of HBr in the lower stratosphere making HBr one of the most abundant species of the bromine family (Figure 5). Figure 4 shows also, the percentage of ozone decrease versus altitude produced by 20 ppt of bromine for a 10% branching ratio of the HBr forming channel and the higher value of k_1 . We

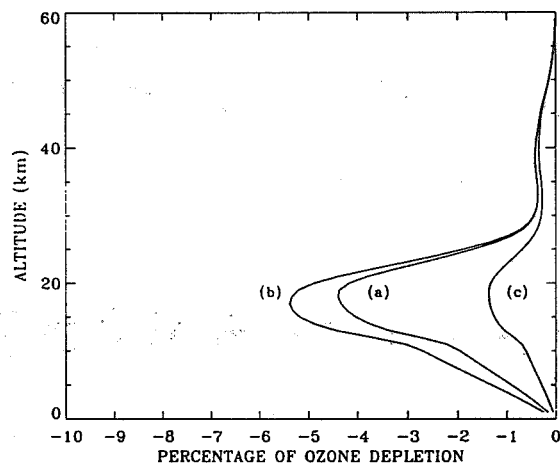


Figure 4: Percentage of ozone depletion produced by 20 ppt of bromine, as a function of altitude. Heterogeneous reaction (5) is included. Case (a): $k_1 = 5.0 \cdot 10^{-12} \text{ cm}^3 \cdot \text{s}^{-1}$, branching ratio for the HBr forming ratio is zero. Case (b): $k_1 = 3.3 \cdot 10^{-11} \text{ cm}^3 \cdot \text{s}^{-1}$, branching ratio is zero. Case (c): $k_1 = 3.3 \cdot 10^{-11} \text{ cm}^3 \cdot \text{s}^{-1}$, branching ratio is 10%.

observe a strong decrease of the ozone reduction. The calculations lead to a decrease of the ozone column density

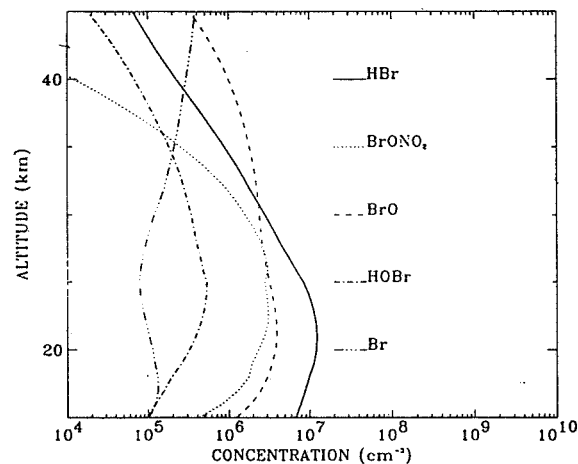
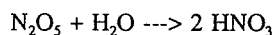


Figure 5: Vertical distribution of the concentration of bromine species, at noon. Reaction (5) is included, $k_1 = 3.3 \cdot 10^{-11} \text{ cm}^3 \cdot \text{molecule}^{-1} \cdot \text{s}^{-1}$, the branching ratio for the HBr forming channel is 10%.

of only 0.75%. These results were expected because HBr is a more efficient reservoir of active bromine than HOBr. We can observe that the inclusion of reaction (5) in the photochemical scheme increases the difference in the reduction of the computed ozone column assuming 10% and 0% for the branching ratio of the HBr forming channel. Using reaction (5) and the higher value of k_1 , the decrease of the reduction of the ozone column is from 2.36% to 0.75%. Neglecting reaction (5), the decrease was only from 1.45% to 0.6%.

3. CONCLUSION

The modelling results presented in this paper, compared with those of Poulet et al. (1992) which did not take into account the heterogeneous reaction:



in the aerosol layer, show that the importance of the catalytic cycle involving the reaction $\text{BrO} + \text{HO}_2$ is reduced compared to the cycle involving the reaction $\text{BrO} + \text{ClO}$, but remains significant. In the present calculations, the ozone column density reduction produced by 20 ppt of total bromine increases from 2.01% (with the lower rate constant k_1) to 2.36% (with the higher rate constant k_1) assuming an aerosol loading twice as high as the "background".

An increase in the aerosol loading would not change significantly these conclusions. Other calculations have been repeated assuming the surface area profile available at Laramie at the maximum of the El Chichon eruption (Hofmann and Solomon, 1989) which was about 25 times as large as the "background". As already pointed out by Rodriguez et al. (1991) the reduction of the ozone column density is not too much affected by this large aerosol loading because the concentration of the NO_x compounds relatively to the concentration of HNO_3 becomes independent of the above heterogeneous reaction when aerosol loading increases. In the presence of this large surface area profile, we calculate a reduction of the ozone column density of 2.6% produced by 20 ppt of bromine with the lower rate constant for the reaction of BrO with HO_2 and a reduction of 3% with the higher rate constant. The cycle involving the reaction $\text{BrO} + \text{HO}_2$ would be therefore significant to deplete ozone even in presence of a large aerosol loading if the new rate constant is taken into account.

The calculations made assuming a 10% branching ratio for the HBr forming channel of reaction $\text{BrO} + \text{HO}_2$ shows an increasing importance of this channel if the above heterogeneous reaction in the aerosol layer is included and when the aerosol loading is increased. This channel would decrease the reduction of the density ozone column produced by bromine species. When the heterogeneous reaction was not included in the photochemical scheme a 10% branching ratio decreases the reduction of the ozone column from 1.45% to 0.6% using the new rate constant, assuming 20 ppt of total bromine. When the heterogeneous reaction is used, the

decrease is from 2.36% to 0.75% with a aerosol loading 2 times as large as the "background" and 3% to 0.85% with a loading 25 times as large as the "background".

Ozone depletion by bromine species is therefore very dependent on the branching ratio for the HBr forming channel of reaction (1). Laboratory investigations are therefore needed, at low temperature, to measure this branching ratio as well as in-situ measurements of HBr. Park et al. (1989) report a far-infrared measurement of 20 ppt at 28 km while Traub et al. (1992) report three measurements and conclude to an upper limit of 4 ppt at 32 km. After Traub et al. (1992), Park and his co-workers now agree that 20 ppt is in fact a tentative upper limit. Our calculations (Figure 5) give 6 ppt at 32 km, assuming a 10% branching ratio. A few percent for this branching ratio would not be therefore inconsistent with the measurements of Traub et al. (1992). Other measurements are obviously needed.

REFERENCES

- De More, W.B., S.P. Sander, D.M. Golden, M.J. Molina, R.F. Hampson, M.J. Kurylo, C.J. Howard and A.R. Ravishankara, Chemical kinetics and photochemical data for use in stratospheric modeling, NASA-JPL Publication 90-1, 1990.
- Hanson, D.R. and A.R. Ravishankara, The reaction probabilities of ClONO_2 and N_2O_5 on 40 to 75% sulfuric acid solutions, *J. Geophys. Res.*, 96, 17307-17314, 1991.
- Hofmann, D.J. and S. Solomon, Ozone destruction through heterogeneous chemistry following the eruption of El Chichon, *J. Geophys. Res.*, 94, 5029-5041, 1989.
- Mac Elroy, M.B., R.J. Salawitch, S.C. Wofsy and J.A. Logan, Reductions of Antarctic ozone due to synergistic interactions of chlorine and bromine, *Nature*, 321, 759-762, 1986.
- Park, J.H., B. Carli and A. Barbis, Stratospheric HBr mixing ratio from far-infrared emission spectra, *Geophys. Res. Lett.*, 16, 787-790, 1989.
- Poulet, G., M. Pirre, F. Maguin, R. Ramaroson and G. Le Bras, Role of the $\text{BrO} + \text{HO}_2$ reaction in the stratospheric chemistry of Bromine, *Geophys. Res. Lett.*, in press.
- Ramaroson, R., M. Pirre and D. Cariolle, A box model for on-line computations of diurnal variations in a 1D model: potential for application in multidimensional cases, *Annales Geophysicae*, 10, 416-428, 1992.
- Rodriguez, J.M., M.K.W. Ko and N.D. Sze, Role of heterogeneous conversion of N_2O_5 on sulphate aerosols in global ozone losses, *Nature*, 352, 134-137, 1991.
- Traub, W.A., D.G. Johnson, K.W. Jucks and K.V. Chance, Upper limit for stratospheric HBr using far-infrared thermal emission spectroscopy, *Geophys. Res. Lett.*, 19, 1651-1654, 1992.
- Wofsy, S.C., M.B. Mac Elroy and Y.L. Yung, The chemistry of atmospheric bromine, *Geophys. Res. Lett.*, 2, 215-218, 1975.
- Yung, Y.L., J.P. Pinto, R.T. Watson and S.P. Sander, Atmospheric bromine and ozone perturbations in the lower stratosphere, *J. Atmos. Sci.*, 37, 339-353, 1980.

303637

THE OZONE DEPLETION POTENTIALS ON HALOCARBONS:
THEIR DEPENDENCE OF CALCULATION ASSUMPTIONS

Igor L. Karol, Andrey A. Kiselev

Main Geophysical Observatory
Karbyshev Str., 7, St.-Petersburg, Russia, 194018

ABSTRACT

The concept of Ozone Depletion Potential (ODP) is widely used in the evaluation of numerous of halocarbons and of their replacements effects on ozone, but the methods, assumptions and conditions used in ODP calculations have not been analyzed adequately.

In this paper a model study of effects on ozone of the instantaneous releases of various amounts of CH_2Cl_3 and of CHF_2Cl (HCFC-22) for several compositions of the background atmosphere are presented, aimed to understand the connections of ODP values with the assumptions used in their calculations.

To facilitate the ODP computation in numerous versions for the long time periods after their releases, the above rather short-lived gases and the one-dimensional radiative photochemical model of the global annually averaged atmospheric layer up to 50 km height are used.

The variation of released gas global mass from 1 Mt to 1 Gt leads to ODP value increase with its stabilization close to the upper bound of this range in the contemporary atmosphere. The same variations are analyzed for conditions of the CFC-free atmosphere of 1960-ies and for anthropogenically loaded atmosphere in the 21st century according to the known IPCC "business as usual" scenario. Recommendations for proper ways of ODP calculations are proposed for practically important cases.

1. INTRODUCTION

Since D. Wuebbles [1983] suggested to use the Ozone Depletion Potential (ODP) of a gas as the measure of its impact on ozone, many publications have been devoted to the ODP calculation problem and to the ODP based recommendations for the replacement of the chlorofluorocarbons (CFCs) by the less dangerous for ozone compounds (e.g. hydrochlorofluorocarbons (HCFCs)), reviewed in [WMO, 1989; WMO/UNEP, 1991].

The simplicity of ODP physical interpretation and its clarity leads to wide use of this concept by non-specialists and to its introduction into such important international treaties as the Montreal Protocol and some other regulations

[WMO, 1988]. Such ODPs universality causes the need to estimate the precision of ODP calculations and its sensitivity to the assumptions used in the model and on conditions of the experiment.

For the definition of ODP of compound A:

- the background steady state atmospheric composition is selected;
- the prescribed instantaneous release of compound A is modelled;
- the atmospheric composition change calculations are continued up to the moment when the initial background atmospheric composition is restored (infinite long by the theory);
- the calculated total ozone changes $\Delta X(t)$ are time integrated (to infinity also by the theory);
- the a-d) steps are repeated for CFC-11 as for compound A;
- the ODP of compound A is the ratio of obtained in item d) integral to similar integral for CFC-11 according to the following mathematical expression:

$$ODP(A) = \frac{\int_0^{\infty} \Delta X_A(t) dt / \Pi(A)}{\int_0^{\infty} \Delta X_{\text{CFC-11}}(t) dt / \Pi(\text{CFC-11})}$$

where $\Pi(A)$ and $\Pi(\text{CFC-11})$ are the compound A and CFC-11 fluxes (releases) into the atmosphere (in mass units).

Since the atmospheric photochemical processes are essentially non-linear and the intensive anthropogenic pollution of the global atmosphere occurs, it is evident that:

- the ODP value of compound A essentially depends on the initial background atmospheric composition (this suggestion is confirmed by S. Solomon et al. [1992], who with aid of modelling and observed data revealed the ODP dependence on the latitude of A injection);
- the ODP value may depend on the scale of the A modelled release;
- the total ozone changes in the atmosphere affected by instantaneous release are not equivalent to the total ozone changes in the continuously affected (more close to reality) atmosphere.

In this paper ODP sensitivity to the background atmospheric composition and to the compound release scale is investigated. The methylchloroform (CH_3CCl_3) and HCFC-22 (CHF_2Cl) are selected as considered compounds, as they have relative short lifetimes and this circumstance allows one to reduce the computer time required for calculations of numerous variants. Consequently the ratio $\text{RDP} = \text{ODP}(\text{CH}_3\text{CCl}_3) / \text{ODP}(\text{CHF}_2\text{Cl})$ instead of the $\text{ODP}(\text{CH}_3\text{CCl}_3)$ and $\text{ODP}(\text{CHF}_2\text{Cl})$ values is considered.

The calculated variants are presented in the Table 1. Three variants of the steady state background atmospheric composition are considered:

P(past), corresponding to 1967 gas composition (with Cl_χ at 40 km equal 0.65 ppbv);

R(recent), corresponding to 1985 gas composition (with Cl_χ at 40 km equal 3.02 ppbv);

F(future), corresponding to 2025 gas composition (with Cl_χ at 40 km equal 4.15 ppbv), the 2025 gas composition was calculated according to "business as usual" (BAU) IPCC scenario [1992 IPCC Supplement].

The four scales of release are considered for each variant, as indicated at the Table 1. Such range of release masses ensures the estimation of sensitivity and suppression of model "noise" influence on the calculation results.

Table 1. The calculated variants and their parameters.

Initial background atmospheric composition		Annual mass release (in Mt/yr)			
Year	(Cl_χ) ₄₀ , ppbv	1.0	17	180	1800
1967	0.65	P1	P2	P3	P4
1985	3.02	R1	R2	R3	R4
2025	4.15	F1	F2	F3	F4
1985-2050	-	-	-	FD3	-

In addition to the steady state variants P, R and F the "dynamic" variant FD3 with continuous changes of atmospheric gas composition in the 1985-2050 period is considered also. The release scale in variant FD3 (180 Mt/yr) allows to obtain the significant effect in spite of the model "noise". The trace gases emissions in variant FD3 is adopted according to BAU IPCC scenario (its 1992 version [1992 IPCC Supplement]). The total ozone change in this variant is the difference between the total ozone deviations in BAU IPCC scenario with and without account of the compound A instantaneous release.

The calculation results have to be considered as the illustration of the system sensitivity to the transient atmospheric photochemistry only. The BAU IPCC scenario is chosen as the most "intensive" and investigated of the known proposed scenarios.

As the qualitative conclusions are the most important, the economically feasible 1-D radiative photochemical model of the annually averaged global

atmosphere is used. This model was successfully compared with the known 1-D LLNL model.

The radiative photochemical model is a combination of the 1-D photochemical model and of the radiative-convective model. The model extends from the Earth's surface to the 50 km with 2 km vertical coordinate differences. In the photochemical block 141 gasphase reactions (including 35 photodissociations) among the 42 compounds of the oxygen, nitrogen, hydrogen, carbon, chlorine and bromine groups in the atmosphere are considered; the photochemical equilibrium is assumed for the 20 short-lived compounds. H_2O is calculated in the stratosphere only, in the troposphere relative humidity is assumed to be constant.

In the radiative-convective model the radiation absorption of CO_2 , H_2O , O_3 , CH_4 , N_2O , NO_2 , HNO_3 , CFC-11 and CFC-12 is considered.

2. THE RESULTS OF MODEL CALCULATIONS

The ratios $\text{RDP} = \text{ODP}(\text{CH}_3\text{CCl}_3) / \text{ODP}(\text{CHF}_2\text{Cl})$ for variants R1-R4 calculated for the finite period of time T in integrals in ODP definition and their dependence on T are presented in Fig.1. The RDP for the t=50 years reaches to 2.01, 2.63 and 2.24 for variants R2, R3 and R4 respectively. It is necessary to emphasize that RDP value change is not linear with the instantaneous release volume increase: its maximum occurs for R3 variant with the common changes of RDP values in about 30%, but this statistics is non-sufficient for the final conclusion. The smallest release of odd chlorine Cl_χ in variant R1 is small and its signal is lost in model "noises". Therefore the $\text{RDP}=0.71$ value for this variant is not significant and not correct.

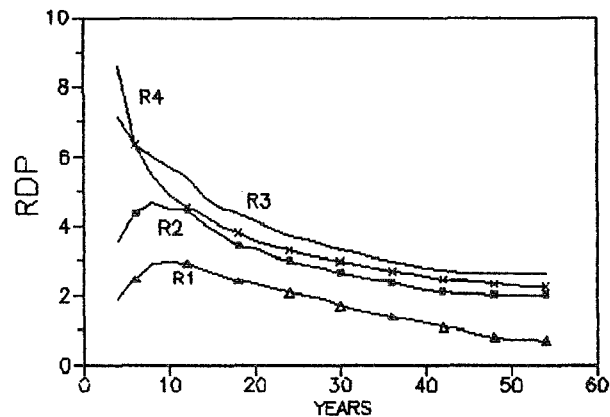


Fig. 1. The time dependence of RDP values for variants R1, R2, R3 and R4 of Table 1.

The Cl_χ mixing ratio at 40 km level is maximal at 9-11th model year for CH_3CCl_3 and at 12-14th model year for CHF_2Cl . The maximal values of the Cl_χ mixing ratio at 40 km are presented in Table 2.

The similar RDP value is shown in the Fig.2 for variants P2, R2 and F2 (i.e. with the same

Table 2. The maximal values of the Cl_x mixing ratio at 40 km (ppbv) for several variants of Table 1.

Gas	CH_2CCl_3					
VARIANT	P2	R1	R2	R3	R4	F2
$(Cl_x)_{40}$	1.98	3.09	4.08	14.3	139	5.04
Gas	CHF_2Cl					
VARIANT	P2	R1	R2	R3	R4	F2
$(Cl_x)_{40}$	1.14	3.05	3.49	7.72	51.4	4.55

release of 17 Mt/yr). The largest RDP value occurs in the "non-freons" atmosphere (variant P). The values of other variants coincide after 10th model year.

The above estimates agree well with ODP values presented in [WMO,1989] and obtained by use of various models. The RDP value changes from 2.0 to 3.2 according to different models. For example:

$$RDP=0.16/0.05=3.2 \text{ (2-D OSLO model),}$$

$$RDP=0.15/0.05=3.0 \text{ (2-D LLNL model),}$$

$$RDP=0.18/0.06=3.0 \text{ (2-D AER model),}$$

$$RDP=(0.1-0.13)/0.05=2.0-2.6 \text{ (1-D RANGE model),}$$

where the numerators and denominators of fractions are the $ODP(CH_2CCl_3)$ and $ODP(CHF_2Cl)$ respectively, estimated by the indicated models.

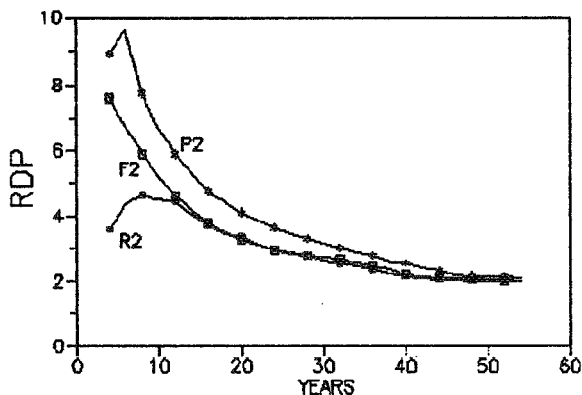


Fig. 2. The time dependence of RDP values for variants P2, R2 and F2 of Table 1.

The total ozone changes for variants R3 and FD3 are compared at the Fig.3. The start of calculations corresponds to 1985 and the years 1990 and 2000 of Fig.3 correspond to 5th and 15th model years and so on. According to the Fig.3, during the first 10-25 years the total ozone changes in steady state variant R3 exceed significantly the same changes of transient "dynamic" variant FD3: in the maximum peak the difference is about 10 D.U. But after the 25-30th model year (2000-2010 in Fig.3) the total ozone changes of FD3 are bigger than the corresponding ones of R3, because of the chlorine atom flow intensity (in the CFCs and HCFCs) in variant FD3 exceed the "conserved" background chlorine content in the stratosphere of the steady

state variant R3. Besides that in the first of them the shares of ozone active chlorine radicals (Cl and ClO) are higher and of passive compounds (HCl , $HOCl$) are lower than in the second variant in the middle and upper stratosphere. The RDP for FD3 variant is in about 1.5 times bigger than for R3 variant all the time and it is equal 3.77 for the year 2050.

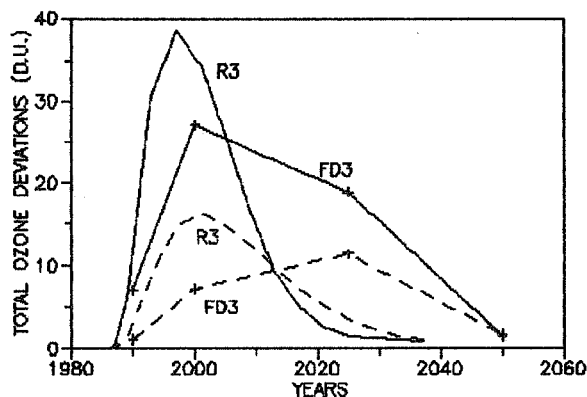


Fig. 3. The total ozone deviations of variants R3 and FD3 of Table 1 for CH_2CCl_3 (solid lines) and for CHF_2Cl (dashed lines).

The calculated lifetimes CH_2CCl_3 and CHF_2Cl for various variants are presented in the Table 3.

Table 3. The lifetimes τ of CH_2CCl_3 and CHF_2Cl (years) and RCLP values (see Text).

VARIANT	$\tau(CH_2CCl_3)$	$\tau(CHF_2Cl)$	RCLP
P2	9	20	0.87
R1	6-7	15	0.78-0.90
R2	5.5-6	15	0.71-0.78
R3	6-7	15	0.78-0.90
R4	5.5-6.5	13-14	0.76-0.97
F2	4-5	10-11	0.71-0.97

Here the lifetime of compound A is the period of the e time decrease of the initial A content. The tendency of the lifetime decrease for the transition to delayed initial background gas composition (i.e. from state P to state R and further to state F) occurs both for CH_2CCl_3 and CHF_2Cl . The obtained lifetimes are in quantitative agreement with their accepted values, which is equal to 6.3 years for CH_2CCl_3 and to 15-17 years for CHF_2Cl [WMO,1989; WMO/UNEP,1990].

Also the relative chlorine loading potentials of the ratio of CH_2CCl_3 and CHF_2Cl are estimated. The chlorine loading potential of compound A is defined in [WMO, 1989; WMO/UNEP,1991] as

$$CLP(A) = \frac{\tau(A)}{\tau(CFC-11)} \cdot \frac{M(CFC-11)}{M(A)} \cdot \frac{n(A)}{n(CFC-11)}$$

where τ , M and n are the lifetime, the molecular weight and the number of chlorine atoms per molecule in compound A or $CFC-11$ correspondingly. Then the ratio of the CH_3CCl_3 and CHF_2Cl chlorine loading potentials is

$$RCLP = \frac{CLP(CH_3CCl_3)}{CLP(CHF_2Cl)} = \frac{\tau(CH_3CCl_3)}{\tau(CHF_2Cl)} \cdot \frac{M(CHF_2Cl)}{M(CH_3CCl_3)} \cdot \frac{n(CH_3CCl_3)}{n(CHF_2Cl)} = 1.944 \cdot \frac{\tau(CH_3CCl_3)}{\tau(CHF_2Cl)}$$

because of values $M(CH_3CCl_3)=133.5$, $M(CHF_2Cl)=86.5$, $n(CH_3CCl_3)=3$ and $n(CHF_2Cl)=1$. The calculated RCLP values in Table 3 are somewhat higher than the corresponding values of other models: RCLP=0.67 (2-D OSLO model), RCLP=0.71 (2-D LLNL model), RCLP=0.62 (2-D AER model), RCLP=0.65 (DuPont), RCLP=0.67 (Solomon,Garcia) [S.Solomon et al., (1992)].

3. SUMMARY AND CONCLUSIONS

The ratio of ODPs and ODPs themselves depend significantly on the mass of the investigated compound release. The ratio of full ODPs slightly depends on initial background gas composition as the total ozone significantly decreases for delayed in time background atmospheric gas composition. This decrease is due to chronological increase (from period P to period F) of Cl_x content in the stratosphere. The background trace gases emission evolution leads to the significant changes of total ozone deviations in time and to RDP transient variant increase in comparison to stationary F3 variant. The large uncertainties in expected trace gases release scenarios requires the caution in application of these results. The lifetimes of CH_3CCl_3 and CHF_2Cl have the tendency to decrease for more anthropogenically loaded background gas composition (because of the OH content changes).

The obtained RDP values have a range about 30-50% for different conditions of the experiment, but this range may be somewhat bigger for other compounds. The obtained results have qualitative character and serve as the base for the further investigations only.

REFERENCES

- IPCC 1990. Houghton J.T., Jenkins G.J., Ephraumis J.J. (Eds.), 1990: Climate Change. The IPCC Scientific Assessment (Cambridge

University Press)

IPCC 1992 Supplement. Scientific Assessment of Climate Change. Submission from Working Group 1. WMO/UNEP

Solomon S., Mills M., Heidt L.E., Pollok W.H., Tuck A.F., 1992: On the Evaluation of Ozone Depletion Potentials, J.Geophys.Res., 97,D1,825-842

WMO 1988. Montreal Protocol on the problem of ozone depleting substances. WMO Bulletin, v.37,N 2,118-120

WMO 1989. Scientific Assessment of Stratospheric Ozone: 1989, v.1. WMO Global ozone Research and Monitoring. Project Rep. N 20

Wuebbles D.J., 1983: Chlorocarbon emission scenarios: Potential impact on stratospheric ozone, J.Geophys.Res., 88,1433

303638

MODEL EVALUATION OF THE RADIATIVE AND TEMPERATURE EFFECTS OF THE OZONE
CONTENT CHANGES IN THE GLOBAL ATMOSPHERE OF 1980-IES

Igor L. Karol, Victor A. Frolkis

Main Geophysical Observatory
Karbyshev Str., 7, St.-Petersburg, 194018, Russia

ABSTRACT

Radiative and temperature effects of the observed ozone and greenhouse gas atmospheric content changes in 1980 - 1990 are evaluated using the two-dimensional energy balance radiative-convective model of the zonally and annually averaged troposphere and stratosphere. Calculated radiative flux changes for standard conditions quantitatively agree with their estimates in WMO/UNEP, 1991 review. Model estimates indicate rather small influence of ozone depletion in the lower stratosphere on the greenhouse tropospheric warming rate, being more significant in the non tropical Southern Hemisphere. The calculated cooling of the lower stratosphere is close to the observed temperature trends there in the last decade.

1. INTRODUCTION

Significant ozone content changes in the lower stratosphere and troposphere as observed in 1980-ies with enhanced intensity during the recent years [WMO/UNEP, 1991] result in variations of radiative and temperature climate of the global atmosphere. The preliminary estimates of these variations have been used for important conclusions about their influence on the rate of greenhouse warming of the global troposphere [WMO/UNEP, 1991; Ramaswamy et al., 1992]. In these publications the meridional distributions of radiative flux variations at the tropopause level are evaluated, as caused by the observed changes of ozone and greenhouse gas content at various latitudes and levels of the global atmosphere in 1980-1990.

As the tropospheric temperature changes only to some extent are determined by the above radiative flux variations, more precise evaluation of the climatic radiative and temperature effects by the comprehensive climatic models is necessary [Ramaswamy et al., 1992]. However, the relative small amplitude of ozone changes makes difficult to reveal the effect "signal" over the considerable "noise" level in such models [IPCC, 1990].

In this paper the mean annual, zonally averaged solar and thermal radiation fluxes and temperature variations at various levels of the global atmosphere are estimated using the two-dimensional Energy Balance Radiative Convective

Model (EBRCM), described in [Karol and Frolkis, 1984]. As indicated in this paper and in [Karol et al., 1986] the radiative and temperature changes caused by the increase of CO₂ concentration in the atmosphere and estimated by EBRCM are very close to those obtained in the three-dimensional comprehensive atmospheric climate models.

In the first part of the paper after the short description of the model, the radiative forcing caused by ozone and greenhouse gases (GG) content changes in conditions used in [WMO/UNEP, 1991; Ramaswamy et al., 1992] are calculated and compared with results in these publications, making in a such way the comparison of the radiative schemes codes and models. Then the annually averaged mean zonal radiative flux and temperature changes are estimated [IPCC, 1990] as caused by the observed GG and ozone content changes for the time period 1980-1990. Some observed evidences of these changes are discussed in the conclusion of the paper.

2. SHORT DESCRIPTION OF THE MODEL

The model is presented in details in [Karol and Frolkis, 1984]. Annually and zonally averaged radiation fluxes and temperature distributions in the global atmosphere up to H=0.64 hPa (50 km) level with prescribed radiatively-active atmospheric constituent concentrations and other parameters are determined by successive approximation up to equilibrium state. At each step the vertical temperature profiles are determined from eight Radiative-Convective Models (RCM) at 80°, 60°, 40°, 15° N and S with 15 horizontal layers, and with surface air temperature T₀, taken from the previous approximation step. These profiles and other information are used for computation of solar and thermal radiation fluxes S_H and F_H at the considered upper atmospheric boundary. T₀ distributions are the solutions of the energy balance equation

$$\frac{d}{dx} j(x) \cdot (1-x^2) \frac{dT_o(x)}{dx} = F_H(x) - S_H(x),$$

where ϕ is the latitude; $x = \sin \phi$; $j(x) = j_0 K(x)$; $j_0 = c_p \cdot p_0 / g R_e^2$; $K(x)$ is the effective horizontal heat transport coefficient. "Heat walls" at the poles are the boundary conditions for this equation solution, which is used for eight RCM at the next

step of successive approximation. Besides the coarse grid of eight zonal belts the fine grid of 36 belts with $\Delta\phi=5^\circ$ is used in computations.

Solar radiation flux calculations are based on the two-stream delta-Eddington scheme. The UV band (197.5-312.5 nm) is divided into 11 spectral intervals, where O_3 , O_3 , NO_2 and aerosol effects are accounted. Visible band contains two spectral intervals with inclusion of O_3 , NO_2 , molecular, aerosol and cloud scattering and reflectance. NIR band (750-4000 nm) is divided into 12 spectral intervals, in which the selective H_2O , CO_2 , O_3 , N_2O and CH_4 absorption is accounted approximated by the Goody transmission function for the statistical model of the absorption band. An original approach is used for the approximate calculation of selective gas absorption and scattering of photons by aerosol and clouds with multiple reflection from the cloud layer boundaries.

The thermal radiation fluxes are calculated for 17 spectral intervals in the 4.4-1000 micrometers band. The transmission functions for the same gas selective absorption are approximated as in NIR with the atmospheric vertical density layering accounted by Curtis-Godson approximation. Weak absorption approach is used for CFCs. H_2O continuum absorption and diffusivity approximation are included, but the cloud and aerosol transmission functions are non-selective. The ground surface and clouds are considered as black bodies.

The external data and conditions, used in the calculations of the radiation flux variations, caused by the GG and ozone changes are presented in Tables 1 and 2. These data are taken from the sources and are the closest to those used in [Ramaswamy et al., 1992], for model comparison. In Table 2 the daily averaged cosine of the solar zenith angle ϕ_* , the clear day relative duration t_* and surface albedo A_s for selected cases used in our calculations are also presented, being not indicated in [WMO/UNEP, 1991; Ch.7 and Ramaswamy et al., 1992]. For comparison purposes the clear sky Mode A with fixed temperature profiles Model I radiative forcing values are used from the above publication.

Table 1. Globally and annually averaged GG tropospheric mixing ratios in 1980 and their increases to 1990 [IPCC, 1990; WMO/UNEP, 1991].

Gas	CO_2	CH_4	N_2O	CFC			
				11	12	113	22
Units	ppmv			ppbv			
1980	337	1.57	302.6	0.158	0.27	0.015	0.05
1980-1990	17	0.15	8.0	0.111	0.17	0.050	0.07

3. RESULTS OF CALCULATIONS.

The radiative forcing (the net total long + short wave radiative flux variations at the tropopause level) is compared in Table 3 for the above conditions as calculated by EBRM and by Mode A, Model I in [WMO/UNEP, 1991]. The radiative forcing caused by ozone, CFC and other GG content change is shown separately. The agreement between

the two model results are good, not only at the tropopause, but at the ground surface also, being the worst for CFC, as in EBRM only the radiative forcing of CFC-11 and 12 are included.

Table 2. Cases selected for radiative forcing calculations due to ozone depletion in the lower stratosphere $\Delta(O_3)$ for standard temperature profiles: tropical-T; midlatitude summer-MLS and winter-MLW; subArctic winter-SAW [WMO/UNEP, 1991]. Daily averaged solar zenith angle ϕ_* , clear day relative duration t_* and surface albedo A_s , which are used in calculations.

No.	Latitude	Month	Temp. Profile	$\Delta(O_3)$ (%)	$\cos\phi_*$	t_*	A_s
1	0°	July	T	-0.5	0.586	0.500	0.076
2	$45^\circ N$	July	MLS	-2.0	0.570	0.640	0.123
3	$45^\circ N$	Feb.	MLW	-8.0	0.301	0.399	0.271
4	$45^\circ S$	Jan.	MLS	-6.0	0.570	0.639	0.067
5	$45^\circ S$	Aug.	MLW	-5.0	0.296	0.396	0.098
6	$70^\circ N$	Mar.	SAW	-17.0	0.134	0.372	0.641
7	$75^\circ S$	Oct.	SAW	-32.0	0.205	0.588	0.799

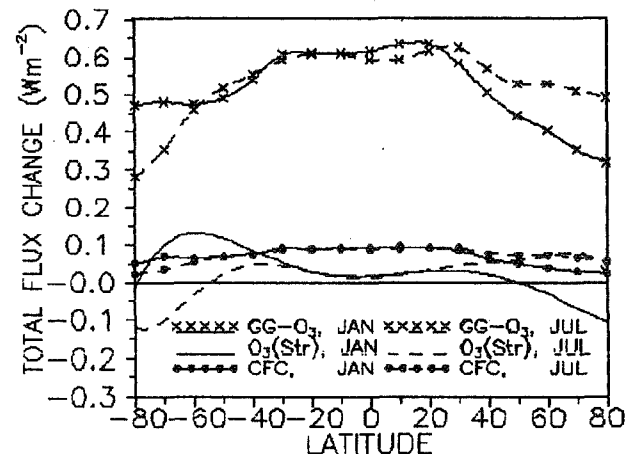


Fig. 1. Total net flux changes at the tropopause level (for Mode A) for January and July due to only O_3 ($O_3(Str)$), to non-ozone GG ($GG-O_3$) and to CFC (CFC) content variations.

Figure 1 demonstrates the meridional distribution of solar and thermal net radiation flux changes at the tropopause level for January and July, calculated by EBRM for ozone and non-ozone GG content variations, indicated in Tables 1 and 2, for Mode A and clear sky conditions.

Ozone depletion leads to increasing of the solar radiation flux coming to the surface-troposphere system at all latitudes throughout the year. The long wave cooling of this system by ozone depletion in Mode A is exceeding its solar warming only in the polar winter. The influence of the atmospheric temperature changes on the radiation

flux variations may be assessed from Table 4 with the meridional variations of annually and zonally averaged changes of solar and thermal radiation fluxes at the tropopause level for Mode C, for the cloudy atmosphere, for GG content increase in Table 1 and for annually averaged ozone depletion estimates in Table 5. The Mode C difference from the Mode B in [WMO/UNEP, 1991; Ramaswamy et al., 1992] is that in Mode C the radiation variations induced by the temperature changes are calculated by EBRCM with account of clouds. In the Mode B the tropospheric temperature and humidity remain unchanged, while the stratospheric temperature is in the radiative equilibrium under the assumption of a so-called Fixed Dynamical Heating concept [WMO/UNEP, 1991].

Table 3. Net radiation flux changes at the tropopause and at the surface levels due to GG and ozone content variations and for the cases and conditions indicated in Table 1 and 2, as evaluated in [WMO/UNEP, 1991, Ch.7]-Mode A and in this work-F.

Cases	CO ₂ +CH ₄ +N ₂ O		CO ₂ +CH ₄ +N ₂ O+CFC		CFC		Ozone	
	Tropopause		Surface		A	F ^a	A	F
	A	F	A	F				
1	.54	.520	.14	.154	.16	.096	.01	.006
2	.51	.460	.20	.231	.13	.074	.08	.024
3	.41	.400	.35	.369	.08	.053	.03	.026
4	.51	.457	-	-	.13	.071	.06	.064
5	.41	.400	-	-	.08	.053	.05	.025
6	.34	.347	.28 ^b	.284 ^b	.05	.034	-.17	-.041
7	.34	.342	.37 ^c	.377 ^c	.05	.033	-.41	-.066

^a/ - For CFC-11 plus CFC-12 only.

^b/ - For SAS temperature profile.

^c/ - For SAM temperature profile.

Figure 2 demonstrates the calculated zonally and annually averaged surface air temperature changes, induced by the radiative forcing due to GG and ozone content changes in Tables 1 and 5, calculated for Mode C conditions and for cloudy atmosphere assumed not to be changing during the period under consideration. The meridional distribution of calculated air cooling in the lower stratosphere, due to ozone depletion being maximal at the 80 mb level is also presented at Fig.2.

4. DISCUSSION OF RESULTS.

The comparison of the net radiation flux variations for the seven standard cases, indicated in the Table 2 and evaluated in [WMO/UNEP, 1991,Ch.7] and in this work as presented in Table

3, reveal the good agreement of calculation results for all cases, bearing in mind the possible deviations in surface short wave albedo, which is not indicated in [WMO/UNEP, 1991, Ch.7]. The agreement of CFC radiative forcing estimates in Table 3 will be improved substantially by increasing our estimates by about 40-60% for account of radiative effects of CFC content increase, other than CFC-11,12.

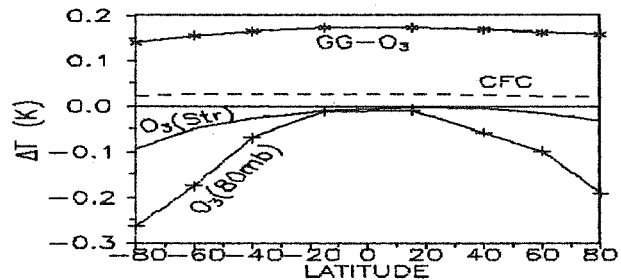


Fig.2. The calculated ΔT_0 obtained for all GG without O₃ (GG-O₃), for CFC only (CFC), for lower stratospheric O₃ only (O₃(Str)) and ΔT at 80 mb level divided by 10 (O₃(80mb)) all for Mode C.

Table 4. The net fluxes of solar ΔS and total ΔR radiation changes (Wm⁻²) at the tropopause level for modes A and C due to gas content variations, indicated in Tables 1 and 5.

Gas	Flux	Southern Latitudes				Northern Latitudes			
		80 ⁰	60 ⁰	40 ⁰	15 ⁰	15 ⁰	40 ⁰	60 ⁰	80 ⁰
Mode A									
O ₃	ΔS	.12	.24	.125	.014	.013	.12	.17	.14
O ₃	ΔR	-.074	.090	.074	.018	.019	.18	.18	-.050
CFCs	ΔR	.022	.034	.046	.056	.058	.048	.037	.029
GG ^a	ΔR	.31	.37	.435	.47	.48	.44	.38	.34
GG ^a	ΔS	.004	-.012	-.025	-.016	-.016	-.024	-.014	-.004
O ₃ ^b	ΔS	.10	.21	.112	.012	.012	.10	.14	.11
O ₃ ^b	ΔR	-.064	.073	.051	.009	.008	.09	.10	-.051
Mode C									
O ₃	ΔS	.012	.25	.13	.015	.013	.12	.18	.15
O ₃	ΔR	-.014	-.14	-.01	.040	.016	.038	.009	-.29
CFCs	ΔR	-.003	-.004	9E-4	.003	.002	.002	-.003	-.002
GG ^a	ΔR	-.0033	.0042	.018	-2E-4	-6E-4	.017	.0012	-.033

^a/ - The sum of greenhouse gases, omitting the ozone variations.

^b/ - Ozone content changes only in the lower stratosphere.

The meridional profiles of radiation flux changes in Fig.1 and in Table 4 are close to relevant curves in Figs. 7.3 and 7.4 in [WMO/UNEP, 1991, Ch.7] for Mode A with fixed atmospheric temperatures. Flux changes are somewhat greater in

the cloudless atmosphere (Mode A) as compared to those in the cloudy atmosphere (Mode C). Therefore our radiation flux calculation schemes and Mode A (fixed temperature) results are close to those in [WMO/UNEP, 1991; Ramaswamy et al., 1992]. The radiative cooling of the lower stratosphere by the ozone depletion effects enhances the negative mean annual total radiation change in the Southern Hemisphere outside of tropics and in the northern polar zone. This ozone caused negative change outweighs by several times the positive (thermal) radiation forcing, caused by the CFC in north polar and south non-tropical latitudes, as it has been found in [WMO/UNEP, 1991], but not in the north temperate latitudes. (The account of other CFCs increases the forcing by 30-50% only [IPCC, 1990] and will not change the above conclusion qualitatively.) Due to above explained differences in temperature change evaluation, the radiation flux variations in the affected temperature fields in EBRCM and in [Ramaswamy et al., 1992] are incomparable in principle and GG and ozone content variation effects assessed by EBRCM may be estimated better by the temperature change analysis.

Table 5. Annually and zonally averaged ozone content changes (%) during 1980-1990 at indicated latitudes and layers, as estimated in [WMO/UNEP, 1991] and used in calculations.

Layer (km)	N, Latitudes			20°N- -20°S	S, Latitudes		
	80°	60°	40°		40°	60°	80°
Troposph.	0	8	8	2	0	0	0
$h_{T_r} - h_{T_r+7}$	-20	-10	-8	-1.6	-10	-20	-30
37 - 45	-10	-5	-3	-0.8	-5	-10	-17

The ΔT_0 -surface air annually averaged "radiative" temperature profiles at Fig.2 demonstrate, that the negative ΔT_0 produced by the observed ozone depletion in the lower stratosphere, surpasses the positive CFC ΔT (underestimated, as pointed out above) only in the polar zones. Maximal ozone produced ΔT_0 around the South Pole attains of about 70% of GG warming in this area, but in the Northern Hemisphere the ozone produced reduction of GG warming does not exceed 25%, being maximal in the North Pole area. This small reduction of the greenhouse warming rate in the lower atmosphere due to observed ozone depletion may be even less in reality with account of the known oceanic thermal inertia effect [IPCC, 1990, Ch.6]. According to several estimates the time delay of the surface air greenhouse warming due to this effect is about 10-20 years [IPCC, 1990; Karol and Jagovkina, 1992] and therefore the actual T_0 increase in 1980-ies is reflecting the greenhouse radiative forcing in previous decades, when ozone depletion forcing was nonsignificant.

The globally averaged $\Delta T_{0a} = 0.129K$ from Fig.2 and $\Delta R_3 = 0.44 Wm^{-2}$ from Table 4 for all GG increase except ozone in 1980-1990 is in good agreement with $\Delta T_{0a} = 0.139K$ and $\Delta R_3 = 0.54 Wm^{-2}$ estimated in [IPCC, 1990]. The negative ΔT_{80a} in the lower stratosphere at Fig.2, when globally averaged is

$\Delta T_3 = -0.58 K$ and it is close to the globally averaged observed temperature negative trend of 0.4 K/decade in the layer between 100 and 50 hPa [WMO/UNEP, 1991, Ch.2].

The observed ozone concentration changes outside the lower stratosphere are much less influencing the radiation and temperature regime in the lower troposphere, as revealed by Table 4, where the solar and net radiation flux changes are compared as caused by all the ozone variations, indicated in Table 4, and by its variations in the lower stratosphere only.

The consequences of "ozone compensation" of the greenhouse warming in the southern polar zone in 1980-ies may result in different changes in the total areas of snow and of ice in the Antarctic and in the Arctic [Cloersen and Campbell, 1991]. While this area decreases in the Arctic, it does not undergo any changes in the Antarctic.

An express Bulletin [GECR, 1992] announced recently that UARS satellite measured 10% lower ozone concentration in 10° S - 20° N zone in January 1992 as a possible result of Mt. Pinatubo volcano aerosol plume effects. Ten percent ozone reduction in the 7 km layer over the tropopause of the 20° S - 20° N zone leads to calculated $\Delta S = 0.13 Wm^{-2}$ and $\Delta R = 0.15 Wm^{-2}$ of solar and total flux changes for Mode A, thus offsetting the tropical minimum of ozone induced change in the flux meridional profile (see Fig. 1 and Table 4). Due to short period radiative forcing, caused by volcano plumes, and its transient effect on the air temperature, the stationary EBRCM is not suited for evaluation of such effects.

REFERENCES

- GECR, 1992: Global Environmental Change Report, v.IV, N3, 2.
- Gloersen P., Campbell W.J., 1991: Recent variations in Arctic and Antarctic sea-ice covers, Nature, 352, 33-36.
- IPCC, 1990: Climate Change. The IPCC Scientific Assessment WMO/UNEP, Cambridge Univ.Press, 365p.
- Karol I.L., Frolkis V.A., 1984: Energy balance radiative-convective model of the global climate, Meteorol. i Gidrol., 8, 59-68 (in Russian).
- Karol et al., 1986: Radiative-photochemical models of the atmosphere (p.p. 51-70), Gidrometeoizdat, Leningrad (in Russian).
- Karol I.L., Frolkis V.A., 1992: Estimation of radiative and temperature consequences of ozone content changes in the global atmosphere in 1980-1990, Doklady of Russian Academy of Sciences, 323, 66-69 (in Russian).
- Karol I.L., Jagovkina S.V. 1992: The estimations of the ocean thermal inertia contribution to the greenhouse warming potentials of the freons, Meteorol. i Gidrol., 7, 45-53 (in Russian).
- Ramaswamy V., Schwarzkopf M.D., Shine K.P., 1992: Radiative forcing of climate from halocarbon induced global stratospheric ozone loss, Nature, 355, 810-812.
- WMO/UNEP, 1991: Scientific Assessment of Ozone Depletion 1991, WMO Global Ozone Res. and Monitoring Project, Rep. N25, Washington D.C.

303639

A Search for Relativistic Electron Induced Stratospheric Ozone Depletion

Arthur C. Aikin

Code 916

NASA Goddard Space Flight Center
Greenbelt, Maryland 20771, USA**Abstract**

Possible ozone changes at 1 mb associated with the time variation and precipitation of relativistic electrons are investigated by examining the NIMBUS 7 SBUV ozone data set and corresponding temperatures derived from NMC data. No ozone depletion was observed in high-latitude summer when temperature fluctuations are small. In winter more variation in ozone occurs, but large temperature changes make it difficult to identify specific ozone decreases as being the result of relativistic electron precipitation.

Introduction

The deposition of energetic electrons and protons in the mesosphere and stratosphere creates N, NO, HNO₃, and OH from molecular oxygen, nitrogen and water. The increase in these minor species causes ozone to be destroyed (Weeks et al, 1972 ; Heath et al, 1977). These initial detections of the ozone-depleting effects of energetic charged particles were associated with energetic protons originating in solar flares. The recovery time for stratospheric and mesospheric ozone was several days. However, these events are the result of the largest proton event, August 1972, and another large flare. Most proton flares produce a measurable effect in the stratosphere, 2 to 0.5 mb, which is much smaller and often lasts for only a few hours (McPeters and Jackman, 1985). The number of such flares is limited to several per year, with some years having very few, depending on solar sunspot cycle (Jackman and McPeters, 1985).

It is well established that the terrestrial radiation belts contain fluxes of relativistic electrons, some with energy in excess of 1 MeV. Such energy is sufficient to allow the electrons to penetrate below 50 km in the atmosphere. These fluxes of electrons exhibit rapid time variation (Nagai, 1988). It has been suggested that the large temporal variations correspond to deposition of these electrons into the atmosphere (Thorne, 1979; Baker et al, 1986, 1987). Direct measurements of relativistic electron flux events have been reported by Herrero et al (1991). It has been suggested that the electron density enhancements below 70 km observed above Scott Base, Antarctica are the result of relativistic electron precipitation (von Biel, 1991). An examination by Aikin (1992) failed to establish any correlation in the summer events studied. Southern hemisphere high-latitude winter and spring ozone changes have been correlated with orbiting electron flux changes (Callis et al, 1991). The present paper is a more extensive investigation of the NIMBUS 7 data set for the effect on ozone of energetic electron events.

Relativistic Electron Fluxes and Their Regions of Precipitation

Large fluxes of electrons with energies greater than 1 MeV are observed in the radiation belts (Baker et al, 1986, 1987). A sample of such observations for parts of 1984 and 1985 is shown in Figure 1., which is adapted from Nagai (1988). Flux changes of several orders of magnitude are observed within a period of several days. These large changes in flux would seem to indicate that the electrons have been deposited in the

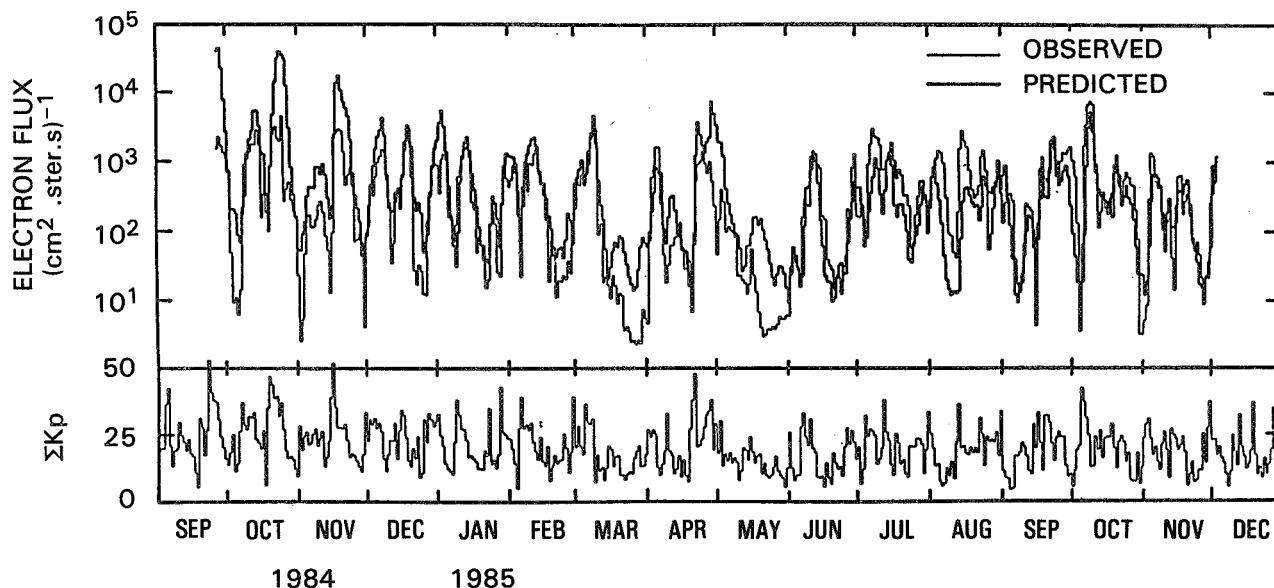


Figure 1 Geosynchronous orbit relativistic electron fluxes for 1984 and 1985 together with predicted flux variations. (Adopted from Nagai, 1988).

atmosphere. Their energies are sufficient in some cases to be deposited at altitudes as low as 45 km.

Analysis of Relativistic Electron Flux Decay Periods for Evidence of Stratospheric Ozone Depletion

The flux changes depicted in Figure 1 are used to identify periods when relativistic electron precipitation should occur. The ozone data set acquired with the SBUV instrument on NIMBUS 7 was used to provide ozone mixing ratios at a pressure level of 1 mb (48 km). Data are averaged over the designated time periods. Since all longitudes are not covered each day, data gaps will be present when only one or two days are considered. Ozone data are displayed in the form of polar projection maps. The ozone amounts at each location are expressed in $\mu\text{g/g}$ and displayed as different colors. The legend for these amounts is included on each color panel.

Using data taken from the NOAA satellites, temperature is also displayed for each period studied for ozone changes. These data termed NMC, are displayed on a polar plot for the pressure level of 1 mb. Depending on season, temperature can exhibit differing degrees of zonal asymmetry and temporal variability. Temperature changes affect ozone through the rate coefficients, which are temperature dependent, so that it is advisable to choose time periods when the temperature

is zonally symmetric between 60° latitude and the north or south poles. Summer is the best season to meet this criterion.

The Event of June 1985

Figure 1 shows that there is a two orders of magnitude change in electron flux, which began in mid-June of 1985. The predicted relativistic electron flux changes are based on a model, which utilizes the magnetic index Kp. Flux decreases begin around 10 June and reach a minimum at 20 June. The beginning of June is characterized by a buildup in radiation belt flux, so large amounts of relativistic electron flux precipitation will be negligible in this period.

During the month of June, the temperature field north of 60° is uniform with the highest global temperatures of the 1 mb pressure surface found in this region. This is illustrated in Figure 2, which presents a series of polar plots covering the periods from 1 to 7, 8 to 14, 21 to 27, and 28 to 30 June 1985. Between 60° and 70° , the temperature distribution is zonally symmetric, with values between 270°K and 275°K . The region between 70° and the pole has temperatures lying between 275°K and 280°K . This picture of a two-temperature spatially uniform representation north of 60° is valid for the entire month of June. Temperature changes are not an important factor in any ozone

change seen at 1 mb during June 1985.

The corresponding polar plots of ozone at 1 mb cover the same time periods in June as the temperature, are also shown in Figure 2. Here the ozone mixing ratio is displayed according to the color legend given on the side of each panel. The ozone distribution north of 60° latitude exhibits a decrease as the month progresses. The maximum decrease is on the order of $50 \times 10^{-2} \mu\text{g/g}$ at latitudes greater than 70°. Zonal symmetry about the north pole is maintained throughout the month. There is no spatial dependence, which might be attributed to relativistic electron precipitation within the auroral zone. This effect may be canceled by a very rapid zonal circulation producing symmetry. Alternatively, it may be that any ozone reduction potential produced by electron of nitric oxide is overwhelmed by the production caused by normal photochemistry in the presence of sunlight.

Other Events Attributed to Relativistic Electron Events

Von Biel (1989) has reported radio wave partial reflection observations of electron densities as large as 10^3 cm^{-3} at 50 km above Scott Base (77°51'S 166°45'E geographic and 79°12'S 315°30'E geomagnetic) near the south geomagnetic pole. Periods of elevated electron densities were compared with ozone maps at 1 and 2 mb by Aikin (1992) to determine if any ozone depletion was associated with these events. Of the events studied. No ozone depletion was found to be associated with the events studied.

Discussion

No ozone depletion was detected in the northern auroral zone during June in spite of

the large relativistic electron flux changes observed by high altitude in situ electron measurements. Since the temperature was well behaved north of 60°, exhibiting no large spatial or temporal excursions, the ozone data need not be corrected for temperature.

One possible explanation is that the pitch angle distribution of the precipitated electrons is restricted to angles greater than 30°. This effect has been observed by Herrero et al (1991). The different altitudes for the effective depths of penetration for a 1 MeV electron with a range of incidence angles from 0° to 70° are summarized in Table I. These depths of penetration do not take into consideration bremsstrahlung, caused by electron deceleration and having energy not exceeding the energy of the electron. The depth of penetration of these x-rays is greater than that of electrons of the same energy. However, the contribution of x-rays is a small fraction of the electrons.

If the electron pitch angles are greater than 30°, then the spectrum of electrons deposited below 50 km is restricted to those electrons with energies greater than 2 MeV for pitch angles of 30°, greater than 3 MeV for pitch angles greater than 45°, and 4 MeV for electrons with an angle of 60°. Those electrons with even greater pitch angles must have energies in excess of 4 MeV, a situation unlikely to occur for these precipitation events. In a recent measurement of electron fluxes between the energies of 0.1 and 3.8 MeV during a relativistic electron event from Poker Flat, Alaska, (65.1°N, 147°W), for an L=5.5, Herrero et al (1991) found that for electrons with energies greater than 0.5 MeV that the flux of electrons with a pitch angle of 90° was about 100 times the flux of electrons with 0° pitch angle. This measurement

Table I
Deposition Height (km) for Electrons With Different Energies and Pitch Angles

Electron Energy (MeV)	Pitch Angle				
	0°	30°	45°	60°	70°
1	54	55.5	57.5	59.5	61.5
2	49	50	51	54.5	57.5
3	48	49	50	53.5	56.5
4	44	46	47.5	50.5	53.5

occurred during a small event. During large events, the spectrum will contain more high energy electrons, which penetrate further into the atmosphere. Nevertheless, one cannot avoid the likelihood that the amount of ionization below 50 km created by relativistic electrons may be less than the isotropic pitch angle. One possibility is to examine higher-altitude ozone data. In the case of SBUV this is difficult. Data at 0.5 mb are much less accurate than at lower altitudes.

Because of the influence of disturbed meteorological conditions and the loss of data in regions where sunlight does not penetrate during winter, only summer data were examined in this study. The increased amount of odd hydrogen produced by sunlight in the summer relative to the winter means that the influence of energetic charged particle deposition is reduced by a factor of 2. This translates into an expected change of 6 to 8% for the predicted ionization rates. While the signal-to-noise ratio is better in summer, the magnitude of the expected ozone decrease is better in winter. These figures are based on studies of solar flare-produced proton events (McPeters and Jackman, 1985 ; Jackman and McPeters, 1985).

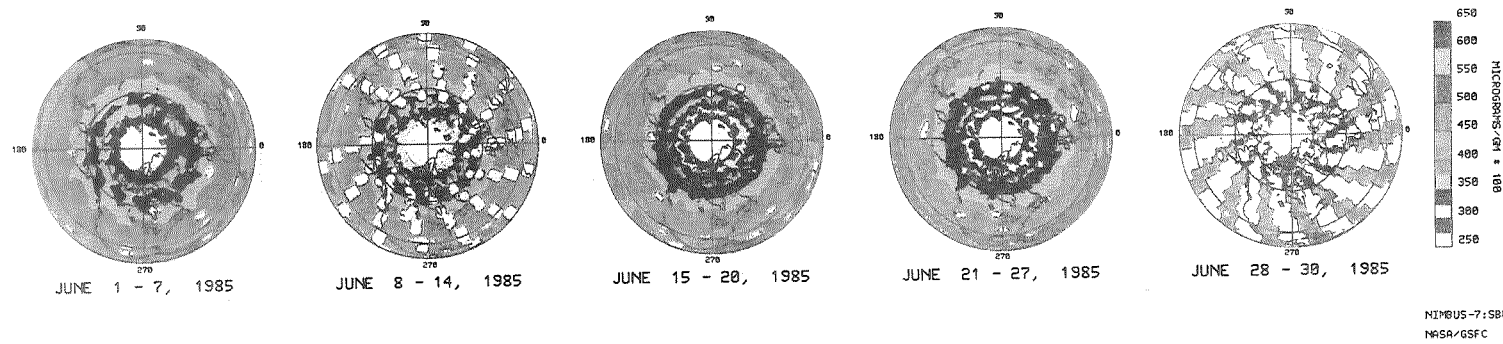
Conclusions

There is no evidence of depletion in the events examined here. This eliminates large-scale ozone changes lasting several days. To correctly identify an ozone depletion caused by relativistic electrons, the following criteria should be met. There should be evidence in the radiation belts of large changes in the flux of orbiting electrons. Corresponding to these flux changes there should be detectable enhancements of the electron densities in the lower ionosphere. One added certainty is to examine conjugate observations of electron density changes. Ozone data need to be corrected for local temperature effects and then examined. Data at altitudes above 45 km is the most important. Short time scale events will be more frequent than long-time scale events. The magnitude of the ozone effect in summer will only be 50% that of winter when the solar zenith angle has increased from 50° to near 80°.

References

- Aikin, A.C., 1992: Stratospheric evidence of relativistic electron precipitation, Planet. Space Sci., 40, 413-431.
- Baker, D.N., et al, 1986: Highly relativistic electrons in the Earth's outer magnetosphere, 1, Lifetimes and temporal history 1979-1984 J. Geophys. Res., 91, 4265-4276.
- Baker, D.N., et al, 1987: Highly relativistic magnetospheric electrons: A role of coupling to the middle atmosphere, Geophys. Res. Lett., 14, 1027-1030.
- Biel von, H.A., 1989: An investigation of the Antarctic mesosphere using partial reflections, Planet. Space Sci., 37, 889-897 .
- Callis, L.B., D.N. Baker, J.B. Blake, J.D. Lambeth, R.E. Boughner, M. Natarajan, R.W. Klesadel, and D.J. Gorney, 1991: Precipitating relativistic electrons: Their long-term effect on stratospheric odd nitrogen levels, J. Geophys. Res., 96, 2939-2976.
- Heath, D.F., A.J. Krueger, and P.J. Crutzen, 1977: Solar proton events: Influence on stratospheric ozone, Science, 197, 886-889.
- Herrero, F.A., D.N. Baker, and R.A. Goldberg, 1991: Rocket measurements of relativistic electrons: New features in fluxes; spectra and pitch angle distributions, Geophys. Res. Lett., 18, 1481-484.
- Jackman, C.H. and R.D. McPeters, 1985: The response of ozone to solar proton events during solar cycle 21: A theoretical interpretation, J. Geophys. Res., 90, 7955-7966.
- McPeters R.D. and C.H. Jackman, 1985: The response of ozone to solar proton events during solar cycle 21: The observations, J. Geophys. Res., 90, 7945-7954.
- Nagai, T., 1988: "Space weather forecast" Prediction of relativistic electron intensity at synchronous orbit, Geophys. Res. Lett., 15, 425-428 .
- Thorne, R.M., 1977.: Energetic radiation belt electron precipitation: A natural depletion mechanism for stratospheric ozone, Science, 195, 287-289.
- Weeks, L.H., R.S. Cuikay, and J.R. Corbin, 1972: Ozone measurements in the mesosphere during the solar proton event of 2 November 1969, J. Atmos. Sci., 29, 1138-1142.

OZONE MONTHLY MEAN FOR 1.0mb



MEAN TEMPERATURE FOR 1.0mb

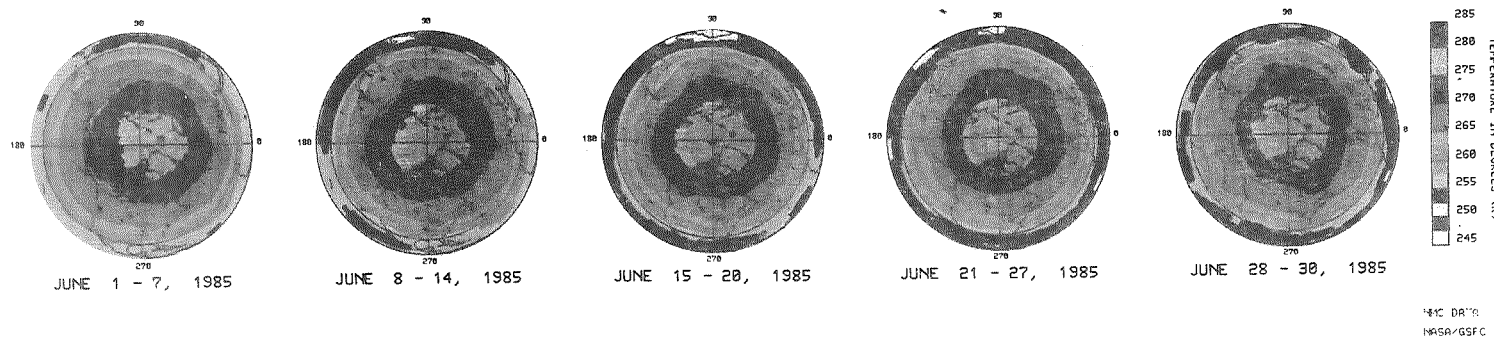


Figure 2 Ozone and temperatures for the month of June 1985 at a pressure level of 1 mb. Temperatures and ozone plots are color-coded with the key given on the side of the plots. Ozone amounts are in units of $\mu\text{g/g} \times 10^2$. Temperatures are displayed in units of $^\circ\text{K}$.

303640

IMPACT OF STRATOSPHERIC AIRCRAFT ON CALCULATIONS
OF NITRIC ACID TRIHYDRATE CLOUD SURFACE AREA DENSITIES
USING NMC TEMPERATURES AND 2D MODEL CONSTITUENT
DISTRIBUTIONS

David B. Considine and Anne R. Douglass
NASA Goddard Space Flight Center
Greenbelt, Maryland 20771

ABSTRACT

A parameterization of NAT (nitric acid trihydrate) clouds is developed for use in 2D models of the stratosphere. The parameterization uses model distributions of HNO_3 and H_2O to determine critical temperatures for NAT formation as a function of latitude and pressure. National Meteorological Center temperature fields are then used to determine monthly temperature frequency distributions, also as a function of latitude and pressure. The fractions of these distributions which fall below the critical temperatures for NAT formation are then used to determine the NAT cloud surface area density for each location in the model grid. By specifying heterogeneous reaction rates as functions of the surface area density, it is then possible to assess the effects of the NAT clouds on model constituent distributions. We also consider the increase in the NAT cloud formation in the presence of a fleet of stratospheric aircraft. The stratospheric aircraft NO_x and H_2O perturbations result in increased HNO_3 as well as H_2O . This increases the probability of NAT formation substantially, especially if it is assumed that the aircraft perturbations are confined to a corridor region.

1. INTRODUCTION

Two dimensional photochemical models of the stratosphere are important tools for the study of stratospheric dynamics and chemistry. They are also the major method for evaluating human influences on the stratosphere because they require less computer time to run and contain a more complete photochemistry than the more complicated three dimensional models. In particular, they are being used to assess the potential effects of a fleet of stratospheric aircraft on stratospheric ozone [e.g., Jackman *et al.*, 1991]. It has been found that model predictions of aircraft-induced ozone depletion differ substantially, depending on whether or not the models include a parameterization of sulfate aerosol heterogeneous processes. Purely gas-phase models generally predict a depletion on the order of several percent. If stratospheric sulfate aerosol effects are added, the predicted depletions are much less, or actually result in a slight increase in stratospheric ozone [Weissenstein *et al.*, 1991].

Heterogeneous reactions are also catalyzed by NAT clouds in the stratosphere. NAT clouds are different from the sulfate aerosols in that the temperature at which they will form depends on the amount of HNO_3 and H_2O in the stratosphere, and are not a ubiquitous feature of the lower stratosphere. NAT clouds are essential components of polar stratospheric chemistry and the properties of such clouds have been studied extensively [e.g., Turco *et al.*, 1989].

Implementing NAT cloud distributions and the heterogeneous reactions they catalyze into zonally averaged models of the stratosphere is difficult. This is because zonally averaged temperatures are generally too high to allow for NAT clouds to form. If one denotes by $\langle c \rangle$ the zonally averaged cloud surface area density, and the zonally averaged temperature by $\langle T \rangle$, then $\langle c(T) \rangle \neq c(\langle T \rangle)$. To get around this difficulty while remaining consistent with the philosophy of a 2D model, we use temperature probability distributions characterizing a particular latitude and pressure level in the model. These distributions are obtained using National Meteorological Center temperature data.

NAT cloud formation depends on the concentrations of HNO_3 and H_2O in addition to the temperature. Because stratospheric aircraft inject both into the stratosphere, it is likely that a stratospheric aircraft fleet will increase the probability of NAT cloud formation. Peter *et al.* [1991] attempted to assess the magnitude of the effect at 70°N , and concluded that the probability of finding an NAT cloud at that latitude might be doubled with the introduction of such a fleet. This paper is in the same spirit as their work, but attempts to develop an annual NAT surface area density climatology for the latitudes and pressure levels of the GSFC 2D model. We do this both with and without the assumption of a stratospheric aircraft fleet in order to allow a 2D model assessment of the chemical effects of stratospheric aircraft on the atmosphere.

2. CRITICAL TEMPERATURES FOR NAT FORMATION

According to Hanson and Mauersberger, [1988], the relationship between the NAT saturation temperature, T_s , the partial pressure of HNO_3 , P_{HNO_3} , and the partial pressure of H_2O , $P_{\text{H}_2\text{O}}$, is given by,

$$\log_{10}(P_{\text{HNO}_3}) = m(T_s) \log_{10}(P_{\text{H}_2\text{O}}) + b(T_s), \quad (1)$$

and

$$m(T_s) = -2.7836 - 0.00088T_s \quad (2)$$

$$b(T_s) = 38.9855 - \frac{11,397.0}{T_s} + 0.009179T_s. \quad (3)$$

The stated range of validity of this equation is for temperatures between 180 K and 200 K. In this study, we assume that the equation is valid up to 210 K, and that NAT clouds will form wherever the temperature is below T_s . This assumption may not be correct, however. Peter *et al.* [1991] have discussed the possibility that a substantial supersaturation on the order of 3 K is required to nucleate the NAT clouds. If this is the case, then using Eq. 1 will result in a prediction of the critical temperatures for NAT cloud condensation that is too high.

Given Eq. 1, and model distributions of HNO_3 and H_2O , a critical temperature distribution can be calculated as a function of latitude and pressure, as shown in Figure 1. In this case, a subsonic aircraft fleet has been assumed, but no stratospheric aircraft fleet. The addition of stratospheric aircraft increases the critical temperatures. The amount of increase depends on the assumptions made about the zonal distribution of HNO_3 . For instance, the dynamics of the stratosphere may be such that aircraft corridors are formed inside of which the constituent concentrations are significantly greater than the zonal mean values. Tracer simulations using the GSFC 3D chemistry and transport model and European Center for Medium Range Weather Forecasting (ECMWF) wind fields suggest maximum concentrations of up to 5 times the zonal mean during the winter [Douglass *et al.*, 1992]. If one considers all of the injected HNO_3 and H_2O from the stratospheric aircraft to be concentrated in a corridor with a width of 72° longitude, the local concentration increase inside the corridor will be 5 times the perturbation to the zonal mean, while outside the corridor the contribution from the aircraft fleet will be 0. Using this assumption, the increase in NAT formation temperatures can be up to 6 K, as shown in Figure 2.

3. TEMPERATURE PROBABILITY DISTRIBUTIONS

As mentioned above, zonally-averaged temperatures are generally too warm to dip below the NAT critical temperatures. If one considers the longitudinal distribution of temperatures at a particular latitude, however, it could be that a substantial fraction of the band is below the condensation temperature, and could support NAT cloud formation. To quantify this effect, we took a month's worth of NMC temperature data, and binned the temperatures into 10° -latitude bands. At each NMC pressure level, the temperatures in the band were used to produce a temperature probability density distribution for each month, $P_m(T, \theta_i, p_j)$, where $\theta_i = (-85, -75, \dots, 85)$ are the latitude coordinates and $\{p_j\}$ are the NMC pressure levels. This distribution is normalized such that PdT gives the probability of finding a temperature between T and $T + dT$. For this paper, NMC temperatures for one year, from May, 1991 to April, 1992, were used. By consider-

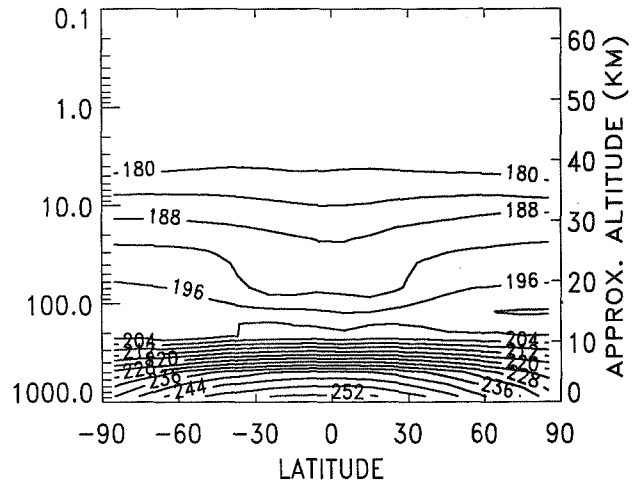


Fig. 1 Critical Temperatures for NAT formation: Assuming the relationship between saturation temperature and distributions of HNO_3 and H_2O given in Hanson and Mauersberger [1988], critical temperature distributions can be calculated. Shown is the January, 1992 distribution, where the HNO_3 and H_2O fields were taken from a model run including sulfate aerosol heterogeneous processes and a subsonic aircraft fleet.

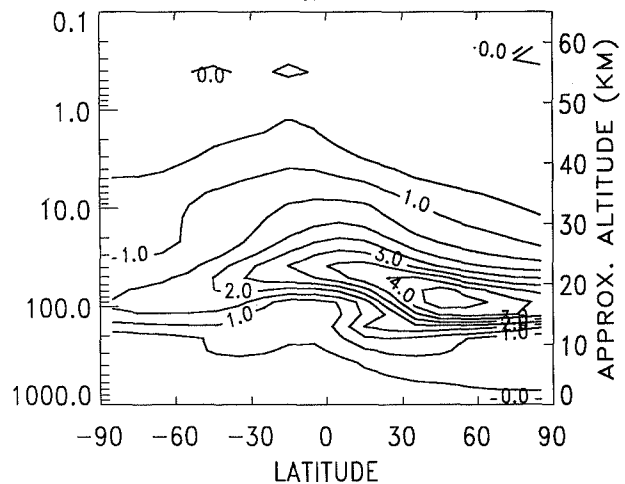


Fig. 2 Increase in critical temperatures from addition of a stratospheric aircraft fleet: The increases in stratospheric HNO_3 and H_2O from stratospheric aircraft can substantially increase the critical temperatures for NAT formation. This effect is on the order of 2 K if the aircraft perturbation is assumed to be distributed zonally. If the aircraft perturbation is assumed to be confined to a tight corridor, concentrations are higher and so is the temperature. The figure above was calculated assuming an aircraft corridor width of 72° longitude.

ing more than one year of NMC data, a better estimate of the climatological temperature distributions could be obtained.

With the critical temperatures calculated using the GSFC 2D model and the NMC temperature distributions, the probability that NAT clouds will be found can be calculated as a function of month, latitude, and pressure. Denoting this fraction by f ,

$$f_m(T_c, \theta_i, p_j) = \int_0^{T_c(\theta_i, p_j)} P_m(T, \theta_i, p_j) dT, \quad (4)$$

where T_c is the condensation temperature for NAT clouds (which we assume is equal to the Hanson and Mauersberger saturation temperature, Eqs. 1-3, above). As shown in Figure 3, which depicts the calculation of f at 50 mb, 65° for January, 1992, f can be a rapidly increasing function of T_c . If T_c increases slightly due to the introduction of stratospheric aircraft, f can increase substantially.

A plot of f for January 1992 is shown in Figure 4. In the case shown, no stratospheric aircraft fleet has been assumed. For this month, the peak probability that an NAT cloud will form occurs in the polar region, and has a magnitude of .2. From the figure, we might expect to see an NAT cloud forming at, say, 70° and 50 mb with a probability of about 0.1, or roughly three days out of the month. This appears to be in fair agreement with the results of the study of Peter *et al.*[1991], which also calculated such probabilities. The figure also indicates a substantial probability that NAT clouds will form in

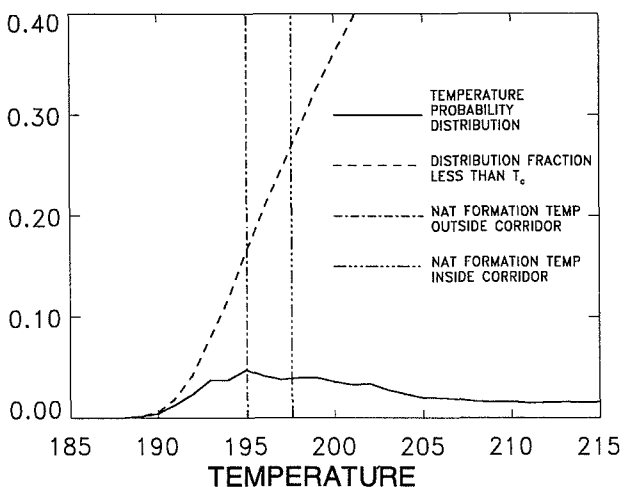


Fig. 3 Calculation of f from T_c and $P(T)$: The solid curve at the bottom of the figure is the temperature probability distribution at 65°N and 50 mb. the dashed line is the integral of this distribution up to the temperature T . The vertical dashed lines show the critical temperatures for NAT condensation inside and outside of an aircraft corridor with a longitudinal width of 72°. Because f can increase rapidly, $f(T_c)$ inside the corridor can be substantially larger than $f(T_c)$ outside of the corridor.

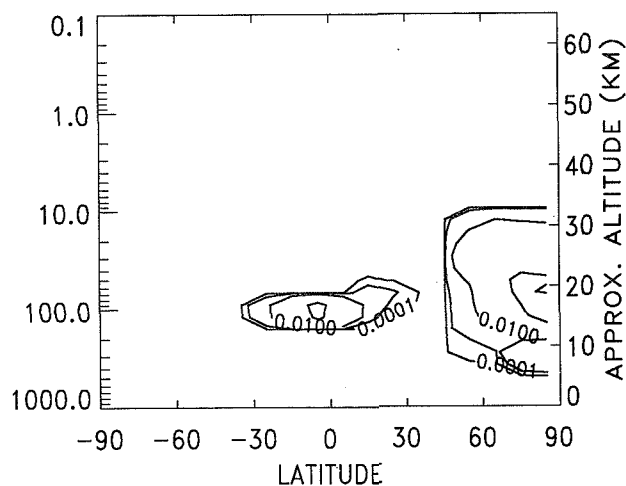


Fig. 4 January 1992 NAT formation probabilities: No stratospheric aircraft are included in this calculation. The peak in the January formation probability occurs near the north pole, at approximately 70 mb. A significant tropical formation probability is also seen, which peaks a bit lower down at approximately 100 mb. Very small probabilities of NAT formation are found in the northern midlatitudes. Temperatures in the southern hemisphere are too warm for NAT clouds to exist there.

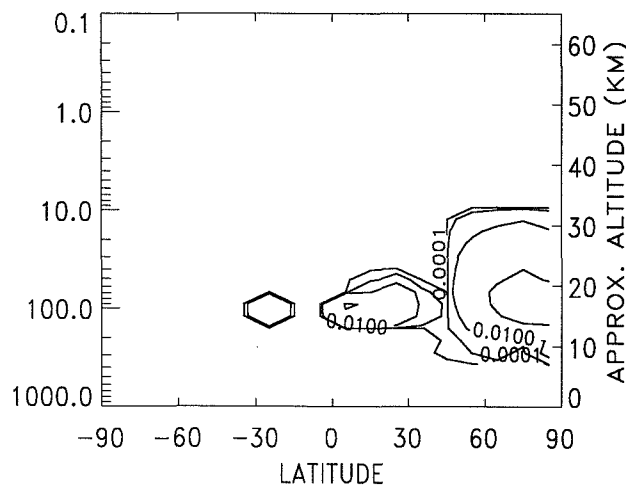


Fig. 5 Increase in January NAT formation probability from the addition of a stratospheric aircraft fleet. Shown is the increase assuming a 72° aircraft corridor, inside the corridor.

the tropics, peaking at about 100 mb, a little lower than the polar peak. The probability of cloud occurrence is a minimum at northern midlatitudes, and is absent in the summer hemisphere, reflecting the warmer temperatures there.

When the NO_x and H_2O perturbations from a stratospheric aircraft fleet are included in the calculations, the resulting probabilities of NAT cloud occurrence are increased. The increase in probability of cloud formation

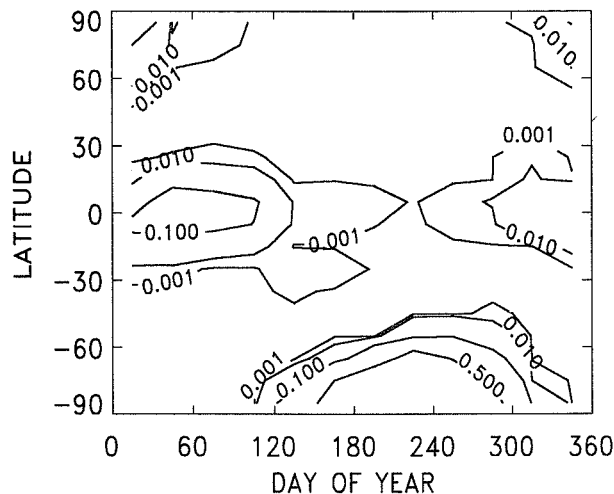


Fig. 6 Seasonal variation of NAT formation probability: Shown is the variation of f as a function of day and latitude, on the 90 mb surface. No stratospheric aircraft perturbation is included. The largest probabilities are in the south polar regions in the months of July, August, and September. Substantial probabilities of occurrence are also found in December/January in the northern high latitudes, and in the tropics in February/March. At 50 mb, no tropical cloud formation is predicted, but the north and south polar distributions are similar to those depicted here.

has somewhat the same morphology as f itself, and has a similar magnitude. If the perturbations are assumed to be confined to a corridor, the increases are larger than if the perturbations are assumed to be distributed zonally (Figure 5).

Distributions similar to Figure 4 can be obtained for each month. Figure 6 depicts the seasonal variation of NAT cloud occurrence probability on the 90 mb surface. The north polar peak in occurrence probability occurs in December/January. The south polar occurrence probability peaks in August, and is large in both July and September. Finally, the tropical probability peaks in February/March, and is at a minimum in October. If one moves to the 50 mb surface, one finds only very small probabilities of tropical cloud formation, while the northern and southern polar regions remain about the same.

If we assume that the NAT cloud that forms has a value of 10^{-8} cm^{-1} , as given by Turco *et al.*, [1989], the distributions define a seasonally-varying NAT cloud surface area density distribution. (This assumption may introduce a substantial uncertainty into the calculation. It should be adequate for a 2D sensitivity study.) The surface area density distribution can then be introduced into the model, and used to calculate the effects of heterogeneous reactions catalyzed by the NAT clouds on constituent distributions. Since the NAT cloud frequency is increased with the addition of a stratospheric aircraft fleet, it appears that including NAT cloud processing in assessments of potential stratospheric aircraft effects on

the stratosphere may result in important changes. These changes remain to be assessed.

ACKNOWLEDGEMENTS

This work was done while D. Considine held a National Research Council-NASA Resident Research Associateship.

REFERENCES

- Douglass, A. R., R. B. Rood, and C. H. Jackman, Three dimensional model calculations of the global dispersion of high speed aircraft exhaust and implications for stratospheric ozone loss, this volume, *Proceedings of the Quadrennial Ozone Symposium*, 1992
- Hanson, D. and K. Mauersberger, Laboratory Studies of the Nitric Acid Trihydrate: Implications for the South Polar Stratosphere, *Geophys. Res. Lett.* **15**, 855-858, 1988.
- Jackman, C. H., A. R. Douglass, K. F. Brueske, and S. A. Klein, The Influence of Dynamics on Two-Dimensional Model Results: Simulations of ^{14}C and Stratospheric Aircraft NO_x Injections, *J. Geophys. Res.* **96**, 22559-22572, 1991.
- Peter, Th., C. Bruhl, and P.J. Crutzen, Increase in the PSC-Formation Probability Caused by High-Flying Aircraft, *Geophys. Res. Lett.* **18**, 1465-1468, 1991.
- Turco, R. P., O. B. Toon, and P. Hamill, Heterogeneous Physicochemistry of the Polar Ozone Hole, *J. Geophys. Res.* **94**, 16493-16510, 1989.
- Weisenstein, D., M. K. W. Ko, J. M. Rodriguez, and N. D. Sze, Impact of heterogeneous chemistry on model-calculated ozone change due to HSCT aircraft *Geophys. Res. Lett.* **18**, 1991-1994, 1991.

303642

THE RESPONSE OF MIDDLE ATMOSPHERIC OZONE TO SOLAR UV
IRRADIANCE VARIATIONS WITH A PERIOD OF 27 DAYS

Li Chen

Department of Physics, University of Colorado, Boulder, Colorado 80309-0391

Guy Brasseur

National Center for Atmospheric Research, Boulder, Colorado 80303-3000

Julius London

Department of Astrophysical, Planetary, and Atmospheric Sciences,
University of Colorado, Boulder, Colorado 80309-0391

ABSTRACT

A one-dimensional photochemical-dynamical-radiative time-dependent model was used to study the response of middle atmospheric temperature and ozone to solar UV irradiance variations with a period of 27 days. The model incorporated the O_x , HO_x , NO_x , and ClO_x families and modeled solar UV variations. The amplitude of the primary temperature response to the solar UV variation is +0.4 K at 85–90 km with a phase lag of about 6 days. A secondary maximum response of +0.3 K at 45–50 km appears with a phase lag of 1 day. There is a maximum positive ozone response to the 27-day solar UV oscillation of 2.5% at 80–90 km with a phase lag of about 10 days after the solar irradiance maximum. At 70 km the ozone response is about 1.2% and is out of phase with the solar variation. In the upper stratosphere (40–50 km) the relative ozone variation is small, about 0.2% to 0.3%, and there is a negative phase of about 4 days between the ozone and solar oscillations. These oscillations are in phase in the middle stratosphere (35–40 km) where there is again a maximum relative response of about 0.6%. The reasons for these ozone amplitude and phase variations are discussed.

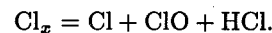
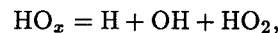
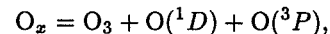
INTRODUCTION

Efforts toward detecting the responses of the middle atmosphere to the solar irradiance variations have been pursued for over 50 years. Understanding of such a response is crucial for (1) fully understanding the photochemical behavior of the middle atmosphere and the coupling between temperature and ozone and (2) detecting possible changes in the atmospheric composition due to anthropogenic effects. Satellite results are now available that show the ozone and temperature responses to solar irradiance variations with a period of 27 days (Keating et al., 1987; Hood, 1986, 1991). The purpose of this paper is to identify, through comparing theoretical results with satellite results, the main processes that control the ozone and temperature

responses to solar irradiance variation. A one-dimensional photochemical-dynamical-radiative time-dependent model extending from 10 to 100 km with a vertical resolution of 0.5 km was used to investigate the responses of ozone and temperature in the middle atmosphere to solar irradiance variations with a period of 27 days.

MODEL DESCRIPTION

The model involves a total of 27 chemical species and 43 chemical reactions. The model uses the following families in order to avoid the mathematically stiff systems that are due to the large dispersion in the chemical lifetimes of the several species:



We used fixed profiles for NO_x and Cl_x (Brasseur and Solomon, 1985) in the model.

The dynamical (vertical diffusion) time constant varies with altitude from 10^5 s at 100 km to 10^7 s at 30 km (Brasseur and Solomon, 1985). For short-lived chemical species with lifetimes shorter than the dynamical time constant, concentrations were derived from photochemical equilibrium:

$$P_i - L_i = 0,$$

where P_i is the production term ($\text{cm}^{-3} \text{s}^{-1}$) for a given constituent i and L_i is the destruction term ($\text{cm}^{-3} \text{s}^{-1}$) of the chemical species i . The species O, $O(^1D)$, NO, NO_2 , ClO, Cl, H, OH, and HO_2 were assumed to be short lived in the model.

For O_x , H_2 , and H_2O , which have long chemical lifetimes and are therefore sensitive to dynamics and chemistry, the following continuity equation was solved:

$$\frac{\partial n_i}{\partial t} = \frac{\partial}{\partial z} \left[K_z n \frac{\partial}{\partial z} \left(\frac{n_i}{n} \right) \right] + P_i - L_i,$$

where n = air density (cm^{-3}), n_i = the number density of a given constituent i , and K_z = the vertical diffusion coefficient ($\text{cm}^2 \text{s}^{-1}$).

The net heat was transported as a tracer with an altitude-dependent vertical-exchange coefficient. The potential temperature was derived from the following energy equation:

$$n \frac{\partial \theta}{\partial t} - \frac{\partial}{\partial z} \left(K_z n \frac{\partial \theta}{\partial z} \right) = n(H - C) \left(\frac{p_0}{p} \right)^\kappa,$$

where θ = potential temperature (K), H = the solar heating rate (K s^{-1}), C = the IR cooling rate (K s^{-1}), p_0 = pressure at the ground (1013 mb), p = pressure (mb), and $\kappa = R/C_p$ (0.286 for dry air).

The solar heating rate based on absorption by molecular oxygen and ozone was modeled after Schoeberl and Strobel (1978). A small contribution from water vapor was prescribed. The cooling rate below 30 km was parameterized from a model developed by Morcrette (Brasseur et al., 1987) after taking into account the emission and absorption of atmospheric radiation by O_3 , CO_2 , and H_2O . Above 40 km, an algorithm to compute the radiative cooling due to carbon dioxide, which has been developed by W. Wehrbein et al. (in preparation), was adopted. This method explicitly includes non-LTE and multiple bands and utilizes the method known as lambda iteration to calculate the populations for each of the energy levels in each atmospheric layer. A wideband model of ozone absorption in the 9.6- μm region (Rosenfield, 1991) was used in the model. A transition between the two models was used for the layer between 30 and 40 km.

The absorption cross sections of O_2 (SRC + Hertzberg bands) and O_3 (Hartley + Huggins + Chappuis + Hertzberg bands) (from WMO, 1985) and the absorption cross sections of H_2O_2 (190–350 nm) and NO_2 (185–410 nm) (from DeMore et al., 1987) were used in the model. The absorption cross section of O_2 over the Schumann-Runge band was calculated according to Allen and Frederick (1982). Values for the photodissociation rates for water vapor (SRB + Lyman- α) and O_2 (Lyman- α) used in the model were taken from Brasseur and Solomon (1985). The solar irradiance at different altitudes was approximated by using Beer's law, and the solar irradiance at the top of the atmosphere was from WMO (1985). The chemical reaction rates given in NASA Reference Publication 1242 (Watson et al., 1990) were used. All of the initial profiles and the vertical diffusion coefficient used to develop the vertical transport for chemical species were taken from Brasseur and Solomon (1985). Boundary conditions used in the model are listed in Table 1.

RESULTS AND DISCUSSION

A 27-day sinusoidal oscillation of the daily average solar irradiance was applied to the model as the external forcing. The amplitude of the solar flux relative variation over a period of 27 days is a strong function of

TABLE 1.

	10 km	100 km
O_x	$\Phi = 0$	$\Phi = 0^*$
H_2	$n = 4.2\text{E} + 12$	$\Phi = 5.\text{E} + 7$
H_2O	$n = 3.06\text{E} + 14$	$\Phi = 0$
θ	$\theta = 288 \text{ K (0 km)}$	$\theta = 12359 \text{ K}$

Note: n is the number density (cm^{-3}) and Φ is the flux ($\text{cm}^{-2} \text{s}^{-1}$).

* $\Phi = 0$ at 100 km is not a realistic boundary condition for O_x . We found, however, that the sponge layer is about 7 km below the upper boundary after using different boundary conditions. Therefore, we only show the results below 90 km.

wavelength. A 23% relative variation of Lyman- α with a period of 27 days was taken in the model. The wavelength dependence of 27-day relative amplitudes for the period of maximum solar irradiance observed by SME (8 July 1982 to 4 August 1982) was taken from London and Rottman (1990). The variation of solar irradiance ($\lambda > 300 \text{ nm}$) was considered to be zero.

The model ran for a time period of 81 days starting from the spring equinox (i.e., from calendar day 80 today 161). The mean solar zenith angle at the equator was calculated each day. The model runs were performed for both constant solar irradiance and a sinusoidal solar irradiance variation with a period of 27 days. The response of the chemical species to the solar irradiance variation was defined as the percent change in species concentration between the two cases:

$$\% \text{ response} = \frac{n_{\text{sinu}} - n_{\text{const}}}{n_{\text{const}}} \times 100\%,$$

where n_{const} = chemical species density for the constant solar irradiance and n_{sinu} = chemical species density for the solar irradiance with sinusoidal variation.

The temperature response to solar irradiance variations, which is defined as the difference between the temperature with a 27-day solar irradiance variation and that with constant solar irradiance, is shown in Figure 1. The primary maximum of the temperature response, about 0.4 K, was found about 85–90 km about 5.8 days after the peak of the solar irradiance oscillation. This maximum results from the increasing absorption of solar irradiance over the Schumann-Runge continuum and the Schumann-Runge bands by molecular oxygen. The secondary maximum, about 0.3 K, occurs at about 45–50 km and is due to increased absorption of solar irradiance over the Hartley band by ozone. A positive phase lag, about 1 day, was observed at about 50 km, which is much shorter than that in the upper layer (above 70 km) and lower layer (below 40 km). This phenomenon occurs because the radiative lifetime of the middle atmosphere (about 3–5 days) is shorter than the

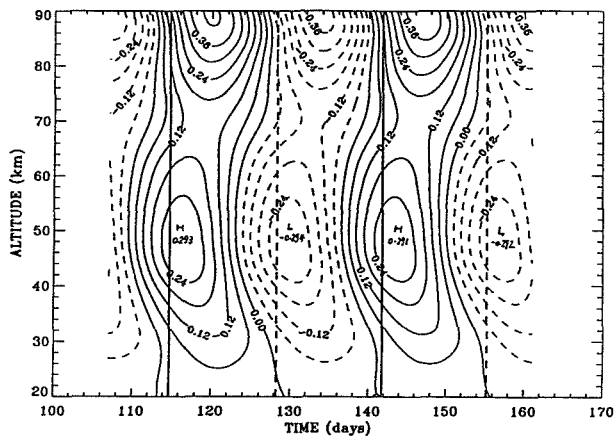


Fig. 1. The temperature difference (K) between the running model with solar irradiance variations and with constant solar irradiance. Only the results of the last 54 days are shown. Time is day of the year starting from 1 January. The solid vertical lines represent the times of solar oscillation maxima, located on days 114.75 and 141.75. The dashed vertical lines represent the times of solar oscillation minima, located on days 128.25 and 155.25. Solid contours represent positive values; dashed contours represent negative values.

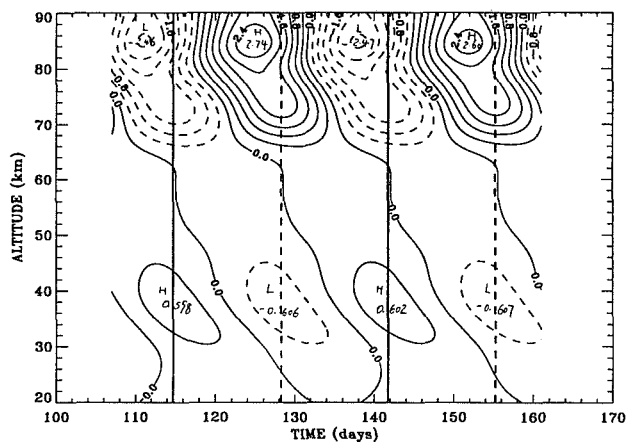


Fig. 2. The ozone response to solar irradiance variations. For complete explanation, see Figure 1.

dynamical time constant (a few weeks). The temperature field at this height, therefore, results largely from a trend toward a radiative equilibrium and is not strongly dependent on transport. Another reason is that the radiative lifetime of the middle and upper stratosphere is shorter than that of the upper mesosphere and the phase lag of the temperature response is dependent on the ratio of the radiative lifetime to the period of solar irradiance oscillation (Hood, 1986). The ozone response with temperature feedback, which is the effect of tem-

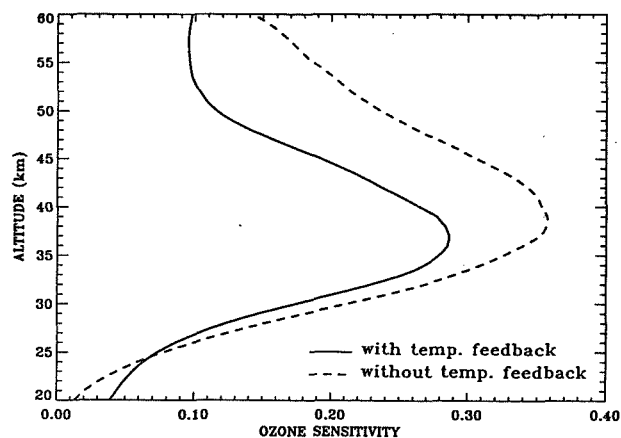


Fig. 3. Ozone sensitivity represents the amplitude of the ozone response corresponding to a change of 1% of the amplitude of the solar irradiance variation at 205 nm. *Without temperature feedback* means holding temperature constant in the model (i.e., using 1976 U.S. standard atmosphere).

perature on the ozone response to solar irradiance variations, is shown in Figure 2. The strong ozone increase at 85–90 km results from photodissociation of molecular oxygen by the Schumann-Runge continuum and Schumann-Runge bands and subsequent recombination of atomic oxygen with molecular oxygen. The phase delay, about 10 days after solar irradiance maximum, occurs because of the low concentrations of third bodies necessary for the three-body recombination process. The ozone decrease at 70–75 km at the time of solar irradiance maximum results from the photodissociation of H_2O at that height by solar Lyman- α . At lower levels (e.g., around 40–50 km), increased photodissociation of molecular oxygen leads to an ozone increase. The negative phase lags (i.e., the peak of the ozone oscillation before the peak of the solar irradiance oscillation) were found in the upper stratosphere and lower mesosphere. The peak of the ozone oscillation is about 7 days before the peak of the solar irradiance oscillation at about 50 km.

The ozone sensitivity, which is here defined as the ozone variation associated with a 1% solar irradiance variation at 205 nm, and the ozone phase lag with temperature feedback were compared with these two parameters without temperature feedback (the temperature profile in the model is not changed with time) in Figures 3 and 4. The value of the ozone response with temperature feedback is generally smaller than that without temperature feedback. An increasing solar irradiance will increase the solar heating rate and hence the temperature. An increasing temperature will cause a higher photochemical destruction rate of ozone and a lower rate of ozone production. The combination of these effects produces a smaller ozone response to

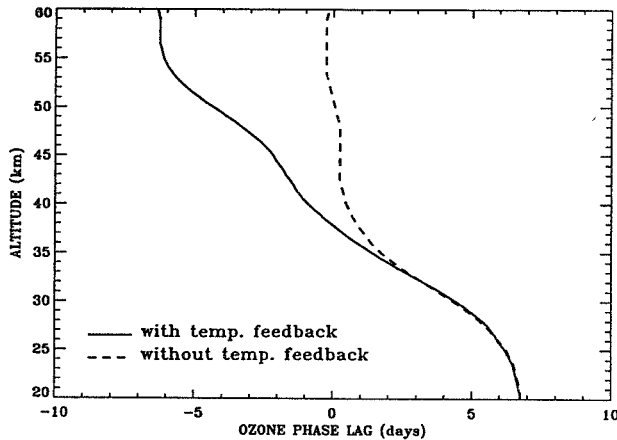


Fig. 4. The phase lag is the difference between the maxima (or minima) of the ozone response and the maxima (or minima) of the solar irradiance oscillation. Twenty-seven days were added to the phase lag above the inflection point. *Without temperature feedback* means holding temperature constant in the model (i.e., using 1976 U.S. standard atmosphere).

solar irradiance oscillations with temperature feedback, as compared to the ozone response without temperature feedback.

When compared with the previous results (Keating et al., 1987; Hood, 1986; Brasseur et al., 1987), the ozone sensitivity from our one-dimensional model agrees qualitatively with observed data (Keating et al., 1987; Hood, 1986) and quantitatively with theoretical values (Brasseur et al., 1987). The difference between the theoretical values and the observed data may be caused by the incomplete treatment of the temperature feedback in our model. We also ran our one-dimensional model with a suggested observed temperature variation associated with observed relative variations at 205 nm (Keating et al., 1987; Hood, 1986; Hood et al., 1991). The agreement between the calculated values and the observed data was improved greatly.

ACKNOWLEDGMENTS

Support is acknowledged from NASA Graduate Student Fellowship NGT-30060 and NASA Contract No. NAS5-27263. The National Center for Atmospheric Research is supported by the National Science Foundation.

REFERENCES

- Allen, Mark, and J. E. Frederick, Effective photodissociation cross section for molecular oxygen and nitric oxide in the Schumann-Runge bands, *J. Atmos. Sci.*, **39**, 2066–2075, 1982.
- Brasseur, Guy, and S. Solomon, *Aeronomy of the middle atmosphere*, D. Reidel Publishing Company, Dordrecht, Holland, 452 p., 1985.
- Brasseur, G. P., A. De Rudder, G. M. Keating, and M. C. Pitts, Response of middle atmosphere to short-term solar ultraviolet variations, *J. Geophys. Res.*, **92**, 903–914, 1987.
- DeMore, W. B., M. J. Molina, S. P. Sander, D. M. Golden, R. F. Hampson, M. J. Kurylo, C. J. Howard, and A. R. Ravishankara, *Chemical kinetics and photochemical data for use in stratospheric modeling, Evaluation number 8*, JPL Publication 87-41, Jet Propulsion Laboratory, Pasadena, California, USA, 196 p., 1987.
- Hood, L. L., Coupled stratospheric ozone and temperature responses to short-term changes in solar ultraviolet flux: An analysis of Nimbus 7 SBUV and SAMS data, *J. Geophys. Res.*, **91**, 5264–5276, 1986.
- Hood, L. L., Z. Huang, and S. W. Bougher, Mesospheric effects of solar ultraviolet variations: Further analysis of SME IR ozone and Nimbus 7 SAMS temperature data, *J. Atmos. Sci.*, **96**, 12,989–13,002, 1991.
- Keating, G. M., M. C. Pitts, G. Brasseur, and A. De Rudder, Response of middle atmosphere to short-term solar ultraviolet variations, *J. Geophys. Res.*, **92**, 889–902, 1987.
- London, J., and G. J. Rottman, Wavelength dependence of solar rotation and solar cycle UV irradiance variations, in K. H. Schatten and A. Arking, eds., *Climate Impact of Solar Variability*, NASA Conference Publications CP-3086, p. 323–327, 1990.
- Rosenfield, J. E., A simple parameterization of ozone infrared absorption for atmospheric heating rate calculations, *J. Geophys. Res.*, **96**, 9065–9074, 1991.
- Schoeberl, M. R., and Q. F. Strobel, The zonally averaged circulation of the middle atmosphere, *J. Atmos. Sci.*, **35**, 577–590, 1978.
- Watson, R. T., M. J. Kurylo, M. J. Prather, and F. M. Ormond, *Present state of knowledge of the upper atmosphere, 1990: An assessment report—Report to Congress*, NASA Reference Publication 1242, 136 p., 1990.
- WMO, *Atmospheric Ozone, 1985*, Volume I, Global Ozone Research and Monitoring Project, Report No. 16, 1985.

303643

WHAT CAN WE LEARN FROM RELAXATION MEASUREMENTS OF A LASER-PERTURBED ATMOSPHERE? A MODELING STUDY

Agostino Clericetti, Hubert van den Bergh and Michel J. Rossi

Laboratory of Atmospheric and Soil Pollution Studies, Institute of Environmental Science and Technology, Ecole Polytechnique Fédérale de Lausanne, CH-1015 LAUSANNE, Switzerland

ABSTRACT

The chemical kinetic aspects of a transient increase in OH and HO₂ by several orders of magnitude are explored in three model tropospheres. This chemical kinetic modeling effort was undertaken to support the operation of a pump-and-probe LIDAR instrument. A powerful excimer laser pulse perturbs the troposphere after which its relaxation back to steady state is examined by remote sensing, for example by DIAL or LIF. Instead of probing ambient levels of key free radicals, a study of the relaxation kinetics in real time enables chemical mechanistic studies *in situ*.

I. INTRODUCTION

For some key species such as tropospheric OH, the *in situ* measurement of its concentration is a difficult problem. One possible way of gaining information on OH radical reactions in the real troposphere has recently been proposed: Pump-and-Probe LIDAR [1]. In this relaxation technique, which is by no means restricted to the measurement of OH, an intense light pulse perturbs the atmosphere. Subsequently the return of [OH] to its steady-state value is observed by optical remote sensing techniques such as DIAL or long path absorption.

The central idea of the Pump-and-Probe LIDAR is to combine the time resolution of the flash photolysis with the spatial resolution of the LIDAR technique to what can be called a real-time *in situ* spatially resolved atmospheric chemical kinetics field experiment. The emphasis is placed on the verification and completion of the chemical mechanisms operative under given atmospheric conditions. In a later phase transport in and out of the irradiated volume will be considered. To test the feasibility of such a Pump-and-Probe LIDAR we have numerically simulated the experiment, and this is the subject of the present work.

We have modeled the following four scenarios: In scenario A) a (hypothetical) pump pulse bleaches NO₂ at $\lambda < 399$ nm in order to "inject" an equivalent quantity of O(³P) whose decay with time is calculated together with all the other chemical species directly affected by it. In scenario B) a model troposphere is perturbed by a powerful pump pulse from a KrF excimer laser at 248 nm which flash photolyzes O₃ to give O(¹D) and O₂(¹D). The electronically excited oxygen atoms insert into H₂O thus generating a transient high concentration of OH radicals. Quenching processes generate significant amounts of O(³P) which is the reason we had to include scenario A. In scenario C) a powerful pump pulse at 308 nm generates H from photolysis of H₂CO and OH from photolysis of O₃ in an unpolluted troposphere rich in CH₄ and H₂CO. In scenario D) both H and OH are generated by

two-photon photodissociation of H₂O at 248 nm at high laser powers. We stress that the present effort relates to the chemical aspect of the troposphere only. Therefore, the necessity of having to include transport properties under given meteorological conditions will be given by its chemical lifetimes which is the primary subject of this paper.

II. METHOD OF CALCULATION

A simplified chemical model of the troposphere including 76 chemical species and 166 reactions was treated using the CHEMKIN II package of programs [2]. This flexible set of programs was chosen because it incorporates the temperature and pressure dependence of all uni-, bi- and termolecular reactions. CHEMKIN II explicitly takes into account the reverse of every elementary reaction. This aspect is important for chemical equilibria such as N₂O₅ \rightleftharpoons NO₃ + NO₂ or CH₃C(O)O₂NO₂ (PAN) \rightleftharpoons CH₃C(O)O₂ + NO₂ where the adduct is weakly bound and where its lifetime thus varies significantly in the temperature range of interest. Most kinetic parameters were taken from kinetic data evaluations for atmospheric chemistry [4] or were estimated [3]. The calculated steady state concentrations for these different tropospheres are given in Table 1.

III. RESULTS AND DISCUSSION

Several different ways of perturbing the atmosphere were considered: The reactions NO₂ + hn \rightarrow NO + O(³P) (scenario A) and O₃ + hn \rightarrow O₂(¹D) + O(¹D) (scenario B) are equivalent to a burst or an instantaneous "injection" of O(³P) and O(¹D), respectively. It leads to transient atom concentrations which are as high as the steady state NO₂ and O₃ concentrations. This has dramatic consequences on other key species as shown below in terms of their relaxation rate. A different type of perturbation is introduced when H atoms are injected into the atmosphere through photolysis of H₂CO (scenario C) or two-photon dissociation of H₂O (scenario D)

Scenario A) Case of Polluted Troposphere: O(³P) Injection

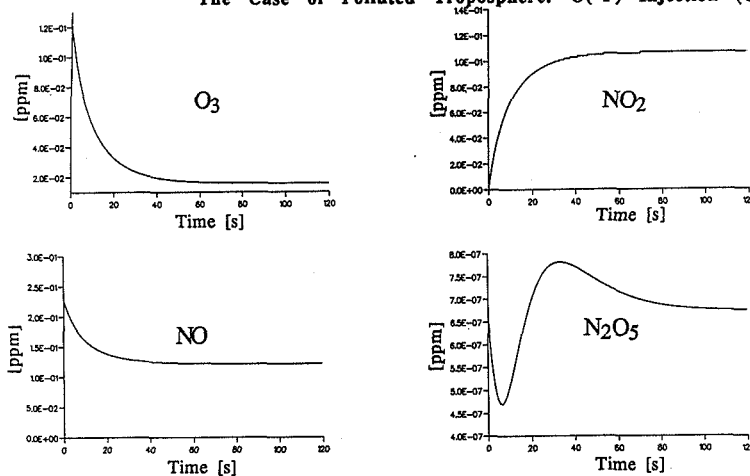
At time $t=0$ a short laser pulse at $\lambda < 398$ nm is assumed to completely bleach NO₂. The degree of bleaching depends on the laser beam fluence and the excitation wavelength. Complete bleaching of NO₂ is difficult to attain but is assumed here in order to simulate that portion of O(¹D) that is converted to O(³P) through collisional quenching of O(¹D) (see scenario B). Figure 1 below shows the recovery/relaxation of O₃, NO₂, N₂O₅, and NO. The recovery of NO and NO₂ is related to the presence of O₃, and

Table : Typical Steady-State Levels of Trace Gas Constituents

Species	Steady State Concentration ¹⁾ [ppm] Polluted Atmosphere	Steady State Concentration ¹⁾ [ppm] Unpolluted Atmosphere	Steady State Concentration ¹⁾ [ppm] Unpolluted Atmosphere - High Level of CH ₂ O
NO	0.121	0.658×10 ⁻²	0.226×10 ⁻⁴
NO ₂	0.107	0.493×10 ⁻²	0.129×10 ⁻³
N ₂	0.772×10 ⁶	0.772×10 ⁶	0.772×10 ⁶
N ₂ O ₅	0.671×10 ⁻⁶	0.206×10 ⁻⁷	0.148×10 ⁻⁸
O ₂	0.208×10 ⁶	0.208×10 ⁶	0.208×10 ⁶
O ₃	0.0157	0.0133	0.0533
H ₂ O ²⁾	0.198×10 ⁵	0.198×10 ⁵	0.198×10 ⁵
CO	0.872	0.198	0.248
CO ₂	0.346×10 ³	0.346×10 ³	0.346×10 ³
CH ₄	1.480	1.480	1.480
C ₂ H ₄ ³⁾	0.247	0.953×10 ⁻²	0.334×10 ⁻²
C ₄ H ₁₀ ³⁾	0.247	0.967×10 ⁻²	0.990×10 ⁻²
HONO	0.402×10 ⁻⁴	0.363×10 ⁻⁴	0.106×10 ⁻⁵
HNO ₃	0.372×10 ⁻²	0.673×10 ⁻³	0.304×10 ⁻²
H ₂ O ₂	0.472×10 ⁻¹²	0.276×10 ⁻¹⁰	0.440×10 ⁻²
CH ₂ O	0.414×10 ⁻²	0.464×10 ⁻³	0.982×10 ⁻²

- 1) The Zenith Angle of the sun was 30° at midlatitudes
- 2) Relative Humidity of 60% at 300K and 1013 mbar
- 3) C₂H₄ and C₄H₁₀ are representative of all the NMHC.

Figure 1 : Concentration [ppm] versus time [s] curves. The Case of Polluted Troposphere: O(³P) Injection (Case A)



occurs on the time scale of several seconds, which is also the time scale of NO₂ photolysis by sunlight. The decay of O(³P) occurs on a very short time scale of several tens of microseconds according to O + O₂ → O₃. The interesting concentration vs. time-curve for N₂O₅ is due to (sequentially): the disappearance of NO₂ by the pump pulse, oxidation of NO₂ to NO₃ by O₃ resulting in an excess of N₂O₅, and finally relaxation to the steady state levels of NO₂ and NO₃.

Scenario B) Case of Unpolluted Troposphere: O(¹D) Injection

At time t=0 a short laser pulse of about 300 mJ/cm² at λ=248 nm completely bleaches O₃ to O₂(¹D) + O(¹D). The latter generates OH free radicals by insertion into H₂O or O(³P) by collisional quenching with air. The maximum OH concentration corresponds to 10¹¹ molec/cm³ which is an enhancement of 2×10⁶ above the steady state concentration.

Low levels of NO_x lead to a significantly longer lifetime of OH (150 ms, Figure 2) compared to a polluted troposphere (7 ms). Surprisingly, the OH density is lingering on for several seconds at levels which are readily observable by DIAL. This "delayed" formation of OH results from the reaction of HO₂ + NO → OH + NO₂ during the HO₂ peak due to CH₄ oxidation by OH (CH₃ + CH₃OO → CH₃O + HO₂ + H₂CO). Methane is thus the true precursor of this "delayed" OH. The OH and CH₃ density vs. time curves track each other as do CH₃O₂ and HO₂.

Scenario C) Case of Unpolluted Troposphere: H and O(¹D) Injection

An intense laser pulse of 300 mJ/cm² at 308 nm generates 2×10⁹ H atoms/cm³ due to photodissociation of 10 ppb of H₂CO and subsequent reaction of HCO with O₂, as well as to 4×10⁹ OH due to O₃ photolysis. The lifetime of H is extremely short and leads instantly to HO₂. Figure 3 displays the response of an unpolluted troposphere with low levels of

Figure 2 : Concentration [ppm] versus time [s] curves.
The Case of Unpolluted Troposphere: O(¹D) Injection (Case B)

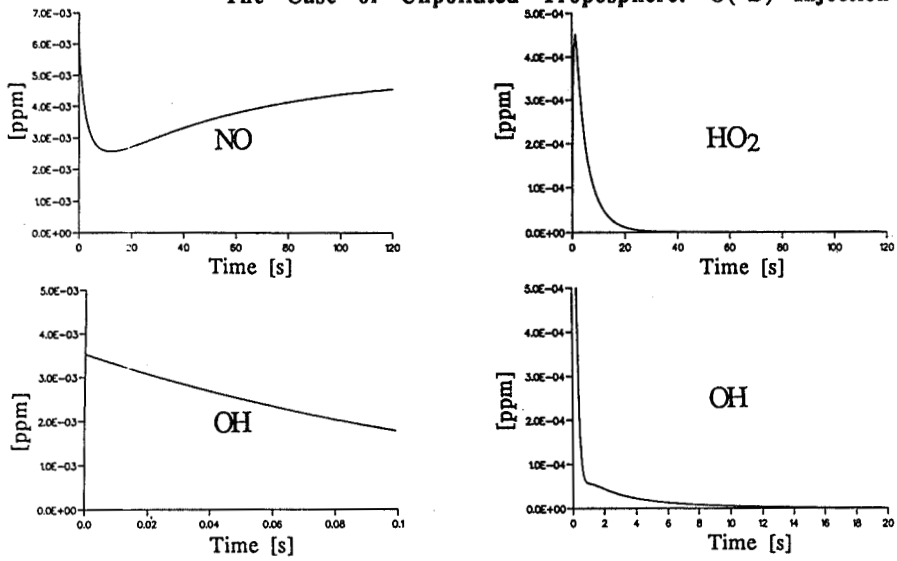


Figure 3 : Concentration [ppm] versus time [s] curves.
The Case of Unpolluted Troposphere (except for high level of CH₂O):
H and O(¹D) Injection (Case C)

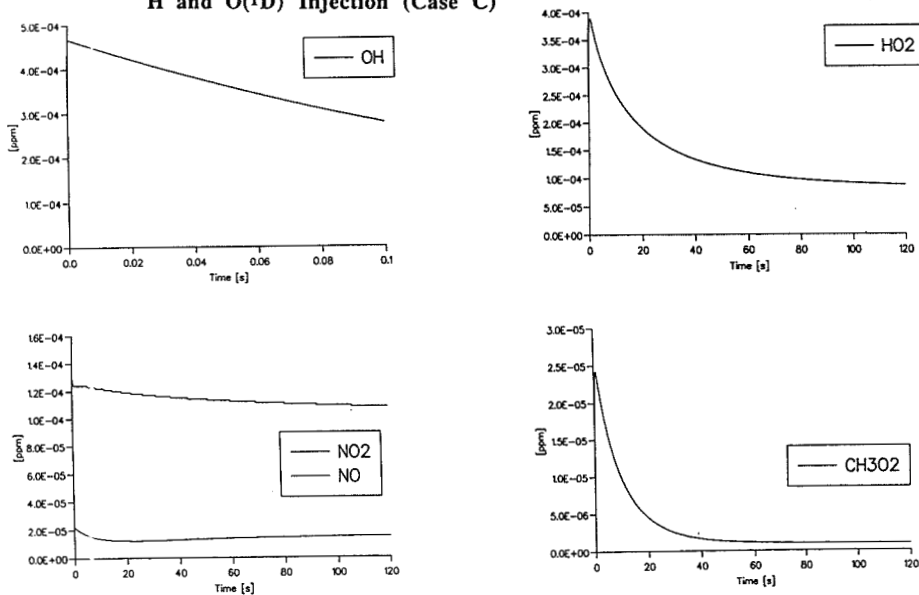
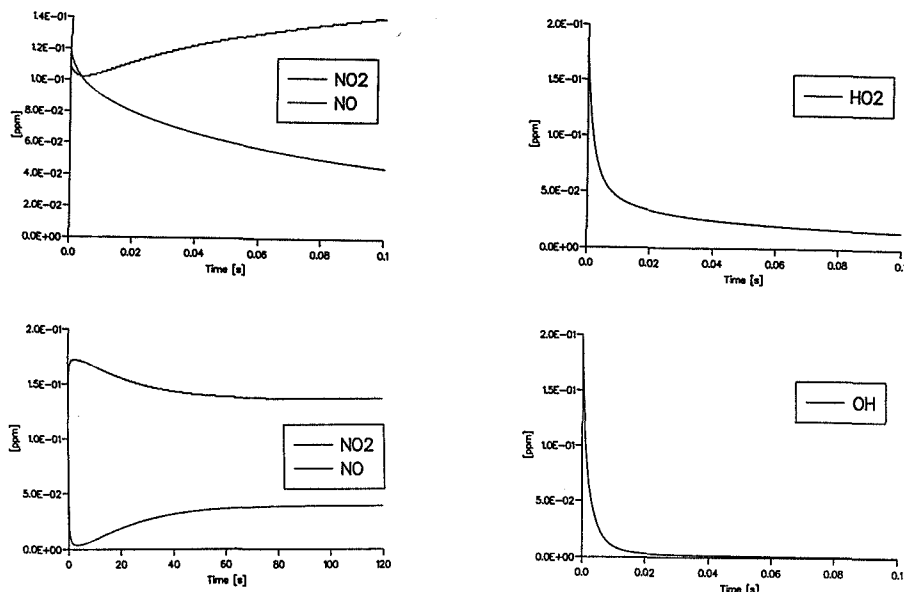


Figure 4 : Concentration [ppm] versus time [s] curves.
The Case of Polluted Troposphere : H and OH Injection (Case D)



NO_x . The OH decays with a time constant of 190 ms, whereas the HO_2 increases from the initially generated level to a maximum at 1 s, mainly because of the reaction $\text{OH} + \text{H}_2\text{CO}$ and $\text{OH} + \text{H}_2\text{O}_2$. The low level of NO in this atmosphere enables the high concentrations of HO_2 and CH_3O_2 . The interaction of two HO_2 affords H_2O_2 that photolyzes into OH which in turn attacks more hydrogen peroxide thus providing a steady source for more HO_2 . The low level of NO and the slow photolysis of H_2O_2 are at the origin of the longevity of HO_2 at elevated concentrations in analogy to the long-lasting OH from scenario B).

Scenario D) Case of Polluted Troposphere: H and OH Injection.

High power laser radiation at 248 nm may lead to two-photon photolysis of atmospheric water vapor to H + OH. We have assumed the extent of the H_2O photolysis to be around 10 ppm of the water vapor (upper limit). Figure 4 displays the response of the polluted atmosphere in which the OH and HO_2 levels initially decay at the same rate to result in the regeneration of H_2O . Due to its high reactivity the OH decays to a larger extent, so that the increased level of HO_2 interacts with the high levels of NO albeit on a much shorter time scale compared to scenario C). At later times the NO and NO_2 levels reach their photostationary state. The peak in NO_2 is due to the reaction $\text{HO}_2 + \text{NO} \rightarrow \text{NO}_2 + \text{OH}$ which leads to a related maximum in O_3 , which in turn is responsible for much of the secondary chemistry at later times.

IV. CONCLUSIONS

→ The relaxation/recovery can occur on very different time scales according to the strength of the perturbation, scenario C) vs. D) or the species observed, for instance OH vs. NO, scenario B).

→ For one observed species different elementary reactions can be important at different times after the relaxation, for instance see N_2O_5 , scenario B).

→ Several transient species may be detected during the recovery of the system back to steady state, for instance OH (10^{11} molec cm^{-3}) or HO_2 (10^{10} molec cm^{-3}) using state-of-the-art detection techniques..

→ Several modes of laser-perturbation lead to direct insight into the hydrocarbon oxidation cycle in the aftermath of a powerful pump pulse under low NO_x conditions, even using a relatively simple reaction mechanism.

→ Radical-radical reactions can become important in the aftermath of the perturbing pulse due to large transient densities of free radicals. For instance $\text{OH} + \text{HO}_2$, scenario D) or $\text{HO}_2 + \text{HO}_2$, scenario C). This interaction is emphasized even more under low NO_x conditions.

ACKNOWLEDGMENT Financial support by the Swiss National Science Foundation under grant 510.087 is gratefully acknowledged.

REFERENCES

- [1] Ph. Gozel and H. van den Bergh, *Entropy* 1991, 164/165, 91-92.
- [2] Kee, R. J., Rupley, F. M. and Miller, J. A., Sandia Report SAND 89-8009, UC-401.
- [3] Benson, S. W., in "Thermochemical Kinetics", 2nd ed., John Wiley and Sons, 1976.
- [4] JPL Publication 90-1, Chemical Kinetic and Photochemical Data for Stratospheric Chemistry, Evaluation No. 9, W. B. DeMore *et al.*

303644

A DETAILED EVALUATION OF HEATING PROCESSES IN THE MIDDLE ATMOSPHERE

Martin Mlynczak

NASA Langley Research Center
Hampton, Virginia 23681-0001 USA

Susan Solomon

NOAA Aeronomy Laboratory
Boulder, Colorado 80303 USA

1. INTRODUCTION

A fundamental problem in the study of the terrestrial middle atmosphere is to calculate accurately the local heating due to the absorption of solar radiation. Knowledge of the heat budget is essential to understanding the atmospheric thermal structure, atmospheric motions, atmospheric chemistry, and their coupling. The evaluation of heating rates is complicated (especially above the stratopause) by the fact that the heating is not a simple one-step process. That is, the absorbed solar energy does not all immediately appear as heat. Rather, substantial portions of the incident energy may appear as internal energy of excited photolysis products (e.g., $O(^1D)$ or $O_2(^1\Delta)$) or as chemical potential energy of product species such as atomic oxygen. The ultimate disposition of the internal and chemical energy possessed by the photolysis products determines the efficiency and thus the rate at which the middle atmosphere is heated. In studies of the heat budget, it is also vitally important to consider transport of long lived chemical species such as atomic oxygen above ~ 80 km. In such cases, the chemical potential energy may be transported great distances (horizontally or vertically) before undergoing a reaction to release the heat. Atomic oxygen influences the heating not only by reactions with itself and with O_2 but also by reactions with odd-hydrogen species, especially those involving OH [Mlynczak and Solomon, 1991a]. Consequently, absorbed solar energy may finally be converted to heat a long time after and at a location far from the original deposition.

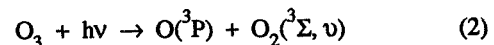
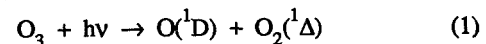
The purpose of this paper is to examine the solar and chemical heating processes and to present parameterizations for the heating efficiencies readily applicable for use in numerical models and heat budget studies. In the next two sections the processes relevant to the heating efficiencies for ozone and molecular oxygen will be reviewed. In Section 4 the processes for the exothermic reactions will be reviewed and parameterizations for the heating efficiencies for both the solar and chemical processes will be presented in Section 5.

2. CALCULATION OF THE SOLAR HEATING EFFICIENCIES FOR OZONE

In this section we develop the formalism for evaluating the heating efficiencies for absorption of solar ultraviolet radiation by ozone. Ozone is dissociated through the absorption of ultraviolet and visible radiation in three bands; the Hartley band (200-300 nm), the Huggins band (310-350 nm), and the Chappuis bands (450-850 nm). The Hartley band is the most significant in terms of heating rate above the stratopause, while all three bands are very important in the

middle and lower stratosphere and the troposphere. Excited photolysis products are generated only by photolysis in the Hartley band. As discussed below, this fact implies that the heating in the Huggins and Chappuis bands occurs at unit efficiency.

Ozone is dissociated by absorption in the Hartley band into one of two "channels"



The "channel" corresponding to Eq. 1 is called the singlet channel in reference to the spin state of the excited oxygen photolysis products. By analogy, the "channel" corresponding to Eq. 2 is called the triplet channel, since triplet oxygen species are formed. Note that the molecular oxygen in the triplet channel may be produced in a vibrationally excited form [Slanger et al., 1988], hence the script v in the notation.

We define the heating efficiency at a given altitude in general terms as the difference between the energy available for heat and the energy lost due to airglow emission, relative to the energy available for heat. That is,

$$\epsilon = \frac{(E_v - E_b) - E_{\text{airglow}}}{E_v - E_b} \quad (3)$$

where E_v is the energy of the incident solar photon, E_b is the energy required to break the chemical bonds of ozone, and E_{airglow} is the energy lost by radiative emission (airglow). The quantity $(E_v - E_b)$ is the energy immediately available for heat. As a consequence of this definition, any heating process in which there is no radiative loss (i.e., $E_{\text{airglow}} = 0$) will have an efficiency of 1.0 as is assumed for the triplet channel of ozone photolysis.

The quantum yields for the singlet and triplet channels are about 0.9 and 0.1, respectively, indicating that the singlet channel is by far the dominant pathway for ozone photolysis. The detailed processes by which the singlet and triplet channels relax are discussed in Mlynczak and Solomon, [1991b] and in Mlynczak and Solomon [1992]. In general, some of the $O(^1D)$ energy is converted to internal energy of O_2 , forming $O_2(^1\Sigma)$, which then radiates. Loss from $O_2(^1\Delta)$ is also quite significant. Based on the work of Harris and Adams [1983], we conclude that energy transfer from $O(^1D)$ to N_2 to CO_2 followed by emission by CO_2 at $4.3 \mu\text{m}$ is only a minor source of energy loss below 100 km.

Before discussing the efficiency calculations we must first consider the disposition of the energy radiated by $O_2(^1\Delta)$ and $O_2(^1\Sigma)$. If sufficient optical mass is present, radiative energy lost from the volume in which the excited species was generated may be absorbed in another other volume some distance away. In such instances, the net gain or loss of photons must also be determined to calculate the local heating. Based on calculations of the escape function [e.g., Andrews et al., 1987] we find that all radiation emitted by $O_2(^1\Delta)$ and $O_2(^1\Sigma)$ either escapes to space or is absorbed in the dense atmosphere with negligible heating upon absorption.

Under steady-state conditions, it is relatively straightforward to show that the heating efficiency is virtually independent of the quantum yield, the ozone concentration, and the photolysis rate. In fact, the efficiency is dependent only on the kinetic and spectroscopic parameters describing the relaxation of the excited species and on the energies of the photons radiated by $O_2(^1\Delta)$, $O_2(^1\Sigma)$, the incident photon energy, and the dissociation energy. This fact will be very important when developing parameterizations of the heating efficiency for use in numerical models.

The heating efficiency for the Hartley band is presented in Figure 1. Below about 50 km, the efficiency is equal to one implying that all internal energy is generated in the singlet channel is locally quenched to release heat.

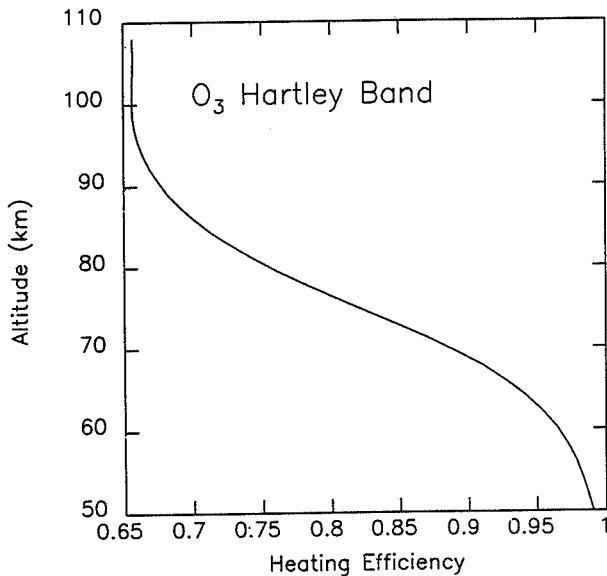


Fig. 1 The heating efficiency of the Hartley band of ozone.

3. HEATING EFFICIENCIES FOR THE PHOTOLYSIS OF MOLECULAR OXYGEN

We turn now to the heating efficiencies associated with the photolysis of molecular oxygen which is dissociated through the absorption of solar ultraviolet radiation in four systems, the Herzberg system, the Schumann-Runge bands, the Schumann-Runge continuum, and the Lyman-alpha band. Only photons in the Schumann-Runge continuum and in the Lyman-alpha band are sufficiently energetic to produce excited atomic oxygen upon dissociation, with one $O(^1D)$ atom and one $O(^3P)$ atom being produced per each photolysis event [Brasseur and Solomon, 1986] in each system. For the altitudes under consideration ($z < 115$ km), radiative loss from $O(^1D)$ is negligible [Harris and Adams, 1983]. Consequently, the only mechanism by which the heating efficiency can be

reduced is by energy transfer to radiatively active species. The $O(^1D)$ energy generated by O_2 photolysis will undergo energy transfer processes identical to that for the $O(^1D)$ generated by O_3 photolysis. Energy can be lost by emission from $O_2(^1\Sigma)$, $O_2(^1\Delta)$, and $CO_2(001)$.

Shown in Figures 2 and 3 are the heating efficiencies for both the Schumann-Runge continuum and the Lyman-alpha band. In both cases illustrated here, it has been assumed that there is negligible loss from emission by CO_2 . These figures demonstrate that very little energy is lost when Lyman-alpha radiation dissociates molecular oxygen in the region where such dissociation is significant (80-100 km), the efficiencies being greater than about 94%. The heating efficiency in the Schumann-Runge Continuum is smaller than in Lyman-alpha band even though both systems produce the same excited photolysis product $O(^1D)$. This apparent contradiction is due to the fact that the amount of energy immediately available for heat ($E_v - E_b$) is larger in the case of Lyman-alpha photolysis than in the Schumann-Runge Continuum.

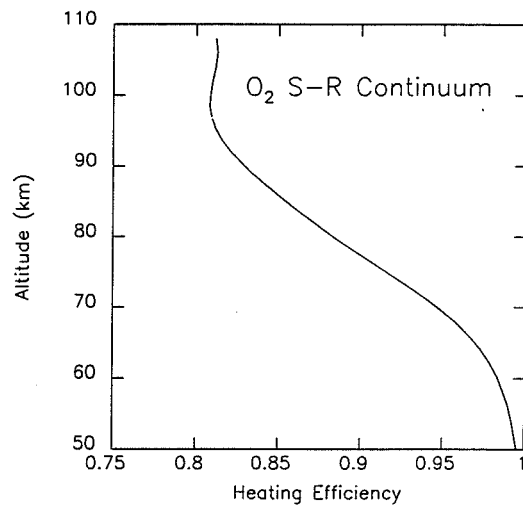


Fig. 2 The heating efficiency of the Schumann-Runge continuum of molecular oxygen.

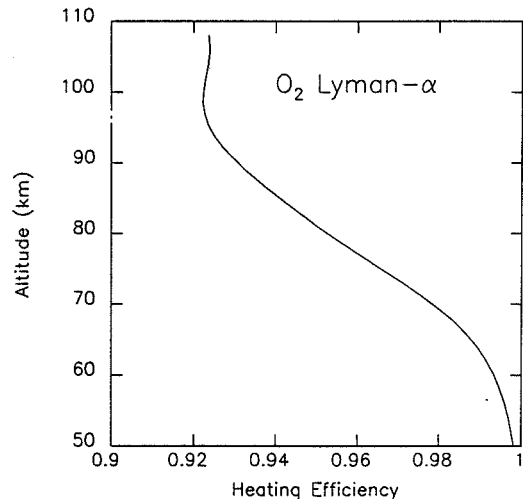


Fig. 3 The heating efficiency in the Lyman-alpha band of molecular oxygen.

4. HEATING DUE TO EXOTHERMIC CHEMICAL REACTIONS

As discussed above, not all of the absorbed solar energy appears as heat in the atmosphere but rather substantial portions of the incident energy are converted to chemical form. This chemical energy is realized as heat during exothermic reactions which take place subsequent in time and potentially far away in space from the location of the initial photon deposition.

Using the constituent concentration fields calculated by the Garcia and Solomon two dimensional model [Garcia and Solomon, 1983; 1985] we have calculated the potential heating rate in Kelvin per day for seven exothermic reactions identified [e.g., Mlynczak and Solomon, 1991a] as being responsible for depositing substantial amounts of heat in the terrestrial middle atmosphere. The latitudinal distribution of the total chemical potential heating from these reactions (at equinox) is shown in Figures 4 and 5. From Figure 4 it can be seen that exothermic reactions are important from the lower stratosphere to the lower thermosphere. Below 60 km, the heating is due almost entirely to the reaction of O and O₂ which forms ozone. Above 60 km, all reactions contribute to the heating. The chemical heating at night (Figure 5) shows a strong contrast to the daytime heating rate. First, there is virtually no chemical heating below ~ 80 km because of the disappearance of atomic oxygen and atomic hydrogen. Secondly, the chemical heating above 80 km is much larger at night owing to the increase in ozone which fuels the fast reaction with atomic hydrogen.

The heating rates in Figures 4 and 5 represent the maximum possible heating based on the model constituent concentrations and reaction rates. The actual heating may be much less than the potential heating rate if any of the reaction products are radiatively active and excited to any extent by the reaction. Chemiluminescent emission is a significant source of energy loss from the atmosphere, particularly in from vibrationally excited OH and possibly from vibrationally excited O₃ [Mlynczak and Solomon, 1991a; Mlynczak 1991]. The energy loss associated with chemiluminescent emission is analogous to the airglow loss discussed for direct solar heating in that it effectively reduces the heating efficiency of the individual reaction.

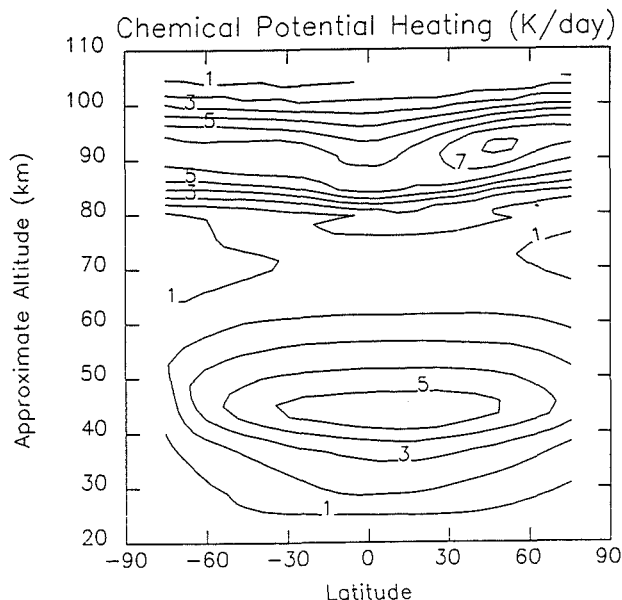


Fig. 4 Chemical potential heating (K/day) for daytime.

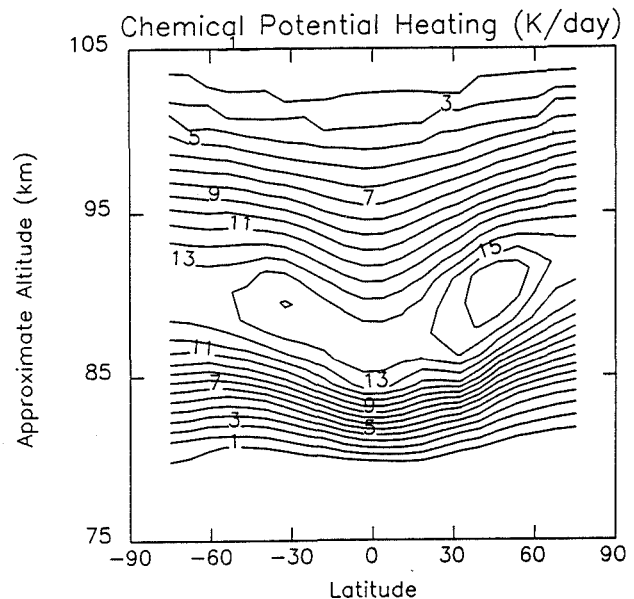


Fig. 5 Chemical potential heating (K/day) for nighttime.

5. HEATING EFFICIENCY PARAMETERIZATIONS

We conclude with a parameterization of the heating efficiencies for the three solar heating processes and the two chemical reactions with potentially significant chemiluminescent emission. For solar heating, the efficiencies are virtually independent of the photolysis rate and of the absorber (i.e., O₃ or O₂) concentration. The chemical heating efficiency is virtually independent of the reactant concentrations and of the rate of reaction. In both cases, the calculated efficiency depends strongly on the kinetic and spectroscopic parameters which describe the removal of energy from the excited product molecules. The rates and mechanisms of energy removal are reasonably well known for the quenching of O(¹D), O₂(¹Δ), and O₂(¹Σ) so that the solar heating efficiencies are calculated with a high degree of confidence. In addition, Mlynczak and Solomon [1991b] demonstrated good agreement between calculated efficiencies and those inferred from airglow observations. The quenching rates and mechanisms of vibrationally excited OH and O₃ are not nearly as well known as are the rates for the oxygen species formed in photolysis events. Consequently, there is uncertainty in the efficiencies which we recommend for the exothermic reactions. The recommended efficiencies are based upon using the latest quenching rates that have been measured in laboratory and reported in the literature.

We have parameterized the heating efficiency in the Hartley band of ozone as a function pressure by fitting a fifth degree Chebyshev polynomial to the efficiency curve shown in Figure 1. The efficiency on a given pressure surface between 10⁻⁴ mb and 1.0 mb can be accurately calculated by the following expression

$$\epsilon(x) = c_0 + c_1x + c_2x^2 + c_3x^3 + c_4x^4 + c_5x^5 \quad (4)$$

where the parameter x is defined by

$$x = \frac{(\log_{10} p + 2)}{2} \quad (5)$$

and p is in mb. The values of constants c_0 through c_5 are 0.75985, 0.29536, 0.13921, - 0.17906, - 0.07893, and - 0.05123, respectively. Calculations of the efficiency using these equations agree with the efficiencies calculated from the detailed kinetics to within 0.5 percent at all pressure levels within the indicated range. The evaluation of the efficiency using this parameterization requires about 15 floating point operations per pressure level, roughly 2.5 times less the number of operations required for direct evaluation using the detailed kinetics. For reference, the efficiencies at 10^{-4} , 10^{-3} , 10^{-2} , 10^{-1} , and 10^0 mb are 0.6526, 0.6627, 0.7598, 0.9166, 0.9876, respectively.

For photolysis of molecular oxygen in the Schumann-Runge continuum, Mlynczak and Solomon [1991b] showed that the heating efficiency is about 0.87 between 95 and 110 km considering only radiative loss from $O_2(^1\Sigma)$ and $O_2(^1\Delta)$. This initial calculation was based on an estimated Schumann-Runge continuum photon at 150 nm. We have revised our recommended efficiency using an actual calculation of the mean photon wavelength (172 nm) in addition to incorporating the Harris and Adams [1983] $O(^1D)$ thermalization profile to account for $CO_2(001)$ loss. We now recommend an efficiency of 0.78, constant with altitude, between 85 and 110 km.

It suffices to simply use a constant efficiency of 0.93 at all altitudes in order to parameterize the heating efficiency of Lyman-alpha radiation. This approximation results in an error of less than 0.01 K/day in the Lyman-alpha heating rate and an error of less than 1 % in the total heating rate at any altitude.

Based on the recent determinations of the quenching rates of OH by O_2 [Dodd et al., 1991], the Einstein coefficients of Nelson et al. [1990], and the reaction rate of OH(1) with O, [Spencer and Glass, 1977], we recommend a heating efficiency of 0.6, constant with altitude over the 80-100 km region, for the reaction of atomic hydrogen with ozone. The efficiency can approach 0.65 to 0.80 if the rate constants derived from OH airglow observations are employed (e.g., those utilized in Lopez-Moreno et al., [1987]). It is a fact that laboratory measurements of the OH quenching rates (e.g., Streit and Johnston, 1976 and Dodd et al., 1991) are generally much smaller than those inferred from airglow measurements. It is also quite likely that interactions between atomic oxygen and vibrationally excited hydroxyl are very important in determining the overall heating efficiency. However, rate constants for such processes are unknown.

The situation is similar with regard to the quenching of vibrationally excited ozone. There have been two different models used in the analysis of ozone limb emission data [Solomon et al., 1986; Rawlins, 1985]. The Rawlins model has a very strongly quenched ozone molecule, while quenching is very weak in the Solomon et al. model. Application of these two models yields much different heating efficiencies [Mlynczak, 1991]. In order to be consistent with our recommendations above, we recommend a unit heating efficiency for the reaction of atomic and molecular oxygen to form ozone. This is based on the laboratory work of Rawlins and Armstrong, [1987] which showed that only about 25% of the available chemical energy is converted to internal energy of ozone, most of which is quenched to release heat.

6. REFERENCES

- Andrews, D. G., J. R. Holton, and C. B. Leovy, Middle Atmosphere Dynamics, 489 pp., Academic Press, Orlando, FL, 1987
- Brasseur, G., and S. Solomon, Aeronomy of the Middle Atmosphere, 452 pp., D. Reidel, Boston, MA, 1986.
- Dodd, J. A., S. J. Lipson, and W. A. M. Blumberg, Formation and vibrational relaxation of $OH(X^2\Pi_1, v)$ by O_2 and CO_2 , *J. Chem. Phys.*, 95, 5752-5762, 1991.
- Garcia, R. R., and S. Solomon, A numerical model of the zonally averaged dynamical and chemical structure of the middle atmosphere, *J. Geophys. Res.*, 88, 1379-1400, 1983
- Garcia, R. R., and S. Solomon, The effect of breaking gravity waves on the dynamics and chemical composition of the mesosphere and lower thermosphere, *J. Geophys. Res.*, 90, 3850-3868, 1985
- Harris, R. D., and G. W. Adams, Where does the $O(^1D)$ energy go?, *J. Geophys. Res.*, 88, 4918-4928, 1983.
- Lopez-Moreno, J. J., R. Rodrigo, F. Moreno, M. Lopez-Puertas, and A. Molina, Altitude distribution of vibrationally excited states of atmospheric hydroxyl at levels $v=2$ to $v=7$, *Planet. Space. Sci.*, 35, 1029-1038, 1987.
- Mlynczak, M. G., and S. Solomon, A detailed evaluation of the heating efficiency of the middle atmosphere, submitted to *J. Geophys. Res.*, 1992.
- Mlynczak, M. G., and S. Solomon, Middle atmosphere heating by exothermic chemical reactions involving odd-hydrogen species, *Geophys. Res. Lett.*, 18, 37-40, 1991a.
- Mlynczak, M. G., and S. Solomon, On the efficiency of solar heating in the middle atmosphere, *Geophys. Res. Lett.*, 18, 1201-1204, 1991b.
- Mlynczak, M. G., Non-local thermodynamic equilibrium processes in ozone: Implications for the energy budget of the mesosphere and lower thermosphere, *J. Geophys. Res.*, 96, 17217-17228, 1991.
- Nelson, D. D., A. Schiffman, D. J. Nesbitt, J. J. Orlando, and J. B. Burkholder, H + O_3 Fourier transform infrared emission and laser absorption studies of $OH(X^2\Pi)$ radical: An experimental dipole moment function and state-to-state Einstein A coefficients, *J. Chem. Phys.*, 93, 7003-7019, 1990.
- Rawlins, W. T., and R. A. Armstrong, Dynamics of vibrationally excited ozone formed by three-body recombination. I. Spectroscopy, *J. Chem. Phys.*, 87, 5202-5208, 1987.
- Rawlins, W. T., Chemistry of vibrationally excited ozone in the upper atmosphere, *J. Geophys. Res.*, 90, 12883-12292, 1985.
- Spencer, J. E., and G. P. Glass, Some reactions of $OH(v = 1)$, *Int. J. Chem. Kinet.*, 9, 111-122, 1977.
- Slinger, T. G., L. E. Jusinski, G. Black, and G. E. Gadd, A new laboratory source of ozone and its potential atmospheric implications, *Science*, 241, 945-950, 1988.
- Solomon, S., J. T. Kiehl, B. J. Kerridge, E. E. Remsberg, and J. M. Russell III, Evidence for non-local thermodynamic equilibrium in the v_3 mode of mesospheric ozone, *J. Geophys. Res.*, 91, 9865-9876, 1986.
- Streit, G. E., and H. S. Johnston, Reactions and quenching of vibrationally excited hydroxyl radicals, *J. Chem. Phys.*, 64, 95-103, 1976.

EFFECTIVE UV RADIATION FROM MODEL CALCULATIONS AND MEASUREMENTS

Uwe Feister and Rolf Grewe

Deutscher Wetterdienst
 Meteorologisches Observatorium Potsdam
 Telegrafenberg, O-1561 Potsdam, Germany

ABSTRACT

Model calculations have been made to simulate the effect of atmospheric ozone and geographical as well as meteorological parameters on solar UV radiation reaching the ground. Total ozone values as measured by Dobson spectrophotometer and Brewer spectrometer as well as turbidity were used as input to the model calculation. The performance of the model was tested by spectroradiometric measurements of solar global UV radiation at Potsdam. There are small differences that can be explained by the uncertainty of the measurements, by the uncertainty of input data to the model and by the uncertainty of the radiative transfer algorithms of the model itself. Some effects of solar radiation to the biosphere and to air chemistry are discussed. Model calculations and spectroradiometric measurements can be used to study variations of the effective radiation in space and time. The comparability of action spectra and their uncertainties are also addressed.

1. INTRODUCTION

Solar UV radiation affects the biosphere, some types of materials and the chemistry of atmospheric trace gases (UNEP 1989, 1991). Due to its dependence on atmospheric ozone, cloudiness and turbidity natural and anthropogenic variations of those parameters can alter the diversity of living species, the air quality in the planetary boundary layer and the climate of the earth. For effects with known action spectra the effective radiation can be determined from model calculations and/or measurements of the spectral distribution of solar radiation.

2. MODEL CALCULATION OF THE EFFECTIVE SOLAR UV RADIATION

A modified version of the radiation model by Green et al. (1974 a, b, 1980) and Schippnick and Green (1982) has been applied to simulate solar UV radiation falling on a horizontal or spherical plane in the UV region using a stepwidth of $\Delta\lambda = 1$ nm. Depending on location and time of the year, solar zenith angles and distances between the earth and the sun were determined from the algorithms given by Sonntag (1989). The extraterrestrial radiation was taken from CIMO (1981), corresponding to a solar constant of 1367 W m^{-2} , and the ozone absorption coefficients from Bass and Paur (1985). Values of the effective radiation $E_x(\Theta, z, A)$ for an effect X were determined by

$$E_x(\Theta, z, A, \tau) = \int_0^{\infty} \epsilon(\lambda) E(\lambda, \Theta, z, A, \tau) d\lambda$$

(λ : wavelength, Θ : solar zenith angle, z : height, A : surface albedo, τ : optical depth of aerosol and gaseous absorbers). $\epsilon(\lambda)$ is the normalized action spectrum of a biological effect X, and $E(\lambda, \Theta, z, A)$ is the spectral radiation falling on a horizontal plane. It should be noted that there are doubts that action spectra can really describe biological effects. On the other hand, action spectra are an excellent tool to simulate the radiation environment and its changes at least to

a first approximation. Equation (1) can also be used to determine the photolysis rate in $[\text{s}^{-1}]$ of a photodissociation process. In that case we have

$$z(\lambda) = \varphi(\lambda) \cdot \sigma(\lambda)$$

with the absorption cross section $\sigma(\lambda)$ of the gas and the quantum yield $\varphi(\lambda)$ of the photodissociation process. In that case, $E(\lambda, \Theta, z, A)$ is the radiation falling on a sphere.

Fig. 1 shows the radiation amplification factors RAF determined from model calculations for UVB radiation and for some effects of UV radiation. The RAF is defined here as the percentage change of effective UV radiation for a 1 % ozone reduction. It can be seen that the RAF depends on the ozone concentration in a non-linear manner, and it also depends on the solar zenith angle (not shown). Therefore, the latitudinal and seasonal effects of ozone changes on daily totals of the effective solar UV radiation reaching the surface should be estimated by model calculations carried out for typical average conditions and assumed changes of atmospheric parameters. Effects with a longer tail of the action spectrum at wavelengths in the UVA, such as erythemal and photocarcinogenic radiation, show a "saturation effect", i.e. a slight decrease of the RAF values with higher total ozone values.

With $\sigma(\lambda)$ in eq. (2) as the absorption cross section of ozone (Bass and Paur 1985) and $\varphi(\lambda)$ the quantum yield (Aleksandrov et al. (1982), equation (1) was applied to determine the photolysis rate of ozone dissociation



which is important for the production of the hydroxyl radical from water vapour in the lower troposphere



Fig. 2 shows the modelled dependence of the O_3 photolysis rate on total ozone and on height above the surface. Due to aerosol absorption, which is strongest in the lower troposphere, the strong increase in upward scattering of the radiation from air molecules and aerosols with height, and due to the decreasing attenuation of solar radiation with increasing height, the photolysis rate increases by two orders of magnitude, with the strongest increase occurring in the lowest 1000 m above the surface. For a decrease of total ozone from 400 D to 200 D the O_3 photolysis rate increases by a factor of 3 to 4.

3. MEASUREMENTS OF SOLAR RADIATION

A spectrometer OL 752/10 (Optronic Laboratories) was used for measurements of solar radiation at Potsdam. The instrument is a double monochromator with dual holographic gratings that allow a spectral resolution of 1.5 nm to 10 nm halfwidth. The spectrometer was calibrated by a 200 W tungsten filament lamp, which is absolutely calibrated against an Eppley Standard Cell at the National Institute of Standards and Technology (NIST). The

spectroradiometric accuracy of the calibration relative to NIST is given as $\pm (2...4)\%$. Due to a straylight problem below 295 nm radiance values with $\lambda < 295$ nm had to be extrapolated from radiances measured at higher wavelengths. The spectrometer was placed on the tower roof platform of the Observatory at a height of 18 m above the ground. A spectral resolution of 1.5 nm was selected with a stepwidth of 2 nm. Fig. 3 shows a spectrum measured on October 11, 1991. The time of measurements corresponds to a solar zenith angle of around 60°. Also shown in Fig. 3 is the result of the model calculation for the respective zenith angle. Atmospheric total ozone, which is needed as input to the model, was taken from measurements with a Dobson spectrophotometer (ADDS) and a Brewer spectrometer (DS) at Potsdam. The measured ozone value was decreased by 2.7 % to account for the inadequate ozone absorption coefficients that were in use before January 1, 1992 (Hudson et al. 1991). The model calculation is thus in two ways based on the Bass and Paur (1985) ozone absorption coefficients. It can be seen from Fig. 3 that the correspondence between model calculation and measurement is quite good.

Erythral radiation [W m ⁻²] _{BRV}	Rel. to BGBl. (1987)	Reference of action spectrum
0.0194	0.69	Coblentz and Stair (1934)
0.0171	0.60	Berger et al. (1968)
0.0257	0.91	Cripps and Ramsay (1970)
0.0159	0.56	Komhyr & Machta (1973)
0.0188	0.66	DIN (1979)
0.0283	1.00	BGBl (1987)
0.0266	0.94	Photocarcinogenesis (CIE 1986)

Table 1 Erythral radiation determined for a spectrum of measured solar global radiation, $\Theta = 59.63^\circ$, $O_3 = 271$ D

However, the uncertainties in the *effective* radiation depend both on the uncertainties in the measured and modelled solar radiation, and on the uncertainties of the action spectrum. As an example, Table 1 shows the erythral radiation determined from one spectrum of solar global radiation (cf. Fig. 3), but using erythral action spectra from different sources. For comparison, the last row in Table 1 shows the result for the photocarcinogenesis. It can be seen that the radiation producing photocarcinogenesis is closest to the latest erythral action spectrum used (BGBl 1987). The different shapes of the action spectra of the erythral effect do not only provide different absolute values of the erythral radiation, but do also produce different dependencies of the effective radiation on atmospheric ozone. If model calculations and measurements are to be compared, there must be a consensus on the action spectra applied. The model has been used to simulate variations of the effective radiation in space and time. As an example, Table 2 shows the percentage ratios of daily totals of UV radiation on June 21, September 23, and December 21, referred to March 21, at the station Arkona. Seasonal averages of total ozone (March: 400 D, June: 360 D, September: 310 D, December: 320 D) and typical surface albedo values of 5 %, 5 %, 5 % (grassland) and 60 % (snow) were used as representative input values. While UV and UVA radiation, which are nearly independent on atmospheric ozone, show a seasonal variation from 20 % to 200 % of the spring time value, the seasonal variations of those effects that are strongly ozone dependent are much higher. They extend from 6 % (winter) to 402 % (summer) for the UVB radiation up to the range 2 % to 950 % of

	June 21	Sept. 23	Dec. 21
UV ($\lambda < 400$ nm)	219	101	18
UVA ($315 < \lambda < 400$)	217	100	19
UVB ($\lambda < 315$ nm)	402	140	6
Erythema (DIN 1979)	488	154	6
Photocarcinogenesis (CIE 1986)	499	156	6
Bactericide (DIN 1979)	716	192	3
Pigmentation (DIN 1979)	221	101	18
Plant response (Caldwell 1971)	606	178	3
Conjunctivitis (DIN 1979)	950	229	2
Photokeratitis (DIN 1979)	385	136	7
Yellowing of PVC (Andrady and Searle 1989, Andrady et al. 1989)	244	105	15

Table 2 Percentage ratios of daily totals of solar global radiation for different effects at the station Arkona (54° 41' N, 13° 26' E) on June 21, September 23, and December 21, referred to March 21

the spring time value for photoconjunctivitis. This phenomenon is similarly reflected in the spatial changes of the radiation effects that can be expected as a result of changes in the total ozone concentration. Fig. 4 shows the modelled percentage increase in zonal averages of UVB radiation and in photoconjunctivitic radiation for a global uniform reduction of total ozone by 10 %. In the first model run (no change), the average latitudinal ozone distribution from London et al. (1976) was used. The vertical distribution of ozone is not changed in the calculation, because such a change could produce different results (Brühl and Crutzen 1989). While the latitudinal gradient for UVB is between 10 % in the tropics to around 30 % at high latitudes in winter, for the photoconjunctivitis, which is highly ozone dependent, the range of changes is between 32 % in the tropics to 60 % at high latitudes. It must be noted here that the *absolute* increase in the effective radiation attains its maximum value in the tropics, where the normal radiation levels are highest. On the other hand, the extent to living matter depends on how much additional effective radiation can be tolerated by the individual species and how they are capable of adapting to it.

4. CONCLUSION

Effects of solar radiation to the biosphere can be studied both by model calculations and measurements. The uncertainties in both approaches do not only arise from inaccurate algorithms, uncertainties of the input parameters to the radiation model and measurement errors, but also from the uncertainties of the action spectra, which describe an "average" or typical behaviour of an individual or a group of species under definite conditions. The different types of erythral action spectra, which produce different values of erythral radiation, are an example of the increasing

knowledge about radiation effects to human skin.

Despite the deficiencies of the approach to use model calculations and spectroradiometric measurements for estimating the effective radiation, they provide an opportunity to study the effects of solar radiation and its changes to different kinds of living species as well as on air chemistry.

REFERENCES

- Aleksandrov, E. L., I. L. Karol', L. R. Rakipova, J. S. Sedunov, A. Ch. Chrgian (1982), *Atmosfernyj ozon i izmenenija global'nogo klimata*. Gidrometeoizdat
- Andrady, A. L., N. D. Searle (1989), *J. Appl. Polymer Sci.* 37, 2789 - 2802
- Andrady, A. L., A. Torikai, K. Fueki (1989), *J. Appl. Polymer Sci.* 37, 935 - 946
- Bass, A. M., R. J. Paur (1985), In: *Atmospheric Ozone*. D. Reidel Publishing Company, 606 - 616
- Berger, D., F. Urbach, R. E. Davies (1968), *Proc. 13. Congressus Internationalis Dermatologicae*, Munich 1967
- BGBl (1987), *Bundesgesundheitsblatt* 30 (Nr. 1), 19 - 31
- Brühl, C., P. J. Crutzen (1989), *Geophys. Res. Lett.* 16, 7, 703 - 706
- CIE (1986), Division 6, Meeting in Budapest 1986
- CIMO (1981), *Abrided Final Report of the Eights Session*. Mexico City. WMO-No 590
- Coblentz, W. W., R. Stair (1934), *Bureau of Standards Journal of Research* 12, 13 - 14
- Cripps, D. J., C. A. Ramsay (1970), *Br. J. Derm.* 82, 584 - 592
- DIN (1979), DIN 5031, Teil 10, November 1979, 1 - 8
- Green, A. E. S., K. R. Cross, L. A. Smith (1980), *Photochemistry and Photobiology* 31, 59 - 65
- Green, A. E. S., T. Mo, J. H. Miller (1974a), *Photochemistry and Photobiology* 20, 473 - 482
- Green, A. E. S., E. P. Shettle (1974b), *Photochemistry and Photobiology* 19, 251 - 259
- Hudson, R. D., W. K. Komhyr, C. L. Mateer, R. D. Bojkov (1991), *Guidance for use of new absorption coefficients in processing Dobson and Brewer spectrophotometer total ozone data beginning 1 January 1992*. Letter to operators at ozone stations. December 1991
- Komhyr, W. D., L. Machta (1973), In: *The perturbed troposphere of 1990 and 2020*. CIAP. Dep. Transportation, Washington, D. C.
- London, J., R. D. Bojkov, S. Oltmans, J. I. Kelley (1976), *Atlas of the global distribution of total ozone*. July 1957 to June 1967, NCAR/TN 113 + STR
- Schippnick, P. F., A. E. S. Green (1982), *Photochemistry and Photobiology* 35, 89 - 101
- Sonntag, D. (1989), *Abhandlungen des MD der DDR*, Nr. 143
- UNEP (1989), *Environmental Effects Panel Report*, November 1989
- UNEP (1991), *Environmental effects of ozone depletion: 1991 update*, November 1991

RADIATION AMPLIFICATION FACTORS THETA=60, IT=6, A=5 %, CLEAR SKY

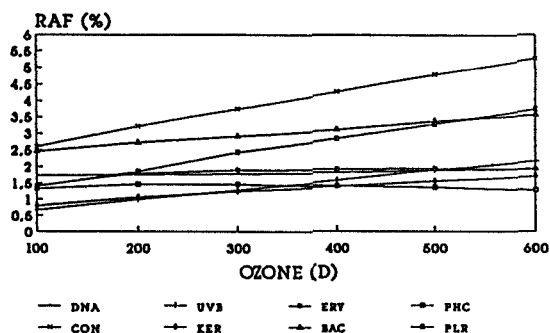


Fig. 1 Radiation amplification factors for biologically effective radiation at the earth's surface in dependence on the total ozone value (DNA: DNA absorption, Sutherland and Griffin 1981; UVB: $\lambda < 315$ nm; ERY: erythematous radiation, PHC: photocarcinogenesis; CON: photoconjunctivitis; KER: photokeratitis; BAC: bactericide effect; PLR: plant response). Solar zenith angle: 60°, surface albedo: 5 %, clear sky.

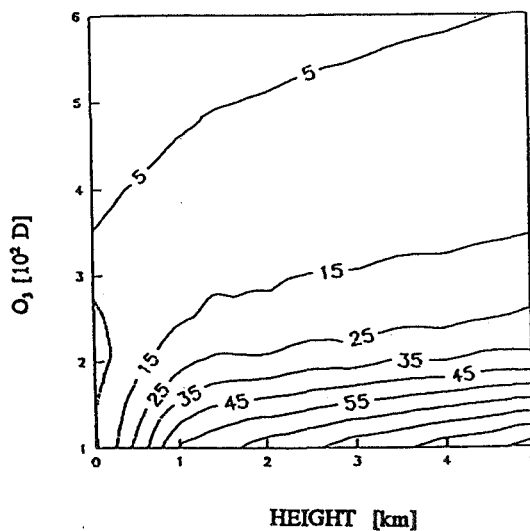


Fig. 2 Photolysis rate of ozone [10^4 s⁻¹] in dependence on total ozone for a solar zenith angle of $\theta = 60^\circ$, surface albedo of 10 %, cloudless conditions and low turbidity

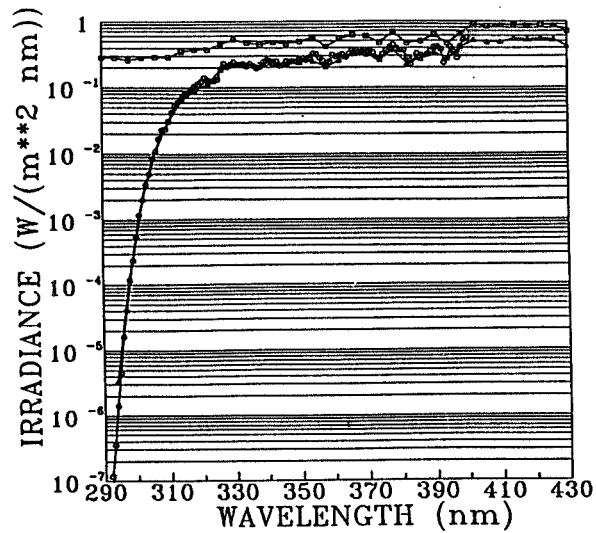


Fig. 3 Solar global radiation at Potsdam (52° 22' N, 13° 5' E) on October 11, 1991, 11.24 CET, $\theta = 59.631^\circ$
 □—□ extraterrestrial radiation from CIMO (1981) corrected for solar zenith angle and distance sun-earth
 ▲—▲ measurements of global solar radiation taken with the spectrometer OL 752/10 at Potsdam 18 m above the ground, clear sky
 ○—○ model calculation of global radiation (direct + diffuse) with $O_3 = 271$ D and an aerosol optical thickness of $\tau = 0.4$ with $\lambda = 350$ nm

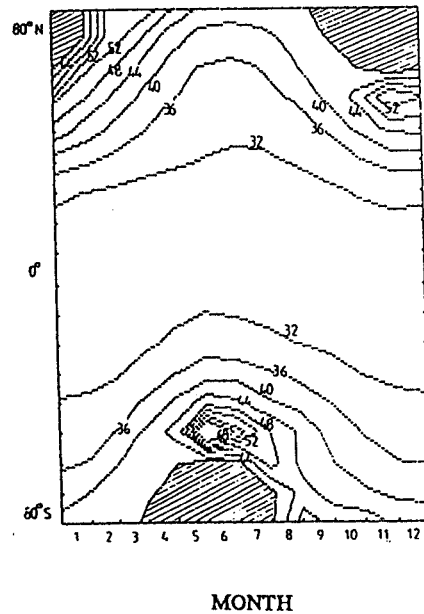
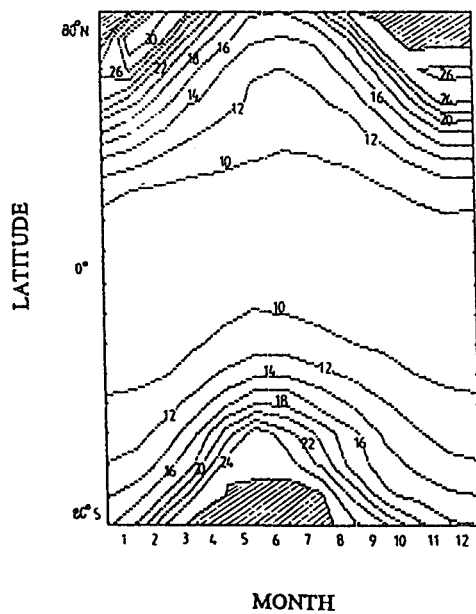


Fig. 4 Latitudinal and seasonal percentage change of UVB ($\lambda < 315$ nm) (a) and photoconjunctivitic (b) radiation modelled for a uniform reduction of total ozone by 10 %

303647

IMPACT OF STRATOSPHERIC AIRCRAFT EMISSIONS ON
OZONE: A TWO DIMENSIONAL MODEL STUDY

M. Natarajan¹, L. B. Callis², R. E. Boughner², and J. D. Lambeth¹

¹ Science Applications International Corporation
Hampton, Virginia 23666, USA.

² Atmospheric Sciences Division, NASA Langley Research Center
Hampton, Virginia 23681, USA.

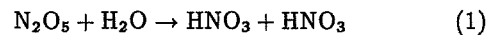
ABSTRACT

Atmospheric perturbations caused by the emission of nitrogen oxides from a projected fleet of stratospheric aircraft are studied with a two dimensional chemistry, transport model. Photochemistry of the lower stratosphere, the region where these aircraft may fly, is now known to be influenced by heterogeneous reactions involving sulfuric acid aerosols. This study examines the sensitivity of the atmospheric effects of aircraft to heterogeneous reactions. Information on background aerosols based on the SAGE II measurements have been used in the parameterization of the heterogeneous conversion rates. It is found that heterogeneous reactions make the lower stratospheric ozone less sensitive to perturbations in the odd nitrogen level. The calculated reduction in global ozone due to NO_x injection from a fleet of Mach 2.4 aircraft is 1.28% if gas phase reactions only are considered in the model, and 0.06% if heterogeneous reactions are included.

1. INTRODUCTION

Recent interest in the development of high speed civil transport aircraft has revived the concerns regarding the effects of aircraft exhaust gases on atmospheric ozone. Results from early model calculations of the perturbation due to a projected fleet of aircraft have been documented by the High Speed Research Program (NASA RP-1272, 1992). Ambient atmosphere with source gas mixing ratios projected for the year 2015 has been used in these studies as the baseline case. Aircraft fuel usage scenario as a function of latitude, and NO_x emission index in the range 5 to 45 gms of NO_x /kg of fuel have been adopted. Model results for NO_x injection at three different altitudes (based on the Mach number of the aircraft) have been reported. The calculated reductions in global ozone for different models ranged from 0.72% to 2.1%, for Mach 2.4 aircraft with an emission index of 15 for NO_x. All these models considered only gas phase reactions. The identification of the heterogeneous reactions on polar stratospheric clouds as a necessary component of the mechanism leading to the springtime ozone loss in the antarctic region, and the subsequent advances in laboratory studies of possible hetero-

geneous reactions on sulfuric acid droplets have revolutionized our understanding of the lower stratospheric photochemistry. Reaction probability for the reaction,



involving sulfuric acid aerosols is believed to be high. Recent work by Hanson and Ravishankara (1991) suggests that the probability of the reaction,



on sulfuric acid aerosols is a function of the acidity of the aerosol, and this reaction could be important under colder temperatures and/or larger aerosol loading. The conversion of reactive odd nitrogen into HNO₃ will also shift the partitioning of odd chlorine species, and recent measurement campaigns have reported data on ClO that are consistent with this theory. It is therefore essential that model studies of the aircraft effects should take into account the heterogeneous reactions on sulfuric acid aerosols. This paper describes one such study. Weisenstein et al. (1991) have also reported a similar study of the impact of reaction (1) on ozone response to aircraft emissions.

2. MODEL DESCRIPTION

The basic tool used in this study is a two dimensional chemistry, transport model developed on a potential temperature - latitude grid. This model extends from the ground to 2700 K surface. Main features of the model have been described by Callis et al.(1991). We have used NMC temperature data and ozone climatology in a radiative transfer code to calculate the monthly averaged diabatic heating rates. The advective fields are derived from these heating rates. Tropospheric fields have been calculated from heating rates based on FGGE data. We have adopted the horizontal mixing coefficients from Yang et al. (1990). The following chemical species are transported in the model: O_x, NO_y, HNO₃, Cl_y, CH₄, H₂O, CO, N₂O, CCl₄, CH₃Cl, CH₃CCl₃, CFCl₃, CF₂Cl₂, HCl, and CHF₂Cl. SAGE II H₂O data have been used in the troposphere. Photochemical and kinetic data are adopted from NASA Evaluation JPL 90-1.

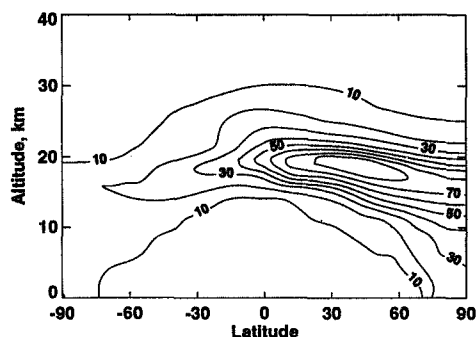


Figure 1: Percent change in total odd nitrogen in July due to NO_x injection from Mech 2.4 aircraft.

For the model with heterogeneous reactions, the distribution of the background aerosol surface area density is based on the information derived from the SAGE II measurements for 1989. γ_1 , the reaction probability for reaction (1) is 0.1, and γ_2 is computed as a function of the acidity of the aerosol (Hanson and Ravishankara, 1991). Heterogeneous reactions involving polar stratospheric clouds have not been included. The boundary values for the source gases are taken from NASA RP-1272, and these are the recommended data to simulate the conditions in the year 2015. The baseline atmosphere in this study includes the NO_x injection from the subsonic aircraft flying in the altitude range 6.1–12.2 km. The fuel usage for the subsonic aircraft is 170×10^9 kg/year and that for the supersonic fleet is 70×10^9 kg/year. The latitudinal distribution of the fuel use is taken from NASA RP-1272. We have considered only the effects of NO_x emission in this study.

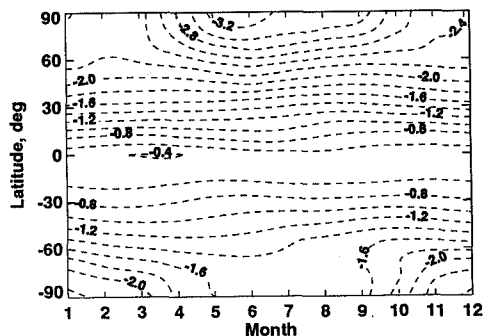


Figure 2: Percent change in total ozone for Model G (gas phase chemistry only) due to NO_x injection from Mech 2.4 aircraft.

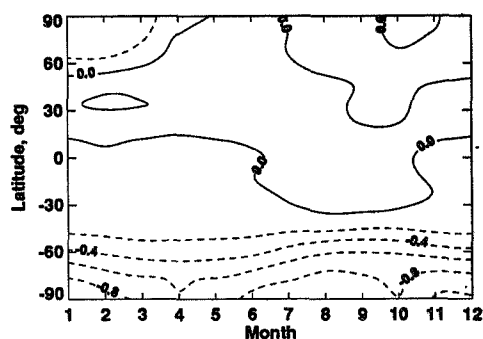


Figure 3: Same as figure 2, for Model H.

3. RESULTS AND DISCUSSION

In the following discussion, ‘Model G’ denotes the case with only gas phase chemistry, and ‘Model H’ includes, in addition, the heterogeneous reactions on the background aerosols. NO_x injection from Mach 2.4 aircraft occurs in the altitude range 16.8–19.8 km. The percent change in the total odd nitrogen due to this injection for July is shown in Figure 1. The maximum change is about 80%, and this occurs between 30° N and 60° N. Total ozone perturbation caused by this increase in NO_y is shown in Figures 2 and 3 for the model G and H respectively. Model G yields ozone reductions at all latitude regions. Maximum reduction of 3.2% occurs in the northern high latitudes. The response of the atmospheric ozone to NO_x injection in the presence of heterogeneous reactions is dramatically different. In this case, most regions in the northern hemisphere show small increases in total ozone. In the high latitude southern hemisphere ozone reductions of 0.8% are seen. It should be noted that the aircraft fuel usage and hence the NO_x input are weighted heavily towards the northern latitudes. The vertical distribution of the ozone perturbation in July are shown in Figures 4 and 5. When only gas phase reac-

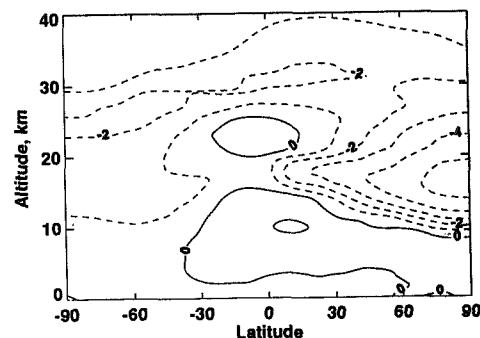


Figure 4: Latitude-Altitude distribution of percent change in ozone due to NO_x injection, Model G.

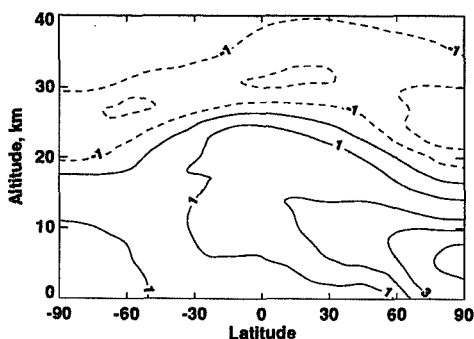


Figure 5: Same as figure 4, for Model H.

tions are considered (model G), ozone losses occur in the region above 10 km where the NO_x catalytic cycle is dominant. There is some increase in the tropospheric ozone which is partly due to increased production from smog reactions. For the model with heterogeneous reactions, ozone reductions are confined to the region between 22 and 35 km. Below this region ozone increases by about 1 to 3%.

The main reason for this change in the ozone response to NO_x injection is the modification of the photochemistry by the heterogeneous reactions, especially reaction (1). By converting reactive NO_x into HNO_3 , this reaction effectively alters the relative importance of various catalytic cycles in destroying odd oxygen. The ratio of the odd oxygen loss rate due to NO_x cycle as a percent of the total odd oxygen loss rate is shown in Figure 6 for July. The solid lines represent results from model H, and the dashed lines represent model G. The contribution of NO_x catalytic cycle is clearly reduced to about 10% in the lower stratosphere because of the heterogeneous reactions. Correspondingly, there are increases in the odd oxygen loss

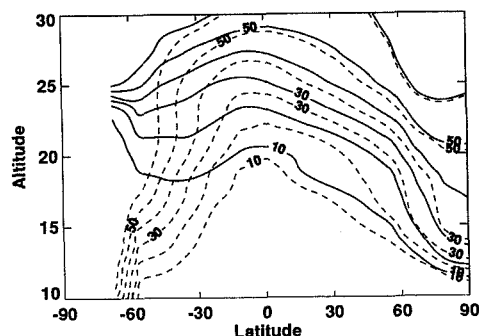


Figure 6: Ratio, in percent, of odd oxygen loss rate due to NO_x catalytic cycle to the total odd oxygen loss rate. Solid lines denote model with heterogeneous chemistry; dashed lines represent model with gas phase chemistry only.

Aircraft Type	Gas Phase Chemistry	Gas Phase + Het. Chemistry
Mach 2.4 (16.8-19.8 km)	-1.28	-0.06
Mach 3.2 (21.3-24.4 km)	-4.5	-2.2

Table I: Calculated percent change in global ozone.

due to Cl_x catalytic cycle. With the reduced significance of the NO_x cycle, the atmosphere with heterogeneous reaction becomes less sensitive to NO_x perturbations from stratospheric aircraft. Ozone increases in the lower altitudes nearly balance the ozone reductions in the upper regions, with the result that there is very little change in the total ozone in model H for the Mach 2.4 case. If the cruise altitude is higher, as in the case of Mach 3.2 aircraft, there will be larger ozone reductions in the mid stratosphere, and some reduction in the total ozone also. But even in this case, total ozone reduction is less for an atmosphere with heterogeneous reactions. The results from our model study are summarized in Table I.

REFERENCES

- Callis, L. B., R. E. Boughner, M. Natarajan, J. D. Lambeth, D. N. Baker, and J. B. Blake, Ozone depletion in the high latitude lower stratosphere: 1979-1990, *J. Geophys. Res.*, 96, 2921-2938, (1991)
- Hanson, D. R., and A. R. Ravishankara, The reaction probabilities of ClONO_2 and N_2O_5 on 40 to 75% sulfuric acid solutions, *J. Geophys. Res.*, 96, 17,307-17,314, (1991)
- NASA Panel for Data Evaluation, Chemical kinetics and photochemical data for use in stratospheric modeling, 9, *JPL Publication 90-1*, (1990)
- NASA RP-1272, The atmospheric effects of stratospheric aircraft: A first program report, (1992)
- Weissenstein, D. K., M. K. W. Ko, J. M. Rodriguez, and N. D. Sze, Impact of heterogeneous chemistry on model-calculated ozone change due to high speed civil transport aircraft, *Geophys. Res. Lett.*, 18, 1991-1994, (1991)
- Yang, H., K. K. Tung, and E. Olaguer, Nongeostrophic theory of zonally averaged circulation. Part II: Eliassen-Palm flux divergence and isentropic mixing coefficient, *J. Atmos. Sci.*, 47, 215-241, (1990)

303648

OZONE AND STRATOSPHERIC HEIGHT WAVES FOR OPPOSITE PHASES OF THE QBO

Kingtse C. Mo

Climate Analysis Center
NMC/NWS/NOAA
Washington D. C. 20233

and

Julia Nogués-Paegle
Department of Meteorology,
University of Utah,
Salt Lake City, Utah 84112

1. Introduction

The stratospheric quasi-biennial oscillation (QBO) provides an important source of interannual variations in the Northern Hemisphere. O'sullivan and Salby (1990) related extra-tropical eddy transports with the phase of the tropical QBO. When the tropical wind is easterly, the zero wind line is shifted into the winter hemisphere. Enhanced wave activity in middle latitudes acts to weaken the polar vortex. When the tropical wind is in the westerly phase the situation reverses. Heights at 30 mb and ozone configurations are contrasted in this paper for these two QBO phases.

When the winter vortex deforms due to the amplification of planetary waves 1 and 2, a band of air is drawn out of the vortex and extends westward and equatorward, the complementary band of low vorticity air spirals in toward the pole from lower latitudes. Sometimes, these planetary waves break (Jukes and McIntyre, 1987) and an irreversible mixing of air takes place between high and mid-latitudes. Global ozone patterns, as obtained from satellite observations, appear to be affected by planetary wave breaking (Leovy et al. 1985). This mixing results on regions with uniform ozone and potential vorticity.

In the Southern Hemisphere (SH), Newman and Randel (1988) using Total Ozone Mapping Spectrometer (TOMS) data and the NMC analyses have found strong spatial correlation between the October mean temperature in the lower stratosphere and total ozone for the 1979 through 1986 years. Recently Nogués-Paegle et al.(1992) analyzed SH ozone and height data from 1986 to 1989. They found that leading empirical orthogonal functions (EOFs) for both ozone and 50 mb heights exhibit zonal wave 1 and 2 and that the correlations between ozone and 50 mb principal components (PCs)

are high. The results were found to be consistent with a linear planetary wave advecting a passive tracer. In this paper, the dominant patterns of variability for 30 mb NMC heights and TOMS total ozone are obtained for the winter to summer transition (January to May) in the Northern Hemisphere (NH) for the years 1987-1990.

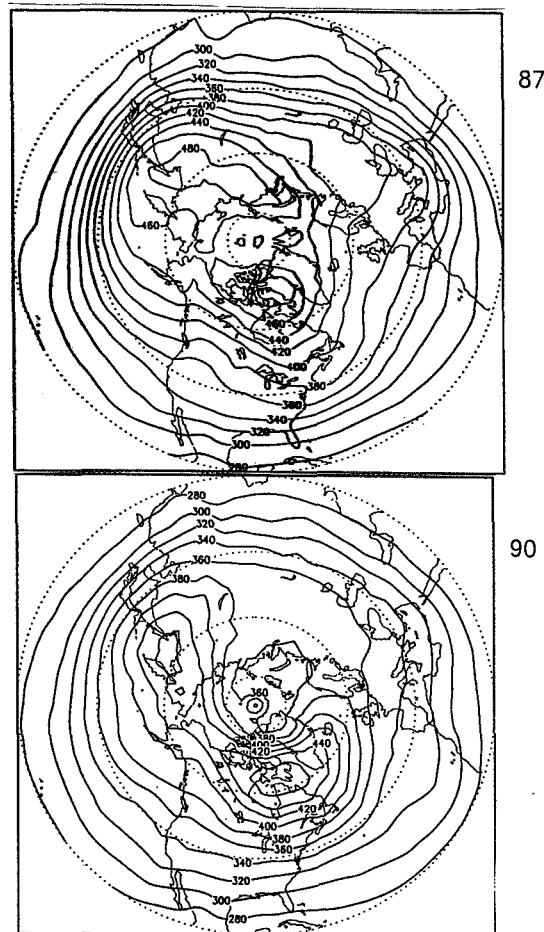


Fig.1: Total column ozone averaged from February to April for (a) 1987 and (b) 1990. Contour interval 20DU

2. General description of ozone variability

Low January ozone values were found for all four years associated with a deep polar vortex. Most of the interannual variability is found from late winter (February) to spring. This is shown in Fig.1. During this period, the 1987 and 1989 years exhibited large ozone values, with peak values over 460 DU over the polar regions. Large ozone values can be found from the Sea of Okhotsk to the opposite side of the Arctic at 80 °W to 75 °N. In contrast, during 1988, regions with more than 460 DU of ozone were smaller than during 1987 and 1989. The 1990 was an ozone depletion year and a large ozone hole centered near the North Pole is apparent in the figure.

The zonal wind at Singapore at 30 mb is used to represent the quasi-biennial oscillation in the tropics and to link this to the ozone distribution. During the 1987 NH winter-spring, the QBO was in the easterly phase, while during 1990 it was in the westerly phase. Both 1988 and 1989 were in the transition phase, but winds were positive during 1988 and turned to negative during 1989. Low/high ozone values were found for the 1990/1987 years respectively. This is consistent with enhanced mid-latitude wave activity during the easterly phase of the tropical QBO. In the rest of the paper, we will examine wave activities in the extratropics and the ozone distribution during two extreme years: 1987 and 1990.

3. The 1987 case.

Fig.2 shows plots of the first two EOFs obtained for the 30 mb heights for each year and the associated PCs. The orthogonality of the PCs permits projection of the ozone grid point time series ($O(x,t)$) onto PCs as follows:

$$O(x,t) = O_{mean}(x) + \sum_k C_k(x) PC_k(t)$$

where $O_{mean}(x)$ is the seasonal mean. The coefficient $C_k(x)$ for $k=1,2$ are given in Fig.2. Interpretation of the results obtained from the EOF analysis is facilitated with longitude-time diagrams of the zonally asymmetric component of the height field at 60 °N (Fig.4a).

PC 1 (Fig.2e) had large negative values during the first 20 days of January. During that period, the height mean shows a slightly off-center polar vortex and an Aleutian anticyclone similar to the EOF 1 pattern. This gives a large wave 1 at 60°N. Fig.4a shows that the wave 1 has both stationary and traveling components. In mid-January (Jan. 21), wave 1 starts to di-

minish and moves eastward. At the same time, the low pressure vortex was displaced to Russian Siberia. During this period, the PC 2 was strongest and the 30 mb height anomalies were similar to EOF 2 pattern (Fig.2b).

The ozone patterns (Fig. 2c, 2d) resemble the height EOFs. The EOF 1 pattern represents a seasonal trend of the 30 mb heights, which shows a weakening vortex as the season progresses. The ozone mean map from January 1 to 21 shows more ozone in the Pacific side and less ozone in the Atlantic side (Fig.2f) where the strong vortex was located. This is consistent with vertically propagating waves which tilt westward with height. As a result, the tropopause is found at low/high altitudes for stratospheric ridges/troughs, indicating a deeper stratosphere and therefore higher values of total ozone in ridges than in troughs. The ozone trend (Fig.2c) indicates that the ozone shifts from the Northern Pacific to the European side as the season shifts from winter to spring and the polar vortex weakens.

4. The 1990 case

The 1990 case is very different from 1987. A strong wave 1 persisted through the end of February (Fig.4b). During this time, large negative PC 1 (Fig.3e) indicated a strong zonal vortex (EOF 1, Fig.3a). A decrease of wave 1 was observed at the end of February with the amplification of PC 2 was large positive. EOF 2 (Fig.3b) also had a wave 1 structure with high pressure over the Atlantic ocean and lowest values close to the North Pole. The composite of heights during this period shows a near symmetric vortex located in the pole (Fig.3f). The vortex started to break during April, when PC 1 turned to large positive. This case displayed marked zonal symmetry and less mean flow-wave interaction than during 1987.

The ozone trend showed that when the vortex broke (Pc 1 becomes positive) during April, the ozone moved into the polar region to fill the ozone hole (Fig.3c).

Acknowledgements: This research has been supported by NASA grant NAG 5 127 and NSF grant 9114073

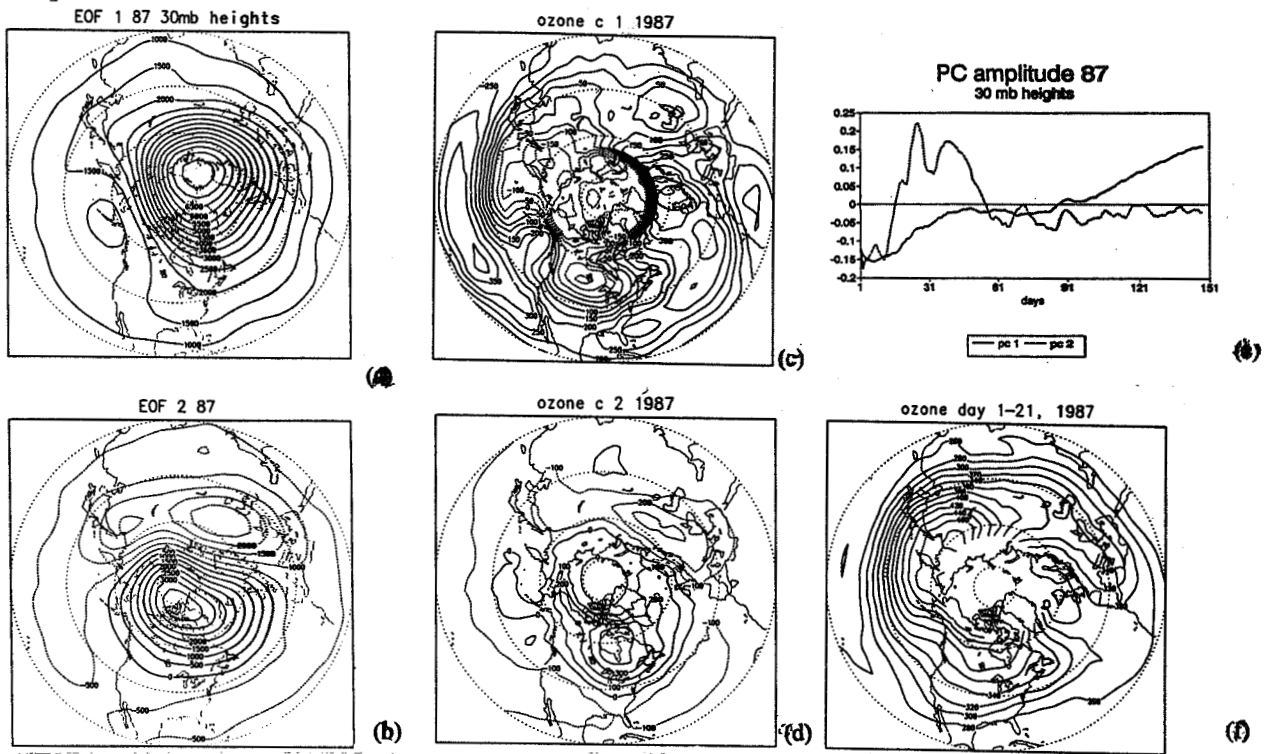


Fig.2: (a) EOF 1 and (b) EOF 2 for 30 mb heights for 1987. (c) C_1 , (d) C_2 , (e) Principal components PC 1 and 2 associated with EOF 1 and 2, and (f) total ozone averaged from January 1 to 21, 87

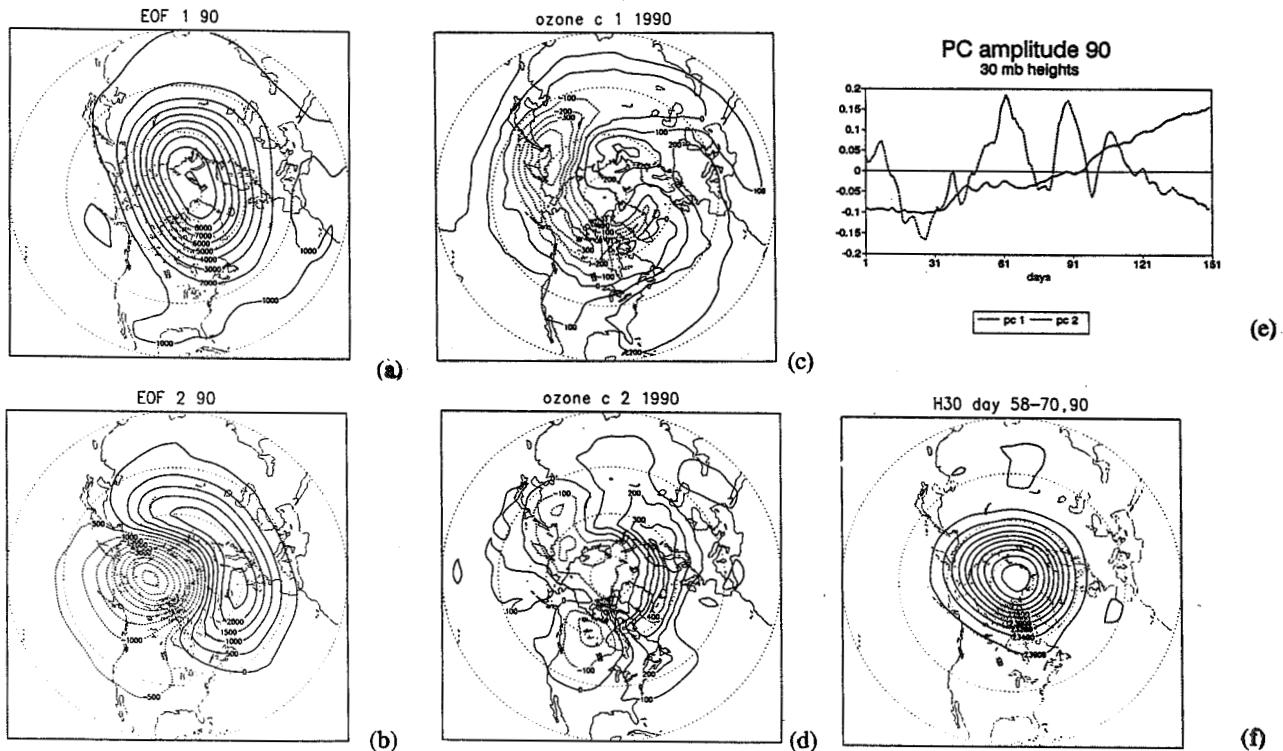


Fig.3: (a) - (e) Same as Fig.2, but for 1990, (f) 30 mb heights averaged over February 27 - March 11, 90

References:

- Juckes, M. N. and M. E. McIntyre, 1987: A high-resolution one-layer model of breaking planetary waves in the stratosphere. *Nature*, Vol. 328, 590-596.
- Leovy, C. B., C. R. Sun, M. H. Hitchman, E. E. Remsberg, J. M. Russell, L. L. Gordley, J. C. Gille and L. V. Lyjak 1985: Transport of ozone in the middle stratosphere: evidence of planetary wave breaking. *J. Atmos. Sci* 42, 230-244
- Newman P. A., W. J. Randel 1988: Coherent ozone-dynamical changes during the Southern Hemisphere spring 1979-1986. *J. Geophys. Res.* 93, 12585-12606
- Nogues-Paegle, J., K. C. Mo and K. P. Callahan 1992: Lower stratosphere waves during 1986-1989 Southern springs. *Tellus*. In press.
- O'Sullivan and M. L. Salby 1990: Coupling of the Quasi biennial oscillation and the extratropical circulation in the stratosphere through planetary wave transport. *J. Atmos. Sci*, 47, 650-673

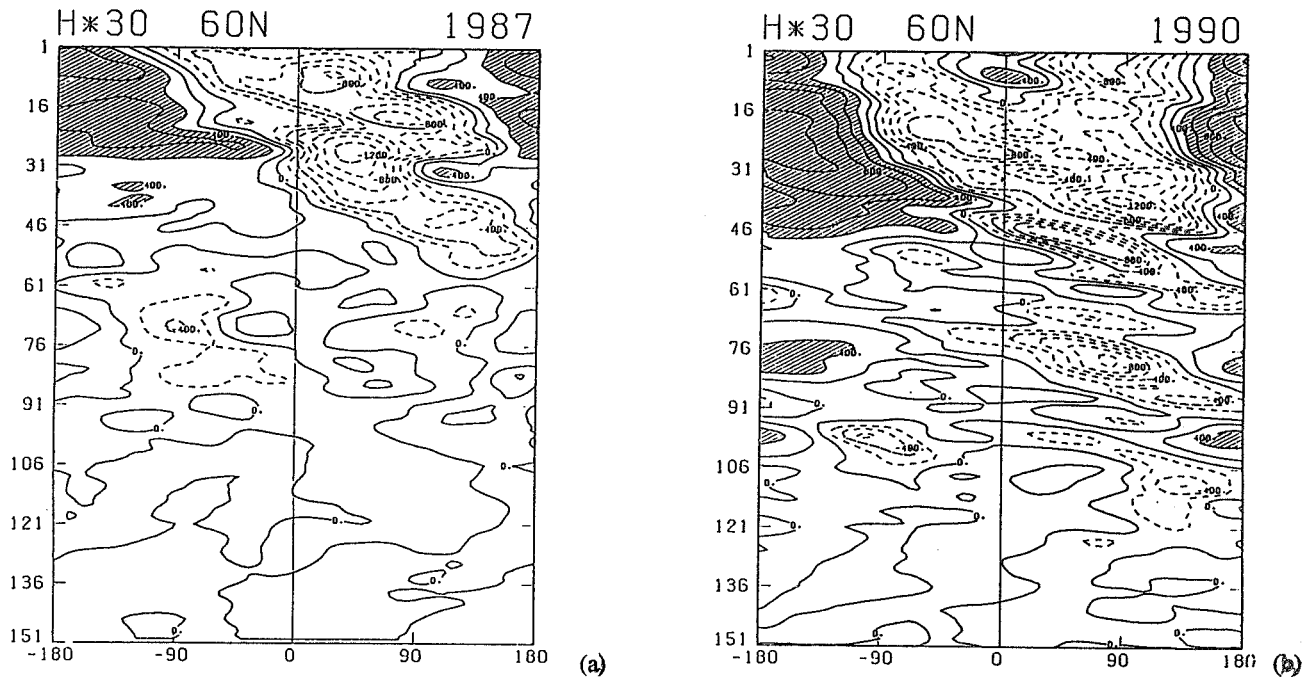


Fig.4 : Longitude-time diagram for the asymmetric part of 30 mb heights at 60N for (a) 1987 and (b) 1990.

INFRARED ABSORPTION CROSS SECTIONS OF ALTERNATIVE CFCs

Cathy Clerboux, Reginald Colin

Laboratoire de Chimie Physique Moléculaire
Université Libre de Bruxelles, CP 160
50 av. F.D. Roosevelt, 1050 Brussels, Belgium

Paul C. Simon

Institut d'Aéronomie Spatiale de Belgique,
3 av. Circulaire, 1180 Brussels, Belgium

ABSTRACT

Absorption cross sections have been obtained in the infrared atmospheric window, between 600 and 1500 cm^{-1} , for 10 alternative hydrohalocarbons: HCFC-22, HCFC-123, HCFC-124, HCFC-141b, HCFC-142b, HCFC-225ca, HCFC-225cb, HFC-125, HFC-134a and HFC-152a. The measurements were made at three temperatures (287K, 270K and 253K) with a Fourier transform spectrometer operating at 0.03 cm^{-1} apodized resolution. Integrated cross sections are also derived for use in radiative models to calculate the global warming potentials.

1 INTRODUCTION

Because of their chemical inertness, chlorofluorocarbons (CFCs) remain in the troposphere for long time periods contributing to the warming of the atmosphere and, after photodissociation in the stratosphere, affect the ozone budget (IPCC, 1990; WMO, 1992). Since the international agreements (Montreal Protocol, 1987 and London Amendment, 1990) have established the phase-out for CFCs, alternative chemicals and technologies are being developed by industries to meet the future needs in refrigeration, foam-blowing, insulation and electronic cleaning and drying processes. The partially halogenated

hydrochlorofluorocarbons (HCFCs) and hydrofluorocarbons (HFCs) were found to have the same physical properties as CFCs and to be environmentally more acceptable compounds. They contain at least one hydrogen atom which lead them to react with hydroxyl radicals in the troposphere, resulting in shorter lifetimes than those of CFCs and consequently lower Ozone Depletion Potential. But these compounds also absorb infrared radiation in the atmospheric window, so that their effectiveness as greenhouse gases must be assessed and compared with that of the CFCs.

Infrared absorption cross sections have been measured, as a function of the temperature, for the 10 alternative compounds given in Table 1.

Table 1. Hydrohalocarbons used as substitutes for CFCs

Hydrohalocarbon	Chemical formula
HCFC-22	CHClF_2
HCFC-123	CHCl_2CF_3
HCFC-124	$\text{CHClF}_2\text{CF}_3$
HCFC-141b	$\text{CH}_3\text{CCl}_2\text{F}$
HCFC-142b	CH_3CClF_2
HCFC-225ca	$\text{CHCl}_2\text{CF}_2\text{CF}_3$
HCFC-225cb	$\text{CClF}_2\text{CF}_2\text{CHClF}$
HFC-125	CHF_2CF_3
HFC-134a	CFH_2CF_3
HFC-152a	CH_3CHF_2

2 EXPERIMENTAL

The spectra have been recorded in the infrared atmospheric window, between 600 and 1500 cm^{-1} , using a Bruker IFS 120HR Fourier Transform Spectrometer. With an apodized resolution of 0.03 cm^{-1} , a hundred scans were necessary to obtain a good signal to noise ratio; the baseline noise does not exceed 0.01 in absorbance units.

The HCFCs and HFCs were supplied by Solvay S.A (Belgium), E.I Du Pont de Nemours (USA) and Asahi Glass Company (Japan). The gas to be studied is introduced in a 5 cm long thermostatic cell closed by two pairs of KBr windows (Hurtmans *et al*, 1992). The cell, stabilized in temperature by a cooled liquid circulating in a double wall, is placed inside the sample chamber of the spectrometer which is then evacuated in order to eliminate infrared absorption interferences from ambient CO_2 and H_2O . Pressure and temperature of the gas are measured inside the cell using respectively an absolute MKS Baratron capacitance gauge and a transducer.

For each gas eighteen spectra have been recorded at six different pressures, ranging from 1 to 4 torrs, and three different temperatures (287K, 270K, 253K).

3 CROSS SECTIONS

According to the Beer-Lambert law, the transmission of radiation through a homogeneous gas sample is described by the relation

$$I(\nu) = I_o(\nu) \exp(-\sigma(\nu)nl) \quad (1)$$

where I and I_o are the intensities of the incident and transmitted radiation at wavenumber ν , n is the concentration of the gas (molec/cm^3) and l is the optical path (cm). σ is the absorption cross section (cm^2/molec) and can be written

$$\sigma(\nu) = \frac{1}{nl} \ln \frac{I_o}{I}(\nu) \quad (2)$$

Cross sections were determined for each spectral data point, 0.0085 cm^{-1} apart, between 600 and 1500 cm^{-1} . In order to increase the accuracy, a linear least square fit was done for each point using all six pressures. For each of the three temperatures, the cross sections are obtained by this procedure. Exemples of the cross sections results can be seen in figures 1 and 2. According to the experimental

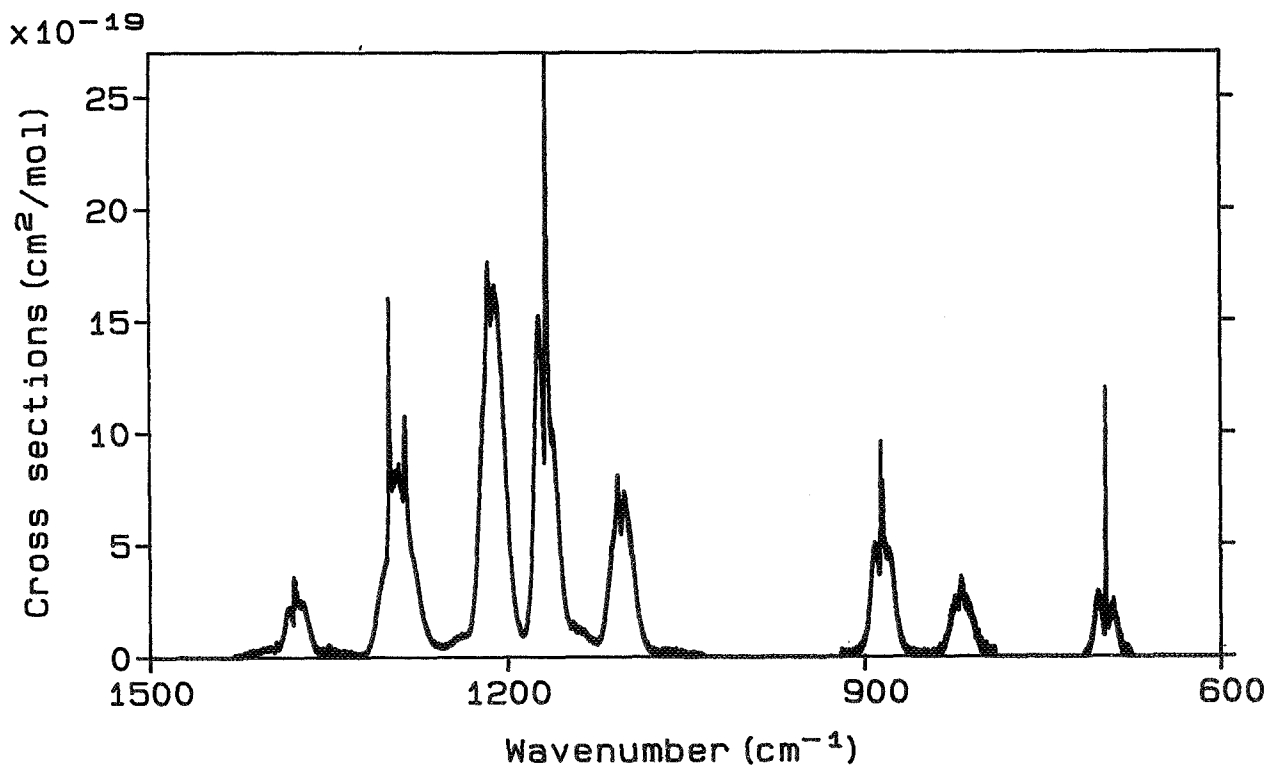


figure 1 : Cross sections ($\text{cm}^2/\text{molec.}$) in the atmospheric window (600 - 1500 cm^{-1}) for HCFC-124 (CHClFCF_3) at 287K

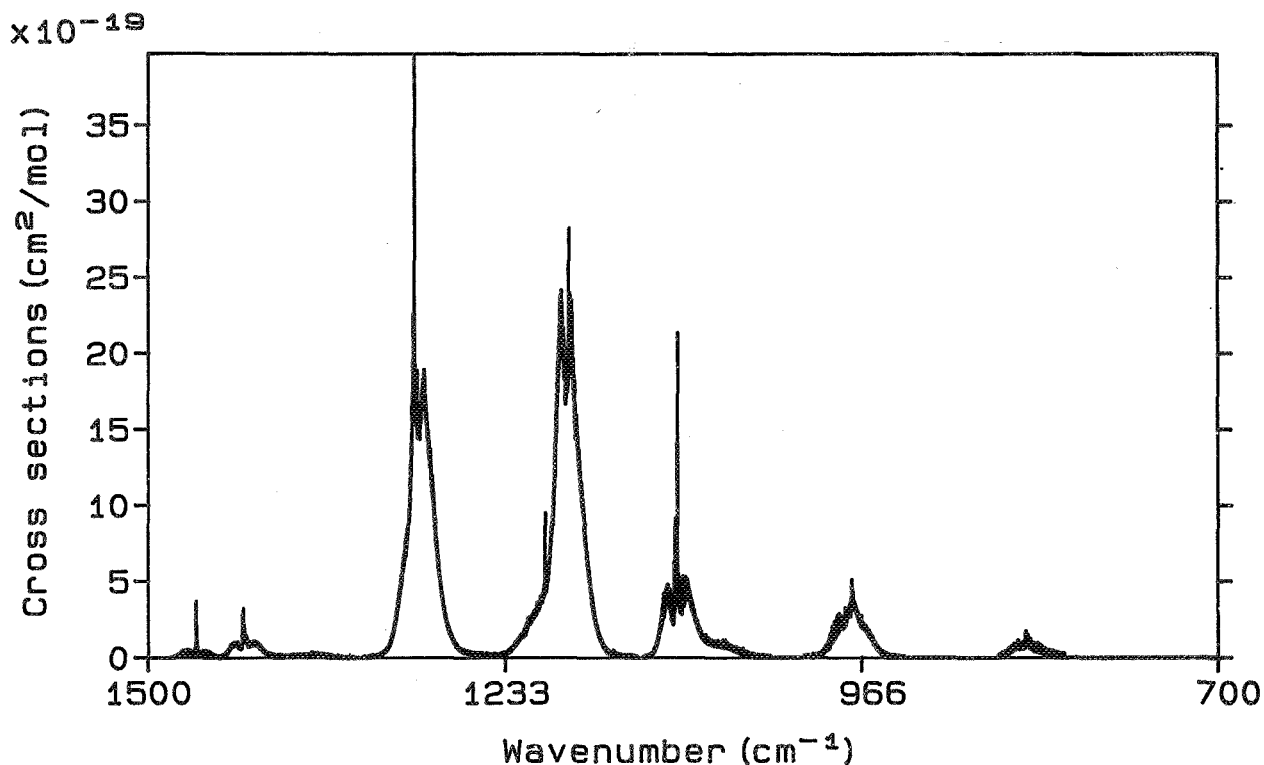


figure 2 : Cross sections ($\text{cm}^2/\text{molec.}$) in the atmospheric window ($600 - 1500 \text{ cm}^{-1}$) for HFC-134a (CFH_2CF_3) at 253K

conditions and the purity of the gas, cross sections are determined with an accuracy of 2% for the strong spectral features and 4% for the weak spectral features.

Table 2. Integrated cross sections ($\text{cm}/\text{molec.} \times 10^{17}$) between 600 and 1500 cm^{-1} for HCFCs and HFCs.

4 INTEGRATED BAND STRENGTHS

Integrated band strengths have been calculated using the formula :

$$\sigma_{int} = \int_{\nu_1}^{\nu_2} \sigma(\nu) d\nu = \sum_{\nu_1}^{\nu_2} \sigma(\nu) \Delta\nu \quad (3)$$

The integration limits ν_1 and ν_2 were chosen in order to cover the main absorption features (each integration region may contain several vibrational bands). To obtain the results presented in Table 2, the integrated cross sections calculated for each region were added to obtain a global estimation for the entire atmospheric window. These results are given with an accuracy of 5%.

Molecule	Integrated cross sections		
	<u>T = 287K</u>	<u>T = 270K</u>	<u>T = 253K</u>
HCFC-22	10.26	10.16	9.98
HCFC-123	12.88	12.56	12.17
HCFC-124	14.43	-	-
HCFC-141b	7.75	7.29	6.83
HCFC-142b	11.13	10.95	10.83
HCFC-225ca	17.71	17.64	17.49
HCFC-225cb	15.58	16.45	16.51
HFC-125	16.11	-	-
HFC-134a	12.61	12.67	12.67
HFC-152a	6.88	7.02	7.07

Acknowledgments. This work has been supported by the Belgian State- Prime Minister's Service- Science Policy Office (*Global Change* and *Eurotrac/Topas* programs).

REFERENCES

- Hurtmans, D., R. Petrisse, D. Lemaître, C. Clerbaux, and J. Vander Auwera, 1992: A thermostatic absorption cell for high accuracy measurement of absolute intensities, *EPA Newsletter* 44, 40-42.
- IPCC, Climate change - The IPCC Scientific Assessment, 1990, Chap.2, Report prepared for the WMO and UNEP Intergovernmental Panel on Climate Change, by working group 1, J.T. Houghton, G.J. Jenkins, and J.J. Ephraums eds., Cambridge Univ. Press, New York, NY.
- WMO, World Meteorological Organization, 1992: Scientific Assessment of Ozone Depletion: 1991, *Global Ozone Research and Monitoring Project*, Report n° 25, Geneva, Switzerland.

303913

**DISTRIBUTION OF OZONE BETWEEN 60 DEGREES NORTH
AND 60 DEGREES SOUTH**

E. Mravlag and M.W.J. Scourfield

Space Physics Research Institute
University of Natal
Durban, South Africa

ABSTRACT

The distribution of total column ozone is investigated, using data from the TOMS (Total Ozone Mapping Spectrometer) experiment aboard the US Nimbus 7 satellite. The region of interest extends from 60° North to 60° South, encircling the earth. Data for several years have been used in order to assess the long-term variations in the distribution of total column ozone. First results are presented on the seasonal variability of total column ozone in each hemisphere. The effects of the seasons are strongest at the highest latitudes but can still be discerned at the equator. While the variations are similar in the two hemispheres, ozone levels in the north are larger than in the south. Strong similarities are also found in the drift patterns of total column ozone in the two hemispheres. These drift patterns are compared to meteorological phenomena. We find an almost stationary ozone distribution for low latitudes at all seasons. At middle latitudes the ozone distribution drifts eastward in both hemispheres and this drift shows a seasonal variation. At very high latitudes (70° and higher) during spring in the southern hemisphere the ozone distribution is once again almost stationary, indicating that these regions are inside the polar vortex.

1. INTRODUCTION

Since 1978 the TOMS instrument onboard the US Nimbus 7 satellite has been measuring daily values of total column ozone. In this paper, we report on the variation of total column ozone in 1985 and 1986, at low and middle latitudes in both hemispheres.

TOMS provides a daily value of total column ozone for each of the global grid points, which are separated by 1° in latitude and by 1.25° in longitude. Note that this implies a time difference

between neighbouring data points of 24 hours at worst.

The ozone distribution for both hemispheres in September 1985 is shown in Figure 1, in the form of Hovmoeller plots. Figure 1(a) shows the summer pattern in the northern hemisphere and Figure 1(b) the winter pattern in the southern hemisphere. Each large square represents one month's worth of data averaged over a 15° latitude strip extending around the earth. The day of the month increases downward on the ordinate. Blocks inside each large square represent total column ozone for one day, averaged over 15° of latitude and 10° of longitude. Four large squares are shown for each hemisphere, numbered 1 to 4, indicating average ozone values for the latitude strips 0° to 15°, 15° to 30°, 30° to 45° and 45° to 60°, respectively.

2. OBSERVATIONS

Plots similar to Figure 1 have been produced, for all months in 1985 and 1986, for both hemispheres. Both years show very similar behaviour. From these plots the following conclusions have been made.

The ozone values in the northern hemisphere are always higher than in the southern hemisphere. The values of total column ozone increase with increasing latitude. The values of ozone appear to be higher in the winter hemisphere than in the summer hemisphere.

In order to determine the zonal bulk drift speed local maxima of ozone were traced. From plots similar to Figure 1 the average bulk drift speed could then be deduced.

Figure 2 shows, for 1985 and 1986, the calculated monthly bulk drift speeds (m s^{-1}) in the four latitude zones for both hemispheres. Eastward drift is shown as positive. Both hemispheres show a rather similar behaviour of the drift

Zonal Drift of Ozone

(1985 and 1986)

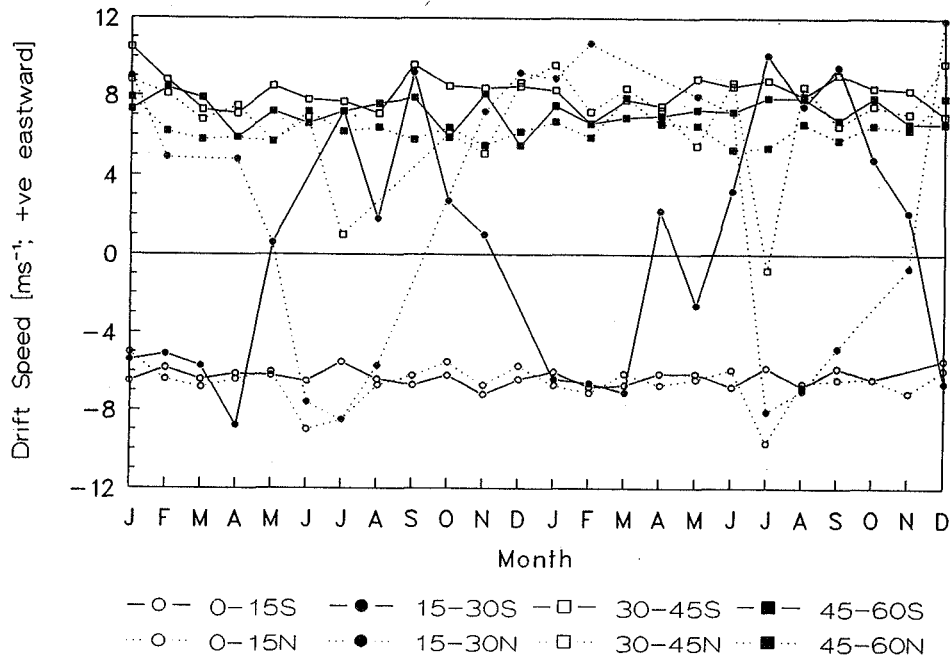


Figure 2. Calculated zonal bulk drift speeds of ozone averaged for each month, for both hemispheres, for the years 1985 and 1986. The key indicates measurements for the four latitude zones in each hemisphere.

speed, but the two hemispheres are out of phase by half a year.

There is a considerable eastward drift at higher latitudes, particularly during the winter months, of the order of 7 to 10 m s^{-1} . This speed tends to be slightly larger in the southern hemisphere than in the northern hemisphere.

The zone of lowest latitudes shows a clear drift, of the order of 6 m s^{-1} . The intermediate zone (15° to 30°) shows a transition from eastward drift in winter to westward drift in summer. It appears that the year is divided equally into four quadrants, two of which correspond to the transitions and one each to a summer and winter pattern.

3. DISCUSSION

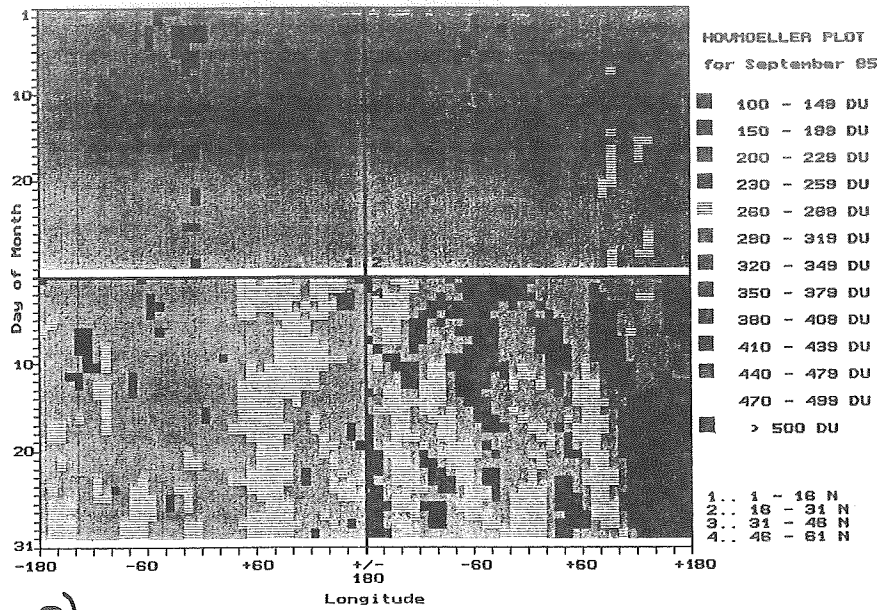
In Figure 1 it is obvious that the annual distribution of total column ozone is, as anticipated, linked to the seasonal change from winter to summer and vice versa. During winter the total column ozone builds up in the polar regions, probably due to the polar vortex

which forms in the winter hemisphere.

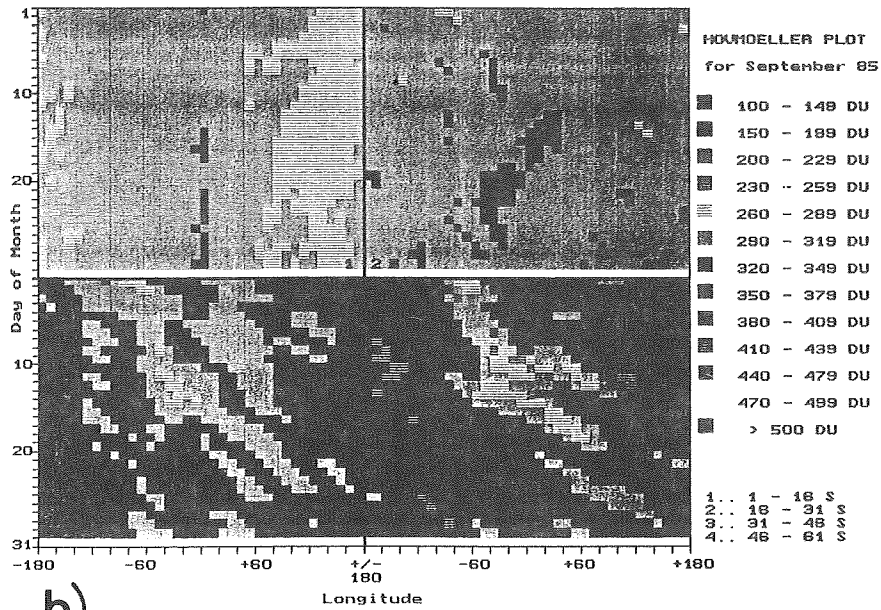
It is also clear that the drift patterns in the winter hemisphere appear to be stronger and more coherent than in the summer hemisphere. From Figure 2 we see, however, that the main change occurs in the middle region between 15° and 30° in latitude. While the higher and the lower latitudes do not change very much, this region suffers a reversal of its drift pattern. This reversal leads to the more pronounced drift patterns in the winter hemisphere (Figure 1). Due to the eastward flow in the intermediate zone during the winter months the eastward bulk drift of ozone is more noticeable in these months.

This is qualitatively consistent with expectations from statistical data (Murgatroyd, 1969; Randel, 1992) and also from modelling (Geller, 1983). In the lower stratosphere, bulk eastward drift in both hemispheres at higher latitudes is expected. In the winter hemisphere this drift extends down to a latitude of about 10°.

In the equatorial zone a westward



a)



b)

Figure 1. Global distribution of total column ozone in both hemispheres for September 1985. In this figure the northern hemisphere (a) shows the summer pattern and the southern hemisphere (b) shows the winter pattern.

drift prevails at all times, which in the summer hemisphere extends to about 25° in latitude. Hence a reversal of the drift for the zone between 15° and 30° is to be expected.

While the direction of the observed bulk ozone drift agrees with the measured and predicted wind speeds, this is not quite the case for the magnitude of the drift speed. Obviously, more work needs to be done before a good understanding of these dynamic phenomena can be achieved.

ACKNOWLEDGEMENTS

The financial assistance of the Foundation for Research and Development and the Department of Environment Affairs is gratefully acknowledged.

The raw data were provided by R.D. McPeters and A.J. Krueger of NASA GSFC and the National Space Science Data Centre/World Data Centre-A for Rockets and Satellites. Their contribution is gratefully acknowledged.

REFERENCES

- Geller, M.A., 1983: Dynamics of the Middle Atmosphere. Space Science Rev., 34, 359.
- Murgatroyd, R.J., 1969: The Global Circulation of the Atmosphere, G.A. Corby, Edt., Roy. Met. Soc..
- Randel, W.J., 1992: Global Atmospheric Circulation Statistics, NCAR Technical Note NCAR/TN-366+STR, National Center for Atmospheric Research, Boulder CO 80307-3000.

3039/4

OZONE MAXIMA OVER SOUTHERN AFRICA : A MID-LATITUDE LINK

Jane Barsby and Roseanne D. Diab

Department of Geographical and Environmental Sciences
University of Natal, King George V Ave, Durban, 4001, South Africa

ABSTRACT

The relationship between patterns of total ozone and day-to-day weather was explored over South Africa for the period 1987 to 1988. Generally, there was a fairly poor relationship (variance less than 20%) between total ozone and the heights of the 100, 300 and 500 hPa geopotential heights at 5 South African stations. However, over a shorter period, October to December 1988, fluctuations in the height of the 300 hPa surface accounted for 53% of the variance in total ozone at Cape Town. High ozone amounts are associated with the lowering of the 300 hPa surface in the presence of an upper-air trough. The role of the mid-latitude westerly waves in this respect is discussed.

1. INTRODUCTION

Dobson et al (1929) were the first to notice the relationship between day-to-day variations in total ozone and surface weather. They found that maximum positive deviations of daily ozone values from monthly means (high ozone values) generally occur to the rear of surface low-pressure systems (west of cyclonic centres), while maximum negative deviations (low ozone values) are found to the rear of surface highs or within anticyclones. Later, Reed (1950) was responsible for describing the relationship between total ozone and weather in more detail. He put forward a model for the Northern Hemisphere in which he attributed the relationship to the effects of horizontal advection and/or vertical motion. More recently, Danielsen (1968), Danielsen and Mohnen (1977), Reiter (1975), Shapiro (1980), Singh et al (1980) and Wakamatsu et al (1989) have studied the dynamics of the tropopause and the injection of stratospheric air into the troposphere in association with upper level-troughs.

Stemming from these findings, it is expected that similar relationships will be found for Southern African data and that the observed variations in total ozone may be explained by the passage of mid-latitude weather systems.

2. DATA

The following data have been utilised in this study:

2.1 TOMS data

Version 6 TOMS data for the period January 1987 to December 1988 for 5 South African stations, namely Cape Town (33° 56'S 18° 28'E), Port Elizabeth (33° 58'S 25° 36'E), Durban (29° 53'S 31'E), Bloemfontein (29° 7'S 26° 14'E) and Pretoria (25° 45'S 28° 12'E); and gridded TOMS data, for the same period for an

area bounded by longitudes 10°W and 50°E and latitudes 0°S and 50°S. The grid spacing used was 5°.

2.2 Meteorological data

Geopotential heights (gpm) of the 500, 300, and 100 hPa surfaces were obtained from radiosonde data for 1987 and 1988 for the 5 stations mentioned above. Gridded ECMWF upper-air data were obtained for 1987 and 1988 for an area bounded by longitudes 10°W and 50°E and latitudes 0°S and 50°S. The grid spacing selected was 5°.

3. RESULTS AND DISCUSSION

The relationship between TOMS total ozone and mid-to upper-tropospheric weather was investigated at 5 South African stations for a two year period, 1987 to 1988. Statistical analysis using simple linear least squares regression and making no allowance for serial autocorrelation in the time series revealed that a negative relationship exists between total ozone and the heights of the 100, 300 and 500 hPa geopotential heights at 5 South African stations. The results are summarised in Table 1.

The relationships are generally poor, with a maximum of 20% of the variance in total ozone explained by the variations in the height of the 300 hPa surface at Cape Town. However, a far better relationship was observed between total ozone and the 300 and 500 hPa geopotential heights for all 5 stations investigated over a shorter period between October to December 1988 (Table 2). The fluctuations in the height of the 300 hPa surface were found to account for between 53% at Cape Town, and 35% at Pretoria, of the variance in total ozone with correlation coefficients ranging between -0.73 to -0.59 respectively.

It appears then, that the lowering of the pressure surfaces is associated with high ozone amounts and that this relationship is strongest for more southerly located stations. This observation may be a function of the time of year for which the analysis has been performed. For instance, the patterns observed may be a reflection of the southward migration of the westerlies between August and December over South Africa. The more northerly located stations of Pretoria (26°S) and Bloemfontein (29°S) will experience the influence of the mid-latitude westerly waves to a lesser degree than the more southerly stations, which exhibit relatively larger r^2 values, and consequently undergo correspondingly smaller day-to-day fluctuations. At the onset of spring, the Inter Tropical Convergence Zone (ITCZ) begins to move southwards and as a result South Africa comes under the influence of air of tropical origin. During this warm season, total ozone values are relatively

STATION	Correlation between TOMS & 100hPa	r ² 100hPa	Correlation between TOMS & 300hPa	r ² 300hPa	Correlation between TOMS & 500hPa	r ² 500hPa
CAPE TOWN	-0.26	6.93	-0.45	20.34	-0.37	14.44
PORT ELIZABETH	-0.21	4.54	-0.37	13.91	-0.31	9.37
DURBAN	-0.15	2.46	-0.25	6.21	-0.20	4.13
BLOEMFONTEIN	-0.16	2.45	-0.28	7.82	-0.21	4.54
PRETORIA	-0.12	1.33	-0.15	2.36	-0.10	1.00

significant at 95% confidence level
r² = percent variance

Relationship between daily TOMS total ozone and the 100, 300 and 500 hPa geopotential heights for 5 South African stations, 1987-1988.

STATION	Correlation between TOMS & 300hPa	r ² 300hPa	Correlation between TOMS & 500hPa	r ² 500hPa
CAPE TOWN	- 0.73	52.97	-0.63	39.45
PORT ELIZABETH	-0.64	41.20	-0.57	32.17
DURBAN	-0.63	39.32	-0.51	26.07
BLOEMFONTEIN	-0.63	39.14	-0.51	25.60
PRETORIA	-0.59	34.59	-0.46	23.11

significant at 95% confidence level
r² = percent variance

Table 2 Relationship between daily TOMS total ozone and the 300 and 500 hPa geopotential heights for 5 South African stations, October to December 1988.

lower throughout the country, and less variability is observed due to the reduced frequency of the transient waves of the mid-latitudes.

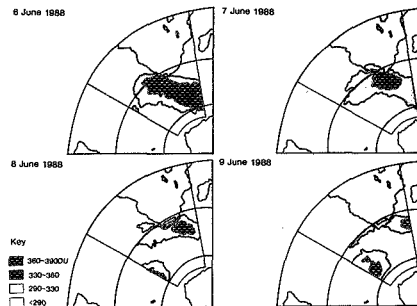


Fig. 1 The distribution of TOMS total ozone (DU) over South Africa, 6-9 June 1988. Illustration compiled by Space Physics Research Institute, University of Natal, Durban, from TOMS data supplied by the NSSDC, U.S.A.

The variability in total ozone associated with the passage of the mid-latitude westerly waves is illustrated in Figure 1, which shows ozone concentrations for four days commencing on 6 June 1988. The west to east movement of an ozone front across South Africa is clearly visible.

The occurrence of ozone maxima was explored in greater detail using gridded data over the entire country for 1987 and 1988. For each day, statistical analysis of the relationship between total ozone and the heights of the 100, 300 and 500 hPa surfaces using simple linear least squares regression and making no allowance for spatial autocorrelation in the time series was undertaken. A strong significant (at the 95% confidence level) negative correlation was evident (Fig. 2).

This analysis revealed that on the majority of the days (approximately 600 days) out of the two year period, between 50% and 95% of the spatial variance in total ozone is explained by the variation in the height of the 100, 300 and 500 hPa surfaces. Again, the relationship was strongest for the 300 hPa surface.

The occurrence of high ozone amounts in association with the lowering of the 300 hPa surface due to the presence of an upper-air trough is clearly depicted in the contour maps for 3 October 1987 (Fig. 3). On 3 October 1987, the synoptic chart (Fig. 3a) depicts a surface cold front moving eastward towards Madagascar and a surface high pressure system ridging in behind the cold front. A further surface cold front is evident to the south-west of

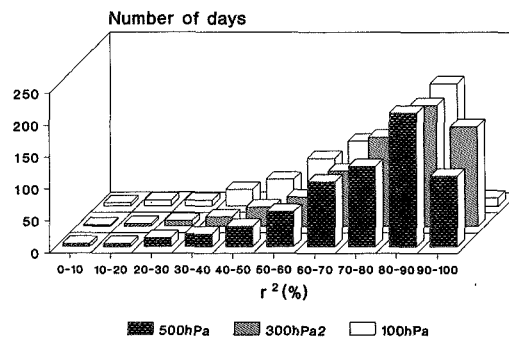


Fig. 2 Relationship between gridded total ozone (TOMS) and the 100, 300 and 500 hPa geopotential heights (ECMWF) over South Africa expressed as r^2 values, January 1987 - December 1988.

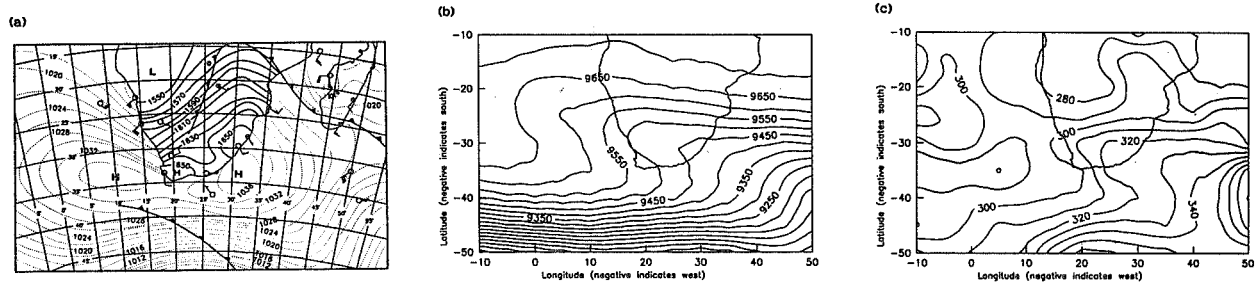


Fig. 3 3 October 1987

a) Surface synoptic chart. Surface pressure expressed as isobars (hPa) over the sea and heights of the 850 hPa (gpm) over the land. Source: SAWB. b) Heights of the 300 hPa surface (gpm). Prepared from the ECMWF data. Source: SAWB. c) Distribution of TOMS total ozone (DU) gridded data. Source: DC, U.S.A.

Cape Town. The upper-air trough at 300 hPa, associated with the first cold front, appears to the rear of the surface front and is aligned west-northwest/east-southeast across the country (Fig. 3b). Total ozone values (Fig. 3c) show a maximum in the vicinity of the well developed 300 hPa trough extending over South Africa with values increasing in a south-easterly direction in association with the lowering of the 300 hPa surface in this region.

5. SUMMARY

Ozone maxima have been related to mid- to upper-tropospheric daily weather patterns over South Africa. It has been shown that an inverse relationship exists between TOMS total ozone and the heights of the 100, 300 and 500 hPa geopotential heights. Although the relationship is poor at individual stations for the two year period between 1987 and 1988, it improves significantly for the three month period between October to December 1988. The relationship appears to be strongest for more southerly located stations such as Cape Town and Port Elizabeth. This may be explained by the extent of the area influenced by the mid-latitude westerly waves.

A strong negative correlation between gridded total ozone data and the heights of the 100, 300 and 500 hPa surfaces was found to exist for an area covering the entire country. Strong evidence was found to support the idea that daily weather patterns play a significant role in influencing total ozone levels in the southern hemisphere mid-latitudes. The fluctuations in the heights of the 100, 300 and 500 hPa surfaces were found to account for between 50% and 95% of the variance in total ozone, for the majority of days investigated in the two year period.

It is suggested, that the origin of ozone maxima over Southern Africa is largely due to dynamics of the atmosphere and that on days showing a weak relationship between total ozone and daily weather, ozone maxima may be explained by mechanisms other than forcing by mid-latitude westerly waves.

6. ACKNOWLEDGEMENTS

The South African Weather Bureau and the European Centre for Medium-range Weather Forecasts for the meteorological data and members of the TOMS Nimbus

Experiment and Ozone Processing Teams, Dr. D. Chesters, the video producer, Dr. A.J. Krueger, the Sensor Scientist, and the National Space Science Data Center.

7. REFERENCES

- Danielsen, E.F. (1968) Stratospheric-tropospheric exchange based on radioactivity, ozone and potential vorticity. *J. Atmospheric Sciences*, 25, 502-518.
- Danielsen, E.F. and Mohnen, V.A. (1977) Project Duststorm report: ozone transport, in situ measurements, and meteorological analyses of tropopause folding. *J. Geophysical Research*, 82, (37), 5867-5877.
- Dobson, G.M.B., Harrison, D.N. and Lawrence, J. (1929) Measurements of the amount of ozone in the earth's atmosphere and in relation to other geophysical conditions. *Proceedings of Royal Meteorological Society of London* 122, 456-486.
- Reed, R.J. (1950) The role of vertical motions in ozone-weather relationships. *J. Meteorology*, 7, 263-267.
- Reiter, E.R. (1975) Stratospheric-tropospheric exchange processes. *Reviews Geophysics and Space Physics*, 13 (4), 459-474.
- Shapiro, M.A. (1980) Turbulent mixing within tropopause folds as a mechanism for the exchange of chemical constituents between the stratosphere and troposphere. *J. Atmospheric Sciences*, 37, 994-1004.
- Singh, H.B., Viezee, W., Johnson, W.B. and Ludwig, F.L. (1980) The impact of stratospheric ozone on tropospheric air quality. *J. Air Pollution Control Association*, 30 (9), 1009-1017.
- Wakamatsu, S., Uno, I. Veda, H. Vehara, K. and Tateishi, H. (1989) Observational study of stratospheric ozone intrusions into the lower troposphere. *Atmospheric Environment*, 23 (8), 1815-1826.

303915

**EFFICIENT OZONE GENERATOR FOR OZONE LAYER
ENRICHMENT FROM HIGH ALTITUDE BALLOON.**

*Igor V. Filiouguine, Sergey V. Kostiouchenko,
Nikolay N. Koudriavtsev, Svetlana M. Starikovskaya.*

Moscow Institute of Physics and Technology,
Moscow Region, Dolgoprudny, MIPT, 141700, Russia.

ABSTRACT

The possibilities of ozone production at low gas pressures by nanosecond high voltage discharge has been investigated. The measurements of ozone synthesis in N_2-O_2 mixtures have been performed. The explanation of experimental results is suggested. The possible ways of ozone yield growth are analyzed.

1. INTRODUCTION

An enrichment of ozone layer hole by generators placed on the high altitude balloon is one of possible way of its efficient restoration. The ozone generators planned to utilize for these purposes should be adjusted according to the following demands: 1. They should efficiency operate at low pressure corresponding to one's in ozone layer (10-30 Torr); 2. They should produce ozone in natural concentration which is not more than 10^{13} cm^{-3} . The production of ozone in much more concentration is unless because its efficiency destruction by UV light. 3. Disturbances of gas parameters must be insufficient. 4. The production of impurities, efficiently destroying ozone layer such as NO, etc. must be seriously restricted.

The efficiency of planned ozone generator must be extremely high. The ozone generators utilizing MW-discharge, corona discharge (impulse and stationary) efficiency operate at gas pressure about 100 Torr and more. A serious restriction of utilizing these types of ozone generators for ozone layer enrichment is in nitrogen oxides production in the significant concentrations.

Also it should be mentioned that only laboratory simulation of ozone kinetics at conditions corresponding to that of in ozone layer are now available because of the difficulties of its reproducing at above means of gas

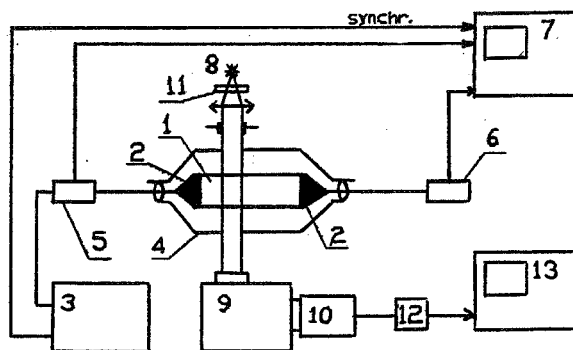
excitation. So the problem of experimental modeling of the ozone layer chemistry at natural conditions is also of great importance.

A breakdown of gas in the form of the sub-light velocity breakdown ionization wave (BIW) propagating through the gas with 10^8-10^9 cm/s velocities (Asinovsky et al., 1983; Loeb, 1965) has some attractive properties permitting to use its afterglow for effective ozone generating. An important property of the BIW which is due to the high reduced electrical field strength in the BIW front ($E/N \geq 100 \text{ Td}$) is an effective electronics and vibrational degrees of freedom excitation of the particles with negligible heating of the gas. So, strongly nonequilibrated, cold plasma with excellent spatial uniformity may be produced in the discharge at wide pressure range (0,1-100 Torr). This feature of the BIWs permit to use them both for production of ozone at low gas pressure and for ozone layer kinetics modeling in wide range of plasma parameters variation corresponding to possible natural conditions in ozone layer of the Earth atmosphere.

In the present study we have investigated possibilities of using electric discharge in the special form of breakdown ionization wave for efficient ozone production from high-altitude balloons and for laboratory simulation of ozone layer chemistry. The ozone synthesis have been performed in BIW's afterglow in O_2-N_2 mixtures in pressure range of 5-40 Torr and reveals the high efficiency of ozone production and so possibilities of practical utilizing this type of generator for ozone layer enrichment from high altitude balloon.

2. EXPERIMENTAL FACILITIES

The experimental setup layout is shown in Fig.1. A quartz discharge tube (1) of 20 cm length and 4,65 cm inner diameter with the plate stainless steel



- 1- quartz discharge tube;
- 2- electrodes;
- 3- nanosecond voltage generator;
- 4- metallic screen;
- 5,6- current shunts;
- 7- oscilloscope;
- 8- UV-lamp; 9- monochromator;
- 10- photomultiplier;
- 11- bandpass filter;
- 12- low frequency electrical filter;
- 13- memory oscilloscope.

Fig.1. The layout of experimental setup.

electrodes at the ends (2) is inserted into the gap of the central wire of the coaxial electrical cable connected with nanosecond voltage generator (3). The coaxial metallic screen (4) surrounding the tube is connected to the screen. The impedance of such system in assumption that the gas gap has an ideal conductivity is equal to the coaxial cable one's ($Z=50 \text{ Ohm}$). Positive and negative polarity voltage pulses with $U=15-20 \text{ kV}$ altitude, 25 ns duration, 8 ns rise time and $f=20-90 \text{ Hz}$ repetition frequency have been used to initialize the BIW developing. The temporal behavior of the supplied to and reflected from the discharge tube electric pulses is monitored with the aid of the calibrated current shunt mounted on the outer shielding conductor of power cable before (5) and after (6) the tube. The signals from the gauges are registered by oscilloscope (7) with 1 GHz transmittance band.

The ozone concentration is measured with accuracy the order of the 10% by using absorption technique at spectral region $250 \pm 5 \text{ nm}$ corresponding to the intensive Hartley's band of O_3 . The radiation of the highly stable UV-lamp (8) passes across the discharge tube perpendicularly to its axis, than selected by monochromator (9) and registered by photomultiplier (10). To avoid the ozone formation as a result of photochemical processes in the ambient air the bandpass filter (11) with $\lambda=250 \pm 9 \text{ nm}$ is used. To prevent the high frequency interferences noise in the electric

circuit the pulse signals from the multiplier are transmitted through low frequency electrical filter (12). This restricts resolution time of the scheme by value of 2 s acceptable for our work. The resulting signal is than recorded by memory oscilloscope (13).

3. EXPERIMENTAL RESULTS

The typical oscillograms of the ozone concentration with time of repetitive discharge operation are represented in Fig.2A-D. The temporal dependence of the ozone formation on the gas pressure has two peculiarities for all investigated gas mixtures. Namely, at gas pressures $P=20-25 \text{ Torr}$ the ozone concentration increases with time while nanosecond generator is turned on up to some value and than remain constant till generator is turned off (Fig.2A). At more high pressure $P \geq 25-30 \text{ Torr}$ ozone concentration has maximum and then slowly drops to the quasistationary value during some tens of seconds (see Fig.2B).

Fig.2C-D represent behavior of ozone concentration after nanosecond generator is turned off. Ozone concentration in O_2-N_2 mixtures decreases to zero (Fig.2C). In technical pure oxygen decreases to some constant value and then drops very slowly to zero (see Fig.2D).

The values of the absolute ozone concentration vs gas pressure are represented for different gas mixtures in Fig.3. The maximal values of ozone

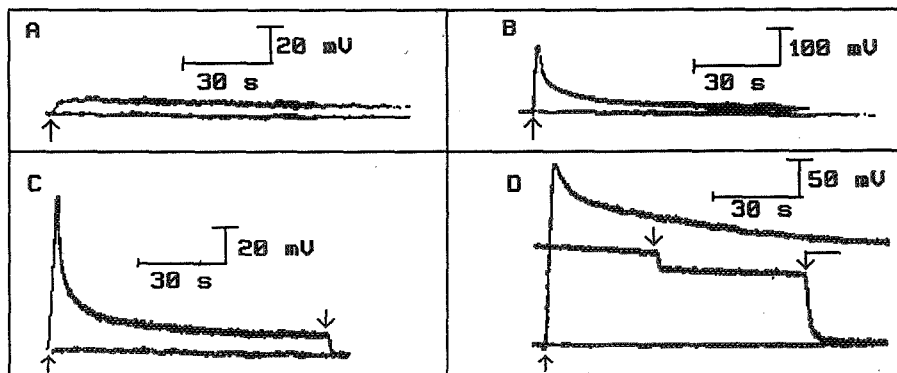


Fig.2. The typical oscillograms from the photomultiplier. Repetition frequency $f=42$ Hz, negative polarity. \uparrow - discharge turned on; \downarrow - discharge turned off; \downarrow - pumping of the discharge tube. (A): 16,2 Torr, 70,5% O_2 mixture; (B): 34,1 Torr, 70,5% O_2 mixture; (C): 30 Torr, 48% O_2 mixture; (D): 30 Torr, technical pure O_2 .

concentration $[O_3]_{\max}$ for all mixtures continuously increases with gas pressure (Fig.3A) to an excellent relative value $\xi=[O_3]/[O_2]=0,5\%$ at highest investigated pressure $P \approx 40$ Torr in technical pure oxygen.

The maximal stationary values of ozone concentration $[O_3]_{st}$ increase in technical pure oxygen both at 42 and 82 Hz repetition frequency. The maximal relative value $\xi=0,2\%$ is achieved at 37 Torr pressure. For all investigated O_2-N_2 mixtures the dependence of stationary ozone concentration upon the pressure has slightly revealed maximum at $P=20-25$ Torr (Fig.3B).

Stopping energy of the gas obtained from the measurements of applied to and reflected from discharge gap electric pulses (Asinovsky, 1983), as well as ozone production efficiency (stopping energy of the gas in one pulse related to O_3 molecules at stationary concentration) also have non monotonous dependence vs pressure, with maximum at pressures $P \approx 10-20$ Torr.

4. DISCUSSION

At the present conditions we may divide the processes in the gas to some stadium:

1. Electrical pulse propagating through the gas gap, production of ions, atoms and excited particles due to high electron density and temperature $T_e \gg T_g$.

Cooling of the electron gas, radiation of short life time excited particles ($t \leq 10^{-7}$ s);

2. Recombination of ions and atoms, quenching of some metastable particles ($t \leq 10^{-4}$ s);

3. Quenching of metastable particles, vibrational recombination, chemical reactions between neutral and excited particles ($t \geq 10^{-4}$ s).

When high voltage pulse propagates through the discharge tube, high reduced electrical field is realized. Under conditions of our experiments E/N is the order of the $30+100$ V/cm·Torr. Electron temperature and concentration could reach values about some electron-volts and $n_e \approx 10^{11}-10^{12}$ cm $^{-3}$ respectively. Under these conditions the intensive dissociation of oxygen and nitrogen take place. Produced atoms take part in chemical reactions of ozone appearance and destruction.

The main reaction of ozone production in discharge is



This reaction is well investigated. According to many of the research, the most of O_3 molecules, created in reaction (1), are vibrationally excited. It could change velocities of ozone destruction reactions.

Characteristic time of atoms O recombination in reaction (1) at pressure $P=30$ Torr and 97% O_2 mixture is

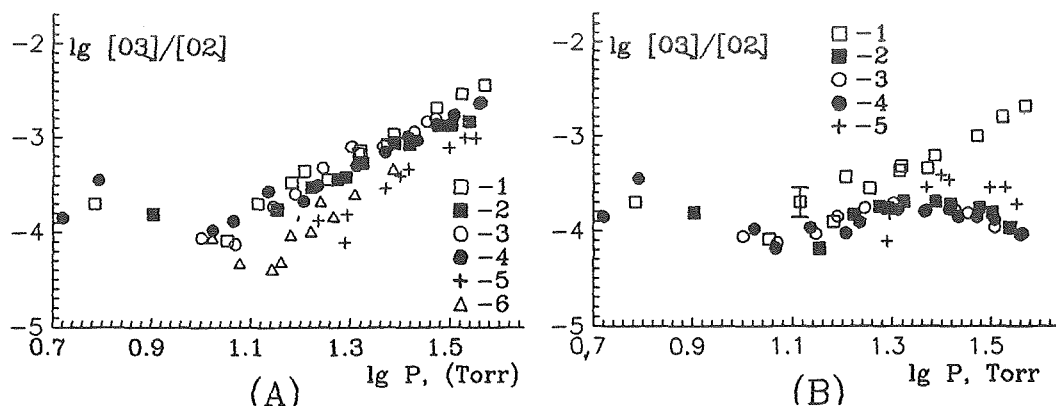
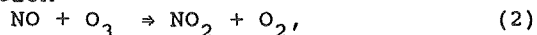


Fig.3. Ozone concentration for different mixtures as a function of gas pressure. (A)- maximal values; (B) - stationary values. 1- technical pure O_2 ; 2- 48% O_2 mixture; 3- 70,5% O_2 mixture; 4- 83,3% O_2 mixture; 5-air.

$\tau_0 \approx k_1 \cdot [O_2] \cdot P \approx 10^{-3} s$, where $k_1 = 7 \cdot 10^{-34} \text{ cm}^6 / s$ - the constant rate of reaction (1). So under our conditions $\tau_0 \ll 1/f$ is justly and velocity of ozone production, observed in experiments with improved time resolution, is limited by velocity of oxygen atoms creation in discharge.

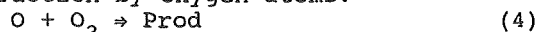
Ozone is mainly destroyed in the reaction



where NO molecules are produced in the reaction of nitrogen atoms with molecules of oxygen:



There are also reactions of ozone destruction by oxygen atoms:



Reaction of O_3 destruction by metastable oxygen $O(^1D)$ is not important in our conditions due to the rapid quenching of oxygen metastable atoms.

Estimation and computer modeling show that production of ozone in our system may be explained by molecular oxygen dissociation in discharge and than O-atoms conversion into ozone. Ozone destruction may be explained by slow accumulation of nitric oxides and its reactions with ozone.

Estimations also show that vibrational excitation of molecules and hydrogen impurities may influence on the ozone production. At low pressures ($P \approx 20$ Torr) diffusion of the O-atoms to the walls of discharge chamber may be

significant.

5. CONCLUSION

Represented experimental results indicate that at the gas pressure in ozone layer 10-30 Torr the discharge in the form of breakdown ionization wave generate efficiently ozone at near natural concentrations.

The efficiency of ozone production permits to enrich ozone layer using this ozone generator situated at high altitude balloons. The estimation show that the utilizing of the set-up, based on the discharge, with an output of 1 kW, allows to product $5 \cdot 10^{12} \text{ cm}^{-3}$ ozone concentration in $V = 35 \text{ m}^3$ volume for one second.

This type of discharge may also be used for the purposes of ozone kinetics laboratory investigation and modeling of ozone layer destroying.

REFERENCES

- Asinovsky E.I., Vasilyak L.M., Markovets V.V, 1983. Wave breakdown of gas gaps. Heat physics of high temperature, V.21, N2,3, 371-381; 577-590 (in Russian).
 Loeb L.B., 1965. Science, 148, 1417-1426.
 Asinovsky E.I, 1983. Experiments of low-attenuation relativistic waves of electrical breakdown. -Proc. XVI ICPIG, Dusseldorf, Invited papers, 224-231.

303916

ON OZONE CORRELATION WITH METEOFIELDS IN THE NORTHERN HEMISPHERE

Tatiana V.Kadygrova, Vitali E.Fioletov

Central Aerological Observatory,
Dolgoprudny, Moscow Region, Russia

with the temperature and geopotential height.

ABSTRACT

The correlation coefficients of temperature and geopotential heights at various levels with total ozone and its vertical distribution have been analyzed, using the ground based and ozone sounding data.

Two independent groups of factors affect total ozone. The first group - the geopotential values of the troposphere - stratosphere border (100-500 mb) manifest themselves most of all in the middle latitudes. Pertaining to this group is the total ozone correlation with the tropopause height and temperature at 500 mb. The correlation coefficients are negative (-0.55..-0.65) and little depend on the season. Related to this factor is a high (up to 0.8) correlation of ozone partial pressure with the temperature in the lower stratosphere.

The second group is the geopotential and temperature values at the 10-30 mb levels. The highest correlation coefficients (up to 0.6) are observed in winter in the subpolar latitudes. In summer they are substantially lower - about 0.1.

1. INTRODUCTION

Total ozone relation to the meteorological processes was discovered during the first years of ozone observations and has been investigated well enough by the present time. Total ozone is inversely correlated with the pressure pattern in the upper troposphere and lower stratosphere (e.g., Craig, 1965; Dutsch, 1969). Besides, total ozone variations are related to the processes occurring in stratospheric layers 15-35 km (e.g., Dobson, 1973). A quantitative estimation of various atmospheric processes' contribution to total ozone variability seems important.

One of the possible solutions is the estimation of ozone values correlation

2. DATA SETS

For the correlation analysis the total ozone daily mean values obtained at 100 Northern Hemisphere ground based ozonometric stations (Dobson and filter) for the period of 1973-1985 as well as ozone sounding data were used. The data are published by AES, Canada, and WMO. The daily data on temperature and geopotential height on 850, 700, 500, 300, 200, 100, 30 and 10 mb levels were used. Before the correlation's computation the initial data series were deseasonalized. Correlation coefficients were computed for four seasons.

3. TOTAL OZONE CORRELATION WITH THE TEMPERATURE AND GEOPOTENTIAL HEIGHT

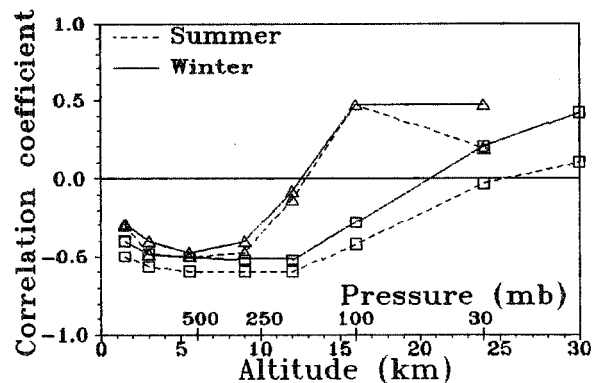


Fig. 1. Correlation coefficients between total ozone and temperature (Δ) and between total ozone and geopotential high (□) for Central Europe.

Figure 1 shows the altitudinal course of the correlation coefficient between total ozone and geopotential height, and between total ozone and temperature for

Central Europe. The largest in absolute value correlation is observed between total ozone and geopotential at 300 mb and between total ozone and temperature at 500 mb and 100 mb. In the polar and tropical latitudes the correlation coefficients altitudinal course remains the same, but the maximum correlation's altitude is somewhat changed.

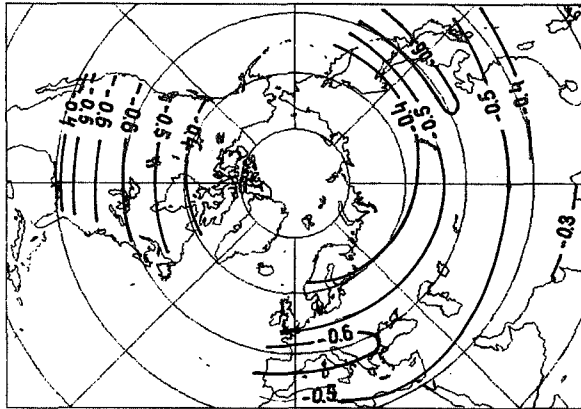


Fig. 2. Correlation coefficient of total ozone and 300 mb geopotential high for Winter.

Figure 2 shows the map of the correlation coefficients between total ozone and the 300 mb geopotential for winter. The maximum correlation (more than 0.6) is observed in the 40°-50°N zone, i.e., between the major jet streams in the region where both Arctic and Antarctic air masses can penetrate. Relatively high correlation of total ozone with temperature and geopotential in the troposphere is accounted for the troposphere - stratosphere border effect.

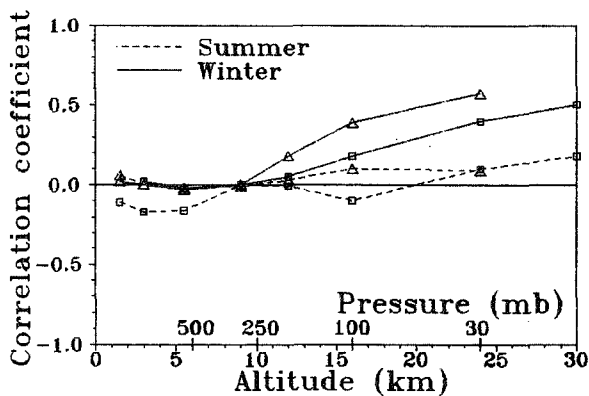


Fig. 3. Partial correlation coefficients (relative to ozone - 300 mb geopotential correlation) between total ozone and temperature (Δ) and between total ozone and geopotential (\square) for Central Europe.

The temperature at 100mb, 500mb; and 200mb and 300mb geopotential heights are closely related to each other. These factors make up the first group of factors affecting to total ozone.

For the examination of other factors affecting total ozone the partial correlation (relative to ozone - 300 mb geopotential correlation) between ozone

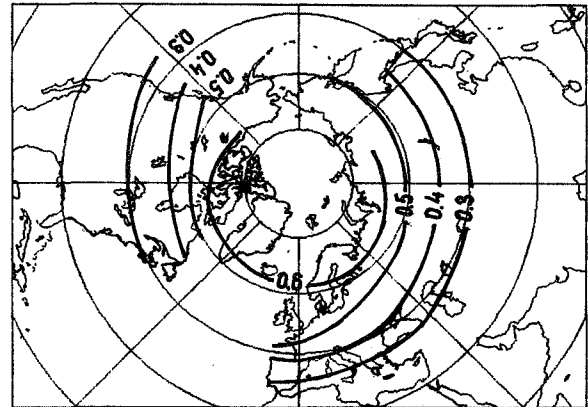


Fig.4. The partial correlation coefficient (relative to ozone - 300 mb geopotential correlation) of total ozone and 10 mb geopotential for Winter.

and meteoroparameters has been considered (Figure 3). The partial correlations' consideration makes the correlation between total ozone and meteoroparameters in the troposphere and lower stratosphere insignificant. Partial correlation with meteoroparameters at 30-10 mb levels remains high, and this suggests their independent origin. Maximum (up to 0.6) particular correlation is observed in winter between total ozone and the 10 mb geopotential. The map of their values is shown in Figure 4.

A monotonic growth of correlation coefficients towards the polar latitudes is observed. This correlation is probable to be accounted for the circumpolar vortex effect on total ozone. Its intensity variation and movement relative to the average long-term position cause geopotential and total ozone variations. Particularly variable in this respect is the circumpolar vortex, and the correlation coefficients are maximum in winter. The temperature variations at 30 mb are related to the geopotential variations at 10 mb (the correlation coefficient reaching 0.85 in winter) and the relation of total ozone to the temperature at 30 mb is probable to have the same reason. These factors make up the second group.

The value of the multiple correlation

between total ozone and geopotential at 300 and 10 mb goes up to 0.7-0.8. It means that these two parameters "account for" more than 50% of the observed total ozone variance. About 15%-25% of variance are accounted for the instrument error of total ozone measurements. Using the 200 mb geopotential and the temperature at 30 mb as predictors lead sometimes to an insignificant improvement.

The factors of the first group well manifest themselves in short time intervals of several days. The second group is characteristic of processes of longer duration.

5. CORRELATION WITH OZONE CONCENTRATION AT DIFFERENT LEVELS

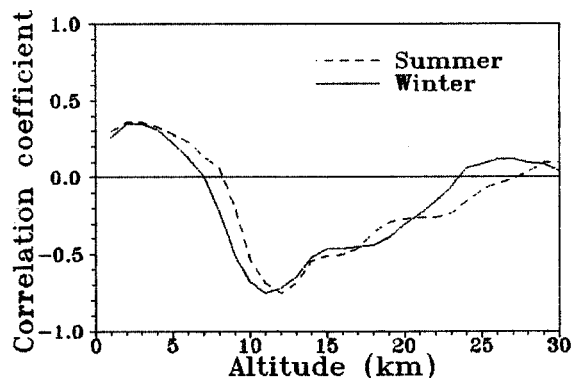


Fig. 5. Correlation coefficient between the temperature at the 6 km level (500mb) and ozone concentration at different altitudes for Hohenpeissenberg.

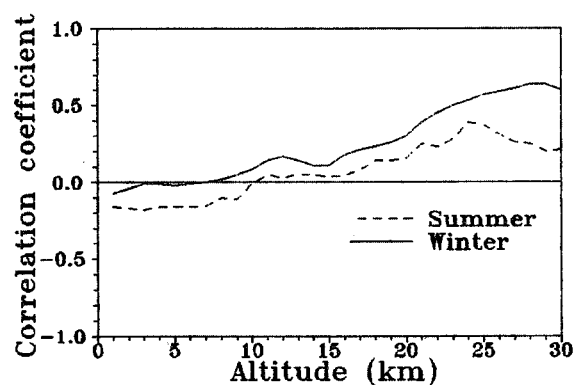


Fig. 6. Correlation coefficient between the temperature at the 24 km level (30mb) and ozone concentration at different altitudes for Hohenpeissenberg.

The ozonesonde measurements enable to

determine the altitudes in the ozone profile with which the mentioned correlation is associated. For this purpose the Hohenpeissenberg station (48°N, 11°E) data were used. The ozone concentration and the temperature in 1 km layers were computed from the observations results, and then for the temperature at each level the correlation coefficients with ozone concentration at all the levels from 1 to 30 km were computed. The largest ones in absolute value are observed between the temperature at 6 km (500 mb) and ozone concentration in the lower stratosphere (Figure 5). This relation accounts for the influence of the first group of factors upon total ozone.

In Figure 6 correlation between the temperature at 24 km (30 mb) and the ozone partial pressure is shown. As the figures show the first factor is associated with the ozone concentrations near the tropopause, the second - in the middle stratosphere.

REFERENCES

- Craig, R.A., 1965, The Upper Atmosphere, Meteorology and Physics, Academic Press, N.Y. and London.
- Dobson, G.M.B., 1973, Atmospheric ozone and the movement of the air in the stratosphere, Pure Appl. Geophys. 106-108.
- Dutsh, H.U., 1969, Atmospheric ozone and ultraviolet radiation, World Survey of Climatology, vol.4, D.F.Rex, ed., Elsevier, New York

303918

MANIFESTATION OF QUASI-BIENNIAL OSCILLATION IN OZONE VERTICAL DISTRIBUTION

Sergey A. Sitnov and Alexander N. Gruzdev

Institute of Atmospheric Physics
 Russian Academy of Sciences, Pyzhevsky per.3
 Moscow 109017, Russia

ABSTRACT

The quasi-biennial oscillations (QBO) in ozone and temperature vertical distributions are studied on the basis of ozonesonde data of 21 stations. Maximum QBO amplitudes in ozone are noted in the 16-20 km layer over Resolute (75N), Aspendale (38S) and in the northern mid-latitude band, but in the 20-24 km layer in the northern subtropical band. In the upper layers the QBO effect is less evident. In the tropospheric layer it is difficult to note the QBO-related effect in all the groups of the data. In all the layers where the QBO effect is noted the positive deviations precede, but the negative deviations follow the time of the maximum of the easterly equatorial wind at 50 mb level. No essential differences in phase or amplitude characteristics of the ozone QBO were noted for the Aspendale data compared with that for the Northern Hemisphere data. The QBO-effect is not noted in the temperature data in the mid-latitudes. Above Resolute and in subtropics the ozone and temperature effects are roughly in phase each with other, except in the 28-32 km layer over subtropics, where they are opposite each to other.

1. INTRODUCTION

There are a lot of studies of the quasi-biennial oscillation (QBO) in total ozone (see e.g. Angell and Korshover, 1983; Hasebe, 1983; Bojkov, 1987; Bowman, 1989, Gruzdev and Mokhov, 1992, and references therein). Less studies deal with the QBO in ozone vertical distribution. Analyzing ozonesonde data, Wilcox et al (1977) calculated the amplitude and phase of 29-month ozone oscillation. Angell and Korshover (1978) analyzed Umkehr data and have noticed the ozone QBO in the 32-46 layer over Australia. Later they (1983) also detected the QBO-related signal both in

Umkehr and ozonesonde data for temperate latitudes of the Northern Hemisphere (NH). Bojkov (1987) analysed ozonesonde and Umkehr data of several European stations and has found that the ozone QBO appears in all layers from the ozone maximum up to 28-30 km. Ling and London (1986) have demonstrated the ozone QBO in the 20-27 km layer using satellite (BUV) measurements. Finally, analyzing satellite (SAGE II) measurements, Zawodny and McCormick (1991) have shown the QBO in stratospheric ozone on a global scale.

2. DATA BASE AND METHOD OF ANALYSIS

The present paper deals with the QBO in ozone and temperature vertical distributions derived from ozone soundings. Ozonesonde data of 21 stations for variable periods from 1969-1990 were obtained from archives "Ozone Data for the World". The ozone contents and layer-mean temperature were calculated in seven 4 km-thick layers centered at 6, 10, 14, 18, 22, 26, and 30 km. Then monthly-means were calculated and the long-term annual means for each station were eliminated. The resulting deviations were smoothed by three-month running averaging. The stations were grouped in two latitude bands of the NH (the subtropical band, 10-40N, and the mid-latitude band, 40-60N). Two stations were considered separately: one subpolar station, Resolute (75N), in the NH, and another subtropical station, Aspendale (38S), in the Southern Hemisphere (SH). For these four groups the average QBO deviations are calculated, which are determined as averages of deseasonalised ozone series around key-0 month, anchored at the months when maxima of easterly equatorial stratospheric wind at 50 mb level were observed.

3. RESULTS OF ANALYSIS

Fig.1 shows the mean ozone deviations around the key-0 month in

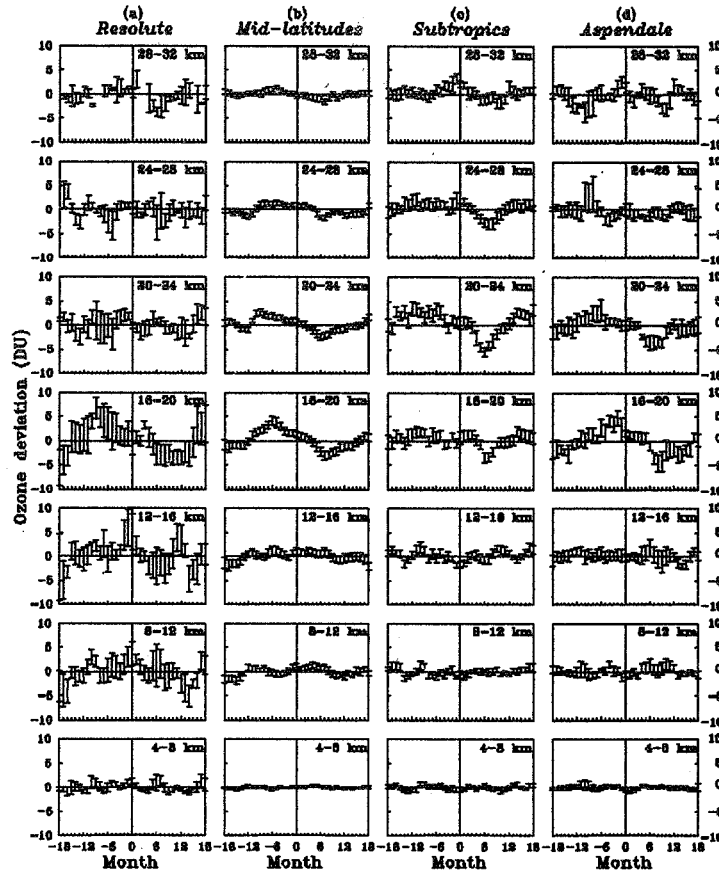


Fig.1. Mean ozone deviations around key-0 month, when maxima of easterly equatorial wind at 50 mb were observed, in layers (from top to bottom) 28-32, 24-28, 20-24, 16-20, 12-16, 8-12, and 4-8 km above (a) Resolute, (b) mid-latitude band, (c) subtropical band, and (d) Aspendale. Vertical segments denote standard deviations.

different layers above Resolute, the NH middle latitudes, NH subtropics and Aspendale. The quasi-biennial effect is most evident in the layers near the maximum ozone concentration level for all the four latitudinal groups of data (in the 16-20 km layer for Resolute and in the two middle layers, 16-20 and 20-24 km, for the three other groups). There the amplitudes of the ozone deviations approach (for the mid-latitude and subtropical bands) and exceed (for Resolute and Aspendale) 3 DU per 4-km thick layer. Note that the height of the maximum deviation decreases with latitude. In the 24-28 km layer, the effect is small (at the mid-latitudes and subtropics) or not evident (above Resolute and Aspendale; above Resolute the effect is not also evident in the lower, 20-24 km, layer). In the upper,

28-32 km, layer the QBO effect is evident in the mid-latitude and subtropical bands. There is also some evidence of the QBO effect in this layer above Resolute and Aspendale. This is surprising because in the lower, 24-28 km, layer the effect is not evident above these stations. In layers lower 16 km the QBO-related effect is not noted in all the groups of the data, although there is a large positive deviation approaching 5 DU near 0-month in the Resolute data (smaller deviation is also seen in the 8-12 km layer). In all the layers where the QBO is noted, for all the four groups of data, the positive deviations precede, but the negative deviations follow the time of the maximum of the easterly equatorial stratospheric wind at 50 mb. Note that there are no essential differences in phase or amplitude of the ozone deviation

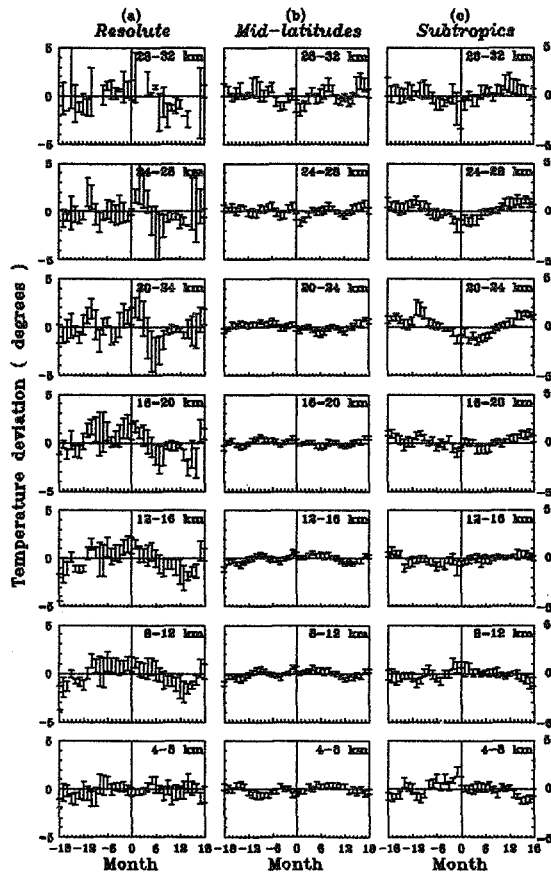


Fig.2. As in Fig.1a,b,c but mean temperature deviations.

between the SH station (Aspendale) and the NH data.

Fig.2 shows the similar deviations of temperature above Resolute, the NH middle latitudes, and NH subtropics (there are no accompanying temperature data for Aspendale). The QBO-related effect in temperature is absent in midlatitudes in all the layers. Above the subtropics it is clearly seen in the stratosphere. At the high NH latitudes (Resolute) the temperature deviations are noted in the two lower-stratospheric, 12-16 and 16-20 km, layers, and, perhaps, also in the 20-24 and 8-12 km layers. In the upper, 28-32 km, layer the negative temperature deviations can only be noted at the time after the 0-month.

The QBO-related ozone and temperature deviations are roughly in phase above Resolute in all the layers where these are seen simultaneously. Above subtropics the ozone and temperature deviations are roughly in phase in the 20-24 km layer, with some

phase shift however, but have opposite phases in the 28-32 km layer. In the intermediate, 24-28 km, layer they are roughly $\pi/2$ out of phase.

4. DISCUSSION

The ozone QBO in the equatorial stratosphere is well known to be the result of the QBO-induced meridional circulation, so that downward (upward) motion during the westerly (easterly) phase of the equatorial stratospheric zonal wind results in the ozone increase (decrease) in the lower and middle stratosphere above the equator (Reed, 1964; Ling and London, 1986). The return branches of the QBO-induced circulation in the tropics have the opposite vertical direction to that at the equator (Reed, 1964), thus resulting in the opposite ozone anomalies in the tropics compared with the anomaly above the equator.

To explain the extratropical QBO, several possible mechanisms have been proposed. First, it may be due to advection of the upper-stratosphere equatorial ozone anomaly (which is of opposite sign to the lower-stratosphere anomaly) by the meridional stratospheric circulation (Holton, 1989). Another mechanism is the transport of the tropical ozone anomaly to higher latitudes by the climatological mean and eddy circulation (Gray and Pyle, 1989). Holton and Tan (1980, 1982) suggested that the zonal wind QBO modulates extratropical planetary wave activity in winters. Such mechanism could effect ozone not only in middle but also in high latitudes.

Fig.1 shows the ozone QBO in extratropical latitudes. The results obtained are in qualitative agreement with the results overviewed in Introduction and with some results of model considerations by Ling and London (1986) and Gray and Pyle (1989). The QBOs in all the four latitudinal groups in Fig.1 are out of phase with the equatorial QBO in total ozone shown by Bowman (1989), and, therefore, they should be in phase with the tropical ozone QBO. The mechanism of the extratropical QBO in Fig.1 cannot be point out here, because this question needs more careful and detailed consideration.

The decrease of the height of the maximum QBO effect in Fig.1 with latitude can be understood, if one takes into account that the maximum in ozone vertical distribution decreases with latitude. QBO-related vertical or/and horizontal motions should cause the largest ozone variations in the domain of large vertical or/and horizontal ozone

gradients, i.e. below the maximum in ozone mixing ratio profile. The latitudinal decrease of height of the maximum ozone QBO has also been noted by Zawodny and McCormick (1991).

Small or absent QBO-related effects in the upper panels in Fig.1 agree well with the results of analysis by Zawodny and McCormick (1991) and with the theoretical consideration by Ling and London (1986). Ozone-temperature phase relationship above subtropics is in qualitative agreement with the Ling and London (1986) results.

REFERENCES

- Angell, J.K., and J. Korshover, 1978: Global ozone variations: An update into 1976. Mon.Wea.Rev., 106, 725-737.
- Angell, J.K., and J. Korshover, 1983: Global variations in total ozone and layer-mean ozone: An update through 1981. J.Clim. Appl.Meteorol., 22, 1611-1627.
- Bojkov, R.D., 1987: The 1983 and 1985 anomalies in ozone distribution in perspective. Mon.Wea.Rev., 115, 2187-2201.
- Bowman, K.P., 1989: Global patterns of the quasi-biennial oscillation in total ozone. J.Atmos.Sci., 46, 3328-3343.
- Gray, L.J., and J.A. Pyle, 1989: A two-dimensional model of the quasi-biennial oscillation of ozone. J.Atmos.Sci., 46, 203-220.
- Gruzdev, A.N., and I.I. Mokhov, 1992: Quasi-biennial oscillation in total ozone field as derived from ground-based measurements. Izvestiya, Atmos.Oceanic Phys., 28, in press.
- Hasebe, F., 1983: Interannual variations of global total ozone revealed from Nimbus 4 UV and ground based observations. J.Geophys.Res., 88, 6819-6834.
- Holton, J.R., 1989: Influence of the annual cycle in meridional transport on the quasi-biennial oscillation in total ozone. J.Atmos.Sci., 46, 1434-1439.
- Holton, J.R., and H.-C. Tan, 1980: The influence of the equatorial quasi-biennial oscillation on the global circulation at 50 mb. J.Atmos.Sci., 37, 2200-2208.
- Holton, J.R., and H.-C. Tan, 1982: The quasi-biennial oscillation in the Northern Hemisphere lower stratosphere. J.Meteorol. Soc.Jap., 60, 140-147.
- Ling, Xiu-De, and J. London, 1986: The quasi-biennial oscillation of ozone in the tropical middle stratosphere: a one dimensional model. J.Atmos. Sci., 43, 3122-3137.
- Naujokat, B., 1986: An update of the observed quasi-biennial oscillation of the stratospheric winds over the tropics. J.Atmos.Sci., 43, 1873-1877.
- Reed, R.J., 1964: A tentative model of 26-month oscillation in tropical latitudes. Quart.J.Roy.Meteorol. Soc., 90, 441-466.
- Wilcox, R.W., G.D. Nastrom, and A.D. Belmont, 1977: Periodic variations of total ozone and its vertical distribution. J.Appl. Meteorol., 16, 290-298.
- Zawodny, J.M., and M.P. McCormick, 1991: Stratospheric Aerosol and Gas Experiment. II. Measurements of the quasi-biennial oscillations in ozone and nitrogen dioxide. J.Geophys. Res., 96, 9371-9377.

303919

QUASI-BIENNIAL OSCILLATION IN TOTAL OZONE: GLOBAL BEHAVIOUR DERIVED FROM
GROUND-BASED MEASUREMENTS*Alexander N. Gruzdev and Igor I. Mokhov*Institute of Atmospheric Physics
Russian Academy of Sciences, Pyzhevsky per.3
Moscow 109017, Russia

ABSTRACT

The quasi-biennial oscillation (QBO) in total ozone (TO) is studied on the basis of TO measurements at the world ground-based ozone network during 1972-1988. The TO content is on the whole greater in the tropical belt and smaller in high latitudes during the westerly phase of the QBO of the equatorial stratospheric 50 mb wind than during the easterly phase in all seasons. The appropriate TO difference (westerly category minus easterly category) displays certain space structures changing during a year. There are regions with the peculiar annual evolution of this difference, particularly in the Arctic and Antarctic. Spectral analysis reveals bimodality of TO power spectra in the frequency range of QBO periods, with spectral maxima corresponding to 17-23 months and 28-35 months. The large period oscillations are predominant on the whole. The small period oscillations are likely the consequence of interaction between an annual cycle and QBO.

1. INTRODUCTION

The QBO in global TO distribution was studied in detail on the basis of zonal mean data (Hasebe, 1983; Tolson, 1981; Hilsenrath and Schlesinger, 1981; Lait et al., 1989). For the more comprehensive study the analysis of latitude-longitude TO field is needed. Gruzdev and Mokhov (1992) have shown that characteristics of the TO QBO are structured on the globe and evolve with season. The aim of this paper is the further analysis of peculiarities in spatial-time distribution of different characteristics of the TO QBO. The monthly mean data of TO measurements at the world ozone measuring network during 1972-1988 (since 1973 for Soviet stations) are used. Stations with a duration of measurements less than 4 years are not considered. The paper

includes: 1) the analysis of spatial distribution and annual evolution of the TO QBO anomalies determined as the long-term three-month mean TO difference (TOD) for the phases of the west and east equatorial stratospheric wind at the 50 mb level (west category minus east category); 2) the analysis of TO power spectra in the QBO frequency range.

2. ANALYSIS OF TOTAL OZONE QBO ANOMALIES

The TOD data were composed for four periods: January-March, April-June, July-September, and October-December. Such, rather than seasonal, composites enables us to separate possible influence of sudden winter stratospheric warmings in the northern extratropical latitudes since these occur primarily in the January-March period.

Fig.1 shows the TOD distribution for the four periods. The zero lines are thickened. Dashed lines correspond to regions with a sparse station distribution or short data series (duration of TO measurements is less than 8 years). All the differences exceeding 10 DU (5 DU in the tropics) by module are statistically significant at the 5% level. The TOD distribution is spatially inhomogeneous. There are seen negative and positive TOD anomalies in Fig.1 which are usually peculiar to certain regions. The anomalies evolve during a year. One can see negative TOD anomalies in the northern extratropical latitudes above the North Atlantic, north-east Asia, Siberia, North America, which are differently displayed in different periods. In the Southern Hemisphere (SH) the negative anomalies are noted over the New-Zealand and South American regions. It should be especially noted the extremely strong negative anomaly over the Antarctic in the October-December (late spring) period.

Positive anomalies are mainly peculiar to the tropics and usually seen

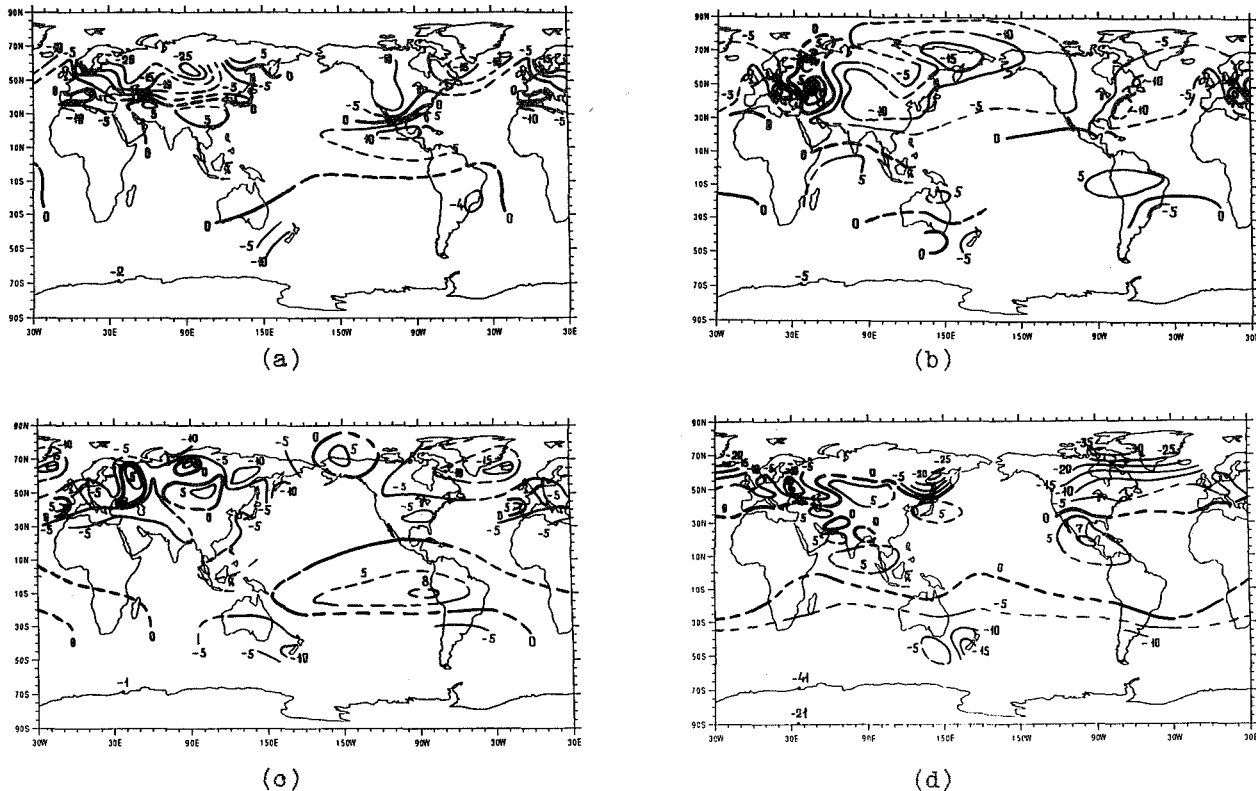


Fig.1. Total ozone difference (westerly category minus easterly category) for (a) January-March, (b) April-June, (c) July-September, and (d) October-December. Units: Dobson units.

over the American and Indian sectors. On the whole, one can distinguish the tropical belt with positive TODs and the areas of the extratropical latitudes, where "westerly" TO is usually less abundant than "easterly" TO. The boundary between the tropical belt and the area of negative TODs is strongly displaced during a year, sometimes stretching to extratropical latitudes.

As it is followed from Fig.1, the TO QBO can be described in the terms of TOD annual evolution. During October-December in the Northern Hemisphere (NH), when the boundary of the tropical area with positive TODs is shifted to the north into the middle latitudes, the strong negative TOD anomaly develops in the high latitudes and Arctic (Fig.1d). During the following January-March and April-June periods the anomaly spreads to the south, weakening in strength and changing zonal structure. A new center of negative TODs appears in January-March over Siberia (Fig.1a). By summer the NH negative anomalies are transformed to the less-scale structures (Fig.1c). The spread of the negative TOD area from the north displaces the tropical area of positive TODs to the south. In SH winter

the negative middle-latitude anomaly in the Australian sector develops (Fig.1c). This, together with the departure of the northern boundary of the tropical positive area from the summer NH, results in penetration of the negative TOD area to the equator. The negative anomaly in the Australian sector retains its position during the following periods, intensifying in spring (Fig.1d), weakening in summer (Fig.1a) and intensifying again in autumn (Fig.1b). Quite different regime of TOD annual evolution is noted in the Antarctic: with very high negative TOD values in late spring and much smaller negative TOD values in all other seasons. The cyclic annual TOD evolution is seen well in Fig.1a-d.

3. SPECTRAL ANALYSIS OF TOTAL OZONE QBO

Annual evolution of the TOD seen in Fig.1 points out the possibility of interaction between the QBO and the annual cycle. This can result in appearing new periodicities in TO time evolution. Indeed, TO power spectra for the most of the stations have bimodal distribution in the frequency range of

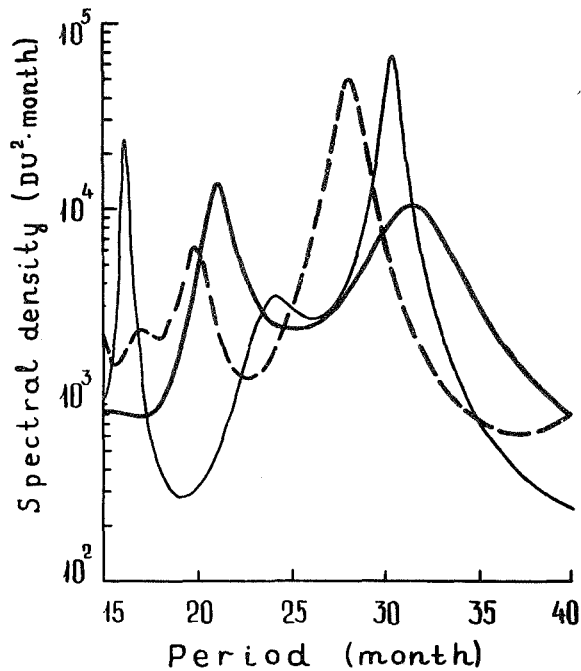


Fig.2. Total ozone power spectra for Boulder (40N, 105W, the thick full curve), Churchill (59N, 94W, the thin full curve), and Edmonton (53N, 114W, the dashed curve) stations.

QBO periods, with spectral maxima corresponding to 17-23 months (the small period (SP)) and 28-35 months (the large period (LP)). The high resolution spectral methods including the maximum entropy method were used for spectra calculations.

Fig.2 shows an example of TO spectra for three stations of the American sector. The detail spatial distributions of the SP and LP are described in Gruzdev and Mokhov (1992). The LP oscillations are predominant on the whole. The SP oscillations are most substantial in the regions where the annual evolution of the boundary between positive and negative TODs is essential (Fig.1). The SP oscillations are supposed to be the result of interaction between the QBO and annual cycle (Gruzdev and Mokhov, 1992).

4. DISCUSSION

The bimodality of TO spectra (in the range of QBO periods) was not found earlier because of insufficient spectral resolution of methods used (Hilsenrath and Schlesinger, 1981; Righter, 1981; Oltmans and London, 1982). Inappropriate spectral methods led some authors

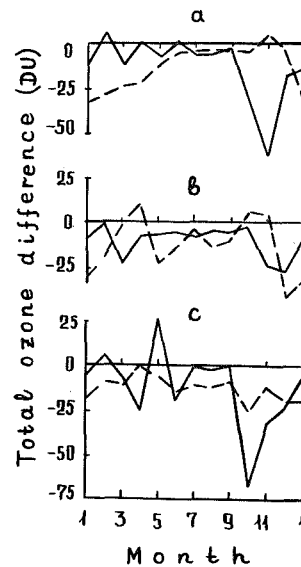


Fig.3. Total ozone difference as a function of month for (a) Resolute (75N, 95W, full curve) and Petropavlovsk-Kamchatsky (53N, 159E, dashed curve), (b) Edmonton (54N, 114W) and Oslo (60N, 11E), and (c) Syowa (69S, 40E) and Invercargill (46S, 168E).

(Hilsenrath and Schlesinger, 1981; Oltmans and London, 1982) to deduction about the latitudinal decrease of the TO QBO.

The TO QBO is related to the QBO in atmospheric circulation. A number of features of the TOD distribution in NH extratropical latitudes in Fig.1 are in agreement with features of the distribution of analogous differences of 50 mb geopotential height (GHD). The January-March negative TOD anomalies over the region of North America and the North Atlantic and over Siberia (Fig.1a) correspond to the "troughs" in the January-March GHD distribution (Holton and Tan, 1982). The areas of positive GHD values over Europe and the North Pacific should be compared with the similar area of positive TODs in Fig.1a.

Different regimes of the TO QBO in the SH middle and polar latitudes are due to dynamical isolation of the Antarctic stratosphere during the period of the winter circumpolar vortex. Intensity and time of the spring reversal of stratospheric circulation (which supplies the SH polar region with ozone) are related to the phase of tropical stratospheric wind. So the quasi-biennial modulation of the spring TO minimum (ozone "hole") over the Antarctic is caused, explaining the high TOD values

just in the same period (Fig.1d).

Existence of the TO QBO in the NH and SH extratropical latitudes in summer may be the consequence of spring anomalies degraded due to photochemical relaxation.

Large negative TOD values in the extratropical latitudes are observed during cold period when the planetary wave activity is large. Strong anomalies occur at different time in different regions (Fig.1). Fig.3 shows some examples of annual cycles of TODs for stations from different regions. Extreme negative TODs can occur in spring, in autumn, both in spring and autumn, when nonstationarity of planetary waves is essential, or in winter when planetary waves are stationary, or both in winter and spring.

REFERENCES

- Gruzdev, A.N., and I.I.Mokhov, 1992: Quasi-biennial oscillation in total ozone field as derived from ground-based measurements. Izvestiya, Atmosph.Oceanic Phys., 28, in press.
- Hasebe, F., 1983: Interannual variations of global total ozone revealed from Nimbus 4 UV and ground based observations. J.Geophys.Res., 88, 6819-6834.
- Hilsenrath, E., and B.M.Schlesinger, 1981: Total ozone seasonal and interannual variations derived from the 7 year Nimbus 7 data set. J.Geophys.Res., 86, 12087-12096.
- Holton, J.R., and H.-C.Tan, 1982: The quasi-biennial oscillation in the Northern Hemisphere lower stratosphere. J.Meteorol. Soc.Jap., 60, 140-147.
- Lait, L.R., M.R.Schoeberl, and P.A.Newman, 1989: Quasi-biennial modulation of the Antarctic ozone depletion. J.Geophys.Res., 94, 11559-11571.
- Oltmans, S.J., and J.London, 1982: The quasi-biennial oscillation in atmospheric ozone. J.Geophys.Res., 87, 8981-8989.
- Righter, P.V., 1981: An analysis of the power spectra of total ozone data. Mon.Wea.Rev., 109, 895-900.
- Tolson, R.H., 1981: Spatial and temporal variations of monthly mean total ozone derived from 7 years of UV data. J.Geophys.Res., 86, 7312-7330.

303920

TOTAL OZONE SEASONAL AND INTERANNUAL VARIATIONS IN THE PRINCIPAL AIR MASSES
OF THE NORTHERN HEMISPHERE IN 1975-1990.

Karol I.L., Klyagina L.P., Shalamyansky A.M., Jagovkina S.V.

Main Geophysical Observatory
Karbyshev Str., 7, St.-Petersburg, 194018, Russia

ABSTRACT

The diurnally mean total ozone X from the Northern Hemisphere ground based 90 stations for 1975-1990 are averaged over the Arctic (\bar{X}_A), Intermediate (\bar{X}_I) and Tropical (\bar{X}_T) air mass areas, divided by the jet stream axes on the isobaric surfaces 300 and 200 mb. The mean square variations of the so averaged X are considerably smaller than of the X , averaged over the corresponding zonal belts.

This property allows one to improve considerably the statistical significance of X trends and changes over various time periods, taking into account the time correlation of data for adjacent time intervals. \bar{X}_A , \bar{X}_I and \bar{X}_T trends are estimated over the periods of solar activity rise and fall in its 21-st and rise in its 22-nd 11 year cycles and over the periods of west and east phases of the known quasibiennial oscillation (QBO). Solar activity variations affect mostly \bar{X}_T , \bar{X}_I trends in summer months, while QBO phases influence the X changes mostly during the cold half year. X are lower in the west QBO phase and their trend is negative in spring during the almost all period considered. The anthropogenic effects on the X is also estimated.

1. INTRODUCTION

Numerous statistical studies of total ozone X variations in space and time have suffered from the high level X variability "noise" of different scales. This essential feature of ozone content fields in the troposphere and lower stratosphere leads to low statistical significance of the ozone content trend and other statistical parameter estimation as indicated in (WMO, 1985; Karol et al., 1987) and in many other publications. A basic cause of such variability is the successive passage of ozone rich and ozone poor air masses over the observing station guided by the planetary atmospheric transport systems.

A new concept of "dynamical" distributing and grouping of the Northern Hemisphere total ozone fields over the known basic planetary air masses: Arctic (AM); Intermediate (IM) and Tropical (TM) as divided by the jet stream axes at the 300 and 200 hPa isobaric surfaces has been introduced and developed by Shalamyansky and Romashkina (1980),

Karol et al. (1987, 1990). These air mass borders, being variable interdiurnally, have regular seasonal courses of their mean monthly positions in the atmosphere, which have been studied in the above publications. Fig. 1, 2 present the examples of seasonal variations of mean monthly values of some of these parameters, based on aerological data for 1962-1980 period. The comparison of the mean square deviations (msd) $\sigma_{\bar{X}}$ of mean monthly total ozone \bar{X} , averaged over the air masses and over the corresponding zonal belts at Fig. 3, reveal a considerable zonal belts $\sigma_{\bar{X}}$ reduction for the air masses. This reflects the almost homogeneous X distributions within the each air mass boundaries with permanent and sufficient X differences in the adjacent air masses.

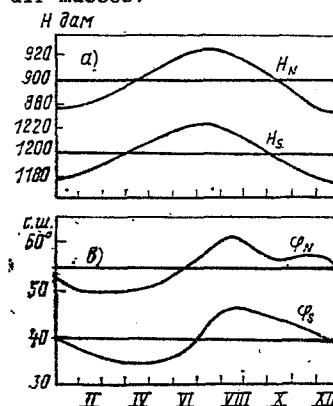


Fig. 1. Seasonal variations of zonally averaged mean monthly: heights of air mass borders h_N and h_S - a; latitudes of air mass borders φ_N and φ_S - b relative to their mean annual values. Bars indicate the mean square deviations (m.s.d.) of the mean.

Such air mass processing was applied to the total ozone data from the Northern Hemisphere ground-based ozonemetering stations with about 50 Dobson's and 40 filter ozonometers for the period 1975-1990. These processed data are used for evaluation of connections of mean monthly X , averaged over the above air masses, with several ozone distribution forming factors of natural origin: eleven year cycle of solar activity (SAC); quasibiennial oscillation (QBO) and of anthropogenic stratospheric chlorine content increase.

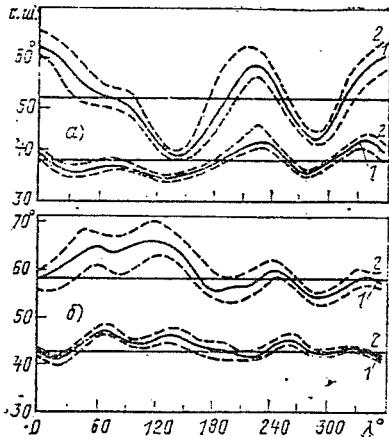


Fig. 2. Longitudinal profiles of mean monthly latitudes of air mass borders φ_N and φ_S for January and July averaged over 1962-1980 period - full lines; φ_N - dashed lines.

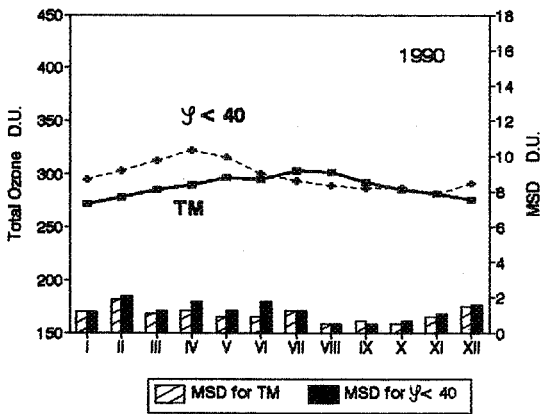
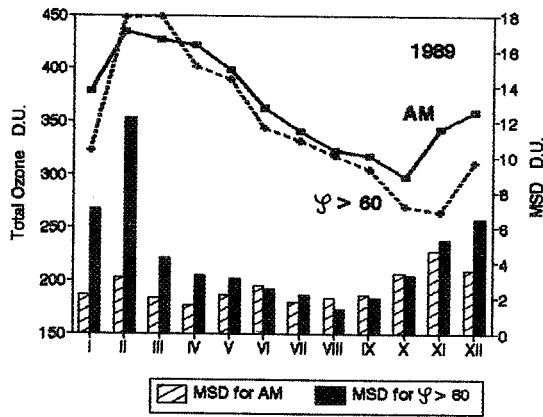


Fig. 3. Seasonal variations of mean monthly total ozone for 1989 and 1990 averaged over the air mass areas - a and over the zonal belts - b. Bars indicate mean square deviations of the mean $\bar{\sigma}_X$.

2. DATA PROCESSING

For the ozone - QBO connections studies the mean monthly \bar{X}_A , \bar{X}_I and \bar{X}_T , averaged over the corresponding Arctic, Intermediate and Tropical air masses are grouped into the east (E) and west (W) QBO phase periods, using the mean monthly zonal winds data at equatorial stations from (Naujokat et al., 1991) and averaged over the same months in each phase. Variances σ_E^2 , σ_W^2 in groups are the sums of all monthly mean variances of monthly \bar{X} , averaged over the period and they are presented at Fig. 4 as bars to seasonal variation profiles. These profiles reveal the evident difference between the \bar{X}_E and \bar{X}_W , which are highly statistically significant in each air mass in the first half of the year. The probability of non-zero difference $\bar{X}_E - \bar{X}_W$ is not less than 85-90% for each month of this period, being 99% in March and April for all air masses.

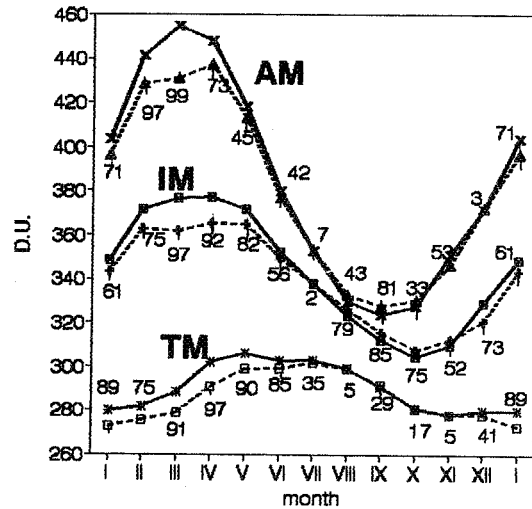


Fig. 4 Seasonal variations of mean monthly total ozone \bar{X}_E and \bar{X}_W averaged over the air mass areas and over periods of E (dotted lines) and W (full lines) of QBO phases. Bars indicate the m.s.d. of the mean $\bar{\sigma}_X$; numbers are the percent probabilities of the non zero difference of \bar{X}_E and \bar{X}_W for 1975-1990 period, according to Student's two sided test.

For evaluation of the interannual monthly \bar{X} covariation, the interannual autocorrelation functions of monthly \bar{X} deviations from their means for the E and W phases are calculated. In both phases during the cold half-year (October-March for AM and IM, November-April for TM) covariation of \bar{X} is weak and they are practically noncorrelating. But during the warm half-year \bar{X} covariation is stronger, and being exponentially approximated as $R(t) = e^{-\alpha t}$, has $\alpha = 1.53; 1.20; 1.15$; for AM, IM and TM correspondingly, with relaxation time $\tau = \alpha^{-1} = 0.66; 0.83; 0.87$ year. The account of \bar{X} interannual correlation according to procedure in (Polyak, 1979) makes only slight corrections in \bar{X}_E

and \bar{X}_W means, their trends and variances, being practically indistinguishable from their noncovariated values.

Linear trends of X are estimated within the groups of E and W QBO phases and also for periods 1975-1986, 1980-1990 of full eleven year cycle of solar activity, according to procedures proposed by Polyak (1979).

3. TOTAL OZONE VARIATIONS IN QBO PHASES

Fig.4 demonstrates that total ozone X in E phase is significantly higher than in W phase for all AM only in January-June. Therefore the linear trends for E and W phases are estimated for these months for periods 1975-1986 and 1980-1990. Analysis of these trends for 1980-1990, presented at Fig.5, reveals the negative trends almost for all masses and months considered, being bigger by value in E phase for TM and IM and in W phase for AM. Comparing this with seasonal X_A variations at Fig.4, one must emphasize that maximal X_A negative trend in March-May for W phase takes place for X_A relative low values with local minimum in these months, reflecting probably the averaged effect of local ozone "mini holes" in Arctic atmosphere (WMO/UNEP, 1989, 1991).

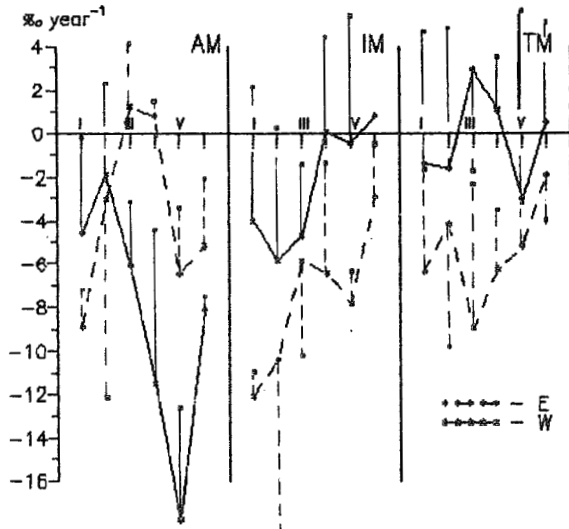


Fig.5. Linear trends (‰ year^{-1}) of \bar{X}_E (dashed lines) and \bar{X}_W (full lines) for January-June 1980-1990. Bars indicate the m.s.d. of the trend value.

Trend distributions at Fig.5 may be well explained by meridional air transport scheme, proposed recently by Trepte and Hitchman (1992) and based on the analysis of SAGE measurements of stratospheric aerosol optical thickness in 1980-ies. In this scheme the QBO E phase conditions are favorable for detrainment of substance from the upper part of lower tropical stratosphere, where the ozone concentration global maximum is situated, and for substance transport to the pole of the winter hemisphere. This enhanced transport may

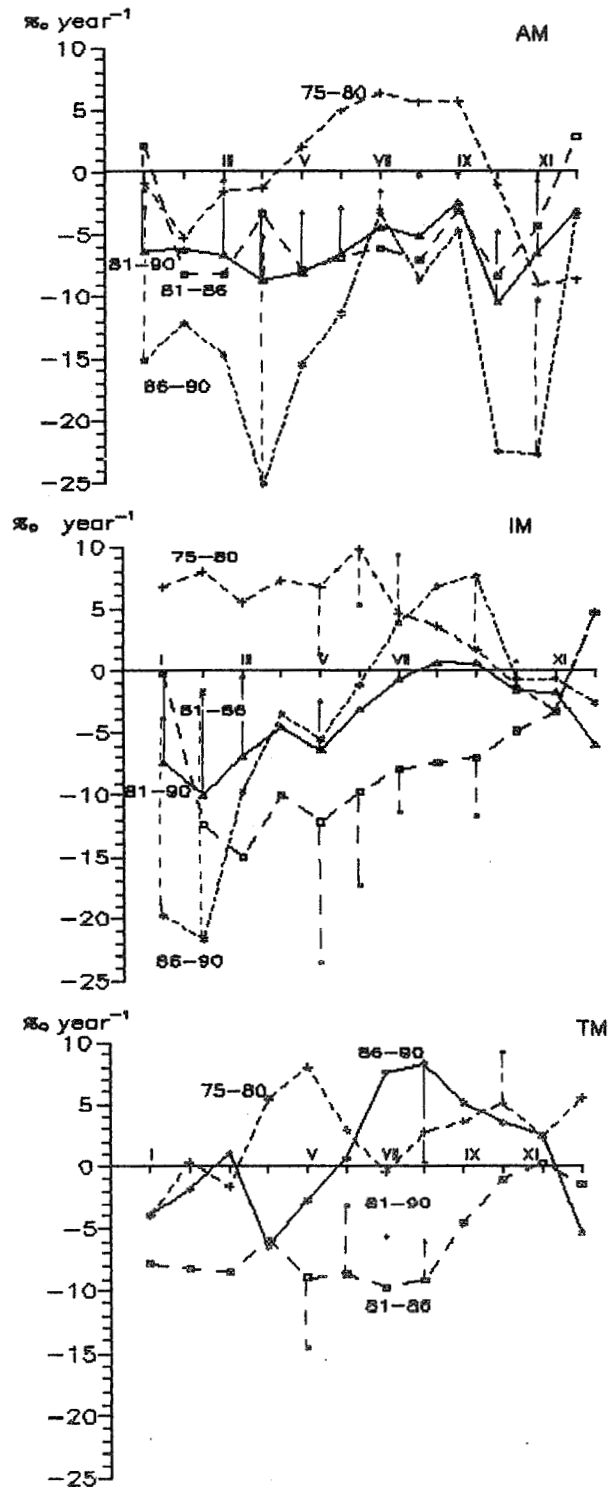


Fig.6. Linear trends (‰ year^{-1}) of mean monthly \bar{X} for the air mass and periods indicated. Bars denote the 90% significant confidence limit of nonzero trend, according to Student's two-sided test.

explain the relatively small X_A trends. Large negative X_A trends in QBO W phase in their turn may be the result of reduced air (and ozone) transport intensity into the polar zone from tropics in winter by the transient planetary waves (WMO/UNEP, 1989). According to Treppe and Hitchman's scheme in the QBO W phase the air and substance are detrained mostly from the lower layer of the tropical lower stratosphere with smaller ozone content, resulting in small and nonsignificant X_T trend. All this explains the Fig.4 and Fig.5 results qualitatively, but quantitative analysis will be necessary in the future.

4. TOTAL OZONE VARIATIONS IN ELEVEN YEAR SOLAR CYCLE.

Fig.6 presents the X_A , X_I , X_T linear trends for the above indicated periods of rise and fall of solar activity in its 21-st (1975-1986) and 22-nd (1986-1997) eleven year cycles. For the period 1975-1980 of solar activity increase, trends are positive for all air masses during the warm half year, being however nonsignificant at 90% confident level for most of months. Negative X_A , X_I and X_T trends for the period 1981-1986 reflect the effect of solar activity and of anthropogenic ozone depletion intensity increase, which becomes almost equal to solar activity variation effect at that period, according to model calculations (Karol et al., 1989). Big negative X_A trends and positive for July-November X_I and X_T trends for the period 1986-1990 reflect evident effect of opposite forcings on the ozone of the above two factors. In the polar ozone the anthropogenic ozone depletion is dominant, but X_A negative trends are minimal in value in the summer months June-September. During these months solar activity increase was dominating over the anthropogenic ozone depletion in intermediate and tropical air masses, where the solar radiation is more intensive.

For the whole decade 1980-1990 X_I and X_T trends are near zero for the second and are small negative for the first half of the year. These negative trends are 90 % confident for X_I (excluding April and June) and nonsignificant at this level for X_T . But X_A trends for decade 1980-1990 are negative and significant at 90% level of confidence for almost all months. All this agrees well with the recent observational results for the total ozone changes in the above decade, when nonsignificant changes have been observed in the tropics and trends of about 3-6% and 4% per decade were estimated in middle and polar northern latitudes (WMO/UNEP, 1991).

5. SUMMARY AND CONCLUSIONS

Total ozone X data from the Northern Hemisphere ground based ozonemetering network for the 1975-1990 are averaged over the principal Arctic, Intermediate and Tropical air mass areas with interdiurnally changing, but when monthly averaged, seasonally regularly varying borders. Due to significant reduction of the mean square deviations of these monthly and area averaged \bar{X} in comparison to regular zonal averaging, more fine and statistically significant variations of monthly

and air mass averaged X are estimated, as affected by QBO and 11-year solar activity cycle.

The trends of total ozone depletion due to anthropogenic influence in 1980-1990 are maximal for Arctic air mass in winter and spring and are close to those estimated for that period from observations in (WMO/UNEP,1991).

The reduced statistical noise and enhanced X_A , X_I , X_T sensitivity to ozone forming factors are promising to use this approach as basement for long term prediction of the total ozone variations.

REFERENCES

- Karol I.L., Klyagina L. P., Shalamyansky A. M., Frolov A.D., 1987 Ozone and temperature fields within air mass borders.- Meteorol.Gidrol.N10, 47-52 (in Russian)
- Karol I.L., Kiselev A.A., Rosanov E.V. 1989. Model assessment of ozone and ozone active atmospheric gas content changes due to anthropogenic influences and to solar activity variations. In "Ozone in the atmosphere (R.Bojkov, P. Fabian eds.) Deepak Publ.
- Karol I.L., Klyagina L.P., Shalamyansky A.M., 1990. Trends of total ozone in Northern Hemisphere principal air masses in 1975 - 1986.- Meteorol. Gidrol., N8,84-88 (in Russian).
- Naujokat B. et al., 1991. Beilagen zu Berliner Wetterkarte (Free Univ. of Berlin) Berlin.
- Polyak I.I.,1979. Methods for the analysis of random processes and fields in climatology, Gidrometizdat Leningrad (in Russian).
- Shalamyansky A.M., Romashkina C.I., 1980. Distribution and transformation of total ozone in various air masses - Trans. USSR Acad. Sci., Atmosph., Ocean. Phys., 6.N12,1258-1267, (in Russian).
- Tepte C.R., Hitchman M.H., 1992. Topical stratospheric circulation deduced from satellite aerosol data.- Nature, 355,626-628.
- WMO, 1985. Atmospheric ozone 1985, v.II. WMO Global Ozone Research and Monitoring Project. Rep.N16, WMO Geneva.
- WMO/UNEP, 1989. Scientific assessment of atmospheric ozone. 1989. WMO Global Ozone Research and Monitoring Project Rep.N20, v.I,WMO, Geneva.
- WMO/UNEP, 1991. Scientific assessment of ozone depletion. 1991, WMO Global Ozone Research and Monitoring Project, Rep.N25, WMO, Geneva.

303921

SOLAR PROTON EFFECTS ON AUSTRAL OZONE DURING THE FINAL MONTHS OF 1989

Judy A. E. Stephenson and Malcolm W. J. Scourfield

Space Physics Research Institute, University of Natal,
Durban, South Africa

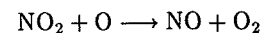
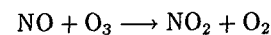
ABSTRACT

Intense solar activity during 1989 prompted six major particle events. Four of these occurred between August and December. Energetic solar protons are a natural source of ozone depletion due to the nitric oxides they produce in the polar atmospheres. In particular, modelling (Reid *et al.*, 1991) of an event that peaked on October 20 (with > 10 MeV proton flux of $73000 \text{ particles cm}^{-2} \text{ s}^{-1} \text{ ster}^{-1}$) yields 55% column density enhancements of NO over the southern polar cap.

Total column ozone data from the TOMS instrument aboard the Nimbus 7 satellite used at times when solar illumination facilitates measurements by TOMS over the entire southern polar regions. The impact of odd nitrogen enhancements on the spatial extent of low total column ozone and of the total ozone mass, over a region extending from 90°S to 70°S , is determined for the period August to December. Comparisons are made with previous years (1984 to 1988) of moderate solar activity. The effect, if any, of these events on ozone during times of heterogeneous chlorine chemistry and dynamic processes is discussed.

INTRODUCTION

Energetic solar protons are a natural source of ozone depletion over the polar caps (Stephenson and Scourfield, 1991). They can penetrate the earth's atmosphere at high latitudes ($> 60^\circ$) where they produce secondary electrons. These secondaries ionize and dissociate N_2 to produce odd nitrogen species which in turn can react with molecular oxygen or ozone to form nitric oxide (Crutzen *et al.*, 1975). Nitric oxide is then able to deplete ozone via the following catalytic reactions:



This paper investigates a means by which odd nitrogen species, produced by solar protons, enhance chlorine-catalysed ozone depletion in the austral spring.

In the last five months of 1989 intense solar activity resulted in four large solar proton events (SPE's). By definition, a solar proton event is said to have occurred when the flux of > 10 MeV protons exceeds 10 particles $\text{cm}^{-2} \text{ s}^{-1} \text{ ster}^{-1}$. Each SPE was characterized by substantial fluxes of high energy protons recorded by the GEOS-7 satellite. The onset dates and fluxes (particles $\text{cm}^{-2} \text{ s}^{-1} \text{ ster}^{-1}$) were: 12 August 9200; 29 September 4500; 19 October 73000 and 30 November 7300. A 2-D coupled dynamical/chemical model (Reid *et al.*, 1991) forecasts 55% column density enhancements in nitric oxide for these four events over the southern polar cap. Jackman (1991) predicts that altitude ranges attained by solar protons of the SPE's in 1989 would promote measurable stratospheric ozone depletion.

TOMS satellite ozone data were processed for the period from late August (day number 240) 1989 to the end of that year. We have calculated the total mass of ozone (at STP), taking into account the cosine dependence of the cell size of TOMS with latitude, from the south pole to latitude 70°S .

RESULTS

A plot of daily ozone mass, from 90°S - 70°S , for day number 240 to 365 (a period during the austral spring that includes the ozone hole) of 1989 is shown as a slender line in Figure 1. Arrows indicate the onset of SPE's the effects of which, since the lifetime of odd nitrogen in the stratosphere is days to months (Reid *et al.*, 1991), may be accumulative. In order to assess any effect the SPE's may have had on

ozone, a typical mass profile of previous periods including chlorine-catalysed ozone holes must be computed. A baseline comprising of five years of daily ozone masses averaged over 1984, 1985, 1986, 1987 and 1988 (all solar quiet years) was evaluated. This is represented as the broad line in Figure 1. The error bars represent the standard deviation, for consecutive 20 day periods, of all the daily ozone masses over five years. Until day number 300 the 1989 ozone mass profile is always well under the lower limit of these standard deviations.

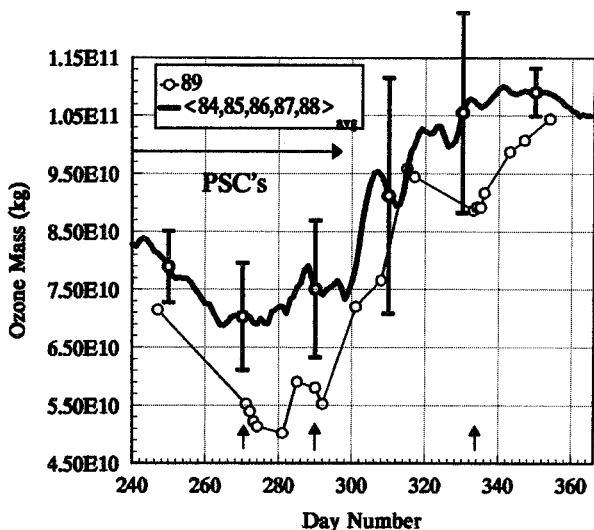


FIGURE 1: The total ozone mass over the zonal band 90°S-70°S for the austral spring of 1989 (slender line) and of a five year average that includes 1984, 85, 86, 87 and 88 (broad line).

Ozone masses are most variable at the time of vortex breakup (whose commencement may vary from year to year), reflected in the high standard deviations, from day number 300 to 340, throughout October and November. Two distinct differences between the 1989 ozone mass profile (slender line) and the 5 year average profile (broad line) are evident. Between day numbers 260 and 305 (end of October) the 1989 ozone hole is considerably deeper than the average profile. A mass difference of 2.2×10^{10} kg around day 280 is over twice the standard deviation. In addition there is a further deviation between the thin and broad lines of Figure 5 from day number 305 to the end of the year. Ozone masses during December 1989 do not recover to those of any of the previous years. A difference of up to $1.9 \pm 1.7 \times 10^{10}$ kg, around day number 333, is evident in this period. Since version 5 (V5) TOMS data were used in computing total ozone mass for 1989 and version 6 (V6) for 1984-88 the slender line representing 1989 data may be 5% too low (Stolarski *et al.*, 1990). High zenith angles, as is the case for polar latitudes in winter, usually result in larger errors. However, in austral spring when ozone levels are very low, these errors are minimized.

DISCUSSION

Two of the SPE's (day numbers 272 and 292) were coincident with the ozone hole. During this period of the year polar stratospheric clouds (PSC's), which form in the extreme cold of the Antarctic middle atmosphere, are surfaces for the heterogeneous conversion of passive chlorine reservoirs into reactive chlorine species. The vast majority of PSC's observed are not pure water ice or nacreous clouds since they have extinctions less than $10^{-2}/\text{km}$ (Hamill *et al.*, 1986). They probably consist of a frozen form of nitric acid with three water molecules ($\text{HNO}_3 \cdot 3\text{H}_2\text{O}$) called nitric acid trihydrate (NAT). These clouds form at a higher temperature (-78°C) than their nacreous counterparts (-83°C). The formation of NAT PSC's results in a highly denitrified stratosphere as removal of reactive nitrogen, which may otherwise trap chlorine into a reservoir molecule ClONO_2 , is converted into nitric acid.

Peter *et al.*, 1991 have modelled the effect that odd nitrogen from exhaust gases of 600 high-flying aircraft may have on NAT PSC formation probabilities. Since increased concentrations of odd nitrogen lead to a higher saturation temperature (in their case an increment of 3°C), PSC's are able to form at higher temperatures. They predict a doubling in occurrence of NAT PSC's and an even stronger increase of ice condensing on NAT particles for northern polar latitudes. Coincidentally, the mass of odd nitrogen produced by the aircraft is similar to that deposited by a large SPE. The purpose of this work is to ascertain what effect odd nitrogen species may have when added directly to low altitudes in the polar stratosphere (thousands of protons with energies > 100 MeV reaching 30 km and below were detected) during the occurrence of the ozone hole.

A study by Steele *et al.* (1983) showed that PSC observations are highly correlated with low temperatures. Cloud is continuous in regions where temperatures are around or below -85°C (McCormick *et al.*, 1985), inferring that the primary prerequisite for PSC formation is temperature. Assuming that NAT PSC's may form at temperatures of -76°C , due to the increased concentrations of odd nitrogen, we infer that from temperature data at 50 hPa for Sanae (70°S , 2°W), Antarctica that days of PSC formation are from day number 155 to 290 in 1989 as indicated by the horizontal arrow in Figure 1. Of course the underlying assumption here is that Sanae is representative of the area under consideration viz 90°S - 70°S .

In order to quantify any effects on ozone concentrations due to additional NAT PSC's we calculated the extent in area of low ozone, < 250 DU within the latitude regions 90°S-70°S and 80°S-70°S. The difference in areas covered by this contour between 1989 and a five year average (1988, 1987, 1986, 1985 and 1984) are shown as thick lines in Figure 2. Solid lines indicate 90°S-70°S and the broken lines 80°S-70°S.

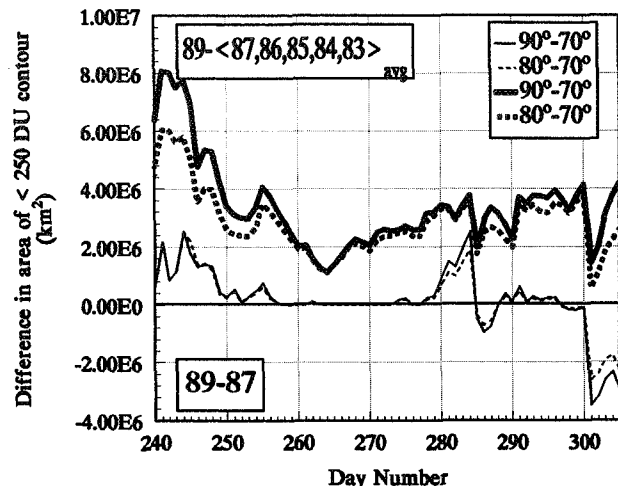


FIGURE 2: The difference in area (km^2) occupied by < 250 DU between 1989 and a five year average (thick lines) and 1987 (thin lines). Solid lines, in both cases, are representative of the difference in area in the latitude region 90°S-70°S, and broken lines 80°S-70°S.

A noticeable feature of the thick lines in Figure 2 is that they are very similar in variance and magnitude, from which we may infer that any changes in area are largely in the zonal band 80°S-70°S. This is what we might expect since lower stratospheric ozone poleward of 80°S is almost totally absent throughout the ozone hole period and the processing by PSC's is therefore saturated. These very low total column values indicate only residual tropospheric and upper stratospheric ozone (Stolarski, 1989). The increase in area of the < 250 DU contour between 80°S and 70°S in 1989, compared with the mean of previous years, varies between 1.3 and $6.0 \times 10^6 \text{ km}^2$, well outside any error that maybe incurred by the difference in data versions. To reaffirm this increase a similar analysis between 1989 and 1987 (thin lines in Figure 2) was performed. Again, the solid line is for the region 90°S-70°S and the broken for 80°S-70°S which once again match each other in variance and magnitude. The year 1987 was chosen as it was the 'worst case' ozone hole in the five year period 1984-1988. Areas of increased ozone depletion can be up to $2.632 \times 10^6 \text{ km}^2$. The accuracy of the results ($\approx 10^3 \text{ km}^2$) is limited only by the TOMS polar latitude cell size since V5 TOMS data were used for both 1987 and 1989 data.

The effect of the final SPE in 1989 (day number 334) is hard to quantify as the vortex began to erode in the last two weeks of October (Stolarski *et al.*, 1989) so that ozone temporal and spatial variations were high. However it is likely that ozone destruction, this time via homogeneous gas phase reactions stated in the beginning of this paper, would have occurred.

In summary, an increase in the spatial extent of the 1989 ozone hole compared to previous years was detected. The enhancement of NO_x concentrations due to SPE's may be seen as a likely source to increase the probability of NAT PSC formation. However, the addition of NO_x may, in some instances, result in larger ice particles rather than increasing the area of coverage of PSC's. In addition, extra odd nitrogen will have no effect in regions where processing of ozone is complete.

REFERENCES

- Crutzen, P. J., I. S. A. Isaksen and G. C. Reid, Solar proton events: stratospheric sources of nitric oxide, *Science*, **189**, 457-459, 1975.
- Hamill, P., O. B. Toon and R. P. Turco, Characteristics of polar stratospheric clouds during the formation of the Antarctic ozone hole, *Geophys. Res. Lett.*, **13**, 1288-1291, 1986.
- Jackman, C. H., Response of the middle atmosphere to solar proton events, *XX General Assembly of IUGG, IAGA Symposium GAM 2.8 held in Vienna, Austria, 1991*.
- McCormick, M. P., P. Hamill and U. O. Farrukh, Characteristics of polar stratospheric clouds as observed by SAM II, SAGE and lidar, *J. Meteor. Soc. Japan*, **63**, 267-276, 1985.
- Peter, Th., C. Brühl and P. J. Crutzen, Increase in PSC-formation probability caused by high-flying aircraft, *Geophys. Res. Lett.*, **18**, 1465-1468, 1991.
- Reid, G. C., S. Solomon and R. R. Garcia, Response of the middle atmosphere to the SPE's of August-December 1989, *Geophys. Res. Lett.*, **18**, 1019-1022, 1991.
- Steele, H. M., P. Hamill, M. P. McCormick and T. J. Swissler, The formation of polar stratospheric clouds, *J. Atmos. Sci.*, **40**, 2055-2067, 1983.
- Stephenson, J. A. E. and M. W. J. Scourfield, Importance of energetic solar protons in ozone depletion, *Nature*, **352**, 137-139, 1991.
- Stolarski, R. S., M. R. Schoeberl, P. A. Newman, R. D. McPeters and A. J. Krueger, The 1989 Antarctic ozone hole as observed by TOMS, *Geophys. Res. Lett.*, **17**, 1267-1270, 1990.

ACKNOWLEDGEMENTS

We thank R. D. McPeters and A. Krueger (NASA/GFSC), members of the TOMS Nimbus Experiment and Ozone Processing teams, and the National Space Data Center-A for Rockets and Satellites for total column ozone data. Data on solar proton events were supplied by NOAA Space Environment Services Center. Temperature profiles at Sanae, Antarctica courtesy of the South African Weather Bureau.

303922

MODEL EVALUATION OF THE RADIATIVE AND TEMPERATURE EFFECTS OF THE OZONE CONTENT CHANGES
IN THE GLOBAL ATMOSPHERE OF 1980-IES

Igor L. Karol, Victor A. Frolkis

Main Geophysical Observatory
Karbyshev Str., 7, St.-Petersburg, 194018, Russia

ABSTRACT

Radiative and temperature effects of the observed ozone and greenhouse gases atmospheric content changes in 1980 - 1990 are evaluated using the two-dimensional energy balance radiative-convective model of the zonally and annually averaged troposphere and stratosphere. Calculated radiative flux changes for standard conditions quantitatively agree with their estimates in WMO/UNEP, 1991 review. Model estimates indicate rather small influence of ozone depletion in the lower stratosphere at the greenhouse tropospheric warming rate, being more significant in the non tropical Southern Hemisphere. The calculated cooling of the lower stratosphere is close to the observed temperature trends there in the last decade.

1. INTRODUCTION

Significant ozone content changes in the lower stratosphere and troposphere as observed in 1980-ies with enhanced intensity during the recent years [WMO/UNEP, 1991] result in variations of radiative and temperature climate of the global atmosphere. The preliminary estimates of these variations have been used for important conclusions about their influence on the rate of greenhouse warming of the global troposphere [WMO/UNEP, 1991; Ramaswamy et al., 1992]. In these publications the meridional distributions of radiative flux variations at the tropopause level are evaluated, as caused by the observed changes of ozone and greenhouse gas content at various latitudes and levels of the global atmosphere in 1980-1990.

As the tropospheric temperature changes only to some extent are determined by the above radiative flux variations, more precise evaluation of the climatic radiative and temperature effects by the comprehensive climatic models is necessary [Ramaswamy et al., 1992]. However, the relative small amplitude of ozone changes makes difficult to reveal the effect "signal" over the considerable "noise" level in such models [IPCC, 1990].

In this paper the mean annual, zonally averaged solar and thermal radiation fluxes and temperature variations at various levels of the global atmosphere are estimated using the two-dimensional Energy Balance Radiative Convective

Model (EBRCM), described in [Karol and Frolkis, 1984]. As indicated in this paper and in [Karol et al., 1986] the radiative and temperature changes, caused by CO₂ concentration increase in the atmosphere estimated by this model, are very close to these, obtained in the three-dimensional comprehensive atmospheric climate models.

In the first part of the paper after the short description of the model, the radiative forcing caused by ozone and greenhouse gases (GG) content changes in conditions used in [WMO/UNEP, 1991; Ramaswamy et al., 1992] are calculated and compared with results in these publications, making in a such way the comparison of the radiative schemes codes and models. Then the annually averaged mean zonal radiative flux and temperature changes are estimated [IPCC, 1990] as caused by the observed GG and ozone content changes for the time period 1980-1990. Some observed evidences of these changes are discussed in the conclusion of the paper.

2. SHORT DESCRIPTION OF THE MODEL

The model is presented in details in [Karol and Frolkis, 1984]. Annually and zonally averaged radiation fluxes and temperature distributions in the global atmosphere up to H=0.64 hPa (50 km) level with prescribed radiatively-active atmospheric constituent concentrations and other parameters are determined by successive approximation up to equilibrium state. At each step the vertical temperature profiles are determined from eight Radiative-Convective Models (RCM) at 80°, 60°, 40°, 15° N and S with 15 horizontal layers, and with surface air temperature T₀, taken from the previous approximation step. These profiles and other information are used for computation of solar and thermal radiation fluxes S_H and F_H at the considered upper atmospheric boundary. To distributions are the solutions of the energy balance equation

$$\frac{d}{dx} j(x) \cdot (1-x^2) \frac{dT_o(x)}{dx} = F_H(x) - S_H(x),$$

where ϕ is the latitude; $x = \sin \phi$; $j(x) = j_0 K(x)$; $j_0 = c_{p0} / g R_0^2$; $K(x)$ is the effective horizontal heat transport coefficient. "Heat walls" at the poles are the boundary conditions for this equation solution, which is used for eight RCM at the next

step of successive approximation. Besides the coarse grid of eight zonal belts the fine grid of 36 belts with $\Delta\phi=5^\circ$ is used in computations.

Solar radiation flux calculations are based on the two-stream delta-Eddington scheme. The UV band (197.5-312.5 nm) is divided into 11 spectral intervals, where O_2 , O_3 , NO_2 and aerosol effects are accounted. Visible band contains two spectral intervals with inclusion of O_3 , NO_2 , molecular, aerosol and cloud scattering and reflectance. NIR band (750-4000 nm) is divided into 12 spectral intervals, in which the selective H_2O , CO_2 , O_3 , N_2O and CH_4 absorption is accounted approximated by the Goody transmission function for the statistical model of the absorption band. An original approach is used for the approximate calculation of selective gas absorption and scattering of photons by aerosol and clouds with multiple reflection from the cloud layer boundaries.

The thermal radiation fluxes are calculated for 17 spectral intervals in the 4.4-1000 micrometers band. The transmission functions for the same gas selective absorption are approximated as in NIR with the atmospheric vertical density layering accounted by Curtis-Godson approximation. Weak absorption approach is used for CFCs. H_2O continuum absorption and diffusivity approximation are included, but the cloud and aerosol transmission functions are non-selective. The ground surface and clouds are considered as black bodies.

The external data and conditions, used in the calculations of the radiation flux variations, caused by the GG and ozone changes are presented in Tables 1 and 2. These data are taken from the sources and are the most close to used in [Ramaswamy et al., 1992], for model comparison. In Table 2 the daily averaged cosine of the solar zenith angle ϕ^* , the clear day relative duration t^* and surface albedo A_s for selected cases used in our calculations are also presented, being not indicated in [WMO/UNEP, 1991; Ch.7 and Ramaswamy et al., 1992]. For comparison purposes the clear sky Mode A with fixed temperature profiles Model I radiative forcing values are used from the above publication.

Table 1. Globally and annually averaged GG tropospheric mixing ratios in 1980 and their increases to 1990 [IPCC, 1990; WMO/UNEP, 1991].

Gas	CO ₂	CH ₄	N ₂ O	CFC			
				11	12	113	22
Units	ppmv			ppbv			
1980	337	1.57	302.6	0.158	0.27	0.015	0.05
1980-1990	17	0.15	8.0	0.111	0.17	0.050	0.07

3. RESULTS OF CALCULATIONS.

The radiative forcings (the net total long + short wave radiative flux variations at the tropopause level) are compared in Table 3 for the above conditions as calculated by EBRM and by Mode A, Model I in [WMO/UNEP, 1991] and caused by ozone, CFC and other GG content change separately. The agreement between the two model results are good,

not only at the tropopause, but at the ground surface also, being the worst for CFC, as in EBRM only the radiative forcing of CFC-11 and 12 are included.

Table 2. Cases selected for radiative forcing calculations due to ozone depletion in the lower stratosphere $\Delta(O_3)$ for standard temperature profiles: tropical-T; midlatitude summer-MLS and winter-MLW; subArctic winter-SAW [WMO/UNEP, 1991]. Daily averaged solar zenith angle ϕ^* , clear day relative duration t^* and surface albedo A_s , which are used in calculations.

No.	Latitude	Month	Temp. Profile	$\Delta(O_3)$ (%)	$\cos\phi^*$	t^*	A_s
1	0°	July	T	-0.5	0.586	0.500	0.076
2	45°N	July	MLS	-2.0	0.570	0.640	0.123
3	45°N	Feb.	MLW	-8.0	0.301	0.399	0.271
4	45°S	Jan.	MLS	-6.0	0.570	0.639	0.067
5	45°S	Aug.	MLW	-5.0	0.296	0.396	0.098
6	70°N	Mar.	SAW	-17.0	0.134	0.372	0.641
7	75°S	Oct.	SAW	-32.0	0.205	0.588	0.799

Fig.1 demonstrates the meridional distribution of solar and thermal net radiation flux changes at the tropopause level for January and July, calculated by EBRM for ozone and non-ozone GG content variations, indicated in Tables 1 and 2, for Mode A and clear sky conditions.

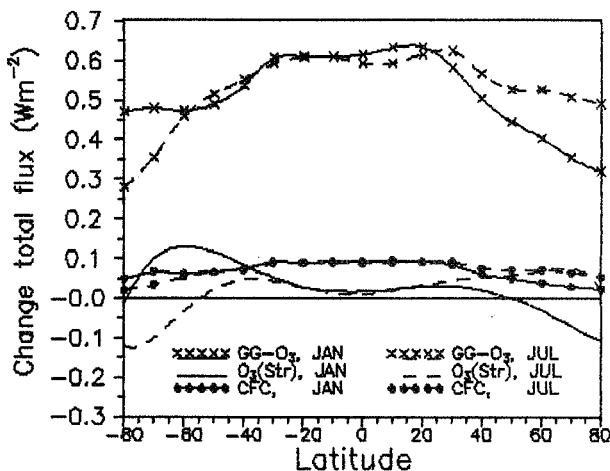


Fig. 1. Total net flux changes at the tropopause level (for Mode A) for January and July due to only O_3 ($O_3(\text{Str})$), to non-ozone GG ($GG-O_3$) and to CFC (CFC) content variations.

Ozone depletion leads to increasing of the solar radiation flux coming to the surface-troposphere system at all latitudes throughout the year. The long wave cooling of this system by ozone depletion in Mode A is exceeding its solar warming only in the polar winter. The influence of the

atmospheric temperature changes on the radiation flux variations may be assessed from Table 4 with the meridional variations of annually and zonally averaged changes of solar and thermal radiation fluxes at the tropopause level for Mode C, for the cloudy atmosphere, for GG content increase in Table 1 and for annually averaged ozone depletion estimates in Table 5. The Mode C difference from the Mode B in [WMO/UNEP, 1991; Ramaswamy et al., 1992]

Table 3. Net radiation flux changes at the tropopause and at the surface levels due to GG and ozone content variations and for the cases and conditions indicated in Table 1 and 2, as evaluated in [WMO/UNEP, 1991, Ch.7]-Mode A and in this work-F.

Case	CO ₂ +CH ₄ +N ₂ O		CO ₂ +CH ₄ +N ₂ O+CFC		CFC		Ozone	
	Tropopause		Surface		A	Fa	A	F
	A	F	A	F				
1	.54	.520	.14	.154	.16	.096	.01	.006
2	.51	.460	.20	.231	.13	.074	.08	.024
3	.41	.400	.35	.369	.08	.053	.03	.026
4	.51	.457	-	-	.13	.071	.06	.064
5	.41	.400	-	-	.08	.053	.05	.025
6	.34	.347	.28 ^b	.284 ^b	.05	.034	-.17	-.041
7	.34	.342	.37 ^c	.377 ^c	.05	.033	-.41	-.066

a/ - For CFC-11 plus CFC-12 only.
 b/ - For SAS temperature profile.
 c/ - For SAN temperature profile.

is that in Mode C the radiation variations induced by the temperature changes are calculated by KBRM with account of clouds. In the Mode B the tropospheric temperature and humidity remain unchanged, while the stratospheric temperature is in the radiative equilibrium under the assumption of a so-called Fixed Dynamical Heating concept [WMO/UNEP, 1991].

Fig. 2 demonstrates the calculated zonally and annually averaged surface air temperature changes, induced by the radiative forcing due to GG and ozone content changes in Tables 1 and 5, calculated for Mode C conditions and for cloudy atmosphere assumed not to be changing during the period under consideration. The meridional distribution of calculated air cooling in the lower stratosphere, due to ozone depletion being maximal at the 80 mb level is also presented at Fig.2.

4. DISCUSSION OF RESULTS.

The comparison of the net radiation flux variations for the seven standard cases, indicated in the Table 2 and evaluated in [WMO/UNEP, 1991, Ch.7] and in this work as presented in Table 3, reveal the good agreement of calculation results for all cases, bearing in mind the possible devi-

ations in surface short wave albedo, which is not indicated in [WMO/UNEP, 1991, Ch.7]. The agreement of CFC radiative forcing estimates in Table 3 will be improved substantially by increasing our estimates by about 40-60% for account of radiative effects of CFC content increase, other than CFC-11,12.

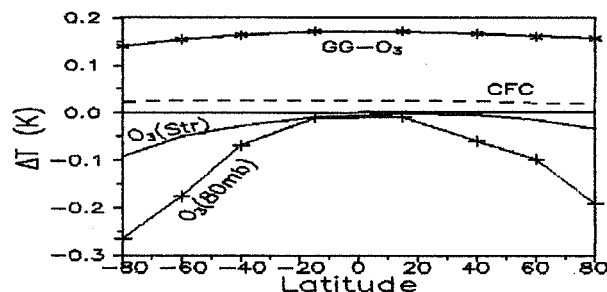


Fig.2. The calculated ΔT_o obtained for all GG without O₃ (GG-O₃), for CFC only (CFC), for lower stratospheric O₃ only (O₃(Str)) and ΔT at 80 mb level divided by 10 (O₃(80mb)) all for Mode C.

Table 4. The net fluxes of solar ΔS and total ΔR radiation changes (Wm^{-2}) at the tropopause level for modes A and C due to gas content variations, indicated in Tables 1 and 5.

Gas	Flux	Southern Latitudes				Northern Latitudes			
		80°	60°	40°	15°	15°	40°	60°	80°
Mode A									
O ₃	ΔS	.12	.24	.125	.014	.013	.12	.17	.14
O ₃	ΔR	-.074	.090	.074	.018	.019	.18	.18	-.050
CFCs	ΔR	.022	.034	.046	.056	.058	.048	.037	.028
GG ^a	ΔR	.31	.37	.435	.47	.48	.44	.38	.34
GG ^a	ΔS	.004	-.012	-.025	-.016	-.016	-.024	-.014	-.004
O ₃ ^b	ΔS	.10	.21	.112	.012	.012	.10	.14	.11
O ₃ ^b	ΔR	-.064	.073	.051	.009	.008	.09	.10	-.051
Mode C									
O ₃	ΔS	.012	.25	.13	.015	.013	.12	.18	.15
O ₃	ΔR	-.14	-.14	-.01	.040	.016	.038	.009	-.28
CFCs	ΔR	-.003	-.004	9E-4	.003	.002	.002	-.003	-.002
GG ^a	ΔR	-.0033	.0042	.018	-2E-4	-6E-4	.017	.0012	-.033

a/ - The sum of greenhouse gases, omitting the ozone variations.
 b/ - Ozone content changes only in the lower stratosphere.

The meridional profiles of radiation flux changes at Fig.1 and in Table 4 are close to relevant curves at Figs. 7.3 and 7.4 in [WMO/UNEP, 1991, Ch.7] for Mode A with fixed atmospheric temperatures. Flux changes are somewhat greater in the cloudless atmosphere (Mode A) as compared to those of a cloudy atmosphere (Mode C). Therefore

our radiation flux calculations schemes and Mode A (fixed temperature) results are close to those in [WMO/UNEP, 1991; Ramaswamy et al., 1992]. The radiative cooling of the lower stratosphere by the ozone depletion effects enhances the negative mean annual total radiation change in the Southern Hemisphere outside of tropics and in the northern polar zone. This ozone caused negative change overweights by several times the positive (thermal) radiation forcing, caused by the CFC in north polar and south non-tropical latitudes, as it has been found in [WMO/UNEP, 1991], but not in the north temperate latitudes. (The account of other CFCs increases the forcing by 30-50% only [IPCC, 1990] and will not change the above conclusion qualitatively.) Due to above explained differences in temperature change evaluation, the radiation flux variations in the affected temperature fields in KBRM and in [Ramaswamy et al., 1992] are incomparable in principle and GG and ozone content variation effects assessed by KBRM may be estimated better by the temperature change analysis.

Table 5. Annually and zonally averaged ozone content changes (%) during 1980-1990 at indicated latitudes and layers, as estimated in [WMO/UNEP, 1991] and used in calculations.

Layer (km)	N. Latitudes			20°N-	S. Latitudes		
	80°	60°	40°	-20°S	40°	60°	80°
Troposph.	0	8	8	2	0	0	0
ht _r -ht _{r+7}	-20	-10	-8	-1.6	-10	-20	-30
37 - 45	-10	-5	-3	-0.8	-5	-10	-17

The ΔT_o -surface air annually averaged "radiative" temperature profiles at Fig.2 demonstrate, that negative ΔT_o produced by the observed ozone depletion in the lower stratosphere, surpass the positive CFC ΔT (underestimated, as pointed out above) only in the polar zones. Maximal ozone produced ΔT_o around the South Pole attains of about 70% of GG warming in this area, but in the Northern Hemisphere the ozone produced reduction of GG warming does not exceed 25%, being maximal in the North Pole area. This small reduction of the greenhouse warming rate in the lower atmosphere due to observed ozone depletion may be even less in reality with account of the known oceanic thermal inertia effect [IPCC, 1990, Ch.6]. According to several estimates the time delay of the surface air greenhouse warming due to this effect is about 10-20 years [IPCC, 1990; Karol and Jagovkina, 1992] and therefore the actual T_o increase in 1980-ies is reflecting the greenhouse radiative forcing in previous decades, when ozone depletion forcing was nonsignificant.

The globally averaged $\Delta T_{oa} = 0.129K$ and $\Delta R_a = 0.50 Wm^{-2}$ from Table 4 for all GG increase except ozone in 1980-1990 is in good agreement with $\Delta T_{oa} = 0.139K$ and $\Delta R_a = 0.54 Wm^{-2}$ estimated in [IPCC, 1990]. The negative ΔT_{oa} in the lower stratosphere at Fig.2, when globally averaged is $\Delta T_a = -0.58 K$ and it is close to the globally averaged observed temperature negative trend of 0.4

K/decade in the layer between 100 and 50 hPa [WMO/UNEP, 1991, Ch.2].

The observed ozone concentration changes outside the lower stratosphere are much less influencing the radiation and temperature regime in the lower troposphere, as revealed by Table 4, where the solar and net radiation flux changes are compared as caused by all the ozone variations, indicated in Table 4, and by its variations in the lower stratosphere only.

The consequences of "ozone compensation" of the greenhouse warming in the southern polar zone in 1980-ies may result in different changes in the total areas of snow and of ice in the Antarctic and in the Arctic [Cloersen and Campbell, 1991]. While this area decreases in the Arctic, it does not undergo any changes in the Antarctic.

An express Bulletin [GECC, 1992] announced recently that UARS satellite measured 10% lower ozone concentration in 10° S - 20° N zone in January 1992 as a possible result of Mt. Pinatubo volcano aerosol plume effects. Ten percent ozone reduction in the 7 km layer over the tropopause of the 20° S - 20° N zone leads to calculated $\Delta S = 0.13 Wm^{-2}$ and $\Delta R = 0.15 Wm^{-2}$ of solar and total flux changes for Mode A, filling up by this the tropical minimum of ozone induced change of flux meridional profile (see Fig. 1 and Table 4). Due to short period radiative forcing, caused by volcano plumes, and its transient effect on the air temperature, the stationary KBRM is not suited for evaluation of such effects.

REFERENCES.

- GECC, 1992: Global Environmental Change Report, v.IV, N3, 2.
- Gloersen P., Campbell W.J., 1991: Recent variations in Arctic and Antarctic sea-ice covers, *Nature*, 352, 33-36.
- IPCC, 1990: Climate Change. The IPCC Scientific Assessment WMO/UNEP, Cambridge Univ.Press, 365p.
- Karol I.L., Frolkis V.A., 1984: Energy balance radiative-convective model of the global climate, *Meteorol. i Gidrol.*, 8, 59-68 (in Russian).
- Karol et al., 1986: Radiative-photochemical models of the atmosphere (p.p. 51-70), Gidrometeoizdat, Leningrad (in Russian).
- Karol I.L., Frolkis V.A., 1992: Estimation of radiative and temperature consequences of ozone content changes in the global atmosphere in 1980-1990, Doklady of Russian Academy of Sciences, 323, 66-69 (in Russian).
- Karol I.L., Jagovkina S.V. 1992: The estimations of the ocean thermal inertia contribution to the greenhouse warming potentials of the freons, *Meteorol. i Gidrol.*, 7, 45-53 (in Russian).
- Ramaswamy V., Schwarzkopf M.D., Shine K.P., 1992: Radiative forcing of climate from halocarbon induced global stratospheric ozone loss, *Nature*, 355, 810-812.
- WMO/UNEP, 1991: Scientific Assessment of Ozone Depletion 1991, WMO Global Ozone Res. and Monitoring Project, Rep. N25, Washington D.C.

TEMPERATURE DEPENDENT ABSORPTION CROSS-SECTIONS OF HNO₃ AND N₂O₅

Oliver V. Rattigan, Matthew H. Harwood, Rod L. Jones and Richard A. Cox

Department of Chemistry, University of Cambridge, Lensfield Road, Cambridge CB2 1EW, UK

Abstract

Absorption cross-sections for HNO₃ and N₂O₅ have been measured in the wavelength region 220-450 nm, using a dual beam diode array spectrometer with a spectral resolution of 0.3 nm. The results for both compounds are in good agreement with recommended values at room temperature. However, the cross-sections of both HNO₃ and N₂O₅ show a marked reduction with decreasing temperature in the range 295-233 K. The calculated photolysis rate of HNO₃ at the low temperatures and high solar zenith angles characteristic of the polar winter and spring is significantly lower than previously estimated.

1. Introduction

Nitric acid and di-nitrogen pentoxide are important reservoir compounds for stratospheric nitrogen oxides. Both compounds sequester stratospheric NO_x, and consequently they play an important role in determining the extent to which high levels of active chlorine oxides are available for ozone destruction in the low stratosphere during polar winter-time (S. Solomon, 1990). The release of NO_x from HNO₃ and N₂O₅ occurs mainly by photodissociation:



In the stratosphere, ozone absorption strongly attenuates solar radiation in the spectral region 220-290 nm. Consequently at high altitudes (above 30 km) the photodissociation of HNO₃ and N₂O₅ is caused principally by light of wavelengths around 200 nm whereas in the lower stratosphere (below 20 km) wavelengths longer than 300 nm become more important (F. Biaume, 1973/74). It is in these spectral regions and at temperatures typical

of the low-stratosphere that it is particularly important to know the absorption cross-sections of HNO₃ and N₂O₅.

There have been few previous investigations of the cross-sections of these species. Currently recommended values (DeMore *et al.*, 1990; Atkinson *et al.*, 1989) are based on the work by Molina and Molina (1981) for HNO₃ and Yao *et al.*, (1982) for N₂O₅. The recommended data for HNO₃ are in good agreement with the earlier results of Biaume (1973/74) and Johnston and Graham (1973) except in the long wavelength tail of the absorption where uncertainties are rather large. There are no previous reported studies of the temperature dependence of the HNO₃ cross-sections. Values of cross-sections for N₂O₅ presented by Yao *et al.*, (1982) are higher than those in the previous studies of Jones and Wulf, (1937) and Johnston and Graham, (1974). The only temperature dependent measurement of the cross-sections for N₂O₅ is reported by Yao *et al.*, (1982) and the data show large scatter in the wavelength region above 340 nm.

We have therefore reinvestigated the ultraviolet absorption spectra of HNO₃ and N₂O₅, with particular emphasis on the determination of the temperature dependencies of the cross-sections in the longer wavelength regions.

2. Experimental Details

Absorption cross-section measurements were made using a dual beam diode array spectrometer which has been described in detail previously (Rattigan *et al.*, 1992). N₂O₅ was produced by the reaction of NO (B.O.C. special gases) with ozonised oxygen, produced by the action of a discharge ozoniser (Argentox GL10) on a flow of O₂ (Distillers M.G.). HNO₃ was prepared by vacuum distillation of a 3:2 mixture of previously cooled sulphuric acid (98%) and nitric acid (70%) held at 273 K, into a trap cooled to 203 K. NO₂ (Cambrian Gases) was mixed with N₂ (Distillers MG) to give a sample suitable for producing NO₂ reference spectra in the ultraviolet

region. The concentration of NO_2 in the mixture was established using the recommended absorption cross-sections for NO_2 at room temperature (DeMore *et al.*, 1990).

The major impurity in the HNO_3 was found to be NO_2 . N_2O_5 samples were contaminated with both NO_2 and HNO_3 . At low temperatures, in both cases significant association of NO_2 into N_2O_4 was expected to occur and the effects of this were also taken into account. Corrections for any NO_2 present in the samples were performed by the scaled subtraction of NO_2 reference spectra, using the characteristic vibrational structure of NO_2 in the region above 320 nm. The effect of N_2O_4 in samples of HNO_3 was taken into account by recording NO_2 reference spectra at each temperature at pressures as close as possible to that of the NO_2 present in the samples. The assumption being that the quantities of N_2O_4 were equal in both samples. In the experiments on N_2O_5 the correction for N_2O_4 was calculated at each temperature using the known equilibrium constant for the self reaction of NO_2 and the measurements of NO_2 reference spectra at different partial pressures. The amount of HNO_3 impurity in the samples of N_2O_5 was calculated using its characteristic infrared absorption bands. Subtraction of the contribution of HNO_3 to the ultraviolet absorbance was then performed using the values of HNO_3 cross-section recommended in this paper.

3. Results

Measurements of HNO_3 absorption spectra from 200-344 nm were made in the temperature range 238-297 K. Figure 1 illustrates the temperature dependence of the cross-section in the region 270-320 nm, using the data at 295 K, 263 K and 238 K. The spectra show a definite decline in the cross-section throughout the region, the effect being particularly noticeable near the long wavelength tail.

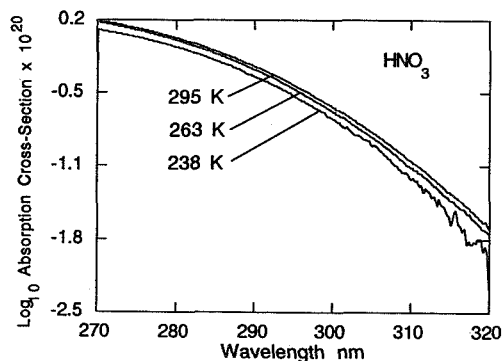


Fig. 1 Temperature dependence of nitric acid absorption cross-section in the wavelength range 270-320 nm.

N_2O_5 absorption spectra were measured in the region 230-450 nm at temperatures from 295 K to 233 K. At each temperature, spectra were measured at several pressures up to the maximum somewhat less than the vapour pressure at that temperature. After the contribution of impurities to the spectra had been removed, the Beer-Lambert law was found to be obeyed by HNO_3 and N_2O_5 providing the absorbance was less than 0.80.

Errors (expressed as one standard deviation) in HNO_3 cross-sections measured at room temperature were approximately 2.5% for wavelengths below 300 nm, increasing to approximately 95% near the limit of detectable absorption at about 335 nm. At the lowest temperature used, HNO_3 cross-sections had errors of 6.5% at 300 nm increasing to 95% at 320 nm. Errors in values of cross-sections for N_2O_5 were calculated from the combined effect of systematic and random errors where random errors are calculated as 95% confidence limits. The errors are 11% for the region 260-360 nm, 12% for 360-380 nm, and 35% for 380-410 nm.

4. Discussion

4.1. Comparison with previous work

The HNO_3 absorption cross-sections measured at 294 K in the present work are in very good agreement with those values reported by Molina and Molina, (1981), Biaueme, (1973/74) and Graham and Johnston, (1973) at wavelengths below 300 nm, see Figure 2.

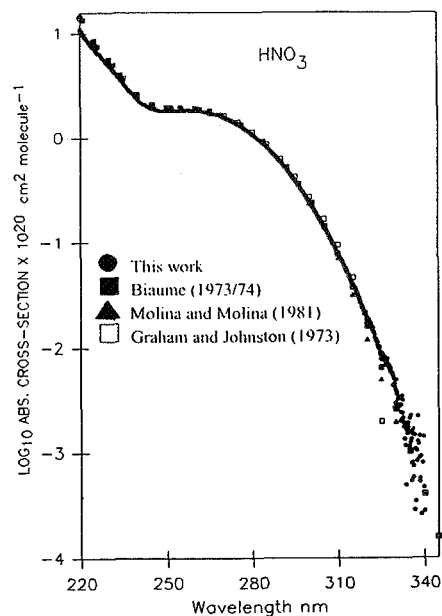


Fig. 2 Comparison of HNO_3 cross-sections at room temperature with previous measurements.

The large uncertainties in the long wavelength region are due to the difficulties involved in correction for the absorbance of NO₂. The present technique provides more spectral information for making this correction, but our samples contained more NO₂ than those measured by Biaueme, (1973/74). Molina and Molina, (1981) did not report details of any corrections made for NO₂. The consistency of the cross-sections determined here with differing amounts of NO₂ gives us confidence in the values we report, which are slightly higher above 310 nm than those recommended by both the NASA (DeMore et al., 1990) and IUPAC (Atkinson et al., 1989) evaluations.

The cross-sections for N₂O₅ from the present work show good agreement with the values of Yao *et al.*, (1982), Table 1. However their NO₂ reference spectra were recorded on a different instrument to that which was used for the N₂O₅ work and the different instrument functions gave rise to a wide scatter in the results above 340 nm where spectral subtraction of NO₂ must be performed. The values of Jones and Wulf, (1937) are lower than those measured here probably due to the presence of HNO₃ in their samples which was not accounted for.

Table 1.
Absorption cross-sections for N₂O₅ /10⁻²⁰ cm² molecule⁻¹

Wavelength nm	295 K		273 K	
	Present work.	Yao <i>et al.</i> (1982)	Present work	Yao <i>et al.</i> (1982)
280	10.5	10.1	9.95	10.0
290	6.46	6.80	6.03	6.44
300	3.76	3.84	3.43	3.43
310	2.10	2.15	1.88	1.83
320	1.17	1.20	0.970	0.98
330	0.645	0.67	0.470	0.52
340	0.347	0.37	0.246	0.28
350	0.198	0.21	0.131	0.15
360	0.115	0.12	0.071	0.080
370	0.068	0.066	0.041	0.043
380	0.040	0.037	0.023	0.023

4.2 Temperature Dependence

The best fit to the temperature dependence of the HNO₃ cross-sections measured here was obtained by plotting log₁₀ (cross-section) versus temperature and by performing a linear least squares analysis fit to the data. This function allowed the extrapolation of absorption cross-sections to any chosen temperature in the range 200-300 K. Table 2 shows recommended cross-sections at 298 K, which were obtained by averaging the data from the present work together with those of Biaueme, (1973/74), Molina and Molina, (1981) and Johnston and Graham, (1973), together with the recommended temperature coefficients from the present work. Cross-sections

at any temperature can then be calculated from the following expression: log₁₀(σ_T) = log₁₀(σ₂₉₈) + B[T-298].

Table 2. Recommended absorption cross-sections for HNO₃.

Wavelength nm	σ ₂₉₈ /10 ⁻²⁰ cm ² molecule ⁻¹	B/10 ⁻³ K ⁻¹
190	1560.0	0
200	661.0	0
210	105.0	1.09
220	14.1	1.09
230	5.45	1.52
240	2.44	1.52
250	1.92	1.52
260	1.86	1.52
270	1.59	1.52
280	1.10	1.52
290	0.613	1.95
300	0.243	2.61
310	0.081	3.91
320	0.017	7.82
330	0.003	>7.82

Data for N₂O₅ was collected at 295, 273, 253, and 233 K. Results from 295 and 273 are displayed in Table 1 and the agreement at both temperatures with the recommended values (DeMore et al., 1990 and Atkinson et al., 1989) is good. Analysis of results at the lowest temperatures which require correction for the presence of N₂O₄ has yet to be performed.

4.3 Atmospheric photolysis rates

Atmospheric photolysis rates for HNO₃ were computed using the cross-section values recommended in Table 2. These calculations were carried out using the model of Lary (1991) for a range of temperatures, altitudes and solar zenith angles (SZA). The results illustrated in Figure 3, show that the photolysis rates decrease monotonically with temperature at all altitudes and SZAs, the decline is most prominent at low altitudes and high SZAs. At lower altitudes and high SZAs ozone strongly attenuates the incoming solar radiation at wavelengths below 290 nm. The remaining light intensity available for photolysis is therefore at longer wavelengths where the HNO₃ cross-section shows the greatest temperature dependence.

These results indicate that the photolysis rate for HNO₃ at temperatures appropriate to the low stratosphere is lower than that using the previous recommended values for the HNO₃ cross-sections (DeMore et al., 1990 and Atkinson et al., 1989). Consequently, reactive chlorine released

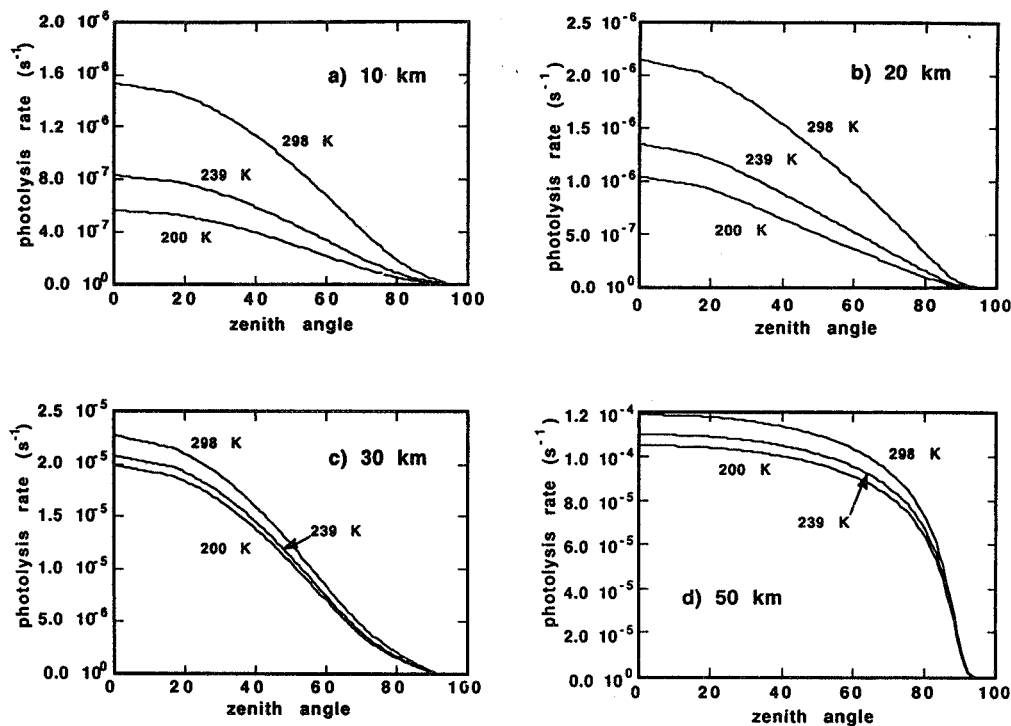


Fig. 3 Dependence of the photolysis rate of HNO_3 on solar zenith angle and temperature at four different altitudes: a = 10 km; b = 20 km; c = 30 km; d = 50 km.

heterogeneously either on background aerosol or polar stratospheric clouds will be longer lived, and a greater ozone loss might be expected through the established mechanisms involving ClO and BrO (Solomon, 1990).

4.4 Future work

Analysis of the low temperature data for N_2O_5 will allow photolysis rates to be calculated in a similar way. Any likely effects on our understanding of the nitrogen partitioning of the atmosphere will then be considered.

5. References

- Atkinson, R., D.L. Baulch, R.A. Cox, R.F. Hampson, J.A. Kerr, and J. Troe, "Evaluated Kinetic and Photochemical data for Atmospheric Chemistry", *J. Phys. Chem. Ref. Data*, 18, 881, (1989).
- Biaume, F., "Nitric acid vapour absorption cross-section spectrum and its photodissociation in the stratosphere", *J. Photochem.*, 2, 139, (1973/74).
- DeMore, W.B., M.J. Molina, S.P. Sander, D.M. Golden, R.F. Hampson, M.J. Kurylo, C.J. Howard, and A.R. Ravishankara, "Chemical Kinetics and Photochemical Data for use in Stratospheric Modelling", *JPL Publications 90-1*, (1990).
- Johnston, H., and R. Graham, "Photochemistry of NO_x and HNO_x compounds", *Can. J. Chem.*, 52, 1415, (1974).
- Johnston, H., and R. Graham, "Gas phase ultraviolet absorption spectrum of HNO_3 vapour", *J. Phys. Chem.*, 77, 62, (1973).
- Jones, E.L., and O.R. Wulf, "The absorption coefficient of N_2O_5 in the ultraviolet and the visible absorption spectrum of NO_3 ", *Chem., Phys.* 5, 873, (1937).
- Lary, D., *Ph.D. Dissertation*, University of Cambridge, 1991.
- Molina, L.T., and M.J. Molina, *J. Photochem.*, 15, 97, (1981).
- Solomon, S., "Progress toward a quantitative understanding of Antarctic ozone depletion", *Nature*, 347, 347, (1990).
- Yao, F., I. Wilson and H. Johnston, "Temperature-dependent ultraviolet absorption spectrum for N_2O_5 ", *J. Phys. Chem.*, 86, 3611, (1982).

303924

RADIATIVE FORCING PERTURBATION DUE TO OBSERVED INCREASES IN TROPOSPHERIC OZONE AT HOHENPEISSENBERG

Wei-Chyung Wang¹, Rumen D. Bojkov², and Yi-Cheng Zhuang¹

1. State University of New York at Albany, New York
2. World Meteorological Organization, Geneva

1. Introduction

The effect on surface temperature due to changes in atmospheric O₃ depends highly on the altitude where the change occurs. Previous sensitivity calculations indicate that ozone changes in the upper troposphere and lower stratosphere are more effective in causing surface temperature change (Wang et al., 1980). Long term ground-based observations show that tropospheric ozone, especially at the tropopause region, has been increasing at middle and high latitudes in the Northern Hemisphere (NATO, 1988; Quadrennial Ozone Symposium, 1992). These increases will enhance the greenhouse effect and increase the radiative forcing to the troposphere-surface system, which is opposite to the negative radiative forcing calculated from the observed stratospheric ozone depletion recently reported in WMO (1992).

We used more than two thousands regularly measured ozonesondes providing reliable vertical O₃ distribution at Hohenpeissenberg (47N; 11E) for the 1967-1990 to study the instantaneous solar and longwave radiative forcing during the two decades 1971-1990 and compare the forcing with those caused by increasing CO₂, CH₄, N₂O, and CFCs. Calculations are also made to compare the O₃ radiative forcing between stratospheric depletion and tropospheric increase. Results indicate that the O₃ changes will induce a positive radiative forcing dominated by tropospheric O₃ increase and the magnitude of the forcing is comparable to that due to CO₂ increases during the two decades. The significant implications of the tropospheric O₃ increase to the global climate are discussed.

2. Ozone Variations

Variations of the O₃ concentration in the stratosphere and troposphere are shown in Fig. 1. Note that the tropopause is assumed to be ~200 and 300 mb for summer and winter, respectively, and ~250 mb for spring and fall. The data indicate that, during this period, O₃ decreases in the stratosphere for all seasons and the decrease is particularly large in winter and spring. On the other hand, tropospheric O₃ has been steadily increasing and the increases are larger in spring and summer. Figure 2 shows the changes of the January and July O₃ vertical distribution between two decades, 1971-80 and 1981-90. On the decadal time scale, the stratospheric O₃ decreases 10-12% around 13-18 km in January while tropospheric O₃ increases 20-30% between 5-8 km for both months. Note that since the tropospheric O₃ amount is about 7-13% of the total column (see Fig. 1), the trend of the total O₃ at Hohenpeissenberg over the whole period show a decline by 2.3%/decade [WMO, 1992].

3. Radiative Forcing

To carry out the solar and longwave radiation calculations, we used (a) the January and July climatological temperature and moisture, (b) incoming solar radiation based on the middle of January and July with corresponding surface albedo 0.4 and 0.2, respectively. For the results shown below, we used clear sky condition.

The effects on the solar and longwave radiative fluxes to the troposphere-surface climate system due to changes in atmospheric O₃ will depend on the

altitudes where O₃ changes. For example, a decrease in stratospheric O₃ is to provide: (a) a warming effect due to increased available solar radiation for absorption and (b) a cooling effect due to decreased downward longwave radiation; the net effect will depend on the location and time of the year. On the other hand, an increase in tropospheric O₃ can warm the troposphere-surface system through increased in absorption of both the solar radiation and longwave radiation. Table 1 shows the calculated solar and longwave radiative forcing due to observed O₃ changes at Hohenpeissenberg. To examine the relative importance of the vertical O₃ changes, we include the calculations of the radiative forcing due to changes in the individual stratosphere and troposphere. Note that in January the total radiative forcing 0.13 Wm⁻² is dominated by the longwave radiative forcing. On the other hand, in July, the total forcing of 0.62 Wm⁻² contributed almost equally from the solar and longwave radiative forcing. Note also that the total longwave radiative forcing is contributed mainly from tropospheric O₃ changes while stratospheric O₃ plays minor role.

Comparison of the radiative forcing between O₃ changes and increases of greenhouse gases CO₂, CH₄, N₂O, and CFCs between the two decades are shown in Table 2. The total radiative forcing is calculated to be 0.5 and 1.1 Wm⁻² respectively for January and July. In January, CO₂ accounts for about 46% of the total forcing while the effect of O₃ is to contribute 26% of the forcing. On the other hand, O₃'s effect in July dominates and accounts for over half of the total forcing.

4. Conclusions and Discussion

It appears that the observed decrease in stratospheric O₃ and increase in tropospheric O₃ during the last two decades at Hohenpeissenberg can contribute substantially to a warming of the local troposphere-surface climate system. The calculations indicate that O₃ changes can account to 26% and 56% respectively of the total January and July radiative forcing of all the greenhouse gases. In addition, the O₃ radiative forcing is dominated by the increases of the tropospheric O₃ while

Table 1 Radiative forcing (Wm⁻²) for the troposphere-surface system due to O₃ changes between the 1971-80 and 1981-90.

Month	Stratosphere		Troposphere		Total	
	SW	LW	SW	LW	SW	LW
January	0.006	0.007	0.001	0.125	0.007	0.130
July	0.213	-0.036	0.110	0.338	0.324	0.302

SW and LW refer to solar and longwave radiation respectively; The tropopause is 300 mb for January and 200 mb for July.

Table 2 Changes of the total radiative forcing (Wm⁻²; SW+LW) for the troposphere-surface system due to O₃ changes and increasing other gases CO₂, CH₄, N₂O, and CFCs between 1971-80 and 1981-90.

Month	O ₃	CFCs	CO ₂	CH ₄	N ₂ O	Total
January	0.137 (26.3)	0.066 (12.7)	0.238 (45.7)	0.064 (12.2)	0.016 (3.1)	0.521
July	0.610 (56.1)	0.105 (9.7)	0.270* (24.8)	0.083 (7.6)	0.019 (1.8)	1.087

Values in parenthesis are percentage of the total.

*The results include a radiative forcing -0.016 Wm⁻² due to changes of SW by CO₂ increases.

stratospheric O₃ decrease plays a minor role. This finding will have broad climate implications since the other ground ozonesonde stations located in middle and high latitudes of the Northern Hemisphere all show an increase of the tropospheric O₃.

References

NATO, 1988: Tropospheric Ozone: Regional and Global Scale Interactions. Ivar S. A. Isaksen (Ed.), NATO Advanced Science Institutes Series, D. Reidel Publ. Co., Dordrecht/Boston/Lancaster/Tokyo, pp 425.

Quadrennial Ozone Symposium, 1992: University of Virginia, Charlottesville, Virginia, June 4-12, 1992.

World Meteorological Organization, 1992: Scientific Assessment of Ozone Depletion: 1991.

Wang, W.-C., J. P. Pinto and Y. L. Yung, 1980: Climatic effects due to halogenated compounds in the earth's atmosphere. J. Atmos. Sci., 37, 333-338.

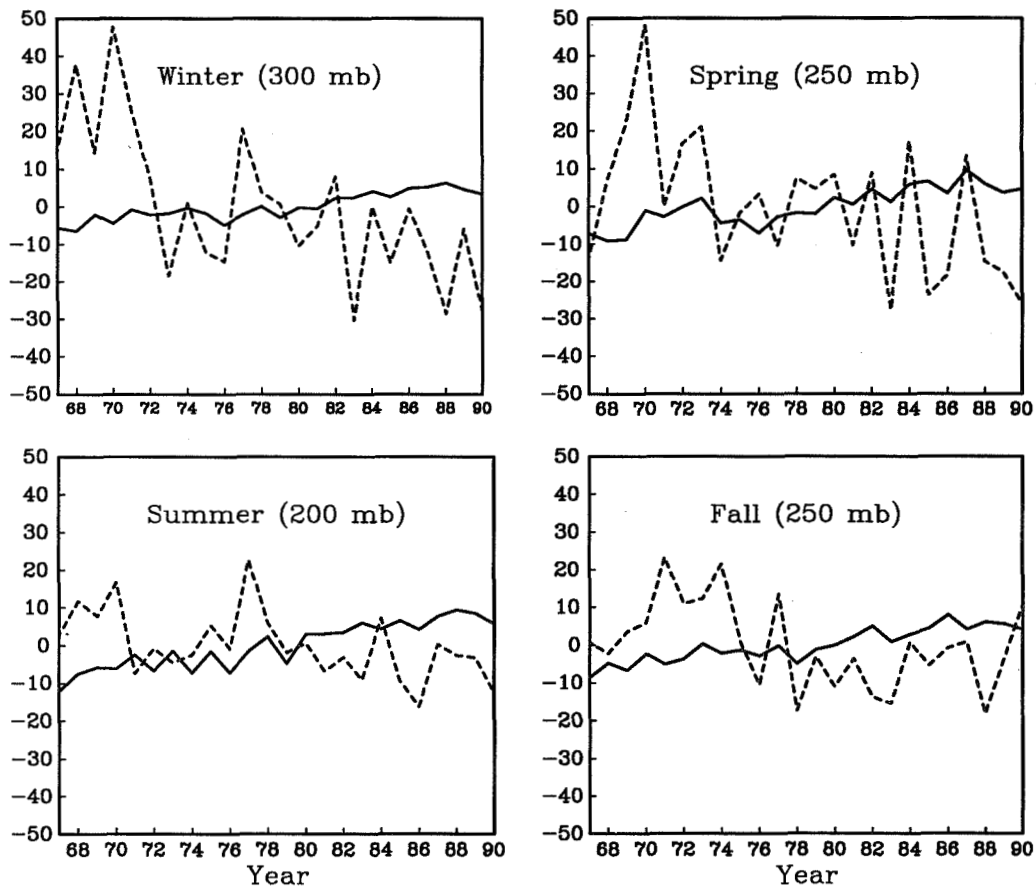


Figure 1: Seasonal variations of O₃ (DU) in the stratosphere (dashed line) and troposphere (solid line) at Hohenpeissenberg for the period 1967-1990. The first number inside the parenthesis is the mean value for the troposphere while the second number is for the stratosphere. The four seasons are winter (December-January-February), spring (March-April-May), summer (June-July-August) and fall (September-October-November). The tropopause is ~200 mb for summer, ~250 mb for spring and fall, and ~300 mb for winter.

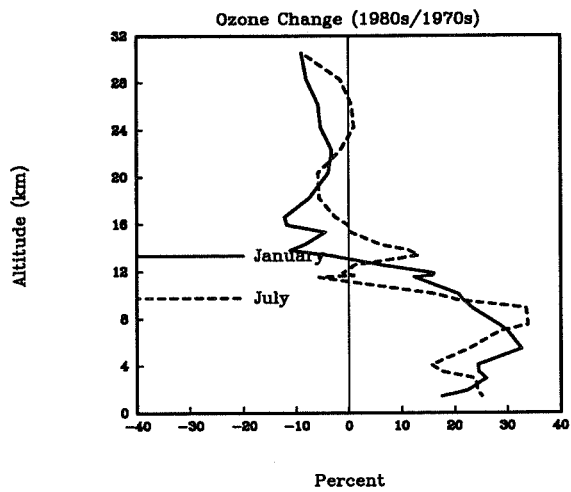


Figure 2: Vertical distribution of change in mean O_3 (%) between the 1971-80 and 1981-1990 at Hohenpeissenberg.

303925

TEMPERATURE DEPENDENCE OF ULTRAVIOLET ABSORPTION
CROSS-SECTIONS OF ALTERNATIVE HYDROCHLOROFLUOROCARBONS.

D. GILLOTAY, P. C. SIMON and L. DIERICKX

INSTITUT D'AERONOMIE SPATIALE DE BELGIQUE.
3, Avenue Circulaire, B-1180 BRUSSELS, BELGIUM.

ABSTRACT

Ultraviolet absorption cross-section of six alternative hydrochlorofluorocarbons (HCFC-21, HCFC-22, HCFC-123, HCFC-124, HCFC-141b and HCFC-142b) and of one alternative hydrobromofluorocarbon (Halon-22b1) have been measured between 170 and 260 nm for temperature ranging from 210 to 295 K. These data are compared with other available determinations performed at room temperature. and their temperature dependence is discussed. Photodissociation coefficients are estimated and their temperature dependence is discussed. Impact of the photodissociation on the total atmospheric destruction of these compounds is illustrated.

I. INTRODUCTION.

Since the 'Montreal Protocole on substances that deplete the ozone layer', alternative CFCs are actively pursued to replace classical CFCs and Halons in many of their applications. Among them, partially hydrogenated halocarbons are relatively vulnerable to OH radical attack at tropospheric altitude which will remove a great part of them before reaching the stratosphere where the remaining HCFC molecules will be photolysed or will react with OH or O(¹D) radicals.

Determination of lifetime and ozone depletion potential of these molecules require an accurate knowledge of the UV absorption cross-sections as a function of wavelength and temperature. The purpose of this paper is to compare available absorption cross-section data of HCFCs, to discuss their temperature dependence and to show the importance of the photolysis in the remove of these alternative compounds in the troposphere and the stratosphere. New investigations of cross-sections of Halon-22b1 will also be presented.

II. EXPERIMENTAL.

Ultraviolet absorption cross-sections and their temperature-dependence were determined by means of a double beam experimental device previously described (Gillotay et al., 1988) which includes a 40W-deuterium lamp or a FEL 1000W tungsten filament lamp as light

source, a 1 m Mc Pherson 225 monochromator, 200 cm and 20 cm thermostated absorption cells (one of them being used as reference channel), EMR type 542 P-09-18 solar blind photomultipliers, and a data acquisition system. The bandwidth is 0.1 nm and the wavelength repeatability ± 0.01 nm. The pressure inside the cell ranging from 2×10^{-3} to 1×10^3 Torr, is measured by means of three capacitance MKS Baratron manometers 170-315 with a 1, 10, and 1000 Torr full scale range. A regular calibration of these manometers allows a precision better than ± 0.1 %. Low temperatures are determined with absolute uncertainties of around ± 1 K and a temperature stability of around ± 0.3 K is usually observed. The purity of the seven compounds is better than 99.5 % as determined by gas phase chromatography.

III. RESULTS.

Numerical values of absorption cross-sections for wavenumber intervals of 500 cm^{-1} have already been reported for the six HCFCs (Simon et al., 1988, Gillotay and Simon, 1991a, 1991b) and are given in table I for Halon-22b1.

In all cases, Beer-Lambert's law was verified for absorption ranging from 10 to 85 %. In such conditions, and according to the error budget previously published, (Simon et al., 1988), the absorption cross-sections reported here are determined with an accuracy of ± 2 % at room temperature and of ± 3 to ± 4 % at the lowest temperature.

Halon-22b1 display a continuous absorption spectra with a maximum around 200nm and a temperature dependence already observed in the case of other Halon, increase of the absorption cross-sections with the temperature for the smaller wavelengths and near the maximum and decrease of these cross-sections for the longer wavelengths.

The relative absorption cross-sections at room temperature of HCFC-123, HCFC-124, HCFC-141b and HCFC-142b are illustrated in Figures 1-4 (Ref = WHO,1990) and show large discrepancies up to 60 % for HCFC-123, for the low values of absorption. In addition, some reported temperature dependence are not coherent with the usual exponential decrease of cross-section values at low temperature. These two issue raise question on the experimental uncertainties when measuring low optical thickness values

IV. DISCUSSION.

Photodissociation coefficients of the molecules have been calculated, neglecting the effects of multiple scattering, for given altitude (z), zenith angle (χ) and wavelengths intervals according to the relation :

$$J(z) = \sigma_{\lambda} q_{\lambda}(z) \quad ; \quad q_{\lambda}(z) = q_{\lambda}(\infty) e^{-\tau_{\lambda}(z)}$$

$$\tau_{\lambda}(z) = \int_z^{\infty} [n(O_2) \sigma_{\lambda}(O_2) + n(O_3) \sigma_{\lambda}(O_3) + n(\text{air}) \sigma_{\text{scatt}}] \sec \chi dz$$

where

z is the altitude,

σ are the absorption cross-sections,

$q_{\lambda}(z)$ and $q_{\lambda}(\infty)$ are the solar irradiance at altitude z or extraterrestrial ($z = \infty$)

n is the number of particles per volume unit.

Calculations are made for solar zenith angle of 0° and 60° ($\sec = 1$ and 2), taking into account the values of $\sigma(O_2)$ and $\sigma(O_3)$ from WMO and Kockarts (1976), σ_{scatt} from Nicolet (1984) and the values of $q(\infty)$ from WMO (1986) and by taking into account the actual values of cross-sections corresponding to the temperature conditions at each altitude.

The loss rates calculated with the WMO rate constants and the photodissociation coefficients corresponding to the temperature conditions at each altitude are represented as a function of altitude in Figures 5-11. These figures show clearly the importance of photolysis relative to the reaction with OH and $O(^1D)$ radicals. At tropospheric altitude, reaction with OH and $O(^1D)$ are in all the cases the main removal mechanisms. Photolysis becomes the main process in the stratosphere for HCFC-123, HCFC-141b and Halon-22b1, but remains of lower or equal importance for all the other compounds.

V. REFERENCE.

- ALLIED-SIGNAL CORPORATION, 1989, in WMO report 20
- GILLOTAY D., A. JENOUVIER, B. COQUART, M.F. MERIENNE, and P.C. SIMON, 1898, Ultraviolet absorption cross-sections of Bromoform in the temperature range 295-240 K., Planet. Space Sci., 37, 1127-1140.
- GILLOTAY D. and P.C. SIMON, 1991a Temperature dependence of ultraviolet absorption cross-sections of alternative chlorofluoroethanes., J. Atmos. Chem., 12, 269-285.
- GILLOTAY D. and P.C. SIMON, 1991b Temperature dependence of ultraviolet absorption cross-sections of alternative chlorofluoroethanes. 2. The 2-chloro-1,1,1,2 tetrafluoro ethane - HCFC-124., J. Atmos. Chem., 13, 289-299.
- HUBRICH, C. and F. STUHL, 1980, The ultraviolet absorption of some halogenated methanes and ethanes of atmospheric interest., J. Photochem., 12, 93-107.
- KOCKARTS G., 1976, Absorption and photodissociation in the Schumann-Runge bands of molecular oxygen in terrestrial atmosphere., Planet. Space Sci., 24, 589-604
- ORLANDO, J.J., J.B. BURKHOLDER, S.S. McKEEN and A.R. RAVISHANKARA, 1990, the atmospheric fade of several hydrochlorofluoroethanes 2. Temperature dependence of UV absorption cross sections and atmospheric lifetimes., J. Geophys. Res., 96, 5013-5023.
- MOLINA M.J. and L.T. MOLINA, 1989, in WMO report 20.
- NICOLET M., 1984, On the molecular scattering in the terrestrial atmosphere : an empirical formula for calculation in the homosphere., Planet. Space Sci., 32, 1467-1468.
- SIMON P.C., D. GILLOTAY, N. VANLAETHEM-MEUREE, and J. WISEMBERG, 1988, Ultraviolet absorption cross-sections of chloro and chlorofluoromethanes at stratospheric temperatures., J. Atmos. Chem., 7, 107-1345.
- WMO, 1986, Atmospheric ozone 1985, WMO global ozone research and monitoring project, Report 14.
- WMO, 1990, Scientific assessment of stratospheric ozone, 1989, Report 20, Volume II.

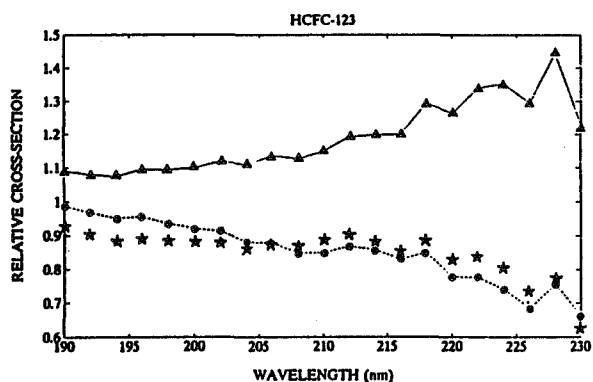


Figure 1

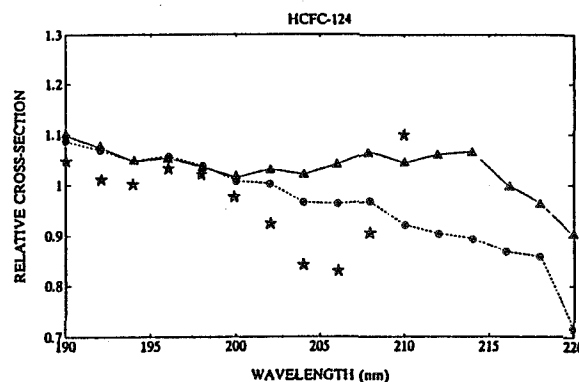


Figure 2

Figures 1-4 Relative absorption cross-sections

- ▲ : Gillotay and Simon, 1991a, 1991b.
- : Molina and Molina, 1989.
- * : Allied-Signal Corporation, 1989.
- + : Hubrigh and Stuhl, 1980.

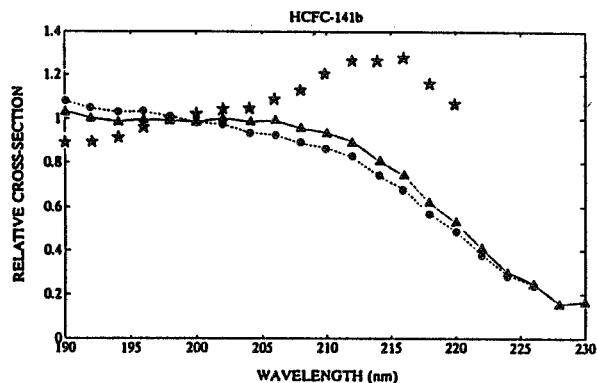


Figure 3

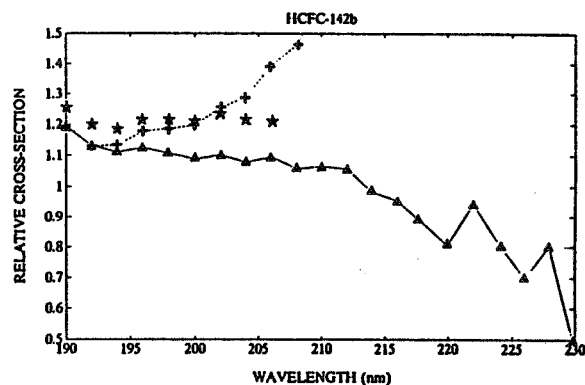


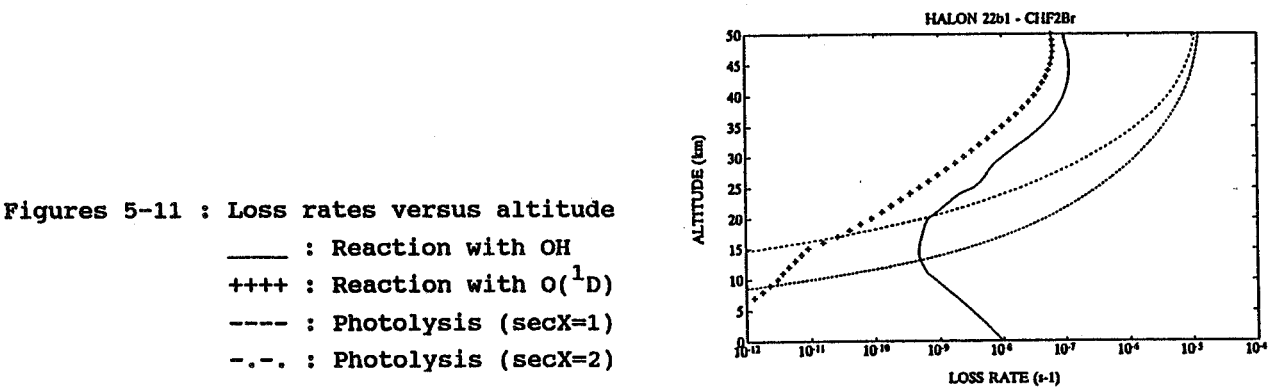
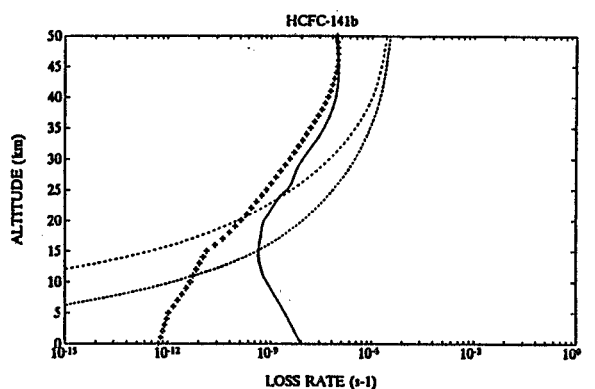
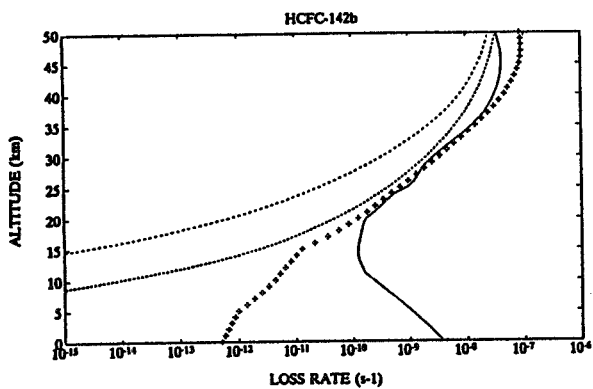
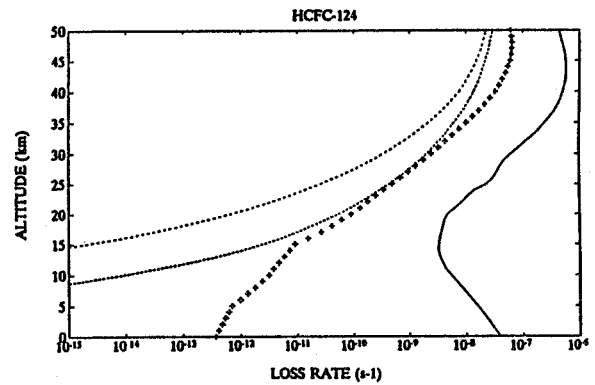
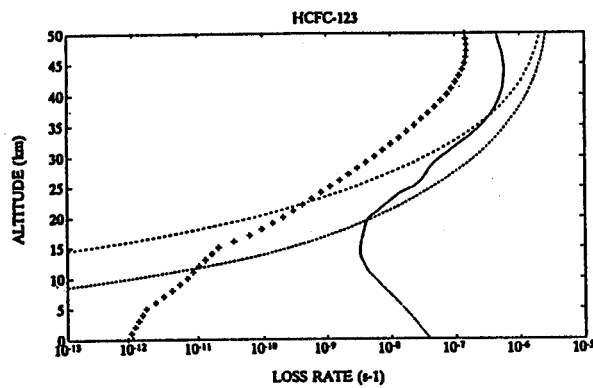
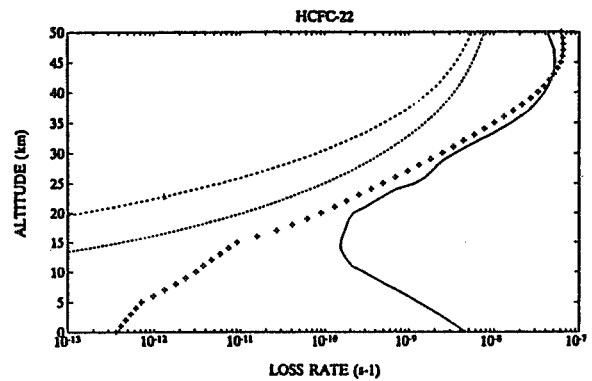
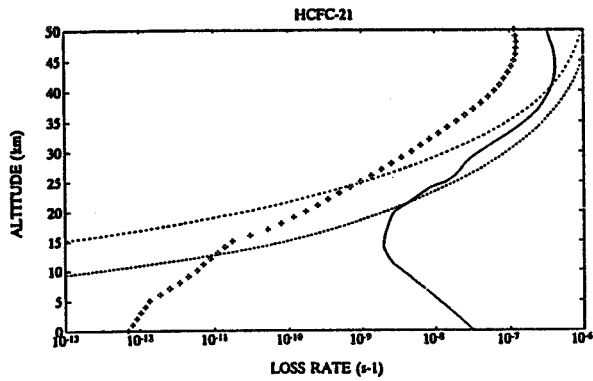
Figure 4

Figures 1-4 Relative absorption cross-sections

- ▲ : Gillotay and Simon, 1991a, 1991b.
- : Molina and Molina, 1989.
- * : Allied-Signal Corporation, 1989.
- + : Hubrish and Stuhl, 1980.

Table I CHF₂Br - Halon 22b1

		$\sigma(\lambda) \times 10^{21} \text{ (cm}^2 \text{ molec.}^{-1}\text{)}$				
N°	(nm)	295K	270K	250K	230K	210K
42	166.7-169.5	39.7	47.2	54.2	62.2	71.5
43	169.5-172.4	82.1	89.9	96.7	104	112
44	172.4-173.9	125	131	137	143	149
45	173.2-175.4	156	162	166	171	175
46	175.4-177.0	188	191	196	200	204
47	177.0-178.6	219	223	226	229	232
48	178.6-180.2	245	249	253	257	260
49	180.2-181.8	266	272	277	282	287
50	181.8-183.5	283	291	298	305	312
51	183.5-185.2	296	304	311	318	325
52	185.2-186.9	306	314	320	327	333
53	186.9-188.7	314	322	328	334	340
54	188.7-190.5	320	327	333	339	346
55	190.5-192.3	323	330	336	343	349
56	192.3-194.2	323	330	336	343	349
57	194.2-196.1	319	327	333	339	346
58	196.1-198.0	312	320	326	332	338
59	198.0-200.0	301	309	315	321	327
60	200.0-202.0	286	294	299	305	311
61	202.0-204.1	268	275	280	286	291
62	204.1-206.2	247	253	258	262	267
63	206.2-208.3	224	229	233	236	240
64	208.3-210.5	200	203	206	209	211
65	210.5-212.8	174	176	177	179	181
66	212.8-215.0	149	149	150	150	151
67	215.0-217.4	124	124	123	123	122
68	217.4-219.8	101	99.6	98.3	97.1	95.9
69	219.8-222.2	80.6	78.3	76.5	74.8	73.1
70	222.2-224.7	62.6	59.9	57.9	55.9	53.9
71	224.2-227.3	47.1	44.3	42.1	40.1	38.2
72	227.3-229.9	34.5	31.7	29.7	27.8	26.1
73	229.9-232.6	24.5	22.1	20.3	18.7	17.2
74	232.6-235.3	16.9	14.9	13.4	12.1	10.9
75	235.3-238.1	11.4	9.73	8.59	7.58	6.69
76	238.1-241.0	7.41	6.17	5.33	4.60	3.97
77	241.0-243.9	4.62	3.73	3.15	2.66	2.24
78	243.9-246.9	2.82	2.22	1.83	1.50	1.24
79	246.9-250.0	1.65	1.26	1.01	0.814	0.655
80	250.0-253.2	0.963	0.715	0.564	0.445	0.351
81	253.2-256.4	0.525	0.381	0.294	0.228	0.176
82	256.4-259.7	0.288	0.205	0.156	0.119	0.0909
83	259.7-263.2	0.148	0.104	0.0788	0.0596	0.0450
84	263.2-266.7	0.0755	0.0533	0.0403	0.0305	0.0231



Figures 5-11 : Loss rates versus altitude
 — : Reaction with OH
 +++ : Reaction with O(¹D)
 ---- : Photolysis (secX=1)
 -.-. : Photolysis (secX=2)

303926

ULTRAVIOLET ABSORPTION CROSS-SECTIONS OF SOME
CARBONYL COMPOUNDS AND THEIR TEMPERATURE DEPENDENCE.

D. GILLOTAY, P. C. SIMON and L. DIERICKX

INSTITUT D'AERONOMIE SPATIALE DE BELGIQUE.
3, Avenue Circulaire B-1180, BRUSSELS, BELGIUM.

ABSTRACT

Ultraviolet absorption cross-section of phosgene (CCl_2O), trichloroacetylchloride ($\text{CCl}_3\text{-CClO}$) and trichloroacetaldehyde ($\text{CCl}_3\text{-CHO}$) have been measured between 170 and 320 nm for temperature ranging from 210 to 295 K with a classical double beam equipment.

These data are compared with other available determinations performed at room temperature. Photodissociation coefficients are estimated and their temperature dependence is discussed. Impact of the photodissociation on the total atmospheric destruction of these compounds is illustrated.

I. INTRODUCTION.

Chemical degradation of alternative hydrochloro-fluorocarbons in troposphere produces a series of carbonyl compounds like phosgene, halo-aldehydes or halo-ketones, which could themselves be removed in three ways : (1) Photodissociation by solar UV radiations to produce potential odd chlorine precursors,

- (2) Reaction with H_2O and
- (3) Reaction with OH.

In order to determine the lifetimes for the photolysis processes, an accurate knowledge of the UV absorption cross-sections is required as a function of wavelength and temperature.

II. EXPERIMENTAL.

Ultraviolet absorption cross sections of phosgene (CCl_2O), trichloroacetylchloride ($\text{CCl}_3\text{-CClO}$) and trichloroacetaldehyde ($\text{CCl}_3\text{-CHO}$) have been measured between 170 and 320 nm for temperature ranging from 210 to 295 K with a classical double beam equipment. (Gillotay et al., 1989). The purity of the three compounds is better than 99.5 % as determined by gas phase chromatography.

III. RESULTS.

Numerical values of absorption cross-sections for wavenumber intervals of 500 cm^{-1} are given in tables I-III. The absorption spectra are illustrated in Figures 1-3 for selected temperatures namely 295, 250 and 210 K and compared with other available data at 295 K.

In all cases, Beer-Lambert's law was verified for absorption ranging from 10 to 85 %. In such conditions, and according to the error budget previously published, (Simon et al., 1988), the absorption cross-sections reported here are determined with an accuracy of $\pm 2\%$ at room temperature and of ± 3 to $\pm 4\%$ at the lowest temperature.

Carbonyl compounds display a continuous absorption in the 170-335 nm range. The presence of two maxima and the temperature dependence observed near the maxima and for the longest wavelengths, seems to indicate that there are two continua, one corresponding to the absorption of the C-Cl bond, with a maximum around 170 nm and the other centred respectively at 240 nm for phosgene, around 260 nm for trichloroacetylchloride and at 290 nm for trichloroacetaldehyde, corresponding to the absorption of the C=O bond.

Absorption cross-sections values change with temperature by a factor, which depends on both the wavelength and the chemical composition of the compound. For each wavelength, an exponential dependence of the absorption cross-section versus temperature is clearly established, with a decrease of absorption cross-sections in the region of low absorptions (up to 80 % at 305 nm and 210 K in the case of CCl_2O) and a small increase near the maximum of absorption (up to 5 %). This effect is the most important at the lowest temperature.

Discrepancies observed between the different set of available data at room temperature have to be discussed in more details in terms of experimental conditions.

IV. DISCUSSION.

Photodissociation coefficients of the molecules have been calculated, neglecting the effects of multiple scattering, for given altitude (z), zenith angle (χ) and wavelengths intervals according to the relation :

$$J(z) = \sigma_{\lambda} q_{\lambda}(z) \quad ; \quad q_{\lambda}(z) = q_{\lambda}(\infty) e^{-\tau_{\lambda}(z)}$$

$$\tau_{\lambda}(z) = \int_z^{\infty} [n(\text{O}_2) \sigma_{\lambda}(\text{O}_2) + n(\text{O}_3) \sigma_{\lambda}(\text{O}_3) + n(\text{air}) \sigma_{\text{scatt}}] \sec \chi dz$$

where

z is the altitude,

σ are the absorption cross-sections,

$q(z)$ and $q(\infty)$ are the solar irradiance at altitude z or extraterrestrial ($z = \infty$)

n is the number of particles per volume unit.

Calculations are made for solar zenith angle of 0° and 60° (sec = 1 and 2), taking into account the values of $\sigma(O_2)$ and $\sigma(O_3)$ from WMO and Kockarts (1976), σ_{scatt} from Nicolet (1984) and the values of $q(\infty)$ from WMO (1986) and by taking into account the actual values of cross-sections corresponding to the temperature conditions at each altitude.

These photodissociation coefficients are illustrated in Figures 4-6 and compared with those calculated with values of absorption cross-sections measured at room temperature.

Stratospheric photodissociation coefficients (for altitude ranging from 15 to 50 km) calculated the temperature dependent absorption cross-sections, are smaller than those calculated with the room temperature values in the 20-35 km region, due to the decrease in the absorption cross-sections in the 200 nm region and the influence of the wavelengths longer than 280nm in the low stratosphere.

Tropospheric photodissociation coefficients for phosgene are very low (between 10^{-9} and 10^{-11} sec $^{-1}$) and are reduced down to 20 % of their room temperature values, using the temperature dependent cross-sections. For the two other compounds, tropospheric photodissociation coefficients are relatively high (between 10^{-7} and 10^{-4} sec $^{-1}$) and show a small temperature dependence. Photolysis is, for these two molecules, a non negligible mechanism for their tropospheric removal.

In conclusion, this work presents a new set of experimental data on the absorption cross-sections of carbonyl compounds in atmospheric temperature condition and highlights a non negligible temperature dependence of their photolysis.

V. REFERENCE.

CHOU, C.C., G. CRECENTINI, H. VERA-RUIZ, W.S. SMITH, and F.S. ROWLAND, 1977, Stratospheric photochemistry of CF_2O , $CClFO$ and CCl_2O , 173rd American Chemical Society Meeting, New Orleans.

GILLOTAY D., A. JENOUVIER, B. COQUART, M.F. MERIENNE, and P.C. SIMON, 1998, Ultraviolet absorption cross-sections of Bromoform in the temperature range 295-240 K., Planet. Space Sci., 37, 1127-1140.

KOCKARTS G., 1976, Absorption and photodissociation in the Schumann-Runge bands of molecular oxygen in terrestrial atmosphere., Planet. Space Sci., 24, 589-604

NICOLET M., 1984, On the molecular scattering in the terrestrial atmosphere : an empirical formula for calculation in the homosphere., Planet. Space Sci., 32, 1467-1468.

RATTINGAN G., and R.A. COX, Spectra and photochemistry of degradation products of hydrochlorofluorocarbons and hydrofluorocarbons, 1991, report to SPA-AFEAS, INC.

SIMON P.C., D. GILLOTAY, N. VANLAETHEM-MEUREE, and J. WISEMBERG, 1988, Ultraviolet absorption cross-sections of chloro and chlorofluoromethanes at stratospheric temperatures., J. Atmos. Chem., 7, 107-1345.

WMO, Atmospheric ozone 1985, WMO global ozone research and monitoring project, Report 14, 1986.

ZABEL, F. et al., 1992, Private communication.

Table I PHOSGENE (CCl_2O)

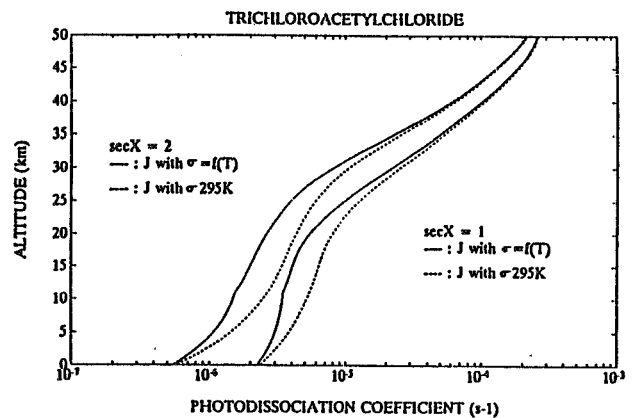
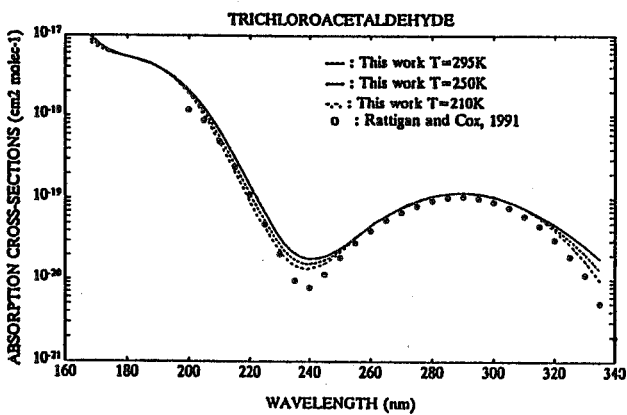
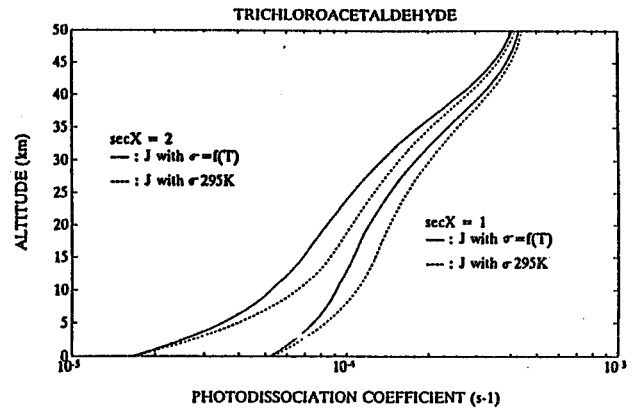
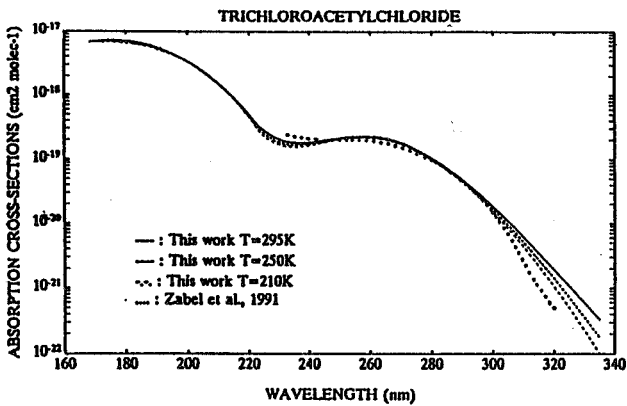
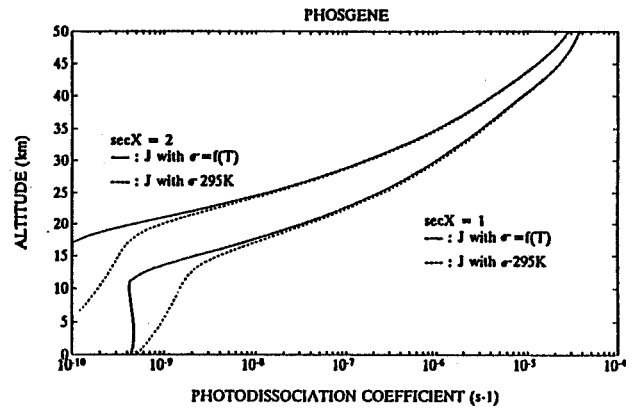
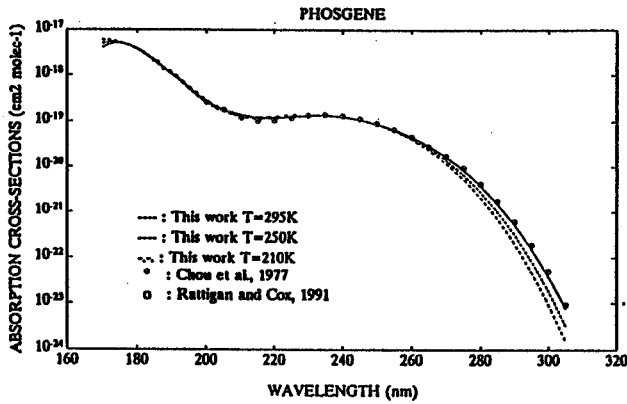
N°	(nm)	$\sigma(\lambda) \times 10^{21}$ (cm 2 molec. $^{-1}$)				
		295K	270K	250K	230K	210K
42	166.7-169.5	2010	2600	4160	4810	5560
43	169.5-172.4	4330	4760	5130	5530	5960
44	172.4-173.9	4930	5160	5360	5560	5770
45	173.2-175.4	5030	5190	5240	5330	5430
46	175.4-177.0	4890	4910	4920	4940	4950
47	177.0-178.6	4540	4490	4460	4420	4380
48	178.6-180.2	4040	3960	3900	3850	3790
49	180.2-181.8	3470	3390	3330	3270	3210
50	181.8-183.5	2890	2820	2760	2710	2660
51	183.5-185.2	2340	2280	2240	2200	2160
52	185.2-186.9	1860	1820	1790	1760	1730
53	186.9-188.7	1460	1440	1410	1390	1370
54	188.7-190.5	1160	1140	1120	1110	1090
55	190.5-192.3	903	888	876	865	854
56	192.3-194.2	715	698	685	673	660
57	194.2-196.1	524	509	498	487	476
58	196.1-198.0	399	386	376	367	357
59	198.0-200.0	312	302	293	285	277
60	200.0-202.0	252	243	236	229	223
61	202.0-204.1	209	202	196	191	185
62	204.1-206.2	179	173	168	163	159
63	206.2-208.3	158	153	149	145	141
64	208.3-210.5	143	139	136	132	129
65	210.5-212.8	133	129	127	124	121
66	212.8-215.0	126	124	121	119	117
67	215.0-217.4	123	121	119	117	115
68	217.4-219.8	122	120	119	117	116
69	219.8-222.2	122	121	120	119	118
70	222.2-224.7	124	124	123	123	122
71	224.7-227.3	127	127	127	127	127
72	227.3-229.9	131	131	131	131	132
73	229.9-232.4	134	134	135	135	135
74	232.4-235.3	136	137	137	137	137
75	235.3-238.1	131	132	132	133	133
76	238.1-241.0	125	125	126	126	127
77	241.0-243.9	116	116	117	117	118
78	243.9-246.8	105	106	106	106	106
79	246.8-250.0	93.1	92.9	92.8	92.7	92.5
80	250.0-253.2	80.5	79.8	79.3	78.8	78.2
81	253.2-256.4	66.5	65.7	64.4	63.4	62.5
82	256.4-259.7	53.4	51.8	50.6	49.4	48.2
83	259.7-263.2	40.3	38.4	37.0	35.7	34.4
84	263.2-266.7	28.9	27.1	25.8	24.5	23.2
85	266.7-270.3	19.8	18.1	16.9	15.8	14.7
86	270.3-274.0	12.6	11.3	10.3	9.45	8.64
87	274.0-277.8	7.36	6.39	5.71	5.10	4.55
88	277.8-281.7	3.92	3.29	2.86	2.48	2.16
89	281.7-285.7	1.93	1.58	1.31	1.11	0.933
90	285.7-289.9	0.931	0.643	0.524	0.426	0.347
91	289.9-294.1	0.316	0.233	0.183	0.143	0.112
92	294.1-298.5	0.105	0.0732	0.0549	0.0413	0.0310
93	298.5-303.0	0.0288	0.0190	0.0136	0.00970	0.00694
94	303.0-307.7	0.00921	0.00298	0.00200	0.00134	0.000899

Table III TRICHLOROACETYLCHLORIDE (CCl₃CClO)

N [*]	(nm)	$\sigma(\lambda) \times 10^{21}$ (cm ² molec. ⁻¹)				
		295K	270K	250K	230K	210K
42	166.7-169.5	6710	6710	6700	6690	6690
43	169.5-172.4	6990	6910	6840	6780	6720
44	172.4-173.9	7120	7000	6900	6810	6710
45	173.2-175.4	7160	7020	6910	6800	6690
46	175.4-177.0	7170	7010	6890	6770	6650
47	177.0-178.6	7140	6970	6840	6710	6580
48	178.6-180.2	7060	6890	6750	6620	6490
49	180.2-181.8	6940	6770	6640	6510	6380
50	181.8-183.5	6770	6610	6480	6360	6240
51	183.5-185.2	6550	6410	6290	6180	6060
52	185.2-186.9	6300	6160	6060	5960	5860
53	186.9-188.7	5990	5880	5790	5710	5620
54	188.7-190.5	5670	5580	5500	5430	5360
55	190.5-192.3	5280	5210	5150	5100	5050
56	192.3-194.2	4870	4810	4790	4750	4710
57	194.2-196.1	4450	4420	4400	4370	4350
58	196.1-198.0	4020	4000	3990	3980	3980
59	198.0-200.0	3580	3580	3580	3580	3580
60	200.0-202.0	3140	3150	3160	3170	3170
61	202.0-204.1	2720	2730	2740	2750	2770
62	204.1-206.2	2310	2330	2340	2350	2370
63	206.2-208.3	1940	1950	1960	1980	1990
64	208.3-210.5	1600	1610	1620	1620	1630
65	210.5-212.8	1290	1290	1290	1300	1300
66	212.8-215.0	1020	1020	1020	1020	1010
67	215.0-217.4	789	783	776	772	767
68	217.4-219.8	595	584	575	566	557
69	219.8-222.2	440	426	415	404	393
70	222.2-224.7	318	302	289	278	266
71	224.7-227.3	258	243	232	222	212
72	227.3-229.9	219	207	198	189	181
73	229.9-232.6	195	186	178	171	164
74	232.6-235.3	183	175	168	162	156
75	235.3-238.1	179	172	166	161	155
76	238.1-241.0	181	174	170	165	160
77	241.0-243.9	187	182	178	174	170
78	243.9-246.9	197	193	189	186	183
79	246.9-250.0	209	205	203	200	197
80	250.0-253.2	218	216	213	211	210
81	253.2-256.4	223	221	220	218	217
82	256.4-259.7	226	223	221	219	217
83	259.7-263.2	223	220	218	215	213
84	263.2-266.7	211	208	205	203	200
85	266.7-270.3	191	188	185	183	181
86	270.3-274.0	166	163	160	158	156
87	274.0-277.8	137	134	132	130	128
88	277.8-281.7	107	105	104	102	100
89	281.7-285.7	81.4	79.5	78.0	76.5	75.0
90	285.7-289.9	58.6	56.9	55.6	54.4	53.1
91	289.9-294.1	40.3	38.9	37.8	36.8	35.7
92	294.1-298.5	26.7	25.5	24.6	23.7	22.8
93	298.5-303.0	16.8	15.8	15.1	14.4	13.7
94	303.0-307.7	9.21	8.48	7.93	7.42	6.95
95	307.7-312.5	6.05	5.46	5.03	4.64	4.27
96	312.5-317.5	3.39	2.96	2.65	2.38	2.14
97	317.5-322.5	1.88	1.57	1.37	1.19	1.03
98	322.5-327.5	1.04	0.830	0.693	0.579	0.484
99	327.5-332.5	0.578	0.436	0.347	0.277	0.221
100	332.5-337.5	0.326	0.230	0.173	0.131	0.0998

Table II TRICHLOROACETALDEHYDE (CCl₃CHO)

N [*]	(nm)	$\sigma(\lambda) \times 10^{21}$ (cm ² molec. ⁻¹)				
		295K	270K	250K	230K	210K
42	166.7-169.5	9880	9310	8880	8470	8070
43	169.5-172.4	7850	7540	7310	7080	6860
44	172.4-173.9	6890	6710	6570	6430	6300
45	173.2-175.4	6420	6300	6210	6120	6030
46	175.4-177.0	6040	5980	5920	5870	5820
47	177.0-178.6	5730	5700	5680	5660	5630
48	178.6-180.2	5480	5480	5470	5470	5470
49	180.2-181.8	5250	5270	5290	5300	5320
50	181.8-183.5	5030	5070	5090	5120	5150
51	183.5-185.2	4820	4850	4880	4920	4950
52	185.2-186.9	4590	4620	4650	4680	4710
53	186.9-188.7	4330	4360	4390	4410	4430
54	188.7-190.5	4070	4080	4100	4110	4120
55	190.5-192.3	3740	3740	3740	3740	3740
56	192.3-194.2	3400	3390	3360	3350	3330
57	194.2-196.1	3030	2990	2960	2930	2900
58	196.1-198.0	2650	2600	2550	2510	2460
59	198.0-200.0	2270	2200	2140	2090	2040
60	200.0-202.0	1890	1810	1750	1700	1640
61	202.0-204.1	1540	1450	1390	1330	1280
62	204.1-206.2	1210	1130	1080	1020	967
63	206.2-208.3	936	865	812	762	715
64	208.3-210.5	703	642	596	554	515
65	210.5-212.8	511	461	424	390	359
66	212.8-215.0	366	326	298	271	248
67	215.0-217.4	257	227	205	186	168
68	217.4-219.8	176	155	139	126	113
69	219.8-222.2	121	106	95.3	85.7	77.0
70	222.2-224.7	82.5	73.2	65.9	59.4	53.5
71	224.7-227.3	57.9	51.3	46.5	42.1	38.2
72	227.3-229.9	39.4	35.2	32.1	29.4	26.8
73	229.9-232.6	28.3	25.3	23.2	21.2	19.4
74	232.6-235.3	22.3	20.1	18.4	17.0	15.6
75	235.3-238.1	19.2	17.4	16.1	14.9	13.8
76	238.1-241.0	17.9	16.4	15.4	14.3	13.4
77	241.0-243.9	18.0	16.8	15.8	14.9	14.1
78	243.9-246.9	19.4	18.3	17.5	16.7	15.9
79	246.9-250.0	22.1	21.2	20.5	19.8	19.2
80	250.0-253.2	26.2	25.5	24.9	24.4	23.8
81	253.2-256.4	32.5	32.0	31.6	31.3	30.9
82	256.4-259.7	40.4	40.2	40.1	39.9	39.8
83	259.7-263.2	50.9	51.0	51.0	51.1	51.2
84	263.2-266.7	60.9	60.6	60.3	60.0	59.7
85	266.7-270.3	72.7	72.0	71.5	71.0	70.4
86	270.3-274.0	84.6	83.7	83.0	82.3	81.6
87	274.0-277.8	96.0	95.1	94.3	93.5	92.8
88	277.8-281.7	106	105	104	104	103
89	281.7-285.7	112	112	111	111	111
90	285.7-289.9	116	116	116	116	116
91	289.9-294.1	115	115	116	116	116
92	294.1-298.5	110	111	111	112	112
93	298.5-303.0	101	102	103	103	103
94	303.0-307.7	87.0	87.1	87.1	87.2	87.3
95	307.7-312.5	76.2	75.8	75.4	75.0	74.6
96	312.5-317.5	61.5	60.1	59.1	58.0	57.0
97	317.5-322.5	47.7	45.5	43.9	42.3	40.7
98	322.5-327.5	35.6	32.8	30.8	28.9	27.1
99	327.5-332.5	25.7	22.6	20.5	18.5	16.8
100	332.5-337.5	17.9	14.9	12.9	11.1	9.61



Figures 1-3 : Ultraviolet absorption cross-sections at 295 K, 250 K and 210 K.

Figures 4-6 : Photodissociation coefficients as a function of altitude.

308927

CLIMATE-CHEMICAL INTERACTIONS AND GREENHOUSE EFFECTS OF TRACE GASES*Guang-yu Shi and Xiao-biao Fan*Institute of Atmospheric Physics
Chinese Academy of Sciences
Beijing 100029, CHINA**ABSTRACT**

A completely coupled one-dimensional radiative-convective (RC) and photochemical-diffusion (PC) model has been developed recently and used to study the climate-chemical interactions. The importance of radiative-chemical interactions within the troposphere and stratosphere has been examined in some detail. We find that increases of radiatively and/or chemically active trace gases such as CO_2 , CH_4 and N_2O have both the direct effects on climate change by modifying the radiation balance through greenhouse effects and the indirect effects on climate change by changing the atmospheric O_3 profile through their interaction with chemical processes in the atmosphere. It is also found that the climatic effect of ozone depends strongly on its vertical distribution throughout the troposphere and stratosphere, as well as on its column amount in the atmosphere.

I. INTRODUCTION

Observations have shown that the concentrations of atmospheric CO_2 and other trace gases (OTG) such as CH_4 , N_2O , and NO_x have been increasing and the trend of increases will most likely continue. It has been suggested that human activities are the major contributions to these increases. Increases of these radiatively and/or chemically active trace gases may have implications for global climate both directly by modifying the earth's radiation budget through their absorption properties and indirectly by changing atmospheric O_3 which is both radiatively and chemically active through the chemical processes in the atmosphere [WMO, 1985]. The greenhouse effect of CO_2 has long since received the most emphasis as a mechanism for climate change, but now the problem concerning the greenhouse effects due to human activities has bordered in scope from the CO_2 -climate problem to the trace-gas-climate problem. As many trace gases are both radiatively and chemically active, the climate effects of OTG are strongly governed by

interactions between chemical, radiative and dynamic processes in the atmosphere. Complexity of the trace-gas-climate problem results also from the fact that the enhanced greenhouse effect due to the increasing CO_2 and the OTG will affect the temperature structure of the atmosphere and in turn the change in temperature profile will change the concentration distribution of many trace gases through their temperature dependence of the chemical reactions. A coupled radiation, chemistry and dynamics model is obviously needed for the trace-gas-climate studies.

II. MODEL DESCRIPTION AND CONTROL CASE

The model used in this study is a completely coupled one dimensional radiative-convective (RC) and photochemical-diffusive (PC) model which extends from 0 to 68 km with a uniform altitude resolution of 2 km. An accurate and efficient radiation transfer scheme, the exponential sum fitting of transmission function (ESFT) is used for the thermal radiation calculation [Shi, 1981], and a combination of the time-marching (TM) method and the Newton-Raphson (NR) iteration is used for finding the equilibrium temperature profile in the RC model [Shi, 1992a,b]. In the PC model, more than 50 species and 100 reactions are taken into account, including the O_x , HO_x , NO_x , BrO_x , and ClO_x chemistry. The chemical reaction rates and the photochemical absorption cross sections used in the calculations are taken from DeMore et al. [1990], and the incident solar flux as a function of wavelength is taken from Hudson et al. [1982]. The model leads to a control climate with the surface temperature of 288.15 K, the surface albedo of 0.102, the planet albedo of 0.316 and the ozone column amount of 0.344 atm-cm, which is a good representation for the present global mean climate.

The vertical temperature profile obtained from the coupled model is shown in fig. 1, along with the U.S. 1976 Standard Atmosphere. The agreement between them is quite good throughout the troposphere and stratosphere, with minor deviations near the tropopause and stratopause. This might mean that the radiative equilibrium

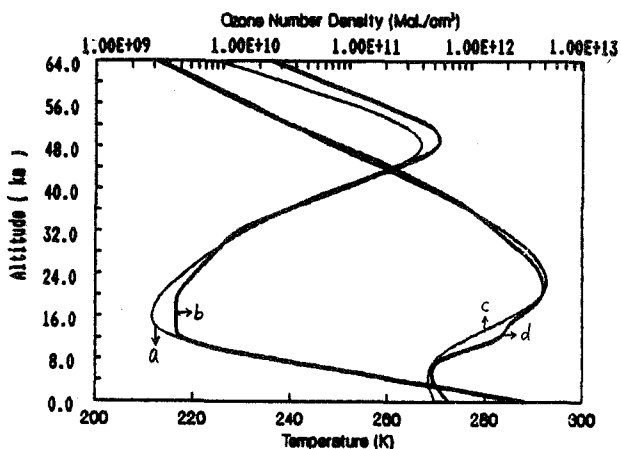


Fig. 1. Temperature (a) and ozone profile (c) obtained by the coupled RC-PC model, and the U.S. 1976 Standard Atmosphere (b and d).

is not a good assumption in these regions. Fig. 1 also shows the ozone profile obtained from the coupled model, and from the U.S. 1976 Standard Atmosphere for comparison. It can be seen from the figure that the overall agreement between the two profiles is satisfactory, except for the troposphere where the model underestimated the ozone. This comes probably from the model's overestimating the reactive radicals HOx which catalyze ozone destruction in the troposphere.

III. RESULTS AND DISCUSSIONS

The results from several case studies on climate-chemical interaction will be presented here. These cases of perturbation in the atmospheric concentration of CO₂, CH₄ and N₂O will most likely occur in the next century.

1. 2xCO₂ (340-680 ppmv)

CO₂ is a radiatively active gas. It governs the magnitude of stratospheric longwave emission and has significant impacts on stratospheric climate. As well known, the infrared emission to space by CO₂ and the absorption of solar radiation by stratospheric O₃ are primarily responsible for the radiative energy budget in the stratosphere. An increase in CO₂ concentration acts to cool the stratosphere while the troposphere warms. This change in temperature structure caused by increasing CO₂ affects the concentration of O₃ through the temperature dependence of chemical reaction related to O₃.

Fig. 2 shows the changes in the temperature and ozone profiles due to a doubled CO₂ concentration, obtained by the RC model and by the coupled RC-PC model, respectively. We can

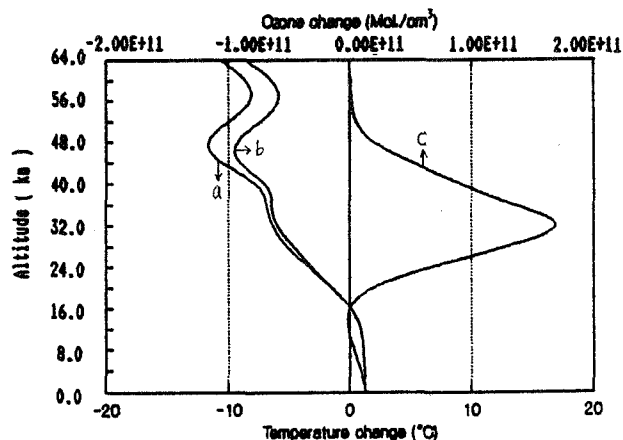


Fig. 2. Changes in temperature and ozone concentration for 2xCO₂ (340 to 680 ppmv). a and b are the temperature changes from RC and RC-PC model, respectively, and c is the ozone concentration calculated from RC-PC model.

see from the figure that, the calculated maximum temperature change (-12.46°C) occurs at 46 km and the calculated surface temperature increase is +1.32°C by the RC model, and the corresponding values by the RC-PC coupled model are -10.30°C and +1.30°C, respectively. This suggests the incorporation of chemical process into RC mitigated somehow the stratospheric cooling and the surface warming due to a doubling CO₂. In fact, as the stratospheric temperature decreases, the temperature dependent ozone destruction reactions, O+O₃ → 2O₂ and NO+O₃ → NO₂+O₂, will be slowed down and the ozone production rate through the reaction, O+O₃ → O₃, will increase. This results in a net increase in stratospheric ozone concentrations. The model calculations indicate, in general, a column O₃ increase of about 3.0% for a doubling of CO₂. This O₃ increase is mainly distributed over above 20km where the enhanced solar heating due to O₃ increase offsetted, more or less, the stratospheric cooling due to CO₂ increase. It means that the chemical feedback gives a negative effect on the stratospheric temperature perturbation and the surface temperature change for the case of CO₂ doubling.

2. 2xCH₄ (1.60-3.20 ppmv)

CH₄ is a radiatively active gas. Just like the radiative nature of CO₂, increase of CH₄ will lead the temperature in the lower atmosphere to increase and the temperature in the upper atmosphere to decrease. By the RC model, the temperature changes at surface and at 56 km are 0.17°C and -0.26°C, respectively, for a doubling of CH₄ (Fig. 3.).

CH₄ is also a chemically active gas. Model result by the RC-PC for a doubling of CH₄ gives

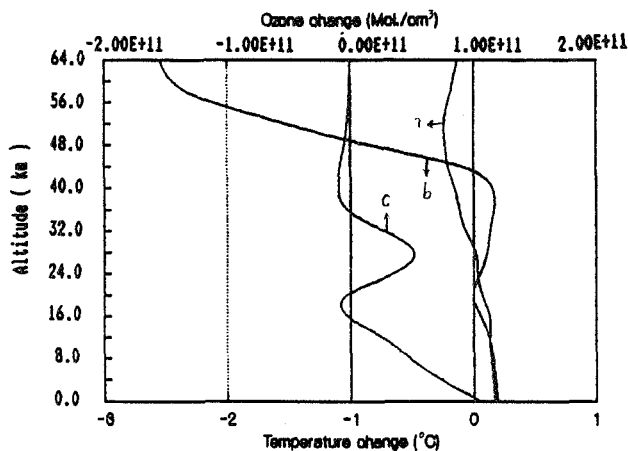


Fig. 3. As in Fig. 2, but for $2xCH_4$ (1.60 to 3.20 ppmv)

an increase of column ozone about 1.2% and the increase ranges from the surface to 36 km, as shown in the figure. We can find from the figure that there are two peaks in the increases of O_3 . One is located near the ground, which is resulted from that the CH_4 oxidation produces O_3 through the CH_4 -NO_x-smog-reactions [Johnston, 1984]; the other is around 28 km, which is caused by the fact that CH_4 provided a sink for Clx and then led to slow down the O_3 destruction catalyzed by Clx.

Compared with the results by the RC, the temperature changes obtained by the RC-PC are $0.19^\circ C$ at the surface and $-2.6^\circ C$ at 56 km, respectively, for a doubling CH_4 . This means that the chemical feedback contributes a positive effect to the stratospheric temperature perturbation and the surface temperature change, as contrasted with the case of doubling CO_2 .

The major sink of atmospheric CH_4 is its reaction with the hydroxyl radical OH while the CH_4 oxidation by OH is the main loss mechanism of OH in the free troposphere. So CH_4 and OH levels are coupled tightly. Increases in CH_4 lead to a decrease in OH and thereby to a further increase in CH_4 levels. With continued increases in CH_4 in the future, this positive feedback could become increasingly important.

3. $1.2xN_2O$ (0.30-0.36 ppmv)

N_2O is also a radiatively and chemically active gas. The results for $1.2xN_2O$ are shown in Fig. 4. In many respects, the radiative consequences due to $1.2xN_2O$ are similar to those of $2xCO_2$ and $2xCH_4$. Increase in the concentration of N_2O causes tropospheric heating and stratospheric cooling. Similar to the case of $2xCH_4$, the chemical feedback gives also a positive effect on the surface temperature change and the stratospheric temperature perturbation.

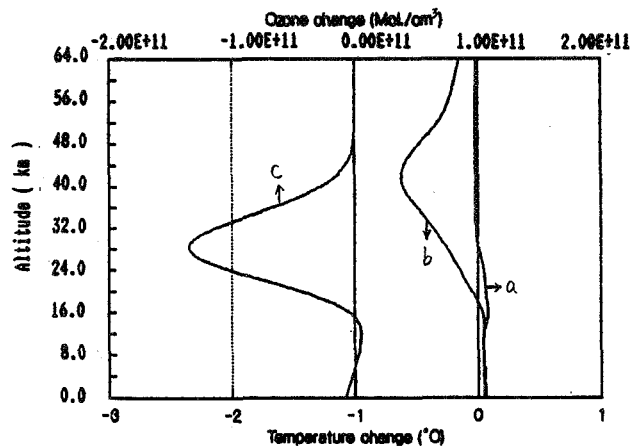


Fig. 4. As in Fig. 2, but for $1.2xN_2O$ (0.30 to 0.36 ppmv)

The chemical effects of increasing atmospheric N_2O arise from the reaction, $O(1D)+N_2O \rightarrow 2NO$, and this reaction provides the major source of odd nitrogen (NO_x) in the middle stratosphere from about 20 to 40 km. Consequently, an increase in atmospheric N_2O level will lead the stratospheric NO_x to increase and subsequently to reduce the stratospheric O_3 by catalytic destruction through the reactions, $NO+O_3 \rightarrow NO_2+O_2$ and $NO_2+O \rightarrow NO+O_2$. Decreased ozone heating will give a lower temperature in the stratosphere. On the other hand, the decreased stratospheric ozone will lead more solar radiation to reach the surface and cause the surface warmer.

4. O_3 -climate problem

It is clear from the results mentioned above that in addition to their direct radiative effects, many of the greenhouse gases also have indirect radiative effects on climate through their interactions with atmospheric chemical processes. As a result of such interactions, the global distribution of ozone in the troposphere and stratosphere was changed.

Ozone plays an important dual role in affecting climate. While CO_2 and OTG are relatively well-mixed in the atmosphere, the climatic effect of ozone depends strongly on its vertical distribution throughout the troposphere and stratosphere, as well as its column amount in the atmosphere. The surface temperature changes calculated by the RC model are shown in Fig. 5 as a function of ozone percentage change and altitude where O_3 is changed. U. S. 1976 Standard Atmosphere is used in the calculations. It can be seen from the figure that changes in ozone in the middle-upper troposphere and lower stratosphere (below 22 km) are most effective in determining the change in surface temperature, with increased ozone leading to a

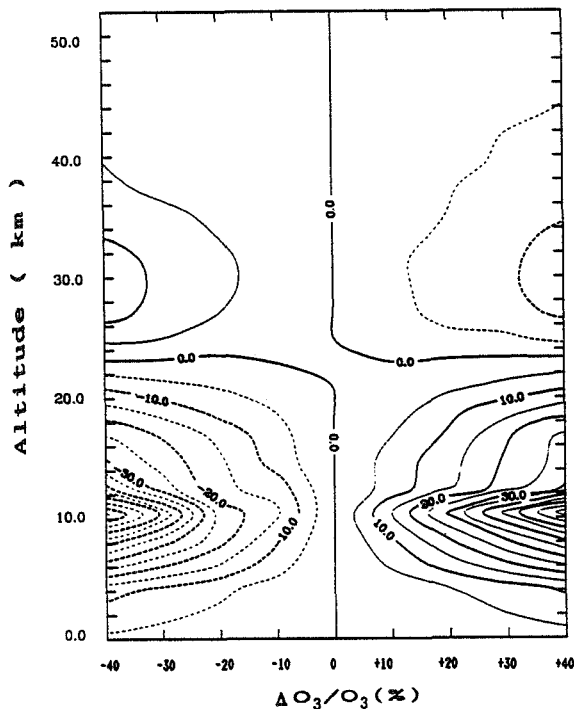


Fig. 5. Computed change in surface temperature ($\times 10^{-3}$ K) due to ozone change (%) as a function of altitude at which ozone is perturbed.

warmer surface (right part of the figure), and vice versa (left part of the figure). This is because the greenhouse effect is directly proportional to the temperature contrast between the level of emission and the levels where radiation is absorbed. This contrast is greatest near the tropopause and the climate sensitivity of ozone change reaches its maximum there. Above about 25 km, added ozone causes a small decrease in surface temperature (right part of the figure) because it absorbs extra solar radiation, effectively robbing the troposphere of direct solar energy that would otherwise warm the surface, and vice versa (left part of the figure).

In summary, ozone is a primary absorber of solar radiation in the stratosphere where it is directly responsible for the increase in temperature with altitude. Ozone is also an important absorber of infrared radiation. It is the balance between these radiative processes that determine the net effect of ozone on climate.

REFERENCE

- DeMore, W. B., et al. (Eds), Chemical Kinetics and Photochemical Data for Use in Stratospheric Modeling, Evaluation Number 9, JPL, Pasadena, California, 1990.
- Hudson, R., et al. (Eds), The Stratosphere 1981: Theory and Measurements, Rep. II, Global Ozone Research and Monitoring Project, WMO, Geneva, 1982.
- Johnston, H.S., Human effects on the global atmosphere, *Ann. Rev. Phys. Chem.*, 35, 481-505, 1984.
- Shi, G. Y., An accurate calculation and representation of the infrared transmission function of the atmospheric constituents, Ph D. Thesis, Dept. of Science, Tohoku University of Japan, 1991.
- Shi, G. Y., Radiative forcing and greenhouse effect due to the atmospheric trace gases, *Science in China (Series B)*, 35(2), 217-229, 1992a.
- Shi, G. Y., Global warming potential due to CFCs and their substitutes, *Scientia Atmospherica Sinica*, 16(3), 345-352, 1992b.
- WMO, Global ozone research and monitoring project, in *Atmospheric Ozone 1985*, Rrp. 16, Geneva, 1985.

**A GENERAL CIRCULATION MODEL STUDY
OF THE CLIMATIC EFFECT
OF OBSERVED STRATOSPHERIC OZONE DEPLETION
BETWEEN 1980 AND 1990**

Michael P. Dudek, Wei-Chyung Wang, Xin-Zhong Liang & Zhu Li

Atmospheric Sciences Research Center
State University of New York at Albany
Albany, New York 12205, USA

1. Introduction

The TOMS and SAGE measurements show a significant reduction in the stratospheric ozone over the middle and high latitudes of both hemispheres between the years 1979 and 1991 (WMO, 1992). This change in ozone will effect both the solar and longwave radiation with climate implications. However, recent studies (Ramaswamy et al., 1992; WMO, 1992) indicate that the net effect depends not only on latitudes and seasons, but also on the response of the lower stratospheric temperature.

In this study we use a general circulation model (GCM) to calculate the climatic effect due to stratospheric ozone depletion and compare the effect with that due to observed increases of trace gases CO₂, CH₄, N₂O, and CFC's for the period 1980-1990. In the simulations, we use the observed changes in ozone derived from the TOMS data. The GCM used is a version of the NCAR community climate model referenced in Wang et al. (1991). For the present study we run the model in perpetual January and perpetual July modes in which the incoming solar radiation and climatological sea surface temperatures are held constant.

2. Model Experiments

Two sets of equilibrium experiments are conducted. In the first case (c1980), we use the atmospheric trace gas concentrations corresponding to 1980 observed conditions (Houghton et al., 1990; see Table 1). In c1980 the standard 23 level GCM ozone distribution, which is dependent on latitude, height and time of year, will be used to run both perpetual January and July simulations. The column ozone amounts calculated from the GCM ozone distribution correspond well to the TOMS distribution observed during the late 1970's and early 1980's.

The second experiment (c1990) uses the trace gas concentrations for 1990 along with a modified ozone distribution which reflects the observed changes in ozone between 1980 and 1990 from TOMS data. Figure 1 shows the time-latitude distribution of ozone change. The middle and high latitudes in both hemispheres show column ozone losses, while the tropics show a slight increase from February to July. The Antarctic ozone hole is evident, with over a 40% reduction in column ozone at the pole in October and November. Note that the TOMS data does not record ozone amount during polar night, so in these regions no change in column ozone is assumed.

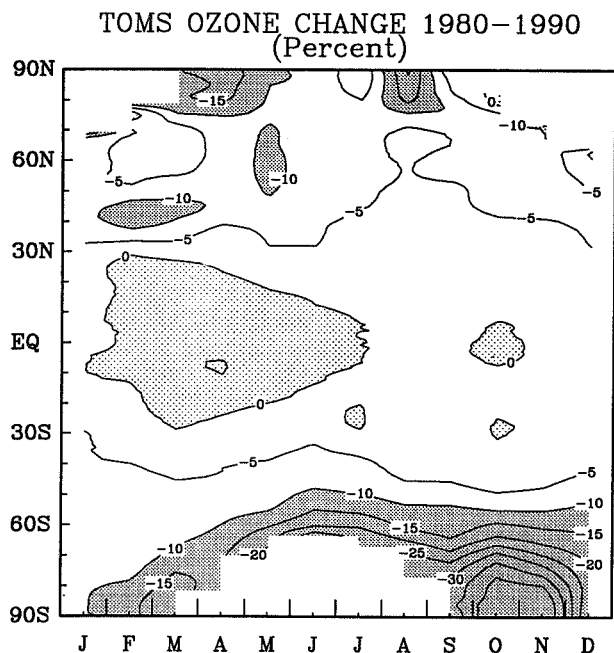


Figure 1. Latitude-time distribution of the percentage change in column ozone measured by TOMS between 1980 and 1990. Months are along the bottom axis. Shaded areas show ozone depletions of greater than 10% and net increases in ozone.

A particular problem for this study was the fact that although the TOMS data produces virtually complete horizontal coverage, it only shows the total column ozone. To derive a consistent ozone dataset for the model, with both horizontal and vertical structure, a procedure had to be devised to use the TOMS data to modify the original GCM ozone distribution. The ozone loss has been observed to occur primarily in the lower stratosphere using both SAGE data and limited ozonesondes (McCormick et al., 1991). To approximate this observed structure, a second-order

polynomial was developed in which all of the change in the column ozone occurs in the lowest 11 km of the stratosphere, while retaining the total column ozone changes shown in Figure 1. A climatologically derived tropopause height is used for this calculation and for the subsequent radiative forcing calculations. Figure 2 shows the vertical cross-section of the percentage change in ozone mixing ratio used in the model experiments. In January a maximum ozone loss occurs between 10 and 16 km poleward of about 30 degrees. The structure is similar in July, but more diffuse in the northern hemisphere, while not extending to the pole in the south. These computed changes are applied to the model zonal ozone distribution and the model is run using 1990 trace gas amounts (c1990, see Table 1).

3. Radiative Forcing

We first compare the radiative forcing induced by changes in the trace gases concentrations. For these calculations a time mean equilibrium state taken from the last 90 days of a 300 day simulation from c1980 are used. Table 2 shows the change in the globally averaged radiative forcing for the troposphere-surface system between c1990 and c1980. The change of total radiative forcing, dominated by the longwave radiative forcing, is calculated to be 0.55 and 0.5 Wm^{-2} in January and July respectively. Ozone changes increase the solar flux into the troposphere while slightly reduce the longwave flux and results in a net warming of 0.14 and 0.08 Wm^{-2} for January and July respectively. These changes are comparable to the warming due to the increase of CFC's. Figure 3 shows the zonal distribution of change in radiative forcing, both for ozone and non-ozone gases. Changes in ozone forcing are dominated by the solar forcing changes, so the summer hemispheres show the largest ozone effect,

Table 1. Uniformly-mixed gas concentrations used in GCM experiments.

Experiment	CO ₂	CH ₄	N ₂ O	CFCl ₃	CF ₂ Cl ₂
c1980	337	1.57	0.30	0.16	0.27
c1990	354	1.72	0.31	0.28	0.48

Concentration unit is ppmv for CO₂, CH₄ and N₂O and ppbv for CFCl₃ and CF₂Cl₂.

Table 2. Changes in the global mean radiative forcing (Wm^{-2}) of the troposphere-surface system.

	January		July		January	July
	LW	SW	LW	SW	Total	Total
All gases	0.434	0.114	0.438	0.066	0.548	0.504
O ₃	-0.040	0.175	-0.042	0.123	0.135	0.081
CFC's	0.117	0.0	0.119	0.0	0.117	0.119

LW refers to longwave radiation and SW to shortwave radiation. All gases include all trace gases listed in Table 1 and ozone. CFC's refers to CFCl_3 and CF_2Cl_2 . The calculation used the January and July equilibrium states from case 1980.

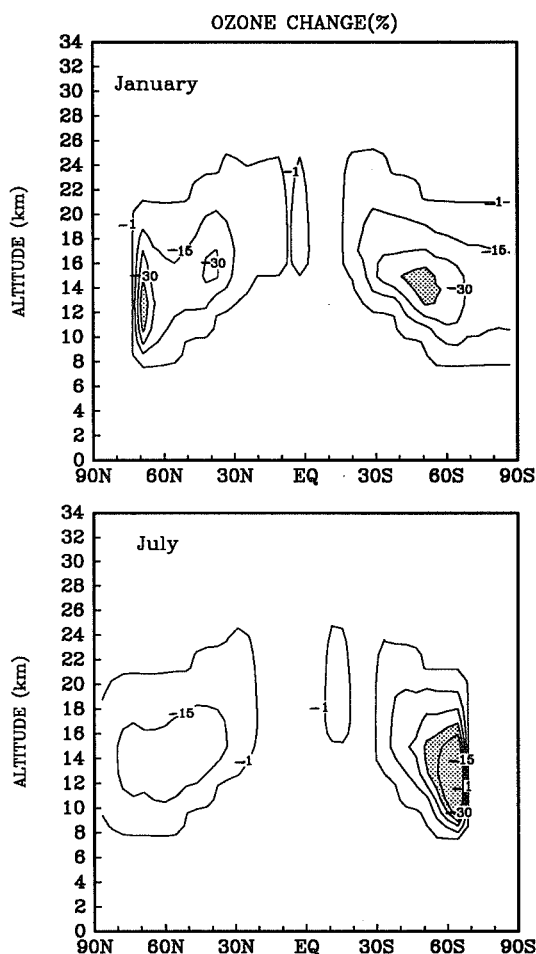


Figure 2. Latitude-height cross-section of the percentage reduction in ozone mixing ratio. The first contour is 1% and the subsequent contour interval is 15%. Shaded areas indicate greater than 45% ozone depletion.

at some latitudes being larger than the non-ozone forcing.

4. Equilibrium Temperature Response

The differences in the zonal mean temperature between c1980 and c1990 are shown in Figure 4. In January, the largest temperature change occurs at high latitudes and is the result of the dynamic response of the polar night stratosphere to the perturbed heating. The temperature is also reduced 1 to 2°C in the lower stratosphere south of 40°S, within the region of maximum ozone loss. The lower stratosphere in the tropics warms about 1°C. In July, there is a more general temperature reduction in the lower stratosphere of 0.5 to 1.0°C. In both months the troposphere is generally slightly warmer, which is consistent with the enhanced net radiative forcing shown in Table 1. Note that the small magnitude of the surface warming is also caused by the fixed sea surface temperature in the two experiments.

References

Houghton, J.T., G.J. Jenkens, and J.J. Ephraums (eds.), 1990: *Climate change: The IPCC Scientific Assessment*, Intergovernmental Panel on Climate Change, pp 365, United Nations Environmental Programme/World Meteorological Organization, Cambridge University Press.

McCormick, M.P., R.E. Veiga, and W.P. Chu, 1992: Stratospheric ozone profile and total ozone trends derived from the SAGE I and SAGE II data, submitted to *Geophys. Res. Lett.*

Ramaswamy, V., M.D. Schwarzkopf and K.P. Shine, 1992: Radiative forcing of climate from halocarbon-induced global stratospheric ozone loss. *Nature*, 355, 810-812.

Wang, W-C., M.P. Dudek, X-Z Liang, and J.T. Kiehl, 1991: Inadequacy of effective CO₂ as a proxy in simulating the greenhouse effect of other radiatively active gases. *Nature*, 350, 573-577.

World Meteorological Organization, 1992: *Scientific Assessment of Ozone Depletion: 1991.*

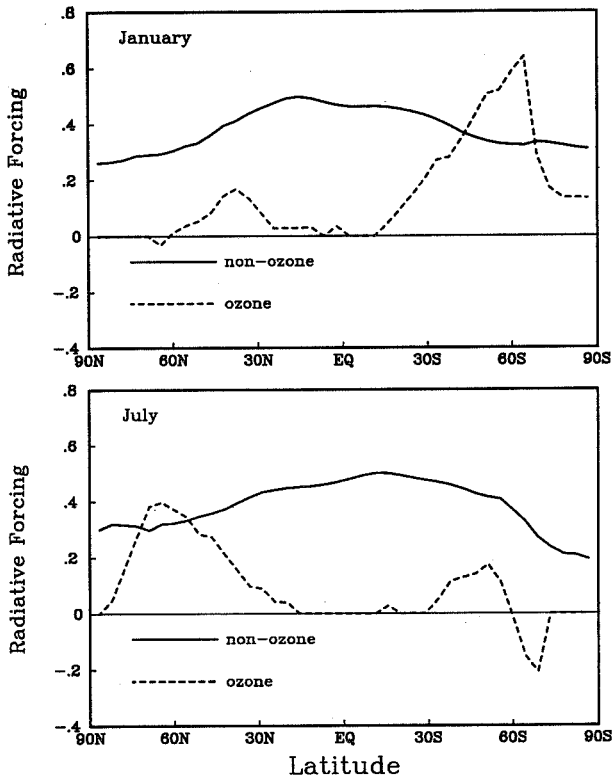


Figure 3. January and July total (both longwave and solar) radiative forcing (Wm^{-2}) due to the 1980 to 1990 increases in all non-ozone gases and that due to ozone changes.

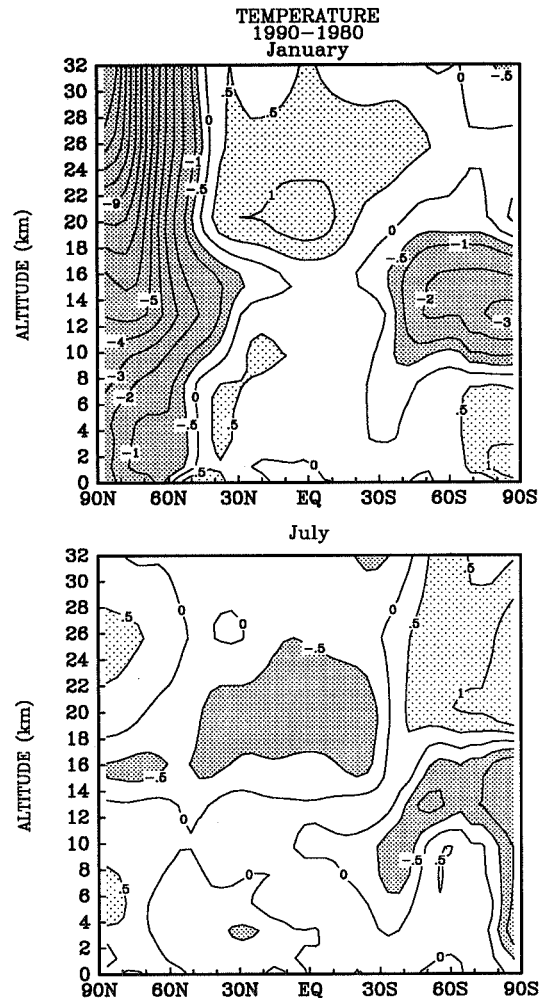


Figure 4. Latitude-height cross-section of the zonal temperature difference between c1990 and c1980 for January and July. Contour interval is every 1°C except for the addition of the -0.5°C and +0.5°C contours. Shaded areas show regions below -0.5°C and above +0.5°C.

APPENDIX

AUTHOR INDEX

Abreu, V.....448
Adrian, G.....524
Ahmad, Z.....877,903,915,942,962
Aikin, A.C.....342
Aimedieu, P.....561
Akagi, K.....582
Alberti, L..... 48
Allaart, M.A.F..... 82
Ancellet, G..... 15,122
Andreae, M.O.....162
Aoki, S.....573
Arabov, A.Y.....675
Archer, C.B..... 45
Aref'ev, V.N.....762
Atkinson, R.J.....594
Austin, J.....467

Bader, J.....186,711
Bais, A.F.....535,786
Balis, D.S.....535
Ballard, J.....439,444,459
Barbe, A.....219
Barnett, J.J.....444
Barsby, J.....382
Barthel, K.....215
Bartlett, L.M.....715
Beagley, S.R..... 78,508
Beaubien, A.E.....766
Beaubien, D.J.....766
Beekmann, M..... 15,122
Berntsen, T..... 62
Bertaux, J.L.....950

Beyerle, G.....	483,512
Bhartia, P.K.....	915,923
Bhatt, P.P.....	934
Blanchette, C.....	619
Blatherwick, R.D.....	610
Blumenstock, T.....	524
Bodeker, G.E.....	598
Boime, R.D.....	938
Bojkov, R.D.....	417,535
Bonasoni, P.....	48,138,707
Borchers, R.....	259,823,827
Borisov, Y.....	877
Boughner, R.E.....	367
Bowman, H.D.....	887
Braathen, G.O.....	504
Brackett, V.G.....	158,631
Brasseur, G.....	351
Browell, E.V.....	115,516,631
Brunke, E.G.....	11
Budiyono, A.....	573
Burley, J.D.....	302
Burrows, J.P.....	958
Butchart, N.....	467
Butler, C.F.....	115,516,631
Byerly, W.....	877
Callis, L.B.....	367
Cariolle, D.....	285,496
Carleer, M.....	166
Carmichael, G.R.....	53, 85
Carter, A.F.....	516
Castagnoli, F.....	479
Cebula, R.P.....	883,927,931,942,946
Cervino, M.....	138,707
Chakrabarty, D.K.....	683,687

Chance, K.V.....	831,958
Chassefiere, E.....	950
Chen, L.....	351
Ching, J.K.S.....	70
Chipperfield, M.....	496
Chronopoulos, G.....	854
Chu, A.....	444
Chu, D.A.....	452,895
Chu, S-H.....	89
Chu, W.P.....	645
Chubachi, S.....	867
Clarmann, Th.V.....	842
Claude, H.J.....	190,807
Clerbaux, C.....	374
Clericetti, A.....	355
Colbeck, I.....	146
Colin, R.....	166,374
Colombo, T.....	138
Connell, P.S.....	302,322,623
Connor, B.J.....	294,444,452,645
Considine, D.B.....	347
Corney, M.....	444,456
Cote, C.....	877
Cox, R.A.....	413
Crist, K.C.....	85
Cros, B.....	631
Crutzen, P.J.....	66,298
Cundari, V.....	138
Cunnold, D.M.....	314,798,895
Da Conceicao, P.....	219
Dahlback, A.....	211
Dalaudier, F.....	950
Das, S.R.....	683
David, C.....	550,561

Davies, T.D.....	3
De Backer, H.....	815
de Grandpre, J.....	78
De Muer, D.....	815
de Zafra, R.L.....	540,543,719
Degorska, M.....	653
del Guasta, M.....	479,561
Deland, M.T.....	927
Delmas, R.....	162
Deshler, T.....	590
Diab, R.D.....	45,382
Dichter, B.K.....	766
Dickerson, R.....	105,134,174
Dierickx, L.....	421,425
Doddridge, B.G.....	134,174
Dosov, V.....	877
Douglass, A.R.....	281,307,347
Dudek, M.P.....	433
Dudhia, A.....	444,456
Eckman, R.S.....	294
Ehhalt, D.H.....	74
Ehlers, J.....	512
Elansky, N.F.....	130,663,675,679,699
Elokhov, A.....	663,695,699
Emery, Y.....	550
Emmons, L.K.....	540,543,719
Evangelisti, F.....	138,707
Evans, R.D.....	195,266,749,962
Evans, W.F.J.....	774,778
Fabian, P.....	823,827,870
Fabian, R.....	483,504,512
Fakhruzzaman, K.M.....	158

Fan, X-B.....	429
Fast, H.....	807
Feister, U.....	363,770
Fenn, M.A.....	115,516,631
Fiedler, F.....	97
Filiouguine, I.V.....	386,835
Fioletov, V.E.....	223,390,535
Fischer, H.....	842
Fish, D.J.....	671,731
Fisher, H.....	524
Fishman, J.....	158,631
Flentje, G.....	870
Flesia, C.....	479,550
Fogal, P.F.....	703
Foreman, M.....	877
Fortezza, F.....	48
Frank, E.....	524
Frank, H.....	663
Freshwater, R.A.....	671,731
Friedl-Vallon, F.....	842
Fritzsche, C.....	842
Froidevaux, L.....	322
Frolkis, V.A.....	338,409
Frolov, A.D.....	754
Fujii, R.....	606
Gelpke, V.....	186
Georgiadis, T.....	48,138
Gerber, L.....	691
Gerhardt, L.....	524
Gillotay, D.....	421,425
Gioulgkidis, K.....	790
Giovanelli, G.....	48,138,707
Gleason, J.F.....	236
Godin, S.....	479,550,561,782

Goldammer, J.....	162
Goldman, A.....	739
Goutail, F.....	561,569,586,602
Grant, K.E.....	623
Grant, W.B.....	115,516,631
Grass, R.D.....	195,266,749,962
Greenhut, G.K.....	150
Grewe, R.....	363
Gruber, A.....	938
Gruzdev, A.N.....	232,393,397,695
Gulde, T.....	524
Gunawardena, R.....	259
Gusten, H.....	127
Haario, H.....	954
Haner, D.....	550
Hare, E.W.....	199
Harries, J.E.....	731
Harwood, M.H.....	413
Hasebe, F.....	310
Hassan, G.K.Y.....	275
Hayashi, M.....	565,573
Hayashida, S.....	635,863
Hayasaka, T.....	635
Hays, P.B.....	448
Heath, D.F.....	962
Heese, B.....	215
Heijboer, L.C.....	82
Heinrich, G.....	127
Helas, G.....	162
Henriksen, K.....	254
Herman, J.R.....	236,244,877,915
Hilsenrath, E.....	883,946
Hoegger, B.....	711
Hofmann, D.J.....	578,590

Hov, O.....215
 Howells, A.....154,290
 Hsu, N.C.....314
 Hudson, R.D.....119,263,877

Ilyas, M..... 33,819
 Isaksen, I.S.A..... 62,109
 Ishov, A.G.....326,667,723,899
 Ismail, S.....516
 Ito, M.....657
 Ito, T.....582,657
 Iwasaka, Y.....565,573

Jackman, C.H.....281
 Jagovkina, S.V.....401
 Jain, S.L.....758
 Jaramillo, M.....719
 Jaross, G.....877,942
 Jayaraman, K..... 24
 Jochum, A.M.....150
 John, K..... 85
 Johnson, D.....831
 Johnson, H.S.....302
 Johnston, P.V.....573,610,615,663,739
 Jones, N.B.....739
 Jones, R.L.....413,671,731
 Jonson, J.E.....109
 Jorgensen, T.S.....504
 Jucks, K.W.....831
 Justice, C.O.....101,158

Kadygrova, T.V.....390
 Kadyshevich, E.A.....679

Kajihara, R.....	657
Kalabokas, P.....	854
Kamenogradsky, N.E.....	762
Kaminski, J.W.....	492,508
Kampfer, N.....	691
Kanakidou, M.....	66
Kann, D.....	448
Kanzawa, H.....	565,606
Karol, I.L.....	334,338,401,409
Kelder, H.....	82,557
Kelly, P.M.....	3
Kendall, J.D.....	101,158
Kenner, R.D.....	471
Kerr, J.B.....	199,663,794,807,858,891
Kerridge, B.J.....	439,444,456,459,958
Kettner, C.....	641
Keys, J.G.....	610,615
Khattatov, V.....	500,535
Kim, J.H.....	119
Kinnison, D.E.....	302,318,322,623
Kiselev, A.A.....	334
Kitaoka, T.....	735
Kjome, N.....	500
Klein, E.....	488
Klenk, K.....	907
Klyagina, L.P.....	401
Kneipp, H.....	479
Knight, R.J.....	439,444
Knudsen, B.....	504
Kobayashi, M.....	657
Koenig, G.L.....	195,266
Kohler, U.....	240,742,807
Koike, M.....	573,849
Kolenda, J.....	479
Komhyr, W.D.....	195,266,578,749,858,962
Kondo, Y.....	565,573,849

Kondratiev, A.....	877
Kooi, S.A.....	115
Korpela, S.....	950
Kosmus, W.....	41
Kostiouchenko, S.V.....	386,835
Koudriavtsev, N.N.....	386,835
Kourtidis, K.....	870
Krola, E.....	954
Krueger, A.....	877,942
Kruger, B.C.....	483,512,827
Krymova, N.V.....	326
Krzyscin, J.W.....	203,207
Kugaenko, B.....	877
Kyro, E.....	479,504,532,807
Kyrola, E.....	950

La Bouar, E.....	561
Laamann, K.....	931
Lacaux, J.P.....	162
Lacoste, A-M.....	782
Lait, L.R.....	101
Lal, M.....	683,687
Lal, S.....	823,827
Lambeth, J.D.....	367
Lambert, A.....	456
Laprise, R.....	78
Lapworth, A.....	249
Larko, D.....	244
Larsen, S.H.H.....	211,254
Lathrop, J.A.....	578,807,858
Le Bras, G.....	330
Leonard, R.K.....	195
Leppelmeier, G.W.....	950
Levrat, G.....	711
Levy II, H.....	19

Li, Z.....	433
Liang, X.Z.....	433
Lienesch, J.H.....	887
Lobert, J.....	162
London, J.....	181,351
Long, C.....	448,631
Lopez-Valverde, M.A.....	444
Low, P.S.....	3
Lowe, R.P.....	790

Maguin, F.....	330
Makar, P.A.....	57
Makarov, O.V.....	130,675
Makino, Y.....	849
Mallison, W.H.....	719
Mantis, H.T.....	535
Marceau, F.J.....	330
Marks, C.J.....	444,452
Marti, J.....	475
Martin, N.A.....	703
Matsubara, K.....	582,657
Matsui, I.....	635,863
Matthews, W.A.....	7,573,739,858
Matthey, R.....	479
Maucher, G.....	524
Mauersberger, K.....	475
Mayor, S.D.....	631
McArthur, L.J.B.....	891
McConnell, J.C.....	57, 78,492,508,619
McDermid, I.S.....	645,649
McElroy, C.T.....	199,663,703,790,794,807,891
McFarlane, N.....	78,508
McKenzie, R.L.....	615,627
McNamara,, D.P.....	101
McPeters, R.D.....	236,244,883,907,911,915,919,923,931

Megie, G.....	15,122,550,561,782,950
Meleti, C.....	535,786
Merat, P.....	950
Merienne, M-F.....	219
Midwinter, C.....	891
Miller, A.J.....	448,887
Minato, A.....	863
Minga, A.....	631
Mitev, V.....	550
Mlynczak, M.....	359
Mo, K.C.....	370
Mokhov, I.I.....	397
Morandi, M.....	479,561
Moreau, G.....	846
Morris, P.....	439,444
Mravlag, E.....	378
Muller, C.....	557
Muller, M.....	488
Muller, R.....	298
Munro, R.....	958
Muramatsu, H.....	142
Murata, I.....	565
Murcray, D.G.....	703
Murcray, F.J.....	610
Naganuma, H.....	582
Nagatani, R.M.....	887
Nakane, H.....	635,863
Natarajan, M.....	367
Neininger, B.....	150
Nelson, W.....	962
Nerushev, A.F.....	37
Neuber, R.....	483,504,512
Newchurch, M.J.....	798
Newman, P.A.....	101

Nganga, D.....631
 Nightingale, T.....444
 Nogues-Paegle, J.....370
 Novelli, P.C.....134
 Nowicki, G.D.....631

Obrazcov, S.P.....754
 Oelhaf, H.....524,842
 Ogawa, T.....811
 Oikarinen, L.....954
 Oldham, D.J.....569,671
 Oltmans, S.J..... 19,134,578,807,858
 Owens, M.A.....174

Pan, L.....877,915
 Papayannis, A.....122
 Parrish, A.....294,645
 Patten Jr., K.O.....322
 Paukkunen, A.....807
 Pellinen, R.....950
 Perner, D.....520
 Perov, S.P.....839
 Pickering, K.E.....101,105
 Piesch, C.....842
 Piquard, J.....528,561
 Pirre, M.....285,330
 Planet, W.G.....263,887
 Pleim, J.E..... 70
 Plumb, I.C.....471
 Plumb, R.A.....594
 Pommereau, J-P.....528,561,569,586,602
 Poulet, G.....330
 Poulida, O.....174
 Price, J.D.....154,290,727

Puckrin, E.....	778
Putz, E.....	41
Quincy, D.M.....	195
Rabus, D.....	842
Rairoux, P.....	479
Rajewska-Wiech, B.....	653
Ramaroson, R.....	285,330,496
Rasmussen, R.A.....	259
Rattigan, O.V.....	413
Ravegnani, F.....	707
Reburn, J.....	439
Reeves, J.M.....	540,543,719
Reid, S.J.....	546
Remedios, J.J.....	439,444,452,456
Remsberg, E.E.....	294,934
Repapis, C.C.....	535
Ribordy, P.....	711
Rinsland, C.P.....	739
Rizi, V.....	550
Robert, C.....	846
Rodgers, C.D.....	444,452,456
Rohrer, F.....	74
Roisin, D.....	444
Roldugin, V.....	254
Rood, R.B.....	281
Roscoe, H.K.....	569,671,731
Roselle, S.J.....	89
Rosen, J.....	500
Rossi, M.J.....	355
Roth, A.....	520
Roth, E.P.....	488
Rudakov, V.....	500

Rummukainen, M.....	504,532
Ryabov, Y.A.....	839
Ryan, K.R.....	471
Ryan, W.F.....	93
Sacco, V.M.....	479
Sakoda, Y.....	582,657
Salichov, R.....	877
Samvelyn, H.....	877
Sandilands, J.W.....	492,508
Sarkissian, A.....	561,569,586,602
Sasano, Y.....	635,863
Savastyuk, V.V.....	675,679
Scala, J.R.....	105
Scheel, H.E.....	11
Schere, K.L.....	89
Scheuer, C.....	444,452
Schiller, C.....	488
Schill, H.....	711
Schmidt, M.....	170
Schmidt, R.W.H.....	127
Schmidt, U.....	488
Schmoe, M.....	649
Schoeberl, M.R.....	101,307
Schrems, O.....	483
Schurath, U.....	127
Scourfield, M.W.J.....	45,378,405,598
Seckmeyer, G.....	641
Seefeldner, M.....	842
Seftor, C.J.....	903,907,919
Seiler, W.....	11
Semyonov, V.K.....	762
Senik, I.A.....	130,675
Shalamyansky, A.M.....	401
Shende, R.R.....	24

Shi, G.Y.....	429
Shibata, S.....	582
Shibasaki, K.....	831
Shimizu, A.....	573
Shindell, D.T.....	540,543,719
Shine, K.P.....	467
Shiotani, M.....	310
Shitamichi, M.....	657
Sidhu, J.S.....	683
Sihvola, E.....	954
Simmons, A.....	146
Simon, P.C.....	166,374,421,425,496
Simpson, J.....	105
Singh, O.N.....	827
Singh, R.E.....	911
Sinyakov, V.P.....	762
Siskind, D.E.....	294,645
Sitnov, S.A.....	393
Sladkovic, R.....	11
Slanger, T.G.....	322
Solomon, S.....	359
Song, G.....	746
Spain, T.G.....	134
Squires, J.A.C.....	569
Sreedharan, C.R.....	24,807
Staehelin, J.....	186,711
Stanek, M.....	229
Starikovskaya, S.M.....	386
Stefanutti, L.....	479,550,561
Stein, B.....	479
Stephenson, J.A.E.....	405
Stevens, A.D.....	439
Stolarski, R.S.....	244,307
Stone, P.....	731
Stowe, L.L.....	631
Strocchi, V.....	48

Subbaraya, B.H.....	823,827
Sugimura, Y.....	849
Sugimoto, N.....	863
Sumi, T.....	735
Sunwoo, Y.....	53
Supperi, A.....	532
Svendby, T.....	211
Svenoe, T.....	254
Swann, N.R.....	703

Taalas, P.....	532
Takao, T.....	582
Tako, T.....	807
Tamminen, J.....	954
Tao, W.K.....	105
Tarasick, D.W.....	794,891
Taylor, F.W.....	439,444,452,456,459
Taylor, S.L.....	907,911,919,923
Terez, E.I.....	254
Terez, G.A.....	254
Thiel, S.....	641
Thomas, P.....	524
Thompson, A.M.....	101,105
Tiwari, V.S.....	24
Tonnessen, F.....	211
Torres, O.....	915
Tourpali, K.....	535
Traub, W.A.....	831
Trieschmann, O.....	524
Tsou, J.J.....	294,645
Tsukagoshi, Y.....	807
Tzoumaka, P.....	535

Uekubo, T.....	657
----------------	-----

Ueno, T.....	657
van den Bergh, H.....	355
Vandaele, A.C.....	166
Vandersee, W.....	190,742
Vanicek, K.....	226,229
Varotsos, C.....	854
Vasiliev, V.I.....	37,271
Vaughan, G.....	154,290,546,715,727
Veiga, R.E.....	631
Venturi, V.....	479
Viatte, P.....	711
Visconti, G.....	550
Vogel, B.....	97
Vogel, H.....	97
Volker, W.....	842
Volkovitsky, O.A.....	762
von der Gathe, P.....	483,504,512
Wahner, A.....	74
Walsh, T.D.....	649
Wang, W-C.....	417,433
Wardle, D.I.....	794,891
Warren, S.G.....	938
Watanabe, T.....	811
Watanabe, Y.....	582
Waters, J.....	322
Weaver, C.J.....	281
Wege, K.....	190
Weidauer, D.....	479
Weiss, H.....	931
Wellemeyer, C.G.....	877,903,907,911,919
Wells, R.J.....	444
Wendt, J.....	870

Woeste, L.....479
Wolf, J.P.....479
Wolfenden, R.....731
Woods, P.T.....703
Wuebbles, D.J.....302,318,322,623

Xiaochun, Z.....746
Xiuji, Z.....746

Yamanouchi, T.....573
Yamanaka, M.D.....606
Yamazaki, K.....606
Yushkov, V.....500

Zaitsev, I.....500
Zerefos, C.S.....535,786
Zhuang, Y.C.....417
Zimmermann, P.H..... 66
Ziomas, I.C.....535,786
Zuccagnoli, L.....479
Zunckel, M..... 45
Zvyaguintsev, A.M.....839

REPORT DOCUMENTATION PAGEForm Approved
OMB No. 0704-0188

Public reporting burden for this collection of information is estimated to average 1 hour per response, including the time for reviewing instructions, searching existing data sources, gathering and maintaining the data needed, and completing and reviewing the collection of information. Send comments regarding this burden estimate or any other aspect of this collection of information, including suggestions for reducing this burden, to Washington Headquarters Services, Directorate for Information Operations and Reports, 1215 Jefferson Davis Highway, Suite 1204, Arlington, VA 22202-4302, and to the Office of Management and Budget, Paperwork Reduction Project (0704-0188), Washington, DC 20503.

1. AGENCY USE ONLY (Leave blank)		2. REPORT DATE April 1994	3. REPORT TYPE AND DATES COVERED Conference Publication	
4. TITLE AND SUBTITLE Ozone in the Troposphere and Stratosphere, Part 1			5. FUNDING NUMBERS 916	
6. AUTHOR(S) Robert D. Hudson, Former Head Atmospheric Chemistry and Dynamics Branch				
7. PERFORMING ORGANIZATION NAME(S) AND ADDRESS(ES) Goddard Space Flight Center Greenbelt, Maryland 20771			8. PERFORMING ORGANIZATION REPORT NUMBER 94B00062	
9. SPONSORING/MONITORING AGENCY NAME(S) AND ADDRESS(ES) National Aeronautics and Space Administration Washington, D.C. 20546-0001			10. SPONSORING/MONITORING AGENCY REPORT NUMBER CP-3266 Part 1	
11. SUPPLEMENTARY NOTES Dr. Robert D. Hudson: University of Maryland				
12a. DISTRIBUTION/AVAILABILITY STATEMENT Unclassified-Unlimited Subject Category 47 Report available from the NASA Center for AeroSpace Information, 800 Elkridge Landing Road, Linthicum Heights, MD 21090; (301) 621-0390.			12b. DISTRIBUTION CODE	
13. ABSTRACT (Maximum 200 words) This is the first part of a 2-part Conference Publication. This document contains papers presented at the 1992 Quadrennial Ozone Symposium held at the Charlottesville, Virginia, from June 4-13, 1992. The papers cover topics in both Tropospheric and Stratospheric research. These topics include ozone trends and climatology, ground based, aircraft, balloon, rocket and satellite measurements, Arctic and Antarctic research, global and regional modeling, and volcanic effects.				
14. SUBJECT TERMS Stratosphere, Troposphere, Measurements, Model results, Ozone, Trends			15. NUMBER OF PAGES 454	
			16. PRICE CODE	
17. SECURITY CLASSIFICATION OF REPORT Unclassified	18. SECURITY CLASSIFICATION OF THIS PAGE Unclassified	19. SECURITY CLASSIFICATION OF ABSTRACT Unclassified	20. LIMITATION OF ABSTRACT Unlimited	

National Aeronautics and
Space Administration
Code JTT
Washington, D.C.
20546-0001

SPECIAL FOURTH-CLASS RATE
POSTAGE & FEES PAID
NASA
PERMIT No. G27

Official Business
Penalty for Private Use, \$300

S2 015 CP-3266-1 940405 S011092 A
NASA
CENTER FOR AEROSPACE INFORMATION
DOCUMENT SUPPLY
800 ELKRIDGE LANDING ROAD
LINTHICUM HEIGHTS MD 210902934



POSTMASTER: If Undeliverable (Section 158,
Postal Manual) Do Not Return